



*polymers*

# Advances in Sustainable Polymeric Materials

---

Edited by  
Cristina Cazan

Printed Edition of the Special Issue Published in *Polymers*

# **Advances in Sustainable Polymeric Materials**



# Advances in Sustainable Polymeric Materials

Editor

**Cristina Cazan**

MDPI • Basel • Beijing • Wuhan • Barcelona • Belgrade • Manchester • Tokyo • Cluj • Tianjin



*Editor*

Cristina Cazan

Product Design, Mechatronics

and Environment Department

Transilvania University of Brasov

Brasov

Romania

*Editorial Office*

MDPI

St. Alban-Anlage 66

4052 Basel, Switzerland

This is a reprint of articles from the Special Issue published online in the open access journal *Polymers* (ISSN 2073-4360) (available at: [www.mdpi.com/journal/polymers/special\\_issues/Adv\\_Sustain\\_Polym\\_Mater](http://www.mdpi.com/journal/polymers/special_issues/Adv_Sustain_Polym_Mater)).

For citation purposes, cite each article independently as indicated on the article page online and as indicated below:

|  |
|--|
| LastName, A.A.; LastName, B.B.; LastName, C.C. Article Title. <i>Journal Name</i> <b>Year</b> , <i>Volume Number</i> , Page Range. |
|--|

**ISBN 978-3-0365-7371-7 (Hbk)**

**ISBN 978-3-0365-7370-0 (PDF)**

© 2023 by the authors. Articles in this book are Open Access and distributed under the Creative Commons Attribution (CC BY) license, which allows users to download, copy and build upon published articles, as long as the author and publisher are properly credited, which ensures maximum dissemination and a wider impact of our publications.

The book as a whole is distributed by MDPI under the terms and conditions of the Creative Commons license CC BY-NC-ND.

# Contents

Preface to "Advances in Sustainable Polymeric Materials" . . . . . ix

**Cristina Cazan**

Advances in Sustainable Polymeric Materials

Reprinted from: *Polymers* **2022**, *14*, 4972, doi:10.3390/polym14224972 . . . . . 1

**Shiou Xuan Tan, Andri Andriyana, Hwai Chyuan Ong, Steven Lim, Yean Ling Pang and Gek Cheng Ngoh**

A Comprehensive Review on the Emerging Roles of Nanofillers and Plasticizers towards Sustainable Starch-Based Bioplastic Fabrication

Reprinted from: *Polymers* **2022**, *14*, 664, doi:10.3390/polym14040664 . . . . . 5

**Shiou Xuan Tan, Andri Andriyana, Steven Lim, Hwai Chyuan Ong, Yean Ling Pang and Gek Cheng Ngoh**

Rapid Ultrasound-Assisted Starch Extraction from Sago Pith Waste (SPW) for the Fabrication of Sustainable Bioplastic Film

Reprinted from: *Polymers* **2021**, *13*, 4398, doi:10.3390/polym13244398 . . . . . 33

**Alberto Di Bartolo, Giulia Infurna and Nadka Tzankova Dintcheva**

A Review of Bioplastics and Their Adoption in the Circular Economy

Reprinted from: *Polymers* **2021**, *13*, 1229, doi:10.3390/polym13081229 . . . . . 53

**Prapaipan Ungprasoot, Papisanee Muanruksa, Varavut Tanamool, James Winterburn and Pakawadee Kaewkannetra**

Valorization of Aquatic Weed and Agricultural Residues for Innovative Biopolymer Production and Their Biodegradation

Reprinted from: *Polymers* **2021**, *13*, 2838, doi:10.3390/polym13172838 . . . . . 79

**Luca Magazzini, Sara Grilli, Seif Eddine Fenni, Alessandro Donetti, Dario Cavallo and Orietta Monticelli**

The Blending of Poly(glycolic acid) with Polycaprolactone and Poly(L-lactide): Promising Combinations

Reprinted from: *Polymers* **2021**, *13*, 2780, doi:10.3390/polym13162780 . . . . . 91

**Ahmed Z. Naser, Ibrahim Deiab, Fantahun Defersha and Sheng Yang**

Expanding Poly(lactic acid) (PLA) and Polyhydroxyalkanoates (PHAs) Applications: A Review on Modifications and Effects

Reprinted from: *Polymers* **2021**, *13*, 4271, doi:10.3390/polym13234271 . . . . . 103

**Giulia Guidotti, Michelina Soccio, Massimo Gazzano, Valentina Siracusa and Nadia Lotti**

Poly(Alkylene 2,5-Thiophenedicarboxylate) Polyesters: A New Class of Bio-Based High-Performance Polymers for Sustainable Packaging

Reprinted from: *Polymers* **2021**, *13*, 2460, doi:10.3390/polym13152460 . . . . . 199

**Yanhui Kang, Fangyu Wang, Zeming Zhang and Jinping Zhou**

Dissolution and Interaction of Cellulose Carbamate in NaOH/ZnO Aqueous Solutions

Reprinted from: *Polymers* **2021**, *13*, 1092, doi:10.3390/polym13071092 . . . . . 217

**Sabzoi Nizamuddin, Yeong Jia Boom and Filippo Giustozzi**

Sustainable Polymers from Recycled Waste Plastics and Their Virgin Counterparts as Bitumen Modifiers: A Comprehensive Review

Reprinted from: *Polymers* **2021**, *13*, 3242, doi:10.3390/polym13193242 . . . . . 231

|  |     |
|--|-----|
| <b>Mihaela Cosnita, Monica Balas and Cristina Cazan</b><br>The Influence of Fly Ash on the Mechanical Properties of Water Immersed All Waste Composites<br>Reprinted from: <i>Polymers</i> <b>2022</b> , <i>14</i> , 1957, doi:10.3390/polym14101957 . . . . .   | 283 |
| <b>Nathapong Sukhawipat, Laksana Saengdee, Pamela Pasetto, Jatupol Junthip and Ekkachai Martwong</b><br>Sustainable Rigid Polyurethane Foam from Wasted Palm Oil and Water Hyacinth Fiber Composite—A Green Sound-Absorbing Material<br>Reprinted from: <i>Polymers</i> <b>2022</b> , <i>14</i> , 201, doi:10.3390/polym14010201 . . . . .                             | 299 |
| <b>Raluca Sanda Komartin, Brindusa Balanuca, Madalina Ioana Necolau, Anca Cojocaru and Raluca Stan</b><br>Composite Materials from Renewable Resources as Sustainable Corrosion Protection Coatings<br>Reprinted from: <i>Polymers</i> <b>2021</b> , <i>13</i> , 3792, doi:10.3390/polym13213792 . . . . .   | 313 |
| <b>Cristina Cazan, Alexandru Enesca and Luminita Andronic</b><br>Synergic Effect of TiO <sub>2</sub> Filler on the Mechanical Properties of Polymer Nanocomposites<br>Reprinted from: <i>Polymers</i> <b>2021</b> , <i>13</i> , 2017, doi:10.3390/polym13122017 . . . . .  | 329 |
| <b>Alexandru Enesca and Cristina Cazan</b><br>Polymer Composite-Based Materials with Photocatalytic Applications in Wastewater Organic Pollutant Removal: A Mini Review<br>Reprinted from: <i>Polymers</i> <b>2022</b> , <i>14</i> , 3291, doi:10.3390/polym14163291 . . . . .   | 353 |
| <b>David Hermann Lamparelli, Magdalena Maria Kleybolte, Malte Winnacker and Carmine Capacchione</b><br>Sustainable Myrcene-Based Elastomers via a Convenient Anionic Polymerization<br>Reprinted from: <i>Polymers</i> <b>2021</b> , <i>13</i> , 838, doi:10.3390/polym13050838 . . . . .  | 373 |
| <b>Zhenyu Wang, Pitchaimari Gnanasekar, Sandeep Sudhakaran Nair, Songlin Yi and Ning Yan</b><br>Curing Behavior and Thermomechanical Performance of Bioepoxy Resin Synthesized from Vanillyl Alcohol: Effects of the Curing Agent<br>Reprinted from: <i>Polymers</i> <b>2021</b> , <i>13</i> , 2891, doi:10.3390/polym13172891 . . . . .                               | 389 |
| <b>Eman M. Allam, Taysser A. Lashen, Saeyda A. Abou El-Enein, Mohamed A. Hassanin, Ahmed K. Sakr and Mohamed Y. Hanfi et al.</b><br>Cetylpyridinium Bromide/Polyvinyl Chloride for Substantially Efficient Capture of Rare Earth Elements from Chloride Solution<br>Reprinted from: <i>Polymers</i> <b>2022</b> , <i>14</i> , 954, doi:10.3390/polym14050954 . . . . . | 403 |
| <b>Claudia Möhl, Timo Weimer, Metin Caliskan, Tom Hager, Stephan Baz and Hans-Jürgen Bauder et al.</b><br>Flax Fibre Yarn Coated with Lignin from Renewable Sources for Composites<br>Reprinted from: <i>Polymers</i> <b>2022</b> , <i>14</i> , 4060, doi:10.3390/polym14194060 . . . . .  | 427 |
| <b>Philip R. Onffroy, Nathan T. Herrold, Harrison G. Goehrig, Kalie Yuen and Katsuyuki Wakabayashi</b><br>Polylactic Acid Chemical Foaming Assisted by Solid-State Processing: Solid-State Shear Pulverization and Cryogenic Milling<br>Reprinted from: <i>Polymers</i> <b>2022</b> , <i>14</i> , 4480, doi:10.3390/polym14214480 . . . . .                            | 443 |
| <b>Vânia Isabel Sousa, Joana Filipa Parente, Juliana Filipa Marques, Marta Adriana Forte and Carlos José Tavares</b><br>Microencapsulation of Essential Oils: A Review<br>Reprinted from: <i>Polymers</i> <b>2022</b> , <i>14</i> , 1730, doi:10.3390/polym14091730 . . . . .  | 459 |

|   |            |
|---|------------|
| <b>Anish Khan, Aftab Aslam Parwaz Khan, Hadi M. Marwani, Maha Moteb Alotaibi, Abdullah M. Asiri and Ayyar Manikandan et al.</b><br>Sensitive Non-Enzymatic Glucose Electrochemical Sensor Based on Electrochemically Synthesized PANI/Bimetallic Oxide Composite<br>Reprinted from: <i>Polymers</i> <b>2022</b> , <i>14</i> , 3047, doi:10.3390/polym14153047 . . . . . | <b>501</b> |
| <b>Mohammad F. Bayan, Saeed M. Marji, Mutaz S. Salem, M. Yasmin Begum, Kumarappan Chidambaram and Balakumar Chandrasekaran</b><br>Development of Polymeric-Based Formulation as Potential Smart Colonic Drug Delivery System<br>Reprinted from: <i>Polymers</i> <b>2022</b> , <i>14</i> , 3697, doi:10.3390/polym14173697 . . . . .                                     | <b>515</b> |





# Preface to “Advances in Sustainable Polymeric Materials”

The field of sustainable materials science is rapidly evolving, with an increasing emphasis on developing new materials and technologies that minimize environmental impact while meeting the needs of society. Polymeric materials are ubiquitous in modern life, but their production and disposal can contribute to significant environmental damage. “Advances in Sustainable Polymeric Materials” aims to address this challenge by presenting the latest research and technological developments in sustainable polymeric materials.

“Advances in Sustainable Polymeric Materials” is a compilation of 22 articles highlighting the recent progress in the research and development of polymeric materials that is both efficient and non-polluting. The growing concern of the environmental impact of traditional manufacturing practices has led to an increasing interest in developing new materials and methods that are more eco-friendly. The articles in this collection address this concern by exploring various aspects of sustainable materials, from their synthesis to their applications in different industries.

This reprint provides a comprehensive overview of sustainable polymeric materials, covering topics such as using renewable resources, biodegradability, recycling, developing new processing techniques, sustainable drug delivery systems, and photocatalytic materials for wastewater treatment and innovative biopolymer production methods. These articles demonstrate the broad scope of research in sustainable materials and the potential for these materials to be used in a wide range of applications.

The contributors to this reprint are global experts in the field of sustainable polymeric materials. They have shared their cutting-edge research and insights to provide readers with a comprehensive overview of this rapidly evolving field. This reprint is intended for researchers, academics, students, and industry professionals interested in developing and applying sustainable polymeric materials.

**Cristina Cazan**  
*Editor*



Editorial

# Advances in Sustainable Polymeric Materials

Cristina Cazan 

Renewable Energy Systems and Recycling Research Center, Transilvania University of Brasov,  
500036 Brasov, Romania; c.vladuta@unitbv.ro

Sustainable polymeric materials are materials of great technological importance and are specially created to meet unique demands regarding: mechanical resistance and rigidity; corrosion resistance; resistance to the action of chemical agents; low weight; dimensional stability; resistance to variable stress, shock and wear; insulating properties; and aesthetics. These characteristics have led to the use of composite materials on an increasingly large scale and stimulated research to discover new types of composite materials with improved properties. Major concerns and realisations of high-performance composite materials exist in all developed countries, due to the desire for continued technological development and the use of qualitatively superior materials achieved through efficient and non-polluting processes and technologies.

This Special Issue includes twenty-two articles highlighting advances in virgin and waste polymeric materials, mainly advancements in the research and development of synthesis, characterisation, processing, morphology, structure, properties and applications for nanocomposites and hybrid polymer composites, blends and polymeric materials for sustainability.

Below is a brief summary of the papers included in this issue, considering the types of advances in sustainable polymeric materials used with applicability in different fields of activity.

In the actual contest of the environment's care and pollution reduction, biodegradable plastics obtained from renewable sources represent a great challenge for the research domain. Xuan Tan et al. [1] highlight the most significant achievements in this research direction, particularly on the role of nanofillers and plasticisers utilised in bioplastic fabrication, focusing on starch-based bioplastics. Xuan Tan et al. [2] optimised a rapid ultrasound-assisted starch extraction from sago pith waste (PSW) to fabricate a sustainable bioplastic film. This process was proven to be more efficient than conventional extraction economically and potentially sustainable for the production of bioplastic film. The ultrasound-extracted sago starch was used to prepare a bioplastic film via the solution-casting method. The article [3] traces a necessary and current state of the art on bioplastics, coherently addressing concepts, classifications, production chain, biodegradability and compostability standards, LCA of bioplastics, and finally, a summary of opportunities and possible challenges. Ungprasoot et al. [4] obtained bioplastic from waste biomass using water hyacinths, bagasse and rice straw via extraction techniques. First, it was synthesised carboxymethylcellulose (CMC) and then used for biopolymer production, using tapioca starch solution and glycerol as a binder and an additive. Biopolymers obtained can be an alternative material to develop into food and drink packaging, being an environmentally friendly product. At the same time, these can be naturally decomposed in a short time, leading to a reduction in pollution from petroleum-based plastics.

Magazzini et al. [5] presented a process of obtaining physical mixtures of biodegradable polymers poly (glycolic acid) (PGA) with poly(L-lactide) (PLLA) and polycaprolactone (PCL) using the melt blending technique. Their morphology, wettability, thermal properties, and degradation behaviour were analysed using SEM, contact angle, DSC, and TGA. Their results show that PGA affected polymer matrices' thermal and degradation behaviour and

**Citation:** Cazan, C. Advances in Sustainable Polymeric Materials. *Polymers* **2022**, *14*, 4972. <https://doi.org/10.3390/polym14224972>

Received: 26 October 2022

Accepted: 14 November 2022

Published: 17 November 2022

**Publisher's Note:** MDPI stays neutral with regard to jurisdictional claims in published maps and institutional affiliations.



**Copyright:** © 2022 by the author. Licensee MDPI, Basel, Switzerland. This article is an open access article distributed under the terms and conditions of the Creative Commons Attribution (CC BY) license (<https://creativecommons.org/licenses/by/4.0/>).

accelerated their degradation, a trait desirable for creating biodegradable and compostable plastics while not increasing the cost substantially.

Naser et al. [6] reviewed modification techniques on the mechanical properties of PLA and PHAs. The main aim of this review article is to widen the applicability of both biopolymers so that they can eventually replace petroleum-based plastics in new potential applications and therefore reduce the amount of waste and pollution.

Recent research studies demonstrated the tremendous potential biodegradability of both thiophene-based homopolymers and copolymeric systems, opening a new method for the industrial recycling of furan and thiophene-based materials. Thus, Guidotti et al. [7] synthesised polycondensation materials suitable for the realisation of rigid and flexible films for packaging applications.

The CarbaCell process is a promising alternative to produce recycled cellulose filaments, membranes, aerogels, and clothing fabrics, using cellulose carbamate as an active intermediate for fibre spinning. The industrialisation of this process is significant for the environment and economic development. Kang et al. [8] detailed the dissolution process of CarbaCell, and the effects of different NaOH and ZnO contents on the dissolution of CC were compared.

The most recent method of valorising recycled polymeric materials is their use of obtaining materials used in the construction field being a low-cost and somehow environmental beneficial solution. Nizamuddin et al. [9] presented the benefits of polymer-modified bitumen and some limitations and challenges that need to be considered when using virgin and recycled plastic to enhance bitumen performance. Different polymers such as HDPE, LDPE, LLDPE, MDPE, PP, PS, PET, EMA, and EVA have been successfully employed for bitumen modification. Different characteristics of plastics-modified bitumen, including chemical, thermal, rheological, structural, and mechanical properties, were investigated.

Cosnita et al. [10] presented the development of new value-added composite materials based on only waste: recycling tire rubber, polyethylene terephthalate (PET), high-density polyethylene (HDPE), wood sawdust, and fly ash. The influence of fly ash on the mechanical properties and water stability of the new “all-waste composites” was assessed, considering their applications as outdoor products in the construction field.

Sukhawipat et al. [11] developed a novel rigid sound-absorbing material made from used palm oil-based polyurethane foam (PUF) and water hyacinth fibre (WHF) composite. This material might be a promising candidate for the sound-absorbing material industry due to its high efficiency with an NCO index of 100 and 1%wt of WHF, mechanical characteristics, flammability and sound absorption.

Komartin et al. [12] presented a relevant study to obtain new sustainable composites based on epoxidised linseed oil and kraft lignin as anticorrosive coatings. The structure, thermal stability, dynamic mechanical behaviour and corrosion protection of carbon steel were investigated. The obtained bio-based epoxy-lignin coatings can mitigate the corrosion processes for carbon steel.

Recent advances in obtaining polymeric materials by improving the interfaces (of inorganic/organic nature) using different fillers and coupling agents have shown strong potential to generate materials. Nanocomposites with polymer matrix were discussed in many studies. Still, Cazan et al. [13] offer excellent opportunities to explore new functionalities of TiO<sub>2</sub> as a reinforcement agent in polymeric nanocomposites beyond those of conventional materials. This review aims to provide specific guidelines on the correlations between the structures and properties of TiO<sub>2</sub> nanocomposites, established and explained based on interfaces realised between the polymer matrix and inorganic filler.

Enesca et al. [14] realised a critical presentation of the photocatalytic activity of TiO<sub>2</sub>, ZnO, WO<sub>3</sub>, Fe<sub>2</sub>O<sub>3</sub>, and Bi<sub>2</sub>MoO<sub>6</sub> from polymer composites against different organic compounds (dyes, active pharmaceutical molecules, phenol, etc.). The effect of other polymeric composites and photocatalytic parameters on the overall photocatalytic efficiency is described. Representative studies were included and correlated with outlining the significance

of polymeric composite composition and testing parameters on the photocatalytic removal of pollutants.

Lamparelli et al. [15] present a relevant study to demonstrate the processability and characterisation of sustainable elastomers by anionic copolymerisation of renewable terpenes in a wide range of compositions with interesting thermal profiles and different polymeric architectures by simply modulating the alimentation feed and the [monomers]/[initiator systems] ratio. Thus, homo- and co-polymerizations of myrcene with styrene and isoprene and terpolymerization of all monomers have been reached using sodium hydride in combination with triisobutylaluminum as the anionic initiating system at 100 °C in toluene.

Wang et al. [16] conducted a systematic study to understand the interactions between vanillyl alcohol-based epoxy better and cross-linkers across-linkerserties of the cured epoxy systems. The authors emphasise the interactions between molecular structure and functionality of the cross-linker and the vanillyl alcohol epoxy resin during the curing process aspects beneficial for optimising bioepoxy formulations targeting industrial applications.

The acquisition of rare earth elements is significant from the point of view of environmental protection and the current state of natural resources. In this regard, Allam et al. [17] reported synthesising and characterising a new polymeric composite based on polyvinyl chloride (PVC). RE ions' desorption/uptake capacity from loaded cetylpyridinium bromide/polyvinylchloride (CPB/PVC) sorbent was investigated. High-extract rare earth elements (REEs) uptake values were achieved, and the optimal sorption conditions were thoroughly investigated.

Möhl et al. [18] provided a comparative study of using lignin-based thermoplastic on commercial flex yarn to improve the tensile properties compared to the flex yarn itself.

Onffroy et al. [19] presented an effective chemical foaming process of polylactic acid (PLA) via the solid-state processing methods of solid-state shear pulverisation (SSSP) and cryogenic milling. The effects of the pre-foaming solid-state processing method and chemical foaming agent (CFA) concentration were investigated.

Polymer materials are also widely used in the medical field. Nowadays, the use of essential oils has increased. Essential oils (EOs) are complex polymeric mixtures of volatile compounds extracted from different parts of plants by other methods. Sousa et al. [20] presented different microencapsulation strategies for general and essential oils, some extraction methods for essential oils, and their applications. Khan et al. [21] highlight an essential issue for the safety and protection of human health, namely, timely and accurate glucose detection and monitoring. The authors developed sensitive and reliable electrochemical sensors for glucose determination to solve this problem using affordable and readily available materials. Thus, a non-enzymatic glucose electrochemical sensor based on an electrochemically synthesised PANI/Bimetallic oxide composite was reported. Polyaniline was synthesised by the electrochemical method, more precisely, the chronoamperometric method. Bayan et al. [22] synthesised a smart drug delivery system based on pH-sensitive polymeric formulations using a free radical bulk polymerisation method with different monomer and crosslinker concentrations. The optimisation of this smart system was investigated to achieve a colon-specific drug delivery, thereby improving the therapeutic efficacy and reducing the dosing frequency and potential side effects.

As the editor of this Special Issue, I recognise that the diversity and innovation of new sustainable polymeric materials rapidly developing in the multidisciplinary research field, sometimes using waste as raw materials, cannot be collected in a single volume. However, I am sure that this collection will contribute to the interest in the research in this area, providing our readers with a broad and updated overview of this topic.

**Funding:** This research received no external funding.

**Acknowledgments:** I acknowledge all the authors and reviewers who have contributed to achieving this Special Issue. In addition, I would like to thank the technical support team at MDPI for their assistance in preparing this Issue.

**Conflicts of Interest:** The author declares no conflict of interest.

## References

1. Tan, S.X.; Andriyana, A.; Ong, H.C.; Lim, S.; Pang, Y.L.; Ngoh, G.C. A Comprehensive Review on the Emerging Roles of Nanofillers and Plasticizers towards Sustainable Starch-Based Bioplastic Fabrication. *Polymers* **2022**, *14*, 664. [CrossRef] [PubMed]
2. Tan, S.X.; Andriyana, A.; Lim, S.; Ong, H.C.; Pang, Y.L.; Ngoh, G.C. Rapid Ultrasound-Assisted Starch Extraction from Sago Pith Waste (SPW) for the Fabrication of Sustainable Bioplastic Film. *Polymers* **2021**, *13*, 4398. [CrossRef] [PubMed]
3. Di Bartolo, A.; Infurna, G.; Dintcheva, N.T. A Review of Bioplastics and Their Adoption in the Circular Economy. *Polymers* **2021**, *13*, 1229. [CrossRef] [PubMed]
4. Ungprasoot, P.; Muanruksa, P.; Tanamool, V.; Winterburn, J.; Kaewkannetra, P. Valorization of Aquatic Weed and Agricultural Residues for Innovative Biopolymer Production and Their Biodegradation. *Polymers* **2021**, *13*, 2838. [CrossRef] [PubMed]
5. Magazzini, L.; Grilli, S.; Fenni, S.E.; Donetti, A.; Cavallo, D.; Monticelli, O. The Blending of Poly(glycolic acid) with Polycaprolactone and Poly(l-lactide): Promising Combinations. *Polymers* **2021**, *13*, 2780. [CrossRef]
6. Naser, A.Z.; Deiab, I.; Defersha, F.; Yang, S. Expanding Poly(lactic acid) (PLA) and Polyhydroxyalkanoates (PHAs) Applications: A Review on Modifications and Effects. *Polymers* **2021**, *13*, 4271. [CrossRef]
7. Guidotti, G.; Soccio, M.; Gazzano, M.; Siracusa, V.; Lotti, N. Poly(Alkylene 2,5-Thiophenedicarboxylate) Polyesters: A New Class of Bio-Based High-Performance Polymers for Sustainable Packaging. *Polymers* **2021**, *13*, 2460. [CrossRef]
8. Kang, Y.; Wang, F.; Zhang, Z.; Zhou, J. Dissolution and Interaction of Cellulose Carbamate in NaOH/ZnO Aqueous Solutions. *Polymers* **2021**, *13*, 1092. [CrossRef]
9. Nizamuddin, S.; Boom, Y.J.; Giustozzi, F. Sustainable Polymers from Recycled Waste Plastics and Their Virgin Counterparts as Bitumen Modifiers: A Comprehensive Review. *Polymers* **2021**, *13*, 3242. [CrossRef]
10. Cosnita, M.; Balas, M.; Cazan, C. The Influence of Fly Ash on the Mechanical Properties of Water Immersed All Waste Composites. *Polymers* **2022**, *14*, 1957. [CrossRef]
11. Sukhawipat, N.; Saengdee, L.; Pasetto, P.; Junthip, J.; Martwong, E. Sustainable Rigid Polyurethane Foam from Wasted Palm Oil and Water Hyacinth Fiber Composite—A Green Sound-Absorbing Material. *Polymers* **2022**, *14*, 201. [CrossRef] [PubMed]
12. Komartin, R.S.; Balanuca, B.; Necolau, M.I.; Cojocar, A.; Stan, R. Composite Materials from Renewable Resources as Sustainable Corrosion Protection Coatings. *Polymers* **2021**, *13*, 3792. [CrossRef] [PubMed]
13. Cazan, C.; Enesca, A.; Andronic, L. Synergic Effect of TiO<sub>2</sub> Filler on the Mechanical Properties of Polymer Nanocomposites. *Polymers* **2021**, *13*, 2017. [CrossRef]
14. Enesca, A.; Cazan, C. Polymer Composite-Based Materials with Photocatalytic Applications in Wastewater Organic Pollutant Removal: A Mini Review. *Polymers* **2022**, *14*, 3291. [CrossRef] [PubMed]
15. Lamparelli, D.H.; Kleybolte, M.M.; Winnacker, M.; Capacchione, C. Sustainable Myrcene-Based Elastomers via a Convenient Anionic Polymerization. *Polymers* **2021**, *13*, 838. [CrossRef]
16. Wang, Z.; Gnanasekar, P.; Nair, S.S.; Yi, S.; Yan, N. Curing Behavior and Thermomechanical Performance of Bioepoxy Resin Synthesized from Vanillyl Alcohol: Effects of the Curing Agent. *Polymers* **2021**, *13*, 2891. [CrossRef]
17. Allam, E.M.; Lashen, T.A.; Abou El-Enein, S.A.; Hassanin, M.A.; Sakr, A.K.; Hanfi, M.Y.; Sayyed, M.I.; Al-Otaibi, J.S.; Cheira, M.F. Cetylpyridinium Bromide/Polyvinyl Chloride for Substantially Efficient Capture of Rare Earth Elements from Chloride Solution. *Polymers* **2022**, *14*, 954. [CrossRef]
18. Möhl, C.; Weimer, T.; Caliskan, M.; Hager, T.; Baz, S.; Bauder, H.-J.; Stegmaier, T.; Wunderlich, W.; Gresser, G.T. Flax Fibre Yarn Coated with Lignin from Renewable Sources for Composites. *Polymers* **2022**, *14*, 4060. [CrossRef]
19. Onffroy, P.R.; Herrold, N.T.; Goehrig, H.G.; Yuen, K.; Wakabayashi, K. Polylactic Acid Chemical Foaming Assisted by Solid-State Processing: Solid-State Shear Pulverization and Cryogenic Milling. *Polymers* **2022**, *14*, 4480. [CrossRef]
20. Sousa, V.I.; Parente, J.F.; Marques, J.F.; Forte, M.A.; Tavares, C.J. Microencapsulation of Essential Oils: A Review. *Polymers* **2022**, *14*, 1730. [CrossRef]
21. Khan, A.; Khan, A.A.P.; Marwani, H.M.; Alotaibi, M.M.; Asiri, A.M.; Manikandan, A.; Siengchin, S.; Rangappa, S.M. Sensitive Non-Enzymatic Glucose Electrochemical Sensor Based on Electrochemically Synthesized PANI/Bimetallic Oxide Composite. *Polymers* **2022**, *14*, 3047. [CrossRef] [PubMed]
22. Bayan, M.F.; Marji, S.M.; Salem, M.S.; Begum, M.Y.; Chidambaram, K.; Chandrasekaran, B. Development of Polymeric-Based Formulation as Potential Smart Colonic Drug Delivery System. *Polymers* **2022**, *14*, 3697. [CrossRef] [PubMed]

Review

# A Comprehensive Review on the Emerging Roles of Nanofillers and Plasticizers towards Sustainable Starch-Based Bioplastic Fabrication

Shiou Xuan Tan <sup>1</sup>, Andri Andriyana <sup>1,2</sup>, Hwai Chyuan Ong <sup>3</sup>, Steven Lim <sup>4,5,\*</sup>, Yean Ling Pang <sup>4,5</sup> and Gek Cheng Ngoh <sup>6,\*</sup>

- <sup>1</sup> Department of Mechanical Engineering, Faculty of Engineering, Universiti Malaya, Kuala Lumpur 50603, Malaysia; kva190014@siswa.um.edu.my (S.X.T.); andri.andriyana@um.edu.my (A.A.)
- <sup>2</sup> Center of Advanced Materials, Faculty of Engineering, Universiti Malaya, Kuala Lumpur 50603, Malaysia
- <sup>3</sup> Future Technology Research Center, National Yunlin University of Science and Technology, 123 University Road, Section 3, Douliou, Yunlin 64002, Taiwan; onghc@yuntech.edu.tw
- <sup>4</sup> Department of Chemical Engineering, Lee Kong Chian Faculty of Engineering and Science, Universiti Tunku Abdul Rahman, Kajang 43000, Malaysia; pangyl@utar.edu.my
- <sup>5</sup> Centre of Photonics and Advanced Materials Research, Universiti Tunku Abdul Rahman, Kajang 43000, Malaysia
- <sup>6</sup> Department of Chemical Engineering, Faculty of Engineering, Universiti Malaya, Kuala Lumpur 50603, Malaysia
- \* Correspondence: stevenlim@utar.edu.my (S.L.); ngoh@um.edu.my (G.C.N.)

**Abstract:** Petroleum-based plastics are associated with environmental pollution problems owing to their non-biodegradable and toxic properties. In this context, renewable and biodegradable bioplastics possess great potential to replace petroleum-based plastics in mitigating these environmental issues. Fabrication of bioplastic films involves a delicate mixture of the film-forming agent, plasticizer and suitable solvent. The role of the plasticizer is to improve film flexibility, whereas the filler serves as a reinforcement medium. In recent years, much research attention has been shifted toward devising diverse methods for enhancing the performance of bioplastics, particularly in the utilization of environmentally benign nanoparticles to displace the conventional hazardous chemicals. Along this line, this paper presents the emergence of nanofillers and plasticizers utilized in bioplastic fabrication with a focus on starch-based bioplastics. This review paper not only highlights the influencing factors that affect the optical, mechanical and barrier properties of bioplastics, but also revolves around the proposed mechanism of starch-based bioplastic formation, which has rarely been reviewed in the current literature. To complete the review, prospects and challenges in bioplastic fabrication are also highlighted in order to align with the concept of the circular bioplastic economy and the United Nations' Sustainable Development Goals.

**Keywords:** starch-based bioplastic; nanofiller; bioplastic fabrication; plasticizer; mechanism

**Citation:** Tan, S.X.; Andriyana, A.; Ong, H.C.; Lim, S.; Pang, Y.L.; Ngoh, G.C. A Comprehensive Review on the Emerging Roles of Nanofillers and Plasticizers towards Sustainable Starch-Based Bioplastic Fabrication. *Polymers* **2022**, *14*, 664. <https://doi.org/10.3390/polym14040664>

Academic Editor: Cristina Cazan

Received: 3 December 2021

Accepted: 21 January 2022

Published: 10 February 2022

**Publisher's Note:** MDPI stays neutral with regard to jurisdictional claims in published maps and institutional affiliations.



**Copyright:** © 2022 by the authors. Licensee MDPI, Basel, Switzerland. This article is an open access article distributed under the terms and conditions of the Creative Commons Attribution (CC BY) license (<https://creativecommons.org/licenses/by/4.0/>).

## 1. Introduction

Fossil-fuel-derived plastics have vast applications ranging from food packaging, bottle drinks, furniture, household appliances and toys to medical equipment and even construction materials [1,2]. The high demand for plastics in these applications can be attributed to their low production cost and favourable properties such as high mechanical strength while maintaining a light weight, high resistance to degradation by water, chemicals, sunlight, and bacteria, as well as their capacity to provide adequate electrical and thermal insulation [3]. However, these conventional plastics are mainly derived from non-renewable petrochemical sources which can be degraded neither by the influence of solar radiation nor by the microbial decomposers [4]. As a consequence, plastic wastes continue to accumulate



in the environment with the excessive usage of petroleum-based plastic products and hazardous chemical additives, which could cause severe impacts to the ecosystem.

Considering their non-biodegradability, for petroleum-based plastic wastes, recycling, landfill and incineration must be resorted to for their disposal [5]. It has been reported that only 7% of the 34 million tons of plastic waste produced per year was being recycled, while the remaining 93% ended up in landfills and oceans [2]. Plastic waste in the ocean could cause serious injuries, deformities or intoxication to marine animals when it is consumed due to the addition of endocrine disruptor compounds to the polymer matrix to enhance flexibility or colour properties [6]. The low recycling effort is mainly due to the high energy consumption of recycling. It was reported by Ross and Evans [7] that 18.9 MJ of energy was required to produce 1 kg of recycled material, which is tantamount to 23.5% of the cost required for manufacturing the same product from the virgin raw materials. On the other hand, the disposal of plastic waste in landfills has several disadvantages. Besides requiring a large land area, the major concerns are emission of toxic gases due to the absence of a gas collection system in normal practice and the probable leaching problem from landfill sites [8,9]. Furthermore, the incineration of plastic waste produces a net increase in carbon dioxide and may also emit hazardous gases such as sulfur dioxide, carbon monoxide and nitric oxide [10]. To solve and alleviate these economic and environmental problems brought about by petroleum-based plastics, considerable efforts have been directed towards the development of bioplastics which are biodegradable and more sustainable.

Bioplastics can be defined as biobased polymers derived from renewable resources or which are biodegradable and/or compostable naturally by microorganisms [11,12]. With growing concern about the economic and environmental problems caused by the utilization of petroleum-based plastics, the demand for bioplastics has increased tremendously in recent years. The global production capacity of bioplastic had increased by 38% per annum between 2003 and 2007, with a further projection that it would reach 3.45 million tonnes in 2020 [13]. The important characteristics of bioplastics include favourable mechanical and thermoforming properties, high gas and water vapor permeability, transparency and availability [14]. More importantly, the biodegradation products are usually non-toxic to the environment [1].

Apart from the generation of plastic waste, food waste generation was also alarming in Malaysia as it contributed up to 70% of the national municipal solid waste [15]. There is no comprehensive food waste management framework being established, which indicates that no specific method is available to dispose of food waste in a sustainable manner [16]. Despite the fact that 90% of food waste is biodegradable, reuse and recycle of the waste remains very low [15,17]. Recently, food wastes with high starch content such as mango seed [18], avocado seed [19], durian seed [20], jackfruit seed [12] and cassava peel [21] that can be utilized as bioplastic matrix has been extensively studied. These food wastes with high starch content have many advantages: they have a large supply availability and are low in price, biodegradable and renewable [22]. Nevertheless, native starch is brittle and has few mechanical properties, leading to poor film-forming capacity. In view of these drawbacks, most researches have focused on enhancing the functional properties and bonding strength of starch-based bioplastics through incorporation of less hazardous plasticizers and fillers to alleviate the brittleness of the materials [23].

As compared with petroleum-based plastics, bioplastics present three main disadvantages: the processing window, the performance and the cost. The narrow processing window, poor gas and water barrier properties, unbalanced mechanical properties, low softening temperature and weak resistivity of plastics have collectively limited their broader applications. Through substantial research work, the above limitations could be overcome by the introduction of nanofillers [24,25]. Meanwhile, the barrier properties of bioplastic could also be improved by incorporating suitable plasticizer. However, the cost of manufacturing bioplastics such as polylactic acid (PLA) and polyhydroxyalkanoate (PHA) is higher than that of conventional plastics. Therefore, blending them with biomaterial such as cellulose is a feasible way to minimize the cost [26].

The present article reviews the main classifications of bioplastics according to the feedstocks, the critical roles of emerging nanofillers and the selection of environmentally benign plasticizers in enhancing the properties of starch-based bioplastics. This is followed by an elucidation of the formation mechanism of starch-based bioplastics to provide a deeper insight into their properties down to the molecular level. The importance of the effects of different synthesizing parameters in the solvent-casting technique on the optical, mechanical and barrier properties of bioplastics is also discussed. Challenges and suggestions for future research are highlighted. These state-of-the-art reviews are still rarely available in the current literature. Therefore, this review could bridge the gap of the relevant scientific information required to transform the bioplastics industry into a more sustainable pathway in line with the circular economy.

## 2. Classifications of Bioplastics

Currently, bioplastics have been developed in three different generations based on the types of feedstock used for the fabrication. The classification of bioplastics with relevant examples is depicted in Figure 1. Each generation of bioplastics has its respective advantages and disadvantages. Therefore, in-depth understanding of the properties of bioplastics is crucial to devise appropriate modification methods to suit different applications.

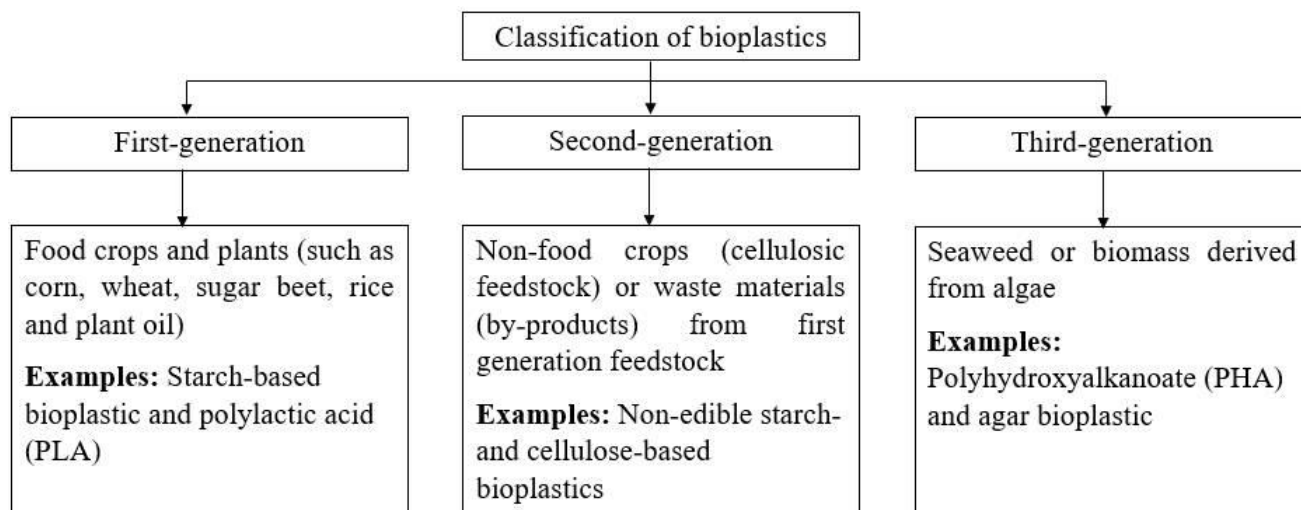


**Figure 1.** Classifications of bioplastics based on feedstock.

### 2.1. First-Generation Bioplastic

The feedstocks of the first-generation bioplastics are usually comprised of edible food crops or carbohydrate-rich plants such as corn or sugarcane. This is the most efficient feedstock since it requires the least land area to produce the highest yield based on highly matured plantation technology. Notable examples include corn, wheat, sugarcane, potato, sugar beet and rice. Starch-based bioplastics and PLA are examples of first-generation bioplastics derived from first-generation feedstocks.

Starch is a type of carbohydrate comprised of carbon, hydrogen and oxygen with a mole ratio of 6:10:5 [27]. It contains two main polysaccharide units: (i) linear chain amylose, which comprises 15–20% of starch; and (ii) branched amylopectin, which composes the majority of the remaining starch. Starch is also a natural semi-crystalline biopolymer of D-glucose [22]. The typical structures of amylose and amylopectin in starch are illustrated in Figure 2. Amylose units form the irregular amorphous region, while the well-ordered amylopectin region contributes to the crystallinity of starch. The concentration of amylose determines the gelling ability of starch, while the concentration of amylopectin controls the water-holding capacity of starch [28]. As the concentration of amylose increases, more starch will be converted into a gel structure and thus increase its elongation at break [27,28].

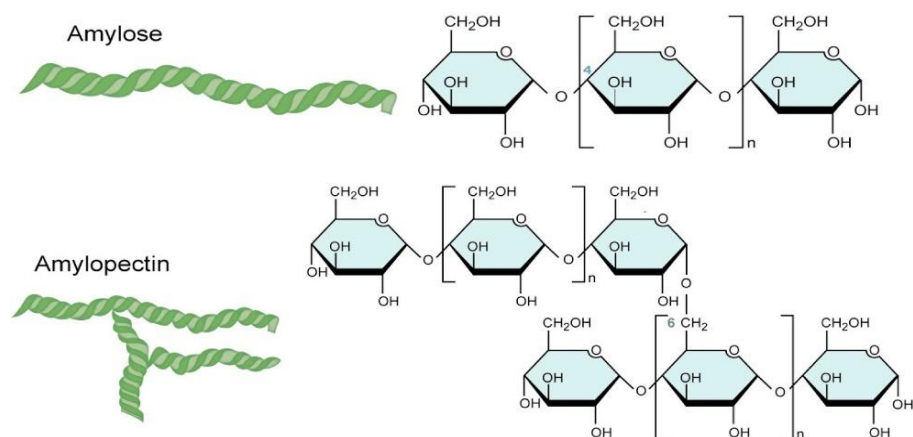


**Figure 2.** Structure of amylose and amylopectin in starch. Reprinted with permission from Ref. [28]. Copyright 2015 Elsevier Ltd.

Native starch is challenging to use due to its brittleness, low mechanical properties and poor film forming capacity, as previously described. Plasticization and blending of starch with other polymers are often adopted to overcome these shortcomings [27]. In the fabrication of starch-based bioplastic, water is often used as a primary plasticizer because of its capability to hydrolyse the molecular bond structure of starch when heated together. The water content will also affect the oxygen permeability (OP) of starch-based bioplastic film. Under low-humidity conditions, the film can serve as an excellent barrier against oxygen transmission [27]. Besides, the hydrophilic nature due to the presence of numerous hydroxyl (O-H) groups and the poor long-term stability of native starch hinder its substitution for conventional plastic film. It has been reported that the crystalline amylopectin region obstructs the binding between plasticizers with the O-H groups, causing the starch matrix to retrograde after a certain period of time [29]. Therefore, fillers such as layered silicates, organic, inorganic and carbonaceous nanofillers can be incorporated into the matrix to reinforce the film, which is discussed in more detail in Section 3 [30].

In a bioplastic composite, starch acts as the matrix and plasticizer and filler as the plasticizing and reinforcement agents, respectively. The formation of starch-based bioplastics is related to starch gelatinization, whereby starch thickens in the presence of water after breaking down the intermolecular bonds of starch molecules. This allows the hydrogen bonding sites to engage with more water molecules. The starch granules dissolve irreversibly in water due to the plasticizer. Gelatinization simply turns a colloidal system from a temporary suspension to a permanent suspension, involving processes such as starch granule swelling, crystal or double helical melting and amylose leaching.

At the initial stage, water molecules enter the amorphous amylose region of starch granules, causing them to swell and expand. They are unable to enter the crystalline amylopectin region at ambient temperature. With an increase in the temperature, the additional heat energy melts the crystalline amylopectin region [31] and dissolves the amylose. Consequently, the number and size of crystalline regions decreases. At gelatinization temperature (75 °C), sufficient heat energy can break the hydrogen bond to allow more water molecules to enter and expand the starch granules. When amylose molecules leach into the surrounding water solvent, the granular structure disintegrates and forms a gel in the amylose matrix. A bioplastic composite process is initiated by mixing cracked starch granules with suitable plasticizer and filler [32]. The plasticizer molecules penetrate the starch granules and enlarge the cavities formed while destroying the inner hydrogen bonds of starch at high temperature with shearing. Starch–starch intermolecular bonding are destroyed and replaced with starch–plasticizer interactions [33]. As a result, the matrix becomes more elastic, which improves its elongation at break. On the other hand, the addition of suitable filler can fill the cavities in the matrix to form a denser bioplastic with strengthened mechanical properties [32].

One of the well-known bioplastics is PLA. PLA is a transparent plastic that possesses similar characteristics to common petrochemical-based plastics, such as polyethylene and polypropylene [34]. A wide variety of PLA structures, from semi-crystalline to totally amorphous, can be obtained depending on the feedstock from which the starch is derived. This bioplastic can be used for packaging applications as it is highly resistant to oil-based products and it can also act as flavour and odour barriers for foodstuffs [27,35]. Moreover, it fulfils the safety requirements for direct food contact with aqueous, acidic and fatty acids. In addition, cups, cutlery and food containers are commonly being manufactured using PLA [24]. However, high brittleness and poor oxygen barrier properties have restricted wider usage of PLA, making it less competitive when compared with conventional plastics, especially in the field of flexible films [24,36]. In order to enhance its properties, nanoclay has been added to promote the oxygen barrier of PLA [24], while various types of plasticizers such as poly(ethylene glycol) (PEG), oligomeric lactic acid (OLA) and tributyl citrate (TBC) can also be employed to reduce the brittleness of PLA [36].

The fabrication of PLA constitutes a multi-step process. The process begins with the fermentation of hydrolysed sugar from starch to produce lactic acid monomers, and ends with the polymerization of lactic acid to produce PLA [27]. Lactic acid can be obtained from renewable carbohydrate sources such as corn, potato, whey and sugarcane through fermentation [37]. The three PLA fabrication routes shown in Figure 3 are (i) direct condensation polymerization; (ii) azeotropic dehydrative condensation; and (iii) ring-opening polymerization of lactide [38]. The direct condensation polymerization of lactic acid yields a brittle polymer with low molecular weight (2000 to 10,000 g/mol). Most of it has little use unless a chain extender is employed [34,38,39]. In the azeotropic dehydrative condensation of lactic acid, high-molecular-weight PLA (>100,000 g/mol) without the aid of chain extenders can be achieved. On the other hand, the ring opening polymerization of the lactide can engage appropriate catalyst to produce desirable PLA with designated molecular weight. As reported, the ratio and sequence of D- and L-lactic acid units in the final polymer chain could be controlled by the monomer and reaction conditions [38].

The first-generation feedstocks are generally rich in carbohydrate and are normally consumed by humans and animals. Continuous processing of the feedstock into bioplastic creates undesirable competition with food and animal feed supply [3,39,40]. Therefore, the second-generation bioplastic was developed to resolve this dilemma.

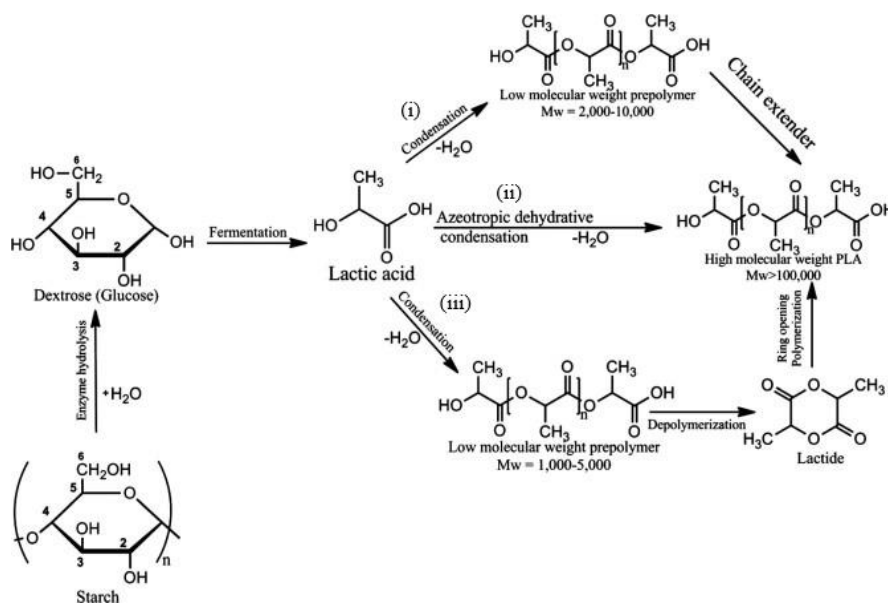


**Figure 3.** Fabrication routes of PLA. Reprinted with permission from Ref. [41]. Copyright 2015 Elsevier Ltd.

## 2.2. Second-Generation Bioplastic

In the fabrication of second-generation bioplastics, the feedstocks utilized are non-food crops such as lignocellulosic biomass. Lignocellulosic biomass derived from plants such as wood, straw, grass and bagasse is the most abundant biomass resource on earth [42]. One of the popular second-generation bioplastics is the cellulose-based bioplastic.

Cellulose is the most abundant natural resource on earth as it can be obtained from various living species such as plants (e.g., cotton, jute, flax, hemp, sisal, coir, ramie, abaca and kenaf), animals (e.g., tunicates), algae (e.g., red, green, grey and yellow-green), bacteria and even amoebas [43]. Cellulose consists of linear chains of D-glucose linked by  $\beta$ -(1,4)-glycosidic bonds and is organized into fibrils, which are surrounded by a matrix of lignin and hemicellulose [24,44]. Cellulose fibres are linked by a number of intra- and intermolecular hydrogen bonds. Since cellulose is insoluble in water and most organic solvents, it presents a challenge to bioplastic fabrication [43]. On the other hand, hemicelluloses located in secondary cell walls and composed of different sugar precursors (pentoses, hexoses and urgonic acids), are easier to hydrolyse as compared to cellulose. This is due to their branched structure (with short lateral chain), lower molecular weight and amorphous structure [44].

There are two major challenges in forming film materials directly from lignocellulosic biomass: its high immiscibility with water and the large amount of non-film forming fractions (lignin and hemicellulose) [42]. Several publications have reported the effectiveness of chemical modification to enhance the film-forming properties of cellulose and hemicellulose [45,46]. Chen and Shi [42] conducted a study in which sugarcane bagasse phthalate film was successfully synthesized via homogeneous esterification of sugarcane bagasse with phthalic anhydride as the inner plasticizer using 1-allyl-3-methylimidazolium chloride as the reaction medium. The thermogravimetric analysis (TGA) results of the study revealed that the modified sugarcane bagasse had lower thermal stability than the original sugarcane bagasse. The contributing factor was the breaking down of the hydrogen bonds that held cellulose, hemicellulose and lignin molecular chains together when subjected to chemical modifications that facilitated the substitution of O-H groups by phthalic anhydrides.

## 2.3. Third-Generation Bioplastic

The most popular feedstocks used in third-generation bioplastic fabrication are algae and seaweed. The feedstocks can be cultivated naturally and they grow into enormous amounts in a short time span [40]. They do not directly compete with food resources and have a high growth rate and high growth tolerance in harsh conditions. These benefits render them a suitable alternative to replace first- and second-generation feedstocks [47,48]. Moreover, the bioplastic film derived from algae was found to be highly transparent, with high mechanical strength and flexibility [40]. Examples of third-generation bioplastics are PHA and agar bioplastic.

PHAs are polymers with desirable properties; they are mainly produced by microorganisms (cyanobacteria) and blue-green algae in the presence of excess carbon sources and a limited supply of essential nutrients such as nitrogen and oxygen [47,49]. PHA is chemically inert and hydrophobic and has a high melting point [49]. Different side chains of the alkanate can be created by manipulating the growth conditions of the microorganism, particularly the composition of cultivation media, producing polymers with desirable properties. Examples of polymers that belong to the group of PHAs are 3-, 4-, 5-, and 6-hydroxyalkanoates, including polyhydroxybutyrate (PHB), polyhydroxyvalerate (PHV), or polyhydroxyhexanate (PHH) [50]. For the family of PHA, PHB and poly(3-hydroxybutyrate-co-hydroxyvalerate) (PHBV) are commercially available and have been produced at an industrial scale [24]. Pure PHB is very brittle and stiff due to its high crystallinity, and it has relatively high melting and glass transition temperatures [50]. As for PHBV, its excellent thermal resistance would have made it a potential replacement candidate for petroleum-based polyolefin. However, its high brittleness, low impact resistance and high production cost have unfavourably limited its application [24].

The other type of third-generation bioplastic is based on agar. Agar is a polysaccharide produced by several families of red seaweed (Rhodophyceae) such as *Gracilariaceae* and *Gelidiaceae*. It consists of two major components: agarose and agaropectin [51]. This type of hydrophilic colloid can form a reversible gel at low temperature [52]. Being the second largest genus of the red seaweed, *Gracilaria* comprised of more than 150 species distributed worldwide [53]. Because of its high gel strength, proteins, fatty acids and bioactive compounds, *Gracilaria changii* is in high demand for applications in the cosmetic, pharmaceutical and food industries [54].

Agar extracted from seaweed has great potential to be used as raw material for bioplastic film fabrication. As demonstrated in the study conducted by Hii et al. [48], agar extracted from red seaweed using the alkali (AEA) and photo-bleached (PBA) methods were added with sago starch and glycerol, respectively, to synthesize the bioplastic film. Both the AEA and PBA bioplastic films gave comparable yield, i.e., 10.68% vs. 9.83%. The employed alkali treatment would remove the sulfate groups such as 4-O-methyl- $\alpha$ -L-galactose and D-galactose-6-sulfate residues, leading to improved gelling ability. Moreover, the AEA method exhibited slightly better thermal stability based on the 74.84% vs. 80.52% weight loss from the TGA analysis (30 °C to 800 °C with nitrogen flow rate of 30 mL/min). Meanwhile PBA bioplastic film showed better tensile strength (3.07 MPa vs. 2.43 MPa) and percent elongation (3.27% vs. 2.48%) than the AEA bioplastic film. These findings confirmed the feasibility of synthesizing bioplastic films from agar.

### 3. Nanofillers for Property Enhancement in Bioplastics

Bioplastics reinforced with filler enhance the mechanical properties of starch but reduce its hydrophilicity [55]. In recent years, utilization of nano-sized fillers has bloomed in the fabrication of bioplastic due to their merits, such as low density, excellent mechanical properties, low abrasive nature and reactive surface for ease of modification [55,56]. Numerous studies had reported that nano-sized fillers have a larger surface area than the conventional micro-sized fillers, thus enhancing the properties due to better interfacial interactions with the polymer matrix [57]. Besides enhancing the mechanical and barrier properties, fillers are also capable of imparting specific functional properties to the bioplastics, e.g., electric conductivity or an antimicrobial character [23]. Another added advantage of filler with nanoscale is in retaining the inherent transparency of the film, especially for the neat matrix [55,58]. Several popular types of nanofillers utilized in starch-based bioplastics are layered silicates (nanoclay, nanosilica and montmorillonites (MMT)), organic nanofillers (cellulose), inorganic nanofillers (metal or metal oxide) and carbonaceous nanofillers (nanotubes, graphene, graphene oxide), which are listed in Table 1.

**Table 1.** List of nanofillers incorporated in starch-based films with the reported findings or properties enhancement.

| Nanofiller                          | Proposed Application | Findings/Enhancement as Compared to the Control Film   | Ref. |
|-------------------------------------|----------------------|--|------|
|                                     |                      | Layered silicates  |      |
| Nanoclay                            | Food packaging film  | Reduction of water vapour permeability (WVP) by 14%<br>Reduction of OP by 15%<br>Presence of microbial growth against <i>C. albicans</i><br>Reduction of microbial growth against <i>S. aureus</i> and <i>E. coli</i> (bacteriostatic effect)  | [59] |
| Nanoclay                            | Packaging material   | Improvement of tensile strength from 5.2 to 6.3 MPa<br>Increase in moisture absorption from 44.44% to 69.58%<br>Complete degradation of thermoplastic starch (TPS)/nanoclay film on the 6th day  | [10] |
| Nanosilica (nano-SiO <sub>2</sub> ) | Packaging material   | TPS film with hydrophilic nano-SiO <sub>2</sub> had lower retrogradation rate than that with hydrophobic nano-SiO <sub>2</sub> .   | [60] |
| MMT                                 | Packaging material   | Improvement of tensile strength by 32% with MMT loading of 5 wt.%<br>Improvement of Young's modulus from 2338 to 3237 MPa<br>Improvement of surface hydrophobicity of film (from 51.97° to 67.77°)<br>Reduction of moisture uptake by 11%  | [61] |
|                                     |                      | Organic nanofillers  |      |
| Cellulose nanofibers (CNF)          | Packaging material   | Improvement of tensile strength by 33% with CNF loading of 3 wt.%<br>Improvement of Young's modulus from 2338 to 3173 MPa<br>Improvement of surface hydrophobicity of film (from 51.97° to 53.89°)<br>Reduction of moisture uptake by 13%  | [61] |
| Cellulose nanocrystals (CNC)        | Packaging film       | Reduction of water absorption and water solubility by 21% and 50% with CNC loading of 20 wt.%, respectively<br>Reduction of WVP by 8% with CNC loading of 15 wt.%; WVP value increased with 20 wt.% CNC loading<br>Optimum tensile strength of 4.59 MPa at 10 wt.% CNC loading; reduction in tensile strength with addition of 15 and 20 wt.% CNC loadings | [62] |
| Cellulose nanocrystals (CNC)        | Food packaging film  | Improvement of tensile strength by 56% with CNC loading of 10 vol.%<br>Reduction of WVP by 17%   | [63] |
| Chitosan                            | Packaging film       | Improvement of tensile strength by 17% with chitosan loading of 10 wt.%<br>Improvement of Young's modulus by 13%<br>Reduction of WVP by 35%<br>TPS/chitosan film had higher opacity than TPS film<br>Reduction of microbial growth against <i>S. aureus</i> and <i>Escherichia coli</i>  | [64] |
| Chitosan                            | Packaging film       | Optimum tensile strength of ~6.79 MPa at TPS/chitosan ratio of 4:6<br>Higher biodegradation rate with increase of starch content   | [1]  |

Table 1. Cont.

| Nanofiller  | Proposed Application  | Findings/Enhancement as Compared to the Control Film   | Ref. |
|---|---|--|------|
| Inorganic nanofillers   |   |  |      |
| Zinc oxide (ZnO) nanorods   | Food packaging film   | Improvement of tensile strength (47 to 90 MPa) and Young's modulus (2.1 to 3.2 MPa)<br>Slight reduction of elongation at break from 50% to 47%.<br>Reduction of WVP by 42%.<br>Improvement of antimicrobial activity against <i>E. coli</i> from $1.5 \times 10^7$ to $9 \times 10^5$ CFU/mL   | [65] |
| Silver nanoparticles (Ag-NP)  | Active packaging film   | Improvement of tensile strength (2.8 to 9.0 MPa) and Young's modulus (50 to 530 MPa)<br>Reduction of EB from 63% to 20%<br>Improvement of antibacterial activity against <i>E. coli</i> from $5.0 \times 10^7$ to $1.5 \times 10^6$ CFU/mL<br>Film with AgNP disintegrated slower than the control film in soil (after 2 weeks vs. after 1 week) | [66] |
| Ag-NP   | Food packaging film   | Reduction of WVP by 16%<br>Reduction of OP by 11%<br>No microorganism growth against <i>S. aureus</i> , <i>E. coli</i> and <i>C. albicans</i> (microbiostatic effect)  | [59] |
| Ag-NP/nanoclay  | Food packaging film   | Reduction of WVP by 33%<br>Reduction of OP by 35%<br>No microorganism growth against <i>S. aureus</i> , <i>E. coli</i> and <i>C. albicans</i> (microbiostatic effect)  | [59] |
| Carbonaceous fillers  |   |  |      |
| Multi-walled carbon nanotubes (MWCNT)   | For packaging and electroconductive applications                            | Improvement of tensile strength by 327% and Young's modulus by 2484% at MWCNT loading of 0.5 wt.%<br>Highest electrical conductivity of 56.3 S/m with 5 wt.% loading as compared to control film ( $1.08 \times 10^{-3}$ S/m)<br>Shifting of thermal degradation temperature to lower temperature with increasing MWCNT loading                  | [67] |
| Multi-walled carbon nanotubes functionalized with cetyltrimethylammonium bromide (MWCNT-CTAB) | Production of conductive film   | Improvement of 2,2'-azino-bis-(3-ethylbenzothiazoline-6-sulfonic acid) (ABTS) radical scavenging activity (from ~2.5% to 30.2% after 1.5 h)<br>Improvement of electrical conductivity (from $2.03 \times 10^{-6}$ S/m to 14.75 S/m)  | [68] |
| Multi-walled carbon nanotubes functionalized with ascorbic acid (MWCNT-AA)                    | As adsorbent for removal of methylene blue (MB) dye from aqueous solution   | Enhancement of thermal stability<br>Suitable to be used as adsorbent for removal of MB dye but not reusable  | [69] |
| Multi-walled carbon nanotubes functionalized with ascorbic acid (MWCNT-AA)                    | As adsorbent for removal of methylene orange (MO) dye from aqueous solution | Enhancement of thermal stability<br>Suitable to be used as adsorbent for removal of MO dye but not reusable  | [70] |
| Multi-walled carbon nanotubes functionalized with fructose (MWCNT-Fr)                         | As adsorbent for dye removal from aqueous solution                          | Film was too brittle for tensile test  | [33] |



Table 1. Cont.

| Nanofiller  | Proposed Application  | Findings/Enhancement as Compared to the Control Film  | Ref. |
|---|---|---|------|
| Multi-walled carbon nanotubes functionalized with Valine (MWCNT-Valine) | As adsorbent for removal of copper ions from aqueous solution | Enhancement of thermal stability<br>Suitable to be used as adsorbent for removal of copper ions but not reusable  | [71] |
| Graphene oxide (GO)   | Food packaging film   | Improvement of tensile strength (from 57.97 to 76.09 MPa) and Young's modulus (from 20.59 to 35.91 MPa).<br>Slight reduction of EB from 6.60% to 3.13%.<br>Enhancement of thermal stability<br>Improvement of surface hydrophobicity of film (from 71.33° to 112.04°)<br>Improvement of water vapour permeability<br>Starch/gelatin/GO film had lower biodegradability than the control film (~30% vs. 50%) after 6 weeks of soil burial degradation. | [72] |

### 3.1. Layered Silicates

Nanoclays are also known as layered silicates [24]. They are readily available, environmentally friendly and of low cost. As a filler with high stiffness, nanoclay improves the mechanical properties of the soft polymer matrix by impeding the free movement of polymer chains. Nanoclay also behaves like a load-bearing constituent if the interfacial adhesion between the filler and the chains is sufficiently strong [73]. This was evidenced by the findings reported by Wahyuningtiyas and Suryanto [74] in which the tensile strength of bioplastic increased from 5.2 MPa to 6.3 MPa in the presence of 5 wt.% nanoclay. Apart from that, the research team discovered that nanoclay could also increase the microbial decomposition rate of bioplastic. For example, only half of the time is required by bioplastic reinforced with nanoclay to fully decompose, compared to a 12-day decomposition period required by the non-reinforced bioplastic. The higher decomposition rate was attributed to the aluminium ions in nanoclay, which acted as Lewis acids to catalyse the hydrolysis process [74]. Li et al. [61] also reported the improvement of the tensile strength of bioplastic from 48.96 MPa to 64.75 MPa after the addition of 5 wt.% of MMT. One point to note is that susceptibility to agglomeration is the unavoidable problem associated with the utilization of nanofiller in polymers. Therefore, ultrasound treatment was employed in the reported studies to disperse the nanofillers in the starch matrix. Homogeneous dispersion of nanofiller in the starch matrix could ensure even transfer of stress between the matrix and the nanofiller, thus enhancing the mechanical properties of polymer nanocomposites [61].

In order to utilize film for food packaging, oxygen and moisture transport must be minimized to extend food shelf-life [59]. In addition to improved mechanical properties, it can be observed from Table 1 that nanoclay showed barrier property (oxygen and moisture) improvement. Incorporation of nanoclay into the matrix would increase the path length and enhance the barrier properties of bioplastic to gases such as oxygen, carbon dioxide, organic vapours and moisture. The uniform dispersion of rigid impermeable nanoclay in the matrix might have hindered the diffusion of permeating molecules by forcing them to traverse and diffuse through a more tortuous path and thus reducing their mass transfer efficiency [24,73]. The antimicrobial effect of nanoclay against bacteria could be related to the release of ammonium salts, which affects bacteria-sensitive targets [75].

In the study by Liu et al. [60], retrogradation behaviour of TPS film was investigated with different surface properties of nano-SiO<sub>2</sub>. TPS film with hydrophilic nano-SiO<sub>2</sub> had a lower retrogradation rate than that with hydrophobic nano-SiO<sub>2</sub>. During gelatinization of starch, the starch granules and crystalline structure were destroyed along with the breakdown of hydrogen bonds and the double helix structure. During short-term retrogradation, the amylose molecules started to crystallize and formed a crystal through a single helix

structure. With longer retrogradation time, the amylopectin molecules gradually formed a crystal through a double helix structure. With the addition of nano-SiO<sub>2</sub>, the starch structure would be affected through interaction between O-H groups of starch and nano-SiO<sub>2</sub>. The addition of hydrophilic nano-SiO<sub>2</sub> produced a V-type starch with a single helix structure. Formation of hydrogen bonds between O-H groups of hydrophilic nano-SiO<sub>2</sub> and starch subsequently destructed the hydrogen bonds between the double helix structure of starch. In contrast, the double helix structure of starch remained with the addition of hydrophobic nano-SiO<sub>2</sub>, which was conducive to the regular arrangement of the double helix structure for crystallization. This indicated that the retrogradation degree of TPS was larger with hydrophobic nano-SiO<sub>2</sub>. Furthermore, the mobility of starch molecules was affected by the different surface properties of nano-SiO<sub>2</sub>. Hydrophilic nano-SiO<sub>2</sub> has many O-H groups on its surface which could form hydrogen bonds with O-H groups of starch and reduce the mobility of starch molecules. On other hand, hydrophobic nano-SiO<sub>2</sub> could not react with starch molecules as there is no O-H group on its surface. Therefore, TPS with hydrophobic nano-SiO<sub>2</sub> had a higher retrogradation rate as a result of the faster movement of starch molecules during retrogradation.

### 3.2. Organic Nanofillers

Cellulose is one of the examples of organic nanofillers. There are three types of cellulose in nanoscale: cellulose nanocrystals (CNC), cellulose nanofiber (CNF) and bacterial nanocellulose [76]. CNC are needle-shaped cellulose particles with a typical diameter of 2–20 nm and a length varying between 100 nm to several micrometres. CNC particles are comprised of 100% cellulose and are highly crystallized, with 54% to 88% crystalline zones. The degree of crystallinity, dimensional diversity and morphology depend on the source of the cellulosic materials, the preparation conditions and the experimental techniques used [77]. The amorphous portion of the cellulose can be easily hydrolysed in strong acidic conditions to generate the individual crystallites. The particle size and properties of the isolated CNCs may vary depending on the cellulosic materials and reaction conditions during hydrolysis [55].

Similar to other fillers, CNCs can increase the stiffness of bioplastic based on their nanoscale dimension, low density, high surface area ( $\geq 100 \text{ m}^2/\text{g}$ ), high aspect ratio of  $\geq 100$ , high crystallinity and high inherent rigidity [56,62]. Xu et al. [63] revealed that CNC-reinforced starch film attained higher tensile strength than that without CNC reinforcement. In this case, a 10 vol.% CNC loading successfully improved the tensile strength of starch film by 129% as well as the barrier property of the starch film, with a 17% reduction in WVP. Another report on bioplastic fabrication by Chiulan et al. [78] revealed that 2 wt.% of bacterial cellulose derived from *G. xylinus* that was used as a reinforcement filler also had increased tensile strength and Young's modulus up to 2 times and 2.1 times, respectively, as compared to that from non-reinforced bioplastic. Similar findings were also obtained in the study conducted by Noshirvani et al. [62]. Indeed, the mechanical properties of TPS-polyvinyl alcohol (PVA) composite film were improved with the addition of CNCs. Even at low loading of 3 wt.%, the uniform dispersion of CNC in the polymer matrix forced the gas molecules to traverse through a more tortuous path to pass through the bioplastic film and thus retarded the gas transmission and increased the mass transfer resistance of CNC-reinforced TPS-PVA composite film to water vapour. However, excessive CNC would cause particle agglomeration and reduce the effective content of CNC and thus facilitate the water vapour permeation.

Chitosan is another example of an organic nanofiller. It can be obtained from the deacetylation of chitin, which can be found in shell waste and skeletal materials of insects and crustaceans [64,79]. It is appealing to employ it as a filler as it serves the purpose of reusing the waste and being a biodegradable material. In addition, it is well-known for its antimicrobial properties. TPS/chitosan film was found to reduce the microbial growth of *S. aureus* and *E. coli*. The reduction of microbial activity was more pronounced at a higher chitosan concentration [64]. However, chitosan is insoluble in water, strong base

solutions and some organic solvents such as alcohol and acetone. Therefore, an aqueous acidic solution such as hydrochloric acid (HCl) or acetic acid is required to dissolve the chitosan [80].

### 3.3. Inorganic Nanofillers

Metal or metal oxides are examples of inorganic nanofillers. Metallic nanoparticles such as Ag-NP are known to have antimicrobial and inhibitory activity against a variety of microorganisms such as bacteria, fungi or viruses [59,81–83]. From Table 1, Ag-NP was reported by Abreu et al. [59] to have a microbial effect against *S. aureus*, *E. coli* and *C. albicans*. Ag-NP would release Ag<sup>+</sup> ions and penetrate into the bacteria, damaging the cell or disrupting the metabolic processes [84]. With the incorporation of hybrid nanofiller of Ag-NP/nanoclay into TPS, both the WVP and OP values were lower than the TPS with Ag-NP only. It was evidenced from the SEM images that incorporation of Ag-NP into nanoclay improved the clay dispersion in the starch matrix, which resulted in higher homogeneity of the film and thus better WVP and OP. Similar to Ag-NP, ZnO nanofillers also exhibit antimicrobial activity. In addition to their ability to be synthesized into different shapes [85], they are suitable to be incorporated into TPS films for food packaging application as they are considered Generally Regarded as Safe (GRAS) by the Food and Drug Administration (FDA) to be used in plastics and food contact materials [65]. From the study by Estevez-Areco et al. [65], TPS/ZnO could not inhibit the bacterial growth completely but it could delay the replication of bacterial growth, which could serve as a bacteriostatic agent.

### 3.4. Carbonaceous Nanofillers

CNT, GO and carbon black are examples of carbonaceous nanofillers. CNT is widely used as nanofiller in starch-based bioplastic owing to its superior mechanical (high tensile strength and Young's modulus), electrical, magnetic, optical and thermal properties [61]. CNT can be produced by rolling sheets of carbon atoms (graphene) to form either single walled or multi-walled CNTs [33]. The study by Domene-López reported that as low as 0.5 wt.% amount of multi-walled CNTs could register an increment up to 327% in tensile strength, 2484% in Young's modulus and also 82% of elongation at break. The augmentation of the mechanical properties was attributed to the good dispersion of multi-walled CNTs in the starch matrix. Furthermore, the findings also indicated that the better interfacial adhesion obtained could avoid the formation of holes and sustain a higher degree of deformation [86].

However, the natural insolubility of CNT in water causes self-association and a strong aggregation tendency, giving rise to low adhesion with the hydrophilic polymer matrix such as the starch matrix [87]. Functionalization of CNT through the adsorption of surfactant is the solution that could help in producing stable CNT dispersion. Alves et al. [68] had investigated the dispersibility of MWCNT by employing three different ionic surfactants, i.e., CTAB, sodium dodecyl sulphate (SDS), and sodium cholate (SC). TPS/MWCNT-SC showed the best dispersibility among them, producing a more homogeneous starch matrix, thus achieving the highest tensile strength and Young's modulus. Nonetheless, the highest antioxidant activity and electrical conductivity were attained by the TPS with MWCNT-CTAB. SC interacted more tightly with the MWCNT surface than CTAB and SDS due to its rigid structure, so that the MWCNT surface was not so exposed. This subsequently reduced the availability of MWCNT to interact with the radical, which resulted in the lowest antioxidant activity [68]. In view of the electrical conductivity, TPS with MWCNT-SDS presented the lowest value, which might be due to agglomeration of nanotubes and weaker dispersibility, as observed in the SEM images. Higher adhesion of SC to the MWCNT surface gave rise to a blocking effect of charge transport in MWCNT network and diminished the contact points between nanotubes [88]. Therefore, the electrical conductivity value was lower. In addition, TPS with functionalized MWCNT could serve as an adsorbent for dye removal. From Table 1, TPS with MWCNT-AA, MWCNT-Fr and MWCNT-Valine was capable of removing dye. They are simple to prepare, cost little and are environmentally

friendly. However, non-reusability is their chief drawback, as the dye adsorbed on the adsorbent surface cannot be separated completely from the adsorbent for next use after dye removal.

#### 4. Plasticizers Applied in Bioplastic Fabrication

Plasticizers consist of polar and low-molecular-weight molecules that are capable of disrupting intermolecular bonds between polymer chains and forming new bonds with O-H groups on the glucosidic units of polysaccharide chains. This facilitates chain movements and produces a more flexible material with a lower glass transition temperature. Thus, starch with added plasticizer can be easily processed to form thermoplastic derivatives. Plasticizers such as water, glycerol and sorbitol are commonly used in bioplastic fabrication [89]. However, it should be noted that the final properties of starch-based bioplastic are highly dependent on the ambient humidity. Hence, water is not recommended to be used directly as plasticizer. Otherwise, the high volatility of the water molecules would often produce a brittle film [30,33]. As for glycerol, it tends to migrate from starch films, leading to starch retrogradation after a prolonged storage period [89]. In a recent development, emerging plasticizers such as vegetable oil-based plasticizer, ionic liquid (IL) and deep eutectic solvent (DES) have attracted increasing attention. These novel plasticizers were reviewed, and their advantages and disadvantages are summarized in Table 2.

**Table 2.** Advantages and disadvantages of plasticizers.

| Plasticizer   | Examples   | Advantages  | Disadvantages  | Ref.       |
|---------------|--|---|--|------------|
| Vegetable oil | <i>Jatropha</i> oil<br>Castor oil  | Biodegradable<br>Renewable  | Edible vegetable oil competes with food supply   | [1,36]     |
| IL            | 1-allyl-3-methylimidazolium chloride<br>1-butyl-3-methylimidazolium chloride | Non-volatile due to negligible vapour pressure<br>Non-flammable<br>Good ionic conductivity<br>High thermal stability<br>High chemical stability<br>High electrochemical stability | Difficult to prepare<br>High production cost (time consuming fabrication and purification) | [90–92]    |
| DES           | Deep eutectic salts based on choline chloride                                | Cheaper to produce<br>Easy to prepare in large quantity<br>Less toxic than IL   | Sometimes biodegradable  | [91,93,94] |

##### 4.1. Vegetable Oil

Vegetable oil is composed primarily of fatty acid and glycerol. It is highly biodegradable and renewable. Many edible vegetable oils such as palm oil, soybean oil and rapeseed oil have been utilized as plasticizers. This has raised a tremendous concern as the use of edible oil, as plasticizer feedstock tends to incur food supply competition leading to a food security threat. Moreover, environmental issues such as deforestation will likely occur if a massive propagation of plants producing edible oil is to take place [36]. To resolve these potential shortcomings, inedible oils have been proposed as alternatives.

Epoxidized vegetable oils are often used as plasticizers instead of pure vegetable oils. The epoxidized vegetable oils have greater molecular weight and a bulkier structure than the pure vegetable oils which have helped to resist migration by minimizing volatility in the polymeric matrix [95]. Epoxidation is an oxidation reaction of adding oxygen atoms to carbon–carbon double bonds to form carbon–oxygen bonds, usually together with an acidic catalyst and H<sub>2</sub>O<sub>2</sub>. Unsaturated fatty acids are the primary target during the epoxidation of vegetable oils due to the higher amount of carbon–carbon double bonds [36]. For example, *Jatropha* oil, which consists of high unsaturated fatty acid, including oleic (C18:1) and linoleic (C18:2) acids, is suitable to be converted into epoxidized *Jatropha* oil before being used as plasticizers in bioplastics fabrication. A typical epoxidation reaction of *Jatropha* oil is presented in Figure 4.

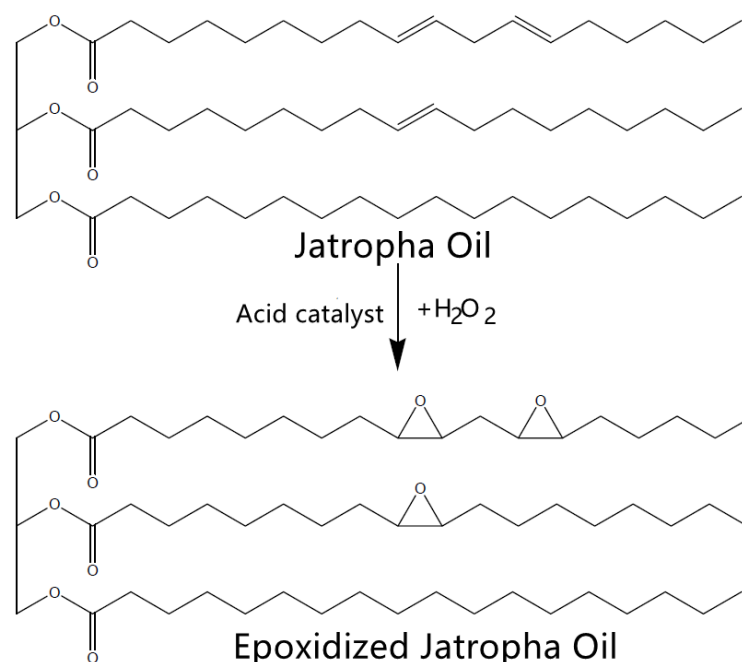


**Figure 4.** Epoxidation of *Jatropha* oil. Reprinted with permission from Ref. [36]. Copyright 2017 MDPI.

Vegetable oil can also be used as an anti-microbial agent. In the algae biofilm synthesized by Othman et al. [40], cinnamon bark oil was utilized as a co-primer and anti-microbial agent to improve the life-span of the biofilm. The oil contained about 50% cinnamaldehyde, an organic compound that occurs naturally as a predominant trans (E) isomer, providing cinnamon with a unique flavour and odour [96]. From the soil burial test, the algae biofilm incorporated with cinnamon bark oil showed less biodegradation potential compared to the normal algae biofilm. The addition of 5% cinnamon bark oil to the biofilm demonstrated a slower biodegradation rate and reduced pore percentage. This has proven the improvement of the insect repellent and the anti-microbial properties of cinnamon in biofilm protection [97].

#### 4.2. Ionic Liquid (IL)

Ionic liquids (ILs) are organic salts of bulky organic cation and a smaller organic or inorganic anion, with a melting point below the boiling point of water at 100 °C [91,98]. Due to their non-volatility (negligible vapour pressure), non-flammable properties, good ionic conductivity, and high thermal, chemical and electrochemical stability, ionic liquids are a superior replacement for organic solvents [90,91]. For instance, the cellulose that could be dissolved in 1-butyl-3-methylimidazolium chloride (BMIMCl) was incorporated with a plasticizer to prepare the cellulose film [98]. The interaction of cellulose and BMIMCl involved oxygen and hydrogen atoms from the hydroxyl (O-H) groups of cellulose [99]. The oxygen and hydrogen atoms from cellulose could serve as electron donors and electron acceptors, respectively. In a corresponding fashion, the BMIM<sup>+</sup> acted as electron acceptor centres while Cl<sup>−</sup> as electron donor centred. Upon interaction, the intermolecular hydrogen bonds were cleaved, resulting in the dissolution of cellulose with BMIMCl [100,101]. It was reported that the quality of the cellulose/BMIMCl composite films depended on the concentration of the ionic liquid retained during water removal from the ionic gel, which in turn played a critical role in determining the mechanical properties of the films [98]. The optimum mechanical properties were attained at 40% BMIMCl concentration. Apart from the hydrogen bonding interactions, the stacking interactions between intra- and inter-sheets of the cellulose layers might have also oriented the cellulose chains [98]. When the cellulose chains were being staked uniformly, the stacking interactions between the cellulose chains would be

enhanced, resulting in an increase in tensile strength and elongation at break [100,102]. It has been reported that when the BMIMCl concentration was increased beyond the optimum level at 40%, the advantages of BMIMCl would diminish to a typical plasticizer. At a higher concentration of more than 40%, BMIMCl would enable the molecules to penetrate the cellulose chains and obscure the interactions between them. This would create the sliding effect in tensile property resulting in decreased tensile strength but increased elongation at break. On the other hand, it was insufficient for the BMIMCl concentration at less than 40% to effectively plasticize the cellulose chains due to the poor distribution of stress and very low elongation at break.

Even though ILs have always been considered as green solvents, uncertainty about their environmental impacts had also been raised [98]. For instance, there was a controversy over the sustainability of pyridinium- or imidazolium-based ILs as they could become more hazardous than other organic solvents. From the ecotoxicological test, pyridinium- and imidazolium-based ILs were found to show moderate ecotoxicity to bacteria, algae, and invertebrates. They would pose harmful impacts to the aquatic ecosystem if released into the open environment [103]. Moreover, ILs are difficult to mass-produce as doing so would incur high production costs due to the time-consuming fabrication and energy-intensive purification steps involved [90]. The effort in searching for alternative green solvents leads to the discovery of deep eutectic solvent (DES), which demonstrates similar physical and chemical properties as IL.

#### 4.3. Deep Eutectic Solvent (DES)

Deep eutectic solvents are mixtures of two or more compounds which consist of hydrogen bond acceptors (e.g., halides salts of quaternary ammonium or phosphonium cations) and hydrogen bond donors (e.g., citric acid, urea or glycerol). The bond acceptors and the bond donors react with each other through strong hydrogen bond interactions to produce DES with a lower melting point and vapour pressure but higher thermal stability than their individual components [90,104]. The charge delocalization, occurring through hydrogen bond formation between the components, is responsible for the lowering of the melting point of the DES compared to its individual components [104].

DES has been employed to replace the traditional imidazolium-based ILs. Although exhibiting similar performances as conventional IL, DES is comparatively cheaper, safer and easier to prepare in large amounts via a simple mixing process [93,94]. Because of its renewable and non-toxic properties, DES has been utilized as plasticizer and crosslinking agent in bioplastic fabrication [93,105]. In particular, choline-chloride-based DESs are favourable for starch modification as they can interact strongly with OH groups from glycosidic units, decrease chain interactions and plasticize the polymer [91]. The employment of a DES plasticizer comprised of choline citrate/glycerol in the fabrication of TPS film was reported by Zdanowicz et al. [89]. They discovered that the tensile strength of the film increased while elongation at break decreased as the choline citrate content in DES was increased. The work reported an inversely proportional relationship between choline citrate content in the TPS film and the sorption degree of the film. In addition, it also indicated a direct correlation whereby the higher amount of citrate anion in the system can lead to a higher degree of crosslinking. The work further confirmed the occurrence of a partial crosslinking reaction between the polysaccharide and DES components via Fourier transform infrared spectroscopy (FTIR) spectra and dynamic mechanical analysis. Among the highlights of the findings reported was the non-retrogradation of the TPS/choline citrate/glycerol film even after 12 months of storage. The covalent-bonded compound could also exert resistance to migration or evaporation from the polymeric matrix, which substantiated the superiority of reactive plasticizer such as DES over the conventional plasticizer (e.g., glycerol). Therefore, it is still inherently safe to apply DESs synthesized bioplastic film in the food packaging or agricultural industry [89].

## 5. Critical Factors Affecting Properties of Bioplastic Using Solvent-Casting Technique

The important optical properties of bioplastic film usually refer to its colour and opacity. The opacity of the film indicates the amount of visible wavelength that can pass through the film [106]. Besides that, the mechanical property of the synthesized film materials is also essential in various applications to prevent films from cracking [42]. Mechanical properties of bioplastic film include the tensile strength, Young's modulus and elongation at break. High tensile strength is generally desirable, and the value can be fine-tuned depending on the proposed application of the film [55]. A lower Young's modulus value is preferred as it imparts higher elasticity to the bioplastic sample [22]. Elongation at break is usually used as an indication of the bioplastic flexibility [18]. Other barrier properties affecting the bioplastic film include WVP, OP and moisture uptake. Several main factors that influence the optical, mechanical and barrier properties of the bioplastic are plasticizer loading, filler loading, processing temperature of bioplastic solution, concentration of chitosan solvent as well as concentration and composition of starch.

### 5.1. Plasticizer Loading

Bioplastic often encounters fragility issues due to its high intermolecular forces, which render it very rigid. With the addition of plasticizer, the moisture content of the starch solution is enhanced, and thus the starch granule can move more freely. The elasticity and flexibility of bioplastic is enhanced through the weakening of the internal hydrogen bonds among polymer chains and increasing the molecular spacing [18,107]. Therefore, plasticizer plays an important role in improving the flexibility, softening and elongation properties of the bioplastic [20]. This had been witnessed in the fabrication of bioplastic film by Lubis et al. [12], whereby an increment in the concentrations of plasticizer sorbitol increased the adsorption intensity of the O-H group on the bioplastics. As the sorbitol molecules slipped between amylose–amylopectin–chitosan chains, the interaction between the polymers weakened and led to a reduction in the tensile strength [108]. A similar trend was observed by Cifriadi et al. [13] on the enhancement in tensile strength of starch-cellulose bioplastic film when the glycerol as plasticizer reached an optimum loading of 37.5%. On the other hand, inadequate plasticizer loading could lead to imperfect plasticizing efficiency causing the starch molecules to become more brittle [21].

Increment of the plasticizer loading during the fabrication of bioplastic increases the elongation at break of bioplastic. This relationship was proven based on the bioplastic synthesized by Ginting et al. [108]. The elongation at break of the bioplastic was found to increase with increasing sorbitol concentrations. They attributed this observation to the low molecular weight of sorbitol when compared to polymeric compounds such as starch and chitosan. The addition of the plasticizer would increase the free movement space for the polymer molecules. The optimum conditions for bioplastic fabrication with various plasticizers are compiled in Table 3. Glycerol and sorbitol are two of the most commonly utilized plasticizers due to their ability in reducing the internal hydrogen bonding of the polymer molecules and thus increasing their intermolecular distance [20]. The range of plasticizer loading to achieve the optimum mechanical properties was reported to be between 1.5 wt.% to 45 wt.%. It can be observed from Table 3 that by using different fillers on the same feedstock and plasticizer, the amount of plasticizer required would also be different. In the bioplastic fabrication using cassava starch as matrix and glycerol as the plasticizer, a higher concentration of glycerol was required for ZnO as compared to that using nanoclay. This was explained by the requirement of higher plasticizer loading to compensate for the lower filler loading. It has been reported by the researchers that the tensile strength of the film was greater by using ZnO instead of nanoclay due to the formations of stronger alkane, C-O, C=C and C-C bonds with the addition of ZnO. In another case involving chitosan as the filler and sorbitol as the plasticizer, durian seed starch bioplastic required higher optimum sorbitol loading compared to sago starch bioplastic (i.e., 45 wt.% vs. 25 wt.%). However, the sago starch bioplastic achieved higher tensile strength than the durian seed starch bioplastic (46.71 MPa vs. 10.63 MPa). The presence of

fat content in the durian seed was believed to form complexes with amylose and to cause the granule surface to be enveloped by hydrophobic fat. Amylose was then inhibited from being released from the granules during gelatinization and the gelling ability of starch was reduced [20,28].

**Table 3.** Optimum reaction conditions for fabrication of starch-based bioplastics using solvent-casting technique.

| Sources of Starch | Filler; Starch to Filler Ratio | Filler; Optimum Loading             | Plasticizer; Optimum Loading | Processing Temperature (°C) | Tensile Strength (MPa) | Young's Modulus (MPa) | Elongation at Break (%) | Moisture Uptake (%) | Ref.  |
|-------------------|--------------------------------|-------------------------------------|------------------------------|-----------------------------|------------------------|-----------------------|-------------------------|---------------------|-------|
| Corn              | -                              | CNC;<br>10 wt.%                     | Glycerol;<br>3 wt.%          | 70                          | 26.80                  | 898                   | 4.20                    | 10                  | [55]  |
| Avocado seed      | Chitosan;<br>7:3               | -                                   | Glycerol;<br>0.2 mL/g        | 90                          | 5.10                   | 36.36                 | 14.03                   | -                   | [19]  |
| Cassava peel      | -                              | MCC<br>Avicel<br>PH101;<br>6 wt./v% | Sorbitol;<br>20 wt.%         | 70                          | 9.12                   | -                     | -                       | 70 *                | [21]  |
| Cassava           | -                              | Nanoclay;<br>5 wt.%                 | Glycerol;<br>1.5 vol.%       | 80                          | 13.50                  | 47                    | -                       | -                   | [10]  |
| Cassava           | -                              | ZnO;<br>0.6 wt.%                    | Glycerol;<br>25 wt.%         | 85 ± 5                      | 22.30                  | -                     | 220 *                   | -                   | [57]  |
| Jackfruit seed    | Chitosan;<br>8:2               | -                                   | Sorbitol;<br>25 wt.%         | 88.82                       | 13.52                  | -                     | -                       | -                   | [12]  |
| Sago              | -                              | Chitosan;<br>20 wt.%                | Sorbitol;<br>25 wt.%         | 70                          | 46.71                  | -                     | 0.32                    | 130.31              | [109] |
| Durian seed       | -                              | Chitosan;<br>15 wt.%                | Sorbitol;<br>45 wt.%         | 70                          | 10.63                  | 129.51                | 8.21                    | -                   | [20]  |
| Yellow pumpkin    | Chitosan;<br>6:4               | -                                   | Castor oil;<br>15 wt.%       | -                           | 6.79                   | 6.09                  | 13.45                   | -                   | [1]   |
| Mango seed        | -                              | Clay;<br>6 wt.%                     | Glycerol;<br>25 wt./v%       | -                           | 5.66                   | -                     | 43.43                   | 32.28               | [18]  |

\* denotes for values estimated from charts presented in the original reference.

### 5.2. Filler Loading

The addition of suitable fillers can affect the optical properties of bioplastic. When Almeida et al. [104] prepared chitosan film using DES as plasticizer and curcumin as the additive, they discovered that an increment in the curcumin concentration caused an increment in the colour parameters (total colour difference ( $\Delta E$ ), chromaticity parameters,  $a^*$  (red-green) and  $b^*$  (yellow-blue)) and a decrement in the lightness ( $L^*$ ). Similar trends were noted in other chitosan films incorporating different additives such as tea polyphenols [110] or cinnamon essential oil [111]. Moreover, the opacity of the film was found to increase with an increase in the curcumin loading. Embedding curcumin pigment into the interspaces of chitosan film obstructed the light transmission. However, Jacquot et al. [112] believed that the colour change in the chitosan film was initiated by the microwave heating process whereby neoformed compounds that appeared in the Maillard reaction were responsible for the film colouration. The Maillard reaction is a very complex reaction between carbonyls and amines which occurs spontaneously during food processing and storage [113].

Unlike plasticizer, the addition of filler could improve tensile strength and Young's modulus while reducing elongation at break. Filler promotes the formation of strong hydrogen bonds between O-H groups on the interface of both the filler and starch matrix. The formation of the stronger molecular bonding increased the tensile strength and Young's modulus of bioplastic. Conversely, elongation at break of bioplastic decreased as intermolecular bonding distance was reduced [18]. Strong filler–matrix compatibility and good filler dispersion also accounts for better reinforcement and thus provides more promising mechanical properties. On the other hand, aggregation of filler should be prevented since it might create an heterogeneous phase, feature discontinuities and decrement in the desired mechanical properties of the film [55].

Modification of property in bioplastic was reported in the work of Agustin et al. [55] using CNCs as filler to reinforce the bioplastic film in various loadings (0 to 15 wt.%). The CNC loading increased the tensile strength and Young's modulus, whereas the elongation at break was decreased from 33.1% (without CNC) to 4.2% (at 10 wt.% maximum loading



of CNC). Expectedly, the increment of the CNC loading increased the stiffness of the film, which then decreased its elasticity [55]. Strong hydrogen bonds between O-H groups from starch and O-H and COOH groups from cellulose in CNC contributed to higher strength and lowered the elongation at break [21]. A similar observation was also obtained by Ginting et al. [19] in their bioplastic film fabrication utilizing chitosan as filler. All the findings reported thus far unanimously agreed that mechanical properties were affected primarily by the number and types of the chemical bonding on the polymer matrix such as covalent, hydrogen and Van der Waals bonds. This was clearly demonstrated by the enhancement of hydrogen bonds and the compactness of intermolecular bonds in the bioplastic with the addition of chitosan to reduce the intermolecular bond distance. This fabrication pathway successfully produced a stronger and more rigid bioplastic [1,19]. Other studies also reported the same findings, which include the fabrication of bioplastic film reinforced with microcrystalline cellulose (MCC) by Maulida and Tarigan [21] and the study undertaken by Wahyuningtiyas and Suryanto [10] using nanoclay. The tensile strength of bioplastic decreased when nanoclay was added beyond its optimum loading of 5 wt.%.

It is worth noting that the density of bioplastic has a large impact on its mechanical properties. A denser bioplastic usually possesses higher tensile strength, which improves its mechanical properties. It is essential to ascertain the density of bioplastic so that the most appropriate packaging and efficiency can be selected [10]. In the study conducted by Wahyuningtiyas and Suryanto [10], the density of bioplastic increased with the addition of nanoclay (filler) as the spatial arrangement of molecules in the composite became more compact [109]. The density of bioplastic is also affected by the degree of crystallinity of the polymer. Maulida and Tarigan [21] obtained a reduction in the density of bioplastic as MCC was added. This anomaly trend was due to the introduction of ultrasonic treatment, which resulted in an increase in the amorphous region in the bioplastic fabrication [114]. A higher amorphous fraction was attributed to a lower density of bioplastic due to non-uniformity and less dense molecules. Lower density bioplastic exhibited more open structures and was more susceptible to penetration by fluids such as H<sub>2</sub>O, O<sub>2</sub> or CO<sub>2</sub> [21].

Minimal moisture uptake of film is favourable, which indicates that the film is water-resistant [55]. Starch-based bioplastics usually have poor resistance to moisture since starch is a hydrophilic polymer [115]. Therefore, the addition of appropriate filler can also improve the water resistance of starch-based bioplastics [55]. Hydrophilic behaviour of starch-based bioplastic can be retarded by mixing starch with hydrophobic biopolymers such as cellulose and chitosan [12]. In the fabrication of bioplastic film conducted by Agustin et al. [55], moisture uptake of the film decreased from 13.8% to 10% with the addition of CNC loading from 0 to 10 wt.%. The decrement in the moisture uptake could be attributed to the formation of hydrogen bonding between O-H groups on the interface of both CNCs and the starch matrix. The resulting hydrogen-bonded network of cellulose with the starch in the composite could prevent the formation of voids, which allows water molecules to pass through [55]. A similar trend was found by Maulida and Tarigan [21], who observed that water uptake decreased as the MCC loading was increased. Furthermore, the cellulose possessed strong hydrogen bonding, which rendered it difficult to bond with water. Another similar observation was discovered by Kartika et al. [18] which showed that increasing the clay content would decrease the water uptake of bioplastics.

The thermal stability of bioplastic film, which can be characterized using TGA, is an indicator of its durability at high temperature applications [55]. A decline in the thermal stability of the bioplastic film was reported when the maximum weight-loss rate temperature ( $T_{max}$ ) decreased from 323.75 °C to 277.26 °C as the CNC loading increased from 0 wt.% to 15 wt.% [55]. This was caused by the inherent low thermal stability of CNCs after being subjected to sulfuric acid hydrolysis. The significant reduction in crystallinity of CNC after sulfuric acid hydrolysis also reduced the thermal stability of bioplastics [116].

The bioplastic synthesized by Anggraini et al. [109] was also more vulnerable to higher processing temperatures with increased chitosan loading. The higher processing

temperature can affect the appearance and mechanical properties of bioplastic with low thermal stability. As reported, bioplastic became more fragile after being heated at 100 °C for 10 min. When heated at a higher temperature of 125 °C for the same duration, the bioplastic started to become more brittle and could be easily broken. Moreover, the colour of bioplastic would turn darker after being heated at the higher processing temperature, which indicated a reduction in mechanical properties. The deterioration of the thermal stability of bioplastic could be explained by the interaction between chitosan and starch in the bioplastics. If the interaction between starch chains is weak and the starch molecules are not in the optimal position, a higher processing temperature can disintegrate or inflict damage on the bioplastics [64].

In a study on TPS film conducted by Salaberria et al. [117], the water vapour transmission rate (WVTR) decreased to around  $85 \text{ g}\cdot\text{mm}\cdot\text{m}^{-2}\cdot\text{day}^{-1}$  from  $114 \text{ g}\cdot\text{mm}\cdot\text{m}^{-2}\cdot\text{day}^{-1}$  with the addition of 5 wt.% chitin nanocrystals in the TPS film. Interestingly, with the same amount of 10 wt.% chitin nanofibers, the WVTR value was on par with the pure TPS film. A further increase of the nanofibers to 20 wt.% would surpass the WVTR value of the pure TPS film. The findings recommended low loading of chitin nanocrystal and nanofiber contents as they could create a more tortuous path to block water molecules from passing through. Otherwise, the presence of excessive contents of chitin nanocrystal and nanofiber would increase the WVTR. With regards to the OP of pure TPS film, its value decreased by roughly 30% and 25% with the addition of 10 wt.% chitin nanocrystal and nanofiber, respectively. Incorporating filler into TPS film has the advantage of imparting the antimicrobial properties against fungi and bacteria. This was proven by the growth inhibition of the *A. niger* exerted by chitin nanocrystal- and nanofiber-reinforced TPS film. At filler loading at 20 wt.%, chitin nanofiber-reinforced TPS film exhibited better inhibition effect compared to the chitin nanocrystal, i.e., fungal growth inhibition (FGI, %), 96% vs. 89%. Unlike the antimicrobial property, the inhibition rate was not affected by the concentration of chitin nano-materials. When chitin nanocrystals of 10 wt.% and 20 wt.% were incorporated into TPS film, there was only a slight FGI difference of 2% (87% vs. 89%, respectively). Furthermore, the mechanism demonstrated by the antimicrobial property of chitin was not conclusive and is still under intense research [117].

### 5.3. Concentration of Chitosan Solvent

Chitosan is commonly incorporated into starch-based bioplastics as a co-polymer or filler to reduce the water sensitivity as well as enhance the mechanical and barrier properties of film [118]. In addition, it is considered as GRAS by the FDA, making it an ideal candidate for food packaging material [79]. Since only chitosan can be dissolved in aqueous acidic solution with a pH of less than 6.3, an aqueous acetic acid solution is commonly used as the chitosan solvent [79]. HCl can also serve the same function as acetic acid. Ginting et al. [20] studied the effect of the concentration of chitosan solvent on the mechanical properties of bioplastic. The chitosan solvent used various HCl concentrations ranging from 0.9 vol.% to 1.3 vol.%. The highest and lowest tensile strengths of 10.63 MPa and 2.65 MPa, respectively, were detected at the two extremes of HCl concentrations. Higher HCl concentration would cause lower solubility of chitosan. Due to the limited solubility of chitosan in inorganic acids, it could dissolve in 1% HCl but not at all in sulfuric acid and acid phosphate. At 0.9 vol.% HCl concentrations, the solvent provided a better distribution of chitosan in the polymer matrix. The chitosan added into the starch solution mixture was able to fill up the voids in the bioplastic to form a dense bioplastic with increased resilience and tensile strength. The interaction between chitosan and starch suspension supports was observed through FTIR based on the increasing number of O-H and N-H groups on bioplastic, which was attributed to the interaction of the amylose–amylopectin–chitosan. The presence of these hydrogen bonds would enhance the tensile strength as well as Young's modulus of the bioplastic. Similar to the trend shown by the tensile strength, the highest Young's modulus of 129.51 MPa and its lowest value at 29.07 MPa were attained at 0.9 vol.% and 1.3 vol.% HCl concentrations, respectively. Since Young's modulus was

inversely proportional to elongation at break, the highest elongation at break was obtained at 1.3 vol.% HCl concentration [20].

#### 5.4. Processing Temperature of Bioplastic Solution

The processing temperature at 90 °C achieved the optimum mechanical properties for bioplastic film as determined by Ginting et al. [19]. Higher processing temperature improved the tensile strength of the film as the intermolecular bond on starch chains weakened and triggered the breaking down of the amylose long chain bond. Moreover, higher processing temperatures promoted homogeneity in the bioplastic which rendered the structure more compact, thus improving the tensile strength. Nevertheless, higher processing temperatures can also have adverse effects on the plasticizer volatilization from the bioplastic. It caused bioplastic to become more arid and easier to be torn. This, in turn, reduced the elasticity of bioplastic and increased the Young's modulus of the bioplastic [19].

It was also discovered that increasing the processing temperature of the bioplastic solution beyond the optimum range deteriorates its tensile strength due to the weakening of the intermolecular bonds in starch chains. Excessive heating would break the glycosidic bonds (bonds between monomers) in amylose [108]. This was agreed by Haryanti et al. [119], in whose study increased processing temperature was found to promote the depolymerization of the amylose chains and subsequently decrease the amylose content. Amylose plays an important role in the gel formation and the production of compact thin layer (film). A reduction in amylose content would lower the cohesiveness of bioplastics formation and thus decrease its tensile strength [108].

For elongation at break, it increases with the increasing processing temperature of the bioplastic solution. As previously discussed, the addition of sorbitol increased the elongation at break of bioplastic [108]. The increase in the kinetic energy of the molecules was attributed to the increase in processing temperature. As the vibrations of the molecules increased, more free volumes are created to allow larger molecular chain rotation [120].

#### 5.5. Concentration and Composition of Starch

As mentioned previously in Section 2.1, starch consists of two main polysaccharide units, namely amylose and amylopectin. Amylose content was reported to have major impacts on the mechanical [121] and optical properties [122] of the synthesized bioplastic film. Sifuentes-Nieves et al. [121] reported that high amylose contents could modify the mechanical properties of glycerol-plasticized starch films to a greater extent, giving higher tensile strength and higher Young's modulus but lower elongation at break. These findings were substantiated through the higher gelatinization and glass transition temperatures of the amylose fraction of starch [123]. However, tensile strength and Young's modulus would decrease while the elongation at break increase with increasing plasticizer concentrations above 15 wt.% regardless of the type of starch employed.

In addition, the amount of lipids in the starch interferes with the opacity of the film. An increase in starch concentration in the film increases the lipid concentration. Meanwhile, the lipid particles could scatter the visible light through the film, causing it to be more opaque [106]. Potato starch film is more transparent than wheat and corn starch films as the latter contains a higher amount of lipids [122]. The opacity and the colour properties of the bioplastic film are dependent on the starch original properties (amylose/amylopectin ratio, size and shape of starch granules) and its concentration. A higher starch concentration contained more amylose in its matrices, and thus the film appeared to be more opaque [122]. The researchers further investigated the effect of starch with different amylose and amylopectin ratios on the optical properties of the synthesized bioplastic film involving corn, wheat and potato starches. Starch with lower amylose content or higher amylopectin content favours the formation of greater homogeneity, as well as denser and thinner film. Among the three types of starch studied, corn starch film was opalescent and thickest at 112 µm, while potato starch film was the least heterogeneous, most transparent and thinnest at 55 µm. Generally, the thinner film is favourable as it

can ease the retraction of starch gel during drying. As a summary, the film thickness is dependent on the amylose/amylopectin ratio, which in turn determines the opacity and transparency of film.

The biodegradability of bioplastic was evaluated by Hasan and Rahmayani [1], who incubated the bioplastic film in the culture medium of *Pseudomonas aeruginosa*. The film which contained higher starch content had a colour change in the media after 10 days of incubation and was completely biodegraded after 30 days. Owing to the presence of glucosidic bonds in the amylose and amylopectin units, bioplastic film with greater starch content could be biodegraded easily through the hydrolysis mechanism.

## 6. Challenges and Potential for Future Sustainable Development

Based on the review presented, nanofiller has a demonstrated ability to enhance the mechanical, optical and barrier properties of bioplastics. However, the scientific literature reporting on the utilization of nanofillers in starch-based bioplastics is still limited. Considering the knowledge gaps waiting to be bridged by the fundamental studies in dealing with the reaction mechanism of nanofiller on starch-based bioplastics, more in-depth and related studies should be carried out. As for the preparation of nanofiller, the process remains complex and not economically feasible. These have restricted the potential of reinforced starch-based bioplastics in replacing conventional petroleum-based plastics [30]. As discussed in Section 5.2, chitin has intrinsic antimicrobial properties against fungi and bacteria, but the associated mechanism leading to the properties has yet to be confirmed [117]. This opens up an opportunity for further exploration to gain an insight into how filler could act as antimicrobial agent besides its reinforcement role. Until now, it is still difficult to obtain insightful information pertaining to economic feasibility on energy consumption and cost analysis for bioplastic fabrication. Hence, it is essential to take into account the thermo-economic aspects of pretreatment and feedstock preparation, including the usage of environmentally benign chemicals in bioplastic fabrication as part of environmental mitigation strategies.

Uniform dispersion of materials is desired when nanofiller is incorporated in bioplastic as its effect can be manifested in its physical and mechanical properties. Nano-sized particles tend to agglomerate with each other, and this problem can be resolved with the aid of ultrasound in dispersing nanomaterials in the polymer [10]. However, scientific data elucidating the effect of ultrasound (for instance, sonication and ultrasonic amplitude) on the dispersion of nanomaterials is rare and not well established. This could prompt more research efforts towards the investigation of ultrasound on mechanical, optical, barrier and biodegradability properties of bioplastic. In addition, the life-cycle assessment analysis of bioplastic from production to its ultimate disposal or recycling is also worth studying to ascertain its sustainability in the context of the circular economy [124,125].

The leaching of plasticizer during storage or end-user applications is also a major concern which could restrict the utilization of plasticizers in essential sectors such as the medical, pharmaceutical and food packaging industries. Plasticizer has comparatively low molecular weight (300–600 g/mol), which could potentially migrate from packaging materials into packaged food, thereby becoming indirect “food additives” [126]. Ideal plasticizers can be derived from renewable sources with desirable properties such as high biodegradability, chemical stability, absence of toxins, and no or little leaching or migration during usage or aging. Nevertheless, the leaching of the plasticizer during storage and its toxicity is still under scrutiny. In view of this, the migration possibility or mechanism in plasticized bioplastics should be investigated so that appropriate remediation or pollutant removal strategies can be devised [36].

When using starch-based bioplastics as food packaging materials, their hydrophilic nature exhibits a low water vapour barrier, which is responsible for poor processing ability, high brittleness, vulnerability to degradation, limited long-term stability and poor mechanical properties [11]. In addition, the potential of nanoparticles to migrate from packaging materials to packaged food should also be taken into consideration [73]. Therefore, risk

assessment such as a toxicology study should be conducted. Storage tests should also be performed for the safe usage of packaging films based on bioplastics before they can be launched into the mass market to replace conventional packaging materials.

## 7. Conclusions

The biodegradable and green starch-based bioplastic is highly desirable to replace the conventional petroleum-based plastic due to its sustainability and environmental friendliness together with its readily available starch sources from food waste. The optical properties of starch-based bioplastics are affected by the amylose and amylopectin contents in starch. Lower amylose or higher amylopectin content resulted in more transparent film. On the other hand, more lipid content in starch can cause the film to become more opaque. The addition of environmentally benign nanofillers in bioplastic fabrication can overcome two main inadequacies of starch-based bioplastics, namely, high water affinity and poor mechanical properties. Filler-incorporated bioplastic has an enhanced tensile strength and Young's modulus due to the large surface area and aspect ratio, which increase the hydrogen bonding between filler–amylose–amylopectin molecular chains. Moreover, barrier properties can be improved by forcing the permeable molecules to follow a more tortuous path which will impede their diffusion. The addition of plasticizer weakens the structure of bioplastic and decreases the tensile strength while increasing the elongation at break of bioplastic. From the collated findings, it can be deduced that tensile strength is closely related to the added fillers, while elongation at break is associated with the addition of plasticizer. Overall, utilizing agricultural or food waste for the production of starch-based bioplastic can maximize their values and reduce the accumulation of hazardous petroleum-based plastic wastes. Commercialization of starch-based bioplastic is highly plausible if it can strike a balance among its mechanical properties, production cost, toxicity and an acceptable level of biodegradability. Therefore, a synergistic relationship between the addition of fillers and plasticizers is crucial to establish in future research studies.

**Author Contributions:** Conceptualization, S.X.T.; investigation, S.X.T.; writing—original draft preparation, S.X.T.; writing—review and editing, A.A., H.C.O., S.L., Y.L.P. and G.C.N.; supervision, A.A., H.C.O., S.L. and G.C.N.; project administration, S.L. and G.C.N.; funding acquisition, S.L. and G.C.N. All authors have read and agreed to the published version of the manuscript.

**Funding:** This work was supported by the Fundamental Research Grant Scheme (FRGS), Ministry of Education, Malaysia [FRGS/1/2018/TK10/UTAR/02/1], Universiti Tunku Abdul Rahman Research Fund (UTARRF/6200-W83), Malaysia and Universiti Malaya, Kuala Lumpur, under the RU Grant (GPF059A-2020).

**Institutional Review Board Statement:** Not applicable.

**Informed Consent Statement:** Not applicable.

**Data Availability Statement:** The data presented in this study are available on request from the corresponding author.

**Conflicts of Interest:** The authors declare no conflict of interest.

## References

1. Hasan, M.; Rahmayani, R. Bioplastic from Chitosan and Yellow Pumpkin Starch with Castor Oil as Plasticizer. In Proceedings of the IOP Conference Series: Materials Science and Engineering, Surakarta, Indonesia, 4–5 September 2017.
2. Pathak, S.; Sneha, C.; Mathew, B.B. Bioplastics: Its timeline based scenario & challenges. *J. Polym. Biopolym. Phys. Chem.* **2014**, *2*, 84–90.
3. Zeller, M.A.; Hunt, R.; Jones, A.; Sharma, S. Bioplastics and their thermoplastic blends from Spirulina and Chlorella microalgae. *J. Appl. Polym. Sci.* **2013**, *130*, 3263–3275. [CrossRef]
4. Khalil, H.A.; Tehrani, M.; Davoudpour, Y.; Bhat, A.; Jawaid, M.; Hassan, A. Natural fiber reinforced poly (vinyl chloride) composites: A review. *J. Reinf. Plast. Compos.* **2013**, *32*, 330–356. [CrossRef]
5. Bilo, F.; Pandini, S.; Sartore, L.; Depero, L.E.; Gargiulo, G.; Bonassi, A.; Federici, S.; Bontempi, E. A sustainable bioplastic obtained from rice straw. *J. Clean. Prod.* **2018**, *200*, 357–368. [CrossRef]

6. Delacuvellerie, A.; Cyriaque, V.; Gobert, S.; Benali, S.; Wattiez, R. The plastisphere in marine ecosystem hosts potential specific microbial degraders including *Alcanivorax borkumensis* as a key player for the low-density polyethylene degradation. *J. Hazard. Mater.* **2019**, *380*, 120899. [CrossRef] [PubMed]
7. Ross, S.; Evans, D. The environmental effect of reusing and recycling a plastic-based packaging system. *J. Clean. Prod.* **2003**, *11*, 561–571. [CrossRef]
8. Wu, C.-S. Renewable resource-based green composites of surface-treated spent coffee grounds and polylactide: Characterisation and biodegradability. *Polym. Degrad. Stab.* **2015**, *121*, 51–59. [CrossRef]
9. Rujnić-Sokele, M.; Pilipović, A. Challenges and opportunities of biodegradable plastics: A mini review. *Waste Manag. Res.* **2017**, *35*, 132–140. [CrossRef]
10. Wahyuningtiyas, N.E.; Suryanto, H. Effect of ultrasonic treatment on morphology and mechanical properties of bioplastic from cassava starch with nanoclay reinforcement. *J. Metastable Nanocrystalline Mater.* **2017**, *29*, 35–41. [CrossRef]
11. Jabeen, N.; Majid, I.; Nayik, G.A. Bioplastics and food packaging: A review. *Cogent Food Agric.* **2015**, *1*, 1–6. [CrossRef]
12. Lubis, M.; Harahap, M.; Manullang, A.; Ginting, M.; Sartika, M. Utilization starch of jackfruit seed (*Artocarpus heterophyllus*) as raw material for bioplastics manufacturing using sorbitol as plasticizer and chitosan as filler. In Proceedings of the International Conference on Computing and Applied Informatics 2016, Medan, Indonesia, 14–15 December 2016.
13. Cifriadi, A.; Panji, T.; Wibowo, N.A.; Syamsu, K. Bioplastic production from cellulose of oil palm empty fruit bunch. In Proceedings of the IOP Conference Series: Earth and Environmental Science, Bogor, Indonesia, 10–11 October 2016.
14. Zhao, X.; Cornish, K.; Vodovotz, Y. Narrowing the Gap for Bioplastic Use in Food Packaging: An Update. *Environ. Sci. Technol.* **2020**, *54*, 4712–4732. [CrossRef] [PubMed]
15. Kasmuri, N.; Zait, M.S.A. Enhancement of Bio-plastic using Eggshells and Chitosan on Potato Starch Based. *Int. J. Eng. Technol.* **2018**, *7*, 110–115. [CrossRef]
16. Lim, W.; Chin, N.; Yusof, A.; Yahya, A.; Tee, T. Food waste handling in Malaysia and comparison with other Asian countries. *Int. Food Res. J.* **2016**, *23*, S1–S6.
17. Reddy, M.V.; Hayashi, S.; Choi, D.; Cho, H.; Chang, Y.-C. Short chain and medium chain fatty acids production using food waste under non-augmented and bio-augmented conditions. *J. Clean. Prod.* **2018**, *176*, 645–653. [CrossRef]
18. Kartika, T.; Harahap, M.B.; Ginting, M.H.S. Utilization of mango seed starch in manufacture of bioplastic reinforced with microparticle clay using glycerol as plasticizer. In Proceedings of the IOP Conference Series: Materials Science and Engineering, Sumatera Utara, Indonesia, 7–8 September 2017.
19. Ginting, M.H.S.; Tarigan, F.R.; Singgih, A.M. Effect of gelatinization temperature and chitosan on mechanical properties of bioplastics from avocado seed starch (*Persea Americana* mill) with plasticizer glycerol. *Int. J. Eng. Sci.* **2015**, *4*, 36–43.
20. Ginting, M.H.S.; Hasibuan, R.; Lubis, M.; Tanjung, D.; Iqbal, N. Effect of Hydrochloric Acid Concentration as Chitosan Solvent on Mechanical Properties of Bioplastics from Durian Seed Starch (*Durio Zibethinus*) with Filler Chitosan and Plasticizer Sorbitol. In Proceedings of the IOP Conference Series: Materials Science and Engineering, Bandung, Indonesia, 16–18 November 2016.
21. Maulida, S.M.; Tarigan, P. Production of starch based bioplastic from cassava peel reinforced with microcrystalline cellulose avicel PH101 using sorbitol as plasticizer. *J. Phys. Conf. Ser.* **2016**, *710*, 012012. [CrossRef]
22. Zuo, Y.; Gu, J.; Yang, L.; Qiao, Z.; Zhang, Y. Study on the preparation of maleated thermoplastic starch by reactive extrusion. *J. Thermoplast. Compos. Mater.* **2016**, *29*, 397–409. [CrossRef]
23. Zdanowicz, M.; Johansson, C. Impact of additives on mechanical and barrier properties of starch-based films plasticized with deep eutectic solvents. *Starch-Stärke* **2017**, *69*, 1700030. [CrossRef]
24. Bhat, A.; Khan, I.; Usmani, M.A.; Rather, J.A. Bioplastics and Bionanocomposites Based on Nanoclays and Other Nanofillers. In *Nanoclay Reinforced Polymer Composites*; Springer: Berlin/Heidelberg, Germany, 2016; pp. 115–139. [CrossRef]
25. Al-Battashi, H.; Annamalai, N.; Al-Kindi, S.; Nair, A.S.; Al-Bahry, S.; Verma, J.P.; Sivakumar, N. Production of bioplastic (poly-3-hydroxybutyrate) using waste paper as a feedstock: Optimization of enzymatic hydrolysis and fermentation employing *Burkholderia sacchari*. *J. Clean. Prod.* **2019**, *214*, 236–247. [CrossRef]
26. Folino, A.; Fazzino, F.; Komilis, D. Preliminary evaluation of the anaerobic biodegradability of three biobased materials used for the production of disposable plastics. *J. Hazard. Mater.* **2019**, *390*, 121653.
27. Ashok, A.; Rejeesh, C.; Renjith, R. Biodegradable polymers for sustainable packaging applications: A review. *Int. J. Bionics Biomater.* **2016**, *2*, 1–11.
28. Zia, F.; Zia, K.M.; Zuber, M.; Kamal, S.; Aslam, N. Starch based polyurethanes: A critical review updating recent literature. *Carbohydr. Polym.* **2015**, *134*, 784–798. [CrossRef] [PubMed]
29. Moran, J.I.; Vazquez, A.; Cyras, V.P. Bio-nanocomposites based on derivatized potato starch and cellulose, preparation and characterization. *J. Mater. Sci.* **2013**, *48*, 7196–7203. [CrossRef]
30. Chan, Y.; Phang, S.; Tee, T.; Lee, T.; Soo, T. Preliminary Study of Mechanical Properties in Thermoplastic Starch (TPS)/Coffee-Waste-Derived Fillers Composites. In Proceedings of the Engineering Undergraduate Research Catalyst Conference (EURECA), Sunway, Selangor, Malaysia, 1–2 July 2015; pp. 1–14.
31. Waterschoot, J.; Gomand, S.V.; Fierens, E.; Delcour, J.A. Production, structure, physicochemical and functional properties of maize, cassava, wheat, potato and rice starches. *Starch-Stärke* **2015**, *67*, 14–29. [CrossRef]

32. Amri, A.; Ekawati, L.; Herman, S.; Yenti, S.; Aziz, Y.; Utami, S. Properties enhancement of cassava starch based bioplastics with addition of graphene oxide. In Proceedings of the IOP Conference Series: Materials Science and Engineering, Pekanbaru-Riau, Indonesia, 29–30 November 2017.
33. Mallakpour, S. Fructose functionalized MWCNT as a filler for starch nanocomposites: Fabrication and characterizations. *Prog. Org. Coat.* **2018**, *114*, 244–249. [CrossRef]
34. Reddy, R.L.; Reddy, V.S.; Gupta, G.A. Study of bio-plastics as green and sustainable alternative to plastics. *Int. J. Emerg. Technol. Adv. Eng.* **2013**, *3*, 76–81.
35. Laadila, M.A.; Hegde, K.; Rouissi, T.; Brar, S.K.; Galvez, R.; Sorelli, L.; Cheikh, R.B.; Paiva, M.; Abokitse, K. Green synthesis of novel biocomposites from treated cellulosic fibers and recycled bio-plastic polylactic acid. *J. Clean. Prod.* **2017**, *164*, 575–586. [CrossRef]
36. Chieng, B.W.; Ibrahim, N.A.; Then, Y.Y.; Loo, Y.Y. Epoxidized jatropha oil as a sustainable plasticizer to poly (lactic acid). *Polymers* **2017**, *9*, 204. [CrossRef]
37. Hu, Y.; Daoud, W.A.; Fei, B.; Chen, L.; Kwan, T.H.; Lin, C.S.K. Efficient ZnO aqueous nanoparticle catalysed lactide synthesis for poly (lactic acid) fibre production from food waste. *J. Clean. Prod.* **2017**, *165*, 157–167. [CrossRef]
38. Lopes, M.; Jardini Filho, A. Synthesis and characterizations of poly (lactic acid) by ring-opening polymerization for biomedical applications. *Chem. Eng.* **2014**, *38*, 331–336.
39. Brodin, M.; Vallejos, M.; Opedal, M.T.; Area, M.C.; Chinga-Carrasco, G. Lignocellulosics as sustainable resources for production of bioplastics—A review. *J. Clean. Prod.* **2017**, *162*, 646–664. [CrossRef]
40. Othman, M.; Rashid, H.; Jamal, N.; Shaharuddin, S.; Sulaiman, S.; Hairil, H.; Khalid, K.; Zakaria, M. Effect of Cinnamon Extraction Oil (CEO) for Algae Biofilm Shelf-Life Prolongation. *Polymers* **2019**, *11*, 4. [CrossRef] [PubMed]
41. Gurunathan, T.; Mohanty, S.; Nayak, S.K. A review of the recent developments in biocomposites based on natural fibres and their application perspectives. *Compos. Part A Appl. Sci. Manuf.* **2015**, *77*, 1–25. [CrossRef]
42. Chen, M.-J.; Shi, Q.-S. Transforming sugarcane bagasse into bioplastics via homogeneous modification with phthalic anhydride in ionic liquid. *ACS Sustain. Chem. Eng.* **2015**, *3*, 2510–2515. [CrossRef]
43. Li, M.-C.; Wu, Q.; Song, K.; Lee, S.; Qing, Y.; Wu, Y. Cellulose Nanoparticles: Structure–Morphology–Rheology Relationships. *ACS Sustain. Chem. Eng.* **2015**, *3*, 821–832. [CrossRef]
44. Mood, S.H.; Golfeshan, A.H.; Tabatabaei, M.; Jouzani, G.S.; Najafi, G.H.; Gholami, M.; Ardjmand, M. Lignocellulosic biomass to bioethanol, a comprehensive review with a focus on pretreatment. *Renew. Sustain. Energy Rev.* **2013**, *27*, 77–93. [CrossRef]
45. Alekhina, M.; Mikkonen, K.S.; Alén, R.; Tenkanen, M.; Sixta, H. Carboxymethylation of alkali extracted xylan for preparation of bio-based packaging films. *Carbohydr. Polym.* **2014**, *100*, 89–96. [CrossRef]
46. Müller, Y.; Tot, I.; Potthast, A.; Rosenau, T.; Zimmermann, R.; Eichhorn, K.-J.; Nitschke, C.; Scherr, G.; Freudenberg, U.; Werner, C. The impact of esterification reactions on physical properties of cellulose thin films. *Soft Matter* **2010**, *6*, 3680–3684. [CrossRef]
47. Özçimen, D.; İnan, B.; Morkoç, O.; Efe, A. A Review on Algal Biopolymers. *J. Chem. Eng. Res. Updates* **2017**, *4*, 7–14. [CrossRef]
48. Hii, S.-L.; LIM, J.; Ong, W.-T.; Wong, C.-L. Agar from Malaysian red seaweed as potential material for synthesis of bioplastic film. *J. Eng. Sci. Technol.* **2016**, *11*, 1–15.
49. Bhatia, S.K.; Gurav, R.; Choi, T.-R.; Jung, H.-R.; Yang, S.-Y.; Moon, Y.-M.; Song, H.-S.; Jeon, J.-M.; Choi, K.-Y.; Yang, Y.-H. Bioconversion of plant biomass hydrolysate into bioplastic (polyhydroxyalkanoates) using *Ralstonia eutropha* 5119. *Bioresour. Technol.* **2019**, *271*, 306–315. [CrossRef] [PubMed]
50. Jost, V.; Langowski, H.-C. Effect of different plasticisers on the mechanical and barrier properties of extruded cast PHBV films. *Eur. Polym. J.* **2015**, *68*, 302–312. [CrossRef]
51. Arvizu-Higuera, D.L.; Rodríguez-Montesinos, Y.E.; Murillo-Álvarez, J.I.; Muñoz-Ochoa, M.; Hernández-Carmona, G. Effect of alkali treatment time and extraction time on agar from *Gracilaria vermiculophylla*. In Proceedings of the Nineteenth International Seaweed Symposium, Kobe, Japan, 26–31 March 2007.
52. Guerrero, P.; Etxabide, A.; Leceta, I.; Peñalba, M.; De la Caba, K. Extraction of agar from *Gelidium sesquipedale* (Rhodophyta) and surface characterization of agar based films. *Carbohydr. Polym.* **2014**, *99*, 491–498. [CrossRef]
53. Brodie, J. Systematics of the Species-Rich Algae: Red Algal Classification, Phylogeny and Speciation. In *Reconstructing the Tree of life: Taxonomy and Systematics of Species Rich Taxa*; CRC Press: Boca Raton, FL, USA, 2007; pp. 323–336.
54. Chu, W.-L.; Mohamed, N.; Phang, S.-M. Fatty acid composition of some Malaysian seaweeds. *Malays. J. Sci.* **2003**, *22*, 21–27.
55. Agustin, M.B.; Ahmmad, B.; Alonzo, S.M.M.; Patriana, F.M. Bioplastic based on starch and cellulose nanocrystals from rice straw. *J. Reinf. Plast. Compos.* **2014**, *33*, 2205–2213. [CrossRef]
56. Ilyas, R.; Sapuan, S.; Sanyang, M.; Ishak, M. Nanocrystalline cellulose reinforced starch-based nanocomposite: A review. In Proceedings of the 5th Postgraduate Seminar on Natural Fiber Composites, Universiti Putra Malaysia, Serdang, Malaysia, 28 December 2016; pp. 82–87.
57. Harunsyah; Yunus, M.; Fauzan, R. Mechanical properties of bioplastics cassava starch film with Zinc Oxide nanofiller as reinforcement. In Proceedings of the IOP Conference Series: Materials Science and Engineering, University of Malaya, Kuala Lumpur, Malaysia, 5–6 April 2017.
58. Pasquini, D.; de Moraes Teixeira, E.; da Silva Curvelo, A.A.; Belgacem, M.N.; Dufresne, A. Extraction of cellulose whiskers from cassava bagasse and their applications as reinforcing agent in natural rubber. *Ind. Crops Prod.* **2010**, *32*, 486–490. [CrossRef]

59. Abreu, A.S.; Oliveira, M.; de Sá, A.; Rodrigues, R.M.; Cerqueira, M.A.; Vicente, A.A.; Machado, A. Antimicrobial nanostructured starch based films for packaging. *Carbohydr. Polym.* **2015**, *129*, 127–134. [CrossRef]
60. Liu, Y.-X.; Liang, Z.-S.; Liang, J.-N.; Liao, L.-Y. Effect of different surface properties of nanosilica on retrogradation behavior and structures of thermoplastic cassava starch. *J. Polym. Res.* **2021**, *28*, 1–12. [CrossRef]
61. Li, J.L.; Zhou, M.; Cheng, G.; Cheng, F.; Lin, Y.; Zhu, P.X. Comparison of mechanical reinforcement effects of cellulose nanofibers and montmorillonite in starch composite. *Starch-Stärke* **2019**, *71*, 1800114. [CrossRef]
62. Noshirvani, N.; Hong, W.; Ghanbarzadeh, B.; Fasihi, H.; Montazami, R. Study of Cellulose Nanocrystal Doped Starch-Polyvinyl Alcohol Bionanocomposite Films. *Int. J. Biol. Macromol.* **2018**, *107*, 2065–2074. [CrossRef]
63. Xu, Y.; Rehmani, N.; Alsubaie, L.; Kim, C.; Sismour, E.; Scales, A. Tapioca starch active nanocomposite films and their antimicrobial effectiveness on ready-to-eat chicken meat. *Food Packag. Shelf Life* **2018**, *16*, 86–91. [CrossRef]
64. Lopez, O.; Garcia, M.A.; Villar, M.A.; Gentili, A.; Rodriguez, M.; Albertengo, L. Thermo-compression of biodegradable thermo-plastic corn starch films containing chitin and chitosan. *LWT-Food Sci. Technol.* **2014**, *57*, 106–115. [CrossRef]
65. Estevez-Areco, S.; Guz, L.; Candal, R.; Goyanes, S. Active bilayer films based on cassava starch incorporating ZnO nanorods and PVA electrospun mats containing rosemary extract. *Food Hydrocoll.* **2020**, *108*, 106054. [CrossRef]
66. Ceballos, R.L.; von Bilderling, C.; Guz, L.; Bernal, C.; Famá, L. Effect of greenly synthesized silver nanoparticles on the properties of active starch films obtained by extrusion and compression molding. *Carbohydr. Polym.* **2021**, *261*, 117871. [CrossRef] [PubMed]
67. Domene-López, D.; Delgado-Marín, J.J.; García-Quesada, J.C.; Martín-Gullón, I.; Montalbán, M.G. Electroconductive starch/multi-walled carbon nanotube films plasticized by 1-ethyl-3-methylimidazolium acetate. *Carbohydr. Polym.* **2020**, *229*, 115545. [CrossRef] [PubMed]
68. Alves, Z.; Abreu, B.; Ferreira, N.M.; Marques, E.F.; Nunes, C.; Ferreira, P. Enhancing the dispersibility of multiwalled carbon nanotubes within starch-based films by the use of ionic surfactants. *Carbohydr. Polym.* **2021**, *273*, 118531. [CrossRef] [PubMed]
69. Mallakpour, S.; Rashidmoghadam, S. Application of ultrasonic irradiation as a benign method for production of glycerol plasticized-starch/ascorbic acid functionalized MWCNTs nanocomposites: Investigation of methylene blue adsorption and electrical properties. *Ultrason. Sonochem.* **2018**, *40*, 419–432. [CrossRef] [PubMed]
70. Mallakpour, S.; Rashidmoghadam, S. Starch/MWCNT-vitamin C nanocomposites: Electrical, thermal properties and their utilization for removal of methyl orange. *Carbohydr. Polym.* **2017**, *169*, 23–32. [CrossRef]
71. Mallakpour, S.; Nezamzadeh Ezhieh, A. Preparation and characterization of starch nanocomposite embedded with functionalized MWCNT: Investigation of optical, morphological, thermal, and copper ions adsorption properties. *Adv. Polym. Technol.* **2018**, *37*, 2195–2203. [CrossRef]
72. Shima, A.; Hossein, B. Investigation the effect of graphene oxide and gelatin/starch weight ratio on the properties of starch/gelatin/GO nanocomposite films: The RSM study. *Int. J. Biol. Macromol.* **2017**, *109*, 1019–1028.
73. Nazir, M.S.; Kassim, M.H.M.; Mohapatra, L.; Gilani, M.A.; Raza, M.R.; Majeed, K. Characteristic Properties of Nanoclays and Characterization of Nanoparticulates and Nanocomposites. In *Nanoclay Reinforced Polymer Composites*; Springer: Berlin/Heidelberg, Germany, 2016; pp. 35–55.
74. Wahyuningtiyas, N.E.; Suryanto, H. Properties of cassava starch based bioplastic reinforced by nanoclay. *J. Mech. Eng. Sci. Technol.* **2018**, *2*, 20–26. [CrossRef]
75. Martins, J.T.; Bourbon, A.L.; Pinheiro, A.C.; Souza, B.W.; Cerqueira, M.A.; Vicente, A.A. Biocomposite films based on  $\kappa$ -carrageenan/locust bean gum blends and clays: Physical and antimicrobial properties. *Food Bioprocess Technol.* **2013**, *6*, 2081–2092. [CrossRef]
76. Jamróz, E.; Kulawik, P.; Kopel, P. The effect of nanofillers on the functional properties of biopolymer-based films: A review. *Polymers* **2019**, *11*, 675. [CrossRef] [PubMed]
77. Brinchi, L.; Cotana, F.; Fortunati, E.; Kenny, J. Production of nanocrystalline cellulose from lignocellulosic biomass: Technology and applications. *Carbohydr. Polym.* **2013**, *94*, 154–169. [CrossRef]
78. Chiulan, I.; Frone, A.N.; Panaitescu, D.M.; Nicolae, C.A.; Trusca, R. Surface properties, thermal, and mechanical characteristics of poly (vinyl alcohol)–starch-bacterial cellulose composite films. *J. Appl. Polym. Sci.* **2018**, *135*, 45800. [CrossRef]
79. Jakubowska, E.; Gierszewska, M.; Nowaczyk, J.; Olewnik-Kruszkowska, E. The role of a deep eutectic solvent in changes of physicochemical and antioxidative properties of chitosan-based films. *Carbohydr. Polym.* **2021**, *255*, 117527. [CrossRef]
80. Azadi, A.; Supriyadi, S.; Herawati, H. Starch Based Biocomposite from Sago (*Metroxylon sagu*) with Nano-Chitosan reinforcement: Mechanical and Thermal Characteristics. *J. Pure Appl. Chem. Res.* **2020**, *9*, 98–107. [CrossRef]
81. Gudikandula, K.; Charya Maringanti, S. Synthesis of silver nanoparticles by chemical and biological methods and their antimicrobial properties. *J. Exp. Nanosci.* **2016**, *11*, 714–721. [CrossRef]
82. Khodashenas, B.; Ghorbani, H. Evaluation of the effective factors on size and anti-bacterial properties of biosynthesized silver nanoparticles. *Int. J. Nano Dimens.* **2015**, *6*, 111–127.
83. Garza-Cervantes, J.A.; Mendiola-Garza, G.; de Melo, E.M.; Dugmore, T.I.; Matharu, A.S.; Morones-Ramirez, J.R. Antimicrobial activity of a silver-microfibrillated cellulose biocomposite against susceptible and resistant bacteria. *Sci. Rep.* **2020**, *10*, 1–7. [CrossRef]
84. Ahmed, S.; Ahmad, M.; Swami, B.L.; Ikram, S. A review on plants extract mediated synthesis of silver nanoparticles for antimicrobial applications: A green expertise. *J. Adv. Res.* **2016**, *7*, 17–28. [CrossRef] [PubMed]






85. Sirelkhatim, A.; Mahmud, S.; Seeni, A.; Kaus, N.H.M.; Ann, L.C.; Bakhori, S.K.M.; Hasan, H.; Mohamad, D. Review on zinc oxide nanoparticles: Antibacterial activity and toxicity mechanism. *Nano-Micro Lett.* **2015**, *7*, 219–242. [CrossRef]
86. Famá, L.M.; Pettarin, V.; Goyanes, S.N.; Bernal, C.R. Starch/multi-walled carbon nanotubes composites with improved mechanical properties. *Carbohydr. Polym.* **2011**, *83*, 1226–1231. [CrossRef]
87. Koh, B.; Cheng, W. Mechanisms of carbon nanotube aggregation and the reversion of carbon nanotube aggregates in aqueous medium. *Langmuir* **2014**, *30*, 10899–10909. [CrossRef] [PubMed]
88. Siljander, S.; Keinänen, P.; Rätty, A.; Ramakrishnan, K.R.; Tuukkanen, S.; Kunnari, V.; Harlin, A.; Vuorinen, J.; Kanerva, M. Effect of surfactant type and sonication energy on the electrical conductivity properties of nanocellulose-CNT nanocomposite films. *Int. J. Mol. Sci.* **2018**, *19*, 1819. [CrossRef] [PubMed]
89. Zdanowicz, M.; Jędrzejewski, R.; Pilawka, R. Deep eutectic solvents as simultaneous plasticizing and crosslinking agents for starch. *Int. J. Biol. Macromol.* **2019**, *129*, 1040–1046. [CrossRef] [PubMed]
90. Khodaverdian, S.; Dabirmanesh, B.; Heydari, A.; Dashtban-Moghadam, E.; Khajeh, K.; Ghazi, F. Activity, stability and structure of laccase in betaine based natural deep eutectic solvents. *Int. J. Biol. Macromol.* **2018**, *107*, 2574–2579. [CrossRef] [PubMed]
91. Zdanowicz, M.; Szychaj, T. Ionic liquids as starch plasticizers or solvents. *Polimery* **2011**, *56*, 861–864. [CrossRef]
92. Zdanowicz, M.; Wilpiszewska, K.; Szychaj, T. Deep eutectic solvents for polysaccharides processing. A review. *Carbohydr. Polym.* **2018**, *200*, 361–380. [CrossRef]
93. Zdanowicz, M.; Johansson, C. Mechanical and barrier properties of starch-based films plasticized with two-or three component deep eutectic solvents. *Carbohydr. Polym.* **2016**, *151*, 103–112. [CrossRef]
94. Tan, Y.T.; Ngoh, G.C.; Chua, A.S.M. Evaluation of fractionation and delignification efficiencies of deep eutectic solvents on oil palm empty fruit bunch. *Ind. Crops Prod.* **2018**, *123*, 271–277. [CrossRef]
95. Hassan, A.A.; Abbas, A.; Rasheed, T.; Bilal, M.; Iqbal, H.M.; Wang, S. Development, influencing parameters and interactions of bioplasticizers: An environmentally friendlier alternative to petro industry-based sources. *Sci. Total Environ.* **2019**, *682*, 394–404. [CrossRef] [PubMed]
96. Webb, H.; Arnott, J.; Crawford, R.; Ivanova, E. Plastic degradation and its environmental implications with special reference to poly (ethylene terephthalate). *Polymers* **2013**, *5*, 1–18. [CrossRef]
97. Nowak, A.P.; Lisowska-Oleksiak, A. Red algae—An alternative source of carbon material for energy storage application. *Int. J. Electrochem. Sci.* **2014**, *9*, 3715–3724.
98. Haq, M.A.; Habu, Y.; Yamamoto, K.; Takada, A.; Ka-dokawa, J.-I. Ionic Liquid Induces Flexibility and Thermoplasticity in Cellulose Film. *Carbohydr. Polym.* **2019**, *223*, 115058. [CrossRef]
99. Feng, L.; Chen, Z.-L. Research progress on dissolution and functional modification of cellulose in ionic liquids. *J. Mol. Liq.* **2008**, *142*, 1–5. [CrossRef]
100. Pang, J.; Liu, X.; Zhang, X.; Wu, Y.; Sun, R. Fabrication of cellulose film with enhanced mechanical properties in ionic liquid 1-allyl-3-methylimidazolium chloride (AmimCl). *Materials* **2013**, *6*, 1270–1284. [CrossRef]
101. Peng, H.; Wang, S.; Xu, H.; Dai, G. Preparations, properties, and formation mechanism of novel cellulose hydrogel membrane based on ionic liquid. *J. Appl. Polym. Sci.* **2018**, *135*, 45488. [CrossRef]
102. Liu, X.; Pang, J.; Zhang, X.; Wu, Y.; Sun, R. Regenerated cellulose film with enhanced tensile strength prepared with ionic liquid 1-ethyl-3-methylimidazolium acetate (EMIMAc). *Cellulose* **2013**, *20*, 1391–1399. [CrossRef]
103. Macário, I.P.; Veloso, T.; Pereira, J.L.; Ventura, S.P.; Coutinho, J.A. Potential Threats of Ionic Liquids to the Environment and Ecosphere. In *Encyclopedia of Ionic Liquids*; Springer: Berlin/Heidelberg, Germany, 2020. [CrossRef]
104. Almeida, C.M.; Magalhães, J.M.; Souza, H.K.; Gonçalves, M.P. The role of choline chloride-based deep eutectic solvent and curcumin on chitosan films properties. *Food Hydrocoll.* **2018**, *81*, 456–466. [CrossRef]
105. Sousa, A.M.; Souza, H.K.; Latona, N.; Liu, C.-K.; Goncalves, M.P.; Liu, L. Choline chloride based ionic liquid analogues as tool for the fabrication of agar films with improved mechanical properties. *Carbohydr. Polym.* **2014**, *111*, 206–214. [CrossRef] [PubMed]
106. Santana, R.F.; Bonomo, R.C.F.; Gandolfi, O.R.R.; Rodrigues, L.B.; Santos, L.S.; dos Santos Pires, A.C.; de Oliveira, C.P.; Fontan, R.d.C.I.; Veloso, C.M. Characterization of starch-based bioplastics from jackfruit seed plasticized with glycerol. *J. Food Sci. Technol.* **2018**, *55*, 278–286. [CrossRef] [PubMed]
107. Ezeoha, S.; Ezenwanne, J. Production of biodegradable plastic packaging film from cassava starch. *IOSR J. Eng.* **2013**, *3*, 14–20. [CrossRef]
108. Ginting, M.H.S.; Kristiani, M.; Amelia, Y.; Hasibuan, R. The effect of chitosan, sorbitol, and heating temperature bioplastic solution on mechanical properties of bioplastic from durian seed starch (*Durio zibehinus*). *Int. J. Eng. Res. Appl.* **2015**, *6*, 33–38.
109. Anggraini, T.; Ulfimarjan; Azima, F.; Yennira, R. The effect of chitosan concentration on the characteristics of sago (*Metroxylon* sp.) starch bioplastics. *Res. J. Pharm. Biol. Chem. Sci.* **2017**, *8*, 1339–1351.
110. Zhang, W.; Jiang, W. Antioxidant and antibacterial chitosan film with tea polyphenols-mediated green synthesis silver nanoparticle via a novel one-pot method. *Int. J. Biol. Macromol.* **2020**, *155*, 1252–1261. [CrossRef]
111. Valizadeh, S.; Naseri, M.; Babaei, S.; Hosseini, S.M.H.; Imani, A. Development of bioactive composite films from chitosan and carboxymethyl cellulose using glutaraldehyde, cinnamon essential oil and oleic acid. *Int. J. Biol. Macromol.* **2019**, *134*, 604–612. [CrossRef]
112. Jacquot, C.; Jacquot, M.; Marques, P.; Jasniewski, J.; Akhtar, M.J.; Didelot, A.S.; Desobry, S. Influence of microwave heating time on the structure and properties of chitosan films. *J. Appl. Polym. Sci.* **2014**, *131*, 40779. [CrossRef]

113. Arihara, K.; Zhou, L.; Ohata, M. Bioactive properties of Maillard reaction products generated from food protein-derived peptides. *Adv. Food Nutr. Res.* **2017**, *81*, 161–185.
114. Zhang, Q.; Benoit, M.; Vigier, K.D.O.; Barrault, J.; Jégou, G.; Philippe, M.; Jérôme, F. Pretreatment of microcrystalline cellulose by ultrasounds: Effect of particle size in the heterogeneously-catalyzed hydrolysis of cellulose to glucose. *Green Chem.* **2013**, *15*, 963–969. [CrossRef]
115. Poovarodom, N.; Permyanwattana, W. Development of starch/shellac-based composites for food contact applications. *J. Thermoplast. Compos. Mater.* **2015**, *28*, 597–609. [CrossRef]
116. Setyaningsih, D.; Muna, N.; Suryawan, N.B.; Nurfauzi, A.A. Cellulose nanofiber isolation from palm oil Empty Fruit Bunches (EFB) through strong acid hydrolysis. In Proceedings of the IOP Conference Series: Earth and Environmental Science, Bogor, Indonesia, 24–25 July 2017.
117. Salaberria, A.M.; Diaz, R.H.; Labidi, J.; Fernandes, S.C. Role of chitin nanocrystals and nanofibers on physical, mechanical and functional properties in thermoplastic starch films. *Food Hydrocoll.* **2015**, *46*, 93–102. [CrossRef]
118. Ren, L.; Yan, X.; Zhou, J.; Tong, J.; Su, X. Influence of chitosan concentration on mechanical and barrier properties of corn starch/chitosan films. *Int. J. Biol. Macromol.* **2017**, *105*, 1636–1643. [CrossRef] [PubMed]
119. Haryanti, P.; Setyawati, R.; Wicaksono, R. Pengaruh Suhu dan Lama Pemanasan Suspensi Pati serta Konsentrasi Butanol terhadap Karakteristik Fisikokimia Pati Tinggi Amilosa dari Tapioka. *Agritech J. Fak. Teknol. Pertan. UGM* **2014**, *34*, 308–315. [CrossRef]
120. Wojciechowska, P. The Effect of Concentration and Type of Plasticizer on the Mechanical Properties of Cellulose Acetate Butyrate Organic-Inorganic Hybrids. In *Recent Advances in Plasticizers*; IntechOpen: London, UK, 2012; pp. 141–164.
121. Sifuentes-Nieves, I.; Flores-Silva, P.C.; Gallardo-Vega, C.; Hernández-Hernández, E.; Neira-Velázquez, G.; Mendez-Montealvo, G.; Velazquez, G. Films made from plasma-modified corn starch: Chemical, mechanical and barrier properties. *Carbohydr. Polym.* **2020**, *237*, 116103. [CrossRef]
122. Basiak, E.; Lenart, A.; Debeaufort, F. Effect of starch type on the physico-chemical properties of edible films. *Int. J. Biol. Macromol.* **2017**, *98*, 348–356. [CrossRef]
123. Wang, H.; Zhu, Q.; Wu, T.; Zhang, M. Glass transition temperature, rheological, and gelatinization properties of high amylose corn starch and waxy cassava starch blends. *J. Food Process. Preserv.* **2020**, *44*, e14682. [CrossRef]
124. Arikan, E.B.; Ozsoy, H.D. A review: Investigation of bioplastics. *Civ. Eng. Archit.* **2015**, *9*, 188–192.
125. Spierling, S.; Knüpffer, E.; Behnsen, H.; Mudersbach, M.; Krieg, H.; Springer, S.; Albrecht, S.; Herrmann, C.; Endres, H.-J. Bio-based plastics-A review of environmental, social and economic impact assessments. *J. Clean. Prod.* **2018**, *185*, 16–491. [CrossRef]
126. Hahladakis, J.N.; Velis, C.A.; Weber, R.; Iacovidou, E.; Purnell, P. An overview of chemical additives present in plastics: Migration, release, fate and environmental impact during their use, disposal and recycling. *J. Hazard. Mater.* **2018**, *344*, 179–199. [CrossRef]



## Article

# Rapid Ultrasound-Assisted Starch Extraction from Sago Pith Waste (SPW) for the Fabrication of Sustainable Bioplastic Film

Shiou Xuan Tan <sup>1</sup>, Andri Andriyana <sup>1</sup>, Steven Lim <sup>2,3,\*</sup> , Hwai Chyuan Ong <sup>4</sup> , Yean Ling Pang <sup>2,3</sup>   
and Gek Cheng Ngoh <sup>5,\*</sup>

- <sup>1</sup> Department of Mechanical Engineering, Faculty of Engineering, Universiti Malaya, Kuala Lumpur 50603, Malaysia; kva190014@siswa.um.edu.my (S.X.T.); andri.andriyana@um.edu.my (A.A.)  
<sup>2</sup> Department of Chemical Engineering, Lee Kong Chian Faculty of Engineering and Science, Universiti Tunku Abdul Rahman, Kajang 43000, Malaysia; pangyl@utar.edu.my  
<sup>3</sup> Centre of Photonics and Advanced Materials Research, Universiti Tunku Abdul Rahman, Kajang 43000, Malaysia  
<sup>4</sup> Future Technology Research Center, National Yunlin University of Science and Technology, Douliou 64002, Taiwan; onghc@yuntech.edu.tw  
<sup>5</sup> Centre of Separation Science and Technology, Department of Chemical Engineering, Faculty of Engineering, Universiti Malaya, Kuala Lumpur 50603, Malaysia  
\* Correspondence: stevenlim@utar.edu.my (S.L.); ngoh@um.edu.my (G.C.N.)

**Abstract:** The present study was conducted to optimize the extraction yield of starch from sago (*Metroxylon sago*) pith waste (SPW) with the assistance of ultrasound ensued by the transformation of extracted starch into a higher value-added bioplastic film. Sago starch with extraction yield of 71.4% was successfully obtained using the ultrasound-assisted extraction, with the following conditions: particle size < 250  $\mu\text{m}$ , solid loading of 10 wt.%, ultrasonic amplitude of 70% and duty cycle of 83% in 5 min. The rapid ultrasound approach was proven to be more effective than the conventional extraction with 60.9% extraction yield in 30 min. Ultrasound-extracted starch was found to exhibit higher starch purity than the control starch as indicated by the presence of lower protein and ash contents. The starch granules were found to have irregular and disrupted surfaces after ultrasonication. The disrupted starch granules reduced the particle size and increased the swelling power of starch which was beneficial in producing a film-forming solution. The ultrasound-extracted sago starch was subsequently used to prepare a bioplastic film via solution casting method. A brownish bioplastic film with tensile strength of  $0.9 \pm 0.1$  MPa, Young's modulus of  $22 \pm 0.8$  MPa, elongation at break of  $13.6 \pm 2.0\%$  and water vapour permeability (WVP) of  $1.11 \pm 0.1 \times 10^{-8}$   $\text{g m}^{-1} \text{s}^{-1} \text{Pa}^{-1}$  was obtained, suggesting its feasibility as bioplastic material. These findings provide a means of utilization for SPW which is in line with the contemporary trend towards greener and sustainable products and processes.

**Keywords:** ultrasound; sago pith waste; sago starch; extraction yield; starch-based bioplastic

**Citation:** Tan, S.X.; Andriyana, A.; Lim, S.; Ong, H.C.; Pang, Y.L.; Ngoh, G.C. Rapid Ultrasound-Assisted Starch Extraction from Sago Pith Waste (SPW) for the Fabrication of Sustainable Bioplastic Film. *Polymers* **2021**, *13*, 4398. <https://doi.org/10.3390/polym13244398>

Academic Editor: Cristina Cazan

Received: 14 November 2021

Accepted: 7 December 2021

Published: 15 December 2021

**Publisher's Note:** MDPI stays neutral with regard to jurisdictional claims in published maps and institutional affiliations.



**Copyright:** © 2021 by the authors. Licensee MDPI, Basel, Switzerland. This article is an open access article distributed under the terms and conditions of the Creative Commons Attribution (CC BY) license (<https://creativecommons.org/licenses/by/4.0/>).

## 1. Introduction

Generally, starch extraction methods can be categorized into chemical and physical techniques. Acid hydrolysis [1,2] and enzymatic hydrolysis [3] are several notable chemical extraction techniques. Acid hydrolysis requires long processing duration of more than 5 days and extra purification steps [4–6]. Meanwhile, enzymatic hydrolysis needs to undergo a lengthy incubation period of more than 24 h to remove protein and fiber prior to the release of starch. Enzymatic hydrolysis is also costly as it requires a pure enzyme and antimicrobial agent to reduce the risk of starch fermentation or degradation [7,8]. Recently, physical techniques such as stirred media milling [9] and high-pressure homogenization [10] had emerged but had constraints such as difficulty in maintaining constant flow at high concentration of starch slurry during milling and the restriction of

low concentration starch slurry application, respectively [5]. Comparatively, ultrasound is a better physical technique for starch extraction in providing strong agitation without any external heating source [11,12]. High extraction yield which can be achieved by the simple and fast ultrasound technique without additional chemical treatment outweighs the shortcomings of the conventional chemical and physical techniques [13]. Therefore, ultrasound is favoured for recovering starch from crops such as taro [8], yam [14], corn [6], pea [15], jicama roots [16] and breadfruit [4].

Similar to the starchy crops mentioned above, the residual starch present in the sago (*Metroxylon sagu*) pith waste (SPW) can be extracted and further converted into higher value-added product. SPW represents an abundant source of agro-industrial waste which is derived from sago starch processing with starch content ranges from 60–80% [17]. Approximately one tonne of SPW is generated for every tonne of sago starch produced (dry weight basis). The total amount of SPW produced in Malaysia had been recorded up to 110 tonnes/year which represented a sizeable amount [18,19]. In the conventional sago starch extraction process, low extraction yield (25–41%) was often reported due to the starch granules that rigidly embedded in the fibrous matrices of the sago pith residue [20,21]. Therefore, SPWs are often dumped into rivers and waterways which threatens the aquatic life [17].

As a matter of fact, the starch extracted from the SPW can be plasticized to produce bioplastics. Development of bioplastics is inspired with the aim to reduce the environmental impacts brought by the utilization of petroleum-based plastics [22,23]. Disposal of petroleum-based plastics threatens the environment with extremely long degradation rate which can last for 100–1000 years [24,25]. Furthermore, the emissions of carbon dioxide and other hazardous gases from the incineration of plastic wastes are also detrimental to the environment and human health. Since bioplastics are produced from renewable agricultural resources and biomass feedstock, they could be degraded naturally as carbon dioxide, water and organic matter which are non-toxic to both the environment and humans [24,26,27].

Considering there is no published report on the exploration of SPW as feedstock for starch extraction using ultrasound to the best knowledge, this study aims to evaluate the effect of various parameters (particle size, solid loading, sonication duration, ultrasonic amplitude and duty cycle) towards the extraction yield of starch from SPW. The investigations of these influencing factors are essential to understand their relationship in obtaining the optimum extraction yield within the shortest duration and minimal use of renewable resources. The effectiveness of the ultrasound technique was subsequently compared with the conventional method in terms of extraction yield, extraction efficiency and chemical composition. The granule structure of the starch extracted from both methods was characterized in detailed by scanning electron microscopy (SEM), particle size distribution, X-ray diffraction (XRD), solubility and swelling power. Subsequently, the ultrasound-extracted starch was used to fabricate bioplastic film to validate its feasibility to be used as value-added product. The film properties were also compared with the bioplastic film fabricated using conventional method extracted starch to gauge its effectiveness.

## 2. Materials and Methods

### 2.1. Materials

SPW was provided by Craun Research Sdn. Bhd., Kuching, Malaysia. Potato amylose (100% purity) was purchased from Sigma-Aldrich Co. (St. Louis, MO, USA). Ethanol (95% purity) from HmbG (Selangor, Malaysia). Sodium hydroxide (99% purity), iodine ( $\geq 99.8\%$ ), potassium iodide (99.5% purity) and acetic acid (100% purity) were obtained from Merck (Darmstadt, Germany). All the chemicals were used as received without further purification. Laboratory formulated distilled water was used throughout the experiments.

## 2.2. Ultrasound-Assisted Starch Extraction from SPW

Starch extraction from SPW was performed following the method of Pinyo et al. [20] with slight modification. Prior to the extraction process, SPW was dried in an oven (SOV70B, Thermo-line, Beijing, China) at 60 °C for 24 h and ground using a blender (Tefal La Moulinette, 1000 W). The SPW powder was then sieved into different particle sizes (smaller than 250 µm, 250–500 µm, 500 µm–1 mm and larger than 1 mm). Starch slurry was prepared by mixing the SPW with distilled water at various solid loadings (5–10 wt.%) and adjusted to a total weight of 200 g. The tip was submerged until half depth of the starch slurry (approximately 1.5 cm to the bottom of the flask). The starch slurry was then subjected to a 500 W one-inch-diameter probe-type ultrasonic processor (model Q500-20, Qsonica LLC, CT, USA) operating at a frequency of 20 kHz. The ultrasound-assisted extraction process was conducted at an auto-induced temperature without temperature control at various amplitudes (50, 60 and 70%), sonication durations (5, 10 and 15 min) and duty cycle (50–100%). The continuous mode (5 s on/0 s off) and 5 different pulse modes (5 s on/1 s off, 5 s on/2 s off, 5 s on/3 s off, 5 s on/4 s off and 5 s on/5 s off) of ultrasonication corresponded to the duty cycle of 100, 83, 71, 63, 56 and 50%, respectively. Upon completion of the ultrasonication, the starch slurry was filtered through a fine filter cloth and the filtrate was allowed to stand for 1 h to precipitate the starch. The supernatant was decanted, and the starch precipitate was dried in an oven at 60 °C for 24 h. Single factor experiment design was adopted to quantify the effects of different factors (particle size, solid loading, ultrasonic amplitude, sonication duration and duty cycle) on the extraction yield of sago starch. The sequence of the factors was decided based on their significance towards the extraction yield found in the literature [28] and the preliminary investigation conducted while minimizing the number of resources required. For control sample, starch was extracted using conventional magnetic stirring approach. Starch slurry was stirred on a magnetic stirrer at 300 rpm and 46 °C for 30 min. The reaction temperature was determined from the reaction conditions for optimum extraction yield using ultrasound technique.

## 2.3. Chemical Composition of Extracted Starch

### 2.3.1. Determination of Amylose Content

Amylose content of starch was determined according to the iodine colorimetric method of Babu and Parimalavalli [29]. A beaker containing the mixture of 0.1 g of starch sample, 1 mL of 95% ethanol and 9 mL of 1 N sodium hydroxide was heated in a boiling water bath for 10 min with occasional mixing to gelatinize the starch. The cooled solution was then topped up with distilled water to a final volume of 100 mL and was shaken thoroughly. A 5 mL of the solution was taken and placed in another 100 mL volumetric flask covered with aluminium foil. One mL of 1 N acetic acid solution and 2 mL of 0.2% iodine solution were added to the flask and made up to the mark with distilled water. The absorbance of the solution was measured using a UV-vis spectrophotometer (SPEKOL 1500, Analytik Jena, Jena, Germany) at 620 nm. The standard curve was plotted using standards of amylose, with absorbance plotted against known amylose concentration. Amylose content was calculated according to Equation (1).

$$\text{Amylose content (\%)} = \frac{C \times DF \times V}{W} \times 100\% \quad (1)$$

where:

C is the sample concentration determined from the standard curve (mg/mL);

DF is the dilution factor;

V is the volume of the sample (mL);

W is the weight of the sample (mg).

### 2.3.2. Determination of Starch Content

Starch content was determined using the enzymatic colorimetric method according to AOAC 920.40 [30]. A measure of 100 mg of the starch sample was incubated with termamyl for 15 min at 100 °C and digested with amyloglucosidase at 60 °C for 30 min. The free glucose content was measured using the spectrophotometer at 510 nm with the aid of the combined glucose oxidase/peroxidase reagent kit. The starch content was calculated by multiplying the free glucose content with a factor of 0.9 [31].

### 2.3.3. Protein Content

Kjeldahl method was adopted to determine the nitrogen content of the sample which involved digestion, distillation and titration steps. One gram of the sample was digested with 30 mL of concentrated sulphuric acid in the presence of 2.0 g of catalyst mixture (potassium sulfate and selenium). The digested solution was subjected to acidic distillation in the presence of 25 mL of boric acid and 25 mL of distilled water. The distillate was neutralized with sodium hydroxide solution before titrating with sulphuric acid. The protein content was determined by multiplying the calculated nitrogen content with a factor of 6.25 [32].

### 2.3.4. Determination of Fat Content

One gram of the dried sample was extracted and refluxed in a Soxhlet extractor with *n*-hexane as the extraction solvent for 6 h. The solvent was evaporated using a rotary vacuum evaporator after completion of the extraction. The fat content was determined from the weight of oil retained in the flask [32].

### 2.3.5. Determination of Ash Content

Two grams of the sample was transferred to a pre-ashed crucible and was combusted over a low burner flame until no more flame was produced. It was then kept in a muffle furnace for overnight at 550 °C. The ash content was determined from the weight of the ash left in the crucible [32].

## 2.4. Determination of Extraction Yield and Extraction Efficiency

Extraction yield was obtained by calculating the amount of dried starch recovered from SPW as expressed in Equation (2) [33].

$$\text{Extraction yield (\%)} = \frac{\text{Weight of dried starch extracted from SPW (g)}}{\text{Weight of SPW (g)}} \times 100\% \quad (2)$$

After determined the optimum conditions, the weight of extracted pure starch was calculated by multiplying the starch content percentage with the weight of dried starch extracted from SPW. Extraction efficiency was calculated according to Equation (3) [33].

$$\text{Extraction efficiency (\%)} = \frac{\text{Weight of extracted pure starch (g)}}{\text{Weight of total starch present in the SPW (g)}} \times 100\% \quad (3)$$

## 2.5. Preparation of Sago Starch Bioplastic Film

The sago starch bioplastic film was prepared following the method of Agustin et al. [27] with slight modification. The starch solution was prepared by mixing 5.0 g of sago starch with 100 mL of distilled water. It was homogenized at 250 rpm and heated at 60 °C for 15 min. A measure of 40 wt.% glycerol (with respect to dried starch) [26] was added into the starch solution and heated at process temperature of 70 °C until it was gelatinized. Upon completion of the reaction, 15.0 g of starch mixture was poured into a square container with dimension of 10 × 10 cm. The mixture was then dried in a heating oven at 60 °C for 24 h and a bioplastic film with thickness of 0.11 ± 0.01 mm was obtained. The film was peeled off and stored in a desiccator with a sealed plastic bag prior to tensile test.

## 2.6. Characterization of Extracted Starch

### 2.6.1. Scanning Electron Microscopy (SEM)

The surface morphology of the control and ultrasound-extracted starch samples was observed using a bench top scanning electron microscope (Phenom ProX, Thermo Fisher Scientific, Breda, The Netherlands). The samples were dried prior to imaging. A single layer of the starch samples was sprinkled evenly on a clean stub attached with double-sided tape without gold coating. The stubs were then placed in the SEM chamber and the images were captured at an accelerating voltage of 15 kV with magnification of 500× [34]. The average size of the extracted starches was measured on 100 particles randomly using Image J software (National Institutes of Health, Bethesda, MD, USA).

### 2.6.2. Particle Size Distribution

Particle size distribution and its cumulative curves of both control and ultrasound-extracted starch samples were determined using a laser particle size analyzer (Malvern Mastersizer MSS, Malvern Instruments, Worcestershire, UK) equipped with a HydroMU sample dispersion unit (Malvern Instruments, Worcestershire, UK) at 25 °C [35]. Prior to the analysis, the particle size analyzer and the laser were powered to warm up for 1 h. Beaker containing distilled water was then pumped through the cell twice using the HydroMU sample dispersion unit to remove impurities from the cell. For sample analysis, the amount of sample added into the beaker containing distilled water was in accordance with the obscuration range required by the laser beam of 10–20%.

### 2.6.3. X-ray Diffraction (XRD) Pattern

The diffraction patterns of the samples were recorded using an X-ray diffractometer (model MiniFlex 300/600, Rigaku, TX, USA). The diffractometer is equipped with a CuK $\alpha$  radiation operating at 45 kV and 30 mA. The diffracted intensity was measured from 3–60° as a function of Bragg angles (2 $\theta$ ) with the scanning speed of 1°/second. Starch crystallinity was calculated according to Equation (4) [16].

$$\text{Crystallinity} = \frac{A_c}{A_c + A_a} \times 100\% \quad (4)$$

where:

$A_c$  is the crystalline area;

$A_a$  is the amorphous area.

### 2.6.4. Solubility and Swelling Power

Solubility and swelling power of the control and ultrasound-extracted starch samples were determined according to the method of Sit et al. [8] with slight modification. Starch of 0.5 g ( $W_0$ ) and 20 mL distilled water were added into a 50 mL centrifuge tube. The tube was kept in a shaking water bath at 70 °C for 30 min. The suspension was then cooled to room temperature and centrifuged at 2000 rpm for 15 min. The supernatant was carefully decanted in a petri dish and dried in an oven to a constant weight ( $W_1$ ) at 103 °C for 2 h. The weight of the swollen granules ( $W_2$ ) was measured after decantation. The solubility and swelling power were calculated according to Equations (5) and (6), respectively.

$$\text{Solubility (\%)} = \frac{W_1}{W_0} \times 100\% \quad (5)$$

$$\text{Swelling power (g gel/g starch)} = \frac{W_2}{W_0 - W_1} \quad (6)$$



## 2.7. Characterization of Fabricated Bioplastic Films

### 2.7.1. Colour Properties

The colour of the bioplastic film was determined using colour spectrophotometer (model CM-5, Konica Minolta, Tokyo, Japan) interfaced with computer operating Spectra Magic NX software (Konica Minolta, Tokyo, Japan). A white standard colour plate was used as the background for the colour measurements. The films were subjected to CIE-Lab system under illuminant D65 and observer 10° where L, a and b represent lightness, redness and yellowness. The total colour difference ( $\Delta E$ ) was calculated using Equation (7) [36]. The average values of the three measurements taken at three different positions of each film were reported.

$$\Delta E = \sqrt{(L - L^*)^2 + (a - a^*)^2 + (b - b^*)^2} \quad (7)$$

where  $L^*$ ,  $a^*$  and  $b^*$  represent the respective values of the white standard colour plate while L, a and b represent the respective values of the film.

### 2.7.2. Tensile Test

Mechanical properties of bioplastic film such as tensile strength, Young's Modulus and elongation at break were determined according to ASTM D882-02 [37] using Universal Testing Machine (Autograph AG-X, Shimadzu, Kyoto, Japan) interfaced with computer operating Trapezium software (Shimadzu, Kyoto, Japan). Measurements were performed with load cell of 500 N, crosshead speed of 5 mm/min and grip separation of 30 mm. Three readings were taken from three random places of each film, measuring  $7 \times 1$  cm. The average values of the three measurements were reported.

### 2.7.3. Water Vapour Permeability (WVP)

A bottle containing 2.0 g of fully dried calcium chloride (0% relative humidity) was sealed on top (11.5 mm in diameter) with the bioplastic film. It was then placed in a desiccator at room temperature of 25 °C with saturated sodium chloride solution (75% relative humidity). The changes in the weight of calcium chloride were recorded for every 1 h interval. The equilibrium state of saturation was reached after 24 h. The WVP of the film was calculated using Equation (8) [38]. Three replicates of each film were performed.

$$\text{WVP} \left( \text{g m}^{-1} \text{s}^{-1} \text{Pa}^{-1} \right) = \frac{w \times d}{A \times t \times P \times (RH_1 - RH_2)} \quad (8)$$

where:

w is the weight gained by calcium chloride (g);

d is the average thickness of the film (m);

A is the area of the film exposed for water vapour permeation ( $\text{m}^2$ );

t is the time (s);

P is the saturation vapour pressure of water at 25 °C (Pa);

$RH_1$  is the relative humidity in the desiccator;

$RH_2$  is the relative humidity inside the bottle.

## 2.8. Statistical Analysis

The experiments were performed in triplicates and all the statistical analysis results were expressed as mean  $\pm$  standard deviation. For results displayed on graph, standard deviation was indicated by an error bar. Significant differences between the mean values ( $p < 0.05$ ) were accessed by one-way analysis of variance (ANOVA) with Tukey test using OriginPro 2018 software (OriginLab, Northampton, MA, USA).

### 3. Results and Discussion

#### 3.1. Effect of Particle Size

Particle size plays an important role in the ultrasound-assisted starch extraction from SPW. Reducing the particle size of the starch increases the number of cells directly exposed to the extraction solvent and the ultrasound cavitation, thus enhancing the extraction yield. This effect could be achieved by grinding the biomass before extraction [39]. Energy consumption increases at lower particle size when the size of the sieve opening changes from coarse to fine [40,41]. Nonetheless, ultrasound could also synergize in breaking down the biomass and prevent agglomeration [39]. Therefore, the smallest particle size adopted in this study was smaller than 250  $\mu\text{m}$  with the purpose of reducing the grinding time and energy. Lower particle size also contributes to higher mass loss and is not economically competitive. Effects of particle size (smaller than 250  $\mu\text{m}$ , 250–500  $\mu\text{m}$ , 500  $\mu\text{m}$ –1 mm and larger than 1 mm) on the starch extraction yield was investigated at a fixed condition (solid loading of 10 wt.%, sonication duration of 10 min, ultrasonic amplitude of 50% and duty cycle of 71.4%). From Figure 1, it can be observed that the starch extraction yield decreased significantly with increasing particle size ( $p < 0.05$ ). The highest extraction yield of  $59.1 \pm 3.0\%$  was achieved at the smallest particle size of smaller than 250  $\mu\text{m}$ . Shorter diffusion path and larger surface area possessed by smaller particle size would facilitate the mass transfer of the starch, thereby achieving higher extraction yield. Furthermore, reduction in the particle size would lead to an increase in the number of starch cells directly exposed to the solvent, thus improving the extraction yield [42,43]. On the other hand, higher mass transfer limitation associated with larger particle size had hampered solvent penetration for starch release as the starch granules were being trapped between the fibrous material structure of sago [17]. The results showed a significant change ( $p < 0.05$ ) in the extraction yield with the increasing particle size from smaller than 250  $\mu\text{m}$  to larger than 1 mm. Particle size of more than 1 mm recorded the lowest extraction yield at  $5.4 \pm 0.1\%$ . A similar trend was observed by Shirsath et al. [43] in the curcumin extraction from *Curcuma amada* using ultrasound by varying four different particle sizes (0.09, 0.106, 0.21 and 0.85 mm). The highest (72%) and lowest (55%) extraction yields were achieved at the smallest (0.09 mm) and biggest (0.85 mm) particle sizes, respectively. In the present study, the weight distribution of SPW increased in the descending order of particle size. By grinding the SPW for 30 s and sieving them into different particle sizes, the weight distribution was as follows: 87.7% (smaller than 250  $\mu\text{m}$ ), 6.8% (250–500  $\mu\text{m}$ ), 4.6% (500  $\mu\text{m}$ –1 mm) and 0.8% (>1 mm). Considering the extraction yield and the weight distribution for particle size smaller than 250  $\mu\text{m}$  were the highest while the weight loss was not very significant which was only approximately 12%, particle size of smaller than 250  $\mu\text{m}$  was selected for the subsequent parameter optimization.

#### 3.2. Effect of Solid Loading

The effect of solid loading on extraction yield was investigated over the range of 5–15 wt.% as depicted in Figure 2. An increase in the solid loading from 5–10 wt.% was able to maintain the extraction yield at  $58.7 \pm 0.7\%$  and  $59.1 \pm 3.0\%$ , respectively with insignificant difference ( $p > 0.05$ ). Theoretically, particle collision frequency would increase with higher solid loading with the aid of ultrasound [44]. This enabled the sonication system to cope with larger throughput at higher solid loading. Consequently, the effect of solid loading on the extraction yield was nominal in the present study. This could also be ascribed to the incomplete interaction of the solvent with the solid when the solvent slowly became saturated with increasing solid loading [45]. The extraction yield decreased to  $46.6 \pm 2.1\%$  when the solid loading was increased to 15 wt.% ( $p < 0.05$ ). This can be explained by the saturation of the solvent beyond the optimum solid loading. The decreasing concentration gradient between the interior starch and the external solvent would lower the mass transfer rate from the solid matrix to the solvent and thus hindered the extraction yield. In addition, different solid loadings will also affect the concentration difference between the inner cells of sago starch and the solvent (water) which subsequently

resulting in different viscosities of starch slurry [43]. Increase in the solid loading would increase the viscosity of the starch slurry and caused the ultrasonic energy delivered to the suspension to be partially attenuated. This would lead to a lower effective ultrasonic energy to disrupt the SPW particles in releasing the starch granules and resulted in lower extraction yield [20,44,46]. This phenomenon was also observed by Patil et al. [47] in the ultrasound-assisted extraction of curcuminoids from *Curcuma longa*. The extraction yield reduced from 86.7–31.3% when the solid loading was increased from 5–20% (*w/v*). At a solid loading of 12.5 wt.%, the amount of starch extracted was 1.2 times higher than that of 10 wt.% solid loading despite its extraction yield was slightly lower ( $57.9 \pm 1.2\%$  vs.  $59.1 \pm 3.0\%$ ). However, more water washing during slurry filtration and longer filtration time were required at solid loading of 12.5 wt.%. Similar extraction yields were also obtained at solid loadings of 5 and 10 wt.%. From the economical point of view, a solid loading of 10 wt.% was chosen for the subsequent parameter study since the final amount of starch produced was doubled compared to the 5 wt.% solid loading.

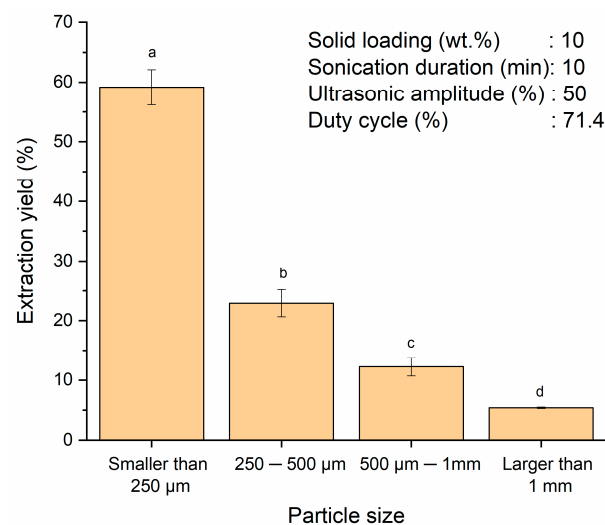


**Figure 1.** Effect of various particle sizes of SPW (smaller than 250 µm, 250–500 µm, 500 µm–1 mm and larger than 1 mm) on extraction yield of starch from SPW. Different letters indicate the values are significantly different ( $p < 0.05$ ).

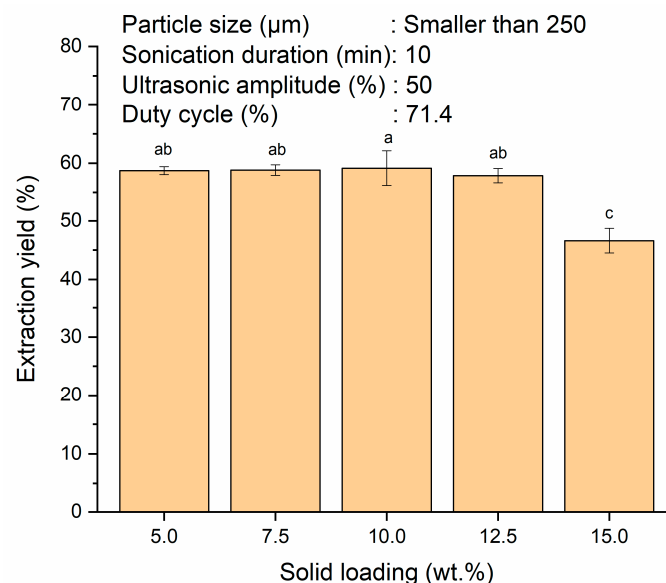


**Figure 2.** Effect of various solid loadings of SPW (5, 7.5, 10, 12.5 and 15 wt.%) on extraction yield of starch from SPW. Different letters indicate the values are significantly different ( $p < 0.05$ ).

### 3.3. Effect of Sonication Duration and Ultrasonic Amplitude

Changes in the extraction yield of starch from the SPW at different sonication durations and ultrasonic amplitudes were investigated on particle size of less than 250  $\mu\text{m}$ , solid loading of 10 wt.% and duty cycle of 71.4%. Increment of the sonication duration had enhanced the extraction yield at constant ultrasonic amplitude as shown in Figure 3. When the sonication duration was increased from 5–15 min, the extraction yields increased in tandem from  $55.7 \pm 1.8\%$  to  $61.2 \pm 0.3\%$  ( $p > 0.05$ ) and from  $60.9 \pm 1.1\%$  to  $66.1 \pm 0.5\%$  ( $p > 0.05$ ) for ultrasonic amplitudes of 50 and 60%, respectively. These results could be related to the dominating effects of both cavitation and thermal effects with increment in sonication duration. Both the cavitation effect and thermal effect are crucial in ultrasound-assisted extraction. The cavitation effect will aid in the imploding of cavitation bubbles while thermal effect will help in the swelling and loosening of the cell structures. Their synergistic effects contribute to the augmented mass transfer of intracellular substances into the solvent [45]. The cavitation effect is associated with more particles breaking down at longer sonication durations which exposes the fibrous material structure of sago to release more starch granules to exterior solvent [20,45,48]. In view of the inherent thermal effect, longer sonication duration would also result in a higher temperature (43–58  $^{\circ}\text{C}$  and 45–63  $^{\circ}\text{C}$  for 50 and 60% ultrasonic amplitudes with sonication duration from 5–15 min, respectively) and a disrupted cell matrix, thus facilitating the starch diffusion from the inner parts of sago to the exterior solvent and enhanced the extraction yield [43,49]. Nonetheless, the increase in the extraction yield with longer sonication duration was not statistically significant ( $p > 0.05$ ) at ultrasonic amplitudes of 50 and 60%.

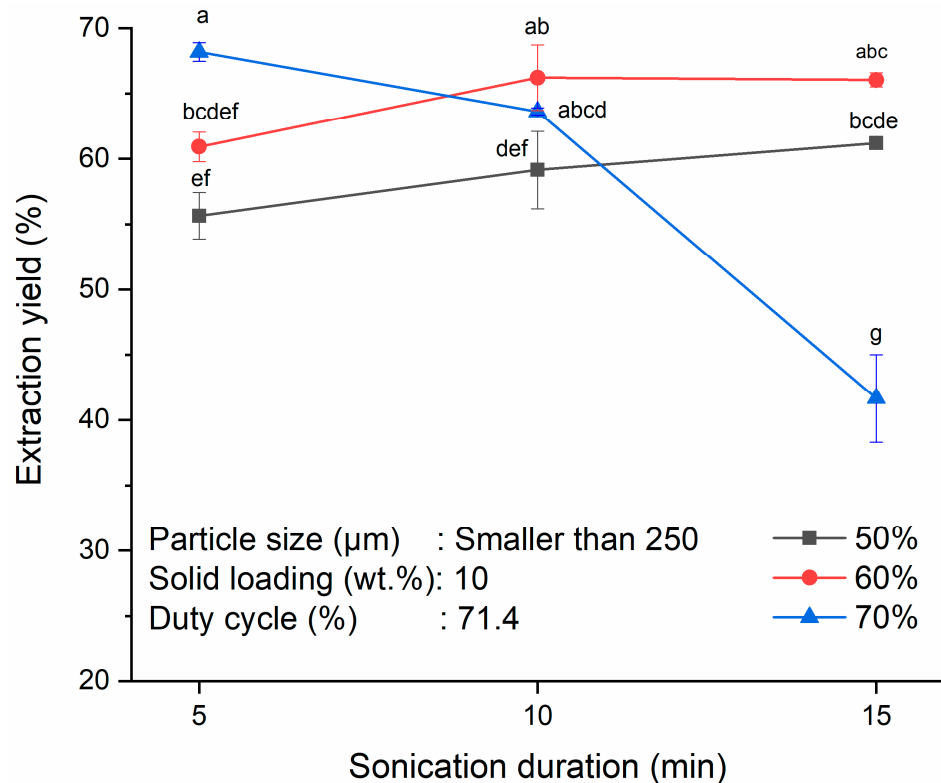


**Figure 3.** Effects of sonication durations (5, 10 and 15 min) and ultrasonic amplitudes (50, 60 and 70%) on extraction yield of starch from SPW. Different letters indicate the values are significantly different ( $p < 0.05$ ).

Conversely, prolonged sonication duration could undermine the extraction yield at high ultrasonic amplitude. This was reflected by the significant decrement in extraction yield at the ultrasonic amplitude of 70% when the sonication duration was increased from 5–15 min ( $p < 0.05$ ). The highest extraction yield of  $68.2 \pm 0.7\%$  was attained at an ultrasonic

amplitude of 70% with sonication duration of 5 min. When the sonication duration was further increased to 15 min, the extraction yield dropped significantly to  $41.7 \pm 3.3\%$  ( $p < 0.05$ ). The decrease in the extraction yield could be related to the negative thermal effect with prolong sonication duration. Heat generated from the frequent asymmetric collapse of cavitation bubbles could increase the temperature to  $66\text{ }^{\circ}\text{C}$  at an ultrasonic amplitude of 70% with sonication time of 15 min. This temperature had exceeded the starch gelatinization temperature of  $64\text{ }^{\circ}\text{C}$ , causing some starch in the suspension started to gelatinize. As a result, some starch granules were trapped in the high viscosity suspension after extraction and could not be separated easily [8,16,20,50]. A similar observation was made by Vasudeo [51] in the ultrasound-assisted extraction of starch from cassava in which the gelatinization of cassava starch took place above  $50\text{ }^{\circ}\text{C}$  which negatively affected the extraction yield.

On the other hand, extraction yield increased with an increase in the ultrasonic amplitude at constant ultrasonic duration. This was because more energy could be transmitted for the cavitation event to occur and thus, cavitation bubbles generated at higher ultrasonic amplitude could collapse at higher intensity, thereby enabling more cracks and fissures to be formed on the starch surface. Impingement by high-speed jets also caused surface erosion and particle fragmentation simultaneously, leading to more channels and spaces for solvent diffusion. When solvent diffused into the particles easily, it facilitated the starch to be released into the solvent [42,43,52]. Nonetheless, extraction yield obtained at an ultrasonic amplitude of 70% after subjected to 15 min of sonication was lower than that at ultrasonic amplitudes of 50% ( $p < 0.05$ ) and 60% ( $p < 0.05$ ) which can be explained by the aforementioned cavitation and thermal effects. Sit et al. [8] also reported the negative effect of increasing ultrasonic amplitude on taro starch extraction yield due to the degradation and solubilization of the starch. Based on the results obtained in the present study, combination of sonication duration of 5 min and ultrasonic amplitude of 70% gave the highest extraction yield of  $68.2 \pm 0.7\%$  without the occurrence of starch degradation or gelatinization.

#### 3.4. Effect of Duty Cycle

Duty cycle is referred as the percentage of ultrasound effective working time to the total ultrasound working time and idling time [53]. It determines the intensity of cavitation effects and prevents excessive burden on the ultrasonicator [54]. Figure 4 shows that as the duty cycle was increased from 50–83%, the extraction yield increased from  $65.1 \pm 0.4\%$  to  $71.4 \pm 0.4\%$  ( $p < 0.05$ ). Pulse inflection of the ultrasound suppressed the formation of degassing bubbles and aided in the clearance of the cavitation area and intensified the sonochemical reactions [55]. Higher duty cycle promoted more intensive cavitation activities and elevated the extraction yield [56]. However, there was no significant ( $p > 0.05$ ) difference in the extraction yield between duty cycles of 83–100%. It had been observed that similar extraction yield of around 71% was achieved for duty cycles of 83 and 100% in pulse and continuous mode, respectively. This might be due to the volumetric oscillation in continuous mode which had restricted the cavitation formation. The transmission of ultrasound might be curtailed by the cloud of degassing bubbles through absorption and scattering of the sound waves. The bubbles would then undergo intensive compression and expansion and restrict the sonochemical reaction [55,57]. The same trend was also reported by Dey and Rathod [45] as well as Pan et al. [58] where similar yields were obtained at both pulse and continuous modes in the ultrasound-assisted extraction of  $\beta$ -carotene from *Spirulina platensis* and antioxidants from pomegranate peel, respectively. Continuous mode usually requires shorter sonication time than pulse mode. However, it could accelerate tip erosion and would not be as energy efficient as the pulse mode [58]. Therefore, duty cycle of 83% was considered as the optimum in the present study.

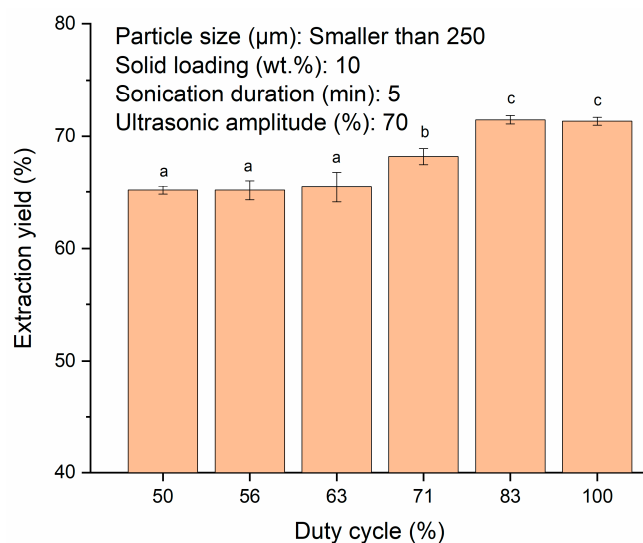


**Figure 4.** Effect of duty cycles (50, 56, 63, 71, 83 and 100%) on extraction yield of starch from SPW. Different letters indicate the values are significantly different ( $p < 0.05$ ).

### 3.5. Comparison between Conventional and Ultrasound-Assisted Extraction

To clearly demonstrate the benefits of the ultrasound technique over the conventional method, their extraction yields were compared under the same optimized conditions of particle size smaller than 250  $\mu\text{m}$ , solid loading of 10 wt.% and temperature of 46  $^{\circ}\text{C}$  (temperature auto-generated at ultrasonic amplitude of 70% with duty cycle of 83%). The extraction efficiency at 89.7% was determined based on the total starch present in the SPW. From Table 1, ultrasound techniques could achieve higher extraction yield and efficiency than the conventional approach i.e., ( $71.4 \pm 0.4\%$  vs.  $60.9 \pm 1.2\%$ ) and ( $89.7 \pm 0.5\%$  vs.  $77.8 \pm 1.5\%$ ), respectively. Moreover, the reaction time could be shortened by as much as 83.3% (5 min vs. 30 min) with the assistance of ultrasound in starch extraction. This could be attributed to the larger interfacial area offered by the shock waves generated from the rapid formation of cavitation bubbles in facilitating the starch diffusion [52]. On the other hand, desirable mixing to achieve higher uniformity was difficult for magnetic stirring as the stirring bar was situated at the bottom of the flask which might have resulted in lower extraction yield [59]. Similar findings in the starch extraction from *Radix Puerariae* was reported by Li et al. [60] with an extraction yield of 45.7% achieved by ultrasound technique in 30 min and an extraction yield of 39.6% by conventional approach using magnetic stirrer in 2 h. Comparatively, the ultrasound technique is more energy and time efficient.

**Table 1.** Comparison between conventional and ultrasound-assisted extraction.

| Parameters                | Ultrasound       | Conventional (Magnetic Stirring) |
|---------------------------|------------------|----------------------------------|
| Extraction yield (%)      | $71.4 \pm 0.4^a$ | $60.9 \pm 1.2^b$                 |
| Extraction efficiency (%) | $89.7 \pm 0.5^a$ | $77.8 \pm 1.5^b$                 |
| Reaction time (min)       | 5 <sup>a</sup>   | 30 <sup>b</sup>                  |
| Amylose content (%)       | $32.1 \pm 0.0^a$ | $37.4 \pm 0.0^b$                 |
| Starch content (%)        | $87.8 \pm 0.1^a$ | $89.3 \pm 0.1^b$                 |
| Protein content (%)       | $0.1 \pm 0.0^a$  | $0.47 \pm 0.1^b$                 |
| Ash content (%)           | $0.7 \pm 0.1^a$  | $0.9 \pm 0.0^b$                  |
| Fat content (%)           | n.d.             | n.d.                             |

Means  $\pm$  standard deviation in the same row with different superscripts are significantly different ( $p < 0.05$ ). n.d. denotes for not detected.

Contrary to the lower extraction yield and efficiency, the chemical composition of the extracted starch from the conventional approach recorded higher amylose content than the ultrasound technique ( $37.4 \pm 0.0\%$  vs.  $32.1 \pm 0.0\%$ ). The longer extraction time (30 min) required in the conventional approach may cause more starch granules to swell

and thus more amylose would be leached out [61]. In addition, a small discrepancy in the starch content was observed between the conventional and the ultrasound techniques, i.e.,  $89.3 \pm 0.1\%$  vs.  $87.8 \pm 0.1\%$ . In the starch extraction from *Radix Puerariae* conducted by Li et al. [60], the starch content reported from the ultrasound approach (99.75%) and that from the conventional approach of 99.52% was almost identical too. Lower starch content of the present study could be due to higher power intensity of the employed ultrasound, i.e.,  $690.34 \text{ kW/m}^2$  as compared to lower power intensity of  $20.38 \text{ kW/m}^2$  used in Li et al. [60]. The high-power intensity might have broken down the SPW into smaller particles and enabled impurities other than starch granules to be purged during washing.

Table 1 shows that ultrasound-extracted starch had lower protein ( $0.1 \pm 0.0\%$  vs.  $0.47 \pm 0.1\%$ ) ( $p < 0.05$ ) and ash contents ( $0.7 \pm 0.1\%$  vs.  $0.9 \pm 0.0\%$ ) ( $p < 0.05$ ) than the control starch, while fat content was not detected in either starches. Lower protein content in the ultrasound-extracted starch could be due to the bond disruptions between protein and starch by ultrasound which eased the starch-protein separation [62]. Park et al. [63] and Zhang et al. [62] also obtained lower protein content of sorghum and corn starches in ultrasound-assisted extraction. Lower ash content is favourable for bioplastic film formation as higher ash content indicates higher mineral content which would hamper the formation of bioplastic film due to the possible interaction between the minerals and amylose, amylopectin and plasticizer [26]. In the present study, ultrasound-extracted starch exhibited lower protein and ash contents which had confirmed its higher starch purity than the control starch extracted by the conventional method.

### 3.6. Comparison of Optimum Reaction Conditions with Existing Literatures

The comparison of the optimum reaction conditions between this study and the reported literatures is presented in Table 2. The extraction yield of starch extracted from waste of sago pith in the present work was comparable with that of Pinyo et al. [20] using sago pith. It is worth to mention that even by utilizing the waste, it was still slightly more energy efficient as the ultrasonic amplitude and sonication duration required in the present study were lower (70 vs. 80%) and shorter (5 vs. 7 min). Moreover, with the extraction yield of more than 71.4%, SPW outperformed other feedstocks such as yam tuber, jicama roots and taro with lower extraction yields ranging from 19.0–32.1%. The low extraction yields reported could be due to the high solid loading used in jicama [16] starch suspension of ~25 wt.%, taro [8] and yam [14] starch suspensions of 50 wt.% which were 2.5 and 5 times higher than that in the present study (10 wt.%), respectively. As previously mentioned in Section 3.2, high solid loading could negatively affect mass transfer and cause a reduction in extraction yield. Apart from the high solid loading, lower duty cycle could be another contributing factor of low extraction yield for taro starch. Although the duty cycle in the present study was 1.7 times greater (83.3 vs. 50%), the extraction yield was 3.8 times higher (71.4 vs. 19.0%) with 2 times shorter sonication duration (5 vs. 10 min). This suggested that a suitable duty cycle is imperative as a high duty cycle would give rise to excessive heating and unnecessary electrical consumption, thus incurring more operational time and cost. Despite the influences of particle size and duty cycle towards extraction yield, they have not been investigated thoroughly in starch extraction thus far. Therefore, a more comprehensive investigation was conducted in the present study to elucidate their effects.

**Table 2.** Comparison of optimum reaction conditions for ultrasound-assisted starch extraction in various studies.

| Feedstock    | Particle Size ( $\mu\text{m}$ ) | Solid Loading (wt.%) | Sonication Duration (min) | Ultrasonic Amplitude (%) | Duty Cycle (%)  | Extraction Yield (%) | Purity (%) | Ref.          |
|--------------|---------------------------------|----------------------|---------------------------|--------------------------|-----------------|----------------------|------------|---------------|
| SPW          | Smaller than 250                | 10                   | 5                         | 70                       | 83.3            | 71.4                 | 87.8       | Present study |
| Sago pith    | -                               | 10                   | 7                         | 80                       | -               | 71.5                 | 95.0       | [20]          |
| Yam tuber    | -                               | 50                   | 15 <sup>a</sup>           | 70 <sup>a</sup>          | -               | 32.1                 | -          | [14]          |
| Jicama roots | -                               | 25                   | 10 <sup>a</sup>           | -                        | -               | 24.0                 | 80.9       | [16]          |
| Taro         | -                               | 50                   | 10 <sup>a</sup>           | 50 <sup>a</sup>          | 50 <sup>a</sup> | 19.0 <sup>*</sup>    | -          | [8]           |

\* amount of pure starch. <sup>a</sup> Parameters investigated.

### 3.7. Characterization of Extracted Starches

#### 3.7.1. Surface Morphology

SEM images of the control starch extracted conventionally and the ultrasound-extracted starches are displayed in Figure 5a,b, respectively. As can be observed from the figure, particle agglomeration was found in both starches. The control starch had larger agglomerates which may be due to the presence of more residual protein content rendering the starch to be more viscous and allowing particles to attach with each other [64]. The residual protein content was evident from the cells that housed the starch granules as indicated by the blue circle shapes in Figure 5 [32]. From Table 1, the control starch was found to have higher protein content than the ultrasound-extracted starch ( $0.47 \pm 0.25$  vs.  $0.1 \pm 0.0\%$ ) which further corroborated the observation found from the SEM images. The granules of the control starch were oval with a temple bell-like shape and exhibited relatively smooth and intact surfaces, whereas in the ultrasound-extracted starch, the granules were of heterogeneous structures including oval, round, trigonal and oval with temple bell-like shapes. The average diameter of ultrasound-extracted starch was roughly 7% smaller than that of the control starch ( $34.1 \pm 7.1 \mu\text{m}$  vs.  $36.7 \pm 7.4 \mu\text{m}$ ). The particle size reduction after subjected to the cavitation effect of ultrasound was consistent with the studies reported by other researchers [65,66]. Incorporating smaller particle size in the preparation of bioplastic film would improve their distribution in the solution and thus producing a film with a more uniform matrix [67].

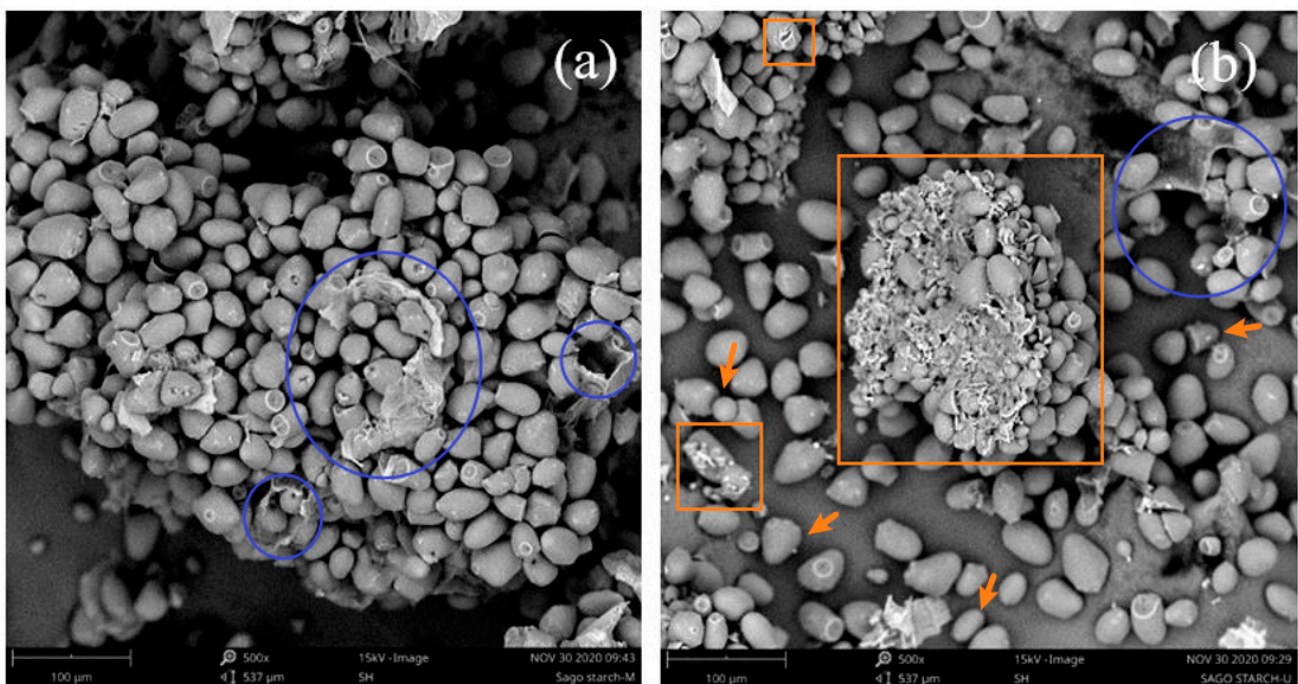


**Figure 5.** SEM micrographs of (a) control sago starch and (b) ultrasound-extracted sago starch at magnification of  $500\times$ . The cells that housed the starch granules were indicated by blue circle shapes; cracks and fissures were indicated by orange square shapes; structures of starch granules were indicated by orange arrows.

After ultrasound-assisted extraction, the starch granules exhibited uneven, disrupted and irregular surfaces with cracks and fissures as indicated by the orange square shapes in Figure 5b. It could be deduced that high-speed jets and violent shock waves produced from the collapsing bubbles had caused surface erosion and particle fragmentation while the starch surface was struck by the shock waves creating microfractures and crevices. This enabled more channels for water diffusion into the starch granules to facilitate the release of more starch contents during the extraction process [68]. This also explained the higher extraction yield obtained from ultrasound-assisted extraction than conventional



extraction. Furthermore, ultrasound-extracted starch demonstrated better water absorption capacity than the control starch as granules breakdown by ultrasound can promote the water penetration into the starch granule [69]. Water absorption capacity is closely related to the swelling power and solubility which would further be discussed in Section 3.7.3.

### 3.7.2. Particle Size Distribution

The particle size distribution and the cumulative particle size distribution curves of control and ultrasound-extracted starches that expressed in volume basis are presented in Figure 6. From the cumulative particle size distribution curves, it is noticed that both curves had reached the plateau for particle size larger than 477  $\mu\text{m}$ . The particle size could be divided into two populations based on the number of peaks present in the particle size distribution curves. One of the populations was ranged from 10.5–88.9  $\mu\text{m}$  and the other ranged from 103.6–477  $\mu\text{m}$ . The control starch had equal size distribution of 47.3% for both the populations. Meanwhile, ultrasound-extracted starch had 51.9% size distribution of 10.5–88.9  $\mu\text{m}$  and the remaining comprised of particle size ranged from 103.6–477  $\mu\text{m}$ . It is important to take note that the particle size distribution data represented the size of isolated particle, minor aggregate and/or agglomerate forms [70] which supported the scenario of particle agglomeration as observed in SEM images.

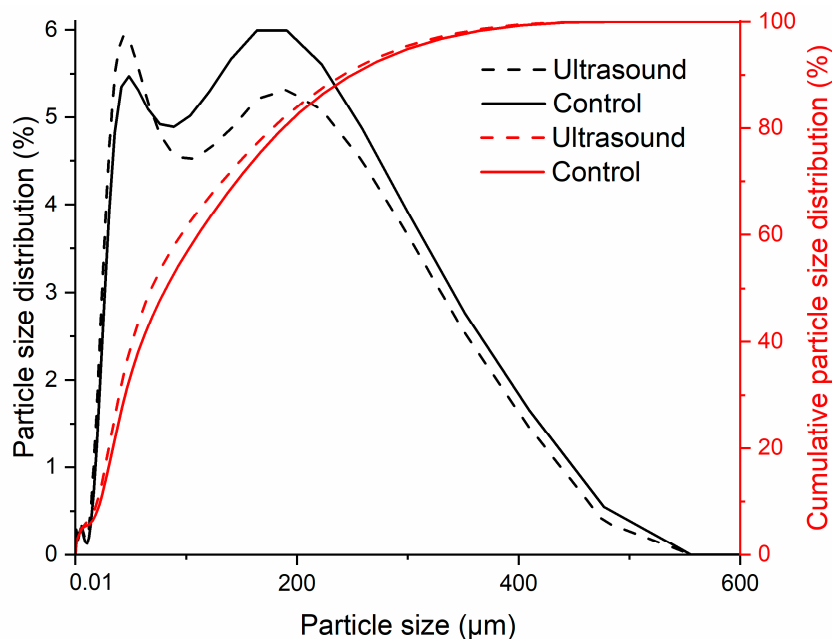


**Figure 6.** Particle size distribution and particle size distribution cumulative curves of control and ultrasound-extracted sago starches.

### 3.7.3. XRD

The XRD patterns of control and ultrasound-extracted starches are displayed in Figure 7. It was observed that sago starch depicted characteristic peaks of C-type starch at  $2\theta$  (5.90, 15.14, 17.05, 18.10 and  $23^\circ$ ). The results were consistent with the results reported by Polnaya et al. [71] and Uthumporn et al. [72] on sago starch in which C-type patterns were also observed. It is evident that the diffraction pattern of ultrasound-extracted starch was similar to that of the control starch indicating that the crystalline structure of the starch remained unaltered after ultrasonication. The noticeable difference between the ultrasound-extracted and control starches was a slight reduction in the intensities of all the diffraction peaks after conventional extraction. The control starch had a slightly lower crystallinity of 2.1% as compared to the ultrasound-extracted starch (19.9 vs. 22.0%). The results obtained in the present study were different from those reported by Li et al. [60] and Zhu et al. [68]. The reason of control starch having lower crystallinity than ultrasound-extracted starch

could be attributed to longer conventional extraction time of 30 min as compared with 5 min ultrasound extraction. Longer extraction duration promoted the swelling of the starch granule and more amylose could be leached out [61]. Since lower crystallinity would indicate higher amylose content, the amylose contents of ultrasound-extracted and control starches were then determined from Table 1. The latter ( $37.4 \pm 0.0\%$ ) was found to have higher amylose content than the former ( $32.1 \pm 0.0\%$ ) which was consistent with the crystallinity results.

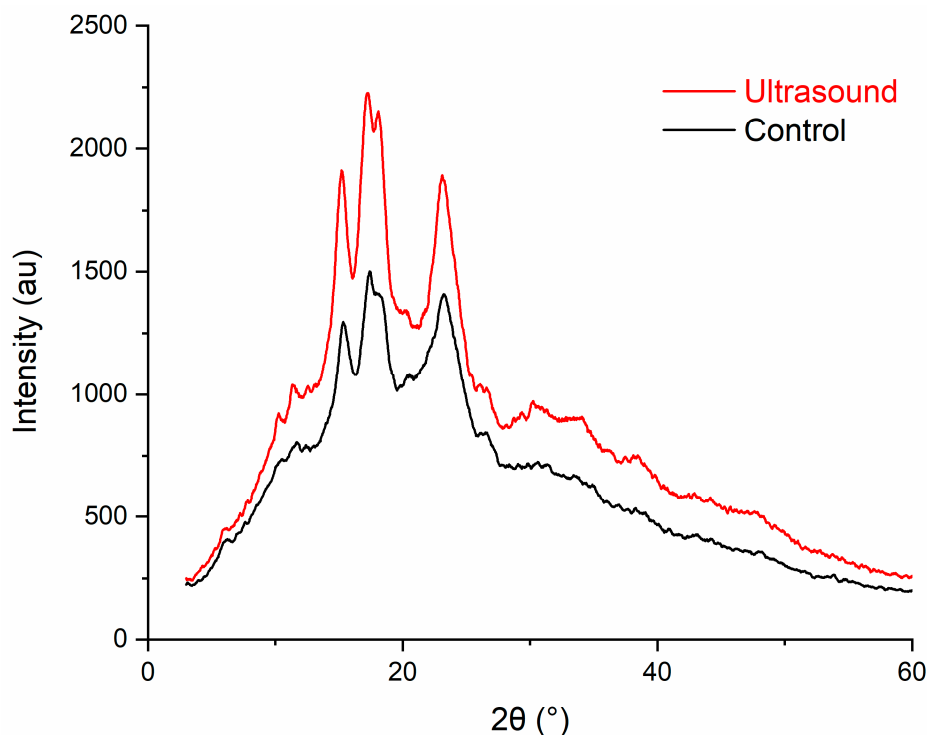


**Figure 7.** XRD patterns of control and ultrasound-extracted sago starches.

#### 3.7.4. Swelling Power and Solubility

Amylose content is also associated with swelling power and solubility of starch in which lower amylose content would have higher swelling power and solubility [15]. The ultrasound-extracted starch exhibited higher swelling power ( $14.5 \pm 0.0$  vs.  $11.8 \pm 0.0$  g gel/g starch) and solubility ( $29.3 \pm 0.0\%$  vs.  $21.7 \pm 0.1\%$ ) than the control starch. This was caused by the cavitation effects of ultrasound that disrupted the covalent bonds of crystalline structure and chains of sago starch as previously discussed. Therefore, more water molecules could bind to the free hydroxyl groups of amylose and amylopectin by hydrogen bonds to increase the swelling power and solubility of starch [69]. High swelling power and solubility of starch would be beneficial in bioplastic film fabrication as they could facilitate starch gelatinization and gel formation and thus obtain a more stable film-forming solution.

### 3.8. Characterization of Fabricated Bioplastic Films

The colour, mechanical and barrier properties of the bioplastic films prepared using control and ultrasound-extracted starches were evaluated in Table 3.

#### 3.8.1. Colour Properties

The photographs of bioplastic films fabricated using control and ultrasound-extracted starches are shown in Figure 8a,b, respectively. Both films were slightly brownish without any visible cracks. The surface exposed to air was rough whereas the surface in contact with the container was smooth and glossy. From Table 3, the film fabricated using ultrasound-extracted starch was found to have significant colour difference ( $\Delta E$ ) with lower  $L$  and  $b$  values than that using control starch ( $p < 0.05$ ). These results indicated

that the film fabricated using ultrasound-extracted starch was darker and less yellowish. This might be caused by the presence of impurities along with the extracted starch after ultrasonication [36].

**Table 3.** Properties of film fabricated using control and ultrasound-extracted starches.

|                       | Film Fabricated Using  | Control Starch          | Ultrasound-Extracted Starch |
|-----------------------|--|-------------------------|-----------------------------|
| Colour properties     | L  | 84.4 ± 0.4 <sup>a</sup> | 80.9 ± 0.0 <sup>b</sup>     |
|                       | a  | 1.14 ± 0.0 <sup>a</sup> | 1.13 ± 0.0 <sup>a</sup>     |
|                       | b  | 12.1 ± 0.1 <sup>a</sup> | 11.9 ± 0.0 <sup>b</sup>     |
|                       | ΔE   | 13.7 ± 0.0 <sup>a</sup> | 15.6 ± 0.1 <sup>b</sup>     |
| Mechanical properties | Tensile strength (MPa)   | 0.9 ± 0.3 <sup>a</sup>  | 0.9 ± 0.1 <sup>a</sup>      |
|                       | Young's Modulus (MPa)  | 22.6 ± 1.1 <sup>a</sup> | 22.0 ± 0.8 <sup>a</sup>     |
|                       | Elongation at break (%)  | 13.8 ± 1.8 <sup>a</sup> | 13.6 ± 2.0 <sup>a</sup>     |
| Barrier property      | WVP × 10 <sup>-8</sup> (g m <sup>-1</sup> s <sup>-1</sup> Pa <sup>-1</sup> ) | 1.13 ± 0.4 <sup>a</sup> | 1.11 ± 0.1 <sup>a</sup>     |

Means ± standard deviation in the same row with different superscripts are significantly different ( $p < 0.05$ ).

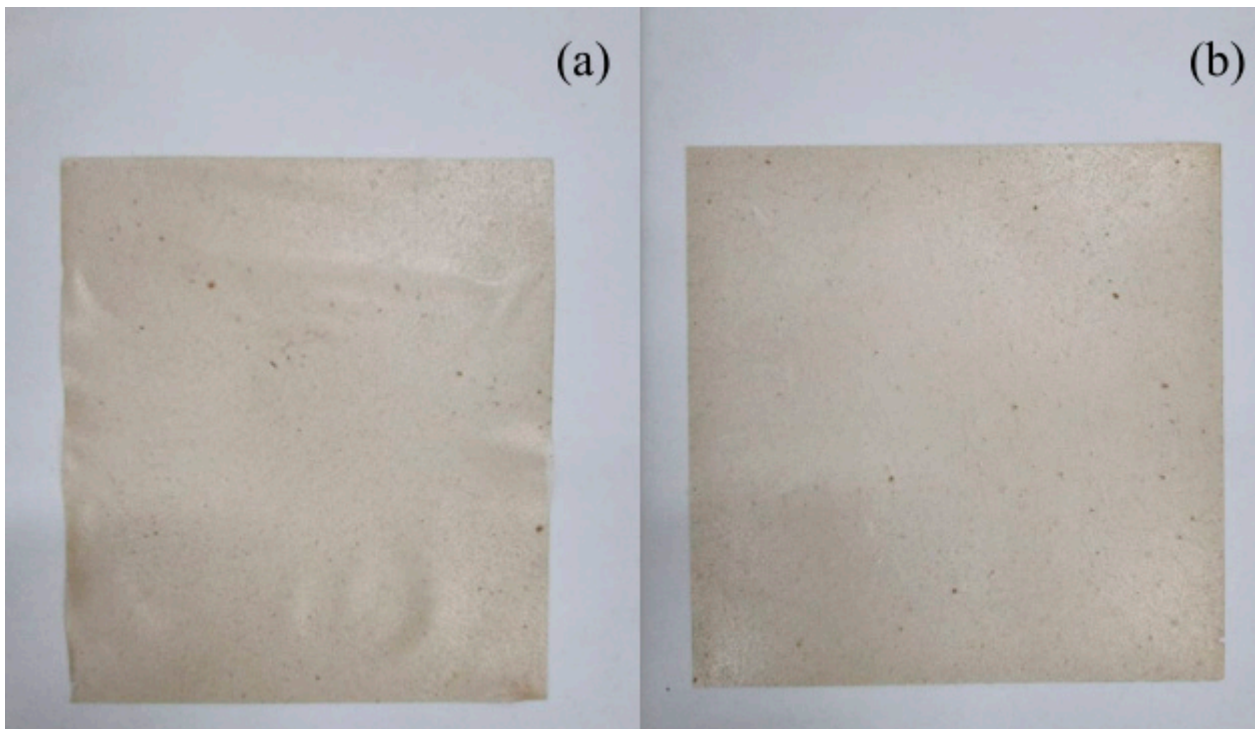


**Figure 8.** Photographs of film fabricated using (a) control starch and (b) ultrasound-extracted starch.

### 3.8.2. Mechanical Properties

Both films prepared using control and ultrasound-extracted starches had comparable mechanical properties ( $p > 0.05$ ) as shown in Table 3. For film with ultrasound-extracted starch, tensile strength of  $0.9 \pm 0.1$  MPa, Young's modulus of  $22.0 \pm 0.8$  MPa and elongation at break of  $13.6 \pm 2.0\%$  were attained at glycerol loading of 40 wt.%. In the preparation of corn starch bioplastic film by Liu et al. [73], tensile strength of  $1.3 \pm 0.0$  MPa, Young's modulus of  $1.8 \pm 0.2$  MPa and elongation at break of  $14.0 \pm 0.4\%$  at glycerol loading of 10 wt.% were recorded. Lower tensile strength in the present study could be due to thinner film (0.11 vs. 0.19 mm) as compared to their study. In brief, the tensile test results revealed that sago starch with starch content of  $87.8 \pm 0.1\%$  was sufficient and feasible to produce a bioplastic film with acceptable mechanical strength.

### 3.8.3. Water Vapour Permeability (WVP)

Both the bioplastic films fabricated using control and ultrasound-extracted starches had comparable WVP of  $1.13 \pm 0.4$  and  $1.11 \pm 0.1 \times 10^{-8} \text{ g m}^{-1} \text{ s}^{-1} \text{ Pa}^{-1}$  ( $p > 0.05$ ), respectively. Slightly lower WVP of film fabricated using ultrasound-extracted starch could be attributed to smaller particle size of starch in producing a film with a uniform matrix. This would then reduce the interstitial spaces between the polymer structure and the diffusion rate of water molecules [74]. In the fabrication of corn starch bioplastic film by Ren et al. [38], the permeability of film was  $7.89 \times 10^{-10} \text{ g m}^{-1} \text{ s}^{-1} \text{ Pa}^{-1}$  which was lower than that of both films in the present study. This could be due to higher glycerol loading used in the present study (40 vs. 20 wt.%) as compared to their study. Addition of glycerol which is more hydrophilic would increase the number of free hydroxyl groups and enhance the interaction with water molecules, making the film more favourable to adsorption and desorption of water molecules, thus increasing the WVP of films [75].

## 4. Conclusions

Ultrasound is a feasible method to extract starch from sago pith waste (SPW). It is not only capable of eliminating mass transfer limitations but also eradicating the needs of separate heating and agitation due to the localized temperature increment and the formation of micro jets. The extraction technique outshines conventional extraction with 17.2% higher extraction yield and much shorter sonication duration. Combination of ultrasound extraction and utilization of low-cost SPW rendered the process to be economically feasible and potentially sustainable for production of bioplastic film.

From the tensile and WVP tests of the bioplastic film fabricated using starch extracted from SPW, tensile strength of 0.9 MPa and WVP of  $1.11 \times 10^{-8} \text{ g m}^{-1} \text{ s}^{-1} \text{ Pa}^{-1}$  were attained which had further confirmed that SPW could serve as an alternative starch source in the bioplastic film industries. Starch extracted from SPW would generate added-value product and close its life cycle and encourage circular economy.

Further improvement in the mechanical properties and WVP of bioplastic film could be achieved by incorporating different types of plasticizer or additives. Future studies could also be directed towards the investigation of factors such as ultrasonic tip placement, size and shape of the sono-reactor that would affect the efficiency of ultrasound, for instance, intensity and energy density. In addition, kinetic modelling of the ultrasound-assisted extraction process could be conducted to determine the proportion of acoustic energy transferred to the medium and thus designing a more efficient process. Furthermore, the possible starch gelatinization effect for large-scale ultrasonication extraction system also requires more studies in the future. This information would be beneficial for scaling the process to the industrial level.

**Author Contributions:** Conceptualization, S.X.T., G.C.N. and S.L.; methodology, S.X.T.; software, S.X.T.; validation, S.X.T.; formal analysis, S.X.T.; investigation, S.X.T.; data curation, S.X.T.; writing—original draft preparation, S.X.T.; writing—review and editing, A.A., G.C.N., H.C.O., S.L. and Y.L.P.; visualization, H.C.O. and Y.L.P.; supervision, A.A., G.C.N. and S.L.; project administration, S.L. and G.C.N.; funding acquisition, S.L. and G.C.N. All authors have read and agreed to the published version of the manuscript.

**Funding:** The research was funded by Fundamental Research Grant Scheme (FRGS), Ministry of Education, Malaysia [FRGS/1/2018/TK10/UTAR/02/1], University of Malaya, Kuala Lumpur under RU Grant (GPF059A-2020) and Universiti Tunku Abdul Rahman Research Grant (UTARRF/6200-W83).

**Conflicts of Interest:** The authors declare no conflict of interest.

## References

- Kim, H.Y.; Lee, J.H.; Kim, J.Y.; Lim, W.J.; Lim, S.T. Characterization of nanoparticles prepared by acid hydrolysis of various starches. *Starch-Stärke* **2012**, *64*, 367–373. [CrossRef]
- Herrera, M.P.; Vasanthan, T. Rheological characterization of gum and starch nanoparticle blends. *Food Chem.* **2018**, *243*, 43–49. [CrossRef]
- Kim, J.-Y.; Lim, S.-T. Preparation of nano-sized starch particles by complex formation with n-butanol. *Carbohydr. Polym.* **2009**, *76*, 110–116. [CrossRef]
- Andrade, I.H.; Otoni, C.G.; Amorim, T.S.; Camilloto, G.P.; Cruz, R.S. Ultrasound-assisted extraction of starch nanoparticles from breadfruit (*Artocarpus altilis* (Parkinson) Fosberg). *Colloids Surf. A Physicochem. Eng. Asp.* **2020**, *586*, 124277. [CrossRef]
- Song, D.; Thio, Y.S.; Deng, Y. Starch nanoparticle formation via reactive extrusion and related mechanism study. *Carbohydr. Polym.* **2011**, *85*, 208–214. [CrossRef]
- Minakawa, A.F.; Faria-Tischer, P.C.; Mali, S. Simple ultrasound method to obtain starch micro-and nanoparticles from cassava, corn and yam starches. *Food Chem.* **2019**, *283*, 11–18. [CrossRef]
- Kringel, D.H.; El Halal, S.L.M.; Zavareze, E.d.R.; Dias, A.R.G. Methods for the Extraction of Roots, Tubers, Pulses, Pseudocereals, and Other Unconventional Starches Sources: A Review. *Starch-Stärke* **2020**, *72*, 1900234. [CrossRef]
- Sit, N.; Misra, S.; Deka, S.C. Yield and functional properties of taro starch as affected by ultrasound. *Food Bioproc. Tech.* **2014**, *7*, 1950–1958. [CrossRef]
- Patel, C.M.; Chakraborty, M.; Murthy, Z. Fast and scalable preparation of starch nanoparticles by stirred media milling. *Adv. Powder Technol.* **2016**, *27*, 1287–1294. [CrossRef]
- Liu, D.; Wu, Q.; Chen, H.; Chang, P.R. Transitional properties of starch colloid with particle size reduction from micro-to nanometer. *J. Colloid Interface Sci.* **2009**, *339*, 117–124. [CrossRef]
- Polachini, T.C.; Hernando, I.; Mulet, A.; Telis-Romero, J.; Cárcel, J.A. Ultrasound-assisted acid hydrolysis of cassava (*Manihot esculenta*) bagasse: Kinetics, acoustic field and structural effects. *Ultrason. Sonochem.* **2021**, *70*, 105318. [CrossRef]
- Hashemi, S.M.B.; Khaneghah, A.M.; Koubaa, M.; Barba, F.J.; Abedi, E.; Niakousari, M.; Tavakoli, J. Extraction of essential oil from *Aloysia citriodora* Palau leaves using continuous and pulsed ultrasound: Kinetics, antioxidant activity and antimicrobial properties. *Process Biochem.* **2018**, *65*, 197–204. [CrossRef]
- Liu, C.-W.; Wang, Y.-C.; Lu, H.-C.; Chiang, W.-D. Optimization of ultrasound-assisted extraction conditions for total phenols with anti-hyperglycemic activity from *Psidium guajava* leaves. *Process Biochem.* **2014**, *49*, 1601–1605. [CrossRef]
- Bernardo, C.O.; Ascheri, J.L.R.; Chávez, D.W.H.; Carvalho, C.W.P. Ultrasound assisted extraction of yam (*Dioscorea bulbifera*) starch: Effect on morphology and functional properties. *Starch-Stärke* **2018**, *70*, 1700185. [CrossRef]
- Karaman, M.; Tuncel, N.B.; Yilmaz Tuncel, N. The effect of ultrasound-assisted extraction on yield and properties of some pulse starches. *Starch-Stärke* **2017**, *69*, 1600307. [CrossRef]
- González-Lemus, L.B.; Calderón-Domínguez, G.; Salgado-Cruz, M.d.I.P.; Díaz-Ramírez, M.; Ramírez-Miranda, M.; Chanona-Pérez, J.J.; Güemes-Vera, N.; Farrera-Rebollo, R.R. Ultrasound-assisted extraction of starch from frozen jicama (*P. erosus*) roots: Effect on yield, structural characteristics and thermal properties. *CyTA-J. Food* **2018**, *16*, 738–746. [CrossRef]
- Lai, J.C.; Rahman, W.A.W.A.; Toh, W.Y. Characterisation of sago pith waste and its composites. *Ind. Crops Prod.* **2013**, *45*, 319–326. [CrossRef]
- Bukhari, N.A.; Loh, S.K.; Bakar, N.A.; Ismail, M. Hydrolysis of residual starch from sago pith residue and its fermentation to bioethanol. *Sains Malays.* **2017**, *46*, 1269–1278. [CrossRef]
- Husin, H.; Ibrahim, M.F.; Kamal Bahrin, E.; Abd-Aziz, S. Simultaneous saccharification and fermentation of sago hampas into biobutanol by *Clostridium acetobutylicum* ATCC 824. *Energy Sci. Eng.* **2019**, *7*, 66–75. [CrossRef]
- Pinyo, J.; Luangpituksa, P.; Suphantharika, M.; Hansawasdi, C.; Wongsagonsup, R. Improvement of sago starch extraction process using various pretreatment techniques and their pretreatment combination. *Starch-Stärke* **2017**, *69*, 1700005. [CrossRef]
- Amin, N.; Sabli, N.; Izhar, S.; Yoshida, H. Sago Wastes and Its Applications. *Pertanika J. Sci. Technol.* **2019**, *27*, 1841–1862.
- Alonso-González, M.; Felix, M.; Romero, A. Development of malt sprout-based bioplastics via injection-moulding. *Ind. Crops Prod.* **2021**, *162*, 113267. [CrossRef]
- Jansens, K.J.; Hong, N.V.; Telen, L.; Brijs, K.; Lagrain, B.; Van Vuure, A.W.; Van Acker, K.; Verpoest, I.; Van Puyvelde, P.; Goderis, B. Effect of molding conditions and moisture content on the mechanical properties of compression molded glassy, wheat gluten bioplastics. *Ind. Crops Prod.* **2013**, *44*, 480–487. [CrossRef]
- Méité, N.; Konan, L.K.; Tognonvi, M.T.; Doubi, B.I.H.G.; Gomina, M.; Oyetola, S. Properties of hydric and biodegradability of cassava starch-based bioplastics reinforced with thermally modified kaolin. *Carbohydr. Polym.* **2020**, *254*, 117322. [CrossRef] [PubMed]
- Amin, M.R.; Chowdhury, M.A.; Kowser, M.A. Characterization and performance analysis of composite bioplastics synthesized using titanium dioxide nanoparticles with corn starch. *Heliyon* **2019**, *5*, e02009. [CrossRef]
- Santana, R.F.; Bonomo, R.C.F.; Gandolfi, O.R.R.; Rodrigues, L.B.; Santos, L.S.; dos Santos Pires, A.C.; de Oliveira, C.P.; Fontan, R.d.C.I.; Veloso, C.M. Characterization of starch-based bioplastics from jackfruit seed plasticized with glycerol. *J. Food Sci. Technol.* **2018**, *55*, 278–286. [CrossRef] [PubMed]
- Agustin, M.B.; Ahmmad, B.; Alonzo, S.M.M.; Patriana, F.M. Bioplastic based on starch and cellulose nanocrystals from rice straw. *J. Reinf. Plast. Compos.* **2014**, *33*, 2205–2213. [CrossRef]

28. Rahman, M.M.; Lamsal, B.P. Ultrasound-assisted extraction and modification of plant-based proteins: Impact on physicochemical, functional, and nutritional properties. *Compr. Rev. Food Sci. Food Saf.* **2021**, *20*, 1457–1480. [CrossRef] [PubMed]
29. Babu, S.A.; Parimalavalli, R. Effect of starch isolation method on properties of sweet potato starch. *Ann. Univ. Dunarea de Jos Galati Fascicle VI-Food Technol.* **2014**, *38*, 48–63.
30. Yoo, J.; Alavi, S.; Vadlani, P.; Amanor-Boadu, V. Thermo-mechanical extrusion pretreatment for conversion of soybean hulls to fermentable sugars. *Bioresour. Technol.* **2011**, *102*, 7583–7590. [CrossRef]
31. Siljeström, M.; Westerlund, E.; Björck, I.; Holm, J.; Asp, N.-G.; Theander, O. The effects of various thermal processes on dietary fibre and starch content of whole grain wheat and white flour. *J. Cereal Sci.* **1986**, *4*, 315–323. [CrossRef]
32. Dutta, H.; Paul, S.K.; Kalita, D.; Mahanta, C.L. Effect of acid concentration and treatment time on acid–alcohol modified jackfruit seed starch properties. *Food Chem.* **2011**, *128*, 284–291. [CrossRef]
33. Vithu, P.; Dash, S.K.; Rayaguru, K.; Panda, M.K.; Nedunchezhiyan, M. Optimization of starch isolation process for sweet potato and characterization of the prepared starch. *J. Food Meas. Charact.* **2020**, *14*, 1520–1532. [CrossRef]
34. Tejavathi, D.; Sujatha, B.; Karigar, C. Physicochemical properties of starch obtained from *Curcuma karnatakensis*—A new botanical source for high amylose content. *Heliyon* **2020**, *6*, e03169. [CrossRef]
35. Klang, V.; Schwarz, J.C.; Matsko, N.; Rezvani, E.; El-Hagin, N.; Wirth, M.; Valenta, C. Semi-solid sucrose stearate-based emulsions as dermal drug delivery systems. *Pharmaceutics* **2011**, *3*, 275–306. [CrossRef]
36. Kyriakidou, A.; Makris, D.P.; Lazaridou, A.; Biliaderis, C.G.; Mourtzinos, I. Physical Properties of Chitosan Films Containing Pomegranate Peel Extracts Obtained by Deep Eutectic Solvents. *Foods* **2021**, *10*, 1262. [CrossRef]
37. ASTM. Standard test method for tensile properties of thin plastic sheeting—D882-02. In *Annual Book of ASTM Standards*; American Society for Testing and Materials: Philadelphia, PA, USA, 2002; pp. 1–9.
38. Ren, L.; Yan, X.; Zhou, J.; Tong, J.; Su, X. Influence of chitosan concentration on mechanical and barrier properties of corn starch/chitosan films. *Int. J. Biol. Macromol.* **2017**, *105*, 1636–1643. [CrossRef]
39. Goula, A.M. Ultrasound-assisted extraction of pomegranate seed oil—Kinetic modeling. *J. Food Eng.* **2013**, *117*, 492–498. [CrossRef]
40. Rozalli, N.M.; Chin, N.; Yusof, Y. Grinding characteristics of Asian originated peanuts (*Arachis hypogaea* L.) and specific energy consumption during ultra-high speed grinding for natural peanut butter production. *J. Food Eng.* **2015**, *152*, 1–7. [CrossRef]
41. Jung, H.; Lee, Y.J.; Yoon, W.B. Effect of moisture content on the grinding process and powder properties in food: A review. *Processes* **2018**, *6*, 69. [CrossRef]
42. Tan, S.X.; Ong, H.C.; Lim, S.; Pang, Y.L.; Milano, J. Process intensification of biodiesel synthesis via ultrasound-assisted in situ esterification of *Jatropha* oil seeds. *J. Chem. Technol. Biotechnol.* **2019**, *94*, 1362–1373. [CrossRef]
43. Shirsath, S.; Sable, S.; Gaikwad, S.; Sonawane, S.; Saini, D.; Gogate, P. Intensification of extraction of curcumin from *Curcuma amada* using ultrasound assisted approach: Effect of different operating parameters. *Ultrason. Sonochem.* **2017**, *38*, 437–445. [CrossRef]
44. Taurozzi, J.S.; Hackley, V.A.; Wiesner, M. Preparation of nanoparticle dispersions from powdered material using ultrasonic disruption. *NIST Spec. Publ.* **2012**, *1200*, 1–15. [CrossRef]
45. Dey, S.; Rathod, V.K. Ultrasound assisted extraction of  $\beta$ -carotene from *Spirulina platensis*. *Ultrason. Sonochem.* **2013**, *20*, 271–276. [CrossRef]
46. Mohammadpour, H.; Sadrameli, S.M.; Eslami, F.; Asoodeh, A. Optimization of ultrasound-assisted extraction of *Moringa peregrina* oil with response surface methodology and comparison with Soxhlet method. *Ind. Crops Prod.* **2019**, *131*, 106–116. [CrossRef]
47. Patil, S.S.; Pathak, A.; Rathod, V.K. Optimization and kinetic study of ultrasound assisted deep eutectic solvent based extraction: A greener route for extraction of curcuminoids from *Curcuma longa*. *Ultrason. Sonochem.* **2021**, *70*, 105267. [CrossRef] [PubMed]
48. Nitayavardhana, S.; Rakshit, S.K.; Grewell, D.; Van Leeuwen, J.; Khanal, S.K. Ultrasound pretreatment of cassava chip slurry to enhance sugar release for subsequent ethanol production. *Biotechnol. Bioeng.* **2008**, *101*, 487–496. [CrossRef]
49. Luo, Y.; Peng, B.; Liu, Y.; Wu, Y.; Wu, Z. Ultrasound extraction of polysaccharides from guava leaves and their antioxidant and antiglycation activity. *Process Biochem.* **2018**, *73*, 228–234. [CrossRef]
50. Ying, Z.; Han, X.; Li, J. Ultrasound-assisted extraction of polysaccharides from mulberry leaves. *Food Chem.* **2011**, *127*, 1273–1279. [CrossRef]
51. Vasudeo, C.G. *Optimization of Ultrasound-Assisted Extraction (UAE) of Starch from Cassava (Manihot esculenta Grantz) using Response Surface Methodology (RSM) Technique*; ICAR-CTCRI: Tamil Nadu, India, 2016.
52. Patil, S.S.; Rathod, V.K. Synergistic effect of ultrasound and three phase partitioning for the extraction of curcuminoids from *Curcuma longa* and its bioactivity profile. *Process Biochem.* **2020**, *93*, 85–93. [CrossRef]
53. Tan, S.X.; Lim, S.; Ong, H.C.; Pang, Y.L. State of the art review on development of ultrasound-assisted catalytic transesterification process for biodiesel production. *Fuel* **2019**, *235*, 886–907. [CrossRef]
54. Joshi, S.M.; Gogate, P.R. Intensifying the biogas production from food waste using ultrasound: Understanding into effect of operating parameters. *Ultrason. Sonochem.* **2019**, *59*, 104755. [CrossRef]
55. More, P.R.; Arya, S.S. Intensification of bio-actives extraction from pomegranate peel using pulsed ultrasound: Effect of factors, correlation, optimization and antioxidant bioactivities. *Ultrason. Sonochem.* **2020**, *72*, 105423. [CrossRef]

56. Mujtaba, M.; Masjuki, H.; Kalam, M.; Ong, H.C.; Gul, M.; Farooq, M.; Soudagar, M.E.M.; Ahmed, W.; Harith, M.; Yusoff, M. Ultrasound-assisted process optimization and tribological characteristics of biodiesel from palm-sesame oil via response surface methodology and extreme learning machine-Cuckoo search. *Renew. Energy* **2020**, *158*, 202–214. [CrossRef]
57. Xu, Y.; Pan, S. Effects of various factors of ultrasonic treatment on the extraction yield of all-trans-lycopene from red grapefruit (*Citrus paradise* Macf.). *Ultrason. Sonochem.* **2013**, *20*, 1026–1032. [CrossRef] [PubMed]
58. Pan, Z.; Qu, W.; Ma, H.; Atungulu, G.G.; McHugh, T.H. Continuous and pulsed ultrasound-assisted extractions of antioxidants from pomegranate peel. *Ultrason. Sonochem.* **2012**, *19*, 365–372. [CrossRef] [PubMed]
59. Yan, W.; Chen, W.; Zhang, S.; Li, B.; Li, J. Evolution of solidification structures and mechanical properties of high-Si Al alloys under permanent magnetic stirring. *Mater. Charact.* **2019**, *157*, 109894. [CrossRef]
60. Li, Y.; Wu, Z.; Wan, N.; Wang, X.; Yang, M. Extraction of high-amylose starch from Radix Puerariae using high-intensity low-frequency ultrasound. *Ultrason. Sonochem.* **2019**, *59*, 104710. [CrossRef] [PubMed]
61. Chan, H.-T.; Bhat, R.; Karim, A.A. Effects of sodium dodecyl sulphate and sonication treatment on physicochemical properties of starch. *Food Chem.* **2010**, *120*, 703–709. [CrossRef]
62. Zhang, Z.; Niu, Y.; Eckhoff, S.R.; Feng, H. Sonication enhanced cornstarch separation. *Starch-Stärke* **2005**, *57*, 240–245. [CrossRef]
63. Park, S.H.; Bean, S.; Wilson, J.; Schober, T. Rapid isolation of sorghum and other cereal starches using sonication. *Cereal Chem.* **2006**, *83*, 611–616. [CrossRef]
64. Zhang, Y.; Li, B.; Xu, F.; He, S.; Zhang, Y.; Sun, L.; Zhu, K.; Li, S.; Wu, G.; Tan, L. Jackfruit starch: Composition, structure, functional properties, modifications and applications. *Trends Food Sci. Technol.* **2020**, *107*, 268–283. [CrossRef]
65. Zhao, Y.; Wen, C.; Feng, Y.; Zhang, J.; He, Y.; Duan, Y.; Zhang, H.; Ma, H. Effects of ultrasound-assisted extraction on the structural, functional and antioxidant properties of *Dolichos lablab* L. Protein. *Process Biochem.* **2021**, *101*, 274–284. [CrossRef]
66. Seo, H.-W.; Kim, J.-H. Ultrasound-assisted fractional precipitation of paclitaxel from *Taxus chinensis* cell cultures. *Process Biochem.* **2019**, *87*, 238–243. [CrossRef]
67. Borah, P.P.; Das, P.; Badwaik, L.S. Ultrasound treated potato peel and sweet lime pomace based biopolymer film development. *Ultrason. Sonochem.* **2017**, *36*, 11–19. [CrossRef]
68. Zhu, J.; Li, L.; Chen, L.; Li, X. Study on supramolecular structural changes of ultrasonic treated potato starch granules. *Food Hydrocoll.* **2012**, *29*, 116–122. [CrossRef]
69. Manchun, S.; Nunthanid, J.; Limmatvapirat, S.; Sriamornsak, P. Effect of Ultrasonic Treatment on Physical Properties of Tapioca Starch. *Adv. Mater. Res.* **2012**, *506*, 294–297. [CrossRef]
70. Ali, M.A.; Razafindralambo, H.L.; Conti, G.; De Coninck, J.I. Bulk and Surface Wettability Characteristics of Probiotic Powders in Their Compressed Disc and Packed-Bed Column Forms. *ACS Omega* **2020**, *5*, 22348–22355. [CrossRef]
71. Polnaya, F.; Marseno, D.; Cahyanto, M. Effects of phosphorylation and cross-linking on the pasting properties and molecular structure of sago starch. *Int. Food Res. J.* **2013**, *20*, 1609–1615.
72. Uthumporn, U.; Wahidah, N.; Karim, A. Physicochemical properties of starch from sago (*Metroxylon Sagu*) palm grown in mineral soil at different growth stages. In *IOP Conference Series: Materials Science and Engineering*; IOP Publishing: Bristol, UK, 2014; p. 012026.
73. Liu, H.; Adhikari, R.; Guo, Q.; Adhikari, B. Preparation and characterization of glycerol plasticized (high-amylose) starch–chitosan films. *J. Food Eng.* **2013**, *116*, 588–597. [CrossRef]
74. Galvis-Sánchez, A.C.; Sousa, A.M.; Hilliou, L.; Gonçalves, M.P.; Souza, H.K. Thermo-compression molding of chitosan with a deep eutectic mixture for biofilms development. *Green Chem.* **2016**, *18*, 1571–1580. [CrossRef]
75. Mei, J.; Yuan, Y.; Wu, Y.; Li, Y. Characterization of edible starch–chitosan film and its application in the storage of Mongolian cheese. *Int. J. Biol. Macromol.* **2013**, *57*, 17–21. [CrossRef] [PubMed]

Review

# A Review of Bioplastics and Their Adoption in the Circular Economy

Alberto Di Bartolo , Giulia Infurna  and Nadka Tzankova Dintcheva \*

Dipartimento di Ingegneria, Università degli Studi di Palermo, Viale delle Scienze, Ed. 6, 90128 Palermo, Italy; alberto.dibartolo@gmail.com (A.D.B.); giulia.infurna@unipa.it (G.I.)

\* Correspondence: nadka.dintcheva@unipa.it

**Abstract:** The European Union is working towards the 2050 net-zero emissions goal and tackling the ever-growing environmental and sustainability crisis by implementing the *European Green Deal*. The shift towards a more sustainable society is intertwined with the production, use, and disposal of plastic in the European economy. Emissions generated by plastic production, plastic waste, littering and leakage in nature, insufficient recycling, are some of the issues addressed by the European Commission. Adoption of bioplastics—plastics that are biodegradable, bio-based, or both—is under assessment as one way to decouple society from the use of fossil resources, and to mitigate specific environmental risks related to plastic waste. In this work, we aim at reviewing the field of bioplastics, including standards and life cycle assessment studies, and discuss some of the challenges that can be currently identified with the adoption of these materials.

**Keywords:** bioplastic; bio-based plastic; biodegradable plastic; bioeconomy; life cycle assessment; sustainability

**Citation:** Di Bartolo, A.; Infurna, G.; Dintcheva, N.T. A Review of Bioplastics and Their Adoption in the Circular Economy. *Polymers* **2021**, *13*, 1229. <https://doi.org/10.3390/polym13081229>

Academic Editor: Cristina Cazan

Received: 22 March 2021

Accepted: 7 April 2021

Published: 10 April 2021

**Publisher's Note:** MDPI stays neutral with regard to jurisdictional claims in published maps and institutional affiliations.



**Copyright:** © 2021 by the authors. Licensee MDPI, Basel, Switzerland. This article is an open access article distributed under the terms and conditions of the Creative Commons Attribution (CC BY) license (<https://creativecommons.org/licenses/by/4.0/>).

## 1. Introduction

The European Green Deal [1] is the action plan outlined by the European Commission (EC) to tackle the ever-growing environment and climate-related challenges our society faces. The plan aims at transforming “the EU into a fair and prosperous society, with a modern, resource-efficient and competitive economy where there are no net emissions of greenhouse gases in 2050 and where economic growth is decoupled from resource use” [1] (p. 2). As also stated in its communication “A new Circular Economy Action Plan for a Cleaner and More Competitive Europe” [2], the EC underlines the utmost importance of shifting towards a circular economy, with a framework of policies that make sustainable products, services, and business models the norm. On the global scale, The United Nations Development Program (UNDP) also stressed the importance of working towards a sustainable economy, with efficient use of natural resources, little to none waste and pollution [3]. In this context, the EC identifies a series of pressing challenges relating to plastic production, (mis-)use and pollution, spanning from single-use items, over-packaging, and littering, to microplastics, high-carbon footprints, and lack of appropriate labeling. The strategy outlined to tackle these challenges includes supporting the bio-based industry and developing a framework for the use of bio-based plastics, “based on assessing where the use of bio-based feedstock results in genuine environmental benefits”, and for the use of biodegradable or compostable plastics, “based on an assessment of the applications where such use can be beneficial to the environment” [2] (p. 9). These plastics, which are either bio-based or biodegradable (or both), are referred to as “bioplastics” and have been the topic of much work and discussion at a global level for some time now. The dwindling of fossil resources provides a strong drive to the development of bio-based products, while the possibility to mitigate environmental pollution or simplify organic waste collection are big motivations behind the development of biodegradable and compostable plastic products. Bioplastics already find applications on the market, particularly as packaging [4–7], carrier and compost bags [5,6]; they are



also applied in the agriculture and horticulture sector [6,8], and in the automotive and electronic industry [6,9]. Furthermore, biodegradable polymers have been long applied in biomedicine [5,10,11]. Still, the production of bio-based plastics is limited to one percent of the worldwide plastic production [7,12] and their adoption comes with uncertainties, as acknowledged in the EC Communication “*A European Strategy for Plastics in a Circular Economy*” [13]. This is exemplified by the research focused on bioplastics sustainability and [8,14–25] biodegradability [26–30], as well as the attention of media to the subject. Excluding the ample literature on biomedical applications, academic research has been focusing on the synthesis of bio-based polymers [31,32], on the life cycle assessment (LCA) of the production and end-of-life (EOL) [20,24,33,34] of different bioplastics, and biodegradation under different conditions [10,14,35].

In this paper, we present the reader with an overview of the bioplastics field, including definitions, polymers on the market, and applications. We discuss biotic and abiotic degradation mechanisms and present standards and certifications that are in place to evaluate the compostability and biodegradability of bioplastics. Recent works on the biodegradability of bioplastics are also reviewed. We report on the standards in place for the LCA of bioplastics and review recent studies on the subject, with particular focus on studies that consider the EOL assessment. Finally, given the material reviewed, we concisely discuss the challenges that can be identified with the adoption of bioplastics, as well as possible solutions, and we draw our conclusions on the topic.

### 1.1. Environmental Impact of Plastics

The generation of plastic waste and subsequent uncontrolled plastic pollution is one of the major environmental problems governments and agencies must face today.

The global production of plastic reached almost 370 million metric tons (Mt) in 2019 [36], almost 60 million of which are produced in Europe. The vast majority of the plastic products that enter the global market are durable materials, in particular, polypropylene and polyethylene are the leading polyolefins on the market, with the production of packaging being the main use of such plastics [36]. As of 2017, it was estimated that 8300 Mt of plastics were produced worldwide while, as of 2015, 79% of all plastic produced had been accumulating in landfills or the environment [37]. The UNEP reports that only 9% of all plastic ever made has been recycled, 12% has been incinerated and the rest accumulates in landfills or nature [38]. Today, 300 Mt of plastic waste are produced every year and around 80% of marine litter is due to plastic debris, with the infamous “*Great Pacific Garbage Patch*” being a dreadful testament to these numbers and with an estimate of 75,000 to 300,000 tons of microplastics entering EU habitats every year [38–41].

Plastic debris in the natural environment is extremely persistent, with degradation in seawater being estimated from hundreds to thousands of years [42,43]. Plastic marine debris results in severe, harmful, impact on the ecosystem [44]. Because of its long half-life and hydrophobic nature, plastic debris provides excellent conditions for the proliferation of diverse microbial communities, forming an ecosystem referred to as “*plastisphere*” [45]. The microbial action, together with mechanical stress, thermal and UV-light degradation, results in the fragmentation of the debris into microplastics, to the point that plastic residues can be found in many aquatic species, as well as birds and other wildlife [46]. In turn, this poses a risk to human health by entering the food chain [47–49].

A great part of the answer to plastic pollution comes from increasing recycling and repurposing of already produced plastics, as well as replacing several classes of plastic items, particularly single-use products, with recyclable alternatives, and from a change in mentality and habits in our society. At the same time, fossil resources are finite and their use results in greenhouse gas (GHG) emissions. As reported by the Ellen MacArthur Foundation in 2016 [50], it can be estimated that by 2050 the plastics sector “*will account for 20% of total oil consumption and 15% of the global annual carbon budget by 2050 (this is the budget that must be adhered to in order to achieve the internationally accepted goal to remain below a 2 °C increase in global warming)*” [50] (p. 7). The production of plastics from renewable

sources has been suggested to achieve a lower carbon footprint, since the raw materials uptake carbon dioxide during their growth, and to alleviate the economy's dependence on fossil fuel [13,41,50]. The application of biodegradable plastics in specific fields, such as soil cover films, carrier bags, and single-use packaging is also suggested as part of technological advancement in the bioeconomy [7,13].

### 1.2. Circular Economy and Bioplastics

Broadly speaking, a circular economy is an economic system and production model aimed at maximizing the reuse and recycling of resources, therefore extending the life cycle of products while minimizing waste. The model was thought of as a response to the traditional economy, the linear economy, where resources are used to manufacture products which are then used and discarded as waste. The *Circular Economy Action Plan* presented by the EC in 2020 [2] outlines the main directions towards which the economic model is being developed. We briefly summarize some of the main points made in the document.

Products should be designed with reusability and recyclability in mind, i.e., they need to be more durable, repairable, recyclable. Packaging is to be reduced, restricted to certain applications, and designed for recyclability. The production of single-use items is to be restricted and the destruction of unsold items is to be banned. Finally, more support to the bio-based sector is also considered as one way to enable greater circularity in industry, though it is also noted that the sourcing, labeling and use of bio-based, biodegradable and compostable plastics, are emerging challenges for which the EC will develop a policy framework [2] (p. 9). The topic of bioplastics is more extensively discussed in a 2018 EC action plan [51] focused on bioeconomy.

Overall, the EC communications suggest that the policy will be to support, e.g., via financial and regulatory incentives, the growth of the bioplastics industry, as one way to move towards a low-carbon economy [41,52,53]. For example, more than 100 million euros have been provided to finance R&D focused on alternative feedstocks, as part of the *Horizon 2020 Research Programme* [52]. The European Committee for Standardization (CEN) has also produced several harmonized standards in the past five years, covering methodologies to claim biodegradability and compostability, and to measure the bio-based content of plastics, to better regulate the bioplastic field. Still, it is acknowledged that more standards are required and that applications of biodegradable plastics can come with both positive and negative implications [53].

## 2. Bioplastics: Definitions and Market

The term bioplastic is often used loosely and synonymously to biodegradable. While some bioplastics are indeed biodegradable, not all are. Bioplastics should be intended as polymers that meet any of two criteria: the polymer is bio-based, the polymer is biodegradable [28,54]. Bio-based means that the polymer is either entirely or partially obtained from biomass, i.e., from any kind of organic renewable material of biological origin as well as organic waste. Biodegradable means that the material can break down into natural substances such as carbon dioxide, water and biomass, due to the action of microorganisms. In a more specific sense, a biodegradable plastic is a plastic material that complies with certain official standards of biodegradability, where a certain amount of degradation needs to be scientifically observed within a certain amount of time and under specific conditions. Similarly, a compostable plastic undergoes biodegradation in industrial composting facilities and has to comply with specific standards.

Bioplastics therefore form three broad groups of polymers: those that are both bio-based and biodegradable, those that are only bio-based and those that are only biodegradable. Some main examples of bioplastics that are both bio-based and biodegradable are polylactic acid (PLA) [55,56], polyhydroxyalkanoates (PHAs) [57] and bio-based polybutylene succinate (bio-PBS) [58], as well as plastics based on starch, cellulose, lignin and chitosan. Examples of bioplastics that are bio-based but not biodegradable are bio-based

polyamides (bio-PP), polyethylene (bio-PE), polyethylene terephthalate (bio-PET) [59]. Finally, examples of biodegradable bioplastics that are based on fossil resources are PBS, polycaprolactone (PCL) [60], polyvinyl alcohol (PVA) [61] and polybutylene adipate terephthalate (PBAT) [62]. Furthermore, polymers like bio-PE, which are bio-based and chemically identical to their fossil-based counterparts, are typically referred to as drop-in polymers. Table 1 lists some bioplastics that are frequently encountered on the market or in research, classified on the basis of the origin of the raw materials and their biodegradability.

**Table 1.** Lists of bioplastics and indication of bio-based origin and biodegradability. In the table, “y” means yes, “n” means no, and “y/n” refers to both statements being valid.

| Polymer                                   | Bio-Based | Biodegradable |
|---|-----------|---------------|
| Polylactic acid (PLA)                     | y         | y             |
| Starch blends, thermoplastic starch (TS)  | y         | y             |
| Polyhydroxyalkanoates (PHAs)              | y         | y             |
| Polybutylene succinate (PBS)              | y/n       | y             |
| Polyurethanes (PURs)                      | y/n       | y/n           |
| Polycaprolactone (PCL)                    | n         | y             |
| Polyvinyl alcohol (PVA)                   | n         | y             |
| Polybutylene adipate terephthalate (PBAT) | n         | y             |
| Polyethylene Furanoate (PEF)              | y         | n             |
| Bio-polypropylene (bio-PP)                | y         | n             |
| Polytrimethylene terephthalate (PTT)      | y         | n             |
| Bio-polyethylene terephthalate (bio-PET)  | y         | n             |
| Bio-polyethylene (bio-PE)                 | y         | n             |
| Bio-polyamides (bio-PAs)                  | y         | n             |

Today’s production volume of bioplastics is relatively small when compared to the numbers of the common plastic industry. According to European Bioplastics, the global production of bioplastics in 2018 was around 2 Mt [12], while the global production for plastics was around 360 Mt. At the same time it is anticipated that the global market for bioplastics will grow steadily for the next five year, increasing in volume by around 40% [12]. Different examples of bioplastics already exist on the market and are produced by companies both in Europe, the USA and Asia, with some of the most important manufacturer being BASF (Germany), Corbion N.V. (Netherlands), NatureWorks LLC (USA), CJ Cheil-Jedang (Korea), Novamont (Italy), Tianjin Guoyun (China). Two historically successful examples are Cellophane<sup>TM</sup>, produced from regenerated cellulose by Futamura Chemical Company (UK), and Nylon-11 produced from castor oil by different manufacturers. More examples are the PLA branded Ingeo<sup>TM</sup> produced by NatureWorks LLC, as well as the Luminy<sup>®</sup> series of PLA resins produced by Total Corbion (fifty-fifty joint venture between Total and Corbion), which is also working on the production of bio-based PEF; Corbion distributes its PURASORB<sup>®</sup> grades of bioresorbable polymers, which include PLA, PCL and copolymers; Danimer Scientific produces the PHA-based bioplastic Nodax<sup>TM</sup>; several compostable polymers are produced by BASF (ecoflex<sup>®</sup>, ecovio<sup>®</sup>); Novamont produces its biodegradable, starch-based, Mater-Bi<sup>TM</sup>; Arkema produces a series of bio-PA (Nylon) under the name Rilsan<sup>®</sup>.

### 2.1. Production Routes of Bio-Based Plastics and Main Examples

As already introduced, bio-based plastics are entirely or partially obtained from some type of biological source, this includes plants, microorganisms, algae, as well as food waste. Some bio-based plastics are obtained from polymers that form directly in nature, within microorganisms and plants. Notably, cellulose—the most abundant organic compound and the main constituent in plant fibers—has been used ever since the 19th century. Other bio-based plastics are relatively novel and are obtained through synthetic routes making use of natural resources to formulate monomers which are then polymerized. In general, we can identify three main routes to produce bio-based plastics: (1) polymerization of

bio-based monomers; (2) modification of naturally occurring polymers; (3) extraction of polymers from microorganisms. Table 2 lists some of the main bio-based polymers grouped by their production route and followed by a brief description of their synthesis.

**Table 2.** List of common bio-based polymers and overview of their production.

| Polymer                | Technology Overview   | Route |
|------------------------|---|-------|
| Polylactic acid        | Fermentation of carbohydrates (e.g., starch) yields lactic acid which polymerizes to low $M_n$ PLA. This depolymerizes to lactide, which polymerizes to high $M_n$ PLA. | 1     |
| Polybutylene succinate | Bacterial fermentation of carbohydrates yields succinic acid, which is esterified to also obtain 1,4-butanediol. The two chemicals polymerize to PBS.                   |       |
| Polyurethanes          | Polyols obtained from plant oils are reacted with isocyanates or bio-isocyanates to yield PURs.   |       |
| Polyamides             | Diacids derived from castor oil are reacted with a diamine to yield PAs. A typical pair is sebacic acid and decamethylenediamine (obtained from the acid).              |       |
| Polyethylene           | Fermentation of saccharides yields bioethanol, then dehydrated to ethylene. Polymerization yields bio-PE.   |       |
| Thermoplastic starch   | Typically obtained by gelatinization of starch (from corn, cassava, etc.) followed by casting or by extrusion of starch pellets and plasticizers.                       | 2     |
| Cellulose acetate      | Cellulose from wood pulp is converted to a triacetate form which is then hydrolyzed to cellulose acetate.   |       |
| Regenerated cellulose  | Cellulose is converted to a soluble form, then regenerated to obtain a film (cellophane) or a fiber (rayon).  |       |
| Polyhydroxyalkanoates  | Intracellularly accumulated by different bacteria. Polyhydroxybutyrate was the first to be discovered.  | 3     |

Today, several bio-based polymers are produced through the polymerization of monomers obtained from natural sources, PLA being the primary example. Polylactic acid is a thermoplastic aliphatic polyester obtained from the fermentation of plant-derived carbohydrates, e.g., sugars obtained from sugarcane or sugar beet, or starch obtained from corn or potato. The fermentation process makes use of various microorganisms, typically *Lactobacilli* strains, which convert sugars to lactic acid [55,63]. If starch is used as feedstock, this is first enzymatically converted to sugars (glucose). Most commonly, the lactic acid is then polymerized to low molecular weight ( $M_n$ ) PLA oligomers, which are in turn depolymerized to yield lactide, the cyclic dimer of PLA. The ring-opening polymerization (ROP) of lactide will then yield high  $M_n$  PLA [55,64,65]. Due to the chiral nature of the monomers, L(-) and D(+), in use during the polymerization process, three stereochemical forms of PLA can be obtained. Depending on the ratio of L- to D-isomers, the resulting polymer can be amorphous or show different degree of crystallinity, with influence on degradation [66] and mechanical properties [67]. PLA processability is comparable to many commodity thermoplastics, which leads to its use as packaging material [56,68]. PLA is also recognized as biodegradable and compostable [55,64,65], it is therefore used in the production of compost bags and disposable tableware, and other applications where recovery of the used product is not feasible. Furthermore, PLA biocompatibility has made it into one of the

most important polymers in biomedicine and tissue engineering [55,64,65,69]. Finally, PLA is one of the main materials in use to produce filaments for fused deposition modeling, a common 3D printing manufacturing process [70].

PBS is another thermoplastic polyester that can be produced from the microbial fermentation of sugars derived from natural feedstocks. The typical route of production for PBS is the esterification of succinic acid with 1,4-butanediol [71], where the succinic acid can be obtained from the anaerobic fermentation of bacteria or yeast and subsequently reduced to 1,4-butanediol. Several microorganisms have been studied for the biosynthesis of succinic acid, e.g., *Anaerobiospirillum succiniciproducens* and *Actinobacillus succinogenes* [72]. The polymerization process proceeds through a first step during which the 1,4-butanediol is reacted with the succinic acid to yield oligomers of PBS, and a second step of polycondensation of the oligomers to yield semicrystalline, high  $M_n$  PBS [58]. PBS shows similar properties to polyethylene terephthalate and polypropylene and finds applications as compostable packaging and bags, as mulch film and hygiene products [58,73]. The use of PBS in biomedical applications has also been attracting significant attention, thanks to its biodegradability and low toxicity profile, though its low flexibility and slow degradability rate need to be circumvented by blending or copolymerization with other polymers, such as PLA [71,73].

Bio-based polyethylene is an aliphatic thermoplastic synthesized from the polymerization of bioethanol. The bioethanol is obtained through the fermentation of sugars from the aforementioned feedstocks (sugarcane, sugar beet, and starch from corn, wheat or potato) [59], yeast or bacteria being used as fermentation agents [74]. The bioethanol is distilled and dehydrated to obtain ethylene which is then polymerized to bio-PE. The polymer is equivalent to fossil-derived polyethylene and the same different types (low and high density, linear and branched) can be obtained, consequently, bio-PE can be used for any of the many applications of PE. It should also be noted that bioethanol can also be used in the synthesis of other important plastics such as polyvinyl chloride, polystyrene and polyethylene terephthalate [59].

Several naturally occurring polymers can be used to produce bio-based and biodegradable plastics, in particular the polysaccharides starch and cellulose.

Among naturally occurring polymers, cellulose is the most abundant one, being ubiquitous in plants. It is a structural polysaccharide based on repeating units of D-glucose. Cellulose has attracted great attention from research and industry due to its abundance, low-cost, biocompatibility and biodegradability. Cellulose is typically obtained from wood through a pulping process and can be converted to different materials, in particular two main cellulose-based plastics (or cellulose derivatives) are regenerated cellulose and cellulose diacetates [75]. In the production of cellulose diacetates, the cellulose is first converted to cellulose triacetate by reaction with acetic anhydride, this is then partially hydrolyzed to obtain a lower degree of substitution. Most typically cellulose diacetates are produced with degree of substitution around 2.5. Cellulose acetates find several applications in the textile industry [76], as fibers in cigarette filters [77], films (e.g., photography) and membranes in separation technologies (e.g., hemodialysis) [78]; manufactured as porous beads they have potential applications in biomedicine and biotechnology [79]. Cellulose diacetate is also biodegradable under different natural conditions with the process being accelerated by hydrolysis [80].

Regenerated cellulose is typically prepared following the viscose process (though other industrial methods exist), in which cellulose is converted to cellulose xanthogenate by reaction with alkali and carbon disulfide. The intermediate is dissolved in NaOH solutions, resulting in a mixture called viscose, which can be processed as films and fibers and treated in acidic solutions to yield regenerated cellulose [81,82]. Regenerated cellulose materials are either already applied or could find applications, in different fields, from textile and packaging, to biotechnology and biomedicine [82]. Rayon and cellophane, which are generic trademarks for regenerated cellulose fibers and films respectively, are materials with great commercial importance. Rayon finds many applications in the textile industry,

from the manufacture of clothing to the production of wound dressings [83]. Cellophane is almost ubiquitous in the food packaging market, but also in the cosmetic (casing, boxes, etc.) and pharmaceutical industry [82].

Starch-based polymers form an important family of bioplastics on the market. Starch is a polysaccharide consisting of two main macromolecules, amylose and amylopectin, and is obtained from feedstocks such as corn, rice, wheat or potato [84,85]. Thermoplastic starch (TPS) is the material obtained from a granular form of native starch, through thermomechanical processing (extrusion) with the addition of gelatinization agents or plasticizers [84–87]. Typical plasticizers in use to improve the processability of TPS are glycerol and other polyols, sugars, amides and amines, and citric acid [84]. TPS can be used on its own, though very often it is used as part of polymeric blends with polymers such as PLA and other polyesters, to improve its properties. Starch-based plastics find different applications in the packaging, food, textile and pharmaceutical industry [88–90].

Bacteria can synthesize and accumulate a large number of biopolymers, many of which can be potentially exploited for industrial applications or as high-value products in the medical field [91]. Polyhydroxyalkanoates are a family of polyesters synthesized by the activity of several types of bacteria, where they accumulate serving the purpose of carbon reserve material. The intracellular accumulation of PHAs is typically promoted by particular culturing conditions and nutrients starvation, which can lead to high concentration of accumulated polymer [71,91–94]. Several renewable feedstocks, as well as carbon dioxide, chemicals and fossil resources, can be used as substrate for the production of PHAs [94]. In a typical process a seed culture containing the chosen bacteria is inoculated in a fermentation vessel containing the fermentation medium. At the end of the culturing period, the polymers can be obtained by solvent extraction, separated from the residual biomass and reprecipitated by mixing with a non-solvent, typically an alcohol [31,71,95]. To this day, more than 150 monomeric units have been identified, which can lead to different polymers with different properties. Polyhydroxybutyrate (PHB) is the simplest PHA and the first one to be discovered in the bacterium *Bacillus megaterium*. PHAs find applications in the packaging, food and chemical industry, though most recently attention has been shifting towards possible agricultural and medical applications [96–98].

## 2.2. Biodegradability and Compostability Standards

As introduced, biodegradable polymers are susceptible to be broken down into simple compounds because of microbial action. Many plastics have been known to undergo this process in a reasonably short time (e.g., six months), and are commonly identified as biodegradable, though to substantiate biodegradability claims, certain standards have been put into place in the past twenty years. These standards present methodologies to evaluate the biodegradability and compostability of a plastic, where compostable refers to the material being degraded under specifically designed conditions and by specific microorganisms, typically in industrial composting facilities. The main standardization bodies involved are the International Organization for Standardization (ISO), European Committee for Standardisation (CEN) and the American Society for Testing and Materials (ASTM). Table 3 reports the main ISO [99] and CEN [100] standards in place, many of which are shared as the CEN standards are often based on the ISO ones. In particular, for a polymer to be marketed as biodegradable or compostable the main standards to conform to are the European EN 13432 or EN 14995 or the international ISO 17088 (other equivalents would be the USA ASTM 6400 or the Australian AS4736). As part of the requirements to pass the standards, the testing methodologies in use to evaluate biodegradability need to be the ones outlined by other official standards, for example EN ISO 14855. The simulated environment, the biodegradability indicator in use, the inoculum in use, test duration, number of replicates required and percentage of evaluated biodegradability to pass the test, are focus points for biodegradability testing standards. It can be noticed that the biodegradability evaluation is carried out by different experimental methodologies, such as release of carbon dioxide and oxygen demand measurements. Indeed, the main

indicators of biodegradation adopted by these standards are the measurement of BOD (the biological oxygen demand) or the measurement of evolved CO<sub>2</sub>, though also mass loss measurements, measurements of CH<sub>4</sub> evolution, as well as surface morphology and spectroscopy analysis are methodologies in use [101]. Biodegradability standards describe a series of well-defined conditions under which biodegradability or compostability tests are to be carried out, for example temperature, microbial activity and humidity. While this is required for reproducibility and repeatability of results, researchers have pointed out the difficulty in encompassing the variability of conditions encountered in natural, open environments [10,14]. In particular, the more environmentally harmful perspective of plastic waste leaking into the natural environment leads to a series of possible environmental conditions that are hard to accurately predict and simulate. For example, plastic debris leaked in the sea is exposed to a wide range of temperatures, depending on climate, biomes, buoyancy, and other characteristics that might very well change over time. Given that the appeal of biodegradable plastics in several applications is their supposed ability to degrade in the environment, completely and harmlessly, it is of utmost importance to understand the validity of these standards outside of laboratory conditions. In a 2018 review of biodegradability standards, Harrison et al. [35] found that the international standards in use would be insufficient to predict the biodegradability of carrier bags in aqueous environments (wastewater, marine and inland waters). They concluded that the standards in use would typically underestimate the time required for polymers to undergo biodegradation in a natural, uncontrolled environment, particularly because of the methods in use relying on artificially modified media and inocula and relatively high temperatures, that do not reflect what is commonly expected in a natural environment. In 2017, Briassoulis et al. [102] come to similar conclusions when reviewing the standards relevant to the biodegradability of plastics in soil, particularly for the agriculture and horticulture environment. They observe that the standard methodologies enhance the conditions for biodegradation of the specimens in a way that may not be representative of the natural environment, where temperature, water content and soil properties can vary considerably. The standards caution the users about the potential difference between laboratory and natural environment results, though it is not clear how the methodologies should be modified to obtain more representative conclusions. In a 2017 work, Emadian et al. [103] reviewed a series of studies on the biodegradation of bioplastics in different conditions. For the same biopolymers, they reported extremely different results across the studies taken into consideration. For example, testing the biodegradability of PLA in compost researchers reported biodegradation values as low as 13% over 60 days [104] and as high as 70% over 28 days [105]. This difference in results is due to different methodologies, conditions and sample geometry and size being in use, and therefore stresses the need for standard procedures being followed during laboratory tests. Though, at the same time, the kind of differences that create this discrepancy, can also be encountered in a natural environment, and further stress the problem of how well biodegradability can be predicted outside of a laboratory. Further problematics can be encountered when considering the biodegradation of polymeric blends instead of homopolymers. In a 2018 paper Narancic et al. [14] reported on the biodegradability of several biopolymers and their blends in different environments, following the relative standards. The paper is extremely thorough, and its full analysis goes beyond the scope of this review, though one conclusion was that the polymeric blends would generally biodegrade well under industrial composting conditions, but they would show poor biodegradation in aquatic environment and soil. Interestingly, the authors observed that, while PLA is generally not home-compostable, when blended with PCL it would result in a material that could undergo biodegradation under home-composting conditions (though not in soil). At the same time, this was not the case for blends of PLA and PHB, which remained not home-compostable.

**Table 3.** Main ISO and CEN standards relating to biodegradability and compostability of plastics.

| Standard                                   | Title   |
|--|---|
| EN ISO 10210:2017                          | Plastics—Methods for the preparation of samples for biodegradation testing of plastic materials (ISO 10210:2012)  |
| EN 14995:2006                              | Plastics—Evaluation of compostability—Test scheme and specifications  |
| EN 13432:2000                              | Packaging—Requirements for packaging recoverable through composting and biodegradation—Test scheme and evaluation criteria for the final acceptance of packaging  |
| EN 14046:2003                              | Packaging—Evaluation of the ultimate aerobic biodegradability of packaging materials under controlled composting conditions—Method by analysis of released carbon dioxide   |
| EN 17033:2018                              | Plastics—Biodegradable mulch films for use in agriculture and horticulture—Requirements and test methods  |
| ISO 17088:2012                             | Specifications for compostable plastics   |
| EN ISO 14855-1:2012<br>EN ISO 14855-2:2018 | Determination of the ultimate aerobic biodegradability of plastic materials under controlled composting conditions—Method by analysis of evolved carbon dioxide—Part 1: General method (ISO 14855-1:2012)—Part 2: Gravimetric measurement of carbon dioxide evolved in a laboratory-scale test (ISO 14855-2:2018) |
| EN ISO 16929:2019                          | Plastics—Determination of the degree of disintegration of plastic materials under defined composting conditions in a pilot-scale test (ISO 16929:2019)  |
| EN ISO 20200:2015                          | Plastics—Determination of the degree of disintegration of plastic materials under simulated composting conditions in a laboratory-scale test (ISO 20200:2015)   |
| ISO 23977-1:2020<br>ISO 23977-2:2020       | Plastics—Determination of the aerobic biodegradation of plastic materials exposed to seawater—Part 1: Method by analysis of evolved carbon dioxide—Part 2: Method by measuring the oxygen demand in closed respirometer   |
| EN ISO 14853:2017                          | Plastics—Determination of the ultimate anaerobic biodegradation of plastic materials in an aqueous system—Method by measurement of biogas production (ISO 14853:2016)   |
| EN ISO 14851:2019                          | Determination of the ultimate aerobic biodegradability of plastic materials in an aqueous medium—Method by measuring the oxygen demand in a closed respirometer (ISO 14851:2019)  |
| EN ISO 14852:2018                          | Determination of the ultimate aerobic biodegradability of plastic materials in an aqueous medium—Method by analysis of evolved carbon dioxide (ISO 14852:2018)  |
| EN 17417:2020                              | Determination of the ultimate biodegradation of plastics materials in an aqueous system under anoxic (denitrifying) conditions—Method by measurement of pressure increase   |
| EN ISO 10634:2018                          | Water quality—Preparation and treatment of poorly water-soluble organic compounds for the subsequent evaluation of their biodegradability in an aqueous medium (ISO 10634:2018)   |
| EN ISO 14593:2005                          | Water quality—Evaluation of ultimate aerobic biodegradability of organic compounds in aqueous medium—Method by analysis of inorganic carbon in sealed vessels (CO <sub>2</sub> headspace test) (ISO 14593:1999)   |
| EN ISO 11733:2004                          | Water quality—Determination of the elimination and biodegradability of organic compounds in an aqueous medium—Activated sludge simulation test (ISO 11733:2004)   |
| EN ISO 17556:2019                          | Plastics—Determination of the ultimate aerobic biodegradability of plastic materials in soil by measuring the oxygen demand in a respirometer or the amount of carbon dioxide evolved (ISO 17556:2019)  |
| EN ISO 11266:2020                          | Soil quality—Guidance on laboratory testing for biodegradation of organic chemicals in soil under aerobic conditions (ISO 11266:1994)   |
| EN ISO 15985:2017                          | Plastics—Determination of the ultimate anaerobic biodegradation under high-solids anaerobic-digestion conditions—Method by analysis of released biogas (ISO 15985:2014)   |
| EN ISO 18830:2017                          | Plastics—Determination of aerobic biodegradation of non-floating plastic materials in a seawater/sandy sediment interface—Method by measuring the oxygen demand in closed respirometer (ISO 18830:2016)   |
| EN ISO 19679:2020                          | Plastics—Determination of aerobic biodegradation of non-floating plastic materials in a seawater/sediment interface—Method by analysis of evolved carbon dioxide (ISO 19679:2020)   |
| ISO 13975:2019                             | Plastics—Determination of the ultimate anaerobic biodegradation of plastic materials in controlled slurry digestion systems—Method by measurement of biogas production  |
| ISO 22404:2019                             | Plastics—Determination of the aerobic biodegradation of non-floating materials exposed to marine sediment—Method by analysis of evolved carbon dioxide  |
| ISO/DIS 23517-1<br>(under development)     | Plastics—Biodegradable mulch films for use in agriculture and horticulture<br>Part 1: Requirements and test methods regarding biodegradation, ecotoxicity and control of constituents   |

Several companies in Europe market their products with labels specifying their biodegradability. Figure 1 summarizes the main certifications in use in Europe, which are released by the Belgian certifier TÜV Austria and German certifier DIN CERTCO. It should be noted that home compostability is yet to be specifically described by EN harmonized standards, though standard prEN 17427:2020 “Packaging-Requirements and test scheme for carrier bags suitable for treatment in well-managed home composting installations” is



pending. Industrial compostability is covered by the standards EN 14995 and EN 13432, and these are used during the certification. Soil biodegradability is also certified by two of the labels through EN 17033, which therefore limits the certification to mulch film. Two labels for biodegradability in water are offered by TÜV but they are independent from EN standards.

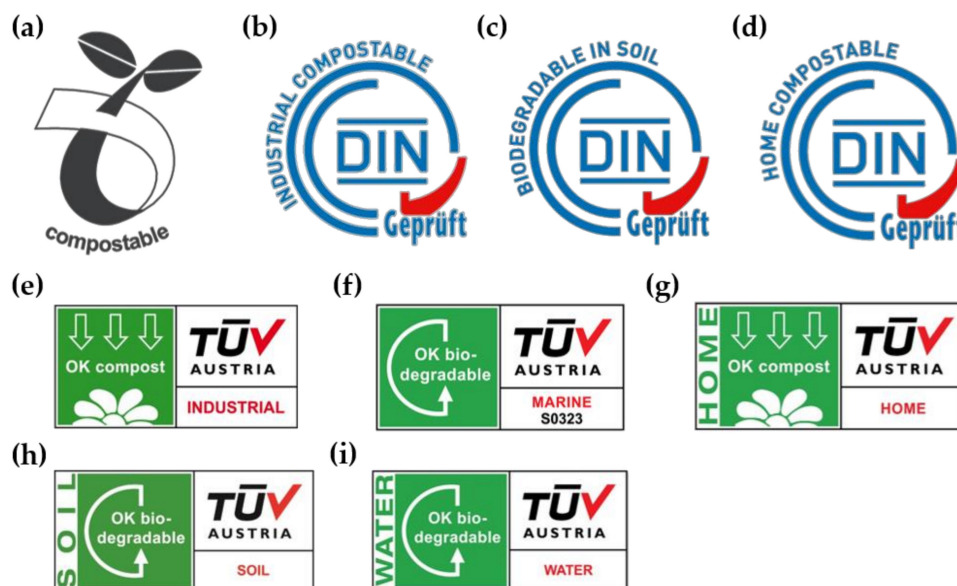


**Figure 1.** Certification labels relating to biodegradability and compostability: (a) seedling logo by *European Bioplastics*, indicates that the product is industrially compostable and complies with EN 13432; (b–d) DIN CERTCO labels for industrial compostability, biodegradability in soil and home compostability, respectively; (e–i) TÜV Austria labels for industrial compostability, marine biodegradability, home compostability, soil biodegradability and freshwater biodegradability, respectively.

### 2.3. Overview of Abiotic and Biotic Degradation Mechanisms

While the official definition of biodegradation is exclusively focused on the biotic phenomena, it is important to remember that abiotic phenomena take place during the biodegradation of a polymeric material, and these can have a strong influence on the overall degradation rate. We can identify three main steps through which biodegradation proceeds, with the process being susceptible to stop at each step [103,106–108].

During a first step referred to as biodeterioration, the material is broken down into smaller fractions due to biotic and abiotic activity. During this step a biofilm is formed on the surface of the material, consisting of a variety of microorganisms embedded in a matrix of water, proteins and polysaccharides produced by the same microorganisms [109,110]. The process of colonization of a polymeric surface by a microbial biofilm is referred to as fouling and follows different steps that lead to the settlement of bacteria and other microorganisms (microfouling) as well as larger organisms (macrofouling) such as larvae [110,111]. During and subsequently the biofilm formation, the microorganisms can infiltrate the surface porosity of the polymer which results in a change of the porous volume and potentially in cracks, furthermore this process facilitates water infiltration and consequentially hydrolysis. Additives and plasticizers can also leach out of the polymer during this step, resulting in embrittlement and rupture.

The microorganisms inhabiting the biofilm secrete enzymes that can be broadly defined as intracellular and extracellular depolymerase [28,101,103,106,110]. These enzymes are responsible for the second step in biodegradation, the depolymerization step, during which the polymer chains are broken down into shorter oligomers and eventually monomers, though this process can also result from abiotic phenomena which are covered later in this section.

The third step of biodegradation comprises of the assimilation and mineralization processes during which monomers and oligomers from the broken-down polymer can reach the cytoplasm and enter the metabolism of the microorganisms, therefore being converted to metabolites, energy and biomass, with the release in the environment gases, organic compounds and salts [106]. This step is of particular importance given that several standardized methodologies rely on the analysis of evolved CO<sub>2</sub> to evaluate biodegradability.

Abiotic degradation phenomena are involved either before or in concomitance with biotic degradation. Typical abiotic degradation phenomena are mechanical, thermal, UV, and chemical degradation.

Mechanical damage, both at macro and microscopical scale, can facilitate and accelerate other types of abiotic and biotic degradation, for example by increasing the available contact surface or creating defects that are easily attacked by chemical infiltration and more susceptible to heat damage.

Heat can further increase mechanical damage by lowering the mechanical properties of the polymer, e.g., if the plastic were to experience temperatures higher than its glass transition or melting temperature, its structural integrity would be quickly compromised under relatively low forces. Conversely, temperatures much lower than the glass transition might result in brittleness and rupture of the polymer. The loss of crystallinity, as well as the transition to the rubbery state, can also increase the permeability of biotic and abiotic agents in the polymeric matrix, therefore accelerating the degradation process. This is particularly important for polyesters, such as PLA, where the degradation process is strongly governed by hydrolysis reactions and therefore will proceed at a much faster rate when water can easily penetrate the polymeric network.

Chemical degradation includes oxidative phenomena due to molecular oxygen and is, therefore, one of the main factors in abiotic degradation. Oxidation often proceeds concomitantly with light degradation phenomena, leading to the formation of free radicals, ultimately decreasing the molecular weight by chain scission as well as causing crosslinking of the polymeric network which often leads to high brittleness. Hydrolysis is the other main factor acting during chemical degradation. Several bioplastics contain hydrolyzable covalent bonds, e.g., ester, ether, carbamide groups. Chemical degradation acts synergistically with all other degradation mechanisms. For example, oxidation and hydrolysis are facilitated by the polymer transitioning to the rubbery state and additionally losing its crystallinity due to exposure to relatively high temperatures.

UV-light degradation, or photodegradation, is also a very common occurrence in everyday life plastics. Photodegradation can typically lead to radicalization, resulting in chain scission and/or crosslinking, as already discussed these phenomena can be concomitant to oxidative degradation. Typically, photodegradation will result in the plastic material break down, which in turn increases the surface area available for biotic degradation to occur, and ultimately speeding up the biodegradation process. It can therefore be expected a large difference in biodegradation times depending on the plastic debris being exposed to sunlight or less; this could be the difference between a plastic bag floating at the sea surface against dense plastic debris sinking to deep-sea level.

### 3. Life Cycle Assessment of Bioplastics

The topic of bioplastics sustainability is very much debated in our society, both at the academic and institutional level. Life cycle assessment (LCA) is the main approach through which researchers and policymakers can investigate the benefits and drawbacks of using bioplastics in place of common plastics. LCA is a standardized methodology, with the prevalent standards being ISO 14,040 and ISO 14044, through which it is possible to analyze the environmental and socio-economic impacts related to the production and use of a certain good. There exist several LCA standards in use at the international level, as well as guidelines that are valid in the EU. The *Product Environmental Footprint* (PEF) and the *Organisation Environmental Footprint* (OEF) [112] are two methodologies compiled by the Joint Research Centre (JRC), the department of the EC focusing on scientific research. The

JRC also authored the technical report *Comparative Life Cycle Assessment (LCA) of Alternative Feedstock for Plastics Production* [113] which builds on the PEF providing scientific guidelines and modeling methodologies for an audience already expert in LCA. These guidelines are themselves based on ISO 14040 and ISO 14044. The two standards describe the various aspects of performing an LCA, from definitions and goals to its main phases of life cycle inventory analysis (LCI) and life cycle impact assessment (LCIA), respectively, the “data collection and calculation procedures to quantify relevant inputs and outputs of a product system” and the process through which the inventory data is associated with specific environmental impact categories [114]. Table 4 reports some of the main ISO and CEN standards relevant to the life cycle assessment of plastics and bioplastics, some of the standards are shared as the EN version is based on the ISO one. Among these standards, ISO 14040 and ISO 14044 are the main ones that define the principles and practices for LCA, providing the basic framework for the assessment but leaving a range of choices to the practitioners. Further guidance is provided by the International Reference Life Cycle Data System (ILCD) which consists of technical documents and a data network aimed at ensuring the validity and consistency of LCA. General definitions and aspects of bio-based plastics are also discussed by the CEN standard EN 17228, as well as in EN 16575 which represents a vocabulary for bio-based products.

The complete LCA of bioplastics needs to take into consideration several impact categories, of environmental, social and economic nature, as well as different options for the product EOL. Typically, this is not the case with most LCA research, as data on the entirety of a certain product’s life might be lacking or because of the intended motivation of the study not requiring assessing the whole life cycle. Depending on the system boundaries, we can identify two main approaches to the LCA of a product: the cradle-to-gate and the cradle-to-grave assessment [113,115,116]. Cradle-to-gate refers to an assessment from the resource extraction stage (cradle) to the factory gate, meaning at the end of production. For bio-based products this includes crops cultivation and biomass pre-processing, and in general, any transportation involved should be included. Additionally, eco-profile is a name in use to describe the cradle to factory gate life cycle inventory assessment of polymers and chemicals. Eco-profiles are used as building blocks in cradle-to-gate LCA studies and many can be found available on PlasticsEurope website [117] as well as on other databases (Sphera, GaBi, openLCA Nexus, SimaPro Industrial Database, Life Cycle Initiative).

The cradle-to-grave assessment takes into consideration the entire life cycle of the product, from the raw material extraction to the EOL management. This includes all aspects taken into consideration by the cradle-to-gate assessment and also the product’s retail, storage, its use by consumers and its disposal.

LCA needs to consider several impact categories and put them into comparable numbers depicting the potential influence on the environment, these categories are therefore standardized in their definitions and units in use [113,115,118,119]. Table 5 reports the main indicators in use for the different impact categories [118]. The global warming potential ( $GWP_{100}$ ) is the main parameter reported by LCA academic studies, it gives an indication of the amount of GHGs produced by the system under assessment and the effect on global warming. Several GHGs are released during the production and distribution of a certain good, each having a different potential for global warming, which is defined by the specific amount of infrared radiation the gas can absorb in the atmosphere. The  $GWP_{100}$  considers the overall global warming potential by converting each mass of gas emitted to the atmosphere, in the mass of equivalent  $CO_2$  that would absorb the same amount of energy. Furthermore, the GWP depends on the number of years over which the energy absorption is calculated. Typically, 100 years are considered, hence the subscript in  $GWP_{100}$ .

**Table 4.** List of CEN and ISO standards, technical reports and specifications, relevant to the life cycle assessment of bioplastics.

| Standard   | Title   |
|--|---|
| EN 17228:2019  | Plastics—Bio-based polymers, plastics, and plastics products—Terminology, characteristics and communication   |
| EN 16760:2015  | Bio-based products—Life Cycle Assessment  |
| EN 16751:2016  | Bio-based products—Sustainability criteria  |
| EN 16575:2014  | Bio-based products—Vocabulary   |
| EN 16640:2017  | Bio-based products—Bio-based carbon content—Determination of the bio-based carbon content using the radiocarbon method  |
| EN 17351:2020  | Bio-based products—Determination of the oxygen content using an elemental analyser  |
| CEN/TR 16957:2016  | Bio-based products—Guidelines for Life Cycle Inventory (LCI) for the End-of-life phase  |
| CEN/TR 16721:2014  | Bio-based products—Overview of methods to determine the bio-based content   |
| CEN/TR 17341:2019  | Bio-based products—Examples of reporting on sustainability criteria   |
| CEN/TR 16208:2011  | Biobased products—Overview of standards   |
| EN ISO 14040:2006  | Environmental management—Life cycle assessment—Principles and framework (ISO 14040:2006)  |
| EN ISO 14044:2006  | Environmental management—Life cycle assessment—Requirements and guidelines (ISO 14044:2006)   |
| EN ISO 14046:2016  | Environmental management—Water footprint—Principles, requirements and guidelines (ISO 14046:2014)   |
| EN ISO 14067:2018  | Greenhouse gases—Carbon footprint of products—Requirements and guidelines for quantification (ISO 14067:2018)   |
| ISO/TS 14072:2014  | Environmental management—Life cycle assessment—Requirements and guidelines for organizational life cycle assessment   |
| ISO/TS 14048:2002  | Environmental management—Life cycle assessment—Data documentation format  |
| ISO/TS 14071:2014  | Environmental management—Life cycle assessment—Critical review processes and reviewer competencies: Additional requirements and guidelines to ISO 14044:2006  |
| ISO 14045:2012   | Environmental management—Eco-efficiency assessment of product systems—Principles, requirements and guidelines   |
| ISO/TR 14069:2013  | Greenhouse gases—Quantification and reporting of greenhouse gas emissions for organizations—Guidance for the application of ISO 14064-1   |
| ISO 22526-1:2020<br>ISO 22526-2:2020<br>ISO 22526-3:2020   | Plastics—Carbon and environmental footprint of biobased plastics—Part 1: General principles—Part 2: Material carbon footprint, amount (mass) of CO <sub>2</sub> removed from the air and incorporated into polymer molecule—Part 3: Process carbon footprint, requirements and guidelines for quantification                  |
| ISO 16620-1:2015<br>ISO 16620-2:2019<br>ISO 16620-3:2015<br>ISO 16620-4:2016<br>ISO 16620-5:2017 | Plastics—Biobased content—Part 1: General principles—Part 2: Determination of biobased carbon content—Part 3: Determination of biobased synthetic polymer content—Part 4: Determination of biobased mass content—Part 5: Declaration of biobased carbon content, biobased synthetic polymer content and biobased mass content |

**Table 5.** Impact category indicators in use in life cycle assessment.

| Indicator   | Units                 | Description   |
|---|-----------------------|---|
| Global Warming Potential, GWP <sub>100</sub>        | kg CO <sub>2</sub> eq | Indicator of the potential global warming due to all greenhouse gas emissions over a period of 100 years; CO <sub>2</sub> as reference  |
| Ozone Depletion Potential, ODP                      | kg CFC-11 eq          | Indicator of the potential destruction of the stratospheric ozone layer due to emissions; freon-11 as reference   |
| Photochemical Ozone Creation Potential, POCP        | kg ethene eq          | Indicator of the photochemical ozone creation potential due to emission of gases; ethene as reference   |
| Acidification Potential, AP                         | kg SO <sub>2</sub> eq | Indicator of the potential acidification of water and soil due to emissions causing acid rain; sulphur dioxide as reference   |
| Eutrophication, EU                                  | kg PO <sub>4</sub> eq | Indicator of the over-supply of nutrients to the ecosystem due to the release of nitrogen and phosphorous containing compounds which leads to algae bloom; phosphate as reference |
| Human Toxicity, HT                                  | kg DCB eq             | Indicator of the impact on human health due to toxic substances release; 1,4-dichlorobenzene as reference   |
| Ecotoxicity, ET                                     | kg DCB eq             | Indicator of the impact on the ecosystem due to toxic substances release; 1,4-dichlorobenzene as reference  |
| Land Use, LU  | m <sup>2</sup>        | Indicator of the land in use by the system under assessment   |
| Water Use, WU                                       | m <sup>3</sup>        | Indicator of the water in use by the system under assessment  |
| Abiotic Resource Depletion, ADP                     | kg Sb eq              | Indicator of the depletion of non-living primary resources such as minerals and metals; antimony as reference   |
| Abiotic Resource Depletion–Fossil fuels, ADP-fossil | MJ                    | Indicator of the fossil energy consumed by the system under assessment  |

LCA studies typically take into consideration environmental impact categories, though also social and economic aspects are of great importance. Social life cycle assessment (S-LCA) looks at how the extraction or production of raw materials, and manufacturing, distribution, use and disposal of goods, can bring negative effects from a social point of view [20]. Life cycle costing (LCC) is also referred to as environmental LCC (E-LCC) [20] when applied in conjunction with LCA. E-LCC takes into account all costs that are involved with the product's life cycle, independently from the party incurring such costs. Environment-related cost factors are taken into consideration, such as ecological taxes and expenses for emissions control.

### 3.1. Life Cycle Assessment Research on Bioplastics

LCA research has already been reviewed in the past years, here we discuss some of the main findings.

In 2018 Spierling et al. [20] presented a review of cradle-to-gate LCA, S-LCA and LCC studies on different bioplastics, and focused their attention not only on the environmental impacts but also on the social and economic impact assessments. Assessing CO<sub>2</sub> emissions related to bio-sourced plastics, the authors underline that since bioplastics are often considered carbon-neutral, the data about carbon content and CO<sub>2</sub> uptake are often omitted. This lack of information leads to an imbalance in modeling, especially if the EOL stage is such that methane or GHGs other than CO<sub>2</sub> are released. The authors observed that many LCA studies did not provide information on important impact categories, such

as acidification, while mostly focusing on GWP and energy depletion. Land use is also reported by different studies, but other than reporting the square meters occupied no related impacts are considered. Overall, the authors could only compare the LCA studies on the GWP basis and estimate potential savings of 241–316 million tons of CO<sub>2</sub>-eq per year by replacing 65.8% of conventional plastics with bio-based ones. Still, the authors acknowledged several limitations and uncertainties and noted that the assessment of the use phase and EOL phase could strongly impact the results. Regarding S-LCA and LCC, the authors report the lack of studies and available data, though the authors could infer a high social risk potential when bioplastics' raw materials are produced in countries with weak legal standards.

In a 2020 review, Walker and Rothman [33] assess the comparative LCA of bio-based and fossil-based plastics, focusing on environmental LCA, cradle-to-grave, studies. The reviewed studies were checked for compliance with the EU PEF, though none of the studies completely met the document requirements. Partially complying papers were therefore selected; seven bio-based polymers and seven fossil-based polymers were compared across seven impact categories for which sufficient data were available. The authors report a lack of agreement between different studies, both for bio-based and fossil-based polymer assessments, with variations as high as 400% for the same impact category and same polymer. Negative values of CO<sub>2</sub> emissions were noted for bio-based systems due to the gas being absorbed during biomass growth. Like in Spierling et al., the authors note that this a controversial point as potential CO<sub>2</sub> or methane emissions during EOL are often not considered. Indeed, the authors underline that in cradle-to-grave studies several impact categories show far worse values than the ones in cradle-to-gate studies, which is due to the emissions and energy consumption during several EOL options. Furthermore, the authors notice that many studies on biodegradable polymers assumed composting as the EOL phase, though assuming incineration would significantly increase particulate emissions. Generally, the authors report similar values for most impact categories across fossil-based and bio-based systems. Finally, they conclude by commenting on the lack of comparability and standard methodologies in the field, stating that “without the ability to compare across studies, LCA has much lower relevance than it could or should have”.

In a recent review, Bishop et al. [34] also compared results from bio-based and fossil-based polymers LCA studies. Similar to the other works discussed, the authors found a lack of impact categories being covered as well as a lack of uncertainty analysis being carried out. Additionally, they noted that most studies did not account for the use of additives and their potential leakage in the environment and suggested that LCI should always include additives in use even if used in small quantities. In line with the other review already discussed, Bishop et al. note that the assumption of bio-based plastics being carbon-neutral can be misleading. In addition to the previous studies, they observe that biogenic CO<sub>2</sub> will spend a period of time in the atmosphere depending on the growth cycles of the biomass. While this might be negligible for fast-growing crops, it can become relevant with an increasing use of lignocellulosic-derived biomass which has long growth cycles. The authors underline that the worst approach to the assessment of bioplastics is to imply a large and permanent CO<sub>2</sub> uptake since most certainly this amount of gas will be released once again to the environment in the 100-year time horizon for which the GWP is typically calculated.

An important issue for bioplastics is their durability in service conditions, i.e., the ability of biopolymers to maintain unchanged the properties and performance in service. To be ensured unchanged properties, the biopolymers are usually added with appropriate stabilizing systems, such as synthetic antioxidants, UV-absorbers, quenchers [120] or naturally occurring molecules having protection actions [121–123]. All stabilizers can protect the biopolymers and improve the oxidative resistance in service conditions, making these materials suitable and durable. Interestingly, as documented, some natural antioxidants can exert concentration dependent anti-/pro-oxidant activity and, if they added at high concentrations, can exert pro-oxidant activity rather than protection action [124–126].

From what already discussed, one very important, though unfortunately overlooked, aspect of LCA is the assessment of the EOL phase. In the following section we report on research focused on the EOL of bioplastics.

### 3.2. End-of-Life Options for Bioplastics

The analysis of the EOL of a product is one of the most important parts of LCA, here we report some of the main research works focused on the topic.

In a 2013 review, Soroudi and Jakubowicz investigated the mechanical recycling of bioplastics and their blends [127]. The authors concluded that the performance and sustainability of recycled bioplastics could not be thoroughly understood given that research in the field was at a preliminary stage. They noticed that additives, such as compatibilizers, would need to be considered for the mechanical recycling of blends of bioplastics, because of the immiscibility of polymeric mixtures. They also noticed that biocomposites' mechanical properties often depend on the microstructure obtained during processing, for example, alignment of fiber fillers, which can be lost after recycling resulting in the loss of mechanical performance. They observe that chemical recycling, as an alternative to mechanical recycling, can be very costly, for example, the depolymerization of PLA requires high temperatures and therefore high energy expenditure. The authors observed that mechanical recycling of plastics with bioplastics might result in increased contamination, therefore affecting the performance of the recycled material.

In a 2016 paper, Cosate de Andrade et al. [128] presented an LCA of PLA comparing chemical recycling, mechanical recycling, and composting. The authors found that mechanical recycling had the least environmental impact, followed by chemical recycling and lastly composting when considering the climate change, human toxicity, and fossil depletion categories. In particular, it was observed that composting was outperformed as EOL option since it does not produce PLA or starting blocks for PLA, and therefore it will cause all the impact associated with producing virgin polymer again.

In a 2017 paper, Hottle et al. [24] investigate the EOL phase of several biopolymers and fossil-based polymers. The three EOL options taken into consideration are recycling, composting, and landfilling. As an important note, the paper takes into consideration the waste collection and transport stages. The two stages are required independently from the EOL option and can strongly influence the overall impact. The authors observed that the EOL stage greatly influences the overall sustainability assessment of a polymer life cycle. Recycling was found to be the most effective way to reduce environmental impacts for the drop-in plastics under assessment. Large, negative, values of GWP, ADP-fossil, and other impact categories are achieved through recycling of these polymers since the original raw material is bio-based (bioethanol) and because it is assumed that the recycled material offsets the fossil-based production of virgin polymers. A worst-case scenario for compostable polymers being landfilled is the uncontrolled release of methane following their biodegradation. In this case, the authors found that the GWP would drastically increase, particularly for PLA. On the other hand, composting would drastically reduce ODP, GWP, as well as eutrophication. Transportation, including international shipping, waste collection, intermediate handling, all largely contributed to higher GWP and ODP. Port-to-port shipping from California to recycling facilities in Hong Kong was considered and resulted in large increases in several impact categories.

In a 2020 review, Lamberti et al. [129] cover the recycling routes of several bio-based polymers. The authors observe that, generally, the best practice is to reuse any plastic as much as possible before recycling, then the plastic should be mechanically recycled until the resulting material is of commercially acceptable grade, finally, the plastic should be chemically recycled to recover part of the original monomers. For example, they observe that mechanical recycling of PLA results in a lower grade polymer that can be reused, though further recycling should be chemical. The authors report that chemical recycling of PLA through alcoholysis generates value-added products (different lactates depending on the alcohol), which can also be converted to lactide which can be directly polymerized

to high  $M_n$  PLA. Furthermore, bio-PET and bio-PE can be mechanically recycled multiple times before being chemically recycled. They identified glycolysis as the best chemical recycling option for bio-PET and pyrolysis as the one for bio-PE. The former results in value-added chemicals and in the least number of steps to polymerize back to PET, while the latter is the only route able to degrade PE resulting in valuable aromatics and fuel (gas and char). The authors conclude that biopolymers' mechanical performance needs to be improved and that better schemes for recycling and waste collection need to be put into place.

Anaerobic digestion is an appealing waste management route for compostable bioplastics. The process converts municipal organic waste to biogas (methane) and can incur the problem of plastic bags contamination. The use of bioplastic bags for municipal organic waste could therefore prove to solve the contamination problems while converting unavoidable plastic waste into energy.

In a 2018 review, Batori et al. [130] reported on the conditions needed for the effective anaerobic degradation of bioplastics. They noted that typical biogas plants operate with a solid retention time of 15 to 30 days and, therefore, bioplastic bags should be able to degrade in this time length. The authors found PBS to be not suitable for the application because the polymer does not degrade under the conditions in use at the plants, they reported that PLA, PCL and PVA do not sufficiently degrade in the time range, but they found PHB to be suitable. It was observed that more standardization for biodegradable bags suitable for organic waste collection is needed, and the authors suggest that the standards should require biodegradation greater than 50% over 1 month. It was pointed out that the plastic bags should also be able to withstand moisture until they reach the fermenter, a property that might not be common in many biodegradable plastics due to the presence of hydrophilic moieties. The authors observe that less resistant bioplastics might be still used and coated in a layer of water-resistant ones.

In the previously referenced work, Narancic et al. [14] tested several bioplastics and blends, observing that the majority would degrade by thermophilic anaerobic digestion with high biogas output. Still, the authors reported that the degradation times were 3 to 6 times longer than the retention times of commercial plants.

In 2018 Zhang et al. [131] reported on the anaerobic biodegradation of 9 bioplastics compliant with standard EN 13432. The plastics, together with organic waste, were fed daily to a digester for 177 days with a retention time of 50 days. The authors found that the digestion process was not inhibited but they also observed that only 4 cellulose-based materials showed substantial biodegradation.

Researchers have also taken into consideration the result of biodegradable plastics entering the recycling process of common plastics. Different research groups investigated the effect of small (5 wt%) amounts of PLA being mixed in the recycling process of PET [132–136]. The results showed that even small quantities of PLA will negatively affect the mechanical and thermal properties of recycled PET, which can cause technological and economic burdens. The main problems are due to the difference in thermal degradation temperatures, with PLA already degrading at the processing temperature of PET and causing yellowing of the product. The polymers are also immiscible, which can cause a lack of homogeneous surfaces, undesired opacity, and defects or failure during injection molding.

Currently published study deals about that the oxidation during burning of biopolymers and synthetic polymers can produce similar amount of  $\text{CO}_2$ . Therefore, a correct waste collection and management is required to solve the environmental troubles arising from the uncontrolled plastic use, release and accumulation of both petroleum-based polymers and bio-based polymers. The sustainable live vs. waste management of polymers and biopolymers depends on accurate end-of-life disposal of these materials and reduction of volumes of used plastics and bioplastics, maybe just articles having short service-life [137].



#### 4. Bioplastics: Summary of Opportunities and Possible Challenges

Table 6 presents a summary of possible advantages and disadvantages related to the adoption of bioplastics, as discussed in the available literature.

**Table 6.** Summary of potential advantages and disadvantages related to the adoption of bioplastics.

| Category                     | Description  |
|------------------------------|--|
| Advantages of bioplastics    | <p>Reducing fossil fuel dependency by using renewable resources, replacing existing plastics with bio-based counterparts (e.g., drop-in plastics)</p> <p>Potential environmental benefits in terms of GWP reduction</p> <p>The use of compostable plastics, in applications where organic contamination is expected, simplifies waste management and returns carbon to soil as compost</p> <p>Anaerobic digestion of biodegradable plastics can produce large specific energy and contribute to achieve an optimal ratio of carbon to nitrogen in the process</p> <p>Biodegradable plastics could replace non-degradable plastics in products that are likely to leak in the environment, potentially mitigating plastic pollution</p> |
| Disadvantages of bioplastics | <p>High production costs and, possibly, lower performance than common plastics</p> <p>Lack of processability with common technologies or lack of know-how</p> <p>Small market volume does not justify major investments nor redesign of production frameworks and waste manager infrastructure</p> <p>Possible feedstock competition with biofuel and food industry</p> <p>Risk of fouling of recycling streams with biodegradable plastics</p> <p>Risk of landfilling biodegradable plastics resulting in GHG emissions</p> <p>Lack of dedicated composting and recycling infrastructure and logistics</p> <p>Uncertainty regarding biodegradability in different open environments</p>   |

While it should be kept in mind that the volume of bioplastics in our economy is still too small to accurately predict all implications resulting from large-scale adoption, one point in favor of their adoption is that fossil resources are limited. The adoption of bio-based plastics can, therefore, prove to be an important way to decouple our economy from an unsustainable model.

Biodegradable plastics might also prove to be beneficial in mitigating some environmental risk scenarios where the leakage of plastics is not easily avoided, nor the use of plastic items can be effectively discontinued. For example, mulch films need to be collected and recycled at the end of their life-cycle. However, they are contaminated with soil and organic material which makes recycling procedures economically unviable. Furthermore, film fragments can accumulate in the soil, causing an environmental risk. Biodegradable mulch films have been on the market since the early 2000s, offering the same performance as common plastic ones, while being biodegradable in soil [138].

Compostable plastic bags for organic waste collection are already in use, which eliminates the need to separate the bag from the waste. Their use in anaerobic digestion facilities—if the material is designed to degrade within the retention time—can also lead to the production of renewable energy.

Figure 2 presents a simplified infographic representing the main steps in plastics linear economy and what the authors consider some important additional steps introduced by bioplastics in the circular economy. The linear economy route proceeds through the collection of resources, the production of plastic goods, their use, and their disposal. The circular economy route adds two important steps of repurposing of goods and recycling (mainly mechanical) to extend the life of the material as much as possible. Durable bio-based plastics, like drop-in plastics, can be recycled and their goods can be repurposed like common plastics. Compostable plastics would be used primarily as food waste collection bags and contribute to the production of biogas and compost in appropriate industrial

facilities. The compost would be used for agricultural purposes, including growing the raw materials for bioplastic production, and the biogas would provide energy, including energy for manufacturing processes. Bioplastic goods that are no longer recyclable would be incinerated to produce energy.

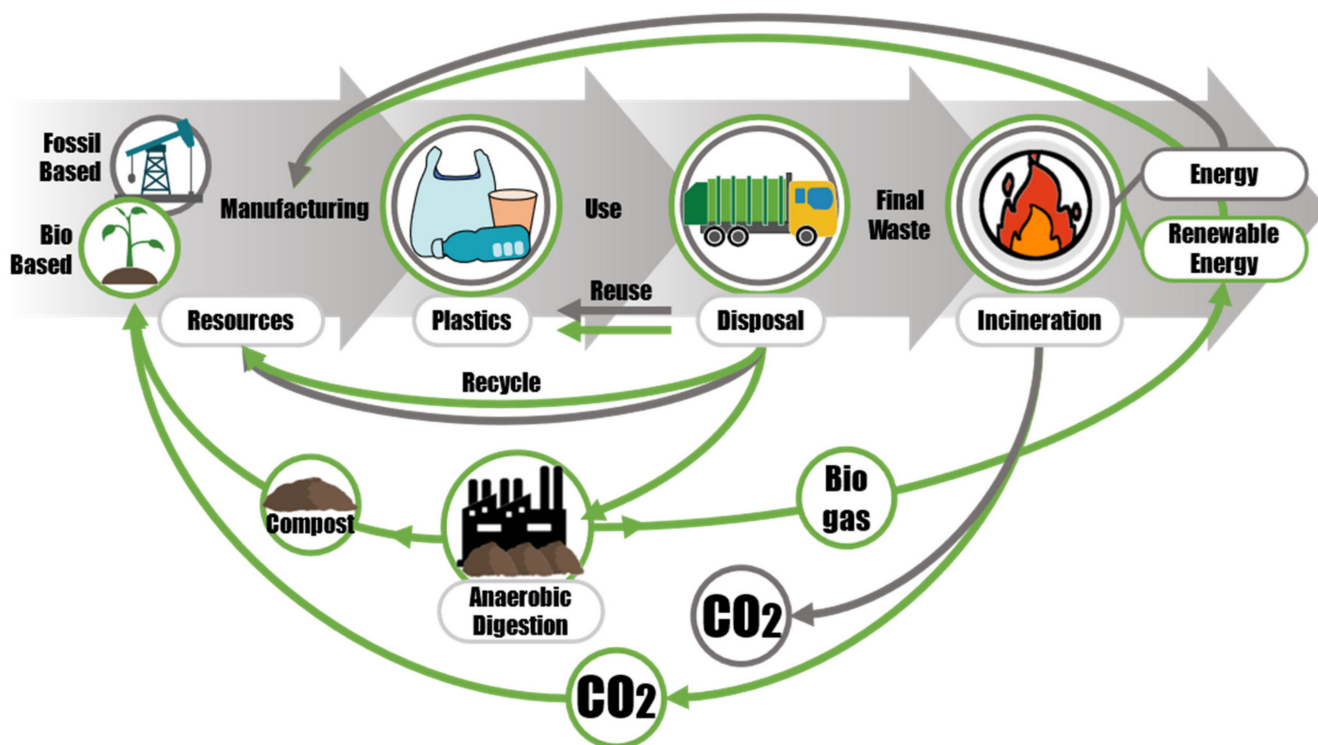


**Figure 2.** A simplified infographic representing the main steps in linear economy (straight arrows) and the additional steps introduced by circular economy with a focus on bioplastics (green arrows), considering anaerobic digestion as EOL option for compostable plastics, reuse and recycling for durable bio-based plastics and incineration as final disposal of any plastic that is no longer recyclable nor reusable.

The bioplastic industry is still very small in volume and relatively new, when compared to the common plastic industry, furthermore regulations about bioplastics have been changing in recent years. Therefore, it is understandable that several present and future challenges related to the adoption of bioplastics can be identified. In the following sections we review the challenges that can be identified from what discussed so far.

#### 4.1. Lack of Comparable LCA Studies

The use of different approaches and methodologies, as well as different reference units and data sources, strongly hinders the comparability of LCA studies. As already discussed, the use and EOL phases are often not taken into consideration, most assessments being cradle-to-gate. Yet, the EOL phase is shown to drastically influence the overall values of most impact categories. Studies that do not consider this stage can also come to the misleading conclusion that the production of a certain bio-based plastic completely removes GHGs from the atmosphere by converting CO<sub>2</sub> to biogenic carbon, while, depending on the EOL, stronger GHGs might be produced. The use of the same reference units is also important to compare different studies. LCA studies of specific products should consider a reference number of items produced. This approach is more comparable across different studies than using mass as reference, because not all polymers are converted to the same number of items per unit of mass.

Moving forward, studies should be thought-out to be comparable so that the overall significance of LCA could be ensured.

#### 4.2. Issues Relating to Standards and Regulations

In the last ten years, a lot of efforts have gone into the production of standards to define and evaluate compostability and biodegradability. While standards on industrial composting can reproduce the designed conditions of these facilities, standards for biodegradation in less controlled or uncontrolled conditions need more development. This is certainly the case for natural environments. Furthermore, home-composting conditions can be expected to vary greatly [139], even on a household-to-household basis. Since this is not an industrially regulated process, there is no confidence about the process conditions and the quality, concentration, and type of microorganisms in use. Additionally, independently from the adoption of bioplastics, home-composting also presents the risk of GHGs emissions [140,141] and therefore its sustainability might need a more thorough assessment.

One problem underlined in literature [35] is that many biodegradability standards require duplicates or at best triplicates of results. Triplicates are generally accepted in academia, where time and resources are often limited, and studies might be of a proof-of-concept nature. Still, the lack of reproducibility in academic studies is a serious topic of discussion [142]. Harmonized standards and official certifications have a great impact at international level and should represent the most reliable piece of information on a certain technical subject. Taking these considerations into account, the use of triplicates to assess statistical significance does not seem acceptable.

Finally, the scientific community, as well as regulatory agencies and certification companies, should consider the possibility that no standards will ever be able to encompass the diverse and dynamic conditions that are found in natural environments, and that producing standards claiming the opposite might mislead consumers on the actual environmental risks associated with plastic products.

#### 4.3. Land and Water Use

One concern that has been expressed is the possible competition between the production of raw materials for the bio-based industry and agricultural production. *European Bioplastics* reports that, in the foreseeable future, bioplastics production will account for less than 0.02% of global agricultural area usage and therefore does not compete with the production of food. On the other hand, a Greenpeace report noted that it is important to consider where the land is situated and if it is concentrated within a few regions [143]. Furthermore, the report offered its own calculation on the effect of replacing plastic packaging with PLA packaging. The calculation suggests that in doing so, 32% of global annual corn production would be needed to be diverted to PLA, accounting for 1% of available agricultural land.

Furthermore, the production of bioplastics requires considerable use of fresh water, due to crop cultivation, e.g., corn farming intended for PLA production [144]. Water footprint analysis of bio-based plastics production is not often carried out in LCA studies, though some alarming results suggest that replacing European packaging production with bioplastics, would increase the related use of water to almost one fifth of the EU's total freshwater withdrawal [18].

#### 4.4. Issues Related to the Waste Disposal System

Europe has been greatly developing its composting capacity ever since the Landfill Directive 1999/31/EC. Still, the distribution of composting facilities at the national level needs to be considered. Looking at the Italian case, there are more than 330 composting facilities at the national level, but most are concentrated in the North of Italy [145]. The result is that compostable waste from the Center and the South needs to be transferred to the North, with additional costs and fuel consumption. Furthermore, if the resulting compost were to be sold in the South the opposite process would need to take place. If we are to adopt larger and larger volumes of compostable plastics, we need to be sure that composting facilities can cover this increase in volume at the regional level.

Biodegradable plastics are designed to completely break down due to microbial action but are also susceptible to degradation phenomena such as hydrolysis and thermal degradation, which generally play an important role in the biodegradation rate. As discussed, contamination of biodegradable plastics in common plastic recycling streams would be detrimental to the properties of the recyclates. The separation and sorting of this additional stream can also be complex and expensive [135]. Therefore, with an increasing use of biodegradable plastics, a reorganization in the recycling framework will be required, as well as informing consumers on the correct way to dispose of such products.

## 5. Conclusions

European governments are working towards a zero-emission economy, decoupled from fossil resources, and focused on sustainability and circularity. Reforming the way plastic products are produced, handled, and disposed of, is an important part of this process. The adoption of bio-based plastics might surely come with risks (use of fertilizers, social risks, etc.) as well as advantages, what seems certain is that it offers an alternative to fossil-based production and might therefore become a necessity in the future. Compostable or biodegradable plastics might result in problems if not sorted out from recycling streams. Still, applications like compost bags offer benefits since bag and content can be co-digested eliminating the need for separation and producing energy and compost. Materials should be designed to ensure effective degradation without causing technological issues while retaining their mechanical properties during the “use” phase. The use of biodegradable plastics to mitigate environmental pollution due to leakage in open environments is another discussed advantage, currently, this seems overly optimistic. Conditions in natural environments are dynamic, they greatly change within geographic regions and seasons, furthermore, the size and density of the plastic debris, as well as agglomeration with other materials, can influence the outcome. Additionally, the economic loss from this plastic waste is not solved by using biodegradable alternatives. In this sense, stricter regulations, promoting an environmental-friendly mentality, and investing in sustainability-focused education at an early age could prove to be a more effective use of resources.

To conclude, it can be expected that the bioplastics industry will receive incentives to grow, develop new technologies and materials, and scale-up its production to greater volumes. Once larger productions are achieved and larger volumes of bioplastics are circulated, more assessment will be undoubtedly required to understand the sustainability of these materials. However, one thing to keep in mind moving forward is that most of the issue lies in our throw-away mentality. Replacing one plastic with another, without replacing the mentality, is not a solution.

**Author Contributions:** All authors listed have made substantial, direct, and intellectual contributions to this work and approved it for publication. All authors have read and agreed to the published version of the manuscript.

**Funding:** This work has been financially supported by MIUR—Italy (Ministry of Education, University and Research of Italy), Grant: CLEAN—PRIN-20174FSRZS\_002.

**Conflicts of Interest:** The authors declare no conflict of interest.

## References

1. European Commission. *The European Green Deal COM(2019) 640 Final*; European Commission: Brussels, Belgium, 2019.
2. European Commission. *A New Circular Economy Action Plan For a Cleaner and More Competitive Europe COM(2020) 98 Final*; European Commission: Brussels, Belgium, 2020.
3. United Nations Sustainable Development Knowledge Platform the 2030 Agenda for Sustainable Development. Available online: <https://sdgs.un.org/2030agenda> (accessed on 5 April 2021).
4. Peelman, N.; Ragaert, P.; De Meulenaer, B.; Adons, D.; Peeters, R.; Cardon, L.; Van Impe, F.; Devlieghere, F. Application of bioplastics for food packaging. *Trends Food Sci. Technol.* **2013**, *32*, 128–141. [CrossRef]
5. Pilla, S. (Ed.) *Handbook of Bioplastics and Biocomposites Engineering Applications*; John Wiley & Sons, Inc.: Hoboken, NJ, USA, 2011; ISBN 9781118203699.

6. George, A.; Sanjay, M.R.; Srisuk, R.; Parameswaranpillai, J.; Siengchin, S. A comprehensive review on chemical properties and applications of biopolymers and their composites. *Int. J. Biol. Macromol.* **2020**, *154*, 329–338. [CrossRef]
7. European Environment Agency. *The Circular Economy and the Bioeconomy—Partners in Sustainability*; European Environment Agency: Copenhagen, Denmark, 2018; ISBN 9789292139742.
8. Razza, F.; Briani, C.; Breton, T.; Marazza, D. Metrics for quantifying the circularity of bioplastics: The case of bio-based and biodegradable mulch films. *Resour. Conserv. Recycl.* **2020**, *159*. [CrossRef]
9. Barillari, F.; Chini, F. Biopolymers—Sustainability for the Automotive Value-added Chain. *ATZ Worldw.* **2020**, *122*, 36–39. [CrossRef]
10. Narancic, T.; Cerrone, F.; Beagan, N.; O'Connor, K.E. Recent advances in bioplastics: Application and biodegradation. *Polymers* **2020**, *12*, 920. [CrossRef]
11. Kaplan, D.L. Introduction to Biopolymers from Renewable Resources. In *Biopolymers from Renewable Resources*; Springer: Berlin/Heidelberg, Germany, 1998; pp. 1–29.
12. European Bioplastics. Bioplastics Market. Available online: <https://www.european-bioplastics.org/market/> (accessed on 1 November 2020).
13. European Commission. *A European Strategy for Plastics in a Circular Economy COM(2018) 28 Final*; European Commission: Brussels, Belgium, 2018.
14. Narancic, T.; Verstichel, S.; Reddy Chaganti, S.; Morales-Gamez, L.; Kenny, S.T.; De Wilde, B.; Babu Padamati, R.; O'Connor, K.E. Biodegradable Plastic Blends Create New Possibilities for End-of-Life Management of Plastics but They Are Not a Panacea for Plastic Pollution. *Environ. Sci. Technol.* **2018**, *52*, 10441–10452. [CrossRef] [PubMed]
15. Shen, L.; Worrell, E.; Patel, M.K. Open-loop recycling: A LCA case study of PET bottle-to-fibre recycling. *Resour. Conserv. Recycl.* **2010**, *55*, 34–52. [CrossRef]
16. Zhu, Y.; Romain, C.; Williams, C.K. Sustainable polymers from renewable resources. *Nature* **2016**, *540*, 354–362. [CrossRef]
17. Kawasaki, J.; Silalertruksa, T.; Scheyvens, H.; Yamanoshita, M. Environmental sustainability and climate benefits of green technology for bioethanol production in Thailand. *J. Int. Soc. Southeast Asian Agric. Sci.* **2015**, *21*, 78–95.
18. Brizga, J.; Hubacek, K.; Feng, K. The Unintended Side Effects of Bioplastics: Carbon, Land, and Water Footprints. *One Earth* **2020**, *3*, 45–53. [CrossRef]
19. Yates, M.R.; Barlow, C.Y. Life cycle assessments of biodegradable, commercial biopolymers—A critical review. *Resour. Conserv. Recycl.* **2013**, *78*, 54–66. [CrossRef]
20. Spierling, S.; Knüpffer, E.; Behnsen, H.; Mudersbach, M.; Krieg, H.; Springer, S.; Albrecht, S.; Herrmann, C.; Endres, H.J. Bio-based plastics—A review of environmental, social and economic impact assessments. *J. Clean. Prod.* **2018**, *185*, 476–491. [CrossRef]
21. Matsuura, E.; Ye, Y.; He, X. Sustainability opportunities and challenges of bioplastics. Master Thesis, School of Engineering, Blekinge Institute of Technology, Karlskrona, Sweden, 2008.
22. Hottle, T.A.; Bilec, M.M.; Landis, A.E. Sustainability assessments of bio-based polymers. *Polym. Degrad. Stab.* **2013**, *98*, 1898–1907. [CrossRef]
23. Álvarez-Chávez, C.R.; Edwards, S.; Moure-Eraso, R.; Geiser, K. Sustainability of bio-based plastics: General comparative analysis and recommendations for improvement. *J. Clean. Prod.* **2012**, *23*, 47–56. [CrossRef]
24. Hottle, T.A.; Bilec, M.M.; Landis, A.E. Biopolymer production and end of life comparisons using life cycle assessment. *Resour. Conserv. Recycl.* **2017**, *122*, 295–306. [CrossRef]
25. Bisinella, V.; Albizzati, P.F.; Astrup, T.F.; Damgaard, A. *Life Cycle Assessment of Grocery Carrier Bags*; Danish Environmental Protection Agency: Copenhagen, Denmark, 2018; pp. 1–144.
26. Rutkowska, M.; Krasowska, K.; Heimowska, A.; Steinka, I.; Janik, H. Degradation of polyurethanes in sea water. *Polym. Degrad. Stab.* **2002**, *76*, 233–239. [CrossRef]
27. Saygin, H.; Baysal, A. Degradation of sub- $\mu$ -sized bioplastics by clinically important bacteria under sediment and seawater conditions: Impact on the bacteria responses. *J. Environ. Sci. Health Part A* **2020**, *56*, 1–12. [CrossRef]
28. Tokiwa, Y.; Calabia, B.P.; Ugwu, C.U.; Aiba, S. Biodegradability of plastics. *Int. J. Mol. Sci.* **2009**, *10*, 3722–3742. [CrossRef]
29. Kale, G.; Auras, R.; Singh, S.P.; Narayan, R. Biodegradability of polylactide bottles in real and simulated composting conditions. *Polym. Test.* **2007**, *26*, 1049–1061. [CrossRef]
30. Accinelli, C.; Saccà, M.L.; Mencarelli, M.; Vicari, A. Deterioration of bioplastic carrier bags in the environment and assessment of a new recycling alternative. *Chemosphere* **2012**, *89*, 136–143. [CrossRef]
31. Babu, R.P.; O'Connor, K.; Seeram, R. Current progress on bio-based polymers and their future trends. *Prog. Biomater.* **2013**, *2*, 8. [CrossRef]
32. Nakajima, H.; Dijkstra, P.; Loos, K. The Recent Developments in Biobased Polymers toward General and Engineering Applications: Polymers that are Upgraded from Biodegradable Polymers, Analogous to Petroleum-Derived Polymers, and Newly Developed. *Polymers* **2017**, *9*, 523. [CrossRef]
33. Walker, S.; Rothman, R. Life cycle assessment of bio-based and fossil-based plastic: A review. *J. Clean. Prod.* **2020**, *261*, 121158. [CrossRef]
34. Bishop, G.; Styles, D.; Lens, P.N.L. Environmental performance comparison of bioplastics and petrochemical plastics: A review of life cycle assessment (LCA) methodological decisions. *Resour. Conserv. Recycl.* **2021**, *168*, 105451. [CrossRef]

35. Harrison, J.P.; Boardman, C.; O'Callaghan, K.; Delort, A.-M.; Song, J. Biodegradability standards for carrier bags and plastic films in aquatic environments: A critical review. *R. Soc. Open Sci.* **2018**, *5*, 171792. [CrossRef]
36. PlasticsEurope Plastics—The Facts. 2020. pp. 1–64. Available online: <https://www.plasticseurope.org/en/resources/publications/4312-plastics-facts-2020> (accessed on 1 November 2020).
37. Geyer, R.; Jambeck, J.R.; Law, K.L. Production, use, and fate of all plastics ever made. *Sci. Adv.* **2017**, *3*, 25–29. [CrossRef] [PubMed]
38. UNEP Web Page—Beat Plastic Pollution. Available online: <https://www.unep.org/interactive/beat-plastic-pollution/> (accessed on 1 November 2020).
39. European Commission. *Proposal for a Directive of the European Parliament and of the Council: On the Reduction of the Impact of Certain Plastic Products on the Environment COM(2018) 340 Final*; European Commission: Brussels, Belgium, 2018.
40. Lebreton, L.; Slat, B.; Ferrari, F.; Sainte-Rose, B.; Aitken, J.; Marthouse, R.; Hajbane, S.; Cunsolo, S.; Schwarz, A.; Levivier, A.; et al. Evidence that the Great Pacific Garbage Patch is rapidly accumulating plastic. *Sci. Rep.* **2018**, *8*, 4666. [CrossRef] [PubMed]
41. European Commission. *A Circular Economy for Plastics—Insights from Research and Innovation to Inform Policy and Funding Decisions*; European Commission: Brussels, Belgium, 2019; ISBN 9789279984297.
42. Gallo, F.; Fossi, C.; Weber, R.; Santillo, D.; Sousa, J.; Ingram, I.; Nadal, A.; Romano, D. Marine litter plastics and microplastics and their toxic chemicals components: The need for urgent preventive measures. *Environ. Sci. Eur.* **2018**, *30*, 13. [CrossRef] [PubMed]
43. UNEP. *Marine Litter Vital Graphics*; UNEP: Nairobi, Kenya, 2016; ISBN 9788277011530.
44. Gregory, M.R. Environmental implications of plastic debris in marine settings—Entanglement, ingestion, smothering, hangers-on, hitch-hiking and alien invasions. *Philos. Trans. R. Soc. B Biol. Sci.* **2009**, *364*, 2013–2025. [CrossRef] [PubMed]
45. Zettler, E.R.; Mincer, T.J.; Amaral-Zettler, L.A. Life in the “plastisphere”: Microbial communities on plastic marine debris. *Environ. Sci. Technol.* **2013**, *47*, 7137–7146. [CrossRef]
46. Andrady, A.L. Microplastics in the marine environment. *Mar. Pollut. Bull.* **2011**, *62*, 1596–1605. [CrossRef]
47. Rochman, C.M.; Tahir, A.; Williams, S.L.; Baxa, D.V.; Lam, R.; Miller, J.T.; Teh, F.-C.; Werorilangi, S.; Teh, S.J. Anthropogenic debris in seafood: Plastic debris and fibers from textiles in fish and bivalves sold for human consumption. *Sci. Rep.* **2015**, *5*, 14340. [CrossRef] [PubMed]
48. Smith, M.; Love, D.C.; Rochman, C.M.; Neff, R.A. Microplastics in Seafood and the Implications for Human Health. *Curr. Environ. Health Rep.* **2018**, *5*, 375–386. [CrossRef]
49. Dehaut, A.; Cassone, A.-L.; Frère, L.; Hermabessiere, L.; Himber, C.; Rinnert, E.; Rivière, G.; Lambert, C.; Soudant, P.; Huvet, A.; et al. Microplastics in seafood: Benchmark protocol for their extraction and characterization. *Environ. Pollut.* **2016**, *215*, 223–233. [CrossRef] [PubMed]
50. Ellen MacArthur Foundation. *The New Plastics Economy: Rethinking the Future of Plastics*; Ellen MacArthur Found: Cowes, UK, 2016; p. 120.
51. European Commission. *A Sustainable Bioeconomy for Europe: Strengthening the Connection between Economy, Society and the Environment*; European Commission: Brussels, Belgium, 2018; ISBN 9789279941450.
52. European Commission. *A European Strategy for Plastics in a Circular Economy*; European Commission: Brussels, Belgium, 2018.
53. Sander, M.; Filatova, T.; Weber, M. *Biodegradability of Plastics in the Open Environment*; ETH Zurich: Zürich, Switzerland, 2020; ISBN 9783982030180.
54. European Commission Directorate-General for Environment. *Plastic Waste in the Environment—Final Report*; European Commission: Brussels, Belgium, 2011; p. 171.
55. Garlotta, D. A Literature Review of Poly(Lactic Acid). *J. Polym. Environ.* **2001**, *9*, 63–84. [CrossRef]
56. Madhavan Nampoothiri, K.; Nair, N.R.; John, R.P. An overview of the recent developments in polylactide (PLA) research. *Bioresour. Technol.* **2010**, *101*, 8493–8501. [CrossRef] [PubMed]
57. Chanprateep, S. Current trends in biodegradable polyhydroxyalkanoates. *J. Biosci. Bioeng.* **2010**, *110*, 621–632. [CrossRef] [PubMed]
58. Xu, J.; Guo, B.H. Poly(butylene succinate) and its copolymers: Research, development and industrialization. *Biotechnol. J.* **2010**, *5*, 1149–1163. [CrossRef]
59. Siracusa, V.; Blanco, I. Bio-Polyethylene (Bio-PE), Bio-Polypropylene (Bio-PP) and Bio-Poly(ethylene terephthalate) (Bio-PET): Recent Developments in Bio-Based Polymers Analogous to Petroleum-Derived Ones for Packaging and Engineering Applications. *Polymers* **2020**, *12*, 1641. [CrossRef] [PubMed]
60. Labet, M.; Thielemans, W. Synthesis of polycaprolactone: A review. *Chem. Soc. Rev.* **2009**, *38*, 3484. [CrossRef]
61. Aslam, M.; Kalyar, M.A.; Raza, Z.A. Polyvinyl alcohol: A review of research status and use of polyvinyl alcohol based nanocomposites. *Polym. Eng. Sci.* **2018**, *58*, 2119–2132. [CrossRef]
62. Ferreira, F.V.; Cividanes, L.S.; Gouveia, R.F.; Lona, L.M.F. An overview on properties and applications of poly(butylene adipate-co-terephthalate)-PBAT based composites. *Polym. Eng. Sci.* **2019**, *59*, E7–E15. [CrossRef]
63. Auras, R.; Lim, L.-T.; Selke, S.E.M.; Tsuji, H. (Eds.) *Poly(Lactic Acid)*; John Wiley & Sons, Inc.: Hoboken, NJ, USA, 2010; Volume 53, ISBN 9780470649848.
64. Drumright, R.E.; Gruber, P.R.; Henton, D.E. Polylactic Acid Technology. *Adv. Mater.* **2000**, *12*, 1841–1846. [CrossRef]
65. Mehta, R.; Kumar, V.; Bhunia, H.; Upadhyay, S.N. Synthesis of poly(lactic acid): A review. *J. Macromol. Sci. Polym. Rev.* **2005**, *45*, 325–349. [CrossRef]

66. Pantani, R.; Sorrentino, A. Influence of crystallinity on the biodegradation rate of injection-moulded poly(lactic acid) samples in controlled composting conditions. *Polym. Degrad. Stab.* **2013**, *98*, 1089–1096. [CrossRef]
67. Perego, G.; Cella, G.D.; Bastioli, C. Effect of molecular weight and crystallinity on poly(lactic acid) mechanical properties. *J. Appl. Polym. Sci.* **1996**, *59*, 37–43. [CrossRef]
68. Auras, R.; Harte, B.; Selke, S. An Overview of Polylactides as Packaging Materials. *Macromol. Biosci.* **2004**, *4*, 835–864. [CrossRef] [PubMed]
69. Castro-Aguirre, E.; Iñiguez-Franco, F.; Samsudin, H.; Fang, X.; Auras, R. Poly(lactic acid)—Mass production, processing, industrial applications, and end of life. *Adv. Drug Deliv. Rev.* **2016**, *107*, 333–366. [CrossRef] [PubMed]
70. Cicala, G.; Giordano, D.; Tosto, C.; Filippone, G.; Recca, A.; Blanco, I. Polylactide (PLA) Filaments a Biobased Solution for Additive Manufacturing: Correlating Rheology and Thermomechanical Properties with Printing Quality. *Materials* **2018**, *11*, 1191. [CrossRef] [PubMed]
71. Meraldo, A. *Introduction to Bio-Based Polymers*; Elsevier Inc.: Amsterdam, The Netherlands, 2016; ISBN 9780323371001.
72. Bechthold, I.; Bretz, K.; Kabasci, S.; Kopitzky, R.; Springer, A. Succinic acid: A new platform chemical for biobased polymers from renewable resources. *Chem. Eng. Technol.* **2008**, *31*, 647–654. [CrossRef]
73. Gigli, M.; Fabbri, M.; Lotti, N.; Gamberini, R.; Rimini, B.; Munari, A. Poly(butylene succinate)-based polyesters for biomedical applications: A review. *Eur. Polym. J.* **2016**, *75*, 431–460. [CrossRef]
74. Aditiya, H.B.; Mahlia, T.M.I.; Chong, W.T.; Nur, H.; Sebayang, A.H. Second generation bioethanol production: A critical review. *Renew. Sustain. Energy Rev.* **2016**, *66*, 631–653. [CrossRef]
75. Vroman, I.; Tighzert, L. Biodegradable polymers. *Materials* **2009**, *2*, 307–344. [CrossRef]
76. Law, R.C. 5. Applications of cellulose acetate 5.1 Cellulose acetate in textile application. *Macromol. Symp.* **2004**, *208*, 255–266. [CrossRef]
77. Rustemeyer, P. 5.2 CA filter tow for cigarette filters. *Macromol. Symp.* **2004**, *208*, 267–292. [CrossRef]
78. Shibata, T. 5.6 Cellulose acetate in separation technology. *Macromol. Symp.* **2004**, *208*, 353–370. [CrossRef]
79. Fischer, S.; Thümmeler, K.; Volkert, B.; Hettrich, K.; Schmidt, I.; Fischer, K. Properties and applications of cellulose acetate. *Macromol. Symp.* **2008**, *262*, 89–96. [CrossRef]
80. Puls, J.; Wilson, S.A.; Höltzer, D. Degradation of Cellulose Acetate-Based Materials: A Review. *J. Polym. Environ.* **2011**, *19*, 152–165. [CrossRef]
81. Rose, M.; Palkovits, R. Cellulose-Based Sustainable Polymers: State of the Art and Future Trends. *Macromol. Rapid Commun.* **2011**, *32*, 1299–1311. [CrossRef]
82. Wang, S.; Lu, A.; Zhang, L. Recent advances in regenerated cellulose materials. *Prog. Polym. Sci.* **2016**, *53*, 169–206. [CrossRef]
83. Chen, J. Synthetic Textile Fibers. In *Textiles and Fashion*; Elsevier: Amsterdam, The Netherlands, 2015; pp. 79–95.
84. Liu, H.; Xie, F.; Yu, L.; Chen, L.; Li, L. Thermal processing of starch-based polymers. *Prog. Polym. Sci.* **2009**, *34*, 1348–1368. [CrossRef]
85. Zhang, Y.; Rempel, C.; Liu, Q. Thermoplastic Starch Processing and Characteristics—A Review. *Crit. Rev. Food Sci. Nutr.* **2014**, *54*, 1353–1370. [CrossRef] [PubMed]
86. Da Róz, A.L.; Carvalho, A.J.F.; Gandini, A.; Curvelo, A.A.S. The effect of plasticizers on thermoplastic starch compositions obtained by melt processing. *Carbohydr. Polym.* **2006**, *63*, 417–424. [CrossRef]
87. Lörcks, J. Properties and applications of compostable starch-based plastic material. *Polym. Degrad. Stab.* **1998**, *59*, 245–249. [CrossRef]
88. Santana, Á.L.; Angela, A.; Meireles, M. New Starches are the Trend for Industry Applications: A Review. *Food Public Health* **2014**, *4*, 229–241. [CrossRef]
89. Mohamad Yazid, N.S.; Abdullah, N.; Muhammad, N.; Matias-Peralta, H.M. Application of Starch and Starch-Based Products in Food Industry. *J. Sci. Technol.* **2018**, *10*. [CrossRef]
90. Samsudin, H.; Hani, N.M. Use of Starch in Food Packaging. In *Starch-Based Materials in Food Packaging*; Elsevier: Amsterdam, The Netherlands, 2017; pp. 229–256.
91. Rehm, B.H.A. Bacterial polymers: Biosynthesis, modifications and applications. *Nat. Rev. Microbiol.* **2010**, *8*, 578–592. [CrossRef] [PubMed]
92. Wang, Y.; Yin, J.; Chen, G.-Q. Polyhydroxyalkanoates, challenges and opportunities. *Curr. Opin. Biotechnol.* **2014**, *30*, 59–65. [CrossRef] [PubMed]
93. Lee, S.Y. Bacterial polyhydroxyalkanoates. *Biotechnol. Bioeng.* **2000**, *49*, 1–14. [CrossRef]
94. Reddy, C.S.K.; Ghai, R.; Kalia, V. Polyhydroxyalkanoates: An overview. *Bioresour. Technol.* **2003**, *87*, 137–146. [CrossRef]
95. Kathiraser, Y.; Aroua, M.K.; Ramachandran, K.B.; Tan, I.K.P. Chemical characterization of medium-chain-length polyhydroxyalkanoates (PHAs) recovered by enzymatic treatment and ultrafiltration. *J. Chem. Technol. Biotechnol.* **2007**, *82*, 847–855. [CrossRef]
96. Keshavarz, T.; Roy, I. Polyhydroxyalkanoates: Bioplastics with a green agenda. *Curr. Opin. Microbiol.* **2010**, *13*, 321–326. [CrossRef]
97. Hazer, B.; Steinbüchel, A. Increased diversification of polyhydroxyalkanoates by modification reactions for industrial and medical applications. *Appl. Microbiol. Biotechnol.* **2007**, *74*, 1–12. [CrossRef]
98. Chen, G.; Wang, Y. Medical applications of biopolyesters polyhydroxyalkanoates. *Chin. J. Polym. Sci.* **2013**, *31*, 719–736. [CrossRef]
99. ISO Online Browsing Platform. Available online: <https://www.iso.org/obp/ui#home> (accessed on 1 November 2020).

100. CEN Online Standards Search. Available online: <https://standards.cen.eu/dyn/www/f?p=CENWEB:105::RESET:::> (accessed on 1 November 2020).
101. Folino, A.; Karageorgiou, A.; Calabrò, P.S.; Komilis, D. Biodegradation of wasted bioplastics in natural and industrial environments: A review. *Sustainability* **2020**, *12*, 6030. [CrossRef]
102. Briassoulis, D.; Degli Innocenti, F. Standards for Soil Biodegradable Plastics. In *Soil Degradable Bioplastics for a Sustainable Modern Agriculture*; Springer: Berlin/Heidelberg, Germany, 2017; pp. 139–168.
103. Emadian, S.M.; Onay, T.T.; Demirel, B. Biodegradation of bioplastics in natural environments. *Waste Manag.* **2017**, *59*, 526–536. [CrossRef] [PubMed]
104. Ahn, H.K.; Huda, M.S.; Smith, M.C.; Mulbry, W.; Schmidt, W.F.; Reeves, J.B. Biodegradability of injection molded bioplastic pots containing polylactic acid and poultry feather fiber. *Bioresour. Technol.* **2011**, *102*, 4930–4933. [CrossRef] [PubMed]
105. Tabasi, R.Y.; Aiji, A. Selective degradation of biodegradable blends in simulated laboratory composting. *Polym. Degrad. Stab.* **2015**, *120*, 435–442. [CrossRef]
106. Lucas, N.; Bienaime, C.; Belloy, C.; Queneudec, M.; Silvestre, F.; Nava-Saucedo, J.E. Polymer biodegradation: Mechanisms and estimation techniques—A review. *Chemosphere* **2008**, *73*, 429–442. [CrossRef] [PubMed]
107. Haider, T.P.; Völker, C.; Kramm, J.; Landfester, K.; Wurm, F.R. Plastics of the Future? The Impact of Biodegradable Polymers on the Environment and on Society. *Angew. Chem. Int. Ed.* **2019**, *58*, 50–62. [CrossRef]
108. Fojt, J.; David, J.; Přikryl, R.; Řezáčová, V.; Kučerík, J. A critical review of the overlooked challenge of determining micro-bioplastics in soil. *Sci. Total Environ.* **2020**, *745*, 140975. [CrossRef] [PubMed]
109. Flemming, H.C. Relevance of biofilms for the biodeterioration of surfaces of polymeric materials. *Polym. Degrad. Stab.* **1998**, *59*, 309–315. [CrossRef]
110. Gu, J.D. Microbiological deterioration and degradation of synthetic polymeric materials: Recent research advances. *Int. Biodeterior. Biodegrad.* **2003**, *52*, 69–91. [CrossRef]
111. Pauli, N.-C.; Petermann, J.S.; Lott, C.; Weber, M. Macrofouling communities and the degradation of plastic bags in the sea: An in situ experiment. *R. Soc. Open Sci.* **2017**, *4*, 170549. [CrossRef] [PubMed]
112. European Commission Joint Research Centre. *EC-JRC Product Environmental Footprint (PEF) Guide*; European Commission Joint Research Centre: Brussels, Belgium, 2012; p. 154.
113. Nessi, S.; Bulgheroni, C.; Konti, A.; Sinkko, T.; Tonini, D.; Pant, R. *Comparative Life-Cycle Assessment of Alternative Feedstock for Plastics Production*; European Commission: Brussels, Belgium, 2020.
114. Technical Committee ISO/TC 207. ISO Environmental Management—Life Cycle Assessment—Principles and Framework (ISO 14040:2006). *Environ. Manag. Syst. Requir.* **2004**, *44*, 32.
115. European Commission—Joint Research Centre—Institute for Environment and Sustainability. *International Reference Life Cycle Data System (ILCD) Handbook—General Guide for Life Cycle Assessment—Detailed Guidance*; European Commission: Brussels, Belgium, 2010; ISBN 9789279190926.
116. Finkbeiner, M. Product environmental footprint—Breakthrough or breakdown for policy implementation of life cycle assessment? *Int. J. Life Cycle Assess.* **2014**, *19*, 266–271. [CrossRef]
117. PlasticsEurope PlasticsEurope Website—Eco-profiles. Available online: <https://www.plasticseurope.org/en/resources/eco-profiles> (accessed on 1 November 2020).
118. Hauschild, M.; Huijbregts, M.A.J. *Life Cycle Impact Assessment*; LCA Compendium—The Complete World of Life Cycle Assessment; Hauschild, M.Z., Huijbregts, M.A.J., Eds.; Springer: Dordrecht, The Netherlands, 2015; ISBN 978-94-017-9743-6.
119. European Commission—Joint Research Centre—Institute for Environment and Sustainability. *Characterisation Factors of the ILCD Recommended Life Cycle Impact Assessment Methods*; European Commission: Brussels, Belgium, 2012; ISBN 9789279227271.
120. Dintcheva, N.T.; La Mantia, F.P. Durability of a starch-based biodegradable polymer. *Polym. Degrad. Stab.* **2007**, *92*, 630–634. [CrossRef]
121. Dintcheva, N.T.; Infurna, G.; Baiamonte, M.; D’Anna, F. Natural compounds as sustainable additives for biopolymers. *Polymers* **2020**, *12*, 732. [CrossRef] [PubMed]
122. Dintcheva, N.; La Mantia, F.P.; Arrigo, R. Natural compounds as light stabilizer for a starch-based biodegradable polymer. *J. Polym. Eng.* **2014**, *34*, 441–449. [CrossRef]
123. Arrigo, R.; Morici, E.; Dintcheva, N.T. Biopolyester-based systems containing naturally occurring compounds with enhanced thermooxidative stability. *J. Appl. Biomater. Funct. Mater.* **2016**, *14*, e455–e462. [CrossRef]
124. Dintcheva, N.T.; Arrigo, R.; Baiamonte, M.; Rizzarelli, P.; Curcuruto, G. Concentration-dependent anti-/pro-oxidant activity of natural phenolic compounds in bio-polyesters. *Polym. Degrad. Stab.* **2017**, *142*, 21–28. [CrossRef]
125. Dintcheva, N.T.; Baiamonte, M.; Spera, M. Assessment of pro-oxidant activity of natural phenolic compounds in bio-polyesters. *Polym. Degrad. Stab.* **2018**, *152*, 280–288. [CrossRef]
126. Dintcheva, N.T.; D’anna, F. Anti-/pro-oxidant behavior of naturally occurring molecules in polymers and biopolymers: A brief review. *ACS Sustain. Chem. Eng.* **2019**, *7*, 12656–12670. [CrossRef]
127. Soroudi, A.; Jakubowicz, I. Recycling of bioplastics, their blends and biocomposites: A review. *Eur. Polym. J.* **2013**, *49*, 2839–2858. [CrossRef]
128. De Andrade, M.F.C.; Souza, P.M.S.; Cavalett, O.; Morales, A.R. Life Cycle Assessment of Poly(Lactic Acid) (PLA): Comparison Between Chemical Recycling, Mechanical Recycling and Composting. *J. Polym. Environ.* **2016**, *24*, 372–384. [CrossRef]



129. Lamberti, F.M.; Román-Ramírez, L.A.; Wood, J. Recycling of Bioplastics: Routes and Benefits. *J. Polym. Environ.* **2020**, *28*, 2551–2571. [CrossRef]
130. Bátori, V.; Åkesson, D.; Zamani, A.; Taherzadeh, M.J.; Sárvári Horváth, I. Anaerobic degradation of bioplastics: A review. *Waste Manag.* **2018**, *80*, 406–413. [CrossRef] [PubMed]
131. Zhang, W.; Heaven, S.; Banks, C.J. Degradation of some EN13432 compliant plastics in simulated mesophilic anaerobic digestion of food waste. *Polym. Degrad. Stab.* **2018**, *147*, 76–88. [CrossRef]
132. La Mantia, F.P.; Botta, L.; Morreale, M.; Scaffaro, R. Effect of small amounts of poly(lactic acid) on the recycling of poly(ethylene terephthalate) bottles. *Polym. Degrad. Stab.* **2012**, *97*, 21–24. [CrossRef]
133. Alaerts, L.; Augustinus, M.; Van Acker, K. Impact of bio-based plastics on current recycling of plastics. *Sustainability* **2018**, *10*, 1487. [CrossRef]
134. Gere, D.; Czigan, T. Future trends of plastic bottle recycling: Compatibilization of PET and PLA. *Polym. Test.* **2020**, *81*, 106160. [CrossRef]
135. Samper, M.D.; Bertomeu, D.; Arrieta, M.P.; Ferri, J.M.; López-Martínez, J. Interference of biodegradable plastics in the polypropylene recycling process. *Materials* **2018**, *11*, 1886. [CrossRef] [PubMed]
136. Cornell, D.D. Biopolymers in the existing postconsumer plastics recycling stream. *J. Polym. Environ.* **2007**, *15*, 295–299. [CrossRef]
137. Dintcheva, N.T.; Infurna, G.; D’Anna, F. End-of-life and waste management of disposable beverage cups. *Sci. Total Environ.* **2020**, 143044. [CrossRef] [PubMed]
138. Pellis, A.; Malinconico, M.; Guarneri, A.; Gardossi, L. Renewable polymers and plastics: Performance beyond the green. *N. Biotechnol.* **2021**, *60*, 146–158. [CrossRef]
139. IChemE. *The Institution of Chemical Engineers Standards for Bio-Based, Biodegradable, and Compostable Plastic: Call for Evidence—Consultation Response from the Institution of Chemical Engineers (IChemE)*; IChemE: London, UK, 2019; pp. 1–25.
140. Andersen, J.K.; Boldrin, A.; Christensen, T.H.; Scheutz, C. Greenhouse gas emissions from home composting of organic household waste. *Waste Manag.* **2010**, *30*, 2475–2482. [CrossRef]
141. Lim, S.L.; Lee, L.H.; Wu, T.Y. Sustainability of using composting and vermicomposting technologies for organic solid waste biotransformation: Recent overview, greenhouse gases emissions and economic analysis. *J. Clean. Prod.* **2016**, *111*, 262–278. [CrossRef]
142. Baker, M.; Penny, D. Is there a reproducibility crisis? *Nature* **2016**, *533*, 452–454. [CrossRef]
143. Jia, Z. *Biodegradable Plastics: Breaking Down the Facts—Production, Composition and Environmental Impact*; Green Peace East Asia: Hong Kong, China, 2020.
144. Korol, J.; Hejna, A.; Burchart-Korol, D.; Chmielnicki, B.; Wypiór, K. Water footprint assessment of selected polymers, polymer blends, composites, and biocomposites for industrial application. *Polymers* **2019**, *11*, 1791. [CrossRef]
145. CIC Raccolta dei Rifiuti Organici: In Italia Raggiunte le 6 Milioni di Tonnellate, ma Servono più Impianti. Available online: <https://www.compost.it/wp-content/uploads/2019/04/CS-1-2019-CIC.pdf> (accessed on 1 December 2020).

## Article

# Valorization of Aquatic Weed and Agricultural Residues for Innovative Biopolymer Production and Their Biodegradation

Prapaipan Ungprasoot<sup>1</sup>, Papasanee Muanruksa<sup>2</sup>, Varavut Tanamool<sup>3</sup>, James Winterburn<sup>4</sup>  
and Pakawadee Kaewkannetra<sup>2,5,\*</sup>

<sup>1</sup> Graduate School, Khon Kaen University, Khon Kaen 40002, Thailand; un\_prapaipan@kkumail.com

<sup>2</sup> Research Center for Environmental and Hazardous Substance Management (EHSM), Faculty of Engineering, Khon Kaen University, Khon Kaen 40002, Thailand; m.papasanee@kkumail.com

<sup>3</sup> Chemistry Program, Faculty of Science and Technology, Nakhon Ratchasima Rajabhat University, Nakhon Ratchasima 30000, Thailand; varavut.t@nrru.ac.th

<sup>4</sup> Department of Chemical Engineering and Analytical Science (CEAS), The University of Manchester, Manchester M13 9PL, UK; James.Winterburn@Manchester.ac.uk

<sup>5</sup> Department of Biotechnology, Faculty of Technology, Khon Kaen University, Khon Kaen 40002, Thailand

\* Correspondence: Pakawadee.kku@gmail.com

**Abstract:** In this work, water hyacinths, bagasse and rice straw were valorized to produce an innovative biopolymer. Serial steps of extraction, bleaching and conversion of cellulose to be carboxymethylcellulose (CMC) as well as the last steps of blending and molding were performed. The CMC was mixed with tapioca starch solution by a ratio of 9:18, and a plasticizer of glycerol was varied at 2%, 4% and 6% by volume. In addition, bioplastic sheets were further determined in their properties and biodegradation. The results revealed that bioplastics with 6% glycerol showed a high moisture content of 23% and water solubility was increased by about 47.94% over 24 h. The effect of temperature on bioplastic stability was found in the ranges of 146.28–169.25 °C. Furthermore, bioplastic sheets with 2% glycerol could maintain their shape. Moreover, for texture analysis, the highest elastic texture in the range of 33.74–38.68% with 6% glycerol was used. Moreover, bioplastics were then tested for their biodegradation by landfill method. Under natural conditions, they degraded at about 10.75% by weight over 24 h after burying in 10 cm soil depth. After 144 h, bioplastics were completely decomposed. Successfully, the application of water, weed and agricultural wastes as raw materials to produce innovative bioplastic showed maximum benefits for an environmentally friendly product, which could also be a guideline for an alternative to replace synthetic plastics derived from petroleum.

**Citation:** Ungprasoot, P.; Muanruksa, P.; Tanamool, V.; Winterburn, J.; Kaewkannetra, P. Valorization of Aquatic Weed and Agricultural Residues for Innovative Biopolymer Production and Their Biodegradation. *Polymers* **2021**, *13*, 2838. <https://doi.org/10.3390/polym13172838>

Academic Editor: Antonio Zuorro

Received: 25 June 2021

Accepted: 17 August 2021

Published: 24 August 2021

**Keywords:** valorization; water hyacinths; sugarcane bagasse; rice straw; biodegradation

**Publisher's Note:** MDPI stays neutral with regard to jurisdictional claims in published maps and institutional affiliations.



**Copyright:** © 2021 by the authors. Licensee MDPI, Basel, Switzerland. This article is an open access article distributed under the terms and conditions of the Creative Commons Attribution (CC BY) license (<https://creativecommons.org/licenses/by/4.0/>).

## 1. Introduction

Currently, the world is facing various environmental pollution problems. According to economic expansion, synthetic plastic derived from petroleum has increased because of its low cost of production and durability. However, it is disposed of in large quantities in the environment. Over the last 10 years in Thailand, the amount of synthetic plastic waste has increased by 2 million tons per year, and this waste has had a huge impact on the environment, is difficult to remove and cannot be decomposed naturally [1]. It could take up to 450 years to decay. Therefore, bioplastics can be a solution to these environmental problems. The raw materials used in production can be obtained from nature and have natural decomposition properties. Currently, bioplastics, made from a polymer of natural acids, are produced by microorganisms through the fermentation process. For instance, polyhydroxyalkanoates (PHAs), polyhydroxybutyrate (PHB), Polylactic acid (PLA), etc. Bioplastics can also be produced from aquatic weeds and agricultural wastes that can be obtained from agricultural residues, the wood industry and livestock waste. Most

of them are crops that can be rotated, planted and replaced in a short period of time, such as corncobs, sugarcane bagasse, cassava, rice straw, water hyacinth, palm bunch, etc. [2–4]. These waste materials are disposed of to decompose by influences from physical, chemical and biological factors. There are natural mechanisms for enzymatic or bacterial biodegradation under proper temperature and humidity. These natural decomposition products include water, biomass, methane and carbon dioxide, which are important for the growth and sustenance of plants.

Biomass waste is an environmentally friendly renewable resource. It is classified as a natural carbon source, which mainly contains cellulose, hemicellulose, lignin, chitin, ash and proteins. Thus, it is particularly suitable to be used as a precursor to prepare innovative carbon-based materials [5]. Recently, biocomposite plastic was developed by blending bioplastic with biomass. Previously, Rodion Kopitzky [6] studied cost effective bio-based plastic production by blending polylactic acid-polybutyrene with succinate-sugar beet pulp particles. In addition, cellulose-based composite material production was also reported by Sun et al. [7]. They used cellulose powder, which was obtained from filter paper pulp, as raw material for cellulose hydrogel production.

Thermoplastic starch (TPS) is an environmentally friendly plastic that can be produced from various natural resources. It provides an advantage in terms of cleaner production, because its production process does not depend on petroleum oil [8–10]. Typically, cassava starch is widely used as renewable material for starch-based plastic production at the industrial scale [11]. However, there are some limitations of TPS due to its poor mechanical properties, high moisture adsorption and unstable structure that is caused by relative humidity [12,13]. Accordingly, one popular strategy to increase the stability of TPS is blending starch with plasticizer. Glycerol is a plasticizer that has high ability to improve the mechanical properties of starch-based plastic [14,15]. Previously, Chen et al. [14] investigated the effect of glycerol on corn starch morphologies and the gelatinization process under warm temperature (65 °C). The results showed that the addition of glycerol to corn starch can enhance the strength of plastic, and starch gelatinization was postponed to higher temperatures. Another strategy that has been used is blending starch with fibers, nanofibers and synthetic polymers to overcome the problems of retrogradation and the poor mechanical properties of starch-based plastic [16–19].

Therefore, water weeds and agricultural waste including water hyacinth, sugarcane bagasse and rice straw were used as natural fiber resources to produce bioplastics that maximize the potential benefits. The carboxymethylcellulose, which was obtained from waste biomass via extraction techniques, acted as innovative material for bio-based plastic production. It was further blended with two bioplasticisers (starch and glycerol) in order to form biocomposite plastic. In addition, its biodegradable characteristic was also investigated by soil burial test. The target of this study was to generate bioplastic which can be naturally decomposed, leading to reduction of pollution from petroleum-based plastics. Finally, applications of biocomposite plastics were also evaluated from this characteristic.

## 2. Materials and Methods

### 2.1. Preparation of Raw Materials

Hyacinth, an aquatic weed, was collected from natural canals and water basins. It was washed with clean water to remove soil attached at its root. Then, it was cut to a size of about 1 × 1 cm and then dried by sunlight for 3 days. Meanwhile, agricultural wastes of sugarcane bagasse and rice straw were also collected from onsite at sugarcane farms and rice fields in Khon Kaen province and nearby provinces. The wastes were then sliced, cut and ground to a small size. Other chemicals used were of analytical grade and purchased from Merk Chemical Co., Ltd., Bangkok, Thailand.

### 2.2. Cellulose Extraction and Bleaching

All prepared raw materials, water hyacinth, sugarcane residue and rice straw, were extracted to obtain cellulose by adding the sample into 1 M sodium hydroxide (NaOH)

solution (15 times by weight of sample). Then, the pulp sample was heated on an electromagnetic stirrer at 90 °C for 30 min, and then it was filtered by thin white cotton cloth. The extracted cellulose was obtained. However, the cellulose sample was rinsed with clean water to remove sodium hydroxide solution until the pH of the sample reached 7. Finally, cellulose pulp obtained from water hyacinth, bagasse and rice straw was bleached with a mixed solution of 35% hydrogen peroxide, 2% sodium silicate and 0.05% magnesium sulphate by sample weight. The pulp pH was adjusted again to be pH 7.0 with one molar of NaOH and then heated at 90 °C for 20 min. The pulp cellulose sample was washed in triplication with clean water, before being dried in a hot air oven at 80 °C for 24 h.

### 2.3. Carboxymethylcellulose Synthesis

The bleached cellulose was converted to carboxymethylcellulose (CMC) by using a mixture solution of 18 g chloroacetic acid (C<sub>2</sub>H<sub>3</sub>ClO<sub>2</sub>) and 350 mL isopropyl alcohol (C<sub>3</sub>H<sub>8</sub>O) and heated by an electromagnetic stirrer at 40 °C for 30 min. Then another 50 mL of NaOH with 40% by volume was also added. The pulp solution was continuously stirred at 40 °C for 60 min. The beaker was sealed with aluminum foil and left in the hot air oven at 55 °C for 2 h 30 min until stratification occurred between the liquid and the cellulose sediment. The translucent part was poured and washed off the cellulose sediment with 70% methanol solution for 70 mL. The mixture was left for 10 min. To wash off the isopropyl alcohol solution, the supernatant was rinsed. Then, 70% ethyl alcohol solution at about 100 mL was added into the sediment. This step was repeated 5 times, pure ethyl alcohol was also added at about 200 mL, and the clear portion was discarded. The carboxymethylcellulose (CMC) precipitate was cured in a hot air incubator at 55 °C for 24 h.

### 2.4. Bioplastic Forming

The procedure method was modified from a previous study [20]. A synthetic CMC powder (9 g) was dissolved in 200 mL of distilled water and heated to 90 °C by an electromagnetic stirrer for 30 min. Subsequently, tapioca starch solution (18% *w/v*) was added and continuously heated for 20 min. Glycerol was added with varying concentrations of 2%, 4% and 6% by volume when all mixtures were of homogeneous viscous consistency. They were then poured into a mold of 90 × 15 mm<sup>2</sup> and dried with a hot air oven at 55 °C for 24 h.

### 2.5. Moisture Analysis

A bioplastic sample weighed approximately 100 g and was placed on an aluminum foil tray. The total weight was recorded ( $M_0$ ) and was then baked at 80 °C for 24 h. It was left to cool down in a desiccant chamber. The sample was weighed and the results recorded ( $M_1$ ), following the ASTM standard E104-02 [21]. The results of the moisture content analysis can be calculated from Equation (1) as follows:

$$\% \text{Moisture} = \frac{M_0 - M_1}{M_0} \times 100 \quad (1)$$

where:  $M_0$  = the total sample weight before drying, and  $M_1$  = the total sample weight after drying.

### 2.6. Water Solubility

A filter paper (Whatman No. 1) was prepared by drying in a hot air oven at 105 °C for 24 h. Then, it was cooled down in a desiccant chamber and weighed. Prior to use for filtration, the paper was soaked in distilled water. Meanwhile, a prepared bioplastic sample sheet (50 × 50 mm) was dried in a hot air oven at 65 °C for 24 h. Then, it was cooled down to obtain stable weight in a desiccant cabinet and weighed, and the results were recorded. The bioplastic sample sheets were immersed in 50 mL of distilled water, left at room temperature for 24 h while filtered with prepared paper, dried at 80 °C for 24 h

and kept to cool down (room temperature) in a desiccator. Both of them were weighed and recorded as  $W_0$  and  $W_1$ . The solubility analysis results from Equation (2) are shown as follows:

$$\text{Water Solubility (\%)} = \frac{W_0 - W_1}{W_0} \times 100 \quad (2)$$

where:  $W_0$  = total weight before testing, and  $W_1$  = total weight after testing.

### 2.7. Thermal Property

For thermal property, bioplastics were tested in their stability by using Differential Scanning Calorimeters (Shimadzu DSC-60A, Kyoto, Japan) [22]. In brief, 10 mg bioplastic sample was prepared and placed in an aluminum dish and packed into the designated position inside the Differential Scanning Calorimeters device (DSC). The initial temperature was set at 10 °C to the final temperature of 200 °C. The temperature increase rate was 5 °C/min using nitrogen gas flow rate of 20 mL/min. All thermal measurements were performed on single sample and used for comparative purposes against the control sample.

### 2.8. Texture Analysis

For texture analysis by texture analyzer (CT3 Texture Analyzer, AMETEK, Berwyn, PA, USA), a bioplastic sample (3 cm × 5 cm) was cut, and then it was attached to the head and tail clamping arms of the machine. The velocity of the stretch probe was set at about 1.00 mm/s. The velocity of probe returning was set at 10.00 mm/s, while distance of the probe was touched at the point of impact (20.00 mm/s) milli. Then, stretch value of the texture and strength of the object were measured and recorded.

### 2.9. Biodegradation of Bioplastics

For biodegradation property test, 5 × 5 cm<sup>2</sup> bioplastic samples were dried at 55 °C in hot air oven for 24 h and then were kept in desiccant chamber until achieving stable weight. The biodegradation test was started by burying the sample in 10 cm deep soil. The samples were weighed and recorded as sample coded as  $D_0$ . The sample, hereafter named as  $D_1$ , was withdrawn from the soil and cleaned once a day. The steps were repeated the same as the  $D_0$  sample explained above. The sample's weight loss over time was utilized to determine the biodegradation test in soil. The degradation rate in terms of percentage was calculated using Equation (3):

$$\text{Degradation Rate (\%)} = \frac{D_0 - D_1}{D_0} \times 100 \quad (3)$$

where:  $D_0$  = total weight before testing, and  $D_1$  = total weight after testing.

## 3. Results and Discussion

### 3.1. Chemical Composition of Bioplastics

Chemical composition analysis of raw materials was measured by the fiber analysis technique (Detergent analysis) using a spectrophotometer. The quantitative analysis of cellulose, hemicellulose and lignin was detected. It was found that water hyacinth, sugarcane residue and rice straw at 100 g contained the quantitative cellulose of 40.33%, 48.59% and 47.10%, respectively (Figure 1). Cellulose pulp was extracted with NaOH solution and was bleached with a solution of hydrogen peroxide. Synthesis of carboxymethylcellulose was done with chloroacetic acid. For bioplastic forming, tapioca starch solution and glycerol were used as a binder at concentrations of 2%, 4% and 6% by volume as additive substances.

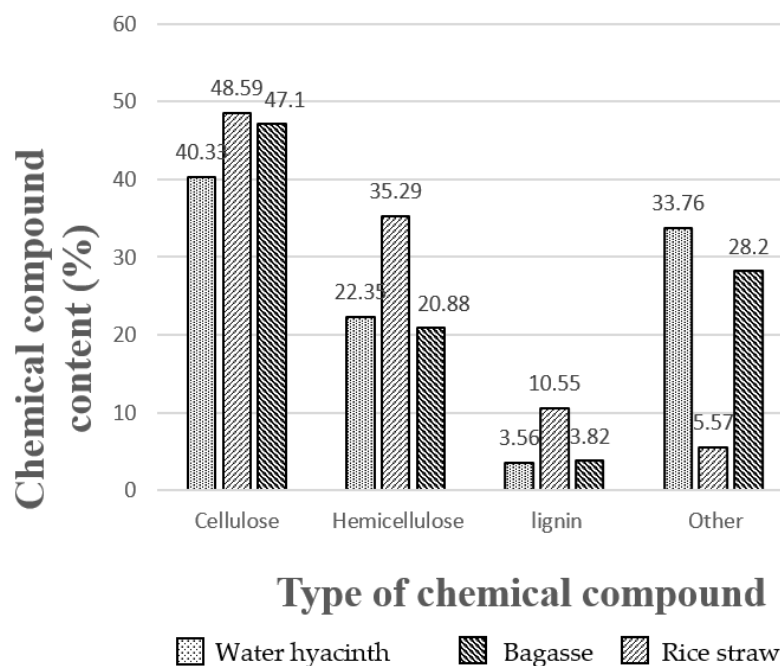


**Figure 1.** Chemical compositions of three different raw materials.

### 3.2. Texture Analysis

Texture properties of bioplastics with variable glycerol concentration show that when bioplastics had a high glycerol concentration of 6% by volume, it was found that at an average tensile strength in the range of 8–50 newtons, bioplastics from water hyacinth, sugarcane bagasse and rice straw showed a higher resilience rate of glycerol. The highest objects were 38.68%, 35.37% and 33.74%, respectively. Unlike bioplastics with low glycerol concentration at 2% by volume, it was found that bioplastics had low material resilience characteristics, and tearing easily accounted for 25.17%, 27.97% and 21.60%, respectively, from the texture analysis of all three types of bioplastics. It was shown that glycerol added to bioplastic samples showed additive properties and increased flexibility in bioplastic samples.

### 3.3. Thermal Property

The thermal characterization was completed by DSC experiments, the results of which are depicted in Figures 2 and 3. It should be noted that the DSC results were shown only for 2 and 6% glycerol concentrations. For temperature analysis affecting the stability of bioplastics obtained from water hyacinth, sugarcane bagasse and rice straw, it was determined in terms of the melting point ( $T_m$ ) of the samples. It was found that when glycerol concentrations by volume were varied at 2, 4 and 6%, the maximal melting point in each sample was reached at 146.28 °C, 169.25 °C and 159.78 °C, respectively. Unlike bioplastics that were blended with 6% glycerol, the lowest melting points were 141.81, 145.74 and 146.08 °C, respectively, due to an increase in the moisture content of the samples caused by the insertion of the glycerol molecule in the bioplastic structure. Previously, the literature [5,6] reported that cellulosic bioplastic can be degraded at high temperatures (190–275 °C). According to results obtained in this work, the samples might easily lose their shapes at low temperatures and provide an environmentally friendly characteristic.

### 3.4. Water Solubility

Water solubility was determined to evaluate the effect on the decomposition of bioplastics derived from water hyacinth, bagasse and rice straw. It was found that water could absorb into all kinds of samples when 2%, 4% and 6% glycerol concentrations were used as shown in Table 1. Some physical changes in the samples were clearly observed

such as swelling, deterioration and loss of morphological stability within 24 h, which was caused by the mixture of carboxymethylcellulose powder and tapioca starch. The starch powder, one of components in the bioplastic sample, showed good water solubility as glycerol concentrations increased up to 6%. Water solubility of 47.94% was found in accordance with the absorption properties of glycerol, though the samples could have absorbed moisture from the atmosphere. In addition, the sample sheet became soft and easy to decompose in a short time.

### 3.5. Moisture Analysis

The disadvantages of using glycerol as an additive in bioplastic samples at different concentrations resulted in high moisture content in all three bioplastic samples because glycerol is a hydrophobic compound that also has good absorbent properties in the atmosphere. Bioplastic samples from water hyacinth, sugarcane bagasse and rice straw with variable glycerol concentration at 2% by volume showed the lowest moisture content of 9.76%, 10.33% and 9.08%, respectively (see Figure 4). When the glycerol concentration used as an additive was increased to 6% by volume, all of the samples showed an increase in moisture content at 23%, 18.45% and 19.33%, respectively. Subsequently, it also caused more moisture absorption in the atmosphere.

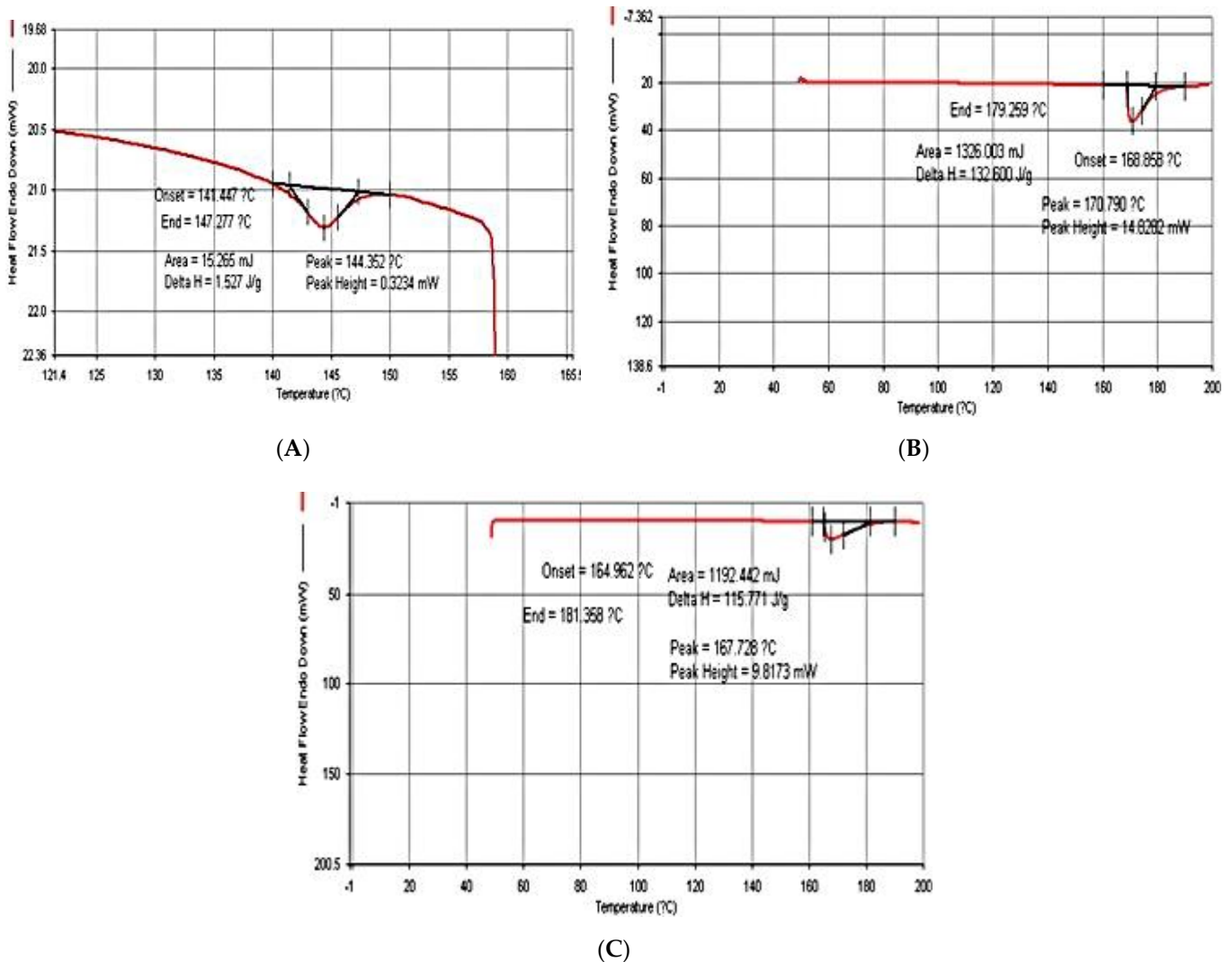


Figure 2. Bioplastic blended with 2% glycerol: (A) water hyacinth; (B) sugarcane bagasse; (C) rice straw.

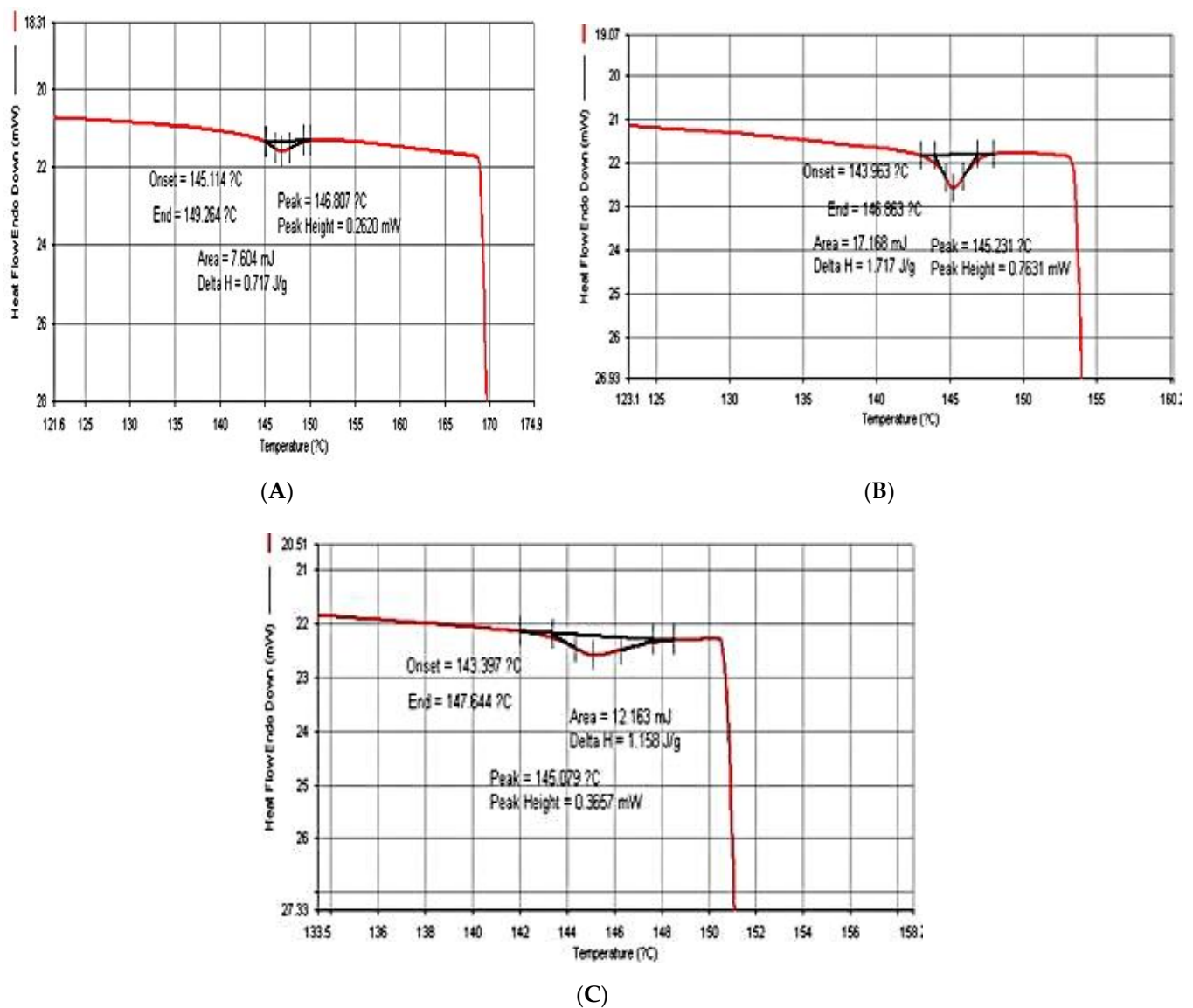


Figure 3. Bioplastic blended with 6% glycerol: (A) water hyacinth; (B) sugarcane bagasse; (C) rice straw.

Table 1. Water solubility of bioplastic derived from water hyacinths, sugarcane bagasse and rice straw.

| Type of Bioplastic | Rate of Water Solubility (%)  |       |       |
|--------------------|-------------------------------|-------|-------|
|                    | Glycerol Concentration (%v/v) |       |       |
|                    | 2                             | 4     | 6     |
| Water hyacinth     | 17.26                         | 31.31 | 40.37 |
| Bagasse            | 29.99                         | 37.91 | 47.94 |
| Rice straw         | 26.37                         | 32.84 | 41.76 |



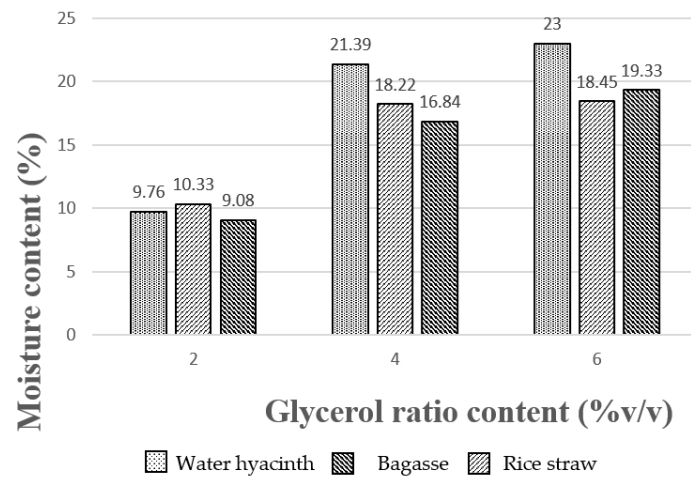


Figure 4. Moisture content of bioplastics obtained from three different raw materials.

### 3.6. Soil Burial Test

Biodegradation of bioplastic samples from water hyacinth, sugarcane residue and rice straw by the landfill method was investigated under a natural environment. However, the burial test results were shown only for 6% glycerol concentration (see Figures 5–7). The results showed that the physical appearance of the samples started biodegrading after 24 h. At 2% glycerol concentration, the degradation rate of bioplastic derived from water hyacinth, sugarcane residue and rice straw was 10.29%, 22.38% and 54.99%, respectively. They were continuously buried up to 120 h. Surprisingly, all of them were found to decompose completely, and no parts were present. This was perhaps caused by various microorganisms, such as soil fungi, which are starch-digesters, turning it into sugar for their growth. On the other hand, bioplastics blended with high glycerol concentration (4–6% glycerol concentrations) required 144 h to be completely degraded in the soil. These results agreed with a previous study [20], which investigated the biodegradation of biocomposite plastic via the soil burial method. The bioplastic sample was made from water hyacinth, starch and glycerol. It was found that 5% glycerol-added biocomposite samples showed a significant weight loss after 15 days, while 20% glycerol-added biocomposite samples presented lower weight loss and took more time for decomposition. This was due to starch and glycerol preventing the decomposition process catalyzed by microorganisms in the soil.

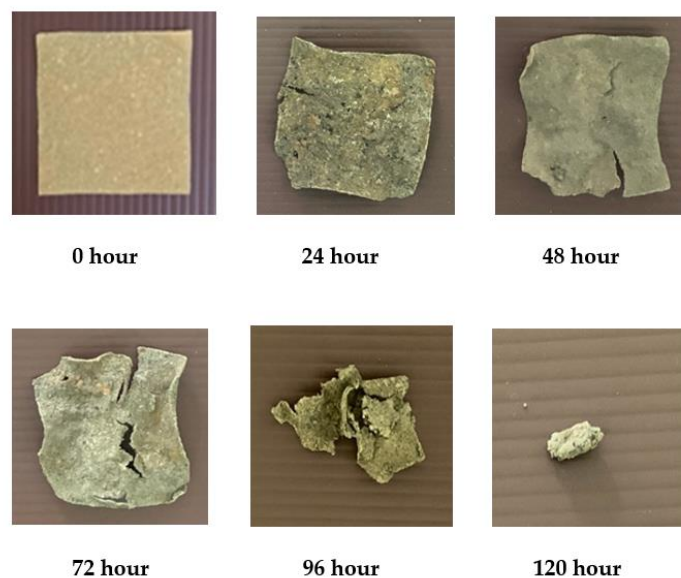


Figure 5. Burial test of bioplastic derived from water hyacinth at 6% glycerol.

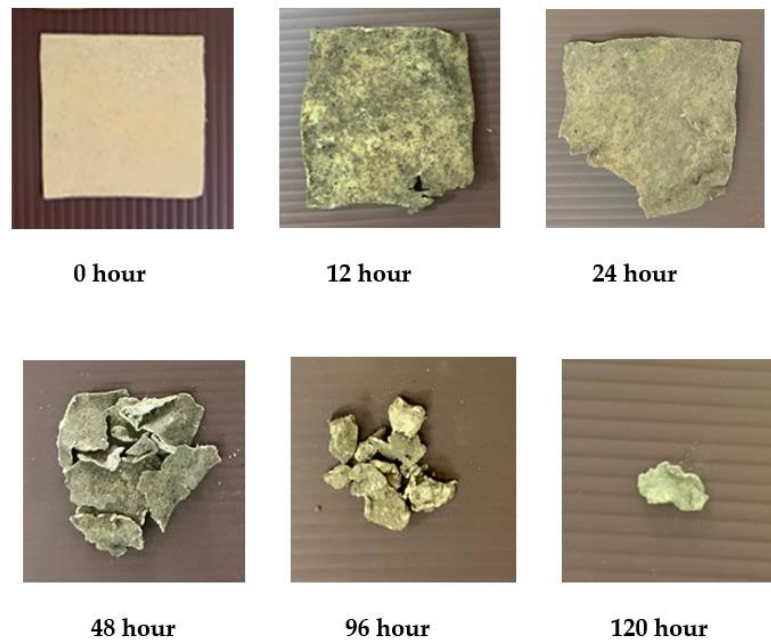


Figure 6. Burial test of bioplastic derived from sugarcane bagasse at 6% glycerol.

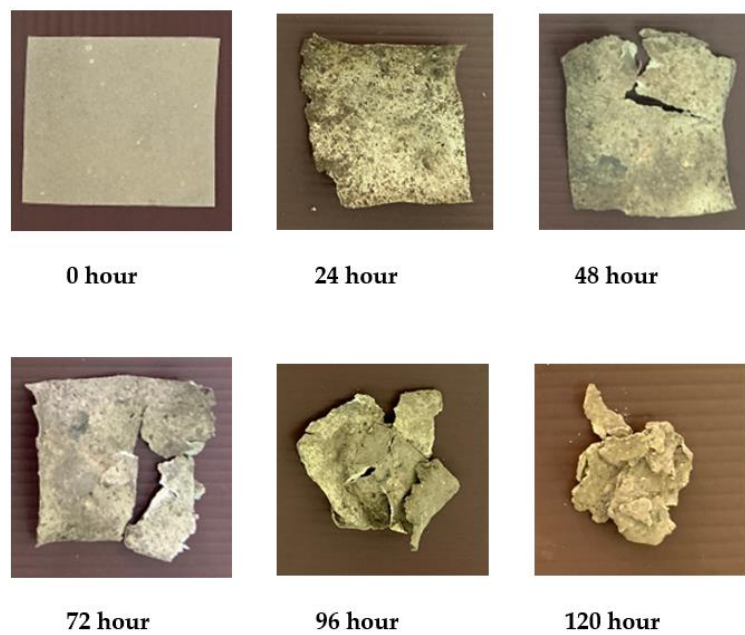


Figure 7. Burial test of bioplastic derived from rice straw at 6% glycerol.

#### 4. Conclusions

Successfully, water hyacinth, sugarcane residue and rice straw are capable as raw materials to convert into carboxymethylcellulose (CMC) and then use for biopolymer production, using tapioca starch solution and glycerol as a binder and an additive. The samples of biopolymer produced were characterized and showed the qualities of a synthetic plastic: an average texture tensile strength of 8 to 50 newtons, the highest flexibility at 38.68% and a melting point of 169.25 °C. In addition, for the decomposition test by water solubility, biopolymers showed an ability to decompose within 24 h after burying them at a 10 cm depth in a landfill for 144 h. Therefore, the biopolymers produced showed good properties such as flexibility, heat resistance and biodegradation. They have high potential and can be an alternative material to develop into food and drink packaging that is safe for humans and is also an environmentally friendly product.

**Author Contributions:** This article was performed as collaborative research among P.U., P.M., V.T., J.W. and P.K.; conceptualization, methodology, resources, data curation, visualization and writing—original draft preparation, P.U. and P.M.; software and formal analysis, V.T.; validation and investigation, J.W.; supervision, project administration, funding acquisition, review and corrections, P.K. All authors have read and agreed to the published version of the manuscript.

**Funding:** This research was mainly funded by the National Research Council of Thailand (NRCT), Bangkok, Thailand, for postgraduate (P. Ungprasoot), as well as co-funded by the Centre of Environmental Hazardous Substance Management (EHSM), Faculty of Engineering, Khon Kaen University, Khon Kaen, Thailand (P. Maunraksa, V. Tanamool and P. Kaewkannetra), and the Newton Fund for Institutional Links, British Council, London, UK (J. Winterburn and P. Kaewkannetra).

**Institutional Review Board Statement:** Not applicable.

**Informed Consent Statement:** Not applicable.

**Data Availability Statement:** The data that support the findings of this study are available from the corresponding author upon reasonable request.

**Acknowledgments:** All authors would like to sincerely thank and gratefully acknowledge all sponsors: the NRCT, Bangkok, Thailand; the EHSM, Khon Kaen University, Khon Kaen, Thailand; and The Newton Fund, London, UK.

**Conflicts of Interest:** The authors declare no conflict of interest.

## References

- Zhao, W.; An, L.; Wang, S. Recyclable high-performance epoxy-anhydride resins with DMP-30 as the catalyst of transesterification reactions. *Polymers* **2021**, *13*, 296. [CrossRef] [PubMed]
- Randrianarison, G.; Ashraf, M.A. Microalgae: A potential plant for energy production. *Geol. Ecol. Landsc.* **2017**, *1*, 104–120. [CrossRef]
- Venkatesan, J.; Anil, S.; Kim, S.K.; Shim, M.S. Seaweed polysaccharide-based nanoparticles: Preparation and applications for drug delivery. *Polymers* **2016**, *8*, 30. [CrossRef] [PubMed]
- Venkatesan, J.; Anil, S.; Kim, S.K. *Seaweed Polysaccharides: Isolation, Biological and Biomedical Applications*, 1st ed.; Elsevier Publications: Amsterdam, The Netherlands, 2017; ISBN 9780128098172.
- Del Sole, R.; Mele, G.; Bloise, E.; Mergola, L. Green Aspects in Molecularly Im-printed Polymers by Biomass Waste Utilization. *Polymers* **2021**, *13*, 2430. [CrossRef] [PubMed]
- Kopitzky, R. Poly(Lactic Acid)–Poly(Butylene Succinate)–Sugar Beet Pulp Composites; Part I: Mechanics of Composites with Fine and Coarse Sugar Beet Pulp Particles. *Polymers* **2021**, *13*, 2531. [CrossRef] [PubMed]
- Sun, L.; Li, L.; An, X.; Qian, X. Nano-Metal Organic Framework for Enhanced Mechanical, Flame Retardant and Ultraviolet-Blue Light Shielding Properties of Trans-parent Cellulose-Based Bioplastics. *Polymers* **2021**, *13*, 2433. [CrossRef] [PubMed]
- Correa, A.C.; Carmona, V.B.; Simão, J.A.; Capparelli, L.H.; Marconcini, J.M. Biodegradable blends of urea plasticized thermoplastic starch (UTPS) and poly( $\epsilon$ -caprolactone) (PCL): Morphological, rheological, thermal and mechanical properties. *Carbohydr. Polym.* **2017**, *167*, 177–184. [CrossRef] [PubMed]
- Ortega-Toro, R.; Contreras, J.; Talens, P.; Chiralt, A. Physical and structural properties and thermal behaviour of starch-poly( $\epsilon$ -caprolactone) blend films for food packaging. *Food Packag. Shelf Life* **2015**, *5*, 10–20. [CrossRef]
- Ortega-Toro, R.; Santagata, G.; Gomez, G.; Cerruti, P.; Talens, P.; Chiralt, A.; Ma-linconico, M. Enhancement of interfacial adhesion between starch and grafted poly( $\epsilon$ -caprolactone). *Carbohydr. Polym.* **2016**, *147*, 16–27. [CrossRef] [PubMed]
- Tappibana, P.; Smith, D.; Triwitayakornb, K.; Bao, J. Recent understanding of starch biosynthesis in cassava for quality improvement: A review. *Trends Food Sci. Technol.* **2019**, *83*, 167–180. [CrossRef]
- Fekete, E.; Bella, É.; Csiszár, E.; Móczó, J. Improving physical properties and retrogradation of thermoplastic starch by incorporating agar. *Int. J. Biol. Macromol.* **2019**, *136*, 1026–1033. [CrossRef] [PubMed]
- Nguyen, H.; Lumdubwong, N. Fabrication of starch blend films with different matrices and their mechanical properties. *Polym. Test.* **2020**, *90*, 106694. [CrossRef]
- Chen, X.; Guo, L.; Du, X.; Chen, P.; Ji, Y.; Hao, H.; Xu, X. Investigation of glycerol concentration on corn starch morphologies and gelatinization behaviours during heat treatment. *Carbohydr. Polym.* **2017**, *176*, 56–64. [CrossRef] [PubMed]
- Basiak, E.; Lenart, A.; Debeaufort, F. How glycerol and water contents affect the structural and functional properties of starch-based edible films. *Polymers* **2018**, *10*, 412. [CrossRef] [PubMed]
- Zhanga, C.-W.; Nair, S.; Chen, H.; Yan, N.; Farnood, R.; Li, F.-Y. Thermally stable, enhanced water barrier, high strength starch biocomposite reinforced with lignin containing cellulose nanofibrils. *Carbohydr. Polym.* **2020**, *230*, 115626. [CrossRef] [PubMed]
- Garalde, R.A.; Thipmanee, R.; Jariyasakoolroj, P. The effects of blend ratio and storage time on thermoplastic starch/poly(butylene adipate-co-terephthalate) films. *Heliyon* **2019**, *5*, e01251. [CrossRef] [PubMed]
- Mina Hernandez, J.H. Effect of the incorporation of polycaprolactone (Pcl) on the retrogradation of binary blends with cassava thermoplastic starch (tps). *Polymers* **2021**, *13*, 38. [CrossRef] [PubMed]

19. Palanisamy, C.P.; Cui, B.; Zhang, H.; Jayaraman, S.; Muthukaliannan, G.K. A comprehensive review on corn starch-based nanomaterials: Properties, simulations, and applications. *Polymers* **2020**, *12*, 2161. [CrossRef] [PubMed]
20. Syafri, E.; Jamaluddin; Wahono, S.; Irwan, A.; Asrofi, M.; Sari, N.H.; Fudholi, A. Characterization and properties of cellulose microfibrils from water hyacinth filled sago starch biocomposites. *Int. J. Biol. Macromol.* **2019**, *137*, 119–125. [CrossRef]
21. ASTM. ASTM. ASTM E104-02. In *Standard Practice for Maintaining Constant Relative Humidity by Means of Aqueous Solutions*; ASTM: West Conshohocken, PA, USA, 2012.
22. Elbayomi, S.M.; Wang, H.; Tamer, T.M.; You, Y. Enhancement of Antioxidant and Hydrophobic Properties of Alginate via Aromatic Derivatization: Preparation, Characterization, and Evaluation. *Polymers* **2021**, *13*, 2575. [CrossRef]



## Article

# The Blending of Poly(glycolic acid) with Polycaprolactone and Poly(L-lactide): Promising Combinations

Luca Magazzini <sup>1</sup>, Sara Grilli <sup>1</sup>, Seif Eddine Fenni <sup>1</sup>, Alessandro Donetti <sup>2</sup>, Dario Cavallo <sup>1,\*</sup>   
and Orietta Monticelli <sup>1,\*</sup>

<sup>1</sup> Dipartimento di Chimica e Chimica Industriale, Università degli Studi di Genova, Via Dodecaneso 31, 16146 Genova, Italy; lucamaga95@gmail.com (L.M.); saragrilli.sg@libero.it (S.G.); seifeddinefenni@gmail.com (S.E.F.)

<sup>2</sup> Natur-World S.p.A., Via Roma 8/2, 16121 Genova, Italy; a.donetti@natur-world.it

\* Correspondence: dario.cavallo@unige.it (D.C.); orietta.monticelli@unige.it (O.M.)

**Abstract:** Poly(glycolic acid) (PGA) holds unique properties, including high gas barrier properties, high tensile strength, high resistance to common organic solvents, high heat distortion temperature, high stiffness, as well as fast biodegradability and compostability. Nevertheless, this polymer has not been exploited at a large scale due to its relatively high production cost. As such, the combination of PGA with other bioplastics on one hand could reduce the material final cost and on the other disclose new properties while maintaining its “green” features. With this in mind, in this work, PGA was combined with two of the most widely applied bioplastics, namely poly(L-lactide) (PLLA) and polycaprolactone (PCL), using the melt blending technique, which is an easily scalable method. FE-SEM measurements demonstrated the formation of PGA domains whose dimensions depended on the polymer matrix and which turned out to decrease by diminishing the PGA content in the mixture. Although there was scarce compatibility between the blend components, interestingly, PGA was found to affect both the thermal properties and the degradation behavior of the polymer matrices. In particular, concerning the latter property, the presence of PGA in the blends turned out to accelerate the hydrolysis process, particularly in the case of the PLLA-based systems.

**Keywords:** PGA; PLA; PCL; blends

**Citation:** Magazzini, L.; Grilli, S.; Fenni, S.E.; Donetti, A.; Cavallo, D.; Monticelli, O. The Blending of Poly(glycolic acid) with Polycaprolactone and Poly(L-lactide): Promising Combinations. *Polymers* **2021**, *13*, 2780. <https://doi.org/10.3390/polym13162780>

Academic Editor: Antonio Zuorro

Received: 28 July 2021

Accepted: 16 August 2021

Published: 18 August 2021

**Publisher's Note:** MDPI stays neutral with regard to jurisdictional claims in published maps and institutional affiliations.



**Copyright:** © 2021 by the authors. Licensee MDPI, Basel, Switzerland. This article is an open access article distributed under the terms and conditions of the Creative Commons Attribution (CC BY) license (<https://creativecommons.org/licenses/by/4.0/>).

## 1. Introduction

The concerns about the accumulating plastic waste pollution as well as the increasing environmental pressure on global warming have stimulated tremendous attention toward bioplastics [1–3]. Among them, poly(glycolic acid) (PGA) holds promising characteristics [4], such as excellent mechanical properties [5], high heat distortion temperature, as well as exceptionally high gas barrier properties [6–8]. Furthermore, the polymer chains, which have a similar chemical structure to poly(lactic acid) (PLA) but without the methyl side group, are tightly packed together, thus producing elevated thermal stability and high degree of crystallinity [4]. The latter unique feature, which affects the PGA properties, was studied in detail. Indeed, by using different characterization techniques, Sato et al. [9] demonstrated that the intermolecular interactions in PGA chains influence the achievable structure, which results in a high melting temperature. Moreover, it was reported that in the crystalline structure, the hydrogen bonds between the oxygen atoms of the ester group and the hydrogen atoms of CH<sub>2</sub> are weak [10]. More recently, Báez et al. [11], comparing the crystallinity, the melting temperature ( $T_m$ ), and the enthalpy of fusion ( $\Delta H_m$ ) of poly(L-lactide) (PLLA) and polycaprolactone (PCL) with those of PGA, observed that with a similar number average molecular weight,  $T_m$  was affected by the polarity of the structural unit of the ester, following the trend: PGA > PLLA > PCL. Clearly, the arrangement of crystalline domains, the intramolecular interactions as well as the conformation of molecular chains affect PGA's mechanical properties. In particular, the structural regularity renders

the polymer more rigid and stiff in comparison with other biopolymers [12]. Indeed, due to its highly crystalline structure, PGA has the strongest mechanical strength but the lowest fracture toughness in comparison to PLA, polylactic-co-glycolic acid (PLGA), and polyethylene terephthalate (PET) [4]. Another interesting feature of the polymer, which affects its extent of hydrolysis, is the relatively high hydrophilicity compared to other biopolymers, such as PLA and PCL [13–16]. As such, PGA hydrolytic degradation, whose rate is quite high, starts with the hydrolysis reaction with water and is followed by the random cleavage of the ester bonds in the polymer chain. Moreover, as occurs for other polyesters, the degradation rate is accelerated by the increase in the carboxylic end groups during the decomposition [17].

Although the aforementioned PGA characteristics make the polymer suitable for high-end applications, such as packaging, electronics, and automobile, so far, it has been mainly used in the biomedical field [18–20]. The main challenge of the application of PGA is related to its high production cost. As such, the development of novel manufacturing approaches, based for instance on the preparation of glycolic acid (GA) from renewable resources and industrial waste gases, could significantly decrease the production cost of PGA [21]. Moreover, the strategy of combining PGA with other biopolymers on one hand could diminish the material cost and on the other take advantage of the synergic properties of the blend components, while maintaining the environmental sustainability of the formulation. Although this approach could overcome some of the PGA drawbacks and enlarge its applicability, only very few studies reported on blends based on PLA and PCL, which are the polymers object of the present work.

Indeed, blends made by the mixing of PGA with PCL were mainly done in fiber/nanofiber form [22,23]. Spearman et al. [22] developed electrospun PCL/PGA nanofibers impregnated with double-stranded deoxyribonucleic acid wrapped single-walled carbon nanotubes and encapsulated by a PCL matrix. *Pseudomonas* lipase, which is used to catalyze the degradation, was found to promote the system degradation within four weeks. The degradation of fibers was also studied by Viera et al. [23], who compared the decomposition rate of neat and blend fibers based on PLA, PCL, PGA, and polydioxane (PDO) in various systems. Hydrolytic degradation was the fastest in the fibers composed by mixing PCL with PGA, whose degradation was more evident under basic conditions with respect to neutral ones.

Concerning PLA, the combination between the two polymers was mainly carried out by the copolymerization reaction, which allows obtaining PLGA, namely a copolymer of lactic acid and GA [24–26]. As for PCL, electrospun nanofiber blends based on PLA and PGA were developed, whose features turned out to be suitable for soft tissue engineering applications [27]. Moreover, a co-continuous phase morphology was obtained during the electrospinning process, and the subsequent extraction of PLA allowed producing porous fibers characterized by a very narrow pore size distribution [28]. Concerning films based on PGA/PLA blends, Ma et al. [29] applied the solution casting method, using the copolymer of PGA and PLA as compatibilizer. It was found that the crystallinity of PGA blended with the copolymer and with PLA decreased with increasing PLA content. In another study, the mechanical properties and degradation of PLA were improved by incorporating PGA fibers in PLA [30]. In this case, PGA fibers acted as reinforcement for PLA and increased the flexural strength and modulus.

It is worth underling that all the above examples are based on the dissolution of PGA by using expensive and highly impacting solvents, such as hexafluoroisopropanol, which is an approach that makes the material exploitation challenging. As such, with the aim of rendering the developed formulations more easily scalable, for the first time, melt blending was applied to develop blends based on PGA, PLA, and PCL. PGA was employed as a minority component in order to limit the costs of the final formulation. The prepared materials were studied in terms of thermal, mechanical, wettability, and degradation properties. Moreover, the influence of the blend composition on the morphology was evaluated by means of Field Emission Scanning Electron Microscopy (FE-SEM) measurements.

## 2. Materials and Methods

### 2.1. Materials

Poly(L-lactide) (PLLA), PLLA 1010 Synterra (average molecular weight  $10^5$  g/mol, MFI = 12 g/10 min), was purchased from Purac (Amsterdam, The Netherlands) in powder form. Polycaprolactone (PCL) was obtained from Perstorp (Malmö, Sweden) (CAPA 6500,  $M_n = 50,000$  g/mol, MFI = 7 g/10 min), while poly(glycolic acid) (PGA), Vytal Resin (MFI = 20 g/10 min), was kindly received from Natur-World (Genoa, Italy).

### 2.2. Blend Preparation

Before accomplishing the blend preparation, in order to remove the moisture, the polymers were dried overnight in a vacuum oven at 60 °C for PLLA and PGA, while in the case of PCL, the temperature was set at 40 °C. Blends were prepared by using a Brabender Plastograph (Duisburg, Germany), mixing the components at 250 °C for 7 min and by applying a mixing speed of 100 rpm. The amount of material was constant in all the systems and corresponded approximately to a filling of 75% of chamber volume. In order to avoid the occurrence of degradation processes, some preliminary experiments allowed verifying the constancy of the torque in the chosen interval of time, as the decrease of the above parameter indicates a decrement of the polymer molecular weight. Moreover, also the neat polymers were treated using the same conditions applied in the blend preparation. The codes, which were assigned to the blends, indicate the ratio of the components (as an example, PCL70/PGA30 indicates a sample based on a ratio PCL/PGA of 70/30 composition).

### 2.3. Material Characterization

Thermal gravimetric analysis (TGA) was performed with a Star<sup>e</sup> System Mettler thermobalance (Milan, Italy). Samples, with weight of 5–8 mg, were heated from 35 to 800 °C at a heating rate of 10 °C/min, under a nitrogen flow of 80 mL/min.

Differential scanning calorimetry (DSC) experiments were performed with a TA Instruments Q20 (Milan, Italy), operating under flow of nitrogen. The samples, having a mass of about 5 mg, were firstly heated from room temperature to 250 °C; then, they were cooled down to 20 °C or –30 °C for PLLA-based and PCL-based blends, respectively. Finally, the samples were heated to 250 °C again. A scanning rate of 10 °C/min was used on both heating and cooling.

The degree of crystallinity ( $X_c$ ) was calculated by using Equation (1) and the enthalpies of fusion of 93 J·g<sup>-1</sup>, 139 J·g<sup>-1</sup>, and 191 J·g<sup>-1</sup> for 100% crystalline PLLA [31], PCL [32], and PGA [33], respectively.

$$X_c(\%) = \frac{\Delta H_m}{\Delta H_0} \times 100 \quad (1)$$

where  $\Delta H_m$  is the measured heat of fusion and  $\Delta H_0$  is the melting enthalpy of the 100% crystalline polymer.

DSC and TGA measurements were conducted in replicate.

Contact angle measurements were performed at room temperature with an Attension contact angle meter (Biolin Scientific, Gothenburg, Sweden) using pure distilled water and diiodomethane as probe liquids. The average static contact angles were obtained by measuring at least three droplets on each film specimen (two films for sample).

In order to obtain the surface energy, the following equation was applied:

$$\frac{\gamma_l(1 + \cos \theta)}{2\sqrt{\gamma_l^d}} = \sqrt{\gamma_s^d} + \sqrt{\gamma_s^p} \frac{\sqrt{\gamma_l^p}}{\sqrt{\gamma_l^d}} \quad (2)$$

where  $\gamma_s^p$  is the sample surface energy polar component and  $\gamma_s^d$  is the sample surface energy-dispersive component. For water:  $\gamma_l = 72$  mN/m;  $\gamma_l^p = 51$  mN/m;  $\gamma_l^d = 21.8$  mN/m. For diiodomethane:  $\gamma_l = 50.8$  mN/m;  $\gamma_l^p = 1.3$  mN/m;  $\gamma_l^d = 49.5$  mN/m.



A Zeiss Supra 40 VP field emission scanning electron microscope equipped with a backscattered electron detector (Oberkochen, Germany) was applied to examine the blend morphologies. The specimens were submerged in liquid nitrogen and fractured cryogenically. All samples were thinly sputter-coated with carbon using a Polaron E5100 sputter coater (Leica Microsystems, Wetzlar, Germany). Statistical analysis of PGA domains was performed by evaluating at least four micrographs at different magnifications for each sample.

To test the hydrolytic degradation, films of the neat polymers and of the blends based on a 70/30 ratio (previously dried overnight), having dimensions of 1 × 1 cm were prepared by a hot-pressing method using a Carver Hydraulic Lab Presses (Wabash, Indiana, USA). The specimens were immersed into 2 mL of distilled water at 50 °C. At different time intervals, the films were removed from water and vacuum dried. Three films were analyzed for each sample.

The (dry) sample weights were determined both before and after the immersion, and the extent of degradation was measured as percentage weight loss of the film as:

$$\text{Weightloss(\%)} = \left[ \frac{W_{dry0} - W_{dry}}{W_{dry0}} \right] \times 100 \quad (3)$$

where  $W_{dry0}$  is the initial weight of the specimens and  $W_{dry}$  is the dry weight of the specimens as measured after the treatment with water for a given time lapse.

### 3. Results

#### 3.1. Blend Morphological Characterization

The morphology of the prepared blends was studied by FE-SEM measurements. The micrographs obtained for the two investigated systems are shown in Figure 1. The PLLA/PGA blends show a typical sea-island morphology, where the spherical domains of PGA are dispersed in the PLLA matrix, thus demonstrating, at least for the analyzed compositions, the immiscibility between the two phases. Considering the dimensions of the PGA domains in the system PLLA/PGA (Figure 2), it is worth underling that their average diameter tends to decrease significantly, reducing the amount of the polymer in the blend, passing from 14 μm in the case of PLLA70/PGA30 sample to 5 μm for the blend PLLA90/PGA10.

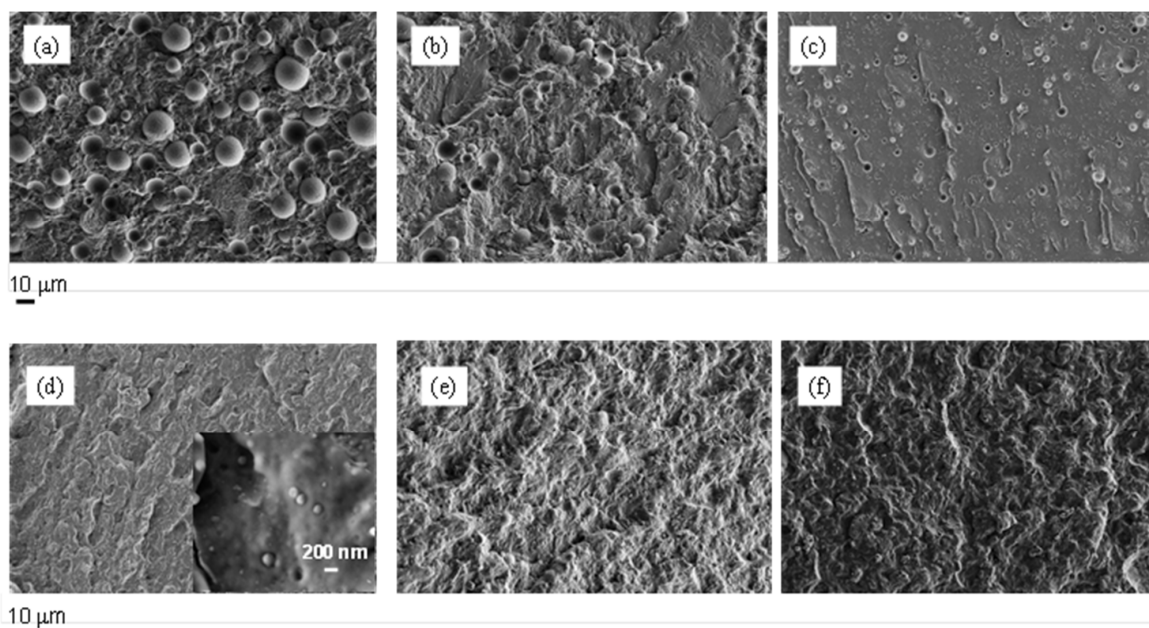


**Figure 1.** FE-SEM micrographs of: (a) PLLA70/PGA30, (b) PLLA80/PGA20, (c) PLLA90/PGA10, (d) PCL70/PGA30, (e) PCL80/PGA20, (f) PCL90/PGA10.

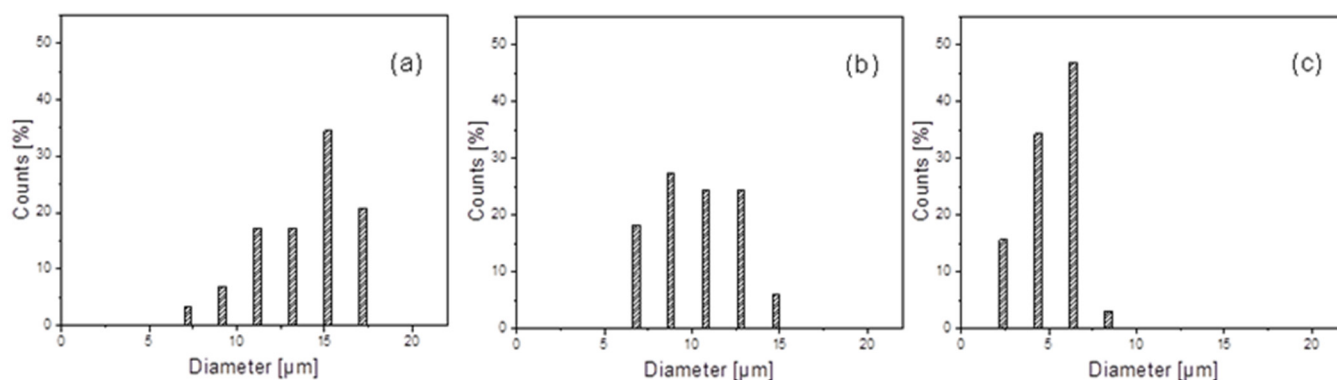


**Figure 2.** Histograms of the PGA domains diameter in the PLLA-based blends: (a) PLLA70/PGA30, (b) PLLA80/PGA20, and (c) PLLA90/PGA10.

On the other hand, in the case of PCL-based blends, the morphological analysis does not reveal the presence of measurable PGA domains. Only for the PCL70/PGA30 sample, considering the measurements carried out at high magnification (see insert of Figure 1d), PGA droplets (characterized by an average diameter of ca. 200 nm and which resulted partially attached to the polymer matrix) are clearly visible.

In order to explain the different behavior of the two investigated polymers, it is worth underling that the morphology of blends is affected by the viscosity and phase elasticity of the components as well as by the shear rate and blend composition [34]. Taking into account that the systems were prepared by applying the same conditions, it is possible to infer that the specific features of the polymers influence the final blend morphology.

### 3.2. Wettability Tests

The wettability of the films based on PLLA, PGA, and PCL was compared with that of the corresponding blends. In particular, to more easily verify the specific effect of PGA on the properties of the systems, blends containing the highest amount of the polymer, namely those with a 70/30 ratio, were studied. In order to evaluate the surface energy of the various systems, the contact angle of water and diiodomethane was measured (Table 1). The water and diiodomethane contact angle of the neat polymer films are in good agreement with those reported in the literature [35–37]. Indeed, the presence of PGA in the blend determines a significant decrease in the water contact angle due to the higher wettability of the above polymer compared to PLLA and PCL. Although the contact angle values are similar for the two systems, interestingly, the polar component of the PLLA-based systems is higher than the PCL/PGA blends. Clearly, this property might affect the behavior of the systems, especially in terms of degradability.

**Table 1.** Water, diiodomethane contact angles, and surface energies of the neat polymers and of the PLLA70/PGA30 and PCL70/PGA30 blends.

| Sample Code  | Water Contact Angle [°] | Diiodomethane Contact Angle [°C] | $\gamma_s$ [mN/m] | $\gamma_s^p$ [mN/m] | $\gamma_s^d$ [mN/m] |
|--------------|-------------------------|----------------------------------|-------------------|---------------------|---------------------|
| PLLA         | 80 ± 1.2                | 44 ± 2.8                         | 41.9              | 8.8                 | 33.1                |
| PCL          | 75 ± 1.3                | 26 ± 2.5                         | 46.8              | 4.6                 | 42.2                |
| PGA          | 50 ± 1.3                | 20 ± 2.1                         | 58.1              | 18.2                | 39.9                |
| PLLA70/PGA30 | 63 ± 3.8                | 41 ± 2.2                         | 47.1              | 13.5                | 33.6                |
| PCL70/PGA30  | 64 ± 1.4                | 22 ± 2.4                         | 49.7              | 7.3                 | 42.4                |

$\gamma_s$  = surface energy,  $\gamma_s^p$  = polar component of surface energy, and  $\gamma_s^d$  = dispersive component of surface energy.

### 3.3. Study of the Hydrolytic Degradation

The hydrolytic degradation of the prepared blends was studied by monitoring the weight loss over time for specimens placed in water. As previously reported, blends with a 70/30 ratio were considered, and with the aim of speeding up the process, the measurements were carried out at 50 °C. Furthermore, the morphology of the surfaces of the films, which underwent a hydrolysis treatment for 80 days, was analyzed by FE-SEM measurements. In order to verify the effect of the presence of PGA, which was dispersed in the two polymer matrices, the behavior of the neat PLLA and PCL films was also analyzed. Indeed, Figure 3 shows the FE-SEM micrographs of the neat PLLA (Figure 3a) and PCL (Figure 3c) treated films and those of the treated blends PLLA70/PGA30 (Figure 3b) and PCL70/PGA30 (Figure 3d), together with the percentage weight loss versus time.

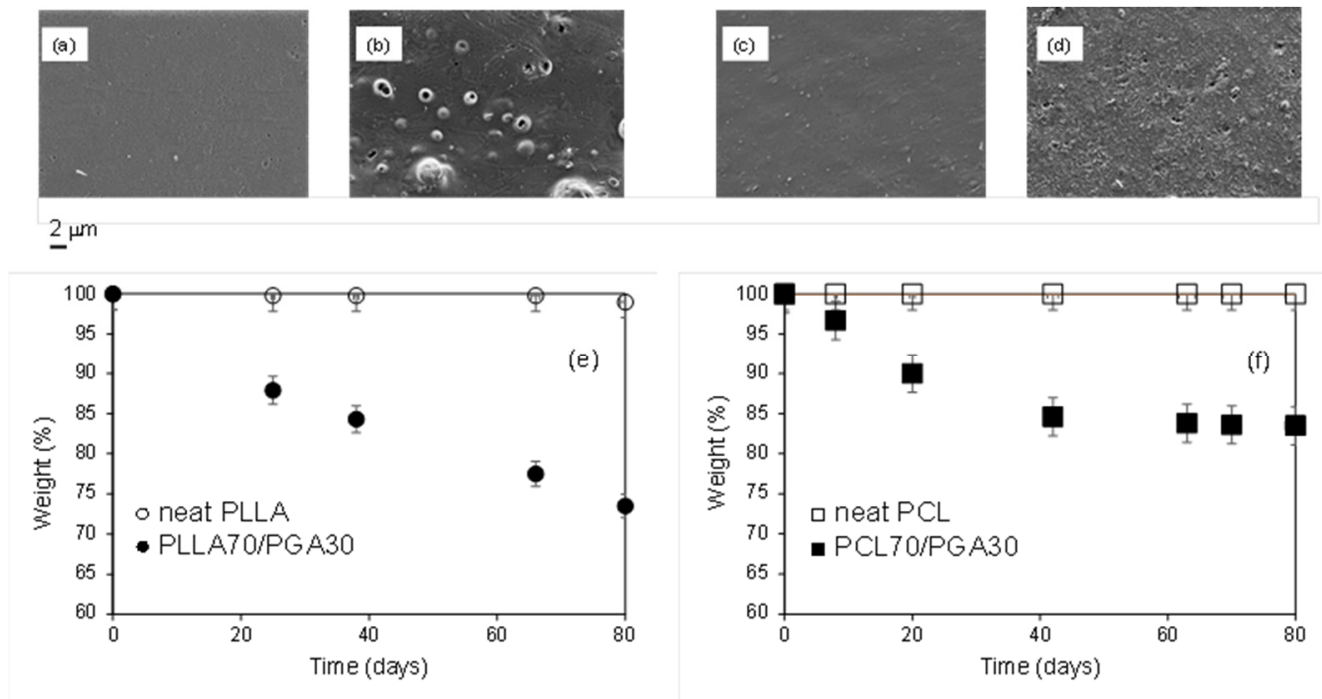


**Figure 3.** FE-SEM micrographs of treated films: (a) neat PLLA, (b) PLLA70/PGA30, (c) neat PCL, and (d) PCL70/PGA30. Weight loss percentage as a function of time of (e) films based on PLLA (○ neat PLLA, ● PLLA70/PGA30) and (f) films based on PCL (□ neat PCL and ■ PCL70/PGA30).

In the analyzed time interval (80 days), the weight loss of the neat PLLA and PCL-based films is practically negligible, and the films' surface appeared homogeneous (Figure 3a,c). It is worth underling that in all the performed experiments, the deviation of the weight loss was within 2%. Indeed, the slow degradation rate of both the polymers, even under very accentuated hydrolysis conditions, that is directly in water and at high temperature, cannot satisfy a wide range of application specific requirements [38,39]. In this regard, it is worth underling that the need to accelerate the degradation process is essential not only for bio-medical applications [40], as an example when the polymer matrices are used as drug carriers, but also in other fields, such as packaging. Considering the trends shown in Figure 3, it is evident that the presence of PGA in the blends significantly modifies the degradation, accelerating the process. Nevertheless, the kinetic of the system decomposition turned out to depend on the polymer matrix, being faster in the case of PLLA-based blends. It is worth noticing that the weight loss kinetic is almost the same for both the blends in the first 40 days, but afterwards, it slows down for those based on PCL.

In order to clarify the above phenomenon, it is necessary to consider the degradation mechanism of PGA as well as the specific properties in terms of morphology, crystallinity,

and wettability of the prepared blends. Concerning the former aspect, it was demonstrated that the degradation of PGA occurs in four stages, which are driven both by the water diffusion and by the hydrolysis rate [13–16,41,42]. Indeed, in the first step, the water diffuses into the polymer, reaching its maximum concentration within a few hours, while in stage two, the diffusion of water becomes slower and the polymer molecular weight decreases steadily as hydrolysis reaction begins. The decrement of molecular weight as well as the plasticizing effect of water lead to an increase of chain mobility in the amorphous phase, which promotes a secondary crystallization. In stage three, the oligomers, formed in stage two, start to diffuse from the polymer surface into the solution. As more spaces are created in the polymer, more water can diffuse through the bulk of the polymer, which is a phenomenon that accelerates the reaction and creates sharp erosion fronts throughout the sample. Indeed, it is possible to hypothesize that the lower crystallinity as well as the higher polar component of the PLLA-based systems favor the water diffusion, resulting in a more constant degradation rate over time than that of the PCL/PGA blends. Furthermore, in the PLLA-based blends, as it appears from the micrograph of the treated sample (Figure 3b), the degradation seems confined in the micrometer-size PGA domains. Conversely, the finer PGA dispersion in the PCL/PGA blends promotes a more distributed erosion (Figure 3d). Summarizing, the effective role of PGA in tuning the degradation of biopolymers was verified by studying systems easily prepared by applying the scalable melt blending technique.

### 3.4. Study of the Thermal Properties

Figure 4 displays the characteristic DSC scans upon cooling and heating PLLA, PGA, and their blends. The thermal properties for all the samples are collected in Table S1 of the Supporting Information. The different crystallizability of the two neat polymers can be noticed. In fact, PGA crystallizes with a large and relatively narrow peak at around 190 °C, while the crystallization of PLLA occurs only for a minor fraction in a broad interval centered at about 100 °C. Moreover, PLLA crystallization is incomplete on cooling, as it can be judged from the cold crystallization event on subsequent heating above the glass transition, again at 100 °C. The initial crystallinity of PLLA, before heating, is ca. 40%. The high crystallinity of PGA ( $X_c$  of ca. 45%) prevents the observation of a distinct glass transition, which should anyhow be present at 35–40 °C [33]. A double melting peak is observed for PGA, and it is tentatively ascribed to melting–recrystallization phenomena, which is typical of many polyesters (see [43] and reference therein).

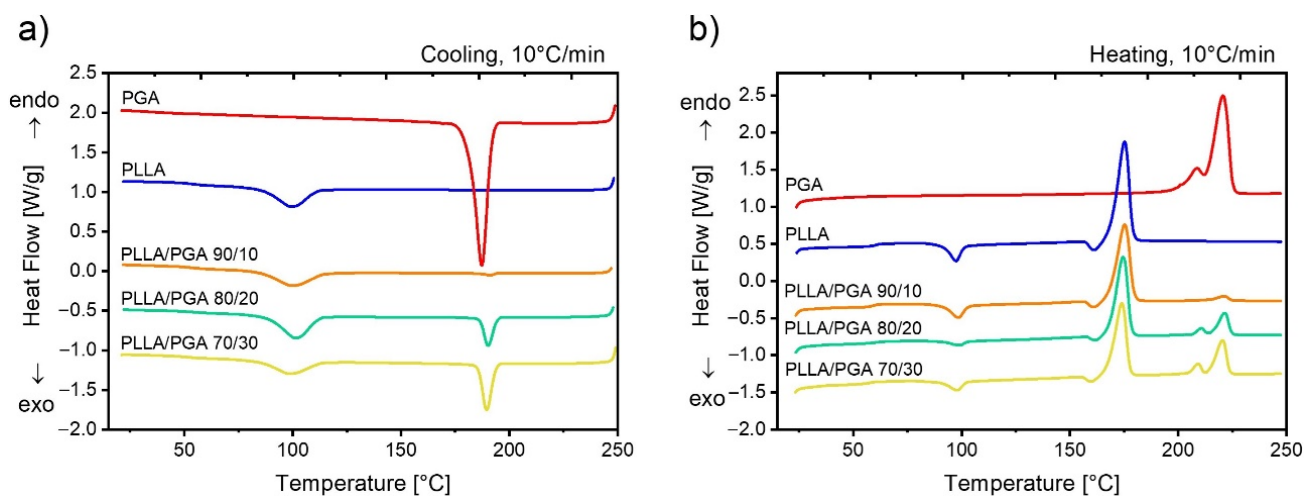


**Figure 4.** DSC cooling (a) and heating (b) scans for the neat polymers and PLLA/PGA blends of indicated compositions.

The DSC scans of the PLLA/PGA blends simply show the thermal features of both polymers to an extent representative of the relative content. In particular, it should be noticed that neither the crystallization temperatures nor the melting temperatures of the

components are affected by the blend composition. This indicates an immiscibility between the two components, which is in line with morphological observation examined via FE-SEM (Figure 1).

Figure 5 shows the differential scanning calorimetry results of PCL/PGA blends, along with those of the respective neat polymers. PGA and PCL are widely separated for what concerns their crystallization and melting temperatures. In fact, a difference of more than 150 °C can be observed between the respective transitions. Moreover, the crystallinity of neat PCL is ca. 45%. Contrary to what has been observed for the case of PLLA/PGA blends, a noteworthy effect of the blending process on the crystallization/melting of the two phases can be observed. Upon cooling, it can be seen that the crystallization of the PGA phase at high temperature is practically suppressed, while the crystallization temperature of PCL is enhanced with respect to that of the neat polymer. The first effect is expected, given the extremely limited size of the PGA domains, and it is almost not resolvable with FE-SEM. As a consequence, a very small number of nucleating impurities is present in the PGA domains, leading to vanishing crystallization kinetics [44]. As a matter of fact, PGA can only crystallize upon the subsequent heating, as evidenced by the cold-crystallization peak observed above the melting temperature of PCL, at around 70 °C. On the other hand, the increase of the crystallization temperature of PCL can be ascribed to a nucleating effect of PGA domains themselves, or to an effective transfer of nucleating impurities from the PGA to the matrix polymer.

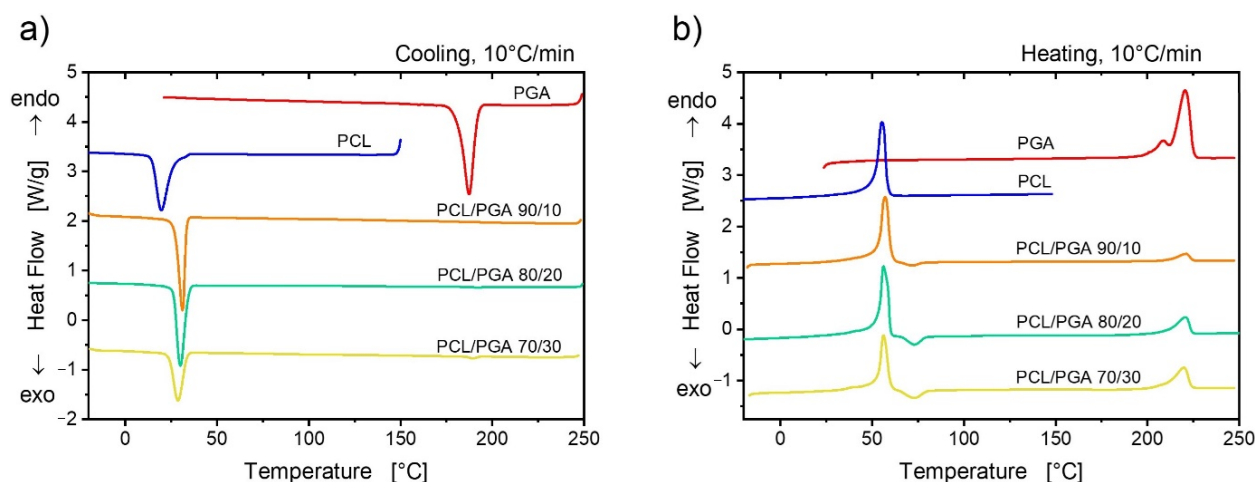


**Figure 5.** DSC cooling (a) and heating (b) scans for the neat polymers and PCL/PGA blends of indicated compositions.

However, despite the observed kinetics effect on crystallization, the melting temperatures of the two phases are unaffected by the blending process. In particular, no evident melting point depression could be detected, indicating once more a thermodynamic immiscibility between the polymers, despite the morphology indicating a quite good compatibility (Figure 1).

The results of thermogravimetric analysis for the PLLA/PGA blends and neat polymers are reported in Figure 6. It can be seen that PGA exhibits a higher thermal stability with respect to PLLA, displaying in particular a similar degradation onset temperature but a ca. 30 °C higher temperature of maximum degradation rate,  $T_{max}$  (Figure 6b). The thermal stability of the blends is not intermediate between the two neat polymers but is instead similar to that of neat PLLA, with a slightly lower onset temperature but identical  $T_{max}$ . These results confirm that during the melt blending process, the molecular features of the PLLA matrix did not undergo substantial changes that could decrease the resistance to temperature.

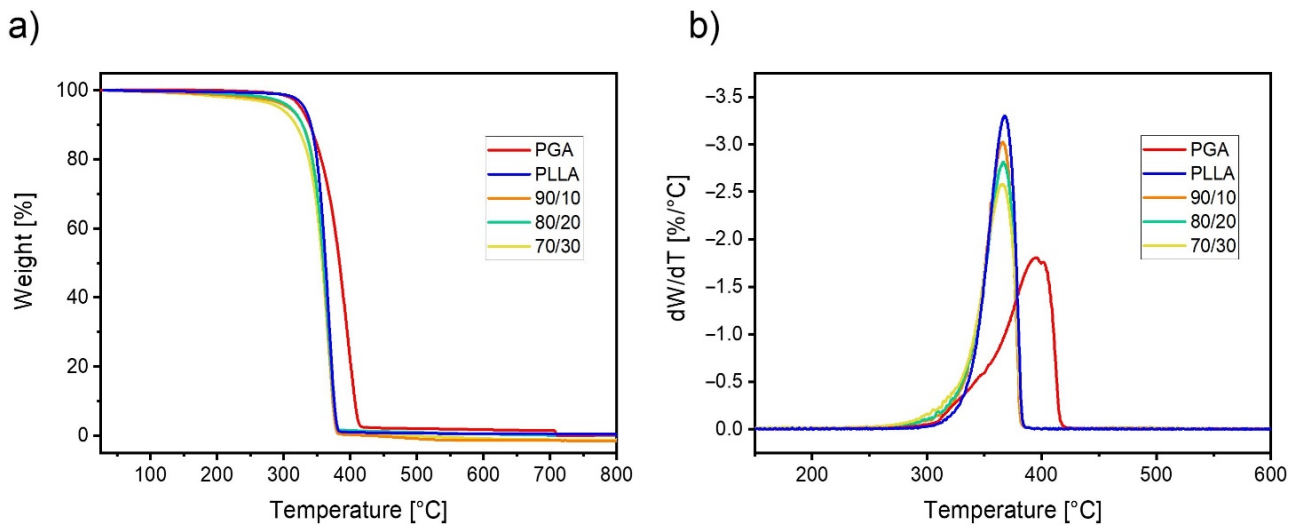


**Figure 6.** Mass loss versus temperature (a) and its derivative (b) for neat PLLA, PGA, and their blends at the indicated compositions.

Thermogravimetric data for the system PCL/PGA are shown in Figure 7. PCL possesses a higher thermal stability with respect to PGA. In particular, the onset of PCL degradation is located approximately 50 °C above that of PGA. In addition, the maximum rate of degradation is shifted to higher temperatures (Figure 7b). The behavior of the blends is somehow intermediate between the two neat polymers. In fact, there is a fraction of the material, increasing with the content of PGA, which degrades earlier than neat PCL, while the majority of the blend thermally degrades in a temperature interval superposed or similar to the one of PCL. As such, the thermal stability of the blend is only partially compromised with respect to the more resistant polymer.

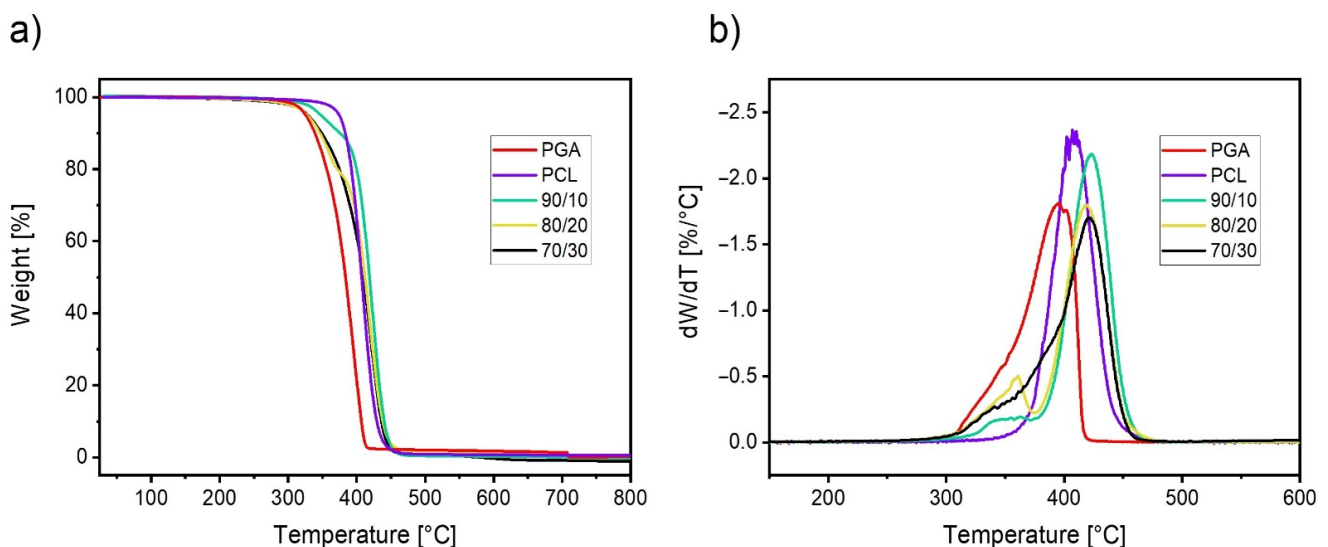


**Figure 7.** Mass loss versus temperature (a) and its derivative (b) for neat PCL, PGA, and their blends at the indicated compositions.

#### 4. Conclusions

In this work, with the aim of verifying the possibility of extending the applicability of PGA, a promising biopolymer suffering from a still high production cost, formulations were developed by combining it, as a minor component, with PLLA and PCL, which are two of the most extensively exploited biopolymers. In order to make the study closer to an industrial development, unlike some works reported in the literature where blends were prepared starting from solutions, the melt blending technique, which is an easily scalable method, was applied. The morphology of the prepared blends strongly depended on the

polymer matrix: the PGA domains, which were not very adherent to both the polymeric matrices, turned out to be extremely smaller in the case of the PCL-based systems compared to the PLLA/PGA blends. Moreover, for both the investigated systems, the wettability increased considerably with the addition of PGA. This caused an interesting increment in the blends degradation rate with respect to that of the polymeric matrices, which is an extremely important feature for a practical application of the developed systems. Furthermore, this phenomenon, which is related to the specific characteristics of the blend as well as of the polymeric matrix such as the crystallinity, the size of PGA domains, and the polar component of the surface energy, was more relevant in the case of blends based on PLLA, demonstrating the possibility of tuning the degradation by properly choosing the system.

For what concerns the crystallization behavior, PLLA and PGA crystallized and melted separately in their relatively coarse blends, at temperatures typical of the pure component, without showing any meaningful interaction. On the other hand, the blending of PCL with PGA caused pronounced mutual effects on the crystallization of the components. In particular, the PCL crystallization temperature was increased, while PGA crystallization in the extremely small domains was hindered, as it occurred only in cold crystallization upon second heating. Thermogravimetric analysis of the prepared blends revealed that the thermal stability of the matrix was not negatively affected by the presence of a low content of PGA, both for the cases of PLLA, which degraded before PGA, and of PCL, with higher thermal stability compared to PGA.

In conclusion, the feasibility of a melt blending approach for the preparation of biobased blends containing PGA was demonstrated. The obtained mixtures exhibited interesting characteristics, especially regarding their hydrolytic degradation behavior, which is tunable with respect to the matrix polymers. This preliminary work will serve as a basis to further explore the characteristics, especially the mechanical properties, and the potential application of these novel materials exploiting the environmentally friendly PGA.

**Supplementary Materials:** The following are available online at <https://www.mdpi.com/article/10.3390/polym13162780/s1>, Table S1: DSC analysis of the neat polymers and polymer blends, Table S2: TGA analysis of the neat polymers and polymer blends.

**Author Contributions:** Conceptualization, O.M., D.C. and A.D.; investigation, L.M., S.G. and S.E.F.; data curation, L.M. and S.G.; writing—review and editing, O.M. and D.C.; supervision, O.M. and D.C. All authors have read and agreed to the published version of the manuscript.

**Funding:** This research received no external funding.

**Institutional Review Board Statement:** Not applicable.

**Informed Consent Statement:** Not applicable.

**Data Availability Statement:** The data that support the findings of this study are available from the corresponding author upon reasonable request.

**Conflicts of Interest:** The authors declare no conflict of interest.

## References

1. Reddy, M.M.; Vivekanandhan, S.; Misra, M.; Bhatia, S.K.; Mohanty, A.K. Biobased plastics and bionanocomposites: Current status and future opportunities. *Prog. Polym. Sci.* **2013**, *38*, 1653–1689. [CrossRef]
2. Di Bartolo, A.; Infurna, G.; Dintcheva, N. A Review of Bioplastics and Their Adoption in the Circular Economy. *Polymer* **2021**, *13*, 1229. [CrossRef]
3. George, A.; Sanjay, M.; Srisuk, R.; Parameswaranpillai, J.; Siengchin, S. A comprehensive review on chemical properties and applications of biopolymers and their composites. *Int. J. Biol. Macromol.* **2020**, *154*, 329–338. [CrossRef] [PubMed]
4. Samantaray, P.K.; Little, A.; Haddleton, D.M.; McNally, T.; Tan, B.; Sun, Z.; Huang, W.; Ji, Y.; Wan, C. Poly(glycolic acid) (PGA): A versatile building block expanding high performance and sustainable bioplastic applications. *Green Chem.* **2020**, *22*, 4055–4081. [CrossRef]
5. Lee, S.; Hongo, C.; Nishino, T. Crystal Modulus of Poly(glycolic acid) and Its Temperature Dependence. *Macromolecules* **2017**, *50*, 5074–5079. [CrossRef]

6. McKeen, L.W. *Permeability Properties of Plastics and Elastomers*, 4th ed.; Elsevier: Amsterdam, The Netherlands, 2012. [CrossRef]
7. Yamane, K.; Sato, H.; Ichikawa, Y.; Sunagawa, K.; Shigaki, Y. Development of an industrial production technology for high-molecular-weight polyglycolic acid. *Polym. J.* **2014**, *46*, 769–775. [CrossRef]
8. Wua, F.; Misra, M.; Mohanty, A.K. Challenges and new opportunities on barrier performance of biodegradable polymers for sustainable packaging. *Progr. Polym. Sci.* **2021**, *117*, 101395. [CrossRef]
9. Sato, H.; Miyada, M.; Yamamoto, S.; Reddy, K.R.; Ozaki, Y. C–H···O (ether) hydrogen bonding along the (110) direction in polyglycolic acid studied by infrared spectroscopy, wide-angle X-ray diffraction, quantum chemical calculations and natural bond orbital calculations. *RSC Adv.* **2016**, *6*, 16817–16823. [CrossRef]
10. Nishimura, F.; Hoshina, H.; Ozaki, Y.; Sato, H. Isothermal crystallization of poly(glycolic acid) studied by terahertz and infrared spectroscopy and SAXS/WAXD simultaneous measurements. *Polym. J.* **2018**, *51*, 237–245. [CrossRef]
11. Báez, J.E.; Marcos-Fernández, A. A Comparison of Three Different Biodegradable Aliphatic Oligoesters (PGA, PLLA, and PCL) with Similar Linear Alkyl End Groups by DSC and SAXS. *Int. J. Polym. Anal. Charact.* **2015**, *20*, 637–644. [CrossRef]
12. Singh, V.; Tiwari, M. Structure-Processing-Property Relationship of Poly(Glycolic Acid) for Drug Delivery Systems 1: Synthesis and Catalysis. *Int. J. Polym. Sci.* **2010**, *2010*, 1–23. [CrossRef]
13. Shawe, S.; Buchanan, F.; Harkin-Jones, E.; Farrar, D. A study on the rate of degradation of the bioabsorbable polymer polyglycolic acid (PGA). *J. Mater. Sci.* **2006**, *41*, 4832–4838. [CrossRef]
14. Hurrell, S.; Milroy, G.E.; Cameron, R.E. The Degradation of Polyglycolide in Water and Deuterium Oxide. Part I: The Effect of Reaction Rate. *Polymer* **2003**, *44*, 1421–1424. [CrossRef]
15. De Oca, H.M.; Farrar, D.; Ward, I.M. Degradation studies on highly oriented poly(glycolic acid) fibres with different lamellar structures. *Acta Biomater.* **2011**, *7*, 1535–1541. [CrossRef]
16. Milroy, G.E.; Smith, R.W.; Hollands, R.; Clough, A.S.; Mantle, M.D.; Gladden, L.F.; Huatan, H.; Cameron, R.E. The Degradation of Polyglycolide in Water and Deuterium Oxide. Part II: Nuclear Reaction Analysis and Magnetic Resonance Imaging of Water Distribution. *Polymer* **2003**, *44*, 1425–1435. [CrossRef]
17. Abou-Zeid, D.-M.; Müller, R.-J.; Deckwer, W.-D. Degradation of natural and synthetic polyesters under anaerobic conditions. *J. Biotechnol.* **2001**, *86*, 113–126. [CrossRef]
18. Matsuda, Y.; Karino, M.; Okui, T.; Kanno, T. Complications of poly-L-lactic acid and polyglycolic acid (PLLA/PGA) osteosynthesis systems for maxillofacial surgery: A retrospective clinical investigation. *Polymers* **2021**, *13*, 889. [CrossRef]
19. Fujimaki, H.; Uchida, K.; Inoue, G.; Matsushita, O.; Nemoto, N.; Miyagi, M.; Inage, K.; Takano, S.; Orita, S.; Ohtori, S.; et al. Polyglycolic acid-collagen tube combined with collagen-binding basic fibroblast growth factor accelerates gait recovery in a rat sciatic nerve critical-size defect model. *J. Biomed. Mater. Res. Part B Appl. Biomater.* **2019**, *108*, 326–332. [CrossRef]
20. Kim, B.N.; Ko, Y.-G.; Yeo, T.; Kim, E.J.; Kwon, O.K.; Kwon, O.H. Guided Regeneration of Rabbit Calvarial Defects Using Silk Fibroin Nanofiber–Poly(glycolic acid) Hybrid Scaffolds. *ACS Biomater. Sci. Eng.* **2019**, *5*, 5266–5272. [CrossRef]
21. DiCosimo, R.; Payne, M.S.; Panova, A.; Thompson, J.; O’Keefe, D.P. Enzymatic Production of Glycolic Acid. U.S. Patent 7,198,927, 29 June 2006.
22. Spearman, S.S.; Irin, F.; Ramesh, S.; Rivero, I.; Green, M.J.; Harrysson, O.L.A. Effect of pseudomonas lipase enzyme on the degradation of polycaprolactone/polycaprolactone-polyglycolide fiber blended nanocomposites. *Int. J. Polym. Mater. Polym. Biomater.* **2018**, *68*, 360–367. [CrossRef]
23. Vieira, A.; Vieira, J.; Guedes, R.; Marques, A. Degradation and Viscoelastic Properties of PLA-PCL, PGA-PCL, PDO and PGA Fibres. *Mater. Sci. Forum* **2010**, *636*, 825–832. [CrossRef]
24. Ajioka, M.; Suizu, H.; Higuchi, C.; Kashima, T. Aliphatic polyesters and their copolymers synthesized through direct condensation polymerization. *Polym. Degrad. Stab.* **1998**, *59*, 137–143. [CrossRef]
25. Li, J.; Stayshich, R.M.; Meyer, T. Exploiting Sequence to Control the Hydrolysis Behavior of Biodegradable PLGA Copolymers. *J. Am. Chem. Soc.* **2011**, *133*, 6910–6913. [CrossRef]
26. Gentile, P.; Chiono, V.; Carmagnola, I.; Hatton, P.V. An Overview of Poly(lactic-co-glycolic) Acid (PLGA)-Based Biomaterials for Bone Tissue Engineering. *Int. J. Mol. Sci.* **2014**, *15*, 3640–3659. [CrossRef] [PubMed]
27. Ramdhanie, L.I.; AuBuchon, S.R.; Boland, E.D.; Knapp, D.C.; Barnes, C.P.; Simpson, D.G.; E Wnek, G.; Bowlin, G.L. Thermal and Mechanical Characterization of Electrospun Blends of Poly(lactic acid) and Poly(glycolic acid). *Polym. J.* **2006**, *38*, 1137–1145. [CrossRef]
28. You, Y.; Youk, J.H.; Lee, S.W.; Min, B.-M.; Lee, S.J.; Park, W.H. Preparation of porous ultrafine PGA fibers via selective dissolution of electrospun PGA/PLA blend fibers. *Mater. Lett.* **2006**, *60*, 757–760. [CrossRef]
29. Ma, Z.; Zhao, N.; Xiong, C. Degradation and miscibility of poly(DL-lactic acid)/poly(glycolic acid) composite films: Effect of poly(DL-lactic-co-glycolic acid). *Bull. Mater. Sci.* **2012**, *35*, 575–578. [CrossRef]
30. Takayama, T.; Daigaku, Y.; Ito, H.; Takamori, H. Mechanical properties of bio-absorbable PLA/PGA fiber-reinforced composites. *J. Mech. Sci. Technol.* **2014**, *28*, 4151–4154. [CrossRef]
31. Simmons, H.; Tiwary, P.; Colwell, J.E.; Kontopoulou, M. Improvements in the crystallinity and mechanical properties of PLA by nucleation and annealing. *Polym. Degrad. Stab.* **2019**, *166*, 248–257. [CrossRef]
32. Balakrishnan, P.B.; Gardella, L.; Forouharshad, M.; Pellegrino, T.; Monticelli, O. Star poly( $\epsilon$ -caprolactone)-based electrospun fibers as biocompatible scaffold for doxorubicin with prolonged drug release activity. *Colloids Surf. B Biointerfaces* **2018**, *161*, 488–496. [CrossRef]



33. Chen, Y.; Xie, K.; He, Y.; Hu, W. Fast-Scanning Chip-Calorimetry Measurement of Crystallization Kinetics of Poly(Glycolic Acid). *Polymers* **2021**, *13*, 891. [CrossRef]
34. Thomas, S.; Grohens, Y.; Jyotishkumar, P. *Characterization of Polymer Blends: Miscibility, Morphology and Interfaces*; Wiley-VCH: Weinheim, Germany, 2015.
35. Li, K.; Fina, A.; Marrè, D.; Carosio, F.; Monticelli, O. Graphite oxide nanocoatings as a sustainable route to extend the applicability of biopolymer-based film. *Appl. Surf. Sci.* **2020**, *522*, 146471. [CrossRef]
36. Tiaw, K.; Goh, S.; Hong, M.; Wang, Z.; Lan, B.; Teoh, S. Laser surface modification of poly( $\epsilon$ -caprolactone) (PCL) membrane for tissue engineering applications. *Biomaterials* **2005**, *26*, 763–769. [CrossRef] [PubMed]
37. Vargha-Butler, E.I.; Kiss, E.; Lam, C.N.C.; Keresztes, Z.; Kálmán, E.; Zhang, L.; Neumann, A.W. Wettability of biodegradable surfaces. *Colloid Polym. Sci.* **2001**, *279*, 1160–1168. [CrossRef]
38. Elsaywa, M.A.; Kim, K.-H.; Park, J.-W.; Deep, A. Hydrolytic degradation of polylactic acid (PLA) and its composites. *Renew. Sustain. Energy Rev.* **2017**, *79*, 1346–1352. [CrossRef]
39. Castilla-Cortázar, I.; Más-Estellés, J.; Meseguer-Dueñas, J.M.; Ivirico, J.E.; Marí, B.; Vidaurre, A. Hydrolytic and enzymatic degradation of a poly( $\epsilon$ -caprolactone) network. *Polym. Degrad. Stab.* **2012**, *97*, 1241–1248. [CrossRef]
40. Tyler, B.; Gullotti, D.; Mangraviti, A.; Utsuki, T.; Brem, H. Polylactic acid (PLA) controlled delivery carriers for biomedical applications. *Adv. Drug Deliv. Rev.* **2016**, *107*, 163–175. [CrossRef]
41. Hurrell, S.; Cameron, R.E. Polyglycolide: Degradation and drug release. Part I: Changes in morphology during degradation. *J. Mater. Sci. Mater. Med.* **2001**, *12*, 811–816. [CrossRef]
42. Hurrell, S.; Milroy, G.E.; Cameron, R.E. The distribution of water in degrading polyglycolide. Part I: Sample size and drug release. *J. Mater. Sci. Mater. Med.* **2003**, *14*, 457–464. [CrossRef]
43. Righetti, M.C.; Marchese, P.; Vannini, M.; Celli, A.; Lorenzetti, C.; Cavallo, D.; Ocando, C.; Müller, A.J.; Androsch, R. Polymorphism and Multiple Melting Behavior of Bio-Based Poly(propylene 2,5-furandicarboxylate). *Biomacromolecules* **2020**, *21*, 2622–2634. [CrossRef]
44. Sangroniz, L.; Wang, B.; Su, Y.; Liu, G.; Cavallo, D.; Wang, D.; Müller, A.J. Fractionated crystallization in semicrystalline polymers. *Prog. Polym. Sci.* **2021**, *115*, 101376. [CrossRef]

Review

# Expanding Poly(lactic acid) (PLA) and Polyhydroxyalkanoates (PHAs) Applications: A Review on Modifications and Effects

Ahmed Z. Naser , Ibrahim Deiab, Fantahun Defersha and Sheng Yang \* 

School of Engineering, University of Guelph, Guelph, ON N1G 2W1, Canada; anaser@uoguelph.ca (A.Z.N.); ideiab@uoguelph.ca (I.D.); fdefersh@uoguelph.ca (F.D.)

\* Correspondence: syang19@uoguelph.ca

**Abstract:** The high price of petroleum, overconsumption of plastic products, recent climate change regulations, the lack of landfill spaces in addition to the ever-growing population are considered the driving forces for introducing sustainable biodegradable solutions for greener environment. Due to the harmful impact of petroleum waste plastics on human health, environment and ecosystems, societies have been moving towards the adoption of biodegradable natural based polymers whose conversion and consumption are environmentally friendly. Therefore, biodegradable biobased polymers such as poly(lactic acid) (PLA) and polyhydroxyalkanoates (PHAs) have gained a significant amount of attention in recent years. Nonetheless, some of the vital limitations to the broader use of these biopolymers are that they are less flexible and have less impact resistance when compared to petroleum-based plastics (e.g., polypropylene (PP), high-density polyethylene (HDPE) and polystyrene (PS)). Recent advances have shown that with appropriate modification methods—plasticizers and fillers, polymer blends and nanocomposites, such limitations of both polymers can be overcome. This work is meant to widen the applicability of both polymers by reviewing the available materials on these methods and their impacts with a focus on the mechanical properties. This literature investigation leads to the conclusion that both PLA and PHAs show strong candidacy in expanding their utilizations to potentially substitute petroleum-based plastics in various applications, including but not limited to, food, active packaging, surgical implants, dental, drug delivery, biomedical as well as antistatic and flame retardants applications.

**Keywords:** poly(lactic acid) (PLA); polyhydroxyalkanoates (PHAs); review; properties; plasticizers; polymer blends; fillers; polymer nanocomposites; degradation; sustainability; 3D printing

**Citation:** Naser, A.Z.; Deiab, I.; Defersha, F.; Yang, S. Expanding Poly(lactic acid) (PLA) and Polyhydroxyalkanoates (PHAs) Applications: A Review on Modifications and Effects. *Polymers* **2021**, *13*, 4271. <https://doi.org/10.3390/polym13234271>

Academic Editor: Cristina Cazan

Received: 5 November 2021

Accepted: 30 November 2021

Published: 6 December 2021

**Publisher's Note:** MDPI stays neutral with regard to jurisdictional claims in published maps and institutional affiliations.



**Copyright:** © 2021 by the authors. Licensee MDPI, Basel, Switzerland. This article is an open access article distributed under the terms and conditions of the Creative Commons Attribution (CC BY) license (<https://creativecommons.org/licenses/by/4.0/>).

## 1. Introduction

Petroleum based polymers have been helpful in meeting mankind's requirements in variety of ways. Based on their composition, petroleum-based polymers can be very durable and disposable. However, the current combustion of fossil fuel has led to an alarming global climate change as a result of the release of carbon dioxide and greenhouse emissions. Wastes made from petroleum-based plastics such as garbage bags, food packaging containers and utensils are adding more burden to the environment. Furthermore, petroleum-based chemicals and solvents are also playing a role in reducing the quality of air. Therefore, finding new methods to secure a sustainable world development is an urgent need. Renewable biomaterials are considered as potential alternatives for petroleum-based products [1]. Polymers made from natural resins, for example shellac, gutta percha and amber, have a long history dating back to Roman times [2]. The official industrial application of natural polymer started in 1940s when Ford Motor Co. began experimenting with soybeans to produce sustainable automobiles [3]. Today, economic and environmental concerns are driving the trend for more utilizations of biopolymers. The current challenge is to develop the required methods necessary to make the revolution of biopolymers that are biodegradable and have renewable sources of feedstocks [4–9]. The level of materials

and chemicals produced from biobased feedstocks has been continuously grown from 12% in 2010, to 18% in 2020 and is expected to reach to around 25% in 2030. It is expected that out of the \$1.5 trillion worldwide chemical industry, two thirds will ultimately be based on renewable resources. A recent roadmap developed by United States Department of Energy and Department of Agriculture has specified a goal of 10% of chemical building blocks developed from agricultural resources by 2020 with ambitious plans to achieve a 50% increase by 2050 [4]. The research in the field of bioplastics has led to the discovery and developments of various new biobased products such as polyurethane products from soy oil, PLA from corn and PHAs from microorganisms [4,10–12].

Recent government policies that are focused on footprint reduction and conservation of energy are considered the driving force towards the use of sustainable and renewable bio-based polymers. For instance, single use plastics that are made from hard to recycle materials are to be banned in Canada by the end of 2021; for the aim to reach to zero plastic wastes by 2030 [13]. Thus, societies have started to switch to green resources to meet the demands of continuously increasing population in a way that does not affect the functioning ecosystems [14]. Among the most studied bio-based polymers to potentially substitute petroleum-based plastics are PLA and PHAs. This is due to their physical properties, barrier properties and stretchability which make them suitable for various applications. However, they suffer from some limitations which need to be overcome if these bioplastics are to compete with petroleum-based plastics. The objective of this work is to review the available materials on the modification's methods of these two bioplastics and present their impacts with a focus on the mechanical properties. Therefore, the use of plasticizers, as well as the preparation of polymer blends and nanocomposites along with their applications have been reviewed. The combination of all these modifications' methods in addition to their applications for both biopolymers is rare. The main aim of this review article is to widen the applicability of both biopolymers so as they can eventually replace petroleum-based plastics in new potential applications and therefore reduce the amount of waste and pollution.

### 1.1. PLA and Its Properties

Figure 1 shows the chemical structure for poly(lactic acid) and polylactide [15]. PLA is an aliphatic linear poly( $\alpha$ -ester) or  $\alpha$ -hydroxyalkanoic polyester that is acid-derived. PLA is produced through the ionic polymerization of lactide. Lactide is a cyclic compound that is produced when two molecules of lactic acid undergo dehydration–condensation. Fermentation of lactic acid from starch and other renewable resources by using different bacteria can also yield lactide. A direct way to obtain PLA is through polycondensation. Nonetheless, this process has two main drawbacks: firstly, the disposal of the solvent and secondly, this process results in low molecular weight polymers. Therefore, the most common technique used today for the production of L-lactide is the lactic acid's two-stage polycondensation to yield an oligomer. This is then followed by depolymerization [15–19].

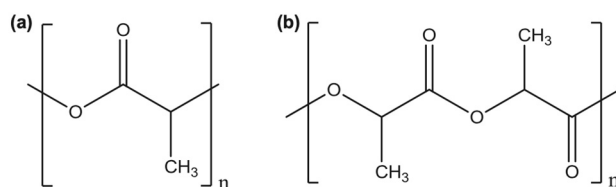


**Figure 1.** The chemical structure for: (a) poly(lactic acid) and (b) polylactide. Reprinted with permission from Elsevier, 2015 [15].

Every molecule of lactic acid has one asymmetric carbon. Lactic acid has two optically active forms which are: L-lactide and D-lactide. Lactide has three isomeric forms as shown in Figure 2a. L-lactide consists of two molecules of L- lactic acid. Two molecules of D- lactic acid yield D-lactide. One molecule of L- lactic acid and another one of D- lactic acid give meso- lactide. L-lactide has a lower cost than D-lactide; this is because it occurs

naturally [15,20]. Similar to L-lactide, meso-lactide is a cyclic diester that has two optically active atoms of carbon in the ring. It is considered as optically inactive because it has an optical R- and S-center. This form of lactide can be distinguished from the other forms by its melting temperature. Both: L-lactide and D-lactide have a melting temperature of 97 °C while the melting temperature for meso-lactide is 54 °C [15]. Yet, meso-lactide is not commercially available. L, D-lactide or rac-lactide is obtained by an equimolar mixture of L- and D-lactide as illustrated in Figure 2b. rac-lactide is produced through melting of equal quantities of L- and D-lactide. The melting temperature of meso-lactide is 129 °C. The most widely used isomeric forms of lactide are L-lactide and rac-lactide [15,20]. PLA can have many types such as: isotactic poly(L-lactide) (PLLA) and isotactic poly(D-lactide) (PDLA). PDLA is only available in small quantities and is very expensive. Other types are poly(meso-lactide) (mesoPLA), poly(rac-lactide) (PDLLA, racPLA), poly(L-lactide-co-D,L-lactide) (PLDLLA), poly(L-lactide-co-D-lactide) (PLDA), isotactic stereocomplex PLA (scPLA) and stereoblock PLA (sbPLA) as well as copolymers with other polymers [15,21].

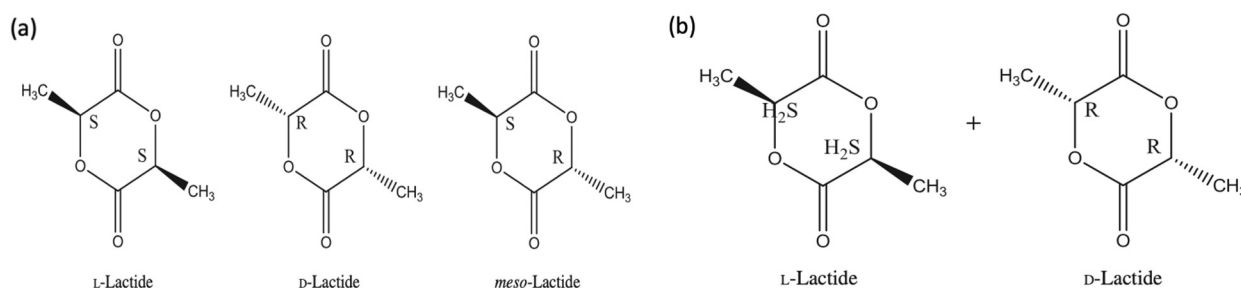


**Figure 2.** (a) Lactide's three stereoisomeric forms and (b) rac-lactide. Reprinted with permission from Elsevier, 2015 [15].

PLA's properties are highly affected by the degree of crystallinity, molecular weight and the comonomer's proportion. Glass transition temperature ( $T_g$ ), melting temperature ( $T_m$ ), Young's modulus and tensile strength all increase at higher molecular weight, nonetheless, percentage elongation decreases. PLA is highly transparent, soluble in organic solvent and exhibits hydrophobic behavior. Different types of PLA show various mechanical properties as well as degradation rates [4,22]. For example, PLLA is a transparent and hard materials with glass transition temperature between 53–63 °C, melting temperature between 160–185 °C and crystallization temperature in the range of 100–120 °C. Due to its biocompatibility, natural renewable origin and its biodegradability, PLA has been gaining a lot of interest. Because it does not lead to a direct raise in the level of carbon dioxide, PLA can be considered as a low environmental impact thermoplastic [15,22]. Figure 3 shows the production steps of PLA along with greenhouse uptake and emissions for 1 kg of PLA [23]. The biodegradation of PLA is useful in terms of forming non-toxic products when PLA based products are composted after their life cycles [24]. Furthermore, PLA's slow degradation rate can be beneficial for some applications to extend their shelf lives. Nonetheless, compared to poly(3-hydroxybutyrate) (P3HB or simply PHB) or Poly( $\epsilon$ -caprolactone) (PCL), the biodegradability of PLA is considerably low [15,25,26]. Although PLA exhibits low melt viscosity that is required for molds' shaping, it suffers from some drawbacks. For instance, PLA exhibits low crystallization rate in long molding cycles and suffers from inferior gas properties. Moreover, PLA demonstrates poor mechanical properties (impact resistance and toughness) as well as thermal resistance when compared to other synthetic polymers. To overcome such limitations, PLA has been blended with other polymers. Furthermore, plasticizers and fillers have been incorporated with PLA. These methods in addition to preparation of PLA nanocomposites have been effective in making PLA more commercially viable. PLA is the mostly widely used biopolymer; as such, PLA is associated with various brand names for different applications as shown in Table 1 [15,27].

**Table 1.** Some of the  $\alpha$ -Hydroxycarboxylic acid derived polyesters along with their manufacturers and applications. Adapted with permission from Elsevier, 2015 [15,28,29].

| Bioplastic    | Company           | Country         | Commercial Name  | Applications/Notes   |
|---------------|-------------------|-----------------|--|--|
| PLA           | NatureWorks LLC   | USA             | <ul style="list-style-type: none"> <li>-Ingeo™ 8000 series, 8052D.</li> <li>-Ingeo™ 7000 series, 7001D TDS and 7032D TDS.</li> <li>-Ingeo™ 6000 series, 6060D TDS, 6201D TDS, 6202D TDS, 6204D TDS, 6251D TDS, 6252D TDS, 6302D TDS, 6400D TDS, 6751D TDS, 6752D TDS.</li> <li>-Ingeo™ 4000 series, 4032D TDS, 4043D TDS, 4060D TDS.</li> <li>-Ingeo™ 3000 series, 3001D SDS, 3052D SDS, 3251D SDS, 3801X SDS.</li> <li>-Ingeo™ 2000 series, 2003D TDS.</li> <li>-Ingeo™ 3D850.</li> </ul> | <ul style="list-style-type: none"> <li>-Foams.</li> <li>-Bottles (7001D TDS and 7032D TDS).</li> <li>-Nonwovens (6060D TDS, 6202D TDS, 6251D TDS, 6252D TDS, 6302D TDS, 6751D TDS, 6752D TDS).</li> <li>-Apparel (6201D TDS, 6204D TDS).</li> <li>-Home textiles (knitted and woven) (6201D TDS, 6202D TDS, 6204D TDS, 6400D TDS).</li> <li>-Cards, folded cartons and films (4032D TDS, 4043D TDS, 4060D TDS).</li> <li>-3D printing (3D850, 4043D).</li> <li>-Durable goods (3001D SDS, 3052D SDS, 3251D SDS, 3801X SDS).</li> <li>-Service war (2003D TDS, 3001D TDS, 3052D TDS, 3251D TDS).</li> <li>-Food packaging (2003D TDS).</li> </ul> |
| PLA, PDLA     | Total Corbion PLA | The Netherlands | <ul style="list-style-type: none"> <li>-Luminy® PLA (L175, L130, L105, LX575, LX530, LX175, LX975, LX930, D120, D070)</li> </ul>   | <ul style="list-style-type: none"> <li>-High heat PLA for demanding applications (L175, L130, L105, LX575, LX530).</li> <li>-Standard PLA for general purpose applications (LX175).</li> <li>-Low heat PLA for usage in seal layers (LX975, LX930).</li> <li>-PDLA utilized to produce full stereocomplex compounds or used as a nucleating agent (D120, D070).</li> </ul>   |
| PLLA          | Purac             | The Netherlands | <ul style="list-style-type: none"> <li>-Purasorb® (PL 18, PL 24, PL 32, PL 38, PL 49, PL 65, PL 10).</li> </ul>  | <ul style="list-style-type: none"> <li>-Medical equipment.</li> </ul>  |
| PLLA, scPLA   | Teijin            | Japan           | <ul style="list-style-type: none"> <li>-Biofront® (HL L201 (PLLA), J20 (scPLA), J201 (scPLA)).</li> </ul>  | <ul style="list-style-type: none"> <li>-Eyeglass frames, sheets, films, fibers, injection molding, medical care, automobiles, electronics, construction and packages.</li> </ul>   |
| Amorphous PLA | Toyobo            | Japan           | <ul style="list-style-type: none"> <li>-Vylcoecol series (BE-400, BE-600, BE-910, HYD-306, BE-450, BE-410, HYD-006).</li> </ul>  | <ul style="list-style-type: none"> <li>-Adhesive, paint, printing ink.</li> <li>-BE-400 in the form of pellet, used as agent for different coating and is a general-purpose resin.</li> <li>-BE-600 in the form of sheet, used as anchor coating for printing ink and vapor deposition films.</li> </ul>   |
| PDLA          | Purac             | The Netherlands | <ul style="list-style-type: none"> <li>-Purasorb®</li> <li>-PD 24</li> <li>-PD 38</li> <li>-Purapol®</li> </ul>  | <ul style="list-style-type: none"> <li>-Medical equipment (Purasorb®).</li> <li>-Nucleating agents for PLLA (Purapol®).</li> </ul>   |

Table 1. Cont.

| Bioplastic                                   | Company                    | Country         | Commercial Name  | Applications/Notes  |
|--|----------------------------|-----------------|--|---|
| PDLLA  | Evonik                     | Germany         | -R 202 H<br>-R 203 H<br>-R 202 S<br>-R 203 S<br>-R 205 S<br>-R 207 S   | -Medical equipment (R 207 S) and drug delivery.   |
| PLDLLA                                       | Purac                      | The Netherlands | -Purasorb® (PLDL 8038, PLDL 8058, PLDL 7028, PLDL 7038, PLDL 7060).  | -Medical equipment.   |
| PLDA   | Purac                      | The Netherlands | -Purasorb® (PLD 9620, PLD 9655).   | -Medical equipment.   |
| PLA<br>(Nature- Works)/<br>copolyester blend | FKuR<br>Kunststoff<br>GmbH | Germany         | -Bio-flex® A4100 CL, Bio-flex® F 1110,<br>Bio-flex® F 1130, Bio-flex® F 1137, Bio-flex® F 2110,<br>Bio-flex® F 2201 CL, Bio-flex® F 6510, Bio-flex® F 6513,<br>Bio-flex® F 6611, Bio-flex® S 5630, Bio-flex® S 6540,<br>Bio-flex® S 9533). | -Flower wrapping, blown film extrusion and packaging (Bio-flex® A4100 CL).<br>-Waste bag, air pillow and carrier bag (Bio-flex® F 1130).<br>-Shopping bags (Bio-flex® F 1137).<br>-Waste bag, netting and deep freeze packaging (Bio-flex® F 2110).<br>-Film (Bio-flex® F 2201 CL).<br>-Multi-layer films (Bio-flex® A4100 CL and Bio-flex® F 2201 CL).<br>-Straws, mugs and ball pen (Bio-flex® F 6510).<br>-Thermoforming (Bio-flex® F 6611).<br>-Injection molding (Bio-flex® F 6513).<br>-Thermoformed inlay (Bio-flex® S 5630).<br>-Cosmetic jars (Bio-flex® S 6540 and Bio-flex® S 9533). |
| PLA/polyether<br>copolymer                   | Toray<br>Industries        | Japan           | -Ecodear® (V554R10, V554X51, V554X52, V751X52, V751X53, V911X51).  | -Bags, films, fibers, packaging, personal care, accessories, office supplies and electronics.   |

Abbreviations: PLA, poly(lactic acid); PDLA, poly (D-lactic acid); PLLA, poly(L-lactide); scPLA; stereocomplex PLA; PDLLA, poly (D, L-lactide); PLDLLA, poly(L-lactide-co-D,L-lactide); PLDA, poly(L-lactide-co-D-lactide).

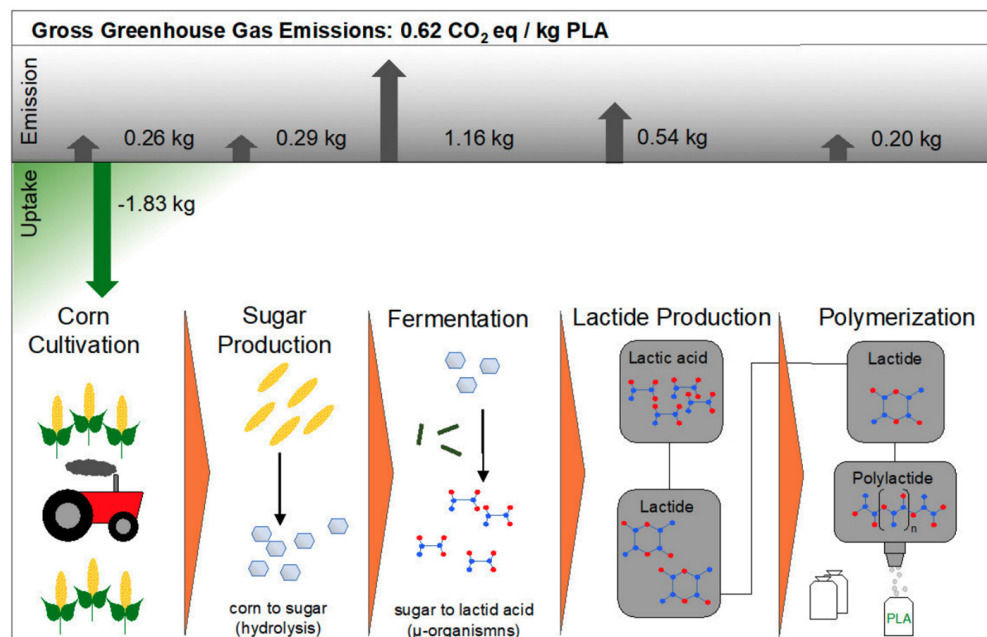


**Figure 3.** PLA's production steps along with greenhouse uptake and emissions for 1 kg of PLA [23].

### 1.2. PHAs and Their Properties

PHAs are known as polyesters of 3-, 4-, 5- and 6- hydroxycarboxylic or hydroxyacids acids. The general chemical structure for PHAs is shown in Figure 4a. The side-alkyl chain's length, the one additional methyl group at carbon atoms between the carboxyl group and hydroxyl group, the hydroxyl group's position relative to the carboxyl group and the large variety of substituents in the side chains all play a role in differentiating between the different types of hydroxyalkanoic acids [30]. This family of biopolymer is produced by various bacteria as intercellular carbon as well as energy storage materials [31]. PHAs can be found as scattered granules inside the cells of bacteria and may take up to 90% of bacteria's dry cell weight. Because they are produced in a natural way via soil bacteria, PHAs degrade when exposed to similar bacteria in compost, marine or soil. Biodegradation initiates when PHAs start to break down to hydroxy acid monomeric units via the different microorganisms on the surface of the biopolymer. The microorganisms then benefit from these hydroxy acid units by using them as sources of carbon for growth. This family of polymers can be also produced chemically [30,32–36]. The monomers for PHAs can range between a three carbon atoms compound (3-hydroxypropionate) to a compound with 14 carbon atoms (3-hydroxytetradecanoate). Based on the number of carbon atoms, this family of biopolymers can be classified to short chain length PHAs (scl-PHA) and PHAs with medium chain length (mcl-PHA). scl-PHA consists of 3–5 carbon atoms, while mcl-PHA contains 6–14 carbon atoms. Due to PHAs' compositional diversity, PHAs can exhibit different physical properties [37].

Today, many bacterial fermentations derived PHAs are commercially available, this include PHB, poly(3-hydroxybutyrate-co-3-hydroxyvalerate) (PHBV or PHBV), poly(3-hydroxybutyrate-co-3-hydroxyhexanoate) (PHBHH<sub>x</sub>) and poly(3-hydroxybutyrate-co-4-hydroxybutyrate) (P3HB4HB). The chemical structures of PHB and PHBV are shown in Figure 4b,c, respectively. Generally, scl-PHA such as PHB are brittle. As the length of monomer chain increases such as Poly(3-hydroxyoctanoate) (P3HO), the material exhibits more flexibility [38]. Because of their flexible properties, PHAs can ultimately substitute polyethylene (PE), PS and PP, which are the major polymers in today's polymer market [39]. Using thermal manufacturing processes such as injection molding, PHAs can be processed well. PHAs can be used in many applications such as, garbage bags, food packaging, diapers, as well as medical equipment [31,40]. This family of biopolymers have been

widely studied to investigate their use in biomedical applications. PHAs have been also used in surgical sutures, lubricating powders, controlled release, bone fracture fixation plates, tissue scaffolds, wound dressings and surgical implants. Table 2 shows some of the commercial PHAs along with their applications [15,41,42].

**Table 2.** Some of the commercial PHAs along with their manufacturers and applications. Adapted with permission from Elsevier, 2015 [15].

| Bioplastic         | Company                              | Country               | Commercial Name  | Applications/Notes  |
|--------------------|--------------------------------------|-----------------------|--|---|
| PHB                | Mitsubishi Gas Chemical Company Inc. | Japan                 | -Biogreen®   | -Cast films and natural latex gloves.   |
| PHB                | PHB Industrial S/A                   | Brazil                | -Biocycle™ (B1000, B18BC-1, B189C-1, B189D-1)          | -Medical devices, films and disposables).   |
| PHB and PHBV       | Biomer Inc.                          | Germany               | -Biomer®300 (P300E, P300F)                             | -Extrusion (P300E)<br>-Extrusion and food contact (P300F).  |
| PHBV and PHBV/PLA  | Tianan Biologic, Ningbo              | China                 | -Enmat™ (Y1000, Y1010, Y1000P, Y3000, Y3000P, F9000P). | -Thermoforming, nonwovens and fiber, injection molding, extrusion and water treatment.  |
| P4HB               | Tepha, Inc.                          | USA                   | -TephaFLEX®  | -Surgical absorbable films and sutures.   |
| PHBHH <sub>x</sub> | Kaneka Co.                           | Japan                 | -Kaneka PHBH<br>-Aonilex®                              | -Foams, fibers, interior automotive materials, electrical equipment, sheets and injection molding.<br>-Containers, bottles, interior automotive materials and electrical equipment. |
| PHBHH <sub>x</sub> | Danimer Scientific                   | USA                   | -Nodax™  | -Coating, laminates, non-woven Fibers and packaging.  |
| P3HB4HB            | Tianjin Green Bio-Science Co./DSM    | China/The netherlands | -GreenBio®   | -Films for wrapping, laminating film, fresh film, heat shrinkable film, garbage bags, food packaging, shopping and gift bags.   |
| Several PHAs       | CJ CheilJedang Corporation           | South Korea           | -CJ PHA®   | -Rigid packaging, 3D printing, paper coating, agriculture and flexible packaging.   |
| Several PHAs       | Alterra Holdings                     | USA                   | -TerraBio®   | -Paper coating, packaging, utensils, straws and disposals.  |

Abbreviations: PHB, polyhydroxybutyrate; PHBV, poly(3-hydroxybutyrate-co-3-hydroxyvalerate); PLA, poly(lactic acid); P4HB, poly(4-hydroxybutyrate); PHBHH<sub>x</sub>, poly(3-hydroxybutyrate-co-3-hydroxyhexanoate); P3HB4HB, poly(3-hydroxybutyrate-co-4-hydroxybutyrate).



PHB, is the most simple and widely used member of the PHAs family [43]. PHB is synthesized and kept within the cells of different microorganisms as a source of energy [44]. PHB's production is usually done in two steps. The first step is fermentation in which various microorganisms store PHB inside their cells after they metabolize the available sugar in the medium. The second step includes extraction and purification of the PHB accumulated inside the microorganisms. PHB is stereoregular structure homopolymer that exhibits high degree of crystallinity. PHB is a stiff and brittle polymer with low melt viscosity and limited processing window. Therefore, the utilization of PHB in various applications is narrow [45]. Yet, many techniques have been used to enhance the ductility of PHB such as: the use of plasticizers, additives, nucleating agents, copolymerization of 3-hydroxybutyrate with 3-hydroxyvalerate (HV) and modification of the processing conditions. PHB has been used in many applications such as: packaging, agriculture for the release of fertilizers and in biomedical devices to regulate the release of drugs. Moreover, it has been used with non-biodegradable polymers as a bio filler to accelerate degradation [15]. The insertion of HV units into PHB biopolymer's backbone through fermentation results in PHBV or PHBHV, which is one of the most promising member in this family of biopolymer [46]. Compared to PHB, PHBV exhibits better toughness and flexibility as well as lower processing temperatures. Currently, PHBV with 15% HV content is commercially available. PHBV with higher HV content is very expensive to produce and therefore not commercially viable [47]. An increase in water permeability, glass transition and melting temperatures, as well as tensile strength is resulted from lowering the content of HV. Yet, percentage elongation at break and impact resistance decrease [48,49]. Due to its similar properties with PP, PHBV is considered as a promising green material. The percentage elongation of PHB and PHBV ranges from around 4 to 42% [15,50]. PHB and PHBV have been used in wound dressing, scaffolds, regeneration of tissue, blood vessels and food packaging [15]. Both PHB and PHBV exhibit some undesirable properties. For example, PHB demonstrates thermal instability, at the same time, both of PHB and PHBV have slow crystallization rates and flow properties. This makes it challenging to process these biopolymers. While processing PHBV, it exhibits a sticky behavior for a long period of time and might stick to itself while processing it into films. As shown in Figure 5, PLA and PHAs are biobased, biodegradable and ecologically friendly polymers with good strength and stiffness. They are intended to replace petroleum-based plastics in various applications. However, they suffer from high brittleness which hinders their utilization in many other potential applications [15].

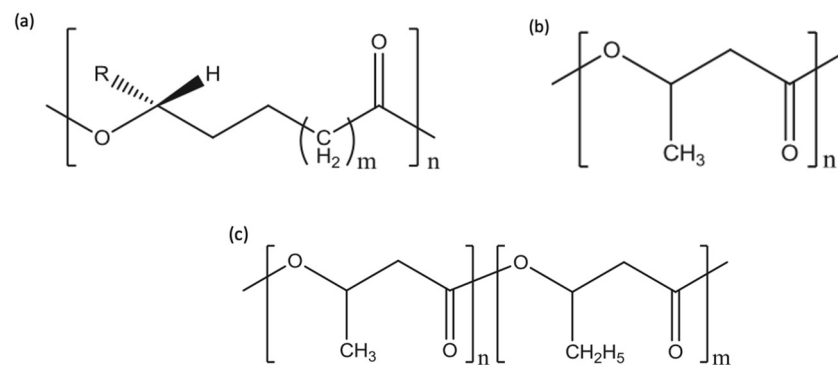


**Figure 4.** (a) The general chemical structure for PHAs,  $m \geq 0$ ,  $R = H$ , (un)substituted alkyl, (b) PHB's chemical structure and (c) PHBV's chemical structure. Reprinted with permission from Elsevier, 2015 [15].

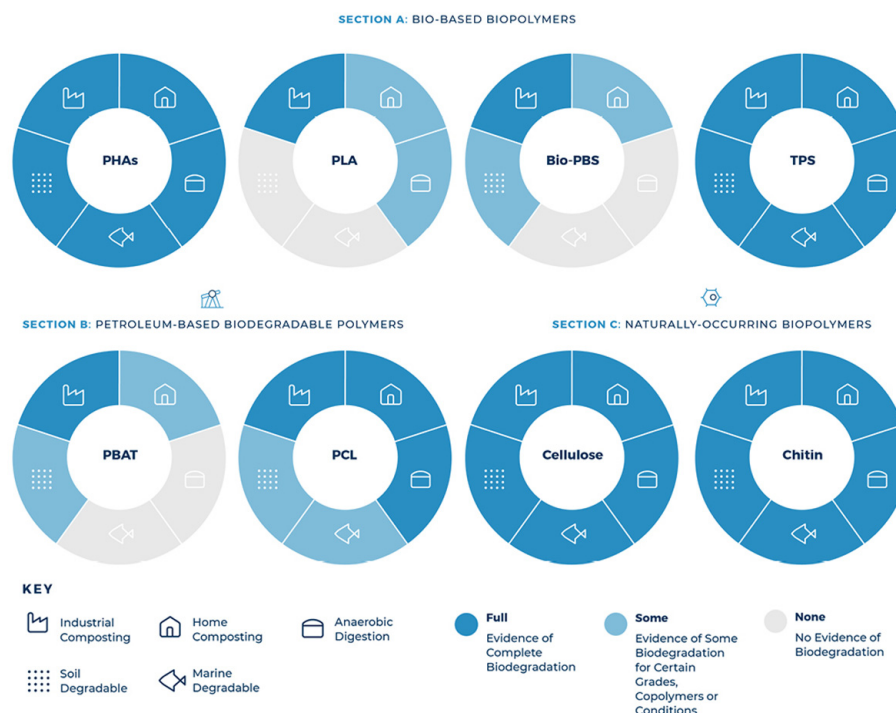


Figure 5. The end-of-life pathways for some plastics alternatives [51].

## 2. PLA’s Modifications

PLA has been reported as one of the most commonly used biodegradable polymers. It has been successfully used in various applications such as food packaging and biomedical devices. Due to its several advantages, PLA is considered as a tempting substitute for petroleum-based nonbiodegradable polymers in such applications. Some of the advantages of PLA include biodegradability, recyclability, biocompatibility and renewable sources (e.g., corn, wheat and rice) [52]. Due to PLA’s nontoxicity and carcinogen-free interaction with human tissues, many biomedical industries have switched their eyes on PLA. Data from different implantation surgeries shows that there has been an absence of any kind of toxic products produced from the degradation of implanted PLA devices. In addition, such produced products did not interfere with the healing process of tissues. Nonetheless, PLA’s use and implementation in food packaging and biomedical applications has been limited due to some of its drawbacks. Some of the important drawbacks of PLA are related to its poor mechanical properties such as, its brittleness, low modulus of elasticity, low percentage elongation at break and low tensile strength [52].

Table 3 shows the mechanical properties along with physical and thermal properties of some PLA developed by NatureWorks LLC [53,54]. Depending on various parameters such as: polymer structure, material formulation (blends, plasticizers, composites, etc.), orientation, crystallinity and molecular weight, the mechanical properties of commercial PLA can be diverse, ranging from elastic soft to stiff, high-strength materials. PLA exhibits some similarity with polystyrene (PS) in which it is a brittle material with low elongation at break and impact strength. However, its Young’s modulus and tensile strength are comparable with polyethylene terephthalate (PET). A comparison between the mechanical properties of PLLA, PS and PET is shown in Table 4. Due to its poor toughness, the use of PLA in applications that requires plastic deformation at higher stress levels has been avoided. For instance, the implementation of PLA in bone surgery as screws and fracture fixation plates has been substantially narrow due to the lack of PLA’s high plastic deformation behavior under high stress level condition [55]. The low stiffness of PLA’s implant devices can hinder the healing process and cause excessive bone motion. This has opened the door to develop various modification techniques to improve the mechanical properties of PLA, specifically its toughness [56].

**Table 3.** Mechanical, thermal and physical properties of some PLA produced by NatureWorks LLC [53,54].

| Properties/Applications                    | Ingeo™ 2003D  | Ingeo™ 3052D  | Ingeo™ 3801X   | ASTM Method |
|--|---|---|--|-------------|
| Specific Gravity                           | 1.24  | 1.24  | 1.25   | D792        |
| Melt Flow Rate, g/10 min (210 °C, 2.16 Kg) | 6   | 14  | 8  | D1238       |
| Relative viscosity                         | NP  | 3.3   | 3.1  | -           |
| Clarity                                    | Transparent   | Transparent   | Opaque   | -           |
| Tensile strength at break, psi (MPa)       | 7700 (53)   | NP  | NP   | D882        |
| Tensile yield strength, psi (MPa)          | 8700 (60)   | 9000 (62)   | 3750 (25.9)  | D882        |
| Tensile modulus, Kpsi (GPa)                | 500 (3.5)   | NP  | 432 (2.98)   | D882        |
| Flexural Strength, psi (MPa)               | NP  | 15,700 (108)  | 6400 (44)  | D790        |
| Flexural Modulus, psi (MPa)                | NP  | 515,000 (3600)  | 413,000 (2850)   | D790        |
| Tensile elongation, %                      | 6.0   | 3.5   | 8.1  | D882        |
| Notched Izod impact, ft-lb/in (J/m)        | 0.3 (16)  | 0.3 (16)  | 2.7 (144)  | D256        |
| Heat distortion temperature (°C)           | 55  | 55  | 65 (at 66 psi)<br>140 (at 16.5 psi)  | E2092       |
| Melt temperature (°C)                      | 210   | 200   | 188  | -           |
| Crystallinity melt temperature (°C)        | NP  | 145–160   | 155–170  | D3418       |
| Glass transition temperature (°C)          | NP  | 55–60   | 45   | D3418       |
| Applications                               | -Designed for fresh food packaging and food service ware applications such as: dairy containers, food service ware, transparent food containers, hinged ware and cold drink cups. | -Designed for injection molding applications that require clarity with heat deflection temperatures lower than 49 °C.<br>-Applications include: cutlery, cups, plates and saucers as well as outdoor novelties. | -Designed for non-food contact injection molding applications that require opaque molded parts with heat deflection temperatures between 65 °C and 140 °C. | -           |

NP: Not provided.

**Table 4.** Mechanical properties of poly(L-lactic acid); poly(styrene) and poly(ethylene terephthalate) [54,56].

| Polymer | Tensile Strength (MPa) | Tensile Modulus (GPa) | Percentage Elongation | Notched Izod (J/m) |
|---------|------------------------|-----------------------|-----------------------|--------------------|
| PLLA    | 59                     | 3.8                   | 4–7                   | 26                 |
| PS      | 45                     | 3.2                   | 3                     | 21                 |
| PET     | 57                     | 2.8–4.1               | 300                   | 59                 |

Abbreviations: PLLA, poly(L-lactic acid); PS, poly(styrene); PET, poly(ethylene terephthalate).

### 2.1. Plasticizers' Effect

PLA is classified as a glassy polymer with a poor elongation at break that is around 10% only. For this reason, various biodegradable and non-biodegradable plasticizers have been used in order to increase its ductility, improve its processability and increase its thermal stability (glass transition temperature) [57]. Such enhancements in the properties of PLA can be achieved through controlling the plasticizers' polarity, end groups and molecular weight. One of the effective monomers for plasticizing PLA is lactide. For example, PLA's elongation at the break can increase up to 288% when 17.3 wt.% of lactide is added to PLA. Nonetheless, lactide suffers from losses and fast migration [58]. Therefore, and since high molecular weight plasticizers do not have a high potential to migrate, they remain the preferable choice.

Different studies in literature have investigated the use of poly(ethylene glycol) (PEG) with different molecular weights as plasticizers for PLA to improve its mechanical properties. In one study, Jacobsen and Fritz [59] studied the effect of PEG with molecular weight 1500 g/mol (PEG1500) on the mechanical properties of PLA. When PEG or glucose monoester were added, there was an increase in the elongation at the break with increasing

the amount of plasticizer. This was not the case when partial fatty acid esters were used as a plasticizer. This variation is attributed to the fact that activation cells that led to crack formation were triggered by the finely distributed partial fatty acid ester. According to the study, PEG is the best plasticizer to be used for enhancing the elongation of PLA. For instance, the addition of 10 wt.% of PEG to PLA can result in an enhancement of the percentage elongation of up to 180%. Results of the impact resistance suggest that high amount (10 wt.% concentration) of PEG can lead to a significant increase in the impact resistance to a point that no break was observed. Nonetheless, the addition of any of the small amounts of PEG, glucose monoester at any concentration or any concentration of partial fatty acid ester resulted in a drop in the impact resistance. This decrease in the impact resistance can be explained by disturbance produced by the plasticizer particles inside the PLA matrix. This disturbance has prevented the sliding of chains to absorb shock energy [59]. The elongation at break was observed to increase with higher concentrations of PEG with molecular weight 400 g/mol or oligomeric lactic acid; however, when 20 wt.% of either of the two plasticizers was added, the highest drops in the modulus of elasticity of 53% and 65% were reported, respectively. At 20 wt.% oligomeric lactic acid, a maximum elongation at break of 200% was reported [60]. In case of PEG with molecular weight of 10,000 g/mol, 20 wt.% of PEG was needed to result in a significant increase in PLA's percentage elongation. Yet, the same change was achieved by incorporating 10 wt.% of PEG with low molecular weight (400 g/mol). Nonetheless, this improvement was at the expense of Young's modulus and tensile strength [61]. For PEG with molecular weights between 200 g/mol and 1000 g/mol, the optimum elongation at break was reported at 20 wt.% [62]. When PEG higher than 20 wt.% was added to the PLA, the modulus of elasticity was found to decrease drastically. It was also found that PLA's physicomechanical properties were not weakened when PEG with molecular weight of 200 g/mol was blended with PLA at a concentration of 10 wt.%. That was also the case when PEG with molecular weights 400 g/mol and 1000 g/mol were blended with PLA at concentrations of 20 wt.% and 30 wt.%, respectively. Due to the lack of cohesion between the separate phases, the blend exhibits a brittle behavior when higher plasticizer content was added. Therefore, the efficiency of the plasticizer is linked to the molecular level miscibility, which is higher for PEG than for other plasticizers used in the same study (acetyl glycerol monolaurate (AGM), dibutyl sebacate (DBS) and poly(1,3-butanediol) (PBOH)). The results suggest that the most effective plasticized formulations that give the best mechanical properties are AGM, PBOH and DBS at concentrations of 20–30%, respectively [62].

Polypropylene glycol (PPG) was reported as an effective plasticizer for PLA. The facts that PPG exhibits low glass transition temperature, does not crystallize in addition to its miscibility with PLA, make PPG a tempting plasticizer to blend with PLA. Mechanical properties suggest that using 12.5 wt.% of lower molecular weight PPG demonstrates the best performance. This is because it gives the highest increase in the elongation at break with the minimum decrease in tensile strength [63].

Nijenhuis et al. [64] found that enhancement of PLA's properties can be obtained using polymeric plasticizers. In their study they have successfully added high molecular weight poly(ethylene oxide) (PEO) to PLLA to enhance its elongation at break. The effect of high molecular weight PEO on the PLLA's elongation at break was mostly prominent at high concentrations exceeding 10 wt.%. For instance, the elongation of PLLA reached up to 500% when 20 wt.% of PEO was added. Nonetheless, when PEO at a concentration of 20 wt.% was used, a reduction in the tensile strength from 58 MPa for the neat PLLA to 24 MPa was observed [64].

Labrecque et al. [65] investigated the use of Citrate esters obtained naturally from citric acid as a potential plasticizer for PLA. The tensile strength significantly dropped to around 50% when the plasticizers were used. The deterioration was higher at larger concentrations. At relatively lower concentrations such as 10 wt.%, there was no major change in the elongation at break; however, when higher concentrations that are more than 20 wt.% were added, a significant increase in the percentage elongation was noticed. When

30 wt.% of triethyl citrate was added, the highest elongation at break value (610%) was reported. Unfortunately, this was accompanied with a major loss in the tensile strength [65].

The feasibility of adding poly(ethylene-*co*-vinyl acetate) (EVA) to PLLA as a plasticizer was studied by Yoon et al. [66]. Results showed a slight increase in the elongation at break for the PLLA/EVA blend when EVA up to 70 wt.% was added. However, a significant enhancement in the elongation at break was reported at 90 wt.% EVA at which a maximum elongation of 209% was reported. On the other hand, both the tensile strength and modulus of elasticity decreased rapidly. This was followed by a more gradual drop as the concentration of EVA increased [66].

Ren et al. [67] have used triacetin and oligomeric poly(1,3-butylene glycol adipate) with low molecular weight in an attempt to plasticize PLA. Results suggest that the resulted blend had a positive impact on improving PLA's elastic properties; however, that was accompanied by a reduction in the tensile strength. The blends were brittle at plasticizer's concentrations less than 5 wt.% but exhibited a ductile behavior at concentrations higher than 5 wt.% [67].

In another study [68], conventional and reactive extrusion was used to blend PLA with limonene (LM) or myrcene (My) bio-based plasticizers. Results showed that both plasticizers were efficient in improving the impact strength and ultimate tensile strength of PLA. This was also accompanied with a reduction in  $T_g$ . The incorporation of a free radical initiator throughout the extrusion of PLA/LM was beneficial for the mechanical properties. The probable formation of local crosslinked regions in the PLA matrix improved the matrix's ultimate tensile strength, yield strength and crystallinity in comparison to the non-reactive PLA/LM blend. However, other properties were retained [68].

The utilization of ozonized soybean oil (OSBO) as a biobased plasticizer for PLA was also investigated [69]. Plasticized PLA samples were made by compounding. OSBO contents in the range of 0 to 15% was added to PLA and the impacts on mechanical and thermal properties were evaluated and studied. Results showed that after the ozonolysis reaction, formation of hydroxyl groups in OSBO as well as an increase in ester groups were observed. As the content of OSBO increased, the impact strength and percentage elongation at break also increased, yet the tensile strength decreased. PLA's  $T_g$ ,  $T_m$  and crystallization temperatures continuously decreased as a function of OSBO content. PLA's crystallinity was also improved due to the presence of OSBO. In summary, at low content, OSBO acted as a plasticizer for PLA; however, at 15% OSBO, there was a formation of fine oil droplets which acted as an impact absorber by energy dissipation [69].

Dominguez-Candela and co-authors [70] have reported a new biobased PLA plasticizer derived from Epoxidized Chia Seed Oil (ECO). PLA with various contents of ECO (0–10 wt.%) was prepared using melt extrusion. Results showed an improvement by 700% in the percentage elongation at break at 10 wt.% ECO. Up to 5 wt.% ECO, plasticized PLA was disintegrated under composting conditions with no delays. Results of the migration tests indicated a very low migration level (lower than 0.11 wt.%), which is of much interest to the packaging industry [70].

In another investigation [71], the use of dibutylmaleate (DBM) and dibutylfumarate (DBF) as biodegradable plasticizers to PLA was studied. Thermal and mechanical properties of plasticized PLA were investigated. Results showed that DBF had a more pronounced plasticization effect exhibiting lower glass transition temperature, yield strength, viscoelastic properties, modulus of elasticity and higher elongation at break. This was attributed to the end-to-end distance of the plasticizer's molecules. The incorporation of 12 wt.% DBF to PLA led to an increase in the elongation at break from 1.3% for neat PLA to around 210.00% [71].

A summary of the various plasticizers reported in literature along with their effects on PLA's mechanical properties at various concentrations is shown in Table 5.

Table 5. Various plasticizers and their effects on the different mechanical properties of PLA along with their applications.

| Plasticizer | Plasticizer's Concentration (wt.%) | PLA's Type and Reference                      | Tensile Strength (MPa) | Young's Modulus (MPa) | Percentage Elongation | Charpy Impact, (MJ/mm <sup>2</sup> ) | Application  | Comments  |
|-------------|------------------------------------|---|------------------------|-----------------------|-----------------------|--------------------------------------|--|---|
| Lactide     | - 25.5%                            | PLA, in the form of films [58].               | - 16.8                 | - 232                 | - 546%                | -                                    | General Packaging.   | Degradation increased with increasing the content of plasticizer. |
|             | - 19.2%                            |   | - 29.2                 | - 658                 | - 536%                |                                      |  |   |
|             | - 17.3%                            |   | - 15.8                 | - 820                 | - 288%                |                                      |  |   |
|             | - 1.3%                             |   | - 51.7                 | - 1993                | - 3.00%               |                                      |  |   |
|             | - 0%                               | PLA (92% L-lactide and 8% meso-lactide) [59]. | - 58                   | - 3800                | - 3%                  | - 32 <sup>b</sup>                    | Applications demanding higher impact resistance and flexibility. | -   |
|             | - PEG 1500 (2.5%)                  |   | - 50                   | - 3200                | - 4%                  |                                      |  |   |
|             | - PEG 1500 (5%)                    |   | - 44                   | - 2500                | - 7%                  |                                      |  |   |
|             | - PEG 1500 (10%)                   |   | - 28                   | - 1200                | - 40%                 |                                      |  |   |
|             | - 0%                               | PLA (92% L-lactide and 8% meso-lactide) [60]. | -                      | - 2050                | - 9%                  | -                                    | -  | Biocompatible plasticizers.                                       |
|             | - m-PEG (10%)                      |   | - 1571                 | - 18%                 |                       |                                      |  |   |
|             | - m-PEG (20%)                      |   | - 1124                 | - 142%                |                       |                                      |  |   |
|             | - PEG 400 (10%)                    |   | - 1488                 | - 26%                 |                       |                                      |  |   |
|             | - PEG 400 (20%)                    |   | - 976                  | - 160%                |                       |                                      |  |   |
| PEG         | - 0%                               | PLA [61].                                     | - 66.0                 | - 3300                | - 1.8%                | -                                    | Medical, personal care and food packaging applications.          | -   |
|             | - PEG 400 (5%)                     |   | - 41.6                 | - 2500                | - 1.6%                |                                      |  |   |
|             | - PEG 400 (10%)                    |   | - 32.5                 | - 1200                | - 140%                |                                      |  |   |
|             | - PEG 400 (12.5%)                  |   | - 18.7                 | - 500                 | - 115%                |                                      |  |   |
|             | - PEG 400 (15%)                    |   | - 19.1                 | - 600                 | - 88%                 |                                      |  |   |
|             | - PEG 400 (20%)                    |   | - 15.6                 | - 500                 | - 71%                 |                                      |  |   |
|             | - PEG 1500 (5%)                    |   | - 52.3                 | - 2900                | - 3.5%                |                                      |  |   |
|             | - PEG 1500 (10%)                   |   | - 46.6                 | - 2800                | - 5.0%                |                                      |  |   |
|             | - PEG 1500 (12.5%)                 |   | - 18.5                 | - 700                 | - 194%                |                                      |  |   |
|             | - PEG 1500 (15%)                   |   | - 23.6                 | - 800                 | - 216%                |                                      |  |   |
|             | - PEG 1500 (20%)                   |   | - 21.8                 | - 600                 | - 235%                |                                      |  |   |
|             | - PEG 10,000 (5%)                  |   | - 53.9                 | - 2800                | - 2.4%                |                                      |  |   |
|             | - PEG 10,000 (10%)                 |   | - 48.5                 | - 2800                | - 2.8%                |                                      |  |   |
|             | - PEG 10,000 (15%)                 |   | - 42.3                 | - 2500                | - 3.5%                |                                      |  |   |
|             | - PEG 10,000 (20%)                 |   | - 22.1                 | - 700                 | - 130%                |                                      |  |   |

Table 5. Cont.

| Plasticizer               | Plasticizer's Concentration (wt.%) | PLA's Type and Reference             | Tensile Strength (MPa) | Young's Modulus (MPa) | Percentage Elongation | Charpy Impact, (MJ/mm <sup>2</sup> ) | Application  | Comments  |
|---------------------------|------------------------------------|--------------------------------------|------------------------|-----------------------|-----------------------|--------------------------------------|--|---|
|                           | - 0%                               |                                      | - 64.0                 | - 2840                | - 3.0%                |                                      |  |   |
|                           | - PEG 200 (10%)                    |                                      | - 30.0                 | - 1700                | - 2.0%                |                                      |  |   |
|                           | - PEG 400 (10%)                    | PLA (92%)                            | - 39.0                 | - 1920                | - 2.40%               |                                      |  |   |
|                           | - PEG 400 (20%)                    | L-lactide and 8%                     | - 16.0                 | - 630                 | - 21.2%               |                                      | Food packaging Applications.                                     | The plasticizers used are food packaging approved.  |
|                           | - PEG 1000 (10%)                   | D-lactide) [62].                     | - 39.6                 | - 1970                | - 2.7%                | -                                    |  |   |
|                           | - PEG 1000 (20%)                   |                                      | - 21.6                 | - 290                 | - 200%                |                                      |  |   |
|                           | - PEG 1000 (30%)                   |                                      | - 4.70                 | - 420                 | - 1.50%               |                                      |  |   |
|                           | - 0%                               |                                      | - 25.5                 |                       | - 64%                 |                                      |  | PPGs increased the ability of   |
|                           | -PEG 600 (5.0%)                    |                                      | - 19.3                 |                       | - 67.0%               |                                      |  | PLA to plastically  |
|                           | - PEG 600 (7.50%)                  | PLA [63].                            | - 17.5                 | -                     | - 360%                |                                      |  | deform in a more  |
|                           | - PEG 600 (10.0%)                  |                                      | - 18.5                 |                       | - 427%                |                                      |  | efficient way than  |
|                           | - PEG 600 (12.50%)                 |                                      | - 19.7                 |                       | - 622%                |                                      |  | PEG.  |
| Glucose monoesters        | - 0%                               |                                      | - 58                   | - 3800                | - 3%                  | - 32 <sup>b</sup>                    |  |   |
|                           | - 2.5%                             |                                      | - 52                   | - 3200                | - 5%                  | - 23 <sup>b</sup>                    |  |   |
|                           | - 5%                               |                                      | - 47                   | - 3000                | - 6%                  | - 24 <sup>b</sup>                    |  |   |
|                           | - 10%                              | PLA (92%)                            | - 39                   | - 2550                | - 12%                 | - 18 <sup>b</sup>                    | Applications requiring higher impact resistance and flexibility. | -   |
| Partial fatty acid esters | - 0%                               | L-lactide and 8% meso-lactide) [59]. | - 58                   | - 3800                | - 3%                  | - 32 <sup>b</sup>                    |  |   |
|                           | - 2.5%                             |                                      | - 52                   | - 3450                | - 14%                 | - 25 <sup>b</sup>                    |  |   |
|                           | - 5%                               |                                      | - 48                   | - 3100                | - 7%                  | - 28 <sup>b</sup>                    |  |   |
|                           | - 10%                              |                                      | - 44                   | - 3000                | - 8%                  | - 22 <sup>b</sup>                    |  |   |
| Oligomeric lactic acid    | - 0%                               | PLA (92%)                            | -                      | - 2050                | - 9%                  | -                                    |  | Biocompatible Plasticizers.   |
|                           | - 10%                              | L-lactide and 8%                     | -                      | - 1256                | - 32%                 | -                                    |  |   |
|                           | - 20%                              | meso-lactide) [60].                  | -                      | - 744                 | - 200%                | -                                    |  |   |
| ATBC                      | - 0%                               |                                      | - 66.0                 | - 3300                | - 1.8%                |                                      |  | ATBC is derived from naturally occurring citric acid. It is also non-toxic and has been approved for use in personal care and medical applications. |
|                           | - 5%                               |                                      | - 53.4                 | - 3200                | - 5.1%                |                                      | Medical, personal care and food packaging applications.          |   |
|                           | - 10%                              | PLA [61].                            | - 50.1                 | - 2900                | - 7.0%                | -                                    |  |   |
|                           | - 12.5%                            |                                      | - 17.7                 | - 100                 | - 218%                |                                      |  |   |
|                           | - 15%                              |                                      | - 21.3                 | - 100                 | - 299%                |                                      |  |   |
|                           | - 20%                              |                                      | - 23.1                 | - 100                 | - 298%                |                                      |  |   |

Table 5. Cont.

| Plasticizer         | Plasticizer's Concentration (wt.%) | PLA's Type and Reference                   | Tensile Strength (MPa) | Young's Modulus (MPa) | Percentage Elongation | Charpy Impact, (MJ/mm <sup>2</sup> ) | Application   | Comments  |
|---------------------|------------------------------------|--|------------------------|-----------------------|-----------------------|--------------------------------------|---|---|
| PBOH                | - 0%                               |  | - 64.0                 | - 2840                | - 3.0%                |                                      |   |   |
|                     | - 10%                              |  | - 56.3                 | - 2350                | - 3.00%               |                                      |   |   |
|                     | - 20%                              |  | - 30.2                 | - 350                 | - 302.5%              | -                                    |   |   |
|                     | - 30%                              |  | - 25.2                 | - 300                 | - 390%                |                                      |   |   |
| AGM                 | - 0%                               | PLA (92% L-lactide and 8% D-lactide) [62]. | - 64.0                 | - 2840                | - 3.0%                |                                      | Food packaging applications.  | The plasticizers used are approved for food packaging.  |
|                     | - 10%                              |  | - 52.1                 | - 2240                | - 32.0%               |                                      |   |   |
|                     | - 20%                              |  | - 27.1                 | - 35.0                | - 335.0%              | -                                    |   |   |
|                     | - 30%                              |  | - 17.9                 | - 107.0               | - 320.0%              |                                      |   |   |
| DBS                 | - 0%                               |  | - 64.0                 | - 2840                | - 3.0%                |                                      |   |   |
|                     | - 10%                              |  | - 39.2                 | - 2000                | - 2.30%               |                                      |   |   |
|                     | - 20%                              |  | - 23.1                 | - 430.0               | - 269.0%              | -                                    |   |   |
|                     | - 30%                              |  | - 18.3                 | - 370.0               | - 333.0%              |                                      |   |   |
| PPG                 | - 0%                               |  | - 25.5                 |                       | - 64%                 |                                      |   |   |
|                     | - PPG 425 (5.0%)                   |  | - 20.7                 |                       | - 19.0%               |                                      |   | PPGs increased the ability of the used PLA to plastically deform in a more efficient way than PEG.                                    |
|                     | - PPG 425(7.5%)                    |  | - 17.7                 |                       | - 107%                |                                      |   |   |
|                     | - PPG 425 (10.0%)                  |  | - 21.0                 |                       | - 524%                |                                      |   |   |
|                     | - PPG 425 (12.5%)                  | PLA [63].                                  | - 21.0                 |                       | - 702%                | -                                    |   |   |
|                     | - PPG 1000 (5.0%)                  |  | - 22.2                 |                       | - 44%                 |                                      |   |   |
|                     | - PPG 1000 (7.5%)                  |  | - 22.6                 |                       | - 329%                |                                      |   |   |
|                     | - PPG 1000 (10.0%)                 |  | - 22.8                 |                       | - 473%                |                                      |   |   |
| - PPG 1000 (12.50%) |                                    | - 21.6                                     |                        | - 496%                |                       |                                      |   |   |
| PEO                 | - 0%                               |  | - 58                   |                       | - 7%                  |                                      | Nerve guides, barriers to tissue adhesion and orbital floor reconstruction. | The initial degradation of PLLA/PEO was more rapid than the neat PLLA and degradation rate increased with increasing the PEO content. |
|                     | - 5%                               |  | - 54.5                 |                       | - 7%                  |                                      |   |   |
|                     | - 10%                              | PLLA [64].                                 | - 54                   |                       | - 11%                 | -                                    |   |   |
|                     | - 15%                              |  | - 35                   |                       | - 50%                 |                                      |   |   |
|                     | - 20%                              |  | - 24                   |                       | - >500%               |                                      |   |   |



Table 5. Cont.

| Plasticizer                          | Plasticizer's Concentration (wt.%)              | PLA's Type and Reference        | Tensile Strength (MPa) | Young's Modulus (MPa) | Percentage Elongation | Charpy Impact, (MJ/mm <sup>2</sup> ) | Application                         | Comments  |
|--------------------------------------|---|---------------------------------|------------------------|-----------------------|-----------------------|--------------------------------------|-------------------------------------|---|
| Triethyl citrate <sup>c</sup>        | - 0%  |                                 | - 51.7                 |                       | - 7%                  |                                      |                                     | Citrates with low molecular weight has increased the rate of eczematous degradation while the degradation rate has decreased when high molecular weight citrates were used. |
|                                      | - 10%   |                                 | - 28.1                 |                       | - 21.3%               |                                      |                                     |   |
|                                      | - 20%   |                                 | - 12.6                 | -                     | - 382%                |                                      |                                     |   |
|                                      | - 30%   |                                 | - 7.2                  |                       | - 610%                |                                      |                                     |   |
| Tributyl citrate <sup>c</sup>        | - 0%  |                                 | - 51.7                 |                       | - 7%                  |                                      |                                     |   |
|                                      | - 10%   |                                 | - 22.4                 | -                     | - 6.2%                |                                      |                                     |   |
|                                      | - 20%   | PLA, in the form of films [65]. | - 7.1                  |                       | - 350%                |                                      |                                     |   |
| Acetyl triethyl citrate <sup>c</sup> | - 0%  |                                 | - 51.7                 |                       | - 7%                  |                                      |                                     |   |
|                                      | - 10%   |                                 | - 34.5                 |                       | - 10%                 |                                      |                                     |   |
|                                      | - 20%   |                                 | - 9.6                  | -                     | - 320%                |                                      |                                     |   |
|                                      | - 30%   |                                 | - 7.6                  |                       | - 228%                |                                      |                                     |   |
| Acetyl tributyl citrate <sup>c</sup> | - 0%  |                                 | - 51.7                 |                       | - 7%                  |                                      |                                     |   |
|                                      | - 10%   |                                 | - 17.7                 | -                     | - 2.3%                |                                      |                                     |   |
|                                      | - 20%   |                                 | - 9.2                  |                       | - 420%                |                                      |                                     |   |
| EVA                                  | - 0%  |                                 | - 55.89                | - 2853.73             | - 4.5%                |                                      |                                     |   |
|                                      | - 10%   |                                 | - 45.11                | - 1804.42             | - 4.7%                |                                      |                                     |   |
|                                      | - 30%   |                                 | - 32.36                | - 1314.09             | - 6.9%                |                                      |                                     |   |
|                                      | - 50%   | PLLA [66].                      | - 16.67                | - 1274.86             | - 10.2%               |                                      |                                     |   |
|                                      | - 70%   |                                 | - 16.67                | - 1284.67             | - 9.0%                |                                      |                                     |   |
|                                      | - 90%   |                                 | - 13.73                | - 627.62              | - 208.9%              |                                      |                                     |   |
| Limonene                             | - 0%  |                                 | - 60.60                | - 2300                | - 7.40%               | - 2.70                               | Transparent packaging applications. | Biobased plasticizers   |
|                                      | - 20%   |                                 | - 15.80                | - 1000                | - 117.50%             | - 5.50                               |                                     |   |
|                                      | - 20% with 1% L101 as a free radical initiator. | PLA [68].                       | - 17.20                | - 1200                | - 120.20%             | - 5.80                               |                                     |   |
| Myrcene                              | - 20%   |                                 | - 18.70                | - 1900                | - 62.70%              | - 12.50                              | Opaque packaging applications.      |   |
|                                      | - 20% with 1% L101.                             |                                 | - 24.80                | - 1700                | - 45.00%              | - 4.90                               |                                     |   |

Table 5. Cont.

| Plasticizer          | Plasticizer's Concentration (wt.%) | PLA's Type and Reference | Tensile Strength (MPa) | Young's Modulus (MPa) | Percentage Elongation | Charpy Impact, (MJ/mm <sup>2</sup> ) | Application   | Comments                    |
|----------------------|------------------------------------|--------------------------|------------------------|-----------------------|-----------------------|--------------------------------------|---|-----------------------------|
| Ozonized soybean oil | - 0%                               | PLA [69].                | - 54.00                | - 1500                | - 5.50%               | - 2.00                               | Applications requiring flexibility and toughness.                 | Biobased plasticizer        |
|                      | - 5%                               |                          | - 46.00                | - 1520                | - 6.50%               | - 2.10                               |   |                             |
|                      | - 10%                              |                          | - 41.00                | - 1400                | - 10.50%              | - 2.20                               |   |                             |
|                      | - 15%                              |                          | - 34.00                | - 1450                | - 8.50%               | - 2.50                               |   |                             |
| ECO                  | - 0%                               | PLA [70].                | - 44.00                | - 3120                | - 8.50%               | -                                    | Packaging applications.   | Biobased plasticizer        |
|                      | - 2.50%                            |                          | - 42.00                | - 3050                | - 17.00%              |                                      |   |                             |
|                      | - 5.00%                            |                          | - 39.00                | - 3070                | - 33.50%              |                                      |   |                             |
|                      | - 7.50%                            |                          | - 36.00                | - 2950                | - 58.00%              |                                      |   |                             |
|                      | - 10.00%                           |                          | - 34.00                | - 2930                | - 64.00%              |                                      |   |                             |
| DBM                  | - 0%                               | PLA [71].                | - 19.00                | - 1672                | - 1.30%               | -                                    | Green alternatives for the production of PLAbased flexible films. | Biodegradable plasticizers. |
|                      | - 7.00%                            |                          | - 45.00                | - 2245                | - 2.80%               |                                      |   |                             |
|                      | - 12.00%                           |                          | - 15.00                | - 1533                | - 3.00%               |                                      |   |                             |
| DBF                  | - 7.00%                            | PLA [71].                | - 30.00                | - 584                 | - 111.90%             | -                                    |   |                             |
|                      | - 12.00%                           |                          | - 10.00                | - 279                 | - 210.00%             |                                      |   |                             |

<sup>a</sup> NP: not provided. <sup>b</sup> All the impact samples used in this study were un-notched. <sup>c</sup> Molecular weights for Triethyl citrate, Tributyl citrate, Acetyl triethyl citrate and Acetyl tributyl citrate are 276 g/mol, 360 g/mol, 318 g/mol and 402 g/mol, respectively. Note: Studies in which no exact values for the mechanical properties were given, the best estimations were provided. Abbreviations: PLA, poly(lactic acid); PEG, poly(ethylene-glycol); m-PEG, PEG monolaurate; ATBC, acetyl tri-n-butyl citrate; PBOH, poly(1,3-butanediol); AGM, acetyl glycerol monolaurate; DBS, dibutyl sebacate; PPG, poly(propylene glycol); PEO, poly(ethylene oxide); PLLA, poly(L-lactic acid); EVA, poly(ethylene-co-vinyl acetate); L101, luperox 101; ECO, epoxidized chia seed oil; DBM, dibutylmaleate; DBF, dibutylfumarate.

## 2.2. Impact Modifiers' Effect

Various impact modifiers can be incorporated into PLA to lower its brittleness while preserving its stiffness. In one study [72], 10 wt.% of Biomax Strong (BS) 100 impact modifier was added into PLA. Results showed an increase in its tensile properties and percentage elongation. Moreover, when 10 wt.% of BS was added, plasticized Cloisite 25A/PLA composites maintained their strength and rigidity while exhibited good ductility [72].

In another study [73], a substantial enhancement in the elongation at break and the notched impact strength of PLA was reported as a result of increasing the content of BS impact modifier up to 50 wt.%. Nonetheless, there was a reduction in the Young's modulus and yield stress of PLA with increasing the amount of BS impact modifier. That was attributed to BS impact modifier's toughening effect which reduced PLA's crystallinity by improving PLA matrix's plastic deformation [73].

The effect of adding Paraloid BPM-515 impact modifier into PLA/talc composites was also investigated. In one study [74], it was found that the toughness of the composite increased as a result of the successful incorporation of 1.8 wt.% of Paraloid BPM-515 impact modifier. This was attributed to the improved compatibility between the talc fillers and the PLA matrix after the addition of the impact modifier [74].

Diaz et al. [75] were able to incorporate Paraloid BPM-515 impact modifier into PLA. Results showed a rapid improvement in the impact strength and a slight increase in the elongation at break of PLA due to the addition of the impact modifier [75].

The synthetization of two transparent impact modifiers—poly(butadiene-*co*-methyl methacrylate-*co*-butyl methacrylate-*co*-butyl acrylate-*co*-hydroxyethyl methacrylate) (known as BMBH copolymer) and poly(butadiene-*co*-lactide-*co*-methyl methacrylate-*co*-butyl methacrylate) (known as BLMB copolymer) as PLA impact modifiers was reported by Choochottiros and Chin [76]. The results showed an improvement in the impact strength and toughness while maintaining the clarity of PLA [76].

Nonetheless, most of PLA's impact modifiers available today are nonbiodegradable. Moreover, they are usually used at a concentration of 10 wt.% for various applications in the industry. Therefore, for applications where the biodegradation of PLA is vital, different studies suggested the use of biodegradable polymers (e.g., PCL, poly(butylenes succinate), poly(propylene carbonate), poly(butylenes adipate-*co*-terephthalate), poly(tetramethylene adipate-*co*-terephthalate) and poly(*p*-dioxanone) (PPD)) as biodegradable impact modifiers for PLA applications [72,77,78]. In their study, Odent et al. [79] found that the addition of poly( $\epsilon$ -caprolactone-*co*- $\delta$ -valerolactone) as a biodegradable impact modifier improved PLA's toughness while maintaining its transparency [79]. Table 6 provides a summary of various impact modifiers that are specifically designed for PLA applications.

**Table 6.** Various PLA's impact modifiers along with their features and applications.

| Impact Modifier and Reference/s          | Company        | Application  | Features   | Comments  |
|--|----------------|--|--|---|
| -Sulkano® PLA im S550 [80].              | -Sulkano Co.   | -Transparent applications such as packaging.                                     | -Highly cost effective.<br>-At a 4% concentration, the impact resistance of PLA can be enhanced by a factor of 10.   | -Compostable and can be used with FDA approved, biodegradable PLA.  |
| -OnCap™BIO Impact T [80,81].             | -PolyOne.      | -Transparent applications such as packaging.                                     | -Improves the impact resistance of PLA while maintaining its transparency.<br>-Improves tear resistance.   | -Designed to improve the applicability of biodegradable and bio-derived polymers.<br>-If used at prescribed loadings, it does not limit the biodegradability or food contact use of the PLA compound. |
| -Biomax® Strong 100 and 120 [80,82,83].  | -DuPont Co.    | -Packaging including food packaging and industrial applications.                 | -Enhance PLA's toughness and impact strength with minimal effect on transparency.<br>-At a 2% concentration, the impact resistance of PLA can be substantially enhanced.   | -Biomax® Strong 100 is designed for non-food applications, while Biomax® Strong 120 is designed for food packaging applications.  |
| -Paraloid™ BPM-500, 515 and 520 [80,84]. | -Dow Chem. Co. | -Packaging, electronics, medical, injection molding and automobile applications. | -Improve the mechanical properties of PLA while maintaining its transparency.<br>-Improvement in flexibility, slitting and cutting.<br>-The addition of only 3% concentration can lead to an improvement in the impact properties of PLA.<br>-Paraloid™ BPM-520 significantly enhances the toughness of PLA and PLA blends with minimal effect on stiffness and heat distortion temperature. Moreover, it features excellent room temperature impact performance. It also provides excellent surface finish and exceptional combinations of color ability and impact strength in opaque PLA and PLA blends applications. | -Paraloid™ BPM-515 is more efficient and FDA approved for up to 5% in food contact resins.  |

**Table 6.** *Cont.*

| Impact Modifier and Reference/s           | Company  | Application   | Features   | Comments |
|---|----------|---|--|----------|
| -Biostrength™ 130, 150, 280 and 200 [80]. | -Arkema. | -Packaging, injection molding, transparent and opaque applications. | <p>-Biostrength™ 130 and 200 are intended to improve PLA's toughness while maintaining its transparency.</p> <p>-Biostrength™ 150 is used in opaque and durable injection molding applications.</p> <p>-Biostrength™ 280 is utilized in applications that require high transparency and toughness.</p> | -        |

Abbreviations: PLA, poly (lactic acid); FDA, Food and Drug Administration.

### 2.3. Blending's Effect

An alternative effective approach that results in new materials with required properties is polymer blending. This approach depends on modifying the available polymer rather than synthesizing entirely new polymers. The ability to blend various polymers and at the same time conserve their distinct properties in the final blend is a tempted and cheaper way for producing new polymers with desirable properties. Preparing blends usually involve the use of twin-screw extruders. To produce a blend with desirable properties, different factors must be taking into consideration. For example, the barrel temperature must be adjusted to be above the  $T_g$  of that of an amorphous polymer or above the  $T_m$  of a semi crystalline polymer. This is crucial to control the viscosity so as to result in an optimal dispersion. The lower limit for PLA blends should be around 180 °C. Thermal degradation of PLA is possible at high temperatures; therefore, polymers that are processed at relatively extreme processing temperatures, that is higher than 270 °C are not preferable candidates for PLA blends. The desired properties resulted from blending of one or more polymers do not always come without a cost. When dealing with miscible blends, one of the biggest challenges is to obtain a good interfacial adhesion among the blending phases. This can directly influence the morphology and, consequently, the mechanical and physical properties. Another issue arises if the added polymer and PLA are not very compatible. In this case, extra subsequent work is required to enhance the compatibility. In case of poor interfacial adhesion, PLA blend can suffer from embrittlement. Furthermore, a significant change in phases' morphology can take place, based on product's design as well as the processing conditions. Another issue can occur when blending PLA with non-biodegradable polymers as this can affect the composability of PLA [4,85,86]. Blending more than two biopolymers does not necessarily yield a biodegradable blend even if one of the blended polymers is biodegradable. The selection of polymer blending partners depends on the desired properties of the final blend. For example, mechanical properties, such as stiffness and toughness, whether the blend should be biodegradable, the rate of biodegradability, the desired chemical and physical properties, crystallinity and miscibility, all play a role in the selection of blending partner. Stiff polymers have higher crystallinity and are brittle while flexible polymers are more amorphous. Hence, when a tough flexible biopolymer is added to a brittle biopolymer, this will increase the impact resistance while at the same time reduce the strength and modulus. Optimized properties and performance are believed to be achieved by blending brittle biopolymers with flexible biopolymers. In biodegradable materials, the two most important points in producing functional biopolymer blends are, (1) the compatibility or miscibility of the blend and (2) the whole biodegradability of the blend and its composition. Polymer blending can be divided into three categories [86]:

Heterogeneous or immiscible polymer blends: In such blends, the polymers exist in separate phases and the respective glass transition temperatures are detected.

Compatible polymer blends: Such blends are immiscible and demonstrate uniform macroscopical physical properties. This can be attributed to the robust interactions between the polymers' component.

Homogeneous or Miscible polymer blends: This type of blends are usually made from polymers that have similar chemical structures. This will lead to a single-phase structure polymer blend with only one glass transition temperature.

#### 2.3.1. PLA/PHAs Blends

PHAs are biodegradable linear polyesters that are obtained by various microorganisms. One of the most common and simplest form of PHAs family is PHB. Because PHAs are produced from renewable natural resources, blends of PHAs/PLA are expected to be completely biodegradable. The miscibility of PLA/PHB blends depends on the PLA's molecular weight. Using a lower molecular weight PLA usually leads to a highly miscible PLA/PHB blend [87–90]. Different studies have investigated the mechanical properties of PHAs/PLA blends.

Blending PLLA with PHBV was investigated by Iannace et al. [91]. The blend was prepared by solution casting of chloroform at room temperature. For the blends with 20 wt.% and 40 wt.% PHBV, results showed a minor increase in the elongation at break. As more PHBV content was used, Young's modulus and tensile strength both reduced. These results were supported by a drop in the crystallinity of the PLLA phase when more PHBV was incorporated [91].

In a similar work [92], the mechanical properties for PLLA/PHBV blends were reported. The study confirmed the trend of the elastic modulus reported from the previous study [91]; however, the tensile strength of PLLA/PHBV blends were lower. The reason behind that was that Iannace et al. [91], obtained dense PLLA films only, while a porous PLLA film was prepared in this study [92].

Yoon et al. [93] investigated the mechanical properties of PLLA/PHB blends after incorporating various types and amounts of compatibilizers. PLLA/PHB blends with a concentration of 50/50 wt.% were blended in 3 wt.% chloroform. Poly(vinyl acetate) (PVAc), PLLA-PEG-PLLA triblock copolymer and PEG PLLA diblock copolymer at 2 wt.% and 5 wt.% were used as compatibilizers. When a compatibilizer was used, all the blends reported improvements in the tensile toughness and percentage elongation for both compositions when compared to the PLLA/PHB blend without a compatibilizer. Nevertheless, when compared with an un-compatibilized PLLA/PHB blend, the modulus of elasticity was lower for all the blends at various amounts of compatibilizer. The values of tensile strength varied according to the type and composition of the compatibilizers. Tensile strength was reduced in both blends with 5 wt.% of diblock and triblock copolymers as well as the PVAc as compatibilizers with respect to the un-compatibilized PLLA/PHB blend. However, a maximum tensile strength of 69.8 Mpa was reported for the blend of 2 wt.% PLLA-PEG-PLLA triblock copolymer, this was followed by a tensile strength value of 65.5 Mpa that was reported for the 2 wt.% PEGPLLA diblock copolymer. PLLA/PHB blend with 2 wt.% of PLLA-PEG-PLLA triblock copolymer reported the best results in terms of percentage elongation, tensile strength and toughness. Moreover, the mechanical properties were better than those of the un-compatibilized PLLA/PHB blend, yet, the modulus of elasticity exhibited a minor reduction [93].

In another work, PLA/PHA blends were prepared by Takagi et al. [94] at various compositions. PLA was blended with PHA as well as with functionalized PHA with 30% epoxy group in its side chains (ePHA). For all compositions, PLA/PHA and PLA/ePHA blends exhibited lower tensile strengths than that of the neat PLA. On the other hand, as the composition of PHA or ePHA increased, Charpy impact strength for both blends increased as well and were higher than that for neat PLA. PLA/ePHA blends reported higher tensile strength and Charpy impact strength compared to the PLA/PHA blends. That was explained by the inserted epoxy side group of ePHA which enhanced the blend's compatibility [94].

Noda et al. [95] were able to prepare PLA/PHA blends via melt mixing using a single-screw extruder. The study used Nodax™ which is poly(3-hydroxybutyrate)-*co*-(3-hydroxyalkanote) in the investigation. When 10 wt.% Nodax™ was added, the blend's toughness improved dramatically. The tensile energy was 10 times more than that of the neat PLA. However, Nodax™'s positive effect was only noticeable up to around 20 wt.%. Further addition of Nodax™ lowered the blend's toughness back to the value of neat PLA. That was explained by the fact that at Nodax™ content less than 20 wt.%, the copolymers dispersed in a fine way in the PLA matrix. The PHA portion of the blend stayed predominantly in a liquid-like amorphous state, therefore crystallization was hindered. The toughness and ductility of the blend were then resulted from the reduced crystallinity [95].

Schreck and Hillmyer [96] reported a similar study of PLLA/Nodax™ blend. A 75 rpm mixer at 190 °C was used for 15 min to compound the blends. The compositions of Nodax™ used in the study was from 0 to 25 wt.%. Similar to the trend reported by Noda et al. [95], enhancements in toughness were reported for the blends for up to 20 wt.% Nodax™. Neat PLLA's impact strength was around 22 J/m whereas the highest impact

strength value was 44 J/m which was reported for the blend with 15 wt.% Nodax™. In an attempt to enhance the binary blend properties, the study also investigated the impact of ternary blends of 81/14 wt.% PLLA/Nodax™ and 5 wt.% oligoNodax-b-poly(L-lactide) diblock copolymers as compatibilizers. There was no reported improvement in toughness with the incorporation of 5 wt.% oligoNodax-b-poly(L-lactide). This is attributed to the weak interfacial adhesion at the particle-matrix interface as a result of low entanglement of oligoNodax with Nodax™, which accordingly lowered the tendency to dissipate and deform impact loads [96].

In another study [43], a melt compound was used to come up with different PLA/PHB-based blends with different weight ratios (100/0, 75/25, 50/50, 25/75, 0/100). Results of the study showed that there was substantial improvement in the tensile properties of the blend in the case of PLA (75 wt.%) to PHB (25 wt.%) blends. This was attributed to the presence of PHB crystals, which acted as a filler and nucleating agent in the polymeric matrix of PLA [43].

Bartczak et al. [97] were able to improve PLA's impact strength and drawability by adding 20 wt% of atactic PHB (a-PHB). Due to the partial miscibility of PLA and PHB, the melting and cold crystallization temperatures of PLA have slightly changed. Results suggest that as the concentration of a-PHB in the blend increased, PLA's glass transition temperature was reduced. Using compression molding or extrusion technique, amorphous foils for food packaging were developed from the PLA/a-PHB blend. As the a-PHB content increased, the yield stress as well as the elastic modulus exhibited a slight drop, yet this was accompanied by an increase in the ultimate strain increased. This was explained by the thick aggregations of diffused crazes observed in PLA. It is believed that such crazes united to form deformation bands and macroscopic neck. Nonetheless, there was an increase in the tensile impact resistance of the thin film from 50 kJ/m<sup>2</sup> in case of neat PLA to around 118 kJ/m<sup>2</sup> for the PLA/a-PHB (80/20 wt.%) blends. The yield strength decreased with increasing the content of a-PHB [97].

Using melt blending technique, Nanda et al. [98] were able to successfully fabricate opaque PHBV/PLA blends for the aim of enhancing PHBV's mechanical and thermal properties. As per the study, there was a 250% and 148% increase in the elongation at break values for virgin PLA and PHBV, respectively [98]. PHBHH<sub>x</sub> which is an mcl-PHA demonstrates better mechanical and thermal properties than the scl-PHAs. Some studies have reported a substantial improvement in the mechanical properties of PLA/PHBHH<sub>x</sub> blends after the incorporation of 20 wt.% of the later [95,99,100].

Another study [101] reported a substantial improvement in the toughness of PLA/PHBHH<sub>x</sub> blends due to the presence of 10 wt.% PHBHH<sub>x</sub>, yet the blend reported to be incompatible [101].

In a similar investigation, Lim et al. [102] were able to fabricate PLA/PHBHH<sub>x</sub> blends. As the amount of PHBHH<sub>x</sub> increased, a drop in the PLA's crystallization was noticed. The investigation suggested that the ductility and toughness of PLA/PHBHH<sub>x</sub> blends for food packaging applications can be improved through the incorporation small quantities of PHBHH<sub>x</sub> to PLA. This is because for small quantities of PHBHH<sub>x</sub>, the tendency of aggregation was found to be insignificant [102].

In another study [103], melt blending was used to come up with a transparent multifunctional PLA, ATBC, cellulose nanocrystals (CNCs), modified CNCs and PHB flexible film for food packaging applications. The developed film demonstrated improved crystallinity, better stretchability, outstanding oxygen barrier properties and enhanced percentage elongation at break. Furthermore, the degradation was improved due to the incorporation of both the plasticizer and CNCs [103].

Moreover, different studies in literature have investigated the impact of different types of plasticizers and their quantity on the resulting blends' mechanical and thermal properties as well as degradation rate [104–108].

PLA/PHB blends (75/25 wt.%) with the incorporation of Lapol 108 as a plasticizer at two different concentrations (5 wt.% and 7 wt.% per 100 parts of the blends) were



produced by Abdelwahab et al. [108]. There was no sign of phase separation in the produced PLA/PHB blend. The blends showed a fine distribution of the main ingredients. Additionally, the miscibility of PLA and PHB with plasticizer was examined using a Differential Scanning Calorimetry (DSC). The DSC curves showed a single glass transition temperature value that exhibited a drop when the plasticizer's quantity increased. Yet, there was no significant variations in the blend's melting temperature and thermal stability for a certain quantity of the plasticizer. However, the PLA/PHB blend's elongation at break was enhanced due to the incorporation of the plasticizer [108].

Sofiane et al. [109] investigated the printability of PLA/PHA blend from physical and structural aspects. The study found that samples printed at higher temperatures and experienced high cooling rates were reported to be more ductile than those printed at low temperatures. This is attributed to the lower degree of crystallinity at high cooling rates. The study has also reported a low amount of porosity (less than 6%) in 3D-printed PLA/PHA blends via Fused Deposition Modeling (FDM). Furthermore, there was a positive impact of the printing temperatures on the tensile performance, density and porosity content. At low printing temperatures, the drop of tensile properties was more pronounced for the percentage elongation than for modulus of elasticity and tensile strength. According to the study, 3D-printed PLA/PHA blends are promising candidates for medical and pharmacological applications [109].

Recently, Olejnik and co-authors [110] blended PLA with PHB at various mixing mass ratios with the aid of an extruder. Results of the investigation showed that there was a drop in the  $T_g$  due to the incorporation of PHB to PLA. Results of the mechanical analysis also showed a drop of the ultimate tensile strength and tensile strength at break as a function of PHB content; however, low PHB content has led to material enhancement. Percentage elongation at break was found to raise in an exponential way as a function of the PHB's content [110].

Table 7 shows the impact of different PLA/PHAs blends at various concentrations on the mechanical properties.

Table 7. The effect of various PLA/PHAs blends at different concentrations on the mechanical properties along with their applications.

| Blend     | Concentration (wt.%)                   | Tensile Strength (MPa) | Young's Modulus (MPa) | Percentage Elongation | Charpy Break Energy/<br>(Notched Izod Break Energy) | Toughness   | Application and/or Reference   |
|-----------|--|------------------------|-----------------------|-----------------------|---|-------------|--|
|           | - 100/0                                | - 71.00                | - 2415                | - 5.60%               |   |             |  |
|           | - 80/20                                | - 54.00                | - 2083                | - 6.20%               |   |             | Biomedical applications [91].  |
|           | - 60/40                                | - 39.00                | - 1552                | - 6.70%               | -   | -           |  |
|           | - 40/60                                | - 29.00                | - 1258                | - 4.10%               |   |             |  |
|           | - 20/80                                | - 24.00                | - 1076                | - 6.90%               |   |             |  |
|           | - 100/0                                | - 29.70                | - 2031                |                       |   |             |  |
|           | - 80/20                                | - 27.80                | - 1761                |                       |   |             | Biomedical applications (surgical implants, sutures and drug delivery) [92]. |
|           | - 60/40                                | - 22.20                | - 1580                | -                     |   | -           |  |
|           | - 40/60                                | - 25.10                | - 1301                |                       |   |             |  |
|           | - 20/80                                | - 24.90                | - 1631                |                       |   |             |  |
|           | - 100/0                                | - 62.00                | - 2700                | - 8.00%               | - (29.00) J/m                                       |             |  |
|           | - 0/100                                | - 22.00                | - 900                 | - 13.00%              | - (49.00) J/m                                       |             |  |
|           | - 50/50                                | - 39.00                | - 1800                | - 7.90%               | - (28.00) J/m                                       |             | [98]   |
|           | - 40/60                                | - 38.00                | - 1700                | - 7.70%               | - (27.00) J/m                                       |             |  |
|           | - 30/70                                | - 33.00                | - 1300                | - 7.60%               | - (27.00) J/m                                       |             |  |
| PLLA/PHBV | - 100/0                                | - 42.00                | - 1400                | - 7.20%               |   |             |  |
|           | - 100/0 with 5% Lapol as a plasticizer | - 14.00                | - 1450                | - 14.40%              |   |             |  |
|           | - 100/0 with 7% Lapol                  | - 16.00                | - 1200                | - 13.70%              |   |             |  |
|           | - 75/25                                | - 16.00                | - 1270                | - 7.10%               | -   | -           |  |
|           | - 75/25 with 5% Lapol                  | - 13.00                | - 1150                | - 15.50%              |   |             | Single use applications such as food packaging [108].                        |
|           | - 75/25 with 7% Lapol                  | - 15.00                | - 1120                | - 15.10%              |   |             |  |
|           | - 50/50                                |                        |                       |                       |   |             |  |
|           | - 50/50 with 2% PLLA-PEG-PLLA triblock | - 49.60                | - 2737                | - 4.40%               |   | - 5.90 N.mm |  |
|           | - 50/50 with 5% PLLA-PEG-PLLA triblock | - 69.80                | - 2291                | - 5.10%               |   | - 9.20 N.mm |  |
|           | - 50/50 with 2% PEG-PLLA diblock       | - 38.50                | - 1921                | - 5.10%               |   | - 7.90 N.mm |  |
|           | - 50/50 with 5% PEG-PLLA diblock       | - 65.50                | - 2581                | - 4.40%               | -   | - 6.50 N.mm | [93]   |
|           | - 50/50 with 5% PEG-PLLA diblock       | - 32.70                | - 2155                | - 5.90%               |   | - 8.30 N.mm |  |
|           | - 50/50 with 2% PVAc                   | - 41.50                | - 1850                | - 4.80%               |   | - 8.40 N.mm |  |
|           | - 50/50 with 5% PVAc                   | - 43.40                | - 2087                | - 4.90%               |   | - 6.60 N.mm |  |

Table 7. Cont.

| Blend      | Concentration (wt.%)   | Tensile Strength (MPa) | Young's Modulus (MPa) | Percentage Elongation | Charpy Break Energy/ (Notched Izod Break Energy) | Toughness  | Application and/or Reference  |
|------------|--|------------------------|-----------------------|-----------------------|--|--|---|
| PLA/PHA    | - 100/0  | - 55.00                | -                     | -                     | - 0.052 J  | -  | Biodegradable blends for applications that require improved impact toughness (impact toughness similar to that of PS and ABS) [94]. |
|            | - 90/10  | - 50.00                | -                     | -                     | - 0.081 J  | -  |   |
|            | - 80/20  | - 37.00                | -                     | -                     | - 0.137 J  | -  |   |
|            | - 70/30  | - 35.00                | -                     | -                     | - 0.161 J  | -  |   |
| PLA/ePHA   | - 90/10  | - 53.00                | -                     | -                     | - 0.089 J  | -  | Ductile and tough plastics applications [95].   |
|            | - 80/20  | - 48.00                | -                     | -                     | - 0.169 J  | -  |   |
|            | - 70/30  | - 37.00                | -                     | -                     | - 0.260 J  | -  |   |
|            | - 100/0  | -                      | -                     | -                     | -  | - 0.30 N.m<br>- 1.90 N.m<br>- 1.40 N.m<br>- 0.30 N.m<br>- 0.20 N.m |   |
| PLA/Nodax™ | - 100/0  | -                      | -                     | -                     | -  | -  | Ductile and tough plastics applications [96].   |
|            | - 90/10  | -                      | -                     | -                     | -  | -  |   |
|            | - 85/15  | -                      | -                     | -                     | -  | -  |   |
|            | - 80/20  | -                      | -                     | -                     | -  | -  |   |
|            | - 75/25  | -                      | -                     | -                     | -  | -  |   |
|            | - 81/14 with 5% <i>oligo</i> Nodax™- <i>b</i> -PLLA diblock copolymer (81/14/5 wt.%)               | -                      | -                     | -                     | -  | -  |   |
|            | - (22.00) J/m<br>- (27.00) J/m<br>- (44.00) J/m<br>- (43.00) J/m<br>- (35.00) J/m<br>- (44.00) J/m | -                      | -                     | -                     | -  | -  |   |

Table 7. Cont.

| Blend                               | Concentration (wt.%)        | Tensile Strength (MPa) | Young's Modulus (MPa) | Percentage Elongation | Charpy Break Energy/ (Notched Izod Break Energy) | Toughness | Application and/or Reference                             |                                |
|-------------------------------------|-----------------------------|------------------------|-----------------------|-----------------------|--|-----------|--|--------------------------------|
| PLA/PHB                             | - 100/0                     | - 26.00                | -                     | - 16.00%              | -  | -         | Applications that require high biodegradation rate [43]. |                                |
|                                     | - 25/75                     | - 2.50                 | -                     | - 6.00%               | -  | -         |  |                                |
|                                     | - 50/50                     | - 8.00                 | -                     | - 11.00%              | -  | -         |  |                                |
|                                     | - 75/25                     | - 32.50                | -                     | - 17.50%              | -  | -         |  |                                |
|                                     | - 100/0                     | - 50.00                | -                     | - 7.25%               | -  | -         | Environmentally friendly packaging [110].                |                                |
|                                     | - 83/17                     | - 47.00                | -                     | - 3.50%               | -  | -         |  |                                |
|                                     | - 57/43                     | - 40.00                | -                     | - 3.85%               | -  | -         |  |                                |
|                                     | - 50/50                     | - 37.50                | -                     | - 3.40%               | -  | -         |  |                                |
|                                     | - 43/57                     | - 35.50                | -                     | - 3.20%               | -  | -         |  |                                |
|                                     | - 29/71                     | - 34.50                | -                     | - 3.20%               | -  | -         |  |                                |
|                                     | - 17/83                     | - 27.00                | -                     | - 3.00%               | -  | -         |  |                                |
|                                     | - 0/100                     | - 26.50                | -                     | - 2.70%               | -  | -         |  |                                |
|                                     | - 100/0                     | - 46.90                | - 1240                | - 41.10%              | -  | -         |  | Biodegradable packaging [103]. |
|                                     | - 75/25                     | - 38.20                | - 1810                | - 13.00%              | -  | -         |  |                                |
|                                     | - 63.75/21.25 with 15% ATBC | - 40.20                | - 550                 | - 90.10%              | -  | -         |  |                                |
| - 60/20 with 5% CNCs and 15% ATBC   | - 27.30                     | - 570                  | - 27.40%              | -                     | -  |           |  |                                |
| - 60/20 with 5% CNCs-m and 15% ATBC | - 28.20                     | - 490                  | 147.70%               | -                     | -  |           |  |                                |
| PLA/aPHB                            | - 100/0                     | - 49.30                | - 3500                | - 6.00%               | - 50.00 <sup>b</sup> KJ/m <sup>2</sup>           | -         | Packaging, especially for food [97].                     |                                |
|                                     | - 98/2                      | - NP <sup>a</sup>      | - NP                  | - NP                  | - 60.00 <sup>b</sup> KJ/m <sup>2</sup>           | -         |  |                                |
|                                     | - 95/5                      | - 46.00                | - 3380                | - 6.00%               | - 60.00 <sup>b</sup> KJ/m <sup>2</sup>           | -         |  |                                |
|                                     | - 90/10                     | - 43.50                | - 3240                | - 7.00%               | - 61.00 <sup>b</sup> KJ/m <sup>2</sup>           | -         |  |                                |
|                                     | - 85/15                     | - 38.30                | - 2910                | - 9.00%               | - 103.00 <sup>b</sup> KJ/m <sup>2</sup>          | -         |  |                                |
|                                     | - 80/20                     | - 30.50                | - 2750                | - 21.00%              | - 118.00 <sup>b</sup> KJ/m <sup>2</sup>          | -         |  |                                |

Table 7. Cont.

| Blend                      | Concentration (wt.%) | Tensile Strength (MPa) | Young's Modulus (MPa) | Percentage Elongation | Charpy Break Energy/ (Notched Izod Break Energy) | Toughness   | Application and/or Reference                                      |
|----------------------------|----------------------|------------------------|-----------------------|-----------------------|--|-------------|---|
| PLA/<br>PHBHH <sub>x</sub> | - 100/0              | - 36.40                | - 1390                | - 13.80%              |  |             |   |
|                            | - 80/20              | - 29.50                | - 1320                | - 99.60%              |  |             | Biomedical applications, such as artificial vascular graft [100]. |
|                            | - 60/40              | - 33.50                | - 1240                | - 7.68%               |  |             |   |
|                            | - 50/50              | - 22.10                | - 910                 | - 7.26%               | -  | -           |   |
|                            | - 40/60              | - 27.70                | - 1250                | - 11.50%              |  |             |   |
|                            | - 20/80              | - 23.60                | - 590                 | - 83.50%              |  |             |   |
|                            | - 0/100              | - 17.60                | - 370                 | - 19.30%              |  |             |   |
|                            | - 100/0              | - 62.20                | - 1603.00             | - 3.60%               |  | - 3.20 MPa  |   |
|                            | - 90/10              | - 54.10                | - 1416.00             | - 7.60%               |  | - 4.00 MPa  | Food packaging and flexible films [102].                          |
|                            | - 80/20              | - 45.30                | - 1265.00             | - 113.10%             |  | - 68.70 MPa |   |
| - 60/40                    | - 40.10              | - 1093.00              | - 37.60%              |                       | - 20.40 MPa                                      |             |   |
| - 0/100                    | - 21.60              | - 309.00               | - 524.80%             |                       | - 160.60 MPa                                     |             |   |

<sup>a</sup> NP: not provided. <sup>b</sup> Impact test was done as per ISO 8256 standard (method A). Note: Studies in which no exact values for the mechanical properties were given, the best estimations were provided. Abbreviations: PLLA, poly(L-lactic acid); PHBV, poly(3-hydroxybutyrate-co-3-hydroxyvalerate); PEG, polyethylene glycol; PVAc, poly (vinyl acetate); PLA, poly(lactic acid); PHA, poly(3-hydroxyalkanoate); ePHA, epoxidized PHA; Nodax™, [poly (3-hydroxybutyrate-co-3-hydroxyhexanoate)]; PHB, poly[<sup>®</sup>-3-hydroxyhexanoate)]; ATBC, acetyl (tributyl citrate); CNCs, cellulose nanocrystals; CNCs-m, modified cellulose nanocrystals; a-PHB, atactic PHB; PHBHH<sub>x</sub>, poly(3-hydroxybutyrate-co-3-hydroxyhexanoate).

### 2.3.2. PLA/PCL Blends

Due to its rubbery characteristics as well as its high elongation at break (roughly 600%), Polycaprolactone (PCL) is considered as a good candidate for toughening PLA [77]. PCL is also a degradable polyester, meaning that blending it with PLA can result in a completely degradable material. Many studies in literature have reported that PLA/PCL blends can result in enhanced elongation at break; however, this is usually accompanied with a reduction in modulus of elasticity and tensile strength.

Hiljanen-Vainio et al. [111] showed that blending 20 wt.% of PCL with PLLA resulted in a lower Young's modulus, tensile strength and shear strength. However, the elongation at break increased from 1.6% for neat PLLA to 9.6%. On the other hand, blending of the elastic poly( $\epsilon$ -caprolactone/L-lactide) (PCL/L-LA) copolymer with PLLA substantially increased the elongation at break to more than 100% compared to both, neat PLLA and the binary blend. Yield deformation was observed for PLA with 5, 10 and 20 wt.% of PCL/L-LA copolymer. A tough rubber-like behavior was reported when the blend contained 30 wt.% of PCL/L-LA copolymer. Initially, the impact strength of PLLA was very poor, however, when 20 wt.% of PCL/L-LA copolymer was added, a quadruple enhancement in the impact strength was obtained [111].

The tensile properties for PLA/PCL blend films were studied by Tsuji and Ikada [112]. The blend films were prepared with a solution casting method using methylene chloride as a solvent. Adding 15 wt.% PCL to PLA resulted in increasing the elongation at break; however, the calculated standard deviation obtained was quite high ( $250\% \pm 200\%$ ) [112].

The elongation at break for PLA/PCL blend was investigated by Wang et al. [77]. Results suggested that the elongation at break for reactive blends of PLA/PCL using triphenyl phosphite as a catalyst increased substantially when compared to neat PLA at certain compositions (PLA/PCL = 80/20 or 20/80). Therefore, the study indicates that reactive blending is a promising technique to enhance the toughness and elongation of PLA. The elongation increased to 127% compared to 28% for the nonreactive binary blend [77].

Maglio et al. [113] reported an enhancement in both the percentage elongation and the notched Charpy impact strength in PLLA/PCL 70/30 wt.% blends compatibilized with PLLA-PCL-PLLA triblock copolymer [113].

PLA/PCL blends were examined by Broz et al. [78]. Only for a PCL content higher than 60 wt.%, a significant increase in the elongation was observed, nonetheless, this was accompanied with a drastic drop in Young's modulus and tensile strength [78].

The addition of diblock copolymer of PLLA-PCL to PLLA/PCL blends was studied by Tsuji et al. [114]. At  $X_{\text{PLLA}}$  ( $X_{\text{PLLA}} = \text{weight of PLLA} / (\text{weight of PLLA and PCL})$ ) of 0.5–0.8, blends' tensile strengths and modulus of elasticities were enhanced due to the addition of the copolymer. Moreover, the elongation at break was also improved for all values of  $X_{\text{PLLA}}$ . These findings indicate that PLLA-CL was miscible with PLLA and PCL, and that the dissolved PLLA-CL in PLLA-rich and PCL-rich phases improved the compatibility between phases [114].

In another study [115], dicumyl peroxide (DCP) was used as a cross-linker in PLA/PCL reactive blend. DCP was used to enhance the elongation at break of the blends. The study reported that the optimum blend ratio of the PLA/PCL blend was 70/30. The elongation at break reached a peak value when low DCP concentrations (around 0.2 phr) was used. In addition, at low DCP content, tensile testing showed yield point and ductile behavior. For the optimum composition, there was a substantial increase in the impact strength [115].

Blends of PLA and a copolymer of caprolactone (CL) as well as trimethylene carbonate (TMC) has been investigated by Grijpma et al. [116]. When 20 wt.% copolymer was incorporated, the notched Izod impact strength increased from 40 J/m to a peak value of 520 J/m. Nonetheless, the same concentration of rubber phase resulted in no enhancement in the notched Izod impact strength in case of homopolymer poly(TMC) and PLA blends [116].

Blends of PLA homopolymer with poly(trimethylene carbonate) [poly (TMC)] copolymers were also studied [117]. In an unnotched impact test, there was no breakage of the blend samples with 21 wt.% of the block of poly(TMC) in PLA. The study also examined

the effect of diblock copolymers of L-lactide and CL blended with PLA on the mechanical properties. When 20 wt.% of diblock copolymer was used, there was an increase from 5 to 50 kJ/m<sup>2</sup> in the blend's unnotched impact strength [117].

Surfactant has also the potential to improve the elongation at break of PLA when added at low quantity. However, such an improvement is accompanied by a drop in both the tensile strength and Young's modulus [118].

According to a study reported by Maglio et al. [113], when a small amount (round 4 wt.%) of PLA-PCL-PLA triblock copolymer was added to PLA/PCL blend with a concentration of 70/30 wt.%, there was an enhancement in the dispersion of PCL. Moreover, an improvement in the resulted blend's ductility was observed. The percentage elongation increased to 53% for the ternary blend from 2% for a PLA/PCL (70:30) blend. This was attributed to the dispersion of PCL domains which after the incorporation of 4 wt.% triblock copolymers were observed to decrease from 10 to 4 µm [113].

PLA/PCL blends with different PCL molecular weights were prepared by Hasook et al. [119]. Out of all the blends, the tensile strength was the highest when PCL (Mw = 40,000 g/mol) was used [119].

The potential to use PLA/PCL blends in Fused Filament Fabrication (FFF) was examined in another work [120]. Using a twin-screw extruder, binary blends of PLA/PCL were prepared at various ratios (20/80 wt.% to 80/20 wt.%). Results of the study showed that the blends were immiscible; however, they showed sign of adhesion between the phases. Tensile properties were compared to those of injection molded blends, and both tensile properties were similar. Blends' ductility was strongly driven by the behavior of its majority phase. 3D-printed blends were reported to have low porosity [120].

By using ROP, a series of linear and star shaped PCL with different arm numbers were successfully synthesized with the initiators having various number of hydroxyl functional groups [121]. After that, a micro compounder at a constant blending ration was used to melt PCL with PLA. Constant 1,4-phenylene diisocyanate (PDI) (1% weight) was also added as a commercial compatibilizer. Results of the study showed that star shaped PCL enhanced PLA's mechanical properties. An increase in the percentage elongation was reported with the addition of star polymers. The percentage elongation increased from 4% to 9%. The three-armed star shaped PCL led to a substantial drop in modulus because of its high molecular chain mobility in comparison to linear, four- and six-armed PCLs. Images of the Scanning electron microscopy (SEM) showed that the immiscibility of the two biodegradable polymers were improved and therefore mechanical improvements were obtained [121].

For the aim of developing a degradable polymer blend for drug delivery applications, Ebrahimifar and Taherimehr [122] tested PCL, PLA, Polyvinylcyclohexane carbonate (PVCHC), in addition to the mixed polymeric matrix of PCL/PVCHC and PLA/PVCHC were tested as carriers for hydrophilic drugs acetaminophen and clindamycin. The highest release efficiency for PCL/PVCHC acetaminophen, PCL-acetaminophen, PLA acetaminophen, PLA/PVCHC clindamycin, PLA clindamycin and PCL clindamycin was found to be 29%, 38%, 39%, 40%, 95% and 96%, respectively [122].

Yang and co-authors [123] reported PLA/PCL blends at various concentrations. This was done using a novel extrusion device, eccentric rotor extruder. The addition of 20 wt.% PCL led to a substantial improvement in the percentage elongation at break to around 476.7%, which is more than 57 times that of the neat PLA. This was accompanied with a drop in tensile strength (20% drop). Due to the enhanced crystallinity of PLA as well as the compatibility of PLA/PCL blends, thermal stability was also improved [123].

Table 8 shows the effect of different PLA/PCL blends at various concentrations on the mechanical properties.

**Table 8.** The effect of various PLA/PCL blends at different concentrations on the mechanical properties along with their applications.

| Blend | Concentration (wt.%)                               | Tensile Strength (MPa) | Young's Modulus (MPa) | Percentage Elongation | Charpy Impact/ (Izod Impact) | Application and/or Reference  |
|-------|--|------------------------|-----------------------|-----------------------|------------------------------|---|
|       | - 100/0  | - 48.26                | - 2275.26             | - 3.0%                |                              |   |
|       | - 80/20  | - 44.19                | - 584.67              | - 28.0%               |                              |   |
|       | - 60/40  | - 19.37                | - 751.52              | - 5.00%               |                              |   |
|       | - 40/60  | - 18.61                | - 164.09              | - 23.0%               |                              | [77]  |
|       | - 20/80  | - 20.13                | - 111.69              | - 44.0%               |                              |   |
|       | - 80/20 with 2% TPP as a coupling agent            | - 33.09                | - 1013.52             | - 127%                | -                            |   |
|       | - 60/40 with 2% TPP                                | - 23.58                | - 710.16              | - 7.00%               |                              |   |
|       | - 40/60 with 2% TPP                                | - 11.44                | - 344.04              | - 3.00%               |                              |   |
|       | - 20/80 with 2% TPP                                | - 17.23                | - 197.87              | - 56.0%               |                              |   |
|       | - 100/0  | - 70                   | - 1500                | - 11.0%               | - (2.00) KJ/m <sup>2</sup>   |   |
|       | - 70/30  | - 55                   | - 1300                | - 20%                 | - (3.80) KJ/m <sup>2</sup>   | High performance applications [115].  |
|       | - 70/30 with 0.1 phr <sup>a</sup> Dicumyl peroxide | - 52                   | - 1200                | - 35%                 | - (3.90) KJ/m <sup>2</sup>   |   |
|       | - 70/30 with 0.2 phr Dicumyl peroxide              | - 49                   | - 1150                | - 160%                | - (4.00) KJ/m <sup>2</sup>   |   |
|       | - 70/30 with 0.3 phr Dicumyl peroxide              | - 48                   | - 1100                | - 149%                | - (4.90) KJ/m <sup>2</sup>   |   |
|       | - 100/0  | - 45.13                | - 3729                | - 2.06%               |                              |   |
|       | - 95/5.0 <sup>b</sup>                              | - 58.62                | - 3631                | - 3.12%               | -                            | [119]   |
|       | - 95/5.0 <sup>c</sup>                              | - 52.21                | - 3422                | - 2.90%               |                              |   |
|       | - 95/5.0 <sup>d</sup>                              | - 44.49                | - 3661                | - 2.32%               |                              |   |
|       | - 0/100  | -                      | - 460                 | -                     | -                            | Biomedical applications [120].  |
|       | - 20/80  | -                      | - 700                 | -                     | -                            |   |
|       | - 30/70  | -                      | - 1220                | -                     | -                            |   |
|       | - 40/60  | -                      | - 1350                | -                     | -                            |   |
|       | - 60/40  | -                      | - 2030                | -                     | -                            |   |
|       | - 70/30  | -                      | - 2500                | -                     | -                            |   |
|       | - 80/20  | -                      | - 2940                | -                     | -                            |   |
|       | - 100/0  | -                      | - 3910                | -                     | -                            |   |
|       | - 0/100  | -                      | - 4600                | - 4.00%               | - (8.00) KJ/m <sup>2</sup>   |   |
|       | - 0/100 with 1% PDI as a compatibilizer            | -                      | - 4200                | - 2.30%               | - (11.50) KJ/m <sup>2</sup>  |   |
|       | - 90/10, linear PCL                                | -                      | - 3400                | - 6.40%               | - (20.00) KJ/m <sup>2</sup>  | Different daily and industrial applications such as, disposable products, biomedical products and food packaging [121]. |
|       | - 90/10, linear PCL with 1% PDI                    | -                      | - 3600                | - 6.43%               | - (17.00) KJ/m <sup>2</sup>  |   |
|       | - 90/10, three-armed star shaped PCL               | -                      | - 2100                | - 8.20%               | - (20.50) KJ/m <sup>2</sup>  |   |
|       | - 90/10, three-armed star shaped PCL with 1% PDI   | -                      | - 2400                | - 8.00%               | - (17.50) KJ/m <sup>2</sup>  |   |
|       | - 90/10, four-armed star shaped PCL                | -                      | - 2250                | - 8.40%               | - (23.00) KJ/m <sup>2</sup>  |   |
|       | - 90/10, four-armed star shaped PCL with 1% PDI    | -                      | - 2800                | - 8.37%               | - (21.00) KJ/m <sup>2</sup>  |   |
|       | - 90/10, six-armed star shaped PCL                 | -                      | - 3450                | - 8.60%               | - (24.50) KJ/m <sup>2</sup>  |   |
|       | - 90/10, six-armed star shaped PCL with 1% PDI     | -                      | - 3500                | - 8.65%               | - (21.00) KJ/m <sup>2</sup>  |   |



Table 8. Cont.

| Blend   | Concentration (wt.%)  | Tensile Strength (MPa) | Young's Modulus (MPa) | Percentage Elongation | Charpy Impact/ (Izod Impact)  | Application and/or Reference                                 |
|---|---|------------------------|-----------------------|-----------------------|---|--|
|   | - 100/0   | - 66.05                | - 1311                | - 8.21%               |   | Applications requiring very high toughness properties [123]. |
|   | - 80/20   | - 53.60                | - 1233                | - 476.70%             |   |  |
|   | - 70/30   | - 50.20                | - 1223                | - 514.60%             | -   |  |
|   | - 60/40   | - 41.30                | - 884                 | - 664.70%             |   |  |
|   | - 100/0   | - 60                   | - 1300                | - 5.0%                |   | [114]  |
|   | - 80/20   | - 30                   | - 1100                | - 175.0%              |   |  |
|   | - 80/20 with 10% poly(L-lactide-co-ε-caprolactone)                      | - 40                   | - 1100                | - 300%                |   |  |
|   | - 100/0   | - 35                   | - 2530                | - 1.6%                | - 41.4 KJ/m <sup>2</sup> at (-)20 °C and 49.2 KJ/m <sup>2</sup> at 23 °C. | Biomedical applications [111]                                |
|   | - 80/20   | - 31.0                 | - 2080                | - 9.60%               | - NP <sup>e</sup>   |  |
|   | - 64/16 with 20% poly(ε-caprolactone/L-lactide)                         | - 11.0                 | - 660                 | - >100%               | - 5.3 KJ/m <sup>2</sup> at (-)20 °C and 10.1 KJ/m <sup>2</sup> at 23 °C.  |  |
|   | - 70/30   | -                      | - 1400                | - 2.00%               | - 1.1 KJ/m <sup>2</sup>   |  |
| PLLA/PCL  | - 70/30 with 4% triblock PLLA -PCL-PLLA as compatibilizing agent        | -                      | - 1400                | - 53.0%               | - 3.7 KJ/m <sup>2</sup>   | Biomedical applications [113].                               |
|   | - 100/0   |                        |                       |                       |   |  |
|   | - 80/20   | - 34.10                | - 19.8                | - 56.30%              |   |  |
|   | - 60/40   | - 41.20                | - 20.7                | - 129.50%             |   |  |
|   | - 50/50   | - 19.30                | - 10.7                | - 152.10%             |   |  |
|   | - 80/20 with copolymer of ethylene oxide and propylene oxide surfactant | - 16.90                | - 8.10                | - 139.60%             |   | Orthopedic and dental applications [118].                    |
|   | - 60/40 with copolymer of ethylene oxide and propylene oxide surfactant | - 20.10                | 9.50                  | - 129.00%             |   |  |
|   | - 50/50 with copolymer of ethylene oxide and propylene oxide surfactant | - 12.90                | - 4.70                | - 130.00%             |   |  |
|   |   | - 10.40                | - 6.60                | - 123.70%             |   |  |
| Triblock copolymer of PLA (85% L-lactide and 15% D-lactide), ε-CL and TMC | - 100/0   | - 56.8                 | -                     | -                     |   | Load bearing devices in biomedical applications [116].       |
|   | - 80/20   | - 36.0                 |                       |                       | - (41.0) J/m<br>- (293–520) J/m   |  |

<sup>a</sup> phr: per hundred of rubber. <sup>b</sup> PCL's molecular weight = 10,000 g/mol. <sup>c</sup> PCL's molecular weight = 40,000 g/mol. <sup>d</sup> PCL's molecular weight = 70,000–10,000 g/mol. <sup>e</sup> NP: not provided. Note: Studies in which no exact values for the mechanical properties were given, the best estimations were provided. Abbreviations: PLA, poly(lactic acid); PCL, poly(ε-caprolactone); TPP, triphenyl phosphite; PDI, 1,4-phenylene diisocyanate; PLLA, poly(L-lactic acid); ε-CL, ε-caprolactone; TMC, trimethylene carbonate.

### 2.3.3. Blends of PLA with Other Biodegradable/Renewable Resource-Based Polymers

Different studies have investigated blending PLA with various biodegradable/renewable resource-based polymers such as PPD [124], poly(propylene carbonate) (PPC) [125], poly(tetramethylene adipate-*co*-terephthalate) (PTAT) [126], poly(butylene adipate-*co*-terephthalate) (PBAT) [127], poly(ethylene/butylene succinate) (Bionolle) [128], poly(butylene succinate) (PBS) [129,130], poly(butylene succinate *co*-L-lactate) (PBSL) [129] and poly(butylene succinate-*co*-butylene adipate) (PBSA) [131].

In a study done by Pezzin et al. [124], PPD, a biodegradable polyester, was blended with PLA. The study showed that the PLLA/PPD blends exhibited higher modulus of elasticity and elongation at break. When only 20 wt.% of PPD was added to the PLLA phase (20/80 wt.% PLLA/PPD), the modulus of elasticity and elongation at break were roughly 1600 Mpa and 55% respectively, whereas these values were around 1400 Mpa and 15% for neat PLLA. On the other hand, the tensile strength of the blend was lower than that of the neat PLLA. Mechanical testing of these blends showed that they were tough and more flexible. Furthermore, the blends showed neck formation during elongation. This enhancement in the mechanical properties was attributed to the plasticizing effect of PPD. However, the mechanical properties of the other blends at compositions of 50/50 wt.% and 20/80 wt.%(PLLA/PPD) were not improved, as compared to neat PLLA. Although the modulus of elasticity at both of these compositions were higher than that of neat PPD, the other values of stress at break, elongation at break, tensile strength and toughness were lower [124].

Blends of PLA and PPC (an amorphous degradable polymer) were prepared at various compositions by Ma et al. [125]. It was observed that for all types of blends, increasing PPC content resulted in a decrease in both Young's modulus and tensile strength. Nonetheless, compared to neat PLA, increasing amounts of PPC resulted in an improvement in the tensile toughness. This increase in toughness was clear in concentrations higher than 40 wt.% PPC. This is due to the reason that when PLA was blended with PPC at a concentration less than 30 wt.%, PLA was the continuous matrix phase; however, for PPC concentrations higher than 40 wt.%, PPC was the continuous phase. Hence, the continuous PPC phase advocates the matrix yielding, therefore more energy was required to break the polymers [125].

PTAT is another biodegradable polyester that was blended with PLLA. Liu et al. [126] prepared PLLA/PTAT blends at different compositions by solution casting from chloroform. The tensile strength and percentage elongation for pure PLLA were 28 Mpa and 19%, respectively. Blend of PLLA/PTAT at a concentration of 75/25 wt.% exhibited a percentage elongation of 97% and a tensile strength of 25 Mpa, whereas the same were reduced to 34% and 7 Mpa, respectively for PLLA/PTAT blend with a concentration of 50/50 wt.%. The reason behind this could be related to the blend's higher amount of phase separation as well as its low miscibility. For the 25/75 wt.% PLLA/PTAT blend, the elongation at break reported was around 285%, which is almost 15 times higher than that of neat PLLA. At the same time, the tensile strength was around 11 Mpa, that is slightly better than what was reported for PLLA/PTAT blend with concentration of 50/50 wt.%. These results suggest that PTAT was able to provide more ductility to the blend [126].

Melt blending of PLA with PBAT was studied by Jiang et al. [127]. PBAT is a biodegradable, flexible, aliphatic-aromatic polyester, with a percentage elongation of 700%. When PBAT was added to PLA at a concentration of 5–20 wt.%, the Young's modulus and tensile strength of the blends decreased. For example, at 20% PBAT content, Young's modulus decreased from 3.4 Gpa for neat PLA to 2.6 Gpa. Similarly, there was a reduction in the tensile strength from 63 Mpa for the pure PLA to 47 Mpa. These results are anticipated due to the fact that PBAT has a lower tensile strength and Young's modulus when compared to PLA. As the content of PBAT increased from 5 to 20 wt.%, an enhancement in the Izod impact strength was observed. Maximum toughening was reported for 20 wt.% PBAT. This was also the case for the elongation at break, as the higher content of PBAT was used, higher elongation at break values were observed. This effect was noticeable even at very low PBAT content. For instance, with the incorporation of only 5 wt.% PBAT, the percentage

elongation observed was more than 200%. As more content of PBAT was incorporated, the failure mode switched from brittle fracture for the neat PLA to a ductile fracture of the blend. This conclusion was supported by the SEM micrographs of the fractured surfaces. The SEM showed that as the content of PBAT increased, more and longer fibrils from the surfaces were spotted [127].

Using a single-screw extruder, different contents of Bionolle were blended with PLA [128]. Bionolle is an aliphatic biodegradable thermoplastic polyester. The percentage elongation for neat PLA was reported to be 2%, while the maximum percentage elongation for the blend was reported to be 8.2% with 40 wt.% Bionolle. On the other hand, as the amount of Bionolle increased, the Young's modulus and tensile strength decreased. That was anticipated as Bionolle's Young's modulus and tensile strength are lower than those of PLA [128].

Shibata et al. [129] investigated the effects of blending PLLA with PBS and PBSL. Melt mixing followed by injection molding were used to blend PLLA with PBS or PBSL. PBSL can be referred to as a relatively new type of PBS. PBSL is a biodegradable polyester. Both the Young's modulus as well as the tensile strength decreased as more concentrations of PBSL or PBS was added with the exception of blend of PLLA with a concentration of 1 wt.% and 5 wt.% of PBS. These blends have exhibited an increase in the Young's modulus and tensile strength in comparison to neat PLLA. Field emission scanning electron microscopy micrographs were used to understand these results. The study attributed the results to the production of finely dispersed blends. Compared to pure PLLA, PBSL and PBS, all the blends exhibited significantly higher percentage elongation over the whole composition range. Overall, lower tensile strength and Young's modulus but higher percentage elongation were observed for PLLA/PBSL in comparison to the PLLA/PBS blends with similar concentration [129].

In another work and for the purpose of enhancing PLLA's mechanical properties, PLLA was blended with PBS [130]. The percentage elongation increased from 6.90% to 320.60% after the incorporation of 25 wt.% PBS.

A Blend of PLLA/PBSA was produced by Chen and Yoon [131]. Results suggested that the brittleness of PLLA was greatly improved at a composition of PLLA/PBSA 75/25 wt.% [131].

Table 9 shows the impact of different PLA blends with various degradable or partial degradable polymers at various concentrations on the mechanical properties.

**Table 9.** The effect of various PLA/other degradable or partial degradable polymers blends at different concentrations on the mechanical properties along with their applications.

| Blend                             | Concentration (wt.%) | Tensile Strength (MPa) | Yield Strength (MPa) | Young's Modulus (MPa) | Percentage Elongation | Break Energy/ (Izod Break Energy)     | Application and/or Reference  |
|-----------------------------------|----------------------|------------------------|----------------------|-----------------------|-----------------------|---------------------------------------|---|
| PLA/PPD                           | -100/0               | -25.30                 | -                    | -1400                 | -14.5%                | -                                     | Medical applications [124].   |
|                                   | -80/20               | -15.60                 | -                    | -1550                 | -55.0%                | NP <sup>a</sup>                       |   |
|                                   | -50/50               | -5.30                  | -                    | -900                  | -3.00%                | -                                     |   |
|                                   | -20/80               | -5.00                  | -                    | -650                  | -4.00%                | -                                     |   |
| PLA/PPC                           | -100/0               | -59.0                  | -59.0                | -3150                 | -                     | -2.00 <sup>b</sup> J/cm <sup>2</sup>  | [125]   |
|                                   | -85/15               | -45.0                  | -49.0                | -2450                 | -                     | -5.00 <sup>b</sup> J/cm <sup>2</sup>  |   |
|                                   | -70/30               | -42.0                  | -46.0                | -2150                 | -                     | -14.00 <sup>b</sup> J/cm <sup>2</sup> |   |
|                                   | -60/40               | -28.0                  | -41.0                | -2050                 | -                     | -55.00 <sup>b</sup> J/cm <sup>2</sup> |   |
|                                   | -50/50               | -26.0                  | -37.0                | -1750                 | -                     | -84.00 <sup>b</sup> J/cm <sup>2</sup> |   |
|                                   | -40/60               | -25.0                  | -36.0                | -1400                 | -                     | -75.00 <sup>b</sup> J/cm <sup>2</sup> |   |
|                                   | -30/70               | -21.0                  | -32.0                | -1050                 | -                     | -72.00 <sup>b</sup> J/cm <sup>2</sup> |   |
|                                   | -15/85               | -14.0                  | -24.0                | -800                  | -                     | -69.00 <sup>b</sup> J/cm <sup>2</sup> |   |
| PLA/PBAT                          | -100/0               | -63.00                 | -                    | -3200                 | -                     | - (2.70) KJ/m <sup>2</sup>            | Applications requiring increased toughness while maintaining degradability [127]. |
|                                   | -95/5                | -58.00                 | -                    | -2900                 | -                     | - (2.75) KJ/m <sup>2</sup>            |   |
|                                   | -90/10               | -55.00                 | -                    | -2850                 | -                     | - (2.90) KJ/m <sup>2</sup>            |   |
|                                   | -85/15               | -51.00                 | -                    | -2700                 | -                     | - (3.50) KJ/m <sup>2</sup>            |   |
|                                   | -80/20               | -47.00                 | -                    | -2600                 | -                     | - (4.40) KJ/m <sup>2</sup>            |   |
| PLA/Bionolle (B1001) <sup>c</sup> | -100/0               | -36.00                 | -                    | -2481                 | -2.00%                | -                                     | Biomedical and food applications [128].   |
|                                   | -95/5                | -32.00                 | -                    | -2471                 | -1.70%                | -                                     |   |
|                                   | -90/10               | -36.00                 | -                    | -2158                 | -2.40%                | -                                     |   |
|                                   | -80/20               | -24.00                 | -                    | -1766                 | -5.00%                | -                                     |   |
|                                   | -70/30               | -28.00                 | -                    | -1704                 | -4.00%                | -                                     |   |
|                                   | -60/40               | -26.00                 | -                    | -1468                 | -5.00%                | -                                     |   |
| PLA/Bionolle (B3010) <sup>c</sup> | -50/50               | -24.00                 | -                    | -1268                 | -4.20%                | -                                     |   |
|                                   | -95/5                | -27.00                 | -                    | -2389                 | -1.50%                | -                                     |   |
|                                   | -90/10               | -31.00                 | -                    | -2292                 | -1.80%                | -                                     |   |
|                                   | -80/20               | -26.00                 | -                    | -1836                 | -2.20%                | -                                     |   |
|                                   | -70/30               | -24.00                 | -                    | -1620                 | -2.40%                | -                                     |   |
| -60/40                            | -22.00               | -                      | -1359                | -8.20%                | -                     |                                       |   |
| -50/50                            | -19.00               | -                      | -1071                | -3.30%                | -                     |                                       |   |

Table 9. Cont.

| Blend                | Concentration (wt.%)                 | Tensile Strength (MPa) | Yield Strength (MPa) | Young's Modulus (MPa) | Percentage Elongation | Break Energy/ (Izod Break Energy) | Application and/or Reference                                      |
|----------------------|--------------------------------------|------------------------|----------------------|-----------------------|-----------------------|-----------------------------------|---|
| PLLA/PTAT            | - 100/0                              | - 28.12                | -                    | -                     | - 19.33%              | -                                 | Medical applications, tissue engineering and drug delivery [126]. |
|                      | - 75/25                              | - 24.62                | -                    | -                     | - 97.00%              | -                                 |   |
|                      | - 50/50                              | - 7.11                 | -                    | -                     | - 34.00%              | -                                 |   |
|                      | - 25/75                              | - 11.11                | -                    | -                     | - 285.33%             | -                                 |   |
| PLLA/PBSL            | - 100/0                              | - 63.00                | -                    | - 2900                | - 2.00%               | -                                 | Packaging applications [132].                                     |
|                      | - 99/1                               | - 61.00                | -                    | - 2800                | - 3.00%               | -                                 |   |
|                      | - 95/5                               | - 62.00                | -                    | - 2650                | - 55.00%              | -                                 |   |
|                      | - 90/10                              | - 55.00                | -                    | - 2450                | - 160%                | -                                 |   |
|                      | - 80/20                              | - 51.50                | -                    | - 2350                | - 120%                | -                                 |   |
|                      | - 99/1 with 10% RKM as a plasticizer | - 35.00                | -                    | - 1900                | - 220%                | -                                 |   |
|                      | - 95/5 with 10% RKM                  | - 29.00                | -                    | - 1150                | - 245%                | -                                 |   |
|                      | - 90/10 with 10% RKM                 | - 28.00                | -                    | - 1000                | - 240%                | -                                 |   |
|                      | - 80/20 with 10% RKM                 | - 30.00                | -                    | - 1250                | - 235%                | -                                 |   |
|                      | - 99/1 with 20% RKM                  | - 22.00                | -                    | - 600                 | - 195%                | -                                 |   |
|                      | - 95/5 with 20% RKM                  | - 21.00                | -                    | - 650                 | - 200%                | -                                 |   |
|                      | - 90/10 with 20% RKM                 | - 21.00                | -                    | - 700                 | - 195%                | -                                 |   |
| - 80/20 with 20% RKM | - 21.00                              | -                      | - 700                | - 170%                | -                     |                                   |   |
| PLLA/PBSA            | - 75/25                              | -                      | - 36.70              | - 1160.90             | - 153.60%             | -                                 | Biodegradable sealing envelope for food packaging [131].          |
| PLLA/PBS             | - 100/0                              | -                      | - 64.60              | - 2214.70             | - 6.90%               | -                                 | [130]   |
|                      | - 0/100                              | -                      | - 32.10              | - 326.30              | - 320.60%             | -                                 |   |
|                      | - 75/25                              | -                      | - 44.70              | - 1075.20             | - 71.80%              | -                                 |   |

<sup>a</sup> NP: not provided. <sup>b</sup> The type of impact test was not provided. <sup>c</sup> Bionolle (B1001) and Bionolle (B3010) are different in the amount of Bionolle. Note: Studies in which no exact values for the mechanical properties were given, the best estimations were provided. Abbreviations: PLA, poly(lactic acid); PPD, poly-*p*-dioxanone; PPC, poly(propylene carbonate); PBAT, poly(butylene adipate-co-terephthalate); Bionolle, poly(ethylene/butylene succinate); PLLA, poly(L-lactic acid); PTAT, poly(tetramethylene adipate-co-terephthalate); PBSL, poly(butylene succinate-co-L-lactate); RKM, Rikemal PL710; PBSA, poly(butylene succinate-co-butylene adipate); PBS, poly(butylene succinate).

## 2.3.4. Features of Various PLA Blends

Blending PLA with PHB was found to improve the impact properties, percentage elongation at break [108,133,134], biodegradation rate [105,134] and barrier properties [107,135]. Enhanced ductility was also reported in case of blending with PBS [136,137] and PCL [138]. Improved barrier properties were also observed in case of blending with PHBV [139], PBS [140] and PBAT [141]. Table 10 shows the advantages of selected studies on PLA blends along with their applications.

**Table 10.** Features of selected studies on PLA blends along with their applications.

| Blend    | Concentration (wt.%)  | Features  | Applications and/or Reference                               |
|----------|---|---|---|
| PLA/PHB  | - 80/20<br>and 60/40  | -Improvement in the percentage elongation at break.   | -Biomedical applications [133].                             |
|          | - 75/25   | -Higher elongation at break with the use of 5% Lapol  | -Single-use applications such as fast-food packaging [108]. |
|          | -   | -Improved biodegradation rate, flexibility and impact properties.   | -Food packaging [134].                                      |
|          | - 75/25   | -Improved barrier and mechanical properties.  | -Food packaging [107].                                      |
|          | - 75/25   | -Biodegradable blend.   | -Biodegradable food packaging [105].                        |
|          | - 85/15   | -Good barrier to water vapor and improved oxygen barrier properties   | -Active food packaging [135].                               |
|          | -   | -Enhanced mechanical and active properties  | -Biodegradable active packaging for chilled salmon [142].   |
| PLA/PHBV | - 75/25<br>and 50/50  | -Improved permeability.   | -Food packaging [139].                                      |
| PLA/PBS  | - 90/10, 80/20<br>and 70/30                                   | -Exceptional combination of ductility, modulus and strength.  | -Green packaging [136].                                     |
|          | - 90/10, 80/20<br>and 70/30                                   | -Enhancement in PLA's water vapor and oxygen permeability.<br>-The levels of migration were maintained below the European legislative limits. | -Biodegradable food packaging [140].                        |
|          | - 80/20   | -Improved elongation at break.  | -Food packaging [137].                                      |
|          | - 90/10   | -Higher antibacterial activity.<br>-Transparent sheets.<br>-Mechanical properties allowed thermoforming for applications of food packaging.   | -Antibacterial food packaging sheets [143].                 |
| PLA/PCL  | - 90/10, 85/15,<br>80/20, 75/25,<br>70/30, 60/40<br>and 50/50 | -Well balanced combination of toughness and stiffness.  | -Packaging, biomedical and agricultural applications [138]. |

Table 10. Cont.

| Blend        | Concentration (wt.%)       | Features   | Applications and/or Reference                               |
|--------------|----------------------------|--|---|
| PLA/PBAT     | - 70/30                    | -Migration levels were below the limit specified by Food contact materials EU NO. 10/2011; therefore, the blend is safe for food contact packaging applications.   | -Food contact materials for containers and packaging [141]. |
| PLA/PHBV/PBS | - 60/30/10<br>and 60/10/30 | -Entirely biodegradable.<br>-An enhancement in the PLA's crystallization, flexibility and toughness was observed in the resulting ternary complex.<br>-Optimum performance with excellent balanced thermal resistance and stiffness-toughness. | [144]   |

Abbreviations: PLA, poly(lactic acid); PHB, polyhydroxybutyrate; PHBV, poly(3-hydroxybutyrate-co-3-hydroxyvalerate); PBS, poly(butylene succinate); PCL, poly( $\epsilon$ -caprolactone); PBAT, poly(butylene adipate terephthalate).

#### 2.4. Composites'/Nanocomposites' Effect

Different studies have suggested the addition of different types of reinforcing fillers such as carbon nanotubes, talc and montmorillonite (MMT) into PLA to enhance its mechanical properties [145,146].

Adding MMT was reported to enhance the modulus of elasticity and flexural modulus of PLA based nanocomposites. Moreover, the molecular mobility of PLA chains can be restricted by the intercalated MMT particles [145–147].

In another investigation [147], the modulus of elasticity increased by 43% after the incorporation of 7.5 wt.% of MMT particles into PLA nanocomposites. The reason behind such enhancement in the stiffness (modulus of elasticity and flexural modulus) of PLA nanocomposites is the effective intercalation of MMT stacked layers in the PLA matrix which resulted in a bigger interfacial area that interacted with the matrix of PLA. Therefore, PLA rigidity resulted from the enhancement in interaction effect between the PLA matrix and MMT particles. In areas of higher interacted interfacial, the applied stress can be effectively transferred from the PLA matrix to the MMT particles. This can subsequently enhance the stiffness of PLA nanocomposites [147].

Balakrishnan et al. [145] investigated the effect of the number of MMT particles on the mechanical properties of PLA nanocomposite. Results showed that the addition of MMT particles into PLA has substantially enhanced the flexural modulus and modulus of elasticity by 18% and 10%, respectively. Results also showed that there was a gradual reduction in the flexural strength and tensile strength of the PLA composites by 25% and 10%, respectively. This was attributed to the increased number of MMT particles in the PLA matrix. This suggests that with the addition of more MMT particles, the particles reduced the interfacial adhesion effect between the MMT particles and PLA matrix because they agglomerated together. The agglomerated MMT particles acted as a stress concentration point in the matrix. Therefore, when they were exposed to an applied stress, they failed to evenly transfer that stress throughout the PLA matrix. Furthermore, the orientation and dispersion of MMT particles in the PLA matrix influence both the flexural strength and tensile strength due to the various orientations of applied stress between flexural bending and tensile straining. The same study showed that the impact strength of the PLA nanocomposite was lowered by 13% when the amount of MMT increased to 4 phr. However, there was a substantial enhancement in the impact strength of PLA/LLDPE nanocomposites by 53% and 21%, respectively, when 2 and 4 phr MMT particles were

added. Results also showed that impact strength was induced when 10 wt.% of LLDPE was added to the MMT/PLA nanocomposites as compared to PLA nanocomposites. Therefore, it was found that a better orientation and dispersion of MMT particles in the PLA matrix was accomplished by the presence of LLDPE. This made the polymer matrix capable of absorbing more energy when subjected to rapid loading [145].

The effect of talc on the mechanical properties of PLA was investigated by Harris and Lee [148]. Both PLA's flexural modulus and strength were substantially enhanced by 25% as a result of the addition of 2 wt.% talc. This was explained by the fact that talc particles acted as a nucleating agent which induced PLA's crystallinity and thus enhanced the toughness of PLA. As a result of talc particles' structure and orientation inside the PLA matrix, the applied stress can be effectively transferred to the PLA matrix from the talc particles. Therefore, the presence of talc particles can offer a reinforcement effect on the toughness and rigidity of the PLA matrix [148].

In another study [149], there was a substantial improvement in both the flexural modulus and strength of neat PLA with the addition of talc. An interesting observation was that when the content of talc increased from 0 to 2.0 wt.%, the flexural modulus and flexural strength of PLA increased rapidly. Such improvement is attributed to the substitution of the PLA matrix with highly rigid talc filler. Therefore, when subjected to external loading, talc filler could efficiently limit the mobility and extendibility of the PLA matrix. SEM analysis of the nanocomposite showed that a good interfacial adhesion effect between the PLA matrix the talc filler existed. Due to this reinforcing and toughening effect, the applied load was transferred evenly throughout the whole polymer matrix. Increasing the talc content to more than 2% wt.% resulted in a slight increase in the flexural modulus and flexural strength. The reason behind this decrease in effectiveness is due to the presence of thicker talc particles which in turn resulted from the insufficient delamination of talc particles. At higher talc filler content, the brittle behavior of the PLA matrix was dominant because the applied load was unable to be efficiently transferred from the polymer matrix to the talc fillers. The reason behind that was the weak interfacial adhesion effect between the PLA matrix and the thicker talc particles. Results from the study have also suggested that at higher content of talc particles (more than 2 wt.%) there was a reduction in the orientation degree of talc particles. It was also found that the orientation direction of talc layers was not parallel to the injection direction. Thus, this has led to a debonding effect of talc particles and the PLA interface. The result was that many microcracks were presented along the direction of fracture [149].

An investigation of the effect of increasing talc and kaolin content on the properties of PLA composites was done by Ouchiar et al. [150]. The reported neat PLA's modulus of elasticity was 2.4 GPa. However, with the addition of 5 wt.% talc content, the modulus of elasticity improved slightly to around 2.6 GPa. The addition of 5 wt.% of kaolin had a similar effect. When the talc and kaolin content increased from 5 to 30 wt.%, the results showed a gradual improvement in the modulus of elasticity of PLA composites. Nonetheless, PLA/talc composite reported a higher modulus of elasticity than kaolin/PLA composites. This is because when compared to kaolin-added PLA composites, an earlier crystallization was demonstrated by PLA/talc composites. This highlights the nucleation effect of talc and its feasibility in inducing the rigidity of PLA composites [150].

In an investigation done by Zhou et al. [151], the effect of using various contents of carbon nanotubes (CNTs) with carboxyl groups (CNTs-COOH) on the mechanical properties of PLA nanocomposites was studied. Results suggest that an increase in Izod impact strength, tensile strength and percentage elongation of PLA nanocomposites could be observed up to CNTs-COOH content of 0.5 wt.%. This demonstrates that enhancements in the impact strength and tensile strength of PLA is feasible with the addition of only a small amount of CNTs. This can be explained by the high stiffness of CNTs with high surface area and aspect ratio which could further enhance the PLA matrix's toughness by efficiently interlocking in the PLA matrix. Due to this interlocking effect, the applied stress can be effectively transferred from the carbon nanotubes particles to the PLA matrix causing



strengthening of the PLA nanocomposites. Another factor that aids in strengthening the PLA matrix is the strong chemical bonds between the PLA matrix and CNT-COOH particles which restricted PLA macromolecular chains' mobility. Nonetheless, a further increase in the CNTs-COOH content above 0.5 wt.% reduced PLA nanocomposites' Izod impact strength and tensile strength [151].

Similar results were also reported for another study [152]. The study showed that when more than 3 wt.% content of CNTs was added, a gradual decrease in the tensile strength of PLA nanocomposites was observed. This reduction in tensile strength can be explained by the increased content of carbon nanotubes in the PLA matrix which agglomerated together into larger carbon nanotube aggregates [151,152]. The presence of such CNTs aggregated in the PLA matrix and worked as point of stress concentration that weakened the applied load transfer throughout the PLA matrix. This has resulted in a reduction in the interfacial adhesion between the PLA matrix and CNTs [152].

Silva and co-authors [153] reported PLA/PHBV blends reinforced with carbon nanotubes. The incorporation of CNTs contributed to the electromagnetic and electrical properties of polymeric nanocomposites. The production of PLA/PHBV blend (80/20 wt.%) and PLA/PHBV blend based nanocomposites with 0.5 and 1.0 wt% of CNTs was reported. The incorporation of CNTs lowered the Izod impact strength, yet flexural properties remained not affected. The incorporation of 1.0 wt% CNTs yielded better electrical properties. Moreover, the nanocomposites demonstrated excellent result as electromagnetic interference shielding material [153].

Both of kenaf fibers and Multi-Walled Carbon Nanotubes (MWCNTs) were used by Chen et al. [154] to reinforce the PLA matrix. Increasing the content of kenaf fibers with the epoxy groups (KF-OX) up to 30 wt.% resulted in a gradual improvement in the MWCNT/PLA nanocomposites' tensile strength prior to and after annealing. The chemical reaction between the PLA matrix and the KF-OX fibers was the main cause behind such improvement in tensile strength. When subjected to annealing, the tensile strength of the PLA nanocomposite became 84% higher than pristine PLA. This can be attributed to the good compatibility of KF-OX and the PLA matrix as well as to the creation of crystalline structure at the interfaces between the KF-OX fibers and PLA matrix which substantially enhanced the tensile strength of PLA nanocomposites. As a result of the outstanding interfacial adhesion effect between the PLA matrix and KF-OX fibers, the presence of transcrystallinity in the PLA matrix was able to deliver a resistance effect against applied external loading [155]. An improvement in the tensile strength was therefore observed due to the superb interfacial adhesion effect between the PLA matrix and KF-OX fibers which allowed the applied straining stress to be transmitted more efficiently to the PLA matrix from the KF-OX fibers. An improvement of KF-OX/MWCNT/PLA nanocomposites' tensile strength was also noticed due to the recrystallization of PLA nanocomposites by the annealing process. Nonetheless, when the KF-OX content increased to above 40 wt.%, there was a drastic decrease in the PLA nanocomposites' tensile strength. This can be explained by the possible obstruction of the recrystallization of PLA chains and weakening of the PLA nanocomposites' stiffness caused by the extremely entangled KF-OX fibers in the PLA matrix [154].

The effect of carbon fiber on the mechanical properties of PLA based composites was also investigated. In one study [156], short carbon fibers were mixed with PLA using FFF technology. The mechanical properties of neat PLA as well as 3D-printed PLA/carbon fibers composites were studied at different printing orientations, namely "upright, on-edge and flat", as shown in Figure 6. Results showed that the incorporation of carbon fibers enhanced the mechanical properties of the produced composites in comparison to the pure PLA. In comparison to the neat PLA, flat PLA/carbon fiber composite samples reported an average increase of 179.9%, 47.1%, 230.95% and 89.75% for tensile stiffness, tensile strength, flexural stiffness and flexural strength, respectively. Overall, the dimensional accuracy was not affected by the addition of short carbon fibers as reinforcements. Furthermore, enhanced surface roughness was reported in case of flat and on-edge PLA/carbon fiber

composite samples. Results suggested that the prepared composite is a promising candidate for applications demanding dimensional stability and higher stiffness [156].

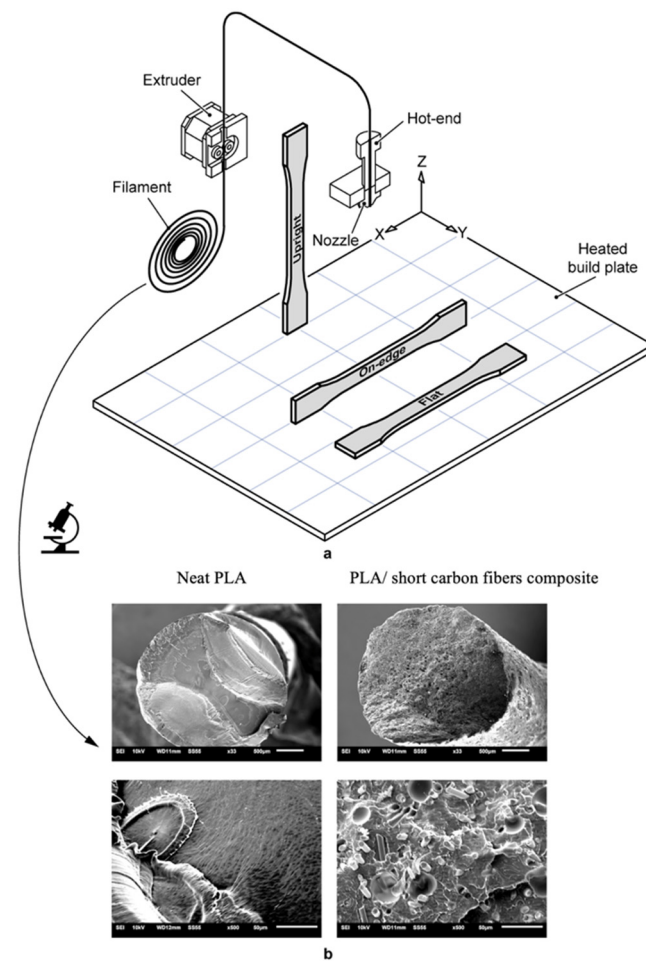


**Figure 6.** (a) A schematic showing the different printing orientations and (b) cross sectional SEM images of printing filaments of neat PLA and PLA/short carbon fibers composite [156].

The effect of Cloisite 30B nanoclay, kenaf fiber and hexagonal boron nitride (h-BN) fillers on PLA composites' mechanical properties was also studied [157]. The study showed that there was a slight increase in the modulus of elasticity of the PLA composite before and after annealing treatment when 5 pph kenaf fiber, Cloisite 30B nanoclay and h-BN were added. When compared to both, Cloisite 30B nanoclay or h-BN, the addition of kenaf fiber resulted in a smaller increase in the Young's modulus. This was attributed to the suitable compatibility between h-BN fillers and Cloisite 30B nanoclay with the PLA matrix. On the other hand, there was a weaker interfacial adhesion effect between the PLA matrix and kenaf fiber. The reason behind that was the absence of polar interaction between the PLA chains and kenaf fiber which ultimately resulted in less rigidity of the PLA composites [157].

A study on the mechanical properties of PLA/PCL and an organoclay nanocomposite was conducted by Hasook et al. [119]. The incorporation of organoclay resulted in an increase in the modulus of elasticity; however, the elongation at break and the strength decreased. With the addition of PCL to the PLA matrix, the modulus of elasticity decreased, whereas there was an increase in the percentage elongation and tensile strength of PLA/organoclay nanocomposites. Out of all the PLA/clay nanocomposite blends, the tensile strength was the highest when PCL ( $M_w = 40,000$  g/mol) was used [119].

In another investigation [130], PLLA was blended with PBS and organoclay. PLLA/PBS at concentration of 75/25 wt.% with treated organoclay, TFC, as well as untreated organ-

oclay, Cloisite 25A, were examined. When various amount of Cloisite 25A and TFC were added to the PLLA/PBS composite, the Young's modulus was higher in comparison to that of PLLA/PBS blend. This shows that both of the Cloisite 25A and TFC exhibited a reinforcing effect due to their platelet structure and high aspect ratio. As the content of TFC clay increased, the Young's modulus of the PLLA/PBS/TFC showed a pronounced effect in comparison to that of PLLA/PBS/Cloisite 25A. When Cloisite 25A was added, the PLLA/PBS composite's percentage elongation decreased drastically. On the other hand, the elongation at break of the PLLA/PBS composite increased with the TFC content. Results showed that the blends with Cloisite 25A exhibited brittle fracture without necking, while composite blends with TFC, demonstrated higher necking. This suggests an increase in the interfacial interaction due to chemical bonds between the epoxy functional groups of the treated organoclay and PLLA/PBS blend which acted as a compatibilizer. Yield strength for the PLLA/PBS was around 44.70 MPa while the yield strength was maximum at a concentration of 10 wt.% of Cloisite 25A and TFC [130].

An investigation was carried out by Chen and Yoon [131] to compare the impact of incorporating treated and untreated organoclay, Cloisite 25A, on the PLLA/PBSA composite's mechanical properties. The composition of PLLA/PBSA was set at 75/25 wt.%. This is because at this blend composition, the brittleness of PLLA was significantly improved. The treated organoclay was produced by reacting (glycidoxypropyl)trimethoxy silane (GPS) with Cloisite 25A to yield functionalized organoclay (TFC). Melt compounding of PLLA and PBSA with the organoclays at 180 °C resulted in the PLLA/PBSA/clay composites. Throughout the entire range of clay compositions, Young's modulus of the PLLA/PBSA/Cloisite 25A/TFC composites was higher than that of the binary blend of PLLA/PBSA. That was anticipated, as the clay was used to reinforce the composite. On the other hand, the composite's percentage elongation, both with organoclay Cloisite 25A and TFC, was significantly less than that of the of PLLA/PBSA blend. An interesting observation is that the composite with treated clay, TFC, exhibited higher modulus of elasticity and percentage elongation than that of untreated clay, C25. The reduction in agglomeration observed in PLLA/PBSA/TFC composite explains the higher elongation at break and Young's modulus of PLLA/PBSA with TFC compared to those of PLLA/PBSA with C25 composite. As a result, this has contributed to more exfoliation and enhanced interaction between the functional groups of PLLA/PBSA and the epoxy group of TFC [131].

The effect of silica (SiO<sub>2</sub>) on the mechanical properties of PLA nanocomposites was investigated by Ahmed et al. [158]. They have used twin extruders to prepare composites of 3D-printed PLA wastes/SiO<sub>2</sub> at various concentrations (95/5, 90/10 and 85/15 wt.%). This was followed by an analysis of the mechanical properties. Figure 7 shows a complete overview of the composites' preparation and fabrication. Results showed that increasing the SiO<sub>2</sub> composition up to 10 wt.% resulted in increasing the tensile strength, yield stress, Young's modulus, ductility and toughness. A further increase of the SiO<sub>2</sub> composition resulted in a drop in these properties. The produced composites can promote the effective recycling of PLA wastes from 3D printing applications [158].

The effect of magnesium oxide particles (nano-Mg) on the PLA nanocomposites' mechanical properties was examined [159]. The authors reported a gradual increase in the Young's modulus and tensile strength of the PLA nanocomposites as a result of increasing nano-MgO's content up to 2 wt.%. Such increase was attributed to the nano-MgO particles' smaller size which offered a higher interfacial area of magnesium oxide nanoparticles by inducing the volume ratio of these particles in the PLA matrix. This high surface interaction between the PLA matrix and the magnesium oxide filler, promoted the transfer of applied stress to nano magnesium oxide filler from the PLA matrix and eventually led to enhancement in the PLA's mechanical properties. On the other hand, upon adding more than to 2 wt.% content of nano-MgO (up to 4 wt.% was used), the PLA nanocomposites' Young's modulus and tensile strength decreased gradually. This can be explained by the fact that higher content of nano-MgO tend to self-agglomerated into larger agglomerated particles which in turn has weakened the interfacial adhesion effect between the PLA

matrix and the agglomerated nano magnesium oxide filler. As a result, the agglomerated nano magnesium oxide fillers were phase-separated from the PLA matrix and worked as a point of stress concentration in the PLA matrix. Thus, the effect of reinforcement of nano magnesium oxide fillers inside the PLA matrix was reduced [159].

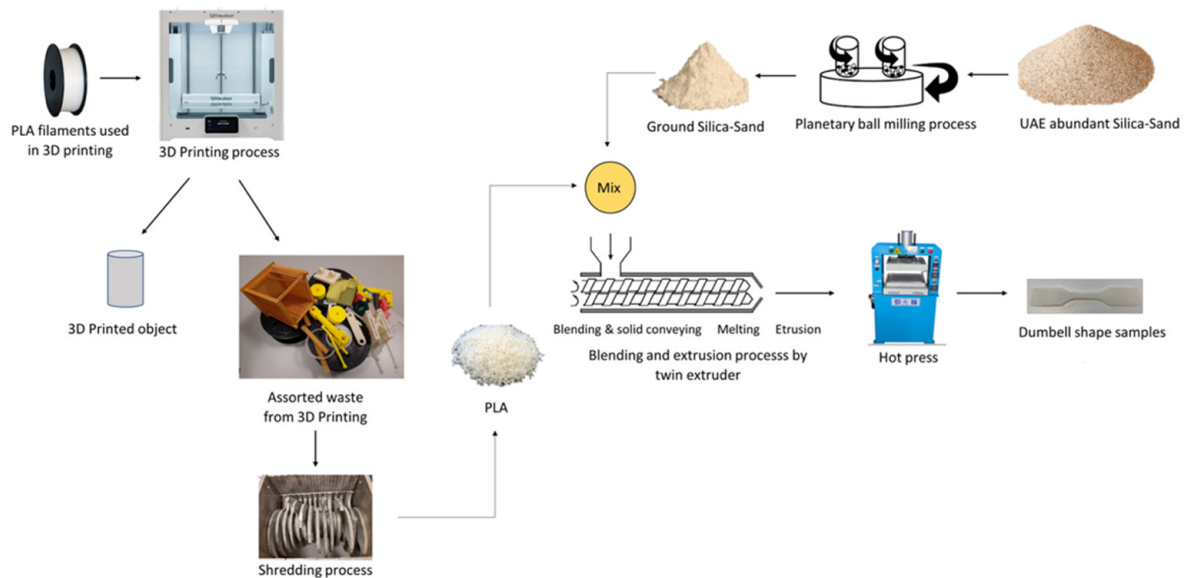


**Figure 7.** Preparation and fabrication of 3D-printed PLA wastes/SiO<sub>2</sub> composites as reported by Ahmed et al. [158].

Different studies in literature have analyzed the effect of natural fibers such as flax and kenaf fibers on PLA's mechanical properties [160–162]. Their low cost, high specific strength, good toughness, biodegradability, renewability and low density have made natural fibers appealing substitutes to conventional reinforcing fillers in PLA composites [161]. Nonetheless, various studies have reported that PLA's mechanical properties were substantially weakened as a result of the low compatibility of hydrophobic PLA with hydrophilic natural fibers [162,163]. This has hindered the use of PLA composites and nanocomposites in many applications.

Foruzanmehr et al. [161] found that the elongation at break and tensile strength were substantially improved after the addition oxidized flax into the PLA matrix. The reason behind that was the enhanced interfacial adhesion between the PLA matrix and fibers which has efficiently transferred the stress between the fibers and the PLA matrix [161].

In another investigation [164], film stacking and hot press compression molding were used to fabricate flax fiber braided yarn plain woven fabric reinforced PLA bio-composites. The impact of fiber weight fraction on the fracture and tensile properties was studied. Results showed that tensile strength and modulus were increased by around 60% and 62%, respectively for 35 wt.% braided fabric in comparison to neat PLA. This is attributed to the high value of plane-strain fracture toughness of braided fabric in comparison to other natural fibers. The interweaving yarns of the braided fabric exhibited high resistance, hence, more energy was required to initiate a crack propagation in comparison to other typical types of reinforcements [164].

The impact of coupling agent 3-glycidoxypropyl trimethoxy silane on the PLA/kenaf fiber composites' mechanical properties was studied by Lee et al. [162]. Results showed a significant enhancement in the interaction between the PLA matrix and kenaf fibers as a result of treating kenaf fibers with 3-glycidoxypropyl trimethoxy silane [162].

The incorporation of wood flour with a surface treatment with different coupling agents,  $\gamma$ -glycidoxypropyltrimethoxy silane (epoxy silane), vinyltrimethoxysilane (vinyl silane),  $\gamma$ -methacryloxypropyltrimethoxysilane (allyl ester silane) and  $\gamma$ -aminopropyl triethoxysilane (amino silane) into the PLA matrix was also investigated [165]. There was a significant improvement in the elongation at break, tensile strength and impact strength of

PLA/wood flour composites due to the incorporation of allyl ester silane, epoxy silane and amino silane. This was attributed to the enhanced interfacial interaction between the wood fibers and the PLA matrix as a result of the addition of silane coupling [165].

PLA/PCL composites using wood powder were prepared by Silva et al. [166] to examine their feasibility to produce disposable cups. Initially, the composites were prepared in a co-rotational twin screw extruder as shown in Figure 8. After that, extruded granules were molded via injection as illustrated in Figure 9. The impact strengths of the bio blend and composites were higher than that of neat PLA. Percentage elongation at break, shore D hardness as well as heat deflection temperature were roughly the same as neat PLA. On the other hand, losses were reported in tensile strength and Young’s modulus. The study concluded that such results are significant in promoting sustainability and recyclability [166].

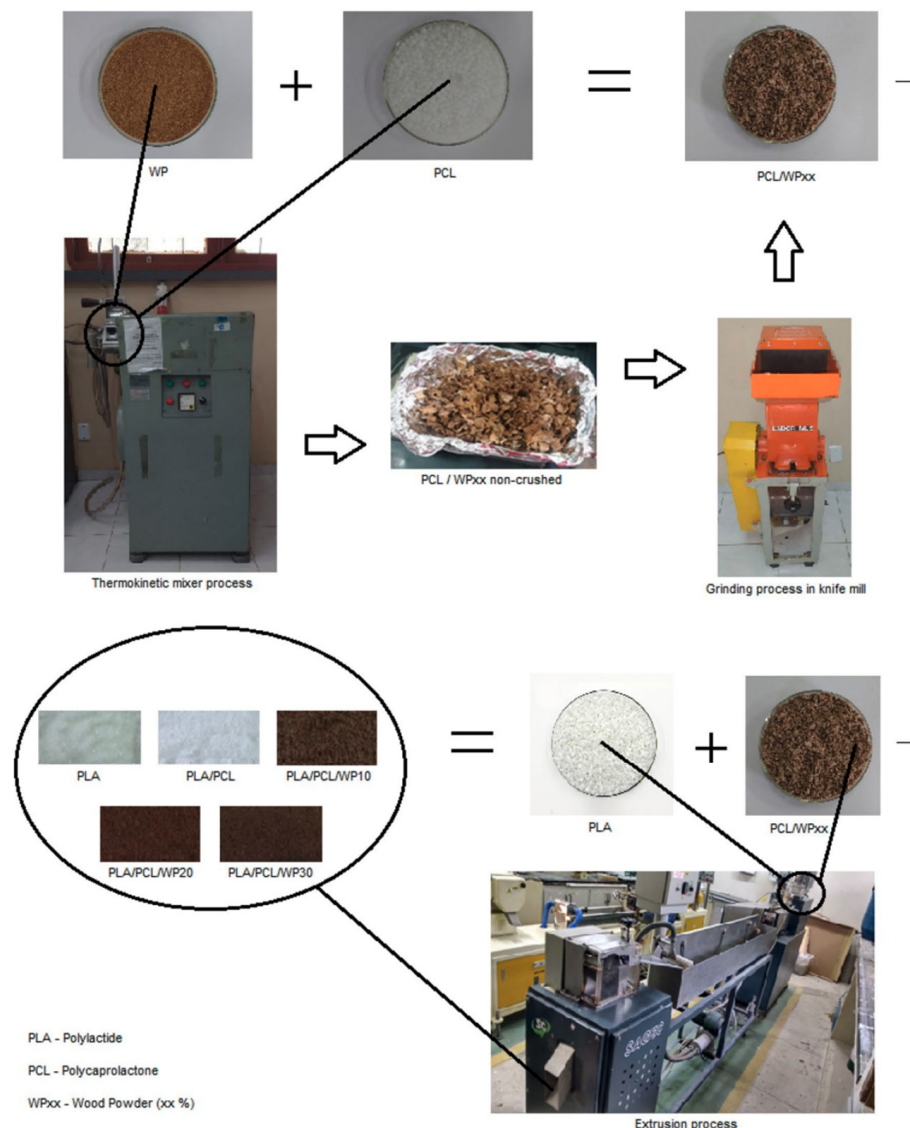


**Figure 8.** Extrusion process of PLA/PCL/wood powder composites. Reprinted with permission from Springer Nature, 2021 [166].

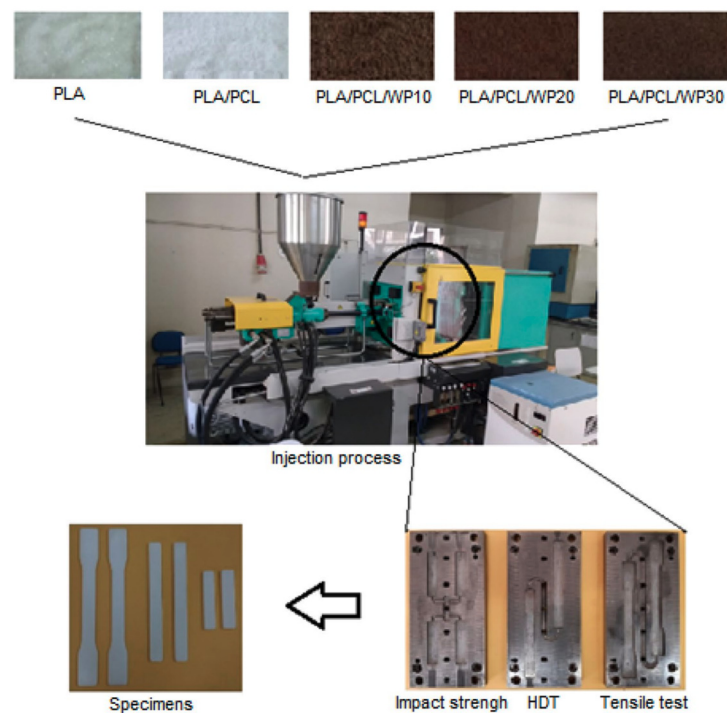


**Figure 9.** Injection molding process of PLA/PCL/wood powder composites. Reprinted with permission from Springer Nature, 2021 [166].

In another investigation [167], PLA/lignin composite filaments were produced by mixing PLA with organosolv lignin at various ratios. Lignin was replaced with PLA up to 20 wt.%. For the aim of enhancing the mechanical properties of the composites, two plasticizers, namely, PEG 2000 and Struktol (TR451) were added in different concentrations. Results showed that at 2 wt.% PEG, the tensile strength and percentage elongation at break were improved by 19% and 35%, respectively. On the other hand, TR451 was capable of improving the percentage elongation at break by 24% [167].

Paul et al. [168] reported the development of PLA/microcrystalline cellulose (MCC) bio composites via melt extrusion and compression molding. Triethylcitrate (TEC) was used as a plasticizer as well as to enhance the dispersion of the microcrystalline cellulose in the PLA matrix. Results showed improvements in crystallinity and ductility. Results of the mechanical and migration properties suggested that PLA/MCC bio composites with 10 wt.% TEC is the most suitable combination for ecofriendly food packaging applications [168].

Rasheed and co-authors [169] have studied the impact of CNCs (natural fiber) from bamboo fiber on the properties of PLA/PBS nanocomposites prepared by melt mixing followed by hot pressing. To improve PLA's properties, they have added 20 wt.% PBS as well as cellulose nanocrystals at different concentrations (0.5, 0.75, 1, 1.5 wt.%). Results showed that the prepared biodegradable PLA/PBS blend had a homogeneous morphology. The nanocomposite showed rod-like cellulose nanocrystals particles embedded in the polymer matrix. Tensile strength, Young's modulus and thermal stability all improved up to 1 wt.% due to the uniform distribution of the cellulose nanocrystals in the nanocomposites; however, percentage elongation at break reduced. According to the study, the developed nanocomposites can be completely degradable in soil, making it a feasible green candidate to conventional packaging materials [169].

Biodegradable nanocomposites prepared from PLA, PHB and CNCs were reported by Frone et al. [170] They have prepared the nanocomposites using a single step reactive blending with DCP as a cross-linking agent. The prepared nanocomposites were then processed using extrusion, compression molding and 3D printing. This was followed by an examination of the thermal, mechanical and morphological properties of these nanocomposites. The addition of DCP resulted in enhanced interfacial adhesion, improved

dispersion of the CNCs in the nanocomposites as well as increased crystallinity. DCP and CNCs exhibited nucleating activity and favored PLA's crystallization, increasing its crystallinity from 16% in PLA/PHB to 38% in DCP crosslinked blend and to 43% in crosslinked PLA/PHB/NC nanocomposite. In comparison to compression molded films, nanocomposites filaments produced by 3D printing and extrusion demonstrated higher storage modulus and onset degradation temperature. The study concluded that PLA/PHB blends and nanocomposites with improved interfacial adhesion, enhanced mechanical properties and thermal stability can be produced following the right choice of processing approach and using DCP and CNCs for properties balance. If processed correctly, such nanocomposites have high potential in meeting the high standards of industrial engineering applications [170].

Alam et al. [171] reported the mechanical properties of 3D-printed novel nanocomposite scaffolds. The scaffolds consisted of a blend of PLA and PCL reinforced with halloysite nanotubes (HNTs). Melt blending was used to develop the nanoengineered filaments while FFF was used to fabricate the nanocomposite scaffolds. The study reported a uniform dispersion of the HNTs inside the blend's matrix. According to the study, the loss in mechanical properties as a result of the incorporation of PCL to PLA was fully recovered by the incorporation of HNTs. Degradation rate, in terms of weight loss, was dropped from 4.6% for neat PLA to 1.3% for PLA/PCL blend. However, that was gradually increased to 4.4% after the addition of 7 wt.% HNTs. Results showed that the mechanical properties, biodegradation rate as well as biological characteristics of the 3D-printed micro architected PLA/PCL/HNT composite scaffolds can be tuned by a suitable combination of PCL and HNTs contents inside the PLA matrix [171].

Recently, Komal et al. [172] were able to fabricate pineapple fibers (PFs)/PLA bio composites using direct injection molding (DIM) without compounding, with compounding using extrusion followed by injection molding (EIM) as well as with compounding using extrusion followed by compression molding (ECM). Figure 10 shows a schematic of the distribution of PFs in each of these composites. Results showed that the mechanical response, crystallinity and viscoelastic response of the EIM composites substantially dominated the composites fabricated by the other two approaches. The study has also reported a severe attrition of fibers during ECM. Nonetheless,  $T_g$ ,  $T_m$  and crystallization temperature were found to be independent of the fabrication approach [172].

In another investigation [173], solution blending was used to fabricate chitosan/PLA composites doped with graphene oxide (GO). GO was added into a PLA solution before blending it with chitosan. Thermal and mechanical properties in addition to the water barriers of various compositions of the chitosan/PLA-GO composites (90/10/2, 70/30/2 and 50/50/2 wt.%) were analyzed. Results suggested enhanced miscibility of chitosan and PLA, improved thermal stability as well as increased tensile strength and modulus due to the addition of GO. Moreover, chitosan/PLA-GO composites reported excellent water barrier properties. The highest decrement in water absorption was for chitosan/PLA-GO (70/30/2 wt.%) composite. The study concluded that the prepared composites with GO have high potential to be used in biomedical applications such as drug delivery. Furthermore, the developed composites can be also utilized in food packaging applications [173].

Table 11 shows the impact of various PLA composites and nanocomposites at various concentrations on the mechanical properties along with their applications.

Table 11. The effect of various PLA nanocomposites at different concentrations on the mechanical properties along with their applications.

| Composite/<br>Nano-<br>Composite | Concent-<br>Ration (wt.%)    | Tensile<br>Strength<br>(MPa) | Young's<br>Modulus<br>(MPa) | Elongation<br>at Break | Charpy Break Energy/<br>(Notched Izod Break<br>Energy)/<br>Toughness | Flexural Strength<br>(MPa) | Flexural Modulus<br>(MPa) | Applications<br>and/or Reference  |                                  |
|----------------------------------|------------------------------|------------------------------|-----------------------------|------------------------|--|----------------------------|---------------------------|-----------------------------------|----------------------------------|
| PLA/MMT                          | - 100/0                      | - 58.0                       | - 3000                      |                        |  | - 109                      | - 3300                    | Structural<br>applications [145]. |                                  |
|                                  | - 100/2 phr <sup>a</sup>     | - 55.0                       | - 3400                      |                        |  | - 84                       | - 3500                    |                                   |                                  |
|                                  | - 100/4 phr                  | - 53.0                       | - 3500                      | -                      |  | - 83                       | - 3850                    |                                   |                                  |
|                                  | - 90/2 phr with 10%<br>LLDPE | - 41.50                      | - 2650                      |                        |  | - 75                       | - 3000                    |                                   |                                  |
|                                  | - 90/4 phr with 10%<br>LLDPE | - 42.50                      | - 2850                      |                        |  | - 66                       | - 3150                    |                                   |                                  |
| PLA/talc                         | - 100/0                      | - 54.0                       |                             | - 2.4%                 |  | - 66.0                     | - 3300                    | Packaging<br>applications [149].  |                                  |
|                                  | - 98/2                       | - 58.5                       |                             | - 2.5%                 |  | - 90.5                     | - 3450                    |                                   |                                  |
|                                  | - 95.5/4.5                   | - 58.4                       |                             | - 2.65%                |  | - 91.0                     | - 4000                    |                                   |                                  |
|                                  | - 90.9/9.1                   | - 58.5                       | -                           | - 3.20%                |  | - 93.0                     | - 4300                    |                                   |                                  |
|                                  | - 87.2/12.8                  | - 58.2                       |                             | - 4.1%                 |  | - 94.0                     | - 4900                    |                                   |                                  |
|                                  | - 81.9/18.1                  | - 59                         |                             | - 5.1%                 |  | - 98.0                     | - 6100                    |                                   |                                  |
|                                  | - 75.7/24.3                  | - 60                         |                             | - 2.4%                 |  | - 103.5                    | - 6750                    |                                   |                                  |
|                                  | - 100/0                      | - 47.0                       | - 2400                      | - 6.70%                |  |                            |                           |                                   | Packaging<br>applications [150]. |
|                                  | - 95/5                       | - 47.0                       | - 2560                      | - 3.0%                 |  |                            |                           |                                   |                                  |
|                                  | - 90/10                      | - 48.0                       | - 3050                      | - 3.0%                 |  |                            |                           |                                   |                                  |
| - 80/20                          | - 46.0                       | - 3650                       | - 2.50%                     |                        |  |                            |                           |                                   |                                  |
| PLA/kaolinite                    | - 70/30                      | - 48.0                       | - 4550                      | - 1.70%                |  |                            |                           | Packaging<br>applications [150].  |                                  |
|                                  | - 100/0                      | - 47.0                       | - 2400                      | - 6.70%                |  |                            |                           |                                   |                                  |
|                                  | - 95/5                       | - 48.0                       | - 2550                      | - 2.4%                 |  |                            |                           |                                   |                                  |
|                                  | - 90/10                      | - 42.0                       | - 2700                      | - 1.90%                |  |                            |                           |                                   |                                  |
|                                  | - 80/20                      | - 42.0                       | - 3100                      | - 1.50%                |  |                            |                           |                                   |                                  |
|                                  | - 70/30                      | - 46.0                       | - 3350                      | - 1.40%                |  |                            |                           |                                   |                                  |



Table 11. Cont.

| Composite/<br>Nano-<br>Composite | Concent-<br>Ration (wt.%) | Tensile<br>Strength<br>(MPa) | Young's<br>Modulus<br>(MPa) | Elongation<br>at Break | Charpy Break Energy/<br>(Notched Izod Break<br>Energy)/<br>Toughness | Flexural Strength<br>(MPa) | Flexural Modulus<br>(MPa) | Applications<br>and/or Reference                          |
|----------------------------------|---------------------------|------------------------------|-----------------------------|------------------------|--|----------------------------|---------------------------|---|
|                                  | - 100/0 <sup>b</sup>      | - 39.50                      |                             | - 22.50%               | - (15.50) KJ/m <sup>2</sup>  |                            |                           |   |
|                                  | - 99/0.1 <sup>b</sup>     | - 40.50                      |                             | - 28.30%               | - (22.60) KJ/m <sup>2</sup>  |                            |                           |   |
|                                  | - 99.5/0.5 <sup>b</sup>   | - 42.80                      | -                           | - 33.60%               | - (27.70) KJ/m <sup>2</sup>  | -                          | -                         | Industrial<br>applications [151].                         |
|                                  | - 99/1 <sup>b</sup>       | - 40.60                      |                             | - 26.70%               | - (20.50) KJ/m <sup>2</sup>  |                            |                           |   |
|                                  | - 98/2 <sup>b</sup>       | - 39.60                      |                             | - 20.50%               | - (8.80) KJ/m <sup>2</sup>   |                            |                           |   |
|                                  |                           | - 60.5 <sup>c</sup>          |                             | - 5.00% <sup>c</sup>   |  |                            |                           |   |
|                                  |                           | - 65.0 <sup>c</sup>          |                             | - 5.60% <sup>c</sup>   |  |                            |                           |   |
|                                  |                           | - 68.0 <sup>c</sup>          |                             | - 5.70% <sup>c</sup>   |  |                            |                           |   |
|                                  | - 100/0                   | - 65.0 <sup>c</sup>          |                             | - 5.70% <sup>c</sup>   |  |                            |                           |   |
|                                  | - 99/1                    | - 63.0 <sup>c</sup>          |                             | - 5.90% <sup>c</sup>   |  |                            |                           |   |
|                                  | - 97/3                    | - 51.0 <sup>d</sup>          | -                           | - 5.00% <sup>d</sup>   |  |                            |                           |   |
|                                  | - 95/5                    | - 58.0 <sup>d</sup>          |                             | - 5.00% <sup>d</sup>   |  |                            |                           |   |
|                                  | - 90/10                   | - 67.5 <sup>d</sup>          |                             | - 7.00% <sup>d</sup>   |  |                            |                           |   |
|                                  |                           | - 64.5 <sup>d</sup>          |                             | - 6.00% <sup>d</sup>   |  |                            |                           |   |
|                                  |                           | - 59.5 <sup>d</sup>          |                             | - 4.80% <sup>d</sup>   |  |                            |                           |   |
| PLA/CNT                          |                           |                              |                             |                        |  |                            |                           |   |
|                                  | - 100/0                   |                              |                             |                        | - (2.14) KJ/m <sup>2</sup>   | - 58.07                    | - 2940                    | Electronic devices<br>and military<br>applications [153]. |
|                                  | - 80/0 with 20% PHBV      |                              |                             |                        | - (4.10) KJ/m <sup>2</sup>   | - 51.60                    | - 3100                    |   |
|                                  | - 80/0.5 with 20% PHBV    | -                            | -                           | -                      | - (2.33) KJ/m <sup>2</sup>   | - 58.66                    | - 3300                    |   |
|                                  | - 80/1 with 20% PHBV      |                              |                             |                        | - (2.46) KJ/m <sup>2</sup>   | - 61.01                    | - 3250                    |   |

Table 11. Cont.

| Composite/<br>Nano-<br>Composite | Concent-<br>Ration (wt.%)                  | Tensile<br>Strength<br>(MPa) | Young's<br>Modulus<br>(MPa) | Elongation<br>at Break | Charpy Break Energy/<br>(Notched Izod Break<br>Energy)/<br>Toughness | Flexural<br>Strength (MPa) | Flexural<br>Modulus (MPa) | Applications and/or<br>Reference  |
|----------------------------------|--|------------------------------|-----------------------------|------------------------|--|----------------------------|---------------------------|---|
|                                  | - 100/0                                    | - 49.70                      |                             |                        | - (17.50) J/m  |                            |                           |   |
|                                  | - 89/10 <sup>e</sup> with 1%<br>MWCNTs     | - 61.60                      |                             |                        | - (30.80) J/m  |                            |                           |   |
|                                  | - 79/20 <sup>e</sup> with 1% MWCNTs        | - 62.80                      |                             |                        | - (36.80) J/m  |                            |                           |   |
|                                  | - 69/30 <sup>e</sup> with 1% MWCNTs        | - 78.50                      |                             |                        | - (37.40) J/m  |                            |                           |   |
|                                  | - 59/40 <sup>e</sup> with 1% MWCNTs        | - 47.70                      |                             |                        | - (43.80) J/m  |                            |                           |   |
|                                  | - 100/0 <sup>f</sup>                       | - 46.80                      |                             |                        | - (30.90) J/m  |                            |                           | Antistatic<br>applications [154].   |
|                                  | - 89/10 <sup>f</sup> with 1% MWCNTs        | - 61.60                      |                             |                        | - (30.30) J/m  |                            |                           |   |
|                                  | - 79/20 <sup>f</sup> with 1% MWCNTs        | - 70.40                      |                             |                        | - (35.50) J/m  |                            |                           |   |
|                                  | - 69/30 <sup>f</sup> with 1% MWCNTs        | - 91.50                      |                             |                        | - (35.40) J/m  |                            |                           |   |
|                                  | - 59/40 <sup>f</sup> with 1% MWCNTs        | - 53.60                      |                             |                        | - (44.90) J/m  |                            |                           |   |
|                                  | - 70/30 <sup>g</sup>                       |                              |                             |                        |  |                            |                           |   |
|                                  | - 100/0                                    | - 63.20                      | - 1410                      | - 6.60%                |  |                            |                           | Packaging<br>applications<br>such as hot boiling<br>water containers [157]. |
|                                  | - 100/0 <sup>f</sup>                       | - 65.30                      | - 1634                      | - 5.30%                |  |                            |                           |   |
|                                  | - PLA/20 pph <sup>h</sup>                  | - 39.50                      | - 1618                      | - 3.50%                |  |                            |                           |   |
|                                  | - PLA/20 pph <sup>f</sup>                  | - 32.70                      | - 1742                      | - 2.50%                |  |                            |                           |   |
| PLA/KF                           | - 90/10                                    |                              |                             |                        |  | - 22.0                     | - 2100                    |   |
|                                  | - 70/30                                    |                              |                             |                        |  | - 40.0                     | - 4000                    |   |
|                                  | - 50/50                                    |                              |                             |                        |  | - 49.0                     | - 4700                    |   |
|                                  | - 30/70                                    |                              |                             |                        |  | - 50.0                     | - 5900                    |   |
|                                  | - 90/10 with 1% GPS as a<br>coupling agent |                              |                             |                        |  | - 38.0                     | - 4700                    |   |
|                                  | - 70/30 with 1% GPS                        |                              |                             |                        |  | - 43.0                     | - 4000                    |   |
|                                  | - 50/50 with 1% GPS                        |                              |                             |                        |  | - 60.0                     | - 5700                    |   |
|                                  | - 30/70 with 1% GPS                        |                              |                             |                        |  | - 63.0                     | - 6800                    |   |
|                                  | - 90/10 with 3% GPS                        |                              |                             |                        |  | - 30.0                     | - 4200                    |   |
|                                  | - 70/30 with 3% GPS                        |                              |                             |                        |  | - 49.0                     | - 4500                    |   |
|                                  | - 50/50 with 3% GPS                        |                              |                             |                        |  | - 64.0                     | - 5800                    |   |
|                                  | - 30/70 with 3% GPS                        |                              |                             |                        |  | - 62.0                     | - 6800                    |   |
|                                  | - 90/10 with 5% GPS                        |                              |                             |                        |  | - 37.0                     | - 4200                    |   |
|                                  | - 70/30 with 5% GPS                        |                              |                             |                        |  | - 48.0                     | - 4650                    |   |
|                                  | - 50/50 with 5% GPS                        |                              |                             |                        |  | - 63.0                     | - 5700                    |   |
|                                  | - 30/70 with 5% GPS                        |                              |                             |                        |  | - 62.0                     | - 6800                    | Prototypes of<br>automobile<br>headliners [162].                            |

Table 11. Cont.

| Composite/<br>Nano-<br>Composite | Concent-<br>Ration (wt.%)   | Tensile<br>Strength<br>(MPa) | Young's<br>Modulus<br>(MPa) | Elongation<br>at Break | Charpy Break Energy/<br>(Notched Izod Break<br>Energy)/<br>Toughness | Flexural<br>Strength<br>(MPa) | Flexural<br>Modulus<br>(MPa) | Applications and/or<br>Reference  |
|----------------------------------|---|------------------------------|-----------------------------|------------------------|--|-------------------------------|------------------------------|---|
|                                  | - 100/0<br>- 100/0 <sup>f</sup>   | - 63.20<br>- 65.30           | - 1410<br>- 1634            | - 6.60%<br>- 5.30%     | -  | -                             | -                            | Packaging<br>applications<br>such as hot boiling<br>water containers [157]. |
|                                  | - PLA with 5 pph Cloisite 30B <sup>®</sup><br>- PLA with 5 pph Cloisite 30B <sup>®f</sup> | - 51.20<br>- 51.60           | - 1599<br>- 1893            | - 5.20%<br>- 3.50%     | -  | -                             | -                            |   |
|                                  | - PLA (100/0)   |                              |                             |                        |  |                               |                              |   |
|                                  | - PLA/PCL <sup>j</sup> /Organoclay 9S-Ben W<br>(90.48/4.76/4.76 wt.%)                     | - 45.13                      | - 3729                      | - 2.06%                |  |                               |                              |   |
|                                  | - PLA/PCL <sup>j</sup> /Organoclay 9S-Ben W<br>(90.48/4.76/4.76 wt.%)                     | - 47.26<br>- 53.91           | - 4371<br>- 4069            | - 2.24%<br>- 3.18%     | -  | -                             | -                            | [119]   |
|                                  | - PLA/PCL <sup>k</sup> /Organoclay 9S-Ben W<br>(90.48/4.76/4.76 wt.%)                     | - 39.94                      | - 4237                      | - 2.00%                |  |                               |                              |   |
|                                  | - PLLA/PBS (100/0)  |                              |                             |                        |  |                               |                              |   |
|                                  | - PLLA/PBS (0/100)  |                              |                             |                        |  |                               |                              |   |
|                                  | - PLLA/PBS (75/25)  |                              |                             |                        |  |                               |                              |   |
| PLA/nano clay or<br>organoclay   | - PLLA/PBS 75/25 with 2% Cloisite<br>25 A <sup>®</sup>                                    |                              | - 2214.70<br>- 326.30       | - 6.90%<br>- 320.60%   |  |                               |                              |   |
|                                  | - PLLA/PBS 75/25 with 5% Cloisite<br>25 A <sup>®</sup>                                    |                              | - 1075.20<br>- 1364.60      | - 71.80%<br>- 4.40%    |  |                               |                              |   |
|                                  | - PLLA/PBS 75/25 with 10% Cloisite<br>25 A <sup>®</sup>                                   |                              | - 1616.60<br>- 1940.10      | - 4.10%<br>- 3.60%     |  |                               |                              | [130]   |
|                                  | - PLLA/PBS 75/25 with 2% TFC  |                              | - 1407.90                   | - 75.50%               |  |                               |                              |   |
|                                  | - PLLA/PBS 75/25 with 5% TFC  |                              | - 1624.60                   | - 100.60%              |  |                               |                              |   |
|                                  | - PLLA/PBS 75/25 with 10% TFC   |                              | - 1990.30                   | - 118.10%              |  |                               |                              |   |
|                                  | - PLLA/PBSA 75/25 with 2%<br>Cloisite 25 A <sup>®</sup>                                   |                              |                             |                        |  |                               |                              |   |
|                                  | - PLLA/PBSA 75/25 with 5% Cloisite<br>25 A <sup>®</sup>                                   |                              | - 1394.10<br>- 1585.00      | - 11.30%<br>- 10.60%   |  |                               |                              |   |
|                                  | - PLLA/PBSA 75/25 with 10%<br>Cloisite 25 A <sup>®</sup>                                  |                              | - 1748.40<br>- 1445.60      | - 5.25%<br>- 69.50%    |  |                               |                              | Biodegradable sealing<br>envelope for food<br>packaging [131].              |
|                                  | - PLLA/PBSA 75/25 with 2% TFC   |                              | - 1698.30                   | - 43.10%               |  |                               |                              |   |
|                                  | - PLLA/PBSA 75/25 with 5% TFC   |                              | - 1780.70                   | - 45.70%               |  |                               |                              |   |

Table 11. Cont.

| Composite/<br>Nano-<br>Composite                     | Concent-<br>Ration (wt.%)   | Tensile<br>Strength<br>(MPa) | Young's<br>Modulus<br>(MPa) | Elongation<br>at Break | Charpy Break Energy/<br>(Notched Izod Break<br>Energy)/<br>Toughness | Flexural<br>Strength<br>(MPa) | Flexural<br>Modulus<br>(MPa) | Applications and/or<br>Reference  |
|--|---|------------------------------|-----------------------------|------------------------|--|-------------------------------|------------------------------|---|
| 3D-printed PLA<br>wastes/SiO <sub>2</sub>            | - 100/0   | - 62.80                      | - 839.60                    | - 11.10%               | - 3.60 MPa   | -                             | -                            | Recycled PLA<br>filaments<br>for 3D printing [158].   |
|  | - 95/5  | - 76.50                      | - 895.10                    | - 12.60%               | - 4.60 MPa   | -                             | -                            |   |
|  | - 90/10   | - 121.00                     | - 1020.70                   | - 15.30%               | - 5.60 MPa   | -                             | -                            |   |
|  | - 85/15   | - 53.90                      | - 793.20                    | - 11.40%               | - 3.10 MPa   | -                             | -                            |   |
| PLA/MgO  | - 100/0   | - 29.10                      | - 1891                      | - 4.40%                | -  | -                             | -                            | Food packaging<br>applications<br>that are transparent<br>and<br>require superior<br>antibacterial<br>efficiency [159]. |
|  | - 99/1  | - 34.00                      | - 2418                      | - 3.30%                | -  | -                             | -                            |   |
|  | - 98/2  | - 37.50                      | - 2470                      | - 3.90%                | -  | -                             | -                            |   |
|  | - 97/3  | - 26.60                      | - 2101                      | - 2.30%                | -  | -                             | -                            |   |
|  | - 96/4  | - 26.20                      | - 1961                      | - 2.40%                | -  | -                             | -                            |   |
| PLA/flax fibers                                      | - 100/0   | - NP <sup>1</sup>            | - 11,000                    | - 3.40%                | - (5.00) KJ/m <sup>2</sup>   | -                             | -                            | [161]   |
|  | - PLA/modified non-<br>cellulose oxidized TiO <sub>2</sub> grafted flax<br>fibers | - 172.00                     | - 9000                      | - 3.80%                | - (16.10) KJ/m <sup>2</sup>  | -                             | -                            |   |
|  | - PLA/modified<br>cellulose oxidized TiO <sub>2</sub> grafted flax<br>fibers      | - 211.00                     | - 105,000                   | - 4.50%                | - (15.70) KJ/m <sup>2</sup>  | -                             | -                            |   |
| PLA/flax fiber<br>braided yarn plain<br>woven fabric | - 100/0   | - 47.00                      | - 820                       | - 6.50%                | -  | -                             | -                            | Housing and<br>automobile interiors<br>such as seat back,<br>door trim and<br>telephone stand [164].                    |
|  | - 82/18   | - 65.00                      | - 1090                      | - 9.00%                | -  | -                             | -                            |   |
|  | - 100/74  | - 73.00                      | - 1190                      | - 9.00%                | -  | -                             | -                            |   |
|  | - 100/65  | - 80.00                      | - 1310                      | - 9.45%                | -  | -                             | -                            |   |

Table 11. Cont.

| Composite/<br>Nano-<br>Composite              | Concent-<br>Ration (wt.%)   | Tensile<br>Strength<br>(MPa) | Young's<br>Modulus<br>(MPa) | Elongation<br>at Break | Charpy Break Energy/<br>(Notched Izod Break<br>Energy)/<br>Toughness | Flexural<br>Strength<br>(MPa) | Flexural<br>Modulus<br>(MPa)       | Applications and/or<br>Reference    |
|---|---|------------------------------|-----------------------------|------------------------|--|-------------------------------|------------------------------------|-------------------------------------|
| PLA/wood flour                                | - 100/0   | - 54.90                      | -                           | - 2.50%                | - (2.30) KJ/m <sup>2</sup>   | -                             | -                                  | Blow molding<br>applications [165]. |
|   | - 100/10 phr  | - 37.40                      | -                           | - 2.60%                | - (3.00) KJ/m <sup>2</sup>   | -                             | -                                  |                                     |
|   | - 100/20 phr  | - 34.00                      | -                           | - 1.80%                | - (2.60) KJ/m <sup>2</sup>   | -                             | -                                  |                                     |
|   | - 100/30 phr  | - 27.60                      | -                           | - 1.30%                | - (2.40) KJ/m <sup>2</sup>   | -                             | -                                  |                                     |
|   | - 100/26 phr with 0.52 phr epoxy<br>silane as a coupling agent and<br>EMAGMA/13 as a compatibilizer | - 31.30                      | -                           | - 6.90%                | - (3.40) KJ/m <sup>2</sup>   | -                             | -                                  |                                     |
|   | - 100/26 phr with 0.52 phr<br>epoxy silane as a coupling agent and<br>EMAGMA/26 as a compatibilizer | - 27.40                      | -                           | - 11.70%               | - (3.80) KJ/m <sup>2</sup>   | -                             | -                                  |                                     |
|   | - 100/26 phr with 0.52 phr<br>epoxy silane as a coupling agent and<br>EMAGMA/52 as a compatibilizer | - 21.00                      | -                           | - 24.40%               | - (4.10) KJ/m <sup>2</sup>   | -                             | -                                  |                                     |
|   | - 100/0   | - 62.00                      | - 1300                      | - 12.20%               | - 30.00 J/mm   | -                             | -                                  |                                     |
|   | - 60/10 with 30% PCL  | - 37.00                      | - 890                       | - 12.45%               | - 60.00 J/mm   | -                             | -                                  |                                     |
|   | - 53.34/20 with 26.66% PCL  | - 35.00                      | - 1000                      | - 11.00%               | - 57.00 J/mm   | -                             | -                                  |                                     |
| PLA/cellulose<br>nanocrystals                 | - 46.66/30 with 23.34% PCL  | - 33.00                      | - 1085                      | - 10.80%               | - 43.00 J/mm   | -                             | -                                  |                                     |
|   | - 80/0 with 20% PBS   | - 75.6                       | - 3200                      | - 17.50%               | -  | -                             | -                                  |                                     |
|   | - 79.5/0.5 with 20% PBS   | - 74.6                       | - 3975                      | - 16.35%               | -  | -                             | -                                  |                                     |
|   | - 79.25/0.75 with 20% PBS   | - 85.1                       | - 6925                      | - 15.25%               | -  | -                             | -                                  |                                     |
|   | - 79/1 with 20% PBS   | - 92.6                       | - 755                       | - 12.90%               | -  | -                             | -                                  |                                     |
| PLA/Lignin                                    | - 78.5/1.5 with 20% PBS   | - 64.6                       | - 3275                      | - 12.45%               | -  | -                             | -                                  |                                     |
|   | - 100/0   | - 56.00                      | - 1800                      | - 4.20%                | -  | -                             | -                                  |                                     |
|   | - 80/20   | - 43.50                      | - 2300                      | - 2.90%                | -  | -                             | -                                  |                                     |
|   | - 78/20 with 2% PEG 2000 as a<br>plasticizer  | - 52.00                      | - 2150                      | - 4.00%                | -  | -                             | -                                  |                                     |
|   | - 75/20 with 5% PEG 2000  | - 44.50                      | - 1600                      | - 3.90%                | -  | -                             | -                                  |                                     |
| - 79.5/20 with 0.5% TR451 as a<br>plasticizer | - 45.50   | - 1700                       | - 3.70%                     | -                      | -  | -                             |                                    |                                     |
| - 79/20 with 1% TR451                         | - 45.00   | - 2150                       | - 3.20%                     | -                      | -  | -                             | 3D printing<br>applications [167]. |                                     |

Table 11. Cont.

| Composite/<br>Nano-<br>Composite | Concent-<br>Ration (wt.%)           | Tensile<br>Strength<br>(MPa) | Young's<br>Modulus<br>(MPa) | Elongation<br>at Break | Charpy Break Energy/<br>(Notched Izod Break<br>Energy)/<br>Toughness | Flexural<br>Strength<br>(MPa) | Flexural<br>Modulus<br>(MPa) | Applications and/or<br>Reference   |
|----------------------------------|-------------------------------------|------------------------------|-----------------------------|------------------------|--|-------------------------------|------------------------------|--|
| PLA/MCC                          | - 100/0                             | - 59.00                      | - 1556                      | - 6.00%                |  |                               |                              | Eco friendly food packaging applications [168].  |
|                                  | - 50/50                             | - 42.00                      | - 2517                      | - 2.00%                |  |                               |                              |  |
|                                  | - 95/0 with 5% TEC as a plasticizer | - 49.00                      | - 1553                      | - 10.00%               |  |                               |                              |  |
|                                  | - 47.5/47.5 with 5% TEC             | - 36.00                      | - 2495                      | - 2.00%                |  |                               |                              |  |
|                                  | - 90/0 with 10% TEC                 | - 46.00                      | - 1366                      | - 13.00%               |  |                               |                              |  |
| PLA/HNTs                         | - 45/45 with 10% TEC                | - 28.00                      | - 563                       | - 26.00%               |  |                               |                              | Bone replacements and regeneration applications [171].   |
|                                  | - 85/0 with 15% TEC                 | - 26.00                      | - 161                       | - 595.00%              |  |                               |                              |  |
|                                  | - 42.5/42.5 with 15% TEC            | - 13.00                      | - 22                        | - 300.00%              |  |                               |                              |  |
|                                  | - 100/0                             | - 17.25                      | - 246.56                    | - 7.18%                |  |                               |                              |  |
|                                  | - 50/1 with 50% PCL                 | - 11.45                      | - 184.10                    | - 12.30%               |  |                               |                              |  |
| PLA/PFs                          | - 50/3 with 50% PCL                 | - 12.87                      | - 213.53                    | - 8.53%                |  |                               |                              | Complex geometries in which the uniform distribution of mechanical performance and fibers are vital [172]. |
|                                  | - 50/5 with 50% PCL                 | - 15.52                      | - 267.65                    | - 9.37%                |  |                               |                              |  |
|                                  | - 50/7 with 50% PCL                 | - 16.62                      | - 281.19                    | - 6.78%                |  |                               |                              |  |
|                                  | - 100/0                             | - 54.00                      | - 1100                      |                        | - (139) J/m  | - 103                         | - 3500                       |  |
|                                  | - NP                                | - 62.00                      | - 1450                      |                        | - (92) J/m   | - 103                         | - 5450                       |  |
| PLA/short carbon fibers          | - 100/0 <sup>m</sup>                | - 47.80                      | - 3350                      |                        |  | 55.60                         | - 2090                       | Applications demanding dimensional stability and higher stiffness [156].                                   |
|                                  | - NP <sup>m</sup>                   | - 70.30                      | - 9210                      |                        |  | - 105.50                      | - 6940                       |  |

<sup>a</sup> phr: per hundred of rubber. <sup>b</sup> PLA/CNT-COOH nanocomposites with Ethylene-butyl acrylate-glycidyl methacrylate (E-BA-GMA) used as a compatibilizer. <sup>c</sup> Testing direction is vertical to the extrusion direction. <sup>d</sup> Testing direction is parallel to the extrusion direction. <sup>e</sup> Modified kenaf fiber. <sup>f</sup> After annealing. <sup>g</sup> Un-modified KF. <sup>h</sup> ppH: part per hundred. <sup>i</sup> PCL's molecular weight = 10,000 g/mol. <sup>j</sup> PCL's molecular weight = 40,000 g/mol. <sup>k</sup> PCL's molecular weight = 70,000–100,000 g/mol. <sup>l</sup> NP: not provided. <sup>m</sup> Tested samples were printed in the flat printing direction. Note: Studies in which no exact values for the mechanical properties were given, the best estimations were provided. Abbreviations: PLA, poly(lactic acid); MMT, montmorillonite; LLDPE, linear low-density polyethylene; CNT-COOH, carbon nanotubes with carboxyl groups; CNT, carbon nanotubes; PHBV, poly(3-hydroxybutyrate-co-3-hydroxyvalerate); KF, kenaf fiber; MWCNTs, modified multi-walled carbon nanotubes; GPS, 3-Glycidioxypropyl trimethoxy silane; PBS, poly(butylene succinate); TFC, twice functionalized organoclay; PBSA, poly(butylene succinate-co-butylene adipate); SiO<sub>2</sub>, silica; MgO, nano-magnesium oxide; TiO<sub>2</sub>, Titanium dioxide; EMAGMA, ethylene-methyl acrylate-glycidyl methacrylate; PCL, poly( $\epsilon$ -caprolactone); PEG, polyethylene glycol; TR451, Struktol; MCC, microcrystalline cellulose; TEC, Triethylcitrate; HNTs, halloysite nanotubes; PFs, pineapple fibers.

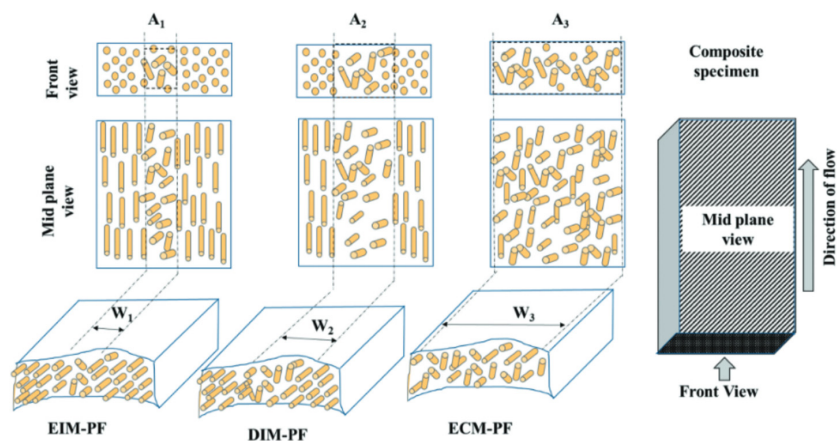


**Figure 10.** A schematic of the distribution of PFs in the various composites, note, “A” is core area. Reprinted with permission from Taylor & Francis, 2021 [172].

### 3. PHAs’ Modifications

PHB shows similar Young’s modulus and tensile strength in comparison to PP. Nonetheless, it suffers from a drastically low percentage elongation (5–10%) [174,175]. HV’s molar ratio affects the mechanical properties of PHBV [176]. Mostly, enhancements in flexibility and toughness can be noticed as a result of increasing the HV fraction, this is accompanied with a gradual decrease in the tensile strength [177]. PHBV with an HV molar ratio of 30 to 60 mol%, exhibits a high degree of softness [175]. The Young modulus of PHAs ranges from the stiffer scl-PHA ( $3.5 \times 10^3$  MPa) to the very ductile mcl-PHA (0.008 MPa) [178]. PHAs’ tensile strength ranges from 8.8 to  $10^4$  MPa [178]. Table 12 shows the mechanical properties of PHB and PHBV as well as of some other commercial polymers. The use of PHB in many applications today is hindered due to its poor mechanical properties, mostly on account of its high fragility [179–181]. PHBV exhibits better mechanical properties such as flexibility, toughness, manufacturability and impact resistance than PHB [182]. Despite some of the improvements it offers over PHB, PHBV exhibits low impact resistance, high fragility and poor thermal stability compared to petroleum-based polymers [183]. Moreover, the high production cost of PHAs with respect to synthetic plastics has hindered their wide in many applications including packaging. Therefore, blending PHAs with other synthetic plastics and nanofillers has been found to tailor PHAs’ properties and overcome such problem by introducing new materials with excellent mechanical and thermal characteristics, better barrier properties and biodegradability [184]

**Table 12.** Typical mechanical properties for PHAs along with other commercial polymers [54,176,177,185].

| Polymer <sup>a</sup> | Tensile Modulus (GPa) | Tensile Strength (MPa) | Percentage Elongation at Break (%) |
|----------------------|-----------------------|------------------------|------------------------------------|
| PHB                  | 1.7–3.5               | 40                     | 3.0–6.0                            |
| PHBV                 | 0.7–2.9               | 30–38                  | 20                                 |
| PLA                  | 1.2–2.7               | 28–50                  | 7.0–9.0                            |
| PCL                  | 0.4                   | 16.0                   | 120–800                            |
| TPS                  | 0.5–1.0 <sup>b</sup>  | 2.6                    | 47.0                               |
| PET                  | 2.2                   | 56.0                   | 70–100                             |
| LDPE                 | 0.2                   | 10–15                  | 300–500                            |
| PP                   | 1.7                   | 35–40                  | 150                                |
| PS                   | 1.6–3.1               | 12–50                  | 3.0–4.0                            |
| PVC                  | 0.3–2.4               | 10–60                  | 12–32                              |

<sup>a</sup> The values for mechanical properties will vary according to different factors such as, polymer crystallinity, molecular weight, orientation, as well as testing conditions. <sup>b</sup> At low water content (5.0–7.0 wt.%). Abbreviations: PHB, polyhydroxybutyrate; PHBV, poly(3-hydroxybutyrate-co-3-hydroxyvalerate); PLA, poly(lactic acid); PCL, poly( $\epsilon$ -caprolactone); TPS, thermoplastic starch; PET, poly(ethylene terephthalate); LDPE, low-density poly(ethylene); PP, poly(propylene); PS, poly(styrene); PVC, poly(vinyl chloride).

### 3.1. Blending's Effect

Due to their nontoxicity, biodegradability and hydrophobicity, PHAs have been widely used in many applications worldwide. Recently, and due to the raised awareness of the environmental concerns, the production of PHA has increased significantly. PHAs are proven to be a good competitor for food packaging applications. Nonetheless, the high production cost of PHAs is the main obstacle for expanding their productions to the commercial scale. Blending PHAs with other polymers has been reported to be a good option to increase their flexibility.

Moreover, PHAs based blends exhibit good degradation rate. In one study [186], the degradation of PHB, PCL and PCL/PHB 70/30 wt.% blend was investigated. Results showed that both neat PCL and PHB samples were degraded with strong erosion of the amorphous zones. After 20 days of incubation, the PCL/PHB 70/30 blend showed that spheres of PCL were bordering with spherulites of PHB demonstrating complete degradation. At various degradation times, the crystallinity content of homopolymers and blend were analyzed. Whereas there was no change in the PCL's crystallinity, the crystallinities of PHB and the blend's PHB-phase have increased [186]. Using solution blending, high molecular weight PHB/PCL and PHB/low-molecular-weight chemically modified PCLs (mPCL) were prepared [187]. The crystallization, morphology as well as the enzymatic degradation of the blends after exposing them to *Aspergillus flavus* were studied. Throughout the entire composition range, high-molecular-weight PHB/PCL blends were found to be immiscible. Results showed a drop in the PHB nucleation density and a fractionated PCL crystallization. PHB/mPCL blends were partially miscible; two phases were formed, but the PHB-rich phase demonstrated clear signs of miscibility. Biodegradation results showed that the blends were degraded more than the homopolymers. The study claimed that the dispersion of the components and their crystallinity can affect the improved degradation rate of the blends. The PHB/mPCL blends exhibited a drop in the degradation rate due to the increased miscibility between the components [187]. Due to their good mechanical and thermal properties, PP and PE have been commonly used in the packaging industries. Nonetheless, they are resistant to microbial degradation. To overcome this limitation, PP and PE have been blended with PHAs. For instance, in one study [188], the biodegradability of various films made out of PE, PHBV as well as PE/PHBV blends was evaluated using a respirometry test after 180 days. Results suggested that the degradation rate was proportional to the quantity of PHBV in contact with PE [188]. In another study [189], melt blending was used to investigate the application of the PHBV copolymer as a biodegradable additive in PP. The study reported a successful production of PHBV/PP blends. The degradation rate of the produced blend was studied in the field as well as in controlled laboratory conditions. Results of the SEM showed biofilm formation due to microbial activity on the surface of the treated films. The degradation of PHBV/PP blends was found to be due to an oxo-biodegradation process. Microorganisms' attachment to PHBV/PP film turns it into material with a higher degree of crystallinity as a result of polymeric chain scission caused by the oxidation process [189].

Blending PHAs with other polymers such as PP [189,190], PE [188,191], poly(ethylene terephthalate-co-1,4-cyclohexanedimethanol terephthalate) (PETG) [192], poly(butylene succinate) (PBS) [144,193] and PLA [43,87,88,101,104–107,194] have been reported to enhance the mechanical properties of PHAs.

Binary blends of PHB and PCL were produced by Garcia et al. [195]. Thermal and mechanical properties of the blends were studied. Moreover, the miscibility and blends morphology were investigated in terms of the blend composition. Binary PHB–PCL blends were developed using melt compounding in a twin screw co-rotating extruder and injection molded. Results claimed that PCL acted as an impact modifier. Therefore, increasing PCL content led to an increase in the blend's flexibility and ductility. Moreover, there was a significant increase in the percentage elongation at break and the energy absorption in impact conditions. Furthermore, when 25 wt.% of PCL was blended with PHB, the resulted blend showed the peak value for the flexural strength and flexural modulus. A drastic drop



in these values was reported when further PCL was added. On the other hand, increasing the content of PCL led to a drop in both the tensile strength and Young's modulus. The study has also reported a clear evidence of the immiscibility of the blend. The same was also reported in another study [196]. Furthermore, an increase in crystallinity of both PHB and PCL was reported for PHB/PCL blends containing 25 wt.% PCL. The study has also reported an increase in the degradation onset of about 30 °C [195].

For the purpose of widening the application of multi-scale instrumental analyses to include biodegradable polymers, plasticized PHA containing 65% PHA, 30% PBS and 5% crosslinking agent were investigated with respect to blending with PCL. The same was also studied after the incorporation of compatibilizers, such as crosslinkers and graft polymers [197]. Results showed that when PHA was blended with more than 30% PCL, there was an increase in the percentage elongation at break as well as the tensile strength in the quasi-static tensile test. On the other hand, impact tensile properties were less enhanced by the addition of PCL. This might be attributed to the molecular mobility suppression as a result of blending. Graft polymers led to a minor decrease in the percentage elongation at break in the quasi-static tensile test while a significant drop was observed in case of crosslinkers. However, with respect to the impact tensile test, both of the graft polymers and crosslinkers led to an increase in the percentage elongation at break and tensile strength [197].

Recently in another study [198], natural medium chain length PHAs (poly(3-hydroxyoctanoate-co-3-hydroxydecanoate (P(3HO-3HD))) was blended with PCL at two concentrations, namely, 75/25 wt.% and 95/5 wt.%. The blends were intended to combine the outstanding ability of PHAs to support the growth and proliferation of mammalian cells with PCL's good processability. The blends were intended to be transformed into a new biomimetic Nerve Guidance Conduit (NGC). The fabricated blends demonstrated superb neuroregenerative properties and a good bio resorption rate. The blends are to be used in the manufacturing of hollow NGCs to support nerve regeneration in 10 mm sciatic nerve gap in rats. Compatibility of the blend with large-scale manufacturing of NGCs was illustrated via the production of porous tubular devices with two wall thickness values. Results showed that the devices exhibited a good porosity/permeability relationship, and therefore permitting excellent nerve regeneration ability whilst maintaining low biodegradation rate and enough stiffness to protect the nerve throughout the whole regenerative process. Results showed that when the content of PCL exceeded 30 wt.%, PCL started to dominate the blends' mechanical properties yielding to substantially stiffer materials than neat P(3HO-3HD) [198].

PBS is a linear, aliphatic, crystalline polyester with excellent mechanical properties and biodegradability. Due to their weak interfacial adhesion, poor compatibility as well as their large particle size, Qiu et al. [199] reported difficulties in fabricating PHB/PBS blends. Yet, in another investigation, Qiu et al. [200] were able to use the solvent casting method to fabricate PHBV and PBS blends (80/20 wt.% and 20/80 wt.%). A drop in the PHBV's crystallization rate was observed as the content of PBS increased. The immiscibility of PHBV with PBS was demonstrated through the lack of change in the glass transition temperature as well as the biphasic melt of the blend [200]. In order to overcome the problem of immiscibility, Ma et al. [193] fabricated PHB/PBS and PHBV/PBS blends using pure PHB, PHBV. *Situ* compatibilization method with DCP which is a free-radical grafting initiator was used. Results showed a significant enhancement in the elongation at break of the PHBV/PBS blends due to the better interfacial adhesion between the PHBV and PBS phases. Furthermore, the deformation, dilatation, as well as the fibrillation of the PBS particles in the polymeric matrix of PHBV led to an improvement in the tensile strength [193].

A ternary blend of entirely biodegradable polymers, namely PLA, PHBV and PBS was fabricated by Zhang et al. [144] via melt compounding. Various blends of PLA/PHBV/PB (60/30/10 wt.% and 60/10/30 wt.%) as well as PHBV/PLA/PBS (60/30/10 wt.% and 60/10/30 wt.%) were produced and examined. The blends' mechanical properties, thermal

properties, thermal resistance, morphology as well as miscibility were studied. Results of the Dynamic Mechanical Analysis (DMA) suggested PHBV and PLA exhibited some limited miscibility with each other, yet PBS was found to be immiscible with PHBV or PLA. A minor phase-separated structure was reported from SEM for all the blends composition except for that of the PHBV/PLA/PBS (60/30/10 wt.%) blend. The same blend was also found to demonstrate a typical core-shell morphology with outstanding stiffness–toughness balance. An enhancement in the PLA’s crystallization, flexibility and toughness was observed in the resulting ternary complex [144].

Using castor oil cake (CC) as a filler, Burlein and Rocha [191], were able to fabricate PHB/LDPE blends by melt mixing. There was a substantial improvement in the LDPE’s modulus of elasticity accompanied by a decrease in the impact resistance and other tensile properties with the incorporation of PHB or CC. This can be explained by the unsatisfactory dispersion of the CC in the LDPE as well as the weak interfacial adhesion between the components of the mixture [191].

Because of its outstanding water and moisture barrier properties, PETG has been widely used in the packaging applications. For the aim of enhancing PHBV’s processability, a twin-screw extruder was used to mix PHB and PETG [192]. When compared to neat PHB, the extruded and injection molded blends were found to exhibit a substantial enhancement in the flexural modulus. This can be attributed to the good dispersion of PETG in the PHB. Blends containing 20 wt.% and 30 wt.% of PETG were found to exhibit an impact resistance that is comparable to the value of that of PHB. Overall, the incorporation of PETG to PHB was proven efficient in enhancing the processability and modulus of elasticity without significant changes in the impact resistance. The biodegradability of PHB was also intact [192].

In another study [201], a newly developed poly(3-hydroxybutyrate-*co*-3-hydroxyvalerate-*co*-3-hydroxy-hexanoate) (P(3HB-*co*-3HV-*co*-3HHx)) fabricated by mixed microbial culture using biomass derived from fruit pulp was mixed with commercial PHBV at concentrations from 10 wt.% to 50 wt.%. Neat PHAs in addition to the produced PHBV/P(3HB-*co*-3HV-*co*-3HHx) blends were subsequently thermo compressed to yield films that were characterized based of their optical characteristics, morphology, mechanical, barrier and thermal properties. This was followed by a detailed analysis to assess their potential in food packaging applications. Results showed good optical properties and interpolymer miscibility. There was no significant impact on the thermal stability of the blend. Moreover, permeability to limonene vapor, water and oxygen gas was reduced in the blends. Furthermore, the blend exhibited more flexibility than the neat rigid PHBV due to the plasticizing effects introduced by the terpolymer. The Young’s modulus and tensile strength of the terpolymer were lower than those of PHBV. This might be attributed to the interference with the crystallization process, the higher the 3HHx fraction in the P(3HB-*co*-3HV-*co*-3HHx), the higher the increase in flexibility. Results have also showed an increase in the percentage elongation at break with increasing the terpolymer content. Therefore, the mechanical response changed from a rigid but fragile to a more ductile behavior after blending PHBV with P(3HB-*co*-3HV-*co*-3HHx) [201].

### 3.2. Composites’/Nanocomposites’ Effect

Nanocomposites are hybrid material containing polymer matrix reinforced with particle, fiber and clay, with at least one component in nanometer scale. Nano clays or nanofillers are usually added to alter the mechanical, thermal and barrier properties of the resulting materials. Furthermore, they are also incorporated to modify the crystallization behavior, rate of degradation as well as the morphology. PHA-based nanocomposites have been fabricated using Cloisite 25A [202], carbon nanotubes (CNTs) [203,204], organ modified montmorillonite (OMMT) [205–207], multi Na-montmorillonite Cloisite Na (Na-MMT), a methyl tallow bis-hydroxyethyl quaternary ammonium-modified MMT Cloisite 30B [208–210], cellulose nanowhiskers (CNWs) [211–213], SiO<sub>2</sub> nanofibers [214], carbon nanofibers (CFs) [215], halloysite nanotube (HNT) [209] and CNCs [103,105–107,216].

Carbon nanotubes can be defined as cylindrical nanostructures in which graphene layers are arranged as stacked cones, cups, or plates. They consist of concentric cylinders of graphite layers [215]. Due to their effectiveness in enhancing the hardness, electrical conductivity as well as the thermal stability of polymer-based composites, CNTs have been incorporated into various PHAs based nanocomposites.

Solution processing was used to develop PHBV/Multiwalled Carbon Nanotubes (MWNTs) nanocomposites by Lai et al. [204]. Results from the investigation suggested that there was an improvement in the nanocomposite's thermal stability due to the homogeneous dispersal of MWNTs inside the PHBV matrix [204].

In another study [203], the crystallization behavior of PHBV after the addition of MWNTs was investigated by Shan et al. The incorporation of the multiwalled carbon nanotubes was found to substantially increase PHBV's crystallinity and crystallite sizes [203].

In their examination, Liao and Wu [217] used melt blending to develop PHB/MWNTs nanocomposite. In order to enhance the compatibility as well as the dispersion of the MWNTs within the PHB matrix, the authors used acrylic acid grafted poly(3-hydroxybutyrate) (PHB-g-AA) and multihydroxyl functionalized MWNTs (MWNTs-OH) as alternatives. The PHB-g-AA/MWNTs-OH blend exhibited a significant improvement in the mechanical and thermal properties of the PHB. It is believed that such an improvement is as a result of the formation of ester carbonyl groups through the reaction between carboxylic acid groups of PHB-g-AA and hydroxyl groups of MWNTs-OH. Due to the incorporation of 1 wt.% MWNTs-OH, there was an increase of 15.1 MPa and 75 °C in both, the tensile strength and the initial decomposition temperature, respectively. The study concluded that a 1 wt.% MWNTs-OH was the optimal amount. A further addition of MWNTs-OH led to separation of the organic and inorganic phases and a reduction in the compatibility of PHB-g-AA and MWNTs-OH [217].

Using solvent casting, Sanchez-Garcia et al. [215] were able to successfully develop PHBV/carbon nanofibers nanocomposites. The study showed that a substantial increase in the thermal, mechanical as well as the barrier properties was obtained due to the addition of the carbon nanofibers. Moreover, an increase in the conductivity of the resulted nanocomposite was also reported [215].

In another investigation [218], carbon nanofibers were chemically modified by *n*-octanol, silane coupling agent (KH-550) as well as nitric acid (HNO<sub>3</sub>) and then then added to poly-3-hydroxybutyrate-co-4-hydroxybutyrate (P3HB-co-4HB). The study reported a significant increase in the crystallinity and the glass transition temperature of the developed nanocomposites due to the addition of small diameters and uniform thickness carbon nanofibers treated with HNO<sub>3</sub> [218].

In a similar work, Gumel et al. [219] reported a substantial increase in the lattice strain (17%), crystallite size (66%) and micromolecular elastic strain (46%) after the incorporation of carbon nanofibers (10% *w/w*) to mcl-PHAs [219].

In another investigation [220], melt blending was used to prepare nanocomposites containing a PHA biopolyester and graphene nanoplatelets (GNPs) or hybrid nanocomposites consisting of a PHA biopolyester, GNPs and carbon nanofibers. Results showed that the fabricated nanocomposites demonstrated good mechanical properties and improved thermal stability. The electrical conductivity has also increased significantly with the best performance obtained at 15 wt.% of the hybrid filler, which was around six times higher than that of the of the pure GNP nanocomposites at the same loading. Hybrid nanocomposites' electromagnetic interference shielding performance was reported to be around 50% better than that of the pure GNP reinforced nanocomposites. Both types of nanocomposites exhibited a significant increase in the thermal conductivity, yet the hybrid nanocomposites reported better performance. Young's modulus and tensile strength were also higher for the hybrid nanocomposites. As a result, the reported nanocomposites can be considered as promising candidates to substitute petroleum-based polymers in thermal and electrical applications [220].

The effect of molecular weight,  $H_x$  content of the PHBH $_x$  as well as the type of SiO $_2$  particles on the poly(3-hydroxybutyrate-*co*-3-hydroxyhexanoate) (PHBH $_x$ )/SiO $_2$ -based nanocomposites' mechanical properties was investigated by Xie et al. [214]. Two different molecular weight (903,000 g/mol and 633,000 g/mol) and  $H_x$  content (6.9 and 7.2 mol%) were used in this study. Furthermore, two types (nominally spheres and fibers) of SiO $_2$  were also examined. There was a 34% and 30% increase in both, the toughness and the modulus of elasticity of the developed nanocomposites due to the incorporation of 1 wt.% SiO $_2$  fibers to the high molecular weight PHBH $_x$  (7.2 mol%  $H_x$ ). On the other hand, the developed nanocomposites reported a slight improvement in thermal stability. In case of nominally spheres SiO $_2$ , the same increase of modulus of elasticity was reported for the high molecular weight PHBH $_x$ , nonetheless, the increase in toughness was limited to only 11%. When more SiO $_2$  fibers (3 wt.%) were incorporated into the PHBH $_x$  matrix, the elongation at break as well as the toughness decreased, yet the modulus of elasticity increased. The authors concluded that in order to enhance the stiffness and the toughness of the PHBH $_x$  nanocomposites, a high molecular weight of the polymer matrix, a good dispersal of the SiO $_2$  nanofillers and a weak interfacial adhesion are essential [214].

Starch has been also added to PHAs for the purpose of reducing their cost. Although other inexpensive fillers such as ground minerals can be used, yet the advantage of starch is that it is already in a fine powder form and it is completely biodegradable. Furthermore, starch can work as a reinforcing filler and therefore can improve the strength and modulus of the nanocomposite. Another advantage of starch is that it can impact the overall degradation rate of PHA/starch blends because starch biodegrades in a very short time [221–225].

Both the mechanical properties and the biodegradation rate of starch-PHBV composites were studied by Ramsay et al. [225]. As the starch content increased, percentage elongation at break and tensile strength exhibited a significant drop. This might be attributed to the weak adhesion between phases. SEM investigation showed a separation of starch granules from the PHA matrix. Yet and due to the rigidity of the starch granules, Young's modulus of the PHA/starch blend demonstrated an increase with increasing the content of the starch [225]. Other studies in literature have also reported similar results [221–224].

For the purpose of improving the adhesion between starch and PHAs, two main methods were used [226]. Firstly, the incorporation of coupling agent. For example, in one study [222], a substantial increase in both of the strength and percentage elongation at break were reported for coated starch with polyethylene oxide (PEO)/PHBV composites. Yet, the values for these mechanical properties were less than that of neat PHBV. The study concluded that PEO can serve as a binding agent because it has a favorable interaction with both starch and PHBV [222]. The second method consists of modifying the starch and/or PHA chemically. For instance, in one investigation [226], a free-radical former (2% bis[tert-butylperoxyisopropyl] benzene) was added to PHBV/starch 80/20 wt.% and 70/20 wt.%. The study reported that due to this addition there was an increase in the impact resistance from 1.8 kJ/m $^2$  for neat PHBV to 2.10 kJ/m $^2$  for PHBV/starch 70/20 wt.%. It is believed that some starch-PHBV graft copolymer was produced via free radical combination reactions and worked as an interfacial binding agent [226].

Another study [227] reported enhanced percentage elongation at break and tensile strength for blends of PHB/starch copolymerized with diisocyanate and propylene glycol. Nonetheless, the values were less than those of neat PHB [227].

Compared to untreated starch/PHBV composite, composites of starch-g-poly (glycidyl methacrylate) (>7% PGMA) and PHBV exhibited substantially higher tensile and flexural strengths [228]. However, there was no significant increase in both of the Young's modulus and percentage elongation at break. All samples were immersed in water for 28 days. The gains in weight for PHBV–starch bars with 25% starch were about 4–5% compared with 0.9% for PHBV alone and 40–50% for starch. After soaking, percentage elongation at break increased, Young's modulus decreased and the tensile strength remained unaffected [228].

Liao and Wu [229] claimed that the tensile strength for composites of starch (50%) with acrylic acid-grafted PHB exhibited 7 MPa increase when compared to the tensile strength value of the unmodified starch/PHB [229].

Blends of starch acetates with PHBV [230,231] were found to be brittle and incompatible. On the other hand, for starch valerate contents lower than 20%, blends of starch valerate and PHBV were believed to be compatible [232].

For the aim of reducing the cost and enhancing the properties of PHB, Godbole et al. [233] investigated PHB's compatibility with starch. All the blends were reported as crystalline. For the blend of PHB/starch, 30/70 wt.%, a substantial improvement in the tensile strength was found in comparison to neat PHB. Due to the low cost of starch, the study claimed that blending PHB with a maximum content of 30 wt.% starch can significantly reduce the cost of PHB while maintaining its physical properties. The study concluded that the developed blend can be used in the food packaging applications such as a coating material on paper or cardboard [233].

In another study [234], casting was used to blend polyhydroxybutyrate-hydroxyvalerate (PHB-HV) with maize starch at various starch contents. Results showed that the tensile strength, modulus of elasticity and percentage elongation at break decreased with increasing the starch content. Results has also suggested that PHB-HV and starch are immiscible [234].

PHB was blended with two types of maize starch, Starch 1 (containing 70% amylose) and Starch 2 (containing 72% amylopectin) [235]. The blends, PHB/starch (70/30 wt.%) were produced via melt compounding. Results of the study showed that starch granules acted as a filler as well as a nucleating agent leading to a very substantial drop in the size of the PHB spherulites. Substantial enhancement in mechanical, rheological and thermal properties were reported. The study showed that the improvements were greater for PHB/starch1 than those of PHB/starch2. This might be due to the improved hydrogen bonding between PHB and Starch 1 with high-amylose content [235].

PHAs and thermoplastic starch were used to come up with novel flexible materials [236]. The starch was initially plasticized with high glycerol content followed by blending with PHBV and PBAT. The investigators claimed that the starch phase was miscible with PHBV and PBAT phases independently. Although the produced material had 70% biobased content, it exhibited excellent mechanical properties that are ideal for flexible packaging [236].

Using coextrusion, glycerol-plasticized starch films laminated with PHBV were developed by Martin et al. [237]. The results showed a gradual decrease of the peel strength as the content of glycerol in the plasticized starch increased. The study has also concluded that thermoplastic starch foams and films laminated with a thin layer of PHA seem to be appropriate for applications involving short-term contact with water. This is was due to the lack of major swelling of the thermoplastic starch films extrusion laminated with polyesters after soaking in water for a few days [237].

Creating a rough interface during the coextrusion process was found to be effective in improving the peel strengths of polyesters on thermoplastic starch. PHBV's adhesion to thermoplastic starch using only water as a plasticizer was greater than when glycerol was incorporated [238].

The use of thermoplastic starch/PHA laminates and foams has been also reported in literature [239]. In such structures, PHA makes up a small component, between 5–20% or less, while the majority of the structure consists of thermoplastic starch. The PHA works as a water-resistant outer coating. Simultaneously, the PHA supports the foam expansion process. Studies on coating starch-based foams and films with PHBV have been also reported [239].

In one investigation [240], foams of extruded starch/PHBV with 5–20% PHBV were developed and their properties were reported. Results suggested that the addition of PHBV has significantly improved the expansion of the foam. The majority of PHBV existed as separate elongated inclusions with a length of approximately 1–5 mm within the starch

matrix. On the other hand, PHBV was found to enrich the surfaces of the foam. This might be attributed to the lower surface energy of PHBV compared to starch. Therefore, the starch/PHBV foams exhibited significantly greater water resistance than starch foams and friability was reduced [240].

Many studies in literature have reported the biodegradation of starch-PHA blends in various environments [224–226,241–250]. A summary of a selected number of these studies is shown in Table 13. In these studies, the biodegradation of PHA was investigated in different environments such as compost, soil, activated sludge under anaerobic and aerobic conditions as well as marine environments. In all of these environments, blends of starch-PHA were found to be biodegradable over a period of weeks to months. Factors such as moisture content, crystallinity and molecular weight of polymers, temperature, presence of starch/PHA degraders, presence of plasticizer, sample thickness and microbial activity were found to affect the biodegradation rate. The biodegradation rates of PHA/starch blends were found to be higher in activated sludge and compost. This might be due to the high temperature as well as the availability of high numbers of PHA depolymerase-producing microorganisms.

**Table 13.** A summary of selected studies for the biodegradation of PHBVs-based/starch composites.

| Percentage of Starch | Biodegradation Environment | Thickness (cm)  | Days | Percentage of Weight Loss | Reference |
|----------------------|----------------------------|-----------------|------|---------------------------|-----------|
| 30%                  | Compost                    | NP <sup>a</sup> | 20   | 100%                      | [226]     |
| 30%                  |                            | 0.05            |      | 100%                      | [245]     |
| 0%                   |                            | 0.05            |      | 60%                       |           |
| 50%                  | Marine                     | 0.05            | 150  | 90–100%                   | [250]     |
| 30%                  |                            |                 |      | 50–90%                    |           |
| 0%                   |                            |                 |      | 10–20%                    |           |
| 50%                  | Soil                       | 0.32            | 125  | 49%                       | [249]     |
| 30%                  |                            |                 |      | 25%                       |           |
| 0%                   |                            |                 |      | 7%                        |           |
| 50%                  | Activated sludge           | 0.08            | 30   | 100%                      | [225]     |
| 25%                  |                            |                 |      | 85%                       |           |
| 0%                   |                            |                 |      | 30%                       |           |

<sup>a</sup> Not provided.

In one study, when compared to PHA degraders, the starch-degrading microorganisms were about 10 times more abundant. Therefore, the starch portion of the PHBV/starch composite degraded far before the PHBV did [250].

In most of the investigations in literature, the rate of biodegradation of PHA-based/starch composites increased with increasing the content of starch. This might be attributed to the creation of more surface area for microbial attack after the removal of the more rapidly degraded starch. Exposing starch/PHBV and PHBV to aqueous environments has led to slow but significant rates of hydrolysis. For long-term applications such as consumer durables, this might be a key factor for PHA blends [244,247]. Despite the fact that biodegradation of starch-PHBV blends is a good option, recycling of the blends back into monomeric hydroxyacids is considered today as a more attractive choice [251,252]. This can be easily done through enzymatic depolymerization. New PHAs can then be biosynthesized from the hydroxyacids and glucose from depolymerized starch. Hence, this might be a tempting option than mineralization back to water and carbon dioxide, especially when the prices of agricultural products continue to increase. Moreover, recycling of PHAs is considered much easier than that of petroleum-based polymers such as polyethylene. This bodes well for the future of PHAs-based/starch composites.

Patel and Narayan [253] have successfully reviewed the sustainability of PHAs and starch blends. The study found that the carbon dioxide emission and energy use resulted from the PHAs' production is almost the same or higher than those associated with petrochemical polymers. As/if the PHAs production becomes efficient, this is expected to change. The study has also highlighted that the carbon dioxide emissions as well as the energy use are substantially lower for starch, thermoplastic starch as well as starch blends than those of polystyrene or polyethylene [253].

Various studies discussing the modification of PHBV's mechanical properties by the addition of nano clays have been reported. PHB and PHBV based nanocomposites were fabricated by adding Montmorillonites (MMTs) and Layered Double Hydroxides (LDHs) by solution casting [202,254–258] or by melt intercalation [184,205,208,259–261] to enhance PHAs' mechanical properties.

Lim et al. was the first to fabricate PHB/MMT nanocomposites through solution casting [202]. In 2003, Maiti and Parkash [262] reported what is believed to be the first fabrication of PHB/Organo-Modified Montmorillonite (OMMT) nanocomposites. A higher storage modulus, that is around 40% higher than that of neat PHB was reported by the developed nanocomposite. Moreover, it has demonstrated an intercalated morphology while maintaining the biodegradability of PHB [262].

Melt extrusion was used by Maiti et al. [205] to prepare PHB-based nanocomposites reinforced using 2 wt.% organo-modified fluoromica or up to 3.6 wt.% MMT. Results showed that the nanocomposites' storage modulus increased and better reinforcing was achieved in case of fluoromica than with MMT. This was proven by the higher amount of polymer degradation in the presence of MMT [205].

The influence of the incorporation of two nanoparticles, namely organomodified montmorillonite Cloisite<sup>®</sup> 30B and a tubular like clay, halloysite (HNT), on the PHBV nanocomposites' morphology, thermal as well as mechanical properties was evaluated by Carli et al. [209]. PHBV/Cloisite<sup>®</sup> 30B demonstrated a structure that is partially exfoliated along with a few tactoids. On the other hand, a substantial enhancement in the modulus of elasticity and higher melting temperature were exhibited by the PHBV/HNT nanocomposites. Nonetheless, both of the impact strength and percentage elongation at break were reduced [209].

In another study [194], the incorporation of nanoclay Cloisite<sup>®</sup> 30B resulted in no major effect on the PLA/PHBV/clay nanocomposites' tensile strength and percentage elongation; however, the tensile modulus increased [194].

Parulekar et al. [259] used modified MMT with neopentyl(diallyl)oxytri (dioctyl)pyrophosphato titanate to come up with PHB nanocomposites. Epoxidised natural rubber was used as an impact modifier and nanocomposites were prepared by extrusion followed by injection molding. Results showed that nanocomposites containing 5 wt% titanate-modified clay showed an improvement of around 400% in impact properties and a reduction of 40% in storage modulus when compared with unreinforced PHB [259].

The effectiveness of two commercial MMTs namely NA-MMT (Cloisite<sup>®</sup> Na+) and the organo-montmorillonite, methyl tallow bis-hydroxyethyl quaternary ammonium-modified MMT (Cloisite<sup>®</sup> 30B-M) as reinforcements to PHB matrix was investigated by Botana et al. [208]. The study showed that Young's modulus of the nanocomposites increased. Nonetheless, there was no significant increase in the tensile strength as the exfoliation/intercalation ratio was not high enough. According to Pavlidou and Paspapyrides [263], the exfoliation/intercalation ratio is the main factor that determine the enhancement in nanocomposites' mechanical properties. Intercalation can ensure that the Young's modulus has increased; however, it is generally the exfoliation/intercalation ratio which determines the effect of the nano-additive on the tensile strength [263]. Cloisite<sup>®</sup> 30B showed better particle exfoliation/intercalation, indicating better compatibility with the PHB matrix in that case [208].

Melt intercalation was used to prepare PHBV/Cloisite<sup>®</sup> 30B nanocomposites [264]. Both X-Ray Powder Diffraction (XRD) and Transmission Electron Microscopy (TEM) anal-

yses confirmed that the intercalated nanostructures were obtained. Clay addition (up to 3 wt.%) has successfully altered the mechanical properties. For instance, the modulus of elasticity increased significantly from 481 to 795 MPa as a result of the strong hydrogen bonding between PHBV and Cloisite<sup>®</sup> 30B. On the other hand, tensile strength barely increased and there was a drop in the elongation at break from 8.5 to 5.6% [264].

In another investigation conducted by Chen and his colleagues [207], solution intercalation with 3 wt% filler content was used to come up with PHBV/OMMT nanocomposites. Results showed that there was a significant drop in tensile properties when higher filler loading (10 wt.%) was used due to clay aggregation. On the other hand, the addition of small quantities of OMMT was found to accelerate the overall rate of PHBV's crystallization in a pronounced way [207].

Zhang et al. [265] prepared poly(3-hydroxybutyrate-co-3-hydroxyhexanoate) or PHB-co-PHH (Nodax<sup>®</sup>TM) with up to 15% Cloisite<sup>®</sup> 20A and Cloisite<sup>®</sup> 25A. Results of the study showed that there was an increase in the elastic modulus, nonetheless, at higher clay loadings, Young's modulus and tensile strength did not improve [265].

In a study conducted by Bruzard and Bourmaud [254], Cloisite<sup>®</sup> 15A was successfully used to come up with PHBV/organoclay nanocomposites using solution intercalation. Cloisite<sup>®</sup> 15A content of 1, 2.5 and 5 (wt.%) was used in this investigation. Results showed an increase in the Young's modulus, tensile stress and hardness with the increase of clay loading. This is attributed to the addition of stiff clay nanofillers into the PHBV matrix. Young's modulus, tensile stress and hardness increased from 633 MPa, 5.9 MPa and 46 MPa for neat PHBV to 1677 MPa, 28.9 MPa and 88 MPa for the nanocomposite containing 5 wt.% Cloisite content, respectively. Furthermore, with the addition of only 2.5 wt.% clay loading, the Young's modulus and hardness were enhanced by 66.9% and 67.4% respectively as compared with the neat PHBV. On the other hand, the elongation at break decreased from 3.3 to 1.4% with increasing clay loading. This indicates that the addition of clay led to an alteration of the plastic deformation of the matrix. All the nanocomposites exhibited greater thermal stability than neat PHBV [254].

The use of LDHs as a reinforcement to prepare PHA-based nanocomposites has been reported by various studies in literature [255,266,267]. The effect of these fillers on the mechanical properties of PHA has been reported by Dagnon et al. [267]. The study showed that the addition of stearic acid-modified Zn-AlNO<sub>3</sub> LDH in PHBV (1–7 wt.%) resulted in more than a 10% improvement in the Young's modulus; however, that was accompanied with a decrease in the elongation at break. Moreover, when up to 3 wt.% LDH was added, the strength increased, yet the strength decreased when further nanofiller was added, probably due aggregation [267].

Hsu et al. [255] were able to prepare PHB/Modified Layered Double Hydroxide (PMLDH) nanocomposites with 2 wt.% and 5 wt.%. Results showed that both the PMLDH content as well as the cooling rates affect the behavior of PHB and PHB/PMLDH composites. With the addition of 2 wt.% of PMLDH, the crystallization rate of the composite increased and the activation energy decreased. On the other hand, the crystallinity of PHB decreased and its activation energy increased when more PMLDH was added to the PHB. This is because the addition of more PMLDH limited the transport ability of the polymer chains [255].

Whilst there are several studies about the addition of inorganic nanofillers to reinforce the PHA matrix, there have been few reports about the use of organic nanofillers such as nanocellulose in PHAs.

Hydrolyzed tunicin cellulose whiskers were used to reinforce medium chain length PHAs [268]. Results showed a significant enhancement in the mechanical properties due to the formation of a transcrystalline network between the whiskers and the semi-crystalline matrix [268].

Using both, solution casting with N, N-dimethylformamide (DMF) as well as extrusion blending and injection molding of PHBV with freeze-dried nano whiskers, Jiang et al. [213] were able to prepare cellulose nano whisker/PHBV nanocomposites. The study reported



that a homogeneous dispersion of the whiskers was attained and the cellulose nano whisker/PHBV nanocomposites exhibited enhanced tensile strength and Young's modulus in case of solvent cast composites. However, the tensile strength reduced during freeze drying due to the agglomeration of whiskers [213].

A number of studies have reported the dynamic mechanical analysis of PHB and PHBV [269–271]. The main objective of such studies was to characterize viscoelastic properties as a function of temperature. It has been generally observed that the storage modulus for PHAs decreases with temperature. It has been also reported that PHB has a storage modulus in the range of 2500–3500 MPa at 20 °C while it is somewhat higher for PHBV [205,270,271]. Various studies in literature have reported the increase of both the storage modulus and the glass transition temperature due to the addition of nanofillers [205,213,269]. The reinforcement influence of nano clay additives reported to be become more prominent above the glass transition temperature, when the materials become soft. This is attributed to the polymer chains' restricted movement [272].

Recently, melt extrusion was used to incorporate different amounts of Coffee Silverskin (CS), an agricultural residue, into a PHBV matrix plasticized by ATBC [273]. In order to examine the feasibility of the produced PHBV/CS-based bio composites to fabricate molded products, morphological, mechanical and thermal properties were examined. Results showed that as the content of CS increased, stiffness, heat deflection temperature and crystallinity all improved. Using injection molding, coffee capsules have been fabricated using the optimized formulation. At a temperature of 100 °C, the overall migration was below the limit (10 mg/dm<sup>2</sup>) required for plastic materials at food contact. The study concluded that CS can be efficiently used to prepare PHBV/CS based bio composites [273].

In another investigation [274], wood flour/PHA composites without additives were prepared using Fused Deposit Molding (FDM) 3D printing system based on micro screw extrusion. The study reported increased melting and crystallization temperatures of the composites. 3D-printed composites were free from warpage. This was attributed to the forming process under pressure and the wood flour/PHA blend. Flexural and tensile strengths of the composites were around 77.30 MPa and 38.70 MPa, respectively. Young's modulus of the blend increased substantially with increasing the wood flour content. The study concluded that FDM has a great potential in the fabrication of 3D-printed bio-based composites [274].

Wu et al. [275] reported a biodegradable composite nanofiber consisting of PHA or modified PHA (MPHA) and treated fish scale powder (TFSP). Using grinding, the powder was prepared after the treatment of FSP with water, acid and heat (450 °C) to produce TFSP. After that, electrospinning (biaxial feed method) was used to produce composite nanofibers of TFSP/PHA and TFSP/MPHA. Figure 11 shows the preparation of the electrospinning solution as well as the fabrication process for the composite nanofibers. Results showed that the serum calcium to phosphorus ratio (Ca/P) of the TFSP was similar to that of the human bone. Moreover, MPHA/TFSP nanofibers exhibited more uniformity and were more strongly bonded in the matrix in comparison to PHA/TFSP composite. Increasing the content of TFSP led to improvement in the tensile strength at failure of the MPHA/TFSP composites. Percentage elongation at break decreased as the content of TFSP increased. The water contact angle reduced with increasing TFSP content in MPHA/TFSP and PHA/TFSP nanofiber membranes. The study reported that TFSP improved the hydrophilic effect of the PHA/TFSP and MPHA/TFSP nanofiber membranes providing a more suitable environment for cell growth [275].

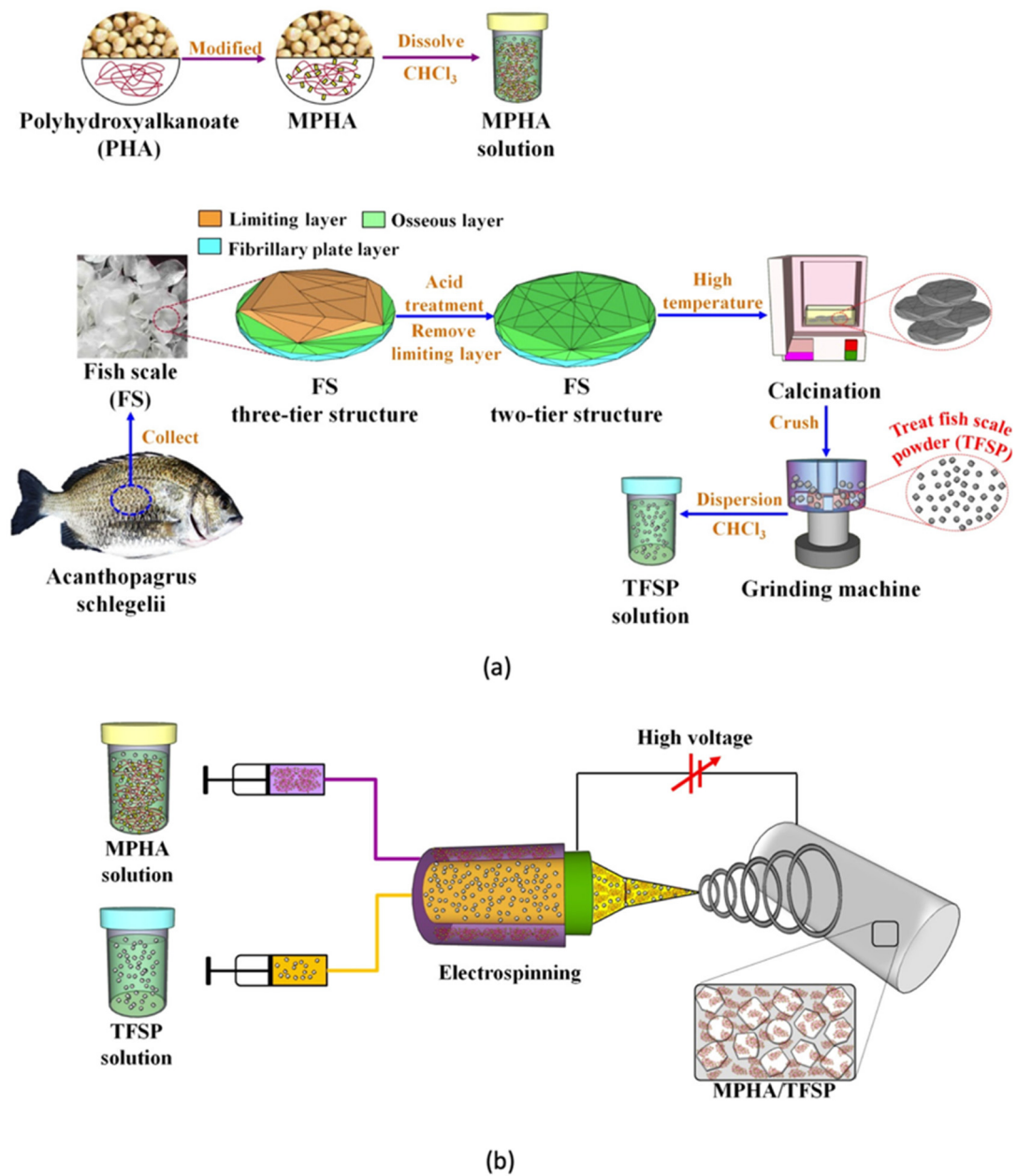


**Figure 11.** (a) The preparation process for the electrospinning modified PHA (MPHA) solution in addition to the treated fish scale powder (TFSP) and (b) The fabrication of electrospun MPHA/TFSP nanofiber. Reprinted with permission from American Chemical Society, 2021 [275].

PHBV based nanocomposites for bone filling and infection treatment were reported by Neto et al. [276]. The nanocomposites were fabricated from PHBV, nano diamond (nD) and nanohydroxyapatite (nHA) loaded with vancomycin (VC). They have prepared the nanocomposites using either a spray dryer or a rotary evaporator. SEM analysis showed a good distribution of the nHA particles. The nanoparticles exhibited a nucleating agent effect increasing the crystallinity of PHBV from 57.1% to 73.3%. The nanocomposites prepared by a spray dryer exhibited stronger interface as well as higher  $T_g$  than those prepared by the rotary evaporator. Furthermore, due to the addition of the nanoparticles, there was an increase by 34% of the flexural elastic modulus matching that reported for the human bone. After 22 days, the nanocomposites prepared by spray dryer and rotary evaporator reported VC release of  $0.42 \pm 0.05$  mg and  $1.38 \pm 0.30$  mg, respectively. These

findings suggest that the developed nanocomposites can be promising candidates for bone defect filling [276].

Shahi and co-authors [277] used the polymer replication method to prepare porous ceramic nanocomposite scaffolds consisting different weight fractions of nano  $\beta$ -tricalcium phosphate (nano- $\beta$ -TCP) (with a particle size of around 50–70 nm) coated with PHB for 30 and 60 s. Results showed that the fabricated scaffold with 50 wt.% nano- $\beta$ -TCP and a coating time of 30 s reflected desirable properties in bone tissue engineering. After examining the bioactivity of this scaffold, bone-like apatite layers were found to be well formed on the nanocomposite scaffold. This nanocomposite scaffold is believed to have a good potential for applications in bone tissue engineering [277].

Recently, Jo et al. [216] have successfully improved the mechanical properties of PHA based composites through the addition of surface-modified CNCs via melt-extrusion. To obtain hydrophobically treated CNCs, double silanization using tetraethyl orthosilicate (TEOS) and methyltrimethoxysilane (MTMS) was conducted. The addition of double silanized CNCs acted as a nucleating agent and improved the elongation at break up to 301% with a minor drop in the tensile modulus. The produced composites are likely appropriate for future utilization in commercial applications demanding high ductility [216].

Table 14 shows the impact of different PHAs blends and nanocomposites at different concentrations on the mechanical properties.

### 3.3. Features of Various PHAs Blends and Nanocomposites

Blending PHB with PCL [195] as well as blending PHBV with PBS [193] and PLA and PBS [144] have been found to enhance the ductility. Improvement in the tensile strength for PHB and the PHBV's tensile strength in the quasi-static tensile test have been found to enhance due to blending with PCL [197] and PBS [193], respectively. Complete degradable blends were obtained via mixing PHB with PCL [186] as well as PHBV with PLA and PBS [144]. Blending PHB with PETG [192] results in a significant improvement in the flexural modulus.

The incorporation of MWCNTs into PHBV improves the thermal stability and crystallinity of PHBV [203,204]. Blending PHBV with CNTs and CNF [215] has been proven to enhance the barrier and mechanical properties of PHBV. Improvement in the crystallinity of P3HB-co-4HB [218] and mcl-PHAs [219] were observed after blending with CNFs. A significant enhancement in the mechanical and thermal properties was reported as a result of blending PHB with MMT [205]. Table 15 shows the advantages and applications of selected studies on PHAs blends and nanocomposites.

Table 14. Mechanical properties of different PHAs blends and nanocomposites at various concentration along with their applications.

| Blend/Composite/<br>Nanocomposite | Concentration (wt.%)  | Tensile Strength<br>(MPa) | Young's Modulus<br>(MPa) | Percentage<br>Elongation | Charpy Impact<br>Strength/(Notched Izod<br>Break Energy) | Applications and/or<br>Reference             |
|-----------------------------------|---|---------------------------|--------------------------|--------------------------|--|--|
| PHB/PCL                           | - 100/0   | - 22.20                   | - 1939                   | - 8.10%                  |  | [195]  |
|                                   | - 75/25   | - 21.40                   | - 1643                   | - 11.20%                 |  |  |
|                                   | - 50/50   | - 19.80                   | - 1387                   | - 17.60%                 |  |  |
|                                   | - 25/75   | - 17.30                   | - 690                    | - >1000%                 |  |  |
| PHA <sup>a</sup> /PCL             | - 70/30   | - 4.0 <sup>b</sup>        |                          | - 4.00% <sup>b</sup>     |  | Medical applications<br>and packaging [197]. |
|                                   | - 50/50   | - 5.0 <sup>b</sup>        | -                        | - 64.00% <sup>b</sup>    |  |  |
|                                   | - 30/70   | - 13.0 <sup>b</sup>       |                          | - 63.00% <sup>b</sup>    |  |  |
| P(3HO-3HD)/PCL                    | - 100/0   | - 14.30                   | - 8.40                   | - 640.00%                |  | Nerve<br>re-generation [198]                 |
|                                   | - 75/25   | - 5.90                    | - 110                    | - 490.00%                |  |  |
|                                   | - 95/5  | - 13.70                   | - 13.70                  | - 620.00%                |  |  |
| PHB/PBS                           | - 100/0   |                           |                          | - 1.00%                  | - (0.60) KJ/m <sup>2</sup>                               | Injection molding<br>applications [193].     |
|                                   | - 80/20   |                           |                          | - 2.00%                  | - (1.50) KJ/m <sup>2</sup>                               |  |
|                                   | - 80/20 with 0.5% DCP as a<br>free-radical grafting initiator |                           |                          | - 4.00%                  | - (3.50) KJ/m <sup>2</sup>                               |  |
|                                   | - 70/30   |                           |                          | - 2.00%                  | - (3.00) KJ/m <sup>2</sup>                               |  |
|                                   | - 70/30 with 0.5% DCP   |                           |                          | - 11.00%                 | - (4.00) KJ/m <sup>2</sup>                               |  |
| PHBV/PBS                          | - 50/50   |                           |                          | - 4.00%                  | - (3.00) KJ/m <sup>2</sup>                               | Injection molding<br>applications [193].     |
|                                   | - 50/50 with 0.5% DCP   |                           |                          | - 15.00%                 | - (5.50) KJ/m <sup>2</sup>                               |  |
|                                   | - 80/20   |                           |                          | - 8.00%                  | - (2.80) KJ/m <sup>2</sup>                               |  |
|                                   | - 80/20 with 0.2% DCP as a<br>free-radical grafting initiator |                           |                          | - 200.00%                | - (3.00) KJ/m <sup>2</sup>                               |  |
|                                   | - 80/20 with 0.5% DCP   |                           |                          | - 400.00%                | - (5.00) KJ/m <sup>2</sup>                               |  |
| PHBV/PLA/PBS                      | - 80/20 with 1% DCP   |                           |                          | - 350.00%                | - (5.50) KJ/m <sup>2</sup>                               | Injection molding<br>applications [193].     |
|                                   | - 0/100/0   | - 70.00                   | - 2750                   | - 5.00%                  | - (17.5) J/m   |  |
|                                   | - 100/0/0   | - 22.00                   | - 1300                   | - 10.00%                 | - (29.00) J/m  |  |
|                                   | - 30/60/10  | - 54.00                   | - 2300                   | - 20.00%                 | - (33.00) J/m  |  |
|                                   | - 10/60/30  | - 55.00                   | - 2150                   | - 51.00%                 | - (36.5) J/m   |  |
| PHBV/PLA/PBS                      | - 60/30/10  | - 34.00                   | - 1750                   | - 62.00%                 | - (30.00) J/m  | Structural<br>materials [144].               |
|                                   | - 60/10/30  | - 28.00                   | - 1200                   | - 82.00%                 | - (32.5) J/m   |  |

Table 14. Cont.

| Blend/Composite/<br>Nanocomposite     | Concentration (wt.%)                  | Tensile Strength<br>(MPa) | Young's Modulus<br>(MPa) | Percentage<br>Elongation | Charpy Impact<br>Strength/(Notched Izod<br>Break Energy) | Applications and/or<br>Reference  |
|---------------------------------------|---------------------------------------|---------------------------|--------------------------|--------------------------|--|---|
| PHB/PETG                              | - 100/0                               | - 58.00                   |                          |                          | - (24.00) J/m  | Applications that require improved processability while minimizing PHB's biodegradability [192].              |
|                                       | - 90/10                               | - 49.00                   |                          |                          | - (13.00) J/m  |   |
|                                       | - 80/20                               | - 42.00                   | -                        | -                        | - (22.00) J/m  |   |
|                                       | - 70/30                               | - 33.00                   |                          |                          | - (27.00) J/m  |   |
|                                       | - 60/40                               | - 33.00                   |                          |                          | - (15.00) J/m  |   |
| PHBV/P(3HB-co-3HV-co-3HHx)            | - 100/0                               | - 34.00                   | - 4000                   | - 2.00%                  |  | Organic recycling food packaging [201].   |
|                                       | - 90/10                               | - 40.00                   | - 3950                   | - 1.800%                 |  |   |
|                                       | - 75/25                               | - 30.00                   | - 2750                   | - 2.60%                  |  |   |
|                                       | - 50/50                               | - 25.00                   | - 2000                   | - 3.30%                  |  |   |
|                                       |                                       |                           |                          |                          |  |   |
| PHB-gAA/MWNTs-OH                      | - 100/0                               | - 16.00                   |                          | - 8.0%                   |  | Applications that require higher performance [217].   |
|                                       | - 99.5/0.5                            | - 23.50                   |                          | - 7.0%                   |  |   |
|                                       | - 99/1                                | - 33.50                   | -                        | - 6.0%                   |  |   |
|                                       | - 97/3                                | - 26.50                   |                          | - 4.0%                   |  |   |
|                                       |                                       |                           |                          |                          |  |   |
| PHB/starch                            | - 100/0                               | - 18.00                   |                          |                          |  | Applications requiring better biodegradation, thermal, mechanical properties as well as processibility [229]. |
|                                       | - 90/10                               | - 14.50                   |                          |                          |  |   |
|                                       | - 80/20                               | - 13.50                   |                          |                          |  |   |
|                                       | - 70/30                               | - 12.00                   |                          |                          |  |   |
|                                       | - 60/40                               | - 8.50                    |                          |                          |  |   |
|                                       | - 50/50                               | - 7.00                    |                          |                          |  |   |
|                                       | - 100/0                               | - 18.29                   | - 1708                   | - 3.32%                  |  |   |
|                                       | - 90/10                               | - 17.20                   | - 1716                   | - 9.80%                  |  |   |
|                                       | - 80/20                               | - 19.70                   | - 1085                   | - 6.00%                  |  |   |
|                                       | - 70/30                               | - 19.23                   | - 949                    | - 9.40%                  |  |   |
|                                       | - 60/40                               | - 7.70                    | - 856                    | - 8.50%                  |  |   |
|                                       | - 50/50                               | - 10.06                   | - 694                    | - 5.27%                  |  |   |
|                                       | - 40/60                               | - 5.24                    | - 686                    | - 3.45%                  |  |   |
|                                       | - 30/70                               | - 4.99                    | - 578                    | - 4.30%                  |  |   |
|                                       | - 70/30 (starch contains 70% amylose) | - 12.50                   | -                        | - 3.90%                  |  |   |
| - 70/30 (starch contains 72% amylose) | - 7.30                                | -                         | - 2.80%                  |                          | - 0.70 KJ/m <sup>2</sup>                                 |   |

Table 14. Cont.

| Blend/Composite/<br>Nanocomposite   | Concentration (wt.%)         | Tensile Strength<br>(MPa) | Young's Modulus<br>(MPa) | Percentage<br>Elongation | Charpy Impact<br>Strength/(Notched Izod<br>Break Energy) | Applications and/or<br>Reference  |
|---|------------------------------|---------------------------|--------------------------|--------------------------|--|---|
| PHB-gAA/starch  | - 100/0                      | - 16.00                   |                          |                          |  | Applications demanding better biodegradation, thermal, mechanical properties as well as processibility [229]. |
|   | - 90/10                      | - 17.00                   |                          |                          |  |   |
|   | - 80/20                      | - 16.00                   | -                        | -                        |  |   |
|   | - 70/30                      | - 15.50                   |                          |                          |  |   |
|   | - 60/40                      | - 15.00                   |                          |                          |  |   |
|   | - 50/50                      | - 14.90                   |                          |                          |  |   |
| - Plasticized 70% amylose corn starch blended with thermoplastic partner (PCL or PBAT) followed by PHB addition.<br>- PHB blended with thermoplastic partner (PCL or PBAT) followed by plasticized 70% amylose corn starch<br>- Addition of PHB with thermoplastic partner (PCL or PBAT) with plasticized 70% amylose corn starch all in one step |                              | - 15.00                   | - 900                    | - 47.00%                 |  | Flexible packaging [236].   |
|   |                              | - 18.00                   | - 1080                   | - 32.00%                 |  |   |
|   |                              | - 21.00                   | - 1020                   | - 114.00%                |  |   |
|   |                              |                           |                          |                          |  |   |
| PHB/ENR/MR/TMC  | - 100/0/0/0                  |                           |                          |                          | - (23.00) J/m  | Applications requiring high impact properties [259].  |
|   | - 60/40/0/0                  |                           |                          |                          | - (25.00) J/m  |   |
|   | - 60/30/10/0                 |                           |                          |                          | - (124.00) J/m   |   |
|   | - 58/30/10/2                 |                           |                          |                          | - (93.00) J/m  |   |
|   | - 55/30/10/5                 |                           |                          |                          | - (116.00) J/m   |   |
|   | - 53/30/10/7                 |                           |                          |                          | - (87.00) J/m  |   |
| PHB/ENR/MR/COC  | - 55/30/10/5                 |                           |                          |                          | - (49.00) J/m  |   |
| PHB/MMT   | - 100/0                      |                           |                          |                          |  | [208]   |
|   | - PHB/Cloisite® Na+          | - 29.60                   | - 3060                   |                          |  |   |
|   | - PHB/modified Cloisite® 30B | - 24.90<br>- 27.00        | - 3200<br>- 3440         |                          |  |   |

Table 14. Cont.

| Blend/Composite/<br>Nanocomposite         | Concentration (wt.%)                                | Tensile Strength<br>(MPa) | Young's Modulus<br>(MPa) | Percentage<br>Elongation | Charpy Impact<br>Strength/(Notched Izod<br>Break Energy) | Applications and/or<br>Reference  |
|---|---|---------------------------|--------------------------|--------------------------|--|---|
| PHBH <sub>x</sub> /SiO <sub>2</sub> fiber | - 100/0 <sup>c</sup>                                | - 23.00                   | - 1000                   |                          |  |   |
|   | - 100/0 <sup>d</sup>                                | - 24.50                   | - 1300                   |                          |  |   |
|   | - 99/1 <sup>c,e</sup>                               | - 24.50                   | - 1300                   |                          |  |   |
|   | - 97/3 <sup>c,e</sup>                               | - 22.50                   | - 1400                   |                          |  |   |
|   | - 95/5 <sup>c,e</sup>                               | - 24.60                   | - 1600                   |                          |  |   |
|   | - 99/1 <sup>c,f</sup>                               | - 23.00                   | - 1300                   |                          |  |   |
|   | - 97/3 <sup>c,f</sup>                               | - 24.50                   | - 1490                   |                          |  |   |
|   | - 95/5 <sup>c,f</sup>                               | - 23.50                   | - 1400                   |                          |  |   |
|   | - 99/1 <sup>d,e</sup>                               | - 24.40                   | - 1300                   |                          |  |   |
|   | - 97/3 <sup>d,e</sup>                               | - 25.00                   | - 1400                   |                          |  |   |
|   | - 95/5 <sup>d,e</sup>                               | - 24.50                   | - 1490                   |                          |  |   |
|   | - 99/1 <sup>d,f</sup>                               | - 25.00                   | - 1400                   |                          |  |   |
|   | - 97/3 <sup>d,f</sup>                               | - 24.50                   | - 1400                   |                          |  |   |
|   | - 95/5 <sup>d,f</sup>                               | - 24.50                   | - 1490                   |                          |  |   |
|   |   |                           |                          |                          |  |   |
| PHBV /wheat starch                        | - 100/0   | - 17.70                   | - 1525                   | - 25.00%                 |  | Complete biodegradable<br>materials with reduced<br>cost [225].                                 |
|   | - 75/25   | - 8.60                    | - 2132                   | - 5.10%                  |  |   |
|   | - 50/50   | - 7.70                    | - 2498                   | - 1.00%                  |  |   |
| PHBV /maize starch                        | - 100/0   |                           |                          |                          |  |   |
|   | - 80/20   |                           |                          |                          |  |   |
|   | - 70/30   |                           |                          |                          |  |   |
|   | - 80/20 with 2% free radical<br>former <sup>8</sup> | -                         | -                        |                          |  |   |
|   | - 70/30 with 2% free radical<br>former <sup>8</sup> | -                         | -                        |                          |  |   |
|   | - 100   | - 18.00                   | - 1200                   | - 2.10%                  |  |   |
|   | - 80/20   | - 6.00                    | - 750                    | - 1.00%                  |  |   |
|   | - 70/30   | - 3.50                    | - 310                    | - 1.10%                  |  |   |
|   | - 60/40   | - 4.00                    | - 305                    | - 1.10%                  |  |   |
|   | - 50/50   | - 2.85                    | - 160                    | - 1.40%                  |  |   |
|   |   |                           |                          |                          |  | Biodegradable<br>disposable<br>plastics with low cost<br>and the required<br>performance [226]. |
|   |   |                           |                          |                          |  | Packaging [234].  |

Table 14. Cont.

| Blend/Composite/<br>Nanocomposite        | Concentration (wt.%)                                      | Tensile Strength<br>(MPa) | Young's Modulus<br>(MPa) | Percentage<br>Elongation | Charpy Impact<br>Strength/(Notched Izod<br>Break Energy) | Applications and/or<br>Reference  |
|--|---|---------------------------|--------------------------|--------------------------|--|---|
| PHBV/corn starch                         | - 75/25 with 5% Acetyl<br>tributyl citrate as plasticizer | - 17.10                   | - 458.00                 | - 15.60%                 | -  | Applications that<br>require improved<br>mechanical<br>properties [228].  |
|  | - 75/25 with 5% Acetyl<br>tributyl citrate as plasticizer | - 23.60                   | - 539.00                 | - 13.00%                 | -  |   |
| PHBV/granular cornstarch                 | - 100/0 with 10% Ttracetin<br>as an additive              |                           |                          |                          |  | Single use applications<br>such as plastic knives<br>and forks [222].   |
|  | - 70/30 with 10% Ttracetin                                | - 24.00                   | - 180                    | - 38.00%                 |  |   |
|  | - 50/50 with 10% Ttracetin                                | - 15.00                   | - 250                    | - 21.00%                 |  |   |
|  | - 70/30 with 10% Ttracetin                                | - 10.00                   | - 300                    | - 11.00%                 |  |   |
|  | and 9% PEO  | - 19.00                   | - 220                    | - 21.00%                 | -  |   |
|  | - 50/50 with 10% Ttracetin<br>and 9% PEO                  | - 18.00                   | - 170                    | - 21.00%                 |  |   |
|  | - 50/50 with 10% Ttracetin<br>and 5% PEO                  | - 15.00                   | - 210                    | - 15.00%                 |  |   |
| - 50/50 with 10% Ttracetin<br>and 2% PEO | - 12.00   | - 280                     | - 10.00%                 |                          |  |   |
| PHBV/Cloisite® 30B                       | - 100/0   | - 37.50                   | - 3500                   | - 3.00%                  | - (20.00) J/m  | Applications that require<br>enhanced processing<br>behaviors, crystallinity,<br>low cost and<br>improved mechanical<br>properties [264]. |
|  | - 99/1  | - 40.60                   | - 5100                   | - 2.40%                  | - (11.00) J/m  |   |
|  | - 97/3  | - 30.70                   | - 4600                   | - 0.70%                  | - (11.00) J/m  |   |
|  | - 95/5  | - 30.40                   | - 7100                   | - 0.60%                  | - (10.00) J/m  |   |
| PHBV/PLA/Cloisite® 30B                   | - 100/0   | - 31.00                   | - 481                    | - 8.50%                  |  | Injection molding<br>applications<br>with high modulus, heat<br>deflection resistance and<br>superior gas barrier<br>properties [194].    |
|  | - 99/1  | - 32.00                   | - 555                    | - 7.60%                  |  |   |
|  | - 98/2  | - 35.00                   | - 730                    | - 7.70%                  | -  |   |
|  | - 97/3  | - 33.00                   | - 795                    | - 5.60%                  |  |   |



Table 14. Cont.

| Blend/Composite/<br>Nanocomposite | Concentration (wt.%)  | Tensile Strength<br>(MPa) | Young's Modulus<br>(MPa) | Percentage<br>Elongation | Charpy Impact<br>Strength/(Notched Izod<br>Break Energy) | Applications and/or<br>Reference  |
|-----------------------------------|---|---------------------------|--------------------------|--------------------------|--|---|
| PHBV/Cloisite® 15A                | - 100/0   | - 5.90                    | - 633.00                 | - 3.30%                  |  | Applications demanding enhanced mechanical properties [254].                        |
|                                   | - 99/1  | - 11.80                   | - 1043.00                | - 2.70%                  |  |   |
|                                   | - 97.5/2.5  | - 18.00                   | - 1311.00                | - 1.80%                  | -  |   |
|                                   | - 95/5  | - 28.90                   | - 1677.00                | - 1.40%                  |  |   |
| PHBV/OMMT                         | - 97/3  | - 26.90                   | - 1373                   | - 4.10%                  |  | Applications that require enhanced crystallization and mechanical properties [207]. |
|                                   | - 90/10   | - 35.60                   | - 1412                   | - 3.90%                  | -  |   |
|                                   |   | - 21.80                   | - 1375                   | - 2.10%                  |  |   |
| PHBV/LDH-SA                       | - 100/0   | - 25.10                   | - 1120                   | - 4.03%                  |  | Medical applications [267].   |
|                                   | - 99/1  | - 28.20                   | - 1230                   | - 3.50%                  |  |   |
|                                   | - 97/3  | - 28.50                   | - 1330                   | - 3.25%                  | -  |   |
|                                   | - 95/5  | - 24.20                   | - 1420                   | - 2.50%                  |  |   |
|                                   | - 93/7  | - 24.40                   | - 1240                   | - 2.70%                  |  |   |
| PHBV/HNT                          | - 100/0   | - 37.50                   | - 3500                   | - 3.00%                  | - (20.00) J/m  | [209]   |
|                                   | - 99/1  | - 39.30                   | - 4000                   | - 3.70%                  | - (19.00) J/m  |   |
|                                   | - 97/3  | - 39.40                   | - 3600                   | - 3.10%                  | - (20.00) J/m  |   |
|                                   | - 95/5  | - 38.70                   | - 5700                   | - 4.10%                  | - (19.00) J/m  |   |
| PHBV/CNW                          | - 100/0   | - 14.10                   | - 820                    | - 12.40%                 |  | Sustainable composite applications [213].   |
|                                   | - 98/2 with PEG as a compatibilizer                             | - 15.50                   | - 1100                   | - 7.10%                  |  |   |
|                                   | - 95/5 with PEG   | - 26.10                   | - 1760                   | - 7.80%                  |  |   |
| PHBV/CS                           | - 100/0   |                           |                          |                          |  | Food contact injection molding applications such as coffee capsules [273].          |
|                                   | - 100/0 with 10% ATBC as a plasticizer and 5% CaCO <sub>3</sub> | - 34.80                   | - 2610                   | - 2.60%                  | - 2.50 KJ/m <sup>2</sup>                                 |   |
|                                   | - 85/5 with 10% ATBC and 5% CaCO <sub>3</sub>                   | - 23.00                   | - 1300                   | - 6.20%                  | - 5.80 KJ/m <sup>2</sup>                                 |   |
|                                   | - 85/7.5 with 10% ATBC and 5% CaCO <sub>3</sub>                 | - 20.80                   | - 1730                   | - 4.00%                  | - 3.70 KJ/m <sup>2</sup>                                 |   |
|                                   | - 85/10 with 10% ATBC and 5% CaCO <sub>3</sub>                  | - 19.70                   | - 1930                   | - 2.90%                  | - 3.70 KJ/m <sup>2</sup>                                 |   |
|                                   | - 85/12.5 with 10% ATBC and 5% CaCO <sub>3</sub>                | - 18.40                   | - 2030                   | - 2.50%                  | - 3.20 KJ/m <sup>2</sup>                                 |   |
|                                   | - 17.30   | - 2050                    | - 2.30%                  | - 3.80 KJ/m <sup>2</sup> |  |   |

Table 14. Cont.

| Blend/Composite/<br>Nanocomposite | Concentration (wt.%) | Tensile Strength<br>(MPa) | Young's Modulus<br>(MPa) | Percentage<br>Elongation | Charpy Impact<br>Strength/(Notched Izod<br>Break Energy) | Applications and/or<br>Reference  |
|-----------------------------------|----------------------|---------------------------|--------------------------|--------------------------|--|---|
| PHA/TFSB                          | - 100/0              | - 1.66                    |                          | - 85.30%                 |  | Biomedical applications,<br>such as bioprotective<br>films,<br>wound healing and bone<br>tissue engineering (e.g.,<br>bone screws, bone joints<br>and tooth roots) [275]. |
|                                   | - 99/1               | - 1.51                    |                          | - 78.80%                 |  |   |
|                                   | - 98/2               | - 1.41                    | -                        | - 73.60%                 | -  |   |
|                                   | - 97/3               | - 1.36                    |                          | - 67.10%                 |  |   |
|                                   | - 96/4               | - 1.22                    |                          | - 62.50%                 |  |   |
| MPHA/TFSB                         | - 95/5               | - 1.08                    |                          | - 57.10%                 |  |   |
|                                   | - 100/0              | - 1.60                    |                          | - 86.10%                 |  |   |
|                                   | - 99/1               | - 1.88                    |                          | - 76.30%                 |  |   |
|                                   | - 98/2               | - 2.13                    | -                        | - 67.80%                 | -  |   |
|                                   | - 97/3               | - 2.43                    |                          | - 59.30%                 |  |   |
| PHA/GNPs                          | - 96/4               | - 2.36                    |                          | - 52.50%                 |  |   |
|                                   | - 95/5               | - 2.24                    |                          | - 39.60%                 |  |   |
|                                   | - 100/0              | - 17.00                   |                          | - 14.00%                 |  |   |
|                                   | - 97.5/2.5           | - 16.40                   |                          | - 10.00%                 |  |   |
|                                   | - 95/5               | - 14.00                   | -                        | - 11.00%                 | -  |   |
| PHA/GNPs and CNFs                 | - 92.5/7.5           | - 18.00                   |                          | - 12.00%                 |  |   |
|                                   | - 90/10              | - 11.00                   |                          | - 3.00%                  |  |   |
|                                   | - 85/15              | - 11.20                   |                          | - 3.00%                  |  |   |
|                                   | - 97.5/2.5           | - 16.40                   |                          | - 12.00%                 |  |   |
|                                   | - 95/5               | - 16.50                   | -                        | - 9.00%                  |  |   |
| PHA/GNPs and CNFs                 | - 92.5/7.5           | - 16.00                   | -                        | - 6.00%                  | -  |   |
|                                   | - 90/10              | - 17.10                   |                          | - 5.50%                  |  |   |
|                                   | - 85/15              | - 17.00                   |                          | - 2.00%                  |  |   |

Table 14. Cont.

| Blend/Composite/<br>Nanocomposite      | Concentration (wt.%)         | Tensile Strength<br>(MPa)     | Young's Modulus<br>(MPa)   | Percentage<br>Elongation            | Charpy Impact<br>Strength/(Notched Izod<br>Break Energy) | Applications and/or<br>Reference                              |
|--|------------------------------|-------------------------------|----------------------------|-------------------------------------|--|---|
| Mixture of P3HB and P4HB<br>/FD-TMCNCs | - 100/0<br>- 95/5<br>- 90/10 | - 25.84<br>- 19.20<br>- 17.02 | - 5.27<br>- 5.52<br>- 3.64 | - 101.33%<br>- 301.00%<br>- 231.00% |  | Commercial applications<br>demanding high<br>ductility [216]. |
| Mixture of P3HB and P4HB<br>/TD-TMCNCs | - 90/10                      | - 15.58                       | - 0.09                     | - 247.67%                           |  |   |

<sup>a</sup> Plasticized PHA containing 65% PHA, 30% PBS and 5% crosslinking agent. <sup>b</sup> Quasi-static tensile testing. <sup>c</sup> Molecular weight of PHBHx = 903,000 g/mol. <sup>d</sup> Molecular weight of PHBHx = 633,000 g/mol <sup>e</sup> SiO<sub>2</sub> fiber. <sup>f</sup> SiO<sub>2</sub> sphere. <sup>g</sup> bis[tert-butylperoxyisopropyl] benzene. Note: Studies in which no exact values for the mechanical properties were given, the best estimations were provided. Abbreviations: PHB, polyhydroxybutyrate; PCL, poly(*ε*-caprolactone); P(3HO-3HD), poly(3-hydroxyoctanoate-*co*-3-hydroxydecanoate); PBS, poly(butylene succinate); DCP, dicumyl peroxide; PHBV, poly(3-hydroxybutyrate-*co*-3-hydroxyvalerate); PETG, poly(ethylene terephthalate-*co*-1,4-cyclohexenedimethanol terephthalate); P(3HB-*co*-3HV-*co*-3HHx), poly(3-hydroxybutyrate-*co*-3-hydroxyvalerate-*co*-3-hydroxy-hexanoate); PHB-*g*-AA, acrylic acid grafted PHB; MWNTs, multiwalled carbon nanotubes; MWNTs-OH, multihydroxyl functionalized MWNTs; PBAT, poly(butylene adipate-*co*-terephthalate); ENR, epoxidized natural rubber; MR, maleated rubber; TMC, titanate modified clay; COC, commercially modified clay; MMT, montmorillonite; Cloisite® Na+, NA-MMT; PHBH<sub>x</sub>, poly(3-hydroxybutyrate-*co*-3-hydroxyhexanoate); SiO<sub>2</sub>, silica; starch-*g*-PGMA, starch-*g*-poly(glycidyl methacrylate); PEO, poly(ethylene oxide); PLA, poly(lactic acid); OMMT, organically modified montmorillonite; LDH, layered double hydroxide; LDH-SA, Zn-Al NO<sub>3</sub> LDH organically modified with stearic acid; HINT, halloysite; CNW, freeze-dried cellulose nano whiskers; PEG, polyethylene glycol; CS, coffee silverskin; ATBC, acetyl tributyl citrate; CaCO<sub>3</sub>, calcium carbonate; TFSB, treated fish scale powder; MPHFA, modified PHA (produced by mixing PHA with 10 phr PHA-*g*-AA, then heating); GNPs, graphene nanoplatelets; CNFs, carbon nanofibers; P3HB, poly-3-hydroxybutyrate; P4HB, poly-4-hydroxybutyrate; CNCs, cellulose nanocrystals; FD-TMCNCs, freeze-dried CNCs with CH<sub>3</sub> ends treated by tetraethyl orthosilicate (TEOS) and methyltrimethoxysilane (MTMS); TD-TMCNCs, thermally-dried CNCs with CH<sub>3</sub> ends treated by TEOS and MTMS.

**Table 15.** Features and applications of some selected studies on PHAs blends and nanocomposites.

| Blend/Nanocomposite | Concentration (wt.%)  | Features   | Applications and/or Reference   |
|---------------------|---|--|---|
| PHB/PLA             | - 80/20 and 60/40   | -Improvement in the percentage elongation at break. Percentage elongation at break for the PHB/PLA 60/40 wt.% was eight time that of the neat PHB.   | -Biomedical applications [133].   |
| PHB/PCL             | - 30/70<br><br>- 75/25, 50/50 and 25/75<br><br>- 65/30 with 5% crosslinking agent | -An increase in the crystallinity of PHB and the blend PHB-phase.<br>-Complete degradation.<br><br>-Increase in the blend's flexibility and ductility.<br>-Significant increase in the percentage elongation at break and the energy absorption in impact conditions.<br><br>-Increase in the percentage elongation at break as well as the tensile strength in the quasi-static tensile test. | -Biotechnological applications [186].<br><br>[195]<br><br>-Multi-scale instrumental analyses [197]. |
| PHBV/PBS            | - 90/10, 80/20 and 70/30  | -Significant enhancement in the elongation at break of the PHBV/PBS blends due to the better interfacial adhesion between the PHBV and PBS phases.<br>-Improvement in tensile strength.  | [193]   |
| PHBV/PLA/PBS        | - 60/30/10 and 60/10/30   | -Entirely biodegradable.<br>-An enhancement in the PLA's crystallization, flexibility and toughness was observed in the resulting ternary complex.<br>-Optimum performance with excellent balanced thermal resistance and stiffness-toughness.   | [144]   |
| PHB/LDPE            | -   | -Substantial improvement in the LDPE's modulus of elasticity.  | [191]   |
| PHBV/PE             | - 10/90 and 30/70   | -The rate of degradation was proportional to the quantity of PHBV in contact with PE.  | [188]   |
| PHB/PETG            | - 80/20, 60/40, 50/50, 40/60 and 20/80  | -Substantial enhancement in the flexural modulus.<br>-Improvement in the processability and modulus of elasticity without significant changes in the impact resistance while keeping the biodegradability of PHB intact.   | [192]   |

Table 15. Cont.

| Blend/Nanocomposite | Concentration (wt.%)  | Features   | Applications and/or Reference   |
|---------------------|---|--|---|
| PHBV/MWNTs          | - 98/2  | -Improvement in thermal stability.   | -Applications that require higher thermal stability, hardness and improved electrical conductivity [204].                         |
|                     | - 99/1, 97/3, 95/5 and 93/7   | -Enhancement in the crystallinity and crystallite sizes of PHBV.   | [203]   |
| PHBV/CNTs           | - 99/1, 97/3, 95/5 and 90/10  | -Improvement in water and oxygen transmission, barrier properties, conductivity and mechanical properties. | -Medicine, aerospace engineering, home appliances, public transportations as well as beverage and food packaging [215].           |
|                     |   |  |   |
| PHBV/CNFs           |   |  |   |
|                     |   |  |   |
| P3HB-co-4HB/CNFs    | - 99/1 treated with <i>n</i> -octanol, silane coupling agent (KH-550) and nitric acid | -Both, the crystallinity and the glass transition temperature increased.                                   | -Biomedical and electronic applications [218].  |
|                     |   |  |   |
| mcl-PHAs/CNFs       | -   | -Improvement in the crystallinity, thermomechanical properties and physical morphology.                    | -Smart biomaterials, such as: biosensors, organic electroconductive materials and stimuli-responsive drug delivery devices [219]. |
|                     |   |  |   |

Table 15. Cont.

| Blend/Nanocomposite                             | Concentration (wt.%)                      | Features   | Applications and/or Reference   |
|---|---|--|---|
| PHBV / plasticized (with Glycerol) wheat starch | -   | -Low cost.<br>-Sufficient adhesion between layers.<br>-Moisture barrier properties.<br>-Satisfactory water resistance.<br>-Improved mechanical properties. | -Compostable multilayers film for disposable articles and food packaging [237]. |
| PHBV/extruded starch                            | - 95/5, 90/10 and 80/20                   | -The expansion of the foam has been reduced.   | -Loose fill packaging applications [240].                                       |
| PHBV/TPS  | -   | -Cost effective.<br>-PHA works as a water-resistant outer coating.   | -Food packaging, insect dyes, controlled drug release and pesticides [239].     |
| PHB/organo-modified fluoromica                  | - 98/2                                    | -Significant enhancement in mechanical and thermal properties as well as the biodegradation rate.  | [205]   |
| PHB/MMT   | - 98.8/1.2, 97.7 and 96.4/3.6             |  |   |
| Nodax <sup>®</sup> TM /clay 20A and clay 25A    | - 99/1, 97/3, 95/5, 93/7, 90/10 and 85/15 | -Improved mechanical properties and a slight enhancement in thermal stability.   | -Applications that Require improved mechanical properties [265].                |
| PHB/PMLDH                                       | - 98/2 and 95/5                           | -Significant enhancement in storage modulus.<br>-An increase in crystallization rate.<br>-A reduction in activation energy.                                | [255]   |
| mcl-PHAs/hydrolyzed tunicin cellulose whiskers  | -   | -Substantial enhancement in mechanical properties.   | [268]   |

Abbreviations: PHB, polyhydroxybutyrate; PLA, poly(lactic acid); PCL, poly( $\epsilon$ -caprolactone); PHBV, poly(3-hydroxybutyrate-co-3-hydroxyvalerate); PBS, poly(butylene succinate); LDPE, low-density polyethylene; PE, poly(ethylene); PETG, poly(ethylene terephthalate-co-1,4-cyclohexenedimethanoterephthalate); MWNTs, multiwalled carbon nanotubes; CNFs, carbon nanofibers; P3HB-co-4HB, poly-3-hydroxybutyrate-co-4-hydroxybutyrate; mcl-PHAs, medium chain length poly-3-hydroxyalkanoate; TPS, thermoplastic starch; MMT, montmorillonite; Nodax<sup>®</sup>TM, [poly(3-hydroxybutyrate-co-3-hydroxyhexanoate)]; clay 20A, Cloisite 20A; clay 25A, Cloisite 25A; PMLDH, modified layered double hydroxide.

#### 4. Trends of PLA and PHAs Applications

##### 4.1. PLA Foams, 3D-printed Scaffolds and Flame Retardancy

One of the ideal materials for various packaging applications is PLA foam. PLA foams are becoming increasingly desired as renewable biopolymer alternatives to petroleum-based polymer foams. This is due to their light weight and good cushioning properties. Polymers foams are produced using different blowing agents, which can be categorized as chemical and physical. The production of foam cells under the impact of pressure/temperature release is done via chemical blowing agents. On the other hand, physical foaming of polymers and composites, results in the production of cellular structures with cell sizes smaller than 10 μm and cell densities greater than 10<sup>9</sup> cells/cm<sup>3</sup>, known as microcellular foams [278,279]. PLA foams can be produced via batch processing, foam injection molding, bead foaming as well as foam extrusion. Foam PLA/natural (lignocellulosic) fiber-reinforced composites are produced mainly using foam injection molding and extrusion. Figures 12–14, show the concept of foam injection molding, foam extrusion and bead foaming, respectively. Such foams exhibit thermal and mechanical properties comparable to those of the currently used petroleum-based foams [23,280]. An improvement of the morphology of the foam cell via modification of polymer melt viscosity is believed to be feasible through the addition of lignocellulosic fibers. For example, the incorporation of lignocellulosic fibers can lower the cell size and increase foam cell density [279,281–286]. Moreover, PLA/natural (lignocellulosic) fiber-reinforced composites were found to enhance specific tensile and flexural moduli. Furthermore, changes in PLA crystallinity prompted by the incorporation of fibers can potentially alter the foam cell characteristics of PLA composites [287].

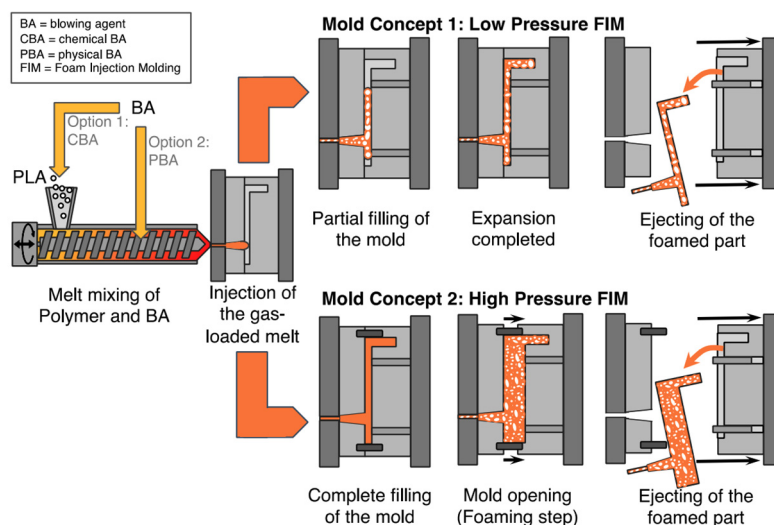


Figure 12. The concept of foam injection molding [23].

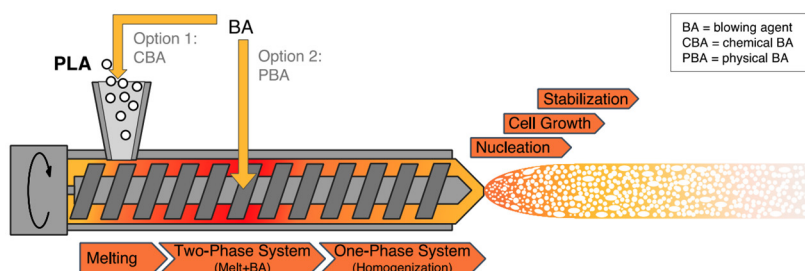
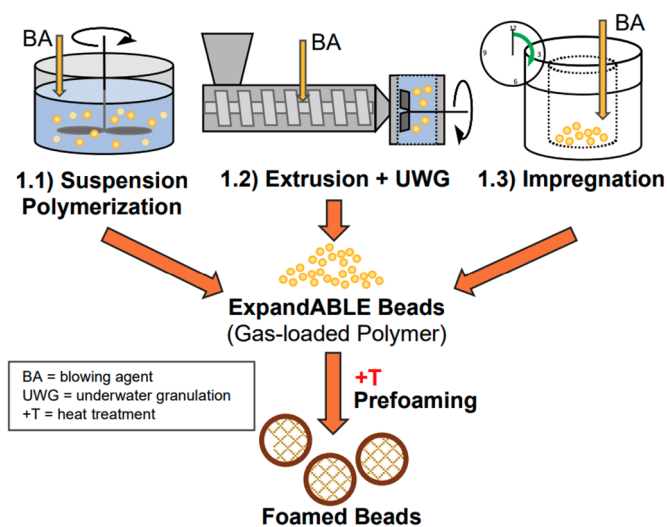


Figure 13. The concept of foam extrusion [23].



**Figure 14.** The various methods for the production of expandable bead foams [23].

In one study [287], microcellular injection molding process was used to produce foamed flax fiber reinforced PLA composites at three various flax concentrations (1, 10 and 20 wt.%). Neat PLA was reported to have an average cell size of 8.4  $\mu\text{m}$ . On the other hand, the cell sizes of PLA/flax composites dropped by around 11%, 47% and 67% at 1, 10 and 20 wt.% flax fiber, respectively. The study has also reported an increase in the specific tensile modulus by around 3%, 10% and 22% for the foamed composites at 1, 10 and 20 wt.% fiber loadings, respectively. This was attributed to the flax fibers' higher modulus in comparison to that of PLA as well as to the restraining impact of fillers on the movement of polymer chain yielding to enhanced stiffness [287].

An investigation of the impact of the addition of willow fiber at 20 wt.% and 30 wt.% concentrations on the mechanical properties of foamed PLA composites was done by Zafar et al. [288]. Neat PLA was reported to have an average cell size of about 33.7  $\mu\text{m}$ . However, the cell sizes of PLA/flax composites dropped to about 20.6  $\mu\text{m}$  at 20 wt.% and 18.1  $\mu\text{m}$  at 30 wt.% willow fiber, respectively. The study reported a slight increase in the flexural modulus and the maximum value was corresponding to that of PLA/30 wt.% willow fiber composite. The specific notched impact strength of PLA/flax composites increased by about 16% at 20% and 45% at 30 wt.% willow fiber, respectively. Moreover, the degree of crystallinity has also increased with the addition of willow fiber [288].

In addition to their use in packaging applications, foamed PLA products have been also utilized in tissue engineering and drug release. PLA is often used in bone or cartilage tissue engineering in the form of 3D-printed scaffolds. One of the most widely used technologies for PLA is additive manufacturing. Generally, a precise control of the 3D printer is essential for the quality of 3D-printed products. A wide range of 3D printers such as Ultimakers and Robo can be used to 3D print PLA filaments [289]. The strength of PLA's printed parts depends mainly on the direction of printing. Therefore, the following points should be given special considerations during the 3D printing. Force application's direction shall not be perpendicular to the printing layer and when printing complex parts, the outer shell thickness, printing pattern, density and the interconnecting parts must be given great considerations as they can lead to premature brittleness. Another important point is to make sure that the platform holds the 3D-printed part firmly so as to avoid the printed spot from being distorted or pulled out. Therefore, it is recommended to use a painter's tape to hold the platform firmly in position [290]. Using a painter's tape will also make it easy to take off the PLA's 3D-printed part as the printed object will stick to the surface of the painter's tape. This will avoid damaging the object when the 3D printing is finished. Another benefit of using a painter's tape is that it can help in avoiding warpage, particularly for semicrystalline PLA which can undertake substantial irregularity in shrinkage when



molten PLA's layers are laid continuously. Moreover, heating the platform can also create a sticking effect. Nevertheless, the platform's temperature shall be kept within the limits that will not cause polymer softening or degradation. The recommended platform and printing temperatures for PLA are 60 °C and 210 °C, respectively. Exposing the PLA filament to high temperatures and moisture can lead to degradation, depolymerization and/or chain scissioning. Therefore, it is recommended to keep the PLA filament stored in a securely sealed condition at a relative humidity less than 10%. Unsealing of the PLA filament is recommended just before the start of printing.

Different studies in literature have reported producing medical implants at a more affordable cost using 3D printing of PLA. Conventional manufacturing techniques such as casting or forging are time consuming and most of the time fail to meet the patients' needs. Three-dimensional printing of scaffolds is one of the mostly suggested medical applications for PLA. For these 3D-printed scaffolds to be able to offer an interconnected network for cell growth as well as transportation of nutrients and waste generated from metabolism, they must meet certain mechanical properties, structural features and durability. Furthermore, these scaffolds are biocompatible with controlled rate of degradation. Therefore, in the long term, there should be no problem for these scaffolds to adhere and match with the tissues [291]. According to Kikuchi et al. [292], to meet the functional requirements of scaffolds, bioactive ceramics such as beta-tricalcium phosphate, hydroxyapatite and calcium phosphate are incorporated with PLA [292]. Niaza et al. [293] investigated 3D printing of porous scaffolds of compounded hydroxyapatite and PLA at an average particle size of 90 nm and 1 µm. FFF technique with a nozzle temperature of 220 °C was used. Results suggested that the modulus of elasticity for PLA with micro-sized hydroxyapatite and nano-sized hydroxyapatite were 2.8 and 4.0 GPa respectively. Knowing that the Young's modulus for the trabecular bone is in the range of 3–5 GPa, it is then very likely to use the 3D-printed PLA- nanosized hydroxyapatite composite bone scaffolding as an alternative to original bone as implants. Moreover, the formation of a high-porosity structure due to the sintering between the layers during 3D printing makes PLA-hydroxyapatite composite a good feasible substitute to original bone [293]. Generally, high porosity is linked to a weaker structure, which in this case weaker PLA-hydroxyapatite composite, nonetheless, such a condition is safe with the addition of nano-sized hydroxyapatite. Various porosities of 3D-printed PLA scaffold structures were studied and compared by Gregor et al. [294]. The investigators were able to 3D print scaffolds with various geometrical structures using FDM. Two types of scaffolds of the defined shape and engineered inner structure that provides regular and sufficient porosity have been successfully printed. The designed 3D-printed scaffolds were subjected to osteosarcoma cells proliferation experiment and mechanical testing. Results suggest that the proliferation of both types of 3D-printed scaffolds with porosity values of 30% and 50% was satisfying with good mechanical durability [294]. Figure 15 shows a schematic of production of filament as well as 3D-printed scaffolds using FFF. According to Alam et al. [171], the process involves (i) solvent casting followed by (ii) filaments fabrication via extrusion and finally (iii) 3D printing of scaffolds.

Various applications (e.g., construction, automobile and electronics) requires high criteria for dripping combustions and flammability, which cannot be satisfied by neat PLA. Therefore, there have been some attempts to enhance PLA's flame retardancy for compact and foamed forms of PLA. In one study [295], an enhancement in compact PLA's flame retardancy was achieved by a synergistic mixture of ammonium polyphosphate (APP) with expandable graphite (EG), an eco-friendly flame retardant. With 15% of this intumescent flame retardant (APP/EG = 3:1), there was an increase in the Limiting Oxygen Index (LOI) from 22 to 36.5. The UL-94-V-0 classification was also reached [295]. In another study [296], the same burning behavior was reported using 30% of a mixture (3:2) of a novel hyperbranched polyamine charring agent (HPCA) together with APP. Tang et al. [297] reported good flame retardancy, anti-dripping effects and high LOI values with synergistic combinations of expanded graphite and aluminum hypophosphite [297]. Other studies were done to enhance foamed PLA's flame retardancy with a phosphorous containing

flame retardant, as well as graphene [298] or starch [299] as a charring agent. UL-94-V-0 classification was reported. Moreover, LOI was significantly increased and anti-dripping effects were observed.

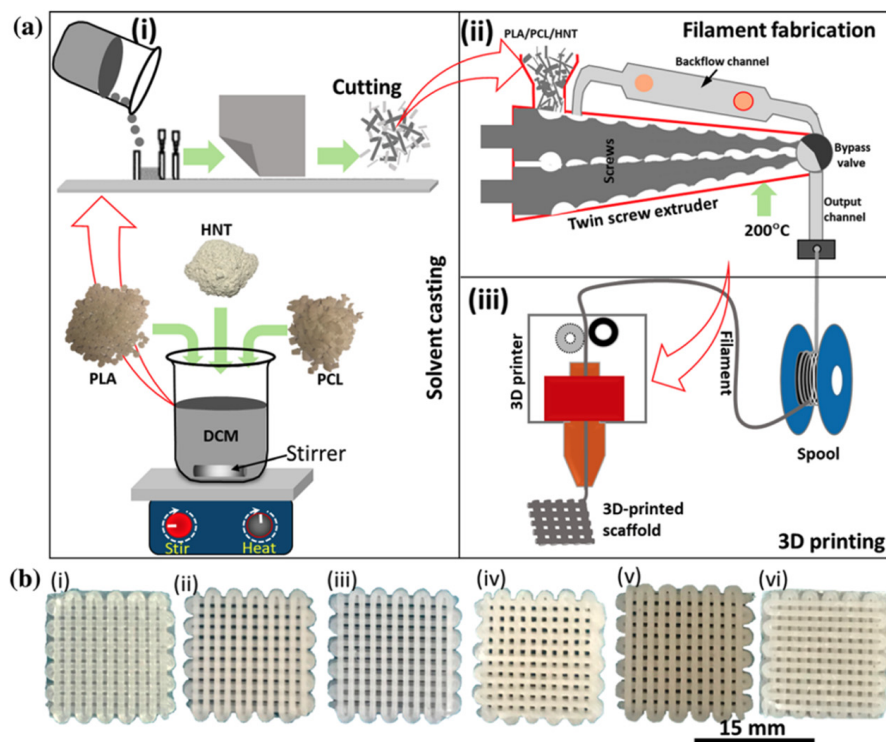


**Figure 15.** (a) Schematic of filament fabrication and 3D printing of scaffolds and (b) optical images of various scaffolds ((i) for neat PLA, (ii) PLA/PCL (50/50 wt.%), (iii) PLA/PCL/HNTs (50/50/1 wt.%), (iv) PLA/PCL/HNTs (50/50/3 wt.%), (v) PLA/PCL/HNTs (50/50/5 wt.%) and (vi) PLA/PCL/HNTs (50/50/7 wt.%) [171].

Vadas and coworkers were able to incorporate a bio-based flame retardant into a PLA extrusion foam [300]. A combination of APP as an intumescent flame retardant and flame retardant treated cellulose (surface treatment with boric acid and diammonium phosphate) as a bio-based charring agent was used to lower PLA foams' flammability. A multifunctional epoxy-based chain extender was utilized and, even at elevated additive loadings, a substantial expansion with void fractions higher than 90% was attainable with carbon dioxide as a blowing agent. With an additive content lower than 20%, superb flame retardancy (LOI of 31.5% and UL-94 V-0) was reported. Moreover, compared to the compact materials, the flame retardant synergism was less noticeable in the expanded foams. This is attributed to the enlarged contact surface as well as the flame retardant's lower volume concentration [298,299].

In another investigation [301], a novel flame retardant and toughened bio-based (PLA)/glycidyl methacrylate-grafted natural rubber (GNR) composite was reported. The interfacial compatibility between PLA/GNR matrix and the charring ability of the PLA/GNR/SiAHP composites as well as the modified aluminum hypophosphite by silane (SiAHP) was enhanced to a certain extent due to the surface modification of AHP. The flame retardancy and toughness of the PLA/GNR/SiAHP composites were slightly greater than those of PLA/GNR/AHP composites. UL-94 V-0 rating and LOI of 26.50% were reported. The promising flame retardancy of the PLA/GNR/SiAHP composites was suggested to be due to the synergistic effect including condensed and gaseous phase flame-retardant mechanisms. High-performance flame-retardant PLA/GNR/SiAHP composites have great potential applications as alternatives to petroleum-based polymers in the building and automotive interior sectors [301].

Li et al. [302] developed a cooperative flame-retardant system based on natural intumescent-grafted bamboo charcoal (BC) and chitosan (CS) for PLA. Figure 16 shows a schematic diagram of the composite preparation and testing. The composite demonstrated minimal decline in strength properties and enhanced flame retardancy. CS as an adhesion promoter enhanced the interfacial compatibility between PLA and graft modified bamboo charcoal resulting in improving the tensile properties by 8.42% and 11.11%, respectively for the Young's modulus and tensile strength. The study found that CS endorses the reorganization of the internal crystal structure. At 3 wt.% CS and 30 wt.% graft-modified bamboo charcoal, the composite's crystallinity was reported to be 43 times that of neat PLA. Flammability tests (UL-94 V-0 rating and LOI of 33.6 vol.%) showed a substantial enhancement in flame retardancy. The reported composite is claimed to meet the requirements for strong, biodegradable and non-toxic PLA packaging products [302].

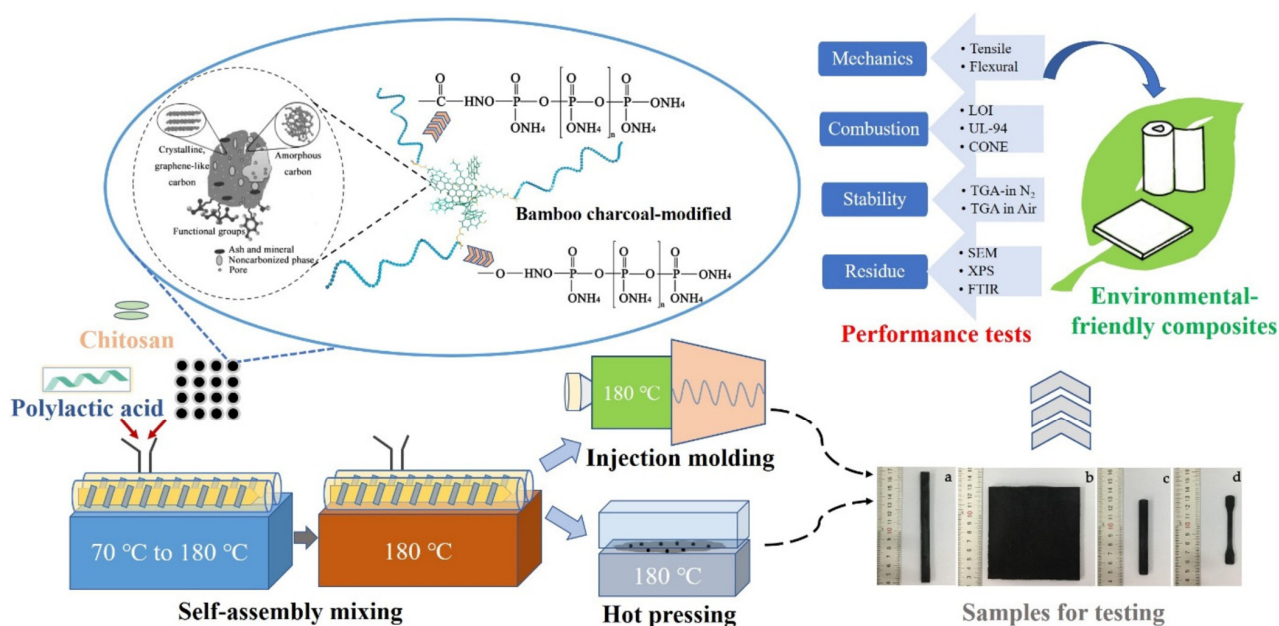


Figure 16. Composite preparation and testing as reported by Li et al. [302].

#### 4.2. PHAs in Active Food Packaging

Technologies that are developed to enhance shelf life, sensory properties and keeps the packaged food safe from mechanical damage as well as microbial contamination are referred to as active food packaging. Bioactive agents (Figure 17) have been used to create edible films with induced desirable functionalities. Figure 18 shows a schematic of active food packaging based on bio nanocomposites with outstanding preservation capability against pathogens and UV irradiation [303]. In one study [304], poly(3-hydroxyalkanoate-co-3-hydroxyalkanoate) (PHAE) (an mcl-PHA) was coated with zosteric acid (nontoxic, antifouling agent) to come up with a PHA-based active food packaging. Exposing the coated PHAE to sewage sludge showed no signs of microbial growth [304]. In another work [305], *Azotobacter chroococcum* 23 was used to synthesize PHB in order to develop a PHA-based active food packaging. Antimicrobial agents, namely chemically synthesized benzoic acid and natural Silbiol were added to the PHB films and PHB-coated paper surface. The PHB films and PHB-coated paper surface exhibited no major antimicrobial activity against Gram-negative and Gram-positive bacterial strains [305]. For the purpose of preventing the antimicrobial agents such as benzoic acid from migrating into the food from the food packaging, Kwiecien et al. [306] produced an active food packaging system based on preservative-oligo (3-HB). Different concentrations of the antimicrobial agent vanillin (4-hydroxy-3-methoxybenzaldehyde) was added to the PHB solution [307]. The antimicrobial potential of the developed films was tested against a variety of bacterial

strains and fungi. Both thermal and mechanical properties of the produced PHB films with and without vanillin were investigated and analyzed. The study concluded that in order to demonstrate antimicrobial activity, the minimum concentration of vanillin required is  $\geq 50 \mu\text{g/g}$  PHB for fungi and  $\geq 80 \mu\text{g/g}$  PHB for bacteria. Furthermore, the elongation at break for the PHB-vanillin exhibited a small increase when compared to that of PHB film. Nonetheless, both of the modulus of elasticity and tensile strength decreased. The rate of migration of vanillin at 37 °C into 50% ethanol and distilled water were 71.736 mg/mL and 65.54 mg/mL, respectively. This might be attributed to the higher temperature and faster migration of vanillin into 50% ethanol than distilled water [307].



Figure 17. Bioactive agents for smart food packaging. Reprinted with permission from Elsevier, 2020 [303].

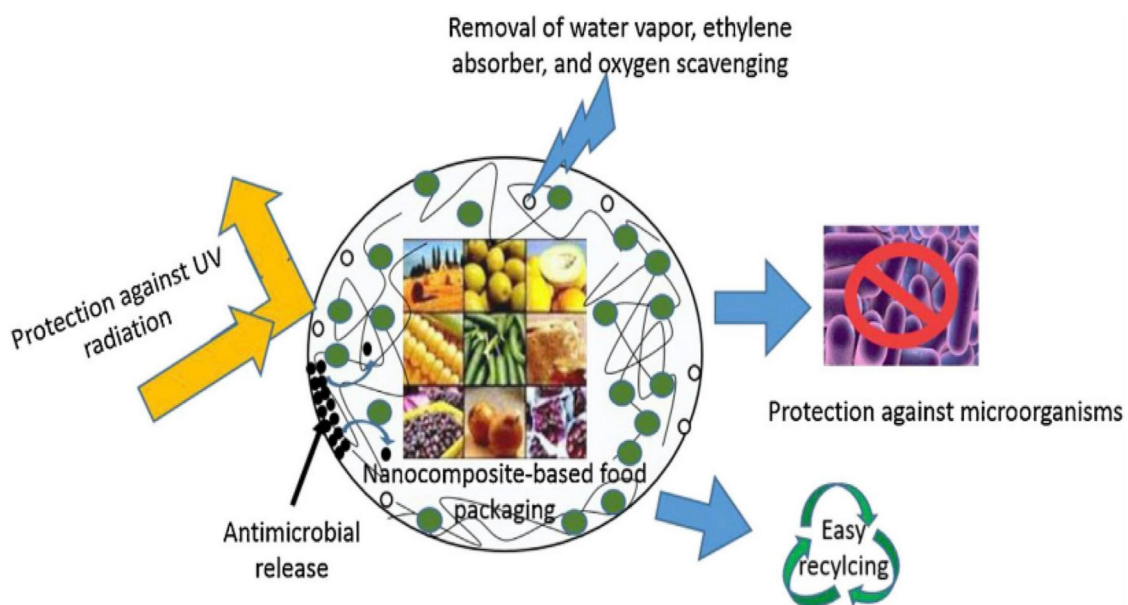


Figure 18. Active food packaging based on bio nanocomposites. Reprinted with permission from Elsevier, 2020 [303].

## 5. Conclusions and Future Insights

PLA is a biodegradable polymer which has a tremendous advantage in overcoming the pollution of plastics following their disposal. PLA can be also produced from agricultural sources which makes it an attractive option over petroleum-based polymers. Due to their nontoxicity, biodegradability and hydrophobicity, PHAs have been widely used in many applications worldwide. Nonetheless, the poor toughness of PLA hinders the widespread use of this polymer in many other applications. PLA-based blends and nanocomposites have been found efficient in enhancing the mechanical properties of PLA. Recently and due to the raised awareness of the environmental concerns, the production of PHAs has been observed to increase significantly. However, the high production cost of PHAs is the main obstacle for expanding their productions to the commercial scale. Blending PHAs with other polymers as well as PHAs based nanocomposites have been reported to be a good option to increase their flexibility and mechanical properties while enhancing/maintaining its biodegradability. The increasing number of additives played a significant role in the development of PLA's and PHAs' physical properties to a high level of performance. Yet, the market for bio-based plastics' additives still lacks solutions for significant properties. For example, investigating the migration behavior of the nano clays, nanoparticles and nanofillers incorporated with PHAs is crucial prior to the use of PHA-based nanocomposites in food packaging. Finally, modified PLA and PHAs have high potential to be used in applications such as drug delivery, tissue engineering, food packaging and bone scaffolds. Furthermore, they have demonstrated good feasibility in structural, automobile, personal care and electronic applications. The wide range of promising properties that these two bio-based polymers offer after modification have paved the way to justify their utilizations today as green biodegradable substitutes to petroleum-based plastics.

**Author Contributions:** Conceptualization, resources, project administration, funding acquisition and supervision, I.D.; methodology, writing—original draft preparation, writing—review and editing, A.Z.N.; editing and review—original and revised drafts, S.Y. and F.D. All authors have read and agreed to the published version of the manuscript.

**Funding:** This research was funded by the Natural Science and Engineering Research Council of Canada (NSERC).

**Acknowledgments:** The authors acknowledge the financial support from The Natural Science and Engineering Research Council of Canada (NSERC). The authors would like to express their sincere gratitude to the editorial team and reviewers for their comments and feedbacks. The first author would like to thank Zeinab Stapić for her support and assistance.

**Conflicts of Interest:** The authors declare no conflict of interest.

## References

1. Sun, X.S. Overview of Plant Polymers: Resources, Demands, and Sustainability. In *Handbook of Biopolymers and Biodegradable Plastics Properties, Processing and Applications*, 1st ed.; Ebnesajjad, S., Ed.; Elsevier: Waltham, MA, USA, 2013.
2. Ashter, S.A. *Introduction to Bioplastics Engineering*, 1st ed.; Elsevier: Cambridge, MA, USA, 2016. [CrossRef]
3. B.F.R. Center. Soybean Car. 1997. Available online: <https://www.thehenryford.org/collections-and-research/digital-resources/popular-topics/soy-bean-car/> (accessed on 10 July 2020).
4. Mohanty, A.K.; Manjusri, M.; Lawrence, T.D. *Natural Fibers, Biopolymers, and Biocomposites*, 1st ed.; CRC Press: Boca Raton, FL, USA, 2005.
5. Gross, R.A.; Kalra, B. Biodegradable polymers for the environment. *Science* **2002**, *297*, 803–807. [CrossRef]
6. Mohanty, A.K.; Misra, M.; Hinrichsen, G. Biofibres, biodegradable polymers and biocomposites: An overview. *Macromol. Mater. Eng.* **2000**, *276–277*, 1–24. [CrossRef]
7. Mohanty, A.K.; Misra, M.; Drzal, L.T. Sustainable Bio-Composites from renewable resources: Opportunities and challenges in the green materials world. *J. Polym. Environ.* **2002**, *10*, 19–26. [CrossRef]
8. Netravali, A.N.; Chabba, S. Composites get greener. *Mater. Today* **2003**, *6*, 22–29. [CrossRef]
9. Rudnik, E. Biodegradability Testing of Compostable Polymer Materials. In *Handbook of Biopolymers and Biodegradable Plastics Properties, Processing and Applications*; Ebnesajjad, S., Ed.; Elsevier: Waltham, MA, USA, 2013.
10. Drumright, R.E.; Gruber, P.R.; Henton, D.E. Polylactic acid technology. *Adv. Mater.* **2000**, *12*, 1841–1846. [CrossRef]

11. Mohanty, A.K.; Wibowo, A.; Misra, M.; Drzal, L.T. Effect of process engineering on the performance of natural fiber reinforced cellulose acetate biocomposites. *Compos. Part A Appl. Sci. Manuf.* **2004**, *35*, 363–370. [CrossRef]
12. Mehta, G.; Mohanty, A.K.; Misra, M.; Drzal, L.T. Biobased resin as a toughening agent for biocomposites. *Green Chem.* **2004**, *6*, 254–258. [CrossRef]
13. Canada One-Step Closer to Zero Plastic Waste by 2030. 2020. Available online: <https://www.canada.ca/en/environment-climate-change/news/2020/10/canada-one-step-closer-to-zero-plastic-waste-by-2030.html> (accessed on 10 April 2021).
14. Clark, J.H.; Deswarte, F.E.I. The Biorefinery Concept-An Integrated Approach. In *Introduction to Chemicals from Biomass*, 1st ed.; John Wiley & Sons Ltd.: Chichester, UK, 2008.
15. Niaounakis, M. *Biopolymers: Applications and Trends*, 1st ed.; Elsevier: Waltham, MA, USA, 2015.
16. Kricheldorf, H.; Dunsing, R. Polylactones, 8. Mechanism of the cationic polymerization of L,L-dilactide. *Die Makromol. Chemie.* **1986**, *187*, 1611–1625. [CrossRef]
17. Maharana, T.; Mohanty, B.; Negi, Y.S. Melt-solid polycondensation of lactic acid and its biodegradability. *Prog. Polym. Sci.* **2009**, *34*, 99–124. [CrossRef]
18. Singhvi, M.S.; Zinjarde, S.S.; Gokhale, D.V. Polylactic acid: Synthesis and biomedical applications. *J. Appl. Microbiol.* **2019**, *127*, 1612–1626. [CrossRef] [PubMed]
19. Gu, S.Y.; Yang, M.; Yu, T.; Ren, T.B.; Ren, J. Synthesis and characterization of biodegradable lactic acid-based polymers by chain extension. *Polym. Int.* **2008**, *57*, 982–986. [CrossRef]
20. Kun, E.; Marossy, K. Effect of crystallinity on PLA's microbiological behaviour. *Mater. Sci. Forum* **2013**, *752*, 241–247. [CrossRef]
21. Tsuji, H.; Ikada, Y. Crystallization from the melt of poly(lactide)s with different optical purities and their blends. *Macromol. Chem. Phys.* **1996**, *197*, 3483–3499. [CrossRef]
22. Garlotta, D. A literature review of poly(lactic acid). *J. Polym. Environ.* **2001**, *9*, 63–84. [CrossRef]
23. Standau, T.; Zhao, C.; Castellón, S.M.; Bonten, C.; Altstädt, V. Chemical modification and foam processing of polylactide (PLA). *Polymers* **2019**, *11*, 306. [CrossRef]
24. Tuominen, J.; Kylmä, J.; Kapanen, A.; Venelampi, O.; Itävaara, M.; Seppälä, J. Biodegradation of lactic acid based polymers under controlled composting conditions and evaluation of the ecotoxicological impact. *Biomacromolecules* **2002**, *3*, 445–455. [CrossRef] [PubMed]
25. Auras, R.; Harte, B.; Selke, S. An overview of polylactides as packaging materials. *Macromol. Biosci.* **2004**, *4*, 835–864. [CrossRef]
26. Massardier-Nageotte, V.; Pestre, C.; Cruard-Pradet, T.; Bayard, R. Aerobic and anaerobic biodegradability of polymer films and physico-chemical characterization. *Polym. Degrad. Stab.* **2006**, *91*, 620–627. [CrossRef]
27. Su, S.; Kopitzky, R.; Tolga, S.; Kabasci, S. Polylactide (PLA) and its blends with poly(butylene succinate) (PBS): A brief review. *Polymers* **2019**, *11*, 1193. [CrossRef]
28. Total Corbion, Our Luminy® PLA Portfolio. 2021. Available online: <https://www.total-corbion.com/luminy-pla-portfolio/> (accessed on 11 September 2021).
29. NatureWorks LLC. Products. 2021. Available online: <https://www.natureworkslc.com/Products> (accessed on 11 September 2021).
30. Loos, K. *Biocatalysis in Polymer Chemistry*, 1st ed.; Wiley-VCH: Weinheim, Germany, 2010. [CrossRef]
31. Griffin, G. *Chemistry and Technology of Biodegradable Polymers*, 1st ed.; Springer: Dordrecht, The Netherlands; London, UK, 1994.
32. Steinbüchel, A.; Valentin, H.E. Diversity of bacterial polyhydroxyalkanoic acids. *FEMS Microbiol. Lett.* **1995**, *128*, 219–228. [CrossRef]
33. Witholt, B.; Kessler, B. Perspectives of medium chain length poly(hydroxyalkanoates), a versatile set of bacterial bioplastics. *Curr. Opin. Biotechnol.* **1999**, *10*, 279–285. [CrossRef]
34. Steinbüchel, A.; Lütke-Eversloh, T. Metabolic engineering and pathway construction for biotechnological production of relevant polyhydroxyalkanoates in microorganisms. *Biochem. Eng. J.* **2003**, *16*, 81–96. [CrossRef]
35. Madison, L.L.; Huisman, G.W. Metabolic Engineering of Poly(3-Hydroxyalkanoates): From DNA to Plastic. *Microbiol. Mol. Biol. Rev.* **1999**, *63*, 21–53. [CrossRef]
36. Shang, L.; Jiang, M.; Chang, H.N. Poly(3-hydroxybutyrate) synthesis in fed-batch culture of *Ralstonia eutropha* with phosphate limitation under different glucose concentrations. *Biotechnol. Lett.* **2003**, *25*, 1415–1419. [CrossRef] [PubMed]
37. Williams, S.F.; Peoples, O.P. Biodegradable plastics from plants. *Chem Tech.* **1996**, *26*, 38–44.
38. Girdhar, A.; Bhatia, M.; Nagpal, S.; Kanampalliwar, A.; Tiwari, A. Process Parameters for Influencing Polyhydroxyalkanoate Producing Bacterial Factories: An Overview. *J. Pet. Environ. Biotechnol.* **2013**, *4*, 1–8. [CrossRef]
39. Lee, S.Y. Plastic bacteria? Progress and prospects for polyhydroxyalkanoate production in bacteria. *Trends Biotechnol.* **1996**, *14*, 431–438. [CrossRef]
40. Chen, G.Q.; Wu, Q. The application of polyhydroxyalkanoates as tissue engineering materials. *Biomaterials* **2005**, *26*, 6565–6578. [CrossRef] [PubMed]
41. Li, Z.; Yang, J.; Loh, X.J. Polyhydroxyalkanoates: Opening doors for a sustainable future. *NPG Asia Mater.* **2016**, *8*, 1–20. [CrossRef]
42. Zinn, M.; Witholt, B.; Egli, T. Occurrence, synthesis and medical application of bacterial polyhydroxyalkanoate. *Adv. Drug Deliv. Rev.* **2001**, *53*, 5–21. [CrossRef]
43. Zhang, M.; Thomas, N.L. Blending polylactic acid with polyhydroxybutyrate: The effect on thermal, mechanical, and biodegradation properties. *Adv. Polym. Technol.* **2011**, *30*, 67–79. [CrossRef]

44. Steinbüchel, A. Perspectives for Biotechnological Production and Utilization of Biopolymers: Metabolic Engineering of Polyhydroxyalkanoate Biosynthesis Pathways as a Successful Example. *Macromol. Biosci.* **2001**, *1*, 1–24. [CrossRef]
45. De Koning, G.J.M.; Lemstra, P.J. Crystallization phenomena in bacterial poly[(R)-3-hydroxybutyrate]: 2. Embrittlement and rejuvenation. *Polymer* **1993**, *34*, 4089–4094. [CrossRef]
46. Rivera-Briso, A.L.; Serrano-Aroca, Á. Poly(3-Hydroxybutyrate-co-3-Hydroxyvalerate): Enhancement strategies for advanced applications. *Polymers* **2018**, *10*, 732. [CrossRef]
47. Fei, B.; Chen, C.; Wu, H.; Peng, S.; Wang, X.; Dong, L.; Xin, J.H. Modified poly(3-hydroxybutyrate-co-3-hydroxyvalerate) using hydrogen bonding monomers. *Polymer* **2004**, *45*, 6275–6284. [CrossRef]
48. Rudnik, E. Compostable polymer materials—Definitions, structures and methods of preparation. In *Compostable Polymer Materials*; Elsevier: Oxford, UK, 2019. [CrossRef]
49. Pilla, S. *Handbook of Bioplastics and Biocomposites Engineering Applications*, 1st ed.; Scrivener Publishing: Beverly, MA, USA, 2011. [CrossRef]
50. Saito, Y.; Doi, Y. Microbial synthesis and properties of poly(3-hydroxybutyrate-co-4-hydroxybutyrate) in *Comamonas acidovorans*. *Int. J. Biol. Macromol.* **1994**, *16*, 99–104. [CrossRef]
51. Goldstein, N. Demystifying Biopolymers And Compostable Packaging. 2020. Available online: <https://www.biocycle.net/demystifying-biopolymers-and-compostable-packaging/> (accessed on 13 June 2021).
52. Farah, S.; Anderson, D.G.; Langer, R. Physical and mechanical properties of PLA, and their functions in widespread applications—A comprehensive review. *Adv. Drug Deliv. Rev.* **2016**, *107*, 367–372. [CrossRef]
53. NatureWorks LLC. *Ingeo™ Biopolymer 2003D, 3052D, and 3801 X Technical Data Sheets*; NatureWorks LLC: Minnetonka, MN, USA, 2018.
54. Naser, A.Z.; Deiab, I.; Darras, B.M. Poly(lactic acid) (PLA) and polyhydroxyalkanoates (PHAs), green alternatives to petroleum-based plastics: A review. *RSC Adv.* **2021**, *28*, 17151–17196. [CrossRef]
55. Daniels, A.U.; Chang, M.K.; Andriano, K.P. Mechanical properties of biodegradable polymers and composites proposed for internal fixation of bone. *J. Appl. Biomater.* **1990**, *1*, 57–78. [CrossRef]
56. Anderson, K.S.; Schreck, K.M.; Hillmyer, M.A. Toughening polylactide. *Polym. Rev.* **2008**, *48*, 85–108. [CrossRef]
57. Mascia, L.; Xanthos, M. An overview of additives and modifiers for polymer blends: Facts, deductions, and uncertainties. *Adv. Polym. Technol.* **1992**, *11*, 237–248. [CrossRef]
58. Sinclair, R.G. The case for polylactic acid as a commodity packaging plastic. *J. Macromol. Sci. Part A Pure Appl. Chem.* **1996**, *33*, 585–597. [CrossRef]
59. Jacobsen, S.; Fritz, H.G. Plasticizing polylactide—The effect of different plasticizers on the mechanical properties. *Polym. Eng. Sci.* **1999**, *39*, 1303–1310. [CrossRef]
60. Martin, O.; Averous, L. Poly(lactic acid): Plasticization and properties of biodegradable multiphase systems. *Polymer* **2001**, *42*, 6209–6219. [CrossRef]
61. Baiardo, M.; Frisoni, G.; Scandola, M.; Rimelen, M.; Lips, D.; Ruffieux, K.; Wintermantel, E. Thermal and mechanical properties of plasticized poly(L-lactic acid). *J. Appl. Polym. Sci.* **2003**, *90*, 1731–1738. [CrossRef]
62. Pillin, I.; Montrelay, N.; Grohens, Y. Thermo-mechanical characterization of plasticized PLA: Is the miscibility the only significant factor? *Polymer* **2006**, *47*, 4676–4682. [CrossRef]
63. Kulinski, Z.; Piorkowska, E.; Gadzinowska, K.; Stasiak, M. Plasticization of poly(L-lactide) with poly(propylene glycol). *Biomacromolecules* **2006**, *7*, 2128–2135. [CrossRef]
64. Nijenhuis, A.J.; Colstee, E.; Grijpma, D.W.; Pennings, A.J. High molecular weight poly(L-lactide) and poly(ethylene oxide) blends: Thermal characterization and physical properties. *Polymer* **1996**, *37*, 5849–5857. [CrossRef]
65. Labrecque, L.V.; Kumar, R.A.; Davé, V.; Gross, R.A.; McCarthy, S.P. Citrate esters as plasticizers for poly(lactic acid). *J. Appl. Polym. Sci.* **1997**, *66*, 1507–1513. [CrossRef]
66. Yoon, J.S.; Oh, S.H.; Kim, M.N.; Chin, I.J.; Kim, Y.H. Thermal and mechanical properties of poly(L-lactic acid)-poly(ethylene co-vinyl acetate) blends. *Polymer* **1999**, *40*, 2303–2312. [CrossRef]
67. Ren, Z.; Dong, L.; Yang, Y. Dynamic mechanical and thermal properties of plasticized poly(lactic acid). *J. Appl. Polym. Sci.* **2006**, *101*, 1583–1590. [CrossRef]
68. Brüster, B.; Adjoua, Y.O.; Dieden, R.; Grysan, P.; Federico, C.E.; Berthé, V.; Addiego, F. Plasticization of polylactide with myrcene and limonene as bio-based plasticizers: Conventional vs. reactive extrusion. *Polymers* **2019**, *11*, 1363. [CrossRef] [PubMed]
69. Chaochanchaikul, K.; Pongmuksuwat, P. Influence of Ozonized Soybean Oil as a Biobased Plasticizer on the Toughness of Polylactic Acid. *J. Polym. Environ.* **2021**, 1–11. [CrossRef]
70. Dominguez-candela, I.; Ferri, J.M.; Cardona, S.C.; Lora, J.; Fombuena, V. Dual plasticizer/thermal stabilizer effect of epoxidized chia seed oil (*Salvia hispanica* L.) to improve ductility and thermal properties of poly(lactic acid). *Polymers* **2021**, *13*, 283. [CrossRef]
71. Llanes, L.C.; Clasen, S.H.; Pires, A.T.N.; Gross, I.P. Mechanical and thermal properties of poly(lactic acid) plasticized with dibutyl maleate and fumarate isomers: Promising alternatives as biodegradable plasticizers. *Eur. Polym. J.* **2021**, *142*, 1–11. [CrossRef]
72. Notta-Cuvier, D.; Odent, J.; Delille, R.; Murariu, M.; Lauro, F.; Raquez, J.M.; Bennani, B.; Dubois, P. Tailoring polylactide (PLA) properties for automotive applications: Effect of addition of designed additives on main mechanical properties. *Polym. Test.* **2014**, *36*, 1–9. [CrossRef]

73. Taib, R.M.; Ghaleb, Z.A.; Mohd Ishak, Z.A. Thermal, mechanical, and morphological properties of polylactic acid toughened with an impact modifier. *J. Appl. Polym. Sci.* **2012**, *123*, 2715–2725. [CrossRef]
74. Barletta, M.; Pizzi, E.; Puopolo, M.; Vesco, S. Design and manufacture of degradable polymers: Biocomposites of micro-lamellar talc and poly(lactic acid). *Mater. Chem. Phys.* **2017**, *196*, 62–74. [CrossRef]
75. Diaz, C.; Pao, H.Y.; Kim, S. Film Performance of Poly(lactic acid) Blends for Packaging Applications. *J. Appl. Packag. Res.* **2016**, *8*, 4.
76. Choochottiros, C.; Chin, I.J. Potential transparent PLA impact modifiers based on PMMA copolymers. *Eur. Polym. J.* **2013**, *49*, 957–966. [CrossRef]
77. Wang, L.; Ma, W.; Gross, R.A.; McCarthy, S.P. Reactive compatibilization of biodegradable blends of poly(lactic acid) and poly( $\epsilon$ -caprolactone). *Polym. Degrad. Stab.* **1998**, *59*, 161–168. [CrossRef]
78. Broz, M.E.; VanderHart, D.L.; Washburn, N.R. Structure and mechanical properties of poly(D,L-lactic acid)/poly( $\epsilon$ -caprolactone) blends. *Biomaterials* **2003**, *24*, 4181–4190. [CrossRef]
79. Odent, J.; Raquez, J.M.; Duquesne, E.; Dubois, P. Random aliphatic copolyesters as new biodegradable impact modifiers for polylactide materials. *Eur. Polym. J.* **2012**, *48*, 331–340. [CrossRef]
80. Liu, H.; Zhang, J. Research progress in toughening modification of poly(lactic acid). *J. Polym. Sci. Part B Polym. Phys.* **2011**, *49*, 1051–1083. [CrossRef]
81. Scaffaro, R.; Morreale, M.; Mirabella, F.; La Mantia, F.P. Preparation and recycling of plasticized PLA. *Macromol. Mater. Eng.* **2011**, *296*, 141–150. [CrossRef]
82. Murariu, M.; Da Silva Ferreira, A.; Duquesne, E.; Bonnaud, L.; Dubois, P. Polylactide (PLA) and highly filled PLA—Calcium sulfate composites with improved impact properties. *Macromol. Symp.* **2008**, *272*, 1–12. [CrossRef]
83. Afrifah, K.A.; Matuana, L.M. Impact modification of polylactide with a biodegradable ethylene/acrylate copolymer. *Macromol. Mater. Eng.* **2010**, *295*, 802–811. [CrossRef]
84. PARALOID™ BPM-520 Impact Modifier. 2021. Available online: <https://www.dow.com/en-us/pdp.paraloid-bpm-520-impact-modifier.185484z.html> (accessed on 29 June 2021).
85. Niaounakis, M. *Biopolymers: Processing and Products*, 1st ed.; Elsevier: Oxford, UK, 2015.
86. Qin, Y. Applications of advanced technologies in the development of functional medical textile materials. In *Medical Textile Materials*, 1st ed.; Woodhead Publishing: London, UK, 2016. [CrossRef]
87. Vogel, C.; Wessel, E.; Siesler, H.W. FT-IR spectroscopic imaging of anisotropic poly(3-hydroxybutyrate)/poly(lactic acid) blends with polarized radiation. *Macromolecules* **2008**, *41*, 2975–2977. [CrossRef]
88. Furukawa, T.; Sato, H.; Murakami, R.; Zhang, J.; Duan, Y.X.; Noda, I.; Ochiai, S.; Ozaki, Y. Structure, dispersibility, and crystallinity of poly(hydroxybutyrate)/poly(L-lactic acid) blends studied by FT-IR microspectroscopy and differential scanning calorimetry. *Macromolecules* **2005**, *38*, 6445–6454. [CrossRef]
89. Ohkoshi, I.; Abe, H.; Doi, Y. Miscibility and solid-state structures for blends of poly[(S)-lactide] with atactic poly[(R,S)-3-hydroxybutyrate]. *Polymer* **2000**, *41*, 5985–5992. [CrossRef]
90. Blümm, E.; Owen, A.J. Miscibility, crystallization and melting of poly(3-hydroxybutyrate)/poly(l-lactide) blends. *Polymer* **1995**, *36*, 4077–4081. [CrossRef]
91. Iannace, S.; Ambrosio, L.; Huang, S.J.; Nicolais, L. Poly(3-hydroxybutyrate)-co-(3-hydroxyvalerate)/Poly-L-lactide blends: Thermal and mechanical properties. *J. Appl. Polym. Sci.* **1994**, *54*, 1525–1536. [CrossRef]
92. Ferreira, B.M.P.; Zavaglia, C.A.C.; Duek, E.A.R. Films of PLLA/PHBV: Thermal, morphological, and mechanical characterization. *J. Appl. Polym. Sci.* **2002**, *86*, 2898–2906. [CrossRef]
93. Yoon, J.S.; Lee, W.S.; Kim, K.S.; Chin, I.J.; Kim, M.N.; Kim, C. Effect of poly(ethylene glycol)-block-poly(L-lactide) on the poly[(R)-3-hydroxybutyrate]/poly(L-lactide) blends. *Eur. Polym. J.* **2000**, *36*, 435–442. [CrossRef]
94. Takagi, Y.; Yasuda, R.; Yamaoka, M.; Yamane, T. Morphologies and mechanical properties of polylactide blends with medium chain length poly(3-hydroxyalkanoate) and chemically modified poly(3-hydroxyalkanoate). *J. Appl. Polym. Sci.* **2004**, *93*, 2363–2369. [CrossRef]
95. Noda, I.; Satkowski, M.M.; Dowrey, A.E.; Marcott, C. Polymer alloys of nodax copolymers and poly(lactic acid). *Macromol. Biosci.* **2004**, *4*, 269–275. [CrossRef]
96. Schreck, K.M.; Hillmyer, M.A. Block copolymers and melt blends of polylactide with Nodax™ microbial polyesters: Preparation and mechanical properties. *J. Biotechnol.* **2007**, *132*, 287–295. [CrossRef] [PubMed]
97. Bartczak, Z.; Galeski, A.; Kowalczyk, M.; Sobota, M.; Malinowski, R. Tough blends of poly(lactide) and amorphous poly[(R,S)-3-hydroxy butyrate]—Morphology and properties. *Eur. Polym. J.* **2013**, *49*, 3630–3641. [CrossRef]
98. Nanda, M.R.; Misra, M.; Mohanty, A.K. The effects of process engineering on the performance of PLA and PHBV blends. *Macromol. Mater. Eng.* **2011**, *273*, 719–728. [CrossRef]
99. Noda, I.; Green, P.R.; Satkowski, M.M.; Schechtman, L.A. Preparation and properties of a novel class of polyhydroxyalkanoate copolymers. *Biomacromolecules* **2005**, *6*, 580–586. [CrossRef] [PubMed]
100. Zhao, Q.; Wang, S.; Kong, M.; Geng, W.; Li, R.K.Y.; Song, C.; Kong, D. Phase morphology, physical properties, and biodegradation behavior of novel PLA/PHBHHx blends. *J. Biomed. Mater. Res. Part B Appl. Biomater.* **2012**, *100*, 23–31. [CrossRef]
101. Rasal, R.M.; Hirt, D.E. Toughness decrease of PLA-PHBHHx blend films upon surface-confined photopolymerization. *J. Biomed. Mater. Res. Part A* **2009**, *88*, 1079–1086. [CrossRef]



102. Lim, J.S.; Park, K.I.; Chung, G.S.; Kim, J.H. Effect of composition ratio on the thermal and physical properties of semicrystalline PLA/PHB-HHx composites. *Mater. Sci. Eng. C* **2013**, *33*, 2131–2137. [CrossRef]
103. Arrieta, M.P.; Fortunati, E.; Dominici, F.; López, J.; Kenny, J.M. Bionanocomposite films based on plasticized PLA-PHB/cellulose nanocrystal blends. *Carbohydr. Polym.* **2015**, *121*, 265–275. [CrossRef]
104. El-Hadi, A.M. Development of novel biopolymer blends based on poly(L-lactic acid), poly((R)-3-hydroxybutyrate), and plasticizer. *Polym. Eng. Sci.* **2014**, *54*, 1394–1402. [CrossRef]
105. Arrieta, M.P.; López, J.; Rayón, E.; Jiménez, A. Disintegrability under composting conditions of plasticized PLA–PHB blends. *Polym. Degrad. Stab.* **2014**, *108*, 307–318. [CrossRef]
106. Arrieta, M.P.; Fortunati, E.; Dominici, F.; Rayón, E.; López, J.; Kenny, J.M. Multifunctional PLA-PHB/cellulose nanocrystal films: Processing, structural and thermal properties. *Carbohydr. Polym.* **2014**, *107*, 16–24. [CrossRef]
107. Arrieta, M.P.; López, J.; Hernández, A.; Rayón, E. Ternary PLA-PHB-Limonene blends intended for biodegradable food packaging applications. *Eur. Polym. J.* **2014**, *50*, 255–270. [CrossRef]
108. Abdelwahab, M.A.; Flynn, A.; Chiou, B.S.; Imam, S.; Orts, W.; Chiellini, E. Thermal, mechanical and morphological characterization of plasticized PLA-PHB blends. *Polym. Degrad. Stab.* **2012**, *97*, 1822–1828. [CrossRef]
109. Guessasma, S.; Belhabib, S.; Nouri, H. Thermal cycling, microstructure and tensile performance of PLA-PHA polymer printed using fused deposition modelling technique. *Rapid Prototyp. J.* **2020**, *26*, 122–133. [CrossRef]
110. Olejnik, O.; Masek, A.; Zawadzko, J. Processability and mechanical properties of thermoplastic polylactide/polyhydroxybutyrate (PLA/PHB) bioblends. *Materials* **2021**, *14*, 898. [CrossRef] [PubMed]
111. Hiljanen-Vainio, M.; Varpomaa, P.; Seppälä, J.; Törmälä, P. Modification of poly(L-lactides) by blending: Mechanical and hydrolytic behavior. *Macromol. Chem. Phys.* **1996**, *197*, 1503–1523. [CrossRef]
112. Tsuji, H.; Ikada, Y. Blends of aliphatic polyesters. I. Physical properties and morphologies of solution-cast blends from poly(DL-lactide) and poly( $\epsilon$ -caprolactone). *J. Appl. Polym. Sci.* **1996**, *60*, 2367–2375. [CrossRef]
113. Maglio, G.; Migliozi, A.; Palumbo, R.; Immirzi, B.; Volpe, M.G. Compatibilized poly( $\epsilon$ -caprolactone)/poly(L-lactide) blends for biomedical uses. *Macromol. Rapid Commun.* **1999**, *20*, 236–238. [CrossRef]
114. Tsuji, H.; Yamada, T.; Suzuki, M.; Itsuno, S. Blends of aliphatic polyesters. Part 7. Effects of poly(L-lactide-co- $\epsilon$ -caprolactone) on morphology, structure, crystallization, and physical properties of blends of poly(L-lactide) and poly( $\epsilon$ -caprolactone). *Polym. Int.* **2003**, *52*, 269–275. [CrossRef]
115. Semba, T.; Kitagawa, K.; Ishiaku, U.S.; Hamada, H. The effect of crosslinking on the mechanical properties of polylactic acid/polycaprolactone blends. *J. Appl. Polym. Sci.* **2006**, *101*, 1816–1825. [CrossRef]
116. Grijpma, D.W.; Van Hofslot, R.D.A.; Supèr, H.; Nijenhuis, A.J.; Pennings, A.J. Rubber toughening of poly(lactide) by blending and block copolymerization. *Polym. Eng. Sci.* **1994**, *34*, 1674–1684. [CrossRef]
117. Joziassse, C.A.P.; Topp, M.D.C.; Pennings, D.W.G.J. Rubber toughened linear and star-shaped. *Polymer* **1998**, *39*, 467–474. [CrossRef]
118. Chen, C.C.; Chueh, J.Y.; Tseng, H.; Huang, H.M.; Lee, S.Y. Preparation and characterization of biodegradable PLA polymeric blends. *Biomaterials* **2003**, *24*, 1167–1173. [CrossRef]
119. Hasook, A.; Tanoue, S.; Lemoto, Y.; Unryu, T. Characterization and mechanical properties of poly(lactic acid)/poly( $\epsilon$ -caprolactone)/organoclay nanocomposites prepared by melt compounding. *Polym. Eng. Sci.* **2006**, *46*, 1001–1007. [CrossRef]
120. Jeantet, L.; Regazzi, A.; Taguet, A.; Pucci, M.F.; Caro, A.S.; Quantin, J.C. Biopolymer blends for mechanical property gradient 3D printed parts. *Express Polym. Lett.* **2021**, *15*, 137–152. [CrossRef]
121. Doganci, M.D. Effects of star-shaped PCL having different numbers of arms on the mechanical, morphological, and thermal properties of PLA/PCL blends. *J. Polym. Res.* **2021**, *28*, 1–13. [CrossRef]
122. Ebrahimi, M.; Taherimehr, M. Evaluation of in-vitro drug release of polyvinylcyclohexane carbonate as a CO<sub>2</sub>-derived degradable polymer blended with PLA and PCL as drug carriers. *J. Drug Deliv. Sci. Technol.* **2021**, *63*, 1–13. [CrossRef]
123. Yang, Z.T.; Yang, J.X.; Fan, J.H.; Feng, Y.H.; Huang, Z.X. Preparation of super-toughened Poly(L-lactide) composites under elongational flow: A strategy for balancing stiffness and ductility. *Compos. Sci. Technol.* **2021**, *208*, 1–8. [CrossRef]
124. Pezzin, A.P.T.; Alberda van Ekenstein, G.O.R.; Zavaglia, C.A.C.; Ten Brinke, G.; Duek, E.A.R. Poly(para-dioxanone) and poly(l-lactic acid) blends: Thermal, mechanical, and morphological properties. *J. Appl. Polym. Sci.* **2003**, *88*, 2744–2755. [CrossRef]
125. Ma, X.; Jiugao, Y.; Wang, N. Compatibility characterization of poly(lactic acid)/poly(propylene carbonate) blends. *J. Polym. Sci. Part B Polym. Phys.* **2006**, *44*, 94–101. [CrossRef]
126. Liu, T.Y.; Lin, W.C.; Yang, M.C.; Chen, S.Y. Miscibility, thermal characterization and crystallization of poly(l-lactide) and poly(tetramethylene adipate-co-terephthalate) blend membranes. *Polymer* **2005**, *46*, 12586–12594. [CrossRef]
127. Jiang, L.; Wolcott, M.P.; Zhang, J. Study of biodegradable polylactide/poly(butylene adipate-co-terephthalate) blends. *Biomacromolecules* **2006**, *7*, 199–207. [CrossRef]
128. Liu, X.; Dever, M.; Fair, N.; Benson, R.S. Thermal and mechanical properties of poly(lactic acid) and poly(ethylene/butylene succinate) blends. *J. Environ. Polym. Degrad.* **1997**, *5*, 225–235. [CrossRef]
129. Shibata, M.; Inoue, Y.; Miyoshi, M. Mechanical properties, morphology, and crystallization behavior of blends of poly(l-lactide) with poly(butylene succinate-co-l-lactate) and poly(butylene succinate). *Polymer* **2006**, *47*, 3557–3564. [CrossRef]
130. Chen, G.X.; Kim, H.S.; Kim, E.S.; Yoon, J.S. Compatibilization-like effect of reactive organoclay on the poly(l-lactide)/poly(butylene succinate) blends. *Polymer* **2005**, *46*, 11829–11836. [CrossRef]

131. Chen, C.X.; Yoon, J.S. Morphology and thermal properties of poly(L-lactide)/poly (butylene succinate-co-butylene adipate) compounded with twice functionalized clay. *J. Polym. Sci. Part B Polym. Phys.* **2005**, *43*, 478–487. [CrossRef]
132. Shibata, M.; Teramoto, N.; Inoue, Y. Mechanical properties, morphologies, and crystallization behavior of plasticized poly(l-lactide)/poly(butylene succinate-co-l-lactate) blends. *Polymer* **2007**, *48*, 2768–2777. [CrossRef]
133. Zhang, L.; Xiong, C.; Deng, X. Miscibility, crystallization and morphology of poly( $\beta$ -hydroxybutyrate)/poly(d,l-lactide) blends. *Polymer* **1996**, *37*, 235–241. [CrossRef]
134. Jandas, P.J.; Mohanty, S.; Nayak, S.K. Sustainability, compostability, and specific microbial activity on agricultural mulch films prepared from poly(lactic acid). *Ind. Eng. Chem. Res.* **2013**, *52*, 17714–17724. [CrossRef]
135. Burgos, N.; Armentano, I.; Fortunati, E.; Dominici, F.; Luzi, F.; Fiori, S.; Cristofaro, F.; Visai, L.; Jiménez, A.; Kenny, J.M. Functional Properties of Plasticized Bio-Based Poly(Lactic Acid)\_Poly(Hydroxybutyrate) (PLA\_PHB) Films for Active Food Packaging. *Food Bioprocess Technol.* **2017**, *10*, 770–780. [CrossRef]
136. Xie, L.; Xu, H.; Niu, B.; Ji, X.; Chen, J.; Li, Z.M.; Hsiao, B.S.; Zhong, G.J. Unprecedented access to strong and ductile poly(lactic acid) by introducing in situ nanofibrillar poly(butylene succinate) for green packaging. *Biomacromolecules* **2014**, *15*, 4054–4064. [CrossRef] [PubMed]
137. Fortunati, E.; Puglia, D.; Iannoni, A.; Terenzi, A.; Kenny, J.M.; Torre, L. Processing conditions, thermal and mechanical responses of stretchable poly (lactic acid)/poly (butylene succinate) films. *Materials* **2017**, *10*, 809. [CrossRef] [PubMed]
138. Ostafinska, A.; Fortelny, I.; Nevoralova, M.; Hodan, J.; Kredatusova, J.; Slouf, M. Synergistic effects in mechanical properties of PLA/PCL blends with optimized composition, processing, and morphology. *RSC Adv.* **2015**, *120*, 98971–98982. [CrossRef]
139. Jost, V.; Kopitzky, R. Blending of polyhydroxybutyrate-co-valerate with polylactic acid for packaging applications—Reflections on miscibility and effects on the mechanical and barrier properties. *Chem. Biochem. Eng. Q.* **2015**, *29*, 221–246. [CrossRef]
140. Luzi, F.; Fortunati, E.; Jiménez, A.; Puglia, D.; Pezzolla, D.; Gigliotti, G.; Kenny, J.M.; Chiralt, A.; Torre, L. Production and characterization of PLA\_PBS biodegradable blends reinforced with cellulose nanocrystals extracted from hemp fibres. *Ind. Crop. Prod.* **2016**, *93*, 276–289. [CrossRef]
141. Songtipya, L.; Limchu, T.; Phuttharak, S.; Songtipya, P.; Kalkornsurapranee, E. Poly(lactic acid)-based Composites Incorporated with Spent Coffee Ground and Tea Leave for Food Packaging Application: A Waste to Wealth. In *IOP Conference Series: Materials Science and Engineering*; IOP Publishing: Bristol, UK, 2019. [CrossRef]
142. Ma, Y.; Li, L.; Wang, Y. Development of PLA-PHB-based biodegradable active packaging and its application to salmon. *Packag. Technol. Sci.* **2018**, *31*, 739–746. [CrossRef]
143. Hongsriphan, N.; Sanga, S. Antibacterial food packaging sheets prepared by coating chitosan on corona-treated extruded poly(lactic acid)/poly(butylene succinate) blends. *J. Plast. Film Sheeting* **2018**, *34*, 160–178. [CrossRef]
144. Zhang, K.; Mohanty, A.K.; Misra, M. Fully biodegradable and biorenewable ternary blends from polylactide, poly(3-hydroxybutyrate-co-hydroxyvalerate) and poly(butylene succinate) with balanced properties. *ACS Appl. Mater. Interfaces* **2012**, *4*, 3091–3101. [CrossRef]
145. Balakrishnan, H.; Hassan, A.; Wahit, M.U.; Yussuf, A.A.; Razak, S.B.A. Novel toughened polylactic acid nanocomposite: Mechanical, thermal and morphological properties. *Mater. Des.* **2010**, *31*, 3289–3298. [CrossRef]
146. Lee, J.H.; Park, T.G.; Park, H.S.; Lee, D.S.; Lee, Y.K.; Yoon, S.C.; Nam, J.D. Thermal and mechanical characteristics of poly(L-lactic acid) nanocomposite scaffold. *Biomaterials* **2003**, *24*, 2773–2778. [CrossRef]
147. Jiang, L.; Zhang, J.; Wolcott, M.P. Comparison of polylactide/nano-sized calcium carbonate and polylactide/montmorillonite composites: Reinforcing effects and toughening mechanisms. *Polymer* **2007**, *48*, 7632–7644. [CrossRef]
148. Harris, A.M.; Lee, E.C. Improving mechanical performance of injection molded PLA by controlling crystallinity. *J. Appl. Polym. Sci.* **2008**, *107*, 2246–2255. [CrossRef]
149. Yu, F.; Liu, T.; Zhao, X.; Yu, X.; Lu, A.; Wang, J. Effects of talc on the mechanical and thermal properties of polylactide. *J. Appl. Polym. Sci.* **2012**, *125*, E99–E109. [CrossRef]
150. Ouchiar, S.; Stoclet, G.; Cabaret, C.; Georges, E.; Smith, A.; Martias, C.; Addad, A.; Gloaguen, V. Comparison of the influence of talc and kaolinite as inorganic fillers on morphology, structure and thermomechanical properties of polylactide based composites. *Appl. Clay Sci.* **2015**, *116–117*, 231–240. [CrossRef]
151. Zhou, Y.; Lei, L.; Yang, B.; Li, J.; Ren, J. Preparation and characterization of polylactic acid (PLA) carbon nanotube nanocomposites. *Polym. Test.* **2018**, *68*, 34–38. [CrossRef]
152. Wang, L.; Qiu, J.; Sakai, E.; Wei, X. The relationship between microstructure and mechanical properties of carbon nanotubes/polylactic acid nanocomposites prepared by twin-screw extrusion. *Compos. Part A Appl. Sci. Manuf.* **2016**, *89*, 18–25. [CrossRef]
153. Silva, A.P.B.; Montagna, L.S.; Passador, F.R.; Rezende, M.C.; Lemes, A.P. Biodegradable nanocomposites based on PLA/PHBV blend reinforced with carbon nanotubes with potential for electrical and electromagnetic applications. *Express Polym. Lett.* **2021**, *15*, 987–1003. [CrossRef]
154. Chen, P.Y.; Lian, H.Y.; Shih, Y.F.; Chen-Wei, S.M.; Jeng, R.J. Preparation, characterization and crystallization kinetics of Kenaf fiber/multi-walled carbon nanotube/polylactic acid (PLA) green composites. *Mater. Chem. Phys.* **2017**, *196*, 249–255. [CrossRef]
155. Quan, H.; Li, Z.M.; Yang, M.B.; Huang, R. On transcrystallinity in semi-crystalline polymer composites. *Compos. Sci. Technol.* **2005**, *65*, 999–1021. [CrossRef]

156. Reverte, J.M.; Caminero, M.Á.; Chacón, J.M.; García-Plaza, E.; Núñez, P.J.; Becar, J.P. Mechanical and geometric performance of PLA-based polymer composites processed by the fused filament fabrication additive manufacturing technique. *Materials* **2020**, *13*, 1924. [CrossRef] [PubMed]
157. Wootthikanokkhan, J.; Cheachun, T.; Sombatsompop, N.; Thumsorn, S.; Kaabbuathong, N.; Wongta, N.; Wong-On, J.; Na Ayutthaya, S.I.; Kositchaiyong, A. Crystallization and thermomechanical properties of PLA composites: Effects of additive types and heat treatment. *J. Appl. Polym. Sci.* **2013**, *129*, 215–223. [CrossRef]
158. Ahmed, W.; Siraj, S.; Al-Marzouqi, A.H. 3d printing pla waste to produce ceramic based particulate reinforced composite using abundant silica-sand: Mechanical properties characterization. *Polymers* **2020**, *12*, 2579. [CrossRef] [PubMed]
159. Swaroop, C.; Shukla, M. Nano-magnesium oxide reinforced polylactic acid biofilms for food packaging applications. *Int. J. Biol. Macromol.* **2018**, *113*, 729–736. [CrossRef]
160. John, M.J.; Anandjiwala, R.D. Recent developments in chemical modification and characterization of natural fiber-reinforced composites. *Polym. Compos.* **2008**, *29*, 187–207. [CrossRef]
161. Foruzanmehr, M.; Vuillaume, P.Y.; Elkoun, S.; Robert, M. Physical and mechanical properties of PLA composites reinforced by TiO<sub>2</sub> grafted flax fibers. *Mater. Des.* **2016**, *106*, 295–304. [CrossRef]
162. Lee, B.H.; Kim, H.S.; Lee, S.; Kim, H.J.; Dorgan, J.R. Bio-composites of kenaf fibers in polylactide: Role of improved interfacial adhesion in the carding process. *Compos. Sci. Technol.* **2009**, *69*, 15–16. [CrossRef]
163. Kumar, R.; Yakabu, M.K.; Anandjiwala, R.D. Effect of montmorillonite clay on flax fabric reinforced poly lactic acid composites with amphiphilic additives. *Compos. Part A Appl. Sci. Manuf.* **2010**, *41*, 1620–1627. [CrossRef]
164. Kanakannavar, S.; Pitchaimani, J. Fracture toughness of flax braided yarn woven PLA composites. *Int. J. Polym. Anal. Charact.* **2021**, *26*, 364–379. [CrossRef]
165. Wang, A.; Qi, R.; Xiong, C.; Huang, M. Effects of coupling agent and interfacial modifiers on mechanical properties of poly(lactic acid) and wood flour biocomposites. *Iran. Polym. J. Engl. Ed.* **2011**, *20*, 281–294.
166. Da Silva, W.A.; Luna, C.B.B.; de Melo, J.B.d.C.A.; Araújo, E.M.; Filho, E.A.d.S.; Duarte, R.N.C. Feasibility of Manufacturing Disposable Cups using PLA/PCL Composites Reinforced with Wood Powder. *J. Polym. Environ.* **2021**, *29*, 2932–2951. [CrossRef]
167. Wasti, S.; Triggs, E.; Farag, R.; Auad, M.; Adhikari, S.; Bajwa, D.; Li, M.; Ragauskas, A.J. Influence of plasticizers on thermal and mechanical properties of biocomposite filaments made from lignin and polylactic acid for 3D printing. *Compos. Part B Eng.* **2021**, *205*, 1–8. [CrossRef]
168. Paul, U.C.; Fragouli, D.; Bayer, I.S.; Zych, A.; Athanassiou, A. Effect of Green Plasticizer on the Performance of Microcrystalline Cellulose/Poly(lactic acid) Biocomposites. *ACS Appl. Polym. Mater.* **2021**, *3*, 3071–3081. [CrossRef]
169. Rasheed, M.; Jawaid, M.; Parveez, B. Bamboo fiber based cellulose nanocrystals/poly(Lactic acid)/poly(butylene succinate) nanocomposites: Morphological, mechanical and thermal properties. *Polymers* **2021**, *13*, 1076. [CrossRef]
170. Frone, A.N.; Batalu, D.; Chiulan, I.; Oprea, M.; Gabor, A.R.; Nicolae, C.A.; Raditoiu, V.; Trusca, R.; Panaitescu, D.M. Morpho-structural, thermal and mechanical properties of PLA/PHB/Cellulose biodegradable nanocomposites obtained by compression molding, extrusion, and 3d printing. *Nanomaterials* **2020**, *10*, 51. [CrossRef]
171. Alam, F.; Verma, P.; Mohammad, W.; Teo, J.; Varadarajan, K.M.; Kumar, S. Architected poly(lactic acid)/poly( $\epsilon$ -caprolactone)/halloy site nanotube composite scaffolds enabled by 3D printing for biomedical applications. *J. Mater. Sci.* **2021**, *56*, 14070–14083. [CrossRef]
172. Komal, U.K.; Lila, M.K.; Singh, I. Processing of PLA/pineapple fiber based next generation composites. *Mater. Manuf. Process.* **2021**, *36*, 1–16. [CrossRef]
173. Mohamad, S.N.K.; Ramli, I.; Abdullah, L.C.; Mohamed, N.H.; Islam, M.S.; Ibrahim, N.A.; Ishak, N.S. Evaluation on structural properties and performances of graphene oxide incorporated into chitosan/poly-lactic acid composites: Cs/pla versus cs/pla-go. *Polymers* **2021**, *13*, 1839. [CrossRef]
174. McChalicher, C.W.J.; Srienc, F. Investigating the structure-property relationship of bacterial PHA block copolymers. *J. Biotechnol.* **2007**, *123*, 296–302. [CrossRef]
175. Sudesh, K.; Iwata, T. Sustainability of biobased and biodegradable plastics. *Clean Soil Air Water* **2008**, *36*, 433–442. [CrossRef]
176. Philip, S.; Keshavarz, T.; Roy, I. Polyhydroxyalkanoates: Biodegradable polymers with a range of applications. *J. Chem. Technol. Biotechnol.* **2007**, *82*, 233–247. [CrossRef]
177. Khanna, S.; Srivastava, A.K. Recent advances in microbial polyhydroxyalkanoates. *Process Biochem.* **2005**, *40*, 607–619. [CrossRef]
178. Rai, R.; Keshavarz, T.; Roether, J.A.; Boccaccini, A.R.; Roy, I. Medium chain length polyhydroxyalkanoates, promising new biomedical materials for the future. *Mater. Sci. Eng. R Rep.* **2011**, *72*, 29–47. [CrossRef]
179. Bugnicourt, E.; Cinelli, P.; Lazzeri, A.; Alvarez, V. Polyhydroxyalkanoate (PHA): Review of synthesis, characteristics, processing and potential applications in packaging. *Express Polym. Lett.* **2014**, *8*, 791–808. [CrossRef]
180. Kushwah, B.S.; Kushwah, A.V.S.; Singh, V. Towards understanding polyhydroxyalkanoates and their use. *J. Polym. Res.* **2016**, *23*, 1–14. [CrossRef]
181. Bucci, D.Z.; Tavares, L.B.B.; Sell, I. PHB packaging for the storage of food products. *Polym. Test.* **2005**, *24*, 564–571. [CrossRef]
182. Aldor, I.S.; Kim, S.W.; Jones Prather, K.L.; Keasling, J.D. Metabolic engineering of a novel propionate-independent pathway for the production of poly(3-hydroxybutyrate-co-3-hydroxyvalerate) in recombinant *Salmonella enterica* serovar typhimurium. *Appl. Environ. Microbiol.* **2002**, *68*, 3848–3854. [CrossRef]

183. Ha, C.S.; Cho, W.J. Miscibility, properties, and biodegradability of microbial polyester containing blends. *Prog. Polym. Sci.* **2002**, *27*, 759–809. [CrossRef]
184. Ohashi, E.; Drumond, W.S.; Zane, N.P.; Barros, P.W.D.F.; Lachtermacher, M.G.; Wiebeck, H.; Wang, S.H. Biodegradable poly(3-hydroxybutyrate) nanocomposite. *Macromol. Symp.* **2009**, *279*, 138–144. [CrossRef]
185. Sudesh, K.; Abe, H.; Doi, Y. Synthesis, structure and properties of polyhydroxyalkanoates: Biological polyesters. *Prog. Polym. Sci.* **2000**, *25*, 1503–1555. [CrossRef]
186. La Cara, F.; Immirzi, B.; Ionata, E.; Mazzella, A.; Portofino, S.; Orsello, G.; De Prisco, P.P. Biodegradation of poly- $\epsilon$ -caprolactone/poly- $\beta$ -hydroxybutyrate blend. *Polym. Degrad. Stab.* **2003**, *79*, 37–43. [CrossRef]
187. Lovera, D.; Márquez, L.; Balsamo, V.; Taddei, A.; Castelli, C.; Müller, A.J. Crystallization, morphology, and enzymatic degradation of polyhydroxybutyrate/polycaprolactone (PHB/PCL) blends. *Macromol. Chem. Phys.* **2007**, *208*, 924–937. [CrossRef]
188. Gonçalves, S.P.C.; Martins Franchetti, S.M. Respirometric evaluation of the biodegradability of films of PE/PHBV blends. *Int. J. Mater. Sci.* **2013**, *11*, 54–60.
189. Masood, F.; Yasin, T.; Hameed, A. Comparative oxo-biodegradation study of poly-3-hydroxybutyrate-co-3-hydroxyvalerate/polypropylene blend in controlled environments. *Int. Biodeterior. Biodegrad.* **2014**, *87*, 1–8. [CrossRef]
190. Gonçalves, S.P.C.; Martins-Franchetti, S.M.; Chinaglia, D.L. Biodegradation of the films of PP, PHBV and its blend in soil. *J. Polym. Environ.* **2009**, *17*, 280–285. [CrossRef]
191. Burlein, G.A.D.; Rocha, M.C.G. Mechanical and morphological properties of LDPE/PHB blends filled with castor oil pressed cake. *Mater. Res.* **2014**, *17*, 97–105. [CrossRef]
192. Quental, A.C.; de Carvalho, F.P.; Rezende, M.L.; Rosa, D.S.; Felisberti, M.I. Aromatic/Aliphatic Polyester Blends. *J. Polym. Environ.* **2010**, *18*, 308–317. [CrossRef]
193. Ma, P.; Hristova-Bogaerds, D.G.; Lemstra, P.J.; Zhang, Y.; Wang, S. Toughening of PHBV/PBS and PHB/PBS blends via in situ compatibilization using dicumyl peroxide as a free-radical grafting initiator. *Macromol. Mater. Eng.* **2012**, *297*, 402–410. [CrossRef]
194. Zhao, H.; Cui, Z.; Wang, X.; Turng, L.S.; Peng, X. Processing and characterization of solid and microcellular poly(lactic acid)/polyhydroxybutyrate-valerate (PLA/PHBV) blends and PLA/PHBV/Clay nanocomposites. *Compos. Part B Eng.* **2013**, *51*, 79–91. [CrossRef]
195. Garcia-Garcia, D.; Ferri, J.M.; Boronat, T.; Lopez-Martinez, J.; Balart, R. Processing and characterization of binary poly(hydroxybutyrate) (PHB) and poly(caprolactone) (PCL) blends with improved impact properties. *Polym. Bull.* **2016**, *73*, 3333–3350. [CrossRef]
196. Chee, M.J.K.; Ismail, J.; Kammer, H.W.; Kummerloöwe, C. Study on miscibility of PEO and PCL in blends with PHB by solution viscometry. *Polymer* **2001**, *43*, 1235–1239. [CrossRef]
197. Nishida, M.; Tanaka, T.; Hayakawa, Y.; Ogura, T.; Ito, Y.; Nishida, M. Multi-scale instrumental analyses of plasticized polyhydroxyalkanoates (PHA) blended with polycaprolactone (PCL) and the effects of crosslinkers and graft copolymers. *RSC Adv.* **2019**, *9*, 1551–1561. [CrossRef]
198. Mendibil, X.; González-Pérez, F.; Bazan, X.; Díez-Ahedo, R.; Quintana, I.; Rodríguez, F.J.; Basnett, P.; Nigmatullin, R.; Lukasiwicz, B.; Roy, I.; et al. Bioresorbable and Mechanically Optimized Nerve Guidance Conduit Based on a Naturally Derived Medium Chain Length Polyhydroxyalkanoate and Poly( $\epsilon$ -Caprolactone) Blend. *ACS Biomater. Sci. Eng.* **2021**, *7*, 672–689. [CrossRef]
199. Qiu, Z.; Ikehara, T.; Nishi, T. Poly(hydroxybutyrate)/poly(butylene succinate) blends: Miscibility and nonisothermal crystallization. *Polymes* **2003**, *44*, 2503–2508. [CrossRef]
200. Qiu, Z.; Ikehara, T.; Nishi, T. Miscibility and crystallization behaviour of biodegradable blends of two aliphatic polyesters. Poly(3-hydroxybutyrate-co-3-hydroxyvalerate) and poly(butylene succinate) blends. *Polymer* **2003**, *44*, 7519–7527. [CrossRef]
201. Meléndez-Rodríguez, B.; Torres-Giner, S.; Reis, M.A.M.; Silva, F.; Matos, M.; Cabedo, L.; Lagarón, J.M. Blends of poly(3-hydroxybutyrate-co-3-hydroxyvalerate) with fruit pulp biowaste derived poly(3-hydroxybutyrate-co-3-hydroxyvalerate-co-3-hydroxyhexanoate) for organic recycling food packaging. *Polymers* **2021**, *13*, 1155. [CrossRef]
202. Lim, S.T.; Hyun, Y.H.; Lee, C.H.; Choi, H.J. Preparation and characterization of microbial biodegradable poly(3-hydroxybutyrate)/organoclay nanocomposite. *J. Mater. Sci. Lett.* **2003**, *22*, 299–302. [CrossRef]
203. Shan, G.F.; Gong, X.; Chen, W.P.; Chen, L.; Zhu, M.F. Effect of multi-walled carbon nanotubes on crystallization behavior of poly(3-hydroxybutyrate-co-3-hydroxyvalerate). *Colloid Polym. Sci.* **2011**, *289*, 1005–1014. [CrossRef]
204. Lai, M.; Li, J.; Yang, J.; Liu, J.; Tong, X.; Cheng, H. The morphology and thermal properties of multi-walled carbon nanotube and poly(hydroxybutyrate-co-hydroxyvalerate) composite. *Polym. Int.* **2004**, *53*, 1479–1484. [CrossRef]
205. Maiti, P.; Batt, C.A.; Giannelis, E.P. New biodegradable polyhydroxybutyrate/layered silicate nanocomposites. *Biomacromolecules* **2007**, *8*, 3393–3400. [CrossRef]
206. Wang, S.; Song, C.; Chen, G.; Guo, T.; Liu, J.; Zhang, B.; Takeuchi, S. Characteristics and biodegradation properties of poly(3-hydroxybutyrate-co-3-hydroxyvalerate)/organophilic montmorillonite (PHBV/OMMT) nanocomposite. *Polym. Degrad. Stab.* **2005**, *87*, 69–76. [CrossRef]
207. Chen, G.X.; Hao, G.J.; Guo, T.Y.; Song, M.D.; Zhang, B.H. Crystallization kinetics of poly(3-hydroxybutyrate-co-3-hydroxyvalerate)/clay nanocomposites. *J. Appl. Polym. Sci.* **2004**, *93*, 655–661. [CrossRef]
208. Botana, A.; Mollo, M.; Eisenberg, P.; Torres Sanchez, R.M. Effect of modified montmorillonite on biodegradable PHB nanocomposites. *Appl. Clay Sci.* **2010**, *47*, 263–270. [CrossRef]

209. Carli, L.N.; Crespo, J.S.; Mauler, R.S. PHBV nanocomposites based on organomodified montmorillonite and halloysite: The effect of clay type on the morphology and thermal and mechanical properties. *Compos. Part A Appl. Sci. Manuf.* **2011**, *42*, 1601–1608. [CrossRef]
210. Misra, M.; Desai, S.M.; Mohanty, A.K.; Drzal, L.T. Novel solvent-free method for functionalization of polyhydroxyalkanoates: Synthesis and characterizations. In Proceedings of the Annual Technical Conference—ANTEC, Chicago, IL, USA, 16–20 May 2004.
211. Martínez-Sanz, M.; Villano, M.; Oliveira, C.; Albuquerque, M.G.E.; Majone, M.; Reis, M.; Lopez-Rubio, A.; Lagaron, J.M. Characterization of polyhydroxyalkanoates synthesized from microbial mixed cultures and of their nanobiocomposites with bacterial cellulose nanowhiskers. *N. Biotechnol.* **2014**, *31*, 364–376. [CrossRef]
212. Ten, E.; Turtle, J.; Bahr, D.; Jiang, L.; Wolcott, M. Thermal and mechanical properties of poly(3-hydroxybutyrate-co-3-hydroxyvalerate)/cellulose nanowhiskers composites. *Polymer* **2010**, *51*, 2652–2660. [CrossRef]
213. Jiang, L.; Morelius, E.; Zhang, J.; Wolcott, M.; Holbery, J. Study of the poly(3-hydroxybutyrate-co-3-hydroxyvalerate)/cellulose nanowhisker composites prepared by solution casting and melt processing. *J. Compos. Mater.* **2008**, *42*, 2629–2645. [CrossRef]
214. Xie, Y.; Kohls, D.; Noda, I.; Schaefer, D.W.; Akpalu, Y.A. Poly(3-hydroxybutyrate-co-3-hydroxyhexanoate) nanocomposites with optimal mechanical properties. *Polymer* **2009**, *50*, 4656–4670. [CrossRef]
215. Sanchez-Garcia, M.D.; Lagaron, J.M.; Hoa, S.V. Effect of addition of carbon nanofibers and carbon nanotubes on properties of thermoplastic biopolymers. *Compos. Sci. Technol.* **2010**, *70*, 1095–1105. [CrossRef]
216. Jo, J.; Kim, H.; Jeong, S.Y.; Park, C.; Hwang, H.S.; Koo, B. Changes in mechanical properties of polyhydroxyalkanoate with double silanized cellulose nanocrystals using different organosiloxanes. *Nanomaterials* **2021**, *11*, 1542. [CrossRef]
217. Liao, H.T.; Wu, C.S. Poly(3-hydroxybutyrate)/multi-walled carbon nanotubes nanocomposites: Preparation and characterizations. *Des. Monomers Polym.* **2013**, *16*, 99–107. [CrossRef]
218. Jin, X.; Fan, Y.; Xue, Y.; Wu, L.; Lu, Y.; Chen, J.; Wang, X.; Dong, D.; Meng, F.; Lu, Y.; et al. Electrospun CF-PHA nanocomposites: Effect of surface modifications of carbon fibers. *Int. J. Polym. Mater. Polym. Biomater.* **2014**, *63*, 262–267. [CrossRef]
219. Gumel, A.M.; Annuar, M.S.M.; Ishak, K.A.; Ahmad, N. Carbon nanofibers-poly-3-hydroxyalkanoates nanocomposite: Ultrasound-assisted dispersion and thermostructural properties. *J. Nanomater.* **2014**, *2014*, 1–10. [CrossRef]
220. Cataldi, P.; Steiner, P.; Raine, T.; Lin, K.; Kocabas, C.; Young, R.J.; Bissett, M.; Kinloch, I.A.; Papageorgiou, D.G. Multifunctional Biocomposites Based on Polyhydroxyalkanoate and Graphene/Carbon Nanofiber Hybrids for Electrical and Thermal Applications. *ACS Appl. Polym. Mater.* **2020**, *2*, 3525–3534. [CrossRef]
221. Kotnis, M.A.; O'Brien, G.S.; Willett, J.L. Processing and mechanical properties of biodegradable Poly(hydroxybutyrate-co-valerate)-starch compositions. *J. Environ. Polym. Degrad.* **1995**, *3*, 97–105. [CrossRef]
222. Shogren, R.L. Poly(ethylene oxide)-coated granular starch-poly(hydroxybutyrate-co-hydroxyvalerate) composite materials. *J. Environ. Polym. Degrad.* **1995**, *3*, 75–80. [CrossRef]
223. Koller, I.; Owen, A.J. Starch-filled PHB and PHB/HV copolymer. *Polym. Int.* **1996**, *39*, 175–181. [CrossRef]
224. Rosa, D.D.S.; Rodrigues, T.C.; Das Graças Fassina Guedes, C.; Calil, M.R. Effect of thermal aging on the biodegradation of PCL, PHB-V, and their blends with starch in soil compost. *J. Appl. Polym. Sci.* **2003**, *89*, 3539–3546. [CrossRef]
225. Ramsay, B.A.; Langlade, V.; Carreau, P.J.; Ramsay, J.A. Biodegradability and mechanical properties of poly-( $\beta$ -hydroxybutyrate-co- $\beta$ -hydroxyvalerate)-starch blends. *Appl. Environ. Microbiol.* **1993**, *59*, 1242–1246. [CrossRef]
226. Avella, M.; Errico, M.E.; Rimedio, R.; Sadocco, P. Preparation of biodegradable polyesters/high-amylose-starch composites by reactive blending and their characterization. *J. Appl. Polym. Sci.* **2002**, *83*, 1432–1442. [CrossRef]
227. Innocentini-Mei, L.H.; Bartoli, J.R.; Baltieri, R.C. Mechanical and thermal properties of poly(3-hydroxybutyrate) blends with starch and starch derivatives. In *Macromolecular Symposia*; Wiley: Weinheim, Germany, 2003.
228. Willett, J.L.; Kotnis, M.A.; O'Brien, G.S.; Fanta, G.F.; Gordon, S.H. Properties of starch-graft-poly(glycidyl methacrylate)-PHBV composites. *J. Appl. Polym. Sci.* **1998**, *70*, 1121–1127. [CrossRef]
229. Liao, H.T.; Wu, C.S. Performance of an acrylic-acid-grafted poly(3-hydroxybutyric acid)/starch bio-blend: Characterization and physical properties. *Des. Monomers Polym.* **2007**, *10*, 1–18. [CrossRef]
230. Koenig, M.F.; Huang, S.J. Biodegradable blends and composites of polycaprolactone and starch derivatives. *Polymer* **1995**, *36*, 1877–1882. [CrossRef]
231. Zhang, L.; Deng, X.; Zhao, S.; Huang, Z. Biodegradable polymer blends of poly(3-hydroxybutyrate) and starch acetate. *Polym. Int.* **1997**, *44*, 104–110. [CrossRef]
232. Seves, A.; Beltrame, P.L.; Selli, E.; Bergamasco, L. Morphology and thermal behaviour of poly(3-hydroxybutyrate-co-hydroxyvalerate)/starch valerate blends. *Angew. Makromol. Chem.* **1998**, *260*, 65–70. [CrossRef]
233. Godbole, S.; Gote, S.; Latkar, M.; Chakrabarti, T. Preparation and characterization of biodegradable poly-3-hydroxybutyrate-starch blend films. *Bioresour. Technol.* **2003**, *86*, 33–37. [CrossRef]
234. Reis, K.C.; Pereira, J.; Smith, A.C.; Carvalho, C.W.P.; Wellner, N.; Yakimets, I. Characterization of polyhydroxybutyrate-hydroxyvalerate (PHB-HV)/maize starch blend films. *J. Food Eng.* **2008**, *89*, 361–369. [CrossRef]
235. Zhang, M.; Thomas, N.L. Preparation and properties of polyhydroxybutyrate blended with different types of starch. *J. Appl. Polym. Sci.* **2009**, *116*, 688–694. [CrossRef]
236. Parulekar, Y.; Mohanty, A.K. Extruded biodegradable cast films from polyhydroxyalkanoate and thermoplastic starch blends: Fabrication and characterization. *Macromol. Mater. Eng.* **2007**, *292*, 1218–1228. [CrossRef]

237. Martin, O.; Schwach, E.; Avérous, L.; Couturier, Y. Properties of biodegradable multilayer films based on plasticized wheat starch. *Starch/Stärke* **2001**, *53*, 372–380. [CrossRef]
238. Wang, L.; Shogren, R.L.; Carriere, C. Preparation and properties of thermoplastic starch-polyester laminate sheets by coextrusion. *Polym. Eng. Sci.* **2000**, *40*, 499–506. [CrossRef]
239. Lawton, J.W. Biodegradable Coatings for Thermoplastic Starch. In *Cereals: Novel Uses and Processes*, 1st ed.; Springer: New York, NY, USA, 1997.
240. Willett, J.L.; Shogren, R.L. Processing and properties of extruded starch/polymer foams. *Polymer* **2002**, *43*, 5935–5947. [CrossRef]
241. Gordon, S.H.; Imam, S.H.; Shogren, R.L.; Govind, N.S.; Greene, R.V. Semiempirical model for predicting biodegradation profiles of individual polymers in starch-poly( $\beta$ -hydroxybutyrate-co- $\beta$ -hydroxyvalerate) bioplastic. *J. Appl. Polym. Sci.* **2000**, *76*, 1767–1776. [CrossRef]
242. Allen, A.L.; Mayer, J.; Stote, R.; Kaplan, D.L. Simulated marine respirometry of biodegradable polymers. *J. Environ. Polym. Degrad.* **1994**, *2*, 237–244. [CrossRef]
243. Vikman, M.; Itävaara, M.; Poutanen, K. Measurement of the biodegradation of starch-based materials by enzymatic methods and composting. *J. Environ. Polym. Degrad.* **1995**, *3*, 23–29. [CrossRef]
244. Yasin, M.; Holland, S.J.; Jolly, A.M.; Tighe, B.J. Polymers for biodegradable medical devices. VI. Hydroxybutyrate-hydroxyvalerate copolymers: Accelerated degradation of blends with polysaccharides. *Biomaterials* **1989**, *10*, 400–412. [CrossRef]
245. Tanna, S.T.; Gross, R.; McCarthy, S.P. Biodegradation of blends of bacterial polyester and starch in a compost environment. *Polym. Mater. Sci. Eng. Proc. ACS Div. Polym. Mater. Sci. Eng.* **1992**.
246. Lauzier, C.; Monasterios, C.; Saracovan, I.; Marchessault, R.; Ramsay, B. Film formation and paper coating with poly( $\beta$ -hydroxyalkanoate), a biodegradable latex. *Tappi J.* **1993**, *76*.
247. Yasin, M.; Tighe, B.J. Strategies for the design of biodegradable polymer systems: Manipulation of polyhydroxybutyrate-based materials. *Plast. Rubber Compos. Process. Appl.* **1993**, *19*, 15–27.
248. Imam, S.H.; Gordon, S.H.; Shogren, R.L.; Greene, R.V. Biodegradation of starch-poly( $\beta$ -hydroxybutyrate-co-valerate) composites in municipal activated sludge. *J. Environ. Polym. Degrad.* **1995**, *3*, 205–213. [CrossRef]
249. Imam, S.H.; Chen, L.; Gordon, S.H.; Shogren, R.L.; Weisleder, D.; Greene, R.V. Biodegradation of injection molded starch-poly(3-hydroxybutyrate-co-3-hydroxyvalerate) blends in a natural compost environment. *J. Environ. Polym. Degrad.* **1998**, *6*, 91–98. [CrossRef]
250. Imam, S.H.; Gordon, S.H.; Shogren, R.L.; Tosteson, T.R.; Govind, N.S.; Greene, R.V. Degradation of starch-poly( $\beta$ -hydroxybutyrate-co- $\beta$ -hydroxyvalerate) bioplastic in tropical coastal waters. *Appl. Environ. Microbiol.* **1999**, *65*, 431–437. [CrossRef] [PubMed]
251. Kaihara, S.; Osanai, Y.; Nishikawa, K.; Toshima, K.; Doi, Y.; Matsumura, S. Enzymatic transformation of bacterial polyhydroxyalkanoates into repolymerizable oligomers directed towards chemical recycling. *Macromol. Biosci.* **2005**, *5*, 644–652. [CrossRef]
252. Reddy, C.S.K.; Ghai, R.; Kalia, V.C. Polyhydroxyalkanoates: An overview. *Bioresour. Technol.* **2003**, *87*, 137–146. [CrossRef]
253. Patel, M.; Narayan, R. How sustainable are biopolymers and biobased products? The hope, the doubts, and the reality. In *Natural Fibers, Biopolymers, and Biocomposites*, 1st ed.; Taylor & Francis: Boca Raton, FL, USA, 2005. [CrossRef]
254. Bruzaud, S.; Bourmaud, A. Thermal degradation and (nano)mechanical behavior of layered silicate reinforced poly(3-hydroxybutyrate-co-3-hydroxyvalerate) nanocomposites. *Polym. Test.* **2007**, *26*, 652–659. [CrossRef]
255. Hsu, S.F.; Wu, T.M.; Liao, C.S. Nonisothermal crystallization behavior and crystalline structure of poly(3-hydroxybutyrate)/layered double hydroxide nanocomposites. *J. Polym. Sci. Part B Polym. Phys.* **2007**, *45*, 995–1002. [CrossRef]
256. Bruno, M.; Tavares, M.I.B.; Motta, L.M.; Miguez, E.; Preto, M.; Fernandez, A.O.R. Evaluation of PHB/clay nanocomposite by spin-lattice relaxation time. *Mater. Res.* **2008**, *11*, 483–485. [CrossRef]
257. Erceg, M.; Kovačić, T.; Klarić, I. Poly(3-hydroxybutyrate) nanocomposites: Isothermal degradation and kinetic analysis. *Thermochim. Acta* **2009**, *485*, 26–32. [CrossRef]
258. Erceg, M.; Kovačić, T.; Sanja, P. Isothermal degradation of poly(3-hydroxybutyrate)/organically modified montmorillonite nanocomposites. *Polym. Compos.* **2010**, *31*, 272–278. [CrossRef]
259. Parulekar, Y.; Mohanty, A.K.; Imam, S.H. Biodegradable nanocomposites from toughened polyhydroxybutyrate and titanate-modified montmorillonite clay. *J. Nanosci. Nanotechnol.* **2007**, *7*, 3580–3589. [CrossRef]
260. Hablot, E.; Bordes, P.; Pollet, E.; Avérous, L. Thermal and thermo-mechanical degradation of poly(3-hydroxybutyrate)-based multiphase systems. *Polym. Degrad. Stab.* **2008**, *93*, 413–421. [CrossRef]
261. Sanchez-Garcia, M.D.; Gimenez, E.; Lagaron, J.M. Morphology and barrier properties of nanobiocomposites of poly(3-hydroxybutyrate) and layered silicates. *J. Appl. Polym. Sci.* **2008**, *108*, 2787–2801. [CrossRef]
262. Maiti, P.; Prakash Yadav, J.P. Renewable plastics: Synthesis and properties of PHB nanocomposites. *Polym. Mater. Sci. Eng.* **2003**, *88*, 58–59.
263. Pavlidou, S.; Papaspyrides, C.D. A review on polymer-layered silicate nanocomposites. *Prog. Polym. Sci.* **2008**, *33*, 1119–1198. [CrossRef]
264. Choi, W.M.; Kim, T.W.; Park, O.O.; Chang, Y.K.; Lee, J.W. Preparation and characterization of poly(hydroxybutyrate-co-hydroxyvalerate)-organoclay nanocomposites. *J. Appl. Polym. Sci.* **2003**, *90*, 525–529. [CrossRef]

265. Zhang, X.; Lin, G.; Abou-Hussein, R.; Hassan, M.K.; Noda, I.; Mark, J.E. Some novel layered-silicate nanocomposites based on a biodegradable hydroxybutyrate copolymer. *Eur. Polym. J.* **2007**, *43*, 3128–3135. [CrossRef]
266. Wu, T.M.; Hs, S.F.; Shih, Y.F.; Liao, C.S. Thermal degradation kinetics of biodegradable poly(3-hydroxybutyrate)/layered double hydroxide nanocomposites. *J. Polym. Sci. Part B Polym. Phys.* **2008**, *46*, 1207–1213. [CrossRef]
267. Dagnon, K.L.; Chen, H.H.; Innocentini-Mei, L.H.; D'Souza, N.A. Poly[(3-hydroxybutyrate)-co-(3-hydroxyvalerate)]/layered double hydroxide nanocomposites. *Polym. Int.* **2009**, *58*, 133–141. [CrossRef]
268. Dufresne, A.; Kellerhals, M.B.; Witholt, B. Transcrystallization in Mcl-PHAs/cellulose whiskers composites. *Macromolecules* **1999**, *32*, 7396–7401. [CrossRef]
269. Chen, G.X.; Hao, G.J.; Guo, T.Y.; Song, M.D.; Zhang, B.H. Structure and mechanical properties of poly(3-hydroxybutyrate-co-3-hydroxyvalerate) (PHBV)/clay nanocomposites. *J. Mater. Sci. Lett.* **2002**, *21*, 1587–1589. [CrossRef]
270. Thellen, C.; Coyne, M.; Froio, D.; Auerbach, M.; Wirsén, C.; Ratto, J.A. A processing, characterization and marine biodegradation study of melt-extruded polyhydroxyalkanoate (PHA) films. *J. Polym. Environ.* **2008**, *16*, 1–11. [CrossRef]
271. Gregorova, A.; Wimmer, R.; Hrabalova, M.; Koller, M.; Ters, T.; Mundigler, N. Effect of surface modification of beech wood flour on mechanical and thermal properties of poly (3-hydroxybutyrate)/wood flour composites. *Holzforschung* **2009**, *63*, 565–570. [CrossRef]
272. Sinha Ray, S.; Okamoto, M. Polymer/layered silicate nanocomposites: A review from preparation to processing. *Prog. Polym. Sci.* **2003**, *28*, 1539–1641. [CrossRef]
273. Gigante, V.; Seggiani, M.; Cinelli, P.; Signori, F.; Vania, A.; Navarini, L.; Amato, G.; Lazzeri, A. Utilization of coffee silverskin in the production of Poly(3-hydroxybutyrate-co-3-hydroxyvalerate) biopolymer-based thermoplastic biocomposites for food contact applications. *Compos. Part A Appl. Sci. Manuf.* **2021**, *140*, 1–10. [CrossRef]
274. Tian, J.; Zhang, R.; Wu, Y.; Xue, P. Additive manufacturing of wood flour/polyhydroxyalkanoates (PHA) fully bio-based composites based on micro-screw extrusion system. *Mater. Des.* **2021**, *199*, 1–14. [CrossRef]
275. Wu, C.S.; Wu, D.Y.; Wang, S.S. Biodegradable Composite Nanofiber Containing Fish-Scale Extracts. *ACS Appl. Bio Mater.* **2021**, *4*, 462–469. [CrossRef]
276. de Almeida Neto, G.R.; Barcelos, M.V.; Ribeiro, M.E.A.; Folly, M.M.; Rodríguez, R.J.S. Formulation and characterization of a novel PHBV nanocomposite for bone defect filling and infection treatment. *Mater. Sci. Eng. C* **2019**, *104*, 1–13. [CrossRef]
277. Shahi, S.; Karbasi, S.; Ahmadi, T.; Naeimi, F.; Goodarzi, V.; Ebrahimi-Barough, S. Evaluation of physical, mechanical and biological properties of  $\beta$ -tri-calcium phosphate/Poly-3-hydroxybutyrate nano composite scaffold for bone tissue engineering application. *Mater. Technol.* **2021**, *36*, 237–249. [CrossRef]
278. Koyama, R.; Kuboki, T.; Ding, W.D.; Adhikary, K.B.; Chen, N.; Park, C.B. Extrusion foaming of cellulose fiber reinforced polylactic acid biocomposites. In Proceedings of the Annual Technical Conference—ANTEC, Boston, MA, USA, 1–5 May 2011.
279. Cho, S.Y.; Park, H.H.; Yun, Y.S.; Jin, H.J. Influence of cellulose nanofibers on the morphology and physical properties of poly(lactic acid) foaming by supercritical carbon dioxide. *Macromol. Res.* **2013**, *21*, 529–533. [CrossRef]
280. Oluwabunmi, K.; D'Souza, N.A.; Zhao, W.; Choi, T.Y.; Theyson, T. Compostable, fully biobased foams using PLA and micro cellulose for zero energy buildings. *Sci. Rep.* **2020**, *10*, 1–20. [CrossRef]
281. Matuana, L.M.; Faruk, O. Effect of gas saturation conditions on the expansion ratio of microcellular poly (lactic acid)/wood-flour composites. *Express Polym. Lett.* **2010**, *4*, 621–631. [CrossRef]
282. Rizvi, R.; Cochrane, B.; Naguib, H.; Lee, P.C. Fabrication and characterization of melt-blended polylactide-chitin composites and their foams. *J. Cell. Plast.* **2011**, *47*, 283–300. [CrossRef]
283. Ding, W.D.; Kuo, P.Y.; Kuboki, T.; Park, C.B.; Sain, M. Foaming of cellulose fiber reinforced polylactic acid composites: The effect of cellulose fiber type. In Proceedings of the Annual Technical Conference—ANTEC, Cincinnati, OH, USA, 22–24 April 2013.
284. Neagu, R.C.; Cuénoud, M.; Berthold, F.; Bourban, P.E.; Gamstedt, E.K.; Lindström, M.; Månson, J.A.E. The potential of wood fibers as reinforcement in cellular biopolymers. *J. Cell. Plast.* **2012**, *48*, 71–103. [CrossRef]
285. Matuana, L.M.; Diaz, C.A. Strategy to produce microcellular foamed poly(lactic acid)/wood-flour composites in a continuous extrusion process. *Ind. Eng. Chem. Res.* **2013**, *52*, 12032–12040. [CrossRef]
286. Bergeret, A.; Benezet, J.C. Natural fibre-reinforced biofoams. *Int. J. Polym. Sci.* **2011**, *2011*, 1–14. [CrossRef]
287. Pilla, S.; Kramschuster, A.; Lee, J.; Auer, G.K.; Gong, S.; Turng, L.S. Microcellular and solid polylactide-flax fiber composites. *Compos. Interfaces* **2009**, *16*, 869–890. [CrossRef]
288. Zafar, M.T.; Zarrinbakhsh, N.; Mohanty, A.K.; Misra, M.; Ghosh, A.K. Biocomposites based on poly(Lactic acid)/willow-fiber and their injection moulded microcellular foams. *Express Polym. Lett.* **2016**, *10*, 176–186. [CrossRef]
289. Noorani, R. *3D Printing Technology, Applications, and Selection*, 1st ed.; CRC Press: Boca Raton, FL, USA, 2018.
290. Horvath, J. *Mastering 3D Printing*, 1st ed.; Apress: New York, NY, USA, 2014.
291. Yan, Q.; Dong, H.; Su, J.; Han, J.; Song, B.; Wei, Q.; Shi, Y. A Review of 3D Printing Technology for Medical Applications. *Engineering* **2018**, *4*, 729–742. [CrossRef]
292. Kikuchi, M.; Suetsugu, Y.; Tanaka, J.; Akao, M. Preparation and mechanical properties of calcium phosphate/copoly-L-lactide composites. *J. Mater. Sci. Mater. Med.* **1997**, *8*, 361–364. [CrossRef]
293. Niaza, K.V.; Senatov, F.S.; Kaloshkin, S.D.; Maksimkin, A.V.; Chukov, D.I. 3D-printed scaffolds based on PLA/HA nanocomposites for trabecular bone reconstruction. In *Proceedings of the Journal of Physics: Conference Series*; IOP Publishing: Bristol, UK, 2016; pp. 1–5.

294. Gregor, A.; Filová, E.; Novák, M.; Kronek, J.; Chlup, H.; Buzgo, M.; Blahnová, V.; Lukášová, V.; Bartoš, M.; Nečas, A.; et al. Designing of PLA scaffolds for bone tissue replacement fabricated by ordinary commercial 3D printer. *J. Biol. Eng.* **2017**, *11*, 1–21. [CrossRef]
295. Zhu, H.; Zhu, Q.; Li, J.; Tao, K.; Xue, L.; Yan, Q. Synergistic effect between expandable graphite and ammonium polyphosphate on flame retarded polylactide. *Polym. Degrad. Stab.* **2011**, *96*, 183–189. [CrossRef]
296. Ke, C.H.; Li, J.; Fang, K.Y.; Zhu, Q.L.; Zhu, J.; Yan, Q.; Wang, Y.Z. Synergistic effect between a novel hyperbranched charring agent and ammonium polyphosphate on the flame retardant and anti-dripping properties of polylactide. *Polym. Degrad. Stab.* **2010**, *95*, 763–770. [CrossRef]
297. Tang, G.; Zhang, R.; Wang, X.; Wang, B.; Song, L.; Hu, Y.; Gong, X. Enhancement of flame retardant performance of bio-based polylactic acid composites with the incorporation of aluminum hypophosphite and expanded graphite. *J. Macromol. Sci. Part A Pure Appl. Chem.* **2013**, *50*, 255–269. [CrossRef]
298. Wang, K.; Wang, J.; Zhao, D.; Zhai, W. Preparation of microcellular poly(lactic acid) composites foams with improved flame retardancy. *J. Cell. Plast.* **2017**, *53*, 45–63. [CrossRef]
299. Wang, J.; Ren, Q.; Zheng, W.; Zhai, W. Improved flame-retardant properties of poly(lactic acid) foams using starch as a natural charring agent. *Ind. Eng. Chem. Res.* **2014**, *53*, 1422–1430. [CrossRef]
300. Vadas, D.; Igricz, T.; Sarazin, J.; Bourbigot, S.; Marosi, G.; Bocz, K. Flame retardancy of microcellular poly(lactic acid) foams prepared by supercritical CO<sub>2</sub>-assisted extrusion. *Polym. Degrad. Stab.* **2018**, *153*, 100–108. [CrossRef]
301. Wu, N.; Yu, J.; Lang, W.; Ma, X.; Yang, Y. Flame retardancy and toughness of poly(lactic acid)/GNR/SiAHP composites. *Polymers* **2019**, *11*, 1129. [CrossRef] [PubMed]
302. Li, W.; Zhang, L.; Chai, W.; Yin, N.; Semple, K.; Li, L.; Zhang, W.; Dai, C. Enhancement of flame retardancy and mechanical properties of polylactic acid with a biodegradable fire-retardant filler system based on bamboo charcoal. *Polymers* **2021**, *13*, 2167. [CrossRef] [PubMed]
303. Asgher, M.; Qamar, S.A.; Bilal, M.; Iqbal, H.M.N. Bio-based active food packaging materials: Sustainable alternative to conventional petrochemical-based packaging materials. *Food Res. Int.* **2020**, *137*, 1–12. [CrossRef] [PubMed]
304. Hany, R.; Böhlen, C.; Geiger, T.; Schmid, M.; Zinn, M. Toward non-toxic antifouling: Synthesis of hydroxy-cinnamic acid-, sulfate-, and zosteric acid-labeled poly[3-hydroxyalkanoates]. *Biomacromolecules* **2004**, *5*, 1452–1456. [CrossRef]
305. Gonta, S.; Savenkova, L.; Krallish, I.; Kirilova, E. Antimicrobial Activity of PHB Based Polymeric Compositions. *Environ. Eng. Manag. J.* **2012**, *11*, 99–104.
306. Kwiecień, I.; Adamus, G.; Bartkowiak, A.; Kowalczyk, M. Synthesis and structural characterization at the molecular level of oligo(3-hydroxybutyrate) conjugates with antimicrobial agents designed for food packaging materials. *Des. Monomers Polym.* **2014**, *17*, 311–321. [CrossRef]
307. Xavier, J.R.; Babusha, S.T.; George, J.; Ramana, K.V. Material Properties and Antimicrobial Activity of Polyhydroxybutyrate (PHB) Films Incorporated with Vanillin. *Appl. Biochem. Biotechnol.* **2015**, *176*, 1498–1510. [CrossRef] [PubMed]





## Article

# Poly(Alkylene 2,5-Thiophenedicarboxylate) Polyesters: A New Class of Bio-Based High-Performance Polymers for Sustainable Packaging

Giulia Guidotti <sup>1</sup>, Michelina Soccio <sup>1,2,\*</sup>, Massimo Gazzano <sup>3</sup>, Valentina Siracusa <sup>4</sup> and Nadia Lotti <sup>1,2,5,\*</sup>

<sup>1</sup> Department of Civil, Chemical, Environmental and Materials Engineering, University of Bologna, Via Terracini 28, 40131 Bologna, Italy; giulia.guidotti9@unibo.it

<sup>2</sup> Interdepartmental Center for Industrial Research on Advanced Applications in Mechanical Engineering and Materials Technology, CIRI-MAM, University of Bologna, 40126 Bologna, Italy

<sup>3</sup> Institute of Organic Synthesis and Photoreactivity, ISOF-CNR, Via Gobetti 101, 40129 Bologna, Italy; massimo.gazzano@isof.cnr.it

<sup>4</sup> Department of Chemical Science, University of Catania, Viale A. Doria 6, 95125 Catania, Italy; vsiracus@dmfci.unict.it

<sup>5</sup> Interdepartmental Center for Agro-Food Research, CIRI-AGRO, University of Bologna, 40126 Bologna, Italy

\* Correspondence: m.soccio@unibo.it (M.S.); nadia.lotti@unibo.it (N.L.)

**Abstract:** In the present study, 100% bio-based polyesters of 2,5-thiophenedicarboxylic acid were synthesized via two-stage melt polycondensation using glycols containing 3 to 6 methylene groups. The so-prepared samples were characterised from the molecular point of view and processed into free-standing thin films. Afterward, both the purified powders and the films were subjected to structural and thermal characterisation. In the case of thin films, mechanical response and barrier properties to O<sub>2</sub> and CO<sub>2</sub> were also evaluated. From the results obtained, it emerged that the length of glycolic sub-units is an effective tool to modulate the chain mobility and, in turn, the kind and amount of ordered phases developed in the samples. In addition to the usual amorphous and 3D crystalline phases, in all the samples investigated it was possible to evidence a further phase characterised by a lower degree of order (mesophase) than the crystalline one, whose amount is strictly related to the glycol sub-unit length. The relative fraction of all these phases is responsible for the different mechanical and barrier performances. Last, but not least, a comparison between thiophene-based homopolymers and their furan-based homologues was carried out.

**Keywords:** 2,5-thiophenedicarboxylic acid; thermal properties; barrier properties; mechanical properties; 2D-ordered structure; structure-property relationship

**Citation:** Guidotti, G.; Soccio, M.; Gazzano, M.; Siracusa, V.; Lotti, N. Poly(Alkylene 2,5-Thiophenedicarboxylate) Polyesters: A New Class of Bio-Based High-Performance Polymers for Sustainable Packaging. *Polymers* **2021**, *13*, 2460. <https://doi.org/10.3390/polym13152460>

Academic Editor: Tzong-Ming Wu

Received: 15 June 2021

Accepted: 20 July 2021

Published: 27 July 2021

**Publisher's Note:** MDPI stays neutral with regard to jurisdictional claims in published maps and institutional affiliations.



**Copyright:** © 2021 by the authors. Licensee MDPI, Basel, Switzerland. This article is an open access article distributed under the terms and conditions of the Creative Commons Attribution (CC BY) license (<https://creativecommons.org/licenses/by/4.0/>).

## 1. Introduction

Plastic waste has become a matter of great concern in recent years and is pushing governments and society to come up with new strategies to face the problem. If the amount of both plastic waste volume and the exploitation of non-renewable sources are analysed, it is immediately clear how the development of sustainable alternatives to traditional plastics is urgent and re-use, where possible, should be encouraged. If it is true that since 2006, the amount of plastic waste recycled has doubled, it is also likely that we are still far from the so called “zero landfilling” needed to achieve the circular economy of plastics, as in many cases plastic waste is sent to landfills or, even worse, is disposed of in marine and terrestrial environments [1].

It is also important to consider that among the principal current applications of plastics, packaging alone covers 39.9% of them [1]: as far as packaging is concerned, petrochemical-based ones are currently largely used thanks to its abundance, great mechanical strength, and barrier properties together with low production costs despite most of it being non-biodegradable. As an alternative, plastics obtained from renewable sources can represent a

valuable solution thanks to their resource efficiency and reduced carbon footprint. This potential is confirmed also by the increasing bioplastics market size and demand: according to the most recent studies, global bioplastics production capacity is estimated to grow from 2.11 million tons in 2019 to about 2.43 million tons in 2024 [2]. However, to date there are still some important drawbacks related to the final properties of these bioplastics, limiting their current applications, such as short-term stability, bad processability, poor mechanical strength, brittleness, or relatively high gas permeability.

Besides the use of renewable sources, also reducing packaging volumes could be a very practical route to reduce environmental impact. For this reason, many efforts have been devoted to the research of optimized flexible solutions in place of rigid and oversized ones, keeping at the same time the pack quality and the product protection, in particular when the product is characterised by a very short life cycle, as in the case of food. For example, vacuum skin packs can provide excellent barrier properties, minimizing volumes while at the same time preserving the product's shelf life. Another issue is related to multilayer materials, commonly used to better preserve food, in which high barrier properties are ensured by the combination of different layers. These strata are intimately overlapped and very thin, and thus very difficult to separate in view of a possible reuse. Therefore, the use of monomaterials, which can provide an effective barrier to gases on one side and can be also easily recovered after use, should be preferred.

Aware of the severity and the complexity of this scenario, the European Commission has adopted both a Waste Framework Directive (2008/98/EC) and an action plan for a circular economy in view of ensuring that all plastic packaging would be recyclable by 2030 [3]. In addition, the U.S. Department of Energy has identified twelve building blocks that can be produced from renewable sources, such as sugars, which can in turn be converted to many high-value bio-based chemicals [4]. Among them, 2,5-furandicarboxylic acid (FDCA) is of particular interest, both academically and industrially, since one of its derived materials, poly(ethylene furanoate) (PEF), is considered the most credible green alternative of the fossil-based poly(ethylene terephthalate) (PET), which is largely employed in packaging applications. Moreover, according to published studies, PEF is more performant than PET in terms of mechanical and barrier response [5–9]. It is known that FDCA can be obtained from sugar dehydration, obtaining 5-hydroxymethyl-furfural (HMF) as an intermediate product [10], with high yield and purity.

In recent years, 2,5-thiophenedicarboxylic acid (2,5-TDCA) has attracted growing attention due to its chemical structure, which is similar to that of FDCA. In addition, 2,5-TDCA can be derived from renewable sources and is already industrially produced from adipic acid, which can be obtained, in turn, from glucaric acid, muconic acid, or lignin [11–14]. As proof of the growing interest in these polyesters, many scientific studies have been recently published, including those conducted outside of our research group, demonstrating the great potential of both thiophene-based homopolymers and copolymeric systems [15–24].

Moreover, since the enzymatic degradability of PET and PEF has already been demonstrated [25–27], more recently the biodegradability of poly(butylene 2,5-furandicarboxylate) PBF and poly(butylene 2,5-thiophenedicarboxylate) PBTF was also investigated. It was proved that *Humicola insolens* (HiC) and *Thermobifida cellulosilytica* (Cut) cutinases can hydrolyse both homopolymers, opening a new way for the industrial recycling of furan- and thiophene-based materials [28].

Considering the above-described scenario, the present work aimed to synthesize by two-step polycondensation four fully bio-based poly(alkylene 2,5-thiophenedicarboxylate)s, starting from dimethyl 2,5-thiophenedicarboxylate, the dimethyl ester of 2,5-TDCA, and glycols of different length (the number of methylene groups changed from 3 to 6). These can be all derived from renewable sources as well as 2,5-TDCA. By acting only on the number of CH<sub>2</sub> groups in the glycol moiety, it was possible to cover a wide range of properties, making the materials obtained particularly suitable for the realisation of rigid as well as flexible films for packaging applications. The polymers synthesized, in the

form of both powders and thin films, were characterised from the molecular, structural, thermal, mechanical, and gas barrier point of view, and correlations between structure and properties were extrapolated. In addition, the presence of a mesophase was hypothesized, and both the amount of ordered domains developed and the mechanism of their formation was compared to those of furan-based analogues [29].

## 2. Materials and Methods

### 2.1. Materials

2,5-thiophenedicarboxylic acid (2,5-TDCA) was purchased from TCI (Tokyo, Japan), titanium tetrabutoxide (TBT), titanium isopropoxide (TIP), 1,3-propanediol (PD), 1,4-butanediol (BD), 1,5-pentanediol (PeD), and 1,6-hexanediol (HD) were purchased from Sigma-Aldrich (Milan, Italy). All reagents were used as received.

### 2.2. Synthesis

Prior to polymer synthesis, dimethyl 2,5-thiophenedicarboxylate (DMTF) was prepared, starting from 2,5-TDCA, according to the procedure described in [18]. Afterward, all the homopolymers were synthesized through two-stage melt polycondensation, starting from DMTF (0.02 mol, 4 g) and PD/BD/PeD/HD (0.04 mol, corresponding to 3.04 g for PD, 3.60 g for BD, 4.17 g for PeD and 4.73 g for HD, respectively), using TBT and TTIP as catalysts (200 ppm of each). In all cases, a diester:glycol molar ratio of 1:2 was used in order to favour the DMTF solubilisation. The syntheses were carried out in a glass reactor put in a thermostated bath. The reaction mixture was kept under continuous stirring by using a two-bladed centrifugal stirrer connected to an overhead motor. Syntheses proceeded in two stages. The first one occurred under pure nitrogen flow at a temperature of 180 °C. This condition was maintained until 90% of the theoretical amount of methanol was distilled off (about 2 h from the solubilisation of the dimethyl ester). During the second stage, pressure was reduced gradually to 0.06 mbar and temperature raised up to 220 °C to favour the removal of the glycolic excess as well as the increasing of molecular weight. Polymerisation was stopped when a constant torque value was reached (after about two additional hours).

Prior to solid-state polymer characterisation, all the samples were purified to remove impurities, oligomers, and catalysts. The polyesters were first dissolved in chloroform (in the case of PPTF some drops of hexafluoro-2-propanol were needed for the complete polymer solubilisation), then precipitated in methanol. Lastly, the purified powders were kept under a vacuum at room temperature for 48 h to remove the residual solvent.

### 2.3. Molecular Characterisation

Chemical structure was confirmed by means of proton nuclear magnetic resonance ( $^1\text{H-NMR}$ ), employing a Varian Inova 400 MHz instrument (Palo Alto, CA, USA). More in detail, each homopolymer was dissolved in deuterated chloroform containing 0.03 vol.% tetramethylsilane (TMS) as an internal standard (solutions' concentration was about 0.5 wt%). For PPTF, a mixture of trifluoroacetic acid and chloroform was used (20% *v/v*). The spectra were recorded at room temperature with a relaxation delay of 1 s, acquisition time of 1 s and up to 64 repetitions.

In order to determine the molecular weight of the synthesized materials, gel permeation chromatography (GPC) was performed at 30 °C using an 1100 HPLC system (Agilent Technologies, Santa Clara, CA, USA) equipped with a PLgel 5-mm MiniMIX-C column. A UV detector was employed, and chloroform was used as an eluent. We used 0.3 mL/min flow and sample concentrations of about 2 mg/mL. Polystyrene standards in the range of 800–100,000 g/mol were used to obtain a calibration curve.

### 2.4. Film by Compression Moulding

Polymeric films of about 100  $\mu\text{m}$  thickness were prepared via compression moulding using a Carver laboratory press (Wabash, IN, USA). The PPTF, PBTF, PPeTF and PHTF samples were melted at temperatures of 205, 180, 95 and 125 °C, respectively, between

two Teflon sheets. Therefore, a pressure of  $7 \text{ ton}\cdot\text{m}^{-2}$  was applied for 2 min. The samples were then ballistically cooled down to room temperature in press, the process taking about 15 min. The as-obtained film pictures are shown in Figure S1. Prior to further tests, the films of the polymers with a glass transition temperature below room temperature (PPeTF and PHTF) were stored at room temperature for 3 weeks in order to let them reach equilibrium crystallinity.

### 2.5. Thermal and Structural Characterisation

Thermal stability and thermal transitions of the homopolymers were investigated by means of thermogravimetric analysis (TGA) and calorimetric measurements (DSC), respectively. In the former case, the analyses were carried out using a Perkin Elmer TGA7 apparatus (gas flow: 40 mL/min), under an inert  $\text{N}_2$  atmosphere (Shelton, CT, USA). Weighed samples of about 10 mg were heated at a constant rate ( $10 \text{ }^\circ\text{C}/\text{min}$ ) from  $40 \text{ }^\circ\text{C}$  up to  $800 \text{ }^\circ\text{C}$ . In this way, it was possible to calculate the temperature corresponding to initial degradation ( $T_{\text{onset}}$ ) as well as the temperature at which maximum weight loss occurs ( $T_{\text{max}}$ ).

As for calorimetric measurements, these ones were carried out on both purified powders and films using a Perkin Elmer DSC6 (Shelton, CT, USA) calibrated with indium and cyclohexane standards. As is known, DSC analysis allows the determination of glass transition temperature ( $T_g$ ), melting and crystallisation temperatures ( $T_m$  and  $T_{cc}$ , respectively), as well as the specific heat increment associated with the glass transition of the amorphous phase ( $\Delta c_p$ ), and the heat of fusion and crystallisation ( $\Delta H_m$  and  $\Delta H_{cc}$ , respectively), relative to the crystalline portion of the polymer.  $T_g$  was calculated as the midpoint of the heat capacity increment related to the glass-to-rubber transition.  $T_m$  and  $T_{cc}$  were considered as the peak values of the endothermal and exothermal phenomena in the DSC curve, respectively,  $\Delta c_p$  was calculated from the vertical distance between the two extrapolated baselines at  $T_g$ , while  $\Delta H_m$  and  $\Delta H_{cc}$  were calculated considering the global area subtended by melting and crystallisation peaks, respectively. In the procedure adopted, polymeric samples of about 8 mg were put in aluminium pans and heated at a constant rate ( $20 \text{ }^\circ\text{C}/\text{min}$ ) from  $-50 \text{ }^\circ\text{C}$  to 210, 200, 160 and  $180 \text{ }^\circ\text{C}$  for PPTF, PBTF, PPeTF and PHTF, respectively, held there for 3 min, and then rapidly cooled ( $100 \text{ }^\circ\text{C}/\text{min}$ ) to  $-50 \text{ }^\circ\text{C}$ . They were then heated again at the same heating rate (II scan).

Wide-angle X-ray scattering (WAXS) patterns of purified powders and films were recorded by means of a PANalytical X'PertPro diffractometer (Almelo, The Netherlands) equipped with a fast solid-state X'Celerator detector and a copper target ( $\lambda = 0.1548 \text{ nm}$ ). The samples were scanned in the range  $2\theta = 5^\circ$  to  $60^\circ$  (step size of  $0.10^\circ$ , acquisition time of 100 s per step). The degree of crystallinity ( $X_c$ ) was calculated dividing the value of the crystalline diffraction area ( $A_c$ ) by the total area of the diffraction pattern ( $A_t$ ),  $X_c = A_c/A_t$ .  $A_c$  was determined by subtracting the amorphous halo from the  $A_t$  value itself.

### 2.6. Mechanical Characterisation

Tensile tests were carried out on rectangular films ( $5 \text{ mm} \times 50 \text{ mm}$ , gauge length of 20 mm) by means of an Instron 5966 testing machine (Norwood, MA, USA) equipped with a rubber grip and a 1KN load cell. Experiments were performed at room temperature with a crosshead speed of 10 mm/min, testing at least seven specimens for each polymeric sample. The so-obtained load-displacement curves were then converted to stress-strain curves. The value of the tensile elastic modulus ( $E$ ) was calculated from the initial linear slope of the stress-strain curve. The values of stress at break ( $\sigma_B$ ) and elongation at break ( $\varepsilon_B$ ) were also determined. The results are reported as the average value  $\pm$  standard deviation.

### 2.7. Gas Barrier Properties Evaluation

In order to evaluate gas transmission rates through polymeric films, permeability tests were performed by using a manometric method (Permeance Testing Device, type GDP-C (Brugger Feinmechanik GmbH, München, Germany)), in accordance with ASTM

1434-82, DIN 53 536, ISO/DIS 15 105-1 and the gas permeability testing manual of the instrument. Each circular film (film area of 78.5 cm<sup>2</sup>) was placed in between two chambers. First, the system was put under high vacuum, and then the upper chamber was filled with the selected gas (CO<sub>2</sub> or O<sub>2</sub> food grade, 0% RH) at 23 °C and atmospheric pressure, with a gas stream of 100 cm<sup>3</sup>/min. Any variation in gas pressure was recorded, as a function of time, by a pressure sensor located in the lower chamber. Gas transmission rate (GTR [cm<sup>3</sup> cm m<sup>-2</sup> d<sup>-1</sup> atm<sup>-1</sup>]), i.e., the value of film permeability, was determined taking into account the pressure increase as a function of time and of the whole volume of the device. The GTR values were normalised for the film thickness, the latter measured as the average value among five different measurements.

### 3. Results and Discussion

#### 3.1. Synthesis and Molecular Characterisation

The chemical structure of the homopolymers under investigation are reported in Figure 1, together with a schematic representation of the synthetic process. All the materials were characterised by a diacid aromatic subunit derived from 2,5-TDCA and by an aliphatic glycolic subunit differing for the number of methylene groups ranging from 3 to 6. It is worth noting from the chemical structure a nonpolar moiety, coming from the aliphatic segment, was combined with a polar one, i.e., thiophene ring, whose dipole moment ( $\mu$ ) was 0.51 D. The starting 2,5-TDCA was esterified because the impurities present in the diacid acting as nucleating agents affected the polymer microstructure and consequently the final polymer properties, such as the mechanical and gas barrier ones [18]. The as-synthesized polymers looked slightly coloured due to the presence of residual catalysts, while after purification, in all cases, white powders were obtained.

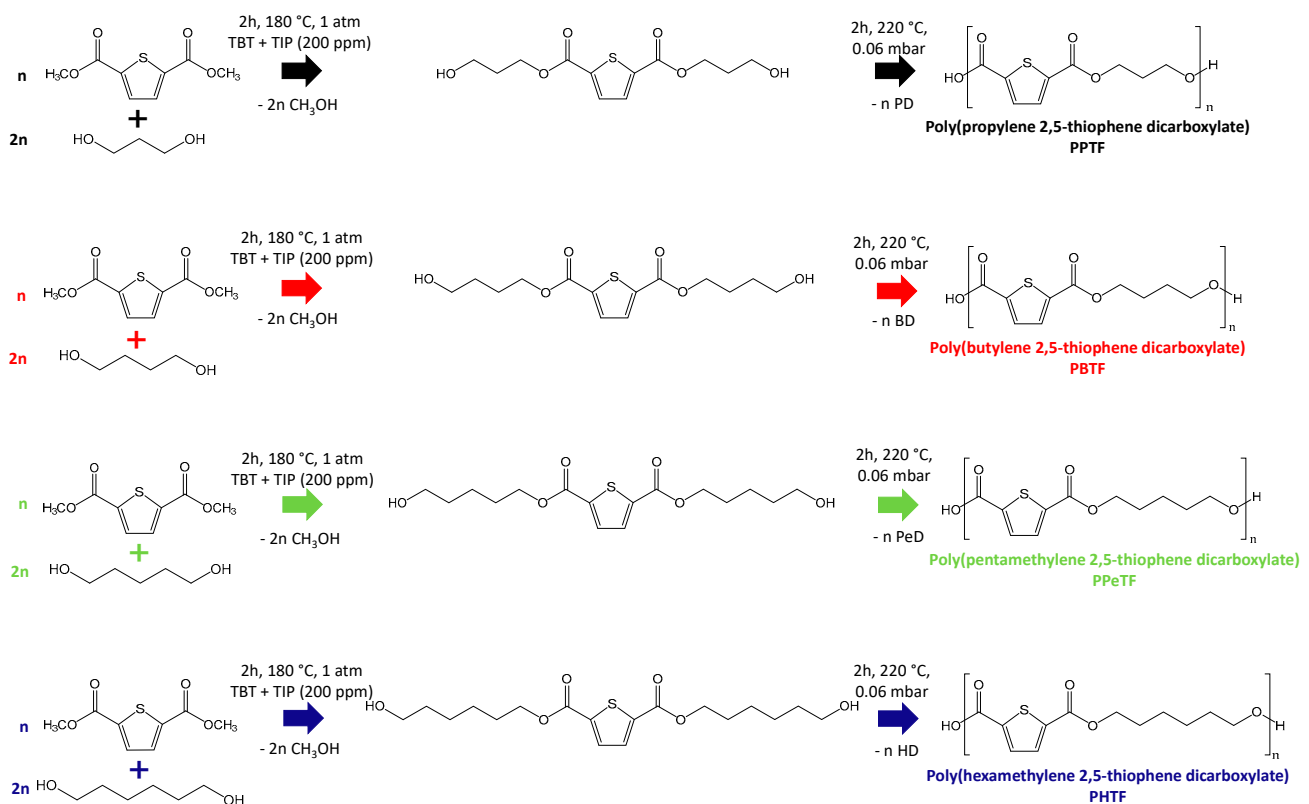


**Figure 1.** Schematic representation of the synthetic process together with the chemical structure of the homopolymers under study: PPTF, PBTF, PPeTF and PHTF.

The chemical structures were confirmed via  $^1\text{H-NMR}$  spectroscopy (Figure 2). Table 1 collects the peak position and multiplicity observed in the NMR spectra. No extra signals were found, proving the absence of impurities in the synthesized samples.

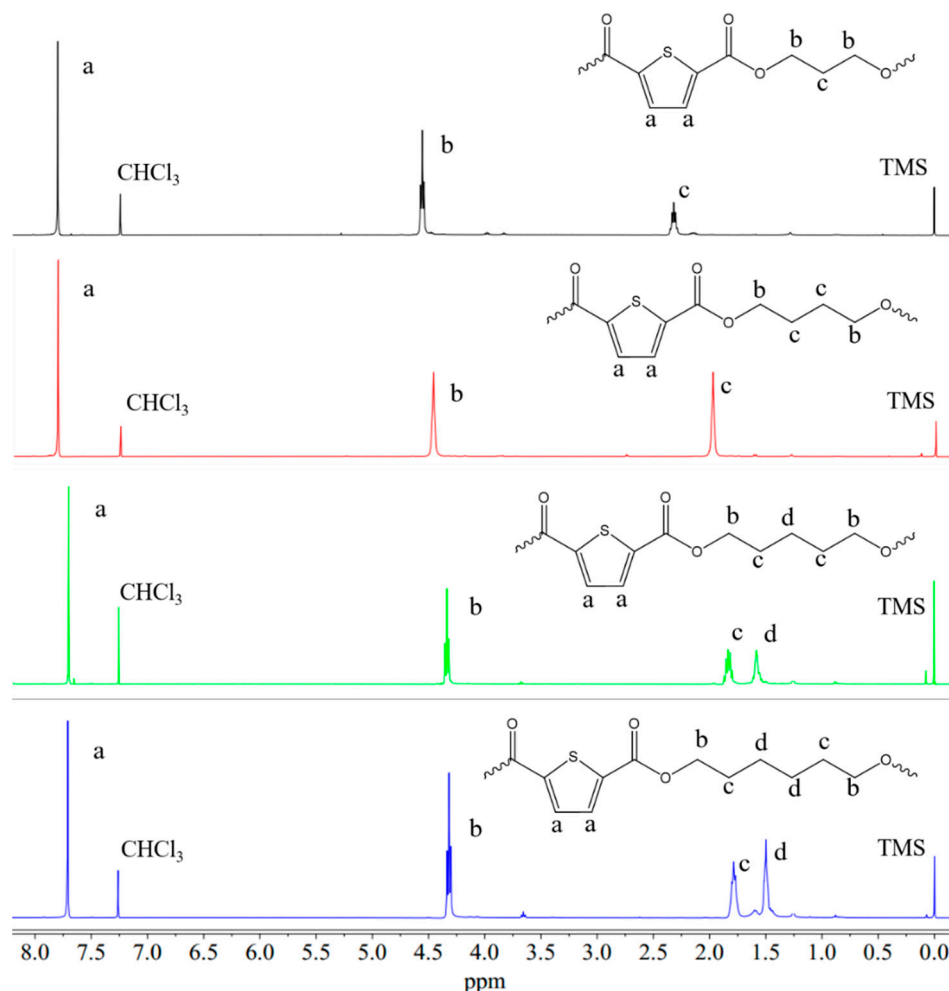


**Figure 2.**  $^1\text{H-NMR}$  spectra of the homopolymers under study together with peaks' assignment.

**Table 1.**  $^1\text{H-NMR}$  peak position and molecular characterisation data for the homopolymers under study.

|       | Peak Position (ppm) |  | $M_n$<br>(Da) | D   |
|-------|---------------------|--|---------------|-----|
|       | Diacid Subunit      | Glycolic Subunit                             |               |     |
| PPTF  | 7.83 (2H, s)        | 2.34 (2H, m)<br>4.60 (4H, t)                 | 26,300        | 2.3 |
| PBTF  | 7.83 (2H, s)        | 1.99 (4H, m)<br>4.48 (4H, t)                 | 39,600        | 2.0 |
| PPeTF | 7.70 (2H, s)        | 1.58 (2H, m)<br>1.82 (4H, m)<br>4.34 (4H, t) | 25,800        | 2.5 |
| PHTF  | 7.70 (2H, s)        | 1.51 (4H, m)<br>1.81 (4H, m)<br>4.32 (4H, t) | 32,400        | 2.3 |

All the materials analysed show high and comparable values of  $M_n$  (see Table 1 and the chromatograms shown in Figure S2) and a polydispersity index (D) around 2, typical

of polyesters obtained by melt polycondensation, corroborating the optimization of the polymerisation process.

### 3.2. Thermal Characterisation

#### 3.2.1. Powder Samples

The first scan DSC curves of powder samples are shown in Figure 3A and the relative data are displayed in Table S1. The DSC traces of all samples present the typical profile of semicrystalline materials with an endothermic baseline deviation related to glass-to-rubber transition, followed by an endothermic phenomenon associated with the melting of crystalline phase. This phase behaviour can be explained due to solvent-induced crystallisation. In PPTF DSC trace, the glass transition phenomenon is not detectable because of its very low intensity due to the high crystallinity degree. Besides the main melting peak, two low and broad endothermic signals can be identified around 60–70 °C, whose origin is not so clear. Broad multiple melting peaks were also detected for PBTF, PPeTF and PHTF samples, suggesting melting–crystallisation–re-melting processes occurring during heating scan or in the presence of different crystalline phases.

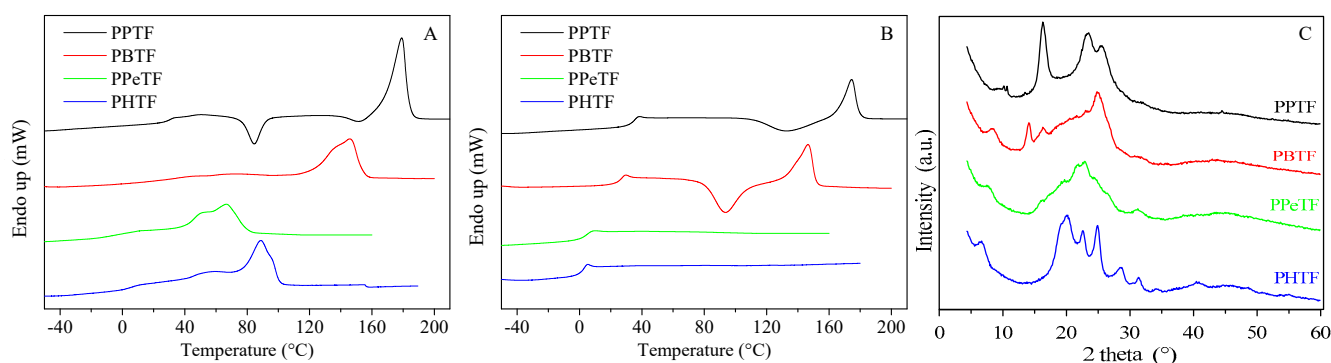


**Figure 3.** (A) I scan; (B) II scan DSC curves; (C) WAXS profiles of PPTF, PBTF, PPeTF and PHTF purified powders.

In general, the position of the main endotherm ( $T_m$ ) moved toward lower temperature as the glycol length increased, with the exception of PPeTF, which exhibited the lowest melting temperature.

As is well known, semicrystalline polymers behave differently from their completely amorphous analogues due to the physical crosslinks provided by crystalline structures, which limit chain mobility, raising the  $T_g$  value [30,31]. Therefore, we decided to perform a DSC scan after rapid cooling from the molten state with the aim of quenching the polymer macromolecules. The relative curves are reported in Figure 3B, while the corresponding calorimetric data are displayed in Table S1. The results demonstrated the effectiveness of the rapid cooling from the melt in quenching the powders, being all the materials amorphous in the II scan. Nevertheless, some differences in the crystallisation capability from the glass could be evidenced. In particular, in the second run PPeTF and PHTF showed just the endothermic jump associated with the glass-to-rubber transition, while PPTF and PBTF powders in addition to the  $T_g$  step presented an endothermic signal together with an exothermic one of equal intensity, demonstrating their chains are capable of rearranging into an ordered structure upon heating. However, since  $\Delta H_c \approx \Delta H_m$ , one can assert rapid cooling from the melt was effective in quenching both PPTF and PBTF powders. Considering the  $T_g$  values, as expected, the higher the number of methylene groups the higher the flexibility of macromolecular chains, i.e., the lower the  $T_g$  value. Moreover, a longer glycol subunit implies fewer stiff aromatic rings along the polymer backbone. More in detail, PPTF was the only glassy material at room temperature, being its  $T_g > RT$ . Conversely, PPeTF and PHTF were in the rubbery state, with  $T_g$  well below room temperature. PBTF was instead characterised by a glass transition temperature near room temperature.



WAXS patterns of powder samples are reported in Figure 3C. At first glance, it is clear that the samples were characterised by different crystallinity degrees,  $X_c$  being equal to 29%, 16%, 9% and 25% for PPTF, PBTF, PPeTF and PHTF, respectively. The profiles showed different shapes with a variation of peak positions on the 2-theta scale and intensities peculiar for each sample. This suggests the crystal phases probably do not share any similarities, i.e., are not isomorphous. By comparing with previous reported data [15], we can ascribe the crystal fraction of the PPTF sample to its  $\beta$ -form. Indeed, the four main peaks at 9.3°, 16.3°, 23.3° and 25.5° were previously reported for a film sample named  $\beta$ -PPTF [15]. As for the PBTF sample, the observed main peaks at 8.2°, 14.0°, 16.2° and 24.8° permitted us to recognize in the PBTF powder the  $\gamma$ -phase [18]. PPeTF showed a very low crystallinity degree with peaks, or better peak clues, at 7.6°, 16.2°, 21.6°, 22.8°, 24.3° and 31.1°. The PHTF profile was characterised by well-defined peaks identified at 6.5°, 19.2°, 20.0°, 22.6°, 24.9°, 28.6° and 31.3°, indicating the presence of a conspicuous amount of crystals. This pattern is compatible with the one reported by authors of another study [19].

### 3.2.2. Compression-Moulded Films

Prior to solid-state characterisation, compression-moulded films were subjected to 3 weeks storage at room temperature to uniform their thermal history since both PPeTF and PHTF are characterised by  $T_g$ s below room temperature, and the  $T_g$  of PBTF is near RT.

Firstly, compression-moulded films (Figure S1) were subjected to thermogravimetric analysis (TGA) under pure nitrogen flux. The temperatures of initial degradation ( $T_{onset}$ ) and of maximum weight loss rate ( $T_{max}$ ) are displayed in Table 2, while the corresponding TGA curves and derivatives are shown in Figure 4A,B, respectively. All the polyesters displayed very good thermal stability, with  $T_{onset}$  above 370 °C and  $T_{max}$  above 400 °C, as clearly evidenced by thermograms' derivatives, the degradation process occurring in all cases in two steps, the main one around 400 °C. The second step was sensibly smaller in all cases and occurred immediately afterward. Lastly, no residual mass at 800 °C was found. Some differences among the samples could be found. PPTF turned out to be the fastest-degrading material, presumably because of the high amount of ester groups, which undergo thermal cleavage more easily, and the presence of 1,3-propanediol, which favours  $\beta$ -scission reactions as previously observed for other polyesters, among these PPF, its furan-based counterpart [29,32]. PBTF was, on the contrary, the most thermally stable among the family, while PPeTF and PHTF were characterised by a very similar thermal stability, intermediate between those of PPTF and PBTF. This trend was slightly different from the one observed in the case of furan-based materials, where PPeF was the most thermally stable [33].

Each thiophene-based polyester was directly compared with its furan-based counterpart (see Figure 4C). As you can see, PPTF and PBTF appeared to be more thermally stable than their furan-based counterparts (PPF and PBF). We hypothesize such a result could be due to the higher resonance energy, p-to-d  $\pi$ -back bonding, and lack of ring strain due to the longer C-S bond of the thiophene ring. Conversely, poly(pentamethylene furanoate) (PPeF) turned out to be more thermally stable than PPeTF, whereas PHF and PHTF showed very similar thermal stability.

**Table 2.** Thermal characterisation (TGA and DSC) data of the homopolymers under study in the form of compression-moulded films.

|       | $T_{onset}$<br>°C | $T_{max}$<br>°C | I Scan      |                       |                |                        |             |                     | II Scan     |                       |                |                        |             |                     |
|-------|-------------------|-----------------|-------------|-----------------------|----------------|------------------------|-------------|---------------------|-------------|-----------------------|----------------|------------------------|-------------|---------------------|
|       |                   |                 | $T_g$<br>°C | $\Delta c_p$<br>J/g°C | $T_{cc}$<br>°C | $\Delta H_{cc}$<br>J/g | $T_m$<br>°C | $\Delta H_m$<br>J/g | $T_g$<br>°C | $\Delta c_p$<br>J/g°C | $T_{cc}$<br>°C | $\Delta H_{cc}$<br>J/g | $T_m$<br>°C | $\Delta H_m$<br>J/g |
| PPTF  | 375               | 402             | 36          | 0.175                 | -              | -                      | 183         | 44                  | 36          | 0.323                 | 120            | 36                     | 183         | 37                  |
| PBTF  | 391               | 410             | 24          | 0.272                 | 87             | 28                     | 148         | 28                  | 24          | 0.291                 | 88             | 27                     | 148         | 27                  |
| PPeTF | 382               | 402             | 8           | 0.144                 | -              | -                      | 52/63       | 19/6                | 8           | 0.308                 | -              | -                      | -           | -                   |
| PHTF  | 384               | 402             | 7           | 0.008                 | -              | -                      | 49/95       | 10/23               | 2           | 0.289                 | -              | -                      | -           | -                   |

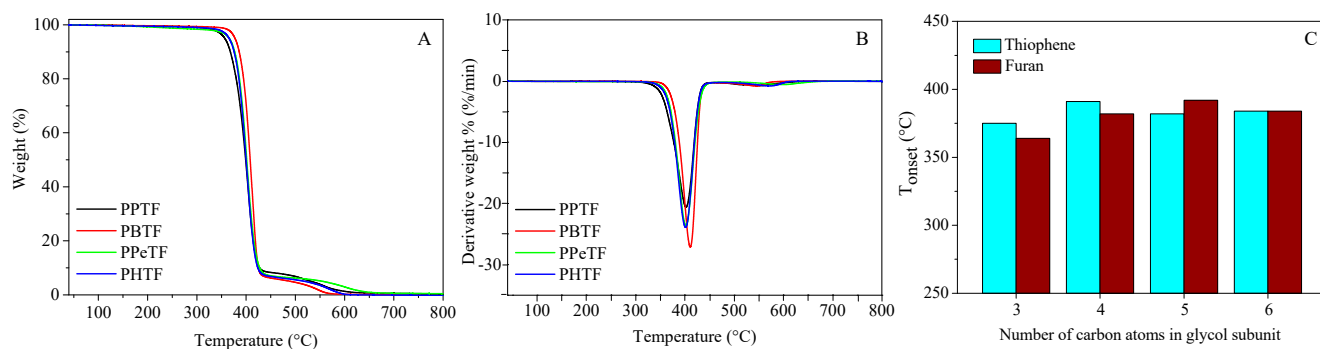


**Figure 4.** (A) TGA curves and (B) TGA derivatives of PPTF, PBTF, PPeTF and PHTF homopolymers; (C) comparison between  $T_{\text{onset}}$  of both thiophene- and furan-based homopolymers.

The highest thermal stability of PPeF within the furan-based family was ascribed to the presence in this polyester of the highest fraction of mesophase, the latter due to the establishment of hydrogen bonds between adjacent macromolecular chains in addition to  $\pi$ - $\pi$  interactions [33]. As previously reported, mesophase formation is favoured in flexible and mobile macromolecular chains and compete with the crystalline 3D phase. PPeF was indeed amorphous with  $T_g$  below room temperature and had very slow crystallising capability [29,33,34]. The authors of the present paper previously investigated PBTF, which was characterised by the presence of a 2D-ordered phase (mesophase) [16,18]. Nevertheless, the mesophase present in thiophene-based polyesters cannot originate from hydrogen bonds between adjacent polymer chains, sulphur atoms being significantly less electronegative than oxygen. In this case, the 2D-ordered structure could arise from thiophene ring  $\pi$ - $\pi$  stacking, as observed also for polythiophenes [35] and for some other aromatic polyesters containing, for example, terephthalic and isophthalic rings [36–38]. As previously reported [16,18], also for the thiophene-based family, the mesophase formed at the expense of the crystalline one, particularly enhanced by compression-moulding treatment.

The DSC analysis discussed below indicates PBTF compression-moulded film is characterised by a very low crystallinity degree, different from the other members of the family. Consequently, we can hypothesize the mesophase fraction, and then the interchain  $\pi$ - $\pi$  stacking interactions, reached the maximum value in the PBTF film, determining the highest thermal degradation temperature.

The first scan DSC traces of compression-moulded films are shown in Figure 5 and the relative data are displayed in Table 2.

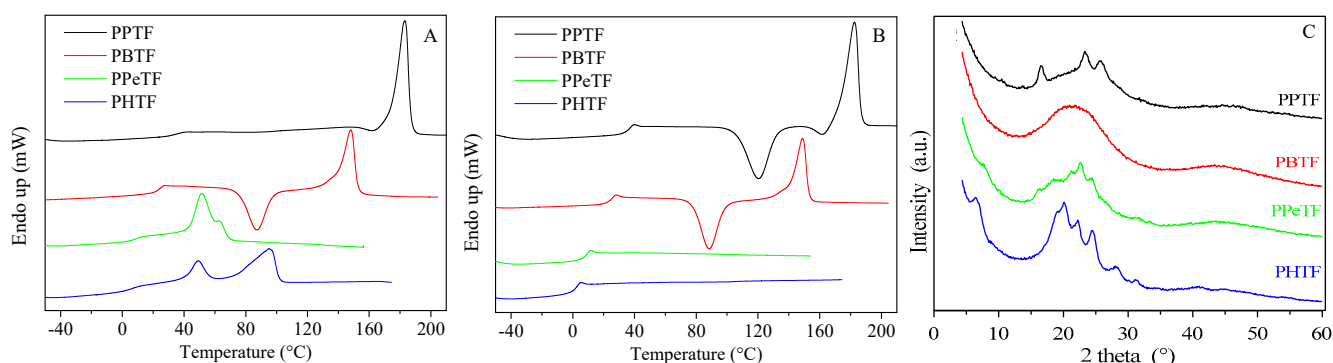


**Figure 5.** (A) I scan; (B) II scan DSC curves; (C) WAXS profiles of PPTF, PBTF, PPeTF and PHTF compression-moulded films.

First of all, it has to be emphasized that some remarkable differences in the thermal behaviour before and after compression moulding were noticed. In all cases, with the exception of PBTF film, the I scan curves show endotherms typical of semicrystalline materials. In the case of PBTF, an additional exothermic peak between  $T_g$  and  $T_m$  could be observed; however, the peak areas were comparable, ( $\Delta H_{\text{cc}} = \Delta H_m$ ), indicating film

processing totally suppressed the development of 3D-crystalline phase in the PBTF sample. As for PPeTF, analogously to powder, a broad endothermic phenomenon could be found. However, in this case, the peak at the lower temperature (52 °C) was more intense than that at the higher temperature (63 °C). Finally, the DSC curve of PHTF film shows two melting peaks, at 49 and 95 °C, very similar to the endotherms measured for purified powder, but again higher intensity for the lower temperature signal was detected. Interestingly, in both PPeTF and PHTF polyesters the first endothermic peak was located at a constant temperature, about 50 °C. It is worth noticing the signal, similar in terms of position even if less intense, previously reported for PBTF film was ascribed to the mesophase isotropisation phenomenon [16]. Such an endotherm is not visible in the calorimetric trace of the PBTF film obtained from dimethyl 2,5-thiophenedicarboxylate [18], probably hidden by the upcoming cold crystallisation peak (as known, the mesophase can act as a precursor of the 3D crystalline phase). Considering this scenario, it can be hypothesized that the endotherms around 50 °C in both PPeTF and PHTF were due to this peculiar 2D microstructure already detected and investigated.

As expected, II scan DSC curves of films are identical to those collected for purified powders.

In Figure 5C, the WAXS profiles of films are reported. From the profile shape, we can state PPTF and PHTF were in the same crystal forms as the respective powders. Indeed, the peak positions of PPTF film were 16.5°, 23.3° and 25.5°, very similar to the powder ones; PHTF showed peaks at 6.5°, 19.1°, 20.0°, 22.2°, 24.4°, 28.2° and 31.2°. For this sample, the position of the peaks was not exactly the same as those observed in the powder sample, but the good crystallinity and the overall match of the pattern allow us to state the powder and the film displayed the same crystal form, the small differences observed being due to different preparations. PBTF film showed only the bell-shaped background, typical of amorphous compounds, in agreement with DSC results. The comparison of PPeTF samples was not easy, the film showing small peaks or shoulders at 7.5°, 16.3°, 18.4°, 21.3° 22.6° and 24.3°. They were roughly at the same positions found in the powder sample. The imperfect coincidence in the position of the peaks as well as the presence of additional peaks could be compatible with the presence of a further phase.

As for sample crystallinity,  $X_c$  values were 18%, 14% and 21% for PPTF, PPeTF and PHTF, respectively.

For the sake of comparison, in Figure S3  $T_g$  and  $T_m$  of the thiophene-based polyesters under study and their furan- and terephthalate-based counterparts are reported as a function of glycolic subunit length. As for  $T_g$  values, regardless of the kind of ring considered, all the families showed a regular decrease of glass transition temperature with the glycolic subunit length. In addition, by fixing the glycol length, the trend observed was  $T_{g,thiophene} < T_{g,benzene} < T_{g,furan}$ , more pronounced for 1,3-propanediol- and 1,4-butanediol-containing polymers, as a result of the different polarity/aromaticity ratio of the three rings. The lower  $T_g$  values of thiophene-based polyesters with respect to those of the furan-based ones can be explained considering that in the former polymer family interchain interactions are weaker because of the lower electronegativity of sulphur atoms with respect to oxygen ones.

As for the melting temperatures, although the same trend can be noticed for all the polymeric families, the decrease of  $T_m$  for thiophene-based samples was shifted at higher  $CH_2$  numbers with respect to their furan- and benzene-based analogues, probably due to differences in the main structural parameters, which led to a less efficient chain packing, i.e., lower  $T_m$ s. PPTF and PPF were exceptions: the higher  $T_m$  of the former polymer can be ascribed to a more perfect crystalline phase as well as to the higher aromaticity of thiophene ring, which promotes chain folding [15].

### 3.3. Mechanical Characterisation

Mechanical properties of the compression-moulded films were evaluated by tensile tests. The values of the elastic modulus ( $E$ ), stress at break ( $\sigma_B$ ), and strain at break ( $\epsilon_B$ ) are displayed in Table 3. The corresponding stress–strain curves are shown in Figure 6.

**Table 3.** Mechanical and gas permeability characterisation data of the compression-moulded films.

|       | $E$<br>(MPa)    | $\sigma_B$<br>(MPa) | $\epsilon_B$<br>(%) | $O_2$ -TR<br>( $cm^3 cm m^{-2} d^{-1} atm^{-1}$ ) | $CO_2$ -TR<br>( $cm^3 cm m^{-2} d^{-1} atm^{-1}$ ) |
|-------|-----------------|---------------------|---------------------|---|--|
| PPTF  | $1550 \pm 125$  | $13 \pm 3$          | $1.2 \pm 0.3$       | $0.021 \pm 0.003$                                 | $0.024 \pm 0.002$                                  |
| PBTF  | $47 \pm 3$      | $19 \pm 2$          | $580 \pm 60$        | $0.003 \pm 0.001$                                 | $0.017 \pm 0.001$                                  |
| PPeTF | $1.9 \pm 0.3^*$ | $0.5 \pm 0.1^*$     | $1650 \pm 110^*$    | $0.288 \pm 0.035$                                 | $0.753 \pm 0.125$                                  |
|       | $391 \pm 26$    | $14 \pm 2$          | $17 \pm 3$          |   |  |
| PHTF  | $3.5 \pm 0.5^*$ | $0.5 \pm 0.1^*$     | $674 \pm 9^*$       | $0.404 \pm 0.101$                                 | $1.62 \pm 0.110$                                   |
|       | $299 \pm 22$    | $15 \pm 1$          | $32 \pm 3$          |   |  |

\* Mechanical data obtained immediately after film moulding.

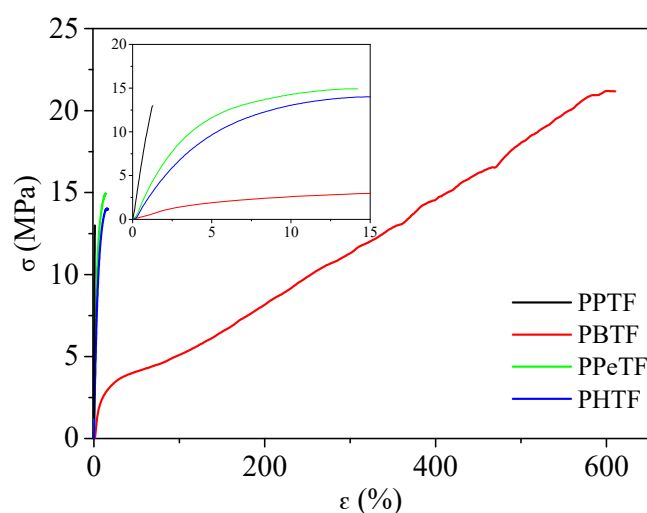


**Figure 6.** Stress–strain curves of PPTF, PBTF, PPeTF and PHTF films after 3 weeks of storage at room temperature.

The results obtained can be explained on the basis of chain flexibility (i.e.,  $T_g$  value) and crystallinity degree, which are the main parameters affecting polymers' mechanical response. More in detail, referring to mechanical characterisation data obtained after three weeks of storage at room temperature, it was possible to notice that PPTF was the most rigid material, with the highest value of  $E$  and the lowest elongation at break. This result was due both to its crystallinity degree, the highest among the family, and its  $T_g$ , the latter being well-above room temperature, which limited macromolecular mobility. Among the thiophene-based family, PBTF, which was amorphous with  $T_g$  around RT, turned out to be the one with the lowest value of  $E$  and the highest of  $\epsilon_B$ , almost 600%. Regarding polymers containing longer and flexible glycols, i.e., PPeTF and PHTF, which are both semicrystalline and in the rubbery state at RT, they were characterised by a mechanical response intermediate between those of PPTF and PBTF. The elongation at break was similar for the two polymers, whereas PPeTF exhibited a higher elastic modulus despite its lower crystallinity degree probably because of its lower chain flexibility (higher  $T_g$ ). Lastly, for all the materials analysed, stress at break was comparable, with values ranging from 13 to 19 MPa.

The unexpected mechanical response of PBTF can be explained as being due to the presence of a mesophase in the polymeric film, as already demonstrated in previous studies carried out by some of the authors of the present paper [16,18]. As reported in the literature,

polymer liquid crystals are characterised by smart mechanical properties, their brittleness being significantly reduced (high values of elongation at break).

In order to support the already-mentioned hypothesis of the presence of a mesophase, stress–strain measurements were carried out on PPeTF and PHTF films immediately after compression moulding, as reported in Figure 7. In these conditions, the two films were completely amorphous, as evidenced by DSC (only the endothermic baseline deviation associated with glass transition was evident in the DSC trace of both polyesters) and WAXS analysis (WAXS profiles of both polymers show only the bell shape halo characteristic of the amorphous phase) (Figure 7B,C,E,F). Nevertheless, it is worth noting that although both materials were in an amorphous rubbery state at room temperature, free-standing films could be obtained. That supports the assumption of the presence, together with the amorphous fraction, of another phase. A similar behaviour was already evidenced for PPeF, the furan-based analogous of PPeTF [29,33], for which the presence of a mesophase was demonstrated. As one can see from Figure 7, the mechanical response of the films tested immediately after moulding was completely different. Both films were characterised by outstanding elongation at break (around 1700% in the case of PPeTF and about 700% for PHTF) and elastic modulus values, about two orders of magnitude lower than those of the same films measured after 3 weeks from moulding (Figure 7A,D). This result further supposes the development of a mesophase in PPeTF and PHTF, too. The storage of the films at room temperature also favoured, of course, the formation of a 3D-crystalline phase. The former is associated with the endothermic phenomenon at constant T around 50 °C, the latter to the fusion process occurring at a higher temperature whose value increases with the number of methylene groups present in the glycol subunit (see Figure 7B,E). Both the films become more rigid (E increases) and stretch much less after 3 weeks at room temperature due to the increment of crystalline fractions and to disclinations between amorphous, 2D and 3D ordered phases.

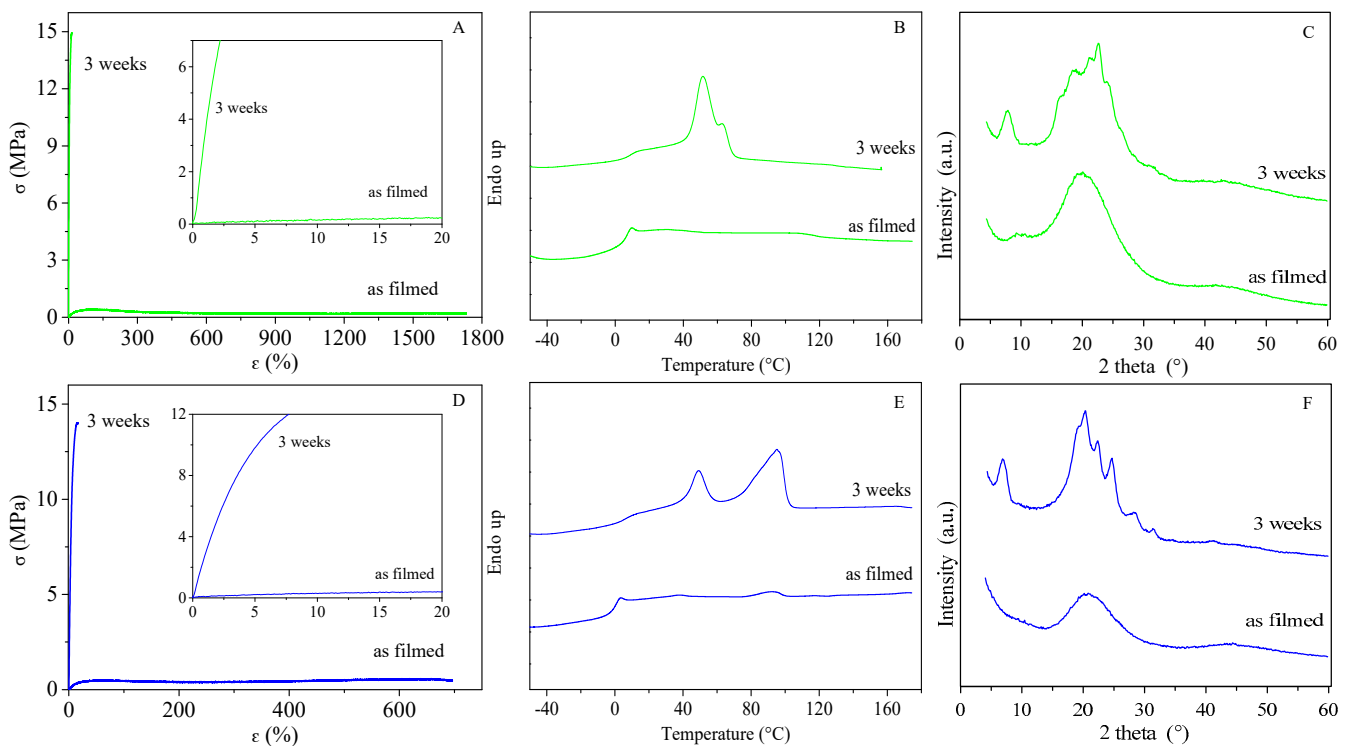


**Figure 7.** (A) Stress–strain curves; (B) DSC curves; (C) WAXS profiles of PPeTF films immediately after moulding and after 3 weeks of storage at room temperature. (D) Stress–strain curves; (E) DSC curves; (F) WAXS profiles of PHTF films immediately after moulding and after 3 weeks of storage at room temperature.

In Figure 8, a comparison between mechanical characterisation data of thiophene-based homopolymers and their furan-based counterparts is shown. As far as the elastic modulus is concerned, an odd–even  $-CH_2-$  number trend was observed: the thiophene-based homopolymers containing a glycol subunit with an odd number of  $-CH_2-$  groups (PPTF and PPeTF) showed a higher elastic modulus with respect to their furan-based counterparts, attributable to their semicrystalline nature. An opposite result was found for the samples containing an even number of C atoms in glycolic subunits (PBTF vs. PBF and PHTF vs. PHF); in fact, the thiophene-based polyesters showed a lower elastic modulus than the furan-based analogous. More in detail, PBF film was semicrystalline, whereas PBTF was fully amorphous and PHF had a higher fraction of crystalline phase compared to PHTF. Moreover, the PHF crystal phase was characterised by a higher melting temperature with respect to PHTF, indicating a higher degree of perfection, i.e., the crystal phase was highly packed.

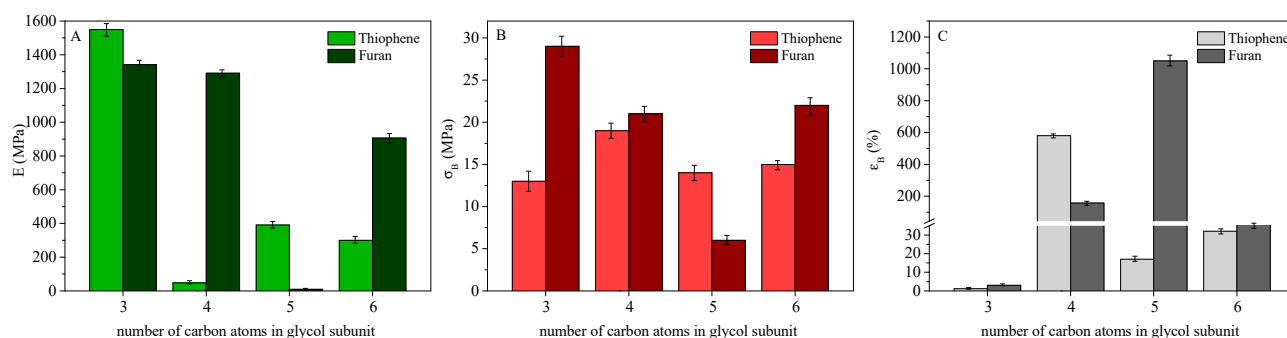


**Figure 8.** Comparison between mechanical characterisation data of thiophene-based homopolymers and their furan-based counterparts: (A) elastic modulus; (B) stress at break; (C) elongation at break.

In the case of stress at break, we measured in general a lower value for thiophene-based polyesters when compared with their furan-based counterparts, with the exception of polyesters of 1,5 pentanediol. For PPeTF and PPeF, exactly the opposite occurred. Interestingly,  $\sigma_{B,PPTF} < \sigma_{B,PPF}$ , despite the semicrystalline nature of the former film and the amorphous nature of the latter one. Such a result can be correlated with the significantly higher  $T_g$  of PPF. For the pair PBTF and PBF, the lower  $\sigma_B$  of the thiophene-based polyester was due to its amorphous nature, PBF being on the contrary semicrystalline. As far as PPeTF and PPeF are concerned,  $\sigma_{B,PPeTF} > \sigma_{B,PPeF}$  because of the semicrystalline nature of thiophene-containing film and the amorphous character of the furan-based one. Lastly, PHF film is characterised by a higher stress at break than the PHTF one due to its higher crystalline degree,  $T_m$  and  $T_g$  values.

The elongation at break was also correlated with the presence in the film of a crystalline phase; in fact,  $\epsilon_{B,PBTF} > \epsilon_{B,PBF}$  (PBTF film was amorphous, while PBF contained a crystal phase). Exactly the opposite happened for the PPeTF and PPeF pair; the former was indeed semicrystalline and the latter was amorphous. Lastly, PHTF and PHF were characterised by a very similar elongation at break, as expected if we considered both polyesters are semicrystalline and in the rubbery state.

### 3.4. Gas Barrier Properties Evaluation

Barrier properties were evaluated with respect to dry  $O_2$  and  $CO_2$  gases. The GTR values normalised for the sample thickness and measured at 23 °C and at 0% of relative humidity are displayed in Table 3. For the sake of comparison, in Figure 9A,B gas permeability values of thiophene-based materials are shown together with those of their furan-based counterparts and with some commonly used traditional fossil-based plastics and other bio-based polymers, respectively.

As is well-known, many factors, such as ordered and amorphous phases amount, glass transition temperature, chain polarity and flexibility, as well as molecular weight

and its distribution, can affect the final barrier properties of materials together with the different characteristics of gas molecules (like size, polarity, inertness). Since gases cannot diffuse and permeate through the highly packed crystalline phase, this parameter plays a key role. Therefore, it is generally assumed that in polymers with higher percentages of crystalline phases the best barrier performances are observed. In addition, it is well-recognized the glassy state offers a higher barrier to gases since it is characterised by reduced chain mobility with respect to the rubbery one, and also by a lower free volume through which gas can diffuse. When mesogenic groups, like thiophene rings, are present together with flexible segments, barrier properties can further improve thanks to the development of a mesophase (1D- or 2D-ordered structure), as this is even more effective than the crystalline phase in hampering gas passage [39]. As already mentioned, meso- and crystalline phases develop one at the expense of the other. Moreover, when both form the amorphous–mesophase–crystal disclination content raises. According to these assumptions, it is not surprising PBTF turned out to be the best-performing material of the family, being the sample in which just the most performant mesophase was present together with the disordered portion, i.e., less interphase percentage.

In addition, previous studies carried out on poly(butylene isophthalate) PBI, which similar to PBTF is aromatic with a  $T_g$  near  $T_{room}$ , have shown this material, if stored at room temperature, develops a very efficiently packed amorphous phase within a few minutes [40,41]. The presence of this peculiar dense amorphous phase can explain the excellent mechanical and barrier properties of PBI. Conversely, in poly(ethylene terephthalate) (PET), another well-known aromatic polyester, a very different behaviour was observed: being PET  $T_g$  is well-above room temperature, it is not capable of quick re-arrangement, and the above-mentioned densification does not occur in short times. All these studies then seem to support the assumption according to which the mesophase presence and the possibility of quickly compacting its mobile amorphous phase are responsible for the outstanding PBTF properties. According to the data reported in Table 3, PPTF is the second-best performing material: it is indeed the only one that showed a  $T_g$  value above room temperature, which means an amorphous glassy phase characterised by a low amount of free volume through which gases can diffuse. As for PPeTF and PHTF, both contained a rubbery amorphous phase at room temperature, coexisting with a mesophase and crystals. Consequently, their higher GTR values can be explained on the basis of the higher fraction of free volume due to  $T_g > RT$  and to the contemporary presence of both 3D and 2D domains causing higher disclination (channels created at the interface between the two ordered regions) density through which gas can easily diffuse. Conversely, there was no significant separation between the mesophase and amorphous regions, as they were characterised by a similar electron density.

Moreover, for all the samples under study,  $CO_2$  was more permeable than  $O_2$ , in agreement with studies carried out in the literature on other similar polymeric systems [42,43] due to reduction of diffusivity with the decreasing of the permeant size (the values of molecular diameter for  $CO_2$  and  $O_2$  were 3.4 Å and 3.1 Å, respectively) [44].

The  $GTR_{CO_2}/GTR_{O_2}$  ratio changed as a function of glycol subunit length; for PPTF (containing 3 methylene groups) it was close to 1, turning almost 2 in the case of PBTF, and 2.5 for PPeTF and PHTF (containing 5 and 6 methylene moieties, respectively).  $GTR_{CO_2}/GTR_{O_2}$  ratio increments can be associated with a decrement of  $CO_2$  solubility in the polymer matrix occurring in samples containing longer glycol subunits.

If thiophene-based homopolymers are compared to their furan-based counterparts, some significant differences can be detected. First, within the thiophene family, the best-performing material was the one containing four carbon atoms in the glycol subunit, unlike what was found for the furan family where PPeF resulted in the best one [29,33]. It is worth noting both the samples were totally amorphous and with a  $T_g$  around RT; it can be supposed that this latter condition favoured the formation of a mesophase. It seems the optimal glycolic length to maximize mesophase formation was different for the two classes, probably because the two mesophases arose from different intermolecular interactions

( $\pi$ - $\pi$  stacking in the case of poly(alkylene 2,5-thiophenedicarboxylate)s,  $\pi$ - $\pi$  stacking and intermolecular hydrogen bonds for poly(alkylene 2,5-furandicarboxylate)s).

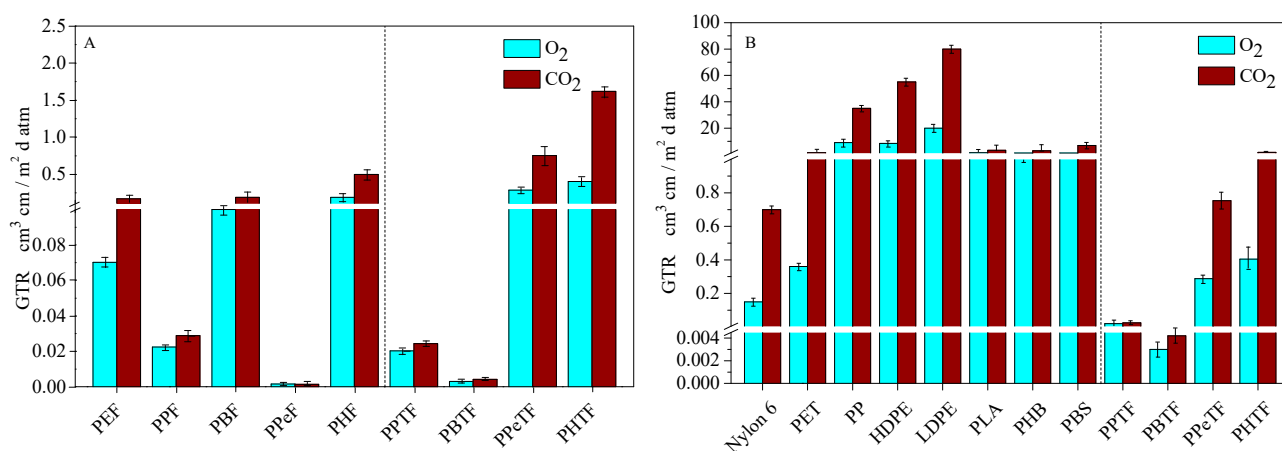


**Figure 9.** GTR values of O<sub>2</sub> and CO<sub>2</sub> through polymeric films ( $T = 23$  °C) compared with those of (A) furan-based homopolymers [29,33]; (B) traditional plastics and principal bio-based polymers [8,18,45].

In addition, by comparing furan- and thiophene-based homopolymers containing a propylene segment, it can be noticed that  $GTR_{PPTF} < GTR_{PPF}$ . Both were in the glassy state, but the former was semicrystalline, the latter amorphous. Mesophase formation was not favoured in both cases, the macromolecular chains being frozen in the glassy state. Considering the butylene moiety-containing polyesters, the results recorded evidence PBTF was more performant than PBF. That was probably due to the presence of a higher amount of mesophase, whose formation was favoured by an amorphous and partially mobile phase (PBF, on the contrary, was glassy and semicrystalline). The five methylene-containing polymers, PPeF and PPeTF, were both in the rubbery state at room temperature, with PPeTF containing also a crystal phase. Nevertheless,  $GTR_{PPeF} \lll GTR_{PPeTF}$  due to the very high mesophase fraction in the PPeF sample. Lastly,  $GTR_{PHF} < GTR_{PHTF}$  is explainable on the basis of a higher  $T_g$  and crystalline fraction for PHF.

Looking at the overall trend, by lengthening the glycol subunit in the poly(alkylene 2,5-thiophenedicarboxylate)s, we can observe a progressive worsening of barrier properties, except for PBTF due to the lowering of  $T_g$  values, unlike furan-based polyesters for which an even-odd trend was observed [29]. It can be assumed that for PPeTF and PHTF, despite the higher amount of mesophase, the worsening effect of both low  $T_g$  value and the high amount of disclinations between the mesophase and 3D domains prevailed.

The homopolymers under study were also compared to the fossil-based traditional materials currently employed in food packaging, as well as to other bio-based polyesters (see Figure 9B). Poly(alkylene 2,5-thiophenedicarboxylate)s turned out to be the more performant of the polyolefins and of PLA, PHB and PBS to both gases. Interestingly, PPTF and PBTF had even better barrier properties than PET and nylon.

#### 4. Conclusions

A new family of fully bio-based homopolymers of 2,5-thiophenedicarboxylic acid were successfully synthesized via melt polycondensation, a green and solvent-free process, starting from dimethyl 2,5-thiophenedicarboxylate and glycols with different lengths.

All solid-state properties appeared to be strongly affected by glycol subunit length; the number of methylene groups present in the flexible aliphatic segment indeed impacted the macromolecular chain flexibility and crystallising ability, in turn, determining different glass transition temperature values and the development of different kinds and fractions of ordered phases (2D mesophase or 3D crystalline phase).

Through the analysis of the effect of glycol subunit length on sample microstructure, we could confirm some results previously reported:



- Mesophase formation is favoured in the case of macromolecular chains, which are mobile at room temperature but have reduced crystallising capability. If the glycol subunit is long enough, 3D crystalline phase formation appears prevalent
- Mesophases and crystalline phases compete with each other, i.e., each one develops at the expense of the other
- Type, number, and amount of ordered phases have a huge impact on the final functional properties (mechanical and gas barrier)

As previously established for furan-based polyesters, the outstanding gas barrier properties are mainly ascribable to mesophase presence. However, due to the lower electronegativity of sulphur atoms with respect to oxygen ones, the 2D-ordered structure present in poly(alkylene 2,5-thiophenedicarboxylate)s could only originate from thiophene ring  $\pi$ - $\pi$  stacking, different from furan-based polyesters where the mesophase also resulted from interchain hydrogen bonds involving furan rings.

This is the reason why the result of the comparison between the functional properties of a thiophene-based polyester and the furan-based analogue with the same length of the glycol subunit changed according to the length of this latter.

Of particular importance is the comparison in terms of functional properties between the best-performing polymer of the thiophene-based family, namely PBTF, and PPeF, the best polymer within the family of 2,5-furandicarboxylic acid. Both polyesters were characterised by outstanding barrier properties, even though some differences, directly related to the nature of interchain interactions responsible of the resulting mesophase, exist: the strong interchain hydrogen bonds established in PPeF in addition to van der Waals  $\pi$ - $\pi$  interactions, also present among thiophene rings, explain the halving of the oxygen GTR value observed for the PPeF, whereas the lower dipole moment of the thiophene ring with respect to the furan one justified the doubling of the permselectivity ratio in the case of PBTF. In both cases, we are dealing with polymers with performances similar to EVOH, which is used as a high gas barrier material in multilayer films.

On the other hand, PBTF is more tough and ductile than PPeF, having an elastic modulus and a stress at break 5 and 3 times higher, respectively, than those of PPeF, the elongation at break being very high (>500%).

**Supplementary Materials:** The following are available online at <https://www.mdpi.com/article/10.3390/polym13152460/s1>, Figure S1: Pictures of compression-moulded films, Figure S2: Chromatograms of the synthesised polymers, Table S1: DSC data of the homopolymers in the form of purified powders, Figure S3:  $T_g$  and  $T_m$  trends as a function of glycolic subunit length for thiophene ring-containing polyesters compared to furan ring- and benzene ring-containing ones.

**Author Contributions:** Conceptualisation, M.S. and N.L.; methodology, G.G., V.S. and M.G.; investigation, G.G., V.S., M.S., M.G. and N.L.; data curation, G.G., V.S., M.S., M.G. and N.L.; writing—original draft preparation, G.G. and N.L.; writing—review and editing, G.G., M.S. and N.L.; supervision, M.S. and N.L. All authors have read and agreed to the published version of the manuscript.

**Funding:** This research received no external funding.

**Institutional Review Board Statement:** Not applicable.

**Informed Consent Statement:** Not applicable.

**Data Availability Statement:** The data that support the findings of this study are available from the corresponding author upon reasonable request.

**Conflicts of Interest:** The authors declare no conflict of interest.

## References

1. Plastics Europe-Plastics the Facts. 2020. Available online: <https://www.plasticseurope.org> (accessed on 12 June 2021).
2. European Bioplastics-Bioplastics Market Data. 2020. Available online: <https://docs.european-bioplastics.org> (accessed on 12 June 2021).
3. European Commission-A European Strategy for Plastics in a Circular Economy. 2015. Available online: <https://ec.europa.eu/environment/circular-economy/pdf/plastics-strategy-brochure.pdf> (accessed on 12 June 2021).

4. Top Value Added Chemicals from Biomass Volume I-Results of Screening for Potential Candidates from Sugars and Synthesis Gas. 2004. Available online: <https://www.nrel.gov/docs/fy04osti/35523.pdf> (accessed on 12 June 2021).
5. Burgess, S.K.; Leisen, J.E.; Kraftschik, B.E.; Mubarak, C.R.; Kriegel, R.M.; Koros, W.J. Chain Mobility, Thermal, and Mechanical Properties of Poly(ethylene furanoate) Compared to Poly(ethylene terephthalate). *Macromolecules* **2014**, *47*, 1383–1391. [CrossRef]
6. Burgess, S.K.; Mikkilineni, D.S.; Yu, D.B.; Kim, D.J.; Mubarak, C.R.; Kriegel, R.M.; Koros, W.J. Water sorption in poly(ethylene furanoate) compared to poly(ethylene terephthalate). Part 1: Equilibrium sorption. *Polymer* **2014**, *55*, 6861–6869. [CrossRef]
7. Burgess, S.K.; Mikkilineni, D.S.; Yu, D.B.; Kim, D.J.; Mubarak, C.R.; Kriegel, R.M.; Koros, W.J. Water sorption in poly(ethylene furanoate) compared to poly(ethylene terephthalate). Part 2: Kinetic sorption. *Polymer* **2014**, *55*, 6870–6882. [CrossRef]
8. Burgess, S.K.; Kriegel, R.M.; Koros, W.J. Carbon Dioxide Sorption and Transport in Amorphous Poly(ethylene furanoate). *Macromolecules* **2015**, *48*, 2184–2193. [CrossRef]
9. Wang, J.; Liu, X.; Jia, Z.; Liu, Y.; Sun, L.; Zhu, J. Synthesis of bio-based poly(ethylene 2,5-furandicarboxylate) copolyesters: Higher glass transition temperature, better transparency, and good barrier properties. *J. Polym. Sci. Part A Polym. Chem.* **2017**, *55*, 3298–3307. [CrossRef]
10. Van Putten, R.J.; Van der Waal, J.C.; De Jong, E.; Rasrendra, C.B.; Heeres, H.J.; De Vries, J.G. Hydroxymethylfurfural, A Versatile Platform Chemical Made from Renewable Resources. *Chem. Rev.* **2013**, *113*, 1499–1597. [CrossRef]
11. Zhi, W.; Hu, Y.; Liang, M.; Liu, Y.; Li, J.; Yin, J.; Shi, Y. Solid-liquid equilibrium and thermodynamic of 2,5-thiophenedicarboxylic acid in different organic solvents. *Fluid Phase Equilib.* **2014**, *375*, 110–114. [CrossRef]
12. Yang, Y.; Zhang, Q.; Cao, C.; Cheng, L.; Shi, Y.; Yang, W.; Hu, Y. Solubility and solution thermodynamics of 2,5-thiophenedicarboxylic acid in (water + ethanol) binary solvent mixtures. *Thermochim. Acta* **2014**, *592*, 52–57. [CrossRef]
13. Polen, T.; Spelberg, M.; Bott, M. Toward biotechnological production of adipic acid and precursors from biorenewables. *J. Biotechnol.* **2013**, *167*, 75–84. [CrossRef]
14. Corona, A.; Bidy, M.J.; Vardon, D.R.; Birkved, M.; Hauschild, M.Z.; Beckham, G.T. Life cycle assessment of adipic acid production from lignin. *Green Chem.* **2018**, *20*, 3857–3866. [CrossRef]
15. Guidotti, G.; Soccio, M.; Lotti, N.; Gazzano, M.; Siracusa, V.; Munari, A. Poly(propylene 2,5-thiophenedicarboxylate) vs. poly(propylene 2,5-furandicarboxylate): Two examples of high gas barrier bio-based polyesters. *Polymers* **2018**, *10*, 785. [CrossRef] [PubMed]
16. Guidotti, G.; Gigli, M.; Soccio, M.; Lotti, N.; Gazzano, M.; Siracusa, V.; Munari, A. Poly(butylene 2,5-thiophenedicarboxylate): An added value to the class of high gas barrier biopolyesters. *Polymers* **2018**, *10*, 167. [CrossRef] [PubMed]
17. Guidotti, G.; Gigli, M.; Soccio, M.; Lotti, N.; Salatelli, E.; Gazzano, M.; Siracusa, V.; Munari, A. Tailoring poly(butylene 2,5-thiophenedicarboxylate) features by the introduction of adipic acid co-units: Biobased and biodegradable aliphatic/aromatic polyesters. *Polymer* **2018**, *145*, 11–20. [CrossRef]
18. Guidotti, G.; Gigli, M.; Soccio, M.; Lotti, N.; Gazzano, M.; Siracusa, V.; Munari, A. Ordered structures of poly(butylene 2,5-thiophenedicarboxylate) and their impact on material functional properties. *Eur. Polym. J.* **2018**, *106*, 284–290. [CrossRef]
19. Wang, G.Q.; Liang, Y.; Jiang, M.; Zhang, Q.; Wang, R.; Wang, H.H.; Zhou, G.Y. Synthesis and characterization of bio-based polyesters from 2,5-thiophenedicarboxylic acid. *Polym. Degrad. Stab.* **2019**, *168*, 108942. [CrossRef]
20. Wang, G.Q.; Jiang, M.; Zhang, Q.; Wang, R.; Liang, Q.D.; Wang, H.H.; Zhou, G.Y. Partially bio-based and tough polyesters, poly(ethylene 2,5-thiophenedicarboxylate-co-1,4-cyclohexanedimethylene 2,5-thiophenedicarboxylate)s. *Express Polym. Lett.* **2019**, *13*, 938–947. [CrossRef]
21. Wang, G.Q.; Liang, Y.; Jiang, M.; Zhang, Q.; Wang, R.; Wang, H.H.; Zhou, G.Y. High T<sub>g</sub> and tough poly(butylene 2,5-thiophenedicarboxylate-co-1,4-cyclohexanedimethylene 2,5-thiophenedicarboxylate)s: Synthesis and characterization. *J. Appl. Polym. Sci.* **2020**, *137*, 48634. [CrossRef]
22. Wang, G.Q.; Jiang, M.; Zhang, Q.; Wang, R.; Liang, Q.D.; Zhou, G.Y. New bio-based copolyesters poly(trimethylene 2,5-thiophenedicarboxylate-co-trimethylene terephthalate): Synthesis, crystallization behavior, thermal and mechanical properties. *Polymer* **2019**, *173*, 27–33. [CrossRef]
23. Wang, G.Q.; Jiang, M.; Zhang, Q.; Wang, R.; Liang, Q.D.; Zhou, G.Y. New bio-based copolyesters derived from 1,4-butanediol, terephthalic acid and 2,5-thiophenedicarboxylic acid: Synthesis, crystallization behavior, thermal and mechanical properties. *Polym. Test.* **2019**, *75*, 213–219. [CrossRef]
24. Wang, J.G.; Zhang, X.Q.; Shen, A.; Zhu, J.; Song, P.A.; Wang, H.; Liu, X.Q. Synthesis and Properties Investigation of Thiophene-aromatic Polyesters: Potential Alternatives for the 2,5-Furandicarboxylic Acid-based Ones. *Chin. J. Polym. Sci.* **2020**, *38*, 1082–1091. [CrossRef]
25. Ferrario, V.; Pellis, A.; Cesugli, M.; Guebitz, G.M.; Gardossi, L. Nature Inspired Solutions for Polymers: Will Cutinase Enzymes Make Polyesters and Polyamides Greener? *Catalysts* **2017**, *6*, 205. [CrossRef]
26. Pellis, A.; Gamerith, C.; Ghazaryan, G.; Aortner, A.; Herrero Acero, E.; Guebitz, G.M. Ultrasound-enhanced enzymatic hydrolysis of poly(ethylene terephthalate). *Bioresour. Technol.* **2016**, *218*, 1298–1302. [CrossRef]
27. Weinberger, S.; Canadell, J.; Quartinello, F.; Yeniad, B.; Arias, A.; Pellis, A.; Guebitz, G.M. Enzymatic Degradation of Poly(ethylene 2,5-furanoate) Powders and Amorphous Films. *Catalysts* **2017**, *7*, 318. [CrossRef]
28. Gigli, M.; Quartinello, F.; Soccio, M.; Pellis, A.; Lotti, N.; Guebitz, G.M.; Licoccia, S.; Munari, A. Enzymatic hydrolysis of poly(1,4-butylene 2,5-thiophenedicarboxylate) (PBTF) and poly(1,4-butylene 2,5-furandicarboxylate) (PBF) films: A comparison of mechanisms. *Environ. Int.* **2019**, *130*, 104852. [CrossRef] [PubMed]

29. Guidotti, G.; Soccio, M.; García-Gutiérrez, M.C.; Ezquerro, T.; Siracusa, V.; Gutiérrez-Fernández, E.; Munari, A.; Lotti, N. Fully Biobased Superpolymers of 2,5-Furandicarboxylic Acid with Different Functional Properties: From Rigid to Flexible, High Performant Packaging Materials. *ACS Sustain. Chem. Eng.* **2020**, *8*, 9558–9568. [CrossRef] [PubMed]
30. Dobbertin, J.; Hensel, A.; Schick, C. Dielectric spectroscopy and calorimetry in the glass transition region of semi-crystalline poly(ethylene terephthalate). *J. Therm. Anal.* **1996**, *47*, 1027–1040. [CrossRef]
31. Sanz, A.; Nogales, A.; Ezquerro, T.A.; Lotti, N.; Munari, A.; Funari, S.S. Order and segmental mobility during polymer crystallization: Poly(butylene isophthalate). *Polymer* **2006**, *47*, 1281–1290. [CrossRef]
32. Soccio, M.; Lotti, N.; Finelli, L.; Munari, A. Thermal characterization of novel aliphatic polyesters with ether and thioether linkages. *e-Polymers* **2009**, *10*, 35.
33. Guidotti, G.; Soccio, M.; García-Gutiérrez, M.C.; Gutiérrez-Fernández, E.; Ezquerro, T.A.; Siracusa, V.; Munari, A.; Lotti, N. Evidence of a 2D-Ordered Structure in Biobased Poly(pentamethylene furanoate) Responsible for Its Outstanding Barrier and Mechanical Properties. *ACS Sustain. Chem. Eng.* **2019**, *7*, 17863–17871. [CrossRef]
34. Martínez-Tong, D.E.; Soccio, M.; Robles-Hernández, B.; Guidotti, G.; Gazzano, M.; Lotti, N.; Alegria, A. Evidence of Nanostructure Development from the Molecular Dynamics of Poly(pentamethylene 2,5-furanoate). *Macromolecules* **2020**, *53*, 10526–10537. [CrossRef]
35. Rudyak, V.Y.; Gavrilov, A.A.; Guseva, D.V.; Tung, S.H.; Komarov, P.V. Accounting for  $\pi$ - $\pi$  stacking interactions in the mesoscopic models of conjugated polymers. *Mol. Syst. Des. Eng.* **2020**, *5*, 1137. [CrossRef]
36. Sago, T.; Itagaki, H.; Asano, T. Onset of Forming Ordering in Uniaxially Stretched Poly(ethylene terephthalate) Films Due to  $\pi$ - $\pi$  Interaction Clarified by the Fluorescence. *Macromolecules* **2014**, *47*, 217–226. [CrossRef]
37. Shanavas, A.; Sathiyaraj, S.; Chandramohan, A.; Narasimhaswamy, T.; Sultan Nasar, A. Isophthalic acid based mesogenic dimers: Synthesis and structural effects on mesophase properties. *J. Mol. Struct.* **2013**, *1038*, 126–133. [CrossRef]
38. Mahendrasingam, A.; Blundell, D.J.; Martin, C.; Urban, V.; Narayanan, T.; Fuller, W. Time resolved WAXS study of the role of mesophase in oriented crystallisation of poly(ethylene terephthalate-co-isophthalate) copolymers. *Polymer* **2005**, *46*, 6044–6049. [CrossRef]
39. Hedenqvist, M.S. Barrier Packaging Materials. In *Handbook of Environmental Degradation of Materials*, 2nd ed.; Kutz, M., Ed.; Elsevier, Inc.: Amsterdam, The Netherlands, 2012; pp. 840–842.
40. Quattrosoldi, S.; Lotti, N.; Soccio, M.; Schick, C.; Androsch, R. Stability of Crystal Nuclei of Poly (butylene isophthalate) Formed Near the Glass Transition Temperature. *Polymers* **2020**, *12*, 1099. [CrossRef] [PubMed]
41. Quattrosoldi, S.; Androsch, R.; Janke, A.; Soccio, M.; Lotti, N. Enthalpy Relaxation, Crystal Nucleation and Crystal Growth of Biobased Poly(butylene Isophthalate). *Polymers* **2020**, *12*, 235. [CrossRef]
42. Genovese, L.; Gigli, M.; Lotti, N.; Gazzano, M.; Siracusa, V.; Munari, A.; Dalla Rosa, M. Biodegradable Long Chain Aliphatic Polyesters Containing Ether-Linkages: Synthesis, Solid-State, and Barrier Properties. *Ind. Eng. Chem. Res.* **2014**, *53*, 10965–10973. [CrossRef]
43. Guidotti, G.; Soccio, M.; Siracusa, V.; Gazzano, M.; Salatelli, E.; Munari, A.; Lotti, N. Novel Random PBS-Based Copolymers Containing Aliphatic Side Chains for Sustainable Flexible Food Packaging. *Polymers* **2017**, *9*, 724. [CrossRef]
44. Robertson, G.L. Optical, Mechanical and Barrier Properties of Thermoplastics Polymers. In *Food Packaging-Principles and Practice*, 3rd ed.; CRC Press: Boca Raton, FL, USA, 2013; pp. 91–130.
45. Mensitieri, G.; Di Maio, E.; Buonocore, G.G.; Nedi, I.; Oliviero, M.; Sansone, L.; Iannace, S. Processing and shelf life issues of selected food packaging materials and structures from renewable resources. *Trends Food Sci. Technol.* **2011**, *22*, 72–80. [CrossRef]

## Article

# Dissolution and Interaction of Cellulose Carbamate in NaOH/ZnO Aqueous Solutions

Yanhui Kang, Fangyu Wang, Zeming Zhang and Jinping Zhou \*

Hubei Engineering Center of Natural Polymers-Based Medical Materials, Key Laboratory of Biomedical Polymers of Ministry of Education, Department of Chemistry, Wuhan University, Wuhan 430072, China; kangyanhui0707@163.com (Y.K.); wangfangyu9527@gmail.com (F.W.); zmzhang0224@163.com (Z.Z.)

\* Correspondence: zhoujp325@whu.edu.cn

**Abstract:** The dissolution and molecular interactions of cellulose carbamate (CC) in NaOH/ZnO aqueous solutions were studied using optical microscopy, differential scanning calorimetry (DSC),  $^1\text{H}$  NMR, dynamic light scattering (DLS), atomic force microscopy (AFM), transmission electron microscopy (TEM), and molecular dynamic simulation. The dissolution of CC in NaOH/ZnO aqueous solutions using the freezing–thawing method was an exothermic process, and the lower temperature was favorable for the dissolution of CC. ZnO dissolved in NaOH aqueous solutions with the formation of  $\text{Zn}(\text{OH})_4^{2-}$ , and no free  $\text{Zn}^{2+}$  ions existed in the solvents. NaOH/ $\text{Na}_2\text{Zn}(\text{OH})_4$  system formed strong interactions with the hydroxyl groups of CC to improve its solubility and the stability of CC solution. The results indicate that 7 wt% NaOH/1.6 wt% ZnO aqueous solution was the most appropriate solvent for the dissolution of CC. This work revealed the dissolution interaction of CC–NaOH/ZnO solutions, which is beneficial for the industrialization of the CarbaCell process.

**Keywords:** cellulose carbamate; NaOH/ZnO aqueous solution; freezing–thawing method; dissolution interaction

**Citation:** Kang, Y.; Wang, F.; Zhang, Z.; Zhou, J. Dissolution and Interaction of Cellulose Carbamate in NaOH/ZnO Aqueous Solutions. *Polymers* **2021**, *13*, 1092. <https://doi.org/10.3390/polym13071092>

Academic Editor: Cristina Cazan

Received: 18 March 2021

Accepted: 28 March 2021

Published: 30 March 2021

**Publisher's Note:** MDPI stays neutral with regard to jurisdictional claims in published maps and institutional affiliations.



**Copyright:** © 2021 by the authors. Licensee MDPI, Basel, Switzerland. This article is an open access article distributed under the terms and conditions of the Creative Commons Attribution (CC BY) license (<https://creativecommons.org/licenses/by/4.0/>).

## 1. Introduction

It is well known that the rapidly growing awareness of environmental pollution has shifted researchers' focus from traditional petroleum-derived synthetic polymers to more environmentally friendly alternatives [1]. As a widely available reproducible organic material, cellulose is a promising substitute to fossil resources because of its renewability, nontoxicity, and environmental friendliness [2]. Furthermore, it has been developed for thousands of years in the production of fiber, paper, film, filters, and textiles [3–5]. However, a large number of intra- and intermolecular hydrogen bonds of cellulose hinder dissolution, which is an impediment to its wide utilization [6]. Nevertheless, the derivatization of cellulose can improve its solubility and enable new functions and applications [7]. Cellulose xanthogenate is an ancient viscose technology that has been used for more than 100 years [8,9]. The traditional viscose process consumes significant time and energy, is expensive, and produces harmful by-products such as  $\text{CS}_2$ ,  $\text{H}_2\text{S}$ , and heavy metals [10,11]. The development of environmentally friendly systems and processes for the regenerated cellulose industry has been highly valuable. To reduce processing steps and minimize harmful by-products, multiple innovative methods and novel solvents for cellulose have been developed [12–17]. However, commercially viable processes are rare.

The CarbaCell process is a promising alternative to the conventional viscose method, and employs cellulose carbamate (CC) as an active intermediate for fiber spinning [18,19]. Cellulose reacts with urea to produce CC, which is soluble in NaOH aqueous solutions [20]. The use of innocuous urea avoids the problem associated with hazardous sulfur-containing compounds. Several means exist to synthesize CC, including esterification reaction in *N,N*-dimethylacetamide (DMAc) [21], the isocyanate-pyridine procedure [22], the “pad-drycure” method [23], supercritical  $\text{CO}_2$ -assisted impregnation [24,25], and electron ra-

diation [26]. In previous work, we reported the fast synthesis of CC in several minutes by microwave heating without using a solvent or catalyst [27–29]. More recently, the low content of urea aqueous solution was used to soak cellulose, and CC was synthesized by conventional heating [30,31]. CC can be dissolved in 9 wt% NaOH aqueous solution [28]. However, a rheological study showed that CC/NaOH aqueous solutions were extremely prone to forming gel at room temperature [27]. To improve the solubility of CC and the stability of spinning dope, researchers have conducted extensive research. For example, it has been found that the addition of a small amount of urea to NaOH aqueous solution can increase the solubility of CC and reduce the viscosity of the solution [20]. CC can also be dissolved in precooled 18 wt% NaOH solution under intensive stirring [32]. However, none of these methods have achieved industrial CarbaCell production. Therefore, the dissolution of CC is particularly important for green and sustainable development [33].

Cellulose can be dissolved in NaOH [34], NaOH/urea [17] and NaOH/zinc nitrate hexahydrate aqueous solutions [35] using the freezing–thawing method to obtain transparent solutions. This can be ascribed to the partial cleavage of hydrogen bonds between the hydroxyl groups of cellulose [35]. Similarly, the desired amount of CC can be dissolved into the NaOH/ZnO aqueous system, and a transparent CC solution can also be obtained by the freezing–thawing method [36]. We found that adding a small amount of ZnO to NaOH aqueous solution can significantly improve the solubility of CC and the stability of the spinning dope. The regenerated cellulose filaments, membranes, and nanocomposites have been successfully prepared from the CC solutions [37,38]. However, the interactions of CC–NaOH/ZnO aqueous solutions have not been explored systematically to date. In this work, the dissolution and interaction of CC in NaOH/ZnO aqueous solutions were investigated in detail. In NaOH aqueous systems, ZnO existed in the form of  $\text{Zn}(\text{OH})_4^{2-}$  hydrates. NaOH/ $\text{Na}_2\text{Zn}(\text{OH})_4$  hydrates can form stronger interactions with the hydroxyl groups of CC compared with the sole NaOH hydrates, thus promoting the dissolution of CC. These stronger interactions may include H-bonding, ionic, and electrostatic interactions.

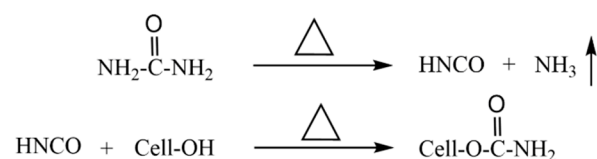
## 2. Experimental Section

### 2.1. Materials

Cotton linter pulps with  $\alpha$ -cellulose content of more than 95% were provided by Hubei Chemical Fiber Co. Ltd. (Xiangyang, China) as the cellulose raw materials. The  $M_w$  in cadoxen was determined by viscometry to be  $7.4 \times 10^4$  g/mol. NaOH, urea, and ZnO of analytical grade (Shanghai Chemical Reagent Co. Ltd., Shanghai, China) were used directly. Deionized water was used throughout the whole experiment.

### 2.2. Oven Heating Synthesis of CC

According to the previous work [38,39], every 100 g of cotton linter pulp was immersed into 2000 g of urea solution with the concentration of 3 wt%. To make the cotton linter pulps fully immersed in the urea solution, the mixtures were stirred every 1 h at 25 °C for 8 h, then filtered, and vacuum dried. Subsequently, the mixtures of cellulose/urea with the urea content of 3.5 wt% were obtained. The cellulose/urea mixtures were heated in an oven at 132.7 °C in a sealed container for 30 min and then heated to 160 °C for 60 min. Finally, the mixtures were washed with deionized water and vacuum-dried at 50 °C. The synthesis of CC from cellulose and urea was as Scheme 1 [18]:



**Scheme 1.** The synthesis process of CC from cellulose and urea.

### 2.3. Dissolution of CC

Based on previous work [30], NaOH and ZnO were directly dissolved in distilled water to obtain the solvents. The contents of NaOH and ZnO were varied from 5 to 10 wt% and 0 to 2 wt%, respectively. ZnO is an amphoteric oxide, which exists as  $\text{Zn}(\text{OH})_4^{2-}$  in the alkali aqueous solution:  $\text{ZnO} + 2\text{OH}^- + \text{H}_2\text{O} \rightarrow \text{Zn}(\text{OH})_4^{2-}$ . The specific composition of the solvent is shown in Table S1.

Subsequently, the desired amount of CC was dispersed into the solvent, cooled to  $-24\text{ }^\circ\text{C}$  in the refrigerator to form a solid for 8 h, and then thawed at ambient temperature. The dissolved and insoluble portions in the solutions were separated by centrifugation at 7000 rpm for 10 min to obtain the clear CC solution.

### 2.4. Characterizations

The intrinsic viscosity ( $[\eta]$ ) of CC in cadoxen at  $25\text{ }^\circ\text{C}$  was determined with an Ubbelohde viscometer [40], and the viscosity-average molecular weight ( $M_\eta$ ) was determined to be  $7.0 \times 10^4$  g/mol. The nitrogen content of CC was ascertained to be 0.832%, which was measured using an elemental analyzer (CHN-O-RAPID Hereaus Co., Hanau, Germany). Then, 500 mL NaOH/ZnO aqueous solution was placed in a glass bottle and sealed for 30 days, waiting for the crystal to precipitate out. Then we poured the solvent out and used the spoon to scrape the crystals off the bottle wall. We washed them with distilled water and froze them to dry. X-ray diffraction (XRD) measurement was performed using an XRD diffractometer (D8-Advance, Bruker, Karlsruhe, Germany). The pattern of Cu  $K\alpha$  radiation ( $\lambda = 0.15418$  nm) at 40 kV and 30 mA was recorded in the  $2\theta$  region from  $10$  to  $80^\circ$  at a scanning speed of  $4^\circ/\text{min}$ .

An optical microscope (ZEISS AXIO SCOPE A1POL) was used to observe the dissolution of CC in the solvent as the freezing time extended. The CC and solvent mixtures were taken out of the refrigerator at different freezing times. Subsequently, an appropriate amount of mixture was directly pressed between the two glass slides, then sealed with paraffin, observed, and photographed. The solubility of CC was determined by observing the CC solutions with the polarized mode. After a certain concentration of CC was obtained, the solution was subjected to polarized microscope observation at room temperature. The area observed in the polarized microscope was a 20 mm diameter circular field. When no fibers were observed, CC was considered to be dissolved at that concentration. Each solubility was tested at least 3 times to confirm the accuracy and repeatability.

Differential scanning calorimetry (DSC) measurements were made using a TA Q20 instrument (New Castle, DE, USA). CC was dispersed in NaOH (5–10 wt%)/ZnO (0–1.6 wt%) hydrates and sealed in a stainless pan. The temperature was programmed from  $20$  to  $-40\text{ }^\circ\text{C}$  and then from  $-40$  to  $20\text{ }^\circ\text{C}$  at a rate of  $1\text{ }^\circ\text{C}/\text{min}$  under  $\text{N}_2$  atmosphere.  $^1\text{H}$  NMR spectra were measured on a Varian INOVA-600 spectrometer in the proton noise-decoupling mode at  $25\text{ }^\circ\text{C}$ . The chemical shifts of protons were referenced to the signals of  $\text{D}_2\text{O}$  and tetramethylsilane (TMS). The CC concentrations for DSC and  $^1\text{H}$  NMR measurements were 5 wt% and 0.3 wt%, respectively.

The hydrodynamic radius ( $R_h$ ) distributions of CC in NaOH/ZnO aqueous solutions were characterized by dynamic light scattering (DLS) on a multi-angle light scattering spectrometer (ALV/SP-125, ALV, Langen, Germany) equipped with an ALV-5000/E multi-digital time correlator. The scattering angle was  $90^\circ$ . The solutions were kept for 10 min at each condition before measurement. All of the CC solutions ( $c = 0.3$  g/L) were optically cleaned through 0.45 and 0.22  $\mu\text{m}$  Millipore filters (Whatman, Inc., Clifton, NJ, USA).

Atomic force microscope (AFM) images were measured with an AFM (Cypher ES, Asylum Research, Santa Barbara, CA, USA) in ac mode at  $25\text{ }^\circ\text{C}$ . Silicon probes with a spring constant of 2 N/m and resonance frequency of 70 kHz (OLTESPA-R3, Bruker, Billerica, MA, USA) were employed. All data from the images were analyzed using AFM accessory software, and the images presented were flattened only when necessary. The CC solution was purified by a 0.22  $\mu\text{m}$  Millipore filter (Whatman, Inc., Clifton, NJ, USA), deposited onto the wafer, and air-dried overnight before imaging. TEM images were obtained using a

JEM-2010(HT) transmission electron microscope (JEOL TEM, Tokyo, Japan). Before TEM observation, the CC solution was cast onto a perforated carbon film, which was supported on a copper grid, and air-dried overnight. The concentration of CC for AFM and TEM measurements was  $1.0 \times 10^{-4}$  g/mL. To make the image clearer, we use distilled water to gently moisten the surface of the sample to remove excess salt particles.

Molecular dynamic simulation software was used to confirm the interaction between CC and solvents. The calculation was performed using Amber 3 force field as implemented in Hyper Chem 8.0.10. A set of 0.1 Kcal/(Å·mol) and a conjugate gradient method (Polak–Ribiere) were used for geometric optimization. During energy minimization, the molecular structure was simulated, in which small changes in geometry can give the most stable configuration. Modeling helped to explore the effect of the non-covalent interactions, specifically the hydrogen bond in the growing polymer chains. The volume of the periodic analog box was  $12 \times 10 \times 8$  Å. In this simulation, 10 repeating units were calculated and  $\text{Zn}^{2+}$ ,  $\text{Na}^+$ ,  $\text{OH}^-$  and  $\text{H}_2\text{O}$  were introduced into the simulation process. The composition of the force field in the simulation included covalent bonds, angles, and twists, in addition to the interaction of electrostatic and hydrogen bonds [41–43].

### 3. Results and Discussion

The optical microscopic images of CC dissolved in 7 wt% NaOH and 7 wt% NaOH/1.6 wt% ZnO solutions with various freezing times are shown in Figure 1. After soaking for a short time at room temperature (freezing 0 min), the morphology of CC, both in 7 wt% NaOH and 7 wt% NaOH/1.6 wt% ZnO aqueous solutions, was not obviously different. CC was lightly swelled in the solvent, and the diameters of fibers were in the range of 15–70  $\mu\text{m}$  (Figure 1a,f). The degree of swelling and dispersion augmented as the freezing time increased from 0 to 5 min. It has been reported that cellulose could expand in strong alkaline media [44,45]. CC began to expand on the fibers' isolated points, forming balloons (Figure 1b,g). The area of the balloons inflated, resulting in the appearance of bead-like structures. The diameter of the fibers expanded until they broke. After the balloons exploded, CC solution coexisted with the undissolved CC in the mixed system. When the freezing time reached 10 min, both CC in 7 wt% NaOH and 7 wt% NaOH/1.6 wt% ZnO systems had analogous clear microscope images and transparent solutions were obtained (Figure 1c,h), indicating the complete dissolution of CC. Although CC can be dissolved in a 7 wt% NaOH system (Figure 1d), the obtained CC/7 wt% NaOH solutions easily changed into gel due to the unstable interaction of CC–NaOH (Figure 1e), and the sol-gel transition was a thermo irreversible process [27]. However, the CC/7 wt% NaOH/1.6 wt% ZnO solutions can be stable for a long period (Figure 1i,j).

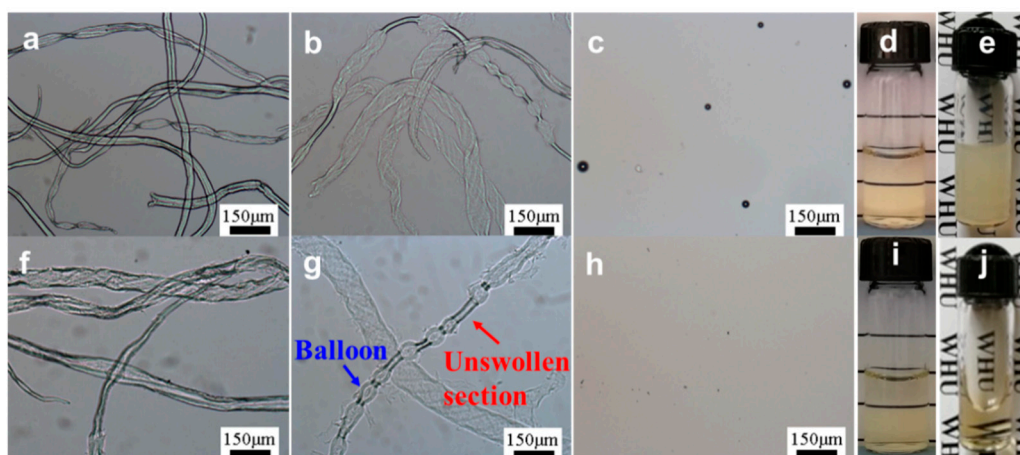


**Figure 1.** Optical microscopic observation of cellulose carbamate (CC) dissolving process in (a–e) 7 wt% NaOH and (f–j) 7 wt% NaOH/1.6 wt% ZnO aqueous solutions at  $-24$  °C for different duration times: (a,f) 0 min; (b,g) 5 min; (c,h) 10 min. (d,i) the new CC solutions and (e,j) CC solutions placed at room temperature for 12 h.

By adding a small amount of ZnO to the NaOH aqueous solutions, the solubility of CC was also significantly improved. Figure S1 shows the solubility of CC increased with an increasing mass fraction of NaOH (5–10 wt%) and ZnO (0–1.6 wt%), whereas the solubility of CC decreased in 7 wt% NaOH/2 wt% ZnO solution. The 7 wt% NaOH/2 wt% ZnO solution was unstable due to the excess of ZnO. As shown in Figure S2, the crystals of orthorhombic  $\text{Zn}(\text{OH})_2$  (JCPDS 38-0385) will precipitate out from the solutions over the storage time at room temperature. The maximum solubility (9 wt%) of CC was obtained in the 7 wt% NaOH/1.6 wt% ZnO system. NaOH aqueous solution can not only dissolve CC, but also provide conversion of ZnO to  $\text{Zn}(\text{OH})_4^{2-}$ , thus improving the solubility of CC and maintaining the stability of CC solution. NaOH/ZnO solutions possessed stronger dissolving capacity than the pure NaOH solution, suggesting that  $\text{Zn}(\text{OH})_4^{2-}$  performed the auxiliary role in the dissolution of CC at the lower temperature.

Dissolution of cellulose has been proven to be a process involved with the thermal effect [46–48]. Figure 2 shows the magnified DSC curves for the cooling (from 15 to  $-20^\circ\text{C}$ ) and heating (from  $-40$  to  $20^\circ\text{C}$ ) processes of the CC mixed with NaOH/ZnO systems. It is worth noting that the subtle exothermic peaks for the dissolution of CC were observed at the temperature range of 15 to  $-20^\circ\text{C}$ . When the ZnO content was 1.6 wt%, the dissolution enthalpy peaks of CC gradually shifted from  $-12.7$  to  $11.9^\circ\text{C}$  as the NaOH content increased from 6 to 10 wt% (Figure 2a), suggesting that the interaction between CC and solvents gradually enhanced with an increase in the NaOH content [47]. The dissolution enthalpy peaks of CC in 5 wt% NaOH/1.6 wt% ZnO aqueous solution could not be observed because it was lower than  $-20^\circ\text{C}$ . The dissolution of CC in NaOH/ZnO aqueous solution indicated a representative exothermic enthalpy-driven process. In the heating process, the melting enthalpy peaks of CC/NaOH/ZnO frozen mass shifted slightly from  $-8.7$  to  $-4.8^\circ\text{C}$  as the NaOH content increased from 5 to 10 wt% (Figure 2c). Analogously, when the NaOH content was 7 wt%, the dissolution enthalpy peaks of CC shifted slightly from  $-7.9$  to  $-3.6^\circ\text{C}$  as the ZnO content increased from 0 to 1.6 wt% (Figure 2b). As a result that the stability of 7 wt% NaOH/2.0 wt% ZnO solvent was lowered, the dissolution enthalpy peak of CC shifted to  $-3.8^\circ\text{C}$ . Moreover, the melting enthalpy peaks of CC/NaOH/ZnO frozen mass gradually shifted from  $-8.2$  to  $-6.2^\circ\text{C}$  as the ZnO content increased from 0 to 1.6 wt%, and then shifted to  $-7.6^\circ\text{C}$  as the ZnO content further increased to 2.0 wt% (Figure 2d).

The corresponding dissolution enthalpies of CC and melting enthalpies of CC/NaOH/ $\text{Na}_2\text{Zn}(\text{OH})_4$  systems are shown in Figure 3. When the ZnO content was 1.6 wt% and the NaOH content increased from 5 to 10 wt%, the dissolution enthalpies of CC increased from 0.28 to 1.85 J/g, and the melting enthalpies of CC/NaOH/ $\text{Na}_2\text{Zn}(\text{OH})_4/\text{H}_2\text{O}$  frozen mass increased from 118.2 to 170.4 J/g. When the NaOH content was 7 wt% and the ZnO content increased from 0 to 1.6 wt%, the dissolution enthalpies of CC gradually increased from 0.58 to 0.78 J/g. Similarly, the melting enthalpies of the frozen mass gradually increased from 128.5 to 143.4 J/g. There was a conspicuous transition in the dissolution and melting enthalpy curves in the light of ZnO content, located at the mass fraction of 7 wt% NaOH/1.6 wt% ZnO. This mass proportion was considered to be the optimum ratio for the dissolution of CC. After further increasing the ZnO content to 2.0 wt%, the dissolution enthalpy of CC and melting enthalpy of CC/NaOH/ $\text{Na}_2\text{Zn}(\text{OH})_4/\text{H}_2\text{O}$  frozen mass declined slightly to 0.74 and 140.4 J/g, respectively. Therefore, excessive ZnO was not conducive to the dissolution of CC. The melting enthalpies were related the amount of melting structures. As shown in Table S1, the quantity of NaOH and  $\text{Na}_2\text{Zn}(\text{OH})_4$  hydrates in the solvent increased with increasing NaOH (5–10 wt%) and ZnO (0–1.6 wt%) content. Therefore, the quantity of CC/NaOH/ $\text{Na}_2\text{Zn}(\text{OH})_4$  hydrates also increased when CC was added into the solvent.



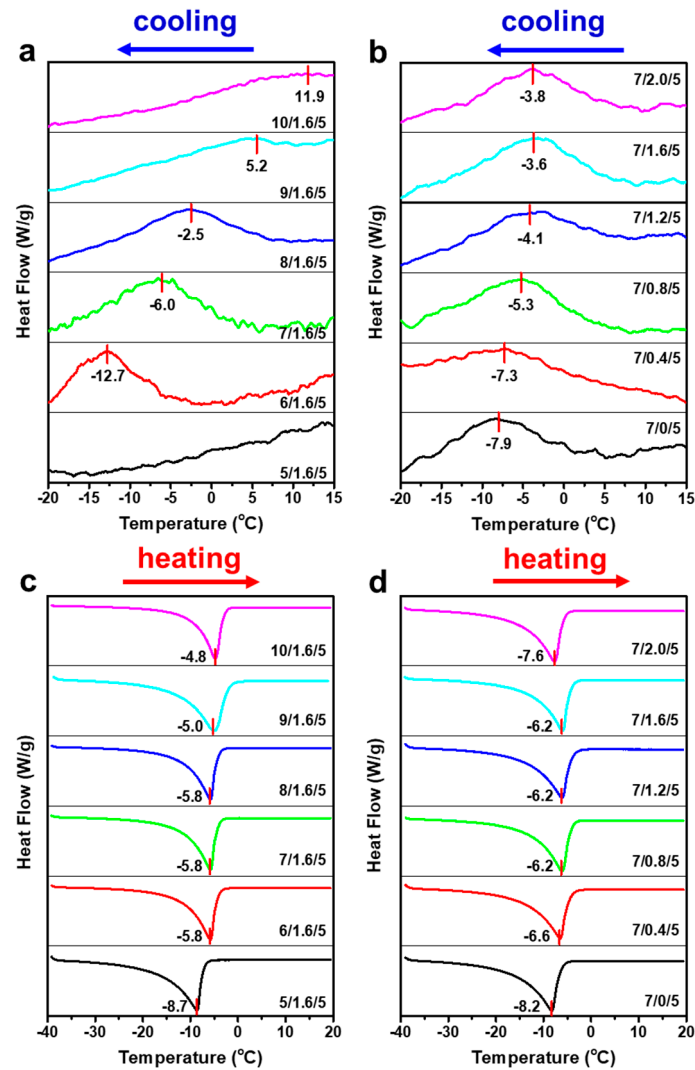


Figure 2. Magnified DSC (a,b) cooling and (c,d) heating thermograms of 5 wt% CC in NaOH/ZnO aqueous solutions with various NaOH and ZnO contents.

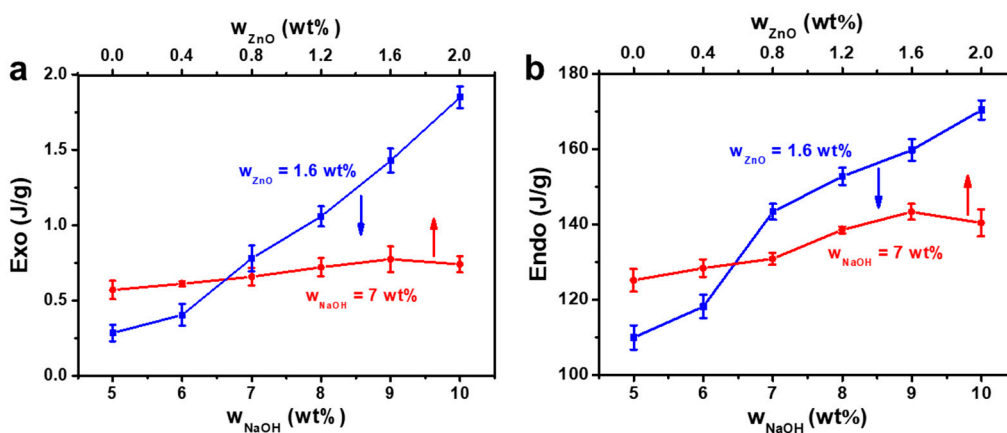
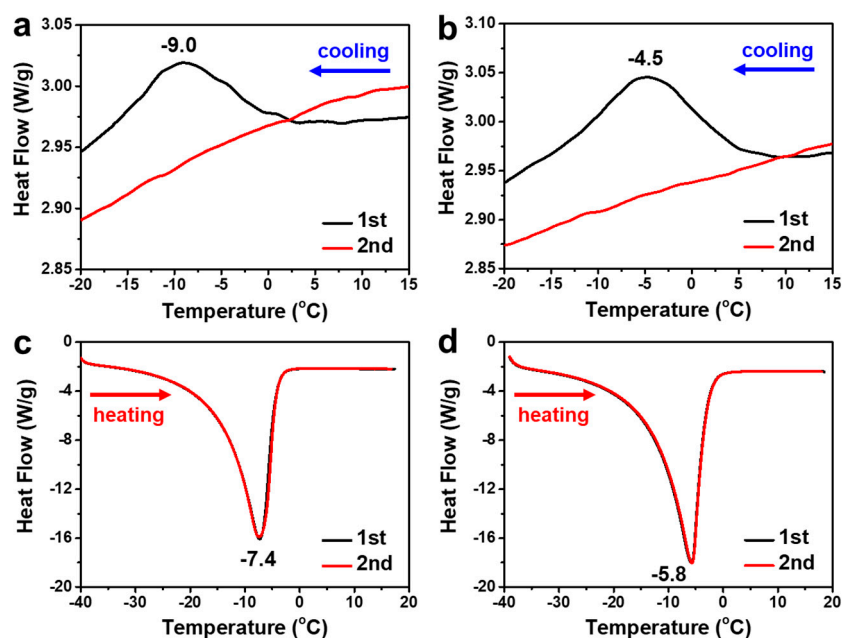


Figure 3. (a) The dissolution enthalpies of CC and (b) The melting enthalpies of CC/NaOH/Na<sub>2</sub>Zn(OH)<sub>4</sub>/H<sub>2</sub>O frozen mass as a function of NaOH and ZnO contents.

The magnified DSC profiles of the cooling and heating processes during two cycles of CC (5 wt%) in 7 wt% NaOH and 7 wt% NaOH/1.6 wt% ZnO systems are dis-

played in Figure 4. It is worth noting that the dissolution enthalpy peaks of CC only appeared in the first cooling cycle, both in NaOH and NaOH/ZnO aqueous solutions ( $-9.0$  and  $-4.5$  °C, respectively). No dissolution enthalpy peak occurred in the second cooling process at the temperature range from 15 to  $-20$  °C, indicating that the complete dissolution of CC was achieved by merely cooling once (Figure 4a,b) [49,50]. In the heating profiles of CC/NaOH and CC/NaOH/ZnO frozen mass, sharp melting enthalpy peaks appeared at  $-7.4$  and  $-5.8$  °C, respectively (Figure 4c,d). Figure S3 shows the melting enthalpies of CC/NaOH and the CC/NaOH/ $\text{Na}_2\text{Zn}(\text{OH})_4$  frozen mass. Whether the first or second cycle, the melting enthalpy of the CC/NaOH/ $\text{Na}_2\text{Zn}(\text{OH})_4$  frozen mass is larger than that of the CC/NaOH frozen mass. When the CC concentration is varied from 1 to 5 wt% (Figure S4a,b), the melting enthalpy peaks gradually shifted from  $-6.9$  to  $-6.2$  °C (CC/NaOH frozen mass) and  $-5.7$  to  $-4.1$  °C (CC/NaOH/ZnO frozen mass). Furthermore, the corresponding melting enthalpies (Figure S4c) also increase from 117.1 to 135.6 J/g and 141.0 to 144.8 J/g, respectively.



**Figure 4.** Magnified DSC profiles of cooling and heating thermograms of 5 wt% CC in (a,c) 7 wt% NaOH and (b,d) 7 wt% NaOH/1.6 wt% ZnO aqueous solutions.

The chemical shifts of NMR spectra are sensitive to the formation and breakage of hydrogen bonding [51]. The proton shift strongly depends on the concentration of electrolytes when they are added into water [52]. Hence,  $^1\text{H}$  NMR was used to study the structure and interaction of CC in the solvent systems (Figure 5). Due to the rapid proton exchange, the chemical shift at 4.78 ppm belonged to the protons of  $\text{D}_2\text{O}$  in the coaxial capillaries as an external reference. The signals distributed in the range of 2.5–4.5 ppm corresponded to the protons of glucose rings of CC [53]. The chemical shifts of H1 (4.3 ppm), H6a (3.8 ppm), H6b (3.6 ppm), H3,4,5 (3.4 ppm), and H2 (3.1 ppm) for CC in 5 wt% NaOH/0.4 wt% ZnO/ $\text{D}_2\text{O}$  were larger than those of H1 (4.1 ppm), H6a (3.6 ppm), H6b (3.4 ppm), H3,4,5 (3.2 ppm), and H2 (3.0 ppm) for CC in 10 wt% NaOH/0.4 wt% ZnO wt%/D<sub>2</sub>O. Clearly, the signals of the protons shifted upfield with an increase in the NaOH content (Figure 5a) [54,55]. Their upfield shift is likely a consequence of a higher extent of hydrogen bonding and deprotonation involving  $-\text{OH}$  groups exerting thus a shielding effect on the C-H protons. The  $\text{OH}^-$  ion acted as strong hydrogen bonding acceptors and formed hydrogen bonding with  $-\text{OH}$  groups in alkali solutions. The higher the concentration of NaOH, the stronger the hydrogen bonding interaction between  $\text{OH}^-$  ion and  $-\text{OH}$  group, resulting in the stronger electro-shielding effect of CC [56]. Therefore, the proton res-

onances were shifted upfield with an increase in the NaOH concentration. Figure 5b shows the  $^1\text{H}$  NMR spectra of CC solutions with different ZnO contents. The chemical shifts of the protons in 7 wt% NaOH/ $\text{D}_2\text{O}$  solutions were H1 (4.2 ppm), H6a (3.6 ppm), H6b (3.5 ppm), H3,4,5 (3.2 ppm), and H2 (3.0 ppm). The signal of the protons moved to the higher field as the ZnO content increased from 0 to 1.6 wt%. After adding ZnO to NaOH(aq),  $\text{Zn}(\text{OH})_4^{2-}$  acted as stronger proton acceptors than  $\text{OH}^-$ , the deprotonation effects of  $-\text{OH}$  groups increased in NaOH/ZnO(aq), and the electro-shielding effect of the protons also increased. As a result, the signals of protons moved upfield upon the addition of ZnO. Moreover, when the ZnO contents were in the range of 1.2–2.0 wt%, the resonances of protons hardly changed, which were H1 (4.0 ppm), H6a (3.5 ppm), H6b (3.3 ppm), H3,4,5 (3.0 ppm), and H2 (2.8 ppm), respectively. Therefore, the ZnO content did not have further influence on the chemical shifts, and thus did not have further influence on the interaction between CC and solvent system. Compared with Figure 5a,b, we can conclude that the hydrogen-bonding and deprotonation effect between CC and the NaOH/ZnO system are stronger than those between CC and the NaOH system.

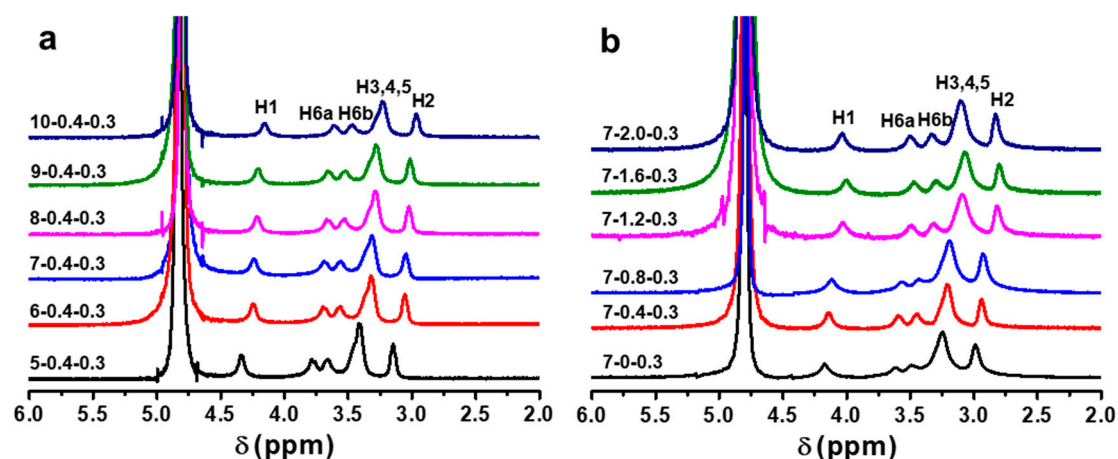


**Figure 5.**  $^1\text{H}$  NMR spectra of CC ( $c = 0.3$  wt%) in NaOH/ZnO/ $\text{D}_2\text{O}$  with different (a) NaOH and (b) ZnO contents.

The dissolved state of CC in NaOH/ZnO aqueous solutions was also verified by DLS, which was evidenced by its  $R_h$  distributions. Figure 6 shows the  $R_h$  distributions of CC in various solvent systems. Only one symmetrical peak existed in the CC solutions. As the NaOH content increased from 5 to 10 wt%, the  $R_h$  distributions of CC gradually narrowed, suggesting that the higher concentration of  $\text{OH}^-$  was beneficial to the dissolution of CC (Figure 6a). As displayed in Figure 6b, the  $R_h$  distributions of CC gradually narrowed as the ZnO content increased from 0 to 1.6 wt%, suggesting that CC was uniformly dissolved in the solvent system. However, when the ZnO content reached 2.0 wt%, the peak was wide, indicating that the excessive ZnO caused uneven dissolution of CC. According to our experiment,  $\text{Zn}(\text{OH})_2$  crystals gradually precipitated out of the CC solution when the solvent was 7 wt% NaOH/2.0 wt% ZnO hydrates. An appropriate amount of ZnO added to the 7 wt% NaOH solution could dissolve a greater quantity of CC. However, excessive ZnO added to the 7 wt% NaOH solution would worsen the dissolution effect. Figure S5 shows the  $R_h$  values of CC in NaOH/ZnO aqueous solutions with various NaOH and ZnO contents. When the ZnO content was 1.6 wt%, the  $R_h$  values of CC decreased from  $37.7 \pm 2.2$  to  $18.0 \pm 1.4$  nm as the NaOH content increased from 5 to 10 wt%. When the NaOH content was fixed at 7 wt%, the  $R_h$  values of CC decreased from  $43.7 \pm 2.8$  to  $21.4 \pm 1.6$  nm as the ZnO content increased from 0 to 1.6 wt%. When the ZnO content attained 2.0 wt%, the  $R_h$  of CC chains increased to  $29.0 \pm 2.1$  nm due to the instability of the solution.  $R_h$  reflects the solvation of CC [57]. The stronger the solvation effect, the more thoroughly the CC was dissolved. This is because the more solvent molecules that CC was exposed to, the better the dissolution of CC at low temperature. Based on the above results, considering that excess NaOH was not conducive to large-scale production

in the plant, it was reasonable to believe that 7 wt% NaOH/1.6 wt% ZnO solution was the most appropriate solvent for CC.

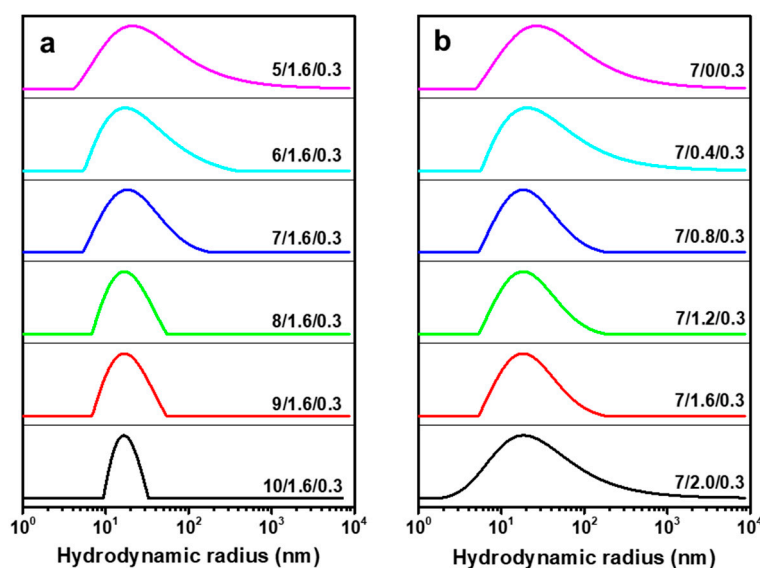


**Figure 6.** Hydrodynamic radius ( $R_h$ ) distributions of CC ( $c = 0.3$  g/L) in NaOH/ZnO aqueous solutions with various contents of (a) NaOH and (b) ZnO at 25 °C.

Under strictly controlled and identical drying conditions, the CC solutions lose water and the CC shrink during the drying process, resulting in the aggregation of nanofibers [51,58]. To indirectly explore the dissolving effect of CC in NaOH and NaOH/ZnO aqueous solutions, the morphology of CC dried from the dilute solution was measured by AFM. As shown in Figure 7a, the aggregation state of CC was obvious. In contrast, Figure 7b shows the better dissolved state of CC. The heights indicated by red and black lines in the AFM images were estimated to be 1.0 to 6.0 nm (Figure 7c,d), which could be defined as the diameter of the CC aggregates [59,60]. The results indicate that the NaOH/ZnO aqueous solution has greater dissolving effect for CC than the NaOH aqueous solution. To provide additional indirect evidence on the dissolution of CC in NaOH and NaOH/ZnO aqueous solutions, TEM was used to observe their morphology. TEM images of the CC dilute solution dried at room temperature are shown in Figure 8. As expected, the images displayed better dissolved state in Figure 8e–h than in Figure 8a–d. It was suggested that the 7 wt% NaOH/1.6 wt% ZnO system had better dissolution ability for CC than the 7 wt% NaOH system. The results further confirm that  $\text{Zn}(\text{OH})_4^{2-}$  hydrates played the auxiliary role in the dissolution of CC.

To further confirm the above discussion on the interactions of CC–NaOH/ZnO solutions, molecular dynamic simulation via modeling software was used [61]; the results are shown in Figure 9. As can be seen, hydroxyl groups of CC and NaOH in the solvent formed new hydrogen bonds. Compared with  $\text{H}_2\text{O}$  (Figure 9a) and NaOH solution (Figure 9b), CC can form a more intensive hydrogen bond network in NaOH/ZnO solution (Figure 9c), leading to intermolecular hydrogen bond cleavage of CC. The dissolution mechanism of CC in NaOH/ZnO aqueous solution is illustrated in Figure 10. In  $\text{H}_2\text{O}$  system (Figure 10a), the crystal structure of the CC chains did not change. The  $R_h$  values of CC in 7 wt% NaOH and 7 wt% NaOH/1.6 wt% ZnO aqueous solutions were determined to be  $43.7 \pm 2.8$  and  $21.4 \pm 1.6$  nm by DLS, respectively. The radii of  $\text{Na}^+$ ,  $\text{Zn}^{2+}$  and  $\text{OH}^-$  were 0.095, 0.074 and 0.176 nm, respectively [62]. Under the effect of small molecules of solvents, the hydrogen bonds of CC were broken at low temperature to obtain a clear solution. In the NaOH/ $\text{H}_2\text{O}$  system (Figure 10b), NaOH maintained the breaking of the hydrogen bonding of CC.  $\text{Na}^+$  combined with water molecules to form hydrated ions. When CC was dissolved in NaOH/ $\text{H}_2\text{O}$  solutions, CC chains were further combined with  $\text{Na}^+$  hydrate through electrostatic interaction. The overall effects in the system result in an exothermic dissolution process for CC. However, the interactions of CC–NaOH were metastable in NaOH aqueous

solution, which was easily entangled and gelled at room temperature. Adding ZnO to the NaOH aqueous solution, ZnO transferred into  $\text{Zn}(\text{OH})_4^{2-}$  hydrates, and CC-NaOH/ZnO interactions could be formed in the solution (Figure 10c). Compared with the NaOH hydrates, NaOH/ZnO hydrates can form stronger interactions with the hydroxyl groups of CC, resulting in enhanced dissolution ability and the stability of the spinning dope.

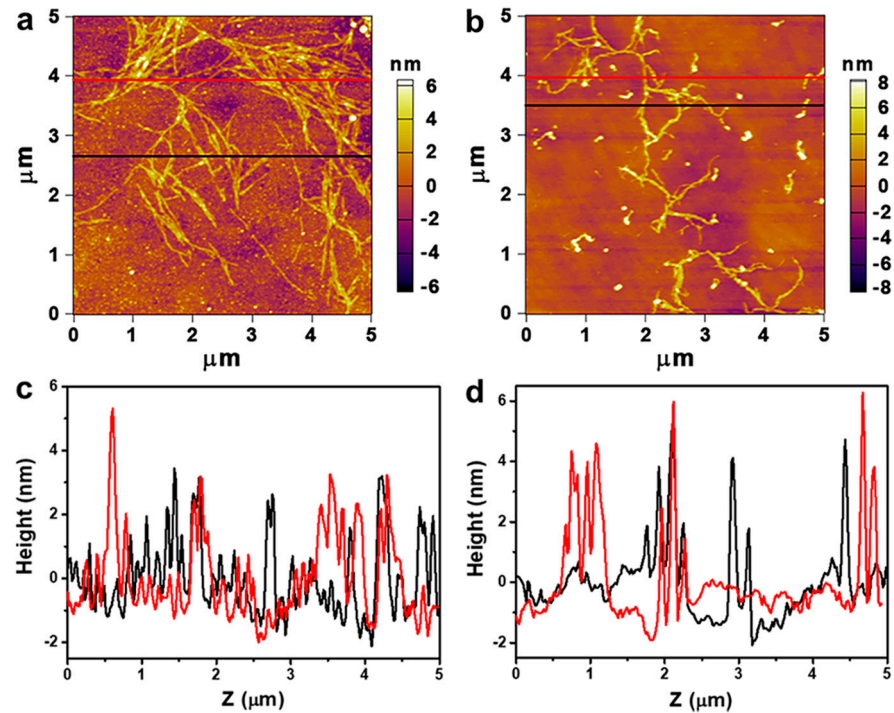


**Figure 7.** Atomic force microscopy (AFM) images of CC in (a) 7 wt% NaOH and (b) 7 wt% NaOH/1.6 wt% ZnO aqueous solutions ( $c = 1.0 \times 10^{-4}$  g/mL). (c,d) the height distributions of CC as indicated by the red and black lines in (a,b).

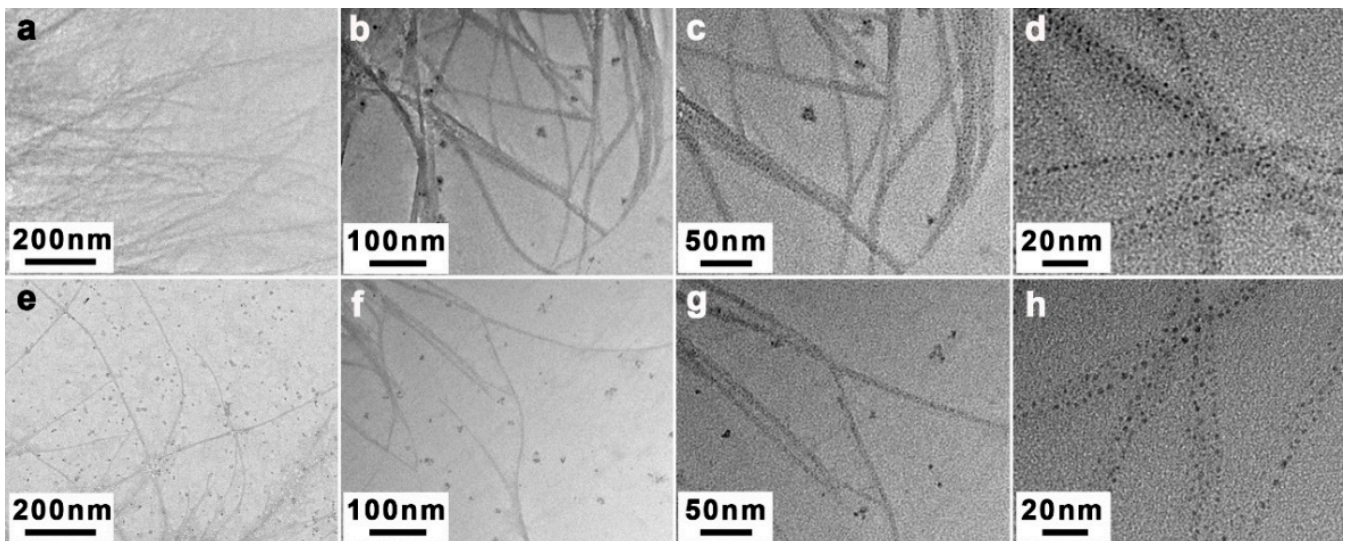


**Figure 8.** TEM images of CC in (a–d) 7 wt% NaOH and (e–h) 7 wt% NaOH/1.6 wt% ZnO aqueous solutions ( $c = 1.0 \times 10^{-4}$  g/mL).

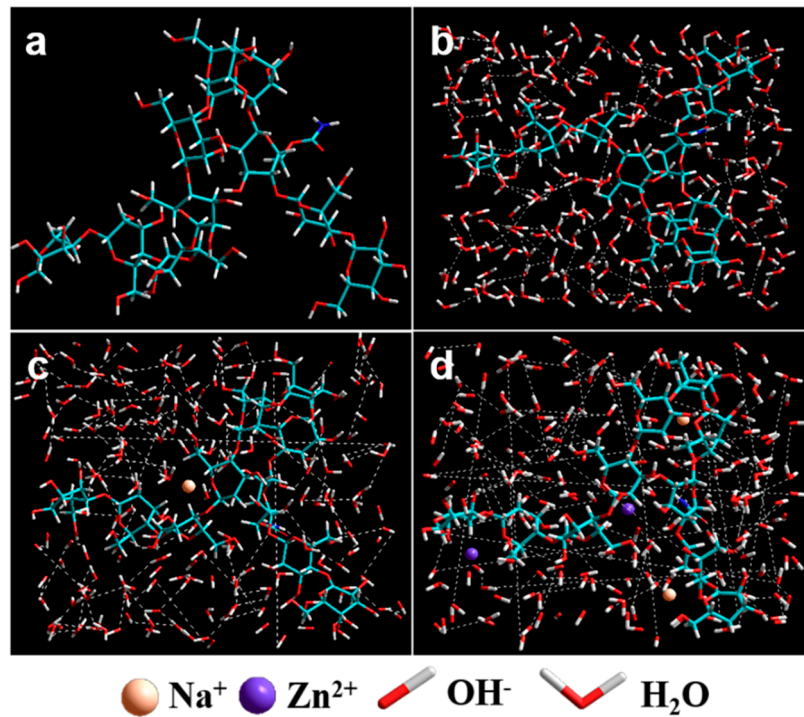


**Figure 9.** The molecular simulation of (a) CC chains, CC in (b) H<sub>2</sub>O, (c) NaOH/H<sub>2</sub>O, and (d) NaOH/ZnO/H<sub>2</sub>O.

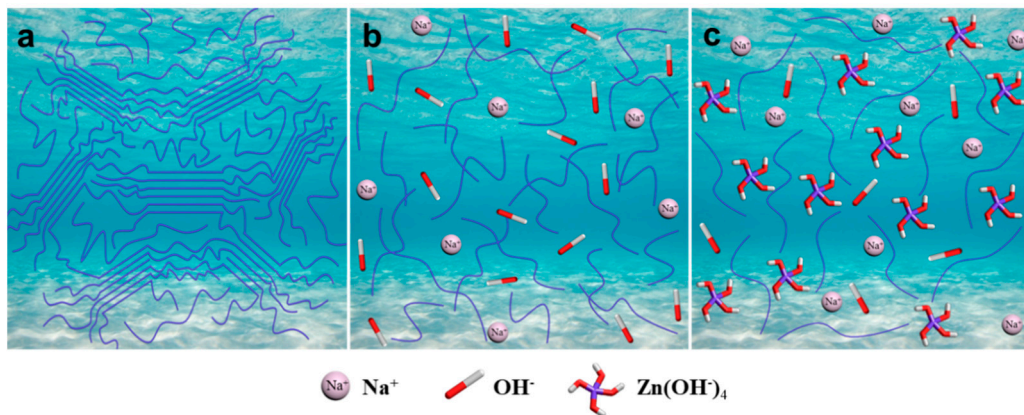


**Figure 10.** Schematic illustration for the dissolution mechanism of CC in (a) H<sub>2</sub>O, (b) NaOH/H<sub>2</sub>O, and (c) NaOH/ZnO/H<sub>2</sub>O.

#### 4. Conclusions

CC can be dissolved in NaOH/ZnO aqueous systems via a freezing–thawing method to form transparent solutions. This was found to be a typical enthalpy-driven process, and low temperature was favorable for the dissolution of CC. With the increase of NaOH and ZnO contents, the amount of hydrates increased; the interaction of CC–NaOH and CC–NaOH/ZnO systems also increased. Thus, the melting enthalpies of the frozen mass increased. ZnO existed as Zn(OH)<sub>4</sub><sup>2−</sup> hydrates in the NaOH aqueous solution. Compared with the sole NaOH system, the NaOH/Na<sub>2</sub>Zn(OH)<sub>4</sub> systems significantly improved the solubility of CC and the stability of CC solution, due to the strong interactions between the Zn(OH)<sub>4</sub><sup>2−</sup> hydrates and the hydroxyl groups of CC. Therefore, 7 wt% NaOH/1.6 wt% ZnO aqueous solution was proven to be the most appropriate solvent for CC, and this work provides a theoretical basis for the application of the CarbaCell process.

**Supplementary Materials:** The following are available online at <https://www.mdpi.com/article/10.3390/polym13071092/s1>, Table S1: Composition and parameters of NaOH/ZnO aqueous solutions; Figure S1: Solubility of CC in NaOH/ZnO aqueous solutions with various NaOH and ZnO contents, Figure S2: XRD pattern of the crystals precipitated out from 7 wt% NaOH/2 wt% ZnO and CC/7 wt% NaOH/2 wt% ZnO aqueous solution over the storage time at room temperature, Figure S3: The melting enthalpies of 5 wt% CC in 7 wt% NaOH and 7 wt% NaOH/1.6 wt% ZnO aqueous solutions during the 1st and 2nd cooling/heating processes (20 °C~−40 °C~20 °C), Figure S4: Magnified DSC heating thermograms of CC (1, 3 and 5 wt%) in (a) 7 wt% NaOH and (b) 7 wt% NaOH/1.6 wt% ZnO aqueous solutions; (c) the corresponding melting enthalpies of the CC solutions, Figure S5: The hydrodynamic radius (Rh) of CC in NaOH/ZnO aqueous solutions with various NaOH and ZnO contents were calculated from the CONTIN analysis.

**Author Contributions:** Conceptualization, J.Z. and Y.K.; methodology, J.Z.; software, Z.Z.; validation, F.W.; formal analysis, J.Z.; investigation, Y.K.; resources, J.Z.; data curation, J.Z.; writing—original draft preparation, Y.K.; writing—review and editing, J.Z.; visualization, Y.K. All authors have read and agreed to the published version of the manuscript.

**Funding:** This work was financially supported by Key Research and Development Program of Hubei Province (2020BCA079) and National Natural Science Foundation of China (51273151).

**Institutional Review Board Statement:** Not applicable.

**Informed Consent Statement:** Not applicable.

**Data Availability Statement:** The data presented in this study are available on request from the corresponding author.

**Conflicts of Interest:** The authors declare no competing financial interest.

## References

- Thongsomboon, W.; Serra, D.O.; Possling, A.; Hadjineophytou, C.; Hengge, R.; Cegelski, L. Phosphoethanolamine cellulose: A naturally produced chemically modified cellulose. *Science* **2018**, *359*, 334–338. [CrossRef] [PubMed]
- Wang, Y.; Liu, L.; Chen, P.; Zhang, L.; Lu, A. Cationic hydrophobicity promotes dissolution of cellulose in aqueous basic solution by freezing–thawing. *Phys. Chem. Chem. Phys.* **2018**, *20*, 14223–14233. [CrossRef] [PubMed]
- Fink, H.-P.; Weigel, P.; Purz, H.; Ganster, J. Structure formation of regenerated cellulose materials from NMMO-solutions. *Prog. Polym. Sci.* **2001**, *26*, 1473–1524. [CrossRef]
- Pohl, M.; Schaller, J.; Meister, F.; Heinze, T. Selectively Dendronized Cellulose: Synthesis and Characterization. *Macromol. Rapid Commun.* **2008**, *29*, 142–148. [CrossRef]
- Zhang, J.; Wu, J.; Yu, J.; Zhang, X.; He, J.; Zhang, J. Application of ionic liquids for dissolving cellulose and fabricating cellulose-based materials: State of the art and future trends. *Mater. Chem. Front.* **2017**, *1*, 1273–1290. [CrossRef]
- Chen, M.; Coasne, B.; Guyer, R.; Derome, D.; Carmeliet, J. Role of hydrogen bonding in hysteresis observed in sorption-induced swelling of soft nanoporous polymers. *Nat. Commun.* **2018**, *9*, 3507. [CrossRef]
- Marson, G.A.; El Seoud, O.A. Cellulose dissolution in lithium chloride/N,N-dimethylacetamide solvent system: Relevance of kinetics of decrystallization to cellulose derivatization under homogeneous solution conditions. *J. Polym. Sci. Part A Polym. Chem.* **1999**, *37*, 3738–3744. [CrossRef]
- Li, N.; Zhou, X.; Jinglan, Y.; Yu, F.; Wang, X. Spinnability of low-substituted hydroxyethylcellulose sodium hydroxide aqueous solutions. *J. Appl. Polym. Sci.* **2010**, *117*, 767–774. [CrossRef]
- Zugenmaier, P. Conformation and packing of various crystalline cellulose fibers. *Prog. Polym. Sci.* **2001**, *26*, 1341–1417. [CrossRef]
- Philipp, B. Organic Solvents for Cellulose as a Biodegradable Polymer and Their Applicability for Cellulose Spinning and Derivatization. *J. Macromol. Sci. Part A* **1993**, *30*, 703–714. [CrossRef]
- Teng, Y.; Yu, G.; Fu, Y.; Yin, C. The preparation and study of regenerated cellulose fibers by cellulose carbamate pathway. *Int. J. Biol. Macromol.* **2018**, *107*, 383–392. [CrossRef]
- Cai, J.; Zhang, L.; Zhou, J.; Li, H.; Chen, H.; Jin, H. Novel Fibers Prepared from Cellulose in NaOH/Urea Aqueous Solution. *Macromol. Rapid Commun.* **2004**, *25*, 1558–1562. [CrossRef]
- Cai, J.; Zhang, L.; Zhou, J.; Qi, H.; Chen, H.; Kondo, T.; Chen, X.; Chu, B. Multifilament Fibers Based on Dissolution of Cellulose in NaOH/Urea Aqueous Solution: Structure and Properties. *Adv. Mater.* **2007**, *19*, 821–825. [CrossRef]
- Semsarilar, M.; Perrier, S. Solubilization and Functionalization of Cellulose Assisted by Microwave Irradiation. *Aust. J. Chem.* **2009**, *62*, 223–226. [CrossRef]
- Swatloski, R.P.; Spear, S.K.; Holbrey, J.D.; Rogers, R.D. Dissolution of Cellose with Ionic Liquids. *J. Am. Chem. Soc.* **2002**, *124*, 4974–4975. [CrossRef]

16. Zhang, H.; Wu, J.; Zhang, J.; He, J. 1-Allyl-3-methylimidazolium Chloride Room Temperature Ionic Liquid: A New and Powerful Nonderivatizing Solvent for Cellulose. *Macromolecules* **2005**, *38*, 8272–8277. [CrossRef]
17. Zhou, J.; Zhang, L. Solubility of Cellulose in NaOH/Urea Aqueous Solution. *Polym. J.* **2000**, *32*, 866–870. [CrossRef]
18. Klemm, D.; Heublein, B.; Fink, H.-P.; Bohn, A. Cellulose: Fascinating Biopolymer and Sustainable Raw Material. *Angew. Chem. Int. Ed.* **2005**, *44*, 3358–3393. [CrossRef]
19. Kunze, J.; Fink, H.-P. Structural Changes and Activation of Cellulose by Caustic Soda Solution with Urea. *Macromol. Symp.* **2005**, *223*, 175–188. [CrossRef]
20. Selin, J.; Huttunen, J.; Turunen, O.; Eklund, V.; Ekman, K. Cellulose Carbamate Solutions. U.S. Patent 4526620, 2 July 1985.
21. Yu, G.; Teng, Y.; Lai, W.; Yin, C. The preparation and study of cellulose carbamates and their regenerated membranes. *Int. J. Biol. Macromol.* **2016**, *93*, 1155–1160. [CrossRef]
22. Labafzadeh, S.R.; Kavakka, J.S.; Vyavaharkar, K.; Sievänen, K.; Kilpeläinen, I. Preparation of cellulose and pulp carbamates through a reactive dissolution approach. *RSC Adv.* **2014**, *4*, 22434–22441. [CrossRef]
23. Vo, L.T.T.; Hajji, F.; Široká, B.; Manian, A.P.; Davis, A.; Foster, T.J.; Bechtold, T. Direct carbamation of cellulose fiber sheets. *Cellulose* **2013**, *21*, 627–640. [CrossRef]
24. Yin, C.; Shen, X. Synthesis of cellulose carbamate by supercritical CO<sub>2</sub>-assisted impregnation: Structure and rheological properties. *Eur. Polym. J.* **2007**, *43*, 2111–2116. [CrossRef]
25. Yin, C.; Li, J.; Xu, Q.; Peng, Q.; Liu, Y.; Shen, X. Chemical modification of cotton cellulose in supercritical carbon dioxide: Synthesis and characterization of cellulose carbamate. *Carbohydr. Polym.* **2007**, *67*, 147–154. [CrossRef]
26. Iller, E.; Stupińska, H.; Starostka, P. Properties of cellulose derivatives produced from radiation—Modified cellulose pulps. *Radiat. Phys. Chem.* **2007**, *76*, 1189–1194. [CrossRef]
27. Guo, Y.; Zhou, J.; Zhang, L. Dynamic viscoelastic properties of cellulose carbamate dissolved in NaOH aqueous solution. *Biomacromolecules* **2011**, *12*, 1927–1934. [CrossRef] [PubMed]
28. Guo, Y.; Zhou, J.; Song, Y.; Zhang, L. An Efficient and Environmentally Friendly Method for the Synthesis of Cellulose Carbamate by Microwave Heating. *Macromol. Rapid Commun.* **2009**, *30*, 1504–1508. [CrossRef] [PubMed]
29. Guo, Y.; Zhou, J.; Wang, Y.; Zhang, L.; Lin, X. An efficient transformation of cellulose into cellulose carbamates assisted by microwave irradiation. *Cellulose* **2010**, *17*, 1115–1125. [CrossRef]
30. Fu, F.; Guo, Y.; Wang, Y.; Tan, Q.; Zhou, J.; Zhang, L. Structure and properties of the regenerated cellulose membranes prepared from cellulose carbamate in NaOH/ZnO aqueous solution. *Cellulose* **2014**, *21*, 2819–2830. [CrossRef]
31. Fu, F.; Lianjie, L.; Liu, L.; Cai, J.; Zhang, Y.; Zhou, J.; Zhang, L. Construction of Cellulose Based ZnO Nanocomposite Films with Antibacterial Properties through One-Step Coagulation. *ACS Appl. Mater. Interfaces* **2015**, *7*, 2597–2606. [CrossRef]
32. Valta, K.; Sivonen, E.; Malm, T. Method for Preparing a Cellulose Carbamate Solution. U.S. Patent 8066903 B2, 29 November 2011.
33. Klemm, D.; Philipp, B.; Heinze, T.; Heinze, U.; Wagenknecht, W. *Comprehensive Cellulose Chemistry, Volume 2, Function-alization of Cellulose*; Wiley-VCH: Weinheim, Germany, 1998; pp. 161–164.
34. Isogai, A.; Atalla, R.H. Dissolution of Cellulose in Aqueous NaOH Solutions. *Cellulose* **1998**, *5*, 309–319. [CrossRef]
35. Wang, S.; Yang, Y.; Lu, A.; Zhang, L. Construction of cellulose/ZnO composite microspheres in NaOH/zinc nitrate aqueous solution via one-step method. *Cellulose* **2019**, *26*, 557–568. [CrossRef]
36. Fu, F.; Zhou, J.; Zhou, X.; Zhang, L.; Li, D.; Kondo, T. Green Method for Production of Cellulose Multifilament from Cellulose Carbamate on a Pilot Scale. *ACS Sustain. Chem. Eng.* **2014**, *2*, 2363–2370. [CrossRef]
37. Fu, F.; Yang, Q.; Zhou, J.; Hu, H.; Jia, B.; Zhang, L. Structure and Properties of Regenerated Cellulose Filaments Prepared from Cellulose Carbamate–NaOH/ZnO Aqueous Solution. *ACS Sustain. Chem. Eng.* **2014**, *2*, 2604–2612. [CrossRef]
38. Fu, F.; Xu, M.; Wang, H.; Wang, Y.; Ge, H.; Zhou, J. Improved Synthesis of Cellulose Carbamates with Minimum Urea Based on an Easy Scale-up Method. *ACS Sustain. Chem. Eng.* **2015**, *3*, 1510–1517. [CrossRef]
39. Zhou, J.; Fu, F. A Method for Modifying Cellulose with Urea without By-Products. China Patent 201510014122.0, 8 April 2015.
40. Brown, W.; Wikström, R. A viscosity-molecular weight relationship for cellulose in cadoxen and a hydrodynamic interpretation. *Eur. Polym. J.* **1965**, *1*, 1–10. [CrossRef]
41. Busato, M.; D’Angelo, P.; Melchior, A. Solvation of Zn<sup>2+</sup> ion in 1-alkyl-3-methylimidazolium bis(trifluoromethylsulfonyl)imide ionic liquids: A molecular dynamics and X-ray absorption study. *Phys. Chem. Chem. Phys.* **2019**, *21*, 6958–6969. [CrossRef]
42. Gashti, M.P.; Shokri, A. Hydrogel-assisted low-temperature synthesis of calcium borate nanoparticles. *J. Aust. Ceram. Soc.* **2018**, *54*, 601–607. [CrossRef]
43. Manna, B.; Ghosh, A. Dissolution of cellulose in ionic liquid and water mixtures as revealed by molecular dynamics simulations. *J. Biomol. Struct. Dyn.* **2019**, *37*, 3987–4005. [CrossRef] [PubMed]
44. Cuissinat, C.; Navard, P.; Heinze, T. Swelling and dissolution of cellulose. Part IV: Free floating cotton and wood fibres in ionic liquids. *Carbohydr. Polym.* **2008**, *72*, 590–596. [CrossRef]
45. Medronho, B.; Lindman, B. Competing forces during cellulose dissolution: From solvents to mechanisms. *Curr. Opin. Colloid Interface Sci.* **2014**, *19*, 32–40. [CrossRef]
46. Roy, C.; Budtova, T.; Navard, P.; Bédoué, O. Structure of Cellulose–Soda Solutions at Low Temperatures. *Biomacromolecules* **2001**, *2*, 687–693. [CrossRef]
47. Egal, M.; Budtova, T.; Navard, P. Structure of Aqueous Solutions of Microcrystalline Cellulose/Sodium Hydroxide below 0 °C and the Limit of Cellulose Dissolution. *Biomacromolecules* **2007**, *8*, 2282–2287. [CrossRef]



48. Egal, M.; Budtova, T.; Navard, P. The dissolution of microcrystalline cellulose in sodium hydroxide-urea aqueous solutions. *Cellulose* **2007**, *15*, 361–370. [CrossRef]
49. Wang, S.; Lyu, K.; Sun, P.; Lu, A.; Liu, M.; Zhuang, L. Influence of cation on the cellulose dissolution investigated by MD simulation and experiments. *Cellulose* **2017**, *24*, 4641–4651. [CrossRef]
50. Wang, S.; Sun, P.; Zhang, R.; Lu, A.; Liu, M.; Zhang, L. Cation/macromolecule interaction in alkaline cellulose solution characterized with pulsed field-gradient spin-echo NMR spectroscopy. *Phys. Chem. Chem. Phys.* **2017**, *19*, 7486–7490. [CrossRef]
51. Jiang, Z.; Fang, Y.; Xiang, J.; Ma, Y.; Lu, A.; Kang, H.; Huang, Y.; Guo, H.; Liu, R.; Zhang, L. Intermolecular Interactions and 3D Structure in Cellulose–NaOH–Urea Aqueous System. *J. Phys. Chem. B* **2014**, *118*, 10250–10257. [CrossRef]
52. Shoolery, J.N.; Alder, B.J. Nuclear Magnetic Resonance in Concentrated Aqueous Electrolytes. *J. Chem. Phys.* **1955**, *23*, 805–811. [CrossRef]
53. Roshind, M.U.; Tahtinen, P.; Niemitz, M.; Sjhohn, R. Complete assignments of the  $^1\text{H}$  and  $^{13}\text{C}$  chemical shifts and  $J(\text{H}, \text{H})$  coupling constants in NMR spectra of D-glucopyranose and all D-glucopyranosyl-D-glucopyranosides. *Carbohydr. Res.* **2008**, *343*, 101–112. [CrossRef]
54. Liu, Z.; Zhang, C.; Liu, R.; Zhang, W.; Kang, H.; Che, N.; Li, P.; Huang, Y. Effects of additives on dissolution of cellobiose in aqueous solvents. *Cellulose* **2015**, *22*, 1641–1652. [CrossRef]
55. Liu, Z.; Zhang, C.; Liu, R.; Zhang, W.; Kang, H.; Li, P.; Huang, Y. Dissolution of cellobiose in the aqueous solutions of chloride salts: Hofmeister series consideration. *Cellulose* **2016**, *23*, 295–305. [CrossRef]
56. Isogai, A. NMR analysis of cellulose dissolved in aqueous NaOH solutions. *Cellulose* **1997**, *4*, 99–107. [CrossRef]
57. Kok, C.M.; Rudin, A. Relationship between the Hydrodynamic Radius and the Radius of Gyration of a Polymer in Solution. *Makromol. Chem. Rapid Commun.* **1981**, *2*, 655–659. [CrossRef]
58. Krishnamachari, P.; Hashaikeh, R.; Tiner, M. Modified cellulose morphologies and its composites; SEM and TEM analysis. *Micron* **2011**, *42*, 751–761. [CrossRef] [PubMed]
59. Meng, Y.; Zou, S.; Jiang, M.; Xu, X.; Tang, B.Z.; Zhang, L. Dendritic nanotubes self-assembled from stiff polysaccharides as drug and probe carriers. *J. Mater. Chem. B* **2017**, *5*, 2616–2624. [CrossRef] [PubMed]
60. Fang, Y.; Duan, B.; Lu, A.; Liu, M.; Liu, H.; Xu, X.; Zhang, L. Intermolecular Interaction and the Extended Wormlike Chain Conformation of Chitin in NaOH/Urea Aqueous Solution. *Biomacromolecules* **2015**, *16*, 1410–1417. [CrossRef] [PubMed]
61. Bialik, E.; Stenqvist, B.; Fang, Y.; Östlund, Å.; Furó, I.; Lindman, B.; Lund, M.; Bernin, D. Ionization of Cellobiose in Aqueous Alkali and the Mechanism of Cellulose Dissolution. *J. Phys. Chem. Lett.* **2016**, *7*, 5044–5048. [CrossRef]
62. Kielland, J. Individual Activity Coefficients of Ions in Aqueous Solutions. *J. Am. Chem. Soc.* **1937**, *59*, 1675–1678. [CrossRef]

Review

# Sustainable Polymers from Recycled Waste Plastics and Their Virgin Counterparts as Bitumen Modifiers: A Comprehensive Review

Sabzoi Nizamuddin, Yeong Jia Boom and Filippo Giustozzi \* 

Civil and Infrastructure Engineering, School of Engineering, RMIT University, Melbourne, VIC 3001, Australia; nizamuddin.nizamuddin@rmit.edu.au (S.N.); s3359878@student.rmit.edu.au (Y.J.B.)

\* Correspondence: filippo.giustozzi@rmit.edu.au; Tel.: +61-3-99252035

**Abstract:** The failure of bituminous pavements takes place due to heavy traffic loads and weather-related conditions, such as moisture, temperature, and UV radiation. To overcome or minimize such failures, a great effort has been put in recent years to enhance the material properties of bitumen, ultimately improving field performance and increasing the pavement service life. Polymer modification is considered one of the most suitable and by far the most popular approach. Elastomers, chemically functionalised thermoplastics and plastomers (\* Note: notwithstanding the fact that in Polymer Science the word ‘plastomer’ indicates a polymer with the simultaneous behaviour of an elastomer and plastics (thermoplastics), this paper uses the term ‘plastomer’ to indicate a thermoplastic polymer as it is more commonly found in Civil and Pavement Engineering.) are the most commonly used polymers for bitumen modification. Plastomers provide several advantages and are commonly acknowledged to improve high-temperature stiffness, although some of them are more prone to phase separation and consequent storage instability. Nowadays, due to the recent push for recycling, many road authorities are looking at the use of recycled plastics in roads. Hence, some of the available plastomers—in pellet, flakes, or powder form—are coming from materials recycling facilities rather than chemical companies. This review article describes the details of using plastomers as bitumen modifiers—with a specific focus on recycled plastics—and how these can potentially be used to enhance bitumen performance and the road durability. Chemical modifiers for improving the compatibility between plastomers and bitumen are also addressed in this review. Plastomers, either individual or in combination of two or three polymers, are found to offer great stiffness at high temperature. Different polymers including HDPE, LDPE, LLDPE, MDPE, PP, PS, PET, EMA, and EVA have been successfully employed for bitumen modification. However, each of them has its own merit and demerit as thoroughly discussed in the paper. The recent push in using recycled materials in roads has brought new light to the use of virgin and recycled plastomers for bitumen modification as a low-cost and somehow environmental beneficial solution for roads and pavements.

**Citation:** Nizamuddin, S.; Boom, Y.J.; Giustozzi, F. Sustainable Polymers from Recycled Waste Plastics and Their Virgin Counterparts as Bitumen Modifiers: A Comprehensive Review. *Polymers* **2021**, *13*, 3242. <https://doi.org/10.3390/polym13193242>

Academic Editor: Cristina Cazan

Received: 18 August 2021

Accepted: 13 September 2021

Published: 24 September 2021

**Publisher’s Note:** MDPI stays neutral with regard to jurisdictional claims in published maps and institutional affiliations.

**Keywords:** recycled plastics; plastomers; asphalt; bitumen; recycling; sustainability



**Copyright:** © 2021 by the authors. Licensee MDPI, Basel, Switzerland. This article is an open access article distributed under the terms and conditions of the Creative Commons Attribution (CC BY) license (<https://creativecommons.org/licenses/by/4.0/>).

## 1. Introduction

Bitumen (or asphalt binder) is a by-product of the petroleum industry obtained by distillation of crude oil. It possesses valuable characteristics including long durability, high adhesion and water proofing abilities, which opened its ways for utilization as a road construction material [1]. In road construction, the bitumen is mixed with aggregates as a binder for producing the asphalt mixture. The performance characteristics and overall durability of asphalt mixtures highly depend upon the performance of the bitumen binder. Failure of asphalt pavements is mostly directly related to the failure of the asphalt binder, which takes place due to either thermal cracking occurring at low temperature, rutting at high temperature resulting in softening of the bitumen and reduced elasticity of the

bitumen, or due to fatigue cracking at intermediate temperature caused by cyclic loads and ageing of the pavement [1].

As maintenance and repair of bitumen pavements are undesirable for socio-environmental and economic reasons, considerable efforts are spent to avoid failures [2]. A large amount of studies focused on investigating the modification of bitumen to obtain enhanced durability and high-quality pavements. Among all investigated modification methods, polymer modification of bitumen is considered one of the most suitable and by far the most popular approach [3]. The polymer is incorporated into the bitumen either by chemical reaction (wet process) or mechanical mixing (dry process) to get polymer-modified bitumen [4,5]—as shown in Figure 1. In the wet process, the polymer and bitumen are directly blended at high temperature for a given time to allow for proper chemical and physical interaction between the constituents. When the polymer is refined from waste plastics, for instance, the wet method incorporates plastic in the form of flakes, pellets, or powder into hot bitumen [6]. With common mixing temperatures of 160–170 °C [7–9], plastics selected for the wet method generally require melting temperatures below the specified range. Generally, polymer modification of bitumen through the wet process enables improvements in the areas of elasticity, adhesion, cohesion, and stiffness, ultimately resulting in higher durability, fatigue life, and resistance to rutting [10,11].

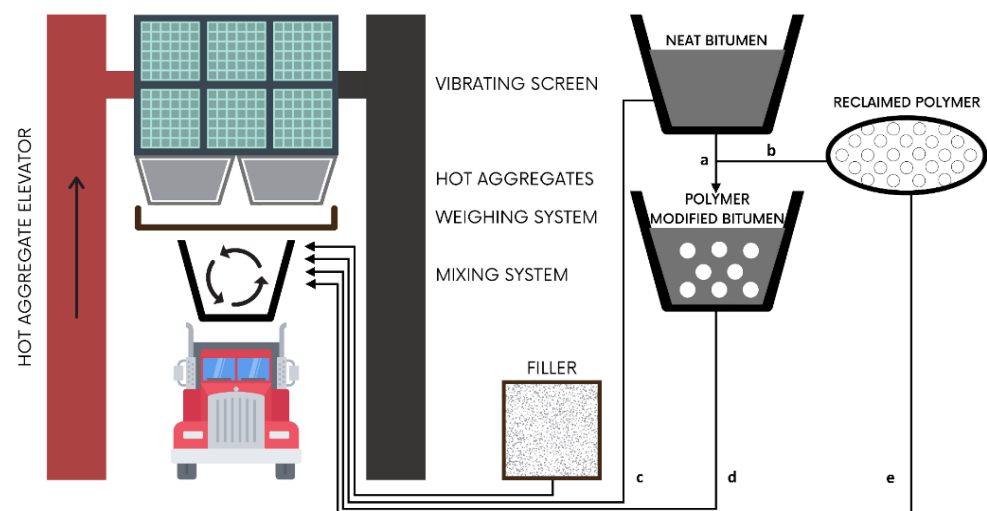


**Figure 1.** Sketch of the dry mixing process (when lines a, b, d are closed and lines c and e are opened) and the wet mixing process (when lines a, b, d are opened and lines c and e are closed) for mixing polymers with bitumen [12].

In the dry process, the polymer and bitumen are not premixed, and the polymer is added directly into the aggregates at the beginning of the mixing process [12,13]. When using waste plastics in the dry method, recycled plastic is incorporated into the bitumen mix as a substitute of the aggregate and it is suggested that its melting temperature is above the bitumen mixing temperature [14,15]; however, several studies have used low-temperature melting point plastics with the dry method as a pre-coating of the hot aggregate before adding the bitumen. The latter is sometimes known as the ‘mixed’ method. The dry method allows using a greater percentage of plastics as it reduces the amount of aggregates to be used in the total mixture. Studies have shown that by adopting this method, stiffness, fatigue life, and Marshall stability characteristics of the road pavement mix are improved [10,11,16,17]. However, several shortcomings have also been identified for both methods (wet and dry) as further described in the following sections.

The blending/mixing process—either chemical or mechanical—has a significant effect on the total cost of the operation and overall properties of the final blend [18,19]. For instance, the resulting blend may experience primary ageing due to the higher blending temperature involved, where degradation of the polymer and oxidation of the maltene compounds in bitumen (i.e., the low molecular weight compounds) can occur [20,21]. In

addition, the difference in polarity and molecular weight of the bitumen and polymer affects the compatibility of the two phases. Further, polymer-modified bitumen blends are not always thermodynamically stable and are prone to phase separation during storage at high temperature [22–25].

Together with the benefits of polymer-modified bitumen, there are some limitations and challenges which need to be taken into consideration such as the high cost of virgin polymers, resistance to ageing, sensitivity to high temperatures for some types of polymer modified bitumen (i.e., waxes-modified bitumen [26]), low elasticity, and poor storage stability [3]. To come up with these shortcomings, several techniques and methods have been suggested such as sulphur vulcanization, saturation, addition of antioxidants, functionalization, application of reactive polymers, and utilization of hydrophobic clay minerals [3,27].

Several review articles have been published on polymer modification of bitumen; some of them focused on the effect of mixing conditions and resulting in modified bitumen properties, whereas others focused on elastomers—the most adopted polymers in the road sector—and reactive polymer applications. However, to the authors' best knowledge, there is minimal comprehensive information published on the utilization and comparison between waste (recycled plastics) and virgin plastomers for road applications. Therefore, the main objective of this paper is to provide an extensive overview on waste (i.e., coming from recycling operations) and virgin plastomer modification of bitumen for pavement applications. The background and physio-chemical characteristics of bitumen are briefly discussed in the following section. Further, the incorporation methods of polymer with bitumen are evaluated. Different characteristics of plastomer-modified bitumen including chemical, thermal, rheological, structural, and mechanical properties are investigated. A description of the processes that lead to the manufacturing of recycled plastics is also provided. Finally, a critical discussion about plastomer-modified bitumen together with conclusions and recommendations for future research work are identified.

A systematic literature review methodology was adopted in this study to systematically review and collect a wide amount of the literature reported in the last decade (2010–2020); however, some of the important literature studies before 2010 are also cited in this study. To conduct the literature survey, three research databases including Scopus, Web of Science, and Google Scholar were used. The keywords used for searching through the literature include 'bitumen', 'bitumen modification', 'polymer modified bitumen', 'PMB', 'virgin and recycled polymers used for bitumen modification', 'performance of PMB', 'hybrid polymer', and 'chemical modifiers', among the most relevant.

## 2. Bitumen

Bitumen is a well-known engineering material and is obtained from the fractional distillation of crude petroleum oil. Although the chemical composition of bitumen is variable and complex, commonly, it is divided into four general fractions including aromatic hydrocarbons (80% carbon, 15% hydrogen [28,29]), asphaltenes, resins, and saturates [1]. Generally, bitumen consists of 11.9–15.8% saturates, 39.6–53.1% aromatics, 22.8–34.8% resins, and 10.3–12.1% asphaltenes (Table 1) depending on the country of origin and refinery process [3]. The reported characteristics of standard paving bitumen in different studies—although these figures may be different worldwide depending on the bitumen source—are shown in Table 1. SARA (Saturate, Aromatic, Resin, and Asphaltene) composition and other basic characteristics of standard bitumen are also listed in Table 1. SARA composition of bitumen can broadly be divided into asphaltenes (q black coloured part of bitumen which is insoluble in n-heptane) and maltenes (the combination of resins, aromatics, and saturated compounds which are soluble in n-heptane) [30].

Due to its properties, bitumen has been used for different applications including adhesives, preservatives, sealants, water proofing agents, and as a construction material for roads and airports [31]. It is reported that 85% of the total consumption of bitumen is used to build pavements of different nature [32] although—in its standard unmodified state—it is still facing challenges due to the lack of suitable mechanical properties in certain

environments, mainly caused by its thermal susceptibility [33]. This suggests adopting techniques for enhancing bitumen performance, such as polymer modification [34]. Synthetic polymer modification of neat bitumen provides significant improvements on a wide range of bitumen properties, enhancing the demand for polymer-modified bitumen [35]. The most commonly used polymers for the modification of bitumen include approximately 75% of elastomers, 15% plastomers, and 10% shredded vehicle tyre rubber and other types of materials [36].

**Table 1.** General characteristics of standard paving bitumen (unmodified).

| Property                     | Value       | References             |
|------------------------------|-------------|------------------------|
| Density (g/cm <sup>3</sup> ) | 1.004–1.019 | [37–40]                |
| Penetration (0.1 mm)         | 59.10–98.0  | [37,41–43]             |
| Penetration index (PI)       | 0.152–0.601 | [44,45]                |
| Softening point (°C)         | 42–65       | [37–39,41,42,44,46,47] |
| Flash Point (°C)             | 240–350     | [37,41,42]             |
| Fire Point (°C)              | 270–376     | [42]                   |
| Ductility (mm)               | 76–720      | [37,41,42,46]          |
| Viscosity @ 135 °C (cP)      | 100–460.35  | [37,41]                |
| Saturates (%)                | 4.0–15.8    |                        |
| Aromatics (%)                | 39.6–69.0   |                        |
| Resins (%)                   | 15.0–34.8   | [7,40]                 |
| Asphaltenes (%)              | 9.0–14.0    |                        |
| Colloidal index              | 0.190–0.333 | [7]                    |

### 3. Modification of Bitumen

The concept of mixing two or more materials—with completely different characteristics than those of the parent materials—to form a new product for paving applications has been in practice since the last few decades [48]. The resultant phase behaviour in terms of homogeneity is considered to determine the chemical, electrical, mechanical, rheological, and other characteristics of the product. The homogeneity/miscibility of mixtures depends upon entropy and heat of mixing. The miscibility or homogeneity of polymers in bitumen can be enhanced by adding compatibilizers, cross-linking agents, and by controlling the phase morphology during the blending process [49].

It is recommended that the substances used for modification of bitumen should possess the following characteristics: (i) not deteriorate at the production temperature of bitumen mixtures, (ii) retain good chemical compatibility with bitumen, (iii) increase the resistance to deformation and reduce thermal susceptibility, and (iv) being physically and chemically stable by means of not changing their characteristics during transportation, storage, processing, and other operations [50]. Polymer additives enhance bitumen's mechanical properties, improve bitumen-aggregate adhesion, and reduce temperature susceptibility, which in turn improves the overall performance of the bitumen mixture, stiffness at high temperature, moisture resistance, enhanced fatigue life and resistance to cracking at low temperature [51–55]. However, the final properties of polymer-modified bitumen highly depend upon the singular properties of the polymer and bitumen, the dosage and type of polymer added to the bitumen as well as the blending process [48]. The reactivity and chemical structure of some polymers also affect the compatibility with bitumen, which is directly related to the properties of polymer-modified bitumen [56]. The compatibility of bitumen with polymer modifiers is controlled by various properties of both the polymer and bitumen. When polymers are blended with bitumen, phase separation can occur due to the high molecular weight of polymers as well as inadequate maltene fractions

for solvation. Phase separation causes the formation of heterogeneous mixture, resulting in poor storage stability and poor compatibility between the polymer and bitumen [57]. These properties include molecular weight, density, solubility, and polarity, among others [58]. The compatibility between polymers and bitumen is reflected in the storage stability of the polymer-modified bitumen, with better polymer-bitumen compatibility generating greater storage stability and easier handling at the bitumen plant [3].

Although polymers have the ability of improving bitumen performance, the blending of bitumen and polymers still poses some challenges due to higher processing temperature and dedicated facilities—hence increased costs at the plant and phase separation due to poor polymer-bitumen compatibility and, sometimes, to the high polymer content. It is suggested that a bitumen modifier should retain the following characteristics: (i) highly soluble into bituminous mixtures to generate a viscous mixture that stays homogenous during storage; (ii) highly resistant to water, thermal stresses, and ultraviolet radiation, (iii) should not release dangerous substances to the environment and (iv) be widely available [22,29,59].

Both virgin and, more recently, recycled polymers have been successfully employed for bitumen modification. Evidently, the research for utilizing recycled plastics in the bitumen industry has significantly increased in the past decade because of the recycling push many countries are putting in place due to growing waste issues such as disposal, environmental and health concerns of plastic wastes. Waste plastics disposal is one of the main growing issues around the world due to rapid increase in plastics consumption rate. The environmental impacts include entrapment and destruction of habitats for wildlife, hazard of ingestion, plastic-facilitated transportation of organisms to eco-system, whereas other health concerns include circulatory, respiratory, and lymphatic system problems for transport with ultimate deposition in kidney, gut, and liver. To minimize the health and environmental issues due to this waste while still improving bitumen performance, there is now great attention to use waste-recycled plastic polymers in roads [60]. It should be noted that research on waste plastics in bitumen started approximately 20 years ago although it did not reach much attention until recently, as governments are heavily investing in recycling and green technology. Research studies [10,16,61] using waste plastics in bitumen roads have found noticeable improvements in tensile strength, water resistance, durability, and overall service life. In addition, utilizing plastics in the bitumen industry, recycling and use of eco-friendly methods to construct road pavements have projected a potential reduction in carbon emission by one third [62,63]. A more recent LCA (life cycle assessment) study found that recycled plastics in bitumen can be beneficial although this depends on the methodology adopted (wet or dry), with more environmental benefits associated with the wet methodology [64].

The polymers used as a bitumen modifier belong to three categories according to their chemical structures and properties [65]; these include plastomers, elastomers, and chemically functionalised thermoplastics [66]. Although it is a fact that polymer modifiers enhance the resistance against thermal susceptibility of bitumen, each type of polymer has a specific effect on bitumen properties [12]. For instance, reactive and plastomer polymers tend to increase the stiffness and resistance to deformation due to load, whereas elastomer polymers improve the elastic properties (resistance to fatigue) of bitumen [67]. It is reported that reactive polymers improve the compatibility between polymer and bitumen as well as require less additives for the stabilisation of the polymer phase. Reactive polymers commonly cause an improvement in the mechanical characteristics, temperature susceptibility and storage stability of the modified binder [68]. Navarro et al. [68] investigated a comparative analysis between reactive and non-reactive polymers on rheological properties of modified binders. They found that reactive polymers caused an evolution in rheological properties ( $G'$  and  $G''$ ), especially at intermediate temperature and low frequency. In addition, the reactive polymer modified binder remains homogenous, consequently offering better storage stability. Among all three types of polymers used for bitumen modification, plastomers are commonly cheaper and offer high stiffness at high temperatures, and hence, resistance to permanent deformation. Additionally, the melting point temperature of com-

mon plastomers is lower than the temperatures used to prepare hot bitumen mixes. Recent research has focussed on recycled plastomers over virgin plastomers for their utilization in road; therefore, the following section expands on recycled plastic waste as possible modification for bitumen.

#### 4. Recycled Plastic Waste and Their Use in Roads

Plastic consumption around the world has been increasing significantly over the last decades [69,70] causing severe environmental pollution with no alternative ways to dispose and recycle [71–73]. In 2017, Victoria in Australia generated 586,300 tons of plastics—only 130,000 tons (22.2%) were recycled while 7200 tons (1.2%) were combusted for energy recovery and the remaining 449,100 tons (76.6%) were sent to landfill. The rate of plastic generation in Victoria was projected to increase by 100,000 tons every 4 years [74]. The US Environmental Protection Agency (EPA) reported that 34.5 million tons of plastics were generated in the United States in 2015. Despite having a recycling rate of 75% from the local citizens, only 3.14 million tons (9.1%) were recycled while 5.35 million tons (15.5%) of plastics were combusted for energy recovery and 26.01 million tons (75.4%) of plastics were sent to landfill. The recycling of polymers and plastic wastes is suggested as a better solution compared to other means of dealing with them such as composting, incineration, or landfilling. Polymers are recycled by two means, i.e., mechanical recycling and chemical recycling. Mechanical recycling is a method of repurposing unmodified plastics into new products [75]. Mechanical recycling comprises of different steps including collection, sorting, shredding, washing or decontamination, extrusion, quenching, and pelletizing (Figure 2). Alternatively, chemical recycling is a method to convert waste plastic into energy or feedstock for fuels and chemicals. There are several methods to chemical recycling including pyrolysis and gasification [76,77]. However, the most commonly adopted method for plastic recycling is mechanical recycling; the outputs generally include clean and pellet-form recycled resins [75].

The recycling process starts with the collection of post-consumer and post-industrial plastic waste. Manufacturing and production firms often seek out collection services by recycling companies as means of disposal to meet environmental safety standards according to ISO standards [78]. Post-industrial plastic wastes are generally recycled more efficiently, as the plastic wastes are collected from each respective company, the source of the plastic wastes is typically the outcome of the processing of specific plastics, which do not require additional sorting. Kerbside collection is a form of post-consumer plastic waste collection method, plastic recycling firms often obtain licenses from local councils to set up collection plans for local households to collect general and recyclable household wastes [79]. Recycling companies also obtain plastic wastes from council regulated municipal waste collection drop-off centres that allows consumers to dispose of personal household plastic wastes as an alternative to kerbside collection. In some countries, post-consumer plastic wastes are sorted according to respective identification categories prior to kerbside collection. Most of the plastics being recycled and reused around the world are predominantly coming from post-industrial plastic streams rather than post-consumer.

After being collected, the waste plastic is shredded. Large pieces of plastics are commonly shredded into smaller chunks and flakes before they are washed or decontaminated [80]. The process of shredding involves a series of rotating blades driven by an electric motor with specific grids for size gradation. Materials are fed into the shredder to produce coarse irregularly shaped plastic flakes [75,76]. As waste plastics come in various forms, predominantly categorised as rigid and flexible plastics, high-end industrial shredders can be designated for specific plastics [75]. However, flexible plastics require specific shredders, due to its soft and film-like form. Film plastics tear is more likely to carry contaminants within pockets of films [81].

# Plastic Product Recycling Process



**Figure 2.** Overall mechanical recycling process of waste plastics.

The process following in the plastic recycling chain requires washing and decontamination. After being decontaminated, plastics are sorted into different categories. Traditionally, for large scale manufacturers, a method of separating polyolefins from common waste is to monitor density differences. Common polyolefins include plastics such as LDPE, LLDPE, HDPE, and PP that have lower density than water [80]. Therefore, polyolefins can be separated in a large tank of water by submerging waste and collecting whatever matter that floats on top. Plastics such as PVC are separated through X-ray fluorescent (XRF), where identifications of chlorine can be traced within the plastic [80]. Optical sorters utilise a series of Near Infra-Red (NIR) cameras to provide Hyper Spectral Imaging Technology. Upon contact with the plastics, the NIR wavelengths emit specific vibrations at a molecular level to indicate certain chemical compositions [75,82]. However, optical sorters can only differentiate certain types of plastics including PET, HDPE, PP, and PE. The excess is normally sorted to a ‘mixed’ category. Another method of sorting plastic involves the transfer of electrons from one particle to another. The electrostatic sorting method employs an electrical charge on to in-fed plastics on a conveyor belt specific to the materials [83,84]. The plastics take on a positive or negative charge reaching a high-tension field, they are then electrostatically separated into pure sorted fractions according to the different charges on each individual plastic particle [83].

Once separated, waste plastics are extruded. Extrusion is employed to homogenise and repurpose reclaimed plastics into convenient materials to work with. The process involves plastic forced along a tubular pipe and shaped through a die mould with an Archimedes screw. The plastics are input through a feeder and require to be in forms of flake, powder, or pellet. The Archimedes screw may vary in different measurements of diameter depending on the required output size. Similarly, the shape of the die mould can be designed differently and interchanged depending on the outcome requirement



of the product. Heating coils are installed on the outer surface of the tubular pipe to ensure plastics are heated to optimum temperature to be shaped accordingly. The extrusion procedure precedes the quenching process where the plastics are cooled before pelletisation.

The rate of cooling ultimately defines the structural properties of the pelletized plastics. Despite rapid cooling or 'quenching', process that cools and hardens the plastics rapidly, the process does not allow the modification of molecular orientation as there would not be adequate time for the chains to have free motion and form crystalline zones [85]. Water quenching and gas quenching are the two main methods employed in this procedure. Water quench involves the plastics to be inserted into a cold-water bath while gas quenching rapidly cools the plastics without oxidation to obtain a higher quality product [86]. Gas quenching is more expensive in comparison to traditional water quenching [87]. On the other hand, if the plastics are cooled at a slow rate, crystallization begins to occur, enabling the molecular orientation of the plastics to develop a more structured and defined form [88].

The final recycling step is the pelletizing which involves hardened plastics fed through an in-feed at a constant line speed, cut between a rotor and a bed knife into rough cylindrical pellets [89]. The size of the pellets will be dependent on the speed of the rotating blades. However, the shape of the pellets will be dependent on the shape of the extruder [90]. Plastic pellets can be subjected to post-treatment processes such as additional drying if the plastics have undergone a water quench, additional cooling if the plastics have undergone a slow cooling process, packaging, and storage.

In combination with the ever-growing asphalt industry, road pavement technicians and scientists are adopting new techniques and methods to improve practices of construction and maintenance with a purpose to minimize damages on the current environment [91,92]. Evidently, the research of utilizing recycled plastics in the asphalt industry has significantly increased in the past decade. Research studies [10,16,61,93,94] in relation to using plastics on roads have found noticeable improvements in the road's physical and mechanical characteristics namely, tensile strength, water resistance, durability, and overall life span, to name a few.

Khurshid et al. [95] investigated the effect of addition of recycled LDPE and HDPE for bitumen modification in a physical analysis experiment. The mixing process concluded that HDPE was insoluble in bitumen even at 0.5% by weight, yielding a non-homogenous mix with prominent solids, while LDPE had a weak solubility in bitumen at mixing temperatures. As a result, HDPE was eliminated, leaving LDPE the only form of polymer utilised in the experiments. The results obtained shows an increase in penetration value with the addition of LDPE enhancing the overall stiffness. LDPE modified bitumen also exhibited a decrease in 16% in penetration value at 2% polymer content in comparison to conventional bitumen. The overall results concluded that the addition of LDPE increased softening point, flash point, and fire point, allowing a greater resistance against high temperatures. Nouali et al. [96] used LDPE from shopping bags to enhance binder characteristics. The results exhibited 15% improvement in softening point and increments in penetration index value while showing a reduction in temperature susceptibility. However, due to the poor compatibility of the bitumen phase and waste plastics, the storage stability was poor at high temperatures. This study also conducted research using the recycled LDPE-modified bitumen in comparison to conventional bitumen in a regular asphalt mix. The results showed that the recycled LDPE-modified bitumen exhibited an increase in water resistance, stiffness modulus and complex modulus by 13%, 20%, and 11%, respectively. Overall, the recycled-LDPE modified bitumen was proved to provide suitable workability and compaction ability for bitumen applications. Another study utilised recycled PE, PP, and PS for polymer modification. It was found that PE aggregate samples achieved the highest resistance against plastic deformation among the three selected polymers. The stiffness of the bitumen mixture was increased by 60% with the addition of recycled PE [97]. The following section discusses in detail about different type of plastomeric polymers (either virgin or recycled) from these categories, which have been widely utilized as a bitumen modifier in past studies.

## 5. Virgin and Waste (Recycled) Plastomers to Improve Bitumen Performance

Plastomers are commonly used as bitumen modifier due to their lower cost—compared to elastomers—as well as their improved stiffness, consequently resisting to permanent deformation at high temperature; namely, rutting. One of the drawbacks in the use of plastomeric modification is the phase separation due to low compatibility of polymers with the bitumen, which results in two separate phases, i.e., asphaltene-rich phase and polymer-rich phase [98]. However, the storage stability is commonly a problem for chemically inert and non-polar plastics such as polyolefins, but when these plastics are co-mingled with polar substituents then the storage stability becomes a smaller issue. The mechanism of phase separation can be better understood by studying the polymer-bitumen interaction. During polymer-bitumen modification, the kinetically stable and thermodynamically unstable system is formed, where the polymer is swollen by the bitumen's maltene fraction [99]. This thermodynamically unstable system persuades phase separation due to the influence of gravitational field, resulting in the settling of heavier asphaltene micelles at the bottom of blends during hot static storage [100]. Pérez-Lepe et al. [25] used high density polyethylene (HDPE) to modify the bitumen binder and found that the modification resulted in an enhanced high temperature performance and decreased storage stability, suggesting that such a type of modification is less effective for pavement applications.

Phase separation is undesirable and limits the applications of these polymers for road pavement applications [65]; therefore, efforts have been put forward to avoid or minimize the phase separation and increase the compatibility between polymer and bitumen. The lower compatibility of plastomers is attributed to the nonpolar chains of the polymers. The compatibility can be improved by either removing or minimizing the non-polar groups, consequently adding polar groups by free radical polymerization with butyl acrylate or vinyl acetate, for instance, which tends to improve the compatibility of polymers with bitumen [101]. The addition of polar functional groups and substituents to the main nonpolar backbone by copolymerizing (e.g., EVA) or grafting (e.g., MA-g-PE) are known as a better solution to enhance the compatibility between plastomers and bitumen. On the other hand, it is reported that recycled plastics provide more polar groups as compared to virgin plastics because when plastic is being recycled it goes through a heating process, which causes ageing of the plastic itself. The polarity of the plastics increases with ageing [102], hence, recycled plastics offer better compatibility with bitumen. It is reported that phase separation of polymer-modified bitumen is influenced by storage conditions such as time and temperature, nature of bitumen binder, and polymer properties and concentration [100,103,104]. Polyethylene and polypropylene are the two most commonly used plastomers [9], other plastomers include ethylene-vinyl acetate, ethylene-butyl acrylate, poly(ethyl methacrylate), polystyrene and polyvinyl chloride [9]. The advantages and disadvantages of employing different plastomers for bitumen modification are shown in Figure 3.

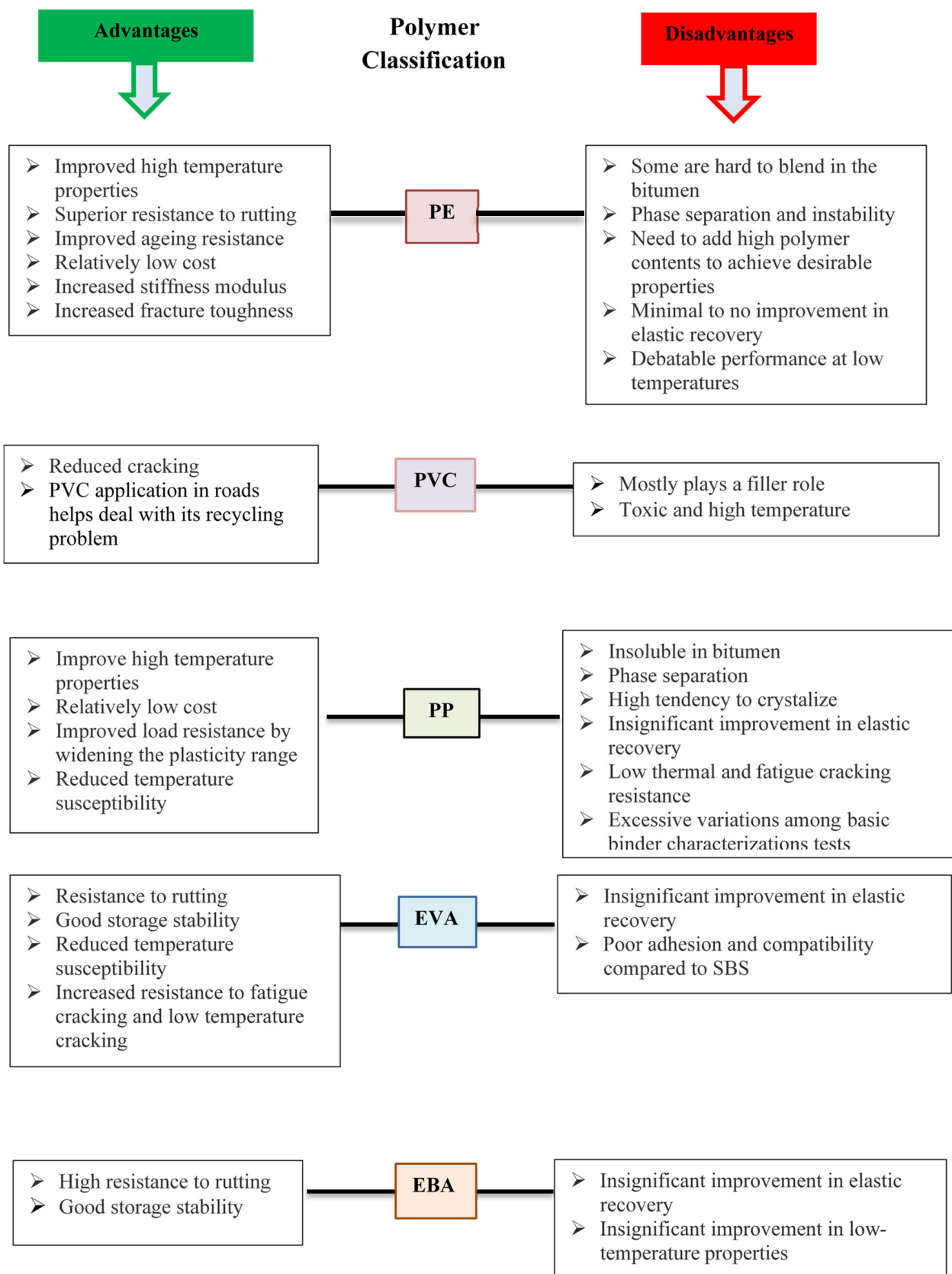


**Figure 3.** Advantages and disadvantages of different types of plastomers as modifiers for bitumen [105].

### 5.1. Polyethylene (PE) Modification of Bitumen

Polyethylene, a long chain hydrocarbon derived from ethylene polymerisation, is a relatively cheap, thermodynamically unstable, and crystalline elastomer [105]. It exists in the form of high-density polyethylene (HDPE), medium-density polyethylene (MDPE), low-density polyethylene (LDPE), very low-density polyethylene (VLDPE), ultra-high molecular weight polyethylene (UHMWPE), and linear low-density polyethylene (L-LDPE) [12] depending on co-polymerization or branching, which varies its density and degree of crystallinity [9]. Metallocene-catalysed PE (m-PE), used to create mainstream PE such as LLDPE and HDPE, have also been used for bitumen modification. All different forms of PE can be evidenced in various objects [106] such as HDPE that can be found in several commercial containers (i.e., milk and shampoo), toys, pipes, and different houseware items; LDPE is found in containers and trays, reusable bags, and agricultural films, whereas L-LDPE can be found in objects such as geomembranes and food packaging films [9]. The basic characteristics of different forms of polyethylene are listed in Table 2. The density ranges between 943 and 961 kg/m<sup>3</sup> for HDPE, 926–948 kg/m<sup>3</sup> for MDPE, 890–953 kg/m<sup>3</sup> for LDPE and approx. 910–940 kg/m<sup>3</sup> for L-LDPE. The softening point ranges between 95 and 127 °C while the melting point of HDPE, MDPE, LDPE and L-LDPE ranges between 129–149 °C, 126–129 °C, 108–120 °C, and 124–128 °C, respectively (Table 2). As the melting temperature is commonly lower than the production temperature used to manufacture hot bitumen mixtures (i.e., 160–170 °C), therefore, these materials can potentially be incorporated in bitumen to obtain polyethylene-modified bitumen [12].

**Table 2.** Basic characteristics of different elastomers including PP, EVA, EBA and PE (HDPE, LDPE, and L-LDPE).

| Properties  | HDPE  | LDPE   | LLDPE   | PP   | EVA   | EBA   | References                         |
|---|---|--|---|--|---|---|------------------------------------|
| Density (kg/m <sup>3</sup> ) @ ASTM 209B          | 938–961                                       | 890–953  | 917–944   | 820–950  | 920–935   | 930   | [34,37,44,107–118]                 |
| Softening point (°C) ASTM D 1525                  | 127   | 95   | 110–115   | 140–150  | 80–150  | 130   | [1,37,119–121]                     |
| Tensile strength (MPa)                            | 3.1–27  | 2.34–10.11                                       | 13–22   | 330–414  | 33  | 20  | [107,109,111,122–124]              |
| Flexural modulus (GN/m <sup>2</sup> ) @ ASTM D790 | 0.307   | 0.203  | -   | -  | 0.02–0.17   | -   | [107,121,125]                      |
| Melting point (°C)                                | 129–149                                       | 106–120  | 124–128   | 130–170  | 54–110  | 76  | [39,107–110,114,116,118,126–136]   |
| Thermal degradation temperature (°C)              | 430–480                                       | 406  | 424–472   | 410–460  | 290–335   | 315   | [50,136–139]                       |
| Elongation at break (%) @ ASTM D412               | 500–560                                       | 300–700  | 650   | 40–350   | 700–1000  | 900   | [5,107,109,110,119,122,140]        |
| Impact strength (J)                               | 0.941   | -  | -   | -  | -   | -   | [9]                                |
| Crystallinity (%)                                 | 52.5–86                                       | 35–47.6  | 48–53   | -  | 40–65   | 10.6  | [110,113,121,141]                  |
| Melting flow index (g/10 min) @ ASTM D1238        | 0.15–20                                       | 0.75–32  | 0.9–20  | 0.2–3  | 6   | 150   | [5,43,110,113,119,120,132,142,143] |
| Chemical structure                                | (C <sub>2</sub> H <sub>4</sub> ) <sub>n</sub> | (CH <sub>2</sub> -CH <sub>2</sub> ) <sub>n</sub> | C <sub>4</sub> H <sub>8</sub> -(CH <sub>2</sub> -CH <sub>2</sub> )-C <sub>5</sub> H <sub>10</sub> | [CH <sub>2</sub> -CH(CH <sub>3</sub> )] <sub>n</sub> | (C <sub>2</sub> H <sub>4</sub> ) <sub>n</sub> -(C <sub>4</sub> H <sub>6</sub> O <sub>2</sub> ) <sub>m</sub> | C <sub>9</sub> H <sub>10</sub> O <sub>3</sub> | [144,145]                          |

Tables 3 and 4 list the mixing conditions and physical, chemical, rheological, and mechanical properties of virgin and waste plastomers modified binders, respectively. Polyethylene is commonly incorporated into bitumen at various percentages (0.1–6% for HDPE, 1–5% for MDPE, 2–10% for LDPE and 4–6% for L-LDPE) by weight of the binder, with mixing temperature ranging from 160 to 185 °C for HDPE, 165 to 170 °C for MDPE, 165 to 185 °C for LDPE, and 150 to 170 °C for L-LDPE; the mixing time is 0.5–6 h for HDPE, 0.2–1.5 h for LDPE, 0.5–1 h for MDPE, and 0.5–2 h for L-LDPE. The mixing speed falls within the range of 2500–4000 rpm for HDPE, 3000–4000 rpm for MDPE, 3000–5000 rpm for LDPE, and 4000 rpm for L-LDPE. The size of polymer added to the binder is also considered as an important parameter for homogenous mixing and the reported particle size for polyethylene-modified bitumen is 0.1–5 mm, as shown in Table 3. Studies suggest washing, drying, and extruding the waste polyethylene before trimming or grinding if it comes directly from post-consumer streams, or it can be directly trimmed or grinded to different sizes if supplied clean [66,146–148]. Post-industrial polyethylene is usually cleaner and of more consistent quality than post-consumer polyethylene.

The addition of polyethylene affects the properties of modified bitumen blends as shown in Table 3. Polyethylene-based polymers have the potential to improve the in-service properties of asphalt mixtures such as resistance to high temperature rutting [104], high temperature behaviour, fatigue life, flexural stiffness, thermo-mechanical resistance, water resistance, adhesion, and elasticity [149–158]. The blending of polyethylene in bitumen tends to improve the glass transition peak of modified blends [159] and crystallizes from blends when it is cooled down because crystallites may crosslink extended polymer chains and form a gel network, which improves the high temperature stiffness until the crystals melt [31]. It is reported that polyethylene is immiscible with bitumen due to bitumen's polar and aromatic nature and has less interaction with bitumen due to its tendency towards crystallization [105]. Although polyethylene-based polymers are insoluble in bitumen binders, they are still capable of flowing and spreading through the binder matrix (i.e., mechanical blending rather than chemical blending), hence improving the properties of the modified blend [160,161]. Different methods and techniques can be implemented to overcome the issues of less miscibility and compatibility of polyethylene-based polymers with bitumen; grafting and chlorination, for instance, are commonly used to disperse the polymer particles into the bitumen [162–165].

**Table 3.** Mixing conditions and physical, chemical, rheological, and mechanical properties of virgin plastomers-modified bitumen. Note: the symbol “-” identifies that no literature studies on bitumen provided quantitative indications of that specific property.

| Mixing Conditions                              | LDPE        | HDPE       | LLDPE      | PP          | EVA            | EBA       | References                    |
|--|-------------|------------|------------|-------------|----------------|-----------|-------------------------------|
| Polymer/binder percentage (%)                  | 3–6         | 0.5–6      | 0.5–6      | 0.5–5       | 1–9            | 2–9       | [35,36,123,140,166–168]       |
| Mixing temperature (°C)                        | 170         | 160–170    | 160–170    | 160–170     | 165–180        | 170–180   | [34,36,118,123,140,166–169]   |
| Mixing time (h)                                | 1–2.5       | 1–2.5      | 1.2–2.5    | 1           | 2–7            | 2–6       | [34,36,118,123,140,166,167]   |
| Mixing speed (rpm)                             | 4000        | 4000       | 4000       | 120         | 1000–3000      | 1000–1200 | [34–36,118,140,166,167,169]   |
| Physical Properties                            |             |            |            |             |                |           |                               |
| Softening point (°C) @ ASTM D-36               | 57–68.5     | 51–79      | 50–67      | 53–76       | 54–62          | 27–72     | [34,36,125,140,168,169]       |
| Penetration (dmm) @ ASTM D-5                   | 23.5–40.8   | 21–36      | 13–41      | 15–35       | 47–53          | 46–75     | [34,36,125,140,168–170]       |
| Penetration index                              | 0.44–1.17   | –2–1.5     | –2–1.5     | 1.96–2.28   | 0.49–1.24      | 0.07–2.92 | [3,115,116,171]               |
| Viscosity (cP) at 135–165 °C @ ASTM D4402      | 200–700     | 270–578    | 380        | 590–687.5   | 980            | 940       | [8,34,44,115,170,172]         |
| Ductility (cm) at 25 °C @ ASTM D-113           | 91–148.5    | 79–133     | 40.25–73.5 | >100        | 5–22           | 10–40     | [7,36,45,125,168,169,173,174] |
| Specific gravity @ ASTM D-70–76                | 1.014–1.042 | 0.935–1.01 | -          | 1.015       | 1.015–1.032    | -         | [36,169,174,175]              |
| Flash point (°C) @ ASTM D 92–02                | 200–240     | 215–257    | -          | 199–292     | 260            | -         | [36,175–177]                  |
| Storage stability (softening point top–bottom) | 0.8–2.5     | 0.96–1.1   | 3          | -           | 1–1.9          | 0–3       | [34,170–172,178,179]          |
| Stability Index                                | 48.1        | 5.42       | 8.43       | -           | -              | -         | [167]                         |
| Rheological Properties                         |             |            |            |             |                |           |                               |
| $G^*/\sin\delta$ (kPa)                         | 0.756–5.911 | 9–12.3     | 1.12–15.20 | 3.7–32.2    | 0.8–1.7        | -         | [163,170,171,180–183]         |
| $G'$ (kPa)                                     | -           | -          | 0.31–29.90 | 0.38–7.04   | -              | 0.62–4.94 |                               |
| $G''$ (kPa)                                    | -           | -          | 6.4–37.5   | 3.7–30.6    | -              | 0.71–7.57 | [180–182,184]                 |
| $G^*$ (kPa) at 10 rad/s                        | 3.97–10.75  | 7.15–23.08 | 6.5–38.9   | 3.72–31.36  | 0.3115–170.790 | 62.3–75.0 |                               |
| $\delta$ (°)                                   | -           | 42.9–83.9  | 71.5–88.1  | 77.01–84.05 | 80–87          | 6.25–64.2 | [180–183]                     |
| SARA Analysis (ASTM D-2006)                    |             |            |            |             |                |           |                               |
| Asphaltene (%)                                 | -           | -          | 17.6–18.8  | 11.1–13.6   | 11.7–14.7      | -         |                               |
| Aromatics (%)                                  | -           | -          | 34.4–41.9  | 31.8–39.6   | 32.5–38.8      | -         |                               |
| Resins (%)                                     | -           | -          | 21.0–27.3  | 41.5–46.1   | 40.3–44.2      | -         | [180,181,185]                 |
| Saturates (%)                                  | -           | -          | 17.3–19.7  | 6.8–8.1     | 8.6–9.2        | -         |                               |

**Table 4.** Mixing conditions and physical, chemical, rheological, and mechanical properties of waste plastomers-modified bitumen. Note: the symbol “-” identifies that no literature studies on bitumen provided quantitative indications of that specific property.

| Mixing Conditions   | LDPE        | HDPE      | LLDPE      | PP        | EVA       | EBA | References                    |
|---|-------------|-----------|------------|-----------|-----------|-----|-------------------------------|
| Polymer/binder percentage (%)                                   | 2–10        | 3–6       | 2–5        | 3–6       | 1–3       | N/A | [35,57,115,117,175,186–188]   |
| Mixing temperature (°C)   | 160–170     | 185       | 180        | 165–170   | 180       | N/A | [8,15,35,57,115,117,186–188]  |
| Mixing time (h)   | 1–2         | 1.5       | 1.5        | 2         | 6         | N/A | [8,35,57,117,175,186,187,189] |
| Mixing speed (rpm)  | 3000–5000   | 4000      | 3750       | 500       | 1800–4000 | N/A | [8,35,57,115,175,186,187,189] |
| Physical Properties   |             |           |            |           |           |     |                               |
| Softening point (°C) @ ASTM D-36                                | 44–68.5     | 43.7–60.5 | 58–70      | 52.05–64  | 26        | N/A | [8,9,115,175,176,186,189,190] |
| Penetration (dmm) @ ASTM D-5                                    | 41–74       | 46–68     | 47–56      | 27–68     | 37        | N/A |                               |
| Penetration index   | 0.08–0.43   | –1.7–0.6  | –1.13–5.81 | –0.8–2.28 | 0.11–2.38 | N/A | [95,115,175,191–193]          |
| Viscosity (cP) at 135–165 °C @ ASTM D4402                       | 200–700     | 600       | 480        | 590–687.5 | 420       | N/A | [8,115,189,190,194]           |
| Ductility (cm) at 25 °C @ ASTM D-113                            | 58–69       | 48–68     | 22–61      | 52–66     | -         | N/A | [176,189]                     |
| Flash point (°C)  | 200–240     | 215–257   | -          | 199–292   | -         | N/A | [176]                         |
| Fire point (°C)   | -           | -         | -          | 345       | -         | N/A | [175]                         |
| Storage stability @ ASTM D-7173 (softening point top to bottom) | 2.8–4.7     | 41.8      | 3.1–4.9    | -         | 0.2–5.2   | N/A | [8,189,191,195]               |
| Rheological Properties  |             |           |            |           |           |     |                               |
| $G^*/\sin\delta$ (kPa)  | 0.09–12     | 2.26      | 1.12–15.20 | 2–47      | 4.08      | N/A | [8,180,190,196,197]           |
| $G^*$ (kPa) at 1 rad/s  | 1.23–11.7   | -         | 6.5–38.9   | -         | -         | N/A |                               |
| $\delta$ (°)  | 70.23–88.12 | 18        | 71.5–88.1  | -         | 19        | N/A | [180,190]                     |
| SARA Analysis   |             |           |            |           |           |     |                               |
| Asphaltene (%)  | 19.0        | 15.4      | -          | -         | 11.7      | N/A |                               |
| Aromatics (%)   | 24.0        | 24.6      | -          | -         | 38.8      | N/A |                               |
| Resins (%)  | 37.8        | 34.9      | -          | -         | 40.3      | N/A | [198,199]                     |
| Saturates (%)   | 19.2        | 25.1      | -          | -         | 9.2       | N/A |                               |

N/A: No data is available on polymer modification of recycled EBA.

The blending conditions and composition of both polymer and binder have a significant effect on properties and performance of plastomers-modified bitumen blends. For instance, the melt flow index, an indirect indicator of molecular weight where higher MFI corresponds to lower molecular weight, is a polymer characteristic that portrays the architecture of the molecular structure of polymers [200] and affects the physical and rheological characteristics of plastomers-modified bitumen. It is suggested that a lower melt flow index resulted in a higher softening point and complex viscosity, lower penetration values, and that a higher mixing temperature increases the melt-flow index, resulting in increased performance of the polyethylene-modified bitumen. On the other hand, low mixing temper-

ature causes incompatibility and dispersion instability and decreases the melt-flow index, hence decreasing the overall performance of blend [201]. It is reported that the molecular weight and distribution of molecular weight of polyethylene or polyethylene-based modifiers are important factors affecting the hot storage stability, low temperature properties, and phase separation of polymer-modified bitumen. Polyethylene-based modifiers with low molecular weight and wide distribution of molecular weight are considered suitable for bitumen modification purposes [202]. The concentration of the polymer also has significant effect on the performance of polyethylene-modified bitumen since high polyethylene concentrations (i.e., 5–15%) causes phase separation, hence 5% (wt%) has been suggested as a maximum limit for pavement applications [188]. Other studies suggested 4% and 6% as optimum weight percentage for polyethylene and polyethylene-based polymers [157,203]. The fluorescent images taken by a UV microscope of polyethylene-modified bitumen at different concentrations of polyethylene are shown in Figure 4a–e. Figure 4a illustrates the scattered spots of 2% polyethylene blended in bitumen; these scattered spots change to a filamentous structure as the concentration of polyethylene is increased from 2% to 4% (Figure 4b). A further increase in polyethylene content to 6% and 8% results in the formation of partly-developed or completed net-like structure (Figure 4c,d), whereas these lines thicken by further increasing the amount of polyethylene up to 10% [204].

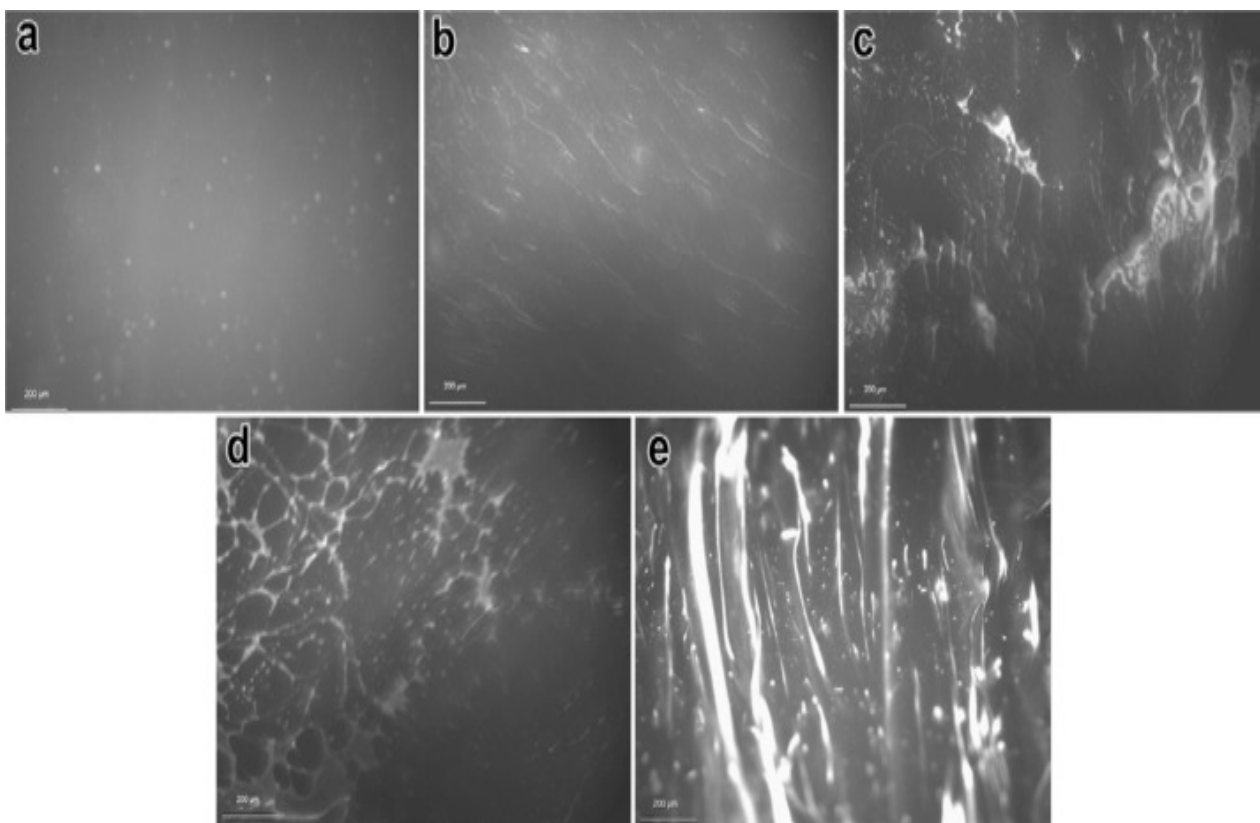


**Figure 4.** Fluorescent images of PE modified images at different concentrations of polyethylene (a) 2%, (b) 4%, (c) 6%, (d) 8%, and (e) 10% [204]. Reused with permission from Elsevier.

The bitumen's softening point increases whereas penetration decreases by increasing the concentration of polyethylene-based modifiers. As shown in Table 3, the reported range of softening point values are 44–68.5 °C, 50–67 °C and 51–79 °C for LDPE, L-LDPE, and HDPE-modified binders while the values of penetration for LDPE, L-LDPE, and HDPE are 23.5–79.1 (0.1 mm), 13–64.7 (0.1 mm), and 21–36 (0.1 mm), respectively. On the other hand, the standard softening point and penetration values of neat bitumen are 42–65 °C and 59.1–98 (0.1 mm), depending on the binder source and type (Table 1). The increase in



softening point and decrease in penetration after addition of polyethylene-based modifiers shows greater consistency of the blends, possibly indicating higher resistance to permanent high-temperature deformations. A very common content used for polyethylene-based modifiers is 3%, which shows 7% to 42% reduction in penetration, whereas the penetration value is reduced by 22–63% for 5% polyethylene-based modifiers [12]. In relation to the softening point, an increase of 2–50% at 3% polyethylene content and 14–91.5% at 5% polyethylene loading was observed [171].

Viscosity is another important characteristic of bitumen and although a greater viscosity can provide improved performance at high temperature (i.e., resistance to flow), it can also hinder the workability and ease of construction of the asphalt mix. It was reported that the viscosity of polyethylene-modified bitumen is higher than that of conventional unmodified bitumen. In addition, viscosity increases by increasing the concentration of polyethylene-based modifiers due to the greater polymer-dominant phase in high-content polyethylene-modified bitumen [194,205]. On the contrary, ductility is decreased by incorporating polyethylene-based modifiers, hence indicating a possible brittle behaviour for polyethylene-modified binders at low temperature [125,174,205]. It was observed that the addition of polyethylene at 5% content resulted in decreasing the ductility up to 97% at 15 °C [206] and up to 35% at 25 °C [174,207]. The rheological characteristics of the polyethylene-modified bitumen suggest that a high concentration of modifier results in greater increments of the complex shear modulus ( $G^*$ ) and reduction of phase angle ( $\delta$ ) values, indicating a shift towards more elastic responses and increased stiffness [12]. Nizamuddin et al. [192] performed MSCR analysis of LLDPE modified bitumen and found that the % recovery was significantly increased whereas Jnr value was decreased by addition of LLDPE. However, the effect was more obvious at low percentages of LLDPE (3% and 6%) as compared to higher percentages of LLDPE. Beena and Bindu [41] added trans-polyoctenamer in LDPE and analysed both % recovery and Jnr value of modified samples; the study found that Jnr value was increasing and % recovery decreasing at lower percentage of additives although the opposite was observed at greater content of trans-polyoctenamer additive. Gama et al. [208] studied MSCR analysis of HDPE modified binder and found that % recovery of the neat binder was approx. 2.4% at 3.2 kPa and 15.7% at 0.1 kPa; these values were increased up to 91.5% at 3.2 kPa and 95.8% at 0.1 kPa, respectively, by adding HDPE, hence confirming the improvement of modified binder to maintain good elastic properties at high traffic levels and temperature. According to some studies, the storage stability of polyethylene modified bitumen is weak as it separates into two distinct phases (polymer-rich phase and bitumen-rich phase) during storage [160,163], even after short periods of time. However, other studies have found that polyethylene-modified bitumen can be considered stable at low to intermediate percentages of polyethylene, such as 5% of LLDPE [66] and 3% of HDPE or LDPE [194], by weight of bitumen.

LLDPE is generally found to be more effective for improving the binder properties and low temperature performance as compared to LDPE and HDPE [118,160,209,210]. HDPE-modified bitumen commonly results in superior strength than LDPE, although the HDPE modification is prone to phase separation problems [25] due to the lower dispersion of HDPE into the bitumen phase compared to LDPE [211]. Fracture toughness of LDPE-modified bitumen was found to be higher than that of unmodified mixes at low temperature [212], which indicates an enhanced resistance to low temperature fracture [105]. Moreover, Marshall stability, fatigue life, resilient modulus, and moisture susceptibility were all improved by adding 2.5% of LDPE.

Metallocene catalysed polyethylene (m-PE) has been proposed as bitumen modifier because of its low cost, high dispersion characteristics, mechanical properties, physical properties, and improved storage stability [213]. It is suggested that the metallocene catalysis controls the molar mass distribution and molecular structure providing polymers with uniform distribution of short chains and narrow molar mass distribution [213]. This results in reducing the melt elasticity and tuning of bulk properties such as crystallinity and viscosity, consequently increasing the dispersion [214]. Spadaro et al. [214] used two different

grades of metallocene catalysed LLDPE for blending with bitumen in order to validate the possible potential use of these polymers as bitumen modifiers. It was observed that the addition of metallocene-catalysed LLDPE enhanced both thermal and mechanical properties of modified bitumen. The glass transition temperature was significantly decreased by increasing the polymer concentration, suggesting advantages related to low temperature flexibility. The modified bitumen blends showed relatively low dynamic shear viscosity at higher concentration of polymers. Another study [213] investigated the rheological and thermal characteristics of metallocene-catalysed LLDPE blended with metallocene-catalysed HDPE. The results of zero shear viscosity, relaxation time and frequency show a linear variation throughout the weight fraction range, suggesting the miscibility of metallocene-catalysed LLDPE/metallocene-catalysed HDPE blends. A research study conducted by González et al. [210] studied the storage stability and viscoelastic characteristic of metallocene-catalysed LLDPE/bitumen blends. The metallocene-catalysed LLDPE/bitumen blends were prepared by loading 1–3% metallocene-catalysed LLDPE into bitumen at 180 °C, 1800 rpm, and 6 h. It was found that metallocene-catalysed LLDPE provided better storage stability by avoiding phase separation at high temperature of storage.

### 5.2. Polyethylene Terephthalate (PET) Modification of Bitumen

PET is most found in water bottles and food packaging and is mostly intended for single use applications although major companies are now reusing up to 100% waste PET to produce new plastic bottles and other products. PET was found as a suitable candidate for its application in asphalt pavements due to its strong chemical resistance to organic materials and water, its high strength-to-weight ratio that makes it a suitable plastic in the asphalt industry to reduce environmental pollution and improve bitumen material characteristics. Unfortunately, PET and recycled PET are very expensive polymers—especially when classified as ‘food grade’—and their uses are predominantly made for containers used in the food industry. The very high melting temperature of PET (i.e., approx. 260 °C) also limits its application as bitumen modifier. However, different studies have reported that the addition of PET as a polymer modifier for bitumen enhances various properties of the mix. Recently a review article was published on application PET for pavement performance [215]. El-Naga and Ragab [216] used PET for bitumen modification and studied its effect on the overall properties of PET-modified bitumen and PET-modified asphalt mixes. The PET modification tends to decrease penetration and increase softening point, ductility [217] and viscosity [218]. Results also showed higher Marshall stiffness modulus, indirect tensile strength and rutting stiffness in comparison to conventional modifiers used in asphalt mixtures [219]. The value of air voids and voids in mineral aggregates increased with the content of PET in the modified asphalt mixture [220]. In addition, the rheological study conducted by Bary et al., found that 4% PET enhanced the complex shear modulus and decreased the phase angle significantly [221]. However, since PET does not melt during the bitumen modification process (i.e., can only act as a filler), its relative size should be carefully considered during DSR tests, especially when a 1 mm gap is used. The PET modification of bitumen improved the  $G^*/\sin\delta$  value, indicating better performance against rutting [222]. Leng et al. [223] studied MSCR characteristics (%recovery and  $J_{nr}$ ) of PET modified bitumen binder at 0.1 kPa and 3.2 kPa. It was observed that the %recovery of modified binder was significantly higher and  $J_{nr}$  value of modified binder was significantly lower than those of pure binder. In addition, the %recovery increased and  $J_{nr}$  decreased by increasing the polymer content. Al-Jumaili [224] utilised PET (from 2.36 mm to 4.75 mm), crumb rubber (same size of PET and added through the dry process) and waste engine oil for bitumen modification. Results showed that 9% crumb rubber content achieved the greatest tensile strength and highest resistance to water damage. The increment of tensile strength values peaked when a greater percentage of PET was added into the bitumen. Overall, the Marshall stability was improved at 9% crumb rubber, 12% PET, and 5% waste engine oil. The study however did not investigate the possible lack of adhesion between the PET particles and bitumen. Another study [225] compared the fatigue properties of SBS

and PET modified bitumen and found that both SBS and PET mixes improved the fatigue response but SBS blends showed better fatigue behaviour than PET blends. According to Cong et al. [226] fatigue behaviour is proportional to the surface energy, as the greater the surface energy, the higher the fatigue life will be. It was also found that the surface energy of SBS modified binder was higher than that of the neat bitumen, hence, SBS modification resulted in improved fatigue life. Arguably, in the same study, PET-modified blend showed higher fatigue behaviour than SBS modified bitumen at 6% PET loading and low strain level. Similarly, it is suggested that PET modification of bitumen has an effect on low temperature cracking, i.e., PET-modified bitumen blends are more susceptible to thermal cracking [227]. The mixing process of PET with bitumen also plays an important role on the overall performance—as discussed earlier there are two approaches for mixing polymers with bitumen, dry process, and wet process. However, the wet process is not considered feasible for PET due to the very high melting temperature of PET, which makes it difficult to achieve homogenous blends [228]; however, there are studies that reported on PET modification of bitumen by wet process. Moghaddam et al. [219] studied the wet mixing of PET and bitumen and found that permanent deformations of PET modified bitumen were improved significantly and a higher PET amount showed better resistance against permanent deformation. Choudhary et al. [228] reported of a dry process and modified dry process (initially heated aggregates were mixed and coated with PET and then bitumen was added and blended) for PET modification of bitumen and found that the modified dry process showed better performance and had high resistance towards moisture-induced damage. Generally, PET-modified bitumen from either of the processes showed greater resistance against deformation with high stability, low flow, and high Marshall quotient.

### 5.3. Polyvinyl Chloride (PVC) Modification of Bitumen

PVC shares about 10.1% of the European plastic production. It is commonly used for the manufacturing of profiles, cable insulation, garden hoses, and window frames [229]. PVC is dubbed as poison plastic because it contains various toxins. Incineration or firing of PVC-based products causes dioxins to be produced [230]. It is reported that PVC emits hydrochloric acid (HCl) in large quantity when it is heated at high temperature. It is suggested that PVC can emit HCl even though it is not actually ignited in a fire. HCl produced by heating of PVC can cause widespread damage to the instruments and environment due to its toxic nature [231]. To deal with the high chlorine content of PVC, it is suggested to partially remove chlorine from PVC through chemical treatment. It is reported that chlorine displacement from the surface of PVC is possible by nucleophilic substitution of ligands such as amines and hydroxy [232]. Considering the 30-year life span of PVCs, there is no absolute safe way of dealing with this hazardous polymer. Additionally, the collection, transportation, and disposal methods are still not conducted properly, especially in developing countries. Uncontrolled dumping of such wastes leads towards serious environmental concerns including ground water pollution [230]. Some studies tested PVC as polymer modification of bitumen although they could not get successful results due to the polymer high melting point (i.e., approx. 298 °C) [194,197,233]. Some other studies used PVC from different origins including window frames, cables, pipes—or not mentioning the origin of PVC—for bitumen modification with limited outcomes [230,234–237]. The mixing conditions for PVC modification of bitumen included 140–190 °C mixing temperature, 20 min to 3 h mixing time, 0.075–2 mm particle size, 1–20% concentration of PVC by weight of the bitumen, and 1300–3750 rpm mixing speed [12,230,234,235].

Although used as a filler to create PVC-based bituminous mastics, it was found that the addition of PVC to bitumen improved the conventional and rheological properties. The penetration value generally decreased whereas the softening point value was significantly increased after PVC addition to the base bitumen. Five percent PVC into the bitumen reduced the penetration value by 57% and increased the softening point by 26% [12]. Viscosity was increased up to 300% while ductility decreased after addition of 5% PVC in bitumen [236,238]. From the rheological perspective, it was noticed that PVC modification

of bitumen resulted in improving the complex shear modulus and reducing the phase angle of the PVC-modified bitumen [230,235]. The increased complex shear modulus and the decreased phase angle helped enhance rutting resistance at high temperature, perhaps indicating greater durability of pavements [12]. There were only a few studies that used additional modifying agents with PVC to modify the base bitumen. For instance, Fang et al. [238] used 0.05%, 0.15%, and 0.25% organic montmorillonite as an agent to improve the properties of PVC-modified bitumen and it was found that the storage stability was improved, specifically at 5% PVC. Another study utilized a chemical modifier with PVC to improve the properties of modified bitumen and found that the dispersion of the polymer in bitumen was improved significantly [230]. No mention in the study was made about the potential fuming and emissions during high temperature heating of PVC.

#### 5.4. Polypropylene (PP) Modification of Bitumen

Polypropylene (PP), currently accounting for 21% of the global plastic production [239] and 19.1% of the European plastic production [229], is commonly found in automotive parts, microwave-proof containers, food packaging, and pipes [229]. PP is a thermoplastic linear hydrocarbon with an intermediate crystalline level between that of HDPE and LDPE [105]. PP has been extensively used as a polymer modifier for bitumen in order to improve its properties. It is reported that PP-modified bitumen blends show increased resistance to rutting and fatigue life when included into the bitumen mixture; PP is also ascribed as to improve stability, Marshall properties, and indirect tensile strength [240–243]. The mixing conditions of PP with bitumen reported in literature are as follows; 165–180 °C mixing temperature, 1–2 h mixing time, 120–4000 rpm mixing speed and 1–6% concentration of PP by weight of the binder (Table 3). The most common dosage values of PP used for polymer modification of bitumen are 3% and 5% [12].

It was found that incorporation of PP into bitumen significantly varies the properties of PP modified bitumen. PP modification of the binder resulted in increasing the softening point while decreasing the penetration value. As mentioned earlier, 3–5% are the most commonly used PP concentrations; the penetration value was observed to drop between 18 and 30% for 3% PP and between 38 and 50% for 5% PP [12]. On the other hand, 4–30% and 11–43.5% increase in softening point was observed for 3% and 5% of PP, respectively [12]. Viscosity was increased and ductility was reduced after the addition of PP into bitumen, and the ductility was diminished by 20% at 5% PP content [244]. Such observations indicate that there are various factors including particle size, mixing duration, and interaction between the binder and modifier, which should be considered before utilizing such kinds of polymers for bitumen modification. In terms of rheological properties, PP modification of bitumen improved the rheological properties of PP-modified bitumen at high temperature and low frequency, resulting in an increased resistance against permanent deformation. The complex shear modulus was increased, the phase angle was decreased, and greater  $G^*/\sin\delta$  values were achieved after PP modification of bitumen [12,245]. Different forms of PP, including aPP, iPP, and sPP, have been successfully employed for bitumen modification [30,246]. Nekhoroshev et al. [247] assessed the aPP modification of bitumen binder and found that adhesion properties were improved, however, aPP has low-crosslink density. Al-Haidri et al. [248] studied the effect of two different grades (atactic polypropylene, aPP, and isotactic polypropylene, iPP) of PP modifiers and found that both iPP and aPP resulted in increasing the resistance to stress, consequently reducing the number of distresses and increasing the in-service life of pavement. However, aPP at 2% concentration provided better results as compared to iPP. Schaur et al. [249] added four different PP polymers including two isotactic polymers with different molecular weights, one isotactic polymer with polar (anhydride) side groups, and one atactic polymer. They found that the long-chain iPP represented heterogeneously distributed polymer whereas the short-chain polymer was finely dispersed. The aPP has less impact on mechanical characteristics of PMB as compared to iPP, establishing a partial network of polymer-rich phase in PMB whereas maPP improved mechanical properties significantly. Awad and Awad and Al-Adday [250]

investigated the utilization of PP as a bitumen modifier and found that PP resulted in greater stability as compared to conventional bitumen in the absence of PP. Various studies reported about storage stability and suggested that the use of PP leads towards phase separation [194,245]. However, to limit this shortcoming, Giavarini et al. [101] suggested adding 3% of polyphosphoric acid (PPA) by weight of bitumen to PP and found acceptable storage stability values. Other modification methods include the incorporation of maleic anhydride to PP and pyrolysis products of PP before using it for binders modification [12]. Although there is a general lack of studies addressing the fatigue performance of PP-modified asphalt mixes, PP has been proved to be a reasonably good polymer—both in its virgin and waste form—to modify bitumen.

### 5.5. Polystyrene (PS) Modification of Bitumen

The global market for PS has been on the climb, increasing its compound annual growth rate (CAGR) by more than 5.5% since 2010 [251]. In comparison, the demand of PS from 2000 to 2010 only grew at 1.4% rate in CAGR. In 2019, the PS global market was recorded at \$42.7 billion and with its current rate of growth, the global market for PS is expected to increase to 9.8% in CAGR by 2023, reaching over \$62 billion. PS is extensively utilized for manufacturing of disposable containers and packaging materials. PS is produced by polymerisation of the monomer styrene and is non-polar as it only contains carbon-hydrogen bonds. It is conveniently recycled multiple times with minimal reduction of its initial properties [252].

Recently, it has been utilized as a modifier for bitumen to form PS-modified bitumen, providing superior conventional physical properties [253]. Fang et al. [254] used expanded polystyrene (EPS) from the packaging industry for bitumen modification and found that the addition of EPS improved viscoelasticity and rutting resistance. A research work was conducted where 5%, 10%, and 15% of PS was added to bitumen and the authors found that the amount of PS has a direct effect on properties of modified bitumen by increasing the softening point, fire point, and flash point and decreasing ductility and penetration [253]. An increase in the softening point at the increasing content of PS shows an improvement in high-temperature stability with the addition of EPS [255]. The effect of extruded PS waste on viscosity of modified bitumen was investigated by Abinaya et al. [256] and it was found that the viscosity increased by increasing the content of PS. Johnson et al. [257] prepared PS/bitumen blends at 1%, 2%, and 3% loading concentration of PS at 180 °C, 600 rpm for 1 h. It was found that the softening point of modified bitumen was increased by 29% for 80/100 grade bitumen and 35% for 60/70 grade bitumen by the addition of PS. The penetration value was decreased up to 20% due to addition of PS. It was concluded that PS increased binder resistance to temperature change as well as the flow resistance, thus indicating enhanced rutting resistance of PS-modified bitumen. It was also observed that the addition of PS in bitumen could potentially provide high resistance against rutting and fatigue as compared to virgin bitumen.

Although PS improves various properties of modified bitumen, it also has some drawbacks such as low mixing compatibility, storage stability problems, and poor elastic and low-temperature properties [258]. Another study proposed the incorporation of nano-clay at 2%, 5%, and 10% weight of PS and observed that the percentage of nano-clay increased the thermal stability and rheological properties [259]. Padhan et al. [258] studied the MSCR performance of PS-modified bitumen with the addition of trans-polyoctenamer at stress levels of 0.1 kPa and 3.2 kPa. It was found that at both stress levels, J<sub>nr</sub> decreased continuously whereas %recovery increased due to PS; the addition of trans-polyoctenamer seemed to suggest that it provides a better recovery of the PP-binder from deformation during loads.

PS is one of the susceptible polymers when it is exposed to the sun (specifically, UV radiation); however, there are very limited studies on UV degradation of PS. UV degradation of PS leads to excessive embrittlement of the plastic, hence potentially leading to significant cracking pattern on the samples. The degradation, embrittlement and cracking

of PS when exposed to the sun (UV) can considerably restrict its application as a bitumen modifier. Therefore, it is recommended to study UV ageing of PS modified binders.

#### 5.6. Ethylene-Vinyl Acetate (EVA) Modification of Bitumen

EVA is a thermoplastic polymer formed by co-polymerization of vinyl acetate and ethylene [133], where the vinyl acetate content is controlled through a copolymerization process [260]. EVA has been used in the modification of bitumen for decades due to the enhancement of molecular bonding between VA and carbonyl linkages that affects the polarity between the two materials [169]. The basic characteristics of EVA reported in different literature studies are provided in Table 2. EVA is similar to LDPE in terms of rigidity and translucency; depending on the VA content EVA can be transparent like rubbers or plasticized PVC and can resemble elastomers for flexibility and softness. EVA is a form of plastomeric polymers used for modification of bitumen where the variation in vinyl acetate content provides interesting characteristics to EVA-modified bitumen. It is suggested that the higher content (i.e., greater than 20% VA) of vinyl acetate in EVA enhances the polarity of the polymer and the elasticity, storage stability, and flexibility of EVA-modified bitumen whereas lower content of vinyl acetate of EVA (i.e., 8–14% VA) increases the degree of crystallinity, leading to stiffer EVA-modified bitumen with enhanced high temperature performance [261]. EVA-based polymers form a rigid and tough bonding with bitumen during its modification to resist the deformation [33]. Unlike many plastomers discussed in the previous sections, EVA—also depending on the VA content—tends to improve the thermal cracking at low temperature and permanent deformation [35].

The mixing temperature for preparing EVA-modified bitumen is commonly 160–200 °C, as shown in Table 3. The lower limit of the temperature range is generally selected at approximately 160 °C due to the fact that the homogeneous mix of EVA in bitumen is difficult to obtain at lower temperature, even after 1 h of mixing time [169]. It is reported that the variation in mixing temperature does not seem to significantly affect penetration, ductility, specific gravity, and softening point of EVA-modified bitumen [169]. The effect of mixing duration for EVA-modified bitumen is listed in Table 3. The overall mixing time reported for mixing of EVA and bitumen is between 20 min to 6 h (Table 3). A study investigated the effect of mixing time on various physical properties of EVA-modified bitumen at 20, 25, and 30 min mixing time and observed that there is no significant change in the physical properties of the final bitumen [169]. Various concentrations of EVA have been used for bitumen blends. Concentrations of EVA at 1–10% are used in different studies (Table 3), where 5% by weight of the bitumen is found to be the most commonly used percentage of EVA. Panda and Mazumdar [169] studied the effect of different concentrations of EVA by varying its loading from 2.5% to 10% by weight of the base bitumen. It was observed that increasing the polymer concentration improves the softening point and lowers ductility and penetration. Another study found that 5% EVA caused an increase of 21.6–53% in softening point and decrease of 33–51% in penetration [12]. However, the increasing level of softening point varies by varying the concentration of the polymer. For instance, the softening point of EVA-modified bitumen as compared to base bitumen increases by 14 °C, 16 °C, and 18 °C at 4%, 5%, and 6% concentration of EVA, respectively [116]. An enhancement in the softening point (showing a stiffening effect of polymer modified bitumen) by addition of EVA polymer can favour the pavement durability in warmer climatic conditions. Similarly, penetration index and ductility values were improved by adding EVA at increasing concentration, which suggest that EVA-modified bitumen is more resistant to rutting and low temperature cracking. The results of storage stability of EVA-modified bitumen indicates that the temperature difference between the top and bottom portion of the cigar tube test (ASTM D7173) sample was less than 2.5 °C, confirming that EVA-modified bitumen is mostly stable at higher temperature [105]. Further, it was suggested that some sort of separation may occur during storage of EVA-modified binders, but EVA gets easily dispersed in bitumen and has relatively high compatibility with binders. EVA with low VA content is expected to provide high storage stability [201]. In order to

further improve the storage stability of EVA-modified bitumen, some stabilizing agents were introduced with EVA, which helped enhancing the overall characteristics of binder. Among others, innovative stabilizing agents include maleic anhydride and nano clays. Addition of maleic anhydride helps decrease penetration, improves storage stability, and increases the ductility and softening point [116]. On the other side, the nano clays result in increasing the softening point and provides stability to binders up to 6% of EVA; the latter content was not stable in the absence of the nano-clay additive [262].

The viscosity of bituminous binders at in-service temperature of asphalt is generally expected to be high to avoid rutting (permanent deformation), whereas it should be very low at handling and manufacturing temperatures, resulting in an easy construction of the pavement. It was observed that the addition of EVA raises the viscosity value when EVA content is greater than 3% [35]. The ductility of bitumen was increased after addition of EVA; for instance, 5% EVA resulted in 20% increment in ductility, which contrasts with other polymers such as PP, PVC, and PE. The higher content (9%) of EVA polymer results in the rheological behaviour of modified bitumen showing better performance as a paving binder [29]. It was found that the phase angle decreases whereas the complex shear modulus increases by increasing the concentration of EVA. It is suggested that the testing temperature, concentration, and nature of the polymer have a significant effect on storage modulus and loss modulus of the polymer-modified bitumen [68]. Liang et al. [261] studied the MSCR of EVA-modified bitumen and found that the VA content in EVA offers higher %recovery whereas increasing temperature and stress load cause a sharp decline in %recovery, meaning that higher temperature associated with heavy loads degrade the recoverable ability of asphalt pavements. Similarly, the VA content of EVA has a significant effect on Jnr value of EVA-modified bitumen due to EVA crystallisation temperature.

The thermogravimetric/differential thermogravimetric (TG/DTG) analysis of base bitumen and EVA-modified bitumen suggests that the TG decomposition stage for bitumen happens at 290–490 °C with 75% mass loss, hence decomposing the asphaltenes to form coke [116]. The DTG curve shows that the maximum weight loss took place at 450 °C. On the other hand, the TG curve for EVA modified bitumen highlights a decomposition peak at 307–492 °C and 462 °C for the DTG curve. The initial and maximum decomposition temperatures of EVA-modified bitumen are higher than that of base bitumen, suggesting that the addition of EVA resulted in increasing the thermal stability of bitumen [116]. The morphological images of EVA-modified bitumen are shown in Figure 5. It can be observed from Figure 5 that the EVA-modified bitumen showed fine dispersion of polymer, which is confirmed by the presence of the polymer network at 5–6% of EVA content [33].

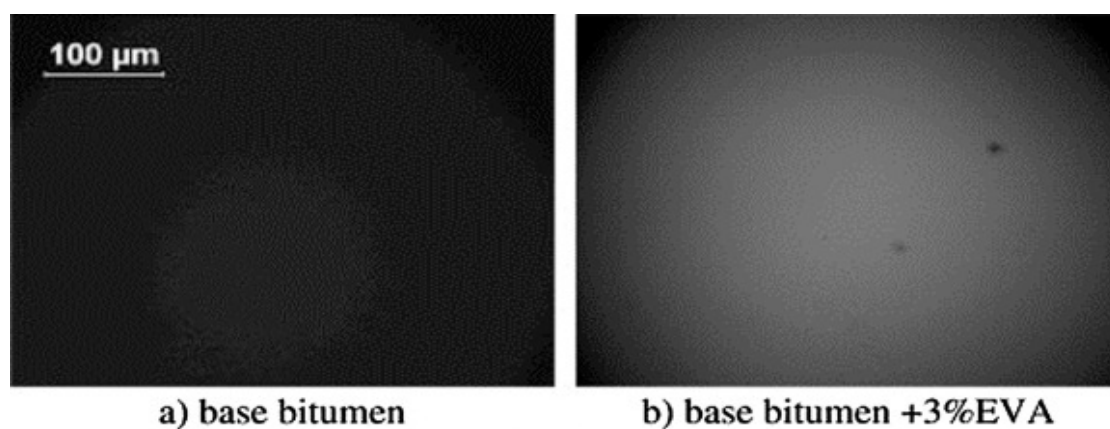
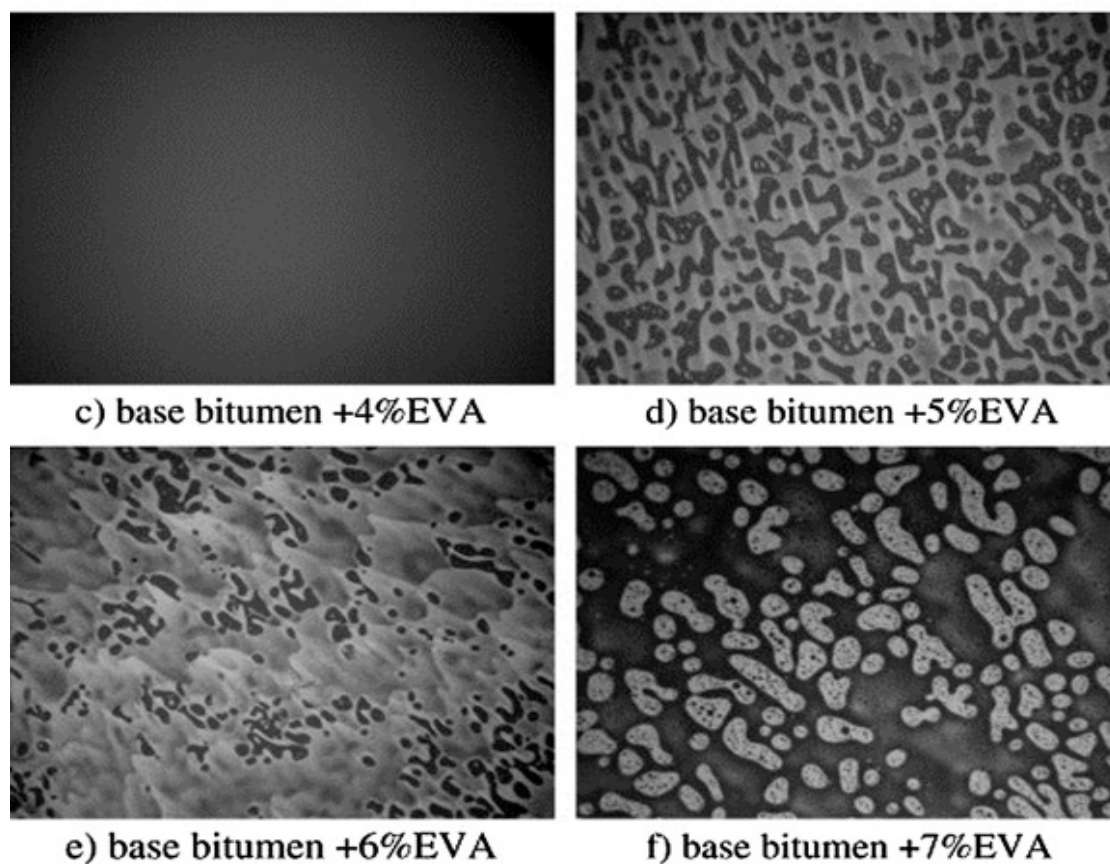


Figure 5. *Conts.*



**Figure 5.** Fluorescent images of EVA-modified bitumen: (a) base bitumen, (b) 3% EVA, (c) 4% EVA, (d) 5% EVA, (e) 6% EVA, and (f) 7% EVA [33]. Reused with permission from Elsevier.

## 6. Co-Mingled Plastomers for Bitumen Modification

Plastics recovered from the post-consumer stream contain many different types of plastomers. As a result, they contribute to most of the co-mingled recycled/waste plastomers in this case [263]. As discussed in the previous sections, each plastomer—whether chemically pure or recycled—has some specific drawbacks, hence, various studies tried to combine different polymers in order to improve the properties of modified bitumen. Various research studies have reported different combination of polymers (mainly elastomers and plastomers) for evaluating the performance of both individual polymers and combined polymers [206,264,265]. The combination of two polymers is carried out either by extruding the polymers before they are added into the bitumen [266,267] or simply by adding the single polymers in a defined proportion and then mixing them with the bitumen [206]. Most of the studies have focused on the combination of elastomers and plastomers such as tyre rubber and PE [268,269], tyre rubber and EVA [270], tyre rubber and PP [265], tyre rubber, EVA and PE [267], and styrene butadiene styrene and PE [271]. Brovelli et al. [266] used two plastomers (i.e., PE and EVA) in combination. However, the most common combinations investigated involve tyre rubber as an elastomer and any of the plastomers to enhance the characteristics of a waste (or recycled) polymer. The addition of rubber with PE-modified binders is suggested to be an effective way of improving both the low and high temperature properties of the blend while maximising the use of recycled products [105]. When combined together, PE helps to enhance the high temperature properties by stiffening the modified bitumen whereas the rubber tends to improve the low temperature properties [161]. It is reported that physical interaction occurs between rubber and PE during combined modification, which helps for homogeneous distribution and size refinement of polyethylene [105].



The mixing conditions for bitumen modification of comingled polymers vary depending upon the type of polymer used. Generally, the mixing temperature found in several studies dealing with co-mingled plastomeric polymers varies between 120 °C and 190 °C, mixing time ranges between 0.5 and 6 h, and 1200–5000 rpm mixing speed [2,265,267,272]. A study by Yuan et al. [273] reported the highest mixing speed of 25,000 rpm with 7–12% of PE, while another study employed a combination of PE and EVA at a mixing speed of 1200–5000 rpm for 6 h [267]. Generally, the penetration value is decreased at a combination of tyre rubber and PE/PP as compared to the base binder but the reduction in penetration value in presence of tyre rubber and plastomer is higher than that of only tyre rubber and lower than that of only plastomer [12]. On the other hand, the changes in softening point commonly exhibit a steeper upward trend with the combination of two polymers compared to the individual polymers. The addition of PE and tyre rubber decreases the ductility of modified bitumen up to a fixed amount of PE, while when the amount of PE is less than tyre rubber, the blend shows improved ductility [206,264]. Adding stabilizing agents—such as furfural extract oil [265], reactive dioctyl phthalate [265], polyphosphoric acid [208], sulphur [274] and maleic anhydride—to the combination of polymers before blending with bitumen generally increases the ductility of the modified bitumen. A study reports that ductility was increased by using maleic anhydride grafted LDPE with styrene butadiene styrene and HDPE before adding them into the bitumen [40].

In terms of rheological properties, it is reported that the addition of hybrid (or combined) polymers tends to enhance the rheological characteristics of modified bitumen by increasing the complex shear modulus and reducing the phase angle [206,275]. A combination of PE with other polymer increased the Superpave parameter  $G^*/\sin\delta$  [208,273], hence indicating greater resistance to rutting. The combination using maleic anhydride grafted LDPE resulted in decreasing the phase angle and improving  $G^*/\sin\delta$  [40]. The addition of a large amount of tyre rubber with plastomers enhances the mechanical characteristics, indicating betterments for low temperature flexibility and resistance to high temperature deformation [265,268]. Regarding storage stability values, mixing 2% styrene-butadiene-styrene to 6% PE (HDPE and LDPE) or mixing 5% styrene-butadiene-styrene, 3.5% PE and 3% furfural extract oil showed good storage stability values [233,275]. Further, the addition of maleic anhydride grafted LDPE to styrene-butadiene-styrene, LDPE and HDPE decreases the phase separation, consequently increasing the compatibility and storage stability [40]. Appiah et al. [276] conducted a physical and rheological study by utilising a combination of HDPE and PP for bitumen modification. The results exhibited an increase in the softening point, a decrease in penetration value while enhancing the overall dynamic and absolute viscosity of the binder in comparison to conventional bitumen. Although no distinct or new findings were observed in the spectroscopic analysis, the study showed a strong bond between polymer strands and the bitumen matrix. Another study investigated the effect of individual PP and HDPE as well as a combination of PP and HDPE at 1:1 ratio and were added to bitumen at 9% weight of bitumen. Marshall test results suggested that HDPE/PP modified bitumen showed 179% improvements in Marshall stability, whereas PP and HDPE increased its value to 156% and 152%, respectively [277].

Manju et al. [278] examined the effect of utilizing combined and recycled polymers including PVC and HDPE pipes, LDPE plastic bags and PET bottles as modifiers for bitumen. Results showed a 40% and 9% decrease in crushing and impact values, respectively, suggesting an increase in strength. The penetration and abrasion test witnessed lower values obtained in comparison to the control sample. The study concluded that the recycled polymer-modified bitumen has shown greater stability in comparison to conventional bitumen. According to Mahmuda et al. [279] hybrid combination of PET and PS showed some potential to enhance the rutting resistance of asphalt. Nkanga [280] studied the incorporation of PET and PS at 1:1 ratio for bitumen modification. A combination of PS and PET increased the specific gravity, softening point, flash, and fire points, while penetration and ductility were decreased. The study concluded that PET and PS improved the road's durability, resistance to deformation, corrugation, and shoving. Another study

employed LDPE, PS, and a blend of both polymers at 1:1 ratio and found that an increase in concentration of polymer from 5% to 15% improved the Marshall stability, flow, bulk density, strength, and fatigue life of the asphalt mix [280]. A study conducted by Chowdhury [281] utilised a combination of polyethylene and polyester; the outcomes showed that the optimum polymer content was 8% by weight of bitumen. The mixing process exhibited a glue and binding effect that improved the physical properties of the aggregates significantly. The stability and ITS (wet-dry, freeze-thaw) of the overall mix increased due to the plastic modification of the mix, specifically on the bond between aggregate and bitumen with the addition of plastic. Yan et al. prepared a blend of bitumen by combining two polymers (tyre rubber and PE) and observed that the modified binder showed uniform distribution between bitumen and polymeric materials [206]. A continuous bitumen phase with dispersed polymer particles by adding a single agent was observed, whereas with the addition of CR and PE under integrate modification, a nearly continuous polymer phase appeared and finally formed two continuous twisted phases [282].

Although comingling of two polymers enhances various properties of modified bitumen, there are some drawbacks which require further investigation—such as low temperature rheological behaviour. In fact, combined polymers could limit the bitumen's ability to relax thermal stress [206]. In the case of crumb rubber being one participant polymer, complex chemical reactions take place during blending and thermal dissociation (or depolymerisation) of crumb rubber can occur [283]. It can be observed that the addition of combined polymers to bitumen has the potential of increasing phase separation due to less compatibility of these polymers in the bitumen. Hence, different additives have been utilized for polymer modification of bituminous binders in an attempt of enhancing the compatibility between bitumen and polymers. The following section discusses the different chemical compatibilizers used for polymer modification of bitumen.

## 7. Enhancements of Plastomer-Modified Bitumen Due to Chemical Modifiers

Many studies tried to address common plastomer drawbacks such as phase separation and thermal instability. Polymers and bitumen become less compatible due to differences in their structure, molecular weight, density, polarity, and viscosity. A difference in density may cause the creaming of polymer particles, which leads to phase separation. Together with the physical blending between bitumen and polymers, chemical modification is also suggested to overcome common drawbacks and improve the properties of modified bitumen. Chemical modification utilizes various chemicals as an additive to the bitumen, extenders of the binder, or modifier to the binder; this section focuses on chemical modifiers to stabilize plastic-modified bitumen. It is suggested that the polymer modifiers should be highly compatible to the binder, hence resulting in homogenous blends and minimizing the phase separation during transportation and storage [105]. Different modifiers play different roles in improving the properties of polymer-modified bitumen; for instance, maleic anhydride improves polarity and decreases crystallinity, which disrupts closely packed crystalline microstructure [99] resulting in increased compatibility and storage stability [100,163,171], organic montmorillonite supports chemical bonding between the bitumen and polymer and polyphosphoric acid enhances the rheological characteristics of the binders at high temperatures [194,284]. To date, various modifiers have been employed to obtain the required compatibility and reduce the phase separation during polymer modification of bitumen. Among the most common modifiers: reactive polymers, polyphosphoric acid, organometallic compounds, sulfonic acid, silanes, maleic anhydride, carboxylic anhydride, thiourea dioxide, sulphur, antioxidants, nanomaterials, clay minerals, plasticizers, and bio-oil [4,105,162,205,210,285–289]. Table 5 lists different the chemical modifiers used for plastomeric bitumen modification.

### 7.1. Chemically Functionalized Polymers

The shortage of butadiene in 2009 hit the SBS market affecting the cost and supply of the most commonly used polymer in bitumen [290]. The high cost of SBS pushed companies to find an economic alternative to SBS, consequently, reactive polymer was recognised as a promising option to potentially substitute SBS [291]. The functionalization of polymers with new functional groups (i.e., acrylic acid and glycidyl methacrylate) leads to new polymer modifiers; i.e., reactive polymers which may crosslink or chemically bond with bitumen molecules through their functional groups [105,292]. In functionalization, different chemical functional groups are added to the polymer for improving the properties of polymer-modified binder, specifically tackling the compatibility of the polymer phase with the bitumen phase for minimizing phase separation. Some examples of such polymers are thermoplastic elastomers functionalized with maleic anhydride and ethylene-based copolymers with epoxy rings [67]. Reactive polymers are mostly based on glycidyl-methacrylate, ethylene, and ester groups—either ethyl, butyl or methyl acrylate, amorphous poly alpha olefins, and trans-polyoctenamer.

Reactive polymers can potentially be utilized as polymer modifiers [293], bitumen modifiers [294], and compatibilizers between polymer and bitumen [57] for improving the mechanical properties, temperature susceptibility, and storage stability of modified bituminous blends and bitumen mixtures [105]. These polymers have a unique characteristic of chemically linking to bitumen to develop a chemical bond with bitumen molecules [65,116]. Reactive polymers contain various functional groups which react by forming a three-dimensional (3D) bonding. This 3D bonding tends to improve the performance and properties of the modified bitumen.

Luo and Chen [116] studied the effect of EVA (plastomer) and EVA-g-MA (reactive polymer) and found that both the polymers improved the softening point and penetration index of bitumen, but EVA-g-MA showed higher softening point temperature than EVA alone. EVA showed 14 °C, 16 °C, and 18 °C increase in softening point whereas EVA-g-MA showed 21 °C, 24 °C, and 27 °C for 4%, 5% and 6% of EVA and EVA-g-MA, respectively than that of unmodified bitumen. Similarly, the penetration index and ductility values of EVA-g-MA modified bitumen were improved compared to EVA-modified bitumen, suggesting that EVA-g-MA modified bitumen is less susceptible to temperature changes and low temperature cracking. It was concluded that a network structure is formed between EVA-g-MA and bitumen due to reactions taking place between the MA group of EVA-g-MA and functional groups of asphaltene in bitumen. This network structure helps reinforce the compatibility between bitumen and EVA-g-MA [116]. The storage stability for EVA-g-MA modified bitumen shows that the temperature difference in top and bottom samples was less than 2.5, confirming that EVA-g-MA modified bitumen is stable at higher temperature according to the storage stability cigar tube test [295]. Another study blended two reactive polymers (Elvaloy AM, containing butylacrylate 28 wt%, glycidylmethacrylate 5.3 wt% and Elvaloy 4170, containing butylacrylate 20 wt%, glycidylmethacrylate 9 wt%) with bitumen to examine the effect of these reactive polymers on storage stability. It was found that all samples exhibited complete homogeneity, suggesting that the reactive polymers guarantee better storage stability and, consequently, better bitumen-polymer compatibility [296]. Yeh et al. confirmed the better compatibility of aPP and bitumen as compared to iPP-bitumen in the presence of reactive polymers [245]. LDPE and LDPE-g-MA were blended with bitumen and it was observed that LDPE-g-MA showed greater stabilizing effect than LDPE [171]. The rheological behaviour of base bitumen and EVA-g-MA modified bitumen in terms of phase angle and complex shear modulus was investigated by [116]. It was observed that the addition of EVA-g-MA in bitumen affected the rheological properties significantly by increasing the complex modulus and reducing phase angle values. The greater the concentration of EVA-g-MA, the more significant the changes in complex shear modulus and lower phase angle. A reduction in phase angle while increasing the polymer content confirms that the elastic properties of modified bitumen have been improved,

whereas an increase in complex shear modulus with increasing polymer content represents the network structure formation.

Although polymer functionalization provides various advantages such as higher reactivity and polarity, it also comes with some drawbacks such as undesired and uncontrolled crosslinking of un-saturated polymers. Hence, it is proposed that the reactive polymers should be used with elastomers (PE and PP) due to their saturated nature [100]. Other than uncontrolled and undesired crosslinking, high cost and gelation problems are also reported as shortcomings of the use of reactive polymers. Various approaches have been suggested to overcome such shortcomings of reactive polymers. One approach is to reduce the content of reactive polymers; the majority of studies suggested using less than 1% concentration whereas very few studies proposed increasing the concentration up to 2–2.5% by weight of bitumen [66]; high loadings of such polymers form infusible and insoluble bitumen gel [67]. Bulatovic et al. [296] studied the effect of different loading percentages of reactive polymers on the properties of bitumen and found that 1.9 wt% reactive polymers resulted in gelification of the binder. Polacco et al. [297] reported that a low percentage of reactive polymers generally has an insignificant effect on the properties of the base binder. Hence, further research is required for optimizing the percentage of reactive polymer by adding co-modifiers and/or catalysts to accomplish improved properties of the binder.

## 7.2. Maleated Bitumen

Maleic anhydride,  $C_4H_2O_3$ , is a five-atom ring, cyclic, and unsaturated compound. It can be used either alone or after creating reactive polymers by adding it to polymers and finally use it for bitumen modification [100]. The chemical interaction between bitumen and maleic anhydride is a complex mechanism coming from Diels-Alder reactions or copolymerization [298,299]. Chemical reactions taking place between maleic anhydride and bitumen were analysed by FTIR and GC-MS analysis, which showed that two acid groups (i.e., HOOC-) were present, which can bond two molecules of bitumen indicating that two anhydrides undergo ring opening to donate the corresponding di-acid. Further, according to the FTIR analysis, a double bond disappeared, which showed the occurrence of chemical reaction between maleic anhydride and bitumen molecules [299]. Possible interaction between maleated bitumen and LDPE is shown in Figure 6 [57].

It is confirmed from various studies that maleic anhydride results in enhanced characteristics of modified bitumen due to its higher reactivity with bitumen molecules. The high reactivity of maleic anhydride will tend to increase the chemical interaction between polymer and bitumen helps to improve the overall characteristics of modified bitumen. Nadkarni et al. [300] studied the effect of different concentrations of maleic anhydride on mechanical and physical properties of modified bitumen. They observed that maleic anhydride improved the cohesive strength at high temperature and enhanced cracking resistance at low temperature. Another study investigated the effect of maleic anhydride grafted polymer (SEBS-g-MA) on the storage stability of modified bitumen and it was found that SEBS-g-MAH-modified bitumen showed better storage stability than the SEBS-modified bitumen [301]. In general, the addition of maleic anhydride improves the properties of modified bitumen significantly due to its high reactivity, which promotes the chemical interaction between bitumen and polymer. However, this high reactivity leads to issues during storage and handling. It is thus suggested to synthesise polymer-maleic anhydride compounds—namely creating a reactive polymer first—and then mix it with bitumen.

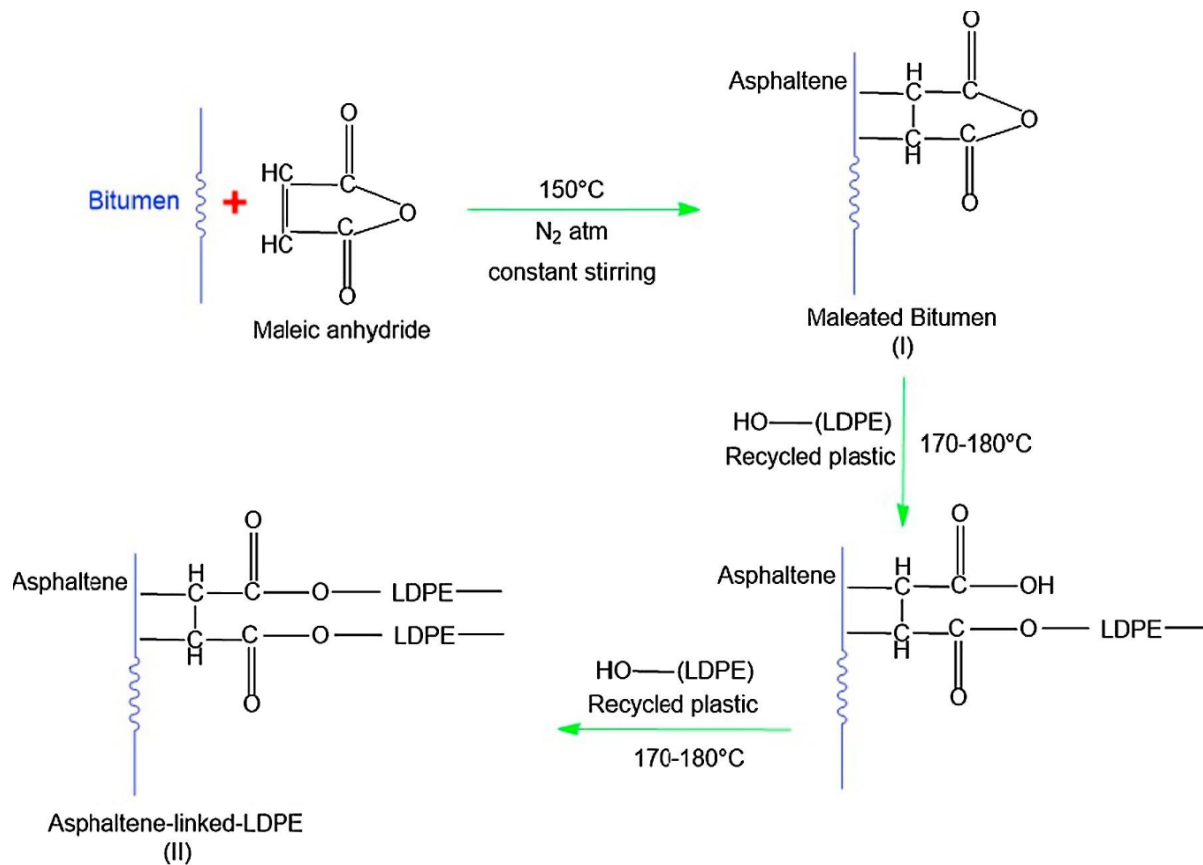


Figure 6. Schematic illustration of interaction occurring between LLDPE and malleated bitumen [57].

### 7.3. Polyphosphoric Acid

Polyphosphoric acid is an oligomer of phosphoric acid ( $H_3PO_4$ ). It has achieved significant importance in the road industry for chemical modification of bitumen as a medium to improve its properties. However, phosphoric acid modification of bitumen is a complex physio-chemical process and the properties of modified bitumen blend may strongly be dependent upon the specific nature of bitumen [100]. However, it is proposed that improvements are also dependent upon the amount of polyphosphoric acid and type and concentration of the polymer [302]. The addition of polyphosphoric acid to bitumen is considered a complex process due to the large number of molecules with different structures and their possible reactions taking place during blending with bitumen. It is reported that the polyphosphoric acid tends to revert back to orthophosphoric acid after blending with bitumen [303]. According to Baumgardner et al. [304], polyphosphoric acid helps neutralize the polar interaction between asphaltene molecules of bitumen through esterification or protonation of basic sites. Other reactions which are expected to take place during mixing of polyphosphoric acid and bitumen are alkyl aromatization and co-polymerization.

It is suggested that polyphosphoric acid plays an important role in improving the thermal, rheological, and other characteristics of modified bitumen. It has been observed that polyphosphoric acid helps improve the storage stability of polymer-modified bitumen. In terms of rheological and thermal properties, it was found that polyphosphoric acid/bitumen blends showed an enhanced high temperature performance whereas it does not significantly alter low temperature properties [305,306]. Another study used three different forms of ethylene-propylene copolymer for modification of bitumen in the presence of polyphosphoric acid and found a remarkable reduction in polymer segregation [101]. Xiao et al. [307] investigated high temperature rheological properties of polymer modified blends in absence and presence of PPA and it was found that the modified binder in presence of PPA showed the highest viscosity values. Another study evaluated the effect of

PPA on EMA-GMA modification of bitumen and compared the results with SBS binder and found that EMA-GMA in presence of PPA increased stiffness as well as elasticity of binders. They claimed that PPA tends to act as a catalyst for promoting chemical reaction between bitumen and EMA-GMA and PPA enhanced the efficiency of EMA-GMA to achieve binders with similar or better performance than SBS binder [9]. PPA is a well-known alternative to be used as binder modifier although some industrial plants are reluctant on using it due its corrosive effect [284].

#### 7.4. Sulphur

Initial applications of sulphur in bitumen were carried out alone without any other material, such as polymers. Hence, it was used in large amounts and it was suggested that the mixing temperature plays a significant role to control the reaction between bitumen and sulphur. A temperature below 140 °C was found to be the ideal temperature for bitumen and sulphur blending, because at this temperature the sulphur can easily penetrate the bitumen molecules and form hydrogen sulphide through dehydrogenation reactions [100]. This promotes reactions between the naphthenic and aromatic components, modifying the colloidal structure and chemical composition of bitumen. It is also suggested that sulphur has the potential to self-polymerize when mixed with bitumen [274]. However, polymers are nowadays added as a main modifier while sulphur is inserted in small quantity (i.e., 0.1% or less by weight of the bitumen) to help chemical reactions happen between the polymer and bitumen. The reaction of polymer/sulphur/bitumen is not fully understood, but it is assumed that the sulphur crosslinks the polymer molecules to chemically link the polymer and bitumen by sulphide and polysulfide bonds. It is also proposed that the addition of sulphur causes vulcanization of bitumen and polymer modifier, creating bitumen-polymer interconnections. These interconnections are supposed to improve the storage stability of the blends through the linking of polymer with bitumen molecules via chemical covalent bond [100].

Several studies have claimed that the addition of sulphur as a chemical modifier in polymer/bitumen blends improves various properties of modified bitumen including elasticity, storage stability, rheological characteristics, and resistance to deformation [307–310]. From a rheological perspective, it is proposed that sulphur-modified polymer/bitumen blends show greater elastic behaviour (lower phase angle at specific temperature and loading frequency) as compared to blends where sulphur is not added [308,311]. Although the addition of sulphur enhances different characteristics of modified bitumen, it also carries a few drawbacks while used as a chemical modifier for polymer/bitumen blends. In fact, sulphur can mainly react with unsaturated polymers due to its reactions taking place with the double bonds of polymers, commonly found in unsaturated polymers. Hence, its range of applications is limited. In addition, sulphur does not distribute throughout the mixture, hence non-homogenous polymer-modified bitumen could be obtained. Another drawback of using elemental sulphur is hydrogen sulphide (hazardous gas) emissions during the preparation of polymer/bitumen blends. A possible solution to this is through the replacement of elemental sulphur by more bitumen soluble polysulfides [312]. Poor recyclability of sulphur-modified polymer/bitumen blends is another shortcoming of the addition of sulphur into polymer-modified bitumen. Alghrafy et al. [313] studied PE modified binders with or without sulphur and found that the viscosity was increased significantly after addition of sulphur and all blends with sulphur met the Superpave viscosity requirements. They observed that sulphur improved the high temperature and aging performance of modified binders for sustainable/economical pavement construction. In another study, the effect of two cross-linking agents, i.e., PPA and sulphur was studied on storage stability and observed that both PPA and sulphur improved the storage stability and performance against fatigue of PE-modified binders [313,314].

### 7.5. Nano-Clay and Nanomaterials

Other than functionalization of polymers, clay minerals in both nano and micro sizes are widely utilized for the modification of neat and polymer-modified bitumen binders and they improve properties such as viscosity, storage stability, stiffness, ageing, and rutting resistance [105,315]. Golestani et al. [315] studied the effect of clay minerals on properties of modified bitumen and found that the added modifiers caused an increase in resistance against rutting. Another study [316] investigated the effect of EVA, nano-clay, and EVA/nano-clay on the properties of modified bitumen and observed that all modifiers improved rheological and physical properties of the binder. Another study found that the polymer nanocomposite can improve the low temperature resistance and rutting resistance of the asphalt binder [317]. Further, both studies confirmed that the nano-composite showed better performance than individual clay mineral and other polymer modifiers. The clay localizes at interfacial polymer/bitumen regions, reducing the interfacial tension, consequently the minor phase-dispersed particles lose their typical round shape where a finer dispersion is obtained [318]. This suggests that clay plays a major role on improving the compatibility between polymer and bitumen [100]. Another study suggests that clay materials enhance the storage stability of polymer-modified bitumen by reducing the density difference between bitumen and polymer; clay also improves the resistance against ageing with barrier properties of the dispersed clay platelets [319,320]. Ouyang et al. [320] fabricated LDPE/nano-silica blends and mixed this blend with bitumen to get LDPE/silica-modified bitumen. It was found that the storage stability was increased for all percentages of nano-silica and this was justified due to clay materials reducing the density gap between asphaltene-rich bitumen phase and polymer-rich phase. The improvement in storage stability is attributed to better compatibility of LDPE and bitumen, suggesting that the clay minerals help enhance the compatibility also. A research study investigated the effect of two different clays on EVA-modified bitumen and found that nano-clay improved the thermo-mechanical properties as well as provided better homogeneity, performance, and stability [321]. In addition to that, polymer dispersion improved with the addition of nanoclay [322] depending upon the concentration and functionality of PE [323].

Together with these advantages, the use of clays also brings some shortcomings mainly due to their hydrophilic nature; therefore, it is hard to disperse small particles of clay into the polymer matrix and it commonly results in two discrete phases separation. It is confirmed that the clay resides in polymer-rich phase, indicating that storage stabilization can be achieved only with pre-formed nano-clay composites. The most commonly used clay minerals for bitumen modification are bentonite, kaolinite, montmorillonite, and organophilic montmorillonite. Among clay minerals, the montmorillonite and organophilic montmorillonite are suggested to be more effective at intermediate and high temperature.

Similar to clay minerals, the addition of any nanomaterial in bitumen—either as a modifier or as an individual component—results in reduced phase angle, increased complex shear modulus, enhanced rheological properties at both high and low temperature, and more homogenous dispersion of the polymer into the bitumen [324–328]. High surface area and low particle size of nanomaterials are responsible for good dispersion of the polymer within the binder, hence producing a compatible system; the reduction in nanomaterial size generally improves the mechanical performance and rheological properties of the modified blends [329]. The nanomaterials used as a modifier for polymer modification of bitumen include nano-clay, nano-calcium tri-oxocarbonate, carbon nanotube, nano-titanium di-oxide, nano-zinc oxide, and nano-silica [47,140,330,331]. Another study [332] used 1% and 2% of carbon nanotube for modification of bitumen binder and found that the modified binder showed better high temperature properties, better resistance to rutting and fatigue than the unmodified binder. It is suggested that among nanomaterial modifiers, the nano-silica and nano-titanium di-oxide have better characteristics in terms of anti-moisture performance and ultraviolet ageing [105,333]. The utilization of nanomaterials in bitumen modification has some limitations such as high cost of nanomaterials and non-homogenous mixing of nanomaterials with polymer/bitumen blends.

### 7.6. Bio-Oil

The bio-oils are produced by hydrothermal liquefaction or pyrolysis of biomass and are composed of complex compounds based on C, H, and O and the main constituents are alcohols, esters, ketones, aldehydes, acids, phenols, and furan [334,335]. Both hydrothermal liquefaction and pyrolysis generate solid, liquid and gases products; where the solid part is termed as biochar, gaseous product is called biogas and liquid product is known as bio-oil. Recently, bio-oil produced from pyrolysis has been proposed as a chemical modifier for bitumen binder, whereas bio-oil from hydrothermal liquefaction still needs to be fully explored as a possible modifier for bitumen.

The most commonly used bio-oils for bitumen applications are produced from pyrolysis of palm oil, soybean oil, vegetable oil, engine oil residue, microalgae, corn stover, grape residue, swine waste, and wood pellets [336–338]. Bio-oils have been utilized for three different purposes in the bitumen industry—i.e., 100% replacement of bitumen (bio-binder), 25–75% replacement of binder (extender), and around 10% replacement (chemical modifier) [336,339,340]. According to Kabir et al. [341] the phase separation of asphalt binders was reduced by 86% after bio-modification.

Sun et al. [342] produced bio-bitumen, a substitute of traditional petroleum bitumen, dissolving bio-oil with styrene to get a homogenous bio-oil solution; this bio-oil solution was uniformly mixed with an accelerator (cobalt naphthenate) and an initiator (tert-butyl peroxybenzoate). The mixture was finally heated in a reactor to produce bio-bitumen. Similarly, another study proposed using switchgrass bio-oil and concluded that the rheological characteristics of the bio-binder were similar to those of bituminous binders [343]. Williams et al. [344] studied bio-oil as an extender for unmodified bitumen and polymer-modified bitumen and suggested that 9% of bio-oil addition results in significant performance improvements of bio-oil modified binders. They reported that the performance of bio-oil modifier depends upon several factors including bio-oil source, amount of bio-oil blended with binder and source and characteristics of the base binder.

Several studies have indeed reported application of bio-oil as a chemical modifier for polymer-modified bitumen binders. It is reported that the addition of bio-oil affects physical, mechanical, rheological, and chemical characteristics of bitumen and improves swelling of the polymer-phase in the binder. Ingrassia et al. [345] added 5%, 10%, and 15% wood bio-oil by weight of bitumen and studied the chemical, morphological, and rheological properties of modified bitumen. It was found from FTIR analysis that the ester and aromatics peaks were developed after bio-oil addition. The morphological analysis confirmed that the bio-binders are completely homogenous, hence there is no risk of phase separation. They concluded that the partial replacement of binder with wood bio-oil is suitable for road applications and provides high performance against thermal and fatigue cracking resistance while also rejuvenating aged bitumen.

The flash point and fire point are considered important tests for transportation and handling of bitumen and modified bitumen and contradictory observations have been reported in literature about the effect of bio-oil addition on the fire point and flash point of modified bitumen. Xinxin et al. [346] reported that as the bio-oil amount increases, both the fire point and flash point decreases whereas some other studies found that fire point and flash point increased when increasing the amount of bio-oil modifier [346,347]. Yang and You [348] investigated the effect of bio-oil addition on rheological properties of polymer-modified bitumen and found that an increase in bio-oil results in an increased complex shear modulus and decreased phase angle. A decrease in phase angle represents the ability of modifier to form a continuous elastic networking between the modifier and bitumen [349]. The  $J_{nr}$  value from multiple stress creep recovery (MSCR) test was decreased by increasing the amount of bio-oil, suggesting that the bio-oil possesses a potential for reducing rutting [9]. From a chemical perspective, it was observed that the addition of bio-oil resulted in a decreased intensity of carbonyl peaks (C=O), whereas the alkyl group (-CO) and alcohol stretching (-OH) appeared on bio-oil modified bitumen. These functional groups are not found in petroleum-based bitumen; hence, they are typical



attributes of bio-oil [350,351]. A reduction in the intensity of carbonyl peaks is attributed to the decrease of the overall asphaltene percentage, consequently decreasing the carbonyl functional groups [352,353]. It was found that the addition of bio-oil caused a significant change in the SARA composition of bitumen, where the resin content was increased and the aromatics were decreased. The addition of bio-oil results in increasing resins and decreasing asphaltenes, saturates and aromatics [344]. A higher amount of resin increases viscosity and lowers shear susceptibility and penetration index [354].

## 8. Critical Discussion

Polymer modification is considered an effective technique to improve the bitumen properties in order to avoid or at least minimize binder failure while increasing the lifetime of the road. The three most commonly used types of polymers—chemically functionalised thermoplastics, elastomers, and plastomers—have been successfully applied for bitumen modification and each type has shown to provide various advantages and disadvantages. However, this review article focuses on the utilization of plastomers; both virgin and waste plastomeric polymers for bitumen modification. An increasing number of research studies are focusing on the application of waste plastomers for bitumen modification due to their abundant availability, easy recycling, low cost, and consistent engineering performance similar to virgin polymers. Plastomers are of various types including EVA, EBA, EMA, PP, PVC, PET, PS, and PE; however, each plastomer has its own advantages and disadvantages over others when mixed with bitumen. After reviewing a large number of studies on plastomeric modification of bitumen, it should be emphasised that some of the polymers only melt at a very high temperature, which can be higher than the bitumen production temperature. Although studies are available that mix high melting temperature plastomers with bitumen, these should be considered as inert fillers rather than active polymers.

**Table 5.** An overview of chemical modifiers used for improving plastomer-bitumen compatibility.

| Modifiers/Compatibilizers  | Method/Weight% of Modifiers   | Key Findings   | References |
|--|---|--|------------|
| Reactive polymer (TOR)   | <ul style="list-style-type: none"> <li>• 2:1 of PE and TOR</li> <li>• 0.1, 0.5 or 1% sulphur was mixed with PE-TOR</li> </ul>   | <ul style="list-style-type: none"> <li>• High stiffness with increased softening point, rotational viscosity, and decreased penetration</li> <li>• Increase storage stability</li> <li>• Increase elastic properties</li> <li>• The modified binder was homogeneous, hence improved rheological properties</li> <li>• Resistant to permanent deformation</li> </ul>  | [41]       |
| Reactive polymer, Amorphous poly alpha olefin (APO)                        | <ul style="list-style-type: none"> <li>• 15% waste tyre rubber, 15% waste polymer and 4% APO, 15% waste polymer and 6% APO</li> </ul>   | <ul style="list-style-type: none"> <li>• APO tends to improve anti-aging properties</li> <li>• Better aging resistance</li> <li>• High resistance to permanent deformation and fatigue cracking</li> <li>• Reduced temperature susceptibility</li> <li>• Improved high temperature performance</li> <li>• High resistance to rutting and high storage stability</li> <li>• Strong molecular network</li> </ul> | [355]      |
| EMA-GMA Terpolymer (ethylene/methylacrylate/glycidyl metacrylate) and HDPE | <ul style="list-style-type: none"> <li>• 1.8% of EMA-GMA</li> <li>• 0.10, 0.30, and 0.50% HDPE</li> <li>• 0.15% and 0.30% polyphosphoric acid</li> </ul>  | <ul style="list-style-type: none"> <li>• EMA-GMA affected the elasticity and stiffness of binder</li> <li>• EMA-GMA with either HDPE and polyphosphoric acid improved both stiffness and elasticity.</li> <li>• Combined EMA-GMA, HDPE and polyphosphoric acid showed better resistance to permanent deformation</li> </ul>  | [9]        |
| Malleated bitumen (Reaction of bitumen with maleic anhydride)              | <ul style="list-style-type: none"> <li>• 1, 2, 3, 5, and 10% of maleic anhydride was added to molten bitumen</li> <li>• 3, 5, 7, and 9% of LDPE was added with malleated bitumen</li> <li>• Finally, an optimized malleated bitumen/LDPE blend was mixed with 1, 2, 3, and 5% SBS, 2, 4, and 6% of natural rubber and 5 and 10% castor oil</li> </ul> | <ul style="list-style-type: none"> <li>• Malleated bitumen minimizes phase separation</li> <li>• Improved storage stability</li> <li>• Adequate softening point and low temperature flexibility</li> </ul>   | [57]       |

Table 5. *Conts.*

| Modifiers/Compatibilizers  | Method/Weight% of Modifiers  | Key Findings   | References |
|--|--|--|------------|
| Maleic anhydride grafted polyethylene (PE-g-MA)Maleic anhydride-grafted ethylene-octene copolymer (POE-g-MA)Maleic anhydride-grafted linear LDPEMaleic anhydride-grafted ethylenevinyl-acetate copolymerMaleic anhydride-grafted styrene-ethylene-butylene-styrene | <ul style="list-style-type: none"> <li>The waste tyre, LDPE and compatibilizer were mixed in HAAKE rheomix at 120 C and 60 rpm for 10 min</li> <li>Then, this mixture was blended with 200 g of bitumen</li> </ul>   | <ul style="list-style-type: none"> <li>PE-g-MA and POE-g-MA provide greater tensile stress and toughness</li> <li>The toughness value of POE-g-MA blend is the largest (2032.3 MJ/ m<sup>3</sup> compared to control 1402.9 MJ/ m<sup>3</sup>)</li> <li>The swelling properties of POE-g-MA blend are the best among the five compatibilizers</li> <li>POE-g-MA should be a good modifier to improve the compatibility between the bitumen and the WTP/LDPE blend</li> </ul> | [356]      |
| LLDPE-g-MA   | <ul style="list-style-type: none"> <li>30%, 50% and 70% HDPE</li> <li>30%, 50% and 70% CR</li> <li>0%, 1%, 3% and 5% LLDPE-g-MA</li> <li>Initially, the HDPE/Cr/LLDPE-g-MA blends were formed by using Rheomix</li> <li>Then 15 wt% of HDPE/Cr/LLDPE-g-MA blend was mixed with bitumen in shear mixer</li> </ul> | <ul style="list-style-type: none"> <li>Higher content of LLDPE-g-MA shows better storage stability</li> <li>Less rutting and permanent deformation</li> <li>Good network and interaction between maleic anhydride and bitumen functional groups, therefore no phase separation at high temperatures</li> </ul>   | [357]      |
| Electron irradiated recycled low-density polyethylene (e-LDPE <sub>R</sub> )   | <ul style="list-style-type: none"> <li>1%, 3%, 5%, 7% and 9% of e-LDPE<sub>R</sub></li> </ul>  | <ul style="list-style-type: none"> <li>Improved rheological properties</li> <li>Improved stiffness</li> <li>Chemical bonding of e-LDPE<sub>R</sub> with bitumen</li> <li>Formation of mixed bitumen/e-LDPE<sub>R</sub> amorphous phase</li> </ul>  | [207]      |
| Electron irradiated recycled high-density polyethylene (e-HDPE <sub>R</sub> )  | <ul style="list-style-type: none"> <li>1%, 3%, 5%, 7% and 9% of e-HDPE<sub>R</sub></li> </ul>  | <ul style="list-style-type: none"> <li>Improvement in temperature susceptibility</li> <li>Enhanced physical properties</li> <li>Chemical interaction between polymer and bitumen</li> </ul>  | [358]      |
| Silane crosslinking agent (Si-XLPE)  | <ul style="list-style-type: none"> <li>0.5, 1, 2 and 3% polymer</li> </ul>   | <ul style="list-style-type: none"> <li>Technical, environmental, and economical benefits</li> <li>More stiffness</li> <li>Improved storage stability, hence, better compatibility</li> </ul>   | [292]      |
| Polyphosphoric acid  | <ul style="list-style-type: none"> <li>0.10, 0.30, and 0.50% HDPE</li> <li>0.15% and 0.30% polyphosphoric acid</li> </ul>  | <ul style="list-style-type: none"> <li>EMA-GMA with either HDPE and polyphosphoric acid improved both stiffness and elasticity</li> <li>Polyphosphoric acid enhanced chemical reactions</li> <li>Combined EMA-GMA, HDPE and polyphosphoric acid showed better resistance to permanent deformation</li> </ul>   | [9]        |

Table 5. *Conts.*

| Modifiers/Compatibilizers                | Method/Weight% of Modifiers  | Key Findings  | References |
|--|--|---|------------|
| Sulphur                                  | <ul style="list-style-type: none"> <li>Hybrid blends of SBS with LLDPE, LDPE, EVA was prepared</li> <li>0.1% sulphur was added</li> </ul>  | <ul style="list-style-type: none"> <li>Sulphur offered chemical cross-linking effect</li> <li>It tends to help chemical bonding</li> <li>Complied with Superpave rutting parameter threshold by addition of sulphur</li> </ul>  | [359]      |
| Sulphur                                  | <ul style="list-style-type: none"> <li>0.15% and 0.25% sulphur were added</li> <li>4.5% and 7.5% of SBS was used as polymer modifier</li> </ul>                                      | <ul style="list-style-type: none"> <li>Sulphur acts as a stabilising agent</li> <li>Sulphur cross-linking creates multi-sulfidic bond</li> <li>Sulphur helped with SBS polymer dispersion</li> </ul>  | [360]      |
| Flake graphite<br>Graphite nanoplatelets | <ul style="list-style-type: none"> <li>5% flake graphite was added</li> <li>The xGNP was used as 2%</li> </ul>   | <ul style="list-style-type: none"> <li>Addition of graphite materials increase thermal conductivity resulting in better light healing</li> <li>The 5% flake graphite modified bitumen mixtures had higher healing performance than 2% graphite nanoplatelets modified bitumen</li> </ul>  | [361]      |
| Rapeseed bio-oil<br>Fish bio-oil         | <ul style="list-style-type: none"> <li>Rapeseed oil and fish oil were used as chemical modifier</li> </ul>   | <ul style="list-style-type: none"> <li>Both oils exhibited solubility issues</li> <li>Fish oil worked better than rapeseed oil for binder modification</li> </ul>   | [354]      |
| Bio-oil from waste wood                  | <ul style="list-style-type: none"> <li>Three types of bio-oil including original bio-oil, de-watered bio-oil and polymer modified bio-oil were used as chemical modifiers</li> </ul> | <ul style="list-style-type: none"> <li>Addition of bio-oil improved high temperature performance of bitumen binders</li> <li>Polymer modified bio-oil had highest stiffness followed by de-watered bio-oil and original bio-oil</li> <li>Original bio-oil showed the lowest effect as compared to other two bio-oils</li> </ul> | [362]      |
| Bio-oil                                  | <ul style="list-style-type: none"> <li>Bio-oil modified bitumen binder was prepared by adding bio-oil into bitumen binder</li> </ul>   | <ul style="list-style-type: none"> <li>Thermal storage stability was decreased by increasing bio-oil content</li> <li>Physical segregation and chemical reactions occurred by adding bio-oil</li> </ul>   | [363]      |

Among the most common plastomers already used by the asphalt industry is EVA. Although this polymer is largely used in combination with bitumen and provides remarkable performance, limited studies have addressed the role of VA content on EVA-modified bitumen. Low VA content increases stiffness and the softening point, whereas it lowers penetration, tensile strength, and elongation values. The contrary is true for high VA content where the polymer behaves more like a rubber than rigid plastic. Additionally, low VA content generates stiffer bituminous blends at high temperature whereas higher VA content shows a similar behaviour to SBS modified bitumen [364]. PP-modified bitumen was found to improve rutting resistance, fatigue life, stability, and Marshall properties; although not extensively studied as polymer for bitumen, PP has demonstrated to retain interesting properties that deserve more investigation. Mainly due to environmental issues during heating at high temperature, PVC is not preferred for road applications; however, a few studies were conducted on PVC modification of bitumen and found that PVC improved physical and rheological characteristics of modified bitumen. PS modification of bitumen, similarly to the other high-melting temperature polymers, generally provided a similar stiffening effect already seen in PVC and PET; most of the studies emphasised betterments at high temperature and lack of miscibility unless modified with additives. Among all plastomers, PE is generally considered the most suitable option for bitumen modification when using recycled plastomers. Due to its low melting point temperature, it has the ability to provide homogeneous mixing with bitumen. This is demonstrated by the large number of research studies that used PE as bitumen modifier over the last two decades. In addition, PE contributes to the largest share of plastomers production worldwide, only followed by PP and PET [223]. PE has robust chemical properties and it takes longer time to degrade than others [41], hence requiring additional attention in terms of potential environmental issues [365].

As shown in Table 3, different percentages (loadings) of plastomers have been used for polymer modification of bitumen; however, 3–6% by weight of binder is considered as an optimal percentage for improving performance while avoiding complications during construction due to excessive viscosity and storage stability issues [192]. If 3–6% of recycled plastics is used in road construction, for instance, then up to 1.5–3 kg recycled plastomers are needed for 1 ton of asphalt, which is enough to pave 2.38 m of 1-lane road, 3.5 m wide, and 50 mm thickness of the bitumen surface layer. Hence, 630–1260 kg of plastomers can effectively be utilised for 1 km road (1 lane). These figures are significant and should carefully be considered by decision makers that foster sustainability. In fact, most of the polyolefins have already been used in the real scale by many contractors in various parts of the world. However, there are more exotic types of plastic such as PVC that are mostly studied at laboratory scale due to emissions, cost, and other problems. To promote a safe and sustainable use of recycled plastics in roads there are some issues that still deserve more investigation: 1) low temperature performance is only addressed by a very small portion of studies, 2) specific stabilisers and compatibilizers should be developed and investigated to solve storage issues, 3) life-cycle assessment studies are needed to exactly quantify the environmental savings if using recycled plastomers, 4) more focus should be put in studying the environmental aspects (i.e., fuming, emissions) of mixing recycled plastomers at high temperature. In addition, the future recyclability of plastomer-modified bitumen/asphalt is an important aspect that requires the attention of policymakers and scientists. In general, the difference in recyclability of polymer-modified bitumen and neat bitumen (if any) is still part of an ongoing research effort.

#### *Drawbacks and Future Works*

While using waste plastic provides an additional option to redirect waste from landfills and a potential enhancement additive as a bitumen modifier, there are several concerns from an environmental perspective when introducing waste plastic on roads—one of them being the possibility of increasing fuming and emissions during bitumen production. While bitumen production is already a known contributor to VOC and PAH emissions, the introduction of waste plastics could potentially affect the total emissions produced. Therefore,

more research is required in this specific field of fuming and emissions when waste plastics are introduced during bitumen production. Additionally, the possibility of microplastic release is also a common environmental concern when introducing new materials in bitumen. While there are studies concerning crumb rubber modified bitumen microplastic leaching, there is no microplastics assessment of waste plastic modified bitumen. Whilst not directly related to bitumen modification, the recyclability of plastic modified asphalt is also an area of concern. Therefore, to fully understand the effects of incorporating waste plastic in road applications, studies only involving mechanical properties are not enough to justify the addition of new foreign materials that could pose a threat in a different form (environmental). More studies related to the topics mentioned above are required before a concise decision can be made.

## 9. Conclusions and Recommendations

The overall performance, durability characteristics as well as the failure of asphalt mixtures are highly dependent upon the characteristics of bitumen. Improved durability and performance of the binder are highly desired, hence considerable efforts are being put into polymer modification of bitumen. Plastomers are commonly used due to their relatively low cost and great stiffness, especially at high temperature. Recently, the use of recycled plastomers is also growing notable interest to possibly contribute to the broader environmental challenges posed by waste plastics.

After reviewing numerous studies, the following conclusions can be drawn.

- The incorporation of recycled LDPE in bitumen saw a decrease in penetration value (approximately 16%) at 2% polymer content—a commonly adopted polymer loading; however, increments to the softening point (approximately 15%), flash point and fire point were also noticed. Moisture resistance and bitumen's complex modulus were also increased by 13% and 11%, respectively;
- Recycled HDPE-modified bitumen results exhibited improvements up to 89% in MSCR tests, hence emphasizing the general rheological betterment at high temperature;
- The use of commingled PE (mainly from post-consumer waste plastics) provided general benefits to the bitumen performance although more variability compared to single-source recycled plastic was noticed;
- The suggested optimum polymer content for polyethylene-based modifiers is 4% by weight of bitumen although greater polymer contents were also evaluated; the greater the polymer content, the higher the chances of phase separation during storage at high temperature;
- PET-modified binders used to make plastic-asphalt exhibited improvements in the Marshall stability by 12%. Despite improvements with the use of PET, the high melting temperature of the plastic does not allow a homogenous blend during the mixing process, therefore, making it unfeasible to be considered as a candidate for bitumen modification;
- The addition of PVC into bitumen saw a reduction in penetration values by 57% and an increment in softening point by 26%. Viscosity was increased by 300% while ductility values dipped. PVC toxicity at high temperature remains a major issue, especially when treated with phthalates of various types;
- PP-modified binders showed a reduction in penetration values by 18% to 30% at 3% polymer content and 38% to 50% at 5% polymer content. However, the softening point was improved between 4% to 30% and 11% to 43.5% at 3% and 5% polymer contents, respectively. Ductility values were reduced by 20% at 5% polymer content;
- The use of PS increased softening points by 29% and 35% for 80/100-grade bitumen and 60/70 grade bitumen, respectively, however decreasing penetration values up to 20%;
- EVA-modified binders exhibited improvements of 22% to 53% in softening point, however decreasing penetration values by 33% to 51%. The ductility of bitumen was improved by 20% at 5% polymer content. Unlike other polymers such as PP, PVC, and PE, EVA-modified binders showed no major rheological drawbacks when polymer contents were increased;

- Commingled plastics modified binders comprising of HDPE/PP exhibited an improvement of up to 179% in Marshall tests on asphalt samples;
- Plastomeric modification of bitumen is mainly achieved by the use of EVA and PE; however, more polymers (especially in their recycled form) are being experimented with in a continuous effort to find a solution to the plastics waste problem;
- Some recycled plastomeric polymers have a melting temperature which is above the bitumen mixing temperature; this implies that their use is mainly as a filler or 'synthetic' aggregate, depending on their size. In these cases, the cost of the filler/aggregate vs. the cost of the polymer used as 'synthetic' aggregate should carefully be considered as the steps involved with recycling contribute to the higher final cost;
- Low melting temperature polymers (i.e., PE, both virgin and recycled) have demonstrated their suitable use as bitumen modifiers. Recycled plastomers are also considered to be cost effective due to their lower prices in comparison to a) chemically virgin plastomers and b) commonly used elastomers. Though, when used as bitumen modifier, their relative quantity in the mix is minimal (i.e., 0.25–0.5% by weight of the asphalt mix) hence reducing the environmental benefits commonly associated with recycling;
- Generally, plastomers provide excellent high-temperature properties and relatively good—depending on the specific polymer—low-temperature behaviour (i.e., EVA at high VA content). However, most of the research studies investigating plastomers are focused on the high-temperature behaviour;
- Plastomers are also acknowledged to be prone to phase separation due to the low compatibility (molecular weight, polarity, and crystallinity) between the polymer and bitumen. However, several commonly adopted elastomers (i.e., SBS) are also not immune from separation issues. New PE-based polymers are now being tested for bitumen applications that show self-crosslinking abilities and greater compatibility with bitumen;
- To improve plastomer-bitumen compatibility, several compounds have been used. These modifiers are reactive polymers, polyphosphoric acid, organometallic compounds, sulfonic acid, silanes, maleic anhydride, carboxylic anhydride, thiourea dioxide, sulphur, antioxidants, nanomaterials, clay minerals, and bio-oils. Despite the persistent use of sulphur and PPA, new additives are being investigated by many authors with promising results (i.e., maleic anhydride to improve polarity and decrease crystallinity, or nanoparticles). The use of nano materials as stabilisers, although appealing to many, have proved to be an expensive exercise, possibly too difficult for being applied on large scale.

Finally, for what specifically concerns the recycled plastomers from waste plastics, several aspects of their inclusion within the bitumen industry still deserve deep investigation. Among these, the use of post-industrial plastics can lead to very different outcomes compared to post-consumer plastics (quality, consistency, presence of contaminants). Fuming and emissions during laboratory blending at high temperature has not been addressed yet although it may deserve a specific focus to avoid unpleasant releases of emissions at the plant and during construction. The use of waste plastomers, especially when substituting the asphalt aggregate fraction (i.e., high melting point plastics), has the potential of generating microplastics on the pavement surface due to wear and tear produced by traffic; studies on the release of microplastics should also tackle the use of waste plastics as a bitumen modifier. Some plastomers are also prone to UV degradation. Finally, the future recyclability of waste plastomer-modified bitumen mixes is also of particular interest due to the full recyclability of standard bitumen.

**Author Contributions:** Conceptualization, F.G., S.N., Y.J.B.; methodology, F.G., S.N., Y.J.B.; formal analysis, S.N., Y.J.B.; data curation, S.N., Y.J.B.; writing—original draft preparation, F.G., S.N., Y.J.B.; writing—review and editing, F.G., S.N., Y.J.B.; visualization, Y.J.B.; supervision, F.G.; project administration, F.G.; funding acquisition, F.G. All authors have read and agreed to the published version of the manuscript.

**Funding:** The authors would like to acknowledge the financial support of Sustainability Victoria through the “Research, Development and Demonstration grants”, project C-11133 “LDPE and crumb rubber in asphalt”.

**Institutional Review Board Statement:** Not applicable.

**Informed Consent Statement:** Not applicable.

**Conflicts of Interest:** The authors have no conflicts of interest to declare that are relevant to the content of this article.

## Abbreviations

|         |  |
|---------|--|
| SARA    | Saturate, Aromatic, Resin and Asphaltene         |
| LCA     | Life Cycle Assessment                            |
| CAGR    | Compound Annual Growth Rate                      |
| PMB     | Polymer Modified Bitumen                         |
| EPA     | Environmental Protection Agency                  |
| PE      | Polyethylene                                     |
| m-PE    | Metallocene-catalysed Polyethylene               |
| LDPE    | Low Density Polyethylene                         |
| VLDPE   | Very Low-Density Polyethylene                    |
| LLDPE   | Linear Low-Density Polyethylene                  |
| MDPE    | Medium Density Polyethylene                      |
| HDPE    | High Density Polyethylene                        |
| UHMWPE  | Ultra-high Molecular Weight Polyethylene         |
| PP      | Polypropylene                                    |
| aPP     | Atactic Polypropylene                            |
| iPP     | Isotactic Polypropylene                          |
| PS      | Polystyrene                                      |
| EPS     | Expanded Polystyrene                             |
| PVC     | Polyvinyl Chloride                               |
| PET     | Polyethylene Terephthalate                       |
| EBA     | Ethylene Butyl Acrylate                          |
| EVA     | Ethylene-Vinyl Acetate                           |
| SBS     | Styrene-butadiene-styrene                        |
| MA-g-PE | Maleic Anhydride grafted Polyethylene            |
| HCL     | Hydrochloric Acid                                |
| PPA     | Polyphosphoric Acid                              |
| XRF     | X-ray fluorescence                               |
| TG/DTG  | Thermogravimetric/Differential Thermogravimetric |
| FTIR    | Fourier Transform Infra-red                      |
| GCMS    | Gas Chromatography and Mass Spectroscopy         |
| MFI     | Melt Flow Index                                  |
| MSCR    | Multiple Stress Creep Recovery                   |
| UV      | Ultraviolet                                      |

## References

1. Tahmoorian, F.; Samali, B.; Yeaman, J. Modified asphalt. In *Evaluation of Structural and Thermal Properties of Rubber and HDPE for Utilization as Binder Modifier*; IntechOpen: London, UK, 2018; pp. 109–130. [CrossRef]
2. Xu, L.; Li, X.; Zong, Q.; Xiao, F. Chemical, morphological and rheological investigations of SBR/SBS modified asphalt emulsions with waterborne acrylate and polyurethane. *Constr. Build. Mater.* **2021**, *272*, 121972. [CrossRef]
3. Zhu, J.; Birgisson, B.; Kringos, N. Polymer modification of bitumen: Advances and challenges. *Eur. Polym. J.* **2014**, *54*, 18–38. [CrossRef]
4. Rezakazemi, M.; Vatani, A.; Mohammadi, T. Synergistic interactions between POSS and fumed silica and their effect on the properties of crosslinked PDMS nanocomposite membranes. *RSC Adv.* **2015**, *5*, 82460–82470. [CrossRef]
5. Farahani, H.Z.; Palassi, M.; Galooyak, S.S. Rheology investigation of waste LDPE and crumb rubber modified bitumen. *Eng. Solid Mech.* **2018**, *6*, 27–38. [CrossRef]



6. Rahi, D.C.; Chandak, R.; Vishwakarma, A. Utilization of liquid plastic waste in bitumen for construction of roads. In Proceedings of the International Conference on Sustainable Materials And Structures For Civil Infrastructures (Smsci2019), Bhopal, India, 14–15 March 2019.
7. Airey, G.D. Rheological evaluation of ethylene vinyl acetate polymer modified bitumens. *Constr. Build. Mater.* **2002**, *16*, 473–487. [CrossRef]
8. Padhan, R.K.; Sreeram, A. Enhancement of storage stability and rheological properties of polyethylene (PE) modified asphalt using cross linking and reactive polymer based additives. *Constr. Build. Mater.* **2018**, *188*, 772–780. [CrossRef]
9. Gama, D.A.; Yan, Y.; Rodrigues, J.K.G.; Roque, R. Optimizing the use of reactive terpolymer, polyphosphoric acid and high-density polyethylene to achieve asphalt binders with superior performance. *Constr. Build. Mater.* **2018**, *169*, 522–529. [CrossRef]
10. Gautam, P.K.; Kalla, P.; Jethoo, A.S.; Agrawal, R.; Singh, H. Sustainable use of waste in flexible pavement: A review. *Constr. Build. Mater.* **2018**, *180*, 239–253. [CrossRef]
11. Angelone, S.; Casaux, M.C.; Borghi, M.; Martinez, F.O. Green pavements: Reuse of plastic waste in asphalt mixtures. *Mater. Struct.* **2015**, *49*, 1655–1665. [CrossRef]
12. Brasileiro, L.; Moreno-Navarro, F.; Tauste-Martínez, R.; Matos, J.; Rubio-Gámez, M.D.C. Reclaimed polymers as asphalt binder modifiers for more sustainable roads: A Review. *Sustainability* **2019**, *11*, 646. [CrossRef]
13. Venturini, L.; Carrara, S.; Giustozzi, F. Pavement and Asset Management. In Proceedings of the World Conference on Pavement and Asset Management (WCPAM 2017), Baveno, Italy, 12–16 June 2017; pp. 433–442.
14. Yadav, S.K.; Srivastava, V. Non-conventional materials in rigid pavement: Effect on mechanical properties. *Int. J. Civ. Eng. Technol.* **2017**, *8*, 10.
15. Kishchynskyi, S.; Nagaychuk, V.; Bezuglyi, A. Improving quality and durability of bitumen and asphalt concrete by modification using recycled polyethylene based polymer composition. *Proc. Eng.* **2016**, *143*, 119–127. [CrossRef]
16. Lambert, S.; Wagner, M. Environmental performance of bio-based and biodegradable plastics: The road ahead. *Chem. Soc. Rev.* **2017**, *46*, 6855–6871. [CrossRef]
17. Bonicelli, A.; Calvi, P.; Martínez-Arguelles, G.; Fuentes, L.; Giustozzi, F. Experimental study on the use of rejuvenators and plastomeric polymers for improving durability of high RAP content asphalt mixtures. *Constr. Build. Mater.* **2017**, *155*, 37–44. [CrossRef]
18. Lu, X.; Isacson, U. Effect of ageing on bitumen chemistry and rheology. *Constr. Build. Mater.* **2002**, *16*, 15–22. [CrossRef]
19. García-Morales, M.; Partal, P.; Navarro, F.J.; Martínez-Boza, F.J.; Gallegos, C. Processing, rheology, and storage stability of recycled EVA/LDPE modified bitumen. *Polym. Eng. Sci.* **2007**, *47*, 181–191. [CrossRef]
20. Fawcett, A.H.; McNally, T. Blends of bitumen with polymers having a styrene component. *Polym. Eng. Sci.* **2001**, *41*, 1251–1264. [CrossRef]
21. Airey, G.D. Styrene butadiene styrene polymer modification of road bitumens. *J. Mater. Sci.* **2004**, *39*, 951–959. [CrossRef]
22. García-Morales, M.; Partal, P.; Navarro, F.J.; Martínez-Boza, F.; Gallegos, C. Linear Viscoelasticity of Recycled EVA-Modified Bitumens. *Energy Fuels* **2004**, *18*, 357–364. [CrossRef]
23. Navarro, F.J.; Partal, P.; Martínez-Boza, F.; Gallegos, C. Thermo-rheological behaviour and storage stability of ground tire rubber-modified bitumens. *Fuel* **2004**, *83*, 2041–2049. [CrossRef]
24. Navarro, F.J.; Partal, P.; Martínez-Boza, F.J.; Gallegos, C. Influence of processing conditions on the rheological behavior of crumb tire rubber-modified bitumen. *J. Appl. Polym. Sci.* **2007**, *104*, 1683–1691. [CrossRef]
25. Pérez-Lepe, A.; Martínez-Boza, F.J.; Attané, P.; Gallegos, C. Destabilization mechanism of polyethylene-modified bitumen. *J. Appl. Polym. Sci.* **2006**, *100*, 260–267. [CrossRef]
26. Giustozzi, F.; Crispino, M.; Toraldo, E.; Mariani, E. Mix design of polymer-modified and fiber-reinforced warm-mix asphalts with high amount of reclaimed asphalt pavement: Achieving sustainable and high-performing pavements. *Trans. Res. Rec.* **2015**, *2523*, 3–10. [CrossRef]
27. Raman, N.A.A.; Hainin, M.R.; Hassan, N.A.; Ani, F.N. A Review on the Application of Bio-oil as an Additive for Asphalt. *J. Teknol.* **2015**, *72*, 105–110. [CrossRef]
28. Hossain, N.; Zaini, J.; Mahlia, T.M.I.; Azad, A.K. Elemental, morphological and thermal analysis of mixed microalgae species from drain water. *Renew. Energy* **2019**, *131*, 617–624. [CrossRef]
29. García-Morales, M.; Partal, P.; Navarro, F.; Martínez-Boza, F.; Gallegos, C.; González, N.; Muñoz, M. Viscous properties and microstructure of recycled eva modified bitumen. *Fuel* **2004**, *83*, 31–38. [CrossRef]
30. Fawcett, A.; McNally, T. Blends of bitumen with various polyolefins. *Polymer* **2000**, *41*, 5315–5326. [CrossRef]
31. Eurobitume, A. *The Bitumen Industry—A Global Perspective: Production, Chemistry, Use, Specification and Occupational Exposure*; Asphalt Institute: Lexington, KY, USA, 2011.
32. McNally, T. *Polymer Modified Bitumen: Properties and Characterisation*, 1st ed.; Woodhead Publishing: Philadelphia, PA, USA, 2011.
33. Sengoz, B.; Topal, A.; Isikyakar, G. Morphology and image analysis of polymer modified bitumens. *Constr. Build. Mater.* **2009**, *23*, 1986–1992. [CrossRef]
34. González, O.; Muñoz, M.; Santamaria, A.; Garcia-Morales, M.; Navarro, F.; Partal, P. Rheology and stability of bitumen/EVA blends. *Eur. Polym. J.* **2004**, *40*, 2365–2372. [CrossRef]
35. Habib, N.Z.; Kamaruddin, I.; Napiah, M.; Isa, M.T. Rheological properties of polyethylene and polypropylene modified bitumen. *Int. J. Civ. Environ. Eng.* **2011**, *3*, 96–100.

36. Khan, I.M.; Kabir, S.; Alhussain, M.A.; Almansoor, F.F. Asphalt design using recycled plastic and crumb-rubber waste for sustainable pavement construction. *Procedia Eng.* **2016**, *145*, 1557–1564. [CrossRef]
37. Onyango, F.; Wanjala, S.R.; Ndege, M.; Masu, L. Effect of rubber tyre and plastic wastes use in asphalt concrete pavement. *Int. J. Civ. Environ. Eng.* **2015**, *2*, 1403–1407.
38. Belsare, C.P.; Kaley, A.A.J.D. Interpretation of bituminous mixes with modified binders. *Int. J. Adv. Eng. Res. Dev.* **2015**, *2*, 1504–1512.
39. Zhang, H.; Wu, X.; Cao, D.; Zhang, Y.; He, M. Effect of linear low density-polyethylene grafted with maleic anhydride (LLDPE-g-MAH) on properties of high density-polyethylene/styrene-butadiene-styrene (HDPE/SBS) modified asphalt. *Constr. Build. Mater.* **2013**, *47*, 192–198. [CrossRef]
40. Gómez, N.H.C.; Oeser, M.; Fleischel, O. Chemical modification of bitumen with novel isocyanate-based additive to enhance asphalt performance. *Cons. Build. Mater.* **2021**, *301*, 124128. [CrossRef]
41. Beena, K.; Bindu, C. Waste plastic as a stabilizing additive in Stone Mastic Asphalt. *Int. J. Eng. Technol.* **2010**, *2*, 379–387.
42. Mohammadiroudbari, M.; Tavakoli, A.; Aghjeh, M.K.R.; Rahi, M. Effect of nanoclay on the morphology of polyethylene modified bitumen. *Constr. Build. Mater.* **2016**, *116*, 245–251. [CrossRef]
43. Zachariah, J.P.; Sarkar, P.P.; Debnath, B.; Pal, M. Effect of polypropylene fibres on bituminous concrete with brick as aggregate. *Constr. Build. Mater.* **2018**, *168*, 867–876. [CrossRef]
44. Gibreil, H.A.; Feng, C.P. Effects of high-density polyethylene and crumb rubber powder as modifiers on properties of hot mix asphalt. *Constr. Build. Mater.* **2017**, *142*, 101–108. [CrossRef]
45. Malarvizhi, G.; Senthul, N.; Kamaraj, C. A study on Recycling of crumb rubber and low density polyethylene blend on stone matrix asphalt. *Int. J. Sci. Res.* **2012**, *2*, 1–16.
46. Bala, N.; Napiah, M.; Kamaruddin, I. Effect of nanosilica particles on polypropylene polymer modified asphalt mixture performance. *Case Stud. Constr. Mater.* **2018**, *8*, 447–454. [CrossRef]
47. Larsen, D.O.; Alessandrini, J.L.; Bosch, A.; Cortizo, M.S. Micro-structural and rheological characteristics of SBS-asphalt blends during their manufacturing. *Constr. Build. Mater.* **2009**, *23*, 2769–2774. [CrossRef]
48. McNally, T. Introduction to polymer modified bitumen (PmB). *Polym. Modif. Bitum.* **2011**, 1–21. [CrossRef]
49. Pyshyev, S.; Gunka, V.; Grytsenko, Y.; Bratychak, M. Polymer modified bitumen. *Chem. Chem. Technol.* **2016**, *10*, 631–636. [CrossRef]
50. Tayfur, S.; Ozen, H.; Aksoy, A. Investigation of rutting performance of asphalt mixtures containing polymer modifiers. *Constr. Build. Mater.* **2007**, *21*, 328–337. [CrossRef]
51. Isacson, U.; Zeng, H. Low-temperature cracking of polymer-modified asphalt. *Mater. Struct.* **1998**, *31*, 58–63. [CrossRef]
52. Gorkem, C.; Sengoz, B. Predicting stripping and moisture induced damage of asphalt concrete prepared with polymer modified bitumen and hydrated lime. *Constr. Build. Mater.* **2009**, *23*, 2227–2236. [CrossRef]
53. Alataş, T.; Yilmaz, M. Effects of different polymers on mechanical properties of bituminous binders and hot mixtures. *Constr. Build. Mater.* **2013**, *42*, 161–167. [CrossRef]
54. Von Quintus, H.L.; Mallela, J.; Buncher, M. Quantification of effect of polymer-modified asphalt on flexible pavement performance. *Trans. Res. Rec.* **2007**, *2001*, 141–154. [CrossRef]
55. Chang, H.-L.; Wong, G.K.; Lin, J.-R.; Yen, T.F. Chapter 9 Electron Spin Resonance Study of Bituminous Substances and Asphaltenes. *Dev. Pet. Sci.* **2000**, *40*, 229–280. [CrossRef]
56. Singh, B.P.; Kumar, L.; Gupta, M.M.; Chauhan, G. Polymer-modified bitumen of recycled LDPE and maleated bitumen. *J. Appl. Polym. Sci.* **2012**, *127*, 67–78. [CrossRef]
57. Wang, T.; Yi, T.; Yuzhen, Z. The Compatibility of SBS-Modified Asphalt. *Pet. Sci. Technol.* **2010**, *28*, 764–772. [CrossRef]
58. Khakimullin, Y.N.; Kimel'Blat, V.I.; Chebotareva, I.G.; Muruzina, E.V.; Murafo, A.V.; Khozin, V.G.; Vol'Fson, S.I. Properties of Bitumens Modified by Thermoplastic Elastomers. *Mech. Compos. Mater.* **2000**, *36*, 417–422. [CrossRef]
59. Cook, C.R.; Halden, R.U. Ecological and health issues of plastic waste. In *Plastic Waste and Recycling*; Academic Press: Cambridge, MA, USA, 2020; pp. 513–527.
60. Wang, J.; Yuan, J.; Xiao, F.; Li, Z.; Wang, J.; Xu, Z. Performance investigation and sustainability evaluation of multiple-polymer asphalt mixtures in airfield pavement. *J. Clean. Prod.* **2018**, *189*, 67–77. [CrossRef]
61. Keijzer, E.E.; Leegwater, G.A.; de Vos-Effting, S.E.; de Wit, M.S. Carbon footprint comparison of innovative techniques in the construction and maintenance of road infra-structure in The Netherlands. *Environ. Sci. Policy* **2015**, *54*, 218–225. [CrossRef]
62. Giustozzi, F.; Crispino, M.; Flintsch, G. Multi-attribute life cycle assessment of preventive maintenance treatments on road pavements for achieving environmental sustainability. *Int. J. Life Cycle Assess.* **2012**, *17*, 409–419. [CrossRef]
63. Santos, J.; Pham, A.; Stasinopoulos, P.; Giustozzi, F. Recycling waste plastics in roads: A life-cycle assessment study using primary data. *Sci. Total. Environ.* **2021**, *751*, 141842. [CrossRef]
64. Jasso, M.; Hampl, R.; Vacin, O.; Bakos, D.; Stastna, J.; Zanzotto, L. Rheology of conventional asphalt modified with SBS, Elvaloy and polyphosphoric acid. *Fuel Process. Technol.* **2015**, *140*, 172–179. [CrossRef]
65. García-Travé, G.; Tauste, R.; Moreno-Navarro, F.; Sol-Sánchez, M.; Rubio-Gámez, M.C. Use of Reclaimed Geomembranes for Modification of Mechanical Performance of Bituminous Binders. *J. Mater. Civ. Eng.* **2016**, *28*, 04016021. [CrossRef]
66. Polacco, G.; Stastna, J.; Biondi, D.; Antonelli, F.; Vlachovicova, Z.; Zanzotto, L. Rheology of asphalts modified with glycidyl-methacrylate functionalized polymers. *J. Colloid Interface Sci.* **2004**, *280*, 366–373. [CrossRef]
67. Li, B.; Li, X.; Kundwa, M.J.; Li, Z.; Wei, D. Evaluation of the adhesion characteristics of material composition for polyphosphoric acid and SBS modified bitumen based on surface free energy theory. *Constr. Build. Mater.* **2021**, *266*, 121022. [CrossRef]

68. Navarro, F.; Partal, P.; García-Morales, M.; Martín-Alfonso, M.; Martínez-Boza, F.; Gallegos, C.; Bordado, J.; Diogo, A. Bitumen modification with reactive and non-reactive (virgin and recycled) polymers: A comparative analysis. *J. Ind. Eng. Chem.* **2009**, *15*, 458–464. [CrossRef]
69. Anwar, M.K.; Shah, S.A.R.; Alhazmi, H. Recycling and Utilization of Polymers for Road Construction Projects: An Application of the Circular Economy Concept. *Polymers* **2021**, *13*, 1330. [CrossRef]
70. Abuaddous, M.; Taamneh, M.M.; Rabab'Ah, S.R. The potential use of recycled polyethylene terephthalate (RPET) plastic waste in asphalt binder. *Int. J. Pavement Res. Technol.* **2021**, *14*, 579–587. [CrossRef]
71. Moore, C.J. Synthetic polymers in the marine environment: A rapidly increasing, long-term threat. *Environ. Res.* **2008**, *108*, 131–139. [CrossRef]
72. Parker, L. A Whopping 91% of Plastic Isn't Recycled. *National Geographic*. 2017. Available online: <https://www.nationalgeographic.com/science/article/plastic-produced-recycling-waste-ocean-trash-debris-environment> (accessed on 12 September 2021).
73. Rahman, T.; Mohajerani, A.; Giustozzi, F. Recycling of Waste Materials for Asphalt Concrete and Bitumen: A Review. *Materials* **2020**, *13*, 1495. [CrossRef] [PubMed]
74. Arulrajah, A.; Naeini, M.; Mohammadinia, A.; Horpibulsuk, S.; Leong, M. Recovered plastic and demolition waste blends as railway capping materials. *Transp. Geotech.* **2020**, *22*, 100320. [CrossRef]
75. Ragaert, K.; Delva, L.; Van Geem, K. Mechanical and chemical recycling of solid plastic waste. *Waste Manag.* **2017**, *69*, 24–58. [CrossRef] [PubMed]
76. Perugini, F.; Mastellone, M.L.; Arena, U. A life cycle assessment of mechanical and feedstock recycling options for management of plastic packaging wastes. *Env. Prog.* **2005**, *24*, 137–154. [CrossRef]
77. Achilias, D.; Roupakias, C.; Megalokonomos, P.; Lappas, A.; Antonakou, E. Chemical recycling of plastic wastes made from polyethylene (LDPE and HDPE) and polypropylene (PP). *J. Hazard. Mater.* **2007**, *149*, 536–542. [CrossRef]
78. Locock, K. *The Recycled Plastics Market: Global Analysis and Trends*; CSIRO: Canberra, Australia, 2017.
79. d'Ambrières, W. Plastics recycling worldwide: Current overview and desirable changes. *J. Field. Act.* **2019**, *19*, 12–21.
80. Goodship, V. Plastic recycling. *Handb. Recycl.* **2007**, *90*, 245–268. [CrossRef]
81. Victoria, S. *Resource Recovery Technology Guide*; Sustainability Victoria: Victoria, Australia, 2018.
82. Hopewell, J.; Dvorak, R.; Kosior, E. Plastics recycling: Challenges and opportunities. *Philos. Trans. R. Soc. B Biol. Sci.* **2009**, *364*, 2115–2126. [CrossRef] [PubMed]
83. Park, C.-H.; Jeon, H.-S.; Yu, H.-S.; Han, O.-H.; Park, J.-K. Application of Electrostatic Separation to the Recycling of Plastic Wastes: Separation of PVC, PET, and ABS. *Environ. Sci. Technol.* **2008**, *42*, 249–255. [CrossRef] [PubMed]
84. Silveira, A.; Cella, M.; Tanabe, E.; Bertuol, D. Application of tribo-electrostatic separation in the recycling of plastic wastes. *Process. Saf. Environ. Prot.* **2018**, *114*, 219–228. [CrossRef]
85. Marand, H.; Xu, J.; Srinivas, S. Determination of the equilibrium melting temperature of polymer crystals: Linear and nonlinear Hoffman–Weeks extrapolations. *Macromolecules* **1998**, *31*, 8219–8229. [CrossRef]
86. Stupp, S.; Supan, T.J.; Belton, D. Ice-water quenching technique for polypropylene. *Ortho. Prosth.* **1979**, *33*, 16–21.
87. Lior, N. The cooling process in gas quenching. *J. Mater. Process. Technol.* **2004**, *155*, 1881–1888. [CrossRef]
88. Cheng, S.Z.; Lotz, B. Enthalpic and entropic origins of nucleation barriers during polymer crystallization: The Hoffman–Lauritzen theory and beyond. *Polymer* **2005**, *46*, 8662–8681. [CrossRef]
89. Urgan Voigt, J. Apparatus for Pelletizing Plastics. U.S. Patent 20100072252A1, 7 June 2011.
90. Boothe, D.A.; Martin, W.J.; Wright, R.B. Apparatus and Method for Controlled Pelletization Processing. U.S. Patent CA2631160C, 15 September 2013.
91. Mohammed, B.; Hassan, R.; Alaswadko, N. The effect of traffic data source on deterioration rates of heavy-duty flexible pavements. *Int. J. Pavement Eng.* **2016**, *19*, 1–15. [CrossRef]
92. Plati, C. Sustainability factors in pavement materials, design, and preservation strategies: A literature review. *Constr. Build. Mater.* **2019**, *211*, 539–555. [CrossRef]
93. Pouranian, M.R.; Shishehbor, M. Sustainability Assessment of Green Asphalt Mixtures: A Review. *Environments* **2019**, *6*, 73. [CrossRef]
94. Shah, A.; Modha, H. Improving the Soil Subgrade with Plastic Waste Reinforcement—An Experimental Study. In Proceedings of the ECE 2020, St. Petersburg, Russia, 19–20 November 2020; pp. 153–161. [CrossRef]
95. Khurshid, M.B.; Qureshi, N.A.; Hussain, A.; Iqbal, M.J. Enhancement of Hot Mix Asphalt (HMA) Properties Using Waste Polymers. *Arab. J. Sci. Eng.* **2019**, *44*, 8239–8248. [CrossRef]
96. Nouali, M.; Derriche, Z.; Ghorbel, E.; Chuanqiang, L. Plastic bag waste modified bitumen a possible solution to the Algerian road pavements. *Road Mater. Pavement Des.* **2019**, *21*, 1713–1725. [CrossRef]
97. Lastra-González, P.; Calzada-Pérez, M.A.; Castro-Fresno, D.; Vega-Zamanillo, Á.; Indacochea-Vega, I. Comparative analysis of the performance of asphalt concretes modified by dry way with polymeric waste. *Constr. Build. Mater.* **2016**, *112*, 1133–1140. [CrossRef]
98. Yusoff, N.I.M.; Mounier, D.; Marc-Stéphane, G.; Hainin, M.R.; Airey, G.; Di Benedetto, H. Modelling the rheological properties of bituminous binders using the 2S2P1D Model. *Constr. Build. Mater.* **2013**, *38*, 395–406. [CrossRef]
99. Polacco, G.; Stastna, J.; Biondi, D.; Zanzotto, L. Relation between polymer architecture and nonlinear viscoelastic behavior of modified asphalts. *Curr. Opin. Colloid Interface Sci.* **2006**, *11*, 230–245. [CrossRef]

100. Porto, M.; Caputo, P.; Loise, V.; Eskandarsefat, S.; Teltayev, B.; Rossi, C.O. Bitumen and Bitumen Modification: A Review on Latest Advances. *Appl. Sci.* **2019**, *9*, 742. [CrossRef]
101. Giavarini, C.; De Filippis, P.; Santarelli, M.L.; Scarsella, M. Production of stable polypropylene-modified bitumens. *Fuel* **1996**, *75*, 681–686. [CrossRef]
102. Liu, P.; Lu, K.; Li, J.; Wu, X.; Qian, L.; Wang, M.; Gao, S. Effect of aging on adsorption behavior of polystyrene microplastics for pharmaceuticals: Adsorption mechanism and role of aging intermediates. *J. Hazard. Mater.* **2020**, *384*, 121193. [CrossRef]
103. Lu, X.; Isacson, U.; Ekblad, J. Phase Separation of SBS Polymer Modified Bitumens. *J. Mater. Civ. Eng.* **1999**, *11*, 51–57. [CrossRef]
104. Zani, L.; Giustozzi, F.; Harvey, J. Effect of storage stability on chemical and rheological properties of polymer-modified asphalt binders for road pavement construction. *Constr. Build. Mater.* **2017**, *145*, 326–335. [CrossRef]
105. Behnood, A.; Gharehveran, M.M. Morphology, rheology, and physical properties of polymer-modified asphalt binders. *Eur. Polym. J.* **2019**, *112*, 766–791. [CrossRef]
106. Ma, Y.; Wang, S.; Zhou, H.; Hu, W.; Polaczyk, P.; Zhang, M.; Huang, B. Compatibility and rheological characterization of asphalt modified with recycled rubber-plastic blends. *Constr. Build. Mater.* **2021**, *270*, 121416. [CrossRef]
107. Attaelmanan, M.; Feng, C.P.; Ai, A.-H. Laboratory evaluation of HMA with high density polyethylene as a modifier. *Constr. Build. Mater.* **2011**, *25*, 2764–2770. [CrossRef]
108. Murphy, M.D.; O'Mahony, M.; Lycett, C.; Jamieson, I. Recycled Polymers for Use as Bitumen Modifiers. *J. Mater. Civ. Eng.* **2001**, *13*, 306–314. [CrossRef]
109. Panda, M.; Mazumdar, M. Utilization of Reclaimed Polyethylene in Bituminous Paving Mixes. *J. Mater. Civ. Eng.* **2002**, *14*, 527–530. [CrossRef]
110. Liang, M.; Xin, X.; Fan, W.; Wang, H.; Jiang, H.; Zhang, J.; Yao, Z. Phase behavior and hot storage characteristics of asphalt modified with various polyethylene: Experimental and numerical characterizations. *Constr. Build. Mater.* **2019**, *203*, 608–620. [CrossRef]
111. Cazan, C.; Cosnita, M.; Duta, A. Effect of PET functionalization in composites of rubber–PET–HDPE type. *Arab. J. Chem.* **2017**, *10*, 300–312. [CrossRef]
112. Kuila, T.; Bose, S.; Mishra, A.K.; Khanra, P.; Kim, N.H.; Lee, J.H. Effect of functionalized graphene on the physical properties of linear low density polyethylene nanocompo-sites. *Polym. Test.* **2012**, *31*, 31–38. [CrossRef]
113. Yousefi, A.A. Polyethylene dispersions in bitumen: The effects of the polymer structural parameters. *J. Appl. Polym. Sci.* **2003**, *90*, 3183–3190. [CrossRef]
114. Al-Hadidy, A. Engineering behavior of aged polypropylene-modified asphalt pavements. *Constr. Build. Mater.* **2018**, *191*, 187–192. [CrossRef]
115. Ahmedzade, P.; Demirelli, K.; Günay, T.; Biryani, F.; Alqudah, O. Effects of Waste Polypropylene Additive on the Properties of Bituminous Binder. *Procedia Manuf.* **2015**, *2*, 165–170. [CrossRef]
116. Luo, W.-Q.; Chen, J.-C. Preparation and properties of bitumen modified by EVA graft copolymer. *Constr. Build. Mater.* **2011**, *25*, 1830–1835. [CrossRef]
117. Jooari, I.B.; Giustozzi, F. Waste tyres crumb rubber as a sustainability enhancer for polymer-modified and hybrid polymer-modified bitumen. *Int. J. Pavem. Eng.* **2021**, 1–15.
118. Liang, M.; Xin, X.; Fan, W.; Zhang, J.; Jiang, H.; Yao, Z. Comparison of rheological properties and compatibility of asphalt modified with various polyethylene. *Int. J. Pavement Eng.* **2021**, *22*, 11–20. [CrossRef]
119. Maddah, H.A. Polypropylene as a promising plastic: A review. *Amer. J. Polym. Sci.* **2016**, *6*, 1–11.
120. Moyano, M.A.; París, R.; Martín-Martínez, J.M. Assessment of the compatibility in hot melts by using different thermoanalytical methods. Ethylene/n-butyl acrylate (EBA) hot melts containing tackifiers of different nature. *J. Therm. Anal. Calorim.* **2017**, *129*, 1495–1503. [CrossRef]
121. Henderson, A. Ethylene-vinyl acetate (EVA) copolymers: A general review. *IEEE Electr. Insul. Mag.* **1993**, *9*, 30–38. [CrossRef]
122. Reddy, N.M.; Venkatasubbaiah, M. Effects of high density polyethylene and crumb rubber powder on properties of asphalt mix. *Int. Res. J. Eng. Technol.* **2017**, *4*, 2572–2578.
123. Lu, X.; Isacson, U. Modification of road bitumens with thermoplastic polymers. *Polym. Test.* **2000**, *20*, 77–86. [CrossRef]
124. Liang, S.; Yang, H.; Wang, K.; Zhang, Q.; Du, R.; Fu, Q. Unique crystal morphology and tensile properties of injection-molded bar of LLDPE by adding HDPE with different molecular weights. *Acta Mater.* **2008**, *56*, 50–59. [CrossRef]
125. Al-Hadidy, A.; Yi-Qiu, T. Effect of polyethylene on life of flexible pavements. *Constr. Build. Mater.* **2009**, *23*, 1456–1464. [CrossRef]
126. Costa, L.M.; Silva, H.M.; Peralta, J.; Oliveira, J.R. Using waste polymers as a reliable alternative for asphalt binder modification—Performance and morpho-logical assessment. *Constr. Build. Mater.* **2019**, *198*, 237–244. [CrossRef]
127. Jun, L.; Yuxia, Z.; Yuzhen, Z. The research of GMA-g-LDPE modified Qinhuangdao bitumen. *Constr. Build. Mater.* **2008**, *22*, 1067–1073. [CrossRef]
128. Ozdemir, D.K.; Topal, A.; McNally, T. Relationship between microstructure and phase morphology of SBS modified bitumen with processing parameters studied using atomic force microscopy. *Constr. Build. Mater.* **2021**, *268*, 121061. [CrossRef]
129. Vargas, M.A.; Vargas, M.A.; Sánchez-Sólis, A.; Manero, O. Asphalt/polyethylene blends: Rheological properties, microstructure and viscosity modeling. *Constr. Build. Mater.* **2013**, *45*, 243–250. [CrossRef]
130. Roman, C.; Cuadri, A.; Liashenko, I.; García-Morales, M.; Partal, P. Linear and non-linear viscoelastic behavior of SBS and LDPE modified bituminous mastics. *Constr. Build. Mater.* **2016**, *123*, 464–472. [CrossRef]

131. Nawang, R.; Danjaji, I.; Ishiaku, U.; Ismail, H.; Ishak, Z.M. Mechanical properties of sago starch-filled linear low density polyethylene (LLDPE) composites. *Polym. Test.* **2001**, *20*, 167–172. [CrossRef]
132. Luyt, A.; Molefi, J.; Krump, H. Thermal, mechanical and electrical properties of copper powder filled low-density and linear low-density polyethylene composites. *Polym. Degrad. Stab.* **2006**, *91*, 1629–1636. [CrossRef]
133. El-Rahman, A.A.; El-Shafie, M.; Mohammedy, M.; Abo-Shanab, Z. Enhancing the performance of blown asphalt binder using waste EVA copolymer (WEVA). *Egypt. J. Pet.* **2018**, *27*, 513–521. [CrossRef]
134. Haddadi, S.; Ghorbel, E.; Laradi, N. Effects of the manufacturing process on the performances of the bituminous binders modified with EVA. *Constr. Build. Mater.* **2008**, *22*, 1212–1219. [CrossRef]
135. Moyano, M.A.; Paris, R.; Martín-Martínez, J.M. Changes in compatibility, tack and viscoelastic properties of ethylene n-butyl acrylate (EBA) copoly-mer-pentaerythritol rosin ester blend by adding microcrystalline wax, Fischer-Tropsch wax and mixture of waxes. *Int. J. Adh. Adhes.* **2016**, *65*, 47–53. [CrossRef]
136. Bockhorn, H.; Hornung, A.; Schawaller, D. Kinetic study on the thermal degradation of polypropylene and polyethylene. *J. Anal. Appl. Pyrolysis* **1999**, *48*, 93–109. [CrossRef]
137. Krupa, I.; Luyt, A. Thermal and mechanical properties of LLDPE cross-linked with gamma radiation. *Polym. Degrad. Stab.* **2001**, *71*, 361–366. [CrossRef]
138. Duquesne, S.; Jama, C.; Le Bras, M.; Delobel, R.; Recourt, P.; Gloaguen, J. Elaboration of EVA–nanoclay systems—characterization, thermal behaviour and fire performance. *Compos. Sci. Technol.* **2003**, *63*, 1141–1148. [CrossRef]
139. Sultan, B.-Åke; Sörvik, E. Thermal degradation of EVA and EBA—A comparison. I. Volatile decomposition products. *J. Appl. Polym. Sci.* **1991**, *43*, 1737–1745. [CrossRef]
140. Bala, N.; Kamaruddin, I.; Napiah, M.; Danlami, N. Rheological and rutting evaluation of composite nanosilica/polyethylene modified bitumen. *IOP Conf. Series: Mater. Sci. Eng.* **2017**, *201*, 12012. [CrossRef]
141. Champion, L.; Gérard, J.-F.; Planche, J.-P.; Martin, D.; Anderson, D. Low temperature fracture properties of polymer-modified asphalts relationships with the morphology. *J. Mater. Sci.* **2001**, *36*, 451–460. [CrossRef]
142. Naddeo, C.; Guadagno, L.; De Luca, S.; Vittoria, V.; Camino, G. Mechanical and transport properties of irradiated linear low density polyethylene (LLDPE). *Polym. Degrad. Stab.* **2001**, *72*, 239–247. [CrossRef]
143. Isacson, U.; Lu, X. Characterization of bitumens modified with SEBS, EVA and EBA polymers. *J. Mater. Sci.* **1999**, *34*, 3737–3745. [CrossRef]
144. Eidesen, H.; Khawaja, H.; Jackson, S. Simulation of the HDPE Pyrolysis Process. *Int. J. Multiphysics* **2018**, *12*, 79–88. [CrossRef]
145. Bureau, E.; Cabot, C.; Marais, S.; Saiter, J.M. Study of the  $\alpha$ -relaxation of PVC, EVA and 50/50 EVA70/PVC blend. *Europ. Polym. J.* **2005**, *41*, 1152–1158. [CrossRef]
146. Fang, C.; Wu, C.; Hu, J.; Yu, R.; Zhang, Z.; Nie, L.; Zhou, S.; Mi, X. Pavement properties of asphalt modified with packaging-waste polyethylene. *J. Vinyl Addit. Technol.* **2014**, *20*, 31–35. [CrossRef]
147. Ahmedzade, P.; Fainleib, A.; Günay, T.; Grygoryeva, O. Modification of bitumen by electron beam irradiated recycled low density polyethylene. *Constr. Build. Mater.* **2014**, *69*, 1–9. [CrossRef]
148. Hu, J.; Fang, C.; Zhou, S.; Jiao, L.; Zhang, M.; Wu, D. Rheological properties of packaging-waste-polyethylene-modified asphalt. *J. Vinyl Addit. Technol.* **2015**, *21*, 215–219. [CrossRef]
149. Jew, P.; Shimizu, J.A.; Svazic, M.; Woodhams, R.T. Polyethylene-modified bitumen for paving applications. *J. Appl. Polym. Sci.* **1986**, *31*, 2685–2704. [CrossRef]
150. Qi, X.; Sebaaly, P.E.; Epps, J.A. Evaluation of Polymer-Modified Asphalt Concrete Mixtures. *J. Mater. Civ. Eng.* **1995**, *7*, 117–124. [CrossRef]
151. Tian, Y.; Li, H.; Sun, L.; Zhang, H.; Harvey, J.; Yang, J.; Yang, B.; Zuo, X. Laboratory investigation on rheological, chemical and morphological evolution of high content polymer modified bitumen under long-term thermal oxidative aging. *Constr. Build. Mater.* **2021**, *303*, 124565. [CrossRef]
152. Punith, V.S.; Veeraragavan, A. Behavior of Asphalt Concrete Mixtures with Reclaimed Polyethylene as Additive. *J. Mater. Civ. Eng.* **2007**, *19*, 500–507. [CrossRef]
153. Aschuri, I.; Woodward, D. Modification of a 14mm asphalt concrete surfacing using RAP and waste HDPE plastic. *Int. J. Pavem.* **2010**, *9*, 70–78.
154. Sui, Y.; Chen, Z. Application and Performance of Polyethylene Modifying Additive in Asphalt Mixture. *ICTE 2011* **2011**, 1915–1919. [CrossRef]
155. Punith, V.S.; Veeraragavan, A.; Amirhanian, S.N. Evaluation of reclaimed polyethylene modified asphalt concrete mixtures. *Int. J. Pavem. Res. Technol.* **2011**, *4*, 1.
156. Punith, V.S.; Suresha, S.N.; Raju, S.; Bose, S.; Veeraragavan, A. Laboratory Investigation of Open-Graded Friction-Course Mixtures Containing Polymers and Cellulose Fibers. *J. Transp. Eng.* **2012**, *138*, 67–74. [CrossRef]
157. Ahmadinia, E.; Zargar, M.; Karim, M.R.; Abdelaziz, M.; Ahmadinia, E. Performance evaluation of utilization of waste Polyethylene Terephthalate (PET) in stone mastic asphalt. *Constr. Build. Mater.* **2012**, *36*, 984–989. [CrossRef]
158. Moghaddam, T.B.; Karim, M.R.; Syammaun, T. Dynamic properties of stone mastic asphalt mixtures containing waste plastic bottles. *Constr. Build. Mater.* **2012**, *34*, 236–242. [CrossRef]
159. Fawcett, A.H.; McNally, T.; McNally, G. An attempt at engineering the bulk properties of blends of a bitumen with polymers. *Adv. Polym. Technol.* **2002**, *21*, 275–286. [CrossRef]

160. Polacco, G.; Berlincioni, S.; Biondi, D.; Stastna, J.; Zanzotto, L. Asphalt modification with different polyethylene-based polymers. *Eur. Polym. J.* **2005**, *41*, 2831–2844. [CrossRef]
161. Fang, C.; Li, T.; Zhang, Z.; Wang, X. Combined modification of asphalt by waste PE and rubber. *Polym. Compos.* **2008**, *29*, 1183–1187. [CrossRef]
162. Li, C.; Zhang, Y.; Zhang, Y. Melt grafting of maleic anhydride onto low-density polyethylene/polypropylene blends. *Polym. Test.* **2003**, *22*, 191–195. [CrossRef]
163. Chen, Z.; Zhang, H.; Liu, X.; Duan, H. A novel method for determining the time-temperature superposition relationship of SBS modified bitumen: Effects of bitumen source, modifier type and aging. *Constr. Build. Mater.* **2021**, *280*, 122549. [CrossRef]
164. Morrison, G.R.; Lee, J.K.; Hesp, S.A.M. Chlorinated polyolefins for asphalt binder modification. *J. Appl. Polym. Sci.* **1994**, *54*, 231–240. [CrossRef]
165. Daly, W.H.; Collier, J.R.; Negulescu, I.I.; Qiu, Z.; Runkle, J. Determination of Significant Factors Controlling Compatibility of Asphalts with Synthetic Polymers. 1995. Available online: <https://rosap.nrl.bts.gov/view/dot/22244> (accessed on 12 September 2021).
166. Bala, N.; Kamaruddin, I. Physical and storage stability properties of linear low density polyethylene at optimum content. In *Engineering Challenges for Sustainable Future, Proceedings of the 3rd International Conference on Civil, Offshore and Environmental Engineering (ICCOEE), Kuala Lumpur, Malaysia, 15–17 August 2016*; CRC Press: Boca Raton, FL, USA, 2016; p. 395.
167. Muhammad, J.; Martinez-Arguelles, G.; Giustozzi, F. Effect of waste tyre rubber size on physical, rheological and UV resistance of high-content rubber-modified bitumen. *Const. Build. Mater.* **2021**, *304*, 124638.
168. Maciejewski, K.; Ramiączek, P.; Chomicz-Kowalska, A. The impact of EBA and ECB polymer modification of 50/70 bitumen. *Struct. Environ.* **2013**, *5*, 15–20.
169. Panda, M.; Mazumdar, M. Engineering Properties of EVA-Modified Bitumen Binder for Paving Mixes. *J. Mater. Civ. Eng.* **1999**, *11*, 131–137. [CrossRef]
170. Kumar, P.; Chandra, S.; Bose, S. Strength characteristics of polymer modified mixes. *Int. J. Pavement Eng.* **2006**, *7*, 63–71. [CrossRef]
171. Kök, B.V.; Aydoğmuş, E.; Yilmaz, M.; Akpolat, M. Investigation on the properties of new palm-oil-based polyurethane modified bitumen. *Constr. Build. Mater.* **2021**, *289*, 123152. [CrossRef]
172. Moran, L.E. Polyethylene Modified Asphalts. CA1316279C, 13 April 1993.
173. Kumar, U.A.; Satyanarayana, P. Studies on Polymer Modified Bitumen—A Laboratory Approach. *Int. J. Civ. Eng. Res.* **2013**, *2*, 123–134.
174. Xia, T.; Chen, X.; Xu, J.; Li, Y.; Zhang, A. Influence of hydrophilic nanosilica premixing method on the property of isocyanate-based polymer modified bitumen. *Constr. Build. Mater.* **2021**, *275*, 122174. [CrossRef]
175. Tapkın, S.; Cevik, A.; Uşar, Ü.; Kurtoğlu, A. Modelling Marshall Design Test Results of Polypropylene Modified Asphalt by Genetic Programming Techniques. *Period. Polytech. Civ. Eng.* **2015**, *59*, 249–265. [CrossRef]
176. Nemade, S.N.; Thorat, P.V. Utilization of polymer waste for modification of bitumen in road construction. *Sci. Rev. Chem. Commun.* **2013**, *2*, 198–213.
177. Yilmaz, M.; Kok, B.V.; Sengoz, B.; Sengur, A.; Avci, E. Investigation of complex modulus of base and EVA modified bitumen with Adaptive-Network-Based Fuzzy Inference System. *Expert Syst. Appl.* **2011**, *38*, 969–974. [CrossRef]
178. Feng, Z.; Cai, F.; Yao, D.; Li, X. Aging properties of ultraviolet absorber/SBS modified bitumen based on FTIR analysis. *Constr. Build. Mater.* **2021**, *273*, 121713. [CrossRef]
179. Saroufim, E.; Celauro, C.; Mistretta, M.C. A simple interpretation of the effect of the polymer type on the properties of PMBs for road paving applications. *Constr. Build. Mater.* **2018**, *158*, 114–123. [CrossRef]
180. Kumar, P.; Garg, R. Rheology of waste plastic fibre-modified bitumen. *Int. J. Pavement Eng.* **2011**, *12*, 449–459. [CrossRef]
181. Oluwasola, E.A.; Hainin, M.R.; Idham, M.K.; Abayomi, M. Workability and rheological properties of eva-modified bitumen compared with PG 76 binder. *J. Teknol.* **2018**, *80*, 117–124. [CrossRef]
182. Lu, X.; Isacson, U.; Ekblad, J. Rheological properties of SEBS, EVA and EBA polymer modified bitumens. *Mater. Struct.* **1999**, *32*, 131–139. [CrossRef]
183. Nejad, F.M.; Gholami, M.; Naderi, K.; Rahi, M. Evaluation of rutting properties of high density polyethylene modified binders. *Mater. Struct.* **2015**, *48*, 3295–3305. [CrossRef]
184. Pérez-Lepe, A.; Martínez-Boza, F.; Gallegos, C.; González, O.; Muñoz, M.; Santamaria, A. Influence of the processing conditions on the rheological behaviour of polymer-modified bitumen. *Fuel* **2003**, *82*, 1339–1348. [CrossRef]
185. Habib, N.Z.; Kamaruddin, I.; Tan, I.M.; Komiyama, M. Investigation on the Effect of Phase Segregation on the Mechanical Properties of Polymer Modified Bitumen Using Analytical and Morphological Tools. Available online: [https://www.mateconferences.org/articles/mateconf/abs/2017/34/mateconf\\_ascm2017\\_07002/mateconf\\_ascm2017\\_07002.html](https://www.mateconferences.org/articles/mateconf/abs/2017/34/mateconf_ascm2017_07002/mateconf_ascm2017_07002.html) (accessed on 12 September 2021).
186. Cuadri, A.; Roman, C.; García-Morales, M.; Guisado, F.; Moreno, E.; Partal, P. Formulation and processing of recycled-low-density-polyethylene-modified bitumen emulsions for reduced-temperature asphalt technologies. *Chem. Eng. Sci.* **2016**, *156*, 197–205. [CrossRef]
187. Gökalp, I. The waste transparent nylon modified bitumen properties: Experimental assessment on physical, rheological properties and storage stability. *Constr. Build. Mater.* **2021**, *303*, 124353. [CrossRef]
188. Audén, C.F.; Sandoval, J.A.; Jerez, A.; Navarro, F.J.; Martínez-Boza, F.J.; Partal, P.; Gallegos, C. Evaluation of thermal and mechanical properties of recycled polyethylene modified bitumen. *Polym. Test.* **2008**, *27*, 1005–1012. [CrossRef]

189. Yu, R.; Fang, C.; Liu, P.; Liu, X.; Li, Y. Storage stability and rheological properties of asphalt modified with waste packaging polyethylene and organic montmorillonite. *Appl. Clay Sci.* **2015**, *104*, 1–7. [CrossRef]
190. Costa, L.; Fernandes, S.R.; da Silva, H.M.R.D.; Oliveira, J.; Miranda, R.F.M. Mechanical analysis of asphalt mixtures produced with waste plastic modified binders. In Proceedings of the 6th International Conference on Mechanics and Materials in Design, Azores, Portugal, 26–30 July 2015; pp. 2053–2062.
191. Saboo, N.; Kumar, P. Optimum Blending Requirements for EVA Modified Binder. *Transp. Res. Procedia* **2016**, *17*, 98–106. [CrossRef]
192. Nizamuddin, S.; Jamal, M.; Gravina, R.; Giustozzi, F. Recycled plastic as bitumen modifier: The role of recycled linear low-density polyethylene in the modification of physical, chemical and rheological properties of bitumen. *J. Clean. Prod.* **2020**, *266*, 121988. [CrossRef]
193. Nazmi, W.M.; Wahab, A.A. Influence of Recycled High Density Polyethylene on the Conventional and Morphology Properties of Bitumen. *J. Eng. Technol.* **2011**, *2*, 67–74.
194. Casey, D.; McNally, C.; Gibney, A.; Gilchrist, M.D. Development of a recycled polymer modified binder for use in stone mastic asphalt. *Resour. Conserv. Recycl.* **2008**, *52*, 1167–1174. [CrossRef]
195. Sharma, S.; Sharma, S.; Upadhyay, N. Composition Based Physicochemical Analysis of Modified Bitumen by High-density polyethylene (HDPE) and Low-density polyethylene (LDPE). *Orient. J. Chem.* **2019**, *35*, 1167. [CrossRef]
196. Zhang, J.; Yao, Z.; Yu, T.; Liu, S.; Jiang, H. Experimental evaluation of crumb rubber and polyethylene integrated modified asphalt mixture upon related properties. *Road Mater. Pavement Des.* **2018**, *20*, 1413–1428. [CrossRef]
197. Dalhat, M.A.; Wahhab, H.I.A.-A. Performance of recycled plastic waste modified asphalt binder in Saudi Arabia. *Int. J. Pavement Eng.* **2017**, *18*, 349–357. [CrossRef]
198. Okhotnikova, E.S.; Ganeeva, Y.M.; Frolov, I.N.; Yusupova, T.N.; Firsin, A.A. Plastic properties and structure of bitumen modified by recycled polyethylene. *Pet. Sci. Technol.* **2018**, *36*, 356–360. [CrossRef]
199. Dehouche, N.; Kaci, M.; Mokhtar, K.A. Influence of thermo-oxidative aging on chemical composition and physical properties of polymer modified bitumens. *Constr. Build. Mater.* **2012**, *26*, 350–356. [CrossRef]
200. Xia, T.; Chen, X.; Xu, J.; Chen, W.; Zhang, A. Effect of annealing method and chemical reaction on the structure and properties of polyethylene/polyethylene glycol modified bitumen. *Constr. Build. Mater.* **2021**, *269*, 121228. [CrossRef]
201. Hussein, I.A.; Iqbal, M.H.; Al-Abdul-Wahhab, H.I. Influence of M w of LDPE and vinyl acetate content of EVA on the rheology of polymer modified asphalt. *Rheol. Acta* **2005**, *45*, 92–104. [CrossRef]
202. Ho, S.; Church, R.; Klassen, K.; Law, B.; MacLeod, D.; Zanzotto, L. Study of recycled polyethylene materials as asphalt modifiers. *Can. J. Civ. Eng.* **2006**, *33*, 968–981. [CrossRef]
203. Punith, V.S.; Veeraragavan, A. Behavior of Reclaimed Polyethylene Modified Asphalt Cement for Paving Purposes. *J. Mater. Civ. Eng.* **2011**, *23*, 833–845. [CrossRef]
204. Fang, C.; Zhang, Y.; Yu, Q.; Zhou, X.; Guo, D.; Yu, R.; Zhang, M. Preparation, Characterization and Hot Storage Stability of Asphalt Modified by Waste Polyethylene Packaging. *J. Mater. Sci. Technol.* **2013**, *29*, 434–438. [CrossRef]
205. Ma, D.; Zhao, D.; Zhao, J.; Du, S.; Pang, J.; Wang, W.; Fan, C. Functionalization of reclaimed polyethylene with maleic anhydride and its application in improving the high temperature stability of asphalt mixtures. *Constr. Build. Mater.* **2016**, *113*, 596–602. [CrossRef]
206. Yan, K.; Xu, H.; You, L. Rheological properties of asphalts modified by waste tire rubber and reclaimed low density polyethylene. *Constr. Build. Mater.* **2015**, *83*, 143–149. [CrossRef]
207. Memon, N.A.; Yusoff, N.I.M.; Jafri, S.F.; Sheeraz, K. Rheological Findings on Storage Stability for Chemically Dispersed Crumb Rubber Modified Bitumen. *Constr. Build. Mater.* **2021**, *305*, 124768. [CrossRef]
208. Gama, D.A.; Júnior, J.M.R.; Melo, T.; Rodrigues, J.K.G. Rheological studies of asphalt modified with elastomeric polymer. *Constr. Build. Mater.* **2016**, *106*, 290–295. [CrossRef]
209. Yousefi, A.A. Rubber-polyethylene modified bitumen. *Iran. Polym. J.* **2004**, *13*, 101–112.
210. González, O.; Muñoz, M.E.; Santamaría, A. Bitumen/polyethylene blends: Using m-LLDPEs to improve stability and viscoelastic properties. *Rheol. Acta* **2005**, *45*, 603–610. [CrossRef]
211. Yeh, P.-H.; Nien, Y.-H.; Chen, W.-C.; Liu, W.-T. Evaluation of thermal and viscoelastic properties of asphalt binders by compounding with polymer modifiers. *Polym. Compos.* **2010**, *31*, 1738–1744. [CrossRef]
212. Kim, K.W.; Kweon, S.J.; Doh, Y.S.; Park, T.-S. Fracture toughness of polymer-modified asphalt concrete at low temperatures. *Can. J. Civ. Eng.* **2003**, *30*, 406–413. [CrossRef]
213. Liu, C.; Wang, J.; He, J. Rheological and thermal properties of m-LLDPE blends with m-HDPE and LDPE. *Polymer* **2002**, *43*, 3811–3818. [CrossRef]
214. Spadaro, C.; Plummer, C.J.G.; Manson, J.-A.E. Thermal and dynamic mechanical properties of blends of bitumen with metallocene catalyzed polyolefins. *J. Mater. Sci.* **2011**, *46*, 7449–7458. [CrossRef]
215. Ben Zair, M.; Jakarni, F.; Muniandy, R.; Hassim, S. A Brief Review: Application of Recycled Polyethylene Terephthalate in Asphalt Pavement Reinforcement. *Sustainability* **2021**, *13*, 1303. [CrossRef]
216. El-Naga, I.A.; Ragab, M. Benefits of utilization the recycle polyethylene terephthalate waste plastic materials as a modifier to asphalt mixtures. *Constr. Build. Mater.* **2019**, *219*, 81–90. [CrossRef]
217. Sojobi, A.; Nwobodo, S.E.; Aladegboye, O.J. Recycling of polyethylene terephthalate (PET) plastic bottle wastes in bituminous asphaltic concrete. *Cogent Eng.* **2016**, *3*, 1133480. [CrossRef]

218. Ashoor, A.; Kareem, M.M.; Al-Baiati, M.N. Improved asphalt binder using recycle polyethylene terephthalate polymer. *IOP Conf. Ser. Mater. Sci. Eng.* **2019**, *571*, 12094. [CrossRef]
219. Moghaddam, T.B.; Soltani, M.; Karim, M.R. Evaluation of permanent deformation characteristics of unmodified and Polyethylene Terephthalate modified asphalt mixtures using dynamic creep test. *Mater. Des.* **2014**, *53*, 317–324. [CrossRef]
220. Ahmad, A.F.; Razali, A.R.; Razelan, I.S.M.; Jalil, S.A.; Noh, M.M.; Idris, A.A. Utilization of polyethylene terephthalate (PET) in bituminous mixture for improved performance of roads. *IOP Conf. Ser. Mater. Sci. Eng.* **2017**, *203*, 12005. [CrossRef]
221. Bary, E.M.A.; Farag, R.K.; Ragab, A.A.; Abdel-Monem, R.M.; Abo-Shanab, Z.L.; Saleh, A.M.M. Green asphalt construction with improved stability and dynamic mechanical properties. *Polym. Bull.* **2020**, *77*, 1729–1747. [CrossRef]
222. Abdelaziz, M.; Mohamed Rehan, K. Rheological evaluation of bituminous binder modified with waste plastic material. In Proceedings of the 5th International Symposium on Hydrocarbons and Chemistry, Sidi Fredj, Algiers, 23–25 May 2010; pp. 1–7.
223. Leng, Z.; Padhan, R.K.; Sreeram, A. Production of a sustainable paving material through chemical recycling of waste PET into crumb rubber modified asphalt. *J. Clean. Prod.* **2018**, *180*, 682–688. [CrossRef]
224. Al-Jumaili, M.A.H. Sustainability of asphalt paving materials containing different waste materials. *IOP Conf. Ser. Mater. Sci. Eng.* **2018**, *454*, 12176. [CrossRef]
225. Modarres, A.; Hamed, H. Effect of waste plastic bottles on the stiffness and fatigue properties of modified asphalt mixes. *Mater. Des.* **2014**, *61*, 8–15. [CrossRef]
226. Cong, L.; Peng, J.; Guo, Z.; Wang, Q. Evaluation of Fatigue Cracking in Asphalt Mixtures Based on Surface Energy. *J. Mater. Civ. Eng.* **2017**, *29*, 4015003. [CrossRef]
227. Moghaddam, T.B.; Soltani, M.; Karim, M.R. Experimental characterization of rutting performance of Polyethylene Terephthalate modified asphalt mixtures under static and dynamic loads. *Constr. Build. Mater.* **2014**, *65*, 487–494. [CrossRef]
228. Choudhary, R.; Kumar, A.; Murkute, K. Properties of Waste Polyethylene Terephthalate (PET) Modified Asphalt Mixes: Dependence on PET Size, PET Content, and Mixing Process. *Period. Polytech. Civ. Eng.* **2018**, *62*, 685–693. [CrossRef]
229. PlasticsEurope Deutschland e.V. *Plastics—The Facts 2016*; PlasticsEurope Deutschland e.V.: Frankfurt, Germany, 2016.
230. Behl, A.; Sharma, G.; Kumar, G. A sustainable approach: Utilization of waste PVC in asphalt of roads. *Constr. Build. Mater.* **2014**, *54*, 113–117. [CrossRef]
231. Chan, H.S.O. Measurement of Hydrochloric Acid Emission from Burning PVC Compounds. *J. Fire Sci.* **1984**, *2*, 106–122. [CrossRef]
232. Padhan, R.K.; Sreeram, A.; Mohanta, C.S. Chemically recycled polyvinyl chloride as a bitumen modifier: Synthesis, characterisation and performance evaluation. *Road Mater. Pavement Des.* **2021**, *22*, 639–652. [CrossRef]
233. Wahhab, H.A.-A.; Dalhat, M.; Habib, M. Storage stability and high-temperature performance of asphalt binder modified with recycled plastic. *Road Mater. Pavement Des.* **2017**, *18*, 1117–1134. [CrossRef]
234. Abdel-Goad, M.A.H. Waste polyvinyl chloride-modified bitumen. *J. Appl. Polym. Sci.* **2006**, *101*, 1501–1505. [CrossRef]
235. Köfteci, S.; Ahmedzade, P.; Kultayev, B. Performance evaluation of bitumen modified by various types of waste plastics. *Constr. Build. Mater.* **2014**, *73*, 592–602. [CrossRef]
236. Rahman, N.; Ahmeduzzaman, M.; Sobhan, M.A.; Ahmed, T.U. Performance Evaluation of Waste Polyethylene and PVC on Hot Asphalt Mixtures. *Am. J. Civ. Eng. Arch.* **2013**, *1*, 97–102. [CrossRef]
237. Ghani, U.; Tanoli, W. Performance evaluation of waste PVC modified bitumen. *Int. J. Adv. Struct. Geotechnol.* **2015**, *4*, 207–210.
238. Fang, C.; Liu, X.; Yu, R.; Liu, P.; Lei, W. Preparation and Properties of Asphalt Modified with a Composite Composed of Waste Package Poly(vinyl chloride) and Organic Montmorillonite. *J. Mater. Sci. Technol.* **2014**, *30*, 1304–1310. [CrossRef]
239. Geyer, R.; Jambeck, J.R.; Law, K.L. Production, use, and fate of all plastics ever made. *Sci. Adv.* **2017**, *3*, e1700782. [CrossRef]
240. Tapkın, S.; Uşar, Ü.; Tuncan, A.; Tuncan, M. Repeated Creep Behavior of Polypropylene Fiber-Reinforced Bituminous Mixtures. *J. Transp. Eng.* **2009**, *135*, 240–249. [CrossRef]
241. Tapkın, S. The effect of polypropylene fibers on asphalt performance. *Build. Environ.* **2008**, *43*, 1065–1071. [CrossRef]
242. Tapkın, S.; Çevik, A.; Uşar, Ü. Accumulated strain prediction of polypropylene modified marshall specimens in repeated creep test using artificial neural networks. *Expert Syst. Appl.* **2009**, *36*, 11186–11197. [CrossRef]
243. Othman, A.M. Impact of Polypropylene Application Method on Long-Term Aging of Polypropylene-Modified HMA. *J. Mater. Civ. Eng.* **2010**, *22*, 1012–1018. [CrossRef]
244. Al-Hadidy, A.; Yi-Qiu, T. Mechanistic approach for polypropylene-modified flexible pavements. *Mater. Des.* **2009**, *30*, 1133–1140. [CrossRef]
245. Yeh, P.-H.; Nien, Y.-H.; Chen, J.-H.; Chen, W.-C.; Chen, J.-S. Thermal and rheological properties of maleated polypropylene modified asphalt. *Polym. Eng. Sci.* **2005**, *45*, 1152–1158. [CrossRef]
246. Nien, Y.-H.; Yeh, P.-H.; Chen, W.-C.; Liu, W.-T.; Chen, J.-H. Investigation of flow properties of asphalt binders containing polymer modifiers. *Polym. Compos.* **2008**, *29*, 518–524. [CrossRef]
247. Nekhoroshev, V.P.; Nekhoroshev, S.; Tarasova, O.I. Chemical modification of road asphalts by atactic polypropylene. *Pet. Chem.* **2017**, *57*, 643–648. [CrossRef]
248. Al-Haidri, H.A.; Tofan, A.S. Evaluation of modified asphalt mixtures with APP and IPP polymers by fatigue distress criteria. *Innov. Infrastruct. Solut.* **2021**, *6*, 131. [CrossRef]
249. Schaur, A.; Unterberger, S.H.; Lackner, R. Impact of molecular structure of PP on thermo-rheological properties of polymer-modified bitumen. *Constr. Build. Mater.* **2021**, *287*, 122981. [CrossRef]



250. Awad, A.; Al-Adday, F. Utilization of waste plastics to enhance the performance of modified hot mix asphalt. *Int. J. Geomate* **2017**, *13*, 132–139. [CrossRef]
251. Hansen, A.P.; da Silva, G.A.; Kulay, L. Evaluation of the environmental performance of alternatives for polystyrene production in Brazil. *Sci. Total Environ.* **2015**, *532*, 655–668. [CrossRef]
252. Maharana, T.; Negi, Y.; Mohanty, B. Recycling of polystyrene. *Polym.-Plast. Technol. Eng.* **2007**, *46*, 729–736. [CrossRef]
253. Baker, M.B.; Abende, R.; Abu-Salem, Z.; Khedaywi, T. Production of sustainable asphalt mixes using recycled polystyrene. *Int. J. Appl. Environ. Sci.* **2016**, *11*, 183–192.
254. Fang, C.; Jiao, L.; Hu, J.; Yu, Q.; Guo, D.; Zhou, X.; Yu, R. Viscoelasticity of Asphalt Modified with Packaging Waste Expanded Polystyrene. *J. Mater. Sci. Technol.* **2014**, *30*, 939–943. [CrossRef]
255. Al-Haydari, I.S.; Jand Masued, G.G. Benefit of using Expanded Polystyrene Packaging Material to Improve Pavement Mixture Properties. *Appl. Res. J.* **2017**, *3*, 332–342.
256. Abinaya, S.; Clement, M.; Shanmugam, S. An experimental study on the properties of extruded Polystyrene waste polymer modified bitumen for flexible pavements. *Int. Res. J. Eng. Technol.* **2016**, *3*, 304–308.
257. Johnson, O.A.; Kamaruddin, I.; Akbar, I. Modification of Malaysia Bituminous Binder Using Waste Polystyrene. In *AWAM International Conference on Civil Engineering*; Springer: Cham, Switzerland, 2019; pp. 1091–1098.
258. Padhan, R.K.; Sreeram, A.; Gupta, A. Evaluation of trans-polyoctenamer and cross-linking agents on the performance of waste polystyrene modified asphalt. *Road Mater. Pavement Des.* **2018**, *21*, 1170–1182. [CrossRef]
259. Kim, T.H.; Lim, S.T.; Lee, C.H.; Choi, H.J.; Jhon, M.S. Preparation and rheological characterization of intercalated polystyrene/organophilic montmorillonite nanocomposite. *J. Appl. Polym. Sci.* **2003**, *87*, 2106–2112. [CrossRef]
260. Stark, W.; Jaunich, M. Investigation of Ethylene/Vinyl Acetate Copolymer (EVA) by thermal analysis DSC and DMA. *Polym. Test.* **2011**, *30*, 236–242. [CrossRef]
261. Liang, M.; Ren, S.; Fan, W.; Xin, X.; Shi, J.; Luo, H. Rheological property and stability of polymer modified asphalt: Effect of various vinyl-acetate structures in EVA copolymers. *Constr. Build. Mater.* **2017**, *137*, 367–380. [CrossRef]
262. Valera-Zaragoza, M.; Ramírez-Vargas, E.; Medellín-Rodríguez, F.; Huerta-Martínez, B. Thermal stability and flammability properties of heterophasic PP-EP/EVA/organoclay nanocomposites. *Polym. Degrad. Stab.* **2006**, *91*, 1319–1325. [CrossRef]
263. Hahladakis, J.N.; Purnell, P.; Iacovidou, E.; Velis, C.A.; Atseyinku, M. Post-consumer plastic packaging waste in England: Assessing the yield of multiple collection-recycling schemes. *Waste Manag.* **2018**, *75*, 149–159. [CrossRef] [PubMed]
264. Ge, D.; Yan, K.; You, Z.; Xu, H. Modification mechanism of asphalt binder with waste tire rubber and recycled polyethylene. *Constr. Build. Mater.* **2016**, *126*, 66–76. [CrossRef]
265. Zhang, F.; Hu, C. The research for crumb rubber/waste plastic compound modified asphalt. *J. Therm. Anal. Calorim.* **2015**, *124*, 729–741. [CrossRef]
266. Brovelli, C.; Crispino, M.; Pais, J.; Pereira, P. Using polymers to improve the rutting resistance of asphalt concrete. *Constr. Build. Mater.* **2015**, *77*, 117–123. [CrossRef]
267. García-Morales, M.; Partal, P.; Navarro, F.; Gallegos, C. Effect of waste polymer addition on the rheology of modified bitumen. *Fuel* **2006**, *85*, 936–943. [CrossRef]
268. Navarro, F.J.; Partal, P.; Martínez-Boza, F.J.; Gallegos, C. Novel recycled polyethylene/ground tire rubber/bitumen blends for use in roofing applications: Thermo-mechanical properties. *Polym. Test.* **2010**, *29*, 588–595. [CrossRef]
269. Jooari, I.B.; Giustozzi, F. Hybrid Polymerisation: An Exploratory Study of the Chemo-Mechanical and Rheological Properties of Hybrid-Modified Bitumen. *Polymer* **2020**, *12*, 945. [CrossRef]
270. Yan, K.; Chen, J.; You, L.; Tian, S. Characteristics of compound asphalt modified by waste tire rubber (WTR) and ethylene vinyl acetate (EVA): Conventional, rheological, and microstructural properties. *J. Clean. Prod.* **2020**, *258*, 120732. [CrossRef]
271. Abed, A.H. Effects of functionalized polyethylene and styrene butadiene styrene polymers on performance grade of local asphalt binder. *J. Eng.* **2012**, *18*, 735–742.
272. Fang, C.; Zhang, M.; Yu, R.; Liu, X. Effect of Preparation Temperature on the Aging Properties of Waste Polyethylene Modified Asphalt. *J. Mater. Sci. Technol.* **2015**, *31*, 320–324. [CrossRef]
273. Yuan, J.; Wang, J.; Xiao, F.; Amirhanian, S.; Wang, J.; Xu, Z. Impacts of multiple-polymer components on high temperature performance characteristics of airfield modified binders. *Constr. Build. Mater.* **2017**, *134*, 694–702. [CrossRef]
274. Syroezhko, A.M.; Begak, O.Y.; Fedorov, V.V.; Gusarova, E.N. Modification of Paving Asphalts with Sulfur. *Russ. J. Appl. Chem.* **2003**, *76*, 491–496. [CrossRef]
275. Luo, W.; Zhang, Y.; Cong, P. Investigation on physical and high temperature rheology properties of asphalt binder adding waste oil and polymers. *Constr. Build. Mater.* **2017**, *144*, 13–24. [CrossRef]
276. Appiah, J.K.; Berko-Boateng, V.N.; Tagbor, T.A. Use of waste plastic materials for road construction in Ghana. *Case Stud. Constr. Mater.* **2017**, *6*, 1–7. [CrossRef]
277. Hendriani, N.; Juliastuti, S.R.; Darmawan, R.; Widjonarko; Aini, F.I.N.; Hakim, M.L. Utilization of plastic waste with mix plastic softening aggregate method as performance of stability and quality asphalt concrete. *IOP Conf. Ser. Mater. Sci. Eng.* **2019**, *543*, 12090. [CrossRef]
278. Manju, R.; Sathya, S.; Sheema, K. Use of plastic waste in bituminous pavement. *Int. J. ChemTech Res.* **2017**, *10*, 804–811.
279. Mahmuda; Sumiati; Flaviana, T.L. Asphalt Modified Plastic Waste to Defend Damage in Asphalt Concrete (Ac-Wc). *J. Phys. Conf. Ser.* **2019**, *1167*, 12011. [CrossRef]

280. Nkanga, U.J.; Joseph, J.A.; Adams, F.V.; Uche, O.U. Characterization of Bitumen/Plastic Blends for Flexible Pavement Application. *Procedia Manuf.* **2017**, *7*, 490–496. [CrossRef]
281. Chowdhury, P.S.; Kumar, S.; Sarkar, D. Performance Characteristic Evaluation of Asphalt Mixes with Plastic Coated Aggregates. In *Transportation Research*; Springer: Berlin/Heidelberg, Germany, 2019; pp. 793–803.
282. Yao, Z.; Zhang, J.; Gao, F.; Liu, S.; Yu, T. Integrated utilization of recycled crumb rubber and polyethylene for enhancing the performance of modified bitumen. *Constr. Build. Mater.* **2018**, *170*, 217–224. [CrossRef]
283. Ding, X.; Ma, T.; Zhang, W.; Zhang, D. Experimental study of stable crumb rubber asphalt and asphalt mixture. *Constr. Build. Mater.* **2017**, *157*, 975–981. [CrossRef]
284. Nuñez, J.Y.M.; Domingos, M.I.; Faxina, A.L. Susceptibility of low-density polyethylene and polyphosphoric acid-modified asphalt binders to rutting and fatigue cracking. *Constr. Build. Mater.* **2014**, *73*, 509–514. [CrossRef]
285. Zhang, F.; Yu, J.; Han, J. Effects of thermal oxidative ageing on dynamic viscosity, TG/DTG, DTA and FTIR of SBS- and SBS/sulfur-modified asphalts. *Constr. Build. Mater.* **2011**, *25*, 129–137. [CrossRef]
286. Masson, J.; Gagné, M. Polyphosphoric acid (PPA)-modified bitumen: Disruption of the asphaltenes network based on the reaction of nonbasic nitrogen with PPA. *Energy Fuels* **2008**, *22*, 3402–3406. [CrossRef]
287. Ortega, F.J.; Navarro, F.J.; García-Morales, M. Dodecylbenzenesulfonic Acid as a Bitumen Modifier: A Novel Approach to Enhance Rheological Properties of Bitumen. *Energy Fuels* **2017**, *31*, 5003–5010. [CrossRef]
288. Peng, C.; Chen, P.; You, Z.; Lv, S.; Zhang, R.; Xu, F.; Zhang, H.; Chen, H. Effect of silane coupling agent on improving the adhesive properties between asphalt binder and aggregates. *Constr. Build. Mater.* **2018**, *169*, 591–600. [CrossRef]
289. Cuadri, A.; Partal, P.; Navarro, F.; García-Morales, M.; Gallegos, C. Bitumen chemical modification by thiourea dioxide. *Fuel* **2011**, *90*, 2294–2300. [CrossRef]
290. Romagosa, H.; Corun, R.; Berkley, R. *SBS Polymer Supply Outlook*; Association of Modified Asphalt Producers (AMAP): Glen Ellyn, IL, USA, 2008.
291. Liu, L.; Xiao, F.; Zhang, H.; Amirkhanian, S. Rheological characteristics of alternative modified binders. *Constr. Build. Mater.* **2017**, *144*, 442–450. [CrossRef]
292. Sarkari, N.M.; Ayar, P.; Oskouei, M.H.; Khosrowshahi, F.K.; Mohseni, M. Silane crosslinkable polyethylene waste as bitumen modifier: A new fortunate destiny by in time recycling of thermoplastic waste before conversion to thermoset end-of-life unrecyclable polymer. *Constr. Build. Mater.* **2021**, *287*, 122999. [CrossRef]
293. Chiono, V.; Filippi, S.; Yordanov, H.; Minkova, L.; Magagnini, P. Reactive compatibilizer precursors for LDPE/PA6 blends. III: Ethylene-glycidylmethacrylate copolymer. *Polymer* **2003**, *44*, 2423–2432. [CrossRef]
294. Ahmedzade, P. The investigation and comparison effects of SBS and SBS with new reactive terpolymer on the rheological properties of bitumen. *Constr. Build. Mater.* **2013**, *38*, 285–291. [CrossRef]
295. EN 13399. *Bitumen and Bituminous Binders—Determination of Storage Stability of Modified Bitumen*; Elsevier: Amsterdam, The Netherlands, 2010.
296. Bulatović, V.O.; Rek, V.; Marković, J. Rheological properties of bitumen modified with ethylene butylacrylate glycidylmethacrylate. *Polym. Eng. Sci.* **2014**, *54*, 1056–1065. [CrossRef]
297. Polacco, G.; Filippi, S.; Merusi, F.; Stastna, G. A review of the fundamentals of polymer-modified asphalts: Asphalt/polymer interactions and principles of compatibility. *Adv. Colloid Interface Sci.* **2015**, *224*, 72–112. [CrossRef]
298. Zher'akova, G.; Kochkan'An, R. Reactivity and structure investigation of coals in reaction with dienophiles. *Fuel* **1990**, *69*, 898–901. [CrossRef]
299. Herrington, P.; Wu, Y.; Forbes, M.C. Rheological modification of bitumen with maleic anhydride and dicarboxylic acids. *Fuel* **1999**, *78*, 101–110. [CrossRef]
300. Nadkarni, V.M.; Shenoy, A.V.; Mathew, J. Thermomechanical behavior of modified asphalts. *Ind. Eng. Chem. Prod. Res. Dev.* **1985**, *24*, 478–484. [CrossRef]
301. Becker, M.Y.; Muller, A.J.; Rodriguez, Y. Use of rheological compatibility criteria to study SBS modified asphalts. *J. Appl. Polym. Sci.* **2003**, *90*, 1772–1782. [CrossRef]
302. Zhang, F.; Hu, C. The research for SBS and SBR compound modified asphalts with polyphosphoric acid and sulfur. *Constr. Build. Mater.* **2013**, *43*, 461–468. [CrossRef]
303. Miknis, F.P.; Thomas, K.P. NMR analysis of polyphosphoric acid-modified bitumens. *Road Mater. Pavement Des.* **2008**, *9*, 59–72. [CrossRef]
304. Baumgardner, G.L.; Masson, J.; Hardee, J.R.; Menapace, A.M.; Williams, A.G. Polyphosphoric acid modified asphalt: Proposed mechanism. *J. Assoc. Asph. Paving Technol.* **2005**, *74*, 283–305.
305. Rossi, C.O.; Spadafora, A.; Teltayev, B.; Izmailova, G.; Amerbayev, Y.; Bortolotti, V. Polymer modified bitumen: Rheological properties and structural characterization. *Colloids Surf. A Physicochem. Eng. Asp.* **2015**, *480*, 390–397. [CrossRef]
306. Thomas, K.P.; Turner, T.F. Polyphosphoric-acid Modification of Asphalt Binders. Impact on Rheological and Thermal Properties. *Road Mater. Pavement Des.* **2008**, *9*, 181–205. [CrossRef]
307. Xiao, F.; Amirkhanian, S.; Wang, H.; Hao, P. Rheological property investigations for polymer and polyphosphoric acid modified asphalt binders at high temperatures. *Constr. Build. Mater.* **2014**, *64*, 316–323. [CrossRef]
308. Wen, G.; Zhang, Y.; Zhang, Y.; Sun, K.; Fan, Y. Rheological characterization of storage-stable SBS-modified asphalts. *Polym. Test.* **2002**, *21*, 295–302. [CrossRef]

309. Chen, J.S.; Huang, C.C. Fundamental characterization of SBS-modified asphalt mixed with sulfur. *J. Appl. Polym. Sci.* **2006**, *103*, 2817–2825. [CrossRef]
310. Sun, D.; Ye, F.; Shi, F.; Lu, W. Storage Stability of SBS-Modified Road Asphalt: Preparation, Morphology, and Rheological Properties. *Pet. Sci. Technol.* **2006**, *24*, 1067–1077. [CrossRef]
311. Gedik, A.; Lav, A.H. Analytical, morphological, and rheological behavior of sulphur-extended-binder. *Can. J. Civ. Eng.* **2016**, *43*, 532–541. [CrossRef]
312. Maldonado, P.; Mas, J.; Phung, T.K. Process for Preparing Bitumen-Polymer Compositions. U.S. Patent 4145322A, 1979.
313. Alghrafy, Y.M.; Alla, E.-S.M.A.; El-Badawy, S.M. Rheological properties and aging performance of sulfur extended asphalt modified with recycled polyethylene waste. *Constr. Build. Mater.* **2021**, *273*, 121771. [CrossRef]
314. Nejad, F.M.; Zarroodi, R.; Naderi, K. Effect of cross-linkers on the performance of polyethylene-modified asphalt binders. *Proc. Inst. Civ. Eng. Constr. Mater.* **2017**, *170*, 186–193. [CrossRef]
315. Golestani, B.; Nam, B.H.; Nejad, F.M.; Fallah, S. Nanoclay application to asphalt concrete: Characterization of polymer and linear nanocomposite-modified asphalt binder and mixture. *Constr. Build. Mater.* **2015**, *91*, 32–38. [CrossRef]
316. Siddig, E.A.; Feng, C.P.; Ming, L.Y. Effects of ethylene vinyl acetate and nanoclay additions on high-temperature performance of asphalt binders. *Constr. Build. Mater.* **2018**, *169*, 276–282. [CrossRef]
317. Mansourian, A.; Goahri, A.R.; Khosrowshahi, F.K. Performance evaluation of asphalt binder modified with EVA/HDPE/nanoclay based on linear and non-linear viscoelastic behaviors. *Constr. Build. Mater.* **2019**, *208*, 554–563. [CrossRef]
318. Vo, L.T.; Giannelis, E.P. Compatibilizing Poly(vinylidene fluoride)/Nylon-6 Blends with Nanoclay. *Macromolecules* **2007**, *40*, 8271–8276. [CrossRef]
319. Galooyak, S.S.; Dabir, B.; Nazarbeygi, A.E.; Moeini, A. Rheological properties and storage stability of bitumen/SBS/montmorillonite composites. *Constr. Build. Mater.* **2010**, *24*, 300–307. [CrossRef]
320. Ouyang, C.; Wang, S.; Zhang, Y.; Zhang, Y. Low-density polyethylene/silica compound modified asphalts with high-temperature storage stability. *J. Appl. Polym. Sci.* **2006**, *101*, 472–479. [CrossRef]
321. Markanday, S.S.; Stastna, J.; Polacco, G.; Filippi, S.; Kazatchkov, I.; Zanzotto, L. Rheology of bitumen modified by EVA-Organoclay nanocomposites. *J. Appl. Polym. Sci.* **2010**, *118*, 557–565. [CrossRef]
322. Roman, C.; García-Morales, M. Comparative assessment of the effect of micro-and nano-fillers on the microstructure and linear viscoelasticity of polyethylene-bitumen mastics. *Constr. Build. Mater.* **2018**, *169*, 83–92. [CrossRef]
323. Islam, M.M.; Shirin, M.S.; Tonoy, T.R.; Sweet, S.A. Modification of Bitumen Properties Using Waste Polymer in Context of Bangladesh. *Int. J. Min. Proc. Extr. Met.* **2021**, *6*, 6.
324. Golestani, B.; Nejad, F.M.; Galooyak, S.S. Performance evaluation of linear and nonlinear nanocomposite modified asphalts. *Constr. Build. Mater.* **2012**, *35*, 197–203. [CrossRef]
325. Shi, X.; Cai, L.; Xu, W.; Fan, J.; Wang, X. Effects of nano-silica and rock asphalt on rheological properties of modified bitumen. *Constr. Build. Mater.* **2018**, *161*, 705–714. [CrossRef]
326. Saltan, M.; Terzi, S.; Karahancer, S. Examination of hot mix asphalt and binder performance modified with nano silica. *Constr. Build. Mater.* **2017**, *156*, 976–984. [CrossRef]
327. Saltan, M.; Terzi, S.; Karahancer, S. Performance analysis of nano modified bitumen and hot mix asphalt. *Constr. Build. Mater.* **2018**, *173*, 228–237. [CrossRef]
328. Vargas, M.; Moreno, L.; Montiel, R.; Manero, O.; Vázquez, H. Effects of montmorillonite (Mt) and two different organo-Mt additives on the performance of asphalt. *Appl. Clay Sci.* **2017**, *139*, 20–27. [CrossRef]
329. Zhang, H.; Gao, Y.; Guo, G.; Zhao, B.; Yu, J. Effects of ZnO particle size on properties of asphalt and asphalt mixture. *Constr. Build. Mater.* **2018**, *159*, 578–586. [CrossRef]
330. Wang, T.; Xu, G.; Shi, C.; Xu, X.; Yu, Y.; Gong, M.; Yang, J. Rheological properties of aged bitumen rejuvenated by polymer modified bio-derived rejuvenator. *Constr. Build. Mater.* **2021**, *298*, 123249. [CrossRef]
331. Bala, N.; Kamaruddin, I.; Napiah, M.; Nahi, M.H. Influence of Nanosilica on Rheological Properties and Oxidative Aging of Polymer Modified Bitumen. *J. Eng. Appl. Sci.* **2017**, *12*, 5990–5996.
332. Fang, C.; Yu, R.; Liu, S.; Li, Y. Nanomaterials Applied in Asphalt Modification: A Review. *J. Mater. Sci. Technol.* **2013**, *29*, 589–594. [CrossRef]
333. De Melo, J.V.S.; Trichês, G.; de Rosso, L.T. Experimental evaluation of the influence of reinforcement with Multi-Walled Carbon Nanotubes (MWCNTs) on the properties and fatigue life of hot mix asphalt. *Constr. Build. Mater.* **2018**, *162*, 369–382. [CrossRef]
334. Li, R.; Xiao, F.; Amirkhanian, S.; You, Z.; Huang, J. Developments of nano materials and technologies on asphalt materials—A review. *Constr. Build. Mater.* **2017**, *143*, 633–648. [CrossRef]
335. Czernik, S.; Bridgwater, A. Overview of applications of biomass fast pyrolysis oil. *Energy Fuels* **2004**, *18*, 590–598. [CrossRef]
336. Mohan, D.; Pittman, C.U.; Steele, P.H. Pyrolysis of Wood/Biomass for Bio-oil: A Critical Review. *Energy Fuels* **2006**, *20*, 848–889. [CrossRef]
337. Su, N.; Xiao, F.; Wang, J.; Cong, L.; Amirkhanian, S. Productions and applications of bio-asphalts—A review. *Constr. Build. Mater.* **2018**, *183*, 578–591. [CrossRef]
338. Lei, Y.; Wang, H.; Chen, X.; Yang, X.; You, Z.; Dong, S.; Gao, J. Shear property, high-temperature rheological performance and low-temperature flexibility of asphalt mastics modified with bio-oil. *Constr. Build. Mater.* **2018**, *174*, 30–37. [CrossRef]

339. Fini, E.H.; Khodaii, A.; Hajikarimi, P. Fractional. Viscoelastic Study of Low-Temperature Characteristics of Biomodified Asphalt Binders. *J. Mater. Civ. Eng.* **2016**, *28*, 4016078. [CrossRef]
340. Metwally, M.; Raouf, M.A. *Development of Non-Petroleum Binders Derived from Fast Pyrolysis Bio-Oils for Use in Flexible Pavement*; Iowa State University: Ames, IA, USA, 2010.
341. Kabir, S.F.; Sukumaran, S.; Moghtadernejad, S.; Barjasteh, E.; Fini, E.H. End of life plastics to enhance sustainability of pavement construction utilizing a hybrid treatment of bio-oil and carbon coating. *Constr. Build. Mater.* **2021**, *278*, 122444. [CrossRef]
342. Sun, Z.; Yi, J.; Feng, D.; Kasbergen, C.; Scarpas, A.; Zhu, Y. Preparation of bio-bitumen by bio-oil based on free radical polymerization and production process optimization. *J. Clean. Prod.* **2018**, *189*, 21–29. [CrossRef]
343. Raouf, M.A.; Williams, C.R. General Rheological Properties of Fractionated Switchgrass Bio-Oil as a Pavement Material. *Road Mater. Pavement Des.* **2010**, *11*, 325–353. [CrossRef]
344. Williams, R.C.; Satrio, J.; Rover, M.; Brown, R.C.; Teng, S. Utilization of fractionated bio oil in asphalt. In Proceedings of the 88th Annual Meeting of the Transportation Research Board, Washington, DC, USA, 11–15 January 2009.
345. Ingrassia, L.P.; Lu, X.; Ferrotti, G.; Canestrari, F. Chemical, morphological and rheological characterization of bitumen partially replaced with wood bio-oil: Towards more sustainable materials in road pavements. *J. Traffic Transp. Eng.* **2020**, *7*, 192–204. [CrossRef]
346. Xinxin, C.; Xuejuan, C.; Boming, T.; Yuanyuan, W.; Xiaolong, L. Investigation on Possibility of Waste Vegetable Oil Rejuvenating Aged Asphalt. *Appl. Sci.* **2018**, *8*, 765. [CrossRef]
347. Al-Omari, A.A.; Khedaywi, T.S.; Khasawneh, M.A. Laboratory characterization of asphalt binders modified with waste vegetable oil using SuperPave specifications. *Int. J. Pavement Res. Technol.* **2018**, *11*, 68–76. [CrossRef]
348. Yang, X.; You, Z. High temperature performance evaluation of bio-oil modified asphalt binders using the DSR and MSCR tests. *Constr. Build. Mater.* **2015**, *76*, 380–387. [CrossRef]
349. Joni, H.H.; Al-Rubae, R.H.; Al-Zerkani, M.A. Rejuvenation of aged asphalt binder extracted from reclaimed asphalt pavement using waste vegetable and engine oils. *Case Stud. Constr. Mater.* **2019**, *11*, e00279. [CrossRef]
350. Cai, X.; Zhang, J.; Xu, G.; Gong, M.; Chen, X.; Yang, J. Internal aging indexes to characterize the aging behavior of two bio-rejuvenated asphalts. *J. Clean. Prod.* **2019**, *220*, 1231–1238. [CrossRef]
351. Chen, A.; Liu, G.; Zhao, Y.; Li, J.; Pan, Y.; Zhou, J. Research on the aging and rejuvenation mechanisms of asphalt using atomic force microscopy. *Constr. Build. Mater.* **2018**, *167*, 177–184. [CrossRef]
352. Li, Y.; Moraes, R.; Lyngdal, E.; Bahia, H. Effect of Polymer and Oil Modification on the Aging Susceptibility of Asphalt Binders. *Transp. Res. Rec.* **2016**, *2574*, 28–37. [CrossRef]
353. Zhang, R.; You, Z.; Wang, H.; Chen, X.; Si, C.; Peng, C. Using bio-based rejuvenator derived from waste wood to recycle old asphalt. *Constr. Build. Mater.* **2018**, *189*, 568–575. [CrossRef]
354. Guarin, A.; Khan, A.; Butt, A.A.; Birgisson, B.; Kringos, N. An extensive laboratory investigation of the use of bio-oil modified bitumen in road construction. *Constr. Build. Mater.* **2016**, *106*, 133–139. [CrossRef]
355. Liu, W.; Yan, K.; Ge, D.; Chen, M. Effect of APAO on the aging properties of waste tire rubber modified asphalt binder. *Constr. Build. Mater.* **2018**, *175*, 333–341. [CrossRef]
356. Ouyang, C.; Gao, Q.; Shi, Y.; Shan, X. Compatibilizer in waste tire powder and low-density polyethylene blends and the blends modified asphalt. *J. Appl. Polym. Sci.* **2011**, *123*, 485–492. [CrossRef]
357. Wang, S.; Yuan, C.; Jiayi, D. Crumb tire rubber and polyethylene mutually stabilized in asphalt by screw extrusion. *J. Appl. Polym. Sci.* **2014**, *131*. [CrossRef]
358. Ahmedzade, P.; Günay, T.; Grigoryeva, O.; Starostenko, O. Irradiated Recycled High Density Polyethylene Usage as a Modifier for Bitumen. *J. Mater. Civ. Eng.* **2017**, *29*, 4016233. [CrossRef]
359. Joohari, I.B.; Giustozzi, F. Chemical and high-temperature rheological properties of recycled plastics-polymer modified hybrid bitumen. *J. Clean. Prod.* **2020**, *276*, 123064. [CrossRef]
360. Yan, C.; Huang, W.; Xiao, F.; Lv, Q. Influence of polymer and sulphur dosages on attenuated total reflection Fourier transform infrared upon Styrene–Butadiene–Styrene-modified asphalt. *Road Mater. Pavement Des.* **2018**, *20*, 1586–1600. [CrossRef]
361. Wang, Z.; Dai, Q.; Guo, S.; Wang, R.; Ye, M.; Yap, Y.K. Experimental investigation of physical properties and accelerated sunlight-healing performance of flake graphite and exfoliated graphite nanoplatelet modified asphalt materials. *Constr. Build. Mater.* **2017**, *134*, 412–423. [CrossRef]
362. Yang, X.; You, Z.; Dai, Q. Performance Evaluation of Asphalt Binder Modified by Bio-oil Generated from Waste Wood Resources. *Int. J. Pavement Res. Technol.* **2013**, *6*, 431–439.
363. Zhang, R.; Wang, H.; Jiang, X.; You, Z.; Yang, X.; Ye, M. Thermal Storage Stability of Bio-Oil Modified Asphalt. *J. Mater. Civ. Eng.* **2018**, *30*, 4018054. [CrossRef]
364. Joohari, I.B.; Giustozzi, F. Effect of different vinyl-acetate contents in hybrid SBS-EVA modified bitumen. *Constr. Build. Mater.* **2020**, *262*, 120574. [CrossRef]
365. Kakar, M.R.; Mikhailenko, P.; Piao, Z.; Bueno, M.; Poulidakos, L. Analysis of waste polyethylene (PE) and its by-products in asphalt binder. *Constr. Build. Mater.* **2021**, *280*, 122492. [CrossRef]



## Article

# The Influence of Fly Ash on the Mechanical Properties of Water Immersed All Waste Composites

Mihaela Cosnita \*, Monica Balas and Cristina Cazan \* 

Renewable Energy Systems and Recycling Research Center, Transilvania University of Brasov, 500036 Brasov, Romania; monica\_balas@unitbv.ro

\* Correspondence: mihaela.cosnita@unitbv.ro (M.C.); c.vladuta@unitbv.ro (C.C.)

**Abstract:** The paper presents new value-added composite materials prepared by recycling tire rubber, polyethylene terephthalate (PET), high-density polyethylene (HDPE), wood sawdust, and fly ash. The composites were manufactured through the compression molding technique for three temperatures (150 °C, 160 °C, and 190 °C) previously optimized. The addition of fly ash as reinforcement in polymer blends is a viable route to improve the composite's properties. The paper aims to assess the effect of fly ash on the mechanical properties and water stability of the new all waste composites considering their applications as outdoor products. The static tensile (stress-strain behavior) and compression properties of the composites were tested. The fly ash composites were characterized in terms of wetting behavior and surface energies (contact angle measurements); chemical structure of the new interface developed between composite's components (FTIR analysis), crystalline structure (XRD analysis), surface morphology and topography (SEM, AFM). The addition of fly ash promoted the development of the hybrid interfaces in the new composites, as FTIR analysis has shown, which, in turn, greatly improved the mechanical and water resistance. The novel all waste composites exhibited lower surface energies, larger contact angles, and smoother morphologies when compared to those with no fly ash. Overall, the study results have revealed that fly ash has improved the mechanical strength and water stability of the composites through the formation of strong hybrid interfaces. The study results show optimal water stability and tensile strength for 0.5% fly ash composites cured at 190 °C and optimal compressive strength with good water stability for 1% fly ash composite cured at 150 °C.

**Keywords:** fly ash; end of life tire rubber; rubber-PET-HDPE-wood composites; wood waste; mechanical properties

**Citation:** Cosnita, M.; Balas, M.; Cazan, C. The Influence of Fly Ash on the Mechanical Properties of Water Immersed All Waste Composites. *Polymers* **2022**, *14*, 1957. <https://doi.org/10.3390/polym14101957>

Academic Editor: Marcin Masłowski

Received: 19 April 2022

Accepted: 9 May 2022

Published: 11 May 2022

**Publisher's Note:** MDPI stays neutral with regard to jurisdictional claims in published maps and institutional affiliations.



**Copyright:** © 2022 by the authors. Licensee MDPI, Basel, Switzerland. This article is an open access article distributed under the terms and conditions of the Creative Commons Attribution (CC BY) license (<https://creativecommons.org/licenses/by/4.0/>).

## 1. Introduction

Nowadays, several worldwide issues derive from the huge amounts of waste disposal, which seriously harms the environment and humanity's health. The reuse of and waste recycling could save 600 billion euros for EU companies. Consequently, gas emissions could be reduced by up to 4% per year [1]. Tire rubber wastes represent an important waste category with a continuous growth rate and negative impact on the environment. Globally, about 1.5 billion tires are discarded per year in addition to the already accumulated large volume [2]. The management of waste tire rubbers is often reduced only at energy recovery by their incineration in a cement kiln, paper plants, etc. [3], but there is a huge loss of materials at the same time that causes a negative impact on the environment. The most sustainable method for recycling rubber tires could be by grinding and blending them with other polymers in order to achieve new polymer composites [4].

On the other hand, plastic-based products are a part of our daily life because of their low cost, density, high strength, and their resistance to corrosion and weathering. Worldwide, the production of plastics doubled from 2000 to 2020, reaching 360 million tons. There are many single-use plastic products (PET, HDPE, PS, PP), and after use, they are

thrown away, thus increasing the environmental burden and causing detrimental effects on the quality of water, soil, and human healthy consequently [5,6].

Government legislative efforts are conducted to recycle end-of-life plastic-based products into value-added products [7].

However, reports on the recycling of plastics in a sustainable way are scarce. Often, the plastic products coming from beverages and the food industry are thrown everywhere, and finally, they reach the sea and endanger marine life.

The use of biomass fillers such as wood, sisal, flax, and so on, to produce composite materials offers a series of advantages, which include a low density, less processing equipment damage, flexibility, biodegradability, and minimal health hazards [8,9].

Wood sawdust, resulting from the exploitation of wood, could harm the environment when there is improper disposal. The strength of wood is 20 times higher than of the HDPE being used as reinforcement in plastic composites. The advantages of using wood in WPC over classic fibers are related to its high availability, low weight and cost, thermal and insulation properties, and a lack of abrasiveness to equipment [10].

There are reports on the development of wood-plastic composites (WPC) and rubber-wood-plastic composites (RubWPC), which have a low density and good mechanical properties [11–16]. The mechanical properties of WPC are determined by the interface adhesion between the wood and the polymer matrix. There are many reported methods for the improvement of polymer-wood compatibilities, such as grafting the maleic anhydride to a polymer, adding coupling agents, treating the wood through mercerizing, plasma, corona, and so on [17–20]. These wood treatments promote the wood-polymer interface adhesion, but they are difficult to be applied on a large scale due to their cost and because they often use toxic chemical compounds.

However, sustainable and economical methods could be applied for the recycling of most discarded waste types (rubber, plastic, wood, etc.) by manufacturing performant and water stability RubWPC through the addition of inorganic fillers.

Moreover, the addition of inorganic fillers in the form of waste into a polymer matrix leads to the formation of the hybrid interfaces, which, in turn, greatly improve the mechanical, physical, thermal, flame retardant, water stability, and durability properties of organic-inorganic (hybrid) composites [21–24].

Silica is often used for improving the wood-polymer interface in order to achieve new value-added products by increasing the synergistic effects of both components' properties [25].

The available FA, the waste generated from heating a power plant (enriched with silica), could be an important candidate for use as a filler in rubber-plastic-wood composites.

Fly ash is widely used as a supplementary cementitious material in concrete manufacturing. It improves the workability and durability of concrete while reducing the costs of concrete products [26–28].

To the best of our knowledge, there are no reports on the influence of FA on water stability and the mechanical properties of all waste composites manufactured from waste rubber, PET, HDPE, and wood.

The new hybrid waste composites, including organic and inorganic fillers in the rubber matrix, could reduce the environmental burden while also providing increased performance products for outdoor applications, such as paving slabs, covers for play and sports grounds, highway walls, and so on.

The paper aims to assess the effect of fly ash on the mechanical properties and water stability of the new all waste composites developed by recycling together most discarded wastes such as tire rubber, PET, HDPE, and wood.

## 2. Experimental Methodology

### 2.1. Materials

The materials used in this study were waste tire rubber from Granutech Recycling (Suceava, RO, USA), PET flakes from used bottles, small amounts of high-density polyethylene

flakes (HDPE, PET from Teli Company), wood sawdust (fir 1–2%, and beech 98–99%) from Wood Engineering Department, Transilvania University of Brasov, Romania, with a natural moisture content of 5.28% and fly ash (FA) coming from the Heating Plant CET Brasov, RO. FA is a cheap material and is a poly-oxide compound with a high weight percentage of SiO<sub>2</sub> (53.32 wt%), Al<sub>2</sub>O<sub>3</sub> (22.05 wt%), and Fe<sub>2</sub>O<sub>3</sub> (8.97 wt%). As per ASTM standard C-618-2a [29], this FA is of F type (the SiO<sub>2</sub>, Al<sub>2</sub>O<sub>3</sub>, and Fe<sub>2</sub>O<sub>3</sub> content exceed 70%) [30]. All of the materials were milled to 1 mm-sized particles.

## 2.2. Methods

All waste rubber-PET-HDPE-wood composites were prepared through the compression molding method using a thermostat oven (type ECv 200–300) for thermal curing. The thermal processing duration was one hour at 150 ± 5 °C (samples 1S type), 160 ± 5 °C (samples 2S type), 190 ± 5 °C (samples 3S type) temperatures optimized in our previous work [31]. The composite components mass ratio previously optimized and the codes of the samples without fly ash (FA) are:

- rubber:PET:HDPE:wood = 80:10:5:5, samples 1S (cured at 150 °C), 2S (cured at 160 °C) and 3S (cured at 190 °C);

The mass ratio of the fly ash composite components is rubber:PET:HDPE:wood:FA = (80 – x):10:5:5:x, with the fly ash weight percentage ranging from 0.5 to 2 wt% with a 0.5 wt% step. The fly ash added composites are denoted as follows in Table 1.

**Table 1.** Codes of fly ash composites.

| Samples Composition [wt%]                    | T [°C] | FA [%] | Samples Code |
|--|--------|--------|--------------|
| rubber:PET:HDPE:wood: FA = (80 – x):10:5:5:x | 150    | 0.5    | 1S_FA—1      |
|  |        | 1      | 1S_FA—2      |
|  |        | 1.5    | 1S_FA—3      |
|  |        | 2      | 1S_FA—4      |
|  | 160    | 0.5    | 2S_FA—1      |
|  |        | 1      | 2S_FA—2      |
|  |        | 1.5    | 2S_FA—3      |
|  |        | 2      | 2S_FA—4      |
|  | 190    | 0.5    | 3S_FA—1      |
|  |        | 1      | 3S_FA—2      |
|  |        | 1.5    | 3S_FA—3      |
|  |        | 2      | 3S_FA—4      |

Two set samples of each series were prepared: the S series (without FA) and the S-FA series (with FA). The two sets of each series of samples without FA and with FA (denoted as S and S\_FA, respectively) were thermally processed at the previously optimized temperatures of 150 °C, 160 °C, and 190 °C [31]. A sample set of each series (S and S-FA, respectively) were kept for three days in laboratory condition, and those from the second set of each composite series were immersed for 5 days in tap water (Total Hardness = 14.5 dGH) and then were dried in an open air laboratory before their characterization. Five representative samples of each series were mechanically tested.

## 2.3. Characterization Techniques

**Mechanical tests:** Tensile strength ( $\sigma_t$ ) and Young modulus (E) were evaluated with Z020, Zwick/Roell equipment (DE) at a traction speed of 100 mm/min. The compression resistance ( $R_C$ ) was tested on the same mechanical testing equipment, according to SR EN ISO 527-4:2000.

**Scanning electron microscopy (SEM) and energy-dispersive X-ray spectroscopy (EDX) analysis:** Micrographs were obtained by using a scanning electron microscope (SEM, JP), Hitachi, S3400N, type II, and quantitative elemental analysis of the samples was



performed with EDX (Thermo, Ultra Dry, Noran System 7, NSS Model, 2000000counts/sec) and the sensitivity down to a few atomic percent.

**Atomic force microscopy (AFM) analysis:** The surface morphology and topography of the nanocomposite were investigated by atomic force microscopy (AFM NT-MDT model NTEGRA PRIMA EC). The images were taken in semi-contact mode with a “GOLDEN” silicon cantilever (NCSG10, force constant 0.15 N/m, tip radius 10 nm).

**Fourier Transforms Infrared Spectroscopy (FTIR) analysis:** was performed using a Spectrum Bruker spectrophotometer (KR); the spectra were recorded in reflectance mode, in the 500 to 4500  $\text{cm}^{-1}$  range, after 16 scans, with a resolution of 4  $\text{cm}^{-1}$ .

**X-ray diffraction (XRD):** The crystallinity data were collected over the range  $2\theta = 10 \sim 60^\circ$  in the fixed time mode, with a step interval of 0.01°, at 25°, using a Bruker Advanced D8 diffractometer ( $\text{CuK}_{\alpha 1}$  radiation, with 1.5406 Å wavelength, at 40 kV, 20 mA).

**Contact angle measurements:** The measurements of the composite surfaces were performed with an OCA-20 Contact Angle System (Data Physics Instruments), based on the sessile drop method. The surface energies were calculated using the Owens, Wendt, Rabel, and Kaelble (OWRK) method [32]. The two liquids used in the experiments were: water ( $\sigma_{\text{H}_2\text{O}} = 72.10 \text{ mN/m}$ ,  $\sigma_{\text{H}_2\text{O}}^{\text{p}} = 52.20 \text{ mN/m}$  and  $\sigma_{\text{H}_2\text{O}}^{\text{d}} = 19.90 \text{ mN/m}$ ) and glycerol ( $\sigma_{\text{glycerol}} = 73.40 \text{ mN/m}$ ,  $\sigma_{\text{glycerol}}^{\text{p}} = 37.00 \text{ mN/m}$  and  $\sigma_{\text{glycerol}}^{\text{d}} = 36.40 \text{ mN/m}$ ) and the total surface energy, polar, and the dispersive components were obtained using Equation (1) [32]:

$$\sigma_{\text{SL}} = \sigma_{\text{S}} + \sigma_{\text{L}} - 2 \left( \sqrt{\sigma_{\text{S}}^{\text{d}} \cdot \sigma_{\text{L}}^{\text{d}}} + \sqrt{\sigma_{\text{S}}^{\text{p}} \cdot \sigma_{\text{L}}^{\text{p}}} \right) \quad (1)$$

$\sigma_{\text{SV}}$ —surface energy;  $\sigma_{\text{S}}$ —surface tension of testing liquid;  $\sigma_{\text{L}}$ —surface tension of solid surface;  $\sigma_{\text{SV}}^{\text{d}}$ ,  $\sigma_{\text{SV}}^{\text{p}}$ —dispersive and polar component of the surface energy.

### 3. Results and Discussions

#### *Mechanical Tests*

Composite materials should meet the required mechanical properties, such as tensile, compressive, and impact strength depending on the targeted applications. The mechanical behavior of the composite materials is strongly influenced by interfacial zone strength. Interfacial adhesion plays a key role that greatly entails the composite’s mechanical, thermal, and durability properties. The interfacial adhesion in composite systems could be tailored mainly by three mechanisms, mechanical, mechanical-chemical, or chemical bonds between the components of the composite system. The nature of the interfacial adhesion in a composite system is strongly dictated by the technological and compositional parameters, filler dispersion degree, filler properties, such as wetting, shape and size, components properties, and so on.

A small amount of fly ash (up to 2%) was added in order to avoid fly ash cluster formation as the filler particle interactions are larger than the interaction of the composite components in the interfacial zone. By adding a small amount of fly ash, cluster formation is avoided. The interfacial linkage between the fly ash and polymer matrix is crucial to the fly ash composite’s mechanical strength [33–35].

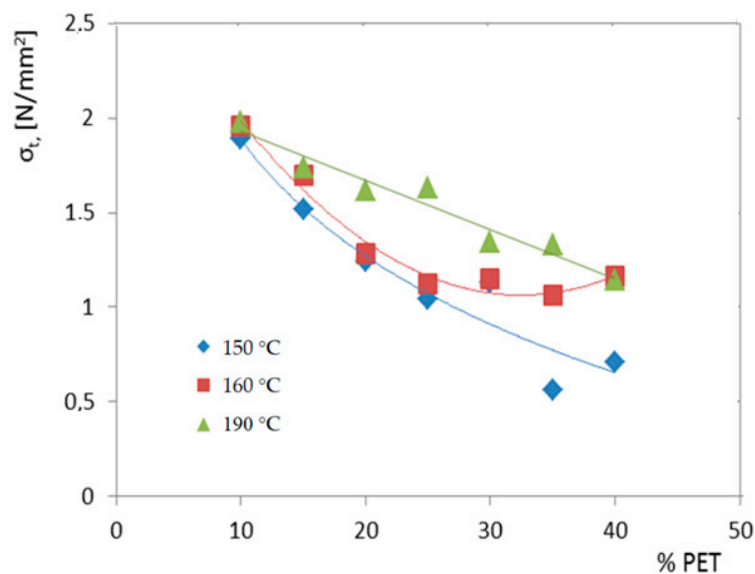
The assessment of the composite behavior under wet conditions represents a prerequisite when outdoor applications are being pursued. That is why the study evaluated the mechanical strength before and after water immersion of the novel hybrid composites.

The previously optimized temperatures valorize the mechanical properties and benefit of the wood incorporated into the rubber-PET-HDPE blend. Wood composites obtained at higher curing temperatures lead to the decomposition of the wood components, thus reducing the binding effect between composite components. Crystalline cellulose from the wood greatly enhances the mechanical properties of the rubber—plastic-based composites when the composite is cured at temperatures below 200 °C [36]. These two series of composites were mechanically tested, and the results are presented in Table 2. The addition of wood sawdust significantly influences the mechanical properties of the rubber–plastic composites.

**Table 2.** Mechanical properties of composites with PET, rubber, HDPE, wood, and ash addition, before and after the water immersion.

| T<br>[°C] | Sample<br>Code | $\sigma_t$<br>[N/mm <sup>2</sup> ]<br>Initial | $\sigma_t$<br>[N/mm <sup>2</sup> ]<br>Immersion | R <sub>c</sub><br>[N/mm <sup>2</sup> ]<br>Initial | R <sub>c</sub><br>[N/mm <sup>2</sup> ]<br>Immersion |
|-----------|----------------|---|---|---|---|
| 150       | 1S_FA—1        | 1.66  | 1.68  | 63.62   | 58.67   |
|           | 1S_FA—2        | 1.51  | 1.52  | 50.34   | 62.80   |
|           | 1S_FA—3        | 1.52  | 1.69  | 55.08   | 50.91   |
|           | 1S_FA—4        | 1.39  | 1.46  | 62.19   | 63.16   |
| 160       | 2S_FA—1        | 1.88  | 1.73  | 52.35   | 62.28   |
|           | 2S_FA—2        | 1.68  | 1.84  | 66.60   | 58.01   |
|           | 2S_FA—3        | 1.63  | 1.72  | 68.69   | 50.05   |
|           | 2S_FA—4        | 1.58  | 1.68  | 66.55   | 53.12   |
| 190       | 3S_FA—1        | 2.09  | 2.07  | 57.42   | 56.52   |
|           | 3S_FA—2        | 1.86  | 1.87  | 55.20   | 57.25   |
|           | 3S_FA—3        | 1.89  | 1.87  | 61.16   | 51.67   |
|           | 3S_FA—4        | 1.71  | 1.94  | 62.78   | 53.37   |

Up to 40 wt% of the PET was incorporated in the rubber matrix for the three optimized temperatures, as is shown in Figure 1.

**Figure 1.** Variation of tensile strength with % PET and processing temperature.

The tensile strength of the all-waste composite drastically decreased when the PET content was increased due to the weakening interface with PET particle agglomerations, Figure 1. The agglomeration of PET at the interface zone hampers the stress transfer from the matrix to filler, as tensile strength tests have revealed. The highest tensile strength was recorded to be 10 wt% for the PET composites. That is why in developing novel composites with rubber, HDPE, wood, and fly ash 10% wt PET was considered.

Five representative samples (with fly ash) of each series (before and after water immersion) were mechanically tested, and the average values are summarized in Table 2.

By comparing the pristine composite series cured at 150 °C, 160 °C, and 190 °C, the tensile strength increased as the curing temperature increased, and we recorded a decreasing trend with the increased amount of FA incorporated into the rubber-plastic-wood blend. Therefore the lowest tensile strength corresponds to 2% in the FA highest

sample obtained at 150 °C (1S\_FA—4), and the highest was recorded for the 0.5% FA composite cured at 190 °C (3S\_FA—1), as is shown in Figure 2.

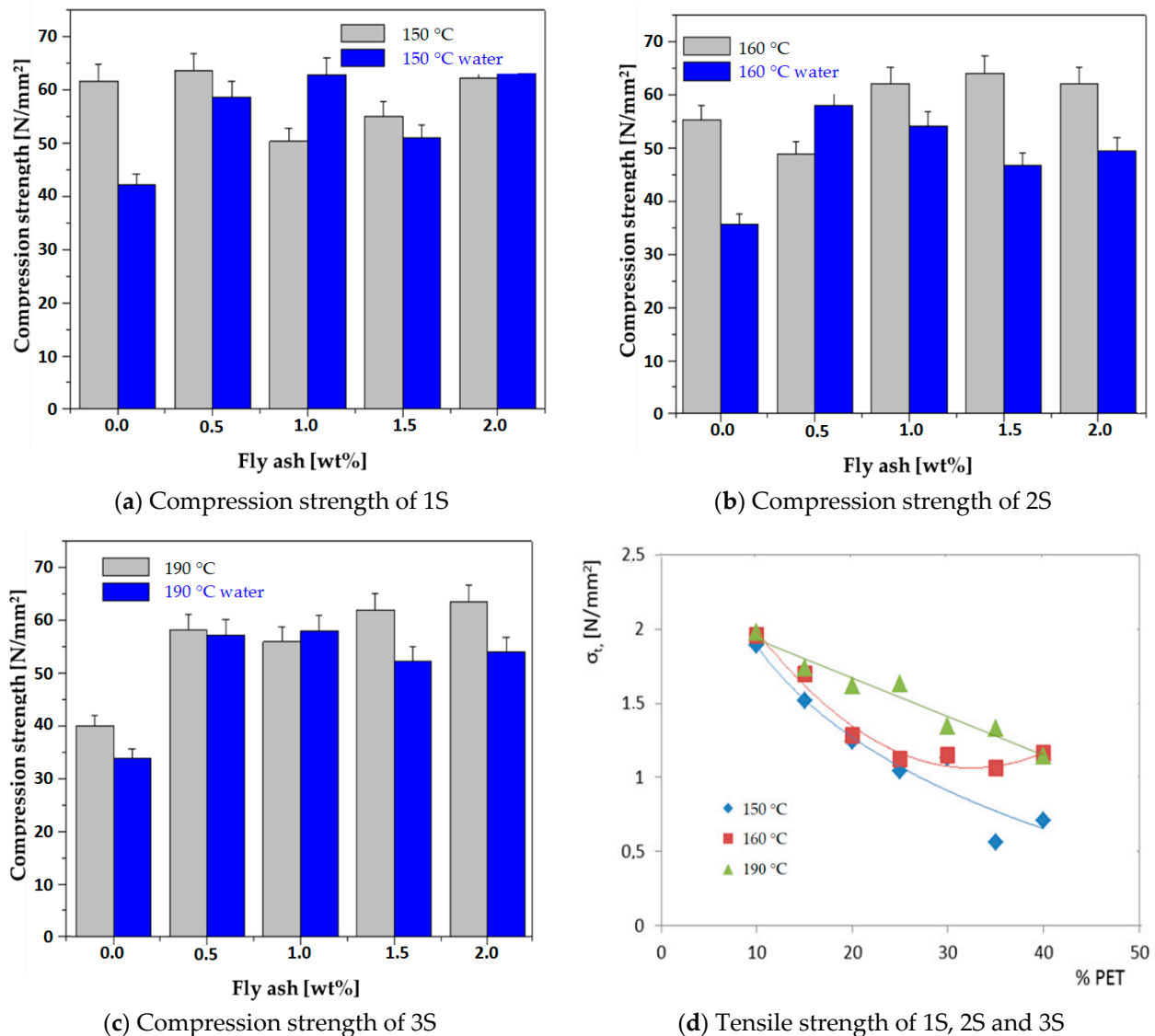


**Figure 2.** Mechanical properties of all waste composites before and after water immersion.

The mechanical properties of a composite system's tensile strength best reflect the interface strength. The curing temperature strongly impacts the composite's mechanical strength. The rubber matrix and HDPE undergo a viscous to fluid phase at the curing temperatures of 150 °C and 160 °C, thus supporting the development of physical–chemical interfaces. Instead, the hydrophilic hemicellulose wood component starts to degrade, and interfaces between rubber, FA, wood, and HDPE are more likely to be formed [31].

The composite cured at 190 °C registered the best tensile strength, and the behavior could be due to the increase in the interface's density. At this temperature, PET undergoes a viscous fluid thermal transition and supports the interface zone extension. The processing temperature of 190 °C compared to the lower ones ensures a tight contact between the composite's components, thus favoring the widening of the interface's zone. The thermal transitions of the rubber, HDPE, and PET alongside the increased amount of hydrophilic wood components degraded favor the development of rubber-PET/HDPE-wood/-rubber-HDPE/rubber-FA interfaces following both mechanisms of physical–chemical bonding and mechanical sticking. The composite's interface is further investigated in the FTIR analysis section.

In the 150 °C and 190 °C composites, we recorded a slight increase in tensile strength, Figure 2. The absorption/desorption mechanism of water molecules that enter the capillary structure, then the micro-cracks, and finally the water diffusion of the composite explain this behavior. The 1S\_FA—2 exhibits good stability in mechanical strength even after water immersion. The water stability of 1S\_FA—2 is entailed by the particular behavior of water molecules, which act as a plasticizing agent when they enter the composite's capillarity structure. The plasticizing water alongside the wood components, which act as a binder in the composite with waste rubber and HDPE [31], enhances the interface strength between the composite's components.

The compressive strength of the pristine series registered an increasing trend as a small fly ash amount was added to the rubber-PET-HDPE-wood blend, Figure 2. The highest compressive strength was assigned to the 2% fly ash composites for all three optimized temperatures. This mechanical behavior is owed to the mechanical strength of fly ash, its rigidity, and especially due to its high SiO<sub>2</sub> content, which exhibits a high affinity for the rubber matrix and thus extending the contact area. There are reports on fly ash's high affinity for rubber matrices [37,38]; thus, hybrid rubber-fly ash interface development is likely to be developed. It is worthy to note that the 160 °C sample recorded the best compression increase after the addition of FA. This behavior was noticed in a previous study for the composite series treated at 160 °C [31]. The rubber-plastic-wood composite produced at T = 160 °C exhibits a particular compression strength increase when inorganic fillers are added. The explanation is related to the composite densification when FA particles enter the sponge-like structure of the rubber-plastic-wood blend, reducing the macromolecular chains' mobility and highly contributing to the increase in the composite's rigidity, as seen in Figure 2. The 190 °C composites with no FA recorded over a 50% lower compression strength compared to those cured at 150 °C and 160 °C, as seen in Figure 2. The decrease in mechanical strength is directly linked to the partial degradation of the wood with a corresponding loss in the composite's mechanical strength. The 3S\_FA—4 registered an outstanding increase in compression strength, with approximately 63 MPa when FA was inserted into the rubber-plastic-wood blend. The composite's resistance increase when fly ash was added could be explained by the rigid and rich silica FA cenospheres, which enter into the composite's capillaries and improve the composite's density.

The water immersion of fly ash composites led to a slight decrease in the compressive strength, as seen in Figure 2. The water immersion of the composites could induce a possible flexibilization of their structure with a subsequent loosening in the structure. However, the samples with 1% fly ash prepared at 150 °C, denoted as 1S\_FA—2, and the 0.5% fly ash sample prepared at 160 °C (2S\_FA—1) registered a significant compression strength increase after their water immersion, 24.75% and 18.96%, respectively. These results prove the synergistic effect of wood, water (plasticizing), and the proper amount of FA on the strength increase in the composite's interface. The FA's cenospheric structure, as was in the SEM analysis section, enters the capillary structure of the composite rubber matrix and leads to a high potential for rubber-FA crosslinking.

The bound water effect (possible with the inorganic filler modifications) is reflected in the tensile strength of composites registered after their immersion in water. The tensile strength of the water immersed composites recorded a slow increase rate, with the highest tensile strength for the 0.5% FA composite prepared at 190 °C, as seen in Figure 2.

These composites could be promising for use in outdoor products (paving slabs, railways, coverings for playgrounds, and sports fields), considering that the matrix can encapsulate the wood components and improve their resistance to humidity and prevent swelling.

#### Surface energy measurements

Considering the outdoor applications of the developed composite based on organic and inorganic phases, the wetting behavior is of the utmost importance because of its influence on aging. The surface energies of the fly ash composites compared to those without FA were determined based on contact angle measurements. The surface energies of composites are strongly influenced by the surface chemical structure, morphology, surface

roughness, the tested liquid type, and the interaction between liquid–surface molecules. The hydrophobic nature of polymer materials with their poor polarity leads to a low contact angle value. The FA composites to be used in outdoor products are required to be resistant to wet environments in order to preserve their interface strength and mechanical characteristics, respectively. The contact angles of the composite surface with both liquid water and glycerol and surface energies  $\sigma_{SV}$  with their components dispersive and polar ( $\sigma_{SV}^d \sigma_{SV}^p$ ) before and after water immersion are summarized in Table 3.

**Table 3.** Surface energies with dispersive and polar components for composites with fly ash unimmersed and water immersed.

| Samples Code | Unimmersed                  |                                |                      |                        |                        | Water Immersed              |                                |                      |                        |                        |
|--------------|-----------------------------|--------------------------------|----------------------|------------------------|------------------------|-----------------------------|--------------------------------|----------------------|------------------------|------------------------|
|              | $\Theta_{\text{water}}$ [°] | $\Theta_{\text{glycerol}}$ [°] | $\sigma_{SV}$ [mN/m] | $\sigma_{SV}^d$ [mN/m] | $\sigma_{SV}^p$ [mN/m] | $\Theta_{\text{water}}$ [°] | $\Theta_{\text{glycerol}}$ [°] | $\sigma_{SV}$ [mN/m] | $\sigma_{SV}^d$ [mN/m] | $\sigma_{SV}^p$ [mN/m] |
| 1S           | 78.40                       | 91.26                          | 81.27                | 11.43                  | 2.56                   | 95.97                       | 88.33                          | 18.80                | 14.56                  | 4.24                   |
| 1S_FA—1      | 104.8                       | 97.9                           | 13.68                | 11.2                   | 2.48                   | 70.26                       | 85.43                          | 43.61                | 40.13                  | 3.48                   |
| 1S_FA—2      | 78.93                       | 103                            | 18.30                | 17.8                   | 0.05                   | 75.6                        | 94.06                          | 55.28                | 47.87                  | 7.41                   |
| 1S_FA—3      | 88.3                        | 103.1                          | 82.51                | 64.75                  | 17.76                  | 96.66                       | 90.83                          | 15.83                | 9.84                   | 5.98                   |
| 1S_FA—4      | 108.1                       | 110.3                          | 12.34                | 0                      | 12.34                  | 94.86                       | 107.96                         | 63.55                | 50.24                  | 13.31                  |
| 2S           | 102.70                      | 94.65                          | 16.63                | 14.45                  | 2.18                   | 88.84                       | 73.47                          | 32.60                | 28.39                  | 4.20                   |
| 2S_FA—1      | 108                         | 99.3                           | 16.06                | 15.14                  | 0.92                   | 82.3                        | 96.16                          | 82.86                | 68.66                  | 14.21                  |
| 2S_FA—2      | 91.2                        | 95.6                           | 12.88                | 12.27                  | 0.61                   | 82.33                       | 86.43                          | 35.16                | 0.04                   | 35.14                  |
| 2S_FA—3      | 107.3                       | 101                            | 11.72                | 9.22                   | 2.51                   | 93.5                        | 96.73                          | 23.73                | 23.72                  | 0.01                   |
| 2S_FA—4      | 108.1                       | 102.2                          | 10.92                | 8.3                    | 2.62                   | 96.06                       | 105.4                          | 42.85                | 37.39                  | 5.46                   |
| 3S           | 86.37                       | 113.61                         | 13.50                | 12.45                  | 1.05                   | 113.3                       | 100.01                         | 28.72                | 28.53                  | 0.19                   |
| 1S_FA—1      | 100.2                       | 90.7                           | 20.94                | 19.22                  | 1.73                   | 95.7                        | 100.36                         | 25.85                | 0.44                   | 25.41                  |
| 1S_FA—2      | 104.2                       | 92                             | 27.83                | 27.68                  | 0.15                   | 92.03                       | 94.53                          | 23.14                | 0.03                   | 23.11                  |
| 1S_FA—3      | 110.7                       | 93.7                           | 47.86                | 46.63                  | 1.43                   | 88.36                       | 94.4                           | 36.39                | 35.31                  | 1.08                   |
| 1S_FA—4      | 111.7                       | 100.8                          | 20.41                | 20.35                  | 0.06                   | 83.7                        | 101.03                         | 52.81                | 52.39                  | 0.42                   |

Almost all of the fly ash composites exhibit low surface energies for all three optimized temperatures. The composites denoted as 1S\_FA—3 and 3S\_FA—3 present a slight surface energy increase compared to all of the others, but it is worthy to note that their dispersive component is prevalent, as seen in Table 3. The contact angle measurement results well match the mechanical tests, which registered good compression strength, thus proving the stiffening effect of FA related to its high content of oxides. The high contact angle values and the low value of the polar components support the FA composite’s hydrophobicity; thus, it has a high potential for application in outdoor products in wet environments. The surface energies and contact angles (with water and glycerol) of water immersed FA composites have shown a similar trend as the unimmersed ones, thus outlining the hydrophobic character of FA composites.

Therefore, poor polarity and low surface energy FA composites well match the requirements of outdoor products (e.g. building materials, tiles, covers for several grounds, pillar sleeves for a carpark and so on).

#### FTIR analysis

The possible hybrid interfaces in the novel all-waste composites were investigated by Fourier Transformed Infrared (FTIR) spectroscopy. During the thermal processing of the polymeric blend with the fly ash, as a result of oxidative processes or reciprocal affinity alongside mechanical adhesion, physical, and/or chemical bonds could be established between the composite’s components.

The FTIR bands of the FA composite with the best combination of mechanical properties (1S\_FA—2) were investigated and compared to that without FA, as shown in Table 4. The FA addition to the rubber-plastic-wood blend brought significant changes to the FTIR spectrum, as can be seen in Figure 3:

- the 1610  $\text{cm}^{-1}$  band assigned to C=C (rubber) or deformation vibration of water from wood disappeared and instead appeared as two bands, 1586 and 1531  $\text{cm}^{-1}$ . The first corresponds to the lignin from wood and the second to the carboxylate group ( $-\text{COO}^-$ ), [32] or C=C from rubber. These changes could be explained by the hybrid interface formation through chemical bonding between rubber, wood, and FA;
- the shift of the of 1458  $\text{cm}^{-1}$  (C=C from rubber) and 1245  $\text{cm}^{-1}$  (C–O–C of PET or wood) to lower wavenumbers 1428 and 1215  $\text{cm}^{-1}$ , respectively; a new band at 1355  $\text{cm}^{-1}$  between the previous occurred and was assigned to wood constituents ( $-\text{CH}_3$  from lignin/hemicellulose/polysaccharide  $-\text{OH}$ ). These results indicate possible chemical interactions between rubber, PET, HDPE, wood, and FA compounds. The shifts of these bands toward lower wavenumbers could explain the interface's flexibilization.
- the appearance of new bands from 1115 (of high intensity) and 537  $\text{cm}^{-1}$  were assigned to silica and other oxides from FA, as seen in Figure 3. These new bands' appearance corresponds to the possible chemical interactions between the matrix and the prevalent silica compounds from fly ash. These results support the mechanical test results, which indicated an increase in the mechanical strength of the composite with fly ash compared to those without fly ash.

**Table 4.** FTIR bands of the composites with and with no FA added.

| FTIR Bands  | 1S   | 1S_FA—2      | Rubber | PET  | HDPE | Wood |
|---|------|--------------|--------|------|------|------|
| OH  | 3354 | 3327         | -      | -    | -    | 3341 |
| aliphatic C–H   | 2911 | 2907         | 2914   |      | 2914 | 2916 |
| $-\text{CH}=\text{CH}_2$                                  | 2845 | 2840         | 2847   | -    | 2847 | -    |
| C=O   | 1714 | 1714         | -      | 1713 | -    | 1721 |
| C=C   | 1610 | 1586<br>1531 | 1617   | -    | -    | -    |
| C=C rubber and HDPE. $-\text{CH}_2$ of PET and CH of wood | 1458 | 1428         | 1431   | 1407 | 1471 | 1421 |
| C–C of rubber. $\text{CH}_3$ of wood                      | -    | 1355         | 1372   | -    | -    | 1369 |
| C–O–C from PET and wood                                   | 1245 | 1215         | -      | 1240 | -    | 1245 |
| C–O–C wood  | 1093 | 1069         |        |      |      |      |
| Si–O stretching vibration (FA)                            |      | 1115         |        |      |      |      |
| C–O–C wood  | 1016 | 1020         |        | 1016 |      | 1025 |
| aromatic nuclei in PET                                    | 837  | 874<br>813   | -      | 872  | -    | -    |
| C–H   | 717  | 717          |        | 723  | 717  | -    |
| FA  |      | 537          |        |      |      |      |

By comparing the FTIR spectra of the 1% FA composite, Figure 4, cured at 150 °C before and after immersion in water, the following changes were noticed, as seen in Table 5.

- The shift to higher wave numbers of 2842, 1722, 1369, 1219, and 719  $\text{cm}^{-1}$  bands. These changes clearly indicate the increased rigidity of the composite structure, as explained by the plasticizing effect of the water in the composite capillaries. The FTIR results confirmed the mechanical test results, which registered an increase in the compression strength and stable tensile strength to water in the 1S\_FA—2 sample.

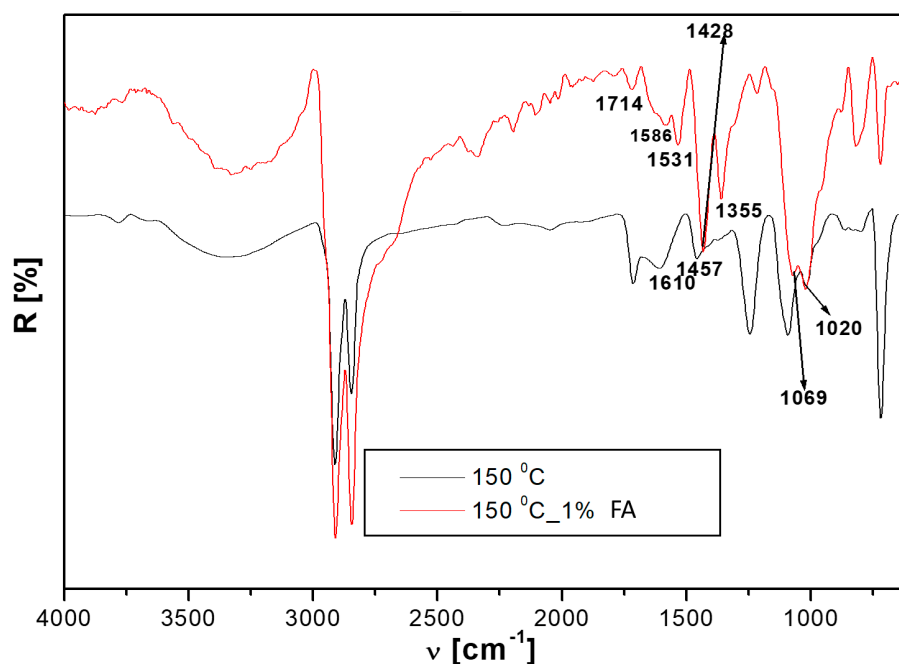


Figure 3. FTIR spectra of samples cured at 150 °C with and without FA, coded as 1S\_FA—2 and 1S.

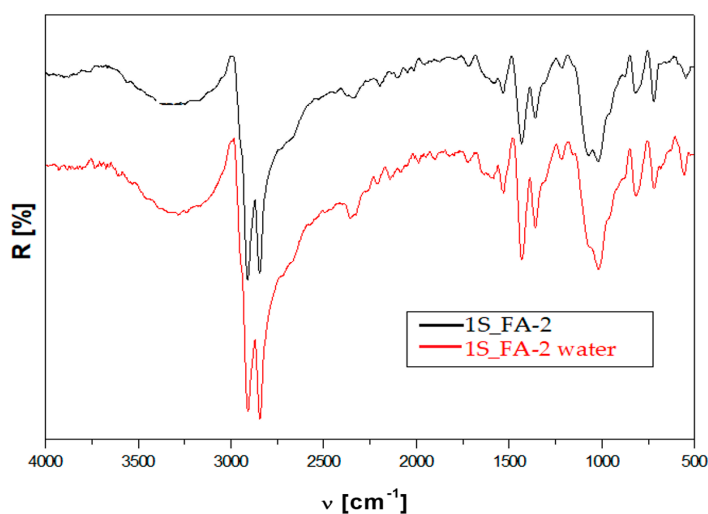


Figure 4. FTIR spectra of 1S\_FA—2 before and after water immersion.

The water immersion of the composite with FA led to some changes; 1069, 1020, and 874  $\text{cm}^{-1}$  bands occurred as a single broader band at 1019  $\text{cm}^{-1}$ . This could be explained by the physical and chemical interactions between PET, wood, and FA made possible through hydrogen bonds. Furthermore, these interactions extend the interface zone, which, in turn, leads to an increase in mechanical strength, as was already noticed in the mechanical test results section.

#### XRD analysis

An XRD investigation was performed to identify the crystalline and amorphous domains of all waste composites with FA and their influence on the mechanical properties. The sample investigated 1S\_FA—2 to explore the best combination of mechanical properties even under humidity and from an economic aspect, being manufactured at the lowest temperature (150 °C). The XRD results are presented compared to samples with no FA addition.

**Table 5.** Representative band values in the IR spectra of water-immersed fly ash composites.

| Specific Groups  | 150 °C | 150 °C. 1% Fly Ash | 150 °C. 1% Fly Ash Immersed | Rubber | PET  | HDPE | Wood |
|--|--------|--------------------|-----------------------------|--------|------|------|------|
| OH   | 3354   | 3327               | 3284                        | -      | -    | -    | 3341 |
| C-H aliphatic  | 2911   | 2907               | 2908                        | 2914   | -    | 2914 | 2916 |
| -CH=CH <sub>2</sub>  | 2845   | 2840               | 2842                        | 2847   | -    | 2847 | -    |
| C=O  | 1714   | 1714               | 1722                        | -      | 1713 | -    | 1721 |
| C=C  | 1610   | 1586<br>1531       | 1584<br>1531                | 1617   | -    | -    | -    |
| C=C rubber and HDPE. -CH <sub>2</sub> in PET și CH in wood | 1458   | 1428               | 1430                        | 1431   | 1407 | 1471 | 1421 |
| C-C in rubber. CH <sub>3</sub> in wood                     | -      | 1355               | 1369                        | 1372   | -    | -    | 1369 |
| C-O-C in PET and wood                                      | 1245   | 1215               | 1219                        | -      | 1240 | -    | 1245 |
| Si-O stretching vibration (FA)                             |        | 1115               | 1118                        |        |      |      |      |
| C-O-C in wood  | 1093   | 1069               |                             |        |      |      |      |
| C-O-C in wood  | 1016   | 1020               | 1019                        |        | 1016 |      | 1025 |
| aromatic nuclei in PET                                     | 837    | 874<br>813         | 815                         | -      | 872  | -    | -    |
| C-H  | 717    | 717                | 719                         |        | 723  | 717  | -    |
| metal oxides   |        | 537                | 552                         |        |      |      |      |

The crystallinity of this composite type is determined by the wood components with their crystalline cellulose and their nucleating agent role on the one hand and on the other hand because of inorganic filler [39–42]. There are reports on the PET nucleating role in wood and HDPE-based composites [43].

The higher crystallinity of the FA composite compared to 1S composites is explained by the increase in the ordered degree as a consequence of the rearrangement of the polymer macromolecular chains. The fly ash, due to its cenospheric shape and high affinity to the matrix, ensures tight contact over a large area with the rubber macromolecular chains. Consequently, the mobility of the macromolecular chains is diminished, which in turn leads to an increase in the ordered degree and a higher crystalline percentage, as shown in the XRD results.

Diffraction patterns of this composite type showed a broad peak due to the amorphous polymer–rubber matrix. The highest intensity peak is assigned to HDPE, with its high symmetry of macromolecules has the largest percentage of crystalline phase.

A slight increase in the crystalline degree was noticed for the water-immersed 1S\_FA—2, as can be seen in Figure 5. This result could be explained by the rearrangement of the macromolecular chains as the water molecules enter the composite capillarity structure.

The crystalline degree of both unimmersed and water immersed 1S\_FA—2 recorded similar values. These XRD results clearly confirm the strong hybrid interface between the components of the composite. These results match the FTIR and mechanical test results, which revealed for 1S\_FA—2 the formation of new chemical bonds and good stability in the mechanical strength even after water immersion.

One may conclude that the crystalline degree could support the composite resistance to water action, conferring thus a rigid matrix that is difficult to weaken or modify.

#### SEM and AFM microscopy

Scanning electron microscopy and atomic force microscopy were performed in order to investigate the quality of the surface morphology and interface structure. Therefore, a low-rugosity surface shows good linking between the composite components and a good interface strength. AFM images were taken over a 50 × 50 μm<sup>2</sup> surface of the composites



with the best combination of mechanical properties (1S\_FA—2) compared to that with no FA (1S).

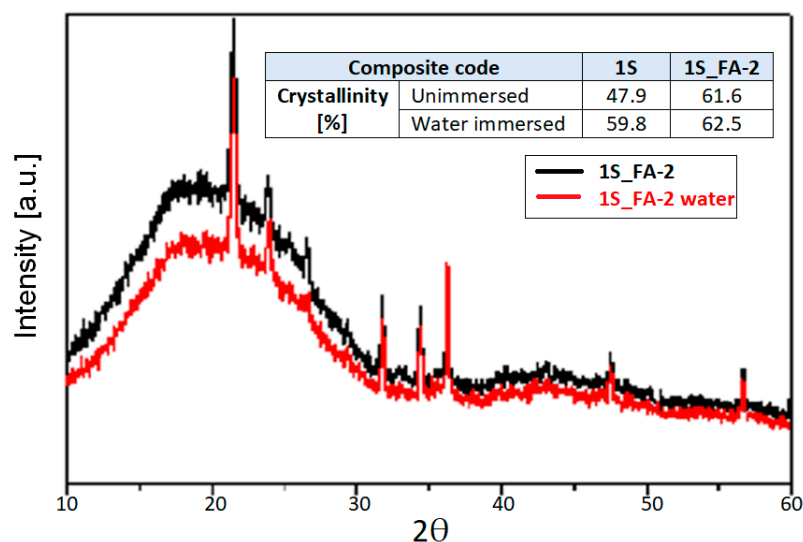


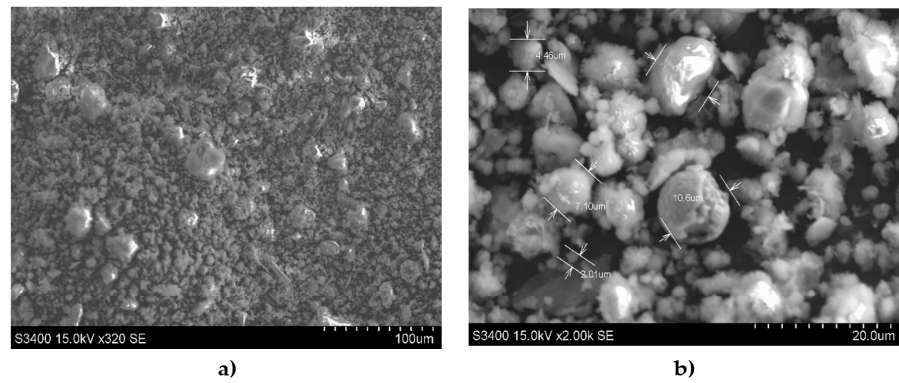
Figure 5. XRD diffractograms of 1S\_FA—2 unimmersed and after water immersion.

The SEM morphology images obtained by the secondary electrons of fly ash evidenced their cenosphere structure with a high specific surface, Figure 6. The FA cenospheres with a 50-times smaller diameter size than the rubber matrix are effective in filling the capillary structure of the rubber-plastic-wood blend, thus enhancing their density. The EDS analysis results pointed out the poly oxides-rich composition of FA with prevalent silica share. These results are in good agreement with the mechanical tests and FTIR results. The first composite strength increase through the composite structure densification due to the addition of FA cenospheres was recorded, and the FTIR results revealed the possible formation of the hybrid interface of rubber-FA type was due to the high silica affinity to the rubber matrix.

The AFM results revealed a decrease in rugosity (RMS = 106.3 nm) for the pristine FA composite (1S\_FA—2) compared to the composite without FA (1S. RMS = 127 nm), Figure 7A,C. The FA composite with the fly ash cenospheres filling the capillarity structure of the composite led to a more compact and homogenous structure for 1S\_FA—2 compared to 1S, as can be seen in Figure 7A,C.

The smoother surface morphology of the FA composite compared to those with no FA may be explained by the good distribution of fly ash cenosphere in the matrix. This behavior is owed to the high affinity between the silica particles and the polymer matrix (rubber) confirmed by the low roughness values, as can be seen in Figure 7C, compared to the composite without FA in Figure 7A. Water-immersed FA composite presents a significant roughness decrease, 20% approximately, compared to that before immersion, Figure 7C,D. The water molecules that enter the capillary structure of the composite act as a plasticizing agent, smoothing the surface of the water-immersed 1S\_FA—2 compared to that of the unimmersed, as can be observed from Figure 7C,D. The increase in surface smoothness of the water-immersed 1S\_F A-2 is explained by the plasticizing effect of water, as can be clearly seen from their topography in the insets of Figure 7C,D.

The decrease in rugosity in the water-immersed 1S\_FA—2 compared to the unimmersed one supports the XRD results, which recorded an increase in the degree of crystallization, and the mechanical tests, which registered an enhancement in the compressive strength.



| Chemical Element | wt. % | At. % |
|------------------|-------|-------|
| O                | 46.85 | 62.81 |
| Na               | 6.89  | 6.42  |
| Mg               | 1.24  | 1.10  |
| Al               | 11.59 | 9.21  |
| Si               | 17.84 | 13.62 |
| S                | 0.42  | 0.28  |
| K                | 1.54  | 0.85  |
| Ca               | 2.68  | 1.43  |
| Ti               | 0.83  | 0.37  |
| Fe               | 10.11 | 3.88  |

Figure 6. SEM morphology of fly ash (a,b) with its chemical elemental composition (c).

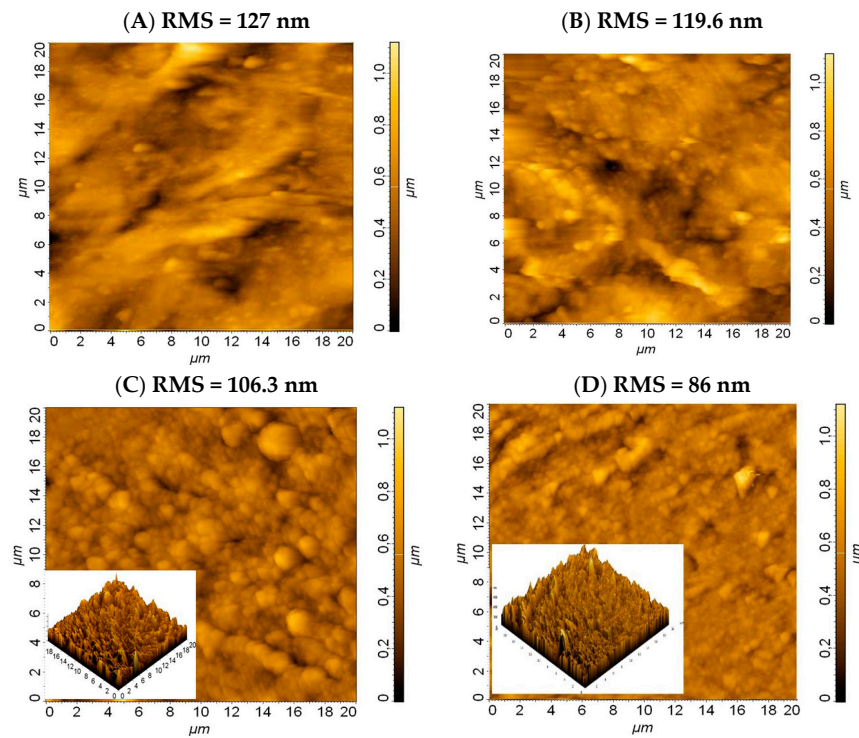


Figure 7. AFM images of 1S\_FA—2 before and after water immersion of: (A) 1S; (B) 1S water immersed; (C) 1S\_FA—2; (D) 1S\_FA—2.

#### 4. Conclusions

The influence of fly ash (FA) cenospheres on the mechanical properties and water stability of the new all-waste composites based on tire rubber, PET, HDPE, and wood sawdust was assessed considering their applications as outdoor products.

The synergistic effect of high stiffness and tensile strength wood alongside rich silica FA with its rigidity was reflected in the superior mechanical properties of the all-waste composites (S-FA type) compared to that without FA (S type). The high FA affinity to the rubber matrix and water as the plasticizer supports strong hybrid interface formation and thus the mechanical strength of rubber-PET-HDPE-wood-FA composites, even in wet conditions. The mechanical performance is well supported by FTIR analyses which outlined hybrid interface formation through chemical bonding. Optimal processing temperature and FA weight ratio in the rubber-PET-HDPE-wood blend are key factors in designing composites with stable mechanical features, even in wet environments.

The best combination of mechanical properties was recorded for 1% FA samples cured at 150 °C and 0.5% FA samples cured at 190 °C.

The water immersion of the rubber-PET-HDPE-wood-FA composite led to a high ordered degree, as the XRD results have shown. The water molecules act as a plasticizer smoothening the composite's surface, as the AFM and contact angle measurements were confirmed by the low rugosity (RMS) and low surface energies, respectively.

The optimal mechanical strength and water stability correspond to the composite cured at 150 °C with 1% fly ash, which could be recommended for outdoor products such as paving slabs, covering playgrounds, and so on.

**Author Contributions:** Conceptualization, M.C. and C.C.; methodology, M.C.; software, M.B.; validation, M.C., C.C. and M.B.; formal analysis, M.C.; investigation, M.C.; resources, M.C. and C.C.; data curation, M.C.; writing—original draft preparation, M.C.; writing—review and editing, M.C.; visualization, M.C., C.C. and M.B.; supervision, M.C.; project administration, M.C. and C.C.; funding acquisition, C.C. All authors have read and agreed to the published version of the manuscript.

**Funding:** This work was supported by a grant from the Romanian National Authority for Scientific Research and Innovation. CCCDI-UEFISCDI. Project number PN-III-P2-2.1-PED-2021-2071. within PNCDI III.

**Conflicts of Interest:** The authors declare no conflict of interest. The funders had no role in the design of the study, in the collection, analyses, or interpretation of data; in the writing of the manuscript or in the decision to publish the results.

#### References





1. Archibong, F.N.; Sanusi, O.M.; Médéric, P.; Aït Hocine, N. An overview on the recycling of waste ground tyre rubbers in thermoplastic matrices: Effect of added fillers. *Resour. Conserv. Recycl.* **2021**, *175*, 105894. [CrossRef]
2. Bowles, A.; Fowler, G.; O'Sullivan, C.; Parker, K. Sustainable rubber recycling from waste tyres by waterjet: A novel mechanistic and practical analysis. *Sustain. Mater. Technol.* **2020**, *25*, e00173. [CrossRef]
3. Fazli, A.; Rodrigue, D. Waste rubber recycling: A review on the evolution and properties of thermoplastic elastomers. *Materials* **2020**, *13*, 782. [CrossRef] [PubMed]
4. Sienkiewicz, M.; Janik, H.; Borzędowska-Labuda, K.; Kucinska-Lipka, J. Environmentally friendly polymer-rubber composites obtained from waste tyres: A review. *J. Clean. Prod.* **2017**, *147*, 560–571. [CrossRef]
5. Grigore, M.E. Methods of Recycling. Properties and Applications of Recycled Thermoplastic Polymers. *Recycling* **2020**, *2*, 24. [CrossRef]
6. Ferdous, W.; Manalo, A.; Siddique, R.; Mendis, P.; Zhuge, Y.; Wong, H.S.; Schubel, P. Recycling of landfill wastes (tyres, plastics and glass) in construction—A review on global waste generation, performance, application and future opportunities. *Resour. Conserv. Recycle.* **2021**, *173*, 105745. [CrossRef]
7. Çınar, M.E.; Kar, F. Characterization of the composite produced from waste PET and marble dust. *Constr. Build. Mater.* **2018**, *163*, 734–741. [CrossRef]
8. Layth, M.; Ansari, M.N.M.; Pua, G.; Jawaid, M.; Islam, M.S. A Review on Natural Fiber Reinforced Polymer Composite and Its Applications. *Int. J. Polym. Sci.* **2015**, *2015*, 243947. [CrossRef]
9. Singh, M.K.; Arora, G.; Tewari, R.; Zafar, S.; Pathak, H.; Sehgal, A.K. Effect of pinecone filler particle size and treatment on the performance of recycled thermoplastics reinforced wood composites. *Mater. Today Proc.* **2022**; *in press*. [CrossRef]

10. Ahmet, S.; Gökhan, H.; Tyagi, V.V. Low cost and eco-friendly wood fiber-based composite phase change material: Development, characterization, and lab-scale thermoregulation performance for thermal energy storage. *Energy* **2020**, *195*, 116983. [CrossRef]
11. Lopez, Y.M.; Gonçalves, F.G.; Paes, J.B.; Gustave, D.; Gutemberg de Alcântara Segundinho, P.; de Figueiredo Latorraca, J.V.; Gomes da Silva, E.S.; Theodoro Nantet, A.C.; Prata Filho, C.M. Comparative study of different technological processes on the physical-mechanical properties and flammability of wood plastic composite. *J. Build. Eng.* **2022**, *52*, 104391. [CrossRef]
12. Chaudemanche, S.; Perrot, A.; Pimbert, S.; Lecompte, T.; Faure, F. Properties of an industrial extruded HDPE-WPC: The effect of the size distribution of wood flour particles. *Constr. Build. Mater.* **2018**, *162*, 543–552. [CrossRef]
13. Zhou, Y.; Wang, Y.; Fan, M. Incorporation of tyre rubber into wood-plastic composites to develop novel multifunctional composites: Interface and bonding mechanisms. *Ind. Crops. Prod.* **2019**, *141*, 111788. [CrossRef]
14. Friedrich, D. Success factors of Wood-Plastic Composites (WPC) as sustainable packaging material: A cross-sector expert study. *Sustain. Prod. Consum.* **2022**, *30*, 506–517. [CrossRef]
15. Martinez, L.Y.; Paes, J.B.; Gustave, D.; Gonçalves, F.G.; Méndez, F.C.; Nantet, A.C.T. Production of wood-plastic composites using cedrela odorata sawdust waste and recycled thermoplastics mixture from the post-consumer products-A sustainable approach for cleaner production in Cuba. *J. Clean. Prod.* **2020**, *244*, 118723. [CrossRef]
16. Zhou, Y.; Hui, D.; Wang, Y.; Fan, M. Nanomechanical and dynamic mechanical properties of rubber-wood-plastic. *Nanotechnol. Rev.* **2022**, *11*, 167–175. [CrossRef]
17. Soccalingame, L.; Bourmaud, A.; Didier, P.; Bénézet, J.C.; Bergeret, A. Reprocessing of wood flour reinforced polypropylene composites: Impact of particle size and coupling agent on composite and particle properties. *Polym. Degrad. Stab.* **2015**, *113*, 72–85. [CrossRef]
18. Lu, J.Z.; Wu, Q.; McNabb, H.S. Chemical coupling in wood fiber and polymer composites: A review of coupling agents and treatments. *Wood Fiber Sci.* **2000**, *32*, 88–104.
19. Gallagher, L.W.; McDonald, A.G. The effect of micron-sized wood fibers in wood-plastic composites. *Maderas Cienc. Technol.* **2013**, *15*, 357–374. [CrossRef]
20. Avramidis, G.; Hauswald, E.; Lyapin, A.; Militz, H.; Viöl, W.; Wolkenhauer, A. Plasma treatment of wood and wood-based materials to generate hydrophilic or hydrophobic surface characteristics. *Wood Mater. Sci. Eng.* **2009**, *4*, 52–60. [CrossRef]
21. Li, M.; Pu, Y.; Thomas, V.M.; Yoo, C.G.; Ozcan, S.; Deng, Y.; Nelson, K.; Ragauskas, A.J. Recent advancements of plant-based natural fiber-reinforced composites and their applications. *Compos. B Eng.* **2020**, *200*, 108254. [CrossRef]
22. Shishkovsky, I.V.; Scherbakov, V.I. Additive manufacturing of polymer composites with nano-titania inclusions. *Laser Phys. Lett.* **2021**, *18*, 066001. [CrossRef]
23. Marwa, A.; Moez, K.; Jamel, M.; Mondher, W.; Fakhreddine, D. Experimental investigation on the mechanical behavior of recycled rubber reinforced polymer composites filled with aluminium powder. *Constr. Build. Mater.* **2020**, *259*, 119845. [CrossRef]
24. Zhou, H.; Wang, X.; Hao, X.; Wang, Q.; Ou, R. Mechanical Properties and Fire Retardancy of Wood Flour/High-Density Polyethylene Composites Reinforced with Continuous Honeycomb-Like Nano-SiO<sub>2</sub> Network and Fire Retardant. *J. Renew. Mater.* **2020**, *8*, 485–498. [CrossRef]
25. Liu, X.; Fu, Z.; Zhang, F.; Wu, M.; Dong, Y. Synthesis of silica Janus nanosheets and their application to the improvement of interfacial interaction in wood polymer composites. *J. Mater. Res. Technol.* **2021**, *15*, 4652–4661. [CrossRef]
26. Abu, S.M.A.; Saif, H.; Munshi, M.I.U.; Elahi, M.M.A.; Sobuz, M.H.R.; Tam, V.W.Y.; Islam, M.S. Assessing the influence of fly ash and polypropylene fiber on fresh mechanical and durability properties of concrete. *J. King Saud Univ. Eng. Sci.* **2021**; in press. [CrossRef]
27. Li, C.; Zhu, H.; Wu, M.; Wu, K.; Jiang, Z. Pozzolanic reaction of fly ash modified by fluidized bed reactor-vapor deposition. *Cem. Concr. Res.* **2017**, *92*, 98–109. [CrossRef]
28. Li, J.; Zhang, W.; Li, C.; Monteiro, P.J.M. Eco-friendly mortar with high-volume diatomite and fly ash: Performance and life-cycle assessment with regional variability. *J. Clean. Prod.* **2020**, *261*, 121224. [CrossRef]
29. Visa, M.; Cosnita, M.; Moldovan, M.; Marin, C.; Mihaly, M. Fly Ash Waste Recycling by Pt/TiO<sub>2</sub> Incorporation for Industrial Dye Removal. *Int. J. Environ. Res.* **2021**, *18*, 3887. [CrossRef]
30. Cosnita, M.; Cazan, C.; Duta, A. Interfaces and mechanical properties of recycled rubber-polyethylene terephthalate-wood composites. *J. Compos. Mater.* **2014**, *48*, 683–694. [CrossRef]
31. Cosnita, M.; Cazan, C.; Duta, A. The influence of inorganic additive on the water stability and mechanical properties of recycled rubber. polyethylene terephthalate. high density polyethylene and wood composites. *J. Clean. Prod.* **2017**, *165*, 630–636. [CrossRef]
32. Vladuta, C.; Voinea, M.; Purghel, E.A.; Duta, A. Correlations between the structure and the morphology of PET-rubber nanocomposites with different additives. *Mater. Sci. Eng. B* **2009**, *165*, 221–226. [CrossRef]
33. Zhang, C.; Tang, Z.; Guo, B.; Zhang, L. Significantly improved rubber-silica interface via subtly controlling surface chemistry of silica. *Compos. Sci. Technol.* **2017**, *156*, S026635381732660X. [CrossRef]
34. Chenchen, T.; Guangyu, C.; Yuxing, F.; Yonglai, L.; Chunmeng, M.; Nanying, N.; Liqun, Z.; Ming, T. Quantitatively identify and understand the interphase of SiO<sub>2</sub>/rubber nanocomposites by using nanomechanical mapping technique of AFM. *Compos. Sci. Technol.* **2019**, *170*, 1–6. [CrossRef]
35. Abbas, Z.M.; Tawfilas, M.; Khani, M.M.; Golian, K.; Marsh, Z.M.; Jhalaria, M.; Simonutti, R.; Stefik, M.; Kumar, S.K.; Benicewicz, B.C. Reinforcement of polychloroprene by grafted silica nanoparticles. *Polymer* **2019**, *171*, 96–105. [CrossRef]

36. Tian, F.; Chen, L.; Xu, X. Dynamical mechanical properties of wood-high density polyethylene composites filled with recycled rubber. *J. Bioresour. Bioprod.* **2021**, *6*, 152–159. [CrossRef]
37. Gunes, I.; Uygunoğlu, T.; Çelik, A.G. Tribological Properties of Fly Ash Blended Polymer Composites. *Matéria (Rio de Janeiro)* **2021**, *26*, e12929. [CrossRef]
38. Stanciu, M.D.; Teodorescu Draghicescu, H.; Tamas, F.; Terciu, O.M. Mechanical and Rheological Behaviour of Composites Reinforced with Natural Fibres. *Polymers* **2020**, *12*, 1402. [CrossRef]
39. Van Krevelen, D.W. *Properties of Polymers*, 3rd ed.; Elsevier: Amsterdam, The Netherlands; Oxford, NY, USA, 1997.
40. Njuguna, J.; Pielichowski, K.; Desai, S. Nanofiller-reinforced polymer nanocomposites. *Polym. Adv. Technol.* **2008**, *19*, 947–959. [CrossRef]
41. Xu, N.; Zhou, W.; Shi, W. Preparation and enhanced properties of poly (propylene)/silica-grafted-hyperbranched polyester nanocomposites. *Polym. Adv. Technol.* **2004**, *15*, 654–661. [CrossRef]
42. Brundle, R.C.; Evans, C.A.; Wilson, S. *Encyclopedia of Materials Characterization*; The Angstrom Laboratory, Materials Analysis Course, Uppsala University, Butterworth-Heinemann: Oxford, UK, 1992.
43. Zhang, L.; Tam, K.C.; Gan, L.H.; Yue, C.Y.; Lam, Y.C.; Hu, X. Effect of nano-silica filler on the rheological and morphological properties of polypropylene/liquid-crystalline polymer blends. *J. Appl. Polym. Sci.* **2003**, *87*, 1484–1492. [CrossRef]

## Article

# Sustainable Rigid Polyurethane Foam from Wasted Palm Oil and Water Hyacinth Fiber Composite—A Green Sound-Absorbing Material

Nathapong Sukhawipat <sup>1,\*</sup>, Laksana Saengdee <sup>2</sup>, Pamela Pasetto <sup>2</sup>, Jatupol Junthip <sup>3</sup>  
and Ekkachai Martwong <sup>4,\*</sup>

- <sup>1</sup> Division of Polymer Engineering Technology, Department of Mechanical Engineering Technology, College of Industrial Technology, King Mongkut's University of Technology North Bangkok, Bangkok 10800, Thailand
- <sup>2</sup> Institut des Molecules et Materiaux du Mans, UMR CNRS 6283, Le Mans Universite, CEDEX 9, 72085 Le Mans, France; laksana.sd@gmail.com (L.S.); Pamela.Pasetto@univ-lemans.fr (P.P.)
- <sup>3</sup> Faculty of Science and Technology, Nakhon Ratchasima Rajabhat University, Nakhon Ratchasima 30000, Thailand; jatupol.j@nrnu.ac.th
- <sup>4</sup> Division of Science, Faculty of Science and Technology, Rajamangala University of Technology Suvarnabhumi, Phra Nakhon Si Ayutthaya 13000, Thailand
- \* Correspondence: nathapong.s@cit.kmutnb.ac.th (N.S.); ekkachai.m@rmutsb.ac.th (E.M.); Tel.: +66-824846930 (N.S.); +66-654516142 (E.M.)

**Abstract:** A novel rigid sound-absorbing material made from used palm oil-based polyurethane foam (PUF) and water hyacinth fiber (WHF) composite was developed in this research. The NCO index was set at 100, while the WHF content was set at 1%wt with mesh sizes ranging from 80 to 20. The mechanical properties, the morphology, the flammability, and the sound absorption coefficient (SAC) of the PUF composite were all investigated. When the WHF size was reduced from 80 to 20, the compression strength of the PUF increased from 0.33 to 0.47 N/mm<sup>2</sup>. Furthermore, the use of small fiber size resulted in a smaller pore size of the PUF composite and improved the sound absorption and flammability. A feasible sound-absorbing material was a PUF composite with a WHF mesh size of 80 and an SAC value of 0.92. As a result, PUF derived from both water hyacinth and used palm oil could be a promising green alternative material for sound-absorbing applications.

**Keywords:** used palm oil; water hyacinth fiber; sound-absorbing material; polyurethane foam

**Citation:** Sukhawipat, N.; Saengdee, L.; Pasetto, P.; Junthip, J.; Martwong, E. Sustainable Rigid Polyurethane Foam from Wasted Palm Oil and Water Hyacinth Fiber Composite—A Green Sound-Absorbing Material. *Polymers* **2022**, *14*, 201. <https://doi.org/10.3390/polym14010201>

Academic Editor: Cristina Cazan

Received: 12 December 2021

Accepted: 2 January 2022

Published: 4 January 2022

**Publisher's Note:** MDPI stays neutral with regard to jurisdictional claims in published maps and institutional affiliations.



**Copyright:** © 2022 by the authors. Licensee MDPI, Basel, Switzerland. This article is an open access article distributed under the terms and conditions of the Creative Commons Attribution (CC BY) license (<https://creativecommons.org/licenses/by/4.0/>).

## 1. Introduction

Polyurethane foam (PUF) is widely used as a sound-absorbing material due to its light weight, ease of manufacture, and tunable properties [1,2]. It has the ability to absorb undesired sound, a serious issue with building structures, affecting human dwellings and comfort [3]. PUF is typically synthesized through the chemical reaction of polyol and isocyanate to form urethane linkage in the presence of a blowing agent. Petroleum-based polyol has been commonly used in the PUF industry. However, the limitations, air pollution, and environmental issues are taken into account. To address these issues, renewable materials including lignin [4], natural rubber [5], and starch [6] could be used as sustainable, and green polyol sources. However, the preparation process is complicated. As a consequence, many researchers are attempting to discover new materials that are easier to produce. Vegetable oils such as soybean oil [7], castor oil [8], rapeseed oil [9], soybean oil [10] and palm oil [11] are promising candidates for PUF synthesis.

Palm oil (PO), which represents the largest global production of vegetable oil, is a low-cost feedstock for PUF preparation and was tried as a replacement for the petroleum-based precursors. Fresh palm oil has been used as a polyol source because of its high activity and easy operation. Chuayjuljit, Sangpakdee and Saravari [12] developed PUF by utilizing PO as the polyol. The stiff PUF was produced, and a closed cell was discovered.

Tanaka et al. [13] developed PUF by combining PO-based polyol, polyethylene glycol (PEG) or diethylene glycol (DEG), and an isocyanate. Because PO-based polyol is a soft segment, it has been claimed that PUF containing a high proportion of PO-based polyol is more flexible. Saifuddin et al. [14] used microwave to make PUF from PO. The finished PUF was hard and rigid. PUF has fairly poor characteristics, which can be enhanced by adding fruit branches and cellulose fiber. The PO-based polyol can even be used as a soft segment of PUF. Palm oil is normally used for cooking. To avoid competition between the uses of palm oil as a food and as a polyol, used palm oil (UPO) is proposed. The UPO benefits include not only reduced environmental waste, but also value-added waste [14–16]. Riyapan et al. [17] prepared PUF from UPO via simultaneous epoxidation and a ring-opening reaction. The PUF sample had low sound absorption coefficients due to its closed-cell and large-cell structure. As a result, the PUF with open-cell and small-cell structures is necessary for effective sound absorption material.

To improve the properties of PUF, organic and inorganic materials have been introduced [10,18]. Although they can improve the properties, their use can lead to pollution and adverse health effects. Therefore, many researchers have attempted to use natural fiber-based cellulose as an additive. According to Berardi and Iannace [19] natural materials such as kenaf, wood, hemp, coconut, straw, and wool have a significant potential to be used in sound absorption applications. Ekici et al. [20] explored the PUF composite with tea leaf addition. The SAC was reported to be enhanced to 0.39 by the addition of 8%wt tea leaf fiber. Jian et al. [21] combined PUF with corn straw powder. The mechanical properties were improved, but close-cell structures were still observed. Chen and Jiang [22] prepared a PUF by adding bamboo leaf particles. It has the potential to improve the characteristics of PUF. Tao, Li and Cai [23] investigated how rice straw fiber and wheat straw fiber affected the sound absorption properties of rigid polyurethane foams. It was discovered that a 5% additive provided effective sound absorption and had a higher open cell. As a consequence, it was discovered that open cell PUF with a low density had significant sound absorption. Thus, incorporating low-density natural-based cellulose into PUF has a promising future. The finding of new low-density cellulose-based material for adding to PUF is the focus.

Water hyacinth fiber (WHF) is stated to be a cellulosic material with low density, high absorption, and a great potential for composite use [24]. WHF is derived from water hyacinth (*Eichhornia crassipes*), a free-floating aquatic plant found worldwide. It has become an environmental issue due to the rapid depletion of minerals and oxygen from water [25]. However, the porous interior structure of the fiber results in a low-density and it has a good prospect for enhancing the characteristics of composite materials. Saratale et al. [26] reported that water hyacinth fiber (WHF) has low-density and high mechanical properties. Abrial et al. [27] validated the mechanical and physical characteristics of WHF once again. It can be used as a polymer addition to increase mechanical and absorption properties. According to the findings, WHF has the potential to be employed as an addition for numerous polymers, including polyester [27] and poly(lactic acid) [28]. Furthermore, the absorption characteristics of WHF are unique due to the porous interior. As a result, it has the absorption applications, in particular the application for heavy metal removal [25]. Sound absorption is another one-of-a-kind use. Setyowati et al. [29] prepared the sound absorption from the water hyacinth and coconut husk based fiber reinforced polymer (FRP) panel. The sound absorption increased accordingly to an SAC of above 0.7. Therefore, many researchers have attempted to use this cellulose as an additive for composite material. For this reason, the focus of this work is on the use of WHF as a PUF additive.

Therefore, this research developed a green rigid sound-absorbing material by combining UPO-based PUF and WHF. The effects of the WHF size on the mechanical properties, morphology and the sound absorption coefficient (SAC) were investigated.

## 2. Materials and Methods

### 2.1. Materials

Used palm oil for preparing recycled palm oil (RPO) was purchased from a Nonthaburi local market, Nonthaburi province (acid value of 1.41 mg KOH/g and iodine value of 40.1 mg I<sub>2</sub>/g). The used palm oil was first filtered before modification. Hydrogen peroxide (H<sub>2</sub>O<sub>2</sub>, 35%) and sodium hydrogen carbonate (NaHCO<sub>3</sub>, >90%) were purchased from Ajax Finechem (Sydney, Australia). Formic acid (HCOOH, 98%) was purchased from Fisher Chemical (Shanghai, China). Ethyl acetate (CH<sub>3</sub>COOC<sub>2</sub>H<sub>5</sub>, >99%) was purchased from RCI Lab-Scan Limited (Bangkok, Thailand). Polymeric diphenylmethane diisocyanate (P-MDI, 31.5% NCO content, functionality = 2.7) was purchased from BASF (Ludwigshafen, Germany). T-12 (dibutyltin dilaurate, 95%) was purchased from Fluka Chemie AG CH-9471 Company (Darmstadt, Germany). Dabco 33LV (33% triethylene diamine in propylene glycol) was purchased from Evonik Goldschmidt GmbH (Essen, Germany). Silicone surfactant (TEGOSTAB<sup>®</sup> B8110) was obtained from Gold-Schmidt (Berlin, Germany). Dried water hyacinth was purchased from Suphanburi province, Thailand. Commercial polyurethane foam, Polyurethane foam/glass fiber, and polyester foam were purchased from a convenience store, Nonthaburi province, Thailand.

### 2.2. Methods

#### 2.2.1. Preparation of Green Polyol from UPO

The green polyol was made from used palm oil (UPO). Both epoxidation and ring-opening reactions were carried out in a single step. Before the reaction, 250 g (0.3 mol) of used palm oil was filtered and dried at 70 °C for 8 h. Dropwise, 57.71 mL (1.5 mol) formic acid was introduced to a 2-L reactor containing the UPO, followed by 50.25 mL hydrogen peroxide (0.75 mol). The mixture was stirred for 4 h at 70 °C at a controlled speed of 200 rpm. The UPO-based polyol was washed with ethyl acetate, saturated NaHCO<sub>3</sub> solution, and NaCl solution, respectively. To obtain pure green polyol or RPO, the sample was evaporated in a rotary evaporator at 40 °C. The iodine value, acid value, and hydroxyl value of the resulting polyol were all determined.

#### 2.2.2. Preparation of WHF Fiber

WHF with mesh sizes of 80, 40, and 20 were provided by starting with a 1 cm length of dried water hyacinth ground with a double blade blender (Thai grinder, Thailand). After grinding, the fine fiber was sieved with 80 mesh, followed 40 mesh, and finally 20 mesh. Before use, all sieved fiber samples were vacuum-dried at 80 °C for 12 h.

#### 2.2.3. Preparation of UPO-Based PUF/WHF Composite

PUF/WHF composites with an NCO index of 100 were prepared in a single step. Table 1 shows the ingredients for all filled foams. A magnetic stirrer set at 250 rpm was used to thoroughly mix the mixtures of RPO, Dabco 33LV, distilled water, and surfactant. WHF was then added to the mixture. The WHF amount was set at 1 mol, and the size of the WHF was varied from 80, 40, and 20 mesh to obtain PUF-WHF-80, PUF-WHF-40, and PUF-WHF-20, respectively. Then, PMDI was added and stirred until the liquid was white. Finally, the completed mixture was transferred to an open mold with a volume of 10 × 10 × 5.5 cm<sup>3</sup> in generating free-rise foam. To finish the polymerization reaction, the PUF composites were completely cured in an oven at 50 °C for 48 h. In this study, neat PUF was made without the addition of WHF to compare with PUF composites.

Figure 1 presents a short overview of the PUF composite preparation process.



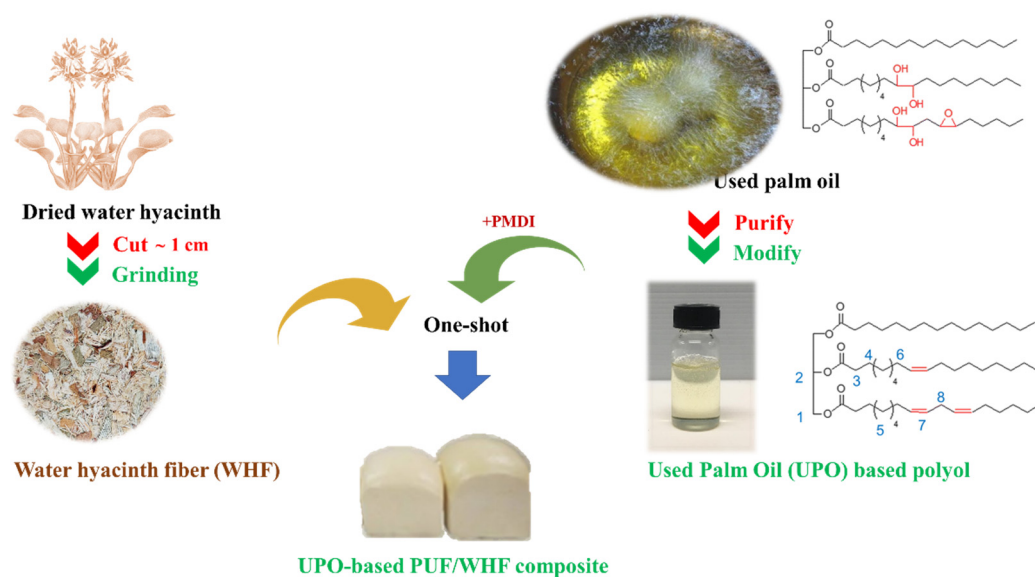


**Figure 1.** A brief overview of the PUF composite preparation process.

**Table 1.** Formulations of UPO-based PUF/WHF composite.

| Sample Name | PUF Precursors (mol) |                  |      | Additives (%wt) |        |        |
|-------------|----------------------|------------------|------|-----------------|--------|--------|
|             | RPO                  | H <sub>2</sub> O | PMDI | WHF-20          | WHF-40 | WHF-80 |
| PUF         | 1                    | 1                | 2    | -               | -      | -      |
| PU-WHF-20   | 1                    | 1                | 2    | 1               | -      | -      |
| PU-WHF-40   | 1                    | 1                | 2    | -               | 1      | -      |
| PU-WHF-80   | 1                    | 1                | 2    | -               | -      | 1      |

### 2.3. Characterization

The iodine values of the RPO were determined by titration to assess the double bonds in the structures, according to ISO3961-2009. The acid values were titrated to analyze the free fatty acids in the oils, according to ISO660-2009. The OH values were titrated to determine the number of OH units in the structures, according to ISO14900-2001.

The chemical structures of UPO and RPO were analyzed by <sup>1</sup>H-NMR with a Bruker 400 Fourier transform spectrometer (Bruker, Berlin, Germany) at 400.13 and 100.62 MHz. All the samples were dissolved in CDCl<sub>3</sub>, using tetramethylsilane (TMS) as the internal standard. Fourier Transform Infrared (FTIR) spectra were recorded with a Nicolet Avatar 370 DTGS FTIR spectrometer (LabX, Midland, ON, Canada) using the range 4000–400 cm<sup>-1</sup>.

The molecular weights of the UPO and RPO samples were analyzed by size exclusion chromatography (SEC) using a Shodex GPC KF-806M column (Shodex, Tokyo, Japan).

The density of the PUF was determined using the ISO4590-2002 test. A Vernier caliper was used to measure the exact dimensions. The density of the specimens was calculated using the equation density = mass/volume.

The compressive stress was measured using Testometric (M500-25AT) on an Instron universal testing machine in accordance with the ISO844-2007 standard (Testometric, Rochdale, UK). All the PUF samples were cut to 50 × 50 × 30 mm<sup>3</sup> size. The crosshead moved at a rate of 2.5 mm/min. The compressive strength was determined using the conventional 10% deformation method. Three duplicates of each sample type were examined, and the average findings were reported in kilopascals (kPa).

The morphology of the PUF composites was examined using a scanning electron microscope (SEM) equipped with a JSM-6510LV (JEOL, Japan) under high vacuum and high voltage settings at 20.00 kV. Before imaging, all of the samples were gold-coated. In addition, to check the structure of the WHF, an optical microscope with a magnification of 5× and Xenon (DN-117M) (Nanjing Jiangnan Novel Optics, Nanjing, China) was utilized.

The moisture absorption of the PUF/WHF composite was studied by placing the sample into the desiccator with a controlled of 60% relative humidity. It was determined in five samples for each formula. The PUF/WHF composite was weighed every day. The moisture absorption rate was calculated by the following Equation (1).

$$A (\%) = W_f - W_i / W_i \times 100 \quad (1)$$

when: A (%) is absorption percentage,  $W_i$  is the initial weight of the PUF/WHF, and  $W_f$  is the weight after obtaining the moisture of the PUF/WHF.

The flammability test was performed according to ASTM D4986. This method is employed for testing the extent and time of the burning of cellular polymeric materials. The foam specimens were burned in a horizontal position with a methane burner. The standard test specimens were  $50 \times 150 \times 13 \text{ mm}^3$ , with the heights 25, 60, and 125 mm marked on them with lines. The time was recorded when the flame reached the 25, 60 and 125 mm marks, and when the specimen extinguishes.

The acoustic characteristics of PUF were investigated in terms of the Sound Absorption Coefficient (SAC) according to ASTM E1050 90, utilizing Kundt's tube, which included an impedance tube, two microphones, and a frequency analyzer (Impedance Measurement Tube Type 4206) (Brüel&Kjær, Nærum, Denmark). The impedance tube equipment contained the B&K Type 1405 Noise generator, the B&K Type 2406 Impedance tube filter and speaker, the B&K Type 2706 power amplifier, the B&K Type 4135 0.25" condenser microphone, a 0.25" microphone calibrator, the B&K Type 2406 small sample tube, the B&K Type 4206 large sample tube, and the 01 dB SYMPHONIE data acquisition hardware. The foam samples were cut to 25 mm diameter and 15 mm thickness and tested with a working frequency range of 500 to 6000 Hz. In this study, commercial polyurethane foam, polyurethane foam/glass fiber, and polyester foam were compared. The SAC was defined as the ratio of the acoustic energy absorbed by the PUF composites ( $I_{\text{incident}} - I_{\text{reflection}}$ ) to the incident acoustic energy ( $I_{\text{incident}}$ ) on the surface, as given in Equation (2).

$$\text{Sound absorption coefficient (SAC), } \alpha = (I_{\text{incident}} - I_{\text{reflection}}) / I_{\text{incident}} \quad (2)$$

where  $I_{\text{incident}}$  is the incident acoustic energy and  $I_{\text{reflection}}$  is the reflected acoustic energy.

### 3. Results

#### 3.1. Characteristic of WHF

Figure 2 shows the physical appearance and optical microscope images of the WHF with different mesh sizes—80, 40, and 20 mesh. The WHFs are a fine, yellowish fiber. The OM images revealed that the WHF fiber of mesh 80, 40, and 20 had a length of 180  $\mu\text{m}$ , 400  $\mu\text{m}$ , and 840  $\mu\text{m}$ , respectively, with a diameter of 20–25  $\mu\text{m}$ . It is relevant to the standard size of the material after sieving in each mesh size. The OM images revealed that the WHF has a porous interior, and this is the point at which WHF should be introduced into the PUF. According to the idea, a material with a high porous structure and a low density can increase the sound absorption qualities [11]. As a result, WHF is one of the best materials for improving sound properties in this study.

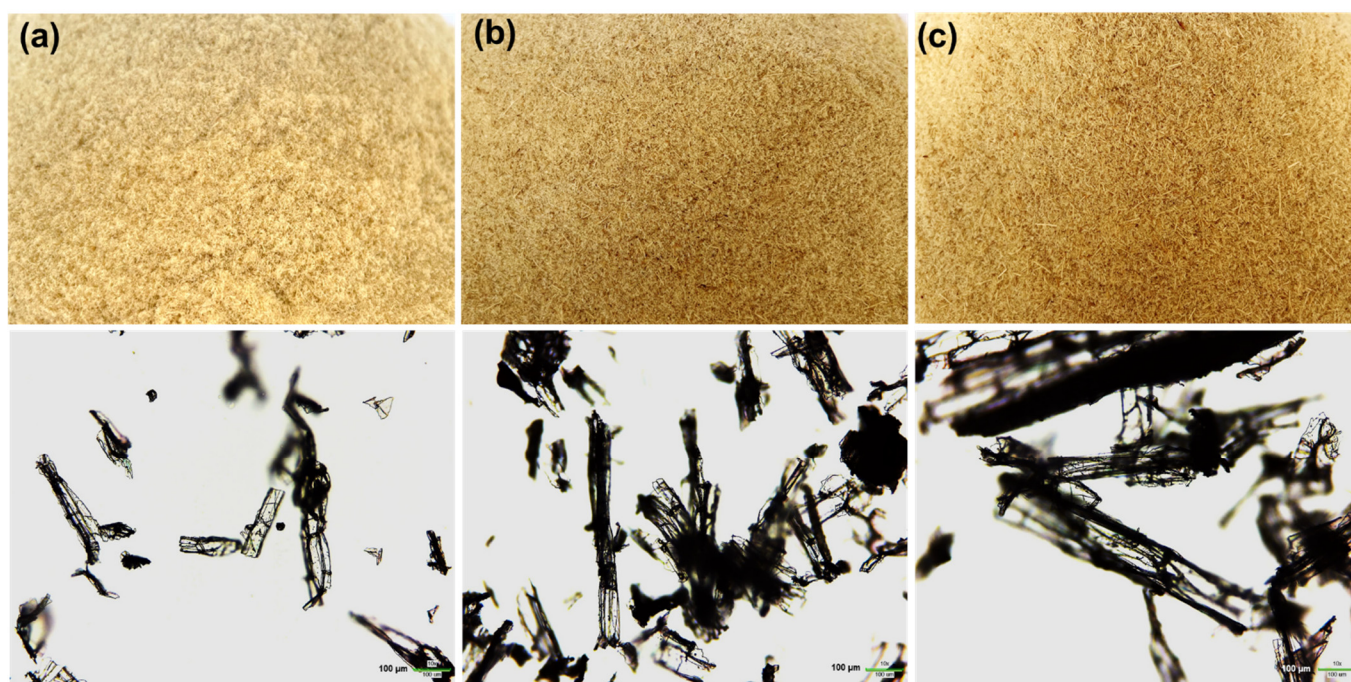


**Figure 2.** Physical appearances (upper) and optical microscope images (lower) of WHF with different mesh size—(a) 80 mesh, (b) 40 mesh and (c) 20 mesh, respectively.

### 3.2. UPO and UPO-Based Polyol

#### 3.2.1. Properties of UPO and UPO-Based Polyol

Table 2 lists the specific properties of the UPO and the RPO precursors of PUF/WHF composites. After conversion of UPO to RPO, the iodine number, which indicates the quantity of double bonds on the oil structure, reduced from 40.1 to 0.51. The OH values, which indicate the presence of a hydroxyl group on the structure of UPO and RPO, increased from 0 to 192.19 mg. KOH/g. After the process, the acid number related to the free acid in the UPO and the residual acid increased slightly from 1.41 to 1.76 mg. KOH/g. These findings revealed that the UPO was effectively changed by oxidation and hydroxylation to form UPO-based polyol, which corresponded to Riyapan et al. [17].

**Table 2.** Properties of UPO and UPO-based polyol.

| Sample Name      | Iodine Number | OH Value (mg. KOH/g) | Acid Number (mg. KOH/g) | Molecular Weight by SEC |               |      |
|------------------|---------------|----------------------|-------------------------|-------------------------|---------------|------|
|                  |               |                      |                         | $M_n$ (g/mol)           | $M_w$ (g/mol) | PDI  |
| UPO              | 40.1          | 0                    | 1.41                    | 2841                    | 3074          | 1.08 |
| UPO-based polyol | 0.51          | 192.19               | 1.76                    | 3073                    | 3150          | 1.02 |

Furthermore, the molecular weight of the UPO and UPO-based polyol was measured using the SEC method. The SEC result is presented in Figure 3. It was found that the molecular weight of polyol-based UPO is higher than that of UPO. Because of the breakage of a double bond to produce OH functional groups on the polyol structure, the  $M_n$  value rose from 2841 to 3073 g/mol. The polydispersity index (PDI) dropped from 1.08 to 1.02. Furthermore, the FTIR and  $^1\text{H-NMR}$  methods were used to validate the chemical structures and functional groups of the UPO and UPO-based polyol.

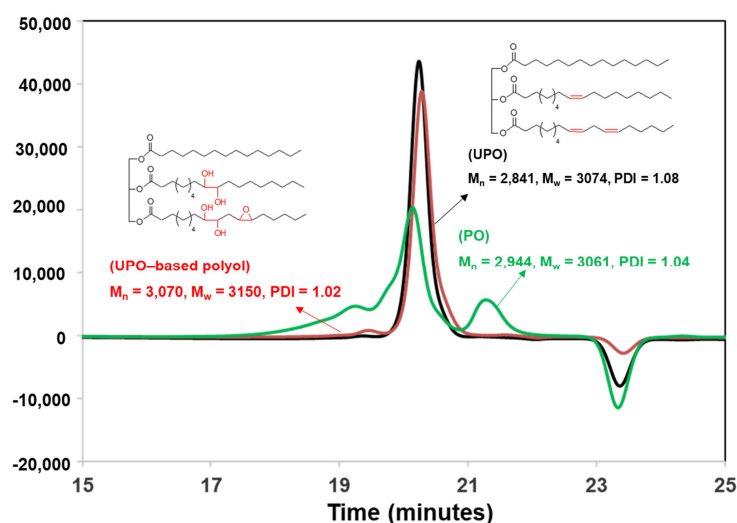


Figure 3. SEC traces of the PO, UPO and UPO-based polyol.

### 3.2.2. Chemical Structure Confirmation

The chemical structure of UPO and polyol-based UPO was confirmed by FTIR and  $^1\text{H-NMR}$ . Figure 4 presents their spectra results. Figure 4a illustrates the  $^1\text{H-NMR}$  spectra results of UPO and UPO-based polyol. The vital peaks at 4.2, 5.1, and 5.3 ppm were assigned to 1, ( $-\text{CH}_2\text{O}(\text{C}=\text{O})$ ), 2 ( $-\text{CHO}(\text{C}=\text{O})$ ), and 7, ( $-\text{CH}=\text{CH}-$ ), respectively. This implied the typical structure of triglyceride. Following the alteration, additional peaks at 3.0 ppm corresponding to methine protons (11, ( $-\text{CH}_2\text{CH}(\text{OH})$ )) were discovered. Furthermore, a peak at 5.3 ppm disappeared due to the absence of the double bond in the triglyceride structures. These findings verified the effective synthesis of the UPO-based polyol.

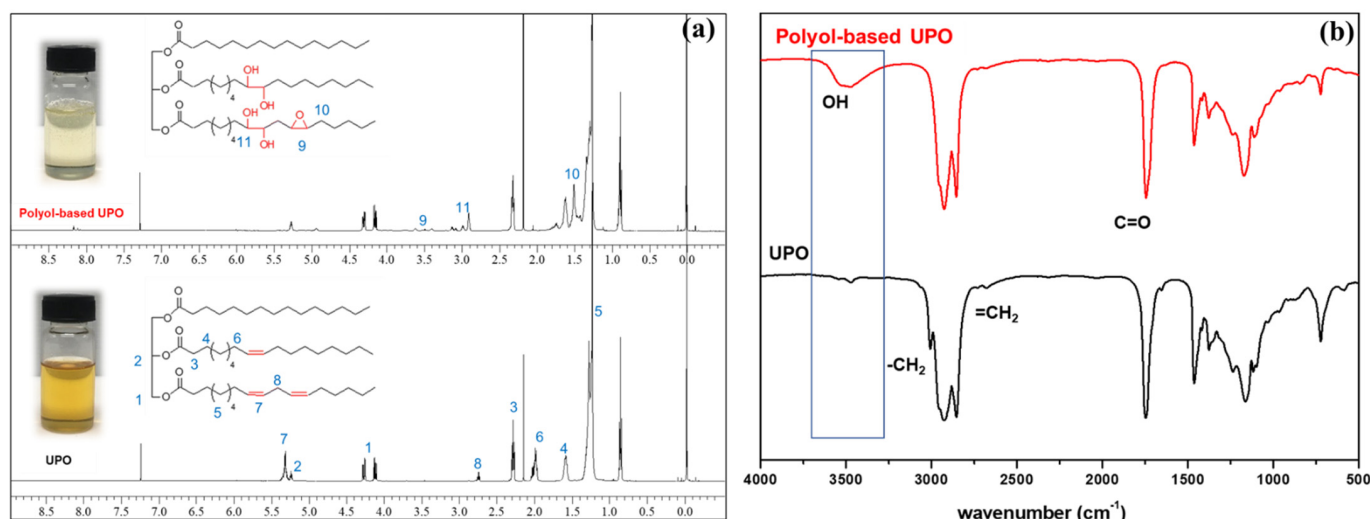


Figure 4. (a)  $^1\text{H-NMR}$  spectra and (b) FTIR spectra of UPO and polyol-based UPO.

Figure 4b presents the FTIR spectra of UPO and UPO-based polyol. The vibration bands of the UPO sample were found at 1150, 1600, 2800–3000, and 3100  $\text{cm}^{-1}$ , which were attributed to the C–O–C, C=O, C–H, and =CH double bonds of triglyceride functional groups, respectively. After the modification, a new broad peak at 3300–3500  $\text{cm}^{-1}$  was observed, indicating the existence of the OH group.

As a result of these chemical structural results, the OH group on the UPO-based polyol may be employed as a green polyol to manufacture the PUF and PUF/WHF composites.

### 3.3. PUF/WHF Composite

#### 3.3.1. Properties of PUF/WHF Composite

Table 3 lists the properties of the PUF/WHF composite. The PUF was compared to the PUF/WHF composites in the blank test. The PUF had a cream time of 12, a rise time of 23, and a track free time of 1282 s. The cream time and the rise time for the PUF/WHF sample rose as the WHF size increased. The cream time and the rise time of the PUF-WHF-80 with the smallest size of WHF were 13 s and 27 s, respectively, whereas the cream time and the rise time of the PUF-WHF-20 were 14 and 35 s. The track-free time of the PUF/WHF composite, on the other hand, reduced as the WHF size increased. The PUF-WHF-80 had a track-free time of 1255 s, while the PUF-WHF-20 had a time of 1154 s. These findings suggested that the size of the WHF might inhibit the production of PUF during the creation of urethane linkages.

**Table 3.** Properties of RPO-based PUF/WHF Composites.

| Sample Name | Cream Time (s) | Rise Time (s) | Track Free Time (s) | Height (cm) | Density (g/mL) | Hardness (Shore OO) | Compressive Strength (kPa) |
|-------------|----------------|---------------|---------------------|-------------|----------------|---------------------|----------------------------|
| PUF         | 12             | 23            | 1282                | 8.4         | 0.095          | 29                  | 0.027 ± 0.003              |
| PUF-WHF-20  | 14             | 35            | 1154                | 6.2         | 0.066          | 33                  | 0.047 ± 0.005              |
| PUF-WHF-40  | 14             | 32            | 1205                | 7.5         | 0.062          | 37                  | 0.042 ± 0.007              |
| PUF-WHF-80  | 13             | 27            | 1255                | 8.0         | 0.061          | 45                  | 0.033 ± 0.003              |

The heights of the PUF, PUF-WHF-80, PUF-WHF-40, and PUF-WHF-20 were 8.4, 8.0, 7.5, and 6.2 cm, respectively. The results showed that the WHF with a large size might reduce the track-free time due to the restriction of the foam growth. Furthermore, the mechanical characteristics of the WHF were superior to those of the PUF due to the greater limit of the PUF expansion. As a result, WHFs with a large size lowered the expansion of the PUF composite and height values.

Another property was the density values. The presence of the WHF reduced the density. Long fiber has a higher density than short fiber, whereas WHF has a lower density than neat PUF. As a result, the density of PUF-WHF-20 is higher than PUF-WHF-80 but lower than that of neat PUF.

The hardness (shore OO) of the PUF composites was also measured. The hardness values of the PUF, PUF-WHF-80, PUF-WHF-40, and PUF-WHF-20 were 29, 45, 37, and 33, respectively. The results revealed that when fine fiber was introduced, the hardness of the PUF composites increased. It is due to the reinforcing effects of the additives. When a smaller fiber with a higher surface area was introduced, the increased hardness was exhibited.

The mechanical characteristics of the PUF/WHF composite were reported in terms of compression strength, as illustrated in Figure 3. The compression strengths of the neat PUF, PU-WHF-80, PU-WHF-40, and PU-WHF-20 were 0.027, 0.033, 0.042, and 0.047 kPa, respectively. This finding indicates that a large size of WHF could increase the compression strength of the PUF/WHF composite, which was relevant with the foam expansion. It is possible that chain entanglement of long fiber might form between the long fibers.

#### 3.3.2. Morphology of PUF/WHF Composite

Figure 5 illustrates the morphological results of the PUF composites. The neat PUF had a closed-cell structure with a large cell size ranging from 0.20 to 1.30 mm. The addition of the WHF resulted in the formation of open-cell foam. During foam expansion, the interface between the WHF and the PUF matrix is weak, and the WHF damages the closed cells of the PUF. As a result, adding WHF to PUF results in more open cells than that of neat PUF. This result is related to the work of Tao et al. [23] and Członka et al. [10]. However, because the strength of the long fiber was greater than the PUF, the biggest additive fiber, PUF-WHF-20, could not expand as much as it could. The short fibers, WHF-40 and WHF-80,

on the other hand, may be well-dispersed in the PUF matrix and generate more open cells for the PUF. The distribution of cell foam in smaller sizes was observed as the short fiber was filled. As a result, the addition of WHF-80 resulted in more open cells and a reduction in the cell size of the PUF composite. Furthermore, it was discovered that when a small size of WHF was applied, the regularity of the cell foam and cell size distribution improved. One of the purposes of this work is to increase the sound absorption capabilities of PUF by using an open cell and a small pore size [30]. As a result, the aim of the PUF composites with a small size and more open cells is achieved.

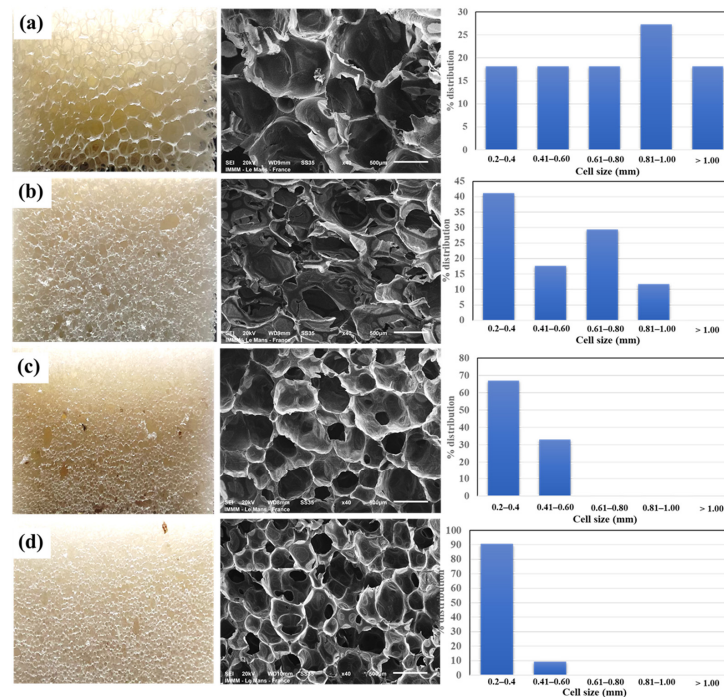


**Figure 5.** (left) Physical appearances, (middle) SEM images of PUF composite series (at a magnification of  $\times 30$ ) and (right) histograms of their cell diameter distributions of PUF composites—(a) PUF, (b) PUF-WHF-20, (c) PUF-WHF-40, and (d) PUF-WHF-80, respectively.

### 3.3.3. Moisture Absorption of PUF/WHF Composite

Moisture absorption was also studied in order to evaluate the behavior of the materials over the use term. In comparison to the real condition, the relative humidity was controlled at 60%. Figure 6 demonstrates the moisture absorption of the PUF compared to the PUF composite. The neat PUF has a moisture-absorption range of 1.1–2.5% after 7 days. The neat PUF is the lowest, whereas adding the WHF enhanced moisture absorption. The PUF/WHF with a lower size of WHF absorbs more than the large size. The PU is normally classified based on its low polarity and water resistance [31]. As a result, it has a low moisture absorption rate. Meanwhile, the addition of WHF results in an open cell and improves the polarity of the PUF composites. Through the open cell, moisture may be delivered into the pore of PUF. It is related to the SEM image of the PUF composites, which exhibits more open cells when the WHF is small compared to when the WHF is large.

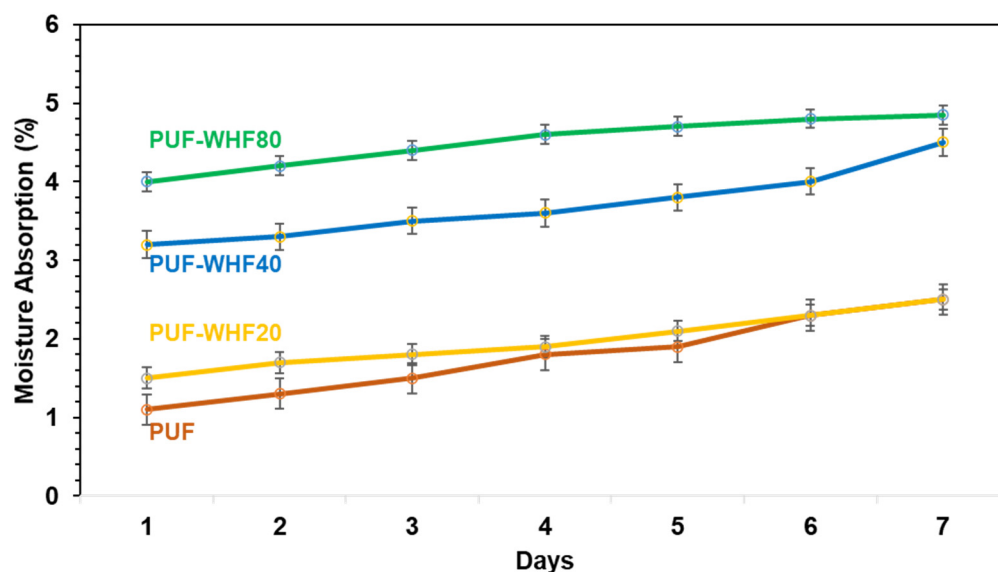
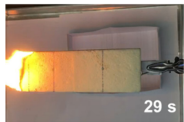













Figure 6. The moisture absorption of PUF and PUF/WHF composite over 7 days.

### 3.3.4. Flammability

Table 4 shows the flammability of the PUF and PUF/WHF composites with varying WHF sizes. It takes around 125 s to burn a PUF sample to 125 mm. Meanwhile, the addition of WHF with mesh sizes of 20 and 40 resulted in a decrease in burning time. The addition of WHF with a mesh size of 80, on the other hand, can increase flame resistance. It takes around 214 s to reach 125 mm. One of the possibilities is that the addition of WHF caused the cell to open, allowing oxygen to flow to the cell. It can effectively use air to support combustion and make a flame spread quickly [32]. However, when fine fiber is burned, the ashes obscure the fire path and make it more difficult to ignite. As a result, PUF/WHF-80 is the most flame resistant.

Table 4. Flammability of PUF and PUF/WHF composites.

| Sample     | Burning Time (s)  |   |   |
|------------|---|---|---|
|            | 25 mm   | 60 mm   | 125 mm  |
| PUF        |  |  |  |
| PUF-WHF-20 |  |  |  |
| PUF-WHF-40 |  |  |  |
| PUF-WHF-80 |  |  |  |

### 3.3.5. Sound Absorption Properties

The sound absorption coefficient (SAC) was used to assess the sound absorption qualities throughout a frequency range of 500 to 6000 Hz. Figure 7 shows the results

of evaluating the PUF/WHF composites compared to the commercial PUF, PUF/glass fiber, and polyester foam. Any material having an SAC greater than 0.4 is defined sound-absorbing material [33]. The average SAC of the PUF composites was more than 0.5, with the PUF-WHF-80 obtaining the highest. The efficiency of the sound absorption could be described by the cell foam number. According to Ji et al. [30], the sound-absorption performance of PUF was controlled by the number of pores, and the more the pores, the greater the sound-absorption performance. Furthermore, the inclusion of low-density material could enhance the SAC at a low frequency range. As a result, the PUF with WHF-80, which has the lowest density and the most cell pores, was the best possible sound-absorbing material. Furthermore, the two-peak tendency on the SAC was discovered in the prepared PUF composites. It is because there are varied cell sizes in the PUF composite and the trend of the SAC spectra is comparable to the findings of Chen and Jiang [22].

In comparison, the commercial PUF and PUF/glass fiber had SACs of 0.4, whereas the polyester foam approached 0.85 in the high frequency range. The prepared PUF composites are therefore superior sound-absorbing materials compared to the commercial ones, based on the efficiency of the SAC findings. Furthermore, PUF-WHF-80 was a suitable sound-absorbing material derived from bio-mass with a high potential for sound absorption and is a prospective option for industrial green manufacturing, with the highest SAC value of 0.92.

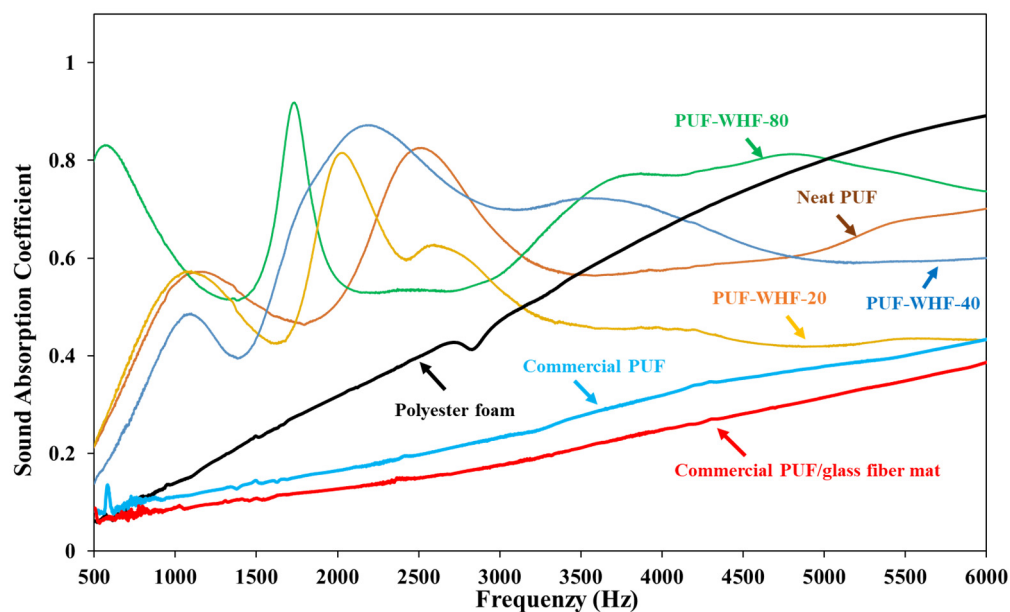


**Figure 7.** SAC spectra of PUF/WHF composites series compared with commercial sound absorption materials.

#### 4. Conclusions

The high efficiency of the UPO-based PUF sound-absorbing material, with an NCO index of 100 and 1%wt of WHF, was successfully developed. The size of a fiber has a significant impact on its morphology, mechanical characteristics, flammability and sound absorption. The manufacture of sound-absorbing material with an SAC value of 0.92 was appropriate for the PUF with an 80 mesh size. Furthermore, a biomass-based substance generated from discarded water hyacinth and UPO might be a promising candidate for the sound-absorbing material industry.



**Author Contributions:** N.S.: conceptualization, investigation, writing—original draft, writing—review & editing, supervision, visualization, funding acquisition; L.S.: writing—review & editing, investigation; P.P.: writing—review & editing, visualization; J.J.: writing—review & editing; E.M.: writing—review & editing, funding acquisition. All authors have read and agreed to the published version of the manuscript.

**Funding:** This research was funded by College of Industrial Technology, King Mongkut's University of Technology North Bangkok (Grant No. Res-CIT0269/2021).

**Institutional Review Board Statement:** Not applicable.

**Informed Consent Statement:** Not applicable.

**Data Availability Statement:** The study did not report any data.

**Acknowledgments:** This research was funded by College of Industrial Technology, King Mongkut's University of Technology North Bangkok (Grant No. Res-CIT0269/2021). The author would like to thank Thanathach Yingshataporn-a-nan, Tanapat Minanandana and Kitchapat Puksuwan for their help. Moreover, the author would like to express our thanks to Nitinart Saetung, Anuwat Saetung and Yeampon Nakaramontri for their suggestions.

**Conflicts of Interest:** The authors declare no conflict of interest.

## References


1. Abdollahi Baghban, S.; Khorasani, M.; Mir Mohamad Sadeghi, G. Soundproofing flexible polyurethane foams: Effect of chemical structure of chain extenders on micro-phase separation and acoustic damping. *J. Cell. Plast.* **2019**, *56*, 167–185. [CrossRef]
2. Cao, L.; Fu, Q.; Si, Y.; Ding, B.; Yu, J. Porous materials for sound absorption. *Compos. Commun.* **2018**, *10*, 25–35. [CrossRef]
3. Rey, R.; Fernandez, J.; Arenas, J.; Sanchis, V. Sound absorbing materials made of recycled polyurethane foam. In Proceedings of the 40th International Congress and Exposition on Noise Control Engineering 2011, INTER-NOISE 2011, Osaka, Japan, 4–7 September 2011; pp. 1–6.
4. Kostopoulos, V.; Kotrotsos, A.; Baltopoulos, A.; Tsantzalis, S.; Tsokanas, P.; Loutas, T.; Bosman, A.W. Bio-based polyurethane prepared from Kraft lignin and modified castor oil. *Express Polym. Lett.* **2016**, *10*, 914–926. [CrossRef]
5. Saetung, A.; Rungvichaniwat, A.; Campistron, I.; Klinpituksa, P.; Laguerre, A.; Phinyocheep, P.; Doutres, O.; Pilard, J.-F. Preparation and physico-mechanical, thermal and acoustic properties of flexible polyurethane foams based on hydroxytelechelic natural rubber. *J. Appl. Polym. Sci.* **2010**, *117*, 828–837. [CrossRef]
6. Kwon, O.-J.; Yang, S.-R.; Kim, D.-H.; Park, J.-S. Characterization of polyurethane foam prepared by using starch as polyol. *J. Appl. Polym. Sci.* **2007**, *103*, 1544–1553. [CrossRef]
7. Fan, H.; Tekeei, A.; Suppes, G.J.; Hsieh, F.-H. Properties of Biobased Rigid Polyurethane Foams Reinforced with Fillers: Microspheres and Nanoclay. *Int. J. Polym. Sci.* **2012**, *2012*, 474803. [CrossRef]
8. Zhang, L.; Zhang, M.; Hu, L.; Zhou, Y. Synthesis of rigid polyurethane foams with castor oil-based flame retardant polyols. *Ind. Crops Prod.* **2014**, *52*, 380–388. [CrossRef]
9. Fourati, Y.; Hassen, R.B.; Bayramoğlu, G.; Boufi, S. A one step route synthesis of polyurethane network from epoxidized rapeseed oil. *Prog. Org. Coatings* **2017**, *105*, 48–55. [CrossRef]
10. Członka, S.; Strąkowska, A.; Strzelec, K.; Kairyte, A.; Kremensas, A. Bio-Based Polyurethane Composite Foams with Improved Mechanical, Thermal, and Antibacterial Properties. *Materials* **2020**, *13*, 1108. [CrossRef]
11. Polaczek, K.; Kurańska, M.; Auguścik-Królikowska, M.; Prociak, A.; Ryszkowska, J. Open-cell polyurethane foams of very low density modified with various palm oil-based bio-polyols in accordance with cleaner production. *J. Clean. Prod.* **2021**, *290*, 125875. [CrossRef]
12. Chuayjuljit, S.; Sangpakdee, T.; Saravari, O. Processing and properties of palm oil-based rigid polyurethane foam. *J. Met. Mater. Miner.* **2017**, *17*, 17–23.
13. Tanaka, R.; Hirose, S.; Hatakeyama, H. Preparation and characterization of polyurethane foams using a palm oil-based polyol. *Bioresour. Technol.* **2008**, *99*, 3810–3816. [CrossRef]
14. Saifuddin, N.M.; Wen, C.; Zhan, W.; Ning, X. Palm Oil Based Polyols for Polyurethane Foams Application. In Proceedings of the International Conference on Advances in Renewable Energy Technologies, Putrajaya, Malaysia, 6–7 July 2010.
15. Kairyte, A.; Kirpluks, M.; Ivdre, A.; Cabulis, U.; Vaitkus, S.; Pundienė, I. Cleaner production of polyurethane foam: Replacement of conventional raw materials, assessment of fire resistance and environmental impact. *J. Clean. Prod.* **2018**, *183*, 760–771. [CrossRef]
16. Used Cooking Oils. Available online: <http://brocklesby.org/used-cooking-oils/> (accessed on 9 October 2021).
17. Riyapan, D.; Saetung, A.; Saetung, N. A Novel Rigid PU Foam Based on Modified Used Palm Oil as Sound Absorbing Material. *J. Polym. Environ.* **2019**, *27*, 1693–1708. [CrossRef]
18. Lin, J.H.; Chuang, Y.C.; Huang, C.H.; Li, T.T.; Lou, C.W. Organic/Inorganic Acoustic-Absorbing/Thermal Insulating Fiber-Reinforced PU Composite Foam Boards. *Appl. Mech. Mater.* **2015**, *749*, 270–273. [CrossRef]

19. Berardi, U.; Iannace, G. Predicting the sound absorption of natural materials: Best-fit inverse laws for the acoustic impedance and the propagation constant. *Appl. Acoust.* **2017**, *115*, 131–138. [CrossRef]
20. Ekici, B.; Kentli, A.; Küçük, H. Improving Sound Absorption Property of Polyurethane Foams by Adding Tea-Leaf Fibers. *Arch. Acoust.* **2012**, *37*, 515–520. [CrossRef]
21. Jiang, D.; Wang, Y.; Li, B.; Sun, C.; Guo, Z. Environmentally friendly alternative to polyester polyol by corn straw on preparation of rigid polyurethane composite. *Compos. Commun.* **2020**, *17*, 109–114. [CrossRef]
22. Chen, S.; Jiang, Y. The acoustic property study of polyurethane foam with addition of bamboo leaves particles. *Polym. Compos.* **2018**, *39*, 1370–1381. [CrossRef]
23. Tao, Y.; Li, P.; Cai, L. Effect of Fiber Content on Sound Absorption, Thermal Conductivity, and Compression Strength of Straw Fiber-filled Rigid Polyurethane Foams. *Bioresources* **2016**, *11*, 4159–4167. [CrossRef]
24. Potluri, R.; Sreenivasa Rao, M. *Water Absorption and Density Tests on the Water Hyacinth-Based Partial Green Composite BT—Advances in Manufacturing Technology*; Hiremath, S.S., Shanmugam, N.S., Bapu, B.R.R., Eds.; Springer: Singapore, 2019; pp. 77–88.
25. Ibrahim, H.S.; Ammar, N.S.; Soylak, M.; Ibrahim, M. Removal of Cd(II) and Pb(II) from aqueous solution using dried water hyacinth as a biosorbent. *Spectrochim. Acta Part A Mol. Biomol. Spectrosc.* **2012**, *96*, 413–420. [CrossRef] [PubMed]
26. Saratale, R.G.; Cho, S.-K.; Ghodake, G.S.; Shin, H.-S.; Saratale, G.D.; Park, Y.; Lee, H.-S.; Bharagava, R.N.; Kim, D.-S. Utilization of Noxious Weed Water Hyacinth Biomass as a Potential Feedstock for Biopolymers Production: A Novel Approach. *Polymers* **2020**, *12*, 1704. [CrossRef] [PubMed]
27. Abrial, H.; Kadriadi, D.; Rodianus, A.; Mastariyanto, P.; Ilhamdi; Arief, S.; Sapuan, S.M.; Ishak, M.R. Mechanical properties of water hyacinth fibers—polyester composites before and after immersion in water. *Mater. Des.* **2014**, *58*, 125–129. [CrossRef]
28. Buasri, A.; Chaiyut, N.; Petsungwan, T.; Boonyuen, Y.; Moonmanee, S. Effect of Surface Treatment on Interfacial and Properties of Water Hyacinth Fiber Reinforced Poly(Lactic Acid) Composites. *Adv. Mater. Res.* **2012**, *463–464*, 449–452. [CrossRef]
29. Setyowati, E.; Yahya, I.; Supriyo, E.; Romadhona, I.C.; Minardi, A. On the Sound Absorption Improvement of Water Hyacinth and Coconut Husk based Fiber Reinforced Polymer Panel. *MATEC Web Conf.* **2018**, *159*, 02035. [CrossRef]
30. Ji, Y.; Chen, S.; Zhu, W. The effect of pore numbers in the cell walls of soybean oil polyurethane foam on sound absorption performance. *Appl. Acoust.* **2020**, *157*, 107010. [CrossRef]
31. Kemona, A.; Piotrowska, M. Polyurethane Recycling and Disposal: Methods and Prospects. *Polymers* **2020**, *12*, 1752. [CrossRef] [PubMed]
32. Ni, X.; Wu, Z.; Zhang, W.; Lu, K.; Ding, Y.; Mao, S. Energy Utilization of Building Insulation Waste Expanded Polystyrene: Pyrolysis Kinetic Estimation by a New Comprehensive Method. *Polymers* **2020**, *12*, 1744. [CrossRef]
33. Building Decorative Stone. In *Woodhead Publishing Series in Civil and Structural Engineering*; Li, Y.; Ren, S.B.T.-B.D.M., Eds.; Woodhead Publishing: Cambridge, UK, 2011; pp. 25–53, ISBN 978-0-85709-257-1.



## Article

# Composite Materials from Renewable Resources as Sustainable Corrosion Protection Coatings

Raluca Sanda Komartin <sup>1,†</sup>, Brindusa Balanuca <sup>1,2,†</sup>, Madalina Ioana Necolau <sup>2</sup>, Anca Cojocaru <sup>3</sup>   
and Raluca Stan <sup>1,\*</sup>

<sup>1</sup> Department of Organic Chemistry “C. Nenitescu”, Faculty of Applied Chemistry and Materials Science, University Politehnica of Bucharest, 1-7 Polizu Street, 011061 Bucharest, Romania; ralu.komartin@gmail.com (R.S.K.); brindusa.balanuca@yahoo.com (B.B.)

<sup>2</sup> Advanced Polymer Materials Group, University Politehnica of Bucharest, 1-7 Polizu Street, 011061 Bucharest, Romania; madalinanecolau@gmail.com

<sup>3</sup> Department of Inorganic Chemistry, Physical Chemistry and Electrochemistry, Faculty of Applied Chemistry and Materials Science, University Politehnica of Bucharest, 1-7 Polizu Street, 011061 Bucharest, Romania; anca.cojocaru@upb.ro

\* Correspondence: rl\_stan2000@yahoo.com

† The authors contributed equally to this work.

**Abstract:** Epoxidized linseed oil (ELO) and kraft lignin (LnK) were used to obtain new sustainable composites as corrosion protection layers through a double-curing procedure involving UV radiation and thermal curing to ensure homogeneous distribution of the filler. The crosslinked structures were confirmed by Fourier-transform infrared spectrometry (FTIR), by comparative monitorization of the absorption band at  $825\text{ cm}^{-1}$ , attributed to the stretching vibration of epoxy rings. Thermal degradation behavior under N<sub>2</sub> gas indicates that the higher LnK content, the better thermal stability of the composites (over 30 °C of Td10% for ELO + 15% LnK), while for the experiment under air-oxidant atmosphere, the lower LnK content (5%) conducted to the more thermo-stable material. Dynamic-mechanic behavior and water affinity of the new materials were also investigated. The increase of the T<sub>g</sub> values with the increase of the LnK content (20 °C for the composite with 15% LnK) denote the reinforcement effect of the LnK, while the surface and bulk water affinity were not dramatically affected. All the obtained composites were tested as carbon steel corrosion protection coatings, resulting in significant increase of corrosion inhibition efficiency (IE) of 140–380%, highlighting the great potential of the bio-based ELO-LnK composites as a future perspective for industrial application.

**Keywords:** epoxidized linseed oil; lignin; composites; anti-corrosion coating

**Citation:** Komartin, R.S.; Balanuca, B.; Necolau, M.I.; Cojocaru, A.; Stan, R. Composite Materials from Renewable Resources as Sustainable Corrosion Protection Coatings. *Polymers* **2021**, *13*, 3792. <https://doi.org/10.3390/polym13213792>

Academic Editor: Cristina Cazan

Received: 12 October 2021

Accepted: 30 October 2021

Published: 2 November 2021

**Publisher's Note:** MDPI stays neutral with regard to jurisdictional claims in published maps and institutional affiliations.



**Copyright:** © 2021 by the authors. Licensee MDPI, Basel, Switzerland. This article is an open access article distributed under the terms and conditions of the Creative Commons Attribution (CC BY) license (<https://creativecommons.org/licenses/by/4.0/>).

## 1. Introduction

Polymer composites are widely used in the fields of engineering due to their performance and versatility, making them adaptable in different industrial sectors. In recent years, numerous studies have been developed for the progress of the bio-based epoxy derivatives, to face out the use of conventional epoxy resins and to achieve great industrial gains [1,2].

Due to their advantages of natural origin, structure versatility, and worldwide availability, vegetable oils (VO) were considered as high-value raw materials in the synthesis of epoxy derivatives (epoxidized vegetable oil–EVO), but there are several drawbacks related to the EVO-based polymeric matrices (e.g., inadequate thermo-mechanical properties or poor mechanical resistance). Many attempts were conducted to solve these issues through the development of different or sophisticated curing procedures or by using reinforcing agents or fillers. For example, mixing different types of conventional epoxy resins with EVO, special design of the crosslinking agents or employing modified vegetable oil structures as crosslinking agents, were reported [2,3].

Literature data present various methods to augment the performances of the conventional resins, using natural curing and co-curing agents as acids, anhydrides, amines, and their derivatives, or natural reinforcing agents like modified cellulose, natural fibers, or powder inorganic fillers [4–6]. One of the important applications related to the epoxy-based coatings is anticorrosion protection, their properties being extensively investigated due to their great advantages in terms of mechanical properties, thermal or chemical stability, and high efficiency upon corrosion inhibition [7–9]. Even if most of them are conventional materials, the frequency of using EVO-based counterparts is continuously growing, different EVO types being successfully used to produce anticorrosion coatings, due to the availability as starting materials, increased hydrophobicity of the resulted layers or convenient reactivity of the epoxy groups [10–12].

Recently, lignin was investigated as potential filler for different anticorrosion coatings, demonstrating a promising inhibition potential in aggressive media [13–15]. Moreover, lignin represents the second natural organic material in terms of occurrence and recent technological development made it available on industrial scale employing industrial waste. Major advantages associated with lignin such as biodegradability, CO<sub>2</sub> neutral, antioxidant, antimicrobial, and stabilizer properties added to the possibility of chemical functionalization are opening new perspectives and a whole new chemistry for applications, association of functionalized lignin's with conventional epoxy resins being recently reported [16].

With the aim to reduce the use of non-renewable resources, this paper provides an investigation of bio-based composite materials obtained from epoxidized linseed oil (ELO) and kraft lignin (LnK) as natural filler, and an investigation of the anticorrosion performance of the obtained coatings in aggressive media. The designed materials' (ELO-LnK) fabrication involved a double-curing procedure to overcome the inconvenience of lignin sedimentation: first, a short-time UV treatment "to catch" the lignin within continuous oil matrix and then a long-term thermal curing to obtain proper polymeric composites with superior yields for the ring-opening reaction in the presence of a commercial crosslinking system. The ELO-LnK composites were investigated by Fourier transform infrared spectrometry (FTIR), thermo-gravimetric analysis (TGA), dynamic mechanical analysis (DMA), contact angle measurements (CA), water absorption degree (WAD), and scanning electron microscopy (SEM). The obtained bio-based epoxy-lignin coatings mitigate the corrosion processes for the carbon steel and a significant improvement of the corrosion inhibition efficiency is observed.

The novelty of the research resides both in association of the two bio-based starting materials, epoxidized linseed oil and kraft lignin, for the synthesis of the new composites and a dual-curing procedure using UV radiation and thermal treatment for hardening the oil-based resin. Thus, a major drawback regarding lignin sedimentation was surpassed reaching adequate features for the studied composite materials in terms of thermal and thermo-mechanical performances and their anticorrosion properties.

## 2. Materials and Methods

### 2.1. Materials

Linseed oil (LO) obtained by cold-pressing process was acquired from PTG Deutschland, Flurstedt, Germany. Kraft lignin (LnK), the photo-initiator triarylsulfonium hexafluoroantimonate (THA) and the solvents and reagents used for the epoxidation of LO were purchased from Sigma-Aldrich (subsidiary of Merck KGaA, Darmstadt, Germany). The dodecyl succinic anhydride hardener (Araldite HY964, HY) and the 2,4,6-tris(dimethylaminomethyl)phenol accelerator (Araldite DY064, DY) were provided by Merck. (Darmstadt, Germany). The products were used as received.

## 2.2. Methods

### 2.2.1. Synthesis of ELO

The epoxidation of the double bonds on the fatty acid structures contained by LO was performed according to procedures described in the literature for LO and other vegetable oils using peracetic acid generated in situ [17–21]. Briefly, the synthesis protocol involves the conversion of the double bonds into epoxy rings using H<sub>2</sub>O<sub>2</sub> and glacial acetic acid (H<sub>2</sub>O<sub>2</sub>/acetic acid/unsaturation molar ratio: 10/2/1), in the presence of H<sub>2</sub>SO<sub>4</sub> (50% solution) as reaction catalyst and toluene as reaction solvent and diluent of the oily phase. After 22 h at 65 °C, under constant magnetic stirring, the reaction was stopped and the product was purified. The purified ELO product (reaction yield~94%) was structurally characterized and used as continuous phase for the composite's fabrication.

### 2.2.2. Preparation of the ELO\_LnK Composite Coatings

A certain amount of ELO and HY964, calculated based on epoxy rings:anhydride molar ratio (2:1), was mixed until visual homogenization. Varying amounts of LnK (5%—sample S1, 10%—sample S2, and 15%—sample S3, respectively, calculated as based on the amount of ELO) were added and homogenized using a Bandelin Sonorex sonication bath for 15 min. The accelerator DY064 (5% wt. with respect to ELO) and the photo-initiator THA (4% wt. against ELO) were then added, manually blended and then sonicated for 5 min [22,23]. A reference sample (Sr) without LnK content was formulated using the same procedure.

To obtain protective layers, carbon steel sheets (15 mm wide × 35 mm long × 0.5 mm thick) were used as substrate for the oil-based coating. Prior to the deposition, the metal sheets were pickled by immersion in HCl solution (10%), then washed with distilled water and finally with isopropanol. The ELO-LnK mixtures (S1–S3 and Sr) were applied on the metal surfaces as uniform and thin films and then subjected to the dual-curing process, with UV irradiation for 15 min ( $\lambda = 365$  nm, power 8 W, maintaining a distance of 10 cm between radiation source and sample surface) and thermal treatment at 80 °C for 23 h. The samples coated with ELO-LnK were tested for anticorrosion performance.

The obtained coated steel plates were tested to define the potential of ELO-LnK composites as anticorrosion protection layers. Likewise, the obtained mixtures were slowly poured in the manufactured silicone molds (20 mm wide × 35 mm long, with respect for the thickness of the layers made on the metal plates, about 0.5 mm) and subjected to the same dual-curing process. The obtained composite materials were subjected to different characterization techniques to establish their general material features.

## 2.3. Characterization

### 2.3.1. Nuclear Magnetic Resonance Spectroscopy (NMR)

<sup>1</sup>H-NMR spectra were recorded on a Bruker Advance III Ultrashield Plus 500 MHz spectrometer (Billerica, MA, USA), operating at 11.74 T, corresponding to the resonance frequency of 500.13 MHz for the <sup>1</sup>H nucleus. Chemical shifts are reported in ppm, using TMS as internal standard.

### 2.3.2. Gel Fraction Measurements (GF)

Tetrahydrofuran extraction (24 h) was made for the obtained ELO-based materials (weight *w*<sub>1</sub>), to determine the soluble fraction. After extraction, materials were dried to constant weight (60 °C; weight *w*<sub>2</sub>). All measurements were performed in triplicate. *GF* was calculated using the equation:

$$GF = \frac{(w_1 - w_2)}{w_1} \times 100 \quad (1)$$

### 2.3.3. Fourier Transform Infrared Spectrometry (FTIR)

FTIR spectra were registered on a Vertex 70 Bruker FTIR spectrometer equipped with an attenuated total reflectance (ATR), at room temperature. Runs with 32 scans in 600–4000  $\text{cm}^{-1}$  wave number region were used.

### 2.3.4. Thermo-Gravimetric Analysis (TGA)

Thermal stability and decomposition profile of the synthesized materials were studied by TGA in both inert and aerobic atmosphere, using a Q500 TA instrument. Thermal degradation was investigated for all samples in the temperature range 25–700 °C, at a heating rate of 10 °C/min under nitrogen/air flow (90 mL/min).

### 2.3.5. Dynamic Mechanical Analysis (DMA)

Thermo-mechanical features of the ELO-LnK composites were measured on a Tritec 2000 instrument, operated in single cantilever bending mode. Rectangular materials (20 mm long  $\times$  10 mm wide  $\times$  5 mm thick) were tested at 1 Hz frequency, ramping the temperature from  $-60$  to  $100$  °C (5 °C/min heating rate).

### 2.3.6. Contact Angle Measurements (CA) and Water Absorption Degree (WAD)

Static CA values were measured for the composite materials at room temperature on DSA100E (KRUSS GMBH) equipment using Drop shape analysis method. Ultrapure water droplets were used with a drop volume of approximately 2  $\mu\text{L}$ . CA values were measured within 10 s of the drop contacts with the surface. Reported values represent the average of three determinations for each specimen. Additionally, WAD was determined in triplicate, using the standard water absorption ASTM D570 method.

### 2.3.7. Scanning Electron Microscopy (SEM)

Composites morphology was explored by scanning electron microscopy, using cross-sections. The samples were manually broken in liquid nitrogen, sputtered with a thin layer of gold, and scanned using a Quanta Inspect F SEM device equipped with a field emission gun with a resolution of 1.2 nm.

### 2.3.8. Electrochemical Measurements

Potentiodynamic polarization measurements and electrochemical impedance spectroscopy (EIS) were performed using a Potentiostat/Galvanostat Voltlab 40 (Radiometer Analytical). Potentiodynamic polarization experiments were performed at a sweep rate of 2.5 mV/s, in the potential range from  $-0.8$  V/SSCS to  $+0.8$  V/SSCS. EIS studies were performed in a frequency range 100 kHz–50 mHz using a sinusoidal perturbation with a voltage amplitude of 10 mV. The impedance spectra were plotted both before the potentiodynamic polarization test in the aggressive environment (after 30 min immersion) and after the accelerated corrosion test. Using EIS data, the electrochemical parameters were calculated, namely the charge transfer resistance ( $R_{ct}$ ) and the double layer capacitance ( $C_{dl}$ ). The electrochemical cell was a thermostated three-electrode one and the experiments were performed in 3.5% NaCl media. The working electrode consisted of the carbon steel samples (wt.%, C: 0.049, Mn: 0.227, Cr: 2.34, S: 0.0005, Fe: rest) coated with the anticorrosive coatings tested (active surface area  $0.5 \text{ cm}^2$ ), the auxiliary electrode was a platinum electrode ( $4.5 \text{ cm}^2$  active surface), and the reference electrode a Ag/AgCl/KCl sat. electrode from Radiometer Analytical (SSCS) immersed into the working solution. All potential values were referred to this reference electrode. All experiments were conducted with naturally aerated solutions at  $25 \pm 1$  °C. Prior to each experiment, the working electrode was immersed in a 3.5% NaCl solution for 30 min to attain a quasi-stationary state.

### 3. Results and Discussion

#### 3.1. ELO Characterization

The epoxidation reaction of the LO was monitored by  $^1\text{H-NMR}$  and FTIR. Structural changes were identified in the  $^1\text{H-NMR}$  spectrum recorded for ELO as compared to the spectrum registered for the crude oil. For ELO compound (Supplementary Material, Figure S1b), new signals at 3.02 and 2.85 ppm, specific to internal and marginal protons belonging to epoxy rings and respectively 1.60 ppm, assigned to the protons from the  $-\text{CH}_2$  groups located between two epoxy rings (originated from linolenic and linoleic acids) were observed. The signal at 5.25 ppm, attributed to the protons of the fatty acid double bonds (unmodified LO, Supplementary Material, Figure S1a) disappear, as a result of the epoxidation [17,19,20]. FTIR analysis (Supplementary Material, Figure S2) confirms the epoxidized structure of the LO monomer, through the appearance of the C–O–C stretching vibration band (epoxy rings) at  $825\text{ cm}^{-1}$ . The absorptions bands at  $3010$  and  $1651\text{ cm}^{-1}$  associated to  $\text{sp}^2$  C–H and to C=C stretching vibrations, respectively, are here relatively weak [17,19,20].

#### 3.2. ELO-LnK Composite Synthesis and Characterization

Diamines and anhydrides were tentatively used as crosslinkers for ELO. In presence of LnK, diamines like hexamethylenediamine (HAD) failed to lead to proper composites. The unsuccessful process can be associated to competing reaction of the functional groups from the lignin structure with the amino groups of HAD leading to polycondensation products, according to literature reports [16,24], resulting in LnK sedimentation and poor crosslinked ELO network. In the absence of LnK we were able to use diamine as crosslinking agent for ELO.

In another approach, cationic photocuring of the ELO-LnK system was performed using THA as a photo-initiator. However, those systems with low LnK content (5%) did not harden, but formed a thin film on the surface after several UV irradiation cycles (at 365 nm). The UV stabilizing effect exerted by the LnK can be an argue, in accordance with the established feature of the kraft lignin as a filler in UV-curable systems to prevent the quenching phenomenon (fluorescence) [25,26]. Thus, the adopted procedure was a double-curing process using UV irradiation at room temperature for 15 min. (ELO homopolymerization), followed by thermal crosslinking at  $80\text{ }^\circ\text{C}$  for 23 h.

#### 3.3. FTIR Spectrometry

The efficiency of the selected curing procedures was assessed by FTIR spectrometry, in  $600\text{--}4000\text{ cm}^{-1}$  wave number region, before and after the dual treatment.

For our discussion, the FTIR spectrum of ELO (Figure 1a) shows a typical absorption at  $825\text{ cm}^{-1}$  attributed to the stretching vibration of epoxy rings. The (b) spectrum (Figure 1b) corresponds to the unreacted mixture ELO-HY-DY-THA, with the expected characteristic bands:  $825\text{ cm}^{-1}$  (typical for the epoxy ring),  $915\text{ cm}^{-1}$  ( $\delta_{\text{C-H, oop}}$  aromatic folding),  $1060\text{ cm}^{-1}$  ( $\delta_{\text{C-O}}$ , HY 964 anhydride),  $1223\text{ cm}^{-1}$  ( $\delta_{\text{C-N}}$ , DY 064),  $1566\text{ cm}^{-1}$  ( $\delta_{\text{C=C}}$ ),  $1787$  and  $1861\text{ cm}^{-1}$  ( $\delta_{\text{C=O}}$ , anhydride). In the (c) spectrum (Figure 1c) of the cured material, the absorption band of the epoxy rings ( $825\text{ cm}^{-1}$ ) and those of the other reactants ( $1060$ ,  $1223$ ,  $1566$ ,  $1787$ , and  $1861\text{ cm}^{-1}$ ) disappeared, as expected after crosslinking and photopolymerization of ELO. The new bands in the range  $1000\text{--}1100\text{ cm}^{-1}$  can be ascribed to the new C–O bonds formed during the two curing processes.



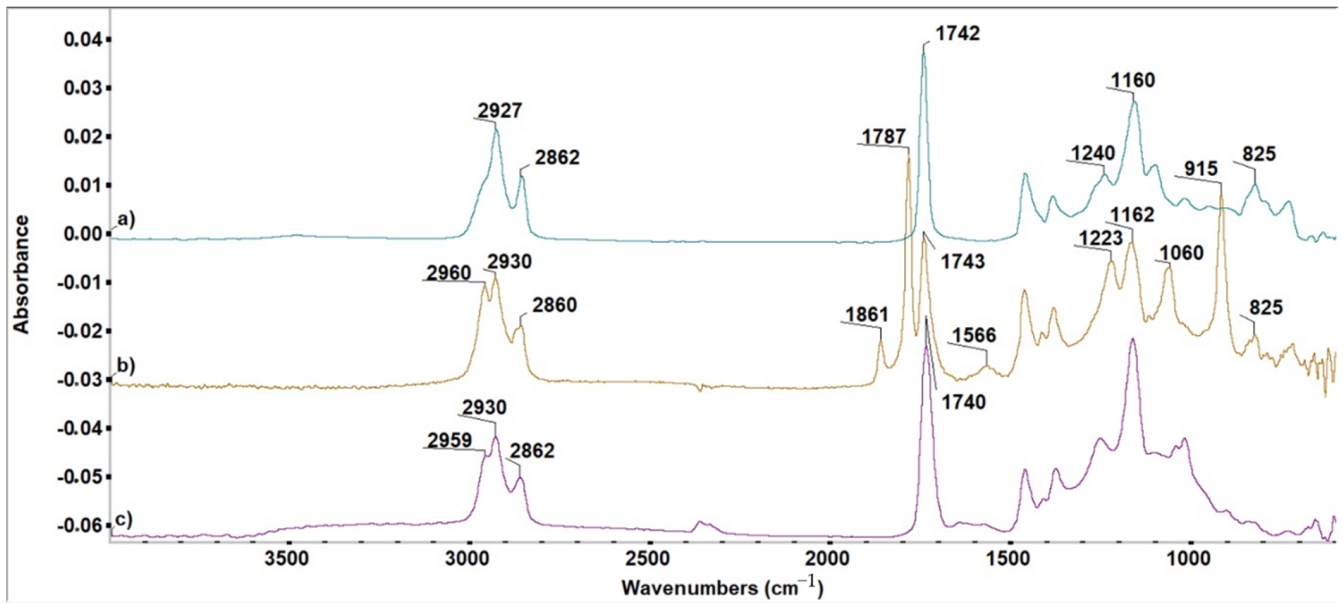


Figure 1. FTIR spectra of (a) ELO; (b) ELO-based formulation before curing; (c) product resulted after curing (Sr).

For the ELO-LnK composites, similar findings were noticed (Figure 2).

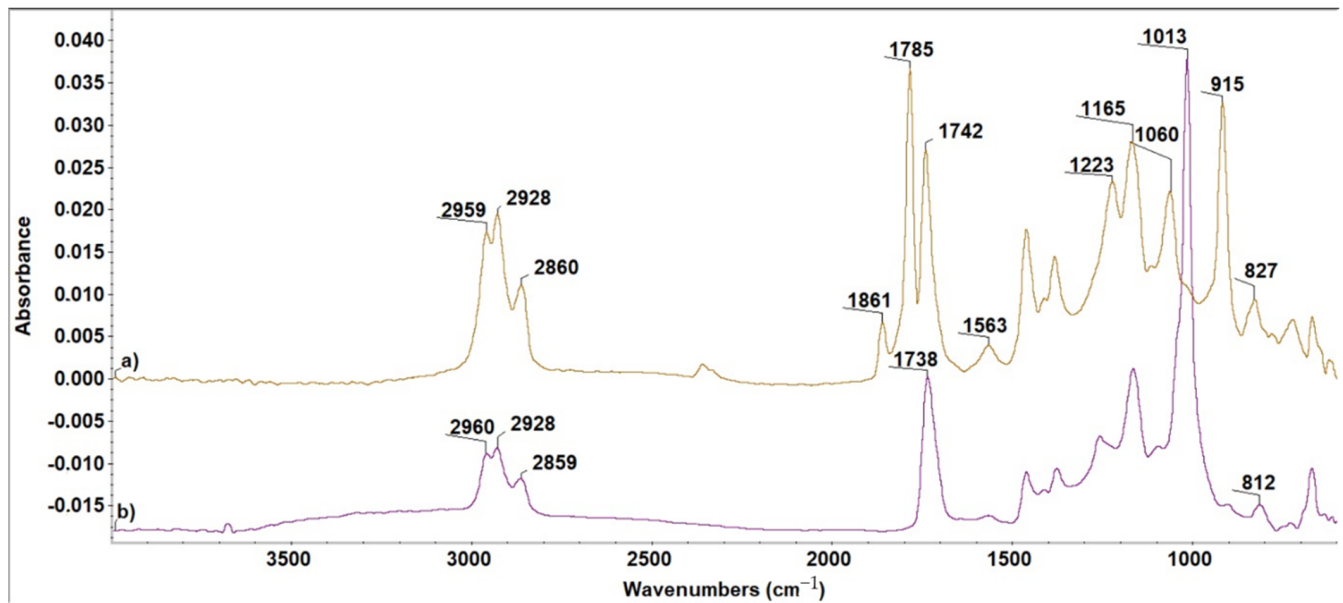


Figure 2. FTIR spectra of the S1 system (ELO + 5%LnK). (a) Before and (b) after dual-curing reaction.

The appearance of the high intensity band at  $1013\text{ cm}^{-1}$  is due to the new C–O bonds formed during the curing processes. Well defined pick shape can be argued by a great number of C–O bonds coming not only from ELO matrix, but also from the new reaction points between ELO and LnK, as a first indication of a reinforcement effect which can be produced by LnK.

Additionally, for all the studied ELO-based materials, *GF measurements* indicate small unreacted fraction (maximum 8%) after the applied dual-treatment (UV irradiation and thermal curing). A slightly increase (3%) of the GF value was noticed for the S3 system compared to the reference sample (Table 2).

### 3.4. Thermogravimetric Analysis

The thermal stability of the composites obtained by dual-curing treatment was investigated by TGA, in N<sub>2</sub> atmosphere as well as in presence of air. Results are summarized in Table 1.

**Table 1.** TGA data of ELO and LnK-based products (N<sub>2</sub> and air).

| N <sub>2</sub> Atmosphere |                             |          |          |          |                               |        |               |                             |                             |
|---------------------------|-----------------------------|----------|----------|----------|-------------------------------|--------|---------------|-----------------------------|-----------------------------|
| Sample Code               | Weight Loss                 |          |          |          | Degradation Steps             |        |               | Weight Change at 700 °C (%) |                             |
|                           | T <sub>d</sub> <sup>a</sup> |          |          |          | T <sub>max</sub> <sup>b</sup> |        |               |                             |                             |
|                           | 3% (°C)                     | 10% (°C) | 30% (°C) | 50% (°C) | 1 (°C)                        | 2 (°C) | 3 (°C)        |                             |                             |
| Sr                        | 185                         | 223      | 320      | 358      | 234                           | 365    | 448 s         | 99                          |                             |
| S1                        | 197                         | 247      | 339      | 366      | 243                           | 365    | 440 s         | 96                          |                             |
| S2                        | 192                         | 242      | 336      | 364      | 230                           | 362    | 448 s         | 91                          |                             |
| S3                        | 197                         | 256      | 343      | 370      | 250                           | 363    | 449 s         | 88                          |                             |
| LnK                       | 159                         | 258      | 355      | 502      | -                             | 353    | -             | 61                          |                             |
| Air Atmosphere            |                             |          |          |          |                               |        |               |                             |                             |
| Sample Code               | Weight Loss                 |          |          |          | Degradation Steps             |        |               |                             | Weight Change at 700 °C (%) |
|                           | T <sub>d</sub> <sup>a</sup> |          |          |          | T <sub>max</sub> <sup>b</sup> |        |               |                             |                             |
|                           | 3% (°C)                     | 10% (°C) | 30% (°C) | 50% (°C) | 1 (°C)                        | 2 (°C) | 3 (°C)        | 4 (°C)                      |                             |
| Sr                        | 193                         | 242      | 336      | 383      | 230                           | 333    | 375 421 s     | 527                         | 88                          |
| S1                        | 199                         | 256      | 346      | 387      | 260                           | 339    | 378 426 s     | 520                         | 85                          |
| S2                        | 191                         | 243      | 332      | 374      | 243                           | 338    | 376 417 s     | 509                         | 98                          |
| S3                        | 182                         | 229      | 325      | 373      | 224                           | 336    | 376 395 429 s | 503                         | 98                          |
| LnK                       | 86                          | 255      | 395      | 436      | -                             | -      | 448           | -                           | 93                          |

a—T<sub>d</sub> = the thermal degradation temperature as the weight loss of material at 3, 10, 30, 50%; b—T<sub>max</sub> = temperature at which the maximum mass decomposition occurs; s—shoulder.

All ELO and ELO-LnK composites show in inert atmosphere a similar behavior, indicating a comparable thermal stability. When LnK is loaded, a lower degradation rate was noticed for all samples (S1–S3) as compared to the reference sample Sr, indicating an improved thermal stability associated with the aromatic structure of the filler. For the S2 system, a slight decrease of T<sub>d</sub> values in the entire temperature range was observed. Such behavior could be explained by a poor LnK dispersion within ELO-based matrix, as a result of an inefficient homogenization. As can be seen from the weight loss curves, above 300 °C, the reference material (Sr) decomposes faster leading to lower residual char at 700 °C (1%), due to the complete decomposition of the LO aliphatic chains. The remaining char quantity is due, probably, to the THA initiator and DY064 accelerator aromatic structures. The increase of residual mass at 700 °C for the S1–S3 composites could be explained by the crosslinked phenolic-type structure of LnK, which does not easily break down [27].

All DTG curves showed a three-step decomposition behavior (Figure 3b). The weight loss onset, up to 300 °C (representing ~20% of sample weight) could be attributed to the volatilization of decomposition products with low molecular weight and low boiling point. The next mass loss stage (of ~65%), with the maximum rate around 365 °C could be attributed to the decomposition of polymeric and oligomeric fragments, whereas the last weight loss (of ~15%), transposed in the DTG curves as a shoulder around 450 °C, probably corresponds to C–C bond cleavage [28].

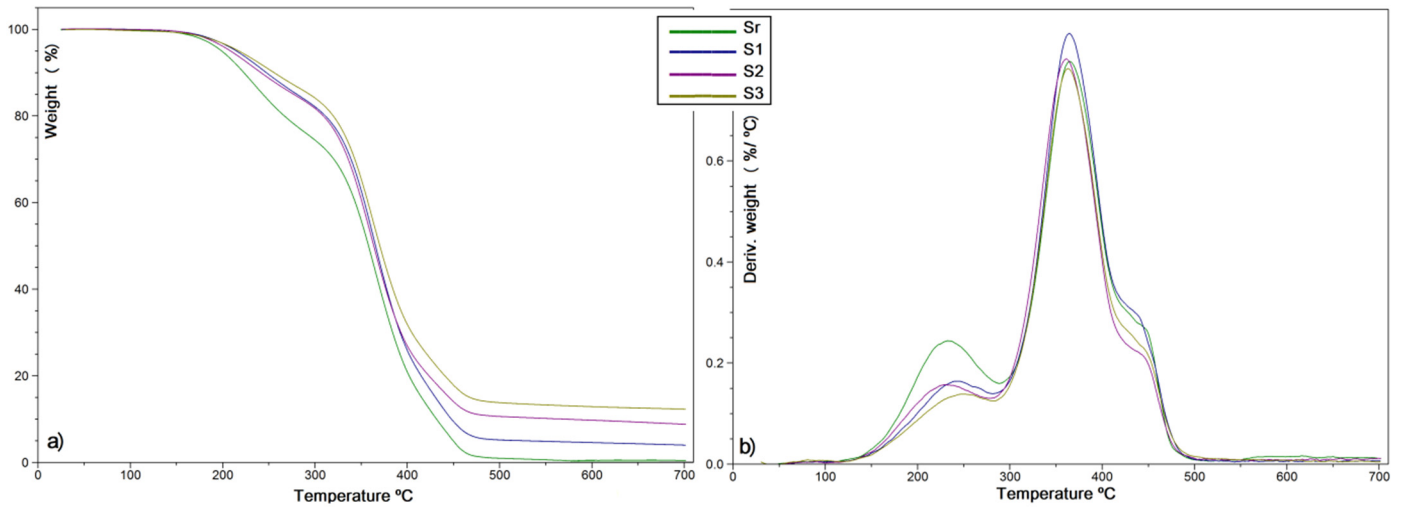


**Figure 3.** (a) TGA and (b) DTG curves for ELO-derived composite materials (N<sub>2</sub>).

TGA studies of the ELO-LnK composites in the presence of air showed a more complex decomposition process (Table 1). Curve shapes are slightly dependent on the LnK proportion in the composite (Figure 4), the decomposition process under thermo-oxidative condition being faster once the concentration of the LnK increases. ELO-based system with lower LnK amount (S1, 5% wt. LnK) seems to be the more thermo-stable material in oxidative environment.

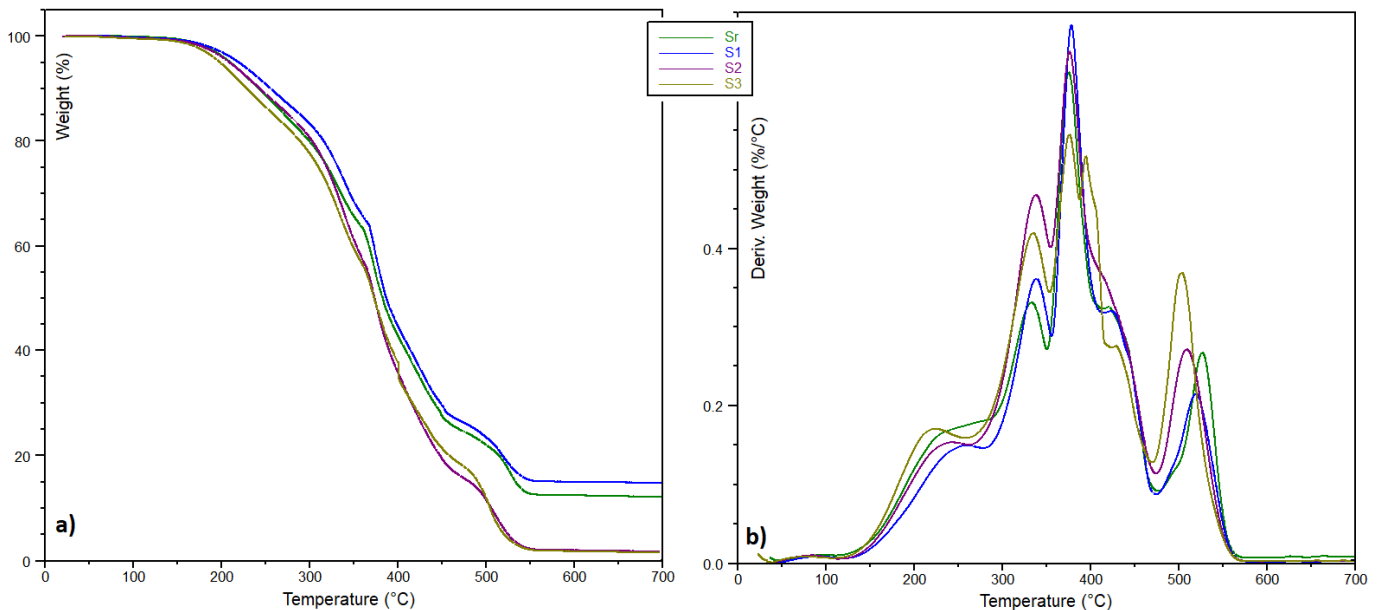


**Figure 4.** Thermal degradation profile (air) of ELO-LnK composites. (a) TGA and (b) DTG curves.

The degradation behavior (Figure 4b) could be related to the LnK amount, but also to the heterogeneity of the triglyceride structure, which means a wider distribution of molecular weight segments within the cross-linked materials.

Decomposition broad peaks, at 150–280 °C ( $T_{\max 1}$ ), are noted for all the samples, which can be explained by moisture elimination but also by loss of volatile compounds and low molecular fragments. At elevated temperatures, two well-defined exothermal peaks are observed (280–450 °C), with shoulder-like peaks around 420–430 °C. These distinct peaks can be explained by degradation processes involving ELO intra-molecular bonds as well as the ELO-LnK inter-unit linkages. When raw LnK was analyzed under the same thermal conditions, a single decomposition peak at 448 °C was registered. Thus,  $T_{\max 2}$  may

be attributed to the fragmentation of the ELO matrix, consisting of more flexible chains, which are easily exposed to oxygen attack.

An influence of LnK upon thermo-oxidation processes is also clearly observed, this stage involving probably degradation of LnK substituents. In case of S3 (15% wt. LnK content), two peaks can be observed at 376 and 395 °C, respectively, and a small shoulder at 429 °C. Such a decomposition profile could be associated with a 3D network with multiple bond types between the oil matrix and LnK as well as with different pyrolysis mechanisms involving LnK aromatic rings substituents, expected to be relatively stable in the first pyrolysis stage [29]. Above 500 °C, a last decomposition peak is observed on the DTG graphs, associated with the ELO matrix, with long tails beyond 570 °C.

### 3.5. Dynamic-Mechanical Analysis

Thermo-mechanical properties of the composites were investigated (Table 2). LnK loading significantly shifts the peaks of  $\tan \delta$ , an increase of 20 °C of the  $\tan \delta$  being observed for the S3 composite, as compared with the neat polymer (Sr). This could be strong evidence of the reinforcing effect involving the aromatic structures. Such interactions could restrict the motion of the long fatty acid chains and thus impart stiffness. We may assume that there are fewer dangling chains available in the network, together with lower molecular weight segments (probably located between crosslinking centers).

**Table 2.** DMA, GF, and contact angle results for ELO-LnK composites.

| Sample | Tg <sup>c</sup> (°C) | GF <sup>d</sup> (%) | $\Theta$ <sup>e</sup> (°) |
|--------|----------------------|---------------------|---------------------------|
| Sr     | 55                   | 92.06 ± 0.54        | 84.82 ± 1.72              |
| S1     | 58                   | 93.13 ± 0.24        | 77.89 ± 4.07              |
| S2     | 62                   | 93.95 ± 0.22        | 73.97 ± 1.46              |
| S3     | 75                   | 94.99 ± 0.30        | 71.38 ± 1.95              |

c—Tg = glass transition temperature considered as the maximum of  $\tan \delta$  plots; d—GF = gel fraction (the average of three measurements and corresponding standard deviation); e— $\theta$  = water contact angle (the average of three measurements and corresponding standard deviation).

### 3.6. Morphology Investigation

Figure 5 shows SEM photographs of the fractured neat ELO material and respectively ELO-LnK composites S1–S3, at 5000× magnification. It can be observed a single-phase morphology for all the investigated specimens, with certain architectural differences associated with the LnK content. The areas of fracture seem to undergo modifications with increasing LnK content.

The fracture surface of the neat epoxy polymer (Figure 5, Sr) is very smooth except for the regular button-shape observed in the cross section, which comes from the incorporated THA photo-initiator. This attribution has been proven by SEM-EDX analysis (Supplementary Material—Figure S4). In contrast, the fracture surfaces of ELO-LnK materials seem rougher (Figure 5 S1–S3). S1 and S3 samples exhibit a network of fine cracks. For S3, we also noticed the disappearance of the button-shape coming from THA.

### 3.7. Water Affinity

Static water contact angle measurements (CA) and water absorption experiments (WAD) were carried out to evaluate the wettability of the composites. The results are shown in Table 2 and Figure 6, respectively.

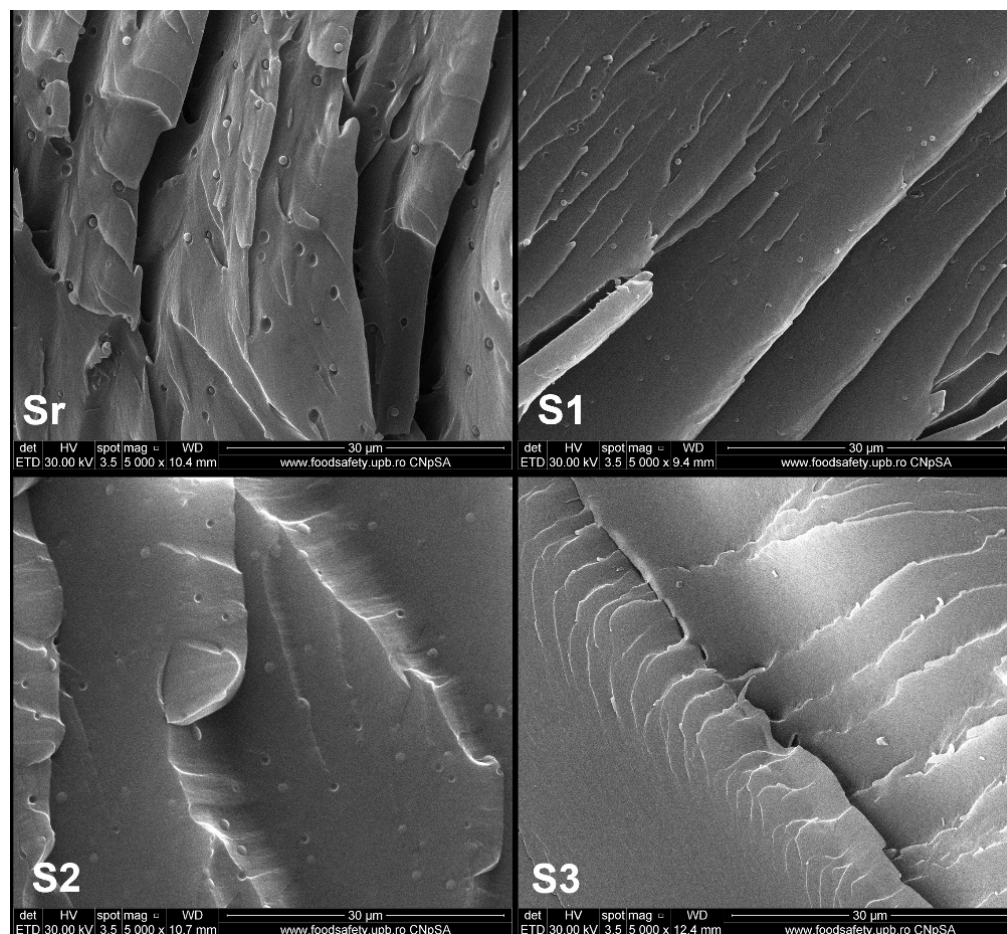


Figure 5. Cross-section SEM images of ELO-LnK composites (5000× magnification). Sr: ELO polymer; S1: ELO+5% wt. LnK; S2: ELO+10% wt. LnK; S3: ELO+15% wt. LnK.

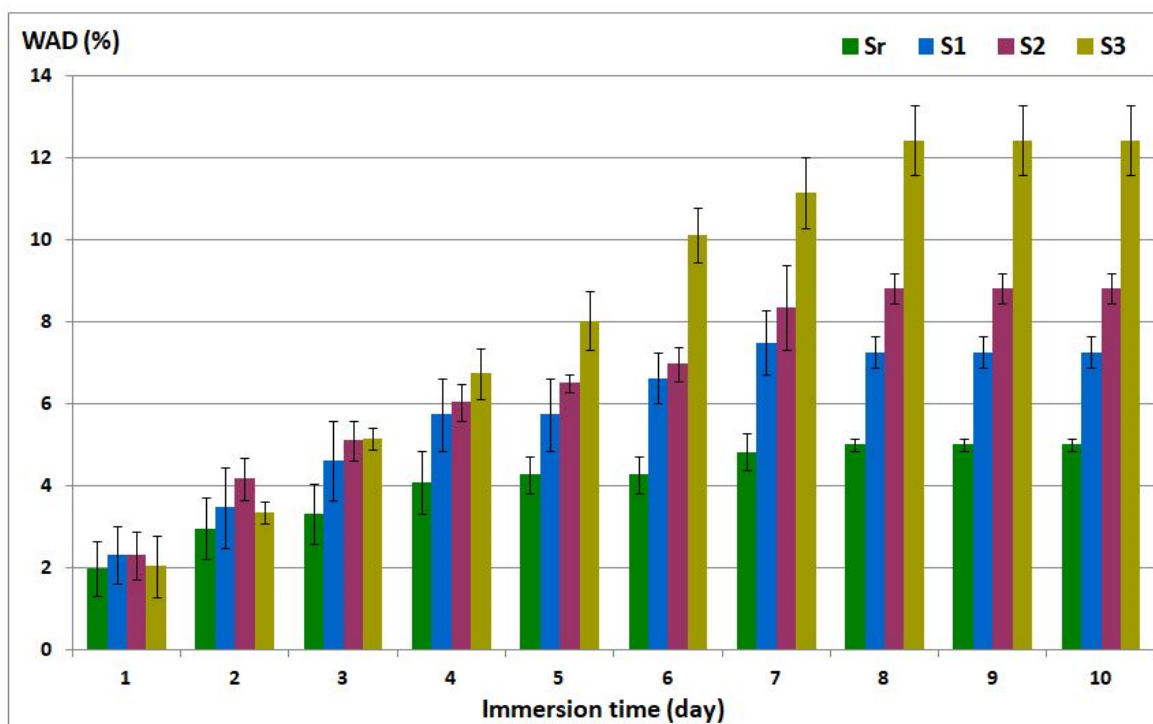


Figure 6. Water absorption degree for ELO-LnK composites.

Generally, water affinity has a direct effect on corrosion susceptibility, more hydrophobic surfaces conferring enhanced resistance against wet corrosion [30].

Lignin, which has both hydrophilic and hydrophobic units, may influence the wetting properties of the final materials in both directions. A highly hydrophobic polymer matrix, as provided by ELO, is expected to reduce the hydrophilic character of the materials, improving at the same time their stability towards thermal degradation and towards corrosive media. CA values can thus be naturally influenced by the LnK concentration and dispersion, the latter influencing the wetting behavior of a surface.

The sample with 15% wt. LnK concentration (S3) registered the lowest contact angle value, around  $71^\circ$ , the differences between the neat Sr sample and S1 (containing 5% wt. LnK) being just  $8^\circ$ . If LnK-loaded composites are compared with the reference sample, the decrease of the CA values is not too high considering the large number of  $-OH$  groups (phenolic and aliphatic) of the LnK structure.

To elucidate the bulk water affinity of the ELO-LnK composites, water absorption degree (WAD) was investigated for ten days, using a ASTM D570 method.

The WAD graph (Figure 6) reveals a low water affinity after ten days of immersion: 7.26% for S1, 8.83% for S2, and 12.42% for S3. These values are promising for the corrosion protection application when compared with other lignin-epoxy composites as anticorrosion coating [31].

### 3.8. Electrochemical Measurements

The anticorrosion performance of ELO-LnK composites was evaluated using coated carbon steel sheets. Figure 7 shows the open circuit potential (OCP) curves vs. time obtained for samples coated with ELO-LnK (Sr, S1, S2, S3) in 3.5% NaCl solution. In the absence of LnK, the initial potential is shifted towards more negative values (curve 2), showing for a short time a shift towards more positive values, maybe due to the porosity of the coating and formation of an oxide film. OCP stabilized gradually with prolonged immersion time up to 600 s. The addition of the LnK leads to a shift of the potential in open circuit towards more positive values. The samples with higher LnK content (S2 and S3—curves 4 and 5) reach a stable potential value shortly after immersion (in about 200 s), while S1 (curve 3) shows a higher potential instability, which might be related to a higher porosity.

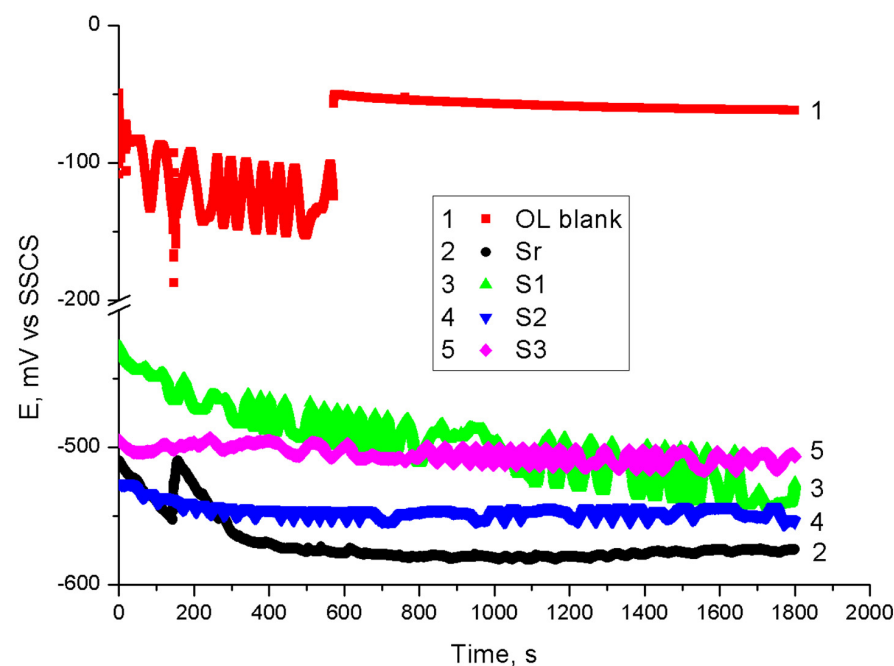


Figure 7. OCP time curves for coated samples Sr (2), S1 (3), S2 (4), and S3 (5).

Potentiodynamic polarizations experiments in 3.5% NaCl solution for 30 min (Figure 8) were conducted to measure parameters such as corrosion potential ( $E_{corr}$ ), corrosion current density ( $i_{corr}$ ), polarization resistance ( $R_p$ ) for the carbon steel sheets coated with ELO-LnK layers. Table 3 shows these results together with cathodic ( $\beta_c$ ) and anodic ( $\beta_a$ ) Tafel slopes and inhibition efficiency ( $IE$ ).

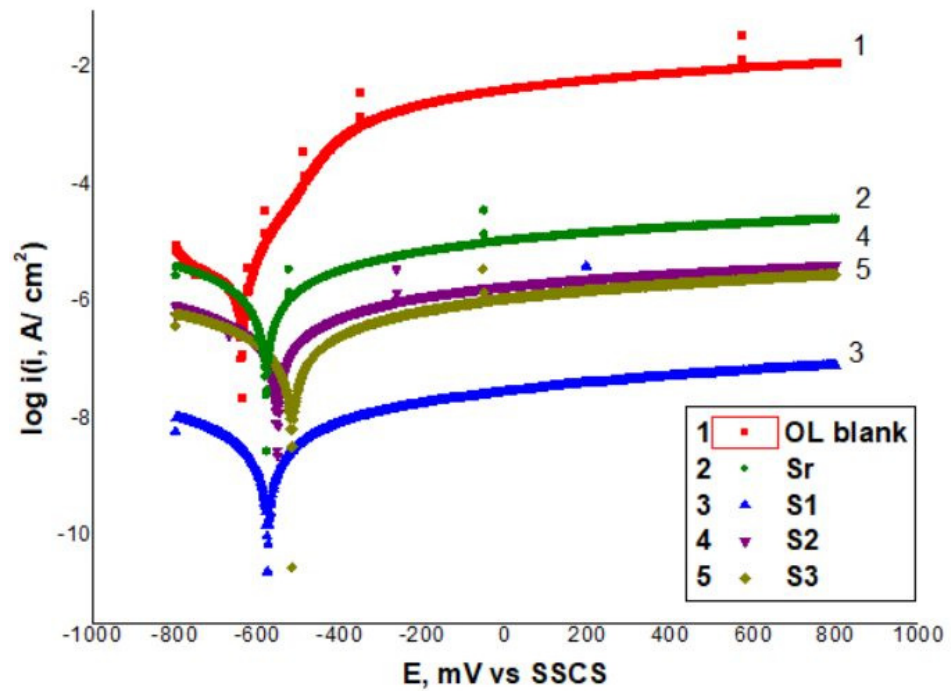


Figure 8. Potentiodynamic polarization (Tafel) curves for uncoated and coated samples in 3.5% NaCl solution at 25 °C (OL—the uncoated sheet/blank sample).

Table 3. Electrochemical parameters calculated from Tafel polarization curves.

| Sample Code | $E_{corr}$ (mV/SSCS) | $i_{corr}$ ( $\mu\text{A}/\text{cm}^2$ ) | $R_p$ (kohm * $\text{cm}^2$ ) | $\beta_a$ (mV) | $-\beta_c$ (mV) | Correlation Coefficient | IE (%) |
|-------------|----------------------|--|-------------------------------|----------------|-----------------|-------------------------|--------|
| OL *        | −646                 | 1.5531                                   | 12.64                         | 75.3           | 257.3           | 0.9999                  | -      |
| Sr          | −584                 | 0.5562                                   | 52.71                         | 180.8          | 185.0           | 0.9977                  | 64.19  |
| S1          | −581                 | 0.0015                                   | 19,930.00                     | 186.1          | 188.3           | 0.9974                  | 99.90  |
| S2          | −558                 | 0.1036                                   | 282.20                        | 185.1          | 183.3           | 0.9977                  | 93.33  |
| S3          | −523                 | 0.0601                                   | 450.26                        | 171.0          | 170.6           | 0.9977                  | 96.13  |

\* OL—the uncoated carbon steel sheets (blank).

The corrosion inhibition efficiency ( $IE$ ) was calculated using Equation (2):

$$IE = \left(1 - \frac{i_{corr}}{i_{corr}^0}\right) \times 100\% \tag{2}$$

where  $i_{corr}^0$  and  $i_{corr}$  are the current densities for steel corrosion in the absence and respectively in the presence of ELO-based coating, in 3.5% NaCl solution.

The graphs in Figure 8 show clearly that all ELO-based coatings exhibit a corrosion inhibition effect, significantly reducing the density of the corrosion current. With or without LnK the coatings lead to a faster passivation of steel surface. With 5% LnK (S1 sample), the corrosion rate is reduced by up to two orders of magnitude compared with the uncoated sample (OL). The highest efficiency against corrosion, namely 99.9%, is exhibited by the S1 sample, while the lowest, 64.19%, by Sr which contains no LnK.

Electrochemical impedance spectroscopy (EIS) measurements were performed on the coated steel samples. Nyquist plots were registered before the potentiodynamic polarization test in aggressive environment (after 30 min immersion) as well as after the test (after accelerated corrosion test) (Figure 9). Electrochemical parameters such as electrolyte resistance (R1), coating resistance (R2), double layer capacitance (Cdl), are presented in Table 4. The inhibition efficiency (IE) was calculated using Equation (3):

$$IE = \left(1 - \frac{R_{ct}^0}{R_{ct}}\right) \times 100\% \tag{3}$$

where  $R_{ct}$  and  $R_{ct}^0$  are the charge transfer resistance for the coated samples and respectively for the uncoated one. The corresponding results are shown in Table 4.

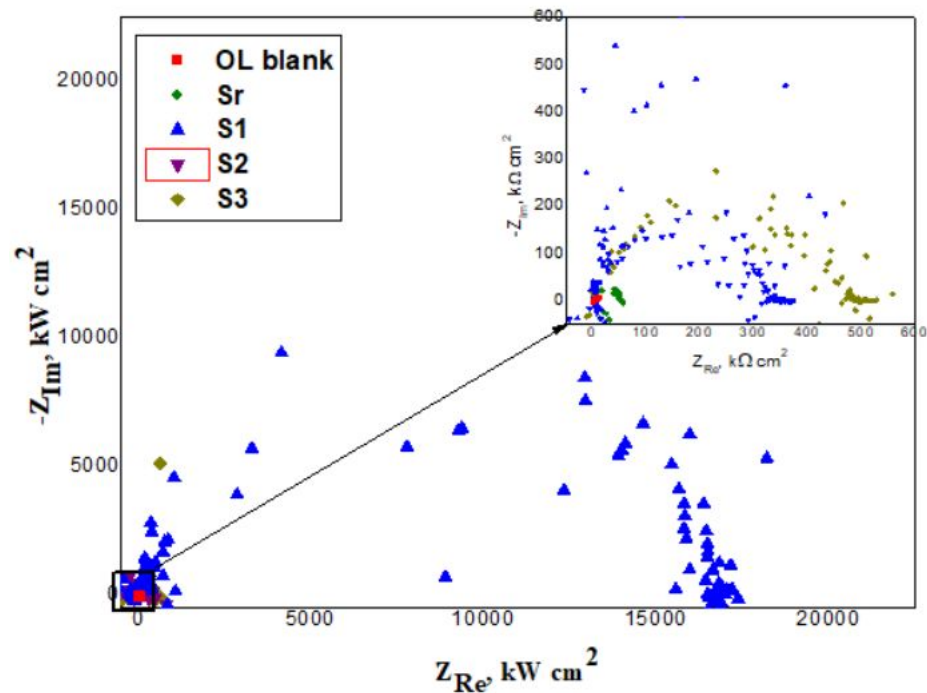


Figure 9. Nyquist plots after accelerated corrosion test in 3.5% NaCl solution at 25 °C.

Table 4. Electrochemical parameters obtained from EIS measurements.

| Sample Code | A *                         |                              |                           |        | B *                         |                              |                           |        |
|-------------|-----------------------------|------------------------------|---------------------------|--------|-----------------------------|------------------------------|---------------------------|--------|
|             | R1 (ohm * cm <sup>2</sup> ) | R2 (kohm * cm <sup>2</sup> ) | Cdl (pF/cm <sup>2</sup> ) | IE (%) | R1 (ohm * cm <sup>2</sup> ) | R2 (kohm * cm <sup>2</sup> ) | Cdl (pF/cm <sup>2</sup> ) | IE (%) |
| OL          | 111.80                      | 6.48                         | 43.69 10 <sup>6</sup>     | -      | 45.83                       | 37.50                        | 84.87 10 <sup>6</sup>     | -      |
| Sr          | 63.83                       | 41.43                        | 307.30                    | 84.35  | 38.52                       | 49.53                        | 321.20                    | 24.29  |
| S1          | 92.99                       | 20,600.00                    | 691.90                    | 99.97  | 41.63                       | 17,350.00                    | 366.80                    | 99.78  |
| S2          | 132.00                      | 405.90                       | 43.90                     | 98.40  | 224.00                      | 596.30                       | 53.37                     | 93.71  |
| S3          | 70.04                       | 390.40                       | 290.10                    | 98.34  | 40.90                       | 501.70                       | 225.80                    | 92.53  |

A: after 30 min immersion in the 3.5% NaCl solution; B: after the accelerated corrosion test in the 3.5% NaCl solution.

As shown in Table 4, after the 30 min immersion required to stabilize the system in the aggressive environment, LnK-loaded coatings indicated a superior corrosion performance, S1 (5% LnK) being the more efficient. The results after accelerated corrosion test are found to be comparable with those obtained after 30 min immersion (Table 4).

The Nyquist recorded spectra (Figure 9), show a semicircle, the higher diameter being associated with the S1 sample (5% LnK). These results are in good agreement with those obtained from Tafel measurements.



#### 4. Conclusions

Considering the global issues regarding the extensive use of petroleum-based raw materials that generate non-biodegradable products, here were formulated, obtained, and tested new composite materials based on renewable resources: vegetable oil and lignin, as anticorrosion protective layers for carbon steel.

The obtained bio-based epoxy resin derived from linseed oil was used further to produce the new composites by loading lignin in different mass ratios. FTIR spectrometry and GF measurements indicated the success of the double-curing procedure involving UV irradiation and thermal treatment, respectively. An improved dispersion of the LnK into the polymer matrix was attained by the double-curing technique. SEM images indicate the good dispersibility of the lignin particle within oil-based network. We intend in a future project to systematically investigate this dual-curing procedure and the polymer thus resulted.

Thermal degradation of the bio-based materials was investigated by TGA in both inert and air-oxidant atmosphere registering higher stability for all the LnK-loaded samples in N<sub>2</sub>, and an improved stability for the sample with 5% wt LnK in aerobic condition. Water affinity was not dramatically influenced when LnK was added, but the thermo-mechanical features were improved indicating the reinforcement effect generated by the rigid aromatic units from the lignin structure.

ELO-LnK composites showed promising anticorrosion protection performance. The sample with 5%-LnK displayed the highest corrosion inhibition efficiency both in Tafel polarization curves and in Nyquist plots.

**Supplementary Materials:** The following are available online at <https://www.mdpi.com/article/10.3390/polym13213792/s1>, Figure S1: <sup>1</sup>H-NMR spectra of (a) crude LO and (b) epoxidized LO; Figure S2—FTIR spectra of crude LO (a) and epoxidized LO (b); Figure S3—Tan delta versus temperature registered for the ELO-LnK materials; Figure S4—Qualitative SEM-EDX for Sr sample (SEM at 1000× magnituded). Insert: quantitative results for ELO-based composites.

**Author Contributions:** Conceptualization: R.S. and B.B.; Methodology: B.B. and A.C.; Investigation: R.S.K., B.B., M.I.N. and A.C.; Formal analysis: M.I.N.; Writing—original draft preparation: B.B. and R.S.K.; Writing—review and editing: R.S. All authors have read and agreed to the published version of the manuscript.

**Funding:** This work is part of a research study supported by the Operational Programme Human Capital of the Ministry of European Funds through the Financial Agreement 51668/09.07.2019, SMIS code 124705. Publishing costs are supported by the University POLITEHNICA of Bucharest, through the project “Engineer in Europe”, project no. 140/GP/19.04.2021.

**Institutional Review Board Statement:** Not applicable.

**Informed Consent Statement:** Not applicable.

**Data Availability Statement:** The data presented in this paper are available on request from the corresponding author.

**Conflicts of Interest:** The authors declare no conflict of interest.

#### References


- Jia, P.; Ma, Y.; Kong, Q.; Xu, L.; Li, Q.; Zhou, Y. Progress in development of epoxy resin systems based on biomass resources. *Green Mater.* **2020**, *8*, 6–23. [CrossRef]
- Ramon, E.; Sguazzo, C.; Moreira, M.G.P.P. A Review of Recent Research on Bio-Based Epoxy Systems for Engineering Applications and Potentialities in the Aviation Sector. *Aerospace* **2018**, *5*, 110. [CrossRef]
- Conti Silva, J.A.; Moreira Grilo, L.; Gandini, A.; Martins Lacerda, T. The Prospering of Macromolecular Materials Based on Plant Oils within the Blooming Field of Polymers from Renewable Resources. *Polymers* **2021**, *13*, 1722. [CrossRef]
- Motta Neves, R.; Ornaghi, H.L., Jr.; José Zattera, A.; Campos Amico, S. Recent studies on modified cellulose/nanocellulose epoxy composites: A systematic review. *Carbohydr. Polym.* **2021**, *255*, 117366. [CrossRef] [PubMed]
- Matykiewicz, D. Hybrid Epoxy Composites with Both Powder and Fiber Filler: A Review of Mechanical and Thermomechanical Properties. *Materials* **2020**, *13*, 1802. [CrossRef] [PubMed]

6. Ding, C.; Matharu, A.S. Recent Developments on Biobased Curing Agents: A Review of Their Preparation and Use. *ACS Sustain. Chem. Eng.* **2014**, *2*, 2217–2236. [CrossRef]
7. Faccini, M.; Bautista, L.; Soldi, L.; Escobar, A.M.; Altavilla, M.; Calvet, M.; Domènech, A.; Domínguez, E. Environmentally friendly anticorrosive polymeric coatings. *Appl. Sci.* **2021**, *11*, 3446. [CrossRef]
8. Hsissou, R. Review on epoxy polymers and its composites as a potential anticorrosive coating for carbon steel in 3.5% NaCl solution: Computational approaches. *J. Mol. Liq.* **2021**, *336*, 116307. [CrossRef]
9. Verma, C.; Olasunkanmi, L.O.; Akpan, E.D.; Quraishi, M.A.; Dagdag, O.; Gouri, M.E.; Sherif, M.E.; Ebenso, E.E. Epoxy resins as anticorrosive polymeric materials: A review. *React. Funct. Polym.* **2020**, *156*, 104741. [CrossRef]
10. Alam, M.; Akram, D.; Sharmin, E.; Zafar, F.; Ahmad, S. Vegetable oil based eco-friendly coating materials: A review article. *Arab. J. Chem.* **2014**, *7*, 469–479. [CrossRef]
11. Noè, C.; Iannucci, L.; Malburet, S.; Graillot, A.; Sangermano, M.; Grassini, S. New UV-Curable Anticorrosion Coatings from Vegetable Oils. *Macromol. Mater. Eng.* **2021**, *306*, 2100029. [CrossRef]
12. Noè, C.; Hakkarainen, M.; Sangermano, M. Cationic UV-Curing of Epoxidized Biobased Resins. *Polymers* **2021**, *13*, 89. [CrossRef] [PubMed]
13. Gao, C.; Wang, S.; Dong, X.; Liu, K.; Zhao, X.; Kong, F. Construction of a Novel Lignin-Based Quaternary Ammonium Material with Excellent Corrosion Resistant Behavior and Its Application for Corrosion Protection. *Materials* **2019**, *12*, 1776. [CrossRef] [PubMed]
14. Marciales, A.; Haile, T.; Ahvazi, B.; Ngo, T.D.; Wolodko, J. Performance of green corrosion inhibitors from biomass in acidic media. *Corros. Rev.* **2018**, *36*, 239–266. [CrossRef]
15. Kulkarni, P.; Ponnappa, C.B.; Doshi, P.; Rao, P.; Balaji, S. Lignin from termite frass: A sustainable source for anticorrosive applications. *J. Appl. Electrochem.* **2021**, *51*, 1491–1500. [CrossRef]
16. Ott, M.W.; Dietz, C.; Trosien, S.; Mehlhase, S.; Bitsch, M.J.; Nau, M.; Meckel, T.; Geissler, A.; Siegert, G.; Huong, J.; et al. Co-curing of epoxy resins with aminated lignins: Insights into the role of lignin homo crosslinking during lignin amination on the elastic properties. *Holzforschung* **2021**, *75*, 390–398. [CrossRef]
17. Balanuca, B.; Stan, R.; Hanganu, A.; Iovu, H. Novel Linseed Oil-Based Monomers: Synthesis and Characterization. *UPB Sci. Bull. B Chem. Mater. Sci.* **2014**, *76*, 129–140.
18. Balanuca, B.; Lungu, A.; Hanganu, A.; Stan, L.R.; Vasile, E.; Iovu, H. Hybrid nanocomposites based on POSS and networks of methacrylated camelina oil and various PEG derivatives. *Eur. J. Lipid Sci. Technol.* **2014**, *116*, 458–469. [CrossRef]
19. Balanuca, B.; Stan, R.; Hanganu, A.; Lungu, A.; Iovu, H. Design of new camelina oil-based hydrophilic monomers for novel polymeric materials. *J. Am. Oil Chem. Soc.* **2015**, *92*, 881–891. [CrossRef]
20. Balanuca, B.; Stan, R.; Lungu, A.; Vasile, E.; Iovu, H. Hybrid networks based on epoxidized camelina oil. *Des. Monomers Polym.* **2017**, *20*, 10–17. [CrossRef]
21. Balanuca, B.; Ghebaur, A.; Stan, R.; Vuluga, D.M.; Vasile, E.; Iovu, H. New hybrid materials based on double-functionalized linseed oil and halloysite. *Polym. Adv. Technol.* **2018**, *29*, 1744–1752. [CrossRef]
22. Healey, P.; Sadleir, R.M.F.S. The construction of rectal electrodes. *J. Reprod. Fertil.* **1966**, *11*, 299–301. [CrossRef]
23. Barker, I.A.; Dove, A.P. Triarylsulfonium hexafluorophosphate salts as photoactivated acidic catalyst for ring-opening polymerization. *Chem. Commun.* **2013**, *49*, 1205–1207. [CrossRef] [PubMed]
24. Santiago-Medina, F.J.; Pizzi, A.; Basso, M.C.; Delmotte, L.; Abdalla, S. Polycondensation Resins by Lignin Reaction with (Poly)amines. *J. Renew. Mater.* **2017**, *5*, 388–399. [CrossRef]
25. Gosselink, R.J.A.; Sniijder, M.H.B.; Kranenbarg, A.; Keijsers, E.R.P.; de Jong, E.; Stigsson, L.L. Characterisation and application of NovaFiber lignin. *Ind. Crops Prod.* **2004**, *20*, 191–203. [CrossRef]
26. Rozman, H.D.; Koay, E.L.; Tay, G.S. Preliminary Study on the Utilization of Lignin as Filler in Ultra-Violet (UV) Curable System. *J. Appl. Polym. Sci.* **2011**, *120*, 2527–2533. [CrossRef]
27. Available online: <https://polymerdatabase.com/polymer%20classes/Lignin%20type.html> (accessed on 26 September 2021).
28. Patil, C.K.; Rajput, S.D.; Marathe, R.J.; Kulkarni, R.D.; Phadnis, H.; Sohn, D.; Mahulikar, P.P.; Gite, V.V. Synthesis of bio-based polyurethane coatings from vegetable oil and dicarboxylic acids. *Prog. Org. Coat.* **2017**, *106*, 87–95. [CrossRef]
29. Kawamoto, H. Lignin pyrolysis reactions. *J. Wood Sci.* **2017**, *63*, 117–132. [CrossRef]
30. Dastpak, A.; Yliniemi, K.; de Oliveira Monteiro, M.C.; Höhn, S.; Virtanen, S.; Lundström, M.; Wilson, B.P. From Waste to Valuable Resource: Lignin as a Sustainable Anti-Corrosion Coating. *Coatings* **2018**, *8*, 454. [CrossRef]
31. Wang, S.; Hu, Z.; Shi, J.; Chen, G.; Zhang, Q.; Weng, Z.; Wu, K.; Lu, M. Green synthesis of graphene with the assistance of modified lignin and its application in anticorrosive waterborne epoxy coatings. *Appl. Surf. Sci.* **2019**, *484*, 759–770. [CrossRef]



Review

# Synergic Effect of TiO<sub>2</sub> Filler on the Mechanical Properties of Polymer Nanocomposites

Cristina Cazan <sup>1,\*</sup>, Alexandru Enesca <sup>2</sup> and Luminita Andronic <sup>2</sup>

<sup>1</sup> Renewable Energy Systems and Recycling Research Center, Transilvania University of Brasov, 500036 Brasov, Romania

<sup>2</sup> Product Design, Mechatronics and Environment Department, Transilvania University of Brasov, 500036 Brasov, Romania; aenesca@unitbv.ro (A.E.); andronic-luminita@unitbv.ro (L.A.)

\* Correspondence: c.vladuta@unitbv.ro

**Abstract:** Nanocomposites with polymer matrix offer excellent opportunities to explore new functionalities beyond those of conventional materials. TiO<sub>2</sub>, as a reinforcement agent in polymeric nanocomposites, is a viable strategy that significantly enhanced their mechanical properties. The size of the filler plays an essential role in determining the mechanical properties of the nanocomposite. A defining feature of polymer nanocomposites is that the small size of the fillers leads to an increase in the interfacial area compared to traditional composites. The interfacial area generates a significant volume fraction of interfacial polymer, with properties different from the bulk polymer even at low loadings of the nanofiller. This review aims to provide specific guidelines on the correlations between the structures of TiO<sub>2</sub> nanocomposites with polymeric matrix and their mechanical properties. The correlations will be established and explained based on interfaces realized between the polymer matrix and inorganic filler. The paper focuses on the influence of the composition parameters (type of polymeric matrix, TiO<sub>2</sub> filler with surface modified/unmodified, additives) and technological parameters (processing methods, temperature, time, pressure) on the mechanical strength of TiO<sub>2</sub> nanocomposites with the polymeric matrix.

**Keywords:** polymer nanocomposites; TiO<sub>2</sub> nanoparticle; organic–inorganic interfaces; surface modification of TiO<sub>2</sub> nanoparticles

**Citation:** Cazan, C.; Enesca, A.; Andronic, L. Synergic Effect of TiO<sub>2</sub> Filler on the Mechanical Properties of Polymer Nanocomposites. *Polymers* **2021**, *13*, 2017. <https://doi.org/10.3390/polym13122017>

Academic Editor: Francesco Lufrano

Received: 9 May 2021  
Accepted: 18 June 2021  
Published: 20 June 2021

**Publisher's Note:** MDPI stays neutral with regard to jurisdictional claims in published maps and institutional affiliations.



**Copyright:** © 2021 by the authors. Licensee MDPI, Basel, Switzerland. This article is an open access article distributed under the terms and conditions of the Creative Commons Attribution (CC BY) license (<https://creativecommons.org/licenses/by/4.0/>).

## 1. Introduction

Polymer nanocomposites represent a new class of composite materials that generally exhibit better properties than traditional microcomposites, in terms of mechanical properties, thermal and dimensional stability, fire and chemical resistance, optical and electrical properties, etc. Polymer nanocomposites with inorganic fillers attracted significant attention due to their unique properties and their numerous applications in modern technology. The properties of polymer nanocomposites are mostly a simple combination of incorporated inorganic nanoparticles and polymeric matrix.

Polymeric materials can be used as matrices in nanocomposites due to their good thermal stability, environmental resistance (durability), and electrical, chemical and mechanical properties [1]. However, it is well known that some polymers (e.g., epoxy resin) are highly brittle. This disadvantage limits the application of these polymers in products that require high impact and fracture strength. Inorganic filler added into polymer matrix improved the mechanical performance of the polymeric nanocomposites. Nanofillers have large surface areas, making them chemically active, and making them interact more easily with the matrix [2]. There are many methods to reinforce polymers with rigid fillers to reduce the cost of production, alleviate some of the polymers limitations and expand their applications [3]. How fillers influence the characteristics of these polymers depends on the polymer nature and the proportion of the filler. Fillers are used to modify many properties

of polymers, such as mechanical [4] (flexural strength, tensile modulus, tensile strength, fracture toughness and impact energy), thermal, electrical, and magnetic properties [5,6].

The polymer mass, chemical structure, semi-crystallinity, chemical solubility, and thermal stability, and the nanoparticle surface area, chemical structure, and dispersion are essential for obtaining polymer nanocomposites and understanding their behavior. There are several methods to obtain polymeric nanocomposites, such as modified emulsion polymerization [7], in situ polymerizations [8,9], via direct blending (mechanical mixing) [10,11], solution dispersion [12–14], the sol-gel method and melt compounding [15,16], selective laser sintering process [17], and melt extrusion and injection molding [18,19]. Each process is specific, but the final morphology of the nanocomposites plays an important role. The morphology depends not only on the method of obtaining the nanocomposites, but also on the polymer–nanoparticle interactions that promote good dispersion and distribution of the nanoparticles in the polymer matrix [20,21].

Polymer nanocomposites have superior mechanical and physical properties over host polymers, due to the large interfacial area between the polymer matrix and nano-fillers.

Among the different fillers used, such as clays, silicas, nanotubes, inorganics, etc., titanium dioxide ( $\text{TiO}_2$ ) play a special role in polymeric matrices, to synthesize high-performance and malleable polymer networks (e.g., improving viscosity, obtaining filaments for 3D printing) [22–24].  $\text{TiO}_2$  is found in many applications due to its good photocatalytic properties, hence it is used in antiseptic and antibacterial compositions, degrading organic contaminants and germs, as a UV-resistant material; this is due to its chemical inertness properties, non-toxicity, low cost, high refractive index, and other advantageous surface properties. In these applications,  $\text{TiO}_2$  is used as a component of various types of nanocomposite materials with special properties, which open up opportunities in the following various fields of applicability: in the production of pharmaceuticals, cosmetics or paints [25], drug delivery systems with controlled release [26], solar cell [27], chemical sensing, luminescent material, and photocatalyst [28]. For example, as materials for obtaining membranes for integration in environmental applications, including water treatment or reducing humidification [29,30]. Polymer nanocomposites find applications in the development of optical and electronic devices, sensors, and bio-sensors [31,32].

The incorporation of  $\text{TiO}_2$  nanoparticles into different types of the polymeric matrix could produce synergistic effects. Studies have been performed on the  $\text{TiO}_2$  nanoparticle effect on several properties of polymeric composite, mainly to figure out whether the application of nanoparticles can enhance the mechanical performance of polymeric composites for applications in various fields.

This paper comprehensively reviews some essential aspects, such as the processing, characterization, and mechanical properties of various nanocomposites with a polymeric matrix and  $\text{TiO}_2$  fillers.

## 2. Polymeric Matrix

### 2.1. Matrix

The main component in the nanocomposite of the polymer matrix is the polymer itself. There are many varieties of polymers used in the preparation of polymeric matrix nanocomposites. These polymers can be thermoplastics, thermosetting, elastomers, natural, and biodegradable polymers. The choice of filler depends on the nature of the polymer, thus obtaining materials with the following specific properties: mechanical, electrical, magnetic, optical biocompatibility, chemical stability, and functionalization. Thermosetting polymer nanocomposites are usually the most common nanocomposites. They are used in many applications, but recently thermoplastic polymer nanocomposites have attracted much of the research interest in industry and academia. The properties of polymers depend mainly on the polymer structure, which in turn depends on the chemical composition, surface morphology, and processing parameters. Polymers are a source of a wide variety of low-priced raw materials, which offer many advantages, such as the following [10]: low specific weight, high material stability against corrosion, good electrical and thermal insu-

lation, ease of shaping and economical mass production, and attractive optical properties. However, they have some deficiencies in strength and stiffness. Fillers are integrated into polymer materials to make up for those deficiencies. These polymers can be epoxy resins, polyester fibreglass resins systems, PURs, PIs, urea, etc.

Theoretically, the associations that can be made between different polymers and the wide range of fillers are infinite. In practice, however, although numerous, the polymer–filler associations are limited. Among the thermoplastic polymers for the processing of which fillers can be introduced, the most important are as follows: polyolefin, polyamides, ABS polymers, polyesters, polycarbonates, and PVC. Elastomers are flexible polymers that comprise a low crosslink density and generally have low Young’s modulus, and by incorporating the fillers, these matrices can be more resistant [11].

## 2.2. Matrix–Filler Interface

The nature of the interface between the matrix and filler is an essential factor influencing the nanocomposite properties. According to Sharpe [33], the interface is defined as an intermediate region of two phases in contact, whose composition, structure, and properties vary throughout the area and are generally different from the two phases. Such phases are rarely devoid of chemical interaction. The volume of material affected by the interface interaction forms a three-dimensional zone, called the interphase. The term interphase is widely used in the adhesion community to indicate the presence of a chemically or mechanically altered zone between adjacent phases [34,35]. The interphase concept, according to Drzal [36], is schematically represented in Figure 1.

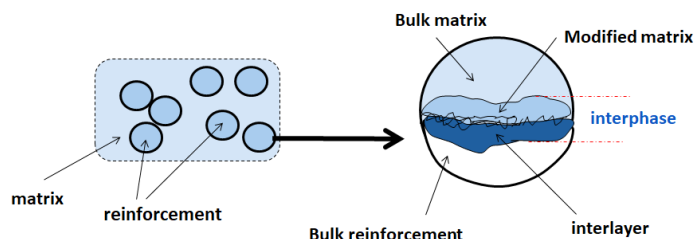


**Figure 1.** Representation of the interphase between matrix and fillers.

Knowledge of the relationship between microstructure and properties in the interface region is essential for the correct use of composite materials. There is no simple quantitative relationship for interface optimization that combines polymeric matrix and fillers [16]; the physicochemical variation and the thermodynamic–mechanical principles are sources of information for the qualitative assessment of the interface phenomena. Numerous researches have been carried out to improve the properties of the composites, particularly the interface when the filling is inorganic, for example,  $\text{TiO}_2$  [17].

Studies have shown [37,38] that the interface has different properties from both the matrix and the filler material. This consists of several layers that can each affect the adhesion of the components. The filler–matrix bonding depends on the following physicochemical aspects of the interfaces of the composite: atomic arrangement, molecular conformation, the chemical constitution of the fillers, matrix and fillers morphological properties, and the diffusivity of the elements in each constituent. The adhesion between the polymeric matrix and the dispersed phase particles was explained in mechanical and thermodynamic adhesion, chemical compatibility, chemical reactions with new bonds, electrostatic attraction forces, and macromolecular interdiffusion, adsorption and watering, as shown in Figure 2 [39]. The mechanical coupling or interlocking adhesion mechanism is based on the adhesive keying into the surface of the substrate [40] and locking the rough irregularities on the surface of the nanocomposites. In many studies, it was shown that the adhesion mechanism was due to interchain entanglement and not chemical bonding between the components of the composites. The mechanical adhesion primarily depends on the forces in the transition region between the non-contacting areas [41,42]. The thermodynamic

mechanism assumes that it does not require a molecular interaction for good adhesion, only an equilibrium process at the interface [43]. In neutral environments, such as air, the thermodynamics of the polymer system will attempt to minimize the surface free energy by orientating the surface into the non-polar region of the polymer. When the polymer surface is in contact with a polar substance, such as water, good adhesion requires that the interfacial tension be minimized [44]. The other theories mentioned above are explained based on the physico-chemical interactions between the components of the composites.

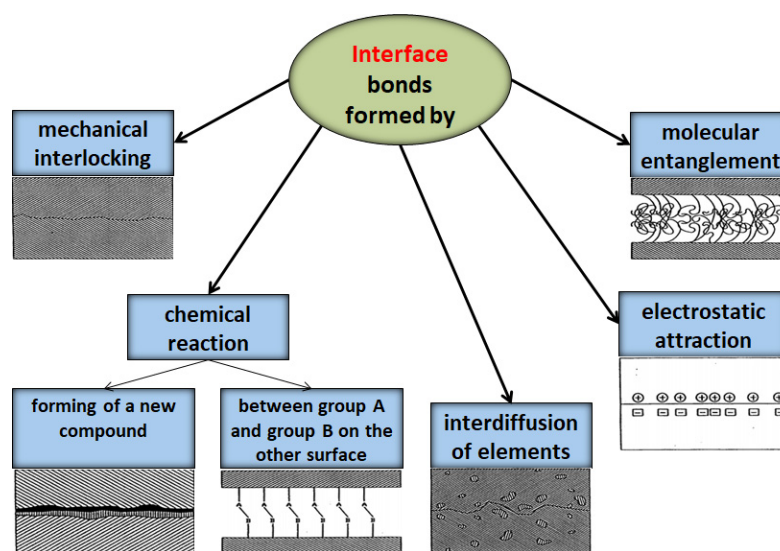


**Figure 2.** The formation of the interface between matrix and filler.

### 2.3. Fillers and Surface Modifications

Composite materials with optimal performances are obtained if an optimal adhesion between the matrix and the filler is achieved. Optimal adhesion is realized between materials of close chemical nature. It is weak between very different materials, from a chemical point of view, such as between the polymer matrix and inorganic fillers. Thus, the adhesion can be improved by treating the surface of the dispersed particles with coupling agents. Surface modification of fillers is becoming more important because of its adhesion improvement on the stress transfer between polymer and filler, which leads to an increase in the dispersion degree [45]. The coupling agent diffusion and adsorption processes at the surface of the filler particles occur at the interface. The properties of the interface and the adhesion of the components can be modified by treating the surface of the fillers before introduction into the polymer matrix. These treatments either remove the weaker layers related to the filler surface of the material or introduce new functional groups capable of influencing the adhesion between the materials.

Surface treatment of the fillers can be achieved by [46,47] the following:

- The chemical interaction of the fillers with compounds that possess functional groups;
- Chemical absorption on the surface of the particles of the filling material of some modifying agents;
- Coating the filler particles with a suitable coupling agent.

These processes are generally laborious and increase the cost of the fillers, but they offer the possibility of considerably increasing the fillers content in mixtures without worsening their characteristics.

Modification of the surface of fillers is becoming more important because of its improvement in adhesion [48]. Hence, it is on the stress transfer between the polymer and filler, leading to an increase in the dispersion degree.

### 3. Titanium Dioxide Nanoparticles

#### 3.1. Size, Shape and Specific Surface Area of the Nanoparticles

Titanium dioxide ( $\text{TiO}_2$ ) is the natural oxide of the element titanium. Titanium dioxide adopts four structures polymorphs found in nature rutile, anatase, brookite, and  $\text{TiO}_2$  (B). An additional four high-pressure forms have been synthesized, as follows:  $\text{TiO}_2$  (II) with the  $\alpha\text{-PbO}_2$  structure,  $\text{TiO}_2$  (H) with hollandite, baddeleyite with  $\text{ZrO}_2$ , and cotunnite with  $\text{PdCl}_2$  [49]. Among the eight structures, rutile and anatase are mostly manufactured in the chemical industry as microcrystalline materials. Thermodynamically, rutile is the most stable phase at all temperatures and pressures below 60 kbar, when  $\text{TiO}_2$  (II) becomes the favourable phase. Particle size influences surface energy and phase stability. Thus, anatase is most stable at sizes less than 11 nm, brookite at sizes between 11 and 35 nm, and rutile at sizes greater than 35 nm. Anatase and brookite are more stable than rutile at nano-size, due to the differences in surface energy. Anatase is more stable than brookite at even smaller sizes [50]. From a commercial point of view, titanium dioxide can be found in the following two common forms that differ in crystal structure: anatase and rutile [51–53].

Titanium dioxide can be prepared in the following various morphologies: nanoparticles, nanowires, nanotubes, and mesoporous structures. There are physical and chemical methods for synthesizing  $\text{TiO}_2$  nanoparticles in the liquid phase, as follows: hydrothermal/solvothermal method, sonochemical method, electrochemical synthesis, sol-gel method, microwave field synthesis, and vapor phase, which includes spraying, atomic deposition of layers, pulsed laser deposition, chemical vapor deposition, physical vapor deposition, and pyrolysis spray [54,55]. The controllable synthesis of  $\text{TiO}_2$  with unusual morphologies and dimensions can give the polymeric matrices with particular features and qualities.

The specific surface area of  $\text{TiO}_2$  increases as the particle size decreases, meaning nanoparticles are attracted due to van der Waal electrostatic forces. With the decreasing particle size, the ratio of surface/volume increases. Therefore, the smaller the particles are, the more important the surface properties will be, influencing agglomeration behavior and interfacial properties as a result of interaction with the polymer matrix [56,57]. The formation of particle agglomerates and non-uniform dispersion has motivated research to better process polymer– $\text{TiO}_2$  nanocomposites. Several methods have been approached to minimize agglomeration and ensure better distribution. Such methods may be as follows: melt mixing, solution mixing in aqueous media or polymer matrices, particle surface modification involving polymer surfactant molecules or other modifiers, which must generate a strong repulsion between nanoparticles, mechanical stirring, and ultrasonic irradiation.

#### 3.2. Surface Modification of $\text{TiO}_2$ Nanoparticles

$\text{TiO}_2$  nanoparticles can be directly added to the organic matrix, but due to the high surface area and high polarity, there is a strong tendency for them to aggregate.  $\text{TiO}_2$  nanoparticles form agglomerates at higher concentrations due to their high surface energy. Surface modification of  $\text{TiO}_2$  nanoparticles effectively reduces their surface energy and improves their dispersion properties in the organic matrix. Therefore, to improve the homogeneous dispersion of nanoparticles, many researchers have focused on the surface modification of nanoparticles and a new method for incorporating inorganic nanofiller into an organic matrix [58–60]. Several ways have been employed to modify the surface of nanoparticles [61,62].

The surface modification of  $\text{TiO}_2$  nanoparticles is often conducted by either a physical or chemical method. The chemical method has attracted the attention of many researchers because the interactions between inorganic nanoparticles and the matrix are much stronger [63]. The surface modification of nanoparticles by chemical treatments is a useful method to improve the dispersion stability of  $\text{TiO}_2$  nanoparticles and the development of interfaces between the organic and inorganic phase. In this regard, the concept of silane coupling agent was reported by Plueddemann and et al. [64]. Researchers found that



organofunctional silanes are silicon chemicals that contain both organic and inorganic reactivity in the same molecule, and which can be used as coupling agents [65,66]. Coupling agents connect resin and fillers, and improve the physical, mechanical and electrical properties of composites. Moreover, they enhance the wetting of inorganic substrates, decrease the viscosity of the resin during mixing, and ensure smoother surfaces of composites [67,68].

The general formulation of the coupling agent molecule is as X–R, where X interacts with the filler and R is compatible with the polymer. Organosilanes are of the form R–Si–(OR')<sub>3</sub>, where OR' can be methoxy, ethoxy, acetoxy, and R can be alkyl, aryl or organofunctional group [56]. According to this structure, the following steps may take place, as shown in Figure 3:

- ✓ Hydrolyzation of alkoxy groups obtaining silanol, which reacts with the mineral surface;
- ✓ The condensation reaction between silanol molecules;
- ✓ Bond formation between TiO<sub>2</sub> nanoparticles and the organofunctional group.

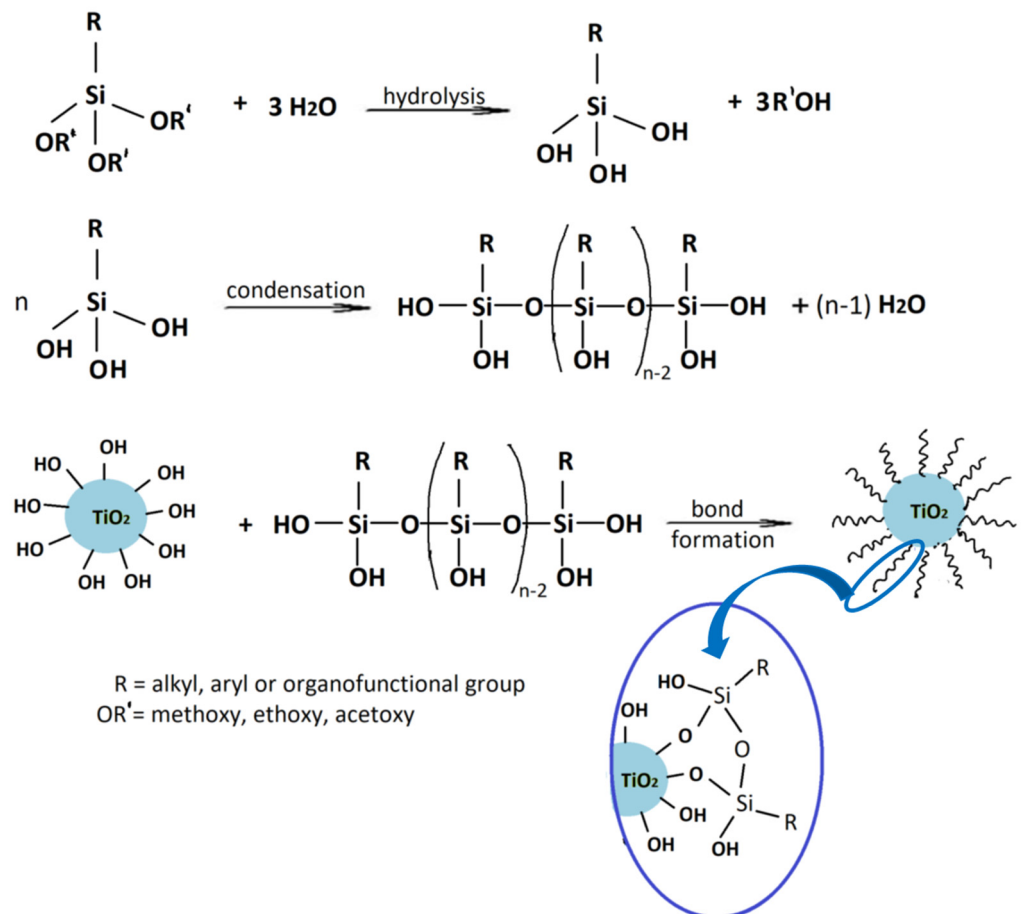


**Figure 3.** The interaction between the coupling agent molecule and the filler.

The choice of organosilane is established, taking into account the polymers chemical structure to be compatible. For example: for a phenolic and epoxy resin an epoxy silane, or an amino silane is recommended and for an unsaturated polyester resin a methacrylsilane. The reactivity of the thermosetting polymers should be close to that of organosilane. For a thermoplastic matrix, bonding occurs by diffusion of the organosilane network in the interphase region of the composite [66].

There were silane coupling agents used, such as 3-methacryloxypropyl-trimethoxysilane (MPS) [68], 3-aminopropyltriethoxysilane (APTES) [69],  $\gamma$ -glycidoxypropyltrimethoxysilane (GPS) [70], n-propyltriethoxysilane and 3-methacryloxypropyltrimethoxysilane [71], which

change the hydrophilic particles into a hydrophobic surface by providing some molecules with certain hydrophobicity.

Some coupling agent recommendations for the surface modification of TiO<sub>2</sub> nanoparticles is given in Table 1.

**Table 1.** Surface modification of TiO<sub>2</sub> nanoparticles.

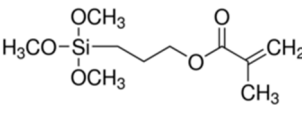
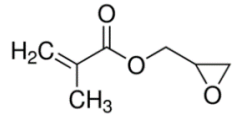
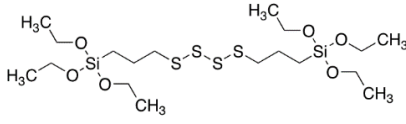
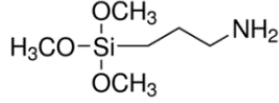
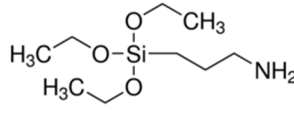
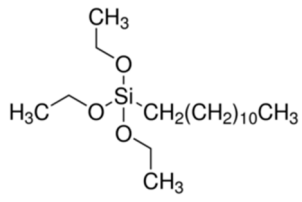
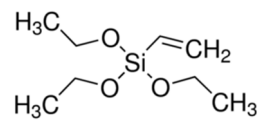
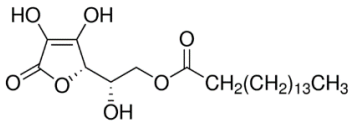
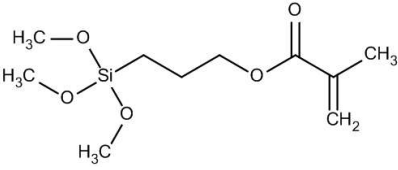
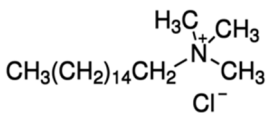
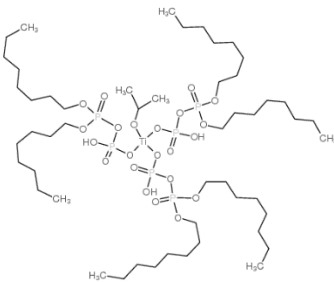
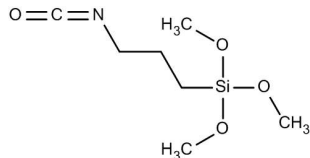
| Modification Agent of TiO <sub>2</sub> Surface    | Chemical Structure  | Polymer-TiO <sub>2</sub> Nanocomposite   | Ref        |
|---|---|--|------------|
| 3-(trimethoxysilyl)propyl methacrylate, KH-570    |    | silicone rubber-TiO <sub>2</sub> nanocomposite   | [72]       |
| fluoro silane                                     | H <sub>3</sub> Si-F   | HDPE-TiO <sub>2</sub> nanocomposite  | [73]       |
| glycidyl methacrylate                             |    | methyl methacrylate-butyl acrylate/dimethylaminoethyl methacrylate-butyl acrylate-acrylic acid-TiO <sub>2</sub> nanoparticles                              | [74]       |
| bis-(3-triethoxysilyl)propyl tetrasulfide (TESPT) |    | rubber-TiO <sub>2</sub> nanocomposite  | [75]       |
| 3-amino propyl trimethoxy silane                  |   | PA11-TiO <sub>2</sub> nanocomposite;PU-TiO <sub>2</sub> composites;  | [76,77]    |
| 3-amino propyl triethoxy silane                   |  | nylon 6/TiO <sub>2</sub> composites;PS-TiO <sub>2</sub> microcomposites;polyurethane-TiO <sub>2</sub> composites;polyamide-TiO <sub>2</sub> nanocomposites | [45,77,78] |
| hexadecyl trimethoxy silane                       |  | PE-TiO <sub>2</sub> nanocomposite  | [79]       |
| vinyl trimethoxy silane (VTMS)                    |  | LDPE-TiO <sub>2</sub> nanocomposite  | [80]       |
| 6-palmitate ascorbic acid                         |  | PMMA-TiO <sub>2</sub> nanocomposite  | [81]       |
| 3-methacryloxy propyl trimethoxy silane           |  | PMMA-TiO <sub>2</sub> nanocomposite;acrylonitrile-styrene-acrylate terpolymer-TiO <sub>2</sub> composite;PS-b-PMMA-TiO <sub>2</sub> nanocomposite          | [82,83]    |

Table 1. Cont.

| Modification Agent of TiO <sub>2</sub> Surface        | Chemical Structure  | Polymer–TiO <sub>2</sub> Nanocomposite   | Ref  |
|---|---|--|------|
| cetyl trimethylammonium chloride (TMAC) amphiphilics  |  | PS-b-PMMA–TiO <sub>2</sub> nanocomposite | [84] |
| isopropyl tri(dioctylpyrophosphate) titanate (TCA201) |  | EP-PU/TiO <sub>2</sub> composite         | [85] |
| 3-isocyanato propyl trimethoxy silane                 |  | polymer–TiO <sub>2</sub>                 | [86] |

Silane coupling agents are usually employed to realize chemical modification. These can offer hydrolyzable groups bonding with the inorganic particles. After bond formation, the organosilane functional groups of silane coupling agents form a hydrophobic layer on the surface of the inorganic nanoparticles. Different coupling agents have been used to modify the surface of TiO<sub>2</sub> and improve the interfacial interactions necessary for the successful incorporation of these hydrophilic nanoparticles into hydrophobic polymer matrices.

The surface modification of TiO<sub>2</sub> has been reported using different silane coupling agents, such as 3-aminopropyltriethoxysilane (APTES). The photocatalytic activity of TiO<sub>2</sub> has been shown to increase with increasing the concentration of APTES used [87]. For example, Mallakpour and Barati [88] reported the surface modification of TiO<sub>2</sub> nanoparticles by the reaction with APTES. The silane coupling agent was adsorbed on the surface of the nanoparticles at its hydrophilic end and interacted with the hydroxyl groups pre-existing on the surface of the nanoparticles. Thus, it was confirmed that the heat stability of the nanocomposite was improved. Shakeri et al. [89] studied the self-cleaning capability of surfaces covered TiO<sub>2</sub> nanoparticles, modified by APTES. They concluded that the surface could degrade the dye used as an organic pollutant due to the obtained coating being stable. Klaysri et al. [90] proposed a one-step synthesis method of APTES-functionalized TiO<sub>2</sub> surface. They showed that obtained nanomaterials are capable of the photocatalytic decolonization of methylene blue.

Modification of the surface of TiO<sub>2</sub> nanoparticles with silane coupling agents was obtained via reflux in an aqueous solution [75,91]. Chen et al. investigated the interactions between 3-aminopropyltrimethoxysilane (APTMS) and phenyltrimethoxysilane with commercially available TiO<sub>2</sub> nanoparticles (Degussa P-25) [91]. They obtained results showing that the silane coupling agents used bind covalently on the surface of the TiO<sub>2</sub> nanoparticles. In another study, Zhao et al. reported the cross-linking and chemical bonding mechanisms of APTMS and 3-isocyanatopropyltrimethoxysilane on TiO<sub>2</sub> nanoparticles [75].

To improve TiO<sub>2</sub> nanoparticles dispersion and enhance the interactions between the nanoparticles and polymeric matrix (polyamide/modified–TiO<sub>2</sub> nanocomposites), the surface of TiO<sub>2</sub> was modified with a 1,3,5-triazine based silane coupling agent [92].

Caris et al. [93] used conventional emulsion polymerization to encapsulate TiO<sub>2</sub> in poly(methyl methacrylate) (PMMA). Sidorenko et al. [84] investigated the radical polymerization of styrene and methyl methacrylate (MMA). This reaction was initiated at the surface of TiO<sub>2</sub> particles by adsorbed hydroperoxide macroinitiators. Erdem et al. [94] encapsulated the TiO<sub>2</sub> nanoparticles by miniemulsion polymerization of styrene, polybutene-succinimide pentamine being used as the stabilizer at the oil/water interface. Rong et al. [95] used the TiO<sub>2</sub> nanoparticles modified by 3-(trimethoxysilyl) propylmethacrylate (MPS) to copolymerize styrene with the methacrylate group of MPS, by free-radical polymerization. Yang and Dan [96] used a similar approach by graft polymerized MMA on the modified surface of the TiO<sub>2</sub> nanoparticles.

Milanesi et al. used a mixture of isomeric octyltriethoxysilanes (OTES), highlighting the hydrophobic layer structure. They concluded that the cross-linking (via Si–O–Si bonds) and chemical bonding (via Ti–O–Si bonds) of silanes onto TiO<sub>2</sub> nanoparticles occurred [97]. Xiang et al. used 3-methacryloxypropyl-trimethoxysilane (MPS) to modify the TiO<sub>2</sub> surface to enhance the compatibility of TiO<sub>2</sub> nanoparticles in the poly(butyl acrylate) (PBA) matrix. The modified TiO<sub>2</sub> presented good compatibility in the PBA matrix [98]. In another study [83], Xiang showed the hydrophobic surface modification of TiO<sub>2</sub> to produce acrylonitrile-styrene-acrylate (ASA) terpolymer–TiO<sub>2</sub> composites for cool materials. Wang et al. [99] functionalized the commercial TiO<sub>2</sub> nanoparticles in an aqueous solution via ultrasonic treatment at room temperature with 3-(trimethoxysilyl)propyl methacrylate.

Godnjavec et al. have coated TiO<sub>2</sub> nanoparticles by 3-glycidyoxypropyltrimethoxysilane (GLYMO) as an additive in a clear polyacrylic coating. According to their results, grafting GLYMO on the nanoparticles surface improved the dispersion, transparency, and UV protection of the clear acrylic coating [100].

Yang et al. [101] reported silanization of TiO<sub>2</sub> particles through a sol-gel method. Based on their results, vinyl triethoxysilane (VTES) as a surface modifier improved the stability of dispersion and suspension in tetrachloroethylene. Dalod et al. [50] modified TiO<sub>2</sub> nanoparticles with amino silane groups using a hydrothermal method and found that the nanoparticles shape and structure depends on the type of silane coupling groups.

Tangchantra et al. [102] investigated the effect of different silane coupling agents on the surface grafting of TiO<sub>2</sub> with hexadecyl trimethoxysilane (HTMS), triethoxyvinylsilane (TEVS), and aminopropyl trimethoxysilane (APS). The results showed that silane coupling agents could modify the surface of TiO<sub>2</sub> nanoparticles via the hydrolytic condensation of titanium isopropoxide. The TEVS agent improved the dispersibility of TiO<sub>2</sub> particles and showed optimum mechanical properties.

The appropriate surface modification on nanoparticles leads to better dispersion and compatibility in the polymer matrix. The formation of chemical and physical interactions with the polymer matrix could guarantee remarkable mechanical properties of polymeric nanocomposites.

### 3.3. Properties, Commercial Products and Applications

At the nanoscale size, the material properties may dramatically change and differ significantly from their bulk counterparts.

Particular attention has been paid, in recent years, to obtaining TiO<sub>2</sub> with photocatalytic properties [103–106], optical properties [107], with applications related to the degradation of pollutants [108–110], and the realization of the photoelectrochemical cells [111]. Also of interest are titanium dioxide films deposited on various substrates to obtain special characteristics, such as surfaces with self-cleaning properties [112,113].

All applications of TiO<sub>2</sub> nanoparticles depend on their crystal structure, morphology, specific surface area, particle size, and form. TiO<sub>2</sub> has been widely used in the industry for many years for its numerous and diverse applications, as shown in Table 2.

**Table 2.** Some properties of TiO<sub>2</sub> and applications.

| Application                                 | Properties   |
|---|--|
| Photocatalysis                              | Particularly in anatase form under ultraviolet light   |
| Self-cleaning and anti-fogging glass        | Spiked with nitrogen ions or droplet with metal oxides under UV–visible light                              |
| Hydrolysis catalyst                         | Super hydrophilicity, deodorizing, sterilizing, anti-fouling; chemical resistance                          |
| Dye-sensitized solar cells                  | Strong oxidative potential for develop OH radicals   |
| Pigments, opacifiers, cosmetic, UV absorber | Brightness, high reflective index, high reflective optical, perfect white, opacity, nontoxic to human life |

The applications that can be mentioned are sensors, photo-conductors, additives in plastics, catalysts, photo-/electrochromics and photovoltaics applications, dye-sensitized solar cells, sunscreens, paints, antimicrobial applications, water purification by photocatalysis processes, biosensing, and drug delivery [114]. TiO<sub>2</sub> nanoparticles incorporated into outdoor building materials, such as paving stones or paints, can reduce volatile organic compounds and nitrogen oxide concentrations.

TiO<sub>2</sub> is a material with multifunctional properties that can be incorporated in polymeric matrices as a filler to develop new nanocomposites with enhanced properties [115].

#### 4. Polymeric Nanocomposites with TiO<sub>2</sub> Filler

##### 4.1. Preparation Methods

Polymeric matrix nanocomposites can be obtained using injection molding, compression molding, in situ polymerization, sol-gel, melt mixing and sintering.

In situ polymerization involves the dispersion of inorganic nanoparticles in a monomer phase as a first step, followed by bulk phase polymerization. This process is mainly used for thermosetting polymers. As a result, unstable nanocomposites can be transform into a different morphology than expected. The in situ polymerization method is a simple and inexpensive method. The nanocomposites with the polymer matrix, and inorganic filler with good filler distribution in the polymer matrix, can be obtained [116].

Most compression molding techniques require pre-treatment of the nanoparticles with curing, but injection molding is the most widely used process for obtaining nanocomposite materials. Injection molding can be used in a variety of applications, in both commercial and research fields [117]. Sintering, powder compaction and sol-gel are all alternative techniques to produce polymeric composites. However, the operating conditions (temperature, pressure, time, etc.) are far more than those of injection molding [118]. Some reports were found in the literature focusing on obtaining TiO<sub>2</sub> nanocomposites with the polymeric matrix, as shown in Table 3.

Studies on polymer–TiO<sub>2</sub> nanocomposites prepared by melt mixing have shown a slight improvement or no change in mechanical properties [119,120]. Somani et al. [121] received highly piezoresistive conducting polyaniline/TiO<sub>2</sub> composite by in situ deposition technique at a low temperature. Feng et al. [122] synthesized a composite of polyaniline-encapsulating TiO<sub>2</sub> nanoparticles by in situ emulsion polymerization. They investigated and explained the interaction between polyaniline and nano-TiO<sub>2</sub> particles, and the nature of chain growth according to Fourier transform infrared (FTIR) spectra. Xia and Wang [123] prepared a polyaniline/nanocrystalline TiO<sub>2</sub> composite by ultrasonic irradiation. They think that ultrasonic irradiation provides a new way to prepare 0–3-dimensional conducting polymer/nanocrystalline composites.

Titanium dioxide has been used to reinforce polypropylene (PP) via extrusion, followed by injection molding, by Alghamdi [124]. There were presented to the mechanical

and structural aspects of PP for different loading of TiO<sub>2</sub> filler (up to 30 wt. %). As the TiO<sub>2</sub> weight percent increases, the impact strength decreases. This behaviour is expected because the PP is incompatible with TiO<sub>2</sub>. The PP phase is non-polar, hydrophobic and has low surface energy, while TiO<sub>2</sub> represent the polar phase, hydrophilic and high surface energy for TiO<sub>2</sub>. The highest resilience value was recorded for the sample with 20% TiO<sub>2</sub> (37.09 ± 5.3 J/m).

Mourad et al. [117] studied HDPE nanocomposites with 5% TiO<sub>2</sub>, obtained by injection molding under the following different processing parameters: temperature, pressure, injection velocity, and injection time. The results showed the influence of processing parameters on the mechanical and thermal properties of HDPE–TiO<sub>2</sub> nanocomposites. Mechanical testing revealed that the tensile strength varied from 22.5 to 26.3 MPa, while the Young modulus increased by 8.6% as the molding temperature increased.

Vladuta et al. [125] investigated the effect of the TiO<sub>2</sub> nanoparticles on the PET–rubber interface in nanocomposites obtained from waste by compression molding. The modifications in surface energy, morphology and crystalline structure were discussed for samples kept under visible light and UV radiation. TiO<sub>2</sub> develops new physical interactions in the composite, but induces, even in visible light, oxidation processes. The results indicated that the optimum concentration for TiO<sub>2</sub> to the composites, for obtaining better interface properties, is 0.25 wt. %.

Regardless of the method of obtaining nanocomposites with the polymeric matrix, it is found that the nature of filler has a significant influence on mechanical properties.

#### 4.2. Mechanical Properties

Titanium dioxide is used as a filler in many polymeric matrices because of the improved physical and mechanical properties it yields. Many studies showed improvements in the mechanical strength and modulus of TiO<sub>2</sub>-filled polymeric nanocomposites compared to the pristine-base matrix. The mechanical properties of the TiO<sub>2</sub> nanocomposites depend significantly on their internal structure. The poor compatibility of hydrophilic TiO<sub>2</sub> nanoparticles with a hydrophobic polymer matrix may lead to particle aggregates and/or agglomerates. The aggregates create defect sites in the nanocomposites, and the improvement in mechanical properties is not observed. More uniform dispersion of nanoparticles is recommended, using one-dimensional nanoparticles, i.e., nanorods, nanotubes or nanoribbons, particles with a high aspect ratio [46]. Several factors that may influence the mechanical properties of composites with a polymer matrix and inorganic fillers are presented in Figure 4.

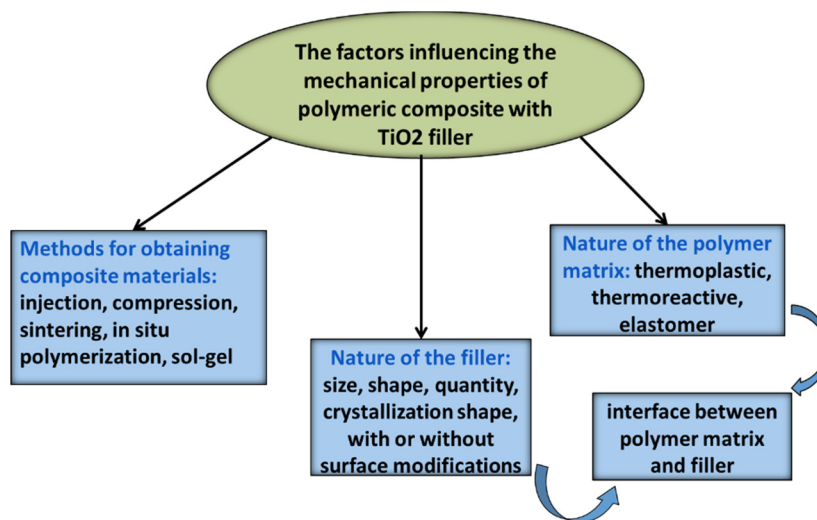


Figure 4. The factors that influence the mechanical properties of composites materials.

#### 4.2.1. The Nature of the Filler

TiO<sub>2</sub> fillers affect the basic mechanical properties of the polymer. The effect of TiO<sub>2</sub> fillers on composites properties depends on the particle size and shape, concentration and the interaction with the matrix, as shown in Table 3. For example, to increase the modulus and hardness of polymers, micrometre-sized inorganic particles are frequently applied. However, a reduction in the material ductility may take place. By diminishing the particle size or by enhancing the particle volume fraction, the strength can be improved. Still, in some cases, the fracture toughness and modulus remain relatively independent of the particle size. The properties of TiO<sub>2</sub> that make it a good filler for composite materials are good dispersibility in the polymer system and good heat stability. Titanium dioxide has a relatively high elastic modulus, which can be frequently combined into various polymers to obtain the composites mechanical gain.

Mikešová and et al. [126] studied the effects of nanoparticles and the properties of the nanocomposites of polypropylene and filler TiO<sub>2</sub>. They used isotactic polypropylene (PP) as a matrix, and as fillers they used TiO<sub>2</sub> in the following different shapes: a commercial titanium dioxide micropowder (mTiO<sub>2</sub>; a mixture of anatase and rutile), a commercial titanium dioxide nanopowder (nTiO<sub>2</sub>; anatase modification), and titanate nanotubes (TiNT). More series of samples were obtained with PP unmodified and with PP modified by electron beam irradiation (PP\*), resulting in PP\*/TiX composites (i.e., PP\*/mTiO<sub>2</sub>, PP\*/nTiO<sub>2</sub>, and PP\*/TiNT). These were prepared by melt mixing of PP\* with 5 wt. % of TiX. The stiffness and microhardness properties of PP\*/TiX systems are improved in the order PP\*/mTiO<sub>2</sub>, PP\*/nTiO<sub>2</sub>, PP\*/TiNT, due to the specific surface of the TiX particles.

Nano-sized TiO<sub>2</sub> was further studied in starch/(poly[vinyl alcohol]) blends by Sreekumar et al. [127]. The nano-sized TiO<sub>2</sub> could provide the composite with superior mechanical properties because of good interfacial adhesion between the polymer matrix and filler.

Bora et al. [128] studied the effect of TiO<sub>2</sub> particle concentrations (up to 25 wt. %) on the properties of polyphenylenesulphide (PPS)–TiO<sub>2</sub> composites. The increase in TiO<sub>2</sub> particle concentrations in the PPS matrix improves the stiffness of the composite. High values of flexural and residual flexural strength were obtained at 10 wt. % TiO<sub>2</sub> particle concentrations. Saluja et al. [129] obtained polyester composites filled with TiO<sub>2</sub> concentrations up to 25 wt. %. This study shows that the addition of TiO<sub>2</sub> particles improves the effective thermal conductivity of polyester–TiO<sub>2</sub> composites, the glass transition temperature (T<sub>g</sub>), and the reduction in the coefficient of thermal expansion (CTE).

The mechanical properties of nanocomposites depend significantly on their internal structure. In the nanocomposite, TiO<sub>2</sub> nanoparticles can appear as agglomerations due to their low compatibility with the hydrophobic polymer matrix.

In this case, the large surface area of the nanowires decreases rapidly, the aggregates create defect sites in the nanocomposites, and no improvement in the mechanical *properties* is observed. A more uniform dispersion of nanoparticles, using one-dimensional (1D) nanoparticles, i.e., nanorods, nanotubes, or nanoribbons, would improve these properties. Compared with the isometric nanoparticles, a large surface-to-volume ratio of the 1D nanoparticle generally improves the nanocomposites properties. Contrary to the anatase polymer nanocomposites, only a few papers concerning polymers filled with titanate nanotubes have been found in the literature [130–132].

The majority of nanoparticle fillers added in the polymer matrix improve mechanical properties such as flexibility, ductility, hardness, and strength and stiffness, even in small amounts.

#### 4.2.2. The Nature of the Polymer Matrix

Polymer–TiO<sub>2</sub> nanocomposites have been successfully synthesized in different polymer matrices such as the following thermoplastic polymers: polyacrylate, poly (methyl methacrylate), polyimide, polystyrene, and polyolefines; the following thermosetting polymers: polycarbonate, polyamide 6, epoxy, unsaturated polyester; and silicone elastomer [77,132].

Saritha et al. [133] studied the incorporation of TiO<sub>2</sub> in rubber composites. The tensile strength, modulus, and tear strength increased with increasing TiO<sub>2</sub> loading. More recently, processing techniques were developed to allow the size of TiO<sub>2</sub> to decrease to the nanoscale. Manap et al. [134] demonstrated that TiO<sub>2</sub> and multi-walled carbon nanotubes (MWCNT) as filler reinforcements could address the agglomeration issue, by exhibiting even distribution of particles in the TPU matrix. The combination of MWCNT and TiO<sub>2</sub> in the TPU matrix enhanced the mechanical and thermal properties significantly, this being a good heat insulator.

In the function of the matrix nature, the percentage by weight of the inorganic filler introduced can remain very low (on the order of 0.5% to 5%) due to the incredibly high surface area-to-volume ratio of the particles. This area can generate a new material behavior, which is widely determined by interfacial interactions, offering unique properties and an entirely new class of materials. Several important types of research in this regard are presented in Table 3.

When designing new polymer–TiO<sub>2</sub> nanoparticle composites, the following aspects should be considered:

- Nature of filler and polymer matrix;
- Amount of filler;
- The distribution of filler, this should not form agglomerates in the samples;
- Concentration of coupling agent for modifying of filler surface;
- The method of obtaining, which is an essential factor.

The impact resistance of polymer matrices with TiO<sub>2</sub> filled is of particular interest to researchers, as long as it represents the weak point of most composite materials. Hardening of thermoplastics by modification with elastomers could be a new way to solve this problem. It is recommended to study new cheaper and more efficient polymer matrices to produce composites with predetermined properties. In this case, we recommend using of polymeric waste as a matrix for obtaining nanocomposites with TiO<sub>2</sub> filler.

Polymer nanocomposites give a new way to overcome the limitations of pure polymers or their traditional composites. Nowadays, polymer nanocomposites with TiO<sub>2</sub> filled represent an area of interest for many researchers. This article contains information on the nature of the polymer matrix (thermoplastic, thermosetting, elastomeric) and the type of TiO<sub>2</sub> filler, processing methods, possible surface modifications of the filler and how they influence the mechanical properties of nanocomposites, thus completing the areas of knowledge for many researchers.

#### *4.3. Advantages, Limits and Applications*

Polymeric materials can be used as matrices in TiO<sub>2</sub> nanocomposites due to their good thermal stability, environmental resistance (durability), and electrical, chemical and mechanical properties. However, it is well known that some polymers (e.g., epoxy resin, polyamides) are highly brittle. This disadvantage limits the application of these polymers in products that require high impact and fracture strength. TiO<sub>2</sub> filler added in the polymer matrix improves the mechanical performance of the polymeric nanocomposites over conventional polymer composites, as shown in Table 4. Finally, typical existing and potential applications are shown in Figure 5.



Table 3. Types of nanocomposites with polymeric matrix and TiO<sub>2</sub> filler.

| Composites                                    | Materials   | Methods   | Results-Mechanical Properties   | Ref.  |
|---|---|---|---|-------|
| Polystyrene (PS)-TiO <sub>2</sub>             | <b>Thermoplastic matrix</b><br><i>Obtaining:</i> mixing of matrix with TiO <sub>2</sub> -coupling agent<br><i>Characterization:</i> mechanical tests, SEM analysis. |   | Values of Young's modulus, tensile strength, elongation at break, flexural strength increase with linearly filler concentration followed by a decrease beyond 15 wt. %.   | [45]  |
|   | <i>Matrix:</i> polystyrene.<br><i>Filler:</i> TiO <sub>2</sub> (0.19 µm)<br><i>Coupling agent:</i> 3-amino ethoxy silane (0.1, 0.5 and 1 wt. %).                    |   |   |       |
| Polyphenylene sulfide (PPS)-TiO <sub>2</sub>  | <i>Matrix:</i> polyphenylenesulphide (PPS)<br><i>Filler:</i> TiO <sub>2</sub> (200 nm; 0, 5, 10, 15, 20, and 25 wt. %)  | <i>Obtaining:</i> injection molding.<br><i>Characterization:</i> solid particle erosion test, three-point bending test, thermal analyzing methods.  | The flexural modulus of composites increased with the increase in TiO <sub>2</sub> concentration up to 10 wt. %, and then it decreases. TiO <sub>2</sub> filler caused to reduce the erosion resistance of the PPS composites.  | [128] |
| Polypropylene (PP)-TiO <sub>2</sub>           | <i>Matrix:</i> PP pellets;<br><i>Filler:</i> TiO <sub>2</sub> (0, 10, 20 and 30 wt. %)  | <i>Obtaining:</i> injection molding<br><i>Characterization:</i> mechanical properties: tensile stress, impact tests; TGA  | The highest resilience value recorded for the sample with 20% TiO <sub>2</sub> (37.09 ± 5.3 J/m). Tensile stress shows a decrease and the E modulus increase as the weight percent of TiO <sub>2</sub> increases.   | [124] |
| Polypropylene (PP)-TiO <sub>2</sub>           | <i>Matrix:</i> polypropylene (PP)<br><i>Filler:</i> TiO <sub>2</sub> micropowder; TiO <sub>2</sub> nanopowder titanate nanotubes (TiNT)                             | <i>Obtaining:</i> melt mixing; samples types PP*/TiX (PP*/mTiO <sub>2</sub> , PP*/nTiO <sub>2</sub> , PP*/TiNT) and samples with PP unmodified.<br><i>Characterization:</i> SEM analysis, TEM analysis, mechanical properties | The stiffness and microhardness of the PP-TiNT nanocomposites increase by 27% and, respectively, 33%. In the PP-nTiO <sub>2</sub> nanocomposites, the increase in these mechanical characteristics is lower.  | [126] |
| Polypropylene (PP)-TiO <sub>2</sub>           | <i>Matrix:</i> PP homopolymer<br><i>Filler:</i> TiO <sub>2</sub> (0–3 wt. %)  | <i>Obtaining:</i> melt compounding;<br><i>Characterization:</i> mechanical properties, thermogravimetric analysis, DSC, SEM analysis  | The addition of TiO <sub>2</sub> nanoparticles increases the mechanical properties of PP fibres. Tenacity is increased by 72.69% for the PP-TiO <sub>2</sub> (3 wt. %) nanoparticle. Elongation at break of the PP fibres with TiO <sub>2</sub> (1.5 wt. %) indicated an increase of 15.79%.  | [135] |
| Polypropylene (PP)-rice husk-TiO <sub>2</sub> | <i>Matrix:</i> polypropylene (PP)<br><i>Filler:</i> rice husk and TiO <sub>2</sub>  | <i>Obtaining:</i> injection molding<br><i>Characterization:</i> mechanical properties, SEM, TGA   | Incorporating inorganic filler TiO <sub>2</sub> into PP/RH significantly enhanced the green hybrid PP/RH/TiO <sub>2</sub> composites mechanical properties and thermal stabilities. The maximum values of tensile strength and Young modulus were 41.2 MPa for PP/RH (10wt. %)/TiO <sub>2</sub> (3wt. %), respectively, for PP/RH (40wt. %)/TiO <sub>2</sub> (3wt. %) | [136] |
| polyurethane (TPU)-TiO <sub>2</sub>           | <i>Matrix:</i> polyurethane (TPU) matrix with multi-walled carbon nanotube (MWCNT);<br><i>Filler:</i> TiO <sub>2</sub> (particle diameter—0.19 µm).                 | <i>Obtaining:</i> injection molding.<br><i>Characterization:</i> mechanical properties: tensile test, DMA, TGA,   | The composites have good mechanical properties: tensile stress was 4.46 MPa, elongation at the break—49%, and Young's Modulus—9.17 MPa.   | [134] |

Table 3. Cont.

| Composites  | Materials  | Methods   | Results-Mechanical Properties  | Ref.  |
|---|--|---|--|-------|
| thermoplastic polyurethane (TPU)-TiO <sub>2</sub>   | Matrix: thermoplastic polyurethane<br>Filler: TiO <sub>2</sub> nano-particles<br>Coupling agent: aminopropyl trimethoxy silane (APS)   | Obtaining: mixing of matrix with filler;<br>Characterization: elemental analysis, FTIR spectroscopy, TGA, mechanical properties.              | For composite with TiO <sub>2</sub> (3 wt.%), tensile strength and Young's modulus were increased by 72% and 48.9, respectively. Higher values were obtained when modified TiO <sub>2</sub> was used, at low percentages (1 wt.%).   | [77]  |
| polybutylene succinate (PBS)-TiO <sub>2</sub>   | Matrix: polybutylene succinate (PBS);<br>Filler: TiO <sub>2</sub> (20 nm; 0, 0.5, 1, 2, 5, and 10 wt. %)   | Obtaining: vane extruder.<br>Characterization: SEM, TEM, XRD, DSC, TGA, DMA; mechanical test, UV transmittance.                               | TiO <sub>2</sub> has little effect on the impact strength of the composite material. The flexural modulus of composites improved by 36.3% with TiO <sub>2</sub> (10 wt. %) addition. The tensile modulus of PBS-TiO <sub>2</sub> (10 wt. %) was higher by 15.5% than that of pristine PBS. | [137] |
| polyetheretherketone (PEEK)-TiO <sub>2</sub>  | Matrix: PEEK.<br>Filler: TiO <sub>2</sub> powder (1, 3, 5 wt.%)  | Obtaining: mixing and extrusion forming;<br>Characterization: density and Melt Flow Index (MFI) measurement, DSC, UV thermal, mechanical test | E modulus increase with TiO <sub>2</sub> content. The PEEK-1% TiO <sub>2</sub> sample has a tensile strength higher than that of pristine PEEK. TiO <sub>2</sub> (5% vol.) particles act effectively as UV blocker retarding the photo-degradation of PEEK.                                | [138] |
| poly(ethylene terephthalate) (PET)-TiO <sub>2</sub><br>Poly(lactic acid) (PLA)-TiO <sub>2</sub> | Matrix: poly(ethylene terephthalate) (PET) and poly(lactic acid) (PLA);<br>Filler: TiO <sub>2</sub> (20 nm);   | Obtaining: extrusion forming;<br>Characterization: analysis—DSC, XRD, SEM, DMTA, UV-Visible test, mechanical test.                            | The mechanical properties of PET-TiO <sub>2</sub> and PLA-TiO <sub>2</sub> composites have maximum values at a loading level of 3% TiO <sub>2</sub> .  | [139] |
| poly(L-lactide-co-ε-caprolactone) (PLCL)-TiO <sub>2</sub> nanocomposites                        | Matrix: PLCL;<br>Filler: TiO <sub>2</sub> (20 nm)<br>Coupling agent: silane coupling agent NH <sub>2</sub> (CH <sub>2</sub> ) <sub>3</sub> Si(OC <sub>2</sub> H <sub>5</sub> ) <sub>3</sub>            | Obtaining: solution casting method.<br>Characterization: analysis—FTIR, DSC, TEM, tensile test, shape memory;                                 | For composite with TiO <sub>2</sub> (5%) the ultimate tensile strength and the elongation at break increase to 35.4 MPa and 444.6%, which are 113% and 11% higher than that of pure PLCL.  | [140] |
| Poly(L-Lactide) (PLLA)-TiO <sub>2</sub>   | Matrix: poly(L-Lactide) (PLLA)<br>Filler: TiO <sub>2</sub> (<25 nm particle size) and Halloysite nanoclay (HNT) (Al <sub>2</sub> Si <sub>2</sub> O <sub>5</sub> (OH) <sub>4</sub> ·2H <sub>2</sub> O); | Obtaining: compression molding.<br>Characterization: mechanical test  | Young modulus had a significant increase ( $p \leq 0.05$ ) with the addition of TiO <sub>2</sub> up to 2.5 g TiO <sub>2</sub> /100 g PLLA. Regarding the tensile strength, better results were also achieved when adding 2.5 g TiO <sub>2</sub> /100g PLLA.                                | [141] |
| Poly(lactic acid) (PLA)-TiO <sub>2</sub>  | Matrix: PLA (4032D, 1.2–1.6% D-isomer lactide)<br>Filler: TiO <sub>2</sub> (20 nm);  | Obtaining: injection molding;<br>Characterization: SEM, TEM, dynamic rheological measurements, DSC, TGA, tensile testing, UV transmittance    | Samples show a higher elongation at break, except for 15 wt. % TiO <sub>2</sub> . Elongations of nanocomposites with 1–2% TiO <sub>2</sub> are about 19.1% and 24% higher than the pristine PLA.   | [142] |

Table 3. Cont.

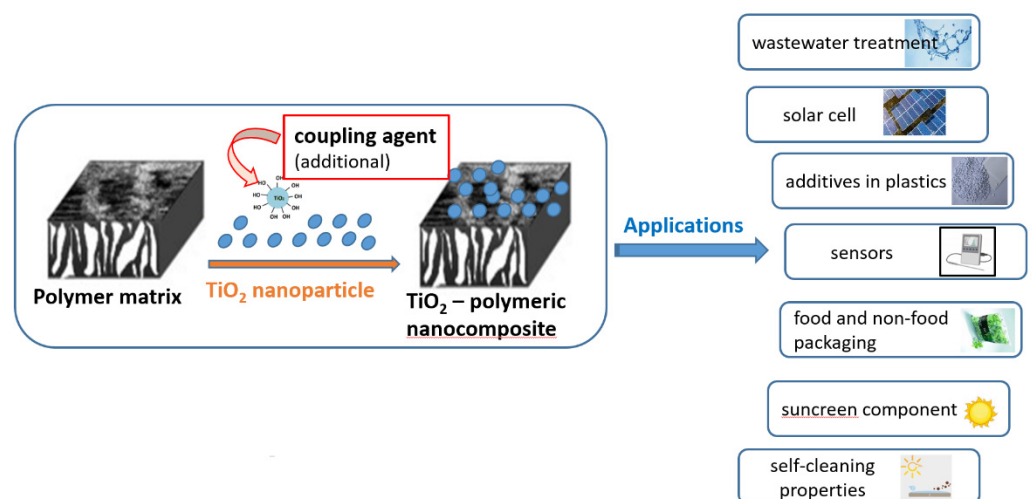
| Composites   | Materials   | Methods  | Results-Mechanical Properties   | Ref.  |
|--|---|--|---|-------|
| Poly(lactic acid) (PLA)-TiO <sub>2</sub>           | <p>Matrix: poly(lactic acid) (PLA)<br/>                     Filler: TiO<sub>2</sub> (1, 3, 5, 10 wt.%)<br/>                     Coupling agent: c-methacryloxy propyltrimethoxy-silane</p>  | <p>Obtaining: in situ polymerization,<br/>                     Characterization: DSC, TGA, XDR, SEM,<br/>                     thermal and mechanical properties</p>              | <p>The tensile strength, elongation at break, and Young's modulus of PLA-TiO<sub>2</sub> (3 wt.%) composites are improved to a certain degree compared with those of pristine PLA.</p>  | [143] |
| <b>Thermosetting matrix</b>                        |   |  |   |       |
| epoxy-TiO <sub>2</sub> nanocomposites              | <p>Matrix: mixture (resin + hardener);<br/>                     Filler: TiO<sub>2</sub> (0.5, 1, 2, 3, 4, 5, 8 and 10% vol.);</p>   | <p>Obtaining: mixing of resin + hardener and filler;<br/>                     Characterization: tensile test, dynamic mechanical analysis;</p>                                   | <p>The incorporation of TiO<sub>2</sub> nanoparticles into the epoxy resin improved flexural stiffness, flexural strength, and fracture toughness of the polymer.</p>   | [144] |
| epoxy-TiO <sub>2</sub> nanocomposites              | <p>Matrix: epoxy resin<br/>                     Filler: TiO<sub>2</sub> (5–40 nm, 0.5–2 wt.%)</p>   | <p>Obtaining: mixing of matrix with filler;<br/>                     Characterization: thermal properties, mechanical properties, morphology, viscoelastic properties.</p>       | <p>TiO<sub>2</sub> composites with dimensions between 5–10 nm showed better properties than those with larger dimensions (20–50 nm).</p>  | [145] |
| epoxy-TiO <sub>2</sub> nanocomposites              | <p>Matrix: mixture (resin+hardener);<br/>                     Filler: TiO<sub>2</sub> (1, 3, 5, 10 wt.%)<br/>                     Coupling agent: methyl isobutyl-ketone; dodecylbenzene-sulfonic acid</p>                          | <p>Obtaining: mixing of matrix, filler and coupling agent;<br/>                     Characterization: FTIR, SEM, XRD, TGA, mechanical tests</p>                                  | <p>The mechanical properties of materials are found to improve with TiO<sub>2</sub>, but degrade if the nano-TiO<sub>2</sub> exceeds 3%.</p>  | [146] |
| epoxy-TiO <sub>2</sub> nanocomposites              | <p>Matrix: epoxy resin (DER 331TM)<br/>                     Filler: TiO<sub>2</sub> (220 nm, 50 nm and 17 nm crystal diameter);<br/>                     Coupling agent: isophorone diamine (IPDA) + salicylic acid.</p>            | <p>Obtaining: mixing of matrix, filler and coupling agent;<br/>                     Characterization: mechanical test, XPS, SEM</p>  | <p>The highest tensile stress values were found at 3 wt. % TiO<sub>2</sub> (17 nm and 50 nm) and 5 wt. % TiO<sub>2</sub> (220 nm). The maximum flexural properties were found at a lower TiO<sub>2</sub> fraction of 1 wt.% only.</p> | [147] |
| epoxy-TiO <sub>2</sub> micro and nanocomposites    | <p>Matrix: epoxy resin:curing agent = 2:1 (wt. %)<br/>                     Filler: TiO<sub>2</sub> (0.2 µm; 1, 5, 10, 15 wt. %); TiO<sub>2</sub> (21 nm; 0.5, 1, 3 wt. %).</p>  | <p>Obtaining: mixing with an electrical stirrer,<br/>                     Characterization: tensile test, tensile creep-recovery test, tensile stress relaxation tests, SEM.</p> | <p>TiO<sub>2</sub> nanocomposites have better strength properties than TiO<sub>2</sub> microcomposites due to the size of the particle.</p>   | [148] |
| vinyl ester resins-TiO <sub>2</sub> nanocomposites | <p>Matrix: vinyl ester:styrene monomers (55:45 wt. %)<br/>                     Filler: TiO<sub>2</sub> (21 nm; 50 m<sup>2</sup>/g; 1, 2.5, and 5 wt. %).<br/>                     Coupling agent: polymeric coupling BYK-C 8000</p> | <p>Obtaining: shear mixing and ultrasonication;<br/>                     Characterization: tensile test, flexural test, impact test, SEM</p>                                     | <p>For nanocomposite with 0–2.5 wt. % TiO<sub>2</sub>, the tensile strength exhibits increasing tendency, while loading more than 2.5 wt. % leads to its decline.</p>   | [149] |

Table 3. Cont.

| Composites  | Materials  | Methods   | Results-Mechanical Properties  | Ref.  |
|---|--|---|--|-------|
| epoxy resin-polyurethane (EP-PU)-TiO <sub>2</sub>               | Matrix: EP-PU epoxy resin;<br>Filler: TiO <sub>2</sub> (0.42 g/cm <sup>3</sup> , 25 nm)<br>Coupling agent: isopropyl tri(dioctylpyrophosphate) titanate (TCA201)   | Obtaining: mixing EP-PU and TCA201-TiO <sub>2</sub><br>Characterization: FT-IR spectroscopy, SEM analysis, TGA analysis, mechanical properties, dielectric constant | The shear strength reached the maximum value (27.14 MPa) for EP-PU/TiO <sub>2</sub> (3 wt. %) and its thermal decomposition temperature increase by 17.48 °C more than that of EP-PU matrix. The dielectric constant and dielectric loss showed 4.27 and 0.02, respectively. | [85]  |
| <b>Elastomeric matrix</b>                                       |  |   |  |       |
| TiO <sub>2</sub> -natural rubber composites                     | Matrix: natural rubber (NR)<br>Filler: TiO <sub>2</sub> (KEMOX RC 800 PG) and the surface-modified nanosilica  | Obtaining: hydraulic press under a pressure<br>Characterization: stress relaxation measurements, SEM, AFM, effect of strain level, effect of ageing                 | The rate of stress relaxation was higher for silica-filled NR than TiO <sub>2</sub> -filled NR. This is due to the high degree of agglomeration in silica compared to TiO <sub>2</sub> . The relaxation rate increased with increasing TiO <sub>2</sub> loading.             | [150] |
| TiO <sub>2</sub> -natural rubber composite                      | Matrix: natural rubber stabilised with ammonia;<br>Filler: TiO <sub>2</sub> dispersion (2, 4 and 6 pphr)   | Obtaining: TiO <sub>2</sub> dispersions added in matrix;<br>Characterisation: tensile test  | The results showed improvement in both elongations at break and tensile strength data at low filler concentration (2 phr).   | [151] |
| TiO <sub>2</sub> -natural rubber composites                     | Matrix: natural rubber latex centrifuged with ammonia;<br>Filler: TiO <sub>2</sub> (3 mm:13 g/mL); TiO <sub>2</sub> (15-40 nm; 4.26 g/mL);<br>aditives: zinc oxide, stearic acid, N-cyclohexyl-benzothiazyl-sulphenamide, N2'-propyl-N-phenylenediamine, and S | Obtaining: TiO <sub>2</sub> dispersion was immersed in natural rubber latex.<br>Characterization: tensile test, SEM, TEM, XRD                                       | The tensile strength of nano-sized TiO <sub>2</sub> -filled natural rubber composites (23.04 MPa) is superior to micro-sized TiO <sub>2</sub> -filled natural rubber composites (19.62 MPa) (for 6 phr of micro- and nano-s)   | [152] |
| TiO <sub>2</sub> -natural rubber composites                     | Matrix: natural rubber;<br>Filler: TiO <sub>2</sub> -15, 25, 45, 85 wt. %<br>aditives: stearic acid, sulfur powder and zinc oxide;   | Obtaining: compression molding;<br>Characterization: mechanical properties; dynamic mechanical properties; thermal stability  | TiO <sub>2</sub> as filler allows obtaining materials with improved mechanical properties and thermal stability compared to the pristine natural rubber vulcanizates.  | [153] |
| TiO <sub>2</sub> -chlorobutyl rubber composites                 | Matrix: chlorobutyl rubber (CBK 150) with 1.2% Cl;<br>Filler: TiO <sub>2</sub> (10-30 phr.)<br>Additives: stearic acid, zinc oxide, sulfur, and zinc   | Obtaining: mixing in a two-roll mill<br>Characterization: mechanical properties, morphology (SEM, AFM), thermophysical measurements, diffusion experiments          | The tensile strength of the composites increases by 250% when the filler loading goes to 40 phr (tensile modulus the same).  | [133] |
| Acrylonitrile-Butadiene-Styrene-TiO <sub>2</sub> nanocomposites | Matrix: acrylonitrile butadiene styrene (ABS)<br>Fillers: TiO <sub>2</sub> (25-50 nm; 0.5, 2.5, 5 and 10 wt. %) and ATO (size < 50 nm)   | Obtaining: mechanical homogeniser.<br>Characterization: SEM, AFM and Raman analysis, thermal properties, tensile test, flexural tests, micro-hardness tests.        | The tensile strength of ABS/TiO <sub>2</sub> and ABS/ATO nanocomposites increased by 7% at the 2.5 wt. % TiO <sub>2</sub> filler, respectively, by 9.2% at 0.50 wt. % ATO filler. The modulus of elasticity increases up to 5 TiO <sub>2</sub> wt. % and then decreases.     | [31]  |

**Table 4.** Advantages of polymer nanocomposites over conventional polymer composites.

| Polymer Nanocomposites   | Conventional Polymer Composites   |
|--|---|
| <ul style="list-style-type: none"> <li>✓ Fillers separation are in nm, and properties will be affected by size effects of nanofiller;</li> <li>✓ Small amounts of TiO<sub>2</sub> filler are enough (less than 10%) to achieve desired properties;</li> <li>✓ Properties are obtained without sacrificing the inherent properties of the polymer or adding excessive weight;</li> <li>✓ Improvements in properties even in low amount is due to nanosized of TiO<sub>2</sub> filler and interphase region;</li> <li>✓ Using nanosized particles can reduce the likelihood of finding defects, such as grain boundaries, voids, dislocations, and imperfections.</li> </ul> | <ul style="list-style-type: none"> <li>✓ Fillers are separated in μm, and there is not that much of size effect;</li> <li>✓ High concentrations should be needed as compared to nanofiller case;</li> <li>✓ Fillers can unfavorably impact other benefits of polymers, such as appearance, ductility and toughness;</li> <li>✓ There is not that much improvement in properties even for a large amount of fillers;</li> <li>✓ It is difficult even observed in conventional polymer composites.</li> </ul> |



**Figure 5.** Applications of the TiO<sub>2</sub> nanocomposites.

### 5. Conclusions

An essential characteristic of polymers is modifying their inherent physical properties by adding fillers, while retaining their characteristic processing ease. By adding inorganic fillers into the polymers matrix, composite materials become stronger, stiffer, electronically conductive, magnetically permeable, flame retardant, more challenging, and more wear-resistant.

After reviewing part of the existing literature on polymeric composites with TiO<sub>2</sub> fillers, it is found that the interfacial connection between the filler and polymer matrix is an important element for determining the mechanical properties of the composite.

The addition of TiO<sub>2</sub> nanoparticles into the polymeric matrix demonstrates their ability to significantly improve important mechanical properties (tensile modulus, tensile strength, toughness and fracture toughness, fracture energies, flexural modulus, flexural strength, elongation at break, fatigue crack propagation resistance, abrasion, pull-off strength, and fracture surface properties), even at low filler contents.

From the literature, one can conclude that the mechanical properties of the composites with the polymer matrix depend on the particle size, and particle–matrix interface adhesion and loading (type, quantity, filler distribution and orientation, and void content). Along

with those properties, the interfacial bonds and the interphase load mechanisms also play an essential role.

Studies performed on polymeric matrix nanocomposites filled with TiO<sub>2</sub> nanoparticles were performed to verify the influence of several variables (shape, size, % loading, surface change, etc.) and also to propose various areas of applicability of these nanocomposites.

**Author Contributions:** Conceptualization, C.C., L.A. and A.E.; methodology, C.C.; validation, C.C., L.A. and A.E.; formal analysis, C.C.; investigation, L.A.; resources, A.E.; data curation, C.C., L.A. and A.E.; writing—original draft preparation, C.C.; writing—review and editing, C.C., A.E., L.A.; visualization, A.E.; supervision, L.A.; project administration, C.C., L.A.; funding acquisition, C.C. All authors have read and agreed to the published version of the manuscript.

**Funding:** This work was supported by a grant from the Romanian National Authority for Scientific Research and Innovation, CCCDI-UEFISCDI, project number 169/2020 ERANET-M.-3D-Photocat, within PNCDI III.

**Institutional Review Board Statement:** Not applicable.

**Informed Consent Statement:** Not applicable.

**Data Availability Statement:** The data presented in this study are available on request from the corresponding author.

**Conflicts of Interest:** The authors declare no conflict of interest.

## References

- Mittal, V. *Optimization of Polymer Nanocomposite Properties*; Wiley: Weinheim, Germany, 2010. [CrossRef]
- Schadler, L.S.; Brinson, L.C.; Sawyer, W.G. Polymer nanocomposites: A small part of the story. *JOM* **2007**, *59*, 53–60. [CrossRef]
- Young, R.; Kinloch, I.A.; Gong, L.; Novoselov, K. The mechanics of graphene nanocomposites: A review. *Compos. Sci. Technol.* **2012**, *72*, 1459–1476. [CrossRef]
- Oliviera, M.; Machado, A. Preparation of Polymer-Based Nanocomposites by Different Routes. In *Nanocomposites: Synthesis, Characterization and Application*; Wang, X., Ed.; NOVA Publishers: Hauppauge, NY, USA, 2013.
- Kumar, R. *Polymer-Matrix Composites Types, Applications & Performance*; Nova Science Publishers Inc.: Hauppauge, NY, USA, 2014.
- Seferis, J. *Role of the Polymeric Matrix in the Processing and Structural Properties of Composite Materials*; Springer: New York, NY, USA, 2013.
- Venditti, I.; D'Amato, R.; Russo, M.V.; Falconieri, M. Synthesis of conjugated polymeric nanobeads for photonic bandgap materials. *Sens. Actuators B Chem.* **2007**, *126*, 35–40. [CrossRef]
- Soares, I.L.; Chimanowsky, J.P.; Luetkmeyer, L.; Da Silva, E.O.; Souza, D.D.H.S.; Tavares, M.I.B. Evaluation of the Influence of Modified TiO<sub>2</sub> Particles on Polypropylene Composites. *J. Nanosci. Nanotechnol.* **2015**, *15*, 5723–5732. [CrossRef] [PubMed]
- Monteiro, M.; Neto, R.C.; Santos, I.C.S.; Da Silva, E.O.; Tavares, M.I.B. Inorganic-organic hybrids based on poly ( $\epsilon$ -Caprolactone) and silica oxide and characterization by relaxometry applying low-field NMR. *Mater. Res.* **2012**, *15*, 825–832. [CrossRef]
- Rubab, Z.; Afzal, A.; Siddiqi, H.M.; Saeed, S. Preparation, Characterization, and Enhanced Thermal and Mechanical Properties of Epoxy-Titania Composites. *Sci. World J.* **2014**, *2014*, 515739. [CrossRef] [PubMed]
- Kierys, A.; Zaleski, R.; Buda, W.; Pikus, S.; Dziadosz, M.; Goworek, J. Nanostructured polymer–titanium composites and titanium oxide through polymer swelling in titania precursor. *Colloid Polym. Sci.* **2012**, *291*, 1463–1470. [CrossRef] [PubMed]
- Suzuki, N.; Kiba, S.; Kamachi, Y.; Miyamoto, N.; Yamauchi, Y. Unusual reinforcement of silicone rubber compounds containing mesoporous silica particles as inorganic fillers. *Phys. Chem. Chem. Phys.* **2012**, *14*, 3400–3407. [CrossRef]
- Da Silva, P.S.R.C.; Tavares, M.I.B. Solvent Effect on the Morphology of Lamellar Nanocomposites Based on HIPS. *Mater. Res.* **2015**, *18*, 191–195. [CrossRef]
- Cunha, A.D.P.C.B.; Tavares, M.I.B.; Silva, E.O.; Zaioncz, S. The Effect of Montmorillonite Clay on the Crystallinity of Poly(vinyl alcohol) Nanocomposites Obtained by Solution Intercalation and In Situ Polymerization. *J. Nanosci. Nanotechnol.* **2015**, *15*, 2814–2820. [CrossRef]
- Motaung, T.; Luyt, A.; Saladino, M.; Caponetti, E. Study of morphology, mechanical properties, and thermal degradation of polycarbonate-titania nanocomposites as function of titania crystalline phase and content. *Polym. Compos.* **2013**, *34*, 164–172. [CrossRef]
- Liaw, W.-C.; Cheng, Y.-L.; Liao, Y.-S.; Chen, C.-S.; Lai, S.-M. Complementary functionality of SiO<sub>2</sub> and TiO<sub>2</sub> in polyimide/silica-titania ternary hybrid nanocomposites. *Polym. J.* **2011**, *43*, 249–257. [CrossRef]
- Shishkovsky, I.V.; Scherbakov, V.I. Additive manufacturing of polymer composites with nano-titania inclusions. *Laser Phys. Lett.* **2021**, *18*, 066001. [CrossRef]
- Sanes, J.; Sánchez, C.; Pamies, R.; Avilés, M.-D.; Bermúdez, M.-D. Extrusion of Polymer Nanocomposites with Graphene and Graphene Derivative Nanofillers: An Overview of Recent Developments. *Materials* **2020**, *13*, 549. [CrossRef]

19. Müller, C.M.; Laurindo, J.B.; Yamashita, F. Composites of thermoplastic starch and nanoclays produced by extrusion and thermopressing. *Carbohydr. Polym.* **2012**, *89*, 504–510. [CrossRef] [PubMed]
20. Kickelbick, G. *Hybrid Materials: Synthesis, Characterization, and Applications*; John Wiley & Sons: Hoboken, NJ, USA, 2007.
21. Almeida, A.D.S.; Tavares, M.I.B.; Da Silva, E.O.; Neto, R.P.C.; Moreira, L.A. Development of hybrid nanocomposites based on PLLA and low-field NMR characterization. *Polym. Test.* **2012**, *31*, 267–275. [CrossRef]
22. Cheraghian, G. Effect of nano titanium dioxide on heavy oil recovery during polymer flooding. *Pet. Sci. Technol.* **2016**, *34*, 633–641. [CrossRef]
23. Vidakis, N.; Petousis, M.; Maniadi, A.; Koudoumas, E.; Liebscher, M.; Tzounis, L. Mechanical Properties of 3D-Printed Acrylonitrile–Butadiene–Styrene TiO<sub>2</sub> and ATO Nanocomposites. *Polymers* **2020**, *12*, 1589. [CrossRef] [PubMed]
24. Vidakis, N.; Maniadi, A.; Petousis, M.; Vamvakaki, M.; Kenanakis, G.; Koudoumas, E. Mechanical and Electrical Properties Investigation of 3D-Printed Acrylonitrile–Butadiene–Styrene Graphene and Carbon Nanocomposites. *J. Mater. Eng. Perform.* **2020**, *29*, 1909–1918. [CrossRef]
25. Nasu, A.; Otsubo, Y. Rheology and UV-protecting properties of complex suspensions of titanium dioxides and zinc oxides. *J. Colloid Interface Sci.* **2007**, *310*, 617–623. [CrossRef]
26. Uddin, M.; Mondal, D.P.; Morris, C.; Lopez, T.; Diebold, U.; Gonzalez, R.D. An in vitro controlled release study of valproic acid encapsulated in a titania ceramic matrix. *Appl. Surf. Sci.* **2011**, *257*, 7920–7927. [CrossRef]
27. Fujihara, K.; Kumar, A.; Jose, R.; Ramakrishna, S.; Uchida, S. Spray deposition of electrospun TiO<sub>2</sub> nanorods for dye-sensitized solar cell. *Nanotechnology* **2007**, *18*, 365709. [CrossRef]
28. Andronic, L.; Enesca, A. Black TiO<sub>2</sub> Synthesis by Chemical Reduction Methods for Photocatalysis Applications. *Front. Chem.* **2020**, *8*, 5489. [CrossRef]
29. Saccà, A.; Carbone, A.; Gatto, I.; Pedicini, R.; Freni, A.; Patti, A.; Passalacqua, E. Composites Nafion-titania membranes for Polymer Electrolyte Fuel Cell (PEFC) applications at low relative humidity levels: Chemical physical properties and electrochemical performance. *Polym. Test.* **2016**, *56*, 10–18. [CrossRef]
30. Fiorati, A.; Bellingeri, A.; Punta, C.; Corsi, I.; Venditti, I. Silver Nanoparticles for Water Pollution Monitoring and Treatments: Ecosafety Challenge and Cellulose-Based Hybrids Solution. *Polymers* **2020**, *12*, 1635. [CrossRef]
31. Pantalei, S.; Zampetti, E.; Macagnano, A.; Bearzotti, A.; Venditti, I.; Russo, M. Enhanced Sensory Properties of a Multichannel Quartz Crystal Microbalance Coated with Polymeric Nanobeads. *Sensors* **2007**, *7*, 2920–2928. [CrossRef]
32. Fratoddi, I.; Cartoni, A.; Venditti, I.; Catone, D.; O’Keeffe, P.; Paladini, A.; Toschi, F.; Turchini, S.; Sciubba, F.; Testa, G.; et al. Gold nanoparticles functionalized by rhodamine B isothiocyanate: A new tool to control plasmonic effects. *J. Colloid Interface Sci.* **2018**, *513*, 10–19. [CrossRef]
33. Sharpe, L.H. *The Interfacial Interactions in Polymeric Composites*; Akovali, G., Ed.; Kluwer: Dordrecht, The Netherlands, 1993.
34. Jesson, D.; Watts, J.F. The Interface and Interphase in Polymer Matrix Composites: Effect on Mechanical Properties and Methods for Identification. *Polym. Rev.* **2012**, *52*, 321–354. [CrossRef]
35. Wang, M.; Wang, Z.; Li, N.; Liao, J.; Zhao, S.; Wang, J.; Wang, S. Relationship between polymer–filler interfaces in separation layers and gas transport properties of mixed matrix composite membranes. *J. Membr. Sci.* **2015**, *495*, 252–268. [CrossRef]
36. Drzal, L.T.; Rich, M.J.; Lloyd, P.F. Adhesion of Graphite Fibers to Epoxy Matrices: I. The Role of Fiber Surface Treatment. *J. Adhes.* **1983**, *16*, 1–30. [CrossRef]
37. Berlin, A.A.; Volfson, S.t.A.; Enikilopian, N.S.; Negmatov, S.S. *Principles of Polymer Composites*; Akademik-Verlag: Berlin, Germany, 1985.
38. Cassidy, P.E.; Yager, B.J. *Coupling Agents As Adhesion Promoters in Reviews in Polymer Technology*; Skeist, I., Ed.; Marcel Dekker Inc.: New York, NY, USA, 1972; Volume 1.
39. Kim, J.-K.; Mai, Y.-W. *Engineered Interfaces in Fiber Reinforced Composites*; Elsevier BV: Amsterdam, The Netherlands, 1998.
40. Fourche, G. An overview of the basic aspects of polymer adhesion. Part I: Fundamentals. *Polym. Eng. Sci.* **1995**, *35*, 957–967. [CrossRef]
41. Morris, H.R.; Turner, J.F.; Munro, B.; Ryntz, R.A.; Treado, P.J. Chemical Imaging of Thermoplastic Olefin (TPO) Surface Architecture. *Langmuir* **1999**, *15*, 2961–2972. [CrossRef]
42. Del Rio, F.W.; De Boer, M.; Knapp, J.A.; Reedy, E.D.; Clews, P.J.; Dunn, M. The role of van der Waals forces in adhesion of micromachined surfaces. *Nat. Mater.* **2005**, *4*, 629–634. [CrossRef]
43. Lipatov, Y. *Polymer Reinforcement*; ChemTec Publishing: Scarborough, ON, Canada, 1995.
44. Qin, R.-Y.; Schreiber, H. Adhesion at partially restructured polymer surfaces. *Colloids Surf. A Physicochem. Eng. Asp.* **1999**, *156*, 85–93. [CrossRef]
45. Selvin, T.P.; Kuruvilla, J.; Sabu, T. Mechanical properties of titanium dioxide-filled polystyrene microcomposites. *Mater. Lett.* **2004**, *58*, 281–289. [CrossRef]
46. De Armit, C.; Rothon, R. Fillers and surface treatment. *Plast. Addit. Compd.* **2002**, *4*, 12–14. [CrossRef]
47. Fronza, B.M.; Lewis, S.; Shah, P.K.; Barros, M.D.; Giannini, M.; Stansbury, J.W. Modification of filler surface treatment of composite resins using alternative silanes and functional nanogels. *Dent. Mater.* **2019**, *35*, 928–936. [CrossRef] [PubMed]
48. Mozetič, M. Surface Modification to Improve Properties of Materials. *Materials* **2019**, *12*, 441. [CrossRef] [PubMed]
49. Chaudhari, S.; Shaikh, T.; Pandey, P. A Review on Polymer TiO<sub>2</sub> Nanocomposites. *Int. J. Eng. Res. Appl.* **2013**, *3*, 1386–1391.

50. Dalod, A.R.M.; Henriksen, L.; Grande, T.; Einarsrud, M.-A. Functionalized TiO<sub>2</sub> nanoparticles by single-step hydrothermal synthesis: The role of the silane coupling agents. *Beilstein J. Nanotechnol.* **2017**, *8*, 304–312. [CrossRef] [PubMed]
51. Chen, X.; Mao, S.S. Synthesis of Titanium Dioxide (TiO<sub>2</sub>) Nanomaterials. *J. Nanosci. Nanotechnol.* **2006**, *6*, 906–925. [CrossRef]
52. Tao, P.; Li, Y.; Rungta, A.; Viswanath, A.; Gao, J.; Benicewicz, B.; Siegel, R.W.; Schadler, L.S. TiO<sub>2</sub> nanocomposites with high refractive index and transparency. *J. Mater. Chem.* **2011**, *21*, 18623–18629. [CrossRef]
53. Díez-Pascual, A.M.; Díez-Vicente, A.L. Nano-TiO<sub>2</sub> Reinforced PEEK/PEI Blends as Biomaterials for Load-Bearing Implant Applications. *ACS Appl. Mater. Interfaces* **2015**, *7*, 5561–5573. [CrossRef] [PubMed]
54. Byranvand, M.M.; Kharat, A.N.; Fatholahi, L.; Beiranvand, Z.M. A review on synthesis of nano-TiO<sub>2</sub> via different methods. *JNS* **2013**, *3*, 1–9. [CrossRef]
55. Wang, Y.; He, Y.; Lai, Q.; Fan, M. Review of the progress in preparing nano TiO<sub>2</sub>: An important environmental engineering material. *J. Environ. Sci.* **2014**, *26*, 2139–2177. [CrossRef] [PubMed]
56. Hanemann, T.; Szabó, D.V. Polymer-Nanoparticle Composites: From Synthesis to Modern Applications. *Materials* **2010**, *3*, 3468–3517. [CrossRef]
57. Laine, R.M.; Choi, J.; Lee, I. Organic–Inorganic Nanocomposites with Completely Defined Interfacial Interactions. *Adv. Mater.* **2001**, *13*, 800–803. [CrossRef]
58. Li, H.; Zhang, Z.; Ma, X.; Hu, M.; Wang, X.; Fan, P. Synthesis and characterization of epoxy resin modified with nano-SiO<sub>2</sub> and  $\gamma$ -glycidoxypropyltrimethoxy silane. *Surf. Coat. Technol.* **2007**, *201*, 5269–5272. [CrossRef]
59. Xu, X.; Li, B.; Lu, H.; Zhang, Z.; Wang, H. The interface structure of nano-SiO<sub>2</sub>/PA66 composites and its influence on material's mechanical and thermal properties. *Appl. Surf. Sci.* **2007**, *254*, 1456–1462. [CrossRef]
60. Li, X.; Cao, Z.; Zhang, Z.; Dang, H. Surface-modification in situ of nano-SiO<sub>2</sub> and its structure and tribological properties. *Appl. Surf. Sci.* **2006**, *252*, 7856–7861. [CrossRef]
61. Iijima, M.; Sato, N.; Lenggoro, I.W.; Kamiya, H. Surface modification of BaTiO<sub>3</sub> particles by silane coupling agents in different solvents and their effect on dielectric properties of BaTiO<sub>3</sub>/epoxy composites. *Colloids Surf. A Physicochem. Eng. Asp.* **2009**, *352*, 88–93. [CrossRef]
62. Balas, F.; Kokubo, T.; Kawashita, M.; Nakamura, T. Surface modification of organic polymers with bioactive titanium oxide without the aid of a silane-coupling agent. *J. Mater. Sci. Mater. Electron.* **2007**, *18*, 1167–1174. [CrossRef]
63. Zhang, Y.; Chen, H.; Wen, Y.; Yuan, Y.; Wu, W.; Liu, C. Tunable wettability of monodisperse core-shell nano-SiO<sub>2</sub> modified with poly(methylhydrosiloxane) and allyl-poly(ethylene glycol). *Colloids Surf. A Physicochem. Eng. Asp.* **2014**, *441*, 16–24. [CrossRef]
64. Plueddemann, E.P. *Silane Coupling Agents*, 2nd ed.; Plenum Press: New York, NY, USA, 1991.
65. Yosomiya, R.; Morimoto, K.; Nakajima, A.; Ikada, Y.; Suzuki, T.; Dharan, C.K.H. Adhesion and Bonding in Composites. *J. Eng. Ind.* **1991**, *113*, 117. [CrossRef]
66. Konakanchi, A.; Alla, R.M.; Guduri, V. Silane Coupling Agents—Benevolent Binders in Composites. *Trends Biomater. Artif. Organs* **2017**, *31*, 108–113.
67. Shokoohi, S.; Arefazar, A.; Khosrokhavar, R. Silane Coupling Agents in Polymer-based Reinforced Composites: A Review. *J. Reinf. Plast. Compos.* **2008**, *27*, 473–485. [CrossRef]
68. Zhang, Y.; Fang, F.; Wang, C.; Wang, L.; Wang, X.; Chu, X.; Li, J.; Fang, X.; Wei, Z.; Wang, X. Hydrophobic modification of ZnO nanostructures surface using silane coupling agent. *Polym. Compos.* **2014**, *35*, 1204–1211. [CrossRef]
69. Mallakpour, S.; Madani, M. The effect of the coupling agents KH550 and KH570 on the nanostructure and interfacial interaction of zinc oxide/chiral poly(amide-imide) nanocomposites containing l-leucine amino acid moieties. *J. Mater. Sci.* **2014**, *49*, 5112–5118. [CrossRef]
70. Liu, Y.-L.; Su, Y.-H.; Lai, J.-Y. In situ crosslinking of chitosan and formation of chitosan–silica hybrid membranes with using  $\gamma$ -glycidoxypropyltrimethoxysilane as a crosslinking agent. *Polymer* **2004**, *45*, 6831–6837. [CrossRef]
71. Lu, Y.; Zhou, S.; Wu, L. De-Agglomeration and Dispersion Behavior of TiO<sub>2</sub> Nanoparticles in Organic Media Using 3-Methacryloxypropyltrimethoxysilane as a Surface Modifier. *J. Dispers. Sci. Technol.* **2012**, *33*, 497–505. [CrossRef]
72. Dang, Z.-M.; Xia, Y.-J.; Zha, J.-W.; Yuan, J.; Bai, J. Preparation and dielectric properties of surface modified TiO<sub>2</sub> /silicone rubber nanocomposites. *Mater. Lett.* **2011**, *65*, 3430–3432. [CrossRef]
73. Xu, Q.F.; Liu, Y.; Lin, F.-J.; Mondal, B.; Lyons, A.M. Superhydrophobic TiO<sub>2</sub>–Polymer Nanocomposite Surface with UV-Induced Reversible Wettability and Self-Cleaning Properties. *ACS Appl. Mater. Interfaces* **2013**, *5*, 8915–8924. [CrossRef] [PubMed]
74. Rahim-Abadi, M.M.; Mahdavian, A.R.; Gharieh, A.; Salehi-Mobarakeh, H. Chemical modification of TiO<sub>2</sub> nanoparticles as an effective way for encapsulation in polyacrylic shell via emulsion polymerization. *Prog. Org. Coat.* **2015**, *88*, 310–315. [CrossRef]
75. Toh-Ae, P.; Junhasavasdikul, B.; Lopattananon, N.; Sahakaro, K. Surface Modification of TiO<sub>2</sub> Nanoparticles by Grafting with Silane Coupling Agent. *Adv. Mater. Res.* **2013**, *844*, 276–279. [CrossRef]
76. Ambrósio, J.D.; Balarim, C.V.M.; De Carvalho, G.B. Preparation, characterization, and mechanical/tribological properties of polyamide 11/Titanium dioxide nanocomposites. *Polym. Compos.* **2014**, *37*, 1415–1424. [CrossRef]
77. Sabzi, M.; Mirabedini, S.M.; Zohuriaan-Mehr, M.J.; Atai, M. Surface modification of TiO<sub>2</sub> nano-particles with silane coupling agent and investigation of its effect on the properties of polyurethane composite coating. *Prog. Org. Coat.* **2009**, *65*, 222–228. [CrossRef]
78. Rusu, G.; Rusu, E. Nylon 6/TiO<sub>2</sub> Composites by in situ Anionic Ring-Opening Polymerization of  $\epsilon$ -Caprolactam: Synthesis, Characterization, and Properties. *Int. J. Polym. Anal. Charact.* **2011**, *16*, 561–583. [CrossRef]




79. Zapata, P.A.; Palza, H.; Delgado, K.; Rabagliati, F.M. Novel antimicrobial polyethylene composites prepared by metallocenic in situ polymerization with TiO<sub>2</sub>-based nanoparticles. *J. Polym. Sci. Part A Polym. Chem.* **2012**, *50*, 4055–4062. [CrossRef]
80. Nguyen, V.G.; Thai, H.; Mai, D.H.; Tran, H.T.; Tran, D.L.; Vu, M.T. Effect of titanium dioxide on the properties of polyethylene/TiO<sub>2</sub> nanocomposites. *Compos. Part B Eng.* **2013**, *45*, 1192–1198. [CrossRef]
81. Džunuzović, E.; Marinović-Cincović, M.; Vuković, J.; Jeremić, K.; Nedeljković, J. Thermal properties of PMMA/TiO<sub>2</sub> nanocomposites prepared by in-situ bulk polymerization. *Polym. Compos.* **2009**, *30*, 737–742. [CrossRef]
82. Yuvaraj, H.; Kim, W.S.; Kim, J.T.; Kang, I.P.; Gal, Y.-S.; Kim, S.W.; Lim, K.T. Synthesis of Poly(methyl methacrylate) Encapsulated TiO<sub>2</sub> Nanocomposite Particles in Supercritical CO<sub>2</sub>. *Mol. Cryst. Liq. Cryst.* **2009**, *514*, 355–365. [CrossRef]
83. Qi, Y.; Xiang, B.; Tan, W.; Zhang, J. Hydrophobic surface modification of TiO<sub>2</sub> nanoparticles for production of acrylonitrile-styrene-acrylate terpolymer/TiO<sub>2</sub> composited cool materials. *Appl. Surf. Sci.* **2017**, *419*, 213–223. [CrossRef]
84. Weng, C.-C.; Wei, K.-H. Selective Distribution of Surface-Modified TiO<sub>2</sub> Nanoparticles in Polystyrene-*b*-poly (Methyl Methacrylate) Diblock Copolymer. *Chem. Mater.* **2003**, *15*, 2936–2941. [CrossRef]
85. Yufei, C.; Zhichao, L.; Junyan, T.; Qingyu, Z.; Yang, H. Characteristics and Properties of TiO<sub>2</sub> /EP-PU Composite. *J. Nanomater.* **2015**, *2015*, 1–7. [CrossRef]
86. Zhao, J.; Milanova, M.; Warmoeskerken, M.M.; Dutschk, V. Surface modification of TiO<sub>2</sub> nanoparticles with silane coupling agents. *Colloids Surf. A Physicochem. Eng. Asp.* **2012**, *413*, 273–279. [CrossRef]
87. Wanag, A.; Sienkiewicz, A.; Rokicka-Konieczna, P.; Kusiak-Nejman, E.; Morawski, A.W. Influence of modification of titanium dioxide by silane coupling agents on the photocatalytic activity and stability. *J. Environ. Chem. Eng.* **2020**, *8*, 103917. [CrossRef]
88. Mallakpour, S.; Barati, A. Efficient preparation of hybrid nanocomposite coatings based on poly(vinyl alcohol) and silane coupling agent modified TiO<sub>2</sub> nanoparticles. *Prog. Org. Coat.* **2011**, *71*, 391–398. [CrossRef]
89. Shakeri, A.; Yip, D.; Badv, M.; Imani, S.M.; Sanjari, M.; Didar, T.F. Self-Cleaning Ceramic Tiles Produced via Stable Coating of TiO<sub>2</sub> Nanoparticles. *Materials* **2018**, *11*, 1003. [CrossRef]
90. Klaysri, R.; Tubchareon, T.; Praserttham, P. One-step synthesis of amine-functionalized TiO<sub>2</sub> surface for photocatalytic decolorization under visible light irradiation. *J. Ind. Eng. Chem.* **2017**, *45*, 229–236. [CrossRef]
91. Chen, Q.; Yakovlev, N.L. Adsorption and interaction of organosilanes on TiO<sub>2</sub> nanoparticles. *Appl. Surf. Sci.* **2010**, *257*, 1395–1400. [CrossRef]
92. Dinari, M.; Haghghi, A. Surface modification of TiO<sub>2</sub> nanoparticle by three dimensional silane coupling agent and preparation of polyamide/modified-TiO<sub>2</sub> nanocomposites for removal of Cr (VI) from aqueous solutions. *Prog. Org. Coat.* **2017**, *110*, 24–34. [CrossRef]
93. Caris, C.; Kuijpers, R.; Van Herk, A.M.; German, A.L. Kinetics of (CO)polymerizations at the surface of inorganic submicron particles in emulsion-like systems. *Makromol. Chem. Macromol. Symp.* **1990**, *35-36*, 535–548. [CrossRef]
94. Erdem, B.; Sudol, E.D.; Dimonie, V.L.; El-Aasser, M.S. Encapsulation of inorganic particles via miniemulsion polymerization. II. Preparation and characterization of styrene miniemulsion droplets containing TiO<sub>2</sub> particles. *J. Polym. Sci. Part A Polym. Chem.* **2000**, *38*, 4431–4440. [CrossRef]
95. Rong, M.Z.; Zhang, M.Q.; Wang, H.B.; Zeng, H.M. Surface modification of magnetic metal nanoparticles through irradiation graft polymerization. *Appl. Surf. Sci.* **2002**, *200*, 76–93. [CrossRef]
96. Yang, M.; Dan, Y. Preparation and characterization of poly(methyl methacrylate)/titanium oxide composite particles. *Colloid Polym. Sci.* **2005**, *284*, 243–250. [CrossRef]
97. Milanese, F.; Cappelletti, G.; Annunziata, R.; Bianchi, C.L.; Meroni, D.; Ardizzone, S. Siloxane–TiO<sub>2</sub> Hybrid Nanocomposites. The Structure of the Hydrophobic Layer. *J. Phys. Chem. C* **2010**, *114*, 8287–8293. [CrossRef]
98. Xiang, B.; Jiang, G.; Zhang, J. Surface modification of TiO<sub>2</sub> nanoparticles with silane coupling agent for nanocomposite with poly(butyl acrylate). *Plast. Rubber Compos.* **2015**, *44*, 148–154. [CrossRef]
99. Wang, C.; Mao, H.; Wang, C.; Fu, S. Dispersibility and Hydrophobicity Analysis of Titanium Dioxide Nanoparticles Grafted with Silane Coupling Agent. *Ind. Eng. Chem. Res.* **2011**, *50*, 11930–11934. [CrossRef]
100. Godnjavec, J.; Znoj, B.; Vince, J.; Steinbacher, M.; Žnidaršič, A.; Venturini, P. Stabilization of rutile TiO<sub>2</sub> nanoparticles with Glymo in polyacrylic clear coating. *Mater. Tehnol.* **2012**, *46*, 19–24.
101. Yang, C.; Yang, C. Preparation of TiO<sub>2</sub> particles and surface silanization modification for electronic ink. *J. Mater. Sci. Mater. Electron.* **2014**, *25*, 3285–3289. [CrossRef]
102. Tangchantra, N.; Krueenate, J.; Aumnate, C.; Sooksomsong, T. The Effect of Surface Modification of TiO<sub>2</sub> on Mechanical Properties of Polyethylene Composite Film. *Adv. Mater. Res.* **2010**, *93-94*, 300–303. [CrossRef]
103. Fujishima, A.; Rao, T.N.; Tryk, D.A. Titanium dioxide photocatalysis. *J. Photochem. Photobiol. C Photochem. Rev.* **2000**, *1*, 1–21. [CrossRef]
104. Herrmann, J.-M. Heterogeneous photocatalysis: Fundamentals and applications to the removal of various types of aqueous pollutants. *Catal. Today* **1999**, *53*, 115–129. [CrossRef]
105. Nada, A.; Barakat, M.; Hamed, H.; Mohamed, N.; Veziroglu, T. Studies on the photocatalytic hydrogen production using suspended modified TiO<sub>2</sub> photocatalysts. *Int. J. Hydrogen Energy* **2005**, *30*, 687–691. [CrossRef]
106. Andronic, L.; Enesca, A.; Cazan, C.; Visa, M. TiO<sub>2</sub>-active carbon composites for wastewater photocatalysis. *J. Sol.-Gel. Sci. Technol.* **2014**, *71*, 396–405. [CrossRef]

107. Sharma, S.K.; Vishwas, M.; Rao, K.N.; Mohan, S.; Reddy, D.S.; Gowda, K. Structural and optical investigations of TiO<sub>2</sub> films deposited on transparent substrates by sol-gel technique. *J. Alloys Compd.* **2009**, *471*, 244–247. [CrossRef]
108. Bayarri, B.; Giménez, J.; Curcó, D.; Esplugas, S. Photocatalytic degradation of 2,4-dichlorophenol by TiO<sub>2</sub> /UV: Kinetics, actinometries and models. *Catal. Today* **2005**, *101*, 227–236. [CrossRef]
109. Gaya, U.I.; Abdullah, A.H. Heterogeneous photocatalytic degradation of organic contaminants over titanium dioxide: A review of fundamentals, progress and problems. *J. Photochem. Photobiol. C Photochem. Rev.* **2008**, *9*, 1–12. [CrossRef]
110. Shimizu, N.; Ninomiya, K.; Ogino, C.; Rahman, M.M. Potential uses of titanium dioxide in conjunction with ultrasound for improved disinfection. *Biochem. Eng. J.* **2010**, *48*, 416–423. [CrossRef]
111. Tuan, N.M.; Nha, N.T.; Tuyen, N.H. Low-temperature synthesis of nano-TiO<sub>2</sub> anatase on nafion membrane for using on DMFC. *J. Phys. Conf. Ser.* **2009**, *187*, 012040. [CrossRef]
112. Armstrong, A.R.; Armstrong, G.; Canales-Vazquez, J.; García, R.; Bruce, P.G. Lithium-Ion Intercalation into TiO<sub>2</sub>-B Nanowires. *Adv. Mater.* **2005**, *17*, 862–865. [CrossRef]
113. Richards, B.S.; Cotter, J.E.; Honsberg, C.B. Enhancing the surface passivation of TiO<sub>2</sub> coated silicon wafers. *Appl. Phys. Lett.* **2002**, *80*, 1123–1125. [CrossRef]
114. Pinto, D.; Bernardo, L.; Amaro, A.; Lopes, S. Mechanical properties of epoxy nanocomposites using titanium dioxide as reinforcement—A review. *Constr. Build. Mater.* **2015**, *95*, 506–524. [CrossRef]
115. Sahu, M.; Satapathy, A. Thermal Characteristics of Polypropylene Composites Filled with TiO<sub>2</sub>. In Proceedings of the ASEAI 2014, Bangkok, Thailand, 11–13 April 2013; Volume 49, pp. 1747–1752.
116. Peng, X.; Ding, E.; Xue, F. In situ synthesis of TiO<sub>2</sub>/polyethylene terephthalate hybrid nanocomposites at low temperature. *Appl. Surf. Sci.* **2012**, *258*, 6564–6570. [CrossRef]
117. Mourad, A.-H.I.; Mozumder, M.S.; Mairpady, A.; Pervez, H.; Kannuri, U.M. On the Injection Molding Processing Parameters of HDPE-TiO<sub>2</sub> Nanocomposites. *Materials* **2017**, *10*, 85. [CrossRef] [PubMed]
118. Zhil'Tsova, T.; Oliveira, M.; Ferreira, J. Relative influence of injection molding processing conditions on HDPE acetabular cups dimensional stability. *J. Mater. Process. Technol.* **2009**, *209*, 3894–3904. [CrossRef]
119. Serrano, C.; Cerrada, M.; Fernandez-Garcia, M.; Ressia, J.; Valles, E.M. Rheological and structural details of biocidal iPP-TiO<sub>2</sub> nanocomposites. *Eur. Polym. J.* **2012**, *48*, 586–596. [CrossRef]
120. Umek, P.; Huskić, M.; Škapin, A.S.; Florjančič, U.; Zupančič, B.; Emri, I.; Arčon, D. Structural and mechanical properties of polystyrene nanocomposites with 1D titanate nanostructures prepared by an extrusion process. *Polym. Compos.* **2008**, *30*, 1318–1325. [CrossRef]
121. Somani, P.R.; Marimuthu, R.; Mulik, U.; Sainkar, S.; Amalnerkar, D. High piezoresistivity and its origin in conducting polyaniline/TiO<sub>2</sub> composites. *Synth. Met.* **1999**, *106*, 45–52. [CrossRef]
122. Feng, W.; Sun, E.; Fujii, A.; Wu, H.; Niihara, K.; Yoshino, K. Synthesis and Characterization of Photoconducting Polyaniline-TiO<sub>2</sub> Nanocomposite. *Bull. Chem. Soc. Jpn.* **2000**, *73*, 2627–2633. [CrossRef]
123. Xia, H.; Wang, Q. Ultrasonic Irradiation: A Novel Approach To Prepare Conductive Polyaniline/Nanocrystalline Titanium Oxide Composites. *Chem. Mater.* **2002**, *14*, 2158–2165. [CrossRef]
124. Alghamdi, M.N. Titanium Dioxide Reinforced Polypropylene Composites: Preparation and Characterization PP-TiO<sub>2</sub> Composites. *Int. J. Eng. Res. Technol.* **2016**, *5*, 633–637.
125. Vladuta, C.; Andronic, L.; Duta, A. Effect of TiO<sub>2</sub>, nanoparticles on the interface in the PET-rubber composites. *J. Nanosci. Nanotechnol.* **2010**, *10*, 2518–2526. [CrossRef] [PubMed]
126. Mikešová, J.; Šlouf, M.; Gohs, U.; Popelková, D.; Vacková, T.; Vu, N.H.; Kratochvíl, J.; Zhigunov, A. Nanocomposites of polypropylene/titanate nanotubes: Morphology, nucleation effects of nanoparticles and properties. *Polym. Bull.* **2014**, *71*, 795–818. [CrossRef]
127. Sreekumar, P.; Al-Harathi, M.A.; De, S. Reinforcement of starch/polyvinyl alcohol blend using nano-titanium dioxide. *J. Compos. Mater.* **2012**, *46*, 3181–3187. [CrossRef]
128. Bora, M.Ö.; Çoban, O.; Avcu, E.; Fidan, S.; Sinmazçelik, T. The effect of TiO<sub>2</sub> filler content on the mechanical, thermal, and tribological properties of TiO<sub>2</sub> /PPS composites. *Polym. Compos.* **2013**, *34*, 1591–1599. [CrossRef]
129. Saluja, P.S.; Tiwari, J.K.; Gupta, G. Preparation and Thermal Behaviour of Polyester Composite Filled with TiO<sub>2</sub>. *Int. Res. J. Eng. Technol.* **2017**, *4*, 3135–3141.
130. Byrne, M.T.; McCarthy, J.E.; Bent, M.; Blake, R.; Gun'Ko, Y.K.; Horvath, E.; Konya, Z.; Kukovecz, A.; Kiricsi, I.; Coleman, J.N. Chemical functionalisation of titania nanotubes and their utilisation for the fabrication of reinforced polystyrene composites. *J. Mater. Chem.* **2007**, *17*, 2351–2358. [CrossRef]
131. Dong, Y.; Gui, Z.; Hu, Y.; Wu, Y.; Jiang, S. The influence of titanate nanotube on the improved thermal properties and the smoke suppression in poly(methyl methacrylate). *J. Hazard. Mater.* **2012**, *209–210*, 34–39. [CrossRef] [PubMed]
132. Alexandru, M. On the morphology and potential application of polydimethylsiloxane-silica-titania composites. *Express Polym. Lett.* **2011**, *5*, 188–196. [CrossRef]
133. Saritha, A.; Joseph, K.; Boudenne, A.; Thomas, S. Mechanical, thermophysical, and diffusion properties of TiO<sub>2</sub>-filled chlorobutyl rubber composites. *Polym. Compos.* **2011**, *32*, 1681–1687. [CrossRef]

134. Manap, A.; Mahalingam, S.; Vaithyalingam, R.; Abdullah, H. Mechanical, thermal and morphological properties of thermoplastic polyurethane composite reinforced by multi-walled carbon nanotube and titanium dioxide hybrid fillers. *Polym. Bull.* **2020**, *1–18*. [CrossRef]
135. Esthappan, S.K.; Kuttappan, S.K.; Joseph, R. Thermal and mechanical properties of polypropylene/titanium dioxide nanocomposite fibers. *Mater. Des.* **2012**, *37*, 537–542. [CrossRef]
136. Awang, M.; Mohd, W.R.W.; Sarifuddin, N. Study the effects of an addition of titanium dioxide (TiO<sub>2</sub>) on the mechanical and thermal properties of polypropylene-rice husk green composites. *Mater. Res. Express* **2019**, *6*, 075311. [CrossRef]
137. Huang, J.; Lu, X.; Zhang, N.; Yang, L.; Yan, M.; Liu, H.; Zhang, G.; Qu, J. Study on the properties of nano-TiO<sub>2</sub> /polybutylene succinate composites prepared by vane extruder. *Polym. Compos.* **2013**, *35*, 53–59. [CrossRef]
138. Bragaglia, M.; Cherubini, V.; Nanni, F. PEEK-TiO<sub>2</sub> composites with enhanced UV resistance. *Compos. Sci. Technol.* **2020**, *199*, 108365. [CrossRef]
139. Farhoodi, M.; Dadashi, S.; Mousavi, S.M.A.; Sotudeh-Gharebagh, R.; Emam-Djomeh, Z.; Oromiehie, A.; Hemmati, F. Influence of TiO<sub>2</sub> Nanoparticle Filler on the Properties of PET and PLA Nanocomposites. *Polym. Korea* **2012**, *36*, 745–755. [CrossRef]
140. Lu, X.-L.; Lü, X.-Q.; Wang, J.-Y.; Sun, Z.-J.; Tong, Y.-X. Preparation and shape memory properties of TiO<sub>2</sub>/PLCL biodegradable polymer nanocomposites. *Trans. Nonferrous Met. Soc. China* **2013**, *23*, 120–127. [CrossRef]
141. Alberton, J.; Martelli, S.M.; Fakhouri, F.M.; Soldi, V. Mechanical and moisture barrier properties of titanium dioxide nanoparticles and halloysite nanotubes reinforced polylactic acid (PLA). *IOP Conf. Ser. Mater. Sci. Eng.* **2014**, *64*, 012010. [CrossRef]
142. Zhang, H.; Huang, J.; Yang, L.; Chen, R.; Zou, W.; Lin, X.; Qu, J. Preparation, characterization and properties of PLA/TiO<sub>2</sub> nanocomposites based on a novel vane extruder. *RSC Adv.* **2015**, *5*, 4639–4647. [CrossRef]
143. Zhuang, W.; Liu, J.; Zhang, J.H.; Hu, B.X.; Shen, J. Preparation, characterization, and properties of TiO<sub>2</sub>/PLA nanocomposites by in situ polymerization. *Polym. Compos.* **2009**, *30*, 1074–1080. [CrossRef]
144. Wetzel, B.; Rosso, P.; Hauptert, F.; Friedrich, K. Epoxy nanocomposites—Fracture and toughening mechanisms. *Eng. Fract. Mech.* **2006**, *73*, 2375–2398. [CrossRef]
145. Chatterjee, A.; Islam, M.S. Fabrication and characterization of TiO<sub>2</sub>–epoxy nanocomposite. *Mater. Sci. Eng. A* **2008**, *487*, 574–585. [CrossRef]
146. Huang, K.S.; Nien, Y.H.; Chen, J.S.; Shieh, T.R.; Chen, J.W. Synthesis and properties of epoxy/TiO<sub>2</sub> composite materials. *Polym. Compos.* **2006**, *27*, 195–200. [CrossRef]
147. Al-Turaif, H.A. Effect of nano TiO<sub>2</sub> particle size on mechanical properties of cured epoxy resin. *Prog. Org. Coat.* **2010**, *69*, 241–246. [CrossRef]
148. Papanicolaou, G.; Kontaxis, L.; Manara, A. Viscoelastic behaviour and modelling of nano and micro TiO<sub>2</sub> powder-epoxy resin composites. *Cienc. Tecnol. Mater.* **2016**, *28*, 138–146. [CrossRef]
149. Salehian, H.; Jahromi, S.A.J. Effect of titanium dioxide nanoparticles on mechanical properties of vinyl ester-based nanocomposites. *J. Compos. Mater.* **2015**, *49*, 2365–2373. [CrossRef]
150. Meera, A.P.; Said, S.; Grohens, Y.; Luyt, A.S.; Thomas, S. Tensile Stress Relaxation Studies of TiO<sub>2</sub> and Nanosilica Filled Natural Rubber Composites. *Ind. Eng. Chem. Res.* **2009**, *48*, 3410–3416. [CrossRef]
151. Ochigbo, S.S.; Luyt, A.S. Mechanical and Morphological Properties of Films Based on Ultrasound Treated Titanium Dioxide Dispersion/Natural Rubber Latex. *Int. J. Compos. Mater.* **2011**, *1*, 7–13. [CrossRef]
152. Hayeemasae, N.; Rathnayake, W.; Ismail, H. Nano-sized TiO<sub>2</sub>-reinforced natural rubber composites prepared by latex compounding method. *J. Vinyl Addit. Technol.* **2017**, *23*, 200–209. [CrossRef]
153. Datta, J.; Kosiorek, P.; Włoch, M. Effect of high loading of titanium dioxide particles on the morphology, mechanical and thermo-mechanical properties of the natural rubber-based composites. *Iran. Polym. J.* **2016**, *25*, 1021–1035. [CrossRef]

Review

# Polymer Composite-Based Materials with Photocatalytic Applications in Wastewater Organic Pollutant Removal: A Mini Review

Alexandru Enesca \* and Cristina Cazan 

Product Design, Mechatronics and Environmental Department, Transilvania University of Brasov, Eroilor 29 Street, 35000 Brasov, Romania

\* Correspondence: aenesca@unitbv.ro

**Abstract:** The development of new technologies using nanomaterials has allowed scientists to design advanced processes with many applications in environmental protection, energy production and storage, and medicinal bio-mediated processes. Due to their significant potential applications in different branches of science, the development of new polymer composites represents a priority, especially for nano-technological processes. Interest in polymeric composites was outlined by the synthesis of a large number of nano- or mezo-scale materials with targeted functional properties for polymer matrix hybridization. The present mini review explores some of the most representative and recent papers reporting the photocatalytic activity of polymer composites toward different organic compounds (dyes, pharmaceutically active molecules, phenol, etc.). The polymer composites were divided based on their composition and photocatalytic activity. TiO<sub>2</sub>- and ZnO-based polymeric composites have been described here in light of their photocatalytic activity toward different pollutants, such as rhodamine B, phenol, or methyl orange. Polymeric composites based on WO<sub>3</sub>, Fe<sub>2</sub>O<sub>3</sub>, or Bi<sub>2</sub>MoO<sub>6</sub> were also described. The influence of different polymeric composites and photocatalytic parameters (light spectra and intensity, pollutant molecule and concentration, irradiation time, and photocatalyst dosage) on the overall photocatalytic efficiency indicates that semiconductor (TiO<sub>2</sub>, ZnO, etc.) insertion in the polymeric matrix can tune the photocatalytic activity without compromising the structural integrity. Future perspectives and limitations are outlined considering the systematic and targeted description of the reported results. Adopting green route synthesis and application can add economic and scientific value to the knowledgebase by promoting technological development based on photocatalytic designs.

**Citation:** Enesca, A.; Cazan, C. Polymer Composite-Based Materials with Photocatalytic Applications in Wastewater Organic Pollutant Removal: A Mini Review. *Polymers* **2022**, *14*, 3291. <https://doi.org/10.3390/polym14163291>

Academic Editor: George Z. Kyzas

Received: 4 July 2022

Accepted: 8 August 2022

Published: 12 August 2022

**Publisher's Note:** MDPI stays neutral with regard to jurisdictional claims in published maps and institutional affiliations.



**Copyright:** © 2022 by the authors. Licensee MDPI, Basel, Switzerland. This article is an open access article distributed under the terms and conditions of the Creative Commons Attribution (CC BY) license (<https://creativecommons.org/licenses/by/4.0/>).

**Keywords:** advanced oxidation; composites; dyes; organic pollutants; pharmaceutical compounds; photocatalysts

## 1. Introduction

The need for available clean and drinking water has significantly increased due to demographic expansion, technological development, and higher comfort standards [1]. These factors put an immense stress on the clean water scarcity which emerges as a global problem threatening human health and future lifestyle. In 2019, the World Health Organization released a report indicating that around 785 million people have no or limited access to drinking water and more than half to the Earth population will encounter drinking water scarcity by 2025 [2,3].

The development of new technologies using nanomaterials has allowed scientists to design advanced process with many applications in environmental protection, energy production and storage, as well as medicinal bio-mediated processes. Due to their significant potentials applications in different branches of science, the development of new polymer composites represents a priority, especially for nano-technological processes [4,5]. Polymers based on nano-composites are considered as hybrid structures composed of organic or inorganic nano-materials coupled with polymers acting as matrices with different sizes

and shapes. Such nano-composite structures exhibit distinctive chemical and physical properties, which cannot be attributed to a stand-alone component and are a consequence of the effects of synergistic dual components. Interest in polymeric composites was outlined by the synthesis of a large number of nano- or mezo-scale materials with targeted functional properties for polymer matrix hybridization. These hybrid materials can be used in different fields, such as organic pollutant removal, energy production and storage, catalytic assisted processes, etc. [6–8]. Polymer-based nanomaterials have been used in the medical field, especially in the total hip implant to improve the mechanical performance of polymers [9].

Persistent organic pollutants (POPs) can be found in many aquatic bodies due to direct release or indirect contamination, and the concentration varies depending on the pollution source. The traditional processes for wastewater treatment are inefficient for the complete removal of POPs and advanced technology is required to address this issue [10]. Bioaccumulation has the disadvantage of moving the pollutant from one site to another, while the main issue remains unsolved. Fenton-based processes use light and cations as driving forces for pollutant removal, but the by-product formation is an important disadvantage. The advanced oxidation process (AOP) is considered as a promising alternative for the complete decomposition of POPs due to its ability to generate oxidative and super-oxidative species when a catalyst is irradiated with different sources (microwave, solar radiation, ultraviolet (UV), visible (vis), or other variants) [11,12]. Mono-component semiconductor metal oxides (such as  $\text{WO}_3$  [13,14],  $\text{TiO}_2$  [15,16],  $\text{ZnO}$  [17,18],  $\text{SnO}_2$  [19,20],  $\text{MnO}_2$  [21,22], etc.) and heterostructures (such as  $\text{ZnO}/\text{CuO}$  [23,24],  $\text{TiO}_2/\text{ZnO}$  [25,26],  $\text{Cu}_2\text{S}/\text{WO}_3$  [27,28],  $\text{TiO}_2/\text{WO}_3/\text{ZnO}$  [29],  $\text{Cu}_2\text{S}/\text{WO}_3/\text{SnO}_2$  [30],  $\text{CuO}/\text{ZnO}/\text{WO}_3$  [31], etc.) have been intensively studied and characterized as suitable candidates for photocatalytic wastewater treatments. However, these materials raise significant issues in large-scale applications due to their limited absorption range, surface warping, interface chemical stability, charge carrier recombination, and mobility [32–34].

Polymeric composites are considered as suitable candidates for AOPs due to their unique physical and chemical properties induced by the formation of the interphase region, fillers, and matrix. Polymeric materials are widely used in the industry, due to their lightweight, versatile processability, high chemical resistance, low cost, and low specific gravity [35,36]. The use of conductive polymers as sensitizing agents in photocatalytic composites have the advantage of improving the photocatalytic efficiency due to p-conjugated systems which contain a high concentration of electron-rich species available for transfer in the semiconductor's conduction band. Consequently, the recombination rate of the photo-generated charge carriers is reduced, while conductive polymers tune the semiconductor's band gap [37,38]. Based on the density functional theory models, the conducting polymers such as poly(1-naphthylamine), polythiophene, polyaniline, polyacetylene, polypyrrole, polycarbazole, or poly(ophenylenediamine) exhibit visible absorption activity due to their low band gap values which make them ideal candidates for extending the semiconductor's light absorption range [39–42]. A systematic review can be used as a tool on designing new experiments to provide more insight on the correlation between the composite composition, testing parameters, and overall photocatalytic activity.

The present mini review explores some of the most representative and recent papers reporting on the photocatalytic activity of polymer composites toward various organic compounds (dyes, pharmaceutically active molecules, phenol, etc.). The literature contains scientific articles presenting similar or different information that was not considered here due to the space limitation or incomplete experimental data. The paper describes the effect of different polymeric composites and photocatalytic parameters (light spectra and intensity, pollutant molecule and concentration, irradiation time, photocatalyst dosage, etc.) on the overall photocatalytic efficiency. Representative studies were included and correlated in order to outline the significance of polymeric composite composition and testing parameters on the photocatalytic removal of pollutants. It can be seen that high light intensity or photocatalyst dosage are not pre-requisites for high photocatalytic activity. Tailoring the

material properties based on their composition as well as the surface chemistry with the pollutant molecules can play an important role.

## 2. Photocatalytic Mechanism of Polymeric Composites

Nanotechnology may represent an alternative solution in solving the issues related to safe drinking water stress and high global demography. The available drinking water sources are inconsistent with the geographical position of high urban density, and so long-term solutions are needed. As a flexible alternative for cost-effective wastewater treatment processes, nanotechnology exhibits high efficiency and multifunctionality and is suitable for large-scale applications [43,44]. Additionally, the photocatalytic process using nanomaterials can integrate renewable resources in the technological wastewater treatment flux as a key component of energy sustainability. The main goal of the photocatalytic process is to induce the pollutant mineralization, leading to non-hazardous products. However, the polymer composite requires large optimization procedures in order to attempt this goal. Moreover, the pollutant is partially decomposed, which may lead to hazardous by-products [45,46].

Photocatalysts based only on metal oxide semiconductors present limitations in terms of charge carrier recombination and mobility, chemical stability, and large band-gaps values, which restrict the light absorption spectrum in the UV region [47–49]. As presented in Figure 1, when coupled with metal oxide semiconductors, the conducting polymers work as photosensitizers due to their high charge mobility properties.

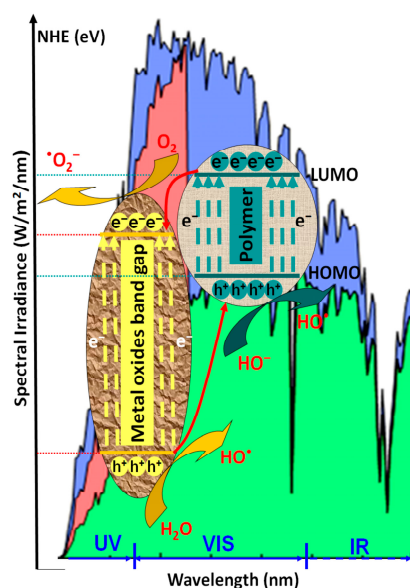
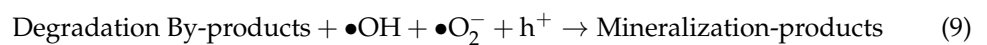
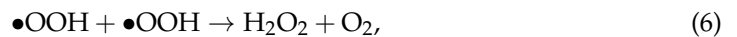
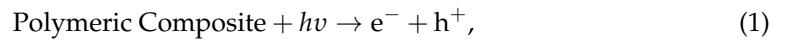


**Figure 1.** The photocatalytic mechanism of polymeric composites.

The polymeric composite exhibits a high-efficiency response in the presence of visible light radiation, thermal and chemical stability, and low charge carrier recombination [49]. During irradiation ( $h\nu$ ), the composite interface behaves as a synergistic active area where the photogenerated electrons ( $e^-$ ) migrate from the lowest unoccupied molecular orbital (LUMO) polymer level to the metal oxide conduction band (CB), while the photo-induced holes ( $h^+$ ) are transferred from the valence energy band (VB) of metal oxide directly to the highest occupied molecular orbital (HOMO) polymer level [50,51]. As presented in Equations (1)–(9), the photocatalytic inter-chain reaction is induced by the formation of hydroxyl radicals ( $\bullet\text{OH}$ ) from water molecules along with the formation of superoxide anion radicals ( $\bullet\text{O}_2^-$ ) from oxygen-dissolved molecules. Both mechanisms require the participation of photogenerated charge carriers ( $h^+$  and  $e^-$ ). The subsequent reactions of  $\bullet\text{O}_2^-$  with photogenerated holes can form hydroperoxyl radicals ( $\bullet\text{OOH}$ ) and  $\text{H}_2\text{O}_2$  [52].

It must be underlined that the direct oxidation of organic pollutants absorbed at the photocatalyst surface is also possible [53].



### 3. Polymer Composite Photocatalytic Materials

Despite the advantages of polymeric materials, their low modulus, low strength, low working temperature, and chemical stability to environmental conditions limit their application in photocatalytic processes. The insertion of a secondary material, such as metals or metallic oxides, as a reinforcement component can provide a unique combination of optical and electrical properties which will enhance photocatalytic activity. Furthermore, the resulting composites possess superior properties compared with stand-alone components, including improved chemical resistance, modulus, strength, and electrical conductivity [54,55].

#### 3.1. Polymer/TiO<sub>2</sub>- or ZnO-Based Composites

Among transition metal oxides, titanium oxide is considered as the most widely used semiconductor due to its high chemical stability, versatile morphology, and high UV sensitivity; however, in recent years, ZnO has earned considerably attention because of its catalytic properties and cost-effective synthesis procedures [56]. As presented in Figure 2, both semiconductors can be coupled with polymers in order to form favorable junction for the photogeneration and transfer of charge carriers, in order to produce oxidative species. Table 1 contains representative studies of polymers/TiO<sub>2</sub> or ZnO composites used in photocatalytic applications.

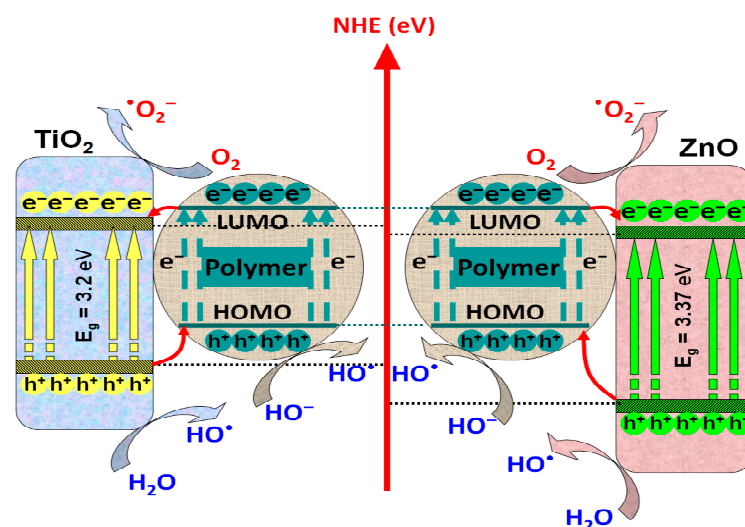


Figure 2. Mechanism of charge photogeneration in polymers/TiO<sub>2</sub> or ZnO composites.

Table 1. Polymer/TiO<sub>2</sub>- or ZnO-based composites.

| Composite Composition   |                      | Pollutant                                      |            | Photocatalytic Properties |                        |                    |                  |                    | Ref. |
|---|----------------------|--|------------|---------------------------|------------------------|--------------------|------------------|--------------------|------|
| Polymer (s)   | Second Material      | Molecule                                       | Conc.      | Radiation Type            | Radiation Intensity    | Exposure Time      | Catalyst Dosage  | Removal Efficiency |      |
| Polyacrylamide  | TiO <sub>2</sub>     | methyl orange                                  | 1.0 mg/L   | UV                        | 3 W                    | 300 min            | np *             | 95%                | [57] |
| Polyurethane  | TiO <sub>2</sub>     | methyl orange                                  | 10 mg/L    | UV                        | 38 W/m <sup>2</sup>    | 50 min             | 0.046 g/3.6 mL   | 100%               | [58] |
| Resorcinol-formaldehyde   | TiO <sub>2</sub>     | methyl orange                                  | 13 mg/L    | UV                        | 36 W                   | 240 min            | 1 mg/3 mL        | 55%                | [59] |
| Polyethylene glycol   | TiO <sub>2</sub>     | methylene blue                                 | 20 mg/L    | UV                        | 300 W                  | 240 min            | 3 g/100 mL       | 100%               | [60] |
| Polytrifluorochloro ethylene  | TiO <sub>2</sub>     | methylene blue                                 | 10 mg/L    | UV                        | 0.5 mW/cm <sup>2</sup> | 270 min            | np               | 100%               | [61] |
| PEG2000-silicone  | TiO <sub>2</sub>     | methylene blue                                 | 3.2 mg/L   | UV                        | 20 W                   | 120 min            | np               | 40%                | [62] |
| Polyvinyl alcohol<br>Polyethylene glycol  | TiO <sub>2</sub>     | acid black                                     | 20 mg/L    | UV                        | 44 W/m <sup>2</sup>    | 120 min            | 50 mg/400 mL     | 55.4%<br>62.8%     | [63] |
| Polythiophene   | TiO <sub>2</sub>     | rhodamine B                                    | 40 mg/L    | UV<br>Vis                 | 10 W<br>320 W          | 180 min<br>600 min | 300<br>mg/300 mL | 76%<br>98%         | [64] |
| Poly-phenylpropenes<br>trans-anethole and<br>N-phenylmaleimide  | TiO <sub>2</sub>     | rhodamine B                                    | 10 mg/L    | UV                        | 600 W                  | 90 min             | 20 mg/20 mL      | 95%                | [65] |
| Chitosan  |                      | tetracycline                                   |            |                           |                        |                    |                  | 97%                |      |
| Polyvinyl alcohol–chitosan  | TiO <sub>2</sub>     | metronidazole                                  | 10 mg/L    | UV                        | 32 W                   | 120 min            | 0.3 g/L          | 100%               | [66] |
| Polyvinyl alcohol   | TiO <sub>2</sub>     | phenol   | 10 mg/L    | Vis                       | 500 W                  | 360 min            | np               | 67.5%              | [67] |
| Poly(vinylidene fluoride)   | TiO <sub>2</sub> /GO | phenol   | 50 mg/L    | UV                        | 100 W                  | 180 min            | np               | 65%                | [68] |
| Polydimethylsiloxane  | TiO <sub>2</sub>     | methylparaben<br>ethylparaben<br>propylparaben | 1 mg/L     | Sun<br>Radiation          | np                     | 120 min            | 140 mg/L         | 50%<br>52%<br>55%  | [69] |
| Polypyrrole   | ZnO                  | methylene blue                                 | 50 mg/L    | UV                        | 100 W                  | 20 min             | 50 mg/50 mL      | 98.12%             | [70] |
| Polypyrrole   | ZnO                  | rhodamine B                                    | 5 mg/L     | Vis                       | 150 W                  | 300 min            | np               | 65%                | [71] |
| Poly(3-hexylthiophene-<br>2,5-diyl)   | ZnO                  | rhodamine B                                    | 0.01 mg/L  | Vis                       | 300 W                  | 80 min             | 20 mg/100 mL     | 99%                | [72] |
| Poly(propylene glycol)-dimethacrylate-<br>methacryloyloxyethyl-<br>N,N-dimethyl-3-<br>(trimethoxysilyl)-propane | ZnO                  | methyl orange                                  | 16.35 mg/L | Vis                       | 4.9 mW/cm <sup>2</sup> | 250 min            | 1 g/50 mL        | 56.12%             | [73] |
|   | ZnO-Ag               |  |            |                           |                        |                    |                  | 95%                |      |

\* not provided.

The photocatalytic removal of methyl orange was evaluated using composites based on polyacrylamide/TiO<sub>2</sub> [57], polyurethane/TiO<sub>2</sub> [58], and resorcinol-formaldehyde/TiO<sub>2</sub> [59]. The polyurethane/TiO<sub>2</sub> could completely remove the methyl orange dye in 50 min from a solution with a 10 mg/L concentration using a catalyst dosage of 0.046 g/3.6 mL. The composite has the advantage of using macroporous supports for TiO<sub>2</sub> insertion which favor the formation of a larger active surface. Consequently, the photo-oxidation rate increases and the mass transfer is reduced. The polyacrylamides/TiO<sub>2</sub> exhibit 95% photocatalytic efficiency after 300 min of UV irradiation with a 3 W light source. The initial concentration of methyl orange solution was significantly lower (1.0 mg/L), which allows higher light penetration during the experiments. The diffusion plays an important role in the photocatalytic efficiency. At low diffusion values, the dye concentration decreases more slowly with time on the outer boundary compared with the case of the fast diffusion. The highest methyl orange concentration (13 mg/L) was used to test the resorcinol-formaldehyde/TiO<sub>2</sub> photocatalytic activity at a 1 mg/3 mL dosage. The sample was irradiated with a 36 W UV lamp for 240 min in order to remove 55% of methyl orange. A lower photocatalytic activity was presumed to be induced by the TiO<sub>2</sub> influence which reduces the apparent polymeric surface, in turn decreasing the number of active sites involved in dye degradation.

The photocatalytic removal of methylene blue was tested using polyethylene glycol/TiO<sub>2</sub> [60], polytrifluorochloro ethylene/TiO<sub>2</sub> [61], and PEG2000–silicone/TiO<sub>2</sub> [62] composites. Both polyethylene glycol/TiO<sub>2</sub> and polytrifluorochloro ethylene/TiO<sub>2</sub> could completely remove the dye, but under different experimental conditions. The polytrifluorochloro ethylene/TiO<sub>2</sub> composite was tested using a 10 mg/L methylene blue concentration and 270 min of UV irradiation (0.5 mW/cm<sup>2</sup>). The overall film roughness was improved due to the TiO<sub>2</sub> nanopowder embedded in the polymer matrix, which maximizes the interface with solution. When roughness increases, these may suggest that the TiO<sub>2</sub> nanoparticles



form aggregates, which can reduce the photocatalytic activity. The concentration of methylene blue solution was double (20 mg/L) for the polyethylene glycol/TiO<sub>2</sub> photocatalytic test and the composite could remove the dye in 240 min under a 300 W UV source using a catalyst dosage of 3 g/100 mL. It is well known that the surface morphologies play an important role in dye adsorption, which is the preliminary step for their degradation. Variations in adsorption capacity were observed due to the PEG increasing the porosity, resulting in an increased interface area with the dye solution. However, when a mixture of PEG2000–silicone/TiO<sub>2</sub> was used, the photocatalytic efficiency decreases at 40%, even if the initial concentration of methylene blue solution was limited at 3.2 mg/L and the UV exposure time was 120 min. In this case, the risk of mechanical collapse was reduced due to the presence of surface hydroxyl groups, allowing the particles to bond tightly to the modified silicone.

The TiO<sub>2</sub> was employed to form composites with polyvinyl alcohol and polyethylene glycol for the photocatalytic removal of acid black dye in similar experimental conditions [63]. The dye solution concentration was 20 mg/L and the catalyst's dosage was 50 mg/400 mL. After 120 min of UV irradiation with 44 W/m<sup>2</sup> irradiance, the polyvinyl alcohol/TiO<sub>2</sub> exhibits 55.4% photocatalytic efficiency, while polyethylene glycol/TiO<sub>2</sub> reaches 62.8% efficiency. It was found that the polyethylene glycol/TiO<sub>2</sub> composite showed higher photocatalytic activity due to the more appropriate calcination temperature, allowing the interaction of Ti-O-C bonds in the structure. Rhodamine B dye photodegradation was also tested with the polythiophene/TiO<sub>2</sub> composite using UV (10 W) and vis (320 W) radiation [64]. The dye solution concentration was 40 mg/L and the catalyst dosage was 300 mg/300 mL. The results indicate that after 180 min of UV radiation, 76% of rhodamine B was removed, while under vis radiation, 600 min were necessary to remove 98% of rhodamine B. Even if the TiO<sub>2</sub> is absorbed in the UV region, surface hybridization in the presence of polythiophene can induce visible light photon absorption. The removal of rhodamine B was also tested with trans-anethole/N-phenylmaleimide/TiO<sub>2</sub> composite poly-phenylpropenes under 600 W UV irradiation using a catalyst dosage of 20 mg/20 mL [65]. After 90 min of irradiation, 95% of the 10 mg/L dye solution concentration was removed. The number of free radicals photogenerated under UV irradiation and the available number of adsorption sites were limited as the dye could saturate a part of them. Increasing the irradiation time can help in generating more oxidative radicals involved in rhodamine B degradation, but the energy consumption will also increase. The same composite and experimental conditions were used for the removal of tetracycline. In this case, the photocatalytic efficiency increased at 97%, indicating that trans-anethole/N-phenylmaleimide/TiO<sub>2</sub> poly-phenylpropenes are versatile composites that can be used to remove different organic pollutant. Another pharmaceutical compound (metronidazole) was considered for photocatalytic degradation using the chitosan polyvinyl alcohol/TiO<sub>2</sub> composite [66] with a 0.3 g/L dosage. The metronidazole was completely removed from the 10 mg/L solution concentration in 120 min under 32 W UV radiation based on the synergetic effect of pseudo-second-order adsorption and pseudo-first-order photocatalytic processes. Density functional theory modeling (DFT) indicates that the assembly of hydroxyl groups will passivate the titanium oxide to the polymer through significant hydrogen bonding. The adsorption of metronidazole molecules on the composite surface is favored by the extensive weak dispersive forces.

Phenol photocatalytic removal was evaluated using polyvinyl alcohol/TiO<sub>2</sub> [67] and poly(vinylidene fluoride)/GO/TiO<sub>2</sub> [68] composites. A visible light source with a 500 W intensity was used to irradiate polyvinyl alcohol/TiO<sub>2</sub> for 360 min. The results indicate that 67.5% of the phenol was removed to form a 10 mg/L solution due to the short diffusion length of excitons, which can induce their dissociation prior recombination. The employment of conjugated PVA will improve the TiO<sub>2</sub> absorption, resulting in higher energy conversion. The dissociation of charge carriers can promote the charge migration from the polymer to the TiO<sub>2</sub> nanoparticles. The poly(vinylidene fluoride)/GO/TiO<sub>2</sub> composite was irradiated with a 100 W UV source for 180 min. The photocatalytic efficiency was

65%, but the initial phenol concentration was five times higher than in the previous case. This is due to the GO presence which serves as an electron receptor and network for the photo-generated charges in TiO<sub>2</sub>. The photo-generated charged carriers migrate through the GO sheets that reduce the electron–hole recombination due to the stereo conductive framework which can alleviate the recombination rate process. The removal of three types of parabens (methylparaben, ethylparaben, and propylparaben) was performed by placing the polydimethylsiloxane/TiO<sub>2</sub> composite under sun radiation for 120 min [69]. Using the same paraben concentration (1 mg/L) and photocatalyst dosage (140 mg/L), the removal efficiency varies up to 50% for methylparaben, 52% for ethylparaben, and 55% for propylparaben. The authors indicate that TiO<sub>2</sub>, when immobilized in the polymeric membranes, is the only component acting for the removal of parabens through the photocatalytic process since no adsorption on the polymeric membranes occurs. Moreover, increasing the TiO<sub>2</sub> concentration favors the nanoparticle agglomeration, which can inhibit the TiO<sub>2</sub> active sites and decrease the available active centers responsible for hydroxyl radical production.

Polymeric composites with ZnO were employed for the photocatalytic removal of dyes such as methylene blue [70], rhodamine B [71,72], or methyl orange [73]. The polypyrrole/ZnO composite was used to remove methylene blue dye from a 50 mg/L concentrated solution [70]. After 20 min of 100 W UV irradiation and a 50 mg/50 mL catalyst dosage, the photocatalytic efficiency was 98.12% due to the suitable charge carrier transfer mechanism between polypyrrole and ZnO nanoparticles that reduce the charge recombination. The study indicates that, at higher temperatures (323 K), photocatalytic efficiency increases to 99.05%, which shows that the degradation process follows an endothermic pathway. A similar composite based on polypyrrole/ZnO was used for rhodamine B photocatalytic removal with a 5 mg/L solution concentration [71]. The sample was irradiated for 300 min with a 150 W vis radiation, and the final photocatalytic efficiency was 65%. During the composite light irradiation, excitons were created. The photo-generated electron in ZnO was transferred from the valence energy band to the CB, and the photo-generated hole migrated to highest occupied molecular orbital (HOMO) of the polymer. Additionally, the photo-generated electron from HOMO migrated to lowest energy unoccupied molecular orbital (LUMO) in the polymer matrix. Finally, from LUMO, the photo-generated electron was transferred to the conduction band of ZnO. When the poly(3-hexylthiophene-2,5-diyl)/ZnO composite was used to remove 0.01 mg/L rhodamine B under 300 W vis radiation, the photocatalytic efficiency increased by 99% after 80 min of irradiation [72]. This result can be attributed to the strengthened vis light absorption and the closely contacted interface between the two components. A comparative study for methyl orange photocatalytic removal was conducted using poly(propylene glycol)-dimethacrylate/methacryloyloxyethyl-N,N-dimethyl-3-(trimethoxysilyl)-propane/ZnO and poly(propylene glycol)-dimethacrylate/methacryloyloxyethyl-N,N-dimethyl-3-(trimethoxysilyl)-propane/ZnO-Ag composites [73]. The samples were irradiated with vis light (4.9 mW/cm<sup>2</sup>) for 250 min in order to remove 16.35 mg/L of methyl orange. The silver-free composite exhibited 56.12% photocatalytic efficiency, while the methacryloyloxyethyl-N,N-dimethyl-3-(trimethoxysilyl)-propane/ZnO-Ag composite reached 95% efficiency. As presented in Figure 3, a lower ZnO-Ag Fermi level relative to the ZnO conduction band energy was established during irradiation, inducing the photo-generated migration of electrons from ZnO to the silver-mediated composite using the potential energy. Consequently, the accumulation of photo-generated electrons occurred in silver particles along with the hole's migration to ZnO surface, inducing the charge carrier's separation. The insertion of silver nanoparticles had a favorable effect on the generation of oxidative radicals, where electrons were adsorbed by the O<sub>2</sub> to form •O<sub>2</sub><sup>−</sup> and holes reacted with OH<sup>−</sup> to form hydroxyl radicals (•OH).

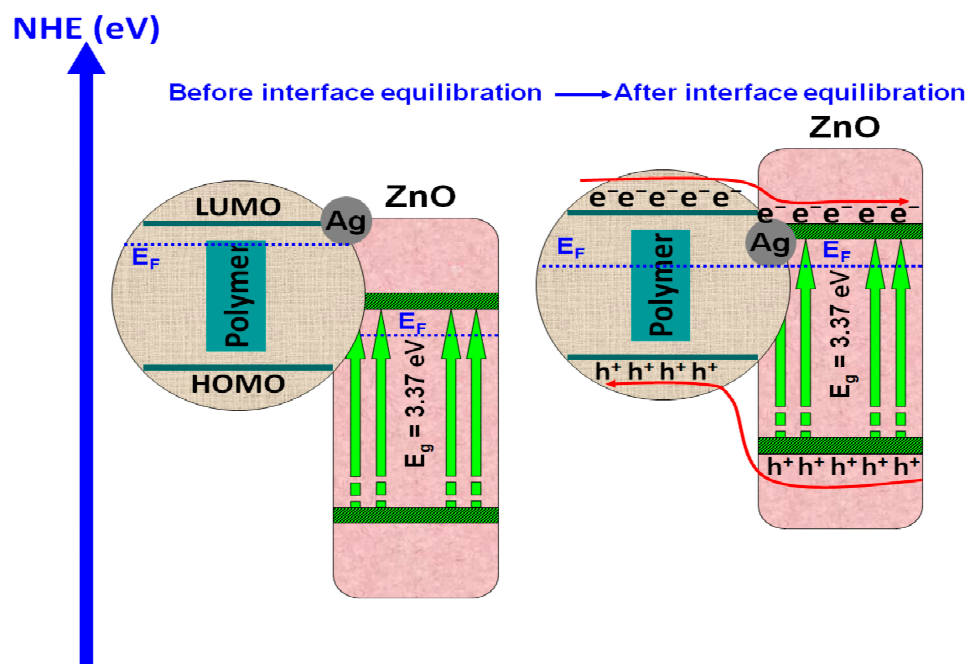


Figure 3. Polymeric composite containing silver coupled ZnO.

### 3.2. Other Polymer Composites Based Materials

Polymers can be combined with one or more components in order to form suitable composites for photocatalytic applications. The components are chosen based on several factors: interface compatibility with the polymeric matrix, chemical stability in the working environment, light sensitivity, and economic costs. Table 2 presents some recent reports on polymeric composites containing tandem semiconductors, metals, or mono-component semiconductors with photocatalytic application for dyes or the removal of pharmaceutically active compounds.

Table 2. Other polymer composite-based materials.

| Composite Composition  |   | Pollutant   |                       | Photocatalytic Properties |                       |               |                 |                                  |      | Ref. |
|--|---|---|-----------------------|---------------------------|-----------------------|---------------|-----------------|----------------------------------|------|------|
| Polymer (s)  | Second Material   | Molecule  | Conc.                 | Radiation Type            | Radiation Intensity   | Exposure Time | Catalyst Dosage | Removal Efficiency               |      |      |
| Poly(vinyl alcohol-g-acrylamide)                               | ZnO/SiO <sub>2</sub>  | methylene blue<br>crystal violet  | 5 mg/L                | UV                        | 18 W                  | 960 min       | 0.1 g/20 mL     | 86%<br>77%                       | [74] |      |
| Polyaniline<br>Polysulphone-styrene maleic anhydride copolymer | Cu <sub>2</sub> O/ZnO<br>Bi <sub>2</sub> S <sub>3</sub> /TiO <sub>2</sub>     | congo red<br>methylene blue   | 30 mg/L<br>20.26 mg/L | UV                        | np *                  | 30 min        | 100 mg/100 mL   | 100%                             | [75] |      |
| Polyvinyl chloride   | Ag-decorated Bi <sub>2</sub> O <sub>3</sub> /Bi <sub>2</sub> O <sub>2.7</sub> | methylene blue  | 12 mg/L               | UV-vis                    | 350 W                 | 180 min       | np              | 95.32%                           | [76] |      |
| Polyppyrrrole  | TiO <sub>2</sub> /V <sub>2</sub> O <sub>5</sub>                               | rhodamine B<br>tetracycline<br>doxycycline<br>oxytetracycline<br>ofloxacin<br>rhodamine B | 50 mg/L               | Vis                       | 300 W                 | 120 min       | 30 mg/50 mL     | 98%<br>96%<br>85%<br>37%<br>100% | [77] |      |
| TX-SCH <sub>2</sub> COOH-DO                                    | Au/Ag   | methylene blue  | 10 mg/L               | UV                        | 100 W                 | 90 min        | 5 mg/5 mL       | 72.5%                            | [79] |      |
| Tris(4-carbazoyl-9-ylphenyl) amine/<br>polyvinylpyrrolidone    | Cu<br>CuO   | methylene blue  | np                    | Vis                       | 300 W                 | 90 min        | 20 mg/15 mL     | 80%<br>90%                       | [80] |      |
| Polyvinyl alcohol  | Au/Pd   | styrene   | 20 mg/L               | Vis                       | 50 mW/cm <sup>2</sup> | 60 min        | np              | 100%                             | [81] |      |

Table 2. Cont.

| Composite Composition  |   | Pollutant       |                    | Photocatalytic Properties |                        |               |                 |                    | Ref.                   |
|--|---|-----------------|--------------------|---------------------------|------------------------|---------------|-----------------|--------------------|------------------------|
| Polymer (s)  | Second Material                                   | Molecule        | Conc.              | Radiation Type            | Radiation Intensity    | Exposure Time | Catalyst Dosage | Removal Efficiency |                        |
| Phenylacetylde   | Ag/Cu   | norfloxacin     | 10 mg/L            | Vis                       | 9 W                    | 40 min        | 10 mg/50 mL     | 100%               | [82]                   |
|  |   | diclofenac      |                    |                           |                        |               |                 | 64.3%              |                        |
| Polypyrrole  | g-C <sub>3</sub> N <sub>4</sub>                   | bisphenol A     | 10 mg/L            | Vis                       | 12 W                   | 120 min       | 0.05 g/50 mL    | 47.6%              | [83]                   |
|  |   | naproxen        |                    |                           |                        |               |                 | 70.5%              |                        |
| Polythiophene  | CdS   | sulfisoxazole   | 10 mg/L            | Vis                       | 75,000–90,000 Lux      | 300 min       | 25 mg/50 mL     | 42%                | [84]                   |
|  |   | methylene blue  |                    |                           |                        |               |                 | 99%                |                        |
| Polyaniline  | rGO/MnO <sub>2</sub>                              | methylene blue  | 5 mg/L             | Vis                       | 150 W                  | 120 min       | 10 mg/50 mL     | 90%                | [85]                   |
|  |   | rhodamine B     | 4.8 mg/L           | Vis                       | 500 W                  | 180 min       | 0.1 g/100 mL    | 62%                |                        |
| Polyaniline  | BiVO <sub>4</sub> /GO                             | methylene blue  | 3.2 mg/L           |                           |                        |               |                 | Vis                | 100 mW/cm <sup>2</sup> |
|  |   | safranine O     | 35 mg/L            | 82%                       |                        |               |                 |                    |                        |
| Polyaniline  | MoSe <sub>2</sub>                                 | methylene blue  | np                 | Vis                       | 500 W                  | 180 min       | 0.1 g/100 mL    | 65%                | [87]                   |
|  |   | methyl orange   | 35 mg/L            |                           |                        |               |                 | 94%                |                        |
| Polyaniline  | LaNiSbWO <sub>4</sub> /GO                         | safranine O     | 1.7 mg/L           | Vis                       | 250 mW/cm <sup>2</sup> | 30 min        | np              | 84%                | [88]                   |
|  |   | gallic acid     | 70 mg/L            |                           |                        |               |                 | 92%                |                        |
| Polyether Tetraacrylate                                      | Nd <sub>0.9</sub> TiO <sub>3</sub>                | Acid Black      | 15 mg/L            | UV                        | 500 W                  | 60 min        | 40 mg/40 mL     | 94%                | [89]                   |
|  |   | Acid Orange 7   | 8 mg/L + 38.7 mg/L | Vis                       | 20 W                   | 120 min       | 10 mg/100 mL    | 95%                |                        |
| Cyclodextrin   | BiOBr   | methylene blue  | 88.2 mg/L          |                           |                        |               |                 | UV                 | 350 W                  |
|  |   | + oxalic acid   | 5 mg/L             | 98%                       |                        |               |                 |                    |                        |
| Polystyrene/divinylbenzene                                   | Fe <sub>2</sub> O <sub>3</sub>                    | oxalic acid     | 30 mg/L            | Vis                       | 300 W                  | 90 min        | 20 mg/100 mL    | 73.6%              | [91]                   |
|  |   | tetracycline    | 10 mg/L            |                           |                        |               |                 | 88.3%              |                        |
| Polypyrrole  | Bi <sub>2</sub> MoO <sub>6</sub>                  | tetracycline    | 10 mg/L            | Vis                       | 0.07 W/cm <sup>2</sup> | 120 min       | np              | 86%                | [92]                   |
|  |   | tetracycline    | 10 mg/L            |                           |                        |               |                 | 81%                |                        |
| 4,7-dibromobenzo thiazole/4-ethynylphenyl amine              | H <sub>3</sub> PMo <sub>12</sub> O <sub>40</sub>  | rhodamine B     | 10 mg/L            | UV                        | 250 mW/cm <sup>2</sup> | 90 min        | 1 g/L           | 86%                | [94]                   |
|  |   | erythrosine B   |                    |                           |                        |               |                 | 81%                |                        |
| Poly(trimethylpropane triacrylate)/bis(acyl)phosphane oxides | H <sub>3</sub> PMo <sub>12</sub> O <sub>40</sub>  | rose bengal     | 15 mg/L            | UV-vis                    | 250 mW/cm <sup>2</sup> | 75 min        | np              | 100%               | [95]                   |
|  |   | ibuprofen       |                    |                           |                        |               |                 | 90%                |                        |
| Poly(trimethylpropane triacrylate)                           | W <sub>10</sub> O <sub>32</sub> (TH) <sub>4</sub> | ciprofloxacin   | 20 mg/L            | Vis                       | 225 W                  | 180 min       | 2.5 g/L         | 86%                | [96]                   |
|  |   | oxytetracycline |                    |                           |                        |               |                 | 50%                |                        |
| Polyimide  | WO <sub>3</sub>                                   | imidacloprid    | 20 mg/L            | Vis                       | 225 W                  | 180 min       | 2.5 g/L         | 73.2%              | [96]                   |

\* not provided.

### 3.2.1. Polymer/Tandem Structure-Based Materials

Tandem structures are composed of at least two semiconductors with suitable disposal of the energy levels, allowing the mobility of charge carriers through the structure and reducing the charge recombination rate. As presented in Figure 4, the tandem structure can be combined with conductive polymeric materials in order to enhance the charge photo-generation, favoring the reduction reactions with e<sup>-</sup> and oxidation reactions by h<sup>+</sup>. These charge carriers will be involved in the oxidative species development, responsible for pollutant mineralization. The non-conductive polymeric matrix can be used to increase the light absorption spectrum, tandem particle dispersion, and the specific surface.

The photocatalytic removal of three dye molecules (methylene blue, crystal violet, and congo red) was studied using the poly(vinyl alcohol-g-acrylamide)/ZnO/SiO<sub>2</sub> composite [74]. The dye's concentration was established at 5 mg/L and the photocatalyst dosage was 0.1 g/20 mL. After 960 min of irradiation with a 18 W UV source, the removal efficiencies were 86% for methylene blue, 77% for crystal violet, and 70% for congo red. The photocatalytic removal efficiency depends on the surface chemistry between the photocatalyst and the dye molecules. When the electrostatic interaction, repelling force, driving force, and hydrogen bonding between dye molecules and composite active sites are in equilibrium, the saturated state facilitates the photocatalytic mineralization reactions. The main driving force for this process is represented by the mass transfer of dye molecules from solution that could reach the available composite active surface sites.

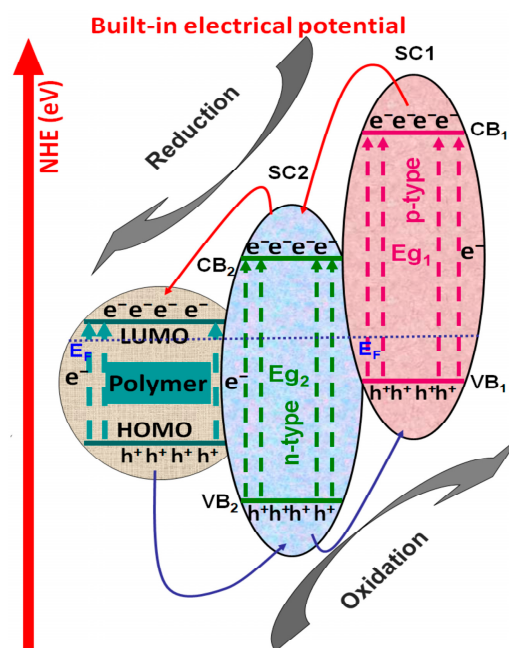


Figure 4. Photocatalytic composite based on polymer/tandem materials.

The total removal of congo red was reached with the polyaniline/Cu<sub>2</sub>O/ZnO composite, using a 30 mg/L dye concentration and a 100 mg/100 mL catalyst dosage [75]. Half an hour was enough to remove the dye due to the insertion of an oxidizing promoter based on ammonium persulfate/potassium permanganate. The composite performance was attributed to the small crystallite sizes (18.5 nm), low bandgap (2.68 eV), reduced and low PL intensity, and large surface area (45.32 m<sup>2</sup>/g). The high photocatalytic removal of methylene blue was reported on polysulphone–styrene maleic anhydride copolymer/Bi<sub>2</sub>S<sub>3</sub>/TiO<sub>2</sub> composites [76]. The catalyst was irradiated for 180 min with a UV–vis (350 W) source and 95% of the 20.25 mg/L dye solution concentration was removed. The composite absorption includes the entire visible-light spectra, due to the Bi<sub>2</sub>S<sub>3</sub>'s small band gap value. Bi<sub>2</sub>S<sub>3</sub> is a direct transition n-type semiconductor with a 1.3 eV band gap energy, which can use the complete visible spectra and enhance the composite light absorption spectrum. The narrower band gap energy of the Bi<sub>2</sub>S<sub>3</sub>-TiO<sub>2</sub> tandem structure stimulates the photo-electric process required to induce the charge carrier's generation. The combined effect of adsorption–migration–photodegradation occurs in the molecular interfacial layers. The reactant's surface and photocatalytic affinity adsorption properties are significant in determining the overall reaction rate.

Rhodamine B photocatalytic removal was evaluated using polyvinyl chloride/Ag-decorated Bi<sub>2</sub>O<sub>3</sub>/Bi<sub>2</sub>O<sub>2.7</sub> [77] and polypyrrole/TiO<sub>2</sub>/V<sub>2</sub>O<sub>5</sub> [78] composites. The polyvinyl chloride/Ag-decorated Bi<sub>2</sub>O<sub>3</sub>/Bi<sub>2</sub>O<sub>2.7</sub> exhibit 97% photocatalytic efficiency after 150 min of irradiation with a low-intensity vis source (5 W). The photocatalytic activity was attributed to the •O<sub>2</sub><sup>−</sup> and h<sup>+</sup> photo-generation based on the synergistic effects of good interface quality; petal-like hierarchical shape; and fast charge separation between Ag particles, β-Bi<sub>2</sub>O<sub>3</sub>, and Bi<sub>2</sub>O<sub>2.7</sub>. If the composite uses the same composition on each side of the heterostructures surface with good lattice fringes matching, then it can establish a suitable and tuned channel for the charges produced during the irradiation. This advantage originates from lower spacing lattice distances between the catalyst partners that may induce lower lattice mismatch, and subsequently decrease the number of defects and interface penetration barriers. The use of the circular band structure provides higher photo-generated carrier migration and separation, due to the minor and potential differences between components. The second composite based on polypyrrole/TiO<sub>2</sub>/V<sub>2</sub>O<sub>5</sub> can completely remove the rhodamine B dye after 120 min of irradiation with a 300 W vis source. The same composite was employed to establish the photocatalytic performance toward four

molecules of pharmaceutically active compounds. Using a 50 mg/L solution concentration and a 30 mg/50 mL photocatalyst dosage, the composite exhibits the following removal efficiencies: 98% for tetracycline, 96% for doxycycline, 85% for oxytetracycline, and 37% for ofloxacin. The presence of  $V_2O_5$  increases the vis light absorption in the 600 nm proximity. The introduction of polypyrrole remarkably broadens the composite absorption region to the total visible light spectrum, which simultaneously enhances the light absorption performance and photocatalytic activities under visible light.

### 3.2.2. Polymer/Metal-Based Materials

Polymer/metal composites are often viewed as suitable materials for the photocatalytic removal of persistent organic pollutants, such as dyes or different pharmaceutical compounds. As presented in Figure 5, the metal nanoparticles penetrate the polymeric matrix and provide a compatible interfacial region. When conductive polymers are used, the composite materials which act as Schottky junctions represent the interface between the metal component and the semiconductor structure, providing an effective pathway to decrease the photo-generated carrier's recombination and even to increase the catalyst spectral absorption.

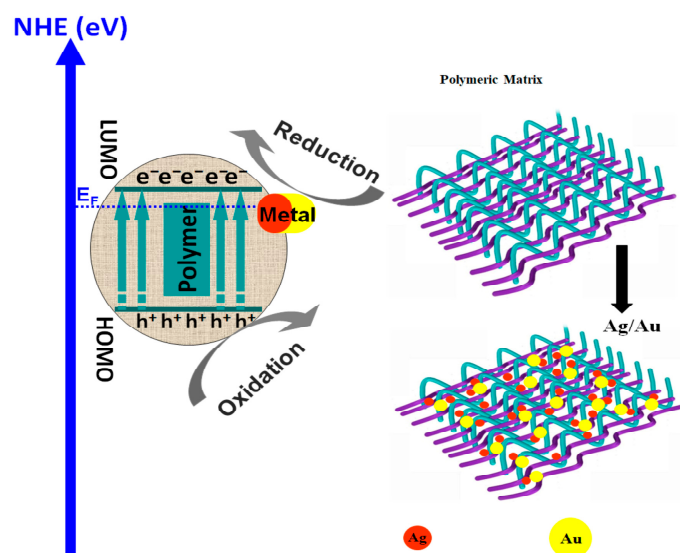


**Figure 5.** Polymer/metal composites for wastewater treatment.

The removal of methylene blue was tested using TX-SCH<sub>2</sub>COOH-DO/Au/Ag [79] and tris(4-carbazoyl-9-ylphenyl) amine/polyvinylpyrrolidone/Cu [80] composites. The first catalyst based on TX-SCH<sub>2</sub>COOH-DO/Au/Ag was tested in the presence of UV radiation provided for 90 min by a 100 W source. Using a catalyst dosage of 5 mg/5 mL, the photocatalytic efficiency reaches 72.5%. When the Au/Ag BNPs composite was irradiated with UV light, due to their high surface plasmon resonance effects, a pair of electrons and holes can be developed. The electrons act to reduce adsorbed molecular oxygen on the composite surface into hydrogen peroxide radicals and superoxide radical. The photo-generated holes could follow two directions: (i) directly oxidizing the adsorbed methylene blue molecules or (ii) producing hydroxyl radicals by interacting with the water molecules or hydroxyl ions adsorbed at the surface. The second composite based on tris(4-carbazoyl-9-ylphenyl) amine/polyvinylpyrrolidone/Cu was irradiated for 90 min with a 300 W vis light source. The photocatalytic activity was 80% when the catalyst dosage was 20 mg/15 mL. If the Cu is replaced with CuO and all others parameters remain unchanged, the photocatalytic efficiency may increase at 90%. Bare CP presents good efficiency for MB removal, as a consequence of the ROS production under visible light. Photoexcited polymers will develop Coulomb-correlated electron-hole pairs, followed by interface diffusion to induce charge-separated states. The Cu presence can improve the

absorption capability of the composite, while CuO can produce light harvesting and charge carrier separation.

The polyvinyl alcohol/Au/Pd composite was tested for styrene photocatalytic removal in the presence of 50 mW/cm<sup>2</sup> irradiance produced by a vis source [81]. The styrene was completely removed in 60 min from the 20 mg/L initial solution concentration. It was observed that the composite catalytic effect increases with increasing light intensity until a certain point where the thermoelectron effect can damage the specific reactions. The core-shell structure of the metallic nanoparticles favors an increase in the local temperature, under visible light illumination. Consequently, the surface plasmon resonances of the localized metal nanoparticles were used to ensure a high catalytic efficiency, induced by the collective oscillations of the electrons on surfaces. High photocatalytic activity under low vis intensity radiation (9 W) was reported for phenylacetylide/Ag/Cu, which can completely remove 10 mg/L of norfloxacin in 40 min [82]. Under the same experimental conditions, the photocatalytic efficiencies decrease at 70.5% for naproxen, 64.3% for diclofenac, 47.6% for bisphenol A, and 42% for sulfisoxazole. Silver nanoparticles insertion endowed the composites with higher dispersion in aqueous solutions, which enhances their adsorption capacity as the first step in the mineralization process. The composite could not directly oxidize hydroxyl ions to radical due to its insufficient valence band potential (0.35 eV). However, the presence of •OH is due to the H<sub>2</sub>O<sub>2</sub> conversion, which was produced by the disproportionation of •O<sub>2</sub><sup>−</sup> following protonation.

### 3.2.3. Other Examples of Polymer Composite-Based Materials

Other materials, such as g-C<sub>3</sub>N<sub>4</sub>, metal sulfides, mixed metal oxides, reduced graphene oxides, etc., have been used to form polymeric-based composites with photocatalytic applications. Metal sulfides and mixed metal oxides have the advantage of larger light absorption spectra and band gap modularity based on their composition. Reduced graphene oxides and g-C<sub>3</sub>N<sub>4</sub> may increase the active surface, providing more sites for oxidative species development. Choosing the right materials ensures a balance between the interface compatibility, light sensitivity, chemical stability, and photocatalytic performance. By coupling polypyrrole with g-C<sub>3</sub>N<sub>4</sub>, Han H. could remove 99% of methylene blue from a 10 mg/L solution [83]. The composite uses low-intensity vis light (12 W) and a dosage of 0.05 g/50 mL to generate the oxidative species. Pure g-C<sub>3</sub>N<sub>4</sub> is a low photocatalytic material, which indicated that polypyrrole addition can enhance the active radical's production via electron separation through the composite structure. Owing to the strong conductivity, the polypyrrole was employed as the electron's transition channel to move onto the g-C<sub>3</sub>N<sub>4</sub> surface, thus inhibiting the photogenerated carrier's recombination. CdS was inserted in three different polymers (polypyrrole, polythiophene, and polyaniline) in order to study the photocatalytic removal of methylene blue from a 10 mg/L solution [84]. Due to the higher gap between the polypyrrole LUMO level and the CdS conduction band energy compared to that of polythiophene and polyaniline, the recombination rate in the polypyrrole/CdS composite was lower, resulting in better photocatalytic efficiency (77% for polypyrrole/CdS, 71% for polythiophene/CdS, and 61% for polyaniline/CdS). During irradiation with a 300 W vis source, the CdS conduction band lay below the polymer's LUMO level (−2.0 eV for polypyrrole, −2.35 eV for polythiophene, and −2.56 eV for polyaniline). The photo-generated electrons from the polymer LUMO level were injected into the CdS conduction band and holes from the CdS valence band migrated to polymers HOMO, inducing the oxidative and reduction reactions required for oxidative species development.

Polyaniline was associated with rGO/MnO<sub>2</sub> [85], BiVO<sub>4</sub>/GO [86], and MoSe<sub>2</sub> [87] in order to evaluate the composite's photocatalytic activity in methylene blue removal. The polyaniline/rGO/MnO<sub>2</sub> composite with a 10 mg/50 mL dosage could remove 90% of the 5 mg/L methylene blue solution after 120 min of irradiation with a 150 W vis source. The second composite based on polyaniline/BiVO<sub>4</sub>/GO (100 mg/100 mL dosage) reached a 73% removal efficiency in 180 min of irradiation with a 500 W vis source. As presented in Figure 6, both composites benefit from the graphene oxide conductive network which

facilitates the charge carrier's dispersion through the surface. The composites use the synergistic effects induced by the electron transfer from GO to polyaniline/ $\text{MnO}_2$  or  $\text{BiVO}_4$  and the limited recombination of photo-generated electron-hole pairs originating from of the ternary composition. Graphene oxide is a promising alternative for photocatalytic application due to its unique properties such as zero band gap and high surface area, as well as its ability to accept electrons in order to limit the charged carrier's recombination. Considering the polyaniline relative energy level ( $\pi$ -orbital and  $\pi^*$ -orbital) and metal oxide-GO band energy, the charges can directly migrate to the  $\pi$ -orbital of PANI. GO serves as the electron migration medium that facilitates the charge transfer and homogeneous metal oxide distribution in the composite. A comparative evaluation of the polyaniline/ $\text{BiVO}_4$ /GO photocatalytic activity toward other dyes shows that the composite can remove 82% of the highly concentrated safranine O solution (35 mg/L) and 62% of rhodamine B (4.8 mg/L) using a similar radiation scenario described for methylene blue. The third composite based on polyaniline/ $\text{MoSe}_2$  was tested for 120 min under  $100 \text{ mW/cm}^2$  vis irradiance and a 20 mg/100 mL catalyst dosage. The results indicate that 65% of methylene blue was removed due to  $\text{MoSe}_2$  posse's large surface area, high chemical stability, high surface activity, and vis-NIR light-driven band gap. Additionally, 94% of methyl orange was removed by the polyaniline/ $\text{MoSe}_2$  composite in 150 min using the same radiation parameters. During irradiation, charge carriers' generation took place in the polyaniline/ $\text{MoSe}_2$  composite due to their narrow band gap energy. The  $\text{MoSe}_2$  valence band and polyaniline HOMO level were positioned at 0.6 eV and 0.8 eV, favoring the hole migration from the polyaniline HOMO level to the  $\text{MoSe}_2$  valence band. Polyaniline was also used to form composites with  $\text{LaNiSbWO}_4$ /GO in order to remove safranine O (35 mg/L) and gallic acid (1.7 mg/L) under radiation produced by a 500 W vis source [88]. The sample exhibits high photocatalytic activity, reaching 84% for safranine O and 92% for gallic acid removal in 180 min. Here, GO is considered as an electron acceptor which can enhance the charge carrier's separation, thereby suppressing their recombination and enhancing the photocatalytic activity. In addition, the GO unpaired  $\pi$  electrons can interact with  $\text{LaNiSbWO}_4$  to increase the light absorption range.

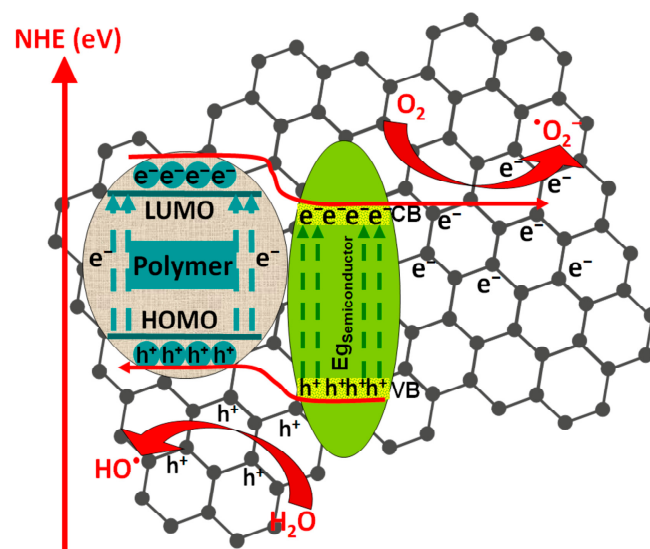


**Figure 6.** Polymer/semiconductor/GO composites with photocatalytic applications.

Polyether tetraacrylate was used to form composites with  $\text{Nd}_{0.9}\text{TiO}_3$  and  $\text{LaTiO}_3$  for acid black dye removal from a 15 mg/L aqueous solution [89]. The photocatalytic efficiency was similar for both composites (94% for polyether tetraacrylate / $\text{Nd}_{0.9}\text{TiO}_3$  and 95% for polyether tetraacrylate/ $\text{LaTiO}_3$ ) after 30 min of exposure to UV light with  $250 \text{ mW/cm}^2$  irradiance. Titanate perovskites are thermally stable materials with remarkable high corrosion resistance, which makes them suitable candidates for acidic environmental photocatalytic



applications. The electrons located on the photocatalyst valence band (O 2p) were excited and transferred to the conduction band ( $Ti^{4+}$ , empty d orbital), which react with  $H_2O$  and dissolved oxygen molecules present in the aqueous solution to produce reactive radicals. The photodegradation of high concentrated acid orange solution (70 mg/L) was studied using the cyclodextrin/BiOBr composite with a catalyst dosage of 40 mg/40 mL [90]. The composite photocatalytic efficiency was 99.2% in 60 min of irradiation with a 500 W vis source. This result is a cumulative action of the porous cyclodextrin polymer characterized by a high specific surface, high adsorption capacities, ultrafast adsorption performances, a wide vis-light response range, and good chemical stability exhibited by BiOBr.

Polystyrene/divinylbenzene/ $Fe_2O_3$  [91] and polypyrrole/ $Bi_2MoO_6$  [92] composites were tested for the removal of methylene blue from an aqueous solution with similar concentration (5–8 mg/L). When the methylene blue solution was mixed with oxalic acid (38.7 mg/L), the polystyrene/divinylbenzene/ $Fe_2O_3$  composite with a 10 mg/100 mL dosage reached 98% photocatalytic efficiency after 120 min of UV irradiation (20 W intensity). However, if the aqueous solution only contains oxalic acid (88.2 mg/L) as pollutant molecule, the photocatalytic efficiency may decrease at 73.6%. The composite exhibits a larger specific surface area (655  $m^2/g$ ) due to the three-dimensional scaffold network which is beneficial for the sorption and holding of different pollutant molecules and improves the photocatalytic overall performance. The porous polymer matrix can adsorb intermediate compounds formed during photodegradation and simultaneously induce a slow release of the organic pollutant and its intermediates into the bulk solution. A similar efficiency (93.6%) was obtained by irradiating the polypyrrole/ $Bi_2MoO_6$  composite with a 35 mg/50 mL dosage for 80 min with a 350 W vis light source. In the same experimental conditions, the composite reached 88.3% photocatalytic efficiency in the tetracycline solution with a 30 mg/L initial concentration. The construction of hierarchical composite photocatalysts combining the  $Bi_2MoO_6$  semiconductor and the polypyrrole conductive polymer presents the advantage of uniform polymeric nanoparticle distribution on the  $Bi_2MoO_6$  nanosheet surface that could effectively accelerate the photo-generated electron–hole pair's separation. The tetracycline photocatalytic removal from a 10 mg/L solution was tested under 90 min of vis irradiation provided by a 300 W source, using 4,7-dibromobenzo thiadiazole/4-ethynylphenyl amine/ $Bi_2WO_6$  as a photoactive composite [93]. The experiment was repeated with a 10 mg/L rhodamine B solution and a 20 mg/100 mL catalyst dosage. The results indicate similar photocatalytic efficiencies for tetracycline (86%) and rhodamine B (84%) due to a tight heterojunction between  $Bi_2WO_6$  and the polymer, extending the light absorption range and increasing the photogenerated charge separation and transport in the heterojunction interface. The mechanism of charge photogeneration corresponds to a Z-scheme electron transfer, where the holes form a  $Bi_2WO_6$  conduction band, oxidizing  $H_2O$  to  $\bullet OH$  radicals, while  $\bullet O_2^-$  radicals are produced by the electrons reacting with the adsorbed  $O_2$ . The enhanced photocatalytic efficiency can be induced by the p-conjugation polymer backbone possessing unique charge separation and mobility properties.

The photocatalytic removal of erythrosine B and rose Bengal dyes was tested by irradiating the poly(trimethyl-propane triacrylate)/bis (acyl) phosphane oxide/ $H_3PMo_{12}O_{40}$  composite with 0.07  $W/cm^2$  UV light [94]. After 120 min, irradiation of the composite shows 81% photocatalytic efficiency for erythrosine B removal and 86% for rose Bengal removal. When submitted to photolysis, the polymer component can generate  $\bullet OH$  radicals in reaction with  $H_2O$  via an oxidative hole trapping mechanism. During the photocatalytic activity, the composite can increase the number of oxidative species due to the photo-generation of simultaneous charge carriers induced by both components. A similar composite based on poly(trimethyl-propanetriacrylate)/ $H_3PMo_{12}O_{40}/W_{10}O_{32}(TH)_4$  was evaluated for the removal of pharmaceutically active compounds from a 15 mg/L aqueous solution concentration [95]. The composite was irradiated with a 250  $mW/cm^2$  UV–vis light source and the ibuprofen was completely removed in 90 min. However, if the irradiation time decreased at 75 min, the photocatalytic efficiency toward ciprofloxacin and

oxytetracycline was 90%, and 86%, respectively. In the first step, the drugs were converted in by-products, such as hydroxylated products or other new functional group intermediates (including alcohols, olefins, and ketones). In 30 min of irradiation, the by-products were completely mineralized by the strong oxidant species generated at the composite surface. The photocatalytic degradation of the imidacloprid pesticide was investigated using a simple polyimide/ $\text{WO}_3$  composite as the photocatalyst [96]. The pesticide concentration was 20 mg/L and the composite was irradiated for 180 min with a 225 W vis light source. The results indicate that the photocatalytic efficiency increases from 50% to 73.2% if the catalyst dosage increases from 1 g/L to 2.5 g/L. The composite exhibits a lamellar structure with a relatively small active surface of 11.49  $\text{m}^2/\text{g}$ . The composite photocatalytic activity is based on the visible-light driven Z-scheme mechanism where the polymer is excited by vis light, and their band potential must be matched in order to ensure the recombination of photo-generated electrons from the polymer LUMO level and holes from the  $\text{WO}_3$  valence band. Then, the useful charge carriers ( $\text{h}^+$  from polymer HOMO level and  $\text{e}^-$  from  $\text{WO}_3$  conduction band) can participate in the oxidative species development. The insertion of phosphorus can improve the efficiency of charge separation and induce the absorption edge redshift.

#### 4. Conclusions and Perspectives

This study has emerged to correlate the photocatalytic activities toward different pollutant molecules with the polymeric composite content and testing conditions. The composite photocatalytic activity depends on catalyst composition/dosage, the active surface area characteristics (active sites, pores size, and volume), the pollutant type/concentration, and the surface chemistry between the pollutant molecule and the catalyst. In processes such as adsorption, decomposition, and diffusion, the desorption kinetics of the degradation products may vary based on the chemically significantly different surfaces and composition. The paper indicates that the balance between all these factors is essential and can provide the pathway for higher photocatalytic efficiencies. Even in the situation of chemically similar materials, the presence of various crystalline forms exhibits drastically different activity. Switching from UV to vis spectra can improve the photocatalytic efficiency of the polythiophene/ $\text{TiO}_2$  composite toward rhodamine B from 76% to 98%. However, higher efficiency was reached with high energy costs considering the use of a 320 W vis light source for 10 h. The silver insertion in different polymeric composites induced a significant increase in the rhodamine B removal rate from 56.12% to 95%, which can be considered as a suitable method to enhance the photocatalytic activity. When pharmaceutically active compounds are used as target molecules, the dependency between the chemical compatibility of drug molecules and catalyst surfaces must be carefully evaluated. The present work has several limitations: (i) the numbers of references were reduced based on the most representative papers, (ii) several papers which may be representative were excluded due to the incomplete experimental description, and (iii) not all the parameters were considered due to the space restrictions.

For future work, the development of catalytic composites via green routes could be attempted, characterized, and compared with other commercially available nanomaterials. The green route application of composite materials is expected to add economic and scientific value to the knowledge by promoting technological development in light of the photocatalytic design. The composite materials could represent the following steps to the a large-scale industrial transition for photocatalytic degradation based on sustainable energy processes. The challenge of scaling up photocatalytic composite applications at the industrial level is one of the main issues not yet sufficiently addressed by the scientific community.

Finally, most of the studies presented in the literature target the effects of temperature, pH, pollutant concentration, or other technological parameters in relation to composite adsorption and photo-degradation capacities, whereas the problem of real wastewater pollutants is very rarely addressed. The wastewater usually contains various pollutant molecules

which are ignored in most studies. The interface chemistry, absorption/desorption kinetics, and photocatalytic activity are different when complex wastewater charge pollution is considered.

**Author Contributions:** Conceptualization, A.E. and C.C.; methodology, A.E.; validation, A.E. and C.C.; formal analysis, C.C.; investigation, A.E. and C.C.; resources, A.E.; data curation, C.C.; writing—original draft preparation, A.E.; writing—review and editing, C.C.; visualization, C.C.; supervision, A.E.; project administration, A.E.; funding acquisition, A.E. All authors have read and agreed to the published version of the manuscript.

**Funding:** This work was supported by a grant of the Ministry of Research, Innovation, and Digitization, CNCS-UEFISCDI, project number PN-III-P4-PCE-2021-1020 (PCE87), within PNCDI III.

**Informed Consent Statement:** Not applicable.

**Data Availability Statement:** Data presented in this study are available upon request from the corresponding author.

**Conflicts of Interest:** The authors declare no conflict of interest.

## References

- Rajlaxmi; Gupta, N.; Behere, R.P.; Layek, R.K.; Kuila, B.K. Polymer nanocomposite membranes and their application for flow catalysis and photocatalytic degradation of organic pollutants. *Mater. Today Chem.* **2021**, *22*, 100600. [CrossRef]
- Zia, J.; Riaz, U. Photocatalytic degradation of water pollutants using conducting polymer-based nanohybrids: A review on recent trends and future prospects. *J. Mol. Liq.* **2021**, *340*, 117162. [CrossRef]
- Pandey, B.; Singh, P.; Kumar, V. Photocatalytic-sorption processes for the removal of pollutants from wastewater using polymer metal oxide nanocomposites and associated environmental risks. *Environ. Nanotechnol. Monit. Manag.* **2021**, *16*, 100596. [CrossRef]
- Ahmad, N.; Anae, J.; Khan, M.Z.; Sabir, S.; Yang, X.J.; Thakur, V.K.; Campo, P.; Coulon, F. Visible light-conducting polymer nanocomposites as efficient photocatalysts for the treatment of organic pollutants in wastewater. *J. Environ. Manag.* **2021**, *295*, 113362. [CrossRef] [PubMed]
- Qian, G.; Zhu, X.; Yao, D. The oil pollution and nitric oxide photocatalytic degradation evaluation of composite nanomaterials for asphalt pavement. *Constr. Build. Mater.* **2022**, *314*, 125497. [CrossRef]
- Baneto, M.; Enesca, A.; Mihoreanu, C.; Lare, Y.; Jondo, K.; Napo, K.; Duta, A. Effects of the growth temperature on the properties of spray deposited CuInS<sub>2</sub> thin films for photovoltaic applications. *Ceram. Int.* **2015**, *41*, 4742–4749. [CrossRef]
- Saleem, H.; Zaidi, S.J.; Goh, P.S. Advances of nanomaterials for air pollution remediation and their impacts on the environment. *Chemosphere* **2022**, *287*, 132083. [CrossRef]
- Zhu, Y.; Xu, F.; Zhang, L. Nanomaterials and plants: Positive effects, toxicity and the remediation of metal and metalloid pollution in soil. *Sci. Total Environ.* **2019**, *662*, 414–421. [CrossRef]
- Jamari, J.; Ammarullah, M.I.; Santoso, G.; Sugiharto, S.; Supriyono, T.; Prakoso, A.T.; Basri, H.; van der Heide, E. Computational Contact Pressure Prediction of CoCrMo, SS 316L and Ti6Al4V Femoral Head against UHMWPE Acetabular Cup under Gait Cycle. *J. Funct. Biomater.* **2022**, *13*, 64. [CrossRef]
- Saravanakumar, K.; Santosh, S.S.; Wang, M.H. Unraveling the hazardous impact of diverse contaminants in the marine environment: Detection and remedial approach through nanomaterials and nano-biosensors. *J. Hazard. Mater.* **2022**, *433*, 128720. [CrossRef]
- Goh, P.S.; Kang, H.S.; Higgins, D. Nanomaterials for microplastic remediation from aquatic environment: Why nano matters? *Chemosphere* **2022**, *299*, 134418. [CrossRef]
- Yu, S.; Tang, H.; Wang, X. MXenes as emerging nanomaterials in water purification and environmental remediation. *Sci. Total Environ.* **2022**, *811*, 152280. [CrossRef]
- Ochiai, T.; Aoki, D.; Saito, H.; Akutsu, Y.; Nagata, M. Analysis of Adsorption and Decomposition of Odour and Tar Components in Tobacco Smoke on Non-Woven Fabric-Supported Photocatalysts. *Catalysts* **2020**, *10*, 304. [CrossRef]
- Enesca, A.; Duta, A.; Schoonman, J. Influence of tantalum dopant ions (Ta<sup>5+</sup>) on the efficiency of the tungsten trioxide photoelectrode. *Phys. Status Solidi A* **2008**, *205*, 2038–2041. [CrossRef]
- Barrocas, B.T.; Ambrožová, N.; Kočí, K. Photocatalytic Reduction of Carbon Dioxide on TiO<sub>2</sub> Heterojunction Photocatalysts—A Review. *Materials* **2022**, *15*, 967. [CrossRef]
- Sciscenko, I.; Mestre, S.; Climent, J.; Valero, F.; Escudero-Oñate, C.; Oller, I.; Arques, A. Magnetic Photocatalyst for Wastewater Tertiary Treatment at Pilot Plant Scale: Disinfection and Enrofloxacin Abatement. *Water* **2021**, *13*, 329. [CrossRef]
- Shafiqul, I.M.; Deep, R.; Lin, J.; Yoshida, T.; Fujita, Y. The Role of Nitrogen Dopants in ZnO Nanoparticle-Based Light Emitting Diodes. *Nanomaterials* **2022**, *12*, 358. [CrossRef]
- Alsharif, A.; Smith, N.; Kozhevnikova, E.F.; Kozhevnikov, I.V. Dehydroisomerisation of  $\alpha$ -Pinene and Limonene to p-Cymene over Silica-Supported ZnO in the Gas Phase. *Catalysts* **2021**, *11*, 1245. [CrossRef]

19. Huang, P.-H.; Zhang, Z.-X.; Hsu, C.-H.; Wu, W.-Y.; Huang, C.-J.; Lien, S.-Y. Chemical Reaction and Ion Bombardment Effects of Plasma Radicals on Optoelectrical Properties of SnO<sub>2</sub> Thin Films via Atomic Layer Deposition. *Materials* **2021**, *14*, 690. [CrossRef]
20. Nasriddinov, A.; Platonov, V.; Garshev, A.; Rumyantseva, M. Low Temperature HCHO Detection by SnO<sub>2</sub>/TiO<sub>2</sub>@Au and SnO<sub>2</sub>/TiO<sub>2</sub>@Pt: Understanding by In-Situ DRIFT Spectroscopy. *Nanomaterials* **2021**, *11*, 2049. [CrossRef]
21. Bridges, L.; Mohamed, R.A.M.; Khan, N.A.; Brusseau, M.L.; Carroll, K.C. Comparison of Manganese Dioxide and Permanganate as Amendments with Persulfate for Aqueous 1,4-Dioxane Oxidation. *Water* **2020**, *12*, 3061. [CrossRef]
22. Dong, Y.; Su, C.; Liu, K.; Wang, H.; Zheng, Z.; Zhao, W.; Lu, S. The Catalytic Oxidation of Formaldehyde by FeO<sub>x</sub>-MnO<sub>2</sub>-CeO<sub>2</sub> Catalyst: Effect of Iron Modification. *Catalysts* **2021**, *11*, 555. [CrossRef]
23. Hessien, M.; Taha, A.; Dana, E. Acacia nilotica Pods' Extract Assisted-Hydrothermal Synthesis and Characterization of ZnO-CuO Nanocomposites. *Materials* **2022**, *15*, 2291. [CrossRef]
24. Cao, C.; Yu, L.; Jin, H. Hydrogen production by supercritical water gasification of lignin over CuO-ZnO catalyst synthesized with different methods. *Int. J. Hydrogen Energy* **2022**, *47*, 8716–8728. [CrossRef]
25. Mahy, J.G.; Tsaffo Mbognou, M.H.; Léonard, C.; Fagel, N.; Woumfo, E.D.; Lambert, S.D. Natural Clay Modified with ZnO/TiO<sub>2</sub> to Enhance Pollutant Removal from Water. *Catalysts* **2022**, *12*, 148. [CrossRef]
26. Jing, Y.; Yin, H.; Yu, S. Fabrication of Pt doped TiO<sub>2</sub>-ZnO@ZIF-8 core@shell photocatalyst with enhanced activity for phenol degradation. *Environ. Res.* **2022**, *203*, 111819. [CrossRef]
27. Peng, F.; Sun, Y.; Yu, W.; Lu, Y.; Hao, J.; Cong, R.; Shi, J.; Ge, M.; Dai, N. Gas Sensing Performance and Mechanism of CuO(p)-WO<sub>3</sub>(n) Composites to H<sub>2</sub>S Gas. *Nanomaterials* **2020**, *10*, 1162. [CrossRef]
28. Patil, A.M.; An, X.; Guan, G. Fabrication of three-dimensionally heterostructured rGO/WO<sub>3</sub>-0.5H<sub>2</sub>O@Cu<sub>2</sub>S electrodes for high-energy solid-state pouch-type asymmetric supercapacitor. *Chem. Eng. J.* **2020**, *403*, 126411. [CrossRef]
29. Ramesh, K.; Gnanavel, B.; Shkir, M. Enhanced visible light photocatalytic degradation of bisphenol A (BPA) by reduced graphene oxide (RGO)-metal oxide (TiO<sub>2</sub>, ZnO and WO<sub>3</sub>) based nanocomposites. *Diam. Relat. Mater.* **2021**, *118*, 108514. [CrossRef]
30. Quy, V.H.V.; Kim, J.H.; Ahn, K.S. Enhanced electrocatalytic activity of electrodeposited F-doped SnO<sub>2</sub>/Cu<sub>2</sub>S electrodes for quantum dot-sensitized solar cells. *J. Power Sources* **2016**, *316*, 53–59.
31. Enesca, A.; Duta, A. Tailoring WO<sub>3</sub> thin layers using spray pyrolysis technique. *Phys. Status Solidi C* **2008**, *5*, 3499–3502. [CrossRef]
32. Chen, H.; Lei, Y.; Zheng, Z. Using a CdS under-layer to suppress charge carrier recombination at the Ag<sub>2</sub>S/FTO interface. *J. Alloys Compd.* **2021**, *879*, 160348. [CrossRef]
33. Madjet, M.E.; Berdiyrov, G.R.; Hamoudi, H. Nonradiative relaxation of charge carriers at molecule-metal interfaces: Nonadiabatic molecular dynamics study. *Surf. Interfaces* **2022**, *30*, 101830. [CrossRef]
34. Govea-Alcaide, E.; Rodríguez-Milanés, J.; Jardim, R.F. Transport of charge carriers across the normal-superconducting interfaces in Bi<sub>1.65</sub>Pb<sub>0.35</sub>Sr<sub>2</sub>Ca<sub>2</sub>Cu<sub>3</sub>O<sub>10+δ</sub> nanoceramics. *Ceram. Int.* **2021**, *47*, 13039–13099. [CrossRef]
35. Ravichandran, J.; Karthikeyan, B.S.; Samal, A. Investigation of a derived adverse outcome pathway (AOP) network for endocrine-mediated perturbations. *Sci. Total Environ.* **2022**, *826*, 154112. [CrossRef]
36. Ganiyu, S.O.; Arslan, M.; El-Din, H.G. Combined solar activated sulfate radical-based advanced oxidation processes (SR-AOPs) and biofiltration for the remediation of dissolved organics in oil sands produced water. *Chem. Eng. J.* **2022**, *433*, 134579. [CrossRef]
37. Wang, N.; He, L.; Bu, Y. The potential environmental behavior and risks of TBEC transformation initiated by reactive oxygen species in natural waters and AOPs. *Ecotoxicol. Environ. Saf.* **2021**, *228*, 113055. [CrossRef]
38. Sun, B.; Zheng, Y.; Yin, R. Concentration-dependent chloride effect on radical distribution and micropollutant degradation in the sulfate radical-based AOPs. *J. Hazard. Mater.* **2022**, *430*, 128450. [CrossRef]
39. Bilińska, L.; Gmurek, M. Novel trends in AOPs for textile wastewater treatment. Enhanced dye by-products removal by catalytic and synergistic actions. *Water Resour. Ind.* **2021**, *26*, 100160. [CrossRef]
40. Zhang, T.; Liu, Y.; Zhang, L. AOPs-based remediation of petroleum hydrocarbons-contaminated soils: Efficiency, influencing factors and environmental impacts. *Chemosphere* **2020**, *246*, 125726. [CrossRef]
41. Esfahani, K.N.; Pérez-Moya, M.; Graells, M. A Hybrid Model Coupling Advanced Oxidation Processes (AOP) and Conventional Bio-processes for the Removal of Recalcitrant Contaminants in Wastewaters. *Comput. Aided Chem. Eng.* **2021**, *50*, 883–889.
42. Mouchaal, Y.; Enesca, A.; Mihoreanu, C.; Khelil, A.; Duta, A. Tuning the opto-electrical properties of SnO<sub>2</sub> thin films by Ag<sup>+1</sup> and In<sup>+3</sup> co-doping. *Mater. Sci. Eng. B* **2015**, *199*, 22–29. [CrossRef]
43. Chen, C.; Feng, H.; Deng, Y. Re-evaluation of sulfate radical based-advanced oxidation processes (SR-AOPs) for treatment of raw municipal landfill leachate. *Water Res.* **2019**, *153*, 100–107. [CrossRef]
44. Zgheib, E.; Gao, W.; Bois, F.Y. Application of three approaches for quantitative AOP development to renal toxicity. *Comput. Toxicol.* **2019**, *11*, 13. [CrossRef]
45. Cako, E.; Gunasekaran, K.D.; Boczkaj, G. Ultrafast degradation of brilliant cresyl blue under hydrodynamic cavitation based advanced oxidation processes (AOPs). *Water Resour. Ind.* **2020**, *24*, 100134. [CrossRef]
46. Miklos, D.B.; Wang, W.L.; Hübner, U. Comparison of UV-AOPs (UV/H<sub>2</sub>O<sub>2</sub>, UV/PDS and UV/Chlorine) for TOC removal from municipal wastewater effluent and optical surrogate model evaluation. *Chem. Eng. J.* **2019**, *362*, 537–547. [CrossRef]
47. Ferreira, L.C.; Fernandes, J.R.; Lucas, M.S. Wireless UV-A LEDs-driven AOP in the treatment of agro-industrial wastewaters. *Environ. Res.* **2021**, *200*, 111430. [CrossRef]
48. Cako, E.; Soltani, R.D.C.; Boczkaj, G. Desulfurization of raw naphtha cuts using hybrid systems based on acoustic cavitation and advanced oxidation processes (AOPs). *Chem. Eng. J.* **2022**, *439*, 135354. [CrossRef]

49. Kolle, S.N.; Landsiedel, R.; Natsch, A. Replacing the refinement for skin sensitization testing: Considerations to the implementation of adverse outcome pathway (AOP)-based defined approaches (DA) in OECD guidelines. *Regul. Toxicol. Pharmacol.* **2020**, *115*, 104713. [CrossRef]
50. Gong, Y.; Wang, Y.; Jiang, W. A two-step process coupling photocatalysis with adsorption to treat tetracycline—Copper(II) hybrid wastewaters. *J. Water Proc. Eng.* **2022**, *47*, 102710. [CrossRef]
51. Liang, Q.; Chen, X.; Luo, H. Efficient removal of Cr(VI) by a 3D Z-scheme TiO<sub>2</sub>-Zn<sub>x</sub>Cd<sub>1-x</sub>S graphene aerogel via synergy of adsorption and photocatalysis under visible light. *J. Environ. Sci.* **2023**, *124*, 360–370. [CrossRef]
52. Fatima, H.; Azhar, M.R.; Shao, Z. Rational design of ZnO-zeolite imidazole hybrid nanoparticles with reduced charge recombination for enhanced photocatalysis. *J. Colloid Interface Sci.* **2022**, *614*, 538–546. [CrossRef] [PubMed]
53. Dudita, M.; Bogatu, C.; Enesca, A.; Duta, A. The influence of the additives composition and concentration on the properties of SnO<sub>x</sub> thin films used in photocatalysis. *Mater. Lett.* **2011**, *65*, 2185–2189. [CrossRef]
54. Li, C.; Li, H.; Yang, Q. One-pot synthesis of mesosilica/nano covalent organic polymer composites and their synergistic effect in photocatalysis. *Chin. J. Catal.* **2021**, *42*, 1821–1830. [CrossRef]
55. Moradeeya, P.G.; Kumar, M.A.; Basha, S. Conductive polymer layered semiconductor for degradation of triclopyr acid and 2,4-dichlorophenoxyacetic acid from aqueous stream using coalesce adsorption-photocatalysis technique. *Chemosphere* **2022**, *298*, 134360. [CrossRef]
56. Liu, Y.; Zhang, Q.; Yuan, H.; Luo, K.; Li, J.; Hu, W.; Pan, Z.; Xu, M.; Xu, S.; Levchenko, I.; et al. Comparative study of photocatalysis and gas sensing of ZnO/Ag nanocomposites synthesized by one- and two-step polymer-network gel processes. *J. Alloys Compd.* **2021**, *868*, 158723. [CrossRef]
57. Mansurov, R.R.; Zverev, V.S.; Safronov, A.P. Dynamics of diffusion-limited photocatalytic degradation of dye by polymeric hydrogel with embedded TiO<sub>2</sub> nanoparticles. *J. Catal.* **2022**, *406*, 9–18. [CrossRef]
58. Uricchio, A.; Nadal, E.; Plujat, B.; Plantard, G.; Massines, F.; Fanelli, F. Low-temperature atmospheric pressure plasma deposition of TiO<sub>2</sub>-based nanocomposite coatings on open-cell polymer foams for photocatalytic water treatment. *Appl. Surf. Sci.* **2021**, *561*, 150014. [CrossRef]
59. Justh, N.; Mikula, G.J.; Bakos, L.P.; Nagy, B.; Laszlo, K.; Parditka, B.; Erdelyi, Z.; Takats, V.; Mizsei, J.; Szilagyi, I.M. Photocatalytic properties of TiO<sub>2</sub>@polymer and TiO<sub>2</sub>@carbon aerogel composites prepared by atomic layer deposition. *Carbon* **2019**, *147*, 476–482. [CrossRef]
60. Liu, X.; Wang, L.; Zhou, X.; He, X.; Zhou, M.; Jia, K.; Liu, X. Design of polymer composite-based porous membrane for in-situ photocatalytic degradation of adsorbed organic dyes. *J. Phys. Chem. Solids* **2021**, *154*, 110094. [CrossRef]
61. Chen, X.; Nie, Q.; Shao, Y.; Wang, Z.; Cai, Z. TiO<sub>2</sub> nanoparticles functionalized borneol-based polymer films with enhanced photocatalytic and antibacterial performances. *Environ. Technol. Innov.* **2021**, *21*, 101304. [CrossRef]
62. Lin, L.H.; Liu, H.J.; Hwang, J.J.; Chen, K.M.; Chao, J.C. Photocatalytic effects and surface morphologies of modified silicone-TiO<sub>2</sub> polymer composites. *Mater. Chem. Phys.* **2011**, *127*, 248–252. [CrossRef]
63. Tekin, D.; Birhan, D.; Kiziltas, H. Thermal, photocatalytic, and antibacterial properties of calcinated nano-TiO<sub>2</sub>/polymer composites. *Mater. Chem. Phys.* **2020**, *251*, 123067. [CrossRef]
64. Xu, S.; Jiang, L.; Yang, H.; Song, Y.; Dan, Y. Structure and Photocatalytic Activity of Polythiophene/TiO<sub>2</sub> Composite Particles Prepared by Photoinduced Polymerization. *Chin. J. Catal.* **2011**, *32*, 536–545. [CrossRef]
65. Li, X.; Raza, S.; Liu, C. Preparation of titanium dioxide modified biomass polymer microspheres for photocatalytic degradation of rhodamine-B dye and tetracycline. *J. Taiwan Inst. Chem. Eng.* **2021**, *122*, 157–167. [CrossRef]
66. Neghi, N.; Kumar, M.; Burkhalov, D. Synthesis and application of stable, reusable TiO<sub>2</sub> polymeric composites for photocatalytic removal of metronidazole: Removal kinetics and density functional analysis. *Chem. Eng. J.* **2019**, *359*, 963–975. [CrossRef]
67. Song, Y.; Zhang, J.; Yang, L.; Cao, S.; Yang, H.; Zhang, J.; Jiang, L.; Dan, Y.; LeRendu, P.; Nguyen, T.P. Photocatalytic activity of TiO<sub>2</sub> based composite films by porous conjugated polymer coating of nanoparticles. *Mater. Sci. Semicond. Process.* **2016**, *42*, 54–57. [CrossRef]
68. Tran, M.L.; Fu, C.C.; Chiang, L.Y.; Hsieh, C.T.; Liu, S.H.; Juang, R.S. Immobilization of TiO<sub>2</sub> and TiO<sub>2</sub>-GO hybrids onto the surface of acrylic acid-grafted polymeric membranes for pollutant removal: Analysis of photocatalytic activity. *J. Environ. Chem. Eng.* **2020**, *8*, 104422. [CrossRef]
69. Gomes, J.; Alves, B.M.P.; Ferreira, P.; Martins, R.C. Immobilization of TiO<sub>2</sub> onto a polymeric support for photocatalytic oxidation of a paraben's mixture. *J. Water Proc. Eng.* **2022**, *46*, 102458. [CrossRef]
70. Singh, A.R.; Dhupal, P.S.; Bhakare, M.A.; Lokhande, K.D.; Bondarde, M.P.; Some, S. In-situ synthesis of metal oxide and polymer decorated activated carbon-based photocatalyst for organic pollutants degradation. *Sep. Purif. Technol.* **2022**, *286*, 120380. [CrossRef]
71. Krishnaswamy, S.; Panigrahi, P.; Kumaar, S.; Nagarajan, G.S. Effect of conducting polymer on photoluminescence quenching of green synthesized ZnO thin film and its photocatalytic properties. *Nano-Struct. Nano-Objects* **2020**, *22*, 100446. [CrossRef]
72. Liu, H.; Li, M.; Yang, J.; Hu, C.; Shang, J.; Zhai, H. In situ construction of conjugated polymer P3HT coupled hierarchical ZnO composite with Z-scheme enhanced visible-light photocatalytic activity. *Mater. Res. Bull.* **2018**, *106*, 19–27. [CrossRef]
73. Podasca, V.E.; Damaceanu, M.D. ZnO-Ag based polymer composites as photocatalysts for highly efficient visible-light degradation of Methyl Orange. *J. Photochem. Photobiol. A Chem.* **2021**, *406*, 113003. [CrossRef]

74. Kongseng, P.; Amornpitoksuk, P.; Chantarak, S. Development of multifunctional hydrogel composite based on poly(vinylalcohol-g-acrylamide) for removal and photocatalytic degradation of organic dyes. *React. Funct. Polym.* **2022**, *172*, 105207. [CrossRef]
75. Mohammed, A.M.; Mohtar, S.S.; Aziz, F.; Aziz, M.; Nasir, M.U. Effects of oxidants on the in-situ polymerization of aniline to form Cu<sub>2</sub>O/ZnO/PANI composite photocatalyst. *Mater. Today Proc.* **2021**, *46*, 2030–2035.
76. Ma, A.; Wei, Y.; Zhou, Z.; Xu, W.; Ren, F.; Ma, H.; Wang, J. Preparation Bi<sub>2</sub>S<sub>3</sub>eTiO<sub>2</sub> heterojunction/polymer fiber composites and its photocatalytic degradation of methylene blue under Xe lamp irradiation. *Polym. Degrad. Stab.* **2012**, *97*, 125–131. [CrossRef]
77. Xu, X.; Wang, Y.; Zhang, D.; Wang, J.; Yang, Z. In situ growth of photocatalytic Ag-decorated β-Bi<sub>2</sub>O<sub>3</sub>/Bi<sub>2</sub>O<sub>2.7</sub> heterostructure film on PVC polymer matrices with self-cleaning and antibacterial properties. *Chem. Eng. J.* **2022**, *429*, 131058. [CrossRef]
78. Liu, J.; Zhou, S.; Gu, P.; Zhang, T.; Chen, D.; Li, N.; Xu, Q.; Lu, J. Conjugate Polymer-clothed TiO<sub>2</sub>@V<sub>2</sub>O<sub>5</sub> nanobelts and their enhanced visible light photocatalytic performance in water remediation. *J. Colloid Interface Sci.* **2020**, *578*, 402–411. [CrossRef]
79. Kazancioglu, E.O.; Aydin, M.; Arsu, N. Photochemical synthesis of bimetallic gold/silver nanoparticles in polymer matrix with tunable absorption properties: Superior photocatalytic activity for degradation of methylene blue. *Mater. Chem. Phys.* **2021**, *269*, 124734. [CrossRef]
80. Djellabi, R.; Ali, J.; Zhao, X.; Saber, A.N.; Yang, B. CuO NPs incorporated into electron-rich TCTA@PVP photoactive polymer for the photocatalytic oxidation of dyes and bacteria inactivation. *J. Water Proc. Eng.* **2020**, *36*, 101238. [CrossRef]
81. Xu, L.; Wang, X.; Ma, T.; Zhao, X. Seed-mediated growth of Au core–Pd shell-structured nanoparticles on a polymer nanofibrous mat as a highly active photocatalytic composite material. *Compos. Commun.* **2020**, *21*, 100406. [CrossRef]
82. Jin, X.; Wu, Y.; Lin, Z.; Liang, D.; Wang, F.; Zheng, X.; Liu, H.; Lv, W.; Liu, G. Plasmonic Ag nanoparticles decorated copper-phenylacetylide polymer for visible-light-driven photocatalytic reduction of Cr(VI) and degradation of PPCPs: Performance, kinetics, and mechanism. *J. Hazard. Mater.* **2022**, *425*, 127599. [CrossRef]
83. Han, H.; Fu, M.; Li, Y.; Guan, W.; Lu, P.; Hu, X. In-situ polymerization for PPy/g-C<sub>3</sub>N<sub>4</sub> composites with enhanced visible light photocatalytic performance. *Chin. J. Catal.* **2018**, *39*, 831–840. [CrossRef]
84. Chaitanya, B.H.; Pawan, K.K.; Priyesh, V.M. Probing the real-time photocatalytic activity of CdS QDs sensitized conducting polymers: Featured PTh, PPy and PANI. *Vacuum* **2018**, *155*, 159–168.
85. Park, Y.; Numan, A.; Ponomarev, N.; Iqbal, J.; Khalid, M. Enhanced photocatalytic performance of PANI-rGO-MnO<sub>2</sub> ternary composite for degradation of organic contaminants under visible light. *J. Environ. Chem. Eng.* **2021**, *9*, 106006. [CrossRef]
86. Biswas, R.D.; Cho, K.Y.; Na, J.D.; Oh, W.C. Highly electro-conductive graphene-decorated PANI-BiVO<sub>4</sub> polymersemiconductor nanocomposite with outstanding photocatalytic performance. *Mater. Sci. Eng. B* **2019**, *251*, 114469. [CrossRef]
87. Mittal, H.; Kumar, A.; Khanuja, M. In-situ oxidative polymerization of aniline on hydrothermally synthesized MoSe<sub>2</sub> for enhanced photocatalytic degradation of organic dyes. *J. Saudi Chem. Soc.* **2019**, *23*, 836–845. [CrossRef]
88. Oh, W.C.; Fatema, K.N.; Liu, Y.; Lim, C.S.; Cho, K.Y.; Jung, C.H.; Biswas, R.D. Sonochemical synthesis of quaternary LaNiSbWO<sub>4</sub>-G-PANI polymer nanocomposite for photocatalytic degradation of Safranin-O and gallic acid under visible light irradiation. *J. Photochem. Photobiol. A Chem.* **2020**, *394*, 112484. [CrossRef]
89. Brahmi, C.; Benlifa, M.; Vaulot, C.; Michelin, L.; Dumur, F.; Airoudj, A.; Morlet-Savary, F.; Raveau, B.; Bousselmi, L.; Lalevee, J. New hybrid perovskites/polymer composites for the photodegradation of organic dyes. *Eur. Polym. J.* **2021**, *157*, 110641. [CrossRef]
90. Du, H.; Wang, X.; Zhang, Y.; Xu, G.; Tu, Y.; Jia, X.; Wu, D.; Xie, X.; Liu, Y. Insights into the photocatalytic activation of peroxymonosulfate by visible light over BiOBr-cyclodextrin polymer complexes for efficient degradation of dye pollutants in water. *Environ. Res.* **2022**, *207*, 112160. [CrossRef]
91. Hojamberdieva, M.; Kadirova, Z.C.; Daminova, S.S.; Yubuta, K.; Razavi-Khosroshahi, H.; Sharipov, K.T.; Miyauchi, M.; Teshima, K.; Hasegawa, M. Amorphous Fe<sub>2</sub>O<sub>3</sub> nanoparticles embedded into hypercrosslinked porous polymeric matrix for designing an easily separable and recyclable photocatalytic system. *Appl. Surf. Sci.* **2019**, *466*, 837–846. [CrossRef]
92. Xie, R.; Fan, J.; Fang, K.; Chen, W.; Song, Y.; Pan, Y.; Li, Y.; Liu, J. Hierarchical Bi<sub>2</sub>MoO<sub>6</sub> microsphere photocatalysts modified with polypyrrole conjugated polymer for efficient decontamination of organic pollutants. *Chemosphere* **2022**, *286*, 131541. [CrossRef]
93. Pan, F.; Wang, Y.; Zhao, K.; Hu, J.; Liu, H.; Hu, Y. Photocatalytic degradation of tetracycline hydrochloride with visible light-responsive bismuth tungstate/conjugated microporous polymer. *Chin. J. Chem. Eng.* **2022**, *41*, 488–496. [CrossRef]
94. Ghali, M.; Benlifa, M.; Brahmi, C.; Elbassi, L.; Dumur, F.; Simonnet-Jegat, C.; Bousselmi, L.; Lalevee, J. LED and solar photodecomposition of erythrosine B and rose Bengal using H<sub>3</sub>PMo<sub>12</sub>O<sub>40</sub>/polymer photocatalyst. *Eur. Polym. J.* **2021**, *159*, 110743. [CrossRef]
95. Brahmi, C.; Benlifa, M.; Ghali, M.; Dumur, F.; Simonnet-Jegat, C.; Valerie, M.; Morlet-Savary, F.; Bousselmi, L.; Lalevee, J. Performance improvement of the photocatalytic process for the degradation of pharmaceutical compounds using new POM/polymer photocatalysts. *J. Environ. Chem. Eng.* **2021**, *9*, 106015. [CrossRef]
96. Meng, P.; Heng, H.; Sun, Y.; Liu, X. In situ polymerization synthesis of Z-scheme tungsten trioxide/polyimide photocatalyst with enhanced visible-light photocatalytic activity. *Appl. Surf. Sci.* **2018**, *428*, 1130–1140. [CrossRef]



## Article

# Sustainable Myrcene-Based Elastomers via a Convenient Anionic Polymerization

David Hermann Lamparelli <sup>1</sup>, Magdalena Maria Kleybolte <sup>2</sup>, Malte Winnacker <sup>2,3,\*</sup>  
and Carmine Capacchione <sup>1,\*</sup>

<sup>1</sup> Department of Chemistry and Biology “Adolfo Zambelli”, University of Salerno, Giovanni Paolo II Str., 84084 Fisciano, Italy; dlamparelli@unisa.it

<sup>2</sup> WACKER-Chair of Macromolecular Chemistry, Technische Universität München, Lichtenbergstraße 4 Str., 85747 Garching bei München, Germany; magdalena.kleybolte@tum.de

<sup>3</sup> Catalysis Research Center (CRC), Ernst-Otto-Fischer-Straße 1, 85748 Garching bei München, Germany

\* Correspondence: malte.winnacker@tum.de (M.W.); ccapacchione@unisa.it (C.C.)

**Abstract:** Soluble heterocomplexes consisting of sodium hydride in combination with trialkylaluminum derivatives have been used as anionic initiating systems at 100 °C in toluene for convenient homo-, co- and ter-polymerization of myrcene with styrene and isoprene. In this way it has been possible to obtain elastomeric materials in a wide range of compositions with interesting thermal profiles and different polymeric architectures by simply modulating the alimentation feed and the (monomers)/(initiator systems) ratio. Especially, a complete study of the myrcene-styrene copolymers (PMS) was carried out, highlighting their tapered microstructures with high molecular weights (up to 159.8 KDa) and a single glass transition temperature. For PMS copolymer reactivity ratios,  $r_{\text{myr}} = 0.12 \pm 0.003$  and  $r_{\text{sty}} = 3.18 \pm 0.65$  and  $r_{\text{myr}} = 0.10 \pm 0.004$  and  $r_{\text{sty}} = 3.32 \pm 0.68$  were determined according to the Kelen–Tudos (KT) and extended Kelen–Tudos (exKT) methods, respectively. Finally, this study showed an easy accessible approach for the production of various elastomers by anionic copolymerization of renewable terpenes, such as myrcene, with commodities.

**Keywords:** myrcene; sodium hydride; anionic polymerization

**Citation:** Lamparelli, D.H.; Kleybolte, M.M.; Winnacker, M.; Capacchione, C. Sustainable Myrcene-Based Elastomers via a Convenient Anionic Polymerization. *Polymers* **2021**, *13*, 838. <https://doi.org/10.3390/polym13050838>

Academic Editor: Cristina Cazan

Received: 22 February 2021

Accepted: 5 March 2021

Published: 9 March 2021

**Publisher's Note:** MDPI stays neutral with regard to jurisdictional claims in published maps and institutional affiliations.



**Copyright:** © 2021 by the authors. Licensee MDPI, Basel, Switzerland. This article is an open access article distributed under the terms and conditions of the Creative Commons Attribution (CC BY) license (<https://creativecommons.org/licenses/by/4.0/>).

## 1. Introduction

In the last two decades, on the one side under globalization pressures there has been an extraordinary planetary expansion of plastics and rubbers manufactured for human use (359 million tons in 2018) [1]; on the other side concerns have grown about environmental problems, dwindling petrochemical reserves and climatic changes, also due to the accumulation of CO<sub>2</sub> in the atmosphere.

Within this scenario, the scientific community and chemical industry have directed their efforts toward more sustainable processes [2] by using feedstock derived from renewable resources as alternatives to petroleum-based products in order to reduce our dependence on fossil raw materials and their adverse effects on the ecosystems [3,4]. Fortunately, nature offers many different compounds, which are excellent building blocks for constructing advanced materials: polysaccharides and their derivatives, lignin, suberin, vegetable oils, tannins, monomers originating from sugars, furan derivatives, lactic acid and fatty acid, which are just a few examples [5,6]. In this context, the large family of terpenes represents a natural, potentially important source of unsaturated hydrocarbons, useful in producing polymers [7–11]. Terpenes are ubiquitous molecules, characterized by the presence of one or more double bonds, found in many plants (mainly conifers), fungi and even some insect, which have both linear and cyclic structures and share 2-methyl-1,4-butadiene (isoprene) (C<sub>5</sub>) as an elementary unit [12]. Among these compounds, β-myrcene (M)—due to the structural similarity to isoprene (I) and butadiene (B) and large availability—has recently aroused a growing attention as building block for the synthesis



of a vast range of polymers, including the elastomer synthesis. Really, the first works on M date back to the 40s of the last century and concern an emulsion polymerization [13] and a study to avoid the deterioration of the monomer during storage due to its reactivity [14]. M, a colorless liquid belongs to the class of acyclic monoterpenes (C<sub>10</sub>), contains three double bonds in its structure, bearing a conjugated diene moiety. Although it is naturally produced by various plants, M is industrially generated by pyrolysis of  $\beta$ -pinene and new developments on its production from microbial synthesis via metabolically engineered *Escherichia coli* were also investigated [15,16].

Recently, homopolymerizations of M and its copolymerization with various comonomers, such as conjugated dienes [17–20], styrene (S) [21–24] and derivatives [25], ethylene and propylene [26], methacrylates [27,28], itaconic acid [29], and lactide [30] by coordinative mechanism [31,32], free [23,33] and controlled radical polymerizations [34–36], cationic [37] and anionic [38–40] polymerization methods have been reported. Very recently, a temperature-controlled one-pot anionic approach for the preparation of diblock copolymers consisting of PS and PM blocks has been described [41]. It has also been reported the synthesis of bifunctional (hydroxyl, furan and pyridine group derivatives) monomers dienes obtained from M and their controlled copolymerization with isoprene via catalytic insertion mechanism [42]. Previously, Cawse and co-workers used hydroxyl-functionalized polymyrcene to modify a polyurethane network leading to improved impact properties and stress–strain behavior [43].

Depending on the polymerization conditions, the polymyrcene can consist of 1,4 *cis/trans*, 1,2 and 3,4 units. However, the most promising application in the large-scale use of these polymers as elastomers has been still lacking. Elastomeric materials play a fundamental role in human life, being used in countless applications ranging from tire to spacecraft seal [44,45].

In the rubber industry, excluding natural rubber (NR), polybutadiene (BR) and styrene-butadiene rubber (SBR) are the two main products [45,46], these latter are produced on a large scale from emulsion (E-SBR) [47,48] and solution (S-SBR) [49] polymerization. S-SBR is synthesized by an anionic polymerization process, which is initiated by organolithiums compounds, such as *sec*-butyl lithium (*sec*-BuLi) or *n*-butyl lithium (*n*-BuLi), soluble in common organic solvents. Indeed, anionic polymerization is still one of the most powerful synthetic tools for the preparation of well-defined polymers, allowing the control of the molecular architecture (molecular weight, molecular weight distribution, composition and microstructure) [50]. Carbanions (or oxanions) with metallic counterions are mostly the active centers, highly sensitive to oxygen, moisture and protic impurities in the chain propagation step.

Alkali metal hydrides (Li, Na, K) can be considered a viable alternative to organolithium compounds as anionic polymerization initiator but have been barely investigated because their low solubility in organic solvents. Notably, the addition of Lewis acid (R<sub>3</sub>Al, R<sub>3</sub>B, R<sub>2</sub>Zn, or R<sub>2</sub>Mg), in particular of trialkylaluminium (Et<sub>3</sub>Al and *i*-Bu<sub>3</sub>Al) to LiH, NaH and KH, allows for their solubilization in non-polar solvents by formation of bimetallic complexes [51–54].

They are compounds quickly available and stable under inert atmosphere in which one or more hydrogen centers have nucleophilic, basic or reducing properties, commonly used as reducing agents in organic synthesis. LiH, NaH and KH have been employed to very limited cases in polymerization [55] and only in recent years systems based on their association with alkyl, alkoxide and hydride derivatives of Al, Mg and Zn in the RAP of styrene and dienes have been explored [56–58]. Deffieux et al. reported that triisobutylaluminium (TIBA) and sodium hydride form soluble heterocomplexes (*i*-Bu<sub>3</sub>Al/NaH) usable as initiating systems for the retarded anionic polymerization (RAP) of S at high temperature in concentrated monomer conditions [56].

The best performances were obtained at ratios  $0.7 < \text{Al}:\text{Na} < 1$ , since for stoichiometric proportion or higher than 1 the system was inactive. As depicted in Figure 1, at ratios  $\text{Al}:\text{Na} \geq 1$ , only the 1:1 complex with an inactive site (S<sub>1</sub>) was formed. Instead, in the

presence of a slight excess of NaH with respect to TIBA, in addition to the 1:1 complex, the formation of the 1:2 complex with an active site was postulated. Furthermore, the addition of tetrahydrofuran (THF) as a second polar additive increased the reactivity of the system and could lead to a mixture of complexes in which the formation of an active Na–H bond ( $S_2$ ) was favored [54,57].

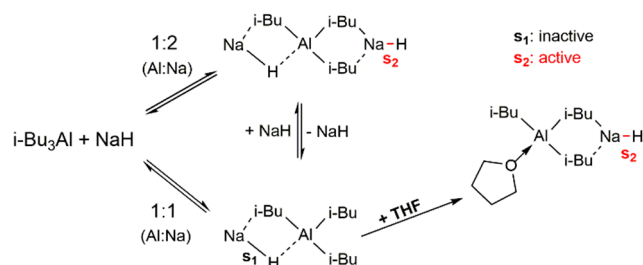


**Figure 1.** Formation of 1:2 and 1:1 Al/Na heterocomplexes of  $i\text{-Bu}_3\text{Al}/\text{NaH}$  system and influence of THF on an inactive 1:1 complex, as suggested by Deffieux et al. [58].

In the present paper, the anionic homo-, co- and ter-polymerization of M, S and I by sodium hydride in combination with TIBA, as anionic initiator heterocomplexes, in highly concentrated monomer media at 100 °C were investigated. These initiating systems can represent a very useful and economical approach for the copolymerization of M with commodities such as S and I, enlarging the armory of techniques that allow the synthesis of more sustainable terpene-based elastomers.

## 2. Materials and Methods

### 2.1. Materials

All chemicals were stored and handled under an argon atmosphere using standard Schlenk techniques or an MBraun glovebox.

All glassware was stored overnight in an oven at 130 °C prior to use.  $\beta$ -myrcene ( $\geq 95\%$ ), isoprene and styrene ( $\geq 99\%$ ) were all purchased from Sigma-Aldrich (Steinheim, Germany) and were purified by overnight stirring over calcium hydride and distillation under reduced pressure. Monomers were stored on molecular sieves at 4 °C and before each set of experiments the amount of water was measured with a Mettler Toledo KF Coulometer DL36 Karl Fischer (Greifensee, Switzerland) instrument (allowed max. 15 ppm  $\text{H}_2\text{O}$ ). Toluene (Sigma-Aldrich) and tetrahydrofuran (Sigma Aldrich) (THF) as solvents dried were obtained with an MBraun MBSPS-800 (Garching, Germany) solvent purification system and were deoxygenized by three freeze-pump-thaw cycles, before storing on molecular sieves. Sodium hydride was stored under argon atmosphere in a drybox. Triisobutylaluminum ( $\text{Al}(i\text{-Bu})_3$ , Sigma-Aldrich) (TIBA) was used as received.

### 2.2. Preparation of NaH/ $i\text{-Bu}_3\text{Al}$ Initiator System

Under argon, NaH (0.096 g,  $4 \times 10^{-3}$  mol) was placed in a glass flask before adding 50 mL of dry and degassed toluene. Then, 3 mL of TIBA solution (25% wt in toluene) was added with a syringe to reach the ratio of  $\text{Al}/\text{Na} = 0.8$ . The final solution was let under vigorous stirring at 50 °C, until NaH was partially solubilized (4 h).

### 2.3. Typical Polymerization Procedure

Polymerizations were carried out under argon at 100 °C in a glass flask for 72 h. 88  $\mu\text{L}$  of  $i\text{-Bu}_3\text{Al}/\text{NaH}$  solutions (ratio  $\text{Al}/\text{Na} = 0.8$ ) and 25  $\mu\text{L}$  of THF were added with a syringe to dry and degassed toluene (0.5 mL). Finally, 0.5 mL of myrcene was added to reaction mixture and the system was maintained under stirring after equilibration at the desired temperature. The polymerization was stopped by adding of methanol containing a little amount of hydrochloric acid and 2,6-bis(1,1-dimethylethyl)-4-methylphenol (BHT) as

stabilizing agent. The polymer was washed and dried under vacuum until constant weight. 230 mg polymer (58% yield,  $M_w = 50.2$  KDa,  $\bar{D} = 1.7$ ).

#### 2.4. Typical Co-polymerization Procedure

Co-Polymerizations were carried out under argon at 100 °C in glass flasks for 72 h. 30  $\mu$ L of *i*-Bu<sub>3</sub>Al/NaH solutions (ratio Al/Na = 0.8) and 9  $\mu$ L of THF were added with a syringe to dry and degassed toluene (0.5 mL). Finally, 0.28 mL of myrcene and 0.19 mL of styrene was sequentially added to reaction mixture and the system was maintained under stirring after equilibration at the desired temperature. The co-polymerization was stopped by adding of methanol containing a little amount of hydrochloric acid and 2,6-bis(1,1-dimethylethyl)-4-methylphenol (BHT) as stabilizing agent. The co-polymer was washed and dried under vacuum until constant weight. 295 mg polymer (75% yield,  $M_w = 151.2$ ,  $\bar{D} = 2.1$ ).

#### 2.5. Preparation of Diblock Copolymer

In a glass flask equipped with magnetic stirrer 30  $\mu$ L of *i*-Bu<sub>3</sub>Al/NaH solutions (ratio Al/Na = 0.8) and 9  $\mu$ L of THF were added with a syringe to dry and degassed toluene (0.5 mL). At 100 °C, the polymerization starts after injection of 0.19 mL of styrene. After 8 h, the glass flask was opened in a drybox and was quickly added 0.28 mL of myrcene. The polymer was coagulated after further 72 h in methanol containing a little amount of hydrochloric acid and 2,6-bis(1,1-dimethylethyl)-4-methylphenol (BHT). The polymer was washed and dried under vacuum at room temperature until constant weight. 366 mg polymer (93% yield,  $M_w = 60.2$ ,  $\bar{D} = 1.8$ ).

#### 2.6. Polymer Characterizations

<sup>1</sup>H and <sup>13</sup>C NMR analysis were recorded Bruker AV III-300, AV HD-400 and AV III-500 spectrometer at room temperature. Chemical shifts  $\delta$  are reported in ppm relative to tetramethylsilane and calibrated to the residual <sup>1</sup>H or <sup>13</sup>C signal of the deuterated solvent.

Diffusion-ordered spectroscopy (DOSY) experiments were carried out at 298 K on a Bruker Avance 600 (Karlsruhe, Germany) spectrometer with the standard Bruker pulse program (ledbpgp2s). The latter used a double stimulated echo sequence and LED, bipolar gradient pulses for diffusion, and two spoil gradients. For the duration of the experiment (about 25 min), the pulse gradients were increased from 5% up to 95% of the maximum gradient strength in a linear ramp. The parameters were set as follows: diffusion times were 2500 ms, the eddy current delay was 5 ms, the gradient recovery delay was 0.2 ms, and the gradient pulse was 1000 ms. Individual rows of the quasi-2D diffusion databases were phased and, after Fourier transformation and baseline correction, the diffusion dimension was processed with the Bruker software Topspin3.2 and Diffusion. By Gaussian fits diffusion coefficients were calculated, using T1/T2 software of Topspin3.2.

Size exclusion chromatography (SEC) measurements were performed using a PolymerLaboratoriesGPC50 Plus (Walnut Creek, CA, USA) chromatograph (calibrated with polystyrene standards) and equipped with Deflection RI detector at 40 °C with THF as the eluent (flow of 1 mL/min).

Differential scanning calorimetry (DSC) analysis was conducted on a DSC Q2000 (New Castle, DE, USA) instrument. 2–5 mg of polymer was sealed into a DSC aluminium pan and heated from –90 to 250 °C at 10 °C/min. The reported values are those determined in the second heating cycle.

Thermal gravimetric analysis (TGA) measurements were performed on a TA Instruments Q5000 SA (New Castle, DE, USA). The heating and cooling rate was adjusted to 10 °C/min and the temperature range measured was 40–600 °C under inert atmosphere of Argon.

Water contact angle measurement (WCA) were performed on a Krüss DropShape Analyzer (Hamburg, Germany). The evaluation was performed with the program ImageJ.

The samples were applied via solvent casting on glass object carriers and measured several times. The average of these values represent the contact angle.

Scanning electron microscope (SEM) measurements were recorded on a JEOL field emission scanning electron microscope JSM-7500F (Garching, Germany). The secondary electrons produced by the electrons of the beam (primary electrons) in interaction with the atoms of the object under investigation served as information source. The samples were examined at different magnifications.

### 3. Results and Discussion

#### 3.1. Homopolymerizations of Myrcene, Styrene and Isoprene

Polymyrcene (PM), polystyrene (PS) and polyisoprene (PI) were synthesized by anionic polymerization using the simple combination of *i*-Bu<sub>3</sub>Al/NaH as initiating systems at 100 °C in degassed and dry toluene solutions (runs 1–9, Table 1). A blank experiment was tried with just NaH and did not provide any results.

**Table 1.** Homopolymerizations of myrcene, styrene and isoprene, using *i*-Bu<sub>3</sub>Al/NaH as initiating systems at 100 °C.

| Run <sup>[a]</sup> | Monomers feed [M,S,I] [mol %] | [NaH]                | $\frac{[mon]}{[NaH]}$ | Time [h] | Yield <sup>[b]</sup> [%] | M <sub>w</sub> <sup>[c]</sup> [KDa] | Đ <sup>[e]</sup> | T <sub>g</sub> <sup>[d]</sup> [°C] | Polymer Composition and Microstructure [%] |     |                               |
|--------------------|-------------------------------|----------------------|-----------------------|----------|--------------------------|-------------------------------------|------------------|------------------------------------|--|-----|-------------------------------|
|                    |                               |                      |                       |          |                          |                                     |                  |                                    | M [1,4/3,4/1,2]                            | S   | I [1,4[ <i>cis</i> ]/3,4/1,2] |
| 1                  | 100,0,0                       | $6.0 \times 10^{-3}$ | 500                   | 24       | 58                       | 50.2                                | 1.7              | −61.8                              | 100<br>[46/52/2]                           | -   | -                             |
| 2 <sup>[e]</sup>   | 100,0,0                       | $6.0 \times 10^{-3}$ | 500                   | 24       | 7                        | 264.9                               | 1.7              | n.d.                               | 100  | -   | -                             |
| "                  | "                             | "                    | "                     | "        | "                        | 7.9                                 | 1.7              | n.d.                               | "  | "   | "                             |
| 3                  | 100,0,0                       | $3.0 \times 10^{-3}$ | 1000                  | 72       | 85                       | 79.6                                | 1.7              | n.d.                               | 100<br>[49/48/3]                           | -   | -                             |
| 4                  | 100,0,0                       | $2.2 \times 10^{-3}$ | 1450                  | 72       | 40                       | 89.3                                | 2.0              | −76.5                              | 100<br>[51/47/2]                           | -   | -                             |
| 5                  | 0,100,0                       | $6.0 \times 10^{-3}$ | 500                   | 8        | 100                      | 151.2                               | 1.4              | 105.5                              | -  | 100 | -                             |
| 6                  | 0,100,0                       | $2.2 \times 10^{-3}$ | 1450                  | 8        | 91                       | 285.1                               | 1.5              | n.d.                               | -  | 100 | -                             |
| 7                  | 0,0,100                       | $6.0 \times 10^{-3}$ | 500                   | 12       | 40                       | 24.9                                | 1.5              | n.d.                               | -  | -   | 100<br>[30[53]/56/14]         |
| 8                  | 0,0,100                       | $6.0 \times 10^{-3}$ | 500                   | 24       | 74                       | 33.4                                | 1.5              | −11.4                              | -  | -   | 100<br>[32[52]/55/13]         |
| 9                  | 0,0,100                       | $3.0 \times 10^{-3}$ | 1000                  | 24       | 55                       | 59.1                                | 1.6              | −14.9                              | -  | -   | 100<br>[35[53]/54/11]         |

<sup>[a]</sup> Reactions were performed in toluene; (monomers) = 3.0; Al/Na = 0.8; tetrahydrofuran (THF)/Na = 50. <sup>[b]</sup> Conversion was determined by gravimetry. <sup>[c]</sup> Determined by size exclusion chromatography (SEC) in THF at 40 °C, calibrated with polystyrene standards. <sup>[d]</sup> Determined by DSC. <sup>[e]</sup> THF/Na = 0. N.d. = not determined.

The effect in terms of efficiency and polymerization control of a second polar additive such as THF was observed in the homopolymerizations of M. Its absence (run 2, Table 1) had negative effects on the polymerization yield (7%) and the molecular weight distribution (MWD) was found bimodal. Reasonably, as already observed in previous studies [56,58], THF increased the reactivity of the system also at ratios  $0.7 < \text{Al:Na} < 1$  and shifted the equilibrium of the complexes, favoring the formation of species with active sites (s<sub>2</sub>) to which propagation reactions are restricted.

According to <sup>1</sup>H NMR analysis of the vinylic proton signals at  $\delta$  4.7–5.2 ppm (see Figure S1 and Equations (E1) and (E2) of supporting information, SI), PM consisted of an almost equimolar mixture of 1,4 *cis/trans* and 3,4 units, since 1,2 units were revealed only in a small percentage (2–3%). The signals between 5.00–5.20 ppm were found assignable to the olefinic protons of 1,4-units (*cis* and *trans*), whereas the doublets at 4.73–4.76 ppm belonged to 3,4-units. The structural irregularity of PM emerged from <sup>13</sup>C {<sup>1</sup>H} NMR spectra (See Figure S2, SI), in which the overlap of some signals did not allow the accurate determination of the *cis* and *trans* geometric isomers for 1,4 units. However, a deeper

analysis of the aliphatic portion of  $^{13}\text{C}$  NMR spectrum (See Figure S3, SI) permitted to detect the presence of many peaks (28.55, 29.89 and 37.23 ppm) related to head-to-head and tail-to-tail regio-irregular 1,4 units along the polymer backbone. These signals have already been reported for samples obtained by cationic and coordination polymerizations of M [21,37]. In the 1980s, pioneering anionic studies have shown that M can be polymerized using sec-butyllithium (sec-BuLi) in nonpolar solvents (e.g., benzene, cyclohexane), obtaining PM with a high amount of the preferable 1,4-units [38,59]. In recent years, the prevalence of 1,4 linkages for M with the same initiator, under different experimental conditions, in both homopolymerizations and copolymerizations has been confirmed [40,60]. At 10 °C in THF, Bolton et al. reported 1,4-, 3,4-, and 1,2-contents of about 30, 60, and 10%, respectively [25]. In the 'green' ether solvents, like cyclopentyl methyl ether and 2-methyltetrahydrofuran, 1,2 and 3,4 units (36–86%) were found enriched [61]. *n*-BuLi in combination with tetramethylethylenediamine (TMEDA) as the modifier provides random copolymer and block copolymer of M and S in which 3,4-units can be found in range 22–39% [62]. However, the presence of a higher percentage of 3,4-addition microstructures, as in our case (47–52%), could make PM more susceptible toward sulfur vulcanization as evidenced by Sarkar et al. [23,63]. This peculiar aspect could be the subject of further investigation in the future.

Size exclusion chromatography (SEC) analysis revealed molecular weights ( $M_w$ ) in the range of 50.2–89.3 KDa, a dispersity index ( $\mathcal{D}$ ) of 1.7–2.0 with monomodal MWD. The broader distribution of  $\mathcal{D}$ , compared to the narrower values generally obtained with anionic polymerizations, can be explained by several factors. Specially, the high operating temperature (100 °C) in experimental conditions could facilitate termination reactions, as well as the presence of a TIBA, which is a chain transfer agent. Yields increased prolonging the polymerization times from 24 h (58%) to 72 h (85%), instead  $M_w$  increased, at the expense of yield, increasing the monomer/NaH ratio. The polymer chains of PM showed low  $T_g$  values (usually below  $-60$  °C) comparable to conventional rubbers.

PS obtained by *i*-Bu<sub>3</sub>Al/NaH heterocomplexes (runs 5–6, Table 1) had characteristic spectra of an atactic polystyrene (for  $^1\text{H}$  and  $^{13}\text{C}$  NMR see Figures S6 and S7 of SI) [64]. This evidence was confirmed by the differential scanning calorimetry (DSC) analysis that showed a  $T_g$  around 105 °C without any  $T_m$ .  $M_w$  followed the same trend of PM, increasing in line with the increase of the monomer/NaH ratio. For the latter set to 1450,  $M_w$  grew up to 285.1 KDa with  $\mathcal{D}$  value (1.5) and yield of over 90% in 8 h. The homopolymerization of isoprene (I) has been reported in literature using similar ternary initiating systems based on alkali metal hydride, trialkylaluminium and alkoxides in cyclohexane at different temperatures (80–120 °C), achieving mainly a mixture of 1,4 and 3,4 isoprene units and small amount of 1,2 units present (3–6%) [65]. Table 1 contains data relating to isoprene polymerizations (runs 7–9). The best monomer conversion (74%) was achieved after 24 h, starting from NaH =  $6.0 \times 10^{-3}$  mol/L and monomer/NaH = 500.

Figure S8 in supporting information displays a typical  $^1\text{H}$  NMR spectrum, in which the resonances above 4.50 ppm were attributed to olefinic protons of 3,4- addition (4.65–4.72 ppm), 1,2- addition (4.80–4.90 ppm), 1,4- (*cis*- and *trans*) addition (5.02 ppm) and 1,2-addition (5.70 ppm). Isoprene polymer compositions were determined by  $^1\text{H}$  and  $^{13}\text{C}$   $\{^1\text{H}\}$  NMR spectroscopy in solution according to Equations (S5)–(S9) (see SI). The contents of 1,4, 3,4-, and 1,2- units in the PI were in the ranges of 30–35%, 54–56% and 11–14%, respectively. The SEC analyses revealed that PI copolymers have  $M_w$  ranging from 24.9 to 59.1 KDa with  $\mathcal{D}$  of 1.5–1.6. The  $T_g$  of polymers measured by DSC ranging from  $-14.9$  to  $-11.4$  °C. TGA curves of PM, PS and PI in argon atmosphere are reported in SI (Figures S38–S40). From the TGA curve it can be clearly seen that below 300 °C there is no noticeable weight loss underlying the thermal stability of the obtained materials. Moreover, plots for myrcene and isoprene conversions versus polymerization time and evolution of molecular weight and  $\mathcal{D}$  versus conversion are shown in the Section S9 of SI.

### 3.2. Synthesis and Characterization of Poly(M-co-S), Poly(M-b-S), Poly(M-co-I) Copolymers and Poly(M-co-S-co-I) Terpolymers

Copolymerization of various monomers is a powerful strategy to modify the properties of manufactured polymers satisfying specific needs, for example modifying  $T_g$ , reducing crystallinity, or changing the molecular architecture of polymer backbone chains in order to obtain new materials with better properties. The polymerizations of M with S and I were performed in toluene, at 100 °C, using a monomers/NaH ratio ranging from 500 to 1450. Table 2 summarizes the main results. Polymer compositions were fully elucidated by  $^1\text{H}$  NMR and  $^{13}\text{C}$  ( $^1\text{H}$ ) NMR spectroscopy according to the methods reported in the supplementary material (See Equations (S1)–(S4) and (S8)–(S13), SI). NMR spectra were recorded in  $\text{CDCl}_3$  and 1,1,2,2 tetrachloroethane- $d_2$  (TCDE) in order to have all the diagnostic samples signals free from deuterated solvent peak. In all copolymers 1,2 units of M were not diagnosed.

**Table 2.** Co- and Ter-Polymerization of myrcene, styrene and isoprene, using  $i\text{-Bu}_3\text{Al}/\text{NaH}$  as initiating systems at 100 °C.

| Run <sup>[a]</sup> | Monomers Feed [M,S,I] [mol %] | [NaH]                | $\frac{[\text{mon}]}{[\text{NaH}]}$ | Time [h] | Yield <sup>[b]</sup> [%] | $M_w$ <sup>[c]</sup> [kDa] | $\bar{D}$ <sup>[e]</sup> | $T_g$ <sup>[f]</sup> [°C] | Polymer Composition and Microstructure [%] |    |    |
|--------------------|-------------------------------|----------------------|-------------------------------------|----------|--------------------------|----------------------------|--------------------------|---------------------------|--|----|----|
|                    |                               |                      |                                     |          |                          |                            |                          |                           | M [1,4/3,4/1,2]                            | S  | I  |
| 10                 | 90,10,0                       | $6.0 \times 10^{-3}$ | 500                                 | 72       | 82                       | 48.1                       | 1.8                      | −47.7                     | 87 [48/52]                                 | 13 | -  |
| 11                 | 90,10,0                       | $2.2 \times 10^{-3}$ | 1450                                | 72       | 45                       | 97.1                       | 1.8                      | −52.2                     | 89 [52/48]                                 | 11 | -  |
| 12                 | 70,30,0                       | $2.2 \times 10^{-3}$ | 1450                                | 72       | 54                       | 142.9                      | 2.1                      | −42.4                     | 65 [55/45]                                 | 35 | -  |
| 13                 | 50,50,0                       | $2.2 \times 10^{-3}$ | 1450                                | 72       | 75                       | 151.2                      | 2.1                      | −4.9                      | 38 [49/51]                                 | 62 | -  |
| 14                 | 30,70,0                       | $2.2 \times 10^{-3}$ | 1450                                | 72       | 91                       | 159.8                      | 1.9                      | 21.3                      | 17 [56/44]                                 | 83 | -  |
| 15                 | 70,0,30                       | $3.0 \times 10^{-3}$ | 1000                                | 72       | 78                       | 71.3                       | 1.7                      | −46.1                     | 55 [59/41]                                 | -  | 45 |
| 16                 | 50,0,50                       | $3.0 \times 10^{-3}$ | 1000                                | 72       | 85                       | 66.5                       | 1.9                      | −37.5                     | 31 [58/42]                                 | -  | 69 |
| 17                 | 30,0,70                       | $3.0 \times 10^{-3}$ | 1000                                | 72       | 80                       | 62.9                       | 1.8                      | −33.0                     | 19 [53/47]                                 | -  | 81 |
| 18                 | 33,33,34                      | $3.0 \times 10^{-3}$ | 1000                                | 72       | 83                       | 98.7                       | 2.7                      | −8.2                      | 17   | 52 | 31 |
| 19                 | 50,40,10                      | $3.0 \times 10^{-3}$ | 1000                                | 72       | 81                       | 145.2                      | 2.2                      | −5.1                      | 33   | 54 | 13 |
| 20                 | 10,40,50                      | $3.0 \times 10^{-3}$ | 1000                                | 72       | 80                       | 90.9                       | 1.7                      | 11.0                      | 8  | 45 | 47 |
| 21 <sup>[e]</sup>  | 50,50,0                       | $3.0 \times 10^{-3}$ | 1000                                | 8 + 72   | 88                       | 60.2                       | 1.8                      | 98.9                      | 36 [46/54]                                 | 64 | -  |
| ,                  | ,                             | ,                    | ,                                   | ,        | ,                        | ,                          | ,                        | −52.5                     | ,  | ,  | ,  |

<sup>[a]</sup> Reactions were performed in toluene; monomers = 3.0; Al/Na = 0.8; THF/Na = 50. <sup>[b]</sup> Conversion was determined by gravimetry. <sup>[c]</sup> Determined by SEC in THF at 40 °C, calibrated with polystyrene standards. <sup>[d]</sup> Determined by DSC. <sup>[e]</sup> Successive monomer additions (1st: styrene; 2nd: myrcene).

Complete assignments of  $^{13}\text{C}$  ( $^1\text{H}$ ) NMR spectra (Figure 2) of synthesized poly(M-co-S) copolymers (PMS) are in agreement with data given in the literature [21,23,37]. The direct comparison of carbon spectra of PMS copolymers and those of PM and PS homopolymers pointed the presence of additional signals (highlighted in Figure 2) that corresponded to the M-S dyads, which were already identified by Hulnik et al. in the emulsion cationic polymerization of M and S using a water-dispersible Lewis acid surfactant combined catalyst (LASC) [37]. It is interesting to observe the C1'' and C2'' signals of the styrenic unit, at higher myrcene contents (Figure 2), almost disappear simultaneously with the formation of the M-S dyads.

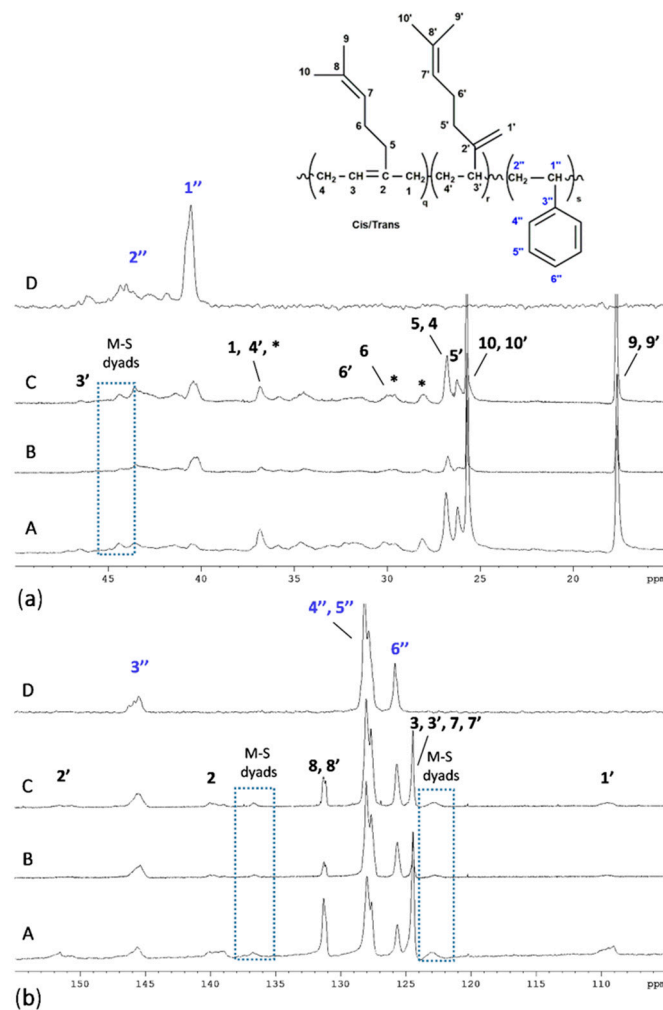


**Figure 2.** Aliphatic (a) and olefinic (b) regions of  $^{13}\text{C}$  NMR spectra (TCDE, 25 °C, 400 Mhz) of PMS, synthesized at different myrcene: styrene ratios, and of PS homopolymer. A) M:S (mol/mol) = 70:30 (run 12, Table 2); B) M:S (mol/mol) = 50:50 (run 13, Table 2); C) M:S (mol/mol) = 30:70 (run 14, Table 2); PS (run 5, Table 1). \* Signals attributed to head-to-head and tail-to-tail regio-irregular 1,4 M units.

Head-to-head and tail-to-tail enchainments bridge of 1,4-*cis* M additions (see Figure S3 in detail, SI), previously observed in the PM, were also visible in all  $^{13}\text{C}$   $\{^1\text{H}\}$  spectra of PMS copolymers. Glass transition temperatures of PMS (runs 10–14) lie between that of the homopolymers (−76.5 and 105.5 °C for polymyrcene and atactic polystyrene, respectively) and are listed in Table 2. All the copolymers, with the exception of run 21, showed a single  $T_g$  value which decreased with increasing amount of M incorporated in the copolymers. This is due to the decrease in the comonomer content of styrene having a rigid benzene ring. For comparison purposes, the Fox equation was applied for the calculation of  $T_g$  values, showing a good correlation between experimental and theoretical data (Figure 3):

$$\frac{1}{T_g} = \sum \frac{W_i}{T_{gi}}$$

where  $W_i$  is weight fraction of component  $i$  and  $T_g$  and  $T_{gi}$  are the glass transition temperatures of the copolymer and of the homopolymer  $i$ , respectively.

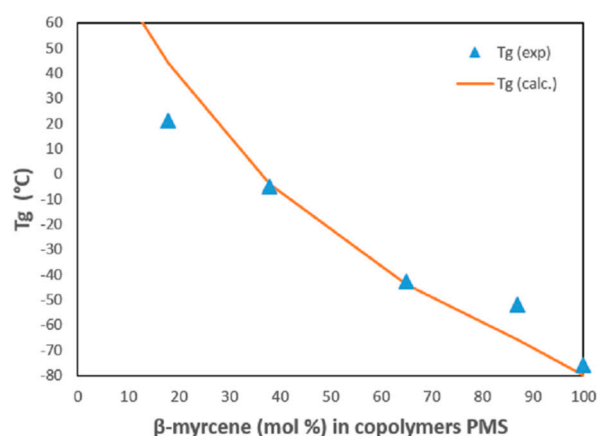


**Figure 3.** Glass transition temperatures ( $T_g$ ) at different  $\beta$ -myrcene content (mol %) incorporated in copolymers.

The reactivity ratios for myrcene-styrene copolymerization were estimated by the Kelen–Tudos (KT) method (See paragraph 2 and Table T3, SI), considering the monomer feed ratios and the copolymer compositions (Table T1, SI). To minimize the composition drift, the copolymerization reactions were stopped after 30 min, corresponding to a monomers conversion of 5–9%. In Figure A2 (SI) is presented the KT plots. The difference in reactivity between myrcene and styrene ( $r_{\text{myr}} = 0.12 \pm 0.003$  and  $r_{\text{sty}} = 3.18 \pm 0.65$ ) indicated that S is more reactive than M. The products of  $r_{\text{myr}}$  and  $r_{\text{sty}}$  were less than the unity ( $r_{\text{myr}} \times r_{\text{sty}} = 0.38$ ). To evaluate the reactivity ratios it was also used modified version of Kelen–Tudos called extended Kelen–Tudos method (exKT). In this method was included a new parameter called Z, by redefining  $\eta$  and  $\xi$  using partial molar conversion of the monomers (see paragraph 2.2, SI). The exKT parameters were shown in the Table T4 of SI. The reactivity of the monomers was found to be  $r_{\text{myr}} = 0.10 \pm 0.004$  and  $r_{\text{sty}} = 3.32 \pm 0.68$  with  $r_{\text{myr}} \times r_{\text{sty}} = 0.33$ .

The two methods (KT and exKT) are in good agreement with each other, revealing that  $r_{\text{sty}} > 1$  and  $r_{\text{myr}} < 1$ . Thus, the polymer chains are enriched in S in the initial stages of polymerization, forming short sequences of styrene units. When the polymerizations proceed to higher monomer conversion, the monomer feed is enriched in the less reactive M favoring its incorporation in the chains. These observations suggested a tendency of S and M to form tapered polymer, as also observed in other recent anionic polymerization works [60].

Keeping in mind the idea of making different PMS architectures, consecutive addition of the two monomers (run 21) produced a poly(M–b-S) diblock copolymer due to the living anionic polymerization character. GPC analysis of synthesized sample was unimodal with  $\bar{D} = 1.8$ , confirming the formation of AB diblock copolymer. More generally, the principal evidence on the copolymeric nature was the marked difference in Mw among poly(M–b-S) and corresponding homopolymers (PM and PS) obtained under the same experimental conditions that led to exclude the formation of a polymer blend. As expected,  $^{13}\text{C}$  NMR spectrum of poly(M–b-S) confirmed the absence of M-S dyads diagnosed for PMS copolymer (Figure S14, SI), showing only the characteristic signals of M and S homosequences. Moreover, high molecular weight (60.2 KDa) did not allow detecting the junction between the two blocks.

DOSY demonstrated definitively the copolymeric nature for the examined samples (Figures S25 and S26, SI).

The DSC curve of poly(M–b-S) displayed two  $T_g$  values (98.9 °C and –52.5 °C) due to the two different long monomer sequences, which are close to those of their homopolymers. Anionic polymerization promoted by *i*-Bu<sub>3</sub>Al/NaH was also applied to produce poly(M–co-I) (PMI). Copolymers of M and I were recently synthesized by lanthanum-based catalyst for coordinative chain transfer polymerization (generating high trans-1,4



microstructure for both M and I) [66], by cationic  $\beta$ -diimidosulfonate lutetium catalyst (obtaining isotactic 3,4-polymyrcene and polyisoprene) [67] and by PN3 type cobalt complexes [18] (obtaining predominantly 1,4-*cis* microstructure—up to 83% for myrcene).

The representative copolymerization data are summarized in Table 2 (runs 15–17). A conversion of 85% was obtained in 72 h at ratio M:I = 50:50 mol/mol of alimentation feed with  $\text{NaH} = 3.0 \times 10^{-3}$  mol/L and  $[\text{M+I}]/\text{NaH} = 1000$ . The typical profile of the  $^1\text{H}$  NMR spectrum of PMI copolymers is shown in Figures S15 and S16 of SI. A comparison among the  $^1\text{H}$  NMR spectra of PM, PI and PMI is reported in Figure S15 (SI). Due to the structural similarity between monomers and the polyisoprenes sequences that contain all possible region-insertions (1,4-*cis*, 1,4-*trans*, 1,2 and 3,4 additions), many peaks of different comonomeric units felt in the same region also in the  $^{13}\text{C}$  ( $^1\text{H}$ ) NMR spectra. Thus, the difficulty in the integration of significant signals involved an uncertainty in determining polymer compositions (see SI, in particular the Equations (E10)–(E13) were based on quaternary carbons of the various concatenating units). Figure 4 shows the  $^{13}\text{C}$  NMR spectra of PMI copolymers which have been produced starting from different initial M:I (mol/mol) ratios. All the main peaks were assigned based on examples in the literature [18,21,37,67,68]. Furthermore, PMI copolymers showed a monomodal and molecular weight distribution in the range 1.7–1.9. Only one  $T_g$  were found for PMI copolymers, and no melting temperatures  $T_m$  were detected.

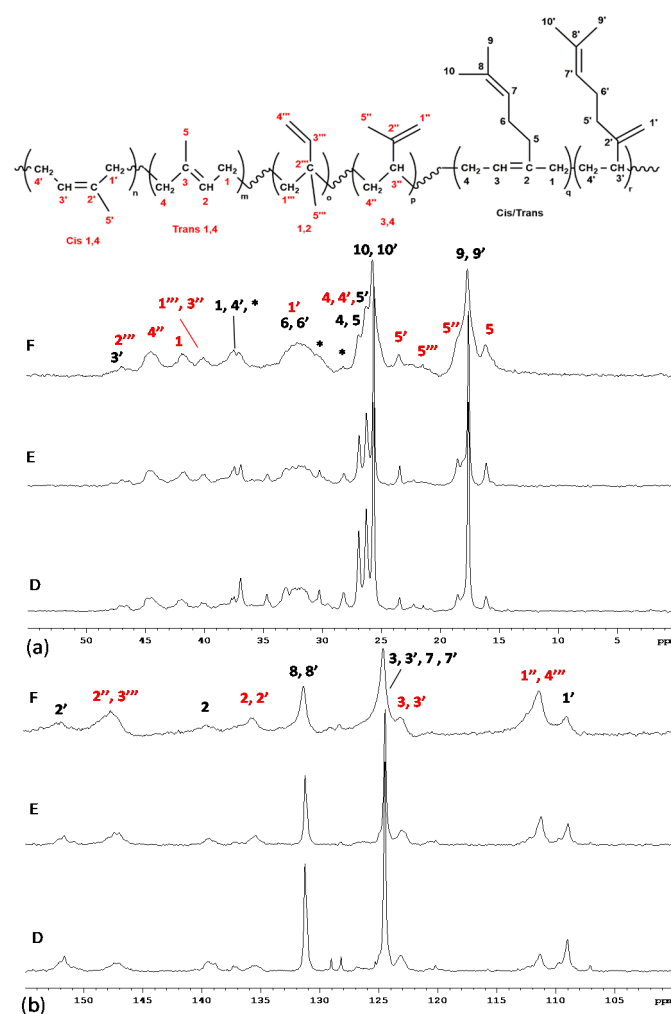


**Figure 4.** Aliphatic (a) and olefinic (b) regions of  $^{13}\text{C}$  NMR spectra (TCDE, 25 °C, 400 Mhz) of PMI, synthesized at different myrcene:isoprene ratios. D) M:I (mol/mol) = 70:30 (run 15, Table 2); E) M:I (mol/mol) = 50:50 (run 16, Table 2); F) M:I (mol/mol) = 30:70 (run 17, Table 2). \* Signals attributed to head-to-head and tail-to-tail regio-irregular 1,4 M units.

Ter-polymerizations of myrcene, isoprene and styrene have been recently achieved by coordinative chain transfer using pentamethylcyclopentadienyl  $\text{La}(\text{BH}_4)_2(\text{THF})_2$  combined with magnesium dialkyl and aluminum dialkyl, obtaining highly stereoregular copolymers in a wide range of compositions [31]. Three experiments (Table 2, runs 18–20) were performed to test anionic initiator systems also in the terpolymerizations of M, I and S and provided a yield on average 80%, Mw in the range of 90–145 KDa and MWD between 1.7 and 2.7 (Table 2, runs 18–20).

The structure of poly(M-co-S-co-I) (PMSI) with the assignments of the main peaks is exhibited in the Figure S21 (SI). In this case, the major complexity of PMSI NMR spectra reflects the microscopic structural irregularity, greatly limiting a depth NMR study.

TGA of copolymers synthesized revealed a good thermal stability for all the samples, with a decomposition temperature close to 350 °C (see Figures S41–S47, SI).

WCA is the most common method for determining the relative hydrophilicity of materials. Figure 5 shows the contact angles for some PMS (a), PMSI (b), PI (c), and PMI (d), respectively (see Table T7, SI). The rise in contact angle from PMS (83.7°) to PMI (122.1°) is evident. Reasonably this trend could be explained by the effect of the greater quantity in the samples of M and I which introduce small side chains in the structure of the copolymers and by their microstructure (mainly 3,4 addition), factors that increase hydrophobicity. The possibility of modulating the surface structure and properties of the copolymers by adjusting the microstructure of the segments has been already observed in previous studies [69,70].

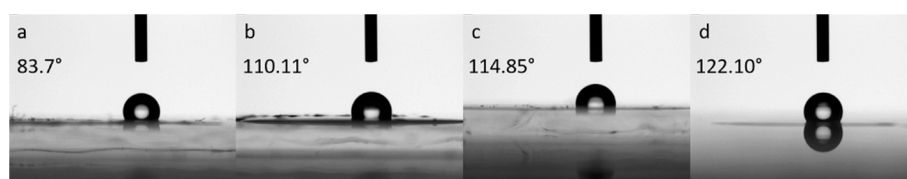


**Figure 5.** Water contact angles (WCA) measured for: PMS from run 14 of Table 2 (a); PMSI from run 19 of Table 2 (b); PI from run 7 of Table 1 (c) PMI from run 17 of Table 2 (d).

SEM is a type of electron microscope that allow to scan the surface of a sample with a high-energy beam of electrons. SEM has the potential to generate images with a few nanometres spatial resolution, and has a relatively large depth of field (up to 100 times that of an optical microscope). This provides valuable information about the surface topography and composition of the scanned objects. The character of the surfaces is very important, as surface properties are of high interest for new elastomers in certain applications, especially such as tires or as sealings.

The morphology of some samples, in particular poly(M-co-S) and poly(M-b-S) obtained, was subsequently investigated by SEM. Figure 6 shows the SEM images of runs 14 (upward) and 21 (below) collected in Table 2. These measurements show rough or wavy surface topographies of these polymers. Interestingly, edges and domains indicate the block structures present, and different dark areas in fine structures can show phase separation here (see Section S8 of the SI for more images).

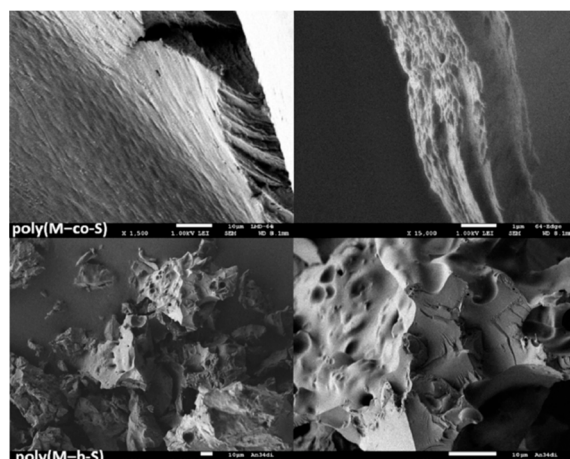


**Figure 6.** Scanning electron microscope (SEM) of poly(M-co-S) from run 14 of Table 2 and poly(M-b-S) from run 21 of Table 2.

#### 4. Conclusions

Homo- and co-polymerizations of myrcene with styrene and isoprene, and terpolymerization of all monomers have been reached using a soluble heterocomplexes consisting of sodium hydride in combination with triisobutylaluminum as anionic initiating system at 100 °C in toluene.

By adjusting the initial feed ratio, it was easily possible to obtain polymers in a wide range of composition with different architectures and various thermal properties. Molecular weights could be well controlled through the regulation of the monomers/NaH ratio.

Materials exhibited a  $T_g$  values in the range requested for an elastomeric material and good thermal stability with a decomposition temperature exceeding 300 °C. Moreover, all the samples were fully characterized by SEC, GPC, and NMR spectroscopy ( $^1\text{H}$ ,  $^{13}\text{C}$  and DOSY experiments). In some cases, to study the surface properties, WCA and SEM characterizations were also performed. A more complete study of myrcene-styrene copolymers (PMS) was carried out, highlighting their tapered microstructures with high molecular weights (ranging from 48.1 to 159.8 KDa) and a single glass transition temperature. Indeed, for PMS the reactivity constants were determined by Kelen–Tudos ( $r_{\text{myr}} = 0.12 \pm 0.003$  and  $r_{\text{sty}} = 3.18 \pm 0.65$ ) and extended Kelen–Tudos ( $r_{\text{myr}} = 0.10 \pm 0.004$  and  $r_{\text{sty}} = 3.32 \pm 0.68$ ) methods from which we supposed the tendency of S and M to form tapered polymer.

In conclusion, here we show a convenient alkyl-lithium-free system for the production of more sustainable elastomers by anionic polymerization, starting from biosourced monoterpenes such as myrcene. Our work is in line with the latest research in the field of elastomeric materials, which aim at the gradual replacement of fossil resources with bio-renewable monomers. The physical and mechanical tests of these myrcene-based elastomers and their behavior toward vulcanization could be the object of possible future developments and investigations.

**Supplementary Materials:** The following are available online at <https://www.mdpi.com/2073-4360/13/5/838/s1>, Figures S1–S25:  $^1\text{H}$ ,  $^{13}\text{C}$  and DOSY NMR of the representative samples; Figures S26–S37: DSC thermograms of representative samples; Figures S38–S47: TGA thermograms of representative samples; Figures S48–S61 GPC curves of representative samples; Figure S61: Conversion vs. time plot for isoprene polymerization; plots of MW (and  $\bar{D}$ ) vs conversion; Figure S62: Conversion vs. time plot for myrcene polymerization; plots of MW (and  $\bar{D}$ ) vs conversion. Table T1: Copolymerization of M and S with  $i\text{-Bu}_3\text{Al}/\text{NaH}$ ; Table T2: Reactivity ratio for copolymerization of M and S; Table S3: FR and KT parameters for PMS copolymers; Table T4: Reactivity ratio for copolymerization of M and S; Table S5: exKT parameters for PMS copolymers; Table T6: Reactivity ratio for copolymerization of M and S; Table T7: Contact angles for tested samples. Equations (E1)–(E16): Analysis of polymer compositions from NMR.

**Author Contributions:** Conceptualization, M.W., C.C. and D.H.L.; methodology, M.W. and D.H.L.; investigation, D.H.L. and M.M.K.; resources, M.W. and C.C.; data curation, D.H.L.; writing—original draft preparation, D.H.L.; writing—review and editing, M.W., C.C. and D.H.L.; funding acquisition, M.W. and C.C. All authors have read and agreed to the published version of the manuscript.

**Funding:** Parts of this work were funded by the Deutsche Forschungsgemeinschaft (DFG, German Research Foundation)—Project Number 445011287—and by FARB Università degli Studi di Salerno ORSA197414.

**Institutional Review Board Statement:** Not applicable.

**Informed Consent Statement:** Not applicable.

**Data Availability Statement:** The data presented in this study are available on request from the corresponding author.

**Acknowledgments:** This work was supported by Ministero dell’Istruzione, dell’Università e della Ricerca, PON 2014-2020 “Dottorati Innovativi con caratterizzazione industriale”. Sergey Vagin, Andrea Causero, Marius Arz and Thomas Pehl are gratefully acknowledged for fruitful discussions and technical assistance. We thank Katia S. Rodewald for her support with the SEM measurements.

**Conflicts of Interest:** The authors declare no conflict of interest.

## References

1. Plastics Europe. Available online: <https://www.plasticseurope.org/en> (accessed on 24 March 2020).
2. Llevot, A.; Meier, M.A.R. Renewability—A Principle of Utmost Importance! *Green Chem.* **2016**, *18*, 4800–4803. [CrossRef]
3. Mathers, R.T.; Meier, M.A.R. *Green Polymerization Methods: Renewable Starting Materials, Catalysis and Waste Reduction*; Wiley: Hoboken, NJ, USA, 2011; ISBN 978-3-527-63617-4.
4. Kristufek, S.L.; Wacker, K.T.; Tsao, Y.-Y.T.; Su, L.; Wooley, K.L. Monomer Design Strategies to Create Natural Product-Based Polymer Materials. *Nat. Prod. Rep.* **2017**, *34*, 433–459. [CrossRef]
5. Gandini, A. Polymers from Renewable Resources: A Challenge for the Future of Macromolecular Materials. *Macromolecules* **2008**, *41*, 9491–9504. [CrossRef]
6. Meier, M.A.R.; Metzger, J.O.; Schubert, U.S. Plant Oil Renewable Resources as Green Alternatives in Polymer Science. *Chem. Soc. Rev.* **2007**, *36*, 1788–1802. [CrossRef]
7. Della Monica, F.; Kleij, A.W. From Terpenes to Sustainable and Functional Polymers. *Polym. Chem.* **2020**. [CrossRef]
8. Winnacker, M. Pinenes: Abundant and Renewable Building Blocks for a Variety of Sustainable Polymers. *Angew. Chem. Int. Ed.* **2018**, *57*, 14362–14371. [CrossRef] [PubMed]
9. Winnacker, M.; Neumeier, M.; Zhang, X.; Papadakis, C.M.; Rieger, B. Sustainable Chiral Polyamides with High Melting Temperature via Enhanced Anionic Polymerization of a Menthone-Derived Lactam. *Macromol. Rapid Commun.* **2016**, *37*, 851–857. [CrossRef]
10. Winnacker, M.; Lamparelli, D.H.; Capacchione, C.; Gungör, H.H.; Stieglitz, L.; Rodewald, K.S.; Schmidt, M.; Gronauer, T.F. Sustainable Polyesteramides and Copolyamides: Insights into the Copolymerization Behavior of Terpene-Based Lactams. *Macromol. Chem. Phys.* **2020**, *221*, 2000110. [CrossRef]
11. Zhao, J.; Schlaad, H. Synthesis of Terpene-Based Polymers. In *Bio-Synthetic Polymer Conjugates*; Schlaad, H., Ed.; Springer: Berlin/Heidelberg, Germany, 2011; Volume 253, pp. 151–190, ISBN 978-3-642-34349-0.
12. Breitmaier, E. *Terpenes: Flavors, Fragrances, Pharmaca, Pheromones*; WILEY-VCH: Weinheim, Germany, 2006; ISBN 978-3-527-31786-8.
13. Johanson, A.J.; McKennon, F.L.; Goldblatt, L.A. Emulsion Polymerization of Myrcene. *Ind. Eng. Chem.* **1948**, *40*, 500–502. [CrossRef]
14. Runckel, W.J.; Goldblatt, L.A. Inhibition of Myrcene Polymerization during Storage. *Ind. Eng. Chem.* **1946**, *38*, 749–751. [CrossRef]
15. Behr, A.; Johnen, L. Myrcene as a Natural Base Chemical in Sustainable Chemistry: A Critical Review. *ChemSusChem* **2009**, *2*, 1072–1095. [CrossRef] [PubMed]
16. Kim, E.-M.; Eom, J.-H.; Um, Y.; Kim, Y.; Woo, H.M. Microbial Synthesis of Myrcene by Metabolically Engineered *Escherichia coli*. *J. Agric. Food Chem.* **2015**, *63*, 4606–4612. [CrossRef]
17. Lamparelli, D.H.; Paradiso, V.; Monica, F.D.; Proto, A.; Guerra, S.; Giannini, L.; Capacchione, C. Toward More Sustainable Elastomers: Stereoselective Copolymerization of Linear Terpenes with Butadiene. *Macromolecules* **2020**. [CrossRef]
18. Li, W.; Zhao, J.; Zhang, X.; Gong, D. Capability of PN<sup>3</sup>-Type Cobalt Complexes toward Selective (Co-)Polymerization of Myrcene, Butadiene, and Isoprene: Access to Biosourced Polymers. *Ind. Eng. Chem. Res.* **2019**, *58*, 2792–2800. [CrossRef]
19. Lamparelli, D.H.; Paradiso, V.; Capacchione, C. New Elastomeric Materials from Biomass: Stereoselective Polymerization of Linear Terpenes and Their Copolymerization with Butadiene by Using a Cobalt Complex With Phosphane Ligands. *Rubber Chem. Technol.* **2020**, *93*, 605–614. [CrossRef]

20. González-Zapata, J.L.; Enríquez-Medrano, F.J.; López González, H.R.; Revilla-Vázquez, J.; Carrizales, R.M.; Georgouvelas, D.; Valencia, L.; Díaz de León Gómez, R.E. Introducing Random Bio-Terpene Segments to High *Cis* -Polybutadiene: Making Elastomeric Materials More Sustainable. *RSC Adv.* **2020**, *10*, 44096–44102. [CrossRef]
21. Naddeo, M.; Buonerba, A.; Luciano, E.; Grassi, A.; Proto, A.; Capacchione, C. Stereoselective Polymerization of Biosourced Terpenes  $\beta$ -Myrcene and  $\beta$ -Ocimene and Their Copolymerization with Styrene Promoted by Titanium Catalysts. *Polymer* **2017**, *131*, 151–159. [CrossRef]
22. Laur, E.; Welle, A.; Vantomme, A.; Brusson, J.-M.; Carpentier, J.-F.; Kirillov, E. Stereoselective Copolymerization of Styrene with Terpenes Catalyzed by an Ansa-Lanthanidocene Catalyst: Access to New Syndiotactic Polystyrene-Based Materials. *Catalysts* **2017**, *7*, 361. [CrossRef]
23. Sarkar, P.; Bhowmick, A.K. Terpene Based Sustainable Elastomer for Low Rolling Resistance and Improved Wet Grip Application: Synthesis, Characterization and Properties of Poly(Styrene-Co-Myrcene). *ACS Sustain. Chem. Eng.* **2016**, *4*, 5462–5474. [CrossRef]
24. Zhang, J.; Lu, J.; Su, K.; Wang, D.; Han, B. Bio-based B-myrcene-modified Solution-polymerized Styrene–Butadiene Rubber for Improving Carbon Black Dispersion and Wet Skid Resistance. *J. Appl. Polym. Sci.* **2019**, *136*, 48159. [CrossRef]
25. Bolton, J.M.; Hillmyer, M.A.; Hoyer, T.R. Sustainable Thermoplastic Elastomers from Terpene-Derived Monomers. *ACS Macro Lett.* **2014**, *3*, 717–720. [CrossRef]
26. Ren, X.; Guo, F.; Fu, H.; Song, Y.; Li, Y.; Hou, Z. Scandium-Catalyzed Copolymerization of Myrcene with Ethylene and Propylene: Convenient Syntheses of Versatile Functionalized Polyolefins. *Polym. Chem.* **2018**, *9*, 1223–1233. [CrossRef]
27. Trumbo, D.L. Free Radical Copolymerization Behavior of Myrcene: I. Copolymers with Styrene, Methyl Methacrylate or p-Fluorostyrene. *Polym. Bull.* **1993**, *31*, 629–636. [CrossRef]
28. Sarkar, P.; Bhowmick, A.K. Terpene Based Sustainable Methacrylate Copolymer Series by Emulsion Polymerization: Synthesis and Structure-Property Relationship. *J. Polym. Sci. Part A Polym. Chem.* **2017**, *55*, 2639–2649. [CrossRef]
29. Lei, W.; Yang, X.; Qiao, H.; Shi, D.; Wang, R.; Zhang, L. Renewable Resource-Based Elastomer Nanocomposite Derived from Myrcene, Ethanol, Itaconic Acid and Nanosilica: Design, Preparation and Properties. *Eur. Polym. J.* **2018**, *106*, 1–8. [CrossRef]
30. Zhou, C.; Wei, Z.; Lei, X.; Li, Y. Fully Biobased Thermoplastic Elastomers: Synthesis and Characterization of Poly(L-Lactide)-b-Polymyrcene-b-Poly(L-Lactide) Triblock Copolymers. *RSC Adv.* **2016**, *6*, 63508–63514. [CrossRef]
31. Georges, S.; Touré, A.O.; Visseaux, M.; Zinck, P. Coordinative Chain Transfer Copolymerization and Terpolymerization of Conjugated Dienes. *Macromolecules* **2014**, *47*, 4538–4547. [CrossRef]
32. You, F.; Zhai, J.; So, Y.-M.; Shi, X. Rigid Acridane-Based Pincer Supported Rare-Earth Complexes for *Cis*-1,4-Polymerization of 1,3-Conjugated Dienes. *Inorg. Chem.* **2021**, *60*, 1797–1805. [CrossRef] [PubMed]
33. Sahu, P.; Sarkar, P.; Bhowmick, A.K. Design of a Molecular Architecture via a Green Route for an Improved Silica Reinforced Nanocomposite Using Bioresources. *ACS Sustain. Chem. Eng.* **2018**, *6*, 6599–6611. [CrossRef]
34. Bauer, N.; Brunke, J.; Kali, G. Controlled Radical Polymerization of Myrcene in Bulk: Mapping the Effect of Conditions on the System. *ACS Sustain. Chem. Eng.* **2017**, *5*, 10084–10092. [CrossRef]
35. Métafiot, A.; Kanawati, Y.; Gérard, J.-F.; Defoort, B.; Marić, M. Synthesis of  $\beta$ -Myrcene-Based Polymers and Styrene Block and Statistical Copolymers by SG1 Nitroxide-Mediated Controlled Radical Polymerization. *Macromolecules* **2017**, *50*, 3101–3120. [CrossRef]
36. Kalita, U.; Samanta, S.; Banerjee, S.L.; Das, N.C.; Singha, N.K. Biobased Thermoplastic Elastomer Based on an SMS Triblock Copolymer Prepared via RAFT Polymerization in Aqueous Medium. *Macromolecules* **2021**, *54*, 1478–1488. [CrossRef]
37. Hulnik, M.I.; Vasilenko, I.V.; Radchenko, A.V.; Peruch, F.; Ganachaud, F.; Kostjuk, S.V. Aqueous Cationic Homo- and Copolymerizations of  $\beta$ -Myrcene and Styrene: A Green Route toward Terpene-Based Rubbery Polymers. *Polym. Chem.* **2018**, *9*, 5690–5700. [CrossRef]
38. Quirk, R.P.; Huang, T.-L. Alkylolithium-Initiated Polymerization of Myrcene New Block Copolymers of Styrene and Myrcene. In *New Monomers and Polymers*; Culbertson, B.M., Pittman, C.U., Eds.; Springer: Boston, MA, USA, 1984; pp. 329–355, ISBN 978-1-4684-4621-0.
39. Matic, A.; Schlaad, H. Thiol-Ene Photofunctionalization of 1,4-Polymyrcene: Thiol-Ene Photofunctionalization of 1,4-Polymyrcene. *Polym. Int.* **2018**, *67*, 500–505. [CrossRef]
40. Wahlen, C.; Blankenburg, J.; von Tiedemann, P.; Ewald, J.; Sajkiewicz, P.; Müller, A.H.E.; Floudas, G.; Frey, H. Tapered Multiblock Copolymers Based on Farnesene and Styrene: Impact of Biobased Polydiene Architectures on Material Properties. *Macromolecules* **2020**. [CrossRef]
41. Bareuther, J.; Plank, M.; Kuttich, B.; Kraus, T.; Frey, H.; Gallei, M. Temperature Variation Enables the Design of Biobased Block Copolymers via One-Step Anionic Copolymerization. *Macromol. Rapid Commun.* **2020**, 2000513. [CrossRef]
42. Gong, D.; Tang, F.; Xu, Y.; Hu, Z.; Luo, W. Cobalt Catalysed Controlled Copolymerization: An Efficient Approach to Bifunctional Polyisoprene with Enhanced Properties. *Polym. Chem.* **2021**. [CrossRef]
43. Cawse, J.L.; Stanford, J.L.; Still, R.H. Polymers from Renewable Sources: 5. Myrcene-Based Polyols as Rubber-Toughening Agents in Glassy Polyurethanes. *Polymer* **1987**, *28*, 368–374. [CrossRef]
44. Spontak, R.J.; Patel, N.P. Thermoplastic Elastomers: Fundamentals and Applications. *Curr. Opin. Colloid Interface Sci.* **2000**, *5*, 333–340. [CrossRef]
45. Bhowmick, A.K.; Stephens, H.L. (Eds.) *Handbook of Elastomers*, 2nd ed.; M. Dekker: New York, NY, USA, 2001; ISBN 978-0-8247-0383-7.

46. Hou, G.; Tao, W.; Liu, J.; Zhang, X.; Dong, M.; Zhang, L. Effect of the Structural Characteristics of Solution Styrene–Butadiene Rubber on the Properties of Rubber Composites. *J. Appl. Polym. Sci.* **2018**, *135*, 45749. [CrossRef]
47. Lewandowski, L.; Sibbald, M.S.; Johnson, E.; Mallamaci, M.P. New Emulsion SBR Technology: Part I. Raw Polymer Study. *Rubber Chem. Technol.* **2000**, *73*, 731–742. [CrossRef]
48. Obrecht, W.; Lambert, J.-P.; Happ, M.; Oppenheimer-Stix, C.; Dunn, J.; Krüger, R. Rubber, 4. Emulsion Rubbers. In *Ullmann's Encyclopedia of Industrial Chemistry*; Wiley-VCH Verlag GmbH & Co. KGaA: Weinheim, Germany, 2011; pp. 623–646, ISBN 978-3-527-30673-2.
49. Brandt, H.-D.; Nentwig, W.; Rooney, N.; LaFlair, R.T.; Wolf, U.U.; Duffy, J.; Puskas, J.E.; Kaszas, G.; Drewitt, M.; Glander, S. Rubber, 5. Solution Rubbers. In *Ullmann's Encyclopedia of Industrial Chemistry*; Wiley-VCH Verlag GmbH & Co. KGaA: Weinheim, Germany, 2011; pp. 649–677, ISBN 978-3-527-30673-2.
50. Hadjichristidis, N.; Hirao, A. (Eds.) *Anionic Polymerization: Principles, Practice, Strength, Consequences and Applications*; Springer Japan: Tokyo, Japan, 2015; ISBN 978-4-431-54185-1.
51. Brown, H.C.; Schlesinger, H.I.; Sheft, I.; Ritter, D.M. Addition Compounds of Alkali Metal Hydrides. Sodium Trimethoxyborohydride and Related Compounds. *J. Am. Chem. Soc.* **1953**, *75*, 192–195. [CrossRef]
52. Ashby, E.C.; Arnott, R.; Srivastava, S. Reactions of Alkali Metal Hydrides with Magnesium Alkyls. Preparation of MMgR<sub>2</sub>H and MMg<sub>2</sub>R<sub>4</sub>H Compounds. *Inorg. Chem.* **1975**, *14*, 2422–2426. [CrossRef]
53. Kubas, G.J.; Shriver, D.F. Nature of Dialkyl- and Diarylzinc Hydride Complexes. *J. Am. Chem. Soc.* **1970**, *92*, 1949–1954. [CrossRef]
54. Ziegler, K.; Köster, R.; Lehmkuhl, H.; Reinert, K. Metallorganische Verbindungen, XXX Neue Komplexverbindungen der Aluminiumalkyle. *Justus Liebigs Ann. Chem.* **1960**, *629*, 33–49. [CrossRef]
55. Needles, H.L. Sodium Hydride-Initiated Polymerizations of Vinyl Monomers in Aprotic Solvents. *J. Polym. Sci. Part A-1 Polym. Chem.* **1969**, *7*, 1437–1445. [CrossRef]
56. Carlotti, S.; Menoret, S.; Desbois, P.; Nissner, N.; Warzelhan, V.; Deffieux, A. Sodium Hydride/Trialkylaluminum Complexes for the Controlled Anionic Polymerization of Styrene at High Temperature. *Macromol. Rapid Commun.* **2006**, *27*, 905–909. [CrossRef]
57. Carlotti, S.; Desbois, P.; Warzelhan, V.; Deffieux, A. Retarded Anionic Polymerization (RAP) of Styrene and Dienes. *Polymer* **2009**, *50*, 3057–3067. [CrossRef]
58. Carlotti, S.; Ménoret, S.; Barabanova, A.; Desbois, P.; Deffieux, A. Sodium Hydride as a New Initiator for the Retarded Anionic Polymerization (RAP) of Styrene. *Polymer* **2007**, *48*, 4322–4327. [CrossRef]
59. Newmark, R.A.; Majumdar, R.N. <sup>13</sup>C-NMR Spectra of Cis-Polymyrcene and Cis-Polyfarnesene. *J. Polym. Sci. A Polym. Chem.* **1988**, *26*, 71–77. [CrossRef]
60. Grune, E.; Bareuther, J.; Blankenburg, J.; Appold, M.; Shaw, L.; Müller, A.H.E.; Floudas, G.; Hutchings, L.R.; Gallei, M.; Frey, H. Towards Bio-Based Tapered Block Copolymers: The Behaviour of Myrcene in the Statistical Anionic Copolymerisation. *Polym. Chem.* **2019**, *10*, 1213–1220. [CrossRef]
61. Glatzel, J.; Noack, S.; Schanzenbach, D.; Schlaad, H. Anionic Polymerization of Dienes in 'Green' Solvents. *Polym. Int.* **2020**, *70*, 181–184. [CrossRef]
62. Zhang, S.; Han, L.; Ma, H.; Liu, P.; Shen, H.; Lei, L.; Li, C.; Yang, L.; Li, Y. Investigation on Synthesis and Application Performance of Elastomers with Biogenic Myrcene. *Ind. Eng. Chem. Res.* **2019**, *58*, 12845–12853. [CrossRef]
63. Sarkar, P.; Bhowmick, A.K. Terpene-Based Sustainable Elastomers: Vulcanization and Reinforcement Characteristics. *Ind. Eng. Chem. Res.* **2018**, *57*, 5197–5206. [CrossRef]
64. Ishihara, N.; Seimiya, T.; Kuramoto, M.; Uoi, M. Crystalline Syndiotactic Polystyrene. *Macromolecules* **1986**, *19*, 2464–2465. [CrossRef]
65. Labbé, A.; Carlotti, S.; Shcheglova, L.; Desbois, P.; Deffieux, A. Dienes Polymerization in the Presence of Metal Hydrides and Triethylaluminum. *Polymer* **2006**, *47*, 3734–3739. [CrossRef]
66. Liu, B.; Liu, D.; Li, S.; Sun, G.; Cui, D. High Trans-1,4 (Co)Polymerization of  $\beta$ -Myrcene and Isoprene with an Iminophosphonamide Lanthanum Catalyst. *Chin. J. Polym. Sci.* **2016**, *34*, 104–110. [CrossRef]
67. Liu, B.; Li, L.; Sun, G.; Liu, D.; Li, S.; Cui, D. Iselective 3,4-(Co)Polymerization of Bio-Renewable Myrcene Using NSN-Ligated Rare-Earth Metal Precursor: An Approach to a New Elastomer. *Chem. Commun.* **2015**, *51*, 1039–1041. [CrossRef] [PubMed]
68. Jia, X.; Zhang, X.; Gong, D. 1,2 Enriched polymerization of isoprene by cobalt complex carrying aminophosphory fused (PN<sup>3</sup>) ligand. *J. Polym. Sci. Part A: Polym. Chem.* **2018**, *56*, 2286–2293. [CrossRef]
69. Ni, H.; Wang, X. Surface Wetting Behavior of the Poly(Styrene-*b*-Isoprene-*b*-Styrene) Triblock Copolymer with Different Chemical Structures of the Polyisoprene Block Chain. *Surf. Sci.* **2007**, *601*, 1560–1565. [CrossRef]
70. Gan, Q.; Xu, Y.; Huang, W.; Luo, W.; Hu, Z.; Tang, F.; Jia, X.; Gong, D. Utilization of Bio-sourced Myrcene for Efficient Preparation of Highly Cis -1,4 Regular Elastomer via a Neodymium Catalyzed Copolymerization Strategy. *Polym. Int.* **2020**. [CrossRef]



## Article

# Curing Behavior and Thermomechanical Performance of Bioepoxy Resin Synthesized from Vanillyl Alcohol: Effects of the Curing Agent

Zhenyu Wang <sup>1,2,3</sup> , Pitchaimari Gnanasekar <sup>3</sup> , Sandeep Sudhakaran Nair <sup>3,4</sup>, Songlin Yi <sup>2,\*</sup> and Ning Yan <sup>3,4,\*</sup>

- <sup>1</sup> Research Institute of Wood Industry, Chinese Academy of Forestry, Beijing 100091, China; wangzhenyu1992@126.com
- <sup>2</sup> Beijing Key Laboratory of Wood Science and Engineering, Beijing Forestry University, Beijing 100083, China
- <sup>3</sup> Department of Chemical Engineering and Applied Chemistry, University of Toronto, Toronto, ON M5S 3E5, Canada; mari.gnanasekar@utoronto.ca (P.G.); sandeepnair217@gmail.com (S.S.N.)
- <sup>4</sup> John H. Daniels Faculty of Architecture, Landscape, and Design, University of Toronto, Toronto, ON M5S 2J5, Canada
- \* Correspondence: ysonglin@126.com (S.Y.); ning.yan@utoronto.ca (N.Y.)

**Abstract:** In order to reduce the dependency of resin synthesis on petroleum resources, vanillyl alcohol which is a renewable material that can be produced from lignin has been used to synthesize bioepoxy resin. Although it has been widely reported that the curing reaction and properties of the cured epoxies can be greatly affected by the molecular structure of the curing agents, the exact influence remains unknown for bioepoxies. In this study, four aliphatic amines with different molecular structures and amine functionalities, namely triethylenetetramine (TETA), Tris(2-aminoethyl)amine (TREN), diethylenetriamine (DETA), and ethylenediamine (EDA), were used to cure the synthesized vanillyl alcohol-based bioepoxy resin (VE). The curing reaction of VE and the physicochemical properties, especially the thermomechanical performance of the cured bioepoxies with different amine functionalities, were systematically investigated and compared using different characterization methods, such as DSC, ATR-FTIR, TGA, DMA, and tensile testing, etc. Despite a higher curing temperature needed in the VE-TETA resin system, the cured VE-TETA epoxy showed a better chemical resistance, particularly acidic resistance, as well as a lower swelling ratio than the others. The higher thermal decomposition temperature, storage modulus, and relaxation temperature of VE-TETA epoxy indicated its superior thermal stability and thermomechanical properties. Moreover, the tensile strength of VE cured by TETA was 1.4~2.6 times higher than those of other curing systems. In conclusion, TETA was shown to be the optimum epoxy curing agent for vanillyl alcohol-based bioepoxy resin.

**Keywords:** bio-based epoxy resin; vanillyl alcohol; aliphatic amines; curing system; thermomechanical properties

**Citation:** Wang, Z.; Gnanasekar, P.; Nair, S.S.; Yi, S.; Yan, N. Curing Behavior and Thermomechanical Performance of Bioepoxy Resin Synthesized from Vanillyl Alcohol: Effects of the Curing Agent. *Polymers* **2021**, *13*, 2891. <https://doi.org/10.3390/polym13172891>

Academic Editor: Emin Bayraktar

Received: 2 August 2021

Accepted: 22 August 2021

Published: 27 August 2021

**Publisher's Note:** MDPI stays neutral with regard to jurisdictional claims in published maps and institutional affiliations.



**Copyright:** © 2021 by the authors. Licensee MDPI, Basel, Switzerland. This article is an open access article distributed under the terms and conditions of the Creative Commons Attribution (CC BY) license (<https://creativecommons.org/licenses/by/4.0/>).

## 1. Introduction

Nowadays, epoxy resin has become an indispensable thermosetting resin for many industrial fields and can be widely used as high-performance coatings, adhesives, and composites, etc., because of its premium physicochemical properties and excellent compatibility with most materials [1]. However, current epoxy resin production is heavily dependent on petroleum-based resources and employs a great amount of reprotoxic bisphenol A which is used as a chemical precursor for more than 80% of the epoxy production worldwide [2,3]. Taking into account the decline in petroleum resources and the rise in environmental awareness, the existing mode of epoxy resin production is inconsistent with the concept of green and sustainable development. Therefore, there is a growing interest in utilizing biobased biomolecules (especially nonharmful monomers containing aromatic bifunctionalities) to produce epoxy polymers.



In recent years, bioepoxies synthesized from natural renewable resources, such as plant oils, rosins, lignin, and lignin derivatives, have been explored [4–9]. Among these biomolecules, lignin, which makes up around 30% of woody biomass, was mostly used as a low-grade fuel by the traditional pulp and paper-making industries. Meanwhile, lignin and lignin derivatives have been regarded as a highly promising raw material for epoxy synthesis, due not only to their wide varieties of sources and excellent commercialization promises, but also to their aromatic and rigid molecular structures which are conducive for obtaining high-performance epoxies [10–13]. However, the direct utilization of lignin in epoxy production is hindered by its large variability and complex chemical structures [14]. As a result, some well-defined and monoaromatic platform chemicals that can be derived from lignin, such as vanillin and vanillin derivatives, have gained significant attention. The interest in vanillin and vanillin derivatives is further fueled by the commercialization of the lignin-to-vanillin process [15–18]. Vanillyl alcohol is a main component of lignin-derived aromatic diols by the reduction of vanillin. Because of the presence of a difunctional hydroxyl group (–OH) in the vanillyl alcohol, it has been used as an attractive chemical platform for the synthesis of renewable epoxies. It has been reported that vanillyl alcohol can be converted into difunctional epoxy monomers by glycidylation and the resulting epoxy resins show satisfying performance and yields [11,19].

For epoxies, a curing agent is required to cure the thermoset resin and to build the desired cross-linking networks that determine the final properties of the cured resins. There are a variety of curing agents, including amines, amides, acid anhydrides, polyphenols, etc., that are commonly used [20]. Currently, amine-based curing agents, as one of the basic types of curing agents, have gained more popularity than other types of curing agents in many fields [21,22]. In particular, aliphatic amines possessing high reactivity and low viscosity at room temperature are widely used to cure epoxy resins [23]. During the formation of cross-linking networks in the curing reaction, a number of parameters, such as curing time, curing temperature, the structure of epoxy, and the curing agent, are known to play a crucial role [21,24–26]. In previous studies, the effects of curing conditions on the conventional epoxy systems have been well investigated [27–31]. Thus, there exists a significant body of knowledge concerning how different types of curing agents affect the structure and property relationship for conventional petroleum-derived epoxy resins. These fundamental understandings contribute greatly to the optimization of epoxy resin formulations targeting specific applications. However, no systematic study has looked into the influence of the molecular structure of the curing agent on the curing behavior and performance of the vanillyl alcohol-based bioepoxy resins. Vanillyl alcohol-based bioepoxies have different molecular structures from the conventional petroleum-based bisphenol A type of epoxy resins, and the crosslinker plays an important role in determining the cross-linking structure of the cured resin. In order to better design these bioepoxy systems for broad adoption by the industry, a thorough understanding of how the structure–property relationship of this type of epoxy resin depends on the structure of the crosslinker is highly necessary.

Therefore, in this study, four common aliphatic amines with a varied quantity of amino groups and different molecular structures (linear vs. branched) were chosen as curing agents to react with a bioepoxy resin synthesized from vanillyl alcohol. The curing agents included triethylenetetramine (TETA), Tris(2-aminoethyl)amine (TREN), diethylenetriamine (DETA), and ethylenediamine (EDA). The comprehensive characteristics of the bioepoxy resin systems, such as curing behavior, chemical structure, chemical resistance, thermal stability, thermomechanical properties, tensile performance, etc., were examined respectively using various analysis techniques including differential scanning calorimetry (DSC), attenuated total reflectance–Fourier transform infrared spectroscopy (ATR–FTIR), thermogravimetric analysis (TGA), dynamic mechanical analysis (DMA), and universal mechanical tester. By investigating the effect of the curing agent on the physicochemical properties of the cured vanillyl alcohol-based bioepoxies, the main focus of the present work is to elucidate the interactions between the bioepoxy and the curing agent to aid the

optimization of the bioepoxy systems to promote industrial applications of these novel bioepoxy resins.

## 2. Materials and Methods

### 2.1. Materials

The chemicals for synthesizing and curing the vanillyl alcohol-based bioepoxy resin (VE) were supplied by Sigma Aldrich or Fisher Chemical. Benzyltriethylammonium chloride (TEBAC, 99%) was selected as the phase transfer catalyst in the etherification reaction between vanillyl alcohol (98%) and epichlorohydrin (99%). The sodium hydroxide (99.1%) was used to initiate the ring-closing reaction of the chlorohydrin ether intermediate to reform oxirane rings in the resulting bioepoxy resin. The structure and molecular weight of the curing agents, namely TETA (97%), TREN (96%), DETA (99%), and EDA (99%), are presented in Figure 1. All the reagents mentioned above were used as received.

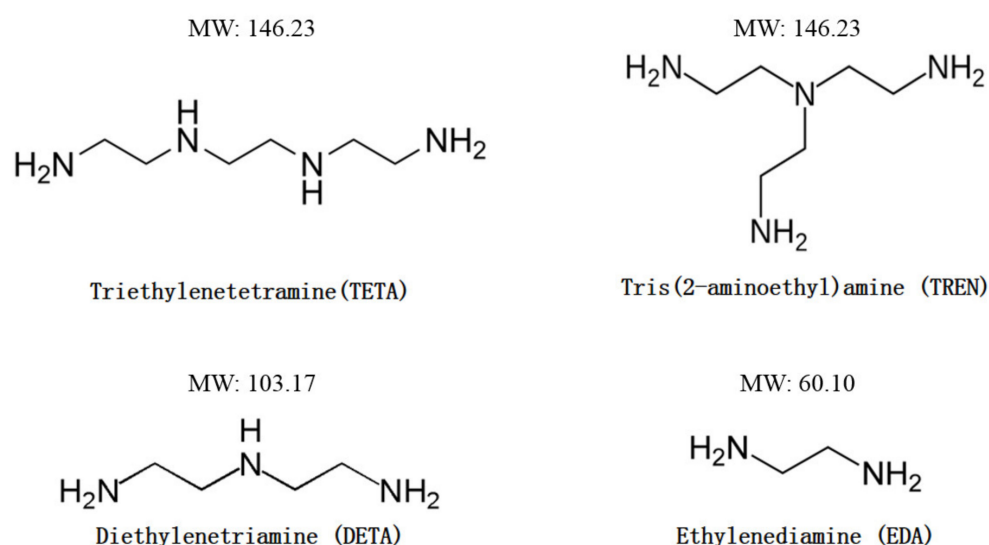


**Figure 1.** Structures of four different aliphatic amine curing agents used in this study.

### 2.2. Synthesis of Vanillyl Alcohol-Based Bioepoxy Resin

The synthesis process of vanillyl alcohol-based bioepoxy resin was carried out by the following procedure. A three-neck round bottom flask equipped with a mechanical stirrer was charged with vanillyl alcohol, TEBAC, and epichlorohydrin in the molar ratio of 1: 1: 10. After 1 h mechanical stirring at room temperature to assure the complete dissolution of reactants, the mixture was gradually heated up to 80 °C and was left under stirring for 0.5 h. Then, the flask was cooled down to room temperature again. For each mole of vanillyl alcohol involved in the reaction system, 0.1 mol TEBAC and 5 mol sodium hydroxide (800 mL aq) were added into the flask, and left to constant stirring for 0.5 h. Afterwards, the ethyl acetate and distilled water were added into the resulting solution in the volume ratio of 1:1. Subsequent to another stirring for several minutes, the two-phase mixture was left to stand for 1 h to separate into two layers. After the completion of separation, the top organic phase layer containing bioepoxy resin was collected and then washed with distilled water. Magnesium sulfate, anhydrous, was used to dry the organic layer, and the precipitate was filtered. The final bioepoxy resin was obtained by evaporating the filtrate on a rotary evaporator to remove the ethyl acetate as well as excess epichlorohydrin in the organic layer. The synthesis approach of the vanillyl alcohol-based bioepoxy resin is shown in Figure 2. The structural information of the synthesized bioepoxy resin has been provided in our previous study [32].

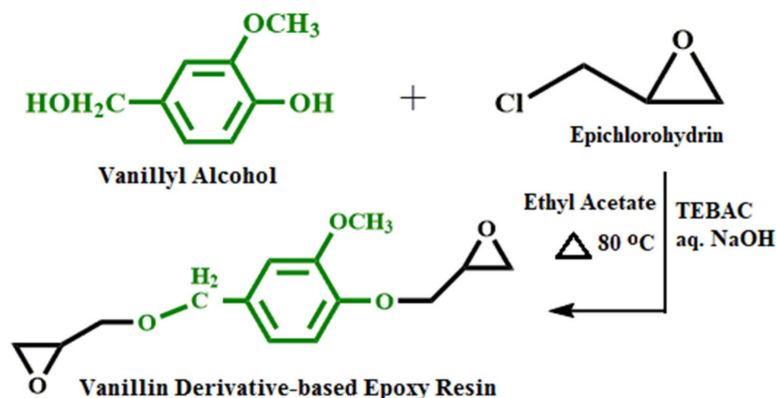


**Figure 2.** Reaction scheme of vanillyl alcohol-based bioepoxy resin synthesis.

### 2.3. Curing Process of the Bioepoxy Resin

Four aliphatic amines with different structures and functionalities were selected to cure the vanillyl alcohol-based bioepoxy resin. Owing to each of the active hydrogens in aliphatic amines supposedly only consuming one epoxide group, the curing agents were added into VE stoichiometrically, and the weight ratios of VE to each curing agent are shown in Table 1. The samples cured with different curing agents were labelled as VE-TETA, VE-TREN, VE-DETA, and VE-EDA, respectively. In order to decrease the viscosity of VE and achieve its full mixing with the curing agents, acetone of the same weight as VE was used as a diluent. After mixing, the mixture of VE and curing agent was magnetically stirred for 4 h, and then the acetone was evaporated by standing the mixture in a fume hood overnight. A drying oven was used to accomplish the curing process as per the following schedule: 0.5 h  $-60\text{ }^{\circ}\text{C}$ , 0.5 h  $-80\text{ }^{\circ}\text{C}$ , 0.5 h  $-100\text{ }^{\circ}\text{C}$ , 0.5 h  $-135\text{ }^{\circ}\text{C}$ , and 1 h  $-180\text{ }^{\circ}\text{C}$ . Prior to further testing, the solid bioepoxies were molded into the required shape and size according to the experimental methods described here.

**Table 1.** Weight ratios of vanillyl alcohol-based epoxy resin to curing agents for different curing systems.

| Curing System | VE/Curing Agent Ratio |
|---------------|-----------------------|
| VE-TETA       | 100.00/18.33          |
| VE-TREN       | 100.00/18.33          |
| VE-DETA       | 100.00/15.51          |
| VE-EDA        | 100.00/11.30          |

### 2.4. DSC Analysis

The curing process of the vanillyl alcohol-based bioepoxy resin with different curing agents was recorded on a Q100 DSC (TA Instruments, USA) analyzer. A high-volume pan was used to seal around 7 mg of VE-curing agent mixtures in the measurement. The experiment was carried out under a nitrogen atmosphere, and the curing temperature was increased from 25 to 250  $^{\circ}\text{C}$  at a heating rate of 10  $^{\circ}\text{C}/\text{min}$ .

### 2.5. ATR-FTIR Analysis

A Nicolet iS50 FTIR (Thermo Fisher Scientific, USA) spectrometer was applied to identify the chemical structure of vanillyl alcohol-based bioepoxy resin cured with different curing agents. Slices of different cured samples with the dimension of nearly 10 mm  $\times$  10 mm  $\times$  0.6 mm were collected to carry out the ATR-FTIR analysis. The spectrum of each curing system was measured in the wavenumber range of 4000 to 400  $\text{cm}^{-1}$  with 64 scans and a resolution of 4  $\text{cm}^{-1}$ .

### 2.6. Swelling and Chemical Resistance Testing

The swelling and chemical resistance studies of different bioepoxy systems were performed on small pieces of cured resin with the same dimension of nearly 10 mm × 10 mm × 0.6 mm. Samples were immersed in sealed vials containing 10 mL of different solvents for 168 h at room temperature. Toluene was used in the testing of swelling ratio and gel content (resistance to organic solvent) [33]. NaOH (3 M) and HCl (3 M) aqueous solution were used to examine the samples' resistance to alkaline and acid medium, respectively. The weights of the dried samples before and after immersion were measured to calculate the mass changes. The samples in the swelling tests were weighed every 24 h to obtain the plots for the swelling ratios. All tests were conducted in triplicate to determine a mean mass change.

### 2.7. Thermogravimetric Analysis

The thermal decomposition behavior of all cured VE samples was investigated with TGA. The measurement was carried out using a Q500 (TA Instruments, USA) thermogravimetric analyzer. Small pieces of the samples of around 10 mg in all experiments were placed in a crucible with a dynamic scan to obtain the thermogravimetric profiles. The temperature increased from room temperature to 600 °C at the heating rate of 10 °C/min with a 60 mL/min nitrogen flow.

### 2.8. Dynamic Mechanical Analysis

The Q800 dynamic mechanical analyzer (TA Instruments, USA) was applied to study thermomechanical responses of the cured resins by operating in a multi-frequency-strain mode. The measurement frequency and oscillation amplitude were set to 1 Hz and 15 µm, respectively. Before the measurement, different cured resin samples were cut into rectangular bars with a dimension of approximately 15 mm × 4 mm × 0.6 mm, and fixed on the clamp. With a heating rate of 3 °C/min, the storage modulus and loss tangent were collected from room temperature to 180 °C.

### 2.9. Tensile Testing

The tensile testing of the cured resin samples was conducted on an Instron 3367 universal testing machine equipped with a 2 kN load cell. After being machined into dog-bone geometry according to ASTM D 638–Type V specifications (63.50 mm in length and 9.53 mm in width), the specimens were mounted on the tester by the clamping jaws with a span of 25 mm. The crosshead speed in testing was set to 10 mm/min<sup>−1</sup>. Five specimens of each VE-curing agent system were measured to obtain the average value.

## 3. Results and Discussion

### 3.1. Curing Behavior of the Synthesized Bioepoxies

In Figure 3, the DSC curves of the heat-flow data versus temperature were plotted to show the curing process of the vanillyl alcohol-based bioepoxy resin with different curing agents. From the two obvious peaks appearing in the curves of every sample, the different polyaddition stages in the curing process can be observed, which were possibly attributable to the reaction between the epoxy group with primary amines and secondary amines. It has been reported that the two types of amine groups coexist during the curing process but differ in reactivity. Primary amines are easier and faster to react than secondary amines [34–36]. In this study, all the reactants were stoichiometrically mixed with each other, thus every hydrogen atom in the two different amine groups was expected to react with one epoxide group. In theory, the reaction of partial hydrogen atoms linked to primary amine would first occur and also form more secondary amines, then the original and/or produced secondary amines would further react until all epoxy groups were exhausted. Consequently, the first peaks of DSC curves at low temperature were mainly corresponding to the reaction between epoxy and highly reactive primary amines, while the second ones were related to the reaction of secondary amines. Furthermore, compared with the second

peak at a higher temperature in the same DSC curve, the first peak usually exhibited a higher reaction heat, which indicates a higher reaction intensity in the early curing stage. This may be also the result of the higher reactivity of primary amines, as well as the lower steric and diffusional restrictions before the completion of a relatively tight cross-linking in the second curing stage.

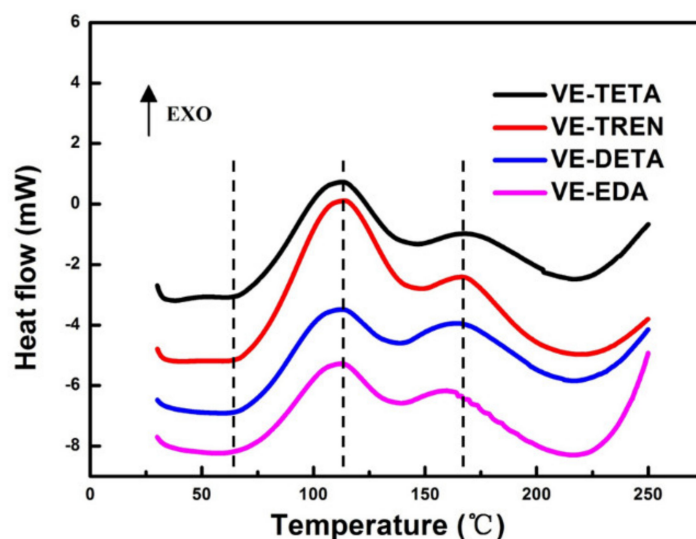


**Figure 3.** DSC curves of vanillyl alcohol-based epoxy with various curing agents.

According to the characteristics of the DSC thermogram in Figure 3, some important points in the curing process, including where the reaction began, peaked, and finished, were determined. The corresponding temperatures were represented by  $T_i$ ,  $T_p$ , and  $T_f$ , respectively, in Table 2. Among the samples cured by the four different amines, the two-stage curing process was not significantly affected by the type of curing agents. However, VE-EDA showed lower initial and peak temperatures than the others. This probably resulted from the higher proportion of primary amines in EDA and the lower molecular weight of EDA, which were both in favor of the reactions occurring at relatively low temperatures [36,37]. This trend was more obvious in the second peak, which also indicated the small molecules of EDA were easier to move and react with VE when parts of the cross-linking network had started to form. In contrast, with the increase of the molecular weight, the  $T_i$  and  $T_p$  in VE-TETA and VE-TREN rose remarkably, suggesting a higher energy consumption than VE-EDA during the curing process.

**Table 2.** Characteristic temperatures from DSC studies of the curing reactions.

|         | $T_i$ (°C) | $T_{p1}$ (°C) | $T_{p2}$ (°C) | $T_f$ (°C) |
|---------|------------|---------------|---------------|------------|
| VE-TETA | 64.42      | 112.71        | 167.30        | 214.60     |
| VE-TREN | 64.89      | 113.75        | 167.84        | 214.58     |
| VE-DETA | 61.81      | 112.18        | 165.20        | 214.04     |
| VE-EDA  | 60.75      | 110.58        | 161.05        | 212.98     |

### 3.2. Chemical Structure and Chemical Resistance of the Cured Bioepoxies

From the ATR-FTIR tests of the cured bioepoxies, the chemical structure of the different VE-curing agent systems was obtained in Figure 4. All cured resins with different curing agents showed a similar spectrum, mainly because all of them were cured by aliphatic amines and the discrepancies in functional groups were limited. It is noteworthy that, after curing, no characteristic peak of epoxide group was found at the wavenumber of  $912\text{ cm}^{-1}$ , which confirmed that most of the oxirane rings were depleted by the curing reaction [38]. However, considering the stoichiometric amount of reactants used in the

curing process, it is hard to guarantee the full contact of every epoxy group with active hydrogens in amines as a result of the steric and diffusional restrictions. Consequently, apart from the reaction between bioepoxies and curing agents, as the curing temperature increased up to 180 °C, it was likely that some epoxide groups were consumed by the hydroxyl–epoxide reaction and/or epoxy homopolymerization [39].

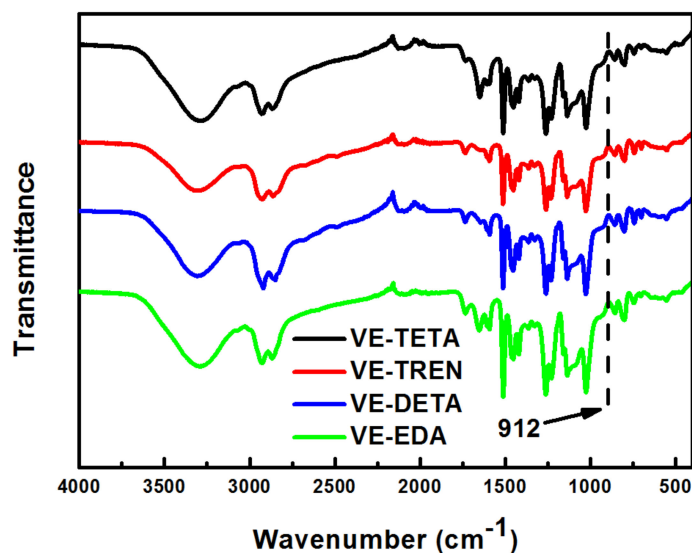


**Figure 4.** ATR–FTIR analysis of vanillyl alcohol–based bioepoxy resin cured by various curing agents.

Additionally, the gel content of the cured bioepoxy resin was also detected to evaluate the degree of the curing process and the resistance of the cured resin to organic solvents. As shown in Figure 5, the gel contents of all cured samples in toluene were more than 99%, indicating that the reactants in the curing process were nearly completely incorporated into the polymer networks and the curing degree of the samples cured with different curing agents was almost the same [40]. Moreover, the resistance of the cured resins to the acidic and alkaline medium was examined. The results are also presented in Figure 5. Immersed in NaOH (3 M) and HCl (3 M) solutions for 168 h, vanillyl alcohol–based bioepoxy resin showed a better resistance to alkaline medium than acidic medium. All the cured systems had a similar weight reduction magnitude of around 7% in NaOH solution. Although there were some changes in the remaining weight between the different curing systems, the differences were small and insignificant. In HCl solution, the weight loss of the cured resins surged to near 13%, except for the VE–TETA samples which exhibited a much higher remaining weight (92.35%) than the others. The better chemical resistance in VE–TETA may be related to a higher cross–linked network and the structural characteristics of TETA [41,42].

In addition to organic, acidic, and alkaline resistance, the swelling ratios of the cured epoxies were determined as a function of immersion time in toluene in Figure 6. Initially (before 24 h), all the samples showed a relatively quick increase in swelling, as a result of the penetration of the solvent into structural defects and cavities on the surface of the samples [42]. Then, a slower and continuous growth of swelling was observed in each sample, indicating the gradual immersion of toluene into the molecule intervals in the network structures. When comparing the differences between the different curing agent systems, after 168 h immersion, the VE–EDA sample showed the highest swelling ratio, while the lowest value could be found for the VE–TETA sample, probably because of a more stable network structure with a stronger crosslinking in the VE–TETA sample.

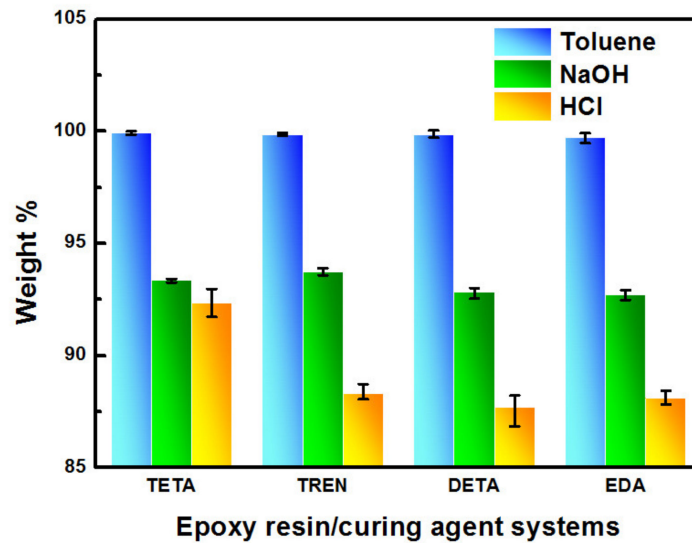


Figure 5. Gel content and acidic and alkaline resistance of the cured bioepoxies with various curing agents.

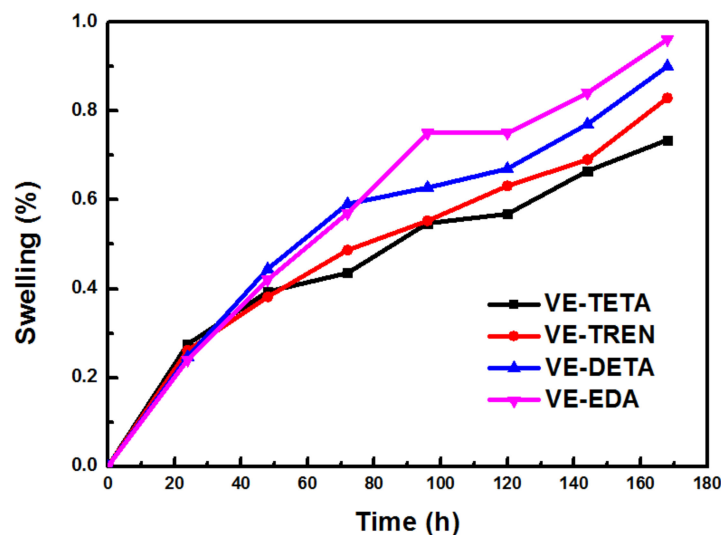


Figure 6. Swelling behaviors of the different vanillyl alcohol-based bioepoxy resin systems.

### 3.3. Thermal Properties of the Cured Bioepoxies

The thermal property testing of the resins cured with different curing agents was conducted by TGA. On the basis of the thermogravimetric (TG) and differential thermogravimetric (DTG) curves shown in Figure 7, the main degradation stage of all samples was concentrated in the 200–400 °C temperature range, and the weight loss rate peaks were generally observed at around 310 °C, accompanied by a high-temperature shoulder peak. As reported by the study of Wu et al., this result of two weight-loss peaks in the DTG curves was largely caused by the rupture of different segments in the polymer networks [43]. The degradation temperatures at 5% ( $T_{5\%}$ ), 10% ( $T_{10\%}$ ), and 50% ( $T_{50\%}$ ) weight loss are depicted in Table 3, and  $T_p$  represents the temperature at which the weight loss rate reached the maximum. Comparing the systems cured with different curing agents, the degradation of VE-EDA illustrated the lowest onset temperature (217.17 °C), indicating a relatively low thermal stability [44]. With the increase of amine groups and active hydrogens in curing agents, the thermal degradation onset temperature of the cured bioepoxies rose gradually, reaching 231.59 °C for VE-DETA, 233.16 °C and 233.24 °C for VE-TETA and VE-TREN, respectively. The rise in initial degradation temperature was mainly due to

the formation of tighter cross-linking networks in the cured resin [45]. Interestingly, the final residue value at 600 °C showed the opposite results to the onset temperature, which was similar to what was reported by Gowda and Mahendra [46]. As the temperature increased during the thermal degradation process, the cross-linked network disintegrated severely, while the basic structure of the polymers played a crucial role in preventing further weight loss, especially at high temperatures. Thus, the higher percentage of thermally stable aromatic structure in the VE-EDA system than others might be the reason for the obvious degradation rate decline in the DTG curves and the highest residue content at 600 °C in Table 3 [47,48]. However, it is worth noting that VE-TETA and VE-TREN were found to have better thermal properties since they showed a relatively higher degradation temperature in almost every stage of the degradation process among all the curing systems.

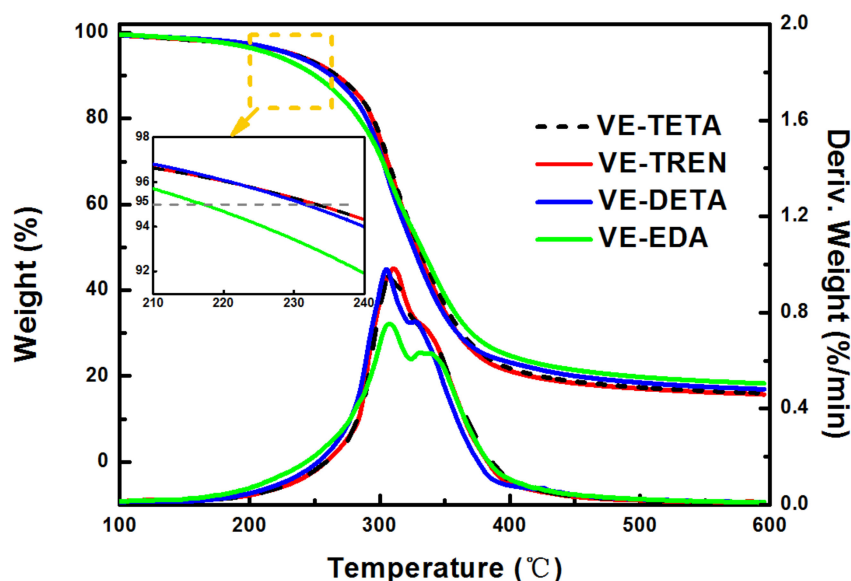


Figure 7. TGA curves of vanillyl alcohol-based bioepoxy resin cured by various curing agents.

Table 3. Thermal properties of vanillyl alcohol-based bioepoxy resin cured by various curing agents.

|         | $T_{5\%}$ (°C) | $T_{10\%}$ (°C) | $T_{50\%}$ (°C) | $T_p$ (°C) | Final Residue (%) at 600 °C |
|---------|----------------|-----------------|-----------------|------------|-----------------------------|
| VE-TETA | 233.16         | 267.05          | 330.17          | 309.13     | 16.04                       |
| VE-TREN | 233.24         | 267.05          | 328.38          | 310.45     | 15.73                       |
| VE-DETA | 231.59         | 262.66          | 325.80          | 305.06     | 16.95                       |
| VE-EDA  | 217.17         | 250.27          | 331.76          | 307.47     | 18.29                       |

### 3.4. Dynamic Mechanical Analysis of the Cured Bioepoxies

The thermomechanical features of the cured bioepoxy networks with different curing agents were determined by DMA. In Figure 8a,b, the storage modulus ( $E'$ ) and loss factors ( $\tan \delta$ ) are respectively plotted versus temperature. Correspondingly, the values relevant to the thermomechanical properties of the cured bioepoxies are presented in Table 4. The  $E'$  represents the rigidity of the material, which was the highest for VE-TETA (3762.48 MPa) and the lowest for VE-EDA (3303.52 MPa). This was most likely attributed to the higher cross-linking density in VE-TETA networks than that in VE-EDA [45,49]. However, the  $E'$  of VE-TREN was also significantly lower than that of VE-TETA, which seemed to be inconsistent with what was found for conventional epoxy resin systems [23]. This phenomenon was probably associated with the side chain of TREN molecules and the damping of the cured epoxy in subglass relaxation.



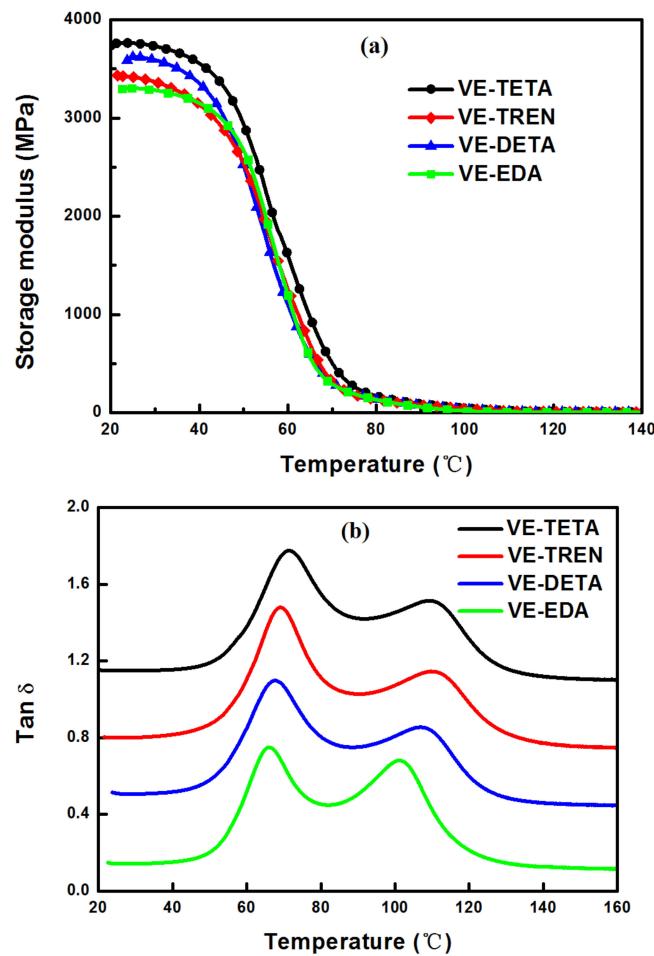


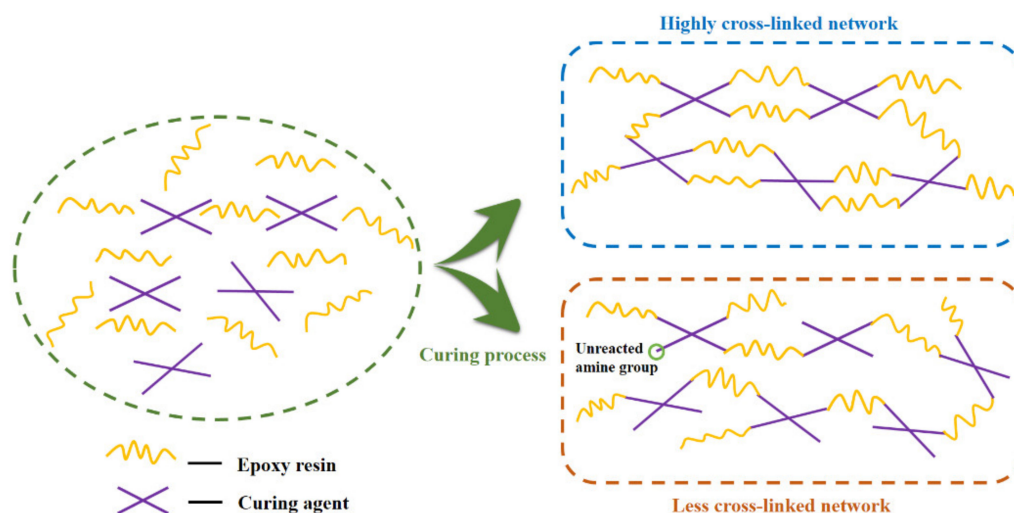
Figure 8. Storage modulus (a) and  $\tan \delta$  (b) curves of cured bioepoxies with different curing agents.

Table 4. Thermomechanical properties of cured bioepoxies.

|         | $E'$ (MPa) | $T_{\alpha 1}$ (°C) | $\tan \delta_1$ | $T_{\alpha 2}$ (°C) | $\tan \delta_2$ |
|---------|------------|---------------------|-----------------|---------------------|-----------------|
| VE-TETA | 3762.48    | 71.37               | 0.69            | 109.21              | 0.43            |
| VE-TREN | 3425.32    | 69.07               | 0.75            | 110.49              | 0.42            |
| VE-DETA | 3619.76    | 67.63               | 0.66            | 107.12              | 0.42            |
| VE-EDA  | 3303.52    | 66.11               | 0.67            | 101.07              | 0.60            |

In Figure 8b, the temperatures corresponding to  $\tan \delta$  peaks were used to determine the relaxation temperatures ( $T_{\alpha}$ ). For all bioepoxy samples, there were two peaks found at around 70 °C and 105 °C, respectively in the  $\tan \delta$  curves, which indicated a heterogeneous polymer network [50,51]. This could be explained by two different regions present in the cured resins, namely the tighter regions with a high cross-linking degree as well as the looser regions with a relatively low cross-linking degree [52]. As discussed in the DSC section, the curing process of all VE-curing agent systems included two stages. During the first stage, highly reactive primary amines took the lead in reacting with epoxide groups, and a looser cross-linking network was built, owing to the incomplete reaction of the curing agents. Since the molecules were much easier to move in loose networks with fewer constraints, the crosslinks formed in this stage were capable of dissipating more energy by distortion [12,23]. Thus, in Figure 8b, the characteristic peak with low  $T_{\alpha}$  corresponded to the looser regions in the whole cross-linked networks and displayed a high  $\tan \delta$ . As for the latter stage, more secondary amines, which had been reported to construct a stronger crosslinked network than the primary amines, started to be involved in the curing

reaction [36]. The tight regions cured in this period were mainly reflected by the second peak in the  $\tan \delta$  curves. In the tight regions, stronger covalent bonds inside the polymer chains could be formed to prevent molecules from moving, thus the second peak displayed a low  $\tan \delta$  at high temperatures [53]. However, although the total amount of secondary amines in the whole curing process prevailed over that of primary amines, the large-scale molecular motions of the cured resin and the drastic decrease of  $E'$  occurred at the same temperature as the first  $\tan \delta$  peak, implying the loose networks seemed to be the dominant structure in the cured systems. This might result from the steric restriction caused by the already formed networks during the curing process, which retarded the full crosslinking of tight networks and led to a high percentage of the loose networks in the entire cured system. The possible schematic representation of the two types of crosslinking systems is shown in Figure 9. When the  $\tan \delta$  curves of the resins cured by different amines were compared with each other, the VE-TETA and VE-TREN samples showed a relatively high  $T_{\alpha}$  in both of the  $\tan \delta$  peaks, indicating a better thermomechanical property of the highly cross-linked VE-curing agent systems. Instead, the VE-EDA sample exhibited a lower  $T_{\alpha}$  with a higher  $\tan \delta$ , which was consistent with the results mentioned in other sections that the VE-EDA cross-linking networks were comparatively weaker than the others.



**Figure 9.** Schematic of the two types of crosslinking systems in the cured vanillyl alcohol-based bioepoxies.

### 3.5. Mechanical Properties of the Cured Bioepoxies

The mechanical performances of vanillyl alcohol-based bioepoxy resins cured by different curing agents are given in Table 5. The tensile strength reached the highest value in VE-TETA (32.94 MPa) and was considerably reduced in the other VE-curing agent systems. The order for tensile strength values was as follows: VE-TETA > VE-TREN > VE-DETA > VE-EDA. Evidently, with the increase in the functionality of the curing agent, a higher mechanical property was observed due to the formation of stronger cross-linking networks. Comparing bioepoxies cured by tetrafunctional TETA and bifunctional EDA, the tensile strength of TETA was more than twice that of EDA. Meanwhile, the influence of the molecular structure of the curing agent on the cured bioepoxy mechanical properties can be clearly revealed from the difference between the VE-TREN and VE-TETA samples. Although having a comparable cross-linking degree with VE-TETA, VE-TREN showed a much lower strength (72.25% of VE-TETA) and modulus (61.13% of VE-TETA) in tensile testing, which was similar to what was observed from the DMA test results. Likewise, this was also related to the branched structure of TREN. It was because the side chains increased the steric hindrance to negatively affect mechanical properties by disturbing the orientation of the molecule chains and causing a larger local stress [54]. These results illustrated

the complex interplay between the type and number of the amine functionality and the molecular structure of the crosslinker in determining the final mechanical properties of the cured resin systems.

**Table 5.** Mechanical properties of different bioepoxy systems.

|         | Tensile Strength (MPa) | Tensile Modulus (GPa) | Strain at Break (%) |
|---------|------------------------|-----------------------|---------------------|
| VE-TETA | 32.94 ( $\pm$ 3.96)    | 2.47 ( $\pm$ 0.30)    | 1.33 ( $\pm$ 0.00)  |
| VE-TREN | 23.80( $\pm$ 3.83)     | 1.51( $\pm$ 0.67)     | 1.67( $\pm$ 0.47)   |
| VE-DETA | 18.92( $\pm$ 1.89)     | 2.84 ( $\pm$ 0.28)    | 0.99 ( $\pm$ 0.47)  |
| VE-EDA  | 12.62 ( $\pm$ 2.28)    | 0.58 ( $\pm$ 0.10)    | 2.00 ( $\pm$ 0.00)  |

#### 4. Conclusions

In this work, renewable vanillyl alcohol was used to synthesize vanillyl alcohol-based bioepoxy resin (VE) without bisphenol A. In order to systematically explore the effects of different curing agents on the bioepoxy curing characteristics and properties of the cured resins, four aliphatic amines with different structures and amine functionalities, including TETA, TREN, DETA, and EDA, were used in the curing process. According to the DSC measurements, chemical resistance and swelling tests, TGA and DMA analysis, and tensile tests, different curing agents had a significant influence on the curing behavior and properties of the cured bioepoxy resins. Among the four curing agents used in this study, TETA was the optimum crosslinker. Although the temperature required for curing was lowest for VE-EDA and rose with the increase in molecular weight of the curing agent, the cured VE-TETA sample exhibited a better overall performance than the other epoxy resin systems, including higher chemical resistance, thermal stability, tensile strength, modulus, and a lower swelling ratio. By analyzing the two-stage resin curing process and comparing the differences of performances between the various curing systems, the superior performance of the VE-TETA epoxy system mainly resulted from the stronger cross-linking networks formed in the curing reaction and the molecular structural characteristics of TETA itself. Since vanillyl alcohol-based bioepoxy has great potential to be used as a substitute for current petroleum-based thermosetting epoxy resins, especially bisphenol A-type epoxy resins, a better fundamental understanding of the epoxy resin and curing agent interactions will help to promote the industrial utilization of these bioepoxies to achieve a higher level of sustainability.

**Author Contributions:** Conceptualization, Z.W., P.G. and N.Y.; methodology, Z.W. and P.G.; software, Z.W.; validation, P.G. and S.S.N.; formal analysis, P.G. and N.Y.; investigation, Z.W. and P.G.; resources, P.G. and N.Y.; data curation, Z.W. and P.G.; writing—original draft preparation, Z.W.; writing—review and editing, P.G., S.S.N., S.Y. and N.Y.; visualization, Z.W.; supervision, S.Y. and N.Y.; project administration, S.Y. and N.Y.; funding acquisition, Z.W. and N.Y. All authors have read and agreed to the published version of the manuscript.

**Funding:** This research was funded by Natural Sciences and Engineering Research Council of Canada (NSERC) Discovery Grant (RGPIN-2017-067) and the scholarship program of China Scholarship Council (No. 201806510028).

**Institutional Review Board Statement:** Not applicable.

**Informed Consent Statement:** Not applicable.

**Data Availability Statement:** Data available on request.

**Conflicts of Interest:** The authors declare no conflict of interest.

#### References





1. Kuo, P.; Sain, M.; Yan, N. Synthesis and characterization of an extractive-based bio-epoxy resin from beetle infested pinus contorta bark. *Green Chem.* **2014**, *16*, 3483–3493. [CrossRef]

2. Mashouf Roudsari, G.; Mohanty, A.K.; Misra, M. Green approaches to engineer tough biobased epoxies: A review. *ACS Sustain. Chem. Eng.* **2017**, *5*, 9528–9541. [CrossRef]
3. Baroncini, E.A.; Kumar Yadav, S.; Palmese, G.R.; Stanzione Iii, J.F. Recent advances in bio-based epoxy resins and bio-based epoxy curing agents. *J. Appl. Polym. Sci.* **2016**, *133*. [CrossRef]
4. Fourcade, D.; Ritter, B.S.; Walter, P.; Schönfeld, R.; Müllhaupt, R. Renewable resource-based epoxy resins derived from multifunctional poly(4-hydroxybenzoates). *Green Chem.* **2013**, *15*, 910–918. [CrossRef]
5. Gnanasekar, P.; Chen, H.; Tratnik, N.; Feng, M.; Yan, N. Enhancing performance of phosphorus containing vanillin-based epoxy resins by P-N non-covalently functionalized graphene oxide nanofillers. *Compos. B Eng.* **2021**, *207*, 108585. [CrossRef]
6. Kuo, P.Y.; de Assis Barros, L.; Sain, M.; Tjong, J.S.Y.; Yan, N. Effects of reaction parameters on the glycidyl etherification of bark extractives during bioepoxy resin synthesis. *ACS Sustain. Chem. Eng.* **2016**, *4*, 1016–1024. [CrossRef]
7. Ma, Q.; Liu, X.; Zhang, R.; Zhu, J.; Jiang, Y. Synthesis and properties of full bio-based thermosetting resins from rosin acid and soybean oil: The role of rosin acid derivatives. *Green Chem.* **2013**, *15*, 1300–1310. [CrossRef]
8. Shou, Z.; Abu-Omar, M.M. Biobased epoxy nanocomposites derived from lignin-based monomers. *Biomacromolecules* **2015**, *16*, 2025–2031. [CrossRef]
9. Niu, H.; Nabipour, H.; Wang, X.; Song, L.; Hu, Y. Phosphorus-free vanillin-derived intrinsically flame-retardant epoxy thermoset with extremely low heat release rate and smoke emission. *ACS Sustain. Chem. Eng.* **2021**, *9*, 5268–5277. [CrossRef]
10. Brazinha, C.; Barbosa, D.S.; Crespo, J.G. Sustainable recovery of pure natural vanillin from fermentation media in a single pervaporation step. *Green Chem.* **2011**, *13*, 2197–2203. [CrossRef]
11. Fache, M.; Darroman, E.; Besse, V.; Auvergne, R.; Caillol, S.; Boutevin, B. Vanillin, a promising biobased building-block for monomer synthesis. *Green Chem.* **2014**, *16*, 1987–1998. [CrossRef]
12. Savonnet, E.; Grau, E.; Grelier, S.; Defoort, B.; Cramail, H. Divanillin-based epoxy precursors as dgeba substitutes for biobased epoxy thermosets. *ACS Sustain. Chem. Eng.* **2018**, *6*, 11008–11017. [CrossRef]
13. Lora, J.H.; Glasser, W.G. Recent industrial applications of lignin: A sustainable alternative to nonrenewable materials. *J. Polym. Environ.* **2002**, *10*, 39–48. [CrossRef]
14. Aouf, C.; Le Guernevé, C.; Caillol, S.; Fulcrand, H. Study of the o-glycidylation of natural phenolic compounds. The relationship between the phenolic structure and the reaction mechanism. *Tetrahedron* **2013**, *69*, 1345–1353. [CrossRef]
15. Bjørsvik, H.R.; Minisci, F. Fine chemicals from lignosulfonates. 1. Synthesis of vanillin by oxidation of lignosulfonates. *Org. Process Res. Dev.* **1999**, *3*, 330–340. [CrossRef]
16. Fache, M.; Boutevin, B.; Caillol, S. Vanillin production from lignin and its use as a renewable chemical. *ACS Sustain. Chem. Eng.* **2016**, *4*, 6379–6401. [CrossRef]
17. Gnanasekar, P.; Feng, M.; Yan, N. Facile synthesis of a phosphorus-containing sustainable biomolecular platform from vanillin for the production of mechanically strong and highly flame-retardant resins. *ACS Sustain. Chem. Eng.* **2020**, *8*, 17417–17426. [CrossRef]
18. Silva, E.A.B.D.; Zabkova, M.; Araújo, J.D.; Cateto, C.A.; Barreiro, M.F.; Belgacem, M.N.; Rodrigues, A.E. An integrated process to produce vanillin and lignin-based polyurethanes from kraft lignin. *Chem. Eng. Res. Des.* **2009**, *87*, 1276–1292. [CrossRef]
19. Fache, M.; Auvergne, R.; Boutevin, B.; Caillol, S. New vanillin-derived diepoxy monomers for the synthesis of biobased thermosets. *Eur. Polym. J.* **2015**, *67*, 527–538. [CrossRef]
20. Li, Y.; Xiao, F.; Wong, C.P. Novel, environmentally friendly crosslinking system of an epoxy using an amino acid: Tryptophan-cured diglycidyl ether of bisphenol A epoxy. *J. Polym. Sci. A Polym. Chem.* **2007**, *45*, 181–190. [CrossRef]
21. Jin, F.L.; Li, X.; Park, S.J. Synthesis and application of epoxy resins: A review. *J. Ind. Eng. Chem.* **2015**, *29*, 1–11. [CrossRef]
22. Jiang, L.; Hu, K.; Liu, Z.; Yuan, Y.; Zhou, C.; Lei, J. Aliphatic diamide as novel asphalt-modified epoxy curing agent for enhanced performance. *Adv. Polym. Technol.* **2018**, *37*, 830–836. [CrossRef]
23. Wan, J.; Li, C.; Bu, Z.-Y.; Xu, C.-J.; Li, B.-G.; Fan, H. A comparative study of epoxy resin cured with a linear diamine and a branched polyamine. *Chem. Eng. J.* **2012**, *188*, 160–172. [CrossRef]
24. Cai, H.; Peng, L.; Gang, S.; Yu, Y.; Gang, L.; Yang, X.; Ryu, S. Curing kinetics study of epoxy resin/flexible amine toughness systems by dynamic and isothermal dsc. *Thermochim. Acta* **2008**, *473*, 101–105. [CrossRef]
25. Chen, W.; Peng, L.; Yu, Y.; Yang, X. Curing kinetics study of an epoxy resin system for T800 carbon fiber filament wound composites by dynamic and isothermal dsc. *J. Appl. Polym. Sci.* **2010**, *107*, 1493–1499. [CrossRef]
26. Montserrat, S.; Málek, J. A kinetic analysis of the curing reaction of an epoxy resin. *Thermochim. Acta* **1993**, *228*, 47–60. [CrossRef]
27. Jin, F.L.; Park, S.J. Thermal properties of epoxy resin/filler hybrid composites. *Polym. Degrad. Stabil.* **2012**, *97*, 2148–2153. [CrossRef]
28. Tucker, S.J.; Fu, B.; Kar, S.; Heinz, S.; Wiggins, J.S. Ambient cure poss-epoxy matrices for marine composites. *Compos. Part A Appl. Sci. Manuf.* **2010**, *41*, 1441–1446. [CrossRef]
29. Ferdosian, F.; Yuan, Z.; Anderson, M.; Xu, C.C. Sustainable lignin-based epoxy resins cured with aromatic and aliphatic amine curing agents: Curing kinetics and thermal properties. *Thermochim. Acta* **2015**, *618*, 48–55. [CrossRef]
30. Balabanovich, A.I.; Hornung, A.; Merz, D.; Seifert, H. The effect of a curing agent on the thermal degradation of fire retardant brominated epoxy resins. *Polym. Degrad. Stabil.* **2004**, *85*, 713–723. [CrossRef]
31. Kornmann, X.; Lindberg, H.; Berglund, L.A. Synthesis of epoxy-clay nanocomposites. Influence of the nature of the curing agent on structure. *Polymer* **2001**, *42*, 4493–4499. [CrossRef]

32. Wang, Z.; Gnanasekar, P.; Sudhakaran Nair, S.; Farnood, R.; Yi, S.; Yan, N. Biobased epoxy synthesized from a vanillin derivative and its reinforcement using lignin-containing cellulose nanofibrils. *ACS Sustain. Chem. Eng.* **2020**, *8*, 11215–11223. [CrossRef]
33. Ahn, B.U.; Su, K.L.; Sang, K.L.; Park, J.H.; Kim, B.K. Uv curable polyurethane dispersions from polyisocyanate and organosilane. *Prog. Org. Coat.* **2008**, *62*, 258–264. [CrossRef]
34. Dusek, K.; Bleha, M.; Lunák, S. Curing of epoxide resins: Model reactions of curing with amines. *J. Polym. Sci. A Polym. Chem.* **2010**, *15*, 2393–2400. [CrossRef]
35. Pham, H.Q.; Marks, M.J. Epoxy resins. In *Ullmann's Encyclopedia of Industrial Chemistry*; Wiley-VCH: Weinheim, Germany, 2000. [CrossRef]
36. Wang, X.; Gillham, J.K. Competitive primary amine/epoxy and secondary amine/epoxy reactions: Effect on the isothermal time-to-vitrify. *J. Appl. Polym. Sci.* **1991**, *43*, 2267–2277. [CrossRef]
37. Jagtap, S.B.; Ratna, D. Effect of molecular weight of curing agents on properties of nanocomposites based on epoxy resin and organoclay with reactive modifier. *J. Appl. Polym. Sci.* **2017**, *134*, 44595. [CrossRef]
38. Shibata, M.; Ohkita, T. Fully biobased epoxy resin systems composed of a vanillin-derived epoxy resin and renewable phenolic hardeners. *Eur. Polym. J.* **2017**, *92*, 165–173. [CrossRef]
39. Mezzenga, R.; Boogh, L.; Månson, J.A.E.; Bo, P. Effects of the branching architecture on the reactivity of epoxy-amine groups. *Macromolecules* **2000**, *33*, 4373–4379. [CrossRef]
40. Lakshmi, M.S.; Srividhya, M.; Reddy, B.S.R. New epoxy resins containing hard-soft segments: Synthesis, characterization and modification studies for high performance applications. *J. Polym. Res.* **2003**, *10*, 259–266. [CrossRef]
41. Kanehashi, S.; Yokoyama, K.; Masuda, R.; Kidesaki, T.; Nagai, K.; Miyakoshi, T. Preparation and characterization of cardanol-based epoxy resin for coating at room temperature curing. *J. Appl. Polym. Sci.* **2013**, *130*, 2468–2478. [CrossRef]
42. Lakshmi, B.; Shivananda, K.; Mahendra, K. Synthesis, characterization and curing studies of thermosetting epoxy resin with amines. *Bull. Korean Chem. Soc.* **2010**, *31*, 2272–2278. [CrossRef]
43. Wu, G.M.; Di, L.; Liu, G.F.; Jian, C.; Huo, S.P.; Kong, Z.W. Thermoset nanocomposites from waterborne bio-based epoxy resin and cellulose nanowhiskers. *Carbohydr. Polym.* **2015**, *127*, 229–235. [CrossRef]
44. Koton, M.; Sazanov, Y.N. Thermal degradation of polypyromellitimides. *Polym. Sci. USSR* **1973**, *15*, 1857–1863. [CrossRef]
45. He, X.; Xu, X.; Wan, Q.; Bo, G.; Yan, Y. Synthesis and characterization of dimmer-acid-based nonisocyanate polyurethane and epoxy resin composite. *Polymers* **2017**, *9*, 649. [CrossRef] [PubMed]
46. Gowda, S.; Mahendra, K.N. Synthesis and reactivity studies of maleimide-epoxy resins with aliphatic amines. *Iran. Polym. J.* **2007**, *16*, 161–171.
47. Madan, R.; Anand, R.; Varma, I. Thermal behaviour of polymers based on nadimides. *J. Therm. Anal. Calorim.* **2000**, *59*, 531–539. [CrossRef]
48. Varma, I.; Gupta, V.; Sini, N. Thermosetting resin-properties. In *Comprehensive Composite Materials II*; Elsevier: Amsterdam, The Netherlands, 2018; pp. 401–468. [CrossRef]
49. Shang, L.; Zhang, X.; Zhang, M.; Jin, L.; Liu, L.; Xiao, L.; Li, M.; Ao, Y. A highly active bio-based epoxy resin with multi-functional group: Synthesis, characterization, curing and properties. *J. Mater. Sci. Technol.* **2018**, *53*, 5402–5417. [CrossRef]
50. Gerard, J.; Galy, J.; Pascault, J.; Cukierman, S.; Halary, J. Viscoelastic response of model epoxy networks in the glass transition region. *Polym. Eng. Sci.* **1991**, *31*, 615–621. [CrossRef]
51. Stanzione III, J.F.; Sadler, J.M.; La Scala, J.J.; Reno, K.H.; Wool, R.P. Vanillin-based resin for use in composite applications. *Green Chem.* **2012**, *14*, 2346–2352. [CrossRef]
52. Feldman, D.; Banu, D.; Natansohn, A.; Wang, J. Structure-properties relations of thermally cured epoxy-lignin polyblends. *J. Appl. Polym. Sci.* **2010**, *42*, 1537–1550. [CrossRef]
53. Poussard, L.; Mariage, J.; Grignard, B.; Detrembleur, C.; Jérôme, C.; Calberg, C.; Heinrichs, B.; De Winter, J.; Gerbaux, P.; Raquez, J.-M. Non-isocyanate polyurethanes from carbonated soybean oil using monomeric or oligomeric diamines to achieve thermosets or thermoplastics. *Macromolecules* **2016**, *49*, 2162–2171. [CrossRef]
54. Yen, M.S.; Chen, P.Y.; Tsai, H.C. Synthesis, properties, and dyeing application of nonionic waterborne polyurethanes with different chain length of ethyldiamines as the chain extender. *J. Appl. Polym. Sci.* **2003**, *90*, 2824–2833. [CrossRef]

## Article

# Cetylpyridinium Bromide/Polyvinyl Chloride for Substantially Efficient Capture of Rare Earth Elements from Chloride Solution

Eman M. Allam <sup>1,\*</sup>, Taysser A. Lashen <sup>1</sup>, Saeyda A. Abou El-Enein <sup>2</sup>, Mohamed A. Hassanin <sup>1</sup>, Ahmed K. Sakr <sup>1</sup> , Mohamed Y. Hanfi <sup>1,3</sup> , M. I. Sayyed <sup>4,5</sup> , Jamelah S. Al-Otaibi <sup>6</sup> and Mohamed F. Cheira <sup>1,\*</sup> 

- <sup>1</sup> Nuclear Materials Authority, El Maadi, Cairo P.O. Box 530, Egypt; ah841873@ucf.edu (T.A.L.); mmsh236@yahoo.com (M.A.H.); akhchemist@gmail.com (A.K.S.); mokhamed.khanfi@urfu.ru (M.Y.H.)
- <sup>2</sup> Department of Chemistry, Faculty of Science, Menoufia University, Shebin El-Kom 32511, Egypt; dr.saeyda\_elenein@yahoo.com
- <sup>3</sup> Institute of Physics and Technology, Ural Federal University, St. Mira, 19, 620002 Yekaterinburg, Russia
- <sup>4</sup> Department of Nuclear Medicine Research, Institute for Research and Medical Consultations (IRMC), Imam Abdulrahman Bin Faisal University (IAU), P.O. Box 1982, Dammam 31441, Saudi Arabia; mabualssayed@ut.edu.sa
- <sup>5</sup> Department of Physics, Faculty of Science, Isra University, Amman 11622, Jordan
- <sup>6</sup> Department of Chemistry, College of Science, Princess Nourah Bint Abdulrahman University, P.O. Box 84428, Riyadh 11671, Saudi Arabia; jsalotabi@pnu.edu.sa
- \* Correspondence: dr\_e.allam@yahoo.com (E.M.A.); mf.farid2008@yahoo.com (M.F.C.)

**Abstract:** A new sorbent cetylpyridinium bromide/polyvinylchloride (CPB/PVC) was prepared and tested to extract rare earth elements (REEs) from their chloride solutions. It was identified by FTIR, TGA, SEM, EDX, and XRD. The impact of various factors such as pH, RE ion initial concentration, contacting time, and dose amount via sorption process was inspected. The optimum pH was 6.0, and the equilibrium contact time was reached at 60 min at 25 °C. The prepared adsorbent (CPB/PVC) uptake capacity was 182.6 mg/g. The adsorption of RE ions onto the CPB/PVC sorbent was found to fit the Langmuir isotherm as well as pseudo-second-order models well. In addition, the thermodynamic parameters of RE ion sorption were found to be exothermic and spontaneous. The desorption of RE ions from the loaded CPB/PVC sorbent was investigated. It was observed that the optimum desorption was achieved at 1.0 M HCl for 60 min contact time at ambient room temperature and a 1:60 solid: liquid phase ratio (S:L). As a result, the prepared CPB/PVC sorbent was recognized as a competitor sorbent for REEs.

**Keywords:** rare earth ions; cetylpyridinium bromide; polyvinylchloride; sorption; desorption

**Citation:** Allam, E.M.; Lashen, T.A.; Abou El-Enein, S.A.; Hassanin, M.A.; Sakr, A.K.; Hanfi, M.Y.; Sayyed, M.I.; Al-Otaibi, J.S.; Cheira, M.F. Cetylpyridinium Bromide/Polyvinyl Chloride for Substantially Efficient Capture of Rare Earth Elements from Chloride Solution. *Polymers* **2022**, *14*, 954. <https://doi.org/10.3390/polym14050954>

Academic Editor: Cristina Cazan

Received: 20 January 2022

Accepted: 24 February 2022

Published: 27 February 2022

**Publisher's Note:** MDPI stays neutral with regard to jurisdictional claims in published maps and institutional affiliations.



**Copyright:** © 2022 by the authors. Licensee MDPI, Basel, Switzerland. This article is an open access article distributed under the terms and conditions of the Creative Commons Attribution (CC BY) license (<https://creativecommons.org/licenses/by/4.0/>).

## 1. Introduction

The rare earth elements (REEs) are the lanthanides series, scandium, and yttrium, except for promethium, all of which occur in nature. The REEs are found fixed in their minerals and act as the same chemical entity [1]. Rare earth elements are not found as individual compounds, but the mineral usually contains all the REEs with some enrichment of them by the cerium group or yttrium group. However, most REEs occur, in principle, only three ore minerals, namely, monazite, bastnasite (as a resource of the cerium group), and xenotime (as a source of the yttrium group) [2].

REEs have evolved into an essential aspect of current life in a wide range of products; thus, their recovery procedures now hold great consideration. The recovery of REEs is a complicated process that involves ore mining, mineral dressing, chemical upgrading, and refining. The crucial refining steps must result in the possible extraction of the REEs existing in the ore with the lowest possible cost [3–6].

Currently, there are great efforts to find innovative materials and technologies to extract RE ions from their solutions. Impregnation techniques have been developed as a substitute for ion exchange or solvent extraction as it overcomes the drawbacks of these

techniques. These techniques depend on the alteration of solid support to extract the desired ions of their complex solutions. Two approaches were exploited for construction; the first method depends on the physical modification of solid support using a suitable reagent, and the second method comprises a chelating ligand toward the solid phase support. A variety of extraction techniques were evolved for selective extraction of RE ions using various solid-phase supports such as benzophenone, activated carbon, SiO<sub>2</sub>, titanium oxide, naphthalene, resins, clay, etc. [7–10].

REEs are recovered from ore materials, requiring some hydrometallurgical functions. Great efforts have been concentrated upon pristine materials to separate REEs. Impregnated resins were produced by altering solid supports for the separation of ions from complex matrices. Two methods were utilized to organize the solid set; one based on the physical modification of a proper solvent at the solid support. The second process implicates attaching the chelating complex to a support material. For individual REE extraction, various solid-extraction approaches have been conceived using solid supports of distinct types such as activated carbon, clays, SiO<sub>2</sub>, polymeric resins, titanium oxide, and naphthalene [10–21]. The extraction of lanthanides from positively acidic wastes has been proposed using a resin, which was developed by a dihexyl succinamic/chloromethylated polymer [22].

Nonionic Amberlite XAD-16 polymeric crosslinked with undiluted tributyl phosphate (TBP) was used to uptake Ce<sup>4+</sup> ions from nitrate solution [23]. Mono aza dibenzo crown ether/Amberlite XAD-4 was employed for the removal of Sm<sup>3+</sup>, La<sup>3+</sup>, and Nd<sup>3+</sup> [24]. A nonionic Amberlite XAD-4 polymeric anchored by vanillinsemicarbazone was used to separate Ce<sup>3+</sup> and La<sup>3+</sup> [25]. Furthermore, La<sup>3+</sup>, along with Ce<sup>3+</sup> ions, were extracted with ethylhexyl phosphonic acid mono-ethylhexyl ester covered by polyvinyl alcohol and linked through divinyl sulfone or glutaraldehyde [26].

Rare earth ion extraction was also investigated using hexyl-ethyl-octyl-isopropylphosphonic acid/resin from HCl solutions [27]. Bis(2-ethylhexyl) phosphoric acid/polyethersulfone polymer was employed to separate rare earth ions from chloride, perchlorate, and sulfate media [28]. Moreover, bis(ethylhexyl)phosphoric acid/resin was utilized to separate Zn, Ca, Pr, Ce, Nd, Fe, Sm, and Al [29]. The rare earth ion separation was initiated by designing a polyethersulfone composite via phase inversion technique [30]. Extraction of La<sub>2</sub>O<sub>3</sub> from monazite was performed in four steps: (a) extraction of lanthanum hydroxide using NaOH; (b) digestion with HNO<sub>3</sub>; (c) precipitation with NH<sub>4</sub>OH; and (d) calcination to La<sub>2</sub>O<sub>3</sub> [31].

The recovery of REEs was examined using silica gel modified with diglycolamic acid [32]. A strong cation exchange resin (Amberlite 1R-120) was used for the adsorption of RE(III) ions from a standard and obtained leach liquor solution from phosphate ore by applying optimum leaching conditions; the optimum conditions for the loading of RE ions onto Amberlite 1R-120 were determined in a batch system [33]. Treated clay impregnated with *m*-aminophenol and amino-hydroxypyrazole was utilized to capture REEs [10].

In this study, polyvinyl chloride (PVC) was impregnated by cetylpyridinium bromide (CPB) to increase its sorption capacity. The physicochemical structure and properties of PVC and CPB/PVC sorbents were first characterized by SEM, XRD, EDX, FTIR, and TGA. Second, the REE sorption properties of these two materials were compared by studying the parameters that affected the sorption process such as pH, initial REE concentration, PVC and CPB/PVC dosage, and contact time. The uptake kinetics and sorption isotherms were also deliberated. Finally, the regeneration and recycling of the two sorbents were examined.

## 2. Materials and Methods

### 2.1. Materials

The REE standard stock solution was prepared by dissolving a mixture of 0.2649 g of LaCl<sub>3</sub>, 0.3989 g of CeCl<sub>3</sub>·7H<sub>2</sub>O, 0.2632 g of PrCl<sub>3</sub>, 0.2606 g of NdCl<sub>3</sub>, 0.3639 g of SmCl<sub>3</sub>·6H<sub>2</sub>O, and 0.3294 g of YCl<sub>3</sub> in 900 mL deionized water acidified by 15.0 mL concentrated HCl (36.5%) to prevent hydrolysis. These salts were supplied through B.D.H. Chem., Poole, England. The salts weights were equivalent to 150 mg/L for each individual La<sup>3+</sup>, Ce<sup>3+</sup>,

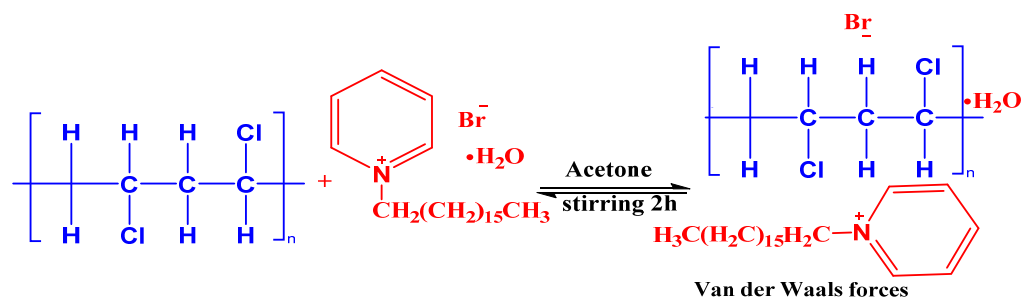
$\text{Pr}^{3+}$ ,  $\text{Nd}^{3+}$ ,  $\text{Sm}^{3+}$ , or  $\text{Y}^{3+}$  ions. However, 900 mg of total RE ions were dissolved in 900 mL distilled water. Hence, RE ion concentration was equivalent to 1 mg/mL ( $1000 \mu\text{g/mL} = 1000 \text{ mg/L}$ ). Polyvinyl chloride ( $(\text{CH}_2\text{CHCl})_n$ ) was supplied by Sigma-Aldrich, St. Louis, MO, USA, it has a molecular weight ( $\approx 48,000 \text{ g/mol}$ ) and its molecular weight of the repeat unit was 62.5 g/mol. Additionally, cetylpyridinium bromide hydrate (CPB), arsenazo III, HCl, and NaOH were gained from Sigma-Aldrich.

A UV-Visible spectrophotometer (UV-2700i, Shimadzu, Kyoto, Japan) with 1.0 cm quartz cell covering the range of 200–1100 nm was used for the spectrophotometric analysis of total REEs by arsenazo III (indicator) at 650 nm as a control analysis for the adsorption process [34]. All pH measurements were carried out using a digital pH-meter, Inolab pH, Xylem Inc., Rye Brook, NY, USA, level 1.0, with an error of  $\pm 0.01$  at ambient laboratory temperature. An inductively coupled plasma-optical emission spectrometer ICP-OES (Agilent 5800, Santa Clara, CA, USA) instrument was employed to measure the concentration of RE ions.

The sorbent's crystal structure was examined by XRD (Empyrean, Malvern Panalytical, Almelo, The Netherlands). The sorbent's morphology was scrutinized via scanning electron microscopy with energy dispersive X-ray analysis (SEM-EDX, Philips XL 30, Eindhoven, The Netherlands). The specific surface area, size of substances, and pore volume were measured using nitrogen sorption at 77 K (Nova 2000 series, Quantachrome Corporation, Boynton Beach, FL, USA). The functional groups of the studied sorbents were evaluated by Fourier transform infrared (FTIR) spectroscopy (IR Prestige-21, Shimadzu, Kyoto, Japan) using IR resolution software via the KBr method. The spectra were recorded in the range of  $400\text{--}4000 \text{ cm}^{-1}$ ,  $4.0 \text{ cm}^{-1}$  resolution, and 50 scans. A thermogravimetric analyzer (TGA 8000, Perkin Elmer, Waltham, MA, USA) was utilized to detect the thermal stability at  $10 \text{ }^\circ\text{C}/\text{min}$  and temperature range of  $25\text{--}900 \text{ }^\circ\text{C}$ .

## 2.2. Preparation of Cetylpyridinium Bromide Hydrate/Polyvinyl Chloride

The dry method was utilized for the modification process. The impregnation conditions were optimized through a series of experiments. A total of 1.0 g cetylpyridinium bromide hydrate was dissolved in 25.0 mL acetone, and then it was added dropwise into a suspended solution of 10.0 g of polyvinyl chloride in 50.0 mL of acetone with stirring for 2.0 h at  $25 \text{ }^\circ\text{C}$  until complete homogenization and dryness. The modified polyvinyl chloride with cetylpyridinium bromide hydrate was physically formed and dried at  $60 \text{ }^\circ\text{C}$  (Scheme 1).



**Scheme 1.** The suggested mechanism of cetylpyridinium bromide hydrate/PVC.

## 2.3. REE Sorption Studies

Many experiments were carried out to identify the applicable parameters affecting the REE extraction from the synthetic solution on both PVC and CPB/PVC adsorbents. The studied factors were solution pH, REE concentration, sorbent dosage, time of sorption, and temperature.

A series of experiments was studied by a different concentration of the REE synthetic solution with constant volume to fix the optimum parameters. The effect of pH on the sorption of REEs was examined with a pH value from 1.0 to 7.0. The pH in all experiments was



adjusted by 0.2 M HCl as well as a 0.2 M NaOH solution. In contrast, the effects of sorbent quantity (10 to 90 mg) and contact time (5–120 min) were investigated. Moreover, different initial concentrations of rare earth ions were designated in 25–400 mg/L. The sorption uptake  $q_e$  (mg/g), efficiency ( $E$ , %), and distribution parameter ( $K_d$ ) were generated by the subsequent equations [35–38].

$$q_e = \frac{(C_o - C_e)V}{m} \quad (1)$$

$$E, \% = \left( \frac{C_o - C_e}{C_o} \right) \times 100 \quad (2)$$

$$K_d = \left( \frac{C_o - C_e}{C_e} \right) \times \frac{V}{m} \quad (3)$$

$C_e$  and  $C_o$  (mg/L) are defined as the equilibrium and initial REE concentration,  $V$  (L) is solution volume, and  $m$  (g) represents the sorbent weight.

#### 2.4. Desorption Studies

The rare earth ions loaded on PVC or CPB/PVC were exposed for stripping process to study the desorption aspects of the rare earth ions. The desorption methods were conducted on either 0.5 g of REE/PVC or REE/CPB/PVC using a 25.0 mL of various concentrations of HCl, NaCl,  $H_2SO_4$ , and  $HNO_3$  in the range from 0.1 to 3.0 M for a 60 min desorption time and then separated by filtration; the filtrate was analyzed to detect the concentration of eluting RE ions. The desorption parameters (the eluting type, the concentration of eluent, desorption time, and temperature) were investigated. After the REE-loaded adsorbent with treated with the eluting agent, it was rinsed carefully with deionized water to prepare it for recycling.

### 3. Results and Discussion

#### 3.1. Depiction of Materials

##### 3.1.1. XRD Investigation

The XRD spectra of PVC, CPB/PVC, REE/PVC, and REE/CPB/PVC are shown in Figure 1. The data in Figure 1a of the PVC show that the polymer exhibited two peaks at  $2\theta$  angles of  $18.0^\circ$  and  $25.0^\circ$  due to its amorphous nature [39]. However, the small peak at  $2\theta = 39.5^\circ$  indicated the polymer semi-crystalline structure [40]. The other peaks were combined into one peak at  $2\theta = 24.0^\circ$  for the CPB/PVC spectrum, and the peak at  $2\theta = 39.5^\circ$  disappeared (Figure 1c). Consequently, it can be concluded that CPB was distributed into PVC to compose CPB/PVC.

The XRD of the REE/PVC spectrum, in Figure 1b was slightly broadened and shifted to  $19.0^\circ$  and  $24.0^\circ$ . Furthermore, the peak at  $2\theta = 39.5^\circ$  in Figure 1a also disappeared due to the PVC polymer structure being amorphous. The data quantified that the rare earth ions were sorbed on the PVC surface. The XRD of REEs/CPB/PVC is shown in Figure 1d. From the XRD of CPB/PVC (Figure 1c), the peak position and peak shape of CPB/PVC at  $2\theta = 24.0^\circ$  was enlarged and had a change in position to  $2\theta = 26.0^\circ$ , and new peaks were gained at  $17.0^\circ$  and  $19.0^\circ$  for the XRD pattern of REE/CPB/PVC in Figure 1d, indicating that the REEs were adsorbed on CPB/PVC.

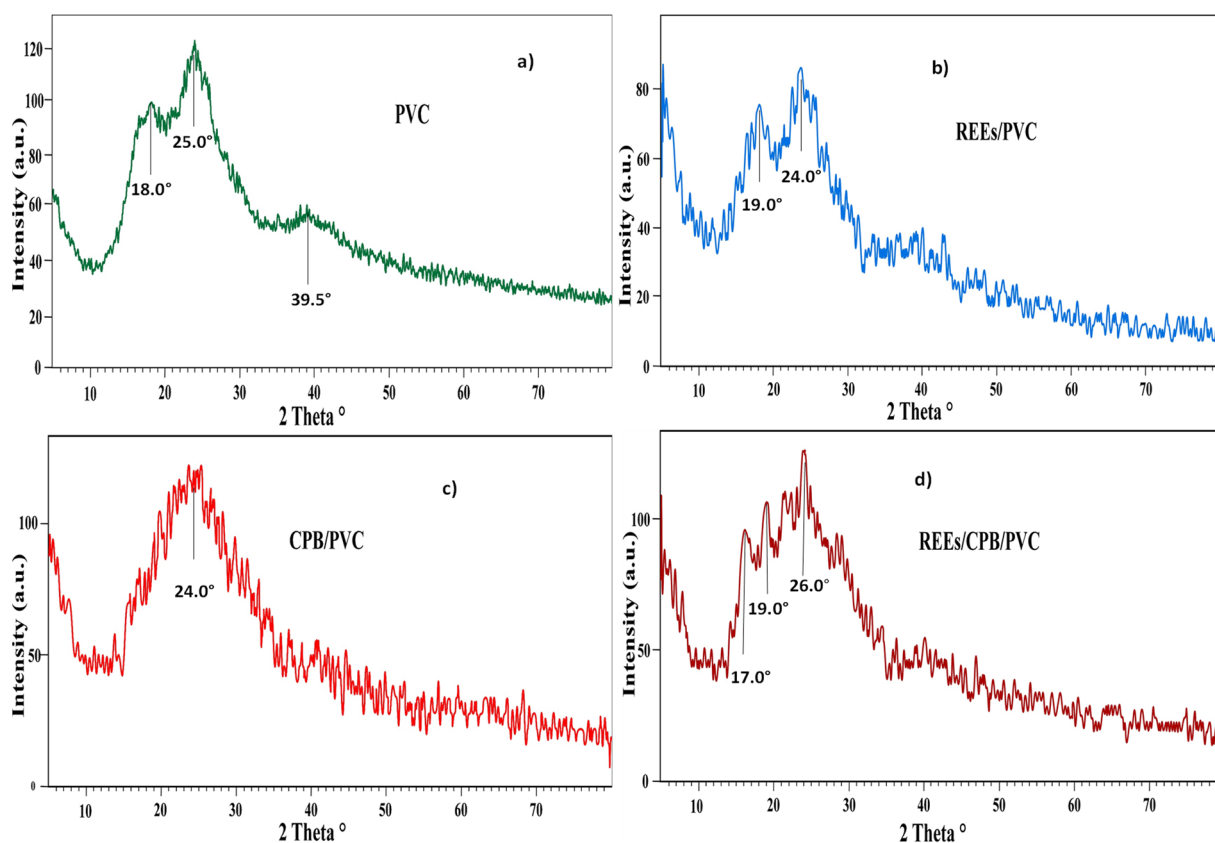


**Figure 1.** XRD analysis of (a) PVC, (b) REEs/PVC, (c) CPB/PVC, (d) REE/CPB/PVC.

### 3.1.2. SEM-EDX Investigations

Figure 2a illustrates that the PVC surface was approximately smooth, spotless, and had no fissures with minor drawbacks due to slight differences in the morphology of the tiny granules of PVC. At the same time, the CPB/PVC image was recognized with few aggregations with structures that seem to be a little globular and regular (Figure 2c). On the other hand, the loaded RE ions on PVC or CPB/PVC images in Figure 2b,d showed that the particles were agglomerated, and RE ions were observed as white spots on the surface of two sorbents. From the results, evident surface morphology changes in the REE/PVC or REE/CPB/PVC sorbents confirmed that the REE sorption onto the studied two sorbents was achieved.

The semi-quantitative EDX investigation of PVC along with CPB/PVC before and after REE sorption was premeditated. From the results, C and Cl bands were accessible in the PVC; furthermore, no additional bands were noticed (Figure 2e). In contrast, the CPB/PVC contained N, C, Cl, and Br peaks (Figure 2g). These results emphasize that the CPB/PVC was established and formed. Therefore, it can be concluded that CPB was distributed into PVC to form CPB/PVC due to the surface electrostatic interaction. After rare earth ion sorption, discrete peaks of some rare earth ions (Y, La, Ce, Pr, Nd, Sm) were found on the two sorbents (Figure 2f,h). The REE peaks were perceived and confirmed REE sorption on PVC and CPB/PVC.

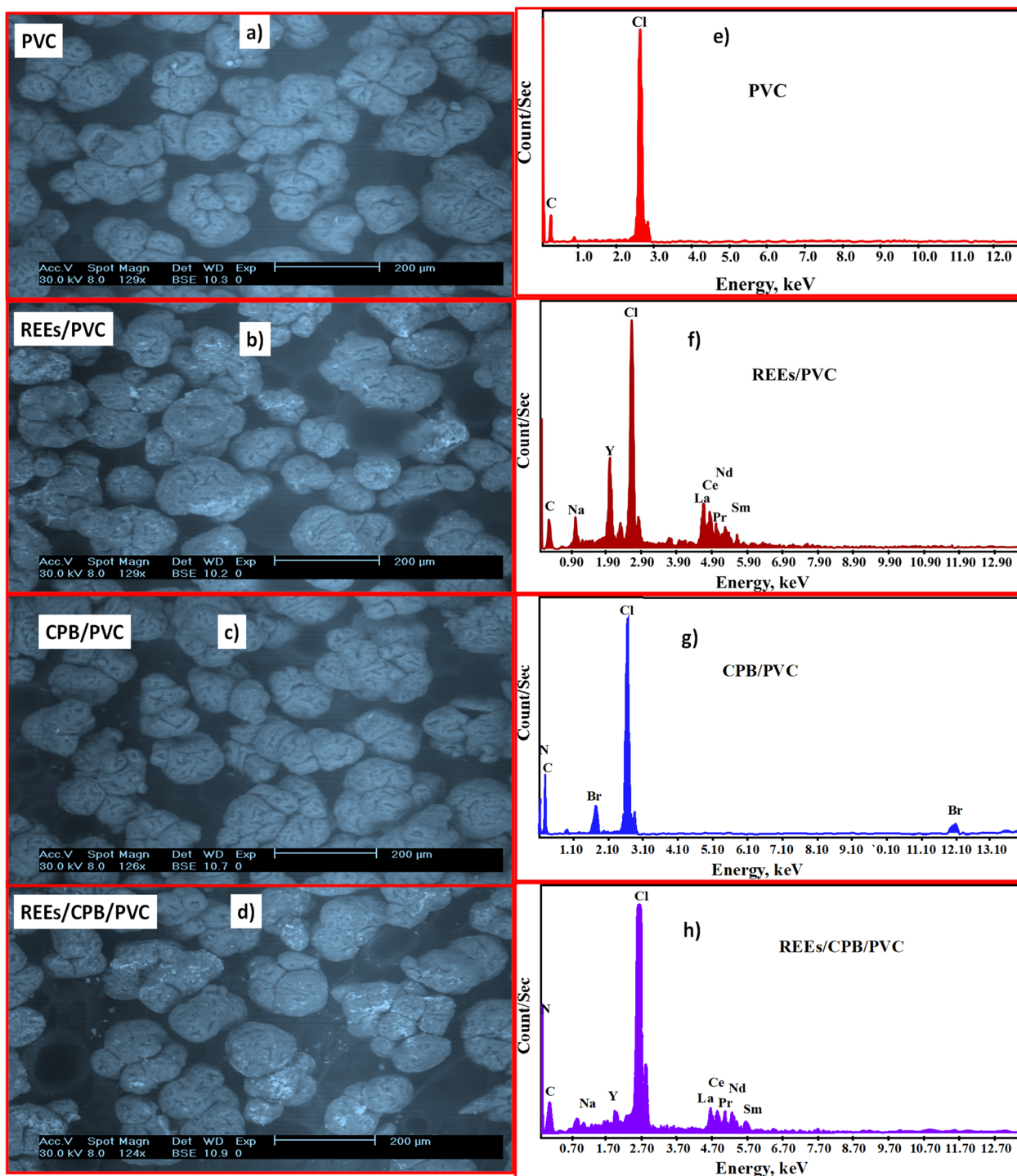


**Figure 2.** SEM pictures of (a) PVC, (b) REE/PVC, (c) CPB/PVC, (d) REE/CPB/PVC and EDX investigation of (e) PVC, (f) REE/PVC, (g) CPB/PVC, (h) REE/CPB/PVC.

### 3.1.3. BET Surface Analysis

The Brunner–Emmett–Teller theory (BET) was utilized to examine the surface area of either solid or porous materials. It provides crucial information about their physical structure, as the area of the solid surface of the substance influences how that solid interacts with its surroundings. During either synthesis or processing, the surface area of a material can be changed. The surface area of a particle increases when pores are created within its interior by decomposition and dissolution as well as other physical or chemical means. A

nitrogen adsorption–desorption analyzer was used to assess the specific surface area and the studied adsorbents' pore size. The four samples were dried before analysis to 60 °C for 2.0 h.

Table 1 and Figure 3a illustrate that PVC surface area, pore size, and volume were 94.06 m<sup>2</sup>/g, 1.94 nm, and 0.091 cc/g. Moreover, the CPB/PVC surface area, pore size, and volume were 68.32 m<sup>2</sup>/g, 2.91 nm, and 0.099 cc/g (Figure 3b). With the addition of CPB to PVC, the surface area of CPB/PVC was decreased. From the result, it may be attributed that CPB was impregnated in PVC. After rare earth ion sorption, the surface area, pore size, and volume of the PVC or CPB/PVC sorbents were decreased because rare earth ions blocked the active sites (Figure 3c,d). The attained results exposed that rare earth ions were more strongly adsorbed on the CPB/PVC than the PVC due to CPB/PVC having more active spots than PVC.

**Table 1.** Surface area, porosity, and pore volume of PVC and CPB/PVC previously and after rare earth ion sorption.

| Materials   | S <sub>BET</sub> , m <sup>2</sup> /g | Pore Size, nm | Pore Volume, cc/g |
|-------------|--------------------------------------|---------------|-------------------|
| PVC         | 94.06                                | 1.94          | 0.091             |
| CPB/PVC     | 68.32                                | 2.91          | 0.099             |
| REE/PVC     | 39.09                                | 1.82          | 0.035             |
| REE/CPB/PVC | 65.19                                | 2.88          | 0.095             |

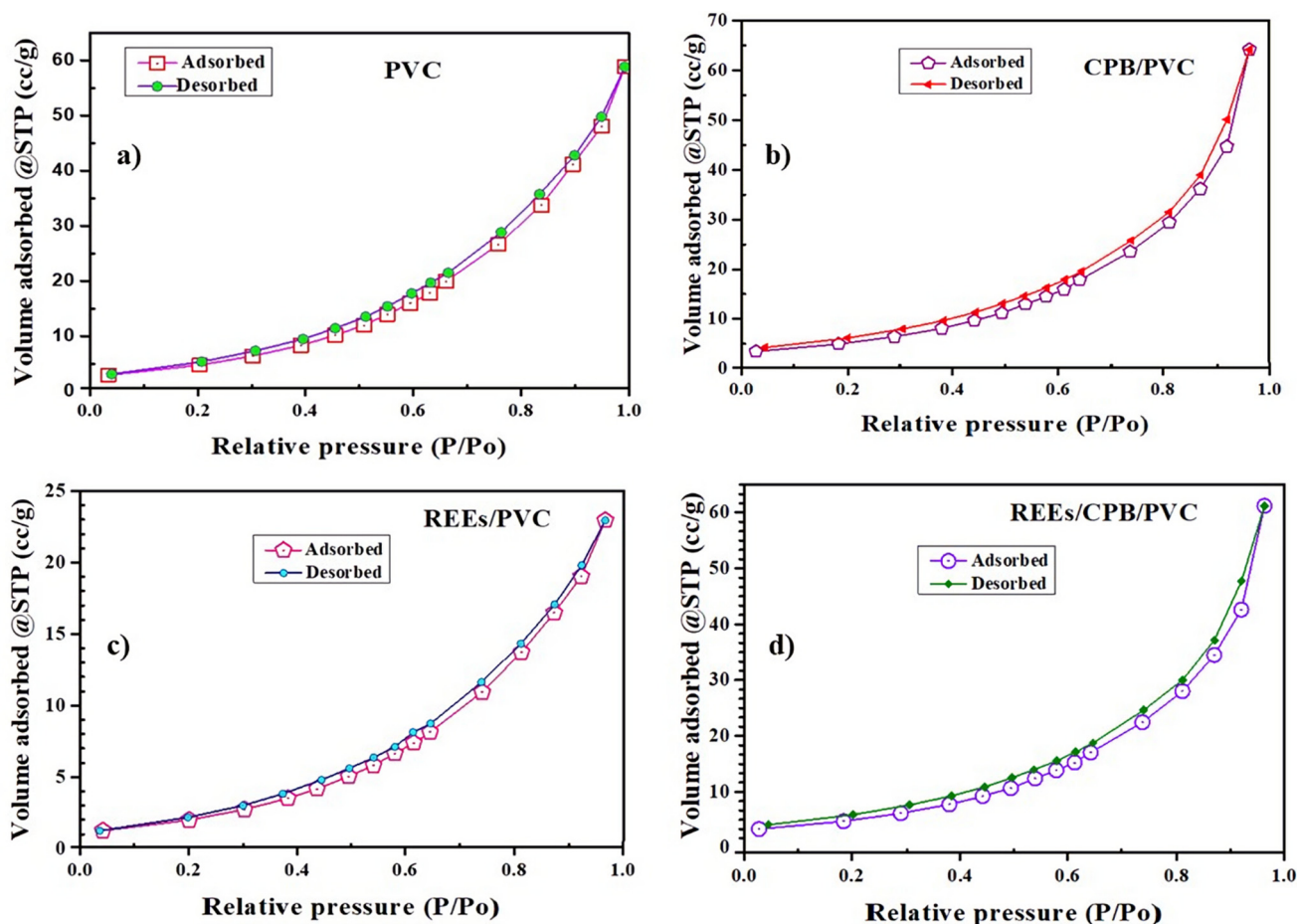


**Figure 3.** N<sub>2</sub> sorption/desorption isotherm of (a) PVC, (b) CPB/PVC, (c) REE/PVC, and (d) REE/CPB/PVC.

### 3.1.4. FTIR Investigation

The functional groups attached to the surface of the materials under study were recognized by FTIR spectroscopy [41]. The PVC spectrum in Figure 4a showed that two peaks at the 606 and 682  $\text{cm}^{-1}$  were related to the C–Cl stretching mode, according to the polymer conformation structure and the locative position of the surrounding atoms according to C–Cl bonds [42]. The peaks at 2911–2969  $\text{cm}^{-1}$  matched  $-\text{CH}_2-$  and  $-\text{CH}$  groups. The assignments at 1250 and 1331  $\text{cm}^{-1}$  indorsed  $-\text{CH}$  in the  $-\text{CHCl}$  group [43]. The intensity of the C–H band was also improved with the impregnation with cetylpyridinium bromide hydrate. Furthermore, the intensity of all of the C–Cl bands was increased.

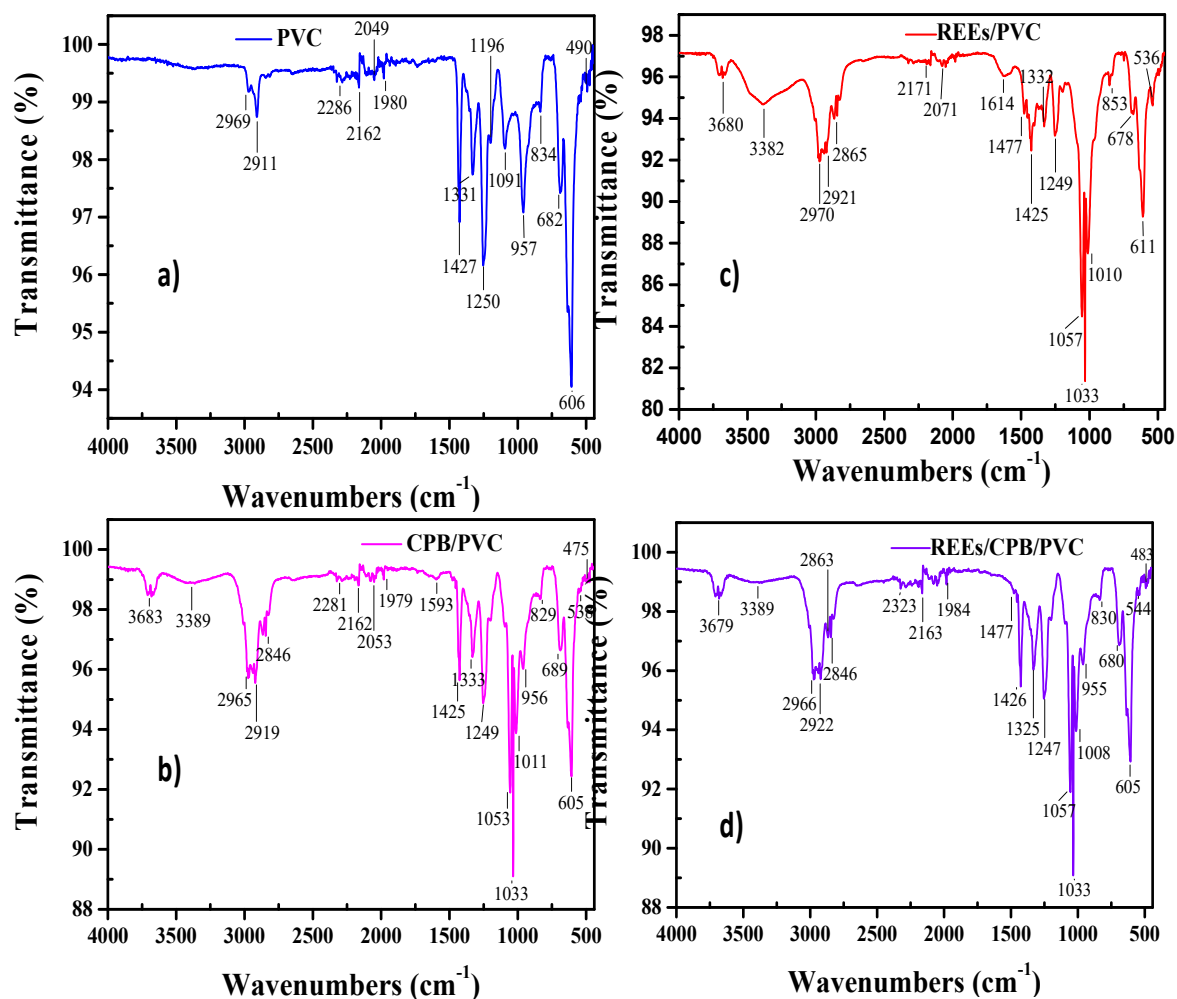


Figure 4. FTIR spectra of (a) PVC, (b) CPB/PVC, (c) REE/PVC, (d) REE/CPB/PVC.

The prepared cetylpyridinium bromide hydrate/polyvinyl chloride spectrum exhibited a band at 3389  $\text{cm}^{-1}$  because of the O–H of hydration (Figure 4b). The vibrational band at 1593  $\text{cm}^{-1}$  confirmed the C=C aromatic of the pyridinium group. The feature at 1425  $\text{cm}^{-1}$  was predictable as O–H of the distortion peak of  $\text{H}_2\text{O}$ . The comparatively broad features at 1250 and 1053  $\text{cm}^{-1}$  indicate the C–N group. In addition, the two features at 605 and 689  $\text{cm}^{-1}$  are due to C–Cl stretching vibration. Hence, the CPB was distributed into PVC to form CPB/PVC because of the electrostatic interaction at the surface (van der Waals forces) due to the presence of C–Cl, imino groups, and most of the peaks in CPB/PVC were shifted 5–10  $\text{cm}^{-1}$ . After REE sorption (Figure 4c,d), the vibration bands of PVC or CPB/PVC were reduced and shifted slightly to 3–11  $\text{cm}^{-1}$ , which could be due to the sorption of rare earth ions on the surface sorbents [44].

### 3.1.5. Thermal Analysis

Thermogravimetric analysis (TGA) is a thermal analysis method for determining changes in both chemical and physical characteristics of the samples. TGA measurements are typically made as a function of temperature rise with a constant heating rate, or as a function of time with mass loss and a constant temperature. TGA measurements are typically made as a function of temperature rise with a constant heating rate, or as a function of time with mass loss with constant temperature. Physical phenomena such as second-order phase transitions, desorption, vaporization, and others can be considered using the TGA. In addition, chemical phenomena such as dehydration and decomposition can be detected. The TGA can easily determine the mass gain or loss of samples due to decomposition, loss of volatile compounds, oxidation, and degradation. Additionally, standardized TGA testing procedures can be used to determine the samples' thermal stability in terms of their resistance to thermal decomposition or degradation [45].

The TGA thermograms of PVC, CBP/PVC, REE/PVC, and REE/CBP/PVC are shown in Figure 5. The TGA curve of the PVC had two weight-loss steps with reference to the two thermal degradation steps that could be discerned in the TGA curve (Figure 5a). The first weight loss step occurred in the range of 220–332 °C and was related to removing the HCl consecutive reaction and forming a conjugated polyene structure. The second step appeared within the range of 445–535 °C due to the thermal degradation of the PVC carbon chain, which yields flammable volatiles [46,47].

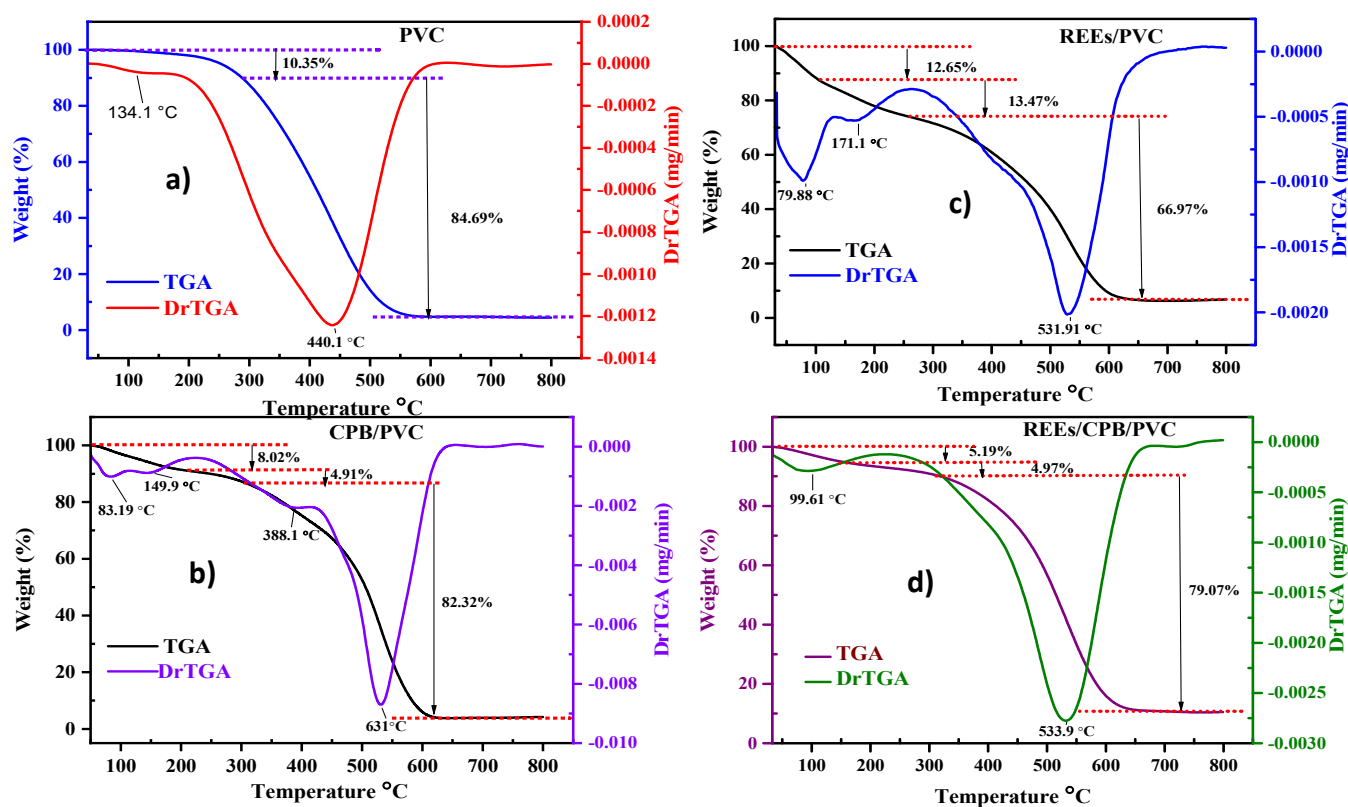


Figure 5. TGA analysis of (a) PVC, (b) CPB/PVC, (c) REEs/PVC, (d) REEs/CPB/PVC.

The thermal stabilities of CPB/PVC and REE/CBP/PVC are also shown in Figure 5b,d, which had three weight loss steps. The first step that appeared at 115 °C was because of the loss of hydration  $H_2O$ . The second step occurred at 255–345 °C due to eliminating HCl, HBr, and  $NH_3$  of the CPB/PVC sorbent. The third step was within a 350–650 °C range due to the thermal degradation of the carbon chains, which generated ignitable volatiles. In contrast, the TGA of REE/PVC exposed three weight loss stages in Figure 5c. The first stage seemed at 110 °C was due to the loss of  $H_2O$  related to REEs. The second stage

occurred at 250 °C due to the removal HCl from the PVC sorbent. The third stage was within the 350–600 °C range because of the thermal decomposition of the carbon chains, which resulted in the production of flammable volatiles.

The remaining residues of PVC and CPB/PVC were 4.96 and 4.75%, respectively. Moreover, the residues of REE/PVC and REE/CBP/PVC were 6.91 and 10.77%, respectively. Hence, the residues of REE/PVC and REE/CBP/PVC were higher than the PVC and CBP/PVC due to the sorption and existence of REEs on the surface of the studied sorbents.

### 3.2. REE Sorption Studies

Batch techniques were executed to investigate the REE sorption on PVC or CPB/PVC as the sorbents from the RE chloride synthetic solution. These were conducted by contacting a mass of PVC or CPB/PVC with a fixed volume (50.0 mL) of RE ion solution. Several experiments on REE sorption efficiency were practically conducted to optimize the pH, sorbent amount, initial RE ion conc., time of contact, and temperature.

#### 3.2.1. Effect of Solution pH

Numerous experiments were carried out with pH values from 1.0 to 7.0. In the meantime, the other procedure parameters were remained stable at a 50.0 mL solution of 200 mg/L REE, 50 mg PVC, or CPB/PVC dose for 30 min at ambient temperature. The gained data from Figure 6a showed that the REE sorption efficiencies were gradually increased from 7.64 and 40.1% to 29.6 and 85.2% for PVC and CPB/PVC, respectively, with an increase in the pH beyond 6.0. However, REE sorption efficiencies were decreased to 24.5% for PVC and 77.18% for CPB/PVC by increasing the pH from 6.0 to 7.0 values. Accordingly, a pH of 5.5–6.0 was determined as the optimal pH value to conduct the succeeding rare earth ion sorption experiments.

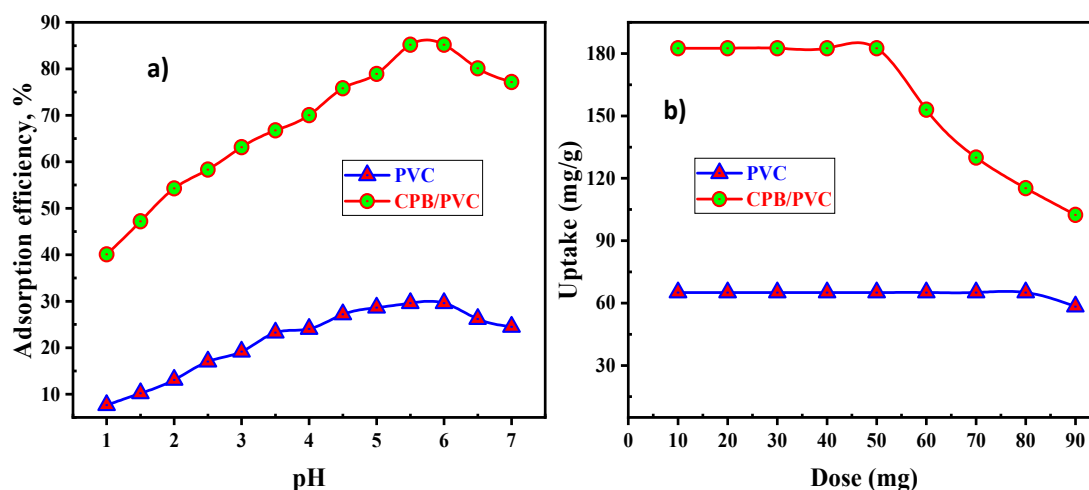


**Figure 6.** Effect of (a) pH and (b) sorbent dose on the REE sorption.

#### 3.2.2. Effect of Sorbent Dose

The effect of sorbent dosage on rare earth ion sorption uptake was studied. The obtained results in Figure 6b revealed that the uptakes of RE ions decreased from 65.12 and 182.6 mg/g to 58.33 and 102.44 mg/g with an increase in the dosage of sorbent material from 10 to 90 mg for PVC and CPB/PVC, respectively. Due to an increase in the surface area, more ion exchange sites exist for ion exchange procedures at a higher dose. Thus, the 50 mg dose was considered as a choice of sorbent dose in the subsequent experiments.

#### 3.2.3. Effect of Contact Time

The influence of agitation time on the RE ion sorption on either PVC or CPB/PVC sorbents was studied from 5–120 min, although the other sorption factors were kept

constant. As observed in Figure 7a, the sorption efficiency of REEs was increased gradually as the sorption time increased until it achieved equilibrium at 60 min, where its uptake was 65.12 mg/g for PVC and remained constant up to 120 min. The sorption uptake of RE ions gradually increased from 49.25 to 182.6 mg/g after 60 min using CPB/PVC, and then equilibrium was achieved.

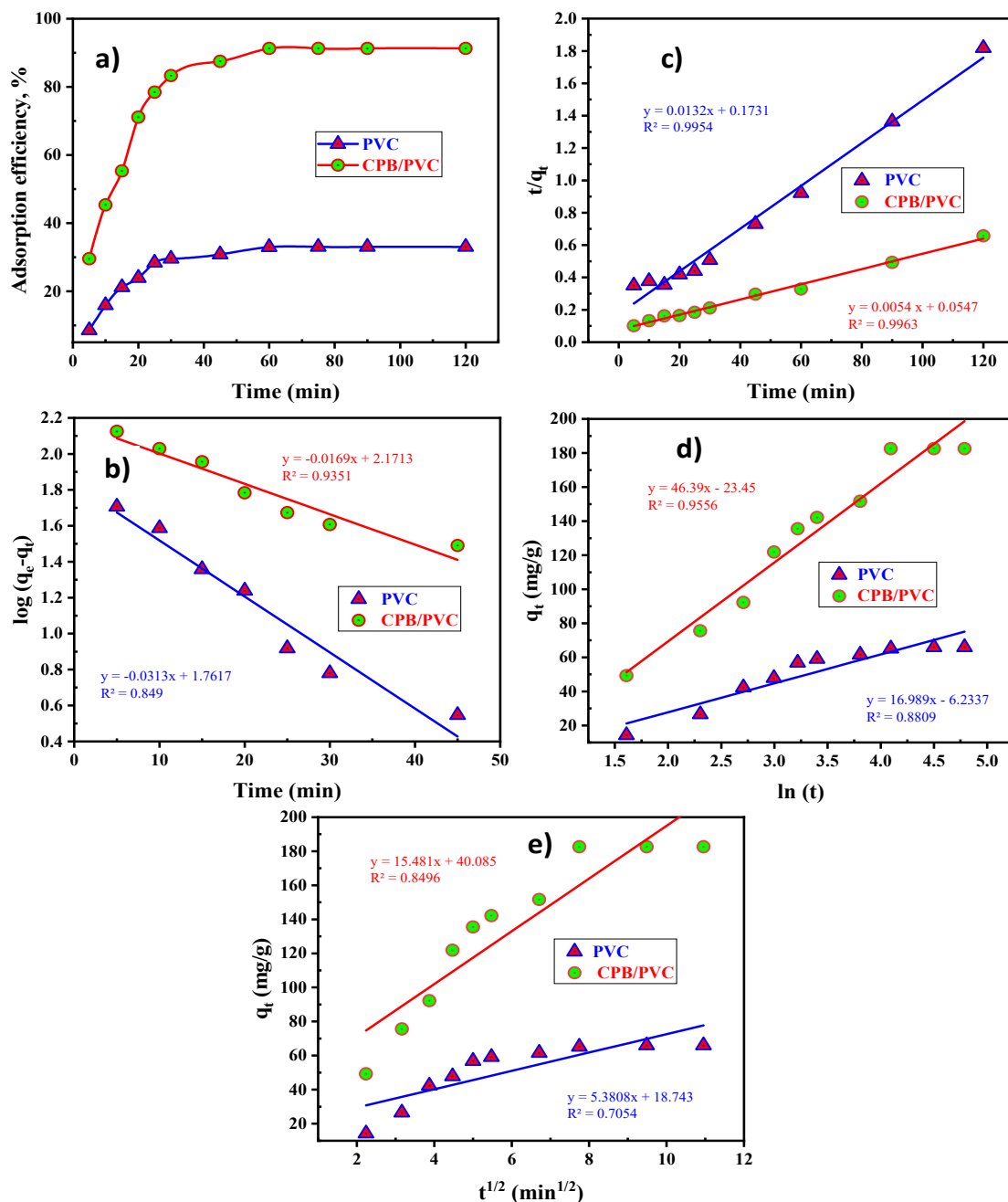


Figure 7. (a) Effect of contact time, (b) Pseudo-first-order, (c) Pseudo-second-order, (d) Elovich, (e) Intra-particle diffusion models of REE sorption on PVC and CPB/PVC.



## Kinetic Characteristics

Different kinetic models were performed for exponential data to assume the RE ion sorption kinetics on PVC or CPB/PVC. The equation of the pseudo-first-order kinetic model was expressed as [48–51]:

$$\log(q_e - q_t) = \log q_e - \left(\frac{k_1 t}{2.303}\right) \quad (4)$$

Both  $q_e$  and  $q_t$  (mg/g) are defined as the adsorbed amount of RE ions at equilibrium and at time  $t$  (min), and  $k_1$  ( $\text{min}^{-1}$ ) represents the pseudo-first-order rate constant. The results obtained from Figure 7b clarified that the  $R^2$  and  $q_{e(\text{cal})}$  values for RE ion sorption on PVC or CPB/PVC did not follow a pseudo-first-order kinetic model.

The pseudo-second-order kinetic model was introduced by [52–54]:

$$\frac{t}{q_t} = \frac{1}{k_2 q_e^2} + \frac{t}{q_e} \quad (5)$$

where  $k_2$  refers to the pseudo-second-order rate constant (g/mg.min). From the data in Figure 7c, the plots exhibited straight lines for PVC and CPB/PVC with a  $R^2$  of about 0.995 and 0.996, respectively, nearly to unity. The sorption processes were right to the pseudo-second-order model, as observed in Table 2. Additionally, the proposed values ( $q_{\text{cal}}$ ) of adsorbed amounts at equilibrium were close to the practical sorption uptakes ( $q_{\text{exp}}$ ). The data show that the RE ion sorption upon PVC or CPB/PVC well obeyed the pseudo-second-order kinetic model.

**Table 2.** Kinetic factors for REE sorption upon PVC and CPB/PVC sorbents.

| Kinetic Models           | Parameters                                 | PVC                   | CPB/PVC               |
|--------------------------|--|-----------------------|-----------------------|
| Pseudo-first-order       | $q_e$ (mg/g)                               | 57.77                 | 148.35                |
|                          | $k_1$ (1/min)                              | 0.075                 | 0.039                 |
|                          | $R^2$                                      | 0.85                  | 0.93                  |
| Pseudo-second-order      | $q_e$ (mg/g)                               | 75.75                 | 185.18                |
|                          | $K_2$ (g/md.min)                           | $1.01 \times 10^{-3}$ | $5.33 \times 10^{-4}$ |
|                          | $R^2$                                      | 0.95                  | 0.996                 |
| Elovich                  | $\alpha$ (mg/g.min)                        | 11.73                 | 27.13                 |
|                          | $\beta$ (g/mg)                             | 0.0589                | 0.022                 |
|                          | $R^2$                                      | 0.881                 | 0.956                 |
| Intra-particle diffusion | $k_{\text{id}}$ (mg/g.min <sup>1/2</sup> ) | 5.38                  | 15.48                 |
|                          | $I$ (mg/g)                                 | 18.74                 | 40.08                 |
|                          | $R^2$                                      | 0.705                 | 0.849                 |
| Practical capacity       | $q_{\text{exp}}$ (mg/g)                    | 65.13                 | 182.60                |

The Elovich kinetic model [55–57] designates the chemical sorption characteristic, and is generally a linear equation according to the following:

$$q_t = \left[\left(\frac{1}{\beta}\right) \ln \alpha \beta\right] + \left[\left(\frac{1}{\beta}\right) \ln t\right] \quad (6)$$

where  $\alpha$  corresponds to the initial sorption rate (mg/g min), while  $\beta$  denotes the Elovich constant (g/mg). From Figure 7d,  $R^2$  was 0.881 and 0.956 for PVC and CPB/PVC, respectively. Hence, it was seen that the Elovich model was not suitable for the sorption processes.

The intraparticle model describes the correlation between the RE ion uptake ( $q_t$ ) sorbed at a time ( $t$ ) vs. the time square root ( $t^{1/2}$ ) linearly and can be expressed as [58]:

$$q_t = k_{\text{id}} t^{1/2} + I \quad (7)$$

where the  $k_{id}$  symbolizes the initial rate constant ( $\text{mg/g}\cdot\text{min}^{1/2}$ ) of intra-particle diffusion; and  $I$  provides a perception of the boundary layer thickness.

The  $K_{id}$  values were estimated using the intra-particle diffusion plot's slope, as seen in Figure 7e. The  $R^2$  values (0.705 and 0.849) showed that the intra-particle diffusion processes were not the rate-limiting stage of the PVC and CPB/PVC sorbents. The obtained parameters for this model are shown in Table 2. This means that intra-particle diffusion models would not be the rate-limiting stage.

### 3.2.4. Effect of Initial REE Concentration

The attained results featured in Figure 8a show that the uptake ( $q_e$ ,  $\text{mg/g}$ ) of RE ions increased with increasing initial RE ions concentration. The maximum uptake was achieved at 200  $\text{mg/L}$  of RE ions. The maximal loading amount of RE ions on the PVC and CPB/PVC sorbents was 65.2 and 182.6  $\text{mg/g}$ , respectively. The loaded REE uptake ( $q_e$ ) was still constant after 200  $\text{mg/L}$  because the two sorbents reached their maximum loading capacities (saturation capacities). RE ions filled all active sites of the two sorbents.

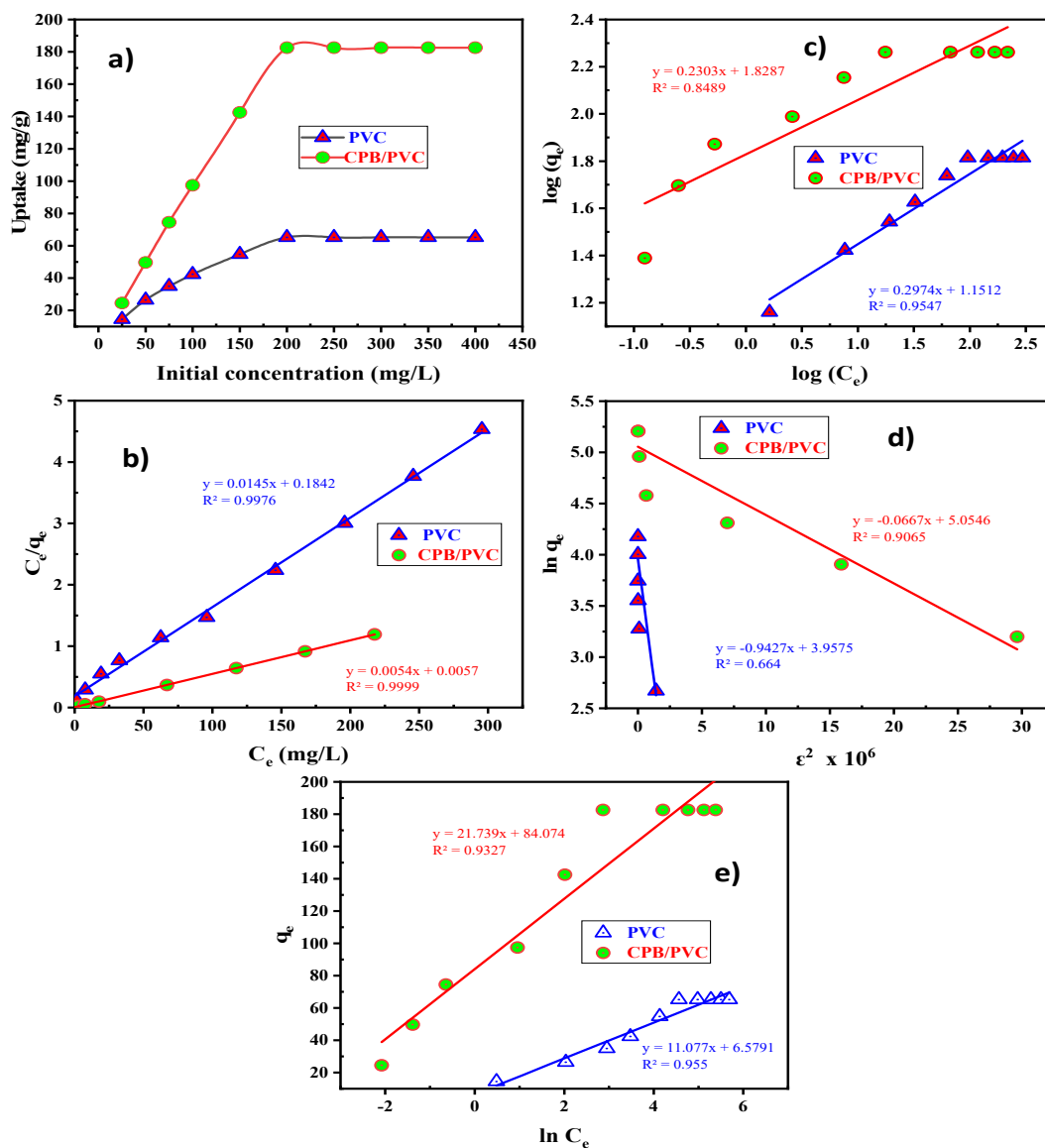


Figure 8. (a) Effect of initial REE concentration on REE uptake, (b) Langmuir, (c) Freundlich, (d) Dubinin and Radushkevich, and (e) Temkin isotherm models of REE sorption on PVC and CPB/PVC.

### Isotherm Characteristics

Studying the sorption isotherm models was necessary to discover the details of the sorption process such as the mechanism, surface properties, and other parameters that affect the sorption procedures.

In accordance with the Langmuir isotherm model, REs ion uptake occurs on a homogeneous surface through the monolayer of RE ions sorbed on the surface of PVC or CPB/PVC sorbents with steady sorption energy. In addition, there should be immobilization of the RE ions on the surface plane [59,60]. The linearized Langmuir isotherm model allowed for the intention of uptake capacity and Langmuir constant as follows:

$$\frac{C_e}{q_e} = \frac{1}{q_{\max} b} + \frac{C_e}{q_{\max}} \quad (8)$$

where  $C_e$  (mg/L) refers to the equilibrium concentration in the aqueous layer, while  $q_e$  and  $q_{\max}$  (mg/g) are the equilibrium and the maximum amount sorbed per unit weight of sorbent, respectively; and  $b$  is a constant correlated to the ability of the binding sites and the sorption energy (L/mg).

The plots of  $C_e/q_e$  vs.  $C_e$  were tabulated in Table 3 and Figure 8b. From the obtained results, the calculated maximum capacities (68.96 and 185.18 mg/g) corresponded more to the practical data (65.13 and 182.60 mg/g), and the  $R^2$  was close to unity for both the PVC and CPB/PVC sorbents. Therefore, the working sorption process could obey the Langmuir sorption model.

**Table 3.** Isotherm restrictions of isotherm modeling for REE sorption upon the PVC and CPB/PVC sorbents.

| Isotherm Models    | Parameters                                 | PVC    | CPB/PVC |
|--------------------|--|--------|---------|
| Langmuir           | $q_{\max}$ (mg/g)                          | 68.96  | 185.18  |
|                    | $b$ (L/mg)                                 | 0.079  | 0.947   |
|                    | $R^2$                                      | 0.997  | 0.999   |
| Freundlich         | $K_f$ (mg/g)                               | 14.16  | 67.41   |
|                    | $1/n$ (mg.min/g)                           | 0.297  | 0.230   |
|                    | $R^2$                                      | 0.955  | 0.849   |
| D–R                | $q_D$ (mg/g.)                              | 52.33  | 156.74  |
|                    | $B_D$ (mol <sup>2</sup> /kJ <sup>2</sup> ) | 0.943  | 0.067   |
|                    | $E$ (kJ/mol)                               | 0.728  | 2.738   |
|                    | $R^2$                                      | 0.664  | 0.906   |
| Temkin             | $b_T$ (J/mol)                              | 223.67 | 113.97  |
|                    | $K_T$ (L/g)                                | 1.81   | 47.79   |
|                    | $R^2$                                      | 0.955  | 0.933   |
| Practical capacity | $q_{\text{exp}}$ (mg/g)                    | 65.13  | 182.60  |

The Freundlich isotherm model was applied to explore the RE ion sorption on the studied sorbent's surface. It supposes that REE sorption takes place with various energetic layers of the active sites [61]. Equation (9) represents the Freundlich isotherm model:

$$\log q_e = \log K_f + \left[ \left( \frac{1}{n} \right) \log C_e \right] \quad (9)$$

where  $K_f$  (mg/g) represents the constant related to overall RE ion sorption uptake and  $n$  is related to surface heterogeneity. The constant  $n$  was deliberated at the slope of  $\log q_e$  against the  $\log C_e$  plot, as demonstrated in Figure 8c.  $K_f$  was calculated from the intercept simultaneously; the  $K_f$  (mg/g) values were less than the two sorbents' experimental capacity of RE ions. The  $1/n$  values were less than 1.0, demonstrating that RE ions preferred

sorption by the PVC and CPB/PVC sorbents, while the  $R^2$  values were 0.955 and 0.849; this revealed that the Freundlich model also did not match the gained experimental results.

The Dubinin–Radushkevich (D–R) isotherm model offers a hypothetical distribution of energy sites. It is an excellent model to distinguish between physisorption and chemisorption [62,63]. It can be stated as follows:

$$\ln q_e = \ln q_D - B_D \varepsilon^2 \quad (10)$$

where  $q_D$  is the monolayer uptake (mg/g);  $B_D$  ( $\text{mol}^2/\text{kJ}^2$ ) is related to the sorption energy constant; and  $\varepsilon$  represents the Polanyi potential correlated to the equilibrium concentration as the subsequent:

$$\varepsilon = RT \ln \left( 1 + \frac{1}{C_e} \right) \quad (11)$$

where  $T$  corresponds to the absolute temperature (K), and  $R$  is associated with the universal gas constant (8.314 J/mol.K). The following relation could calculate the free energy ( $E$ ):

$$E = \frac{1}{\sqrt{2 B_D}} \quad (12)$$

where the  $q_D$  and  $B_D$  constants are inferred from the relation  $\ln q_e$  vs.  $\varepsilon^2$  plots (Table 3 and Figure 4d). The sorption process is chemical if the magnitude of  $E$  is in the variety of 8.0–16.0 kJ/mol whereas the sorption process is physical if  $E$  is less than 8.0 kJ/mol [36,37]. The calculated  $E$  was less than 1.0 kJ/mol for RE ion sorption of the two studied sorbents, demonstrating that RE ions sorption proceeds via physisorption. However, ( $R^2$ ) values were 0.664 and 0.906 for PVC and CPB/PVC, respectively. Consequently, the (D–R) model did not suit the RE ion sorption on PVC and CPB/PVC.

The Temkin isotherm model postulated linear reduction in the sorption energy as the achievement rate of the sorption process toward the sorbent increases. Because of the sorbent–REEs interfaces, the sorption heat of all ions in the layer is regularly reduced with coverage. Moreover, the sorption process was described by a constant dispersal of binding energies, ready for maximum binding energy [64]. The Temkin isotherm could be indicated as follows:

$$q_e = \left[ \left( \frac{RT}{b_T} \right) \ln K_T \right] + \left[ \left( \frac{RT}{b_T} \right) \ln C_e \right] \quad (13)$$

where  $b_T$  (kJ/mol) is defined as a constant interrelated to sorption heat; and  $K_T$  (L/g) points to the equilibrium binding constant. Both  $b_T$  and  $K_T$  were obtained by plotting  $q_e$  vs.  $\ln C_e$  as shown in Table 3 and Figure 8e. From the obtained data, the values of  $R^2$  were 0.955 and 0.933 for the PVC and CPB/PVC sorbents, respectively. The data assumed that the sorption processes did not obey the Temkin isotherm model.

### 3.2.5. Effect of Temperature

The influence of system temperature on RE ion sorption was examined from 25–60 °C. As demonstrated in Figure 9a, the REE sorption uptake of PVC and CPB/PVC diminished from 65.13 and 182.60 mg/g to 55.37 and 150.20 mg/g with an increase in the temperature due to the decomposition of the sorbent structure and decreased active sites. As a result, the ambient temperature was selected as the optimum temperature for RE ion sorption on the two sorbents.

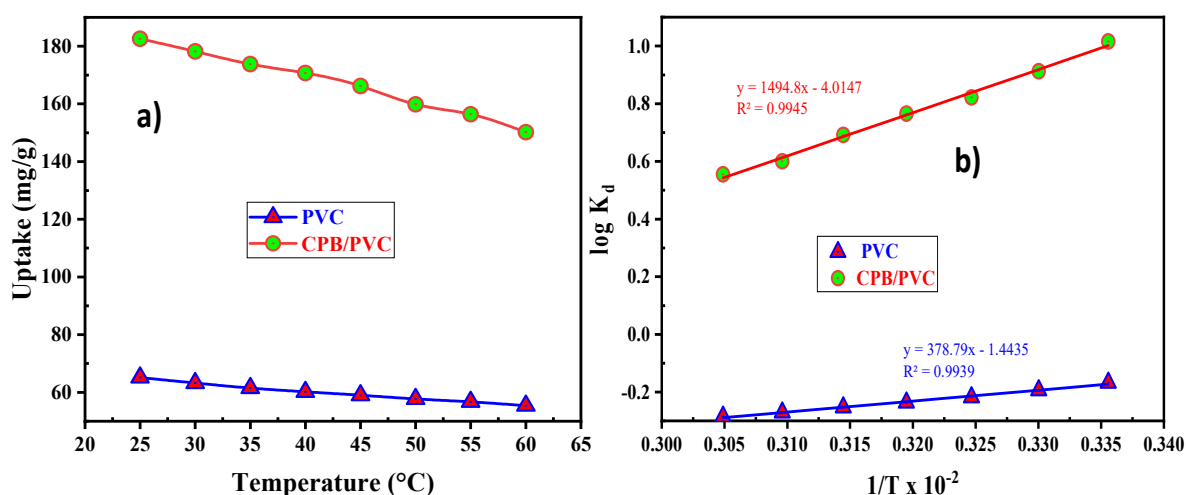


**Figure 9.** (a) Effect of temperature on REE uptake, and (b) log  $K_d$  vs.  $1/T$  relation of REE sorption on PVC, and CPB/ PVC.

#### Thermodynamic Studies

The effectiveness of temperature on the RE ions sorption process was examined to investigate the thermodynamic factors and identify the nature of the sorption process. It was detected that the sorption efficiencies of the two sorbents were reduced with an increase in temperature. The experimental data were utilized to determine the change in entropy ( $\Delta S^\circ$ ), enthalpy ( $\Delta H^\circ$ ), and thermodynamic parameters of RE ions sorption on PVC and CPB/PVC were described from successive equations [65–67].

$$\log K_d = \frac{\Delta S^\circ}{2.303R} - \frac{\Delta H^\circ}{2.303RT} \tag{14}$$

$$\Delta G^\circ = \Delta H^\circ - T\Delta S^\circ \tag{15}$$

where  $K_d$  refers to the RE ion sorption constant (L/g);  $\Delta H^\circ$  is the enthalpy changes (kJ/mol);  $\Delta S^\circ$  symbolizes for the changes in the entropy of RE ions sorption (J/mol.K);  $\Delta G^\circ$  corresponds to Gibbs free energy (kJ/mol); and  $T$  represents the absolute temperature (K). Both  $\Delta S^\circ$  and  $\Delta H^\circ$  can be gained from the intercept and slope of  $\log K_d$  vs.  $1/T$  plot (Figure 9b). The  $\Delta H^\circ$ ,  $\Delta S^\circ$ , and  $\Delta G^\circ$  values for the two sorbents can be found in Table 4. The positive  $\Delta G^\circ$  values of the PVC sorbent proved that the RE ion sorption process is non-spontaneous. Nonetheless, the negative  $\Delta G^\circ$  value verified the spontaneous behavior of RE ion sorption on the CPB/PVC. Furthermore, the process was favorable for forming an electrostatic interaction between RE ions and CPB/PVC sorbent.

**Table 4.** Thermodynamic parameters of REE sorption on the PVC and CPB/PVC.

| Parameters                  | Temperature, K | PVC     | CPB/PVC |
|-----------------------------|----------------|---------|---------|
| $\Delta G^\circ$ , kJ/mol   | 298.0          | 0.9748  | −5.7038 |
|                             | 303.0          | 1.1128  | −5.3193 |
|                             | 308.0          | 1.2508  | −4.9348 |
|                             | 313.0          | 1.3888  | −4.5503 |
|                             | 318.0          | 1.5268  | −4.1658 |
|                             | 323.0          | 1.6648  | −3.7813 |
|                             | 328.0          | 1.8028  | −3.3968 |
| $\Delta H^\circ$ , kJ/mol   | 333.0          | 1.9408  | −3.0123 |
|                             |                | −7.25   | −28.62  |
| $\Delta S^\circ$ , kJ/mol.K |                | −0.0276 | −0.0769 |

The negative  $\Delta H^\circ$  values might propose the exothermic sorption process. Additionally, the negative  $\Delta S^\circ$  values indicated the probability of the sorption processes and the decrease in randomness at the connection point between the sorbent/sorbate during the sorption processes of RE ions on PVC and CPB/PVC.

### 3.3. Desorption Studies

The desorption of metal ions is decisive in designing a sorption system; this step is intended to improve the desired metal ion concentration for final recovery. Moreover, this process is also vital in testing the recyclability of the sorbent, which is a significant feature for economic competitiveness.

#### 3.3.1. Type of Eluting Agent

Impact of eluting agents on the desorption process of rare earth ions from the loaded PVC and CPB/PVC was explored through the batch technique by shaking different eluting agents (NaCl, HCl, HNO<sub>3</sub>, and H<sub>2</sub>SO<sub>4</sub>) while the other parameters were still constant at 0.5 M of the eluting agent at a 1:50 S:L phase ratio (0.1 g of sorbent and 5.0 mL of eluting agent) for 30 min at ambient temperature. As seen in Figure 10a, it was observed that the desorption efficiency of RE ions from loaded PVC or CBP/PVC using 0.5 M hydrochloric acid reached maximum desorption efficiencies, attaining 57.5 and 62.4%, respectively. Therefore, it was concluded that hydrochloric acid can be used to desorb REEs quantitatively from the surfaces of the two sorbents.

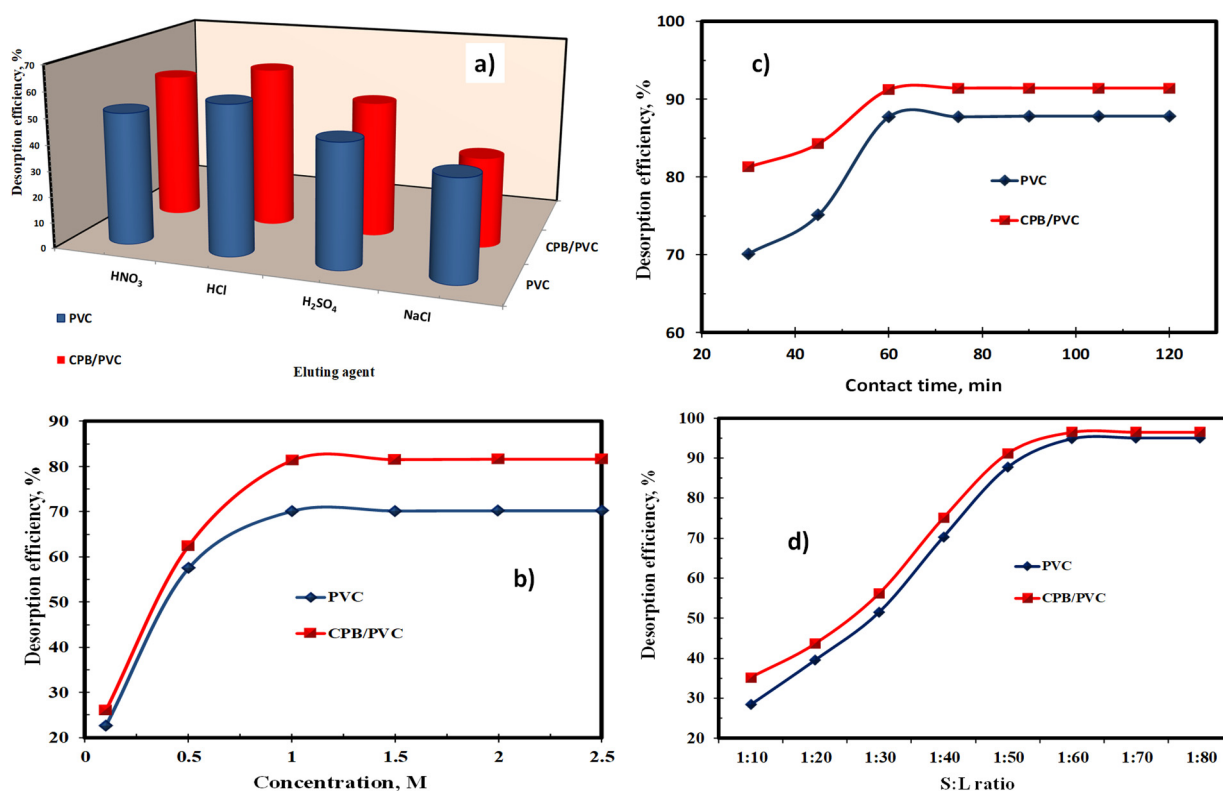


**Figure 10.** Effect of (a) eluting agents, (b) HCl concentration, (c) desorption time, and (d) S:L ratio upon REE desorption efficiency for the PVC and CPB/PVC sorbents.

#### 3.3.2. HCl Concentration

The REE stripping from their loaded sorbents was studied using a concentration range of HCl from 0.1–2.5 M. The other factors were kept constant using 0.1 g loaded sorbents and 5.0 mL of the eluting solution for 30 min at 25 °C room temperature. The gained data represented in Figure 10b illustrates that the desorption efficacy of RE ions

improved with an increase in the concentration of HCl up to 1.0 M. In contrast, the optimum values of desorption were achieved at 70.1 and 81.3% for the PVC and CBP/PVC sorbents, respectively. Consequently, it can be concluded that 1.0 M HCl is recommended for the elution process of rare earth ions.

### 3.3.3. Desorption Time

The influence of desorption time on the RE ion desorption was examined. For this purpose, 0.1 g REE/sorbent (REE/PVC, or REE/CPB/PVC) were mixed with 5.0 mL of 1.0 M HCl by different contact times ranging from 30 to 120 min at ambient temperature. According to the data represented in Figure 10c, it was clear that 60 min of contact time was required for the maximum RE ion desorption efficiencies at 87.7% and 91.2% for the PVC and CPB/PVC sorbents, respectively.

### 3.3.4. S:L Phase Ratio

The influence of S:L phase ratio on REE desorption from their loaded sorbents was examined in the range of 1:10 to 1:80 to investigate the minimum volume of eluting agent required. It was observed that the rare earth ion desorption efficiency was improved by raising the S:L ratio to 1:60; following this, the REE desorption efficiencies were nearly constant at 94.8 and 96.5% for the PVC and CBP/PVC sorbents, respectively (Figure 10d). Therefore, the 1:60 S:L ratio of the studied sorbents was optimized for the subsequent experiments.

### 3.4. Regeneration

The PVC or CBP/PVC were regenerated by 1.0 M of HCl and 1:60 S:L ratio at room temperature for 60 min contact time to be recycled and reused to another sorption experiment. The sorption and desorption processes were recurrent until the desorption efficiency was decreased from 94.8 and 96.5% to 76.0 and 78.0% for the PVC and CBP/PVC, respectively, after eight consecutive sequences. It was decided that there was good sorption constancy of the two considered sorbents for REE recovery.

### 3.5. Case Study

The studied sample consisted of lamprophyre dikes collected from the area of Abu Rusheid in the South-Eastern Desert of Egypt. Lamprophyre dikes are mainly comprised of kaolinite, muscovite, K-feldspars, quartz, biotite, and plagioclases [68]. The sample of lamprophyre dikes was wholly analyzed by suitable techniques to specify major as well as trace ions. The data clearly show that analysis of SiO<sub>2</sub>, Fe<sub>2</sub>O<sub>3</sub>, Al<sub>2</sub>O<sub>3</sub>, K<sub>2</sub>O, CaO, and P<sub>2</sub>O<sub>5</sub> assayed 46.3, 15.36, 16.8, 2.8, 2.3, and 1.02%, respectively. The sample had 3274 mg/kg of yttrium and 400 mg/kg of uranium. Furthermore, individual rare earth ions were analyzed using the ICP-OES technique (Table 5) [69].

The leach liquor of REEs was prepared by treating 2.0 kg of a milled sample of lamprophyre dike with 8.0 L of 3.0 M HCl for 3.0 h at ambient temperature [69]. The residue was then filtered, and the leach solution was analyzed, as shown in Tables 6 and 7.

After preparing and analyzing leach liquor according to the studied optimum condition, PVC and CBP/PVC were used to carefully remove rare earth ions from the treated leachate under optimal conditions. Furthermore, the sorption efficiencies of 48.1 and 87.5% were obtained for PVC and CPB/PVC, respectively. The REE sorption efficiency from leach liquor was slightly lower than the maximum sorption efficiency of PVC and CBP/PVC sorbents from the pure synthetic solution due to impurities in leach liquor.

**Table 5.** Chemical analysis of lamprophyre dike ore.

| Major Oxides                   | Wt., % | Metal Ions       | mg/kg | REE Ions         | mg/kg |
|--------------------------------|--------|------------------|-------|------------------|-------|
| SiO <sub>2</sub>               | 46.30  | U <sup>6+</sup>  | 400   | Y <sup>3+</sup>  | 3274  |
| Al <sub>2</sub> O <sub>3</sub> | 16.80  | Ba <sup>2+</sup> | 167   | Ce <sup>3+</sup> | 160   |
| Fe <sub>2</sub> O <sub>3</sub> | 15.36  | Pb <sup>2+</sup> | 596   | La <sup>3+</sup> | 90    |
| TiO <sub>2</sub>               | 3.40   | V <sup>5+</sup>  | 240   | Nd <sup>3+</sup> | 143   |
| K <sub>2</sub> O               | 2.80   | Cu <sup>2+</sup> | 367   | Sm <sup>3+</sup> | 26    |
| Na <sub>2</sub> O              | 0.48   | Ni <sup>2+</sup> | 86.7  | Gd <sup>3+</sup> | 60    |
| CaO                            | 2.30   | Cd <sup>2+</sup> | 49.5  | Ho <sup>3+</sup> | 171   |
| MnO                            | 0.65   | Zn <sup>2+</sup> | 6348  | Er <sup>3+</sup> | 145   |
| P <sub>2</sub> O <sub>5</sub>  | 1.02   | Th <sup>4+</sup> | 39    | Yb <sup>3+</sup> | 550   |
| MgO                            | 0.06   |                  |       | Lu <sup>3+</sup> | 65    |
| LOI*                           | 8.75   |                  |       | Pr <sup>3+</sup> | 170   |
| Total                          | 97.92  |                  |       |                  |       |

LOI\*: Loss of ignition (1000 °C).

**Table 6.** Chemical investigation of metal ions in the leach liquor.

| Metal Ions       | Conc. (g/L) | Metal Ions       | Conc. (mg/L) |
|------------------|-------------|------------------|--------------|
| Si <sup>4+</sup> | 1.35        | U <sup>6+</sup>  | 94.0         |
| Al <sup>3+</sup> | 2.34        | REEs             | 1140.0       |
| Ti <sup>4+</sup> | 0.32        | Ba <sup>2+</sup> | 44.0         |
| Fe <sup>3+</sup> | 3.57        | Pb <sup>2+</sup> | 103.0        |
| Mn <sup>2+</sup> | 0.50        | V <sup>5+</sup>  | 51.0         |
| Mg <sup>2+</sup> | 0.31        | Cu <sup>2+</sup> | 85.0         |
| Ca <sup>2+</sup> | 0.67        | Ni <sup>2+</sup> | 19.0         |
| K <sup>+</sup>   | 0.73        | Th <sup>4+</sup> | 5.0          |
| Na <sup>+</sup>  | 0.99        | Zn <sup>2+</sup> | 620.0        |
| P <sup>5+</sup>  | 0.12        |                  |              |

**Table 7.** Chemical investigation of RE ions in the leach liquor.

| Metal Ions       | Conc. (mg/L) | Metal Ions       | Conc. (mg/L) |
|------------------|--------------|------------------|--------------|
| La <sup>3+</sup> | 21.0         | Tb <sup>3+</sup> | 0.0          |
| Ce <sup>3+</sup> | 37.0         | Dy <sup>3+</sup> | 0.0          |
| Pr <sup>3+</sup> | 40.0         | Ho <sup>3+</sup> | 40.0         |
| Nd <sup>3+</sup> | 34.0         | Er <sup>3+</sup> | 34.0         |
| Sm <sup>3+</sup> | 6.0          | Tm <sup>3+</sup> | 0.0          |
| Eu <sup>3+</sup> | 0.0          | Yb <sup>3+</sup> | 129.0        |
| Gd <sup>3+</sup> | 14.0         | Lu <sup>3+</sup> | 16.0         |
| Y <sup>3+</sup>  | 769.0        |                  |              |

Loaded sorbents (REE/PVC and REE/CPB/PVC) were subjected to desorption under the studied optimum conditions (1.0 M HCl, 1:60 S:L ratio, 60 min desorption time, 25 °C). Desorption efficiencies of 94.8 and 96.5% of REE/PVC and REE/CPB/PVC were obtained, respectively. After desorption and preconcentration, oxalic acid was used to precipitate RE ions as RE oxalates. The RE ions were precipitated using 20.0% oxalic acid (H<sub>2</sub>C<sub>2</sub>O<sub>4</sub>) as a rare earth oxalate precipitate [70,71]. The obtained precipitates of the two sorbents were analyzed and confirmed using SEM-EDX along with ICP-OES to detect their individual REEs distribution, as presented in Table 8 and Figure 11.



**Table 8.** Chemical analysis of RE oxalate products obtained from REEs loaded on two sorbents using ICP-OES.

| Metal Ions       | Conc. (mg/kg) |           |
|------------------|---------------|-----------|
|                  | PVC           | CPB/PVC   |
| La <sup>3+</sup> | 2415.394      | 7171.722  |
| Ce <sup>3+</sup> | 4546.624      | 13,499.71 |
| Pr <sup>3+</sup> | 4830.788      | 14,343.44 |
| Nd <sup>3+</sup> | 4120.378      | 12,234.11 |
| Sm <sup>3+</sup> | 568.328       | 1687.464  |
| Gd <sup>3+</sup> | 1776.025      | 5273.325  |
| Ho <sup>3+</sup> | 4901.829      | 14,554.38 |
| Yb <sup>3+</sup> | 17,476.09     | 51,889.52 |
| Lu <sup>3+</sup> | 1989.148      | 5906.124  |
| Y <sup>3+</sup>  | 99,457.4      | 295,306.2 |
| Total            | 142,082       | 421,866   |

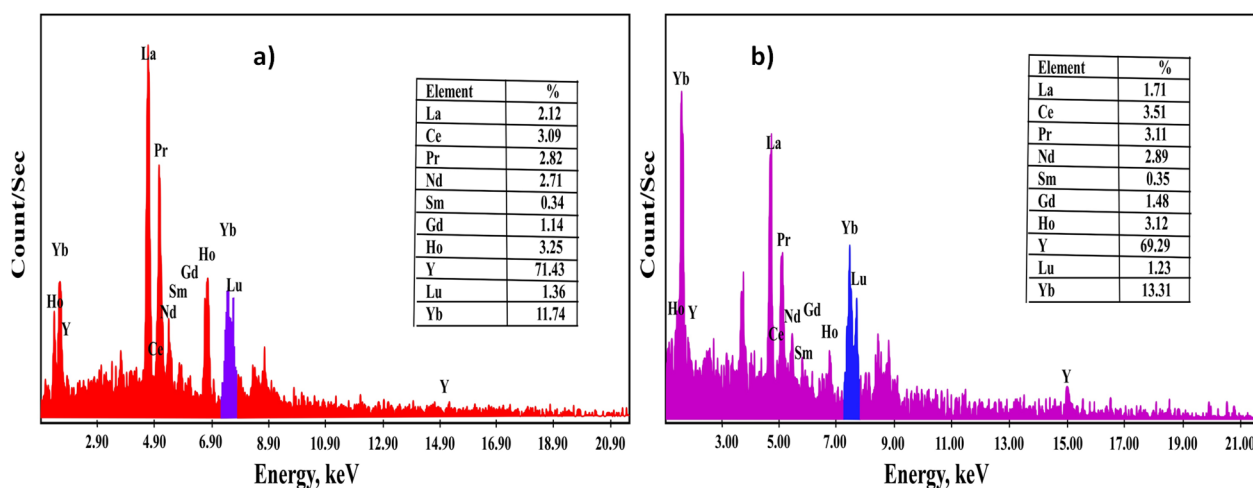


**Figure 11.** (a) The environmental scanning electron microscope of rare earth oxalate from REEs/PVC. (b) The environmental scanning electron microscope of rare earth oxalate from REEs/CPB/PVC.

### 4. Conclusions

Polyvinyl chloride was treated with cetylpyridinium bromide to obtain a highly efficient, low-cost sorbent with outstanding results for RE ion sorption. The PVC and CPB/PVC were utilized to enhance the RE ion uptake from a chloride solution. The optimum sorption conditions were pH 6.0, 60 min equilibrium time, and 25 °C. The uptake of RE ions upon PVC and CPB/PVC were 65.13 and 182.6 mg/g, respectively. The RE ion sorption well obeyed the Langmuir isotherm model, and the pseudo-second-order model proved that the sorption occurred through chemical interaction. Additionally, the thermodynamic studies proved that the sorption of RE ions was exothermic and spontaneous for the CPB/PVC sorbent, and the maximum elution of RE ions from the loaded sorbent was obtained at the 1:60 S:L ratio and 1.0 M HCl for 60 min at ambient temperature. Thus, the CPB/PVC sorbent was recognized as a competitive sorbent for REE recovery.

**Author Contributions:** Conceptualization, E.M.A. and M.A.H.; Methodology, E.M.A. and M.A.H.; Software, E.M.A., A.K.S., and M.F.C.; Validation, M.Y.H. and M.I.S.; Formal analysis, E.M.A.; Investigation, E.M.A., A.K.S., and M.A.H.; Resources, E.M.A.; Data curation, E.M.A., and A.K.S.; Writing—original draft preparation, E.M.A.; Writing—review and editing, E.M.A., A.K.S., and M.F.C.; Visualization, E.M.A. and M.F.C.; Supervision, M.A.H., M.F.C., T.A.L., and S.A.A.E.-E.; Project administration, T.A.L., and S.A.A.E.-E.; Funding acquisition, J.S.A.-O. All authors have read and agreed to the published version of the manuscript.

**Funding:** The authors express their gratitude to Princess Nourah bint Abdulrahman University Researchers Supporting Project number (PNURSP2022R13), Princess Nourah bint Abdulrahman University, Riyadh, Saudi Arabia.

**Institutional Review Board Statement:** Not applicable.

**Informed Consent Statement:** Not applicable.

**Data Availability Statement:** Not applicable.

**Acknowledgments:** The authors express their gratitude to Princess Nourah bint Abdulrahman University Researchers Supporting Project number (PNURSP2022R13), Princess Nourah bint Abdulrahman University, Riyadh, Saudi Arabia.

**Conflicts of Interest:** The authors declare no conflict of interest.

## References

1. Yang, X.; Salvador, D.; Makkonen, H.T.; Pakkanen, L. Phosphogypsum Processing for Rare Earths Recovery—A Review. *Nat. Resour.* **2019**, *10*, 325–336. [CrossRef]
2. Bau, M.; Dulski, P. Comparative study of yttrium and rare earth element behaviors in fluorine-rich hydrothermal fluids. *Contrib. Mineral. Petrol.* **1995**, *119*, 213–223. [CrossRef]
3. Wang, X.; Lei, Y.; Ge, J.; Wu, S. Production forecast of China's rare earths based on the Generalized Weng model and policy recommendations. *Resour. Policy* **2015**, *43*, 11–18. [CrossRef]
4. Cheira, M.F.; Mira, H.I.; Sakr, A.K.; Mohamed, S.A. Adsorption of U(VI) from acid solution on a low-cost sorbent: Equilibrium, kinetic, and thermodynamic assessments. *Nucl. Sci. Tech.* **2019**, *30*, 156. [CrossRef]
5. Sakr, A.K.; Mohamed, S.A.; Mira, H.I.; Cheira, M.F. Successive leaching of uranium and rare earth elements from El Sela mineralization. *J. Sci. Eng. Res.* **2018**, *5*, 95–111.
6. Moustafa, M.I.; Abdelfattah, N.A. Physical and Chemical Beneficiation of the Egyptian Beach Monazite. *Resour. Geol.* **2010**, *60*, 288–299. [CrossRef]
7. Wu, S.; Bie, C.; Su, H.; Gao, Y.; Sun, X. The effective separation of yttrium and other heavy rare earth elements with salicylic acid derivatives. *Miner. Eng.* **2022**, *178*, 107396. [CrossRef]
8. Alakhras, F.A.; Dari, K.A.; Mubarak, M.S. Synthesis and chelating properties of some poly(amidoxime-hydroxamic acid) resins toward some trivalent lanthanide metal ions. *J. Appl. Polym. Sci.* **2005**, *97*, 691–696. [CrossRef]
9. Jeon, J.H.; Yoon, H.-S.; Kim, C.-J.; Chung, K.W.; Jyothi, R.K. Environmentally sound technology development for processing of rare earth elements from waste permanent magnets synthetic leach solutions: Recovery and separation perspectives. *Sep. Purif. Technol.* **2021**, *275*, 119225. [CrossRef]
10. Sakr, A.K.; Cheira, M.F.; Hassanin, M.A.; Mira, H.I.; Mohamed, S.A.; Khandaker, M.U.; Osman, H.; Eed, E.M.; Sayyed, M.I.; Hanfi, M.Y. Adsorption of Yttrium Ions on 3-Amino-5-Hydroxypyrazole Impregnated Bleaching Clay, a Novel Sorbent Material. *Appl. Sci.* **2021**, *11*, 10320. [CrossRef]
11. Alcaraz, L.; Largo, O.R.; Alguacil, F.J.; Montes, M.Á.; Baudín, C.; López, F.A. Extraction of Lanthanum Oxide from Different Spent Fluid Catalytic Cracking Catalysts by Nitric Acid Leaching and Cyanex 923 Solvent Extraction Methods. *Metals* **2022**, *12*, 378. [CrossRef]
12. García, A.C.; Latifi, M.; Amini, A.; Chaouki, J. Separation of Radioactive Elements from Rare Earth Element-Bearing Minerals. *Metals* **2020**, *10*, 1524. [CrossRef]
13. Liu, C.; Yan, Q.; Zhang, X.; Lei, L.; Xiao, C. Efficient Recovery of End-of-Life NdFeB Permanent Magnets by Selective Leaching with Deep Eutectic Solvents. *Environ. Sci. Technol.* **2020**, *54*, 10370–10379. [CrossRef] [PubMed]
14. Zhang, W.; Feng, D.; Xie, X.; Tong, X.; Du, Y.; Cao, Y. Solvent extraction and separation of light rare earths from chloride media using HDEHP-P350 system. *J. Rare Earth.* **2022**, *40*, 328–337. [CrossRef]
15. Moldoveanu, G.; Papangelakis, V. Chelation-Assisted Ion-Exchange Leaching of Rare Earths from Clay Minerals. *Metals* **2021**, *11*, 1265. [CrossRef]
16. Choubey, P.K.; Singh, N.; Panda, R.; Jyothi, R.K.; Yoo, K.; Park, I.; Jha, M.K. Development of Hydrometallurgical Process for Recovery of Rare Earth Metals (Nd, Pr, and Dy) from Nd-Fe-B Magnets. *Metals* **2021**, *11*, 1987. [CrossRef]
17. Chen, Z.; Li, Z.; Chen, J.; Kallem, P.; Banat, F.; Qiu, H. Recent advances in selective separation technologies of rare earth elements: A review. *J. Environ. Chem. Eng.* **2022**, *10*, 107104. [CrossRef]
18. Jia, Q.; Tong, S.; Li, Z.; Zhou, W.; Li, H.; Meng, S. Solvent extraction of rare earth elements with mixtures of sec-octylphenoxy acetic acid and bis(2,4,4-trimethylpentyl) dithiophosphinic acid. *Sep. Purif. Technol.* **2009**, *64*, 345–350. [CrossRef]
19. Jorjani, E.; Shahbazi, M. The production of rare earth elements group via tributyl phosphate extraction and precipitation stripping using oxalic acid. *Arab. J. Chem.* **2016**, *9*, S1532–S1539. [CrossRef]
20. Khawassek, Y.K.; Eliwa, A.A.; Gawad, E.A.; Abdo, S.M. Recovery of rare earth elements from El-Sela effluent solutions Peer review under responsibility of The Egyptian Society of Radiation Sciences and Applications. *J. Radiat. Res. Appl. Sci.* **2015**, *8*, 583–589. [CrossRef]


21. Hamza, M.F.; Salih, K.A.M.; Abdel-Rahman, A.A.H.; Zayed, Y.E.; Wei, Y.; Liang, J.; Guibal, E. Sulfonic-functionalized algal/PEI beads for scandium, cerium and holmium sorption from aqueous solutions (synthetic and industrial samples). *Chem. Eng. J.* **2021**, *403*, 126399. [CrossRef]
22. Raju, C.S.K.; Subramanian, M.S. A novel solid phase extraction method for separation of actinides and lanthanides from high acidic streams. *Sep. Purif. Technol.* **2007**, *55*, 16–22. [CrossRef]
23. Helaly, O.S.; Abd El-Ghany, M.S.; Moustafa, M.I.; Abuzaid, A.H.; Abd El-Monem, N.M.; Ismail, I.M. Extraction of cerium(IV) using tributyl phosphate impregnated resin from nitric acid medium. *Trans. Nonferrous Met. Soc. China* **2012**, *22*, 206–214. [CrossRef]
24. Dave, S.R.; Kaur, H.; Menon, S.K. Selective solid-phase extraction of rare earth elements by the chemically modified Amberlite XAD-4 resin with azacrown ether. *React. Funct. Polym.* **2010**, *70*, 692–698. [CrossRef]
25. Jain, V.K.; Pandya, R.A.; Pillai, S.G.; Agrawal, Y.K.; Kanaiya, P.H. Solid-phase extractive preconcentration and separation of lanthanum(III) and cerium(III) using a polymer-supported chelating calix [4] arene resin. *J. Anal. Chem.* **2007**, *62*, 104–112. [CrossRef]
26. Nishihama, S.; Kohata, K.; Yoshizuka, K. Separation of lanthanum and cerium using a coated solvent-impregnated resin. *Sep. Purif. Technol.* **2013**, *118*, 511–518. [CrossRef]
27. Wang, Z.H.; Ma, G.X.; Lu, J.; Liao, W.P.; Li, D.Q. Separation of heavy rare earth elements with extraction resin containing 1-hexyl-4-ethyl-octyl isopropylphosphonic acid. *Hydrometallurgy* **2002**, *66*, 95–99. [CrossRef]
28. Yadav, K.K.; Singh, D.K.; Anitha, M.; Varshney, L.; Singh, H. Studies on separation of rare earths from aqueous media by polyethersulfone beads containing D2EHPA as extractant. *Sep. Purif. Technol.* **2013**, *118*, 350–358. [CrossRef]
29. Lee, G.S.; Uchikoshi, M.; Mimura, K.; Isshiki, M. Separation of major impurities Ce, Pr, Nd, Sm, Al, Ca, Fe, and Zn from La using bis(2-ethylhexyl)phosphoric acid (D2EHPA)-impregnated resin in a hydrochloric acid medium. *Sep. Purif. Technol.* **2010**, *71*, 186–191. [CrossRef]
30. Saito, T.; Sato, H.; Motegi, T. Recovery of rare earths from sludges containing rare-earth elements. *J. Alloy Compd.* **2006**, *425*, 145–147. [CrossRef]
31. Soe, N.N.; Shwe, L.T.; Lwin, K.T. Study on Extraction of Lanthanum Oxide from Monazite Concentrate. *World Acad. Sci. Eng. Technol. Int. J. Chem. Mol. Nucl. Mater. Metall. Eng.* **2008**, *2*, 226–229.
32. Ogata, T.; Narita, H.; Tanaka, M. Adsorption behavior of rare earth elements on silica gel modified with diglycol amic acid. *Hydrometallurgy* **2015**, *152*, 178–182. [CrossRef]
33. Helfferich, F.G. *Ion. Exchange*; Courier Corporation: Chelmsford, MA, USA, 1995.
34. Marczenko, Z.; Balcerzak, M. Chapter 39—Rare-earth elements. In *Analytical Spectroscopy Library*; Marczenko, Z., Balcerzak, M., Eds.; Elsevier: Amsterdam, The Netherlands, 2000; Volume 10, pp. 341–349.
35. Lahsen, T.; Mohamed, S.; Cheira, M.; Zaki, D.; Allam, E. Leaching and Recovery of Rare Earth Elements from Altered Alkaline Granite Rock from Nusab El-Balgum Area, South Western Desert, Egypt. *Res. Artic.* **2016**, *4*, 787–801.
36. Cheira, M.F.; Rashed, M.N.; Mohamed, A.E.; Zidan, I.H.; Awadallah, M.A. The performance of Alizarin impregnated bentonite for the displacement of some heavy metals ions from the wet phosphoric acid. *Sep. Sci. Technol.* **2020**, *55*, 3072–3088. [CrossRef]
37. Cheira, M.F.; Rashed, M.N.; Mohamed, A.E.; Hussein, G.M.; Awadallah, M.A. Removal of some harmful metal ions from wet-process phosphoric acid using murexide-reinforced activated bentonite. *Mater. Today Chem.* **2019**, *14*, 100176. [CrossRef]
38. Cheira, M.F. Performance of poly sulfonamide/nano-silica composite for adsorption of thorium ions from sulfate solution. *SN Appl. Sci.* **2020**, *2*, 398. [CrossRef]
39. Behboudi, A.; Jafarzadeh, Y.; Yegani, R. Polyvinyl chloride/polycarbonate blend ultrafiltration membranes for water treatment. *J. Membr. Sci.* **2017**, *534*, 18–24. [CrossRef]
40. Ahmad, N.; Kausar, A.; Muhammad, B. An investigation on 4-aminobenzoic acid modified polyvinyl chloride/graphene oxide and PVC/graphene oxide based nanocomposite membranes. *J. Plast. Film Sheet.* **2016**, *32*, 419–448. [CrossRef]
41. Li, L.; Sakr, A.K.; Schlöder, T.; Klein, S.; Beckers, H.; Kitsaras, M.-P.; Snelling, H.V.; Young, N.A.; Andrae, D.; Riedel, S. Searching for Monomeric Nickel Tetrafluoride: Unravelling Infrared Matrix Isolation Spectra of Higher Nickel Fluorides. *Angew. Chem. Int. Ed.* **2021**, *60*, 6391–6394. [CrossRef]
42. Sneddon, G.; McGlynn, J.C.; Neumann, M.S.; Aydin, H.M.; Yiu, H.H.P.; Ganin, A.Y. Aminated poly(vinyl chloride) solid state adsorbents with hydrophobic function for post-combustion CO<sub>2</sub> capture. *J. Mater. Chem. A* **2017**, *5*, 11864–11872. [CrossRef]
43. Giannoukos, K.; Salonitis, K. Study of the mechanism of friction on functionally active tribological Polyvinyl Chloride (PVC) – Aggregate composite surfaces. *Tribol. Int.* **2020**, *141*, 105906. [CrossRef]
44. Salih, K.A.M.; Hamza, M.F.; Mira, H.; Wei, Y.; Gao, F.; Atta, A.M.; Fujita, T.; Guibal, E. Nd(III) and Gd(III) Sorption on Mesoporous Amine-Functionalized Polymer/SiO<sub>2</sub> Composite. *Molecules* **2021**, *26*, 1049. [CrossRef]
45. Parameshwaran, R.; Sari, A.; Jalaiah, N.; Karunakaran, R. Chapter 13—Applications of Thermal Analysis to the Study of Phase-Change Materials. In *Handbook of Thermal Analysis and Calorimetry*; Vyazovkin, S., Koga, N., Schick, C., Eds.; Elsevier Science, B.V.: Amsterdam, The Netherlands, 2018; Volume 6, pp. 519–572.
46. Lv, Y.; Liu, J.; Luo, Z.; Wang, H.; Wei, Z. Construction of chain segment structure models, and effects on the initial stage of the thermal degradation of poly(vinyl chloride). *RSC Adv.* **2017**, *7*, 37268–37275. [CrossRef]
47. Roy, K.J.; Anjali, T.V.; Sujith, A. Asymmetric membranes based on poly(vinyl chloride): Effect of molecular weight of additive and solvent power on the morphology and performance. *J. Mater. Sci.* **2017**, *52*, 5708–5725. [CrossRef]

48. Lagergren, S. About the Theory of so Called Adsorption of Soluble Substances. *K. Sven. Vetensk. Handl.* **1898**, *24*, 1–39.
49. Sayed, A.S.; Abdeltmottaleb, M.; Cheira, M.F.; Abdel-Aziz, G.; Gomaa, H.; Hassanein, T.F. Date seed as an efficient, eco-friendly, and cost-effective bio-adsorbent for removal of thorium ions from acidic solutions. *Aswan Univ. J. Environ. Stud.* **2020**, *1*. [CrossRef]
50. Lin, J.; Wang, L. Comparison between linear and non-linear forms of pseudo-first-order and pseudo-second-order adsorption kinetic models for the removal of methylene blue by activated carbon. *Front. Environ. Sci. Eng. China* **2009**, *3*, 320–324. [CrossRef]
51. Mahmoud, N.S.; Atwa, S.T.; Sakr, A.K.; Abdel Geleel, M. Kinetic and thermodynamic study of the adsorption of Ni (II) using Spent Activated clay Mineral. *N. Y. Sci. J.* **2012**, *5*, 62–68. [CrossRef]
52. Ho, Y.S.; McKay, G. Pseudo-second order model for sorption processes. *Process. Biochem.* **1999**, *34*, 451–465. [CrossRef]
53. Cheira, M.; Awadallah, M.; Rashed, M.; Mohamed, A.E. The use of Alizarin modified bentonite for removal of some heavy metals ions from the wet process phosphoric acid. *J. Sci. Res. Sci.* **2018**, *35*, 483–505. [CrossRef]
54. Gado, M.A.; Atia, B.M.; Cheira, M.F.; Elawady, M.E.; Demerdash, M. Highly efficient adsorption of uranyl ions using hydroxamic acid-functionalized graphene oxide. *Radiochim. Acta* **2021**, *109*, 743–757. [CrossRef]
55. Juang, R.-S.; Chen, M.-L. Application of the Elovich Equation to the Kinetics of Metal Sorption with Solvent-Impregnated Resins. *Ind. Eng. Chem. Res.* **1997**, *36*, 813–820. [CrossRef]
56. Wu, F.-C.; Tseng, R.-L.; Juang, R.-S. Characteristics of Elovich equation used for the analysis of adsorption kinetics in dye-chitosan systems. *Chem. Eng. J.* **2009**, *150*, 366–373. [CrossRef]
57. McLintock, I.S. The Elovich Equation in Chemisorption Kinetics. *Nature* **1967**, *216*, 1204–1205. [CrossRef]
58. Ding, L.P.; Bhatia, S.K.; Liu, F. Kinetics of adsorption on activated carbon: Application of heterogeneous vacancy solution theory. *Chem. Eng. Sci.* **2002**, *57*, 3909–3928. [CrossRef]
59. Langmuir, I. The Adsorption of Gases on Plane Surfaces of Glass, Mica and Platinum. *J. Am. Chem. Soc.* **1918**, *40*, 1361–1403. [CrossRef]
60. Gomaa, H.; Cheira, M.F.; Abd-Elmottaleb, M.A.; Saef El-Naser, T.A.; Zidan, I.H. Removal of uranium from acidic solution using activated carbon impregnated with tri butyl phosphate. *Biol. Chem. Res.* **2016**, *126*, 313–340.
61. Gomaa, H.; Shenashen, M.A.; Elbaz, A.; Kawada, S.; Saef El-Nasr, T.A.; Cheira, M.F.; Eid, A.I.; El-Safty, S.A. Inorganic-organic mesoporous hybrid segregators for selective and sensitive extraction of precious elements from urban mining. *J. Colloid Interface Sci.* **2021**, *604*, 61–79. [CrossRef]
62. Akar, T.; Kaynak, Z.; Ulusoy, S.; Yuvaci, D.; Ozsari, G.; Akar, S.T. Enhanced biosorption of nickel(II) ions by silica-gel-immobilized waste biomass: Biosorption characteristics in batch and dynamic flow mode. *J. Hazard. Mater.* **2009**, *163*, 1134–1141. [CrossRef]
63. Mittal, A.; Kaur, D.; Mittal, J. Batch and bulk removal of a triarylmethane dye, Fast Green FCF, from wastewater by adsorption over waste materials. *J. Hazard. Mater.* **2009**, *163*, 568–577. [CrossRef]
64. Heshmati, H.; Torab-Mostaedi, M.; Ghanadzadeh Gilani, H.; Heydari, A. Kinetic, isotherm, and thermodynamic investigations of uranium(VI) adsorption on synthesized ion-exchange chelating resin and prediction with an artificial neural network. *Desalin. Water Treat.* **2015**, *55*, 1076–1087. [CrossRef]
65. Hassanin, M.A.; Negm, S.H.; Youssef, M.A.; Sakr, A.K.; Mira, H.I.; Mohammaden, T.F.; Al-Otaibi, J.S.; Hanfi, M.Y.; Sayyed, M.I.; Cheira, M.F. Sustainable Remedy Waste to Generate SiO<sub>2</sub> Functionalized on Graphene Oxide for Removal of U(VI) Ions. *Sustainability* **2022**, *14*, 2699. [CrossRef]
66. Foo, K.Y.; Hameed, B.H. Insights into the modeling of adsorption isotherm systems. *Chem. Eng. J.* **2010**, *156*, 2–10. [CrossRef]
67. Abdel Geleel, M.; Atwa, S.T.; Sakr, A.K. Removal of Cr (III) from aqueous waste using Spent Activated Clay. *J. Am. Sci.* **2013**, *9*, 256–262. [CrossRef]
68. Ibrahim, M.E.; Saleh, G.M.; Dawood, N.A.; Aly, G.M. Ocellar lamprophyre dyke bearing mineralization, Wadi Nugrus, eastern desert, Egypt: Geology, mineralogy and geochemical implications. *Chin. J. Geochem.* **2010**, *29*, 383–392. [CrossRef]
69. Allam, E.M.; Lashen, T.A.; Abou El-Enein, S.A.; Hassanin, M.A.; Sakr, A.K.; Cheira, M.F.; Almuqrin, A.; Hanfi, M.Y.; Sayyed, M.I. Rare Earth Group Separation after Extraction Using Sodium Diethyldithiocarbamate/Polyvinyl Chloride from Lamprophyre Dykes Leachate. *Materials* **2022**, *15*, 1211. [CrossRef]
70. Habashi, F. Extractive metallurgy of rare earths. *Can. Metall. Q.* **2013**, *52*, 224–233. [CrossRef]
71. Habashi, F. The recovery of the lanthanides from phosphate rock. *J. Chem. Technol. Biotechnol. Chem. Technol.* **1985**, *35*, 5–14. [CrossRef]



## Article

# Flax Fibre Yarn Coated with Lignin from Renewable Sources for Composites

Claudia Möhl <sup>1,\*</sup>, Timo Weimer <sup>1</sup>, Metin Caliskan <sup>1</sup>, Tom Hager <sup>1</sup>, Stephan Baz <sup>1</sup>, Hans-Jürgen Bauder <sup>1</sup>, Thomas Stegmaier <sup>1</sup>, Werner Wunderlich <sup>1</sup> and Götz T. Gresser <sup>1,2</sup> 

<sup>1</sup> German Institutes of Textile and Fibre Research (DITF), Körsschtalstrasse 26, 73770 Denkendorf, Germany

<sup>2</sup> Institute for Textile and Fibre Technologies (ITFT), University of Stuttgart, Pfaffenwaldring 9, 70569 Stuttgart, Germany

\* Correspondence: claudia.moehl@ditf.de

**Abstract:** The present experimental work analyses the potential of lignin as a matrix for materials made from renewable resources for composite components and the production of hybrid semi-finished products by coating a flax fibre yarn. Natural fibres, due to their low density, in combination with lignin can be a new renewable source for lightweight products. For this purpose, the extrusion process was adapted to lignin as a matrix material for bio-based composites and coating of natural fibre yarns. A commercial flax yarn is the basis for the lignin coating by extrusion. Subsequently, the coated flax yarn was characterised with regard to selected yarn properties. In order to produce composite plates, the lignin-coated flax yarn was used as warp yarn in a bidirectional fabric due to its insufficient flexibility transversely to the yarn axis. The commercial flax yarn was used as weft yarn to increase the fibre volume content. The tensile and flexural properties of the bio-based composite material were determined. There was a significant difference in the mechanical properties between the warp and weft directions. The results show that lignin can be used as matrix material for bio-based natural fibre composites and the coating of natural fibre yarns is an alternative to spun hybrid yarns.

**Keywords:** flax yarn; lignin; bio-based thermoplastics; bio-based matrix material; yarn coating; extrusion; natural fibre; composite

**Citation:** Möhl, C.; Weimer, T.; Caliskan, M.; Hager, T.; Baz, S.; Bauder, H.-J.; Stegmaier, T.; Wunderlich, W.; Gresser, G.T. Flax Fibre Yarn Coated with Lignin from Renewable Sources for Composites. *Polymers* **2022**, *14*, 4060. <https://doi.org/10.3390/polym14194060>

Academic Editor: Cristina Cazan

Received: 30 August 2022

Accepted: 25 September 2022

Published: 27 September 2022

**Publisher's Note:** MDPI stays neutral with regard to jurisdictional claims in published maps and institutional affiliations.



**Copyright:** © 2022 by the authors. Licensee MDPI, Basel, Switzerland. This article is an open access article distributed under the terms and conditions of the Creative Commons Attribution (CC BY) license (<https://creativecommons.org/licenses/by/4.0/>).

## 1. Introduction

Using plant and animal resources for clothing, everyday objects, and tools is as old as humanity itself. Wood, resins, fibres, leather and other naturally available materials were used to construct items that contributed significantly to the survival and development of the human species. This changed only when petroleum-based polymers and modern fibre-reinforced composites were developed. Favoured by low production costs due to the parallel introduction of mass production and adapted properties, demand for polymers and modern fibre-reinforced composites grew exponentially. Between 2010 and 2019, global plastics production increased by around 100 million tonnes to 368 million tonnes to meet the needs of construction, automotive, aerospace, textile, packaging, pharmaceutical and many other industries [1,2]. The consequences of the extensive use and the “take, make and dispose” approach include overflowing landfills, improper disposal in forests, rivers and oceans, contamination of soils and water bodies, the release of greenhouse gases, air pollution from incineration, and threats to biodiversity and mankind itself [3,4]. In this context, the research and development of fully bio-based fibre-reinforced composites that have a lower environmental impact from production to disposal has become an important and pressing goal of our time. Therefore, in this study, the suitability of lignin as a thermoplastic matrix from renewable resources is evaluated and an alternative semi-finished product manufactured by coating flax fibre yarns is investigated.

Lignin is the second most abundant polymer in nature after cellulose. Lignin is an amorphous, three-dimensional, cross-linked heteropolymer, it always consists of the same three main phenylpropane units (guaiacyl, syringyl and p-hydroxyphenyl), which, however, occur in different proportions depending on the biological influencing factors and the starting material used [5]. The annual production volume of lignin from the pulp and paper industry is around 70 million tonnes worldwide, which would make its use possible for various industrial applications. However, it is difficult to develop higher-quality materials from lignin [6]. The heterogenic and the aromatic structure with an even distribution of the molecular weight of the lignin leads to a poor solubility in most known organic solutions, because lignin sterically prevent the reactive sites [7]. That explains why only 2% of lignin produced is currently used as a source for chemicals or materials, while the rest is burned for energy production [8]. A new approach to solving lignin and making lignin processable and usable for products is the use of ionic liquids. Lignin can be dissolved in ionic liquids and the ionic liquids is also reusable [5]. Lignin, with its special properties such as high thermal stability, high carbon content, good ultra violet absorption, low material costs, and above all, biodegradability, is a potential sustainable component for bio-based composites [9,10]. Therefore, lignin was researched years ago as an additive for polymers [11–13], as a reinforcing component in composite materials [14] and as a thermoplastic as well as a thermosetting matrix material [15–17]. It has been used in various applications such as biosurfactant, antimicrobial agents, active packaging, activated carbon, and supercapacitor make this abundant material promising low-cost additive [18]. Recently, research on lignin has focused more on its use as a raw material for bio-based carbon fibres and on the production of biodegradable composites from renewable raw materials.

In addition to the properties already mentioned, blending lignin with other biopolymers is attractive, because of the variety of modifications possible due to its chemical structure [19]. Therefore, many studies on the production of bioplastics focus on the incorporation of lignin into natural biopolymers such as polylactic acid (PLA) [20], polyhydroxybutyrate (PHB) [21] and polybutylene succinate (PBS) [22]. The addition of lignin as a reinforcing material usually lowers costs and water absorption [21]. In addition, lignin has significant antioxidant properties, as the phenolic hydroxyl groups can scavenge free radicals [23]. The compatibility between cellulose and other hydrophobic biopolymers could be greatly enhanced by lignin with its polar phenolic hydroxy groups and non-polar hydrocarbon groups [24]. The addition of lignin could improve the compatibility between cellulose and matrix [25,26]. In [24], it is described that impact strength decreased after the addition of lignin, while Young's modulus and tensile strength improved significantly. In cellulose-lignin bio-composites, the cellulose-containing component enhances the mechanical strength of the composites, while lignin improves the thermal stability of the polymer matrix and ensures good dispersion of the cellulose in the biopolymers [27,28].

By using fully bio-based composites, the ecological disadvantages of glass fibre reinforced plastics and carbon fibre reinforced plastics can be eliminated and, as an alternative, equally high-performance and durable fibre composite components can be produced. Compared to carbon and glass fibres, natural fibres are renewable, sustainable, do not splinter and consume less energy during production [29]. In addition, natural fibres offer high potential for lightweight construction and good insulating properties due to their low density [30].

Yarn coating is used in the textile industry to enhance the functional properties of yarns. One field of application is the sizing of yarns. In this process, the yarn is covered with a starch or synthetic component-based coating to protect the yarn from yarn breakage and production losses in subsequent processing operations such as weaving. The yarn coating is used when an additional functional feature is imparted to the yarn as an end product or when finishing the end product is not possible. Special functions such as abrasion resistance, flame retardancy, antibacterial properties, dirt repellence, electrical conductivity,

UV protection can be added. Coated yarns serve for special niche markets, such as sewing yarns, used in fly screens, cord and more technical applications.

Often, the mechanical yarn characteristics and the sensitivity against moisture prevents the use of natural fibre yarn in composites [31]. Researchers are already working on fibres and yarns coated with matrix material for the production of thermoplastic fibre composite materials [32]. The disadvantages of the natural fibre yarns can be improved or adapted to the respective area of application by means of a targeted yarn coating for the adaptation of the yarn properties and the extension of the yarn functionality. This can be very different in terms of process technology, adapted to the respective application of the yarn. While classic aqueous coatings are mostly applied by dipping and squeezing systems, thermoplastic granulates are extruded and applied to the yarn via nozzles. The desired yarn properties have a wide range and are determined by the subsequent application. The functional coatings can be applied individually according to customer requirements.

A thorough analysis of the literature shows that lignin is mainly used as a filler or in small quantities as an admixture for thermoplastic polymers. It is currently used as a main component in thermoplastics exclusively in the form of granules for injection moulding and extrusion applications. The present experimental study investigates lignin as a coating for natural fibre yarns and its utilisation in textile processes to produce a semi-finished textile product for sustainable fibre reinforced plastic applications.

## 2. Materials and Methods

### 2.1. Materials

For this feasibility study, commercially available flax yarn from N.V. JOS VANNESTE S.A., Harelbeke, Belgium, and ARBOFORM<sup>®</sup> L V100 from TECNARO GmbH, Ilsfeld, Germany were acquired. ARBOFORM<sup>®</sup> L V100 consists of lignin or lignin derivatives, biodegradable polyester from natural sources, lignocellulose fibres, natural resins and waxes. The main parameters of both materials are given in Table 1.

**Table 1.** Materials used.

| Parameter                            | Commercial Flax Yarn   | Lignin Granule               |
|--------------------------------------|------------------------|------------------------------|
| Manufacturer                         | N.V. JOS VANNESTE S.A. | TECNARO GmbH                 |
| Product name                         | Flax yarn              | ARBOFORM <sup>®</sup> L V100 |
| Fineness                             | 205 tex $\pm$ 5 tex    |                              |
| Density                              |                        | 1.29 g/cm <sup>3</sup>       |
| Melt volume rate<br>(190 °C/2.16 kg) |                        | 30 cm <sup>3</sup> /10 min   |

### 2.2. Coating of the Commercial Flax Yarn and Parameters

Extrusion coating was carried out on a Thermo Scientific Eurolab 16 twin screw extruder (Figure 1a) with the software Prism Eurolab 16 from Thermo Fisher Scientific, Karlsruhe, Germany. In the twin-screw extruder, seven conveying zones can be heated independently of each other. In the case of temperature-sensitive thermoplastics, the melting process from the inlet to the nozzle can be precisely adjusted. The coating process was carried out horizontally at the head of the extruder through a modified sheathing nozzle. This sheathing nozzle consists of three individual nozzles (inner nozzle, outlet nozzle, stripper nozzle) with different tasks (Figure 1b). The yarn to be coated passes through an inner nozzle with an adjusted diameter and is coated with the molten matrix material by the outlet nozzle. The coated yarn is given its final diameter in a final stripping process with a stripper nozzle.

The yarn material used was a commercially available flax yarn (FL commercial yarn) and were coated with thermoplastic lignin. Before being used the thermoplastic granules were dried in a drying oven at 50 °C for 4 h. The die diameters were adapted to the yarn in the preliminary tests. The following criteria were considered when choosing the nozzle diameter. The nozzle had to have just enough size that the yarn can pass through



the inner nozzle without any resistance but not generate vibrations due to excess space. Initially, the inner nozzle diameter was reduced from 1.2 mm to 1.0 mm. The outlet nozzle applied the matrix coating material to the yarn. The final diameter of the coated yarn was brought down from 1.6 mm to 1.4 mm by a stripper nozzle at the end of the sheathing nozzle. A further reduction in the nozzle diameters was not possible because of increasing yarn breakages.

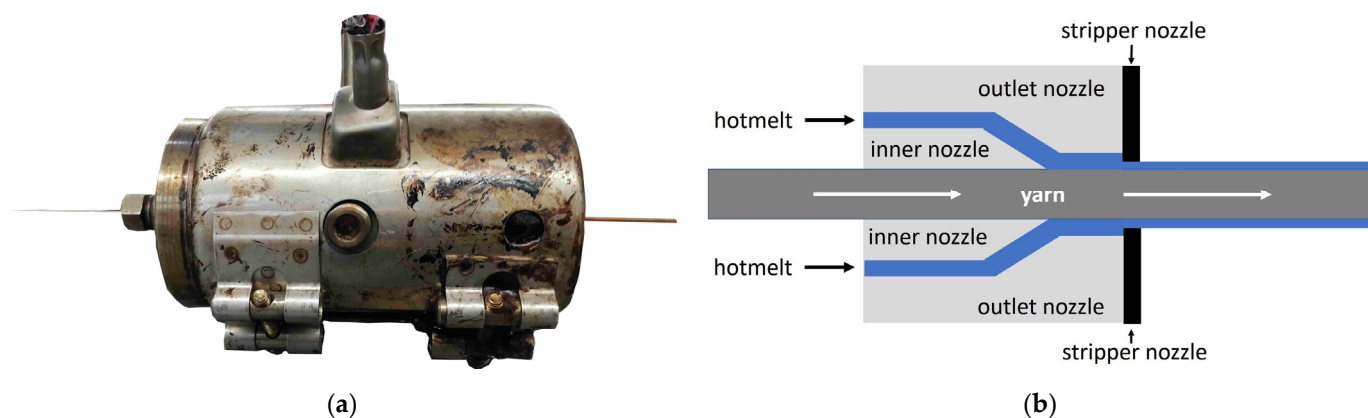


**Figure 1.** (a) Picture of the sheathing nozzle; (b) functional sketch of the sheathing nozzle.

The selection of the die diameter in conjunction with the temperature and pressure setting in the extruder, as well as the throughput speed (production speed) proved to be very demanding. The compliance with the very narrow temperature processing range of the thermoplastic coating material was equally challenging. The following two factors made a continuous yarn coating process difficult: the flax yarn to be coated had (1) many splices with larger diameters. These caused blockages in the sheathing nozzle and ultimately yarn breaks and a production stop (Figure 2a). The other problematic factor was (2) the very narrow temperature range of the thermoplastic coating material. There are differences in the production pressure and in the viscosity behaviour in a range from 180 °C to 184 °C. Especially when the ideal processing temperature of 182 °C was briefly exceeded, deposits formed in the sheathing nozzle due to thermoplastic segregation.

Figure 2b show the uncoated yarn bobbin, while Figure 2c depicts the coated flax yarn (1600 m), which was produced with the settings given in Tables 2 and 3. Figure 2d reveals in a close-up view the sawtooth-like structure of the lignin coated flax yarn (FL-LI coated yarn).

**Table 2.** Parameters of extruder for production of FL-LI coated yarn.

| Production Parameters   | Value      |
|-------------------------|------------|
| Nozzle diameter inside  | 1.0 mm     |
| Nozzle diameter outside | 1.4 mm     |
| Winding speed           | 10 m/min   |
| Delivery volume         | 6.98 g/min |

**Table 3.** Temperature zones of the extruder.

| Temperature Zone | Temperature |
|------------------|-------------|
| Inlet (funnel)   | 178 °C      |
| Zone 1           | 182 °C      |
| Zone 2           | 182 °C      |
| Zone 3           | 182 °C      |
| Zone 4           | 180 °C      |
| Zone 5           | 180 °C      |
| Head (nozzle)    | 180 °C      |



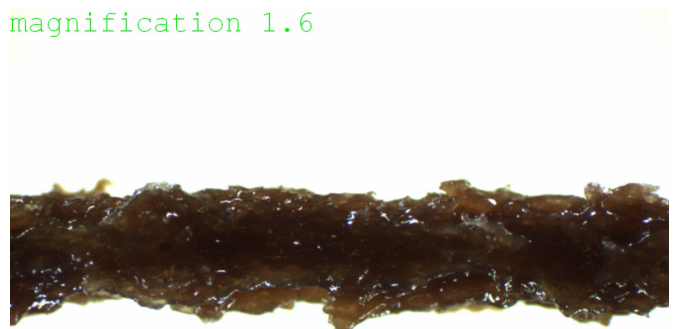
(a)



(b)



(c)



(d)

**Figure 2.** (a) Example of breakage in flax yarn; (b) bobbin of flax yarn (FL) without coating; (c) bobbin of flax yarn with lignin (FL-LI coated yarn); (d) close-up view of FL-LI coated yarn (the magnification is 1.6).

### 2.3. Weaving Process and Parameters

The warping process of the lignin coated flax yarn took place on the mini warping machine SW550, from the CCI Tech Inc., New Taipei City, Taiwan. The FL-LI coated yarn had to be used as the warp because of the stiffness and strength of the yarn. The yarn cannot be cut and is therefore not suitable as weft yarn. During the warping process the tension and the speed had to be adjusted to avoid yarn breakages. The speed during the warping process had to be chosen low, as the yarn is very stiff. The tension during the warping process too had to be chosen low. This eventually means that the warp tension of the individual threads is inhomogeneous, but it prevents the brittle FL-LI coated yarn from breaking. To avoid damaging during the warping process, the yarn was fed with a positive creel, CCI Tech Inc., New Taipei City, Taiwan. The warp length was 3.60 m because of the mechanical limitations of the mini warping machine SW550.

The FL-LI coated yarn was woven on the sample weaving loom Evergreen II (Figure 3) form CCI Tech Inc., New Taipei City, Taiwan. The weaving parameters are given in Table 4.



**Figure 3.** Weaving with FL-LI coated yarn (warp) and FL commercial yarn (weft).

**Table 4.** Weaving parameters.

| Weaving Parameters   | Value   |
|----------------------|---|
| Warp material        | Lignin coated flax yarn (FL-LI coated yarn) 1099 ± 15 tex |
| Warp density         | 6 yarns/cm  |
| Warp tension         | 25 cN   |
| Weft material        | Flax yarn (FL commercial yarn) 205 ± 5 tex                |
| Weft density         | 5 yarns/cm  |
| Weft insertion speed | 3 picks/min   |
| Width                | 0.50 m  |
| Type of fabric       | Twill 2/2   |

The weft insertion speed, and the raising and lowering speed of the shafts had to be set to as slow as possible due to the roughness and sharpness of the FL-LI coated yarn. The faster the weft insertion speed, the more likely the weft yarn breaks as shown in Figure 4a. The lignin coating breaks along the last inserted weft when the shafts move, as seen in Figure 4b. The warp tension has to be raised because of the inhomogeneous warp beam. The raising of the warp tension further led to warp breaks due to the brittleness of the FL-LI coated yarn (Figure 4c). The roughness of the yarn resulted in abrasion of the lignin coating, and high wear of the weaving reed and the weaving healds. Another problem was the partially inhomogeneous lignin coating on the yarn (Figure 4). The partially inhomogeneous lignin coating on the yarn led to yarn breakages due to unsteady yarn tension and the tangling of the yarn in the healds. The length of the finished fabric was 2.70 m.

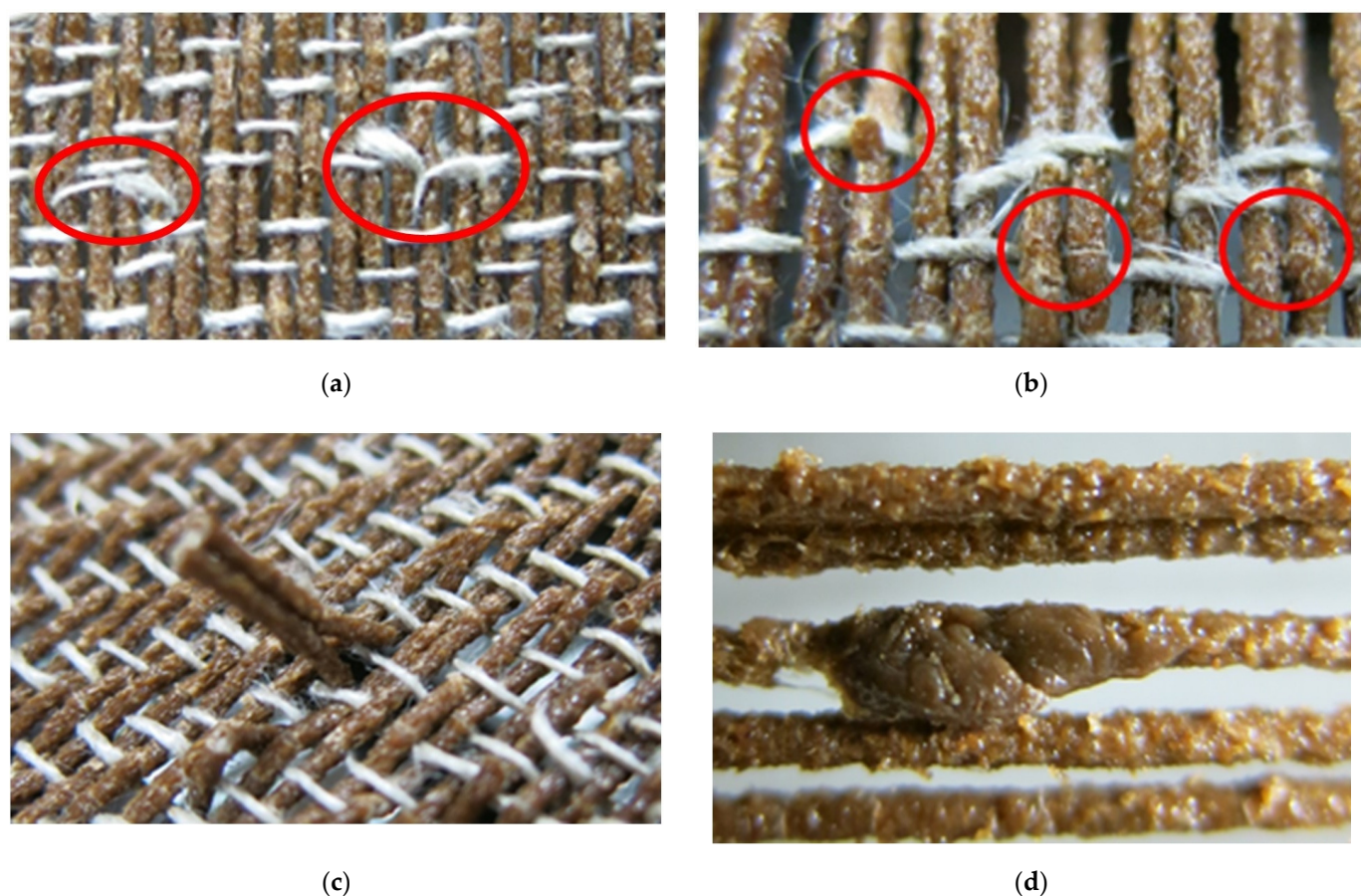


**Figure 4.** (a) Broken weft yarn; (b) broken lignin coating of the warp yarns; (c) broken Warp yarn; (d) in-homogeneous lignin coating of the warp yarn.

#### 2.4. Composite Fabrication

Samples measuring 400 mm × 400 mm were cut out from the flax lignin fabric and pre-dried for 2 h at 80 °C in an oven. Afterwards the fabric pieces were stacked in three layers and consolidated in a VCP500 vacuum hot press from Maschinenfabrik Lauffer GmbH & Co. KG, Horb, Germany. In all layers, warp (FL-LI coated yarn) and weft (FL commercial yarn) yarns were aligned in the same direction. Two sheets were produced for the extraction of specimens according to the two directions warp and weft.

The same pressing parameters, which were determined and applied in [33], were used. They are given in Table 5. Figure 5 shows the pressing cycle for both flax-lignin composite plates (FL-LI composite). Temperature and vacuum pressure are plotted on the left axis and compressive pressure on the right axis. One of the composite plates can be seen in Figure 6a. The weft (0°) and warp (90°) directions are given in Figure 6b.

**Table 5.** Pressing parameters.

| Pressing Parameter     | Value   |
|------------------------|---------|
| Temperature            | 180 °C  |
| Holding time           | 10 min  |
| Vacuum                 | 10 kPa  |
| Compression pressure   | 3.1 MPa |
| Pre-drying temperature | 80 °C   |
| Pre-drying time        | 120 min |
| Venting phase          | None    |

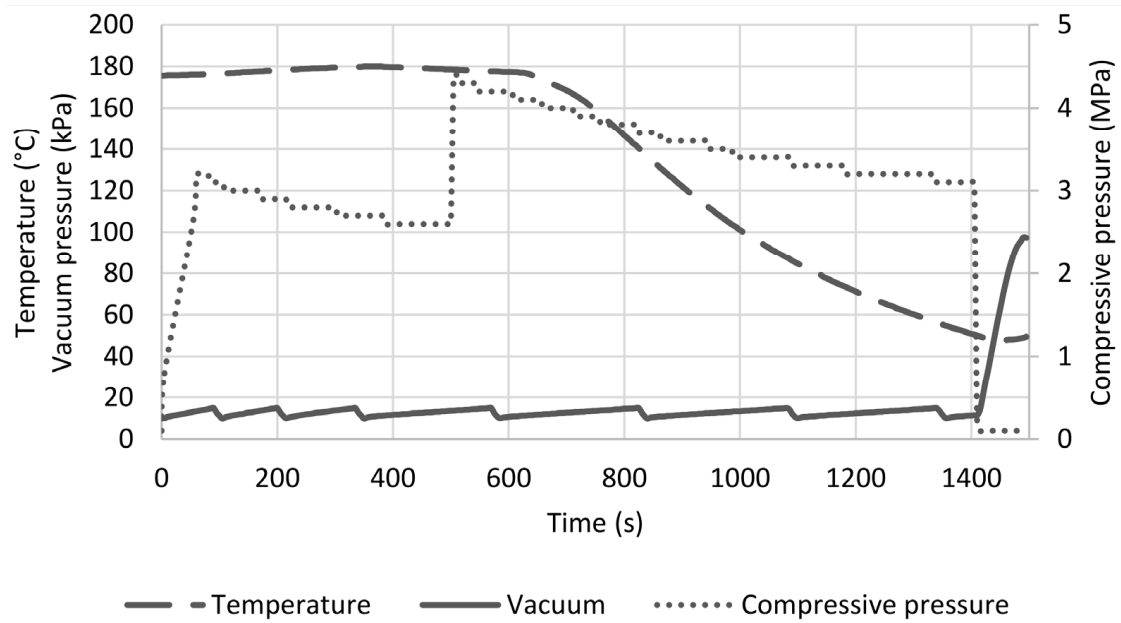
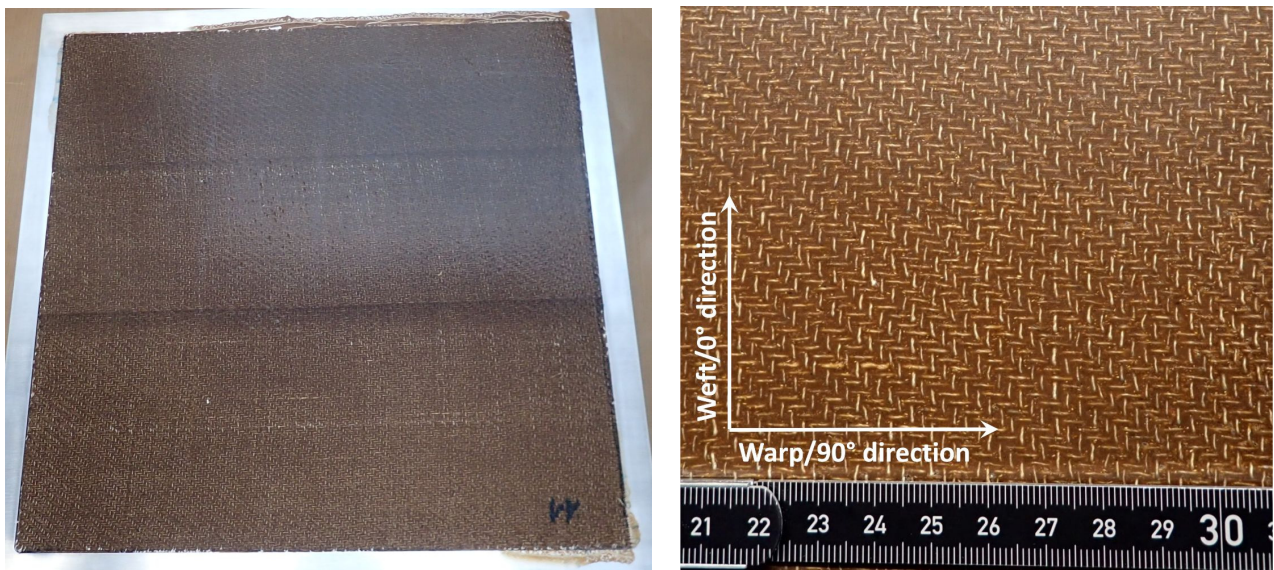


Figure 5. Hot pressing cycle of FL-LI composite plates.



(a)

(b)

Figure 6. (a) Consolidated FL-LI composite plate with aluminium press frame; (b) warp (90°) and weft (0°) direction of composite plate.

## 2.5. Characterisation

### 2.5.1. Determination of Yarn Coating

The determination of the yarn coating add-on is conducted gravimetrically based on DIN EN ISO 2060 textiles—yarn from packages—determination of linear density (mass per unit length), by the skein method. A reeling machine from Zweigle Textilprüfmaschinen GmbH & Co. KG, Reutlingen, Germany, was used to remove 2 times 50 m of yarn from a bobbin. Then, the obtained skeins of yarns were weighed with a scale from Mettler Toledo PM 200, Gießen, Germany.

To calculate the add-on, the mean value was determined from two skeins of 50 m yarns. From the difference value of the weight of the uncoated yarn and the coated yarn, the coating add-on was calculated in per cent.

The tests were conducted at a temperature of  $20\text{ }^{\circ}\text{C} \pm 2\text{ }^{\circ}\text{C}$  and relative humidity of  $65\% \pm 2\%$  (according to DIN EN ISO 139) on samples conditioned for 24 h at standard climate.

#### 2.5.2. Tensile Properties of Yarn

The tensile tests of the FL commercial yarn and FL-LI coated yarn were carried out according to DIN ISO 2062 with the universal testing machine Zwick 1455 ZMART.PRO from ZwickRoell GmbH & Co. KG, Ulm, Germany. The length of the yarn samples was 500 mm. The pre-tension force was set to 0.5 cN/tex and the test speed to 500 mm/min. The tensile force was recorded as a function of deformation. The scope of measurement was 20 samples and the average value for each type of yarn variant was determined.

The tests were conducted on samples conditioned for 24 h at standard climate (temperature of  $20\text{ }^{\circ}\text{C} \pm 2\text{ }^{\circ}\text{C}$  and relative humidity of  $65\% \pm 2\%$  according to DIN EN ISO 139).

#### 2.5.3. Fibre Mass Fraction and Fibre Volume Fraction at Absolute Dry Weight

The standard DIN EN ISO 1833-1 describes the extraction of bast fibres from cellulose-free components from textiles and textile products using sodium hydroxide. To determine the mixing ratio at absolute dry weight, 1 g of the sample was dried with a weighed filter crucible for 16 h at  $105\text{ }^{\circ}\text{C} \pm 3\text{ }^{\circ}\text{C}$  in a drying oven and weighed after cooling. Sodium hydroxide solution (1.5 mol/l solution) was boiled in a flask equipped with a re-flux condenser for at least 15 min and after separating the air from the solution (due to boiling), the sample was placed in the flask and boiling was continued for 1 h. Then the sample was dried and weighed after cooling. Afterwards, the sample was rinsed with water by continuous suction for at least 5 min and immersed in an acetic acid solution of 0.1 mol/l for 10 min. The contents of the flask were then filtered, rinsed with water until neutralised and dried, after which they were weighed. Two samples (double determination) per process step were tested.

Based on the mass fractions and the known densities (flax fibre =  $1.5\text{ g/cm}^3$ ), the volume fraction of the natural fibre was calculated for the lignin granule, coated yarns, woven fabrics and the bio-based composites.

#### 2.5.4. Analysis of Mechanical Properties of Bio-Based Composite

Using a Z100 universal testing machine from ZwickRoell GmbH & Co. KG, Ulm, Germany, with special wedge grips and an external optical strain gauge, tensile tests were performed according to DIN EN ISO 527-5. The dimensions of the specimens were  $250\text{ mm} \times 25 \pm 0.2\text{ mm} \times 2.3 \pm 0.2\text{ mm}$ . The preload was set to 0.1 MPa and the test speed to 1 mm/min. Six measurements were made in which the tensile force was recorded as a function of deformation and the average value was considered. The stress-strain behaviour was evaluated with the software testXpert®II (version 3.71).

With a Zwick Z020 from ZwickRoell GmbH & Co. KG, Ulm, Germany, the bending properties of the manufactured composite were determined in a 4-point bending test (method B) once in warp and once in weft direction according to the standard DIN EN ISO 14125. The specimen measurement and the automatic calculation of the cross-sectional area-specific bending modulus were carried out using testXpert®II software (version 3.71). The radius of the loading and support member was  $2 \pm 0.2\text{ mm}$ . The preload was set to 0.2 MPa and the test speed to 2 mm/min. For each direction, 6 specimens with the dimensions  $60 \pm 0.2\text{ mm} \times 15 \pm 0.2\text{ mm} \times 2.3 \pm 0.2\text{ mm}$  were tested.

All tests were carried out in accordance with the standard DIN EN ISO 139 at standard climate (temperature of  $20 \pm 2\text{ }^{\circ}\text{C}$  and relative humidity of  $65 \pm 2\%$ ) on specimens conditioned for 24 h.

### 3. Results and Discussion

#### 3.1. Yarn Properties

The add-on of the lignin coated yarn was 336%, and therefore 111% over the desired add-on of 225%. The desired add-on was calculated to achieve a fibre mass fraction of

50%. Due to the processing properties of the lignin granulate, the short processing time, the temperature sensitivity during the coating process and therefore low possibility to vary the viscosity, a higher add-on was received. Additionally, the diameter of the stripper nozzle was responsible for the outer diameter of the coated yarn. After testing several nozzle diameter variants, it was found that an even coating could only be achieved with a stripper nozzle of 1.4 mm diameter.

The mechanical properties of the FL-LI coated yarn and the FL commercial yarn are given in Table 6 and in Figure 7. The yarn count increases approximately fivefold from 205 tex for FL commercial yarn to 1099 tex for the coated yarn due to the high proportion of lignin in the process. The reinforcing fibre content of the FL-LI coated yarn is thus 24.88 wt.%. This difference can also be seen in the fineness-related maximum tensile strength between coated flax lignin and FL commercial yarn. Through the lignin coating and the thus reduced proportion of reinforcing fibres, the strength of the entire yarn is reduced by about 78% from 23.06 cN/tex to 5.00 cN/tex. A comparison of the absolute values of the maximum tensile strength shows an increase from 46.72 N for the uncoated yarn to 54.92 N for the coated yarn. The influence of the rather brittle lignin coating can also be seen in the values of elongation. The elongation is reduced from 3.17% for the FL commercial yarn to 2.16% for the FL-LI coated yarn.

**Table 6.** Linear density and fibre mass fraction of yarns.

| Yarn               | Linear Density | Natural Fibre Mass Fraction |
|--------------------|----------------|-----------------------------|
| FL commercial yarn | 205 ± 5 tex    | 100%                        |
| FL-LI coated yarn  | 1099 ± 15 tex  | 24.88%                      |

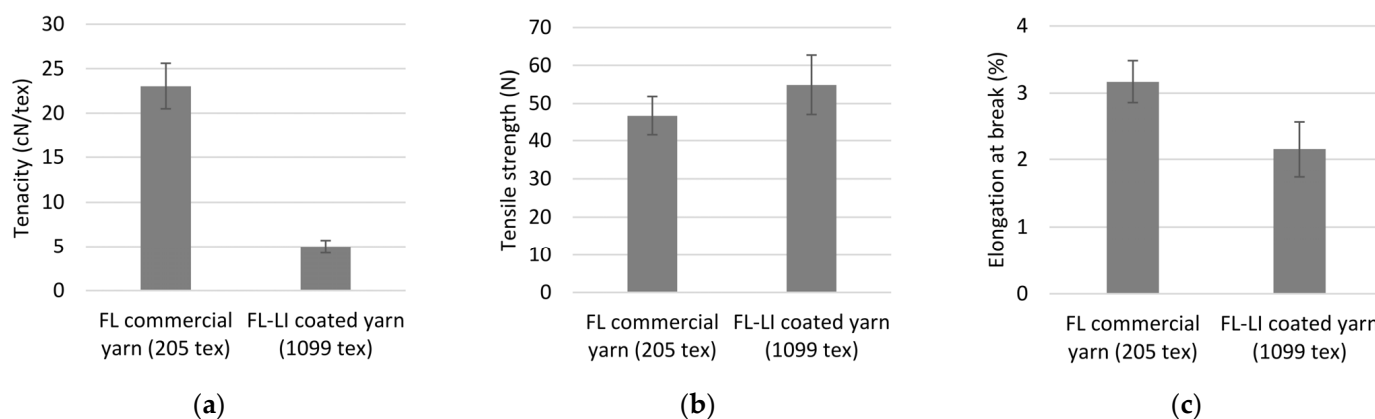


**Figure 7.** (a) Fineness-related tensile strength of yarns; (b) tensile strength of yarns (c) elongation at break of yarns.

### 3.2. Fabric Properties

The warp beam production faced difficulties due to the stiffness and brittleness of the yarn, and resulted in an inhomogeneous warp beam. In Table 7, the properties of the woven fabric are given. The grammage values are calculated from 400 mm × 400 mm pieces. In the experimental study, the weft yarn density with five threads per cm was found to be the best choice. A low weft insertion speed at three picks per minute was chosen, because of the sharpness of the warp yarn as the sawtooth-like structure can damage the weft yarn.

**Table 7.** Textile properties of the woven fabric.

| Woven Fabric    | Grammage                | Fibre Mass Fraction | Fibre Volume Fraction |
|-----------------|-------------------------|---------------------|-----------------------|
| FL-LI twill 2/2 | 894.31 g/m <sup>2</sup> | 34.47%              | 30.81%                |

### 3.3. Fibre Volume Fraction

The fibre volume fractions (FVF) of the semi-finished products for the process steps from the initial material (lignin granulates; 14.32 vol.%) to yarn (23.38 vol.%), fabric (34.47 vol.%) and finally to the composite material (30.81 vol.%). Due to the very high proportion of matrix material in the yarn due to the process, instead of a unidirectional (UD) fabric, a bidirectional one was produced. The coated yarn was used as warp yarn and the FL commercial yarn as weft yarn, thus increasing the FVF by about 10 vol.%. The drop in FVF of 3.66 vol.% between the fabric and the composite is particularly noticeable. Since no loss of fibre material could be detected during the consolidation process, the cause could possibly lie in the test method used according to DIN EN ISO 1833-1. Even though the standard is specifically for the extraction of bast fibres from cellulose-free components, the result suggests that in addition to the lignin, components of the flax fibres are also decomposed. It is therefore conceivable that due to the time required to dissolve the consolidated composite compared to the non-consolidated coated yarn or woven fabric, additional components such as hemicelluloses, lignin, pectin and/or waxes are dissolved out of the bast fibres, thereby reducing the FVF of the composite.

### 3.4. Composites

The bidirectional fabric was cut to size, stacked into three layers each and consolidated into a total of two composite sheets. One was examined in the 0° direction (weft yarn; FL-LI 0°) and one was examined in the 90° direction (warp yarn; FL-LI 90°) with regard to its mechanical properties. In addition, the characteristic values of a unidirectional flax-poly lactide composite (FL-PLA UD composites) were compared for classification, as no composites made from coated natural fibre yarns could be found in the literature [33]. With the exception of the tensile and flexural elongation, the difference in mechanical properties between bidirectional and quasi-unidirectional fabric is clearly evident.

#### 3.4.1. Tensile Properties

The results of the tensile test according to DIN EN ISO 527-5 are shown in Figure 8a–c. The values for FL-LI 0° (weft yarn) for tensile modulus (6.23 GPa), tensile strength (45.06 MPa) and elongation (1.93%) are higher than those of FL-LI 90° (warp yarn; 3.92 GPa, 15.31 MPa, 0.65%). Due to 6 and 5 yarns per cm in in warp and weft directions, respectively, approximately equal, if not opposite characteristic values were expected. The reason for the higher tensile modulus, the higher tensile strength values and the higher tensile elongation were found to be the yarn course of warp-weft system in the fabric. The FL-LI yarns of the warp system laid stretched in the fabric, because they are very stiff due to their coating and have therefore, hardly any undulation after the weaving process (Figure 9a). In the weft direction, the yarn undulates over and under the warp threads and has a meandering yarn course in the fabric (Figure 9b). Due to the undulations, the weft yarn in the composite is longer and has thereby a larger contact area with the matrix system as well as a larger clamping length than the warp yarns. When the consolidated sample is subjected to tension during the tensile test, the weft yarns can therefore absorb more load (Figure 10). The meandering yarn course in the weft direction is also helpful against the weft yarns being pulled out of the matrix. The higher elongation can also be explained by the increased load transfer from the weft yarns to the matrix system. The undulation of the weft yarns is reduced during the tensile test in 0° direction, which results in a plastic deformation of the sample along the diagonal twill weave lines (Figures 11a and 12a), compared to the tensile test in 90° with straight warp yarns where no plastic deformation takes place (Figures 11b and 12b).



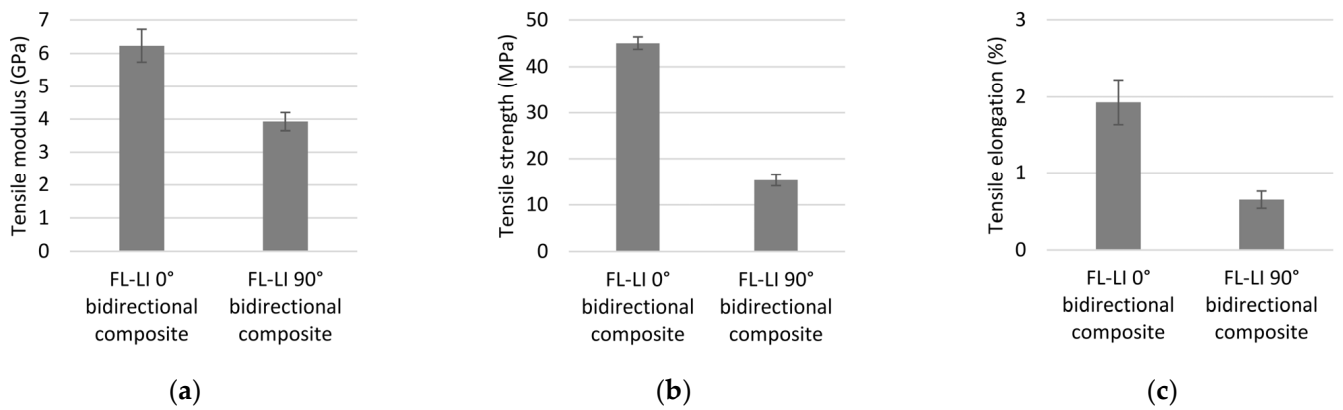


**Figure 8.** (a) Tensile modulus of FL-LI composites; (b) tensile strength of FL-LI composites; (c) elongation of FL-LI composites.

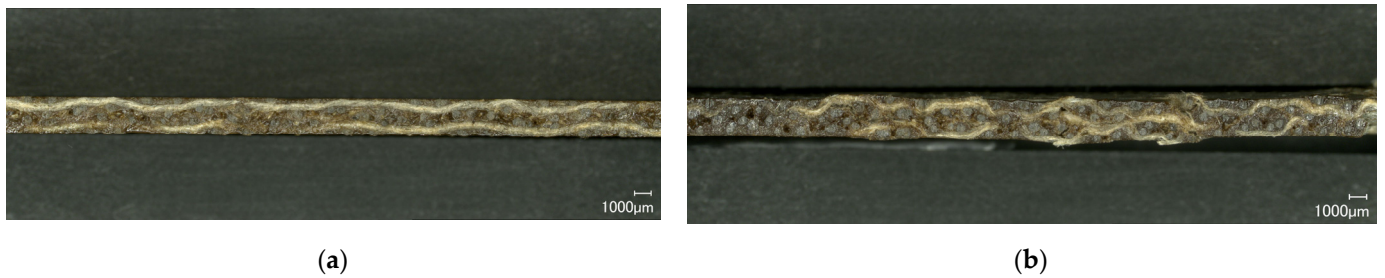


**Figure 9.** (a) Cross section showing the course of warp yarn of the FL-LI composite; (b) cross section showing the course of weft yarn of the FL-LI composite.

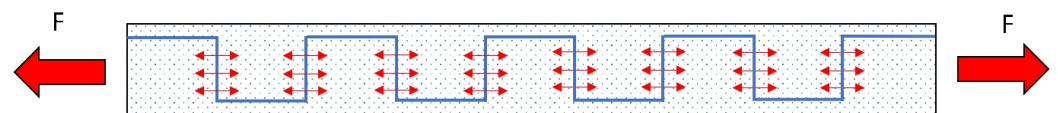


**Figure 10.** Load transfer directions of the weft yarn during the tensile test with idealised yarn course. The red arrows indicate the force (F). The blue line shows the weft yarn in the matrix background.

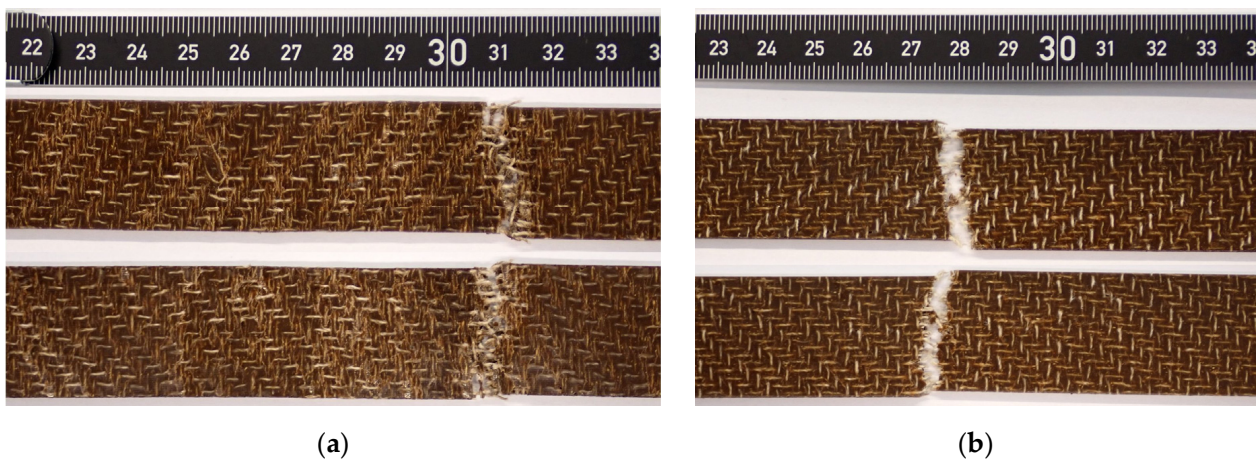


**Figure 11.** Fracture zones of selected tensile test specimens (a) in 0° (weft direction, above front view and below back view); (b) in 90° (warp direction, above front view and below back view).

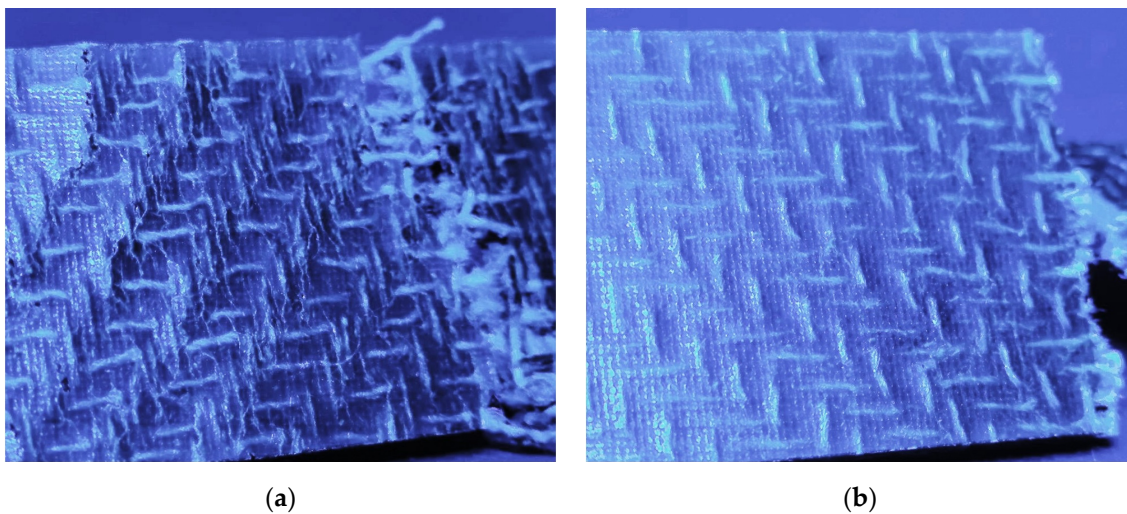


**Figure 12.** Blue coloured detailed view on the structure of the fracture zones of selected tensile test specimens: (a) tensile test in weft direction with plastic deformation along the diagonal twill weave lines; (b) tensile test in warp direction without plastic deformation.

### 3.4.2. Flexural Properties

The bending properties of the FL-LI composites were determined in a 4-point bending test according to DIN EN ISO 14125 and are shown in Figure 13a–c. The flexural modulus of elasticity of FL-LI 90° is only slightly lower at 3.52 GPa compared to that of FL-LI 0° at 4.43 GPa. Due to higher yarn density in warp direction (6 yarns per cm) compared to that in the weft direction (5 yarns per cm) of the FL-LI fabric, a higher flexural modulus in the warp direction (90°) was expected than in the weft direction (0°). However, the 4-point bending tests proved a higher flexural modulus in the weft direction. The higher flexural modulus in the weft direction (0°) is due to the fact that the weft yarns are located further outside the central neutral bending axis, in the FL-LI composite, than the warp yarns (90°). Below the neutral bending line, the yarns are subjected to tensile stress, and above it, to compressive stress. Thus, the weft yarns, which are further away from the neutral bending line are significantly more stressed during the 4-point bending test. The higher flexural modulus in the weft direction is therefore mainly generated by the weft yarns below the neutral bending line.

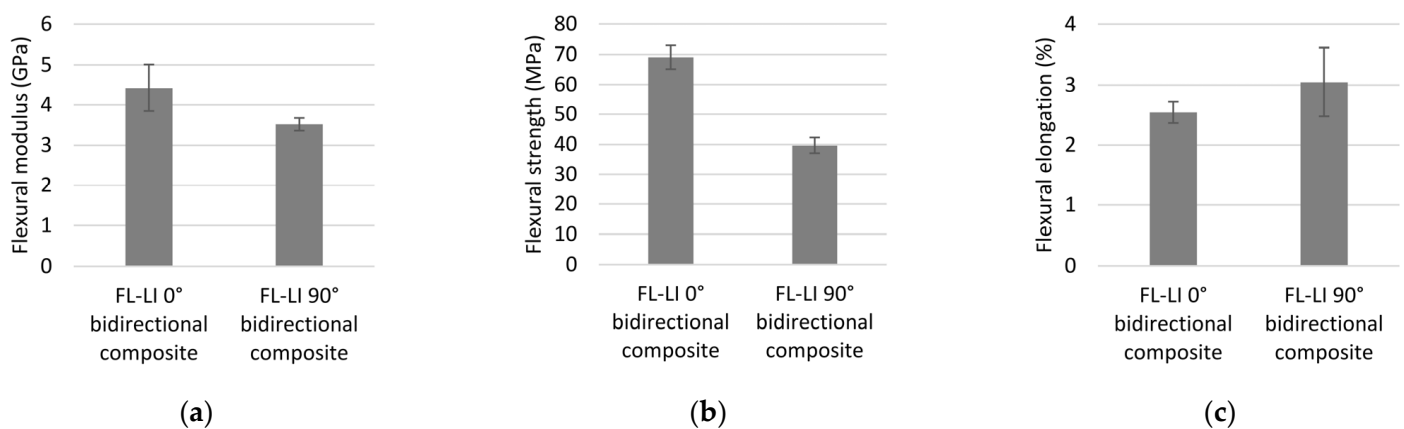


**Figure 13.** (a) Flexural modulus of FL-LI composites; (b) flexural strength of FL-LI composites; (c) elongation of FL-LI composites.

The same effects as for the flexural modulus are evident in the flexural strength tests. The FL-LI composite has a higher flexural strength in the weft direction (69.05 MPa) than

that in the warp direction (39.63 MPa). The weft yarns, which are located more off-centre than the warp yarns in the composite, generate a higher section modulus than the warp yarns. The further the weft yarns are displaced under the neutral bending line of the FL-LI composite, the greater their influence on a higher flexural strength.

Elongations of 2.54% and 3.05% are achieved in the weft and warp directions, respectively. The more even distribution of the warp yarns in the FL-LI composite increases the elongation in the warp direction, because the warp yarns are closer to the neutral bending line than the weft yarns. In contrast to the weft yarns, the yarns in the warp direction are not stressed as much in the 4-point bending test. Therefore, the warp yarns only break at a larger deflection.

#### 4. Conclusions

This paper presents an experimental study on the use of lignin as a matrix material and as a coating of yarns as an alternative for the semi-finished production of composite components. A commercial flax yarn is coated with a lignin matrix using an extrusion process. This coated yarn was processed into a woven fabric and consolidated into composite panels. The semi-finished products thus produced, yarn and composite material, were examined and analysed with regard to their characteristic properties.

The coating by thermal extrusion of flax yarn with lignin was successful. The lignin product passes quickly from the liquid to the solid aggregate state and make the yarn very stiff. Temperature adjustments in the individual extruder zones, as well as varying the production speed result in an acceptable but not satisfactory coating process. To increase uniformity of the coated yarn in future work, a yarn without splices will be used to prevent yarn breakage during the coating process. Furthermore, the lignin formulation has to be improved regarding a longer processing time, a wider temperature processing range and for a smooth surface of coated yarn in addition with reduced add-on. A coating degree of 336% was attained. However, this could not be brought down to the desired 225%.

The coated flax yarns exhibited moderate elongation behaviour and good strength with a fibre volume content of nearly 35 vol.%. These properties allow for further processing by weaving, but the low flexibility transverse to the yarn axis and the saw wire-like surface structure posed a considerable challenge.

The fabrics were produced with the lignin coated flax yarn ( $1099 \pm 15$  tex) in the warp direction and the commercially flax yarn ( $205 \pm 5$  tex) in the weft direction. The warp and weft densities are 6 and 5 yarns per cm, respectively. The lignin coated yarn is very brittle and therefore, gentle and slow processing are required. Nevertheless, the processing of the coated yarn remains intricate. To minimise damage to the yarn, the weaving shed should be reduced in size and the warp tension should be as low as possible. The width of the woven fabric is 500 mm. Another problem is the sharp-edged nature of the lignin coated flax yarn. This causes increased wear on the healds and the weaving reed. Large healds and a coarser weaving reed could bring improvement.

The analysis of the composite material with regard to the tensile and bending properties showed clear differences between the weft (FL-LI  $0^\circ$ ) and the warp (FL-LI  $90^\circ$ ) direction, which can be attributed to the position and orientation of the flax yarns in the warp and weft directions in the composite. In addition, investigations are needed on the general fibre-matrix adhesion between flax yarn and lignin as well as on the influence of the extrusion process on the fibre-matrix adhesion. Furthermore, the penetration depth of the lignin matrix into a compact structure, such as the flax yarn, has to be analysed.

To summarise, the use of lignin as a matrix offers a possibility for the cascading use of biomass, in which the use of by-products or waste products contributes to closing material cycles instead of their purely thermal utilisation, and leads to new advanced bio-based materials. Coating of (natural fibre) yarns with lignin presents an alternative way to manufacture hybrid yarns, which can be used to produce semi-finished products for composite components.

**Author Contributions:** Conceptualization, C.M.; methodology, C.M., M.C., T.W., T.H., H.-J.B., T.S.; investigation, C.M., M.C., T.H.; validation, C.M., M.C., T.W., T.H.; writing—original draft preparation, C.M., T.W., T.H.; visualization, C.M., T.W., T.H.; project administration, C.M.; writing—review and editing, S.B., H.-J.B., T.S., W.W., G.T.G.; supervision: S.B., H.-J.B., T.S., G.T.G. All authors have read and agreed to the published version of the manuscript.

**Funding:** This research was funded by the German Institute of Textile and Fibre Research (DITF).

**Institutional Review Board Statement:** Not applicable.

**Informed Consent Statement:** Not applicable.

**Data Availability Statement:** Data are contained within this article.

**Conflicts of Interest:** The authors declare no conflict of interest.

## References

1. Tiseo, I. Market Size of Plastics Worldwide from 2016 to 2028. Available online: <https://www.statista.com/statistics/1060583/global-market-value-of-plastic/> (accessed on 5 July 2022).
2. Tiseo, I. Annual Production of Plastics Worldwide from 1950 to 2020. Available online: <https://www.statista.com/statistics/282732/global-production-of-plastics-since-1950/> (accessed on 5 July 2022).
3. Shamsuyeva, M.; Endres, H.-J. Plastics in the context of the circular economy and sustainable plastics recycling: Comprehensive review on research development, standardization and market. *Compos. Part C Open Access* **2021**, *6*, 100168. [CrossRef]
4. Varyan, I.; Kolesnikova, N.; Xu, H.; Tyubaeva, P.; Popov, A. Biodegradability of Polyolefin-Based Compositions: Effect of Natural Rubber. *Polymers* **2022**, *14*, 530. [CrossRef]
5. Xia, Z.; Li, J.; Zhang, J.; Zhang, X.; Zheng, X.; Zhang, J. Processing and valorization of cellulose, lignin and lignocellulose using ionic liquids. *J. Bioresour. Bioprod.* **2020**, *5*, 79–95. [CrossRef]
6. Kumar, B.; Agumba, D.O.; Pham, D.H.; Latif, M.; Dinesh; Kim, H.C.; Alrobei, H.; Kim, J. Recent Research Progress on Lignin-Derived Resins for Natural Fiber Composite Applications. *Polymers* **2021**, *13*, 1162. [CrossRef]
7. Li, H.; Liang, Y.; Li, P.; He, C. Conversion of biomass lignin to high-value polyurethane: A review. *J. Bioresour. Bioprod.* **2020**, *5*, 163–179. [CrossRef]
8. Gandini, A.; Lacerda, T.M. Monomers and Macromolecular Materials from Renewable Resources: State of the Art and Perspectives. *Molecules* **2021**, *27*, 159. [CrossRef]
9. Naseem, A.; Tabasum, S.; Zia, K.M.; Zuber, M.; Ali, M.; Noreen, A. Lignin-derivatives based polymers, blends and composites: A review. *Int. J. Biol. Macromol.* **2016**, *93*, 296–313. [CrossRef]
10. Vásquez-Garay, F.; Carrillo-Varela, I.; Vidal, C.; Reyes-Contreras, P.; Faccini, M.; Teixeira Mendonça, R. A Review on the Lignin Biopolymer and Its Integration in the Elaboration of Sustainable Materials. *Sustainability* **2021**, *13*, 2697. [CrossRef]
11. Guilhen, A.; Gadioli, R.; Fernandes, F.C.; Waldman, W.R.; De Paoli, M.A. High-density green polyethylene biocomposite reinforced with cellulose fibers and using lignin as antioxidant. *J. Appl. Polym. Sci.* **2017**, *134*, 45219. [CrossRef]
12. Çalgeris, İ.; Çakmakçı, E.; Ogan, A.; Kahraman, M.V.; Kayaman-Apohan, N. Preparation and drug release properties of lignin-starch biodegradable films. *Starch* **2012**, *64*, 399–407. [CrossRef]
13. Thielemans, W.; Can, E.; Morye, S.S.; Wool, R.P. Novel applications of lignin in composite materials. *J. Appl. Polym. Sci.* **2002**, *83*, 323–331. [CrossRef]
14. Barzegari, M.R.; Alemdar, A.; Zhang, Y.; Rodrigue, D. Mechanical and rheological behavior of highly filled polystyrene with lignin. *Polym. Compos.* **2012**, *33*, 353–361. [CrossRef]
15. Ramires, E.C.; Megiatto, J.D.; Gardrat, C.; Castellan, A.; Frollini, E. Valorization of an industrial organosolv-sugarcane bagasse lignin: Characterization and use as a matrix in biobased composites reinforced with sisal fibers. *Biotechnol. Bioeng.* **2010**, *107*, 612–621. [CrossRef]
16. Ko, H.-U.; Kim, J.W.; Kim, H.C.; Zhai, L.; Kim, J. Esterified PVA-lignin resin by maleic acid applicable for natural fiber reinforced composites. *J. Appl. Polym. Sci.* **2020**, *137*, 48836. [CrossRef]
17. Jablonskis, A.; Arshanitsa, A.; Arnautov, A.; Telysheva, G.; Evtuguin, D. Evaluation of Ligno Boost™ softwood kraft lignin epoxidation as an approach for its application in cured epoxy resins. *Ind. Crops Prod.* **2018**, *112*, 225–235. [CrossRef]
18. Solihat, N.N.; Sari, F.P.; Falah, F.; Ismayati, M.; Lubis, M.A.R.; Fatriasari, W.; Santoso, E.B.; Syafii, W. Lignin as an Activ Biomaterial: A review. *J. Sylva Lestari* **2021**, *9*, 1–22. [CrossRef]
19. Mimini, V.; Sykacek, E.; Syed Hashim, S.N.A.; Holzweber, J.; Hettegger, H.; Fackler, K.; Potthast, A.; Mundigler, N.; Rosenau, T. Compatibility of Kraft Lignin, Organosolv Lignin and Lignosulfonate With PLA in 3D Printing. *J. Wood Chem. Technol.* **2019**, *39*, 14–30. [CrossRef]
20. Gordobil, O.; Delucis, R.; Egüés, I.; Labidi, J. Kraft lignin as filler in PLA to improve ductility and thermal properties. *Ind. Crops Prod.* **2015**, *72*, 46–53. [CrossRef]
21. Vaidya, A.A.; Collet, C.; Gaugler, M.; Lloyd-Jones, G. Integrating softwood biorefinery lignin into polyhydroxybutyrate composites and application in 3D printing. *Mater. Today Commun.* **2019**, *19*, 286–296. [CrossRef]

22. Sahoo, S.; Misra, M.; Mohanty, A.K. Enhanced properties of lignin-based biodegradable polymer composites using injection moulding process. *Compos. Part A Appl. Sci. Manuf.* **2011**, *42*, 1710–1718. [CrossRef]
23. Domínguez-Robles, J.; Martín, N.K.; Fong, M.L.; Stewart, S.A.; Irwin, N.J.; Rial-Hermida, M.I.; Donnelly, R.F.; Larrañeta, E. Antioxidant PLA Composites Containing Lignin for 3D Printing Applications: A Potential Material for Healthcare Applications. *Pharmaceutics* **2019**, *11*, 165. [CrossRef]
24. Graupner, N. Application of lignin as natural adhesion promoter in cotton fibre-reinforced poly(lactic acid) (PLA) composites. *J. Mater. Sci.* **2008**, *43*, 5222–5229. [CrossRef]
25. Thakur, V.K.; Thakur, M.K.; Raghavan, P.; Kessler, M.R. Progress in Green Polymer Composites from Lignin for Multifunctional Applications: A Review. *ACS Sustain. Chem. Eng.* **2014**, *2*, 1072–1092. [CrossRef]
26. Lahtinen, M.H.; Ojala, A.; Wikström, L.; Nättinen, K.; Hietala, S.; Fiskari, J.; Kilpeläinen, I. The impact of thermomechanical pulp fiber modifications on thermoplastic lignin composites. *Compos. Part C Open Access* **2021**, *6*, 100170. [CrossRef]
27. Ma, Y.; Asaadi, S.; Johansson, L.-S.; Ahvenainen, P.; Reza, M.; Alekhina, M.; Rautkari, L.; Michud, A.; Hauru, L.; Hummel, M.; et al. High-Strength Composite Fibers from Cellulose-Lignin Blends Regenerated from Ionic Liquid Solution. *ChemSusChem* **2015**, *8*, 4030–4039. [CrossRef]
28. Liu, R.; Peng, Y.; Cao, J.; Chen, Y. Comparison on properties of lignocellulosic flour/polymer composites by using wood, cellulose, and lignin flours as fillers. *Compos. Sci. Technol.* **2014**, *103*, 1–7. [CrossRef]
29. Graupner, N. Naturfaser Verstärkte Biopolymere: Auf Dem Weg Zum Nachhaltigen LEICHTBAU. In Proceedings of the InnoMateria—Innovative Werkstoffe von Heute Für Die Produkte von Morgen, Cologne, Germany, 16 March 2011.
30. FNR. Composites: Leicht—Modern—Nachhaltig. Available online: <https://biowerkstoffe.fnr.de/composites> (accessed on 25 May 2022).
31. Pott, G.T. Reduction of Moisture Sensitivity in Natural Fibres. *MRS Online Proc. Libr.* **2001**, *702*, 361. [CrossRef]
32. Stegmaier, T.; König, S.; Kreis, P.; Hager, T.; Wunderlich, W.; von Arnim, V.; Selvarayan, S.K.; Milwich, M.; Möhl, C.; Ausheyks, L.; et al. Polypropylenkompatible Schichten für Recycling-Carbonfasern aus CFK End-of-Life-Bauteilen: Schlussbericht iGF-Vorhaben 20092 N/1 /N/2, 2021.
33. Möhl, C.; Weimer, T.; Caliskan, M.; Baz, S.; Bauder, H.-J.; Gresser, G.T. Development of Natural Fibre-Reinforced Semi-Finished Products with Bio-Based Matrix for Eco-Friendly Composites. *Polymers* **2022**, *14*, 698. [CrossRef]

## Article

# Polylactic Acid Chemical Foaming Assisted by Solid-State Processing: Solid-State Shear Pulverization and Cryogenic Milling

Philip R. Onffroy , Nathan T. Herrold, Harrison G. Goehrig, Kalie Yuen and Katsuyuki Wakabayashi \* 

Department of Chemical Engineering, Bucknell University, Lewisburg, PA 17837-2029, USA

\* Correspondence: kw025@bucknell.edu; Tel.: +1-(570)-577-3778

**Abstract:** A chemical foaming process of polylactic acid (PLA) was developed via the solid-state processing methods of solid-state shear pulverization (SSSP) and cryogenic milling. Based on the ability of solid-state processing to enhance the crystallization kinetics of PLA, chemical foaming agents (CFA) are first compounded before foaming via compression molding. Specifically, the effects of the pre-foaming solid-state processing method and CFA concentration were investigated. Density reduction, mechanical properties, thermal behavior, and cell density of PLA foams are characterized. Solid-state processing of PLA before foaming greatly increases the extent of PLA foaming by achieving void fractions approximately twice that of the control foams. PLA's improved ability to crystallize is displayed through both dynamic mechanical analysis and differential scanning calorimetry. The solid-state-processed foams display superior mechanical robustness and undergo low stress relaxation. The cell density of the PLA foams also increases with solid-state processing, especially through SSSP. Additionally, crosslinking of PLA during the pre-foaming processing step is found to result in the greatest enhancement of crystallization but decreased void fraction and foam effectiveness. Overall, SSSP and cryogenic milling show significant promise in improving chemical foaming in alternative biopolymers.

**Citation:** Onffroy, P.R.; Herrold, N.T.; Goehrig, H.G.; Yuen, K.; Wakabayashi, K. Polylactic Acid Chemical Foaming Assisted by Solid-State Processing: Solid-State Shear Pulverization and Cryogenic Milling. *Polymers* **2022**, *14*, 4480. <https://doi.org/10.3390/polym14214480>

Academic Editor: Cristina Cazan

Received: 30 September 2022

Accepted: 17 October 2022

Published: 22 October 2022

**Publisher's Note:** MDPI stays neutral with regard to jurisdictional claims in published maps and institutional affiliations.



**Copyright:** © 2022 by the authors. Licensee MDPI, Basel, Switzerland. This article is an open access article distributed under the terms and conditions of the Creative Commons Attribution (CC BY) license (<https://creativecommons.org/licenses/by/4.0/>).

**Keywords:** solid-state shear pulverization; cryogenic milling; polylactic acid; foams; processing; semicrystalline polymers; compression molding

## 1. Introduction

Polymer foams have widespread valuable applications, including packaging, safety padding, and insulation [1]. Polymer foams are created by incorporating pressurized gas into a molten polymer and subsequently solidifying the polymer-gas composite. In the case of semicrystalline polymers, gas is captured both by entanglement in the polymer chains and by polymer crystallites [2–4]. Today, nearly all polymers in commercial foams are derived from non-renewable fossil fuels and do not degrade easily [5]. Their ubiquitous use can be an environmental challenge. In the pursuit of developing bio-based and/or biodegradable polymers to replace petroleum-based polymers in foams, a variety of strategies have been taken, ranging from plant-based materials to microorganism-produced polymers [6–9]. One of the most studied bio-based polymers is polylactic acid (PLA), a condensation polymer derived through the fermentation of sucrose from cornstarch into lactic acid [10–12]. PLA, known to be more compostable than petroleum-based plastics in accordance with ASTM D6691 [13,14], is becoming a prevalent sustainable material of choice in biomedical, packaging, and additive manufacturing applications [11].

Polymer foams can be created through physical pressurized gas injection or by incorporating gas generated from chemical reactions. To date, most PLA-foaming studies with high levels of success are limited to the former physical foaming method [2,15,16]. However, physical foaming tends to produce unevenly distributed foams with less versatility in product shape than chemical foaming and can be expensive due to the need for high-pressure gas sources and precision transport systems [17,18]. Chemical foaming,

which uses small molecular additives known as chemical foaming agents (CFAs) that break down into gas when heated above their activation temperature [2,19], can circumvent the physical foaming concerns and enable a thoroughly consistent, in situ foam through common polymer processing methods, such as extrusion, injection molding, and compression molding [3]. However, the limited success of chemical foaming of PLA has been reported to date [18,20,21].

Creating an effective PLA foam is challenging partly due to PLA's slow crystallization kinetics, which allows the foaming gas to predominantly escape from the system rather than being secured by PLA's crystallizing chains as the temperature cools to shape a product [2,22]. Additionally, PLA is shear-sensitive in the melt state, suffering from molecular, viscosity, and physical property degradation compared to petroleum-based analogs [2]. Incorporating other polymers, such as polyethylene into a blend with PLA overcomes these challenges, but significantly lessens the sustainable nature of the output [23]. Another potential solution is crosslinking PLA chains via chemical crosslinking agents; however, the crosslinking often still must be accompanied by blending PLA with another polymer such as poly(butylene succinate) to achieve an adequate foam [24].

In previous studies, an alternative processing method called solid-state shear pulverization (SSSP) has shown promising results in increasing the crystallization kinetics of PLA [25–27], which is considered key for better control of the foam cell structure [2]. SSSP is a form of twin screw extrusion conducted under chilled conditions, and it has previously been used to modify homopolymers [28,29], compatibilize polymer blends [30–32], disperse additives [33,34], and create nanocomposites [35–39]. The foci of SSSP have been at the forefront of polymer sustainability, ranging from mechanical recycling [40,41] and natural fiber/renewable feedstock composites [42–44], to PLA/starch blends [45] and PLA crystallinity studies [25,26]. Specifically, the mechanochemistry of SSSP leads to scission and imperfections in PLA chains, which increase the material's rate of nucleation and growth [25]. Another solid-state processing method called cryogenic milling (cryomilling), has also been employed alongside SSSP [46–48] and has contributed to previous sustainable PLA processing research [49,50].

This is the first study in the literature to use SSSP and cryomilling to facilitate the chemical foaming of PLA, aiming to develop a more sustainable biopolymer foam. PLA foams are prepared by first incorporating a CFA with neat polymer pellets via a solid-state process, and subsequently compression-molding it into a specimen. These SSSP and cryomill techniques are compared to a control prepared via manual blending. An additional set of crosslinked PLA foams processed through cryomilling is introduced to investigate the combination of crosslinking and solid-state processing. Void fractions for the different sets of PLA foams are first measured. The foam morphology characterization through scanning electron microscopy (SEM) imaging is followed by thermal analysis of the foams via differential scanning calorimetry (DSC) and mechanical property evaluation with static compression testing and dynamic mechanical analysis (DMA). The processing-structure-property relationships of pre-foaming solid-state compounding of the CFA and the biopolymer are explored.

## 2. Materials and Methods

### 2.1. Materials

The PLA material used in this study was Ingeo Biopolymer 2003D with an L-lactide to D-lactide ratio of 96/4, supplied by NatureWorks, LLC [51]. This extrusion grade material is reported by the manufacturer to have a density of 1.24 g/cm<sup>3</sup>, a melt flow rate of 6 g/10 min at 210 °C, tensile yield strength of 60 MPa, and a heat distortion temperature of 55 °C [51]. Due to PLA's hygroscopic nature, it was dried for at least 2 h at 90 °C in a Moretto XD1 Dryer before all procedures.

The CFA used for this study was an azodicarbonamide (ADCA)-based CFA custom formulated by Avient Corporation. This CFA came in viscous liquid form and its formulation consisted of 54 wt% ADCA with the remainder being carrier, active, surfactant, and

clay thickener. This ADCA CFA activates and releases nitrogen ( $N_2$ ), carbon monoxide (CO), and ammonia ( $NH_3$ ) in an exothermic event [18]. The activation temperature of approximately 205 °C, determined via in-house thermogravimetric analysis testing, is key, as the activation temperature is higher than PLA's measured melting point of around 170 °C; the higher activation temperature ensures that the PLA is molten and able to contain and dissolve the gas [52]. The crosslinking agents used in the final portion of this study were triallyl isocyanurate (TAIC) and dicumyl peroxide (DCP) [53], purchased from Sigma Aldrich.

## 2.2. Pre-Foaming Processing Methods

Both SSSP and cryomilling were used as the primary processing methods for compounding CFA with PLA before foaming. PLA pellets manually blended with CFA were designated as the third control formulation, modeling a traditional process where polymer pellets and additives were directly fed into a molding machine without any solid-state preprocessing step. The fourth formulation of crosslinked PLA was prepared by first crosslinking PLA through single-screw melt extrusion followed by cryomill-compounding with CFA. For the balance of this paper, the SSSP-processed foam set will be referred to as SP, the cryomill-processed set as CM, the melt blended control set as CT, and the crosslinked/cryomill-processed set as XL. For each of the four sets of pre-foam processing modes, a CFA content parametric study was carried out to determine the relationships between the weight percentage of CFA and the physical properties of the resulting foams. The nominal concentrations of CFA for the six series tested were 0.5 wt%, 1.0 wt%, 2.0 wt%, 3.5 wt%, 5.0 wt%, and 6.5 wt%.

For foam set SP, CFA was compounded with PLA pellets through SSSP. The SSSP processing method is based on a KraussMaffei Berstorff ZE25-UTX intermeshing, co-rotating twin screw extruder with a screw diameter of 25 mm and the length-to-diameter ratio of 34. The extruder barrels were chilled to low temperatures using a circulation of  $-12$  °C-ethylene glycol/water solution, provided by Budzar Industries BWA-AC10 chiller. Figure 1 outlines the screw configuration, taken from a previous study [25], which employed a balance of harsh and mild screw elements to disperse the CFA additives while preventing premature polymer decomposition during the SSSP process. PLA pellets were manually coated in the liquid CFA and fed into the SSSP barrel using a Brabender Technologie Volumetric RotoTube feeder with the assistance of pressurized air through the center of the feeder hopper to ensure a continuous flow of 50 g/h. The SSSP screw speed was set to 200 rpm based on a previous parametric study on SSSP processing-structure-property relationships [54].

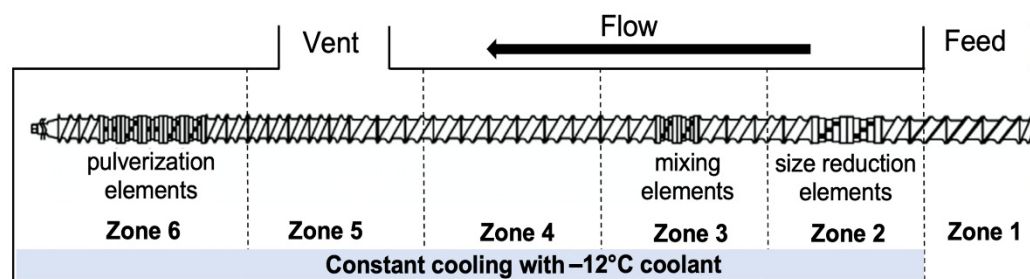


**Figure 1.** The SSSP screw design used in this study contains 9 bilobe kneading discs distributed among conveying elements for size reduction, mixing, and pulverization purposes.

For foam set CM, the cryomill processing method achieved a similar low-temperature mechanochemical compounding effect as SSSP, in a batch setting [55]. Each cryomill run was composed of a 12-g total sample of PLA with CFA, run through a SPEX SamplePrep 6870 Freezer/Mill. The cryomill procedure started with a 15-min cooldown period followed by 5 cycles of 4 min of pulverization and 4 min of cooldown between each cycle. After the final cycle, the sample contents were thawed to room temperature and stored.



For control foam set CT, PLA pellets were manually blended with CFA with a 20-g total sample size in a glass container. This mixture was prepared and stored at room temperature.

Foam set XL followed a two-step preparation process. The first part involved melt-compounding PLA pellets with 0.1 wt% TAIC and 0.1 wt% DCP crosslinking agents through a Killion Model KLB075 single-screw extruder. The screw speed was set to 15 RPM, and an extruder temperature of 180 °C was used because that is above both the melting temperature of PLA and the activation temperature of the crosslinking agents. The crosslinked polymer extrudate was cooled to ambient temperature and pelletized. The second step was to compound the crosslinked PLA with CFA in a cryomill in the same manner as foam set CM.

### 2.3. Compression Molding Foaming Process

After the four pre-foaming preparation methods were completed, the foaming procedure was carried out in a consistent fashion using compression molding. A 5.0 g sample of each formulation was added into a custom, cylindrical stainless steel mold with a 7.6 cm inner diameter and 6.4 cm height. The mold was loaded into an automated Carver Auto-Four 30-15 HC Press. Under an initial 5 MPa of pressure, the sample was pressed at 220 °C and held isothermally for 8 min; during this process, pressure increase was observed inside the mold as CFA activated between 190–210 °C. The pressure was released, and the mold was cooled at an average rate of approximately 10 °C/min on a steel cooling surface with convective air cooling from two AC Infinity Model AI-MPF120P2 dual fans. After at least 20 min of cooling and resting, the foam sample was removed from the mold and stored.

### 2.4. Foam Analysis Methods

The density reduction measurements of the foam samples were conducted following the ASTM D792 standard using an OHAUS Density Determination Kit and Adventurer Model AX324 scale. The density of the sample was first calculated as:

$$\rho_{foam} = \frac{A}{A - B}(\rho_0 - \rho_L) + \rho_L \quad (1)$$

where  $A$  is the weight of the sample in air,  $B$  is the weight of the sample in water, air density ( $\rho_L$ ) equals 0.00119 g/cm<sup>3</sup>, and water density ( $\rho_0$ ) equals 0.997 g/cm<sup>3</sup> at 25 °C. The void fraction ( $\phi$ ) of the foam samples, which is the volume expansion ratio of the material caused by foaming [21,56], was then calculated using the following equation:

$$\phi = \frac{V_{void}}{V_{sample}} = 1 - \frac{\rho_{foam}}{\rho_{PLA}} \quad (2)$$

In Equation (2),  $\rho_{foam}$  is the density of the foam sample calculated via Equation (1), PLA density ( $\rho_{PLA}$ ) equals 1.24 g/cm<sup>3</sup>,  $V_{void}$  represents the volume taken up by gas cells inside the sample, and  $V_{sample}$  is the overall volume of the sample.

Scanning electron microscopy (SEM) was conducted using a Hitachi SU 5000 Field Emission Scanning Electron Microscope. Surfaces of cryogenically fractured PLA foam samples were sputter-coated with gold using a Denton Desk IV. SEM images were taken under a high vacuum with an electron beam voltage of 3.0 kV and at a magnification of  $\times 70$ . These SEM images were used to quantitatively compare the gas cell distribution in samples using the software program ImageJ [57]. The cell density ( $N_C$ ), defined as the number of cells per volume of non-foamed base PLA material, was calculated for each SEM micrograph following Equation (3):

$$N_C = \left(\frac{n * M^2}{A}\right)^{\frac{3}{2}} * \frac{1}{1 - \phi} \quad (3)$$

In Equation (3),  $\phi$  is the void fraction,  $n$  is the number of cells counted in each micrograph image,  $A$  is the cross-sectional area of the foam in the image, and  $M$  is the magnification factor of the image.

Differential scanning calorimetry (DSC) was performed on foam samples using a TA Instruments Q2000, calibrated with indium. A standard heat-cool-reheat run between 0 °C and 220 °C was programmed with a ramp rate of 10 °C/min.

Dynamic mechanical analysis (DMA) was conducted in a compression mode where a 12.7 mm diameter cylindrical cut-out of each foam sample was placed on a custom stainless-steel platform and subjected to oscillatory compressive stress by a cylindrical steel plunger. The compression deformation mode was chosen because it most closely resembles the mechanical strain a polymer foam material would undergo in applications such as packaging. Each compression DMA run was conducted at an oscillation frequency of 1 Hz in a dynamic temperature ramp mode between −20 °C and 170 °C. Additionally, static compression and stress relaxation runs for each sample were conducted at room temperature. The compression strain rate was 0.003/s and the initial static load for stress relaxation was set at 200 kPa [58].

### 3. Results and Discussion

#### 3.1. Density Reduction

Density reduction measurements were conducted on the compression-molded samples to obtain average  $\phi$  values, which are presented as a function of CFA concentration in Figure 2. As the CFA content increased, the void fraction increased for all samples up to a maximum plateau value. The plateau in each set indicates that there is an upper limit to the number of gas cells that a compression-molded PLA foam can successfully contain upon foam expansion, even as an increasing amount of gas is released inside the polymer melt. The different plateau values shown in Figure 2 for each of the four sets reveal that the solid-state processing of PLA before foaming makes a significant difference to the maximum void fraction a foam sample can achieve with compression molding. The manually blended control set CT reached a void fraction plateau of about 35% at a relatively low CFA concentration of 1.0 wt%, whereas the SSSP and cryomill sets (SP and CM, respectively) reached void fraction plateaus of approximately 70% at a CFA concentration of 5.0 wt%.

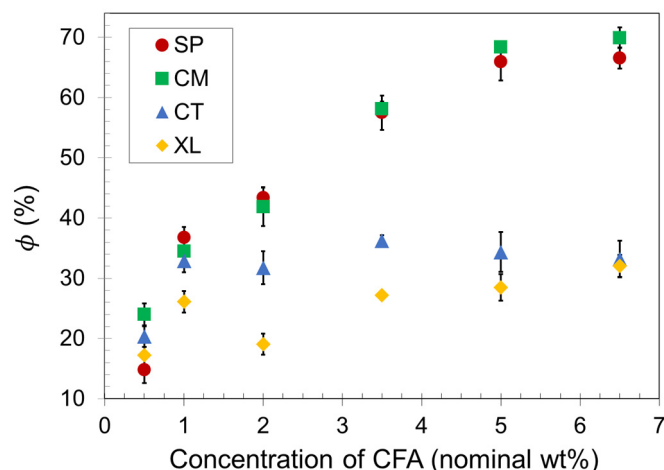


**Figure 2.** Void fraction of SSSP-processed (SP), cryomilled (CM), manually blended control (CT), and crosslinked/cryomilled (XL) PLA foam samples.

Polymer foaming technology often employs crosslinking to effectively capture gas cells and impart prototypical slow recovery foam behavior [59,60]. This study included a crosslinked analog of set CM to investigate the combination of crosslinking and cryogenic milling. Figure 2 reveals that the crosslinked foam set XL resulted in significantly lower void fraction values than set CM. PLA is a relatively brittle polymer at room temperature, and crosslinking may have constrained the chains of the material to such a great extent

that fewer gas cells could be contained, as the XL set reached a void fraction plateau of approximately 30%.

### 3.2. Foam Morphology

The cross-sectional gas cell morphology was evaluated with SEM, for different concentrations of CFA across four pre-foaming processing methods. Figure 3 displays how the four processing methods resulted in different gas cell shapes and size distributions, in a representative comparison of the 6.5 wt% CFA loading series. The non-crosslinked, solid-state-processed foams in Figure 3(SP) and Figure 3(CM) showed similarly high areas of coverage by closed cells. The SP samples displayed smaller gas cells than the CM samples across different CFA concentrations despite similar cell area coverage and  $\phi$  values from an earlier analysis. When comparing the SP and CM samples to the CT sample in Figure 3, it appears the control foam also exhibited closed cells. However, cell area coverage in CT foams was lower than those of the solid-state-processed foams, revealing one major reason why the control foams had lower void fraction values. In addition, the cells in the CT foams were concentrated in clusters around the sample rather than distributed evenly, for example, clustering at the top of Figure 3(CT).

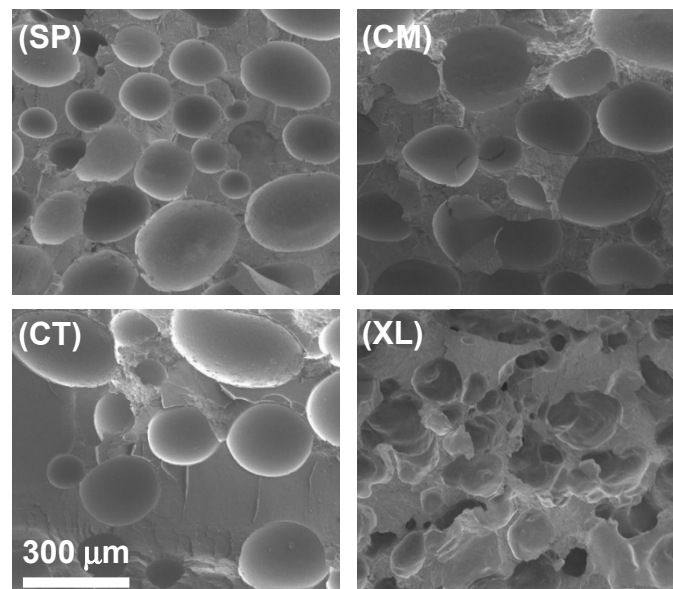


**Figure 3.** SEM images of SSSP-processed (SP), cryomilled (CM), manually blended control (CT), and crosslinked/cryomilled (XL) PLA foams with 6.5 wt% CFA.

A combination of the results so far indicates that PLA compounded with CFA in SP and CM methods were able to be compression-molded into consistent and physically expanded foams, containing a greater amount of gas in closed cells, compared to the CT foams. One explanation is that the mechanochemical modification of the PLA chains enabled enhanced crystallization kinetics [25], leading to a higher effect in trapping gas in closed cells upon solidification. Another explanation is that the intimate and homogeneous mixing in SSSP and cryomilling increased the CFA distribution and its contact level with PLA prior to the foaming process [36,37,42,47].

The crosslinked foams, such as shown in Figure 3(XL), displayed cross-sectional morphology significantly different from the other sets in that open cells were formed instead of closed cells. Open cell structure is a common characteristic of polymer foams with high void fractions [61]. Despite the apparent network structure and moderate open cell concentration, the XL foams did not expand in the mold as much as the SP and CM foams. This indicates that the crosslinking agents made the material too strong and tough

to be able to contain as much gas as the other foams, contributing to its significantly lower  $\phi$  values [62].

Quantitatively, the cell density for each foam was calculated using Equation (3). The average  $N_C$  values are plotted as a function of CFA concentration in Figure 4. For a given CFA concentration, the cell density values generally reflect the visual trends observed in the SEM images. However, the standard deviation ranges overlap for many data points in Figure 4, and therefore we refrain from making definitive remarks but rather provide general observed trends.

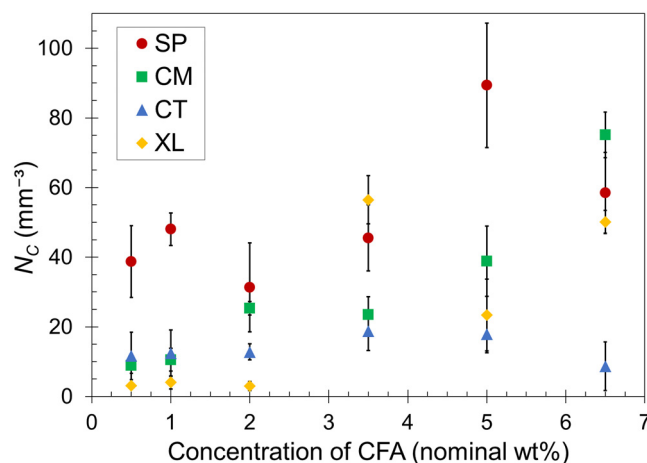


**Figure 4.** Calculated cell density versus CFA concentration for SP, CM, CT, and XL foams. The error bars indicate one standard deviation. The data points that do not show error bars have deviation ranges smaller than the point size.

Both sets of solid-state-processed foams displayed greater cell density than the CT and XL foam sets in most cases, confirming the enhanced ability of the pre-foaming solid-state processing to generate and capture the gas in closed cells. The SP foams tended to have greater gas cell density than CM foams, particularly at low CFA concentrations. At higher CFA content, the CM set began to achieve similarly high  $N_C$  values as the SP set. Perhaps the shearing nature of SSSP is more conducive to dispersing CFA than impact-based cryomilling at low concentrations. As CFA concentration increases, this nuanced difference becomes less relevant because the amount of gas being released is high and the effect of enhanced solidification rate dominates the level of CFA dispersion in these materials. The XL samples experienced the most inconsistent trend, with the majority of  $N_C$  values remaining low except for high jumps observed for 3.5–6.5 wt% CFA. The inconsistency of the XL foam results can be attributed to the open-cell nature of the crosslinked foams causing less consistent cell formation compared to the other closed cell foams.

Lastly, it might be expected that the plateauing trend of  $\phi$  in Figure 2 would correspond to a similarly plateauing trend of cell density in Figure 4. This may be occurring for the SP and CT sets but is not the case for the CM set. Perhaps the fine powder nature of CM formulations after cryomilling enabled gas cell formation more consistent with CFA content than other sets. In contrast, the XL samples showed a delayed increase in cell density while  $\phi$  is relatively steady in Figure 3. Further investigation on the relationship between  $\phi$  and cell density is warranted, but one definitive takeaway is that consistent PLA foams with practical density reduction are reliably achievable with CFA concentrations at around 5–6.5 wt%. These CFA loadings are considerably higher than a typical industry polymer foam CFA concentration of around 1.0 wt% [63].

### 3.3. Differential Scanning Calorimetry

We turned to thermal characterization by DSC to examine the PLA crystal development that occurred in the compression-molded foams. Figure 5 compares the thermograms of the first heat of as-compression-molded foam samples of the 6.5 wt% CFA concentration

grouping. The key thermal events occurring during the first heat curves are the glass transition at  $T_g = 60\text{ }^\circ\text{C}$ , cold crystallization at  $T_{cc} = 100\text{ }^\circ\text{C}$ , and melting at  $T_m = 150\text{ }^\circ\text{C}$ .

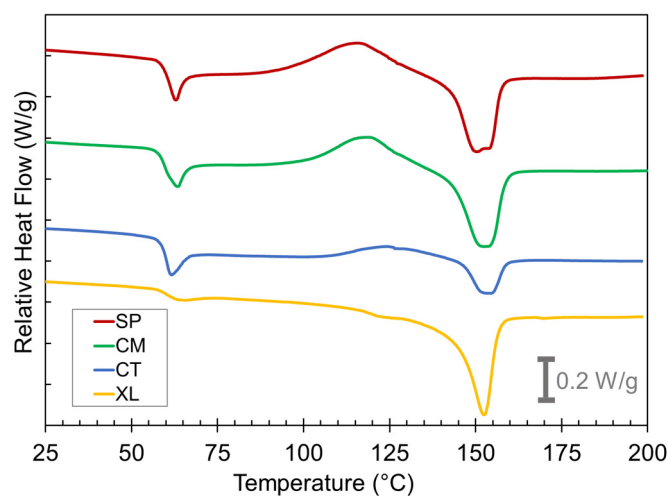


**Figure 5.** DSC first heat curves for the SP, CM, CT, and XL foams with 6.5 wt% CFA (exo up).

The thermogram shape of the XL foams at  $T_g$  is a typical step change expected for reversible glass transition whereas the CT, CM, and SP foams record a  $T_g$  overshoot peak in their thermograms at  $\sim 60\text{ }^\circ\text{C}$ . These overshoots were caused by the devitrification of additional mobile amorphous phase PLA in the sample after cooling during the foaming process [25]. The reasoning behind this will be explained later in this section.

Significant cold crystallization exotherms occurred beginning at  $\sim 100\text{ }^\circ\text{C}$  for the SP and CM foams. Conversely, the CT samples displayed only a shallow cold crystallization peak, and the peak shifted to a higher temperature range than the solid-state-processed samples. The XL samples showed no cold crystallization. These findings indicate that solid-state-processed foams show a higher potential to crystallize whereas the CT and XL samples either have a lower capacity to crystallize or have already crystallized to their full extent before  $100\text{ }^\circ\text{C}$ . The melt peak characteristics reveal more about which of these is occurring. Clear differences can immediately be seen between the different melting endotherms at  $T_m \sim 150\text{ }^\circ\text{C}$ . The melting peaks for the solid-state-processed samples were much larger than for the CT sample. This indicates that the solid-state-processed samples underwent a significant level of total crystallization prior to melting, whereas the CT samples were less able to crystallize comprehensively, resulting in a small melting peak. The double peak nature of the SP sample melt peaks has been attributed to reflecting the recrystallization and reorganization process in a previous study [25]. Despite the XL samples also displaying little evidence of cold crystallization, they still had large melting peaks, indicating that any crystallization in the XL foams happened during the initial foaming process rather than the DSC's first heat run. These contrastive thermogram features between SP, CM, CT, and XL samples were observed at all CFA concentrations.

The differences in the relative latent heat of melting ( $\Delta H_m$ ) vs. cold crystallization ( $\Delta H_{cc}$ ) are worth further investigating. Table 1 lists the two latent heats from the first heat thermograms, and further calculates the effective latent heat of "melt crystallization" ( $\Delta H_{mc}$ ) during the respective foaming process, i.e., the measure of the extent that the PLA was able to crystallize during the cooling step of the compression molding after the CFA has been activated [25]. This value was calculated by subtracting  $\Delta H_{cc}$  from  $\Delta H_m$ . Table 1 reveals that in every case,  $\Delta H_{mc}$ ,  $\Delta H_{cc}$ , and  $\Delta H_m$  are all greater for the SP and CM samples than for the CT samples. The  $\Delta H_{mc}$  values for SP and CM foams were recorded in the range of 5.0–8.5 J/g, compared to 0.5–3.0 J/g for CT foams. While there appears to be no significant correlation between CFA concentration and enthalpy values, the higher ranges in SP and CM confirm substantial PLA crystallite development during their cooling process

in the compression mold, which led to more effective containment of chemically induced gas in the foams.

**Table 1.** Crystallization characteristics extrapolated from DSC first heat curves, with the top number in each cell being  $\Delta H_m$ , the middle, subtracted number being  $\Delta H_{cc}$ , and the resulting number (shaded) being  $\Delta H_{mc}$ . Note: all values are reported in J/g.

| Processing Type  | Enthalpy Type (J/g) | Concentration of CFA (Nominal wt%) |         |         |         |         |         |
|------------------|---------------------|------------------------------------|---------|---------|---------|---------|---------|
|                  |                     | 0.5 wt%                            | 1.0 wt% | 2.0 wt% | 3.5 wt% | 5.0 wt% | 6.5 wt% |
| SSSP (SP)        | $\Delta H_m$        | 15.5                               | 16.1    | 17.2    | 15.7    | 17.1    | 14.0    |
|                  | $\Delta H_{cc}$     | 10.0                               | 9.0     | 9.6     | 8.3     | 9.2     | 8.0     |
|                  | $\Delta H_{mc}$     | 5.5                                | 7.1     | 7.6     | 7.4     | 7.9     | 6.0     |
| Cryomill (CM)    | $\Delta H_m$        | 14.8                               | 16.6    | 16.0    | 14.2    | 17.2    | 15.0    |
|                  | $\Delta H_{cc}$     | 6.7                                | 8.8     | 7.5     | 7.8     | 12.0    | 8.6     |
|                  | $\Delta H_{mc}$     | 8.1                                | 7.8     | 8.5     | 6.4     | 5.2     | 6.4     |
| Control (CT)     | $\Delta H_m$        | 3.1                                | 5.3     | 5.2     | 5.5     | 4.4     | 4.7     |
|                  | $\Delta H_{cc}$     | 1.4                                | 2.7     | 4.7     | 3.2     | 3.5     | 2.2     |
|                  | $\Delta H_{mc}$     | 1.7                                | 2.6     | 0.5     | 2.3     | 0.9     | 2.5     |
| Crosslinked (XL) | $\Delta H_m$        | 17.4                               | 19.0    | 16.5    | 20.5    | 16.4    | 17.7    |
|                  | $\Delta H_{cc}$     | 2.1                                | 4.7     | 1.3     | 2.5     | 2.0     | 0.7     |
|                  | $\Delta H_{mc}$     | 15.3                               | 14.3    | 15.2    | 18.0    | 14.4    | 17.0    |

Interestingly, the XL foams did not display large cold crystallization peaks but still exhibited significantly large melting curves, suggesting that much of the crystallization occurred during foam cooling, to an extent even larger than those of SP and CM samples. Despite the significant crystallization enhancement caused by crosslinking, Section 3.1 showed how the XL foam void fraction values remain significantly lower than the non-crosslinked analogs in the CM set. This suggests that while a moderate amount of crystallization during foaming is desirable, exemplified by solid-state processing cases, excessive crystallization inhibits foaming by over-stiffening the PLA matrix. A similar inhibition of PLA foaming by excessive crystallinity has also previously been observed in physical foaming contexts [62,64].

### 3.4. Dynamic Mechanical Analysis Results

Temperature ramp DMA was conducted to observe the mechanical properties of the foams as a function of temperature, as well as to verify the crystallization behavior that was inferred from the DSC study above. We first focus on the changes in storage modulus ( $E'$ ) in Figure 6 based on a representative set. The 6.5 wt% CFA samples were selected because their substantial density reductions provided the highest contrast of DMA curves between the four contrastive foam samples within the series. The same thermal transition events and relative  $E'$  position trends were observed in other series of CFA concentrations. We limit the following discussion to qualitative comparisons.

The stiffness of the PLA foams remained relatively constant from room temperature up to the  $T_g$  ~60 °C, above which the foams lose stiffness as their chains become mobile. Note that the relative  $E'$  positions of the four samples switch between the pre- and post- $T_g$  plateaus in Figure 6. In the region between glass and cold crystallization temperatures, the SP and CM samples exhibited lower  $E'$  values. With higher void fraction and cell density, the two solid-state-processed foams displayed a suppressed solid-like behavior, especially because their crystallinity during this region was only modest. In contrast, the XL sample did not experience a drastic decrease in stiffness after  $T_g$ , as it was supported by the crosslinks and significant crystallinity that had already developed.

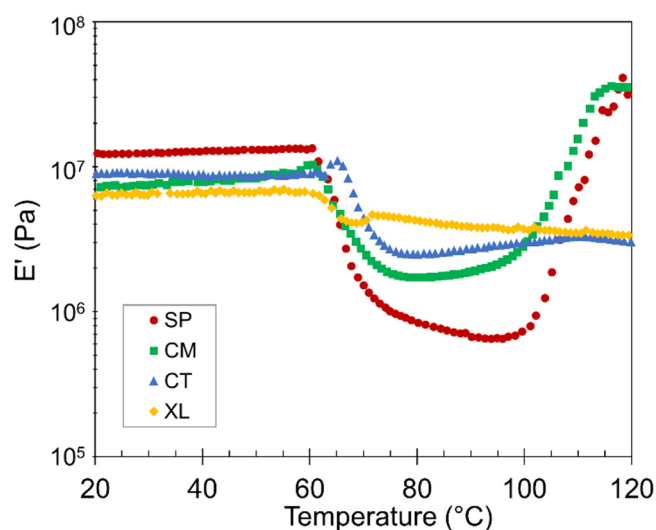


**Figure 6.** Representative plots of  $E'$  versus temperature for SP, CM, CT, and XL foams with 6.5 wt% CFA.

The 100–120 °C region corresponds to cold crystallization. A gradual modulus recovery correlates with the increasing number of developing crystals, as the crystalline phase is stiffer than the amorphous component above the  $T_g$  [65]. Figure 6 reveals that the solid-state-processed SP and CM samples experienced significant cold crystallization, to a level higher than any CT stiffness value and even surpassing their own original  $E'$ , having raised their crystalline potential [25]. On the other hand, the CT and XL samples showed little to no cold crystallization, corroborating the DSC results.

Often, one of the most valuable properties of foam material is its ability to absorb energy [66,67]. The  $\tan \delta$  plot of the temperature ramp DMA can be used to observe the material damping factor of the samples [68,69]. The higher the value of  $\tan \delta$  at a given temperature, the more the material will absorb energy [68]. Figure 7 compares  $\tan \delta$  curves between the 1.0 wt% and 6.5 wt% CFA series of the four foam sets. A major peak in  $\tan \delta$  at  $T_g$  associated with PLA devitrification was observed in each sample, as expected from a previous study on compression DMA of polymer foams [70]. The height of the  $\tan \delta$  peak varied slightly depending on the pre-foaming processing method. The most noticeable difference was between the XL foams and the SP, CM, and CT foams, which suggests that the XL foams remained too rigid through the  $T_g$  and deviated from a typical foam behavior in its mechanical response to the oscillatory motion. A peak height difference was also observed between the 6.5 wt% and 1.0 wt% samples of a given foam set. The fact that the higher CFA content foams constantly displayed a higher damping factor in the SP, CM, and CT sets confirms the effectiveness of employing higher CFA loading in preparing PLA foams. Again, the XL foams did not follow the same trend because their foam structure and rigidity properties are fundamentally different from the other sets.

A second, shallower, and broader  $\tan \delta$  peak appeared around 100 °C most distinctly in the solid-state-processed samples. The CT foams showed a continuously gradual increase without peaking, while the XL foams did not show any evidence of a significant second peak. As discussed above with  $E'$  transitions, the SP, CM, and CT samples developed more liquid-like and damping behaviors above their devitrification points. This typical and desired foam property caused  $\tan \delta$  to remain high until cold crystallization occurs in the respective sample, at which point stiff solid-like behavior returns and lowers the damping factor. The CT curve continued to display high  $\tan \delta$  due to a lack of cold crystallization. The XL foams were already stiff and crystalline before  $T_g$ , causing the  $\tan \delta$  curve to remain low.

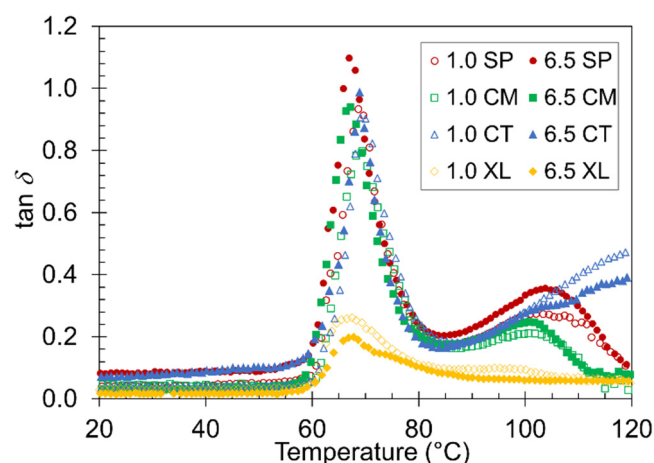


**Figure 7.** Representative plots of  $\tan \delta$  versus temperature for the four contrastive foams with 1.0 wt% and 6.5 wt% CFA.

### 3.5. Static Compression Testing

As polymer foams are likely used in practical applications at ambient temperatures, room-temperature static compression tests were carried out to determine the stress-strain relationships and stress relaxation tendencies. Based on the representative foam set of 6.5 wt% CFA, Figure 8a reveals that the SP and CM samples both displayed stress-strain relationships with higher slopes than the CT set. The solid-state-processed PLA foam samples were significantly stiffer and more mechanically robust than manually blended foam samples at room temperature, due to their higher as-molded crystallinity, as observed earlier by the  $\Delta H_{mc}$  values. The stiffness difference may also reflect that in the foam morphology, as Section 3.2 established that the solid-state-processed samples displayed higher cell density and more spatially consistent closed cell structure. The XL samples exhibited high stiffness because of their enhanced crystallinity through crosslinking and cryomilling; crosslinking has previously been shown to make PLA stiffer [53]. However, the XL sample's stress-strain curve had a lower slope than the SSSP and cryomill stress-strain plots perhaps due to the open-cell nature of the crosslinked foam [71].

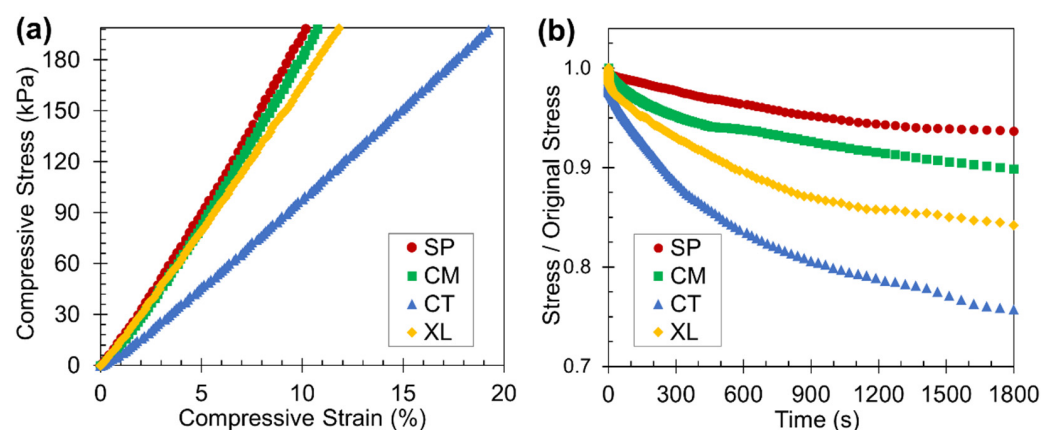


**Figure 8.** Results from the static compression testing displaying the (a) stress-strain curves (truncated at a compressive stress of 200 kPa) and (b) stress relaxation curves of the four foam samples with 6.5 wt% CFA at room temperature.

The stress relaxation results in Figure 8b reveal that SP and CM foams relaxed to a lesser extent than CT foams when subject to a constant initial static load of 200 kPa. In the context of static loading, foams that undergo less stress relaxation are better able to retain their initial shape after being compressed to some reasonable deformation level, enabling



sustainable usage in various applications. For certain packaging applications, an ideal foam can be defined as one that continuously applies a consistent force on an object [72], which the solid-state-processed foams exhibit. While the XL foams had high crystalline properties, their open cell foam structure nonetheless caused significant stress relaxation to occur.

#### 4. Conclusions

An effective PLA chemical foaming method has been established through solid-state processing, via either SSSP or cryomilling, followed by compression molding. Solid-state-processing PLA achieved foams with void fraction values approximately double those of the control foams (70% versus 35%) and consistently higher cell density. Though unusual, a relatively high CFA loading of around 6 wt% is recommended with solid-state processing, as increasing CFA concentration resulted in a corresponding increase in void fraction up until a plateau value. DSC and DMA findings indicated that the shearing and pulverization effects of solid-state processing resulted in enhanced melt crystallization and cold crystallization enthalpies. Additionally, solid-state-processed foams proved more robust and displayed less stress relaxation than crosslinked and control foam sets, enabling better reusability for sustainable applications. The crosslinked foams, which were also solid-state processed, achieved the highest level of melt crystallization but achieved low void fraction values (~30%) and inconsistent cell density, disproving that combining solid-state processing and crosslinking is an effective strategy for PLA foam development.

In the future, a better understanding of the optimal compression molding foaming heating and cooling rates should be established to ensure the most effective foaming method for PLA foams. One potential route is an in-depth investigation into the interplay between foaming and crystallization at different solidification rates. The chemical foaming method developed in this study complements existing physical foaming methods for PLA and contributes toward the widespread application of sustainable foams in our society.

**Author Contributions:** Conceptualization, P.R.O. and K.W.; methodology, P.R.O., H.G.G. and K.W.; software, P.R.O., K.Y. and K.W.; validation, N.T.H. and K.W.; formal analysis, P.R.O. and K.W.; investigation, P.R.O., N.T.H., H.G.G., K.Y. and K.W.; resources, K.W.; data curation, P.R.O. and K.W.; writing—original draft preparation, P.R.O. and K.W.; writing—review and editing, N.T.H., H.G.G. and K.Y.; visualization, P.R.O.; supervision, K.W.; project administration, K.W.; funding acquisition, K.W. All authors have read and agreed to the published version of the manuscript.

**Funding:** The SSSP instrument was funded by a National Science Foundation Major Research Instrumentation grant, CMMI-0820993.

**Institutional Review Board Statement:** Not applicable.

**Informed Consent Statement:** Not applicable.

**Data Availability Statement:** The data presented in this study are available upon request from the corresponding author.

**Acknowledgments:** The authors are grateful to the Avient Corporation for providing the chemical foaming agent. PRO was supported by the Presidential Scholars Program at Bucknell University. We additionally acknowledge our Bucknell colleagues Seth A. Pletcher and Prism Li for preliminary background experiments, Ethan Blumer for valuable technical discussions, and Diane Hall, Dan Johnson, and Tim Baker for supporting the laboratory instruments.

**Conflicts of Interest:** The authors declare no conflict of interest.

#### References

1. Doyle, L.; Weidlich, I. Mechanical Behaviour of Polylactic Acid Foam as Insulation under Increasing Temperature. *Environ. Clim. Technol.* **2019**, *23*, 202–210. [CrossRef]
2. Nofar, M.; Park, C.B. Poly (Lactic Acid) Foaming. *Prog. Polym. Sci.* **2014**, *39*, 1721–1741. [CrossRef]
3. Lee, C.H.; Lee, K.-J.; Jeong, H.G.; Kim, S.W. Growth of Gas Bubbles in the Foam Extrusion Process. *Adv. Polym. Technol.* **2000**, *19*, 97–112. [CrossRef]

4. Altan, M. Thermoplastic Foams: Processing, Manufacturing, and Characterization. In *Recent Research in Polymerization*; Cankaya, N., Ed.; InTech: London, UK, 2018; pp. 117–137.
5. Chamas, A.; Moon, H.; Zheng, J.; Qiu, Y.; Tabassum, T.; Jang, J.H.; Abu-Omar, M.; Scott, S.L.; Suh, S. Degradation Rates of Plastics in the Environment. *ACS Sustain. Chem. Eng.* **2020**, *8*, 3494–3511. [CrossRef]
6. Song, J.H.; Murphy, R.J.; Narayan, R.; Davies, G.B.H. Biodegradable and Compostable Alternatives to Conventional Plastics. *Phil. Trans. R. Soc. B* **2009**, *364*, 2127–2139. [CrossRef]
7. Zhu, Y.; Romain, C.; Williams, C.K. Sustainable Polymers from Renewable Resources. *Nature* **2016**, *540*, 354–362. [CrossRef]
8. Zhao, S.; Malfait, W.J.; Guerrero-Albuquerque, N.; Koebel, M.M.; Nyström, G. Biopolymer Aerogels and Foams: Chemistry, Properties, and Applications. *Angew. Chem. Int. Ed.* **2018**, *57*, 7580–7608. [CrossRef]
9. Gama, N.V.; Soares, B.; Freire, C.S.R.; Silva, R.; Neto, C.P.; Barros-Timmons, A.; Ferreira, A. Bio-Based Polyurethane Foams toward Applications beyond Thermal Insulation. *Mater. Des.* **2015**, *76*, 77–85. [CrossRef]
10. Dorgan, J.R.; Lehermeier, H.; Mang, M. Thermal and Rheological Properties of Commercial-Grade Poly(Lactic Acid)s. *J. Polym. Environ.* **2000**, *8*, 1–9. [CrossRef]
11. Cheng, Y.; Deng, S.; Chen, P.; Ruan, R. Polylactic Acid (PLA) Synthesis and Modifications: A Review. *Front. Chem. China* **2009**, *4*, 259–264. [CrossRef]
12. Carothers, W.H.; Dorough, G.L.; van Natta, F.J. Studies of Polymerization and Ring Formation. X. The Reversible Polymerization of Six-Membered Cyclic Esters. *J. Am. Chem. Soc.* **1932**, *54*, 761–772. [CrossRef]
13. ASTM D6691; Test Method for Determining Aerobic Biodegradation of Plastic Materials in the Marine Environment by a Defined Microbial Consortium or Natural Sea Water Inoculum. ASTM International: Conshohocken, PA, USA, 2009.
14. Greene, J. *PLA and PHA Biodegradation in the Marine Environment*; California Department of Resources Recycling and Recovery: Sacramento, CA, U.S.A, 2012.
15. Larsen, Å.; Neldin, C. Physical Extruder Foaming of Poly(Lactic Acid)-Processing and Foam Properties. *Polym. Eng. Sci.* **2013**, *53*, 941–949. [CrossRef]
16. Rokkonen, T.; Peltola, H.; Sandquist, D. Foamability and Viscosity Behavior of Extrusion Foamed PLA–Pulp Fiber Biocomposites. *J. Appl. Polym. Sci.* **2019**, *136*, 48202. [CrossRef]
17. Lee, S.-T.; Ramesh, N.S. (Eds.) *Polymeric Foams: Mechanisms and Materials*; CRC Press: Boca Raton, FL, USA, 2004.
18. Kmetty, Á.; Litauszki, K.; Réti, D. Characterization of Different Chemical Blowing Agents and Their Applicability to Produce Poly(Lactic Acid) Foams by Extrusion. *Appl. Sci.* **2018**, *8*, 1960. [CrossRef]
19. Yuan, H.; Liu, Z.; Ren, J. Preparation, Characterization, and Foaming Behavior of Poly(Lactic Acid)/Poly(Butylene Adipate- Co -Butylene Terephthalate) Blend. *Polym. Eng. Sci.* **2009**, *49*, 1004–1012. [CrossRef]
20. Seo, J.-H.; Han, J.; Lee, K.S.; Cha, S.W. Combined Effects of Chemical and Microcellular Foaming on Foaming Characteristics of PLA (Poly Lactic Acid) in Injection Molding Process. *Polym.-Plast. Technol. Eng.* **2012**, *51*, 455–460. [CrossRef]
21. Matuana, L.M.; Faruk, O.; Diaz, C.A. Cell Morphology of Extrusion Foamed Poly(Lactic Acid) Using Endothermic Chemical Foaming Agent. *Bioresour. Technol.* **2009**, *100*, 5947–5954. [CrossRef] [PubMed]
22. Wang, J.; Zhu, W.; Zhang, H.; Park, C.B. Continuous Processing of Low-Density, Microcellular Poly(Lactic Acid) Foams with Controlled Cell Morphology and Crystallinity. *Chem. Eng. Sci.* **2012**, *75*, 390–399. [CrossRef]
23. Zhao, M.; Ding, X.; Mi, J.; Zhou, H.; Wang, X. Role of High-Density Polyethylene in the Crystallization Behaviors, Rheological Property, and Supercritical CO<sub>2</sub> Foaming of Poly (Lactic Acid). *Polym. Degrad. Stab.* **2017**, *146*, 277–286. [CrossRef]
24. Campuzano, J.F.; Lopez, I.D. Study of the Effect of Dicumyl Peroxide on Morphological and Physical Properties of Foam Injection Molded Poly(Lactic Acid)/Poly(Butylene Succinate) Blends. *Express Polym. Lett.* **2020**, *14*, 673–684. [CrossRef]
25. Blumer, E.M.; Lynch, B.B.; Fielding, A.S.; Wakabayashi, K. Crystallinity and Property Enhancements in Neat Polylactic Acid by Chilled Extrusion: Solid-state Shear Pulverization and Solid-state/ Melt Extrusion. *Polym. Eng. Sci.* **2019**, *59*, E286–E295. [CrossRef]
26. Lynch, B.B. The Crystallization Kinetics of Polylactic Acid (PLA) Processed Through Solid-State/Melt Extrusion. B.S. Thesis, Bucknell University, Lewisburg, PA, USA, 2014.
27. Brunner, P. Overcoming Sustainability and Energy Challenges in Polymer Science Via Solid-State Shear Pulverization. Ph.D. Thesis, Northwestern University, Evanston, IL, USA, 2013.
28. Ganglani, M.; Torkelson, J.M.; Carr, S.H.; Khait, K. Trace Levels of Mechanochemical Effects in Pulverized Polyolefins. *J. Appl. Polym. Sci.* **2001**, *80*, 671–679. [CrossRef]
29. Diop, M.F.; Torkelson, J.M. Novel Synthesis of Branched Polypropylene via Solid-State Shear Pulverization. *Polymer* **2015**, *60*, 77–87. [CrossRef]
30. Lebovitz, A.H.; Khait, K.; Torkelson, J.M. In Situ Block Copolymer Formation during Solid-State Shear Pulverization: An Explanation for Blend Compatibilization via Interpolymer Radical Reactions. *Macromolecules* **2002**, *35*, 9716–9722. [CrossRef]
31. Tao, Y.; Lebovitz, A.H.; Torkelson, J.M. Compatibilizing Effects of Block Copolymer Mixed with Immiscible Polymer Blends by Solid-State Shear Pulverization: Stabilizing the Dispersed Phase to Static Coarsening. *Polymer* **2005**, *46*, 4753–4761. [CrossRef]
32. Diop, M.F.; Burghardt, W.R.; Torkelson, J.M. Well-Mixed Blends of HDPE and Ultrahigh Molecular Weight Polyethylene with Major Improvements in Impact Strength Achieved via Solid-State Shear Pulverization. *Polymer* **2014**, *55*, 4948–4958. [CrossRef]
33. Tao, Y.; Kim, J.; Torkelson, J.M. Achievement of Quasi-Nanostructured Polymer Blends by Solid-State Shear Pulverization and Compatibilization by Gradient Copolymer Addition. *Polymer* **2006**, *47*, 6773–6781. [CrossRef]

34. Walker, A.M.; Tao, Y.; Torkelson, J.M. Polyethylene/Starch Blends with Enhanced Oxygen Barrier and Mechanical Properties: Effect of Granule Morphology Damage by Solid-State Shear Pulverization. *Polymer* **2007**, *48*, 1066–1074. [CrossRef]
35. Iyer, K.A.; Lechanski, J.; Torkelson, J.M. Green Polypropylene/Waste Paper Composites with Superior Modulus and Crystallization Behavior: Optimizing Specific Energy in Solid-State Shear Pulverization for Filler Size Reduction and Dispersion. *Compos.-A Appl. Sci. Manuf.* **2016**, *83*, 47–55. [CrossRef]
36. Wakabayashi, K.; Pierre, C.; Dikin, D.A.; Ruoff, R.S.; Ramanathan, T.; Brinson, L.C.; Torkelson, J.M. Polymer-Graphite Nanocomposites: Effective Dispersion and Major Property Enhancement via Solid-State Shear Pulverization. *Macromolecules* **2008**, *41*, 1905–1908. [CrossRef]
37. Pujari, S.; Ramanathan, T.; Kasimatis, K.; Masuda, J.; Andrews, R.; Torkelson, J.M.; Brinson, L.C.; Burghardt, W.R. Preparation and Characterization of Multiwalled Carbon Nanotube Dispersions in Polypropylene: Melt Mixing versus Solid-State Shear Pulverization. *J. Polym. Sci. B Polym. Phys.* **2009**, *47*, 1426–1436. [CrossRef]
38. Wakabayashi, K.; Brunner, P.J.; Masuda, J.; Hewlett, S.A.; Torkelson, J.M. Polypropylene-Graphite Nanocomposites Made by Solid-State Shear Pulverization: Effects of Significantly Exfoliated, Unmodified Graphite Content on Physical, Mechanical and Electrical Properties. *Polymer* **2010**, *51*, 5525–5531. [CrossRef]
39. Iyer, K.A.; Torkelson, J.M. Novel, Synergistic Composites of Polypropylene and Rice Husk Ash: Sustainable Resource Hybrids Prepared by Solid-State Shear Pulverization. *Polym. Compos.* **2013**, *34*, 1211–1221. [CrossRef]
40. Miu, E.V.; Fox, A.J.; Jubb, S.H.; Wakabayashi, K. Morphology and Toughness Enhancements in Recycled High-Density Polyethylene (rHDPE) via Solid-State Shear Pulverization (SSSP) and Solid-State/Melt Extrusion (SSME). *J. Appl. Polym. Sci.* **2016**, *133*, 43070. [CrossRef]
41. Khait, K.; Torkelson, J.M. Solid-State Shear Pulverization of Plastics: A Green Recycling Process. *Polym. -Plast. Technol. Eng.* **1999**, *38*, 445–457. [CrossRef]
42. Iyer, K.A.; Torkelson, J.M. Green Composites of Polypropylene and Eggshell: Effective Biofiller Size Reduction and Dispersion by Single-Step Processing with Solid-State Shear Pulverization. *Compos. Sci. Technol.* **2014**, *102*, 152–160. [CrossRef]
43. Iyer, K.A.; Flores, A.M.; Torkelson, J.M. Comparison of Polyolefin Biocomposites Prepared with Waste Cardboard, Microcrystalline Cellulose, and Cellulose Nanocrystals via Solid-State Shear Pulverization. *Polymer* **2015**, *75*, 78–87. [CrossRef]
44. Wakabayashi, K.; Vancoillie, S.H.E.; Assfaw, M.G.; Choi, D.H.; Desplentere, F.; Van Vuure, A.W. Low-temperature Compounding of Flax Fibers with Polyamide 6 via Solid-state Shear Pulverization: Towards Viable Natural Fiber Composites with Engineering Thermoplastics. *Polym. Compos.* **2019**, *40*, 3285–3295. [CrossRef]
45. Brunner, P.J.; Torkelson, J.M. Microcrystalline Cellulose Composites of Poly(Lactic Acid)/Poly(Ethylene Glycol) or Polypropylene Created via Solid-State Shear Pulverization. *ANTEC Proc.* **2011**, *1*, 655–660.
46. Henry, M.F. Solid-State Compatibilization of Immiscible Polymer Blends: Cryogenic Milling and Solid-State Shear Pulverization. M.S. Thesis, Bucknell University, Lewisburg, PA, USA, 2010.
47. Hubert, P.J.; Kathiresan, K.; Wakabayashi, K. Filler Exfoliation and Dispersion in Polypropylene/as-Received Graphite Nanocomposites via Cryogenic Milling. *Polym. Eng. Sci.* **2011**, *51*, 2273–2281. [CrossRef]
48. Gabriel, M.C.; Mendes, L.B.; de Melo Carvalho, B.; Pinheiro, L.A.; Capochi, J.D.T.; Kubaski, E.T.; Cintho, O.M. High-Energy Mechanical Milling of Ultra-High Molecular Weight Polyethylene (UHMWPE). *Mater. Sci. Forum* **2010**, *660–661*, 325–328. [CrossRef]
49. Segura González, E.A.; Olmos, D.; González-Gaitano, G.; Orgaz, B.; González-Benito, J. Effect of Kaolin Nanofiller and Processing Conditions on the Structure, Morphology, and Biofilm Development of Polylactic Acid. *J. Appl. Polym. Sci.* **2015**, *132*, 42676. [CrossRef]
50. Candau, N.; Oguz, O.; León Albiter, N.; Förster, G.; Maspoch, M.L. Poly (Lactic Acid)/Ground Tire Rubber Blends Using Peroxide Vulcanization. *Polymers* **2021**, *13*, 1496. [CrossRef]
51. *Ingeo Biopolymer 2003D Technical Data Sheet*; NatureWorks LLC: Minnetonka, MN, USA, 2015.
52. Bhatti, A.S.; Goddard, R.J.; O'Donnell, G. The Thermal Decomposition of Azodicarbonamide. *Thermochim. Acta* **1984**, *76*, 63–77. [CrossRef]
53. Yang, S.; Wu, Z.-H.; Yang, W.; Yang, M.-B. Thermal and Mechanical Properties of Chemical Crosslinked Poly lactide (PLA). *Polym. Test.* **2008**, *27*, 957–963. [CrossRef]
54. Onffroy, P.R.; Miu, E.V.; Confer, W.J.; Darkes-Burkey, C.M.; Holler, W.C.; Wakabayashi, K. Residence Time Distribution and Specific Mechanical Energy in Solid-state Shear Pulverization: Processing-structure-property Relationships in a Chilled Extruder. *Polym. Eng. Sci.* **2020**, *60*, 503–511. [CrossRef]
55. Katiyar, N.K.; Biswas, K.; Tiwary, C.S. Cryomilling as Environmentally Friendly Synthesis Route to Prepare Nanomaterials. *Int. Mater. Rev.* **2021**, *66*, 493–532. [CrossRef]
56. Matuana, L.M.; Diaz, C.A. Study of Cell Nucleation in Microcellular Poly(Lactic Acid) Foamed with Supercritical CO<sub>2</sub> through a Continuous-Extrusion Process. *Ind. Eng. Chem. Res.* **2010**, *49*, 2186–2193. [CrossRef]
57. Reglero Ruiz, J.A.; Vincent, M.; Agassant, J.-F.; Sadik, T.; Pillon, C.; Carrot, C. Polymer Foaming with Chemical Blowing Agents: Experiment and Modeling. *Polym. Eng. Sci.* **2015**, *55*, 2018–2029. [CrossRef]
58. Miltz, J.; Ramon, O. Characterization of Stress Relaxation Curves of Plastic Foams. *Polym. Eng. Sci.* **1986**, *26*, 1305–1309. [CrossRef]
59. Khemani, K.C. (Ed.) *Polymeric Foams: Science and Technology*; American Chemical Society: Washington, DC, USA, 1997.

60. Jang, L.K.; Fletcher, G.K.; Monroe, M.B.B.; Maitland, D.J. Biodegradable Shape Memory Polymer Foams with Appropriate Thermal Properties for Hemostatic Applications. *J. Biomed. Mater. Res.* **2020**, *108*, 1281–1294. [CrossRef] [PubMed]
61. Wang, L.; Hikima, Y.; Ohshima, M.; Yusa, A.; Yamamoto, S.; Goto, H. Development of a Simplified Foam Injection Molding Technique and Its Application to the Production of High Void Fraction Polypropylene Foams. *Ind. Eng. Chem. Res.* **2017**, *56*, 13734–13742. [CrossRef]
62. Zhai, W.; Ko, Y.; Zhu, W.; Wong, A.; Park, C.B. A Study of the Crystallization, Melting, and Foaming Behaviors of Polylactic Acid in Compressed CO<sub>2</sub>. *Int. J. Mol. Sci.* **2009**, *10*, 5381–5397. [CrossRef]
63. Barzegari, M.R.; Rodrigue, D. The Effect of Injection Molding Conditions on the Morphology of Polymer Structural Foams. *Polym. Eng. Sci.* **2009**, *49*, 949–959. [CrossRef]
64. Standau, T.; Zhao, C.; Murillo Castellón, S.; Bonten, C.; Altstädt, V. Chemical Modification and Foam Processing of Polylactide (PLA). *Polymers* **2019**, *11*, 306. [CrossRef]
65. Liu, G.; Zhang, X.; Wang, D. Tailoring Crystallization: Towards High-Performance Poly(Lactic Acid). *Adv. Mater.* **2014**, *26*, 6905–6911. [CrossRef]
66. Tomin, M.; Kmetty, Á. Polymer Foams as Advanced Energy Absorbing Materials for Sports Applications—A Review. *J. Appl. Polym. Sci.* **2022**, *139*, 51714. [CrossRef]
67. Yang, B.; Zuo, Y.; Chang, Z. Evaluation of Energy Absorption Capabilities of Polyethylene Foam under Impact Deformation. *Materials* **2021**, *14*, 3613. [CrossRef]
68. Shaid Sujon, M.A.; Islam, A.; Nadimpalli, V.K. Damping and Sound Absorption Properties of Polymer Matrix Composites: A Review. *Polym. Test.* **2021**, *104*, 107388. [CrossRef]
69. Bizhani, H.; Katbab, A.A.; Lopez-Hernandez, E.; Miranda, J.M.; Lopez-Manchado, M.A.; Verdejo, R. Preparation and Characterization of Highly Elastic Foams with Enhanced Electromagnetic Wave Absorption Based On Ethylene-Propylene-Diene-Monomer Rubber Filled with Barium Titanate/Multiwall Carbon Nanotube Hybrid. *Polymers* **2020**, *12*, 2278. [CrossRef]
70. Zhang, L.; Jeon, H.K.; Malsam, J.; Herrington, R.; Macosko, C.W. Substituting Soybean Oil-Based Polyol into Polyurethane Flexible Foams. *Polymer* **2007**, *48*, 6656–6667. [CrossRef]
71. Song, P.; Zhang, Y.; Luo, Y.; Liao, X.; Tang, W.; Yang, J.; Tian, C.; Li, G. Design of Lightweight Silicone Rubber Foam for Outstanding Deformation Recoverability Based on Supercritical CO<sub>2</sub> Foaming Technology. *J. Mater. Sci.* **2022**, *57*, 2292–2304. [CrossRef]
72. Miltz, J.; Ramon, O. Energy Absorption Characteristics of Polymeric Foams Used as Cushioning Materials. *Polym. Eng. Sci.* **1990**, *30*, 129–133. [CrossRef]



Review

# Microencapsulation of Essential Oils: A Review

Vânia Isabel Sousa , Joana Filipa Parente , Juliana Filipa Marques, Marta Adriana Forte   
and Carlos José Tavares \* 

Physics Center of Minho and Porto Universities (CF-UM-PT), Campus of Azurém, University of Minho, 4804-533 Guimarães, Portugal; vaniafernandesousa@gmail.com (V.I.S.); joanacp\_17@hotmail.com (J.F.P.); juliana.g.marques@hotmail.com (J.F.M.); martadrianaff@gmail.com (M.A.F.)

\* Correspondence: ctavares@fisica.uminho.pt

**Abstract:** Essential oils (EOs) are complex mixtures of volatile compounds extracted from different parts of plants by different methods. There is a large diversity of these natural substances with varying properties that lead to their common use in several areas. The agrochemical, pharmaceutical, medical, food, and textile industry, as well as cosmetic and hygiene applications are some of the areas where EOs are widely included. To overcome the limitation of EOs being highly volatile and reactive, microencapsulation has become one of the preferred methods to retain and control these compounds. This review explores the techniques for extracting essential oils from aromatic plant matter. Microencapsulation strategies and the available technologies are also reviewed, along with an in-depth overview of the current research and application of microencapsulated EOs.

**Keywords:** essential oils; extraction techniques; microencapsulation; controlled release; microcapsules; pharmacology

**Citation:** Sousa, V.I.; Parente, J.F.; Marques, J.F.; Forte, M.A.; Tavares, C.J. Microencapsulation of Essential Oils: A Review. *Polymers* **2022**, *14*, 1730. <https://doi.org/10.3390/polym14091730>

Academic Editor: Cristina Cazan

Received: 18 March 2022

Accepted: 18 April 2022

Published: 23 April 2022

**Publisher's Note:** MDPI stays neutral with regard to jurisdictional claims in published maps and institutional affiliations.



**Copyright:** © 2022 by the authors. Licensee MDPI, Basel, Switzerland. This article is an open access article distributed under the terms and conditions of the Creative Commons Attribution (CC BY) license (<https://creativecommons.org/licenses/by/4.0/>).

## 1. Introduction

Essential oils (EOs) are liquid products present in plants and can be defined as complex natural mixtures of volatile secondary lipophilic metabolites that give plants and spices their essence and colour [1,2]. These compounds can be obtained by hydrodistillation, solvent extraction, and supercritical CO<sub>2</sub> extraction, among other methods that can also be used for essential oil extraction [1]. These oils can be extracted from different parts of the plant, such as the flowers, leaves, stems, roots, fruits, and bark, and have different biological and pharmaceutical properties [3]. Due to their versatile nature, the oils can be utilised for several purposes, from contact toxicant and fumigant to attractive or repellent applications [4]. However, there are many factors that affect the chemical composition of essential oils, including genetic variation, type or variety of plants, plant nutrition, fertilizer applications, geographical location of the plant, climate, seasonal variations, stress during growth or maturation, as well as post-harvest drying and storage.

EOs that have antimicrobial properties are alternatives to the use of antibiotics and chemical additives [5]. As they have been used worldwide in many industries, their prices differ due to the supply of raw materials, issues related to harvesting, climate factors, and extraction yields. Some of these EOs also have antioxidant properties, with studies reporting that EOs from celery, citronella, cloves, oregano, parsley, tarragon, and thyme seeds were able to inhibit 50% of the 2,2-diphenylpicliryl-hydrazil (DPPH) radical elimination activity [6]. The application of EOs as antioxidants has been evaluated in different types of foods, and research is currently being conducted to optimise the process [7].

Essential oils have gained renewed interest in several areas over the years. Its use was expanded to the medical field due to its biocidal activities (bactericides, viricides, and fungicides) and medicinal properties [8]. The use of natural compounds has become popular in the food industry, with EOs being used as preservatives and food additives due to their antioxidant and antimicrobial properties and pleasant flavour. EOs are included

in the composition of many dosage forms in pharmaceutical products. Studies have been carried out on the many biological activities of essential oils (Figure 1) and their components, and particular interests have also been established to elucidate their modes of action, allowing for the improved and targeted intervention in new drugs [9].

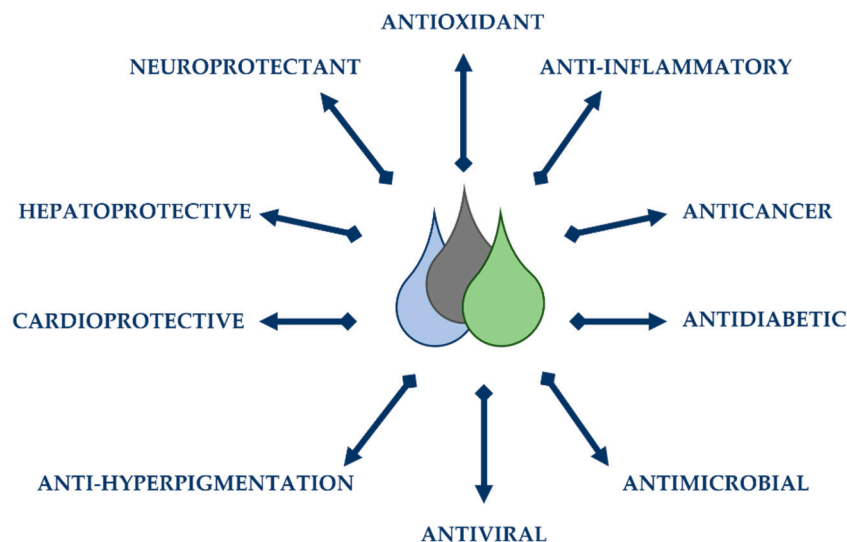


**Figure 1.** Biological activities of essential oils.

EOs are unstable and highly susceptible to changes caused by external factors, such as light, temperature, oxygen, and humidity [10]. The high volatility and reactivity of these compounds represent challenges for the application of essential oils in several industries [11]. To overcome these limitations, the microencapsulation technique is often used to maintain the functional and biological characteristics of these compounds and to control their release [12].

Microencapsulation is a technology based on the coating of solid, liquid, or gaseous particles through an encapsulating agent that acts as a barrier, completely isolating the core material from the external environment [13]. Most microcapsules have a diameter within the range 1–1000  $\mu\text{m}$  [14]. The shell material can be a film of a natural, semi-synthetic, or synthetic polymer and its choice has a key role in the stability of core material [15]. Arabic gum, agar, alginate, proteins, and dextrans are some of the materials used as encapsulating agents in the microencapsulation process [16].

Due to the enormous interest of the scientific community and the industry in the microencapsulation of active substances, several microencapsulation methods have been developed over time. Encapsulation processes are usually divided into three main categories: physicochemical, mechanical, and chemical processes [17]. In this review article, some of these methods, which are used in EO microencapsulation, are described and an outlook of scientific works developed in this area is approached.

## 2. Essential Oils

Essential oils are defined, according to the *European Pharmacopoeia*, as an “odorous product, usually of complex composition, obtained from a botanically defined plant raw material by steam distillation, dry distillation, or a suitable mechanical process without heating. EOs are usually separated from the aqueous phase by a physical process that does not significantly affect their composition” [18]. EOs are extracted from aromatic plant materials such as oily aromatic liquids, and they can be biosynthesised in different plant organs as secondary metabolites, such as flowers, herbs, buds, leaves, fruits, branches, bark, zest, seeds, wood, rhizomes, and roots.

Essential oils are complex mixtures of highly volatile aromatic compounds named after the plant from which they are derived. Within the different species of plants, only 10%

contain EOs and are called aromatic plants. These natural products exert the function of protecting the plants, guaranteeing the growth of the plant and the propagation of species. Essential oil provides the essence, odour, or flavour of the plant and some of the functions that it performs in plants can also be made in living organisms [19]. EOs are generally liquid at room temperature and are hydrophobic (immiscible with water) and lipophilic (miscible with other oils and organic solvents) substances [20]. In general, essential oils are a mixture of compounds with their own physicochemical characteristics that, when combined, give the oil a particular odour. The different aroma of oils is fundamentally due to variations in the volatility and relative concentration of its constituents [21].

### 2.1. Chemistry of Essential Oils

The chemical composition of EOs can be complex due to the number of different components, which can have promising chemical and biological properties [22]. Essential oils are complex mixtures that can contain over 300 different compounds. Most EOs are characterised by two or three main components in reasonably high concentrations (20–70%) compared to other components present in small amounts [8]. The organic constituents have a low molecular weight, and their vapour pressure (at atmospheric pressure and at room temperature) is high enough for them to be partially in vapour state [23].

Chemically, EOs mainly belong to two classes of compounds: terpenes and phenylpropanoids (Table 1). The terpene family is predominant, and phenylpropanoids, when they appear, are responsible for the characteristic odour and taste [24].

#### 2.1.1. Terpenoids

Terpenes, also called terpenoids, constitute the largest class of natural products with several structurally diversified known compounds [25]. Their structures contain carbon skeletons and are formed by isoprene units, being classified according to the number of these units that compose their structure. They can be classified as hemiterpenes (1 isoprene unit; 5 carbons), monoterpenes (2 isoprene units; 10 carbons), sesquiterpenes (3 isoprene units; 15 carbons), diterpenes (4 isoprene units; 20 carbons), triterpenes (6 isoprene units; 30 carbons), and tetraterpenes (8 isoprene units; 40 carbons), among others. Monoterpenes and sesquiterpenes are mostly found in volatile essential oils. Terpenes can present aromatic, aliphatic, and cyclic structures and can contain oxygen atoms, being called terpenoids (Figure 2) [26].

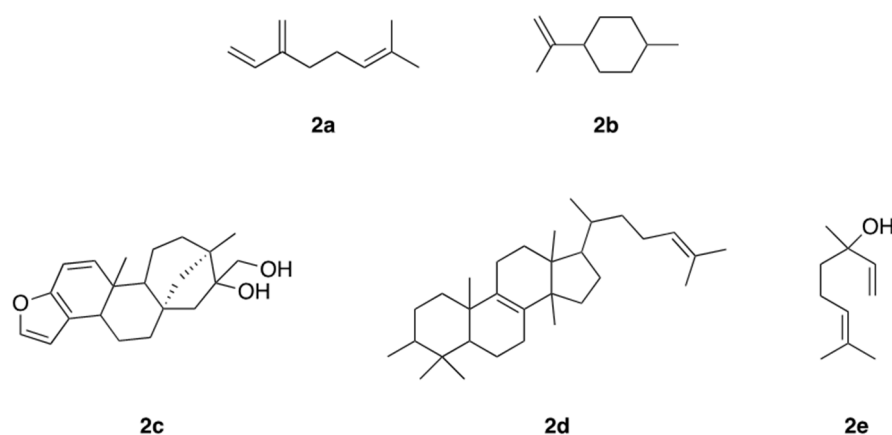


**Figure 2.** Structures of terpenes and terpenoids: acyclic monoterpenes (2a), cyclic monoterpenes (2b), diterpenes (2c), triterpenes (2d), and terpenoids (2e).

#### 2.1.2. Phenylpropanoids

Phenylpropanoids are natural substances commonly found in plants and consist of a six-carbon aromatic ring joined to a three-carbon side chain. This side chain contains a double bond and the aromatic ring may be substituted. These compounds are biosynthesised



from shikimic acid, which forms the basic units of cinnamic and *p*-coumaric acids. These units, through enzymatic reductions, produce propenylbenzenes and/or allylbenzenes and, through oxidations with side chain degradation, generate aromatic aldehydes [27,28].

**Table 1.** Composition of compounds found in essential oils [29].

| Essential Oil Compounds |  |  |
|-------------------------|--|--|
| Classes                 | Constituents   |  |
| Terpenes                | Monoterpene  | (-)-Camphene, p-cymene, (+)-limonene, $\beta$ -ocimene $\alpha$ -phellandrene, $\alpha$ -pinene, $\alpha$ -terpinene, terpinoleneorange,                                 |
|                         | Sesquiterpene  | (-)- $\beta$ -isabolene, $\alpha$ -cadinene, $\beta$ -caryophyllene, $\alpha$ -copaene, $\beta$ -elemene, $\alpha$ -farnesene, $\alpha$ -humulene, $\alpha$ -zingiberene |
| Phenylpropanoids        | (E)-Anethole, cinnamaldehyde, cinnamic acid cinnamic alcohol, eugenol, methyleugenol, myristicin |  |

## 2.2. Extraction Methods

Aromatic herbs or parts thereof, such as leaves, flowers, bark, seeds, and fruits, are subjected to extraction processes after being collected at specific stages of maturity and stored under controlled conditions (light, temperature, and humidity).

Extraction techniques are essentially divided into classical and conventional methods and innovative methods. Classical methods are based on the distillation of water by heating, to extract the EOs from the plant matter. Hydrodistillation, steam distillation, hydrodiffusion, organic solvent extraction, and cold pressing are some of these methods. New extraction technologies have been developed in order to overcome some of the disadvantages of conventional methods. Methods such as ultrasound-assisted extraction and microwave-assisted extraction use energy sources that make the process more environmentally friendly. On the other hand, methods such as supercritical fluid extraction and subcritical liquid extraction allow the non-polar components from the material to be extracted [30].

### 2.2.1. Hydrodistillation

Hydrodistillation is the oldest and simplest method for extracting OEs. This method is characterised by direct contact between the solvent and the plant material, that is, the raw material is submerged in boiling water (Figure 3) [31].

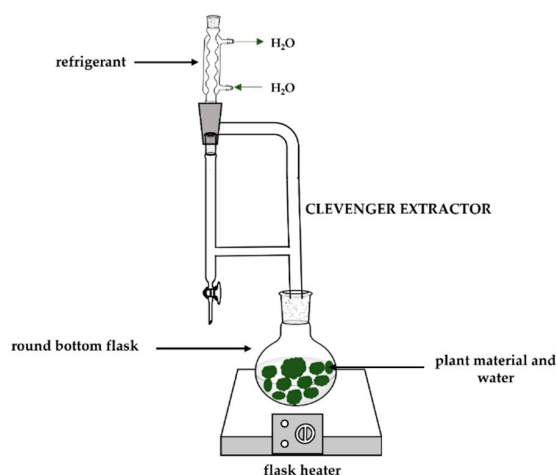


**Figure 3.** Schematic representation of hydrodistillation.

In this procedure, the cell walls are broken, and the oil is evaporated together with the water, and then condensed into a mixture of water vapour and volatile compounds of vegetable raw material. However, these two phases (volatile compounds and water) are immiscible, rendering possible an additional separation according to the difference in density [32]. This technique is inexpensive, but, at the same time, it is not selective because of the waste of large amounts of the compound in the solvent (part of the extract can be lost in the aqueous phase) and can provide low yields [33,34]. Despite being the oldest method, hydrodistillation is still used today for extracting oils from different matrices. Essential oils from *Rosmarinus officinalis* L. [35], *Ziziphora clinopodioides* L. [36], *Citrus latifolia* Tanaka [37], and *Zingiber officinale* [38] are some of the medicinal plants where EOs can be extracted by hydrodistillation.

### 2.2.2. Steam Distillation

Steam distillation is one of the preferred methods of extracting EOs. The extraction procedure is based on the same principles as hydrodistillation. The difference essentially lies in the absence of contact between the substrate to be extracted and the water, which causes a reduction in the extraction time.

The sample is placed in a column where the bottom part is connected to a flask with water under heating (Figure 4). The top part is connected to a condenser, where the steam produced passes through the sample, taking essential oils to the condenser. This process causes the condensation of the water–oil mixture, and this mixture can be separated by liquid–liquid extraction [39].

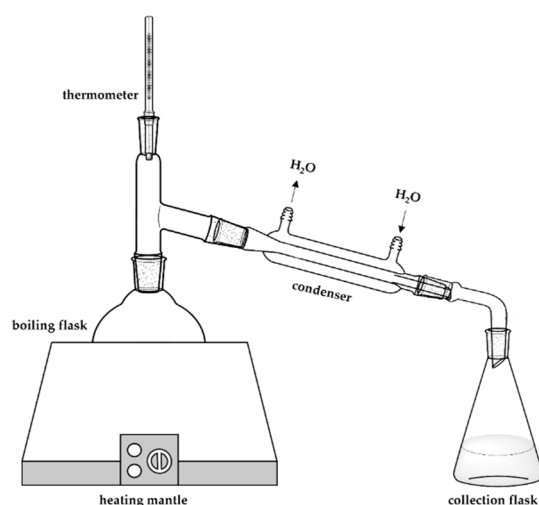


**Figure 4.** Experimental setup used in steam distillation.

This method is applied commercially and on a large scale in the extraction of essential oils from hops [40] and in the extraction of several EOs such as lavender [41] and patchouli essential oil [42].

### 2.2.3. Organic Solvent Extraction

Some essential oils (such as rose and jasmine) have low thermal stability and are unable to withstand high temperatures. In these cases, organic solvents that have a low boiling temperature, are chemically inert, and have low cost can be used.

In organic solvent extraction, the sample is placed in contact with the organic solvent (which can be hexane, benzene, toluene, or petroleum ether, among others) for a period that allows the transfer of the soluble content of the sample. The extracted matrix is concentrated by evaporating the solvent present in the liquid phase. This method allows the sample to be permanently in contact with a quantity of fresh solvent and, at the end of the process, it is not necessary to carry out filtration, as long as there are high yields [34]. Solvent extraction

is the most-used conventional method in the cosmetic industry [43–45]. Figure 5 represents the extraction of organic solvents through a Soxhlet extraction [32,46].

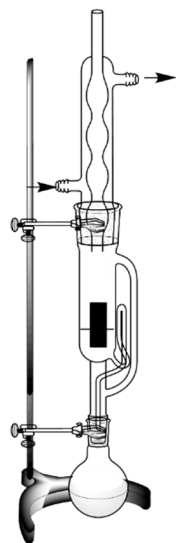


**Figure 5.** Schematic representation of organic solvent extraction using the Soxhlet method.

#### 2.2.4. Cold Pressing

Essential oils are mechanically removed by cold pressing, where the oil glands are broken and volatile oils are released. In this process, an aqueous emulsion is formed, where the oil present can be obtained through centrifugation, decantation, or fractional distillation [13]. The cold pressing method is essentially used to extract oils from citrus fruits [47–49].

#### 2.2.5. Supercritical Fluid Extraction (SCFE)

Supercritical fluid extraction is an efficient, environmentally friendly, and clean technique for isolating EOs. In this technique, supercritical fluids are used as extraction agents due to the supercritical state of fluids, conferring excellent characteristics for the extraction process, such as low viscosity, high density (close to that of a liquid), and high diffusivity (high penetration power).

Several substances can be used as supercritical solvents, such as water, carbon dioxide (CO<sub>2</sub>), methane, ethylene, and ethane. However, CO<sub>2</sub> is the most-used solvent due to its critical point being easily reached (low temperature and pressure, 31.2 °C and 72.9 atm, respectively), low toxicity and reactivity, low cost, and non-flammability. After selecting the ideal temperature and pressure for extraction, supercritical fluid passes through the sample and the oils are dissolved and extracted. Subsequently, the extraction solution is maintained at a pressure below the critical point and as the pressure decreases, the supercritical fluid passes to the gaseous state and loses its solvating capacity, being recycled [50]. This method is increasingly used commercially, being applied in the extraction of EOs from the leaves of laurel [51], rosemary [52], sage [53], flowering plants [54], and horseradish tree [55].

#### 2.2.6. Microwave-Assisted Extraction (MAE)

Due to the need to use more ecological and energy-efficient extraction methods, microwave-assisted extraction has become an alternative to conventional methods. The sample is placed in a microwave reactor without any solvent, where the electromagnetic energy that is converted into heat increases the internal temperature of sample cells due to the evaporation of the moisture present. The internal pressure increases, the glands rupture, and the essential oil is released [56]. Several EOs were extracted from plant matrices through this technique, such as orange [57], laurel [58], lemon [59], mint [60], rosemary [61], and basil [62].

### 2.2.7. Ultrasound-Assisted Extraction (UAE)

Ultrasound energy allows the intensification of EO extraction [63]. Therefore, it is usually combined with other extraction techniques in order to accelerate the extraction process and increase the speed of mass transfer. The sample is submerged in a solvent while being subjected to ultrasound. This method, through rapid solvent movements, induces a mechanical vibration of the walls and membranes of the sample that causes the release of essential oils. In some areas, it is already considered a large-scale application method, such as in the medical and food industry, where it is used to increase the quality of the extracted substrate, reduce working time, and increase the yield [64].

In general, alternative methods have emerged to overcome some of the disadvantages and limitations of conventional methods. Traditional methods have long extraction times (4 to 6 h), high energy consumption, and use solvents that increase environmental pollution. Furthermore, they can cause chemical changes to the EOs that are thermally unstable, causing a decrease in the quality of the extracted oils and changes in the chemical nature of compounds. The 'greener' alternatives are more sustainable and economical due to reduced water and energy consumption and reduced CO<sub>2</sub> emissions. However, these methods are not easily accessible, and the initial investment is higher.

Therefore, currently, the hydrodistillation method continues to be the most-used extraction technique in laboratory due to its accessibility, simplicity, and lower cost [46]. Table 2 summarises the advantages and disadvantages of the different EO extraction methods.

## 2.3. Essential Oils Application

### 2.3.1. Essential Oils in Plants

EOs are stored in specific parts of plants, acting in extraordinarily different ways. Some aromatic plants have been widely explored due to their properties, such as bay laurel (*Laurus nobilis*). This plant is an aromatic tree, and laurel oil is extracted from the dry leaves and branches, appearing as a greenish yellow liquid with a powerful medicinal odour. In addition to being used in cuisine, the laurel tree leaves are used in medicine for having antioxidant [65], antibacterial [65,66], and antifungal [22] properties. According to the literature, laurel has also been proven to be an insect repellent [67,68]. However, it can cause dermatitis in some individuals, and due to the possible narcotic properties attributed to methyleugenol, this oil should be used in moderation.

*Cymbopogon nardus*, commonly known as citronella, is an aromatic and perennial herb. Citronella oil can also be produced from Java or Maha Pengiri citronella (*C. winterianus*) [69]. Citronella leaves are used for their aromatic and medicinal value in many cultures, such as in the treatment of fever, intestinal parasites, and digestive and menstrual problems, as well as for use as an insect stimulant and repellent [69–72]. Citronella is also used in traditional Chinese medicine for rheumatic pain, and it has antifungal [73], antioxidant, and antibacterial [74] properties. It is non-toxic and non-irritating, but it can cause dermatitis in some people [69].

Regarding the medical properties of hops (*Humulus lupulus*), these are better known for treatments associated with nerves, insomnia, nervous tension, neuralgia, and for sexual neurosis in both sexes [5]. It has antibacterial [75,76], antifungal [76], anti-cancer [76,77], and repellent [78,79] properties. In China, it is used for pulmonary tuberculosis and cystitis treatment. It can also be used to make beer. It is non-toxic and non-irritating, but it can cause sensitivity in some individuals, and people with depression should avoid this oil [76].

Lemon balm (*Melissa officinalis*) is a herbaceous perennial from the mint family and it has antibacterial, antifungal [80], sedative, antipyretic, antispasmodic, anti-hypertensive, anti-Alzheimer, and antiseptic properties [81]. In addition to the treatment of several gastrointestinal, liver, and nervous system disorders, it has also been reported that lemon balm is useful in the treatment of asthma, bronchitis, coughs, and several pains [82]. Furthermore, this plant is notably marked by its antimicrobial applications in different medicines, exemplified by its use in insect bites (wasps and bees) and poisonous or infectious bites [81,83].

**Table 2.** Advantages and disadvantages of each essential oil extraction method [46].

| Type of Method | Method                         | Advantages  | Disadvantages   |
|----------------|--------------------------------|---|---|
| Conventional   | Hydrodistillation              | <ul style="list-style-type: none"> <li>- Versatile and simple;</li> <li>- Easy implementation;</li> <li>- Selectivity.</li> </ul>   | <ul style="list-style-type: none"> <li>- Complete extraction is not possible;</li> <li>- High energy consumption;</li> <li>- Long extraction time.</li> </ul>   |
|                | Steam distillation             | <ul style="list-style-type: none"> <li>- Extraction time and loss of polar molecules are reduced (compared with hydrodistillation).</li> </ul>  | <ul style="list-style-type: none"> <li>- Longer extractions;</li> <li>- Present non-appreciable and higher cost compounds due to the long process time.</li> </ul>  |
|                | Organic solvent extraction     | <ul style="list-style-type: none"> <li>- Simple, cheap, and reasonably efficient;</li> <li>- Appropriate for small scale.</li> </ul>  | <ul style="list-style-type: none"> <li>- Time consuming;</li> <li>- High solvent consumption;</li> <li>- Does not allow agitation to speed up the process;</li> <li>- Organic solvents can cause chemical changes or toxic effects in final product.</li> </ul> |
|                | Cold pressing                  | <ul style="list-style-type: none"> <li>- Simple and inexpensive;</li> <li>- Suitable for the production of citrus oils.</li> </ul>  | <ul style="list-style-type: none"> <li>- Oil extraction is not complete;</li> <li>- Not feasible for low-oil samples.</li> </ul>  |
| Innovative     | Supercritical fluid extraction | <ul style="list-style-type: none"> <li>- Reduced time;</li> <li>- Low toxicity solvents;</li> <li>- Solvent-free extract.</li> </ul>  | <ul style="list-style-type: none"> <li>- High cost of equipment, installation, and maintenance operations.</li> </ul>   |
|                | Microwave-assisted extraction  | <ul style="list-style-type: none"> <li>- High reproducibility;</li> <li>- Simple manipulation;</li> <li>- Low solvent consumption;</li> <li>- Lower energy input;</li> <li>- Improved extraction yield.</li> </ul>  | <ul style="list-style-type: none"> <li>- Filtration or centrifuging required at the end.</li> </ul>   |
|                | Ultrasound-assisted extraction | <ul style="list-style-type: none"> <li>- Simple and inexpensive (compared to SCFE and MAE);</li> <li>- Reduced extraction time;</li> <li>- Low solvent consumption;</li> <li>- Mass transfer intensification;</li> <li>- Improvement of solvent penetration.</li> </ul> | <ul style="list-style-type: none"> <li>- Difficult to scale up;</li> <li>- High power consumption.</li> </ul>   |

*Azadirachta indica*, better known as neem, is an ancient tree that has been used for centuries for the most varied purposes. The plant provides a great number of secondary metabolites with biological activity. The plant has gained great importance in several areas, such as agriculture, livestock, and medicine [84]. It is used as an insecticide [85], antiviral [86], antibacterial [87], and antimicrobial [88], among others. Neem oil is very effective for acne, psoriasis, and eczema treatments, but it can also be applied as a support in the treatment of topical fungal or viral conditions, such as nail fungus, athlete's foot, warts, or wounds. The natural antihistamines contained in neem oil are effective in relieving the itching and burning caused by, for example, bee, mosquito, and spider bites. The main constituent of neem is azadiractin, found in the leaves, fruits, and seeds.

*Mentha pulegium*, better known as pennyroyal or mint (Brazil), is one of the best-known species of the genus *Mentha*. Pennyroyal extracts are good insect repellents [89–92]. There are several studies that show that these extracts also have other properties, such as antimicrobial [92–94], antioxidant [92,93,95], antibacterial [95,96], and anti-tumour [96] uses. It is still current in the *British Herbal Pharmacopoeia*, indicated for flatulent dyspepsia, intestinal colic, common cold, delayed menstruation, skin rashes, and gout [69].

*Illicium verum*, popularly known as star anise, is a plant considered a spice for medicinal and culinary use. The extraction of *Illicium verum* has carminative, stomach, stimulating, and diuretic properties and is used as a pharmaceutical supplement [97]. The extracted

shikimic acid is one of the main ingredients of the antiviral drug Tamiflu® (oseltamivir) that is used to treat symptoms caused by avian influenza [98]. It has also been reported to have antimicrobial properties [99] and antioxidant properties [100], as well as significant anti-cancer potential [101]. There are studies in which star anise has been used as an insect repellent, such as for the Indian flour moth (*P. interpunctella larvae*) [102,103]. The main constituent of star anise is trans-anethole (Table 3) (80–90%) and when used in large doses, it is narcotic and slows down circulation, which can lead to brain disorders [69].

**Table 3.** Essential oil plants, species, and main components, and their molecular structure and biological properties.

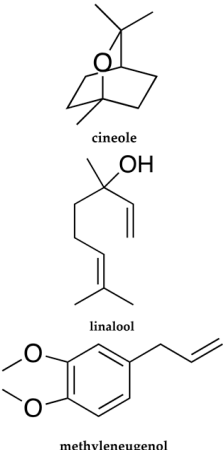
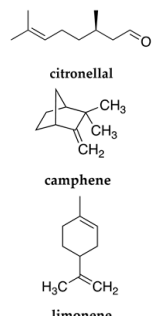
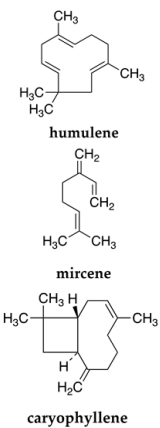
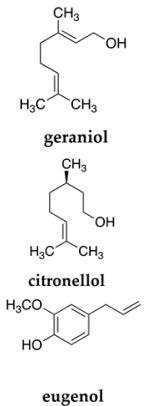
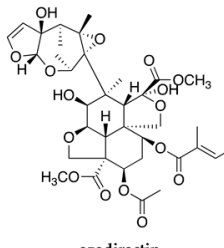
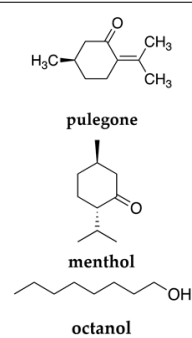
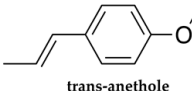
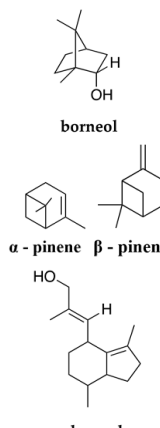
| Plant      | Species                  | EO Major Components  | Chemical Structures of EOs Components  | Some Biological Properties  |
|------------|--------------------------|--|--|---|
| Bay Laurel | <i>Laurus nobilis</i>    | Cineol, pinene, linalool, terpineol acetate, methyleugenol |  <p>The structures shown are: cineole (a bicyclic ether), linalool (a branched chain with two hydroxyl groups and a terminal vinyl group), and methyleugenol (a benzene ring with two methoxy groups and a propenyl group).</p> | Antioxidant, antibacterial, antifungal, insect repellent                              |
| Citronella | <i>Cymbopogon nardus</i> | geraniol, citronellal, geranyl acetate, limonene, camphene |  <p>The structures shown are: citronellal (an aliphatic chain with a terminal aldehyde group), camphene (a bicyclic hydrocarbon), and limonene (a monocyclic diene).</p>   | Antimicrobial, antifungal, antioxidant, antibacterial, insect and stimulate repellent |
| Hops       | <i>Humulus lupulus</i>   | Humulene, myrcene, caryophyllene, farnesene                |  <p>The structures shown are: humulene (a tricyclic sesquiterpene), myrcene (an acyclic diene), and caryophyllene (a bicyclic sesquiterpene).</p>  | Antibacterial, antifungal, anti-cancer, repellent                                     |

Table 3. Cont.

| Plant      | Species                      | EO Major Components   | Chemical Structures of EOs Components  | Some Biological Properties  |
|------------|------------------------------|---|--|---|
| Lemon Balm | <i>Melissa officinalis</i>   | Geraniol, citral, citronellol, eugenol, linalyl acetate                   |  <p>geraniol</p> <p>citronellol</p> <p>eugenol</p>   | Antibacterial, antifungal, antimicrobial, sedative, antipyretic, antispasmodic, anti-hypertensive, anti-Alzheimer, antiseptic |
| Neem       | <i>Azadirachta indica</i>    | Azadiractin   |  <p>azadiractin</p>   | Insecticide, antiviral, antibacterial, antimicrobial  |
| Pennyroyal | <i>Mentha Pulegium</i>       | Pulegone, menthol, iso-mentone, octanol, piperitenone, trans-iso-pulegone |  <p>pulegone</p> <p>menthol</p> <p>octanol</p>   | Insect repellent, antimicrobial, antioxidant, antibacterial, anti-tumour  |
| Star Anise | <i>Illicium verum</i>        | Trans-anethole  |  <p>trans-anethole</p>   | Antimicrobial, antioxidant, diuretic, anti-cancer potential, insect repellent   |
| Valerian   | <i>Valeriana officinalis</i> | Borneol, camphene, $\alpha$ and $\beta$ -pinene, valeranone, valerenol    |  <p>borneol</p> <p><math>\alpha</math>-pinene <math>\beta</math>-pinene</p> <p>valerenol</p> | Antibacterial, antimicrobial, antifungal, antioxidative, sedative   |

Valerian is a perennial flowering plant with many chemical constituents, with more than 150 constituents identified in its essential oil [104]. Regarding therapeutic indications, it is advisable for people with nervous agitation, mild anxiety, and difficulties in sleeping [105,106]. There are also studies that demonstrate its antibacterial [107] and antimicrobial [108] properties. It is non-toxic, non-irritating, and can cause sensitisation. Table 3 describes the main components of the EOs present in plants, as well as their chemical structures and some of the biological properties.

### 2.3.2. Pharmacological and Medical Applications

Essential oils have a wide range of biological properties, and there has been a growing interest in clinical applications (Table 4). Some of the properties include the chemopreventive effects of cancer [109], antifungal [110], antiviral [111], antimicrobial, analgesic, anti-inflammatory [112], and antiparasitic activities [113].

**Table 4.** Some pharmacological actions of essential oils [114].

| Condition  | Essential Oil  |
|--|--|
| Anxiety, agitation, stress, challenging behaviours | Angelica, labdanum, bergamot, sweet orange, palmarosa, lavender, basil, geranium, and valerian                               |
| End-of-life agitation                              | Lavender, sandalwood, and frankincense   |
| Fatigue  | Labdanum, grapefruit, coriander, citronella, black peppermint, gully gum, spearmint, geranium, Scots pine, clary, and ginger |
| Insomnia   | Angelica, lemon, mandarin, sweet orange, lavender, lemon balm, myrtle, basil, sweet marjoram, and valerian                   |
| Mental exhaustion, burnout                         | Peppermint, basil, and everlasting   |
| Memory loss  | May Chang, peppermint, and rosemary  |
| Pain management                                    | Gully gum, lavender, German chamomile, sweet marjoram, rosemary, and ginger  |

An extensive range of EOs have antibacterial activity against Gram-positive and Gram-negative bacteria, along with antifungal properties. These compounds have been studied and have shown very promising results in salmonella, staphylococci, and other oral pathogens, and can be an alternative to antibiotics providing they are properly studied for these effects [115,116]. EOs that have shown antibacterial potential are basil [117], manuka oil (more potent among eucalyptus oil, rosmarinus, lavandula, and tea tree) [118], melaleuca oil [119], and essential leaf oils *P. undulatum* and *Hedychium gardnerianum*.

With regard to antifungal activity, melaleuca oil showed positive results for all of its constituents, especially against dermatophytes and filamentous fungi [120]. In a reported study, germinated conidia of *Aspergillus niger* were more susceptible to non-germinated ones, with EOs of *Melaleuca ericifolia*, *Melaleuca armillaris*, *Melaleuca leucadendron*, and *Melaleuca styphelioides* exhibiting good activity against this fungus [120]. These same oils were evaluated for their antiviral activity in African green monkey kidney cells through the plaque reduction assay in the herpes simplex virus type 1 [121]. Other plants that have good antifungal activity are *M. piperita*, *Brassica nigra*, *Angelica archangelica*, *Cymbopogon nardus*, *Skimmia laureola*, *Artemisia sieberi*, and *Cuminum cyminum* [122–127].

Regarding antioxidant activity, the essential oil of the seeds of *Nigella sativa* L. showed considerable activity in the elimination of hydroxyl radicals. The essential oil of *M. armillaris* has marked antioxidant potential, changing the parameters of superoxide dismutase, and improving the concentrations of vitamin E and vitamin C [128]. However, there have been promising insect repellency/toxicity results from the essential oils of *Nepeta parnassica*, in *Culex pipiens molestus* [129]. Geranial, neral, geraniol, nerol, and trans-anethole are well established to stimulate the estrogenic response, and citrus (a combination of geraniol,



nerol, and eugenol) is effective in replacing [ $^3\text{H}$ ] 17 $\beta$ -estradiol at the oestrogen receptors in recombinant yeast cells [130,131].

Cancer is a growing health problem worldwide and is the second leading cause of death. Essential oil constituents play an important role in cancer prevention and treatment as alternatives to synthetic drugs. Mechanisms such as antioxidant, antimutagenic, and antiproliferative properties, enhancement of immune function and surveillance, enzyme induction and enhancing detoxification, modulation of multidrug resistance, and the synergistic mechanism of EO constituents are accountable for their chemo-preventive properties [132]. It has been reported that mitochondrial damage and apoptosis/necrosis in the yeast *Saccharomyces cerevisiae* were reduced by essential oils [133]. Recently, some studies demonstrated that certain EOs exhibited antimutagenicity towards mutations caused by UV light [8]. Jaganathan et al. reported that the active constituent eugenol from *Syzygium aromaticum* (cloves), nutmeg, basil, cinnamon, and bay leaves showed antiproliferative activity against several cancer cell lines in animal models [134].

In addition to medicinal and pharmacological applications, essential oils are used in perfumes, cosmetics, hygiene products, disinfectants, repellents, candles, phytochemicals, preservatives, and food additives.

### 2.3.3. Food Applications

In food, cosmetics, and personal care products, EOs are used as a natural aroma due to their chemical properties. In the food industry, EOs are being used as a food preservative because one of the main concerns is the preservation of food to prolong its useful life, ensuring safety and quality [11]. An expiration date is defined as the period of time during which the food product will remain safe. This ensures the maintenance of sensory, chemical, physical, microbiological, and functional characteristics. For example, spices can be encapsulated to extend their shelf life, maintain their properties, and inhibit reactions with other compounds [135]. Cinnamaldehyde, the aromatic agent present in cinnamon, has antimicrobial properties, and when encapsulated can slow the growth of yeasts in bakery products. Thus, the use of cinnamon in encapsulated form allows the product to be flavoured without interfering with the leavening process [136].

As the unpleasant taste and instability limit the application of EOs, the use of these encapsulated compounds can allow their application for several purposes. One of them is the intensification of the flavour of food products, where capsules can be used that release the product quickly when introduced into the mouth [20].

The packaging has the function of delaying deterioration, maintaining the quality and safety of packaged foods. For the packaging material to be satisfactory, it must be inert and scratch resistant, and must not allow molecular transfer to or from the packaging materials. Active packaging technologies extend the shelf life and control the quality of food products, decreasing microbial, biochemical, and enzymatic reactions through different strategies, such as adding chemical additives/preservatives, removing oxygen, controlling humidity and/or temperature, or a combination of these [137]. Oregano oil contains a high amount of carvacrol and is considered one of the most active plant extracts against pathogens due to its antimicrobial activity. Therefore, it has been used to preserve a variety of foods such as pizza, fresh beef [138], and cheddar cheese [139]. For the same purpose, limonene is reported for the preservation of strawberries [140], rosemary in chicken breast cuts [141], and cinnamon in pastries [142].

### 2.3.4. Cosmetic and Cleaning Applications

In the detergent and cosmetics industry, microcapsules of essential oils are used in many products such as perfumes, creams, and deodorants where the controlled release of EOs is essential, increasing the duration of fragrance and the properties of the EOs [45]. Aroma ingredients such as patchouli (*Pogostemoncablin*), citronella (*Cymbopogon winterianus*), sandalwood (*Santalum album*), bergamot (*Citrusaurantium*), rosemary (*Rosmarinus officinalis*), mint (*Mentha piperita*), and vetiver (*Chrysopogon zizanioides*) are frequently

used [4]. Regarding the EOs from flowers, *Lavandula officinalis*, rose, jasmine, tuberose, narcissus, and gardenia are those most commonly exploited for cosmetic applications [143]. Products such as detergents, soaps, shampoos, and softeners are largely produced using these natural compounds.

Over the years, EOs have also been used against nosocomial infections, as a cleaning liquid for disinfecting equipment and medical surfaces [9], or as an aerosol in operating rooms and waiting rooms to limit contamination [10].

### 2.3.5. Agrochemical Applications

The loss of quality of agricultural products is caused by the presence of insect pests. The presence of these pests leads to reduced quality, low yield, and economic losses. Furthermore, human and animal health is compromised due to the production of carcinogenic secondary metabolites. To overcome this problem, chemical insecticides were used to excess. Despite being highly efficient, their overuse caused physiological resistance in several insect species and irreversible damage to the environment. Essential oils have emerged as a natural plant alternative to protect agricultural products from pests [144]. The use of EOs has intensified, mainly in gardens and homes, for pest control (Table 5), being important due to their toxic (pesticide) effect. EOs can be inhaled, ingested, or absorbed through the skin of insects. Monoterpenoids are an important group of chemical compounds in essential oils that interfere with the octopaminergic system of insects, which represent a target for insect control. As vertebrates do not have octopamine receptors, most chemicals in EOs are relatively safe to use. The special regulatory status together with the availability of essential oils has made the commercialisation of EO-based pesticides possible. Microencapsulation technology is used to produce these natural pesticides in order to mimic chemical compartmentalisation in plants, by protecting essential oils from degradation [145].

**Table 5.** Pests/pesticides and their corresponding essential oil [145].

| Pests        | Essential Oil                             |
|--------------|---|
| Ants         | Peppermint, mint                          |
| Aphids       | Cedar, hyssop, peppermint, mint           |
| Beetles      | Peppermint, thyme                         |
| Caterpillars | Peppermint, mint                          |
| Mites        | Lavender, lemongrass, sage, thyme         |
| Fleas        | Peppermint, lemon grass, mint, lavender   |
| Flies        | Lavender, mint, rosemary, sage            |
| Mosquitoes   | Patchouli, mint                           |
| Lice         | Cedar, peppermint, mint                   |
| Moths        | Cedar, hyssop, lavender, peppermint, mint |
| Slugs        | Cedar, hyssop, pine                       |
| Snails       | Cedar, pine, patchouli                    |
| Spiders      | Peppermint, mint                          |
| Ticks        | Lavender, lemongrass, sage, thyme         |

### 2.3.6. Textile Applications

Essential oils are used in medical and technical fabrics. The technique used in industrial processes is encapsulation, which is used to give finishes and properties to textiles that were not possible or economical. The main application for encapsulation is durable fragrances and skin softeners, and other applications may include insect repellents, dye,

vitamins, microbial agents, and phase-change materials, and medical applications, such as antibiotics, hormones, and other medications.

The functionalisation of textiles with EOs with anti-mosquito repellent properties is a revolutionary way to protect human beings from insect bites and, thus, from many diseases such as malaria and dengue [146]. Plants, whose OEs have been reported to have repellent properties, include citronella, cedar, geranium, pine, cinnamon, basil, thyme, garlic, and mint. Khanna et al. performed the synthesis of a modified cyclodextrin host ( $\beta$ -CD CA) for inclusion complexation with the essential oils of cedarwood, clove, eucalyptus, peppermint, lavender, and jasmine for the assessment of repellent efficacy against *Anopheles Stephensi* in cotton. It was concluded that jasmine EO is the weakest against mosquitoes, as it worked as an attractant simulating flower nectar. Eucalyptus and clove are the feeding deterrents. On the other hand, lavender and peppermint are potential mosquito repellents, and cedarwood is an effective mosquito killer [147]. Soroh et al. reported that textiles treated with the Litsea and lemon EO microemulsion showed potential mosquito-repellent properties [148]. In general, citronella remains the most promising as an insect repellent and, therefore, is the most-incorporated EO in tissue functionalisation for this purpose. Specos et al. demonstrated citronella essential oil's mosquito-repellent action, especially against *Aedes aegypti* [148]. Microcapsules with citronella are commonly incorporated into matrices such as cotton and polyester [149]. Another report determined that bio-based citronella oil has a better insect repellent effect than synthetic agents. Sariisik et al. concluded that, after washing, the insect repellent activity of the printing and coating method was increased, and the fabrics still showed repellency after five washing cycles [150].

### 3. Microencapsulation

Microencapsulation is the protection of small solid, liquid, or gaseous particles through a coating system (1–1000 nm) [151]. The encapsulated material is called the core and the material that forms the coating of particle is the wall or encapsulating agent [152]. Wall material can be a natural, synthetic, or semi-synthetic polymeric coating. In this technology, microparticles are formed, which can be classified in relation to their size and morphology, according to the encapsulating agent and microencapsulation method used [153].

Microparticles can be distinguished according to their form: they are classified as a reservoir-type system, 'microcapsules', when the core (encapsulated material) is concentrated in the central region, coated by a continuous wall material (encapsulating agent); or a monolithic system, 'microspheres', when the active agent (core) is dispersed in a matrix system (Figure 6). In general, the main difference is that in microspheres, part of the encapsulated material is exposed on the surface of the microparticle [154].

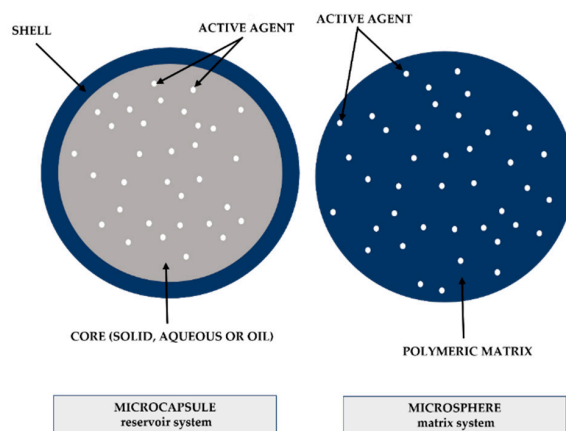


**Figure 6.** Schematic representation of a microcapsule and a microsphere.

The physicochemical characteristics of the microcapsule are defined by the encapsulating agent and the active agent. The wall material must form a cohesive film that bonds with the encapsulated material [155]. Several materials can be used for the coating, with

proteins, carbohydrates, and lipids being frequently used. Furthermore, the materials must be chemically compatible and the encapsulating agent chemically inert, so as not to react with the core [156].

Microencapsulation technologies achieve several objectives (Figure 7) and they are particularly used to protect the core active agent's sensitivity to oxygen, light, and moisture, or to prevent interaction with other compounds. However, the most important reason for encapsulating an active agent is to obtain a controlled release [157].

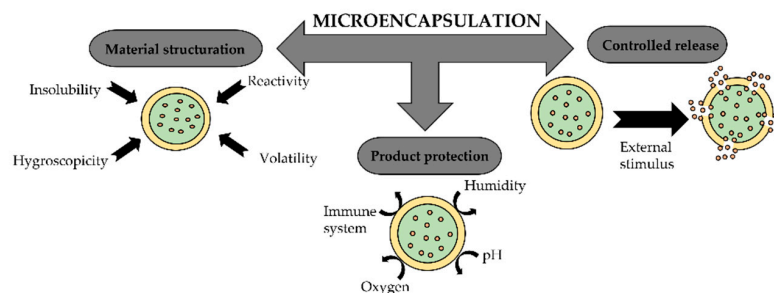


Figure 7. Objectives of microencapsulation.

The process of defining a microencapsulation system is mainly dependent on the purpose of the microcapsules. Characteristics such as shape, size, permeability, biodegradability, or biocompatibility are defined depending on the application of this material. Other physical and mechanical properties of the microcapsule, such as strength and flexibility, must also be defined [158].

One of the great advantages of microencapsulation is the mechanism of the controlled, sustained, or targeted release of the active agent. This release can occur at a certain defined time or not, through a mechanism of diffusion through or rupture of the wall. The release can be activated through temperature variations, solubility, pH changes, or even the biodegradability of the wall material [159].

Depending on the nature of the interaction of the encapsulating and encapsulated material, microencapsulation methods can be distinguished as chemical, physicochemical, and mechanical (Figure 8) [160]. In general, a microencapsulation method must be fast, easy, reproducible, and easily scalable for industry. The most-used microencapsulation methods are spray drying and coacervation, and these approaches will be mentioned in more detail below.

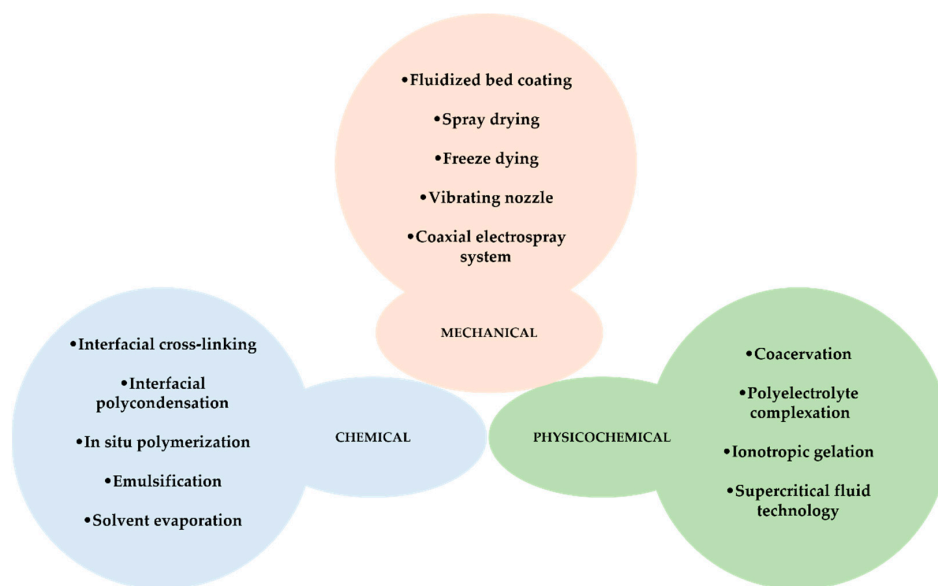


Figure 8. Main microencapsulation methods.

### 3.1. Emulsification

Emulsification is a fundamental step in oil microencapsulation, being used in a wide variety of food and pharmaceutical products. It is applied for the encapsulation of bioactive substances in aqueous solutions, which can be used directly in liquid or dried (spray- or freeze-drying) to form powders.

An emulsion consists of at least two immiscible liquids, with one of the liquids being dispersed as small spherical drops in the other. As can be seen in Figure 9, there are four systems, consisting of:

1. Oil-in-water emulsion (O/W);
2. Water-in-oil emulsion (W/O);
3. Oil-in-water-in-oil emulsion (O/W/O);
4. Water-in-oil-in-water emulsion (W/O/W).

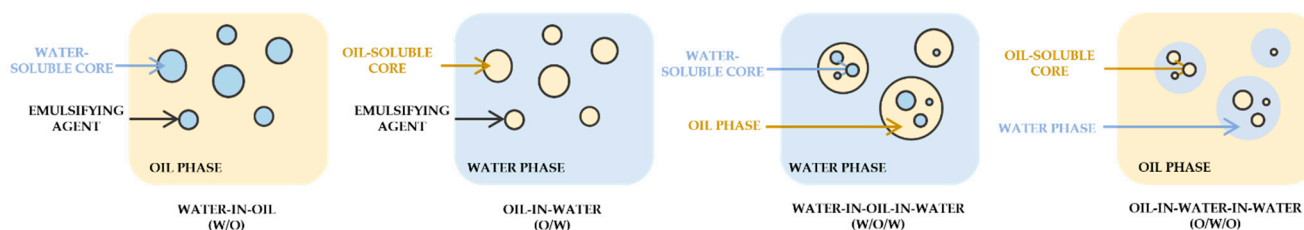


**Figure 9.** Illustration of emulsion systems.

In these systems, the droplet diameters can vary from 0.1 to 100  $\mu\text{m}$  [161] and have been extensively revised by scientists [162]. The O/W emulsion consists of small oil droplets that are dispersed in an aqueous medium, being the droplets wrapped in a thin interfacial layer. Its advantages are the ease of preparation and low cost, with some disadvantages such as physical instability and limited control [162]. Through modifications of the emulsifiers, features can be added, such as the use of Maillard reaction products. These products can increase encapsulation efficiency and are able to protect the microencapsulation oil and other oils from oxidation [163].

A straightforward method for obtaining small droplets with a stratum size distribution is the evaporation/extraction of the emulsifying substance. This method is used in the preparation of biodegradable and non-biodegradable polymeric microparticles and in the microencapsulation of a wide variety of liquid and solid materials [164]. However, it is an expensive method with a low encapsulation efficiency, leading to residual solvent amounts [165].

### 3.2. Coacervation

Coacervation is one of the most widely used microencapsulation techniques. The technique is based on oppositely charged polyelectrolyte polymers that interact and form a wall covering the active agent. The coacervation process can be classified as simple and complex if one or two (or more) polymers are used, respectively. Generally, this technique is defined by the separation of two liquid phases in a colloidal solution, where one phase is rich in polymer (coacervated phase) and the other phase does not contain polymer (equilibrium phase) [46].

Complex coacervation involves the interaction of two oppositely charged colloids, where the neutralisation of charges induces a phase separation. A polysaccharide and a protein are usually used as the different polymers. Wall material systems that are most widely investigated include gelatin/gum arabic, gelatin/alginate, gelatin/glutaraldehyde, gelatin/chitosan and gelatin/carboxymethyl cellulose [166].

In the process of the microencapsulation of hydrophobic materials (Figure 10), the emulsification of the encapsulated agent in an aqueous solution containing two different polymers occurs, usually at a temperature and pH above the gel and isoelectric point of the protein. Then, the separation into two liquid phases (polymer-rich phase and

aqueous phase) follows, which results from the electrostatic interaction of the polymers. Subsequently, a microcapsule wall is formed as the deposition of the polymer-rich phase occurs around the hydrophobic particles of the active agent, due to controlled cooling below the gelation temperature. Finally, the microcapsule walls harden through the addition of a crosslinking agent [167].

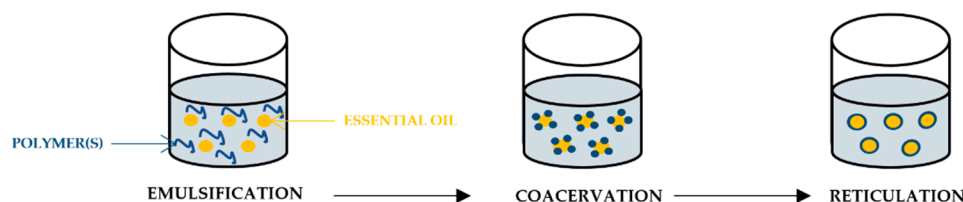


**Figure 10.** Schematic illustration of the coacervation method.

Simple coacervation has advantages over complex coacervation in terms of the associated cost, as cheap inorganic salts are used to induce the separation phase, while expensive hydrocolloids are applied in the complex method. Furthermore, complex coacervation is more sensitive to small variations in pH. However, compared to other microencapsulation methods, complex coacervation is a simple, scalable, inexpensive, reproducible, and solvent-free method, enabling its industrial use [166].

### 3.3. In Situ Polymerisation

In situ polymerisation (Figure 11) is based on the formation of a wall through the addition of a reagent inside or outside the core material [168], becoming one of the most-used methods in the preparation of microcapsules and functional fibres. Polymerisation takes place in the continuous phase and not on both sides of the interface between the core material and the continuous phase. Microcapsule formation occurs through an oil emulsion in a solution of melamine–formaldehyde resin and a sonication process to emulsify the oil in the aqueous phase. Then, resin is added under agitation and the pH is adjusted, with the formation of shells, thus promoting the reaction of the melamine with the formaldehyde at the interface of the oil droplets. This type of microcapsule is used in fragrances, insect repellents, food packaging, and footwear. The microcapsules result in smooth surface morphologies and are able to preserve the encapsulated scented oils for a sufficient period of time. They also have good thermal and controlled release properties [168,169].

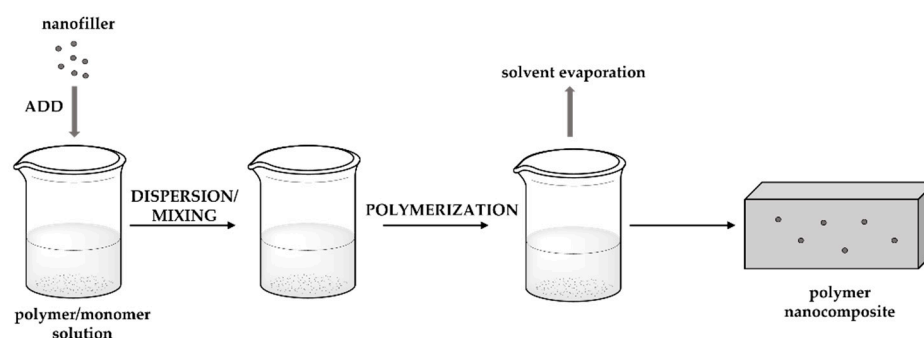


**Figure 11.** Schematic illustration in situ polymerisation method (adapted from [168]).

Using a polymer as a microcapsule wrapper is considered a good addition due to its high strength and stability [170]. On the other hand, using a copolymer to prepare microcapsules with a low molecular weight of formaldehyde–melamine avoids the toxicity of formaldehyde [171].

In situ polymerisation is a method of rapid and easy expansion [172] and, at the same time, provides high encapsulation efficiency. However, the polymerisation reaction is

difficult to control [173] and requires a large amount of solvent, making the monomers non-biodegradable and/or non-biocompatible [174].

### 3.4. Spray Drying

Spray drying is the most-used technology in the microencapsulation of essential oils. It is mainly used on an industrial scale, as it allows simple, reproducible, continuous, and low-cost production. Being used more frequently in the food industry, this process is also utilised in the cosmetics, pesticides, and pharmaceutical industries [175]. This technique allows encapsulated and powdered Eos to be obtained due to the ability to dry them in just one operation. In this process, the atomisation of emulsions occurs in a drying chamber with relatively high temperatures, where the evaporation of the solvent takes place and, consequently, microcapsules are formed [176].

The spray-drying technique involves four steps (Figure 12), where the preparation of dispersion first occurs, i.e., the wall materials are dissolved in water with agitation and controlled temperature. Still in the same step, the addition of the EOs follows and, if necessary, the emulsifier can be added. Afterwards, the dispersion is homogenised to be injected into the equipment through an atomising nozzle, where small droplets are formed. In the third step, emulsion atomisation occurs, where the formed droplets enter the drying chamber with a flow of hot air present. Finally, the dehydration of the atomised microparticles is done through the evaporation of the solvent, which dries the microparticles, which can then be recovered in the form of powder in a collector or filter [177].

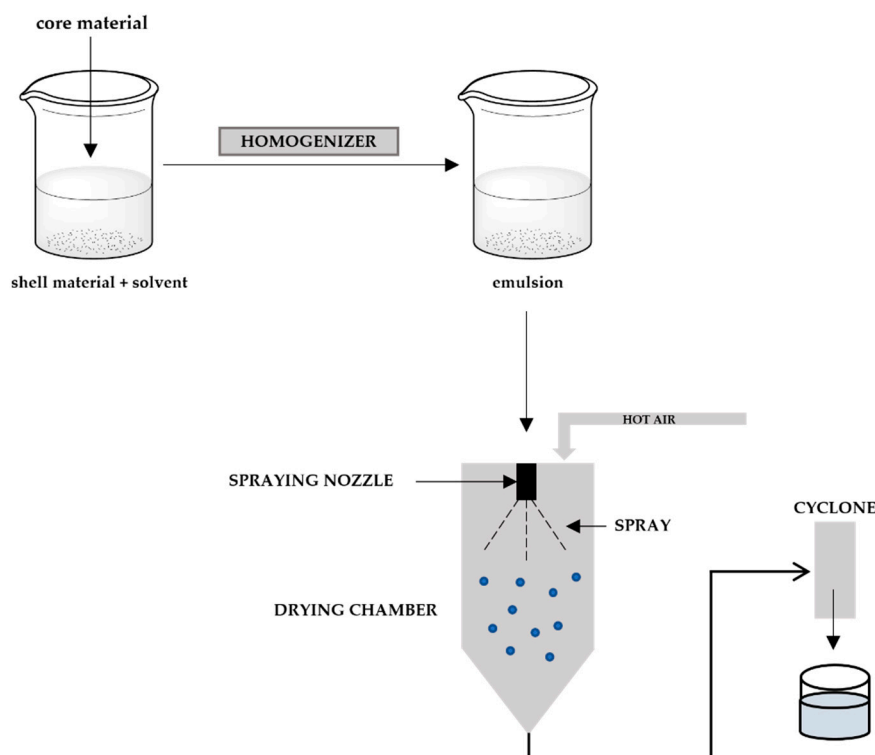


**Figure 12.** Schematic representation of spray drying.

The main limitations of this technique are related to the wall material, which must have good water solubility, and to the number of encapsulating agents available. In addition, some materials may be sensitive to the high temperatures introduced in the atomisation process. In addition, the production of microcapsules in fine powder form can cause agglomeration and an additional process may be required [166].

### 3.5. Freeze Drying

Freeze drying, also known as lyophilisation, is a simple process (Figure 13) that is used to dehydrate most materials sensitive to heat and aromas such as oils. Sublimation is the major principle involved in this drying process, where water passes directly from a solid state to a vapour state without passing through the liquid state. Before starting this process, the oil is dissolved in water and frozen [178]. Afterwards, the pressure is reduced and heat is added to allow the frozen water to sublimate the material directly from the solid phase to the gas phase. Freeze-dried materials appear to have the maximum retention of volatile compounds compared to spray drying, and this technique is used to microencapsulate some oils, with high yields [179]. This method helps to better preserve the EO content in many types of herbs and spices compared with other preservation techniques [180]. Lyophilisation is simple and easy to operate, showing that lyophilised samples are more resistant to oxidation and less efficient in microencapsulation [181]. The process disadvantages include high energy use, long processing time, and high production costs [182].

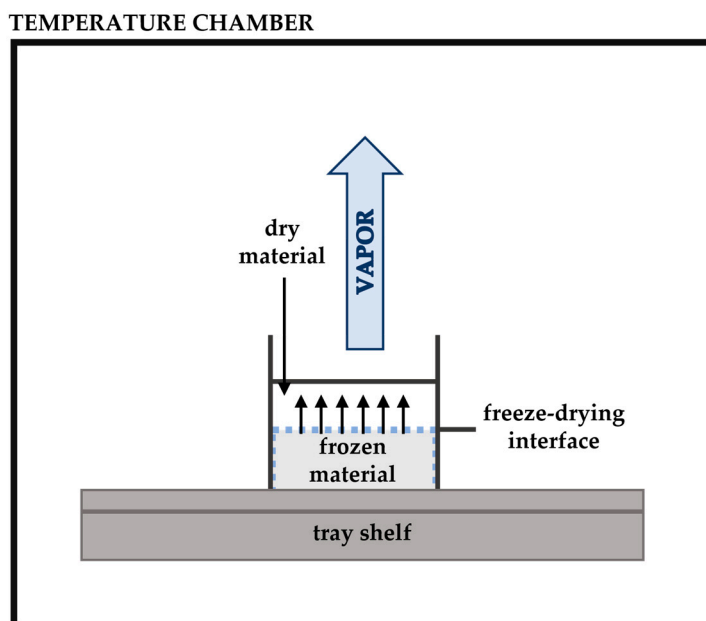


**Figure 13.** Schematic diagram of a freeze dryer (adapted from [163]).

### 3.6. Supercritical Fluid (SCF) Technology

Many pharmaceutical, cosmetic, and food industries use supercritical fluid technology (Figure 14) to form the microcapsules of essential oils due to their inherent advantages. The use of a wide variety of materials that produce controlled particle sizes and morphologies, the easy solvent removal, the non-degradation of the product, and being a non-toxic method are some of the many advantages of SCF technology.

The methods used for supercritical fluids are the precipitation of gas anti-solvent, particles of saturated gas solutions, the extraction of fluid emulsions, and the rapid expansion of supercritical solutions [183,184]. The supercritical solvent impregnation process has proven to be successful in a wide variety of substances (essential oils, fragrances, active pharmaceutical compounds, and dyes) and matrices (wood, polymers, cotton, and contact lenses).

An alternative to spray drying (that degrades oils at high temperatures) is impregnation with supercritical solvent, as it is an ecological process where supercritical carbon dioxide is used as a green solvent.



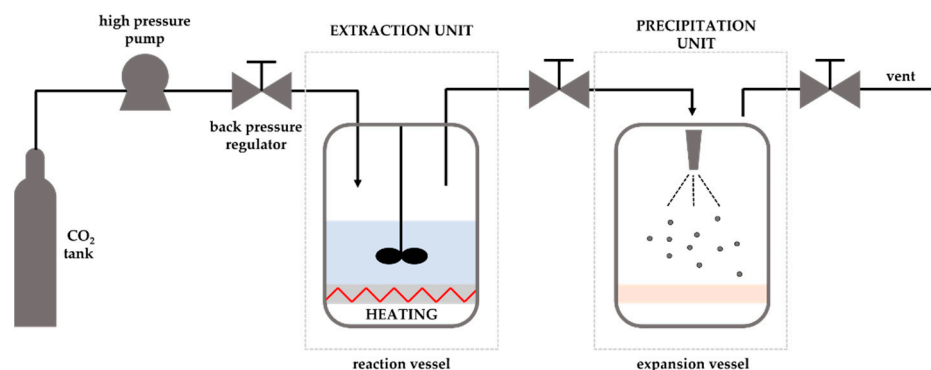


**Figure 14.** Flow chart of supercritical fluid technology.

### 3.7. Coaxial Electro spray System

The food, cosmetic, and pharmaceutical industries use a new technology to encapsulate oils, called coaxial electro spraying (Figure 15) [185,186]. This system is used in two phases, with external and internal solutions being sprayed coaxially and simultaneously through two feed channels separated by a nozzle.

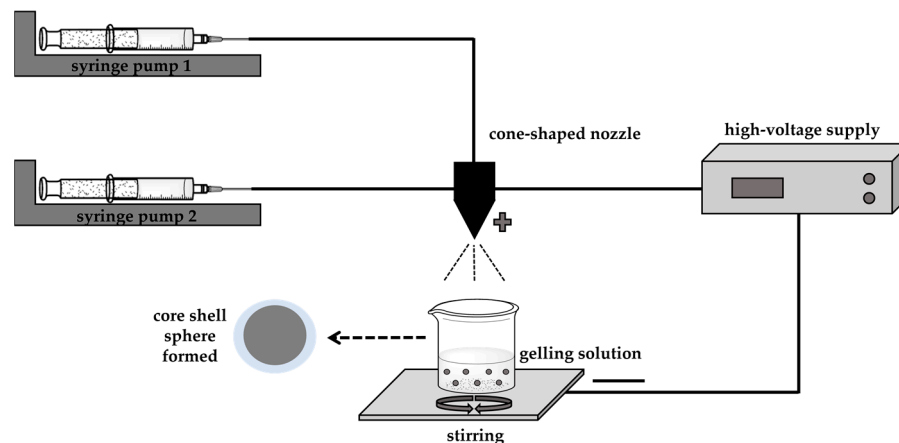


**Figure 15.** Schematic representation of microencapsulation process by coaxial electro spraying (adapted from [144]).

In the electro spray process, the Taylor cone is composed of a core-shell structure that is formed at the top of the spray nozzle, ending up with the polymeric solution encapsulating the internal liquid. This method is distinguished by its ease and efficiency, and the maximum speed of the core material. The coaxial electro spray system provides a uniform size distribution, a high encapsulation efficiency, and an effective protection of bioactivity. However, the encapsulation efficiency and the stability of the microcapsules are affected by the wall materials [186]. Furthermore, controlling the process in coaxial electro spraying is difficult to some extent [187].

In experimental terms, the reported work on coaxial electro spray is based on individual laboratory experiments, consisting of specific combinations of materials and empirical process parameters. The fabrication of polymeric microparticles and nanoparticles is hampered by the lack of standard protocols. Regarding the collection of particles, the methodology cannot facilitate the hardening of the shell or maintain the morphology of particle, or even prevent its aggregation. On the theoretical side, many existing process models are empirical or semi-quantitatively empirical. The simulated results are not enough for the quantitative control of the process, as numerical simulations, such as computational fluid dynamics modelling, have been used to simulate the formation of the liquid cone and atomisation in a single axial electro spray process [188]. In summary, more experimental and

theoretical study is needed to better understand the physical nature of coaxial electro-spray and to provide quantitative guidance for process control.

### 3.8. Fluidized Bed Coating

Fluidised bed coating is one of the most efficient coating methods, in which the ingredients can be mixed, granulated, and dried in the same container. Consequently, the handling and processing time of the material is reduced. This approach was recently used to encapsulate fish oil by spraying and coating it (Figure 16) [189]. Fluidised bed coating is carried out by suspending the solid particles of the core material by an air stream under controlled temperature and humidity and then sprayed, building, over time, a thin layer on the surface of the suspended particles. This material must have an acceptable viscosity for atomisation, and the pumping should be able to form an appropriate film and be thermally stable [190].

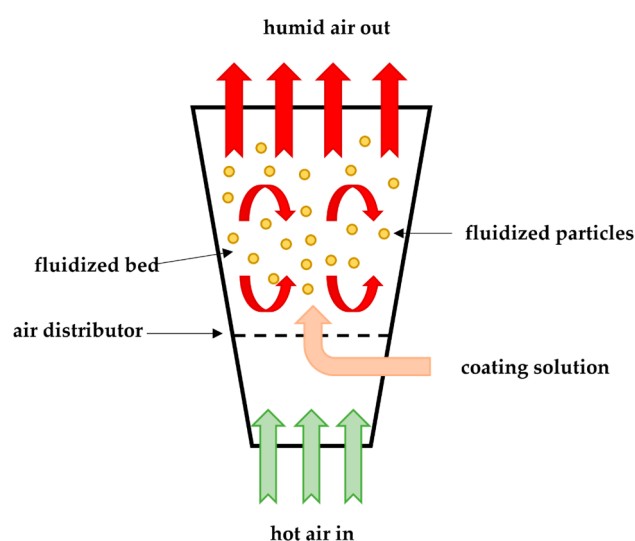


**Figure 16.** Schematic representation of bottom spray fluidised bed coating process (adapted from [166]).

There are several methods used in fluidised bed coating, including top spray, bottom spray, and tangential spray methods. In the top spray system, the coating solution is sprayed in the opposite direction with air in the fluid bed. The opposite flows lead to an increase in the efficiency of encapsulation and the prevention of agglomerates formation, achieving microcapsules with a size between 2 and 100  $\mu\text{m}$ . The bottom spray, known as the Wurster system, uses a coating chamber that has a cylindrical steel nozzle (used to spray the coating material) and a cribriform bottom plate, coating small particles (100  $\mu\text{m}$ ). This multilayer coating procedure helps to reduce particle defects, although it is a time-consuming process. On the other hand, tangential spray consists of a coating chamber with a rotating bottom of the same diameter as the chamber. During the process, the drum is raised to create a space between the edge of the chamber and the drum. A tangential nozzle is placed above the rotating drum, where the coating material is released. Then, the particles move through the space into the spray zone and are finally encapsulated [191]. During this process, there are three mechanical forces, namely, centrifugal force, lifting force, and gravity.

The particles to be coated must be spherical and dense, and must have a narrow size distribution and perfect fluidity, with the non-spherical particles having the largest possible surface area and requiring more coating material.

This technique has a low operating cost and a high thermal efficiency process, allowing total temperature control. However, it can be time consuming, which becomes a disadvantage [173].

### 3.9. Layer-by-Layer Self-Assembly

Layer-by-layer (LbL) is a relatively simple and promising technique for the encapsulation, stabilisation, storage, and release of several active compounds [192]. This method consists of alternating the adsorption of oppositely charged wall materials through many intermolecular interactions onto a charged substrate (Figure 17). The microcapsules have good chemical and mechanical stability through a formation mechanism constituted by irreversible electrostatic interactions that allow the adsorption of successive layers of polyelectrolytes [193]. The adsorption of the layers is normally carried out by immersing the suspension in alternate solutions of cationic and anionic polymers, with washing processes being carried out after the deposition of each layer [194]. This technique has significant advantages over other microencapsulation methods, because it allows the control of the permeability, morphology, composition, size, and wall thickness of the microcapsules by adjusting the number of layers and experimental conditions [195]. Controlling these parameters allows a better adaptation of the microcapsule to its functionality in the target application. However, most LbL systems have some restrictions in terms of biocompatibility [196].

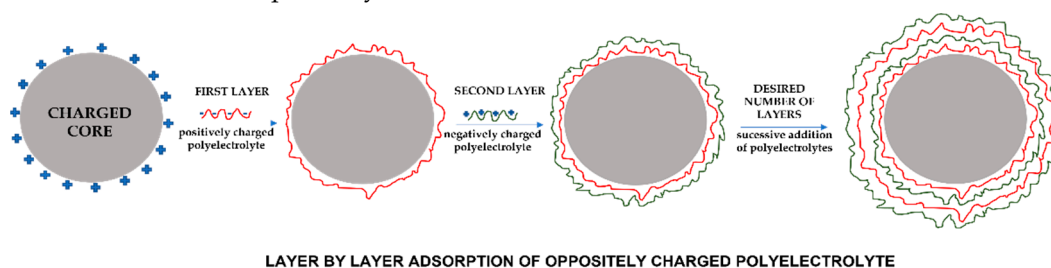


Figure 17. Layer-by-layer (LbL) self-assembly microcapsules (adapted from [197]).

## 4. Microencapsulation of Essential Oils

Microencapsulation is an alternative that can be utilised to overcome several limitations in the application of essential oils. This application is profoundly affected by the high volatility and chemically unstable nature of EOs [198]. In addition, EOs are compounds that can be easily degraded due to interactions with other chemical components and exposure to several factors such as light, temperature, and oxygen [166].

Essential oils can be “trapped” in microcapsules, which act as micro-reservoirs, ensuring excellent protection [199]. The encapsulation process, where small particles are enclosed in solid carriers to increase their protection, has the ability to reduce evaporation, promote easier handling, and control the release of essential oils during storage and application [199]. Furthermore, through microencapsulation, it is possible to change the appearance of EOs (which behave like a powder), without changing their structure and properties [177].

In EO microencapsulation, the first step is often to emulsify or disperse the essential oils in an aqueous solution of a wall material, which also acts as an emulsifier. This process happens because the EOs exist in liquid form at room temperature. Then, the resulting microcapsules must be dried under controlled conditions, so that the loss of the encapsulated material by volatilisation is reduced [177]. One of the areas that has also aroused interest in the microencapsulation of EOs is in the agrochemical industry. Yang et al. prepared and characterised microcapsules based on polyurea, containing essential oils as an active agent for possible applications in the controlled release of agrochemical compounds [200]. The microcapsules were synthesised by O/W emulsion interfacial polymerisation and the synthetic conditions that showed the best results were used to encapsulate four essential oils (lemongrass, lavender, sage, and thyme), capable of interfering with the seed germination and root elongation of some plants. In cases of pest control, biological pesticides must be more effective than synthetic pesticides.

Bagle et al. reported success in encapsulating neem oil, an effective biological insecticide, in phenol formaldehyde (PF) microcapsules [201]. The microcapsules were obtained using an in situ polymerisation process in an O/W emulsion and their size was determined

using a particle size analyser. Controlled release was monitored by measuring optical observations in the UV range. Figure 18 shows scanning electron microscopy (SEM) micrographs of PF microcapsules containing neem oil. It was possible to visualise that the PF microcapsules were spherical and globular, with diameters between 30 and 50  $\mu\text{m}$  at 400–500 rpm. The microcapsules' surface was considered quite smooth and can be useful regarding the protection and sustained release of the neem oil inside.

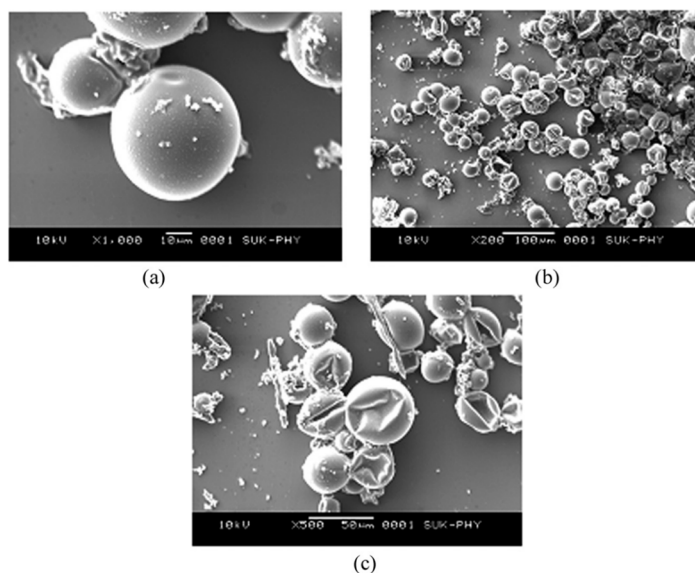


**Figure 18.** SEM micrographs (a–c) of phenol formaldehyde microcapsules containing neem oil [201].

The chemical constitution of synthesised microcapsules was confirmed by Fourier-transform infrared spectroscopy (FTIR), and it was found to be a good thermal stability of MCs needed for the long-term preservation of the core, and it was concluded that neem oil can be better preserved in PF microcapsules.

The controlled release behaviour of PF microcapsules containing neem oil was studied and the experimental data are shown in Figure 19. A release of about 30% was observed after 6 h, confirmed by the decrease in absorbance over time.

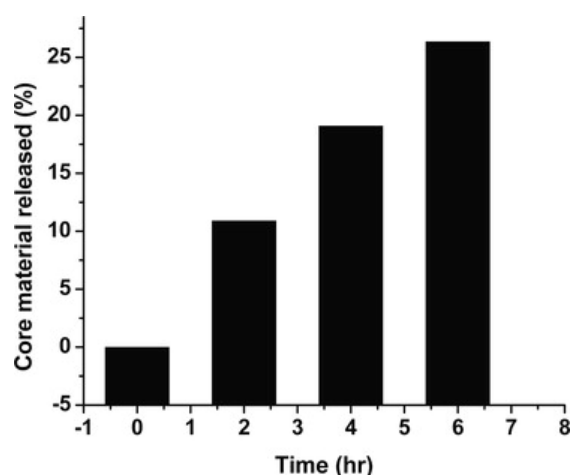


**Figure 19.** Controlled release of core material over time [201].

Like neem oil, other essential oils also have insecticidal properties, such as *Rosmarinus officinalis* and *Zataria multiflora* (Lamiaceae), that can be used as pesticides for stored-product pests. In the study carried out by Ahsaei et al., these oils were encapsulated in octenyl succinic anhydride (OSA) starch to test their insecticidal activity against *Tribolium confusum*. The microcapsules were obtained using an O/W emulsion and dried using the

spray drying technique [202]. The solid formulations were characterised by particle size, encapsulation efficiency, and water activity. The release rate under storage conditions was measured over a period of 40 days, and the insecticidal activity against *T. confusum* was determined using specific bioassays. It was concluded that the encapsulation efficiency depends directly on the surfactant-to-oil ratio. Regarding the morphology of microcapsules loaded with OEs, SEM micrographs reveal the presence of oval and spherical microcapsules with irregular surfaces. The microcapsules appear to be devoid of cracks or fractures, which is an advantageous feature for protecting the oil. The results also showed an optimised release of pesticides from controlled release formulations, which maximises their biological activity for a longer time.

The food sector is probably the sector where the microencapsulation of essential oils is most explored, with the encapsulation of flavours being one of the great interests of this industry. Flavours are necessary for some foods, to promote consumer satisfaction and the consumption of those products. Nevertheless, the flavour stability in foods has been a challenge for this sector in order to achieve quality and acceptability.

For the encapsulation of a flavour, Fernandes et al. evaluated, by spray drying, the effects of the partial or total substitution of arabic gum with modified starch, maltodextrin, and inulin in the encapsulation of rosemary essential oil [203].

Regarding the characterisation of microcapsules, moisture content, wettability and solubility, density and apparent density, and oil retention was determined. From SEM observations (Figure 20), the authors found that there was no evidence of cracking in the particles using any of the encapsulating formulations, ensuring low gas permeability and thus better protecting the EO of rosemary. Differences were observed in the surface of each type of particle, showing that the particles have a spherical shape. It was concluded that the total substitution of arabic gum with modified starch or a mixture of modified starch and maltodextrin did not affect the efficiency of the encapsulation, increasing the possibility of developing new formulations of encapsulants. With the addition of inulin, the oil retention of particles decreased. However, the combination of modified starch and inulin was shown to be a viable substitute for arabic gum in foods.

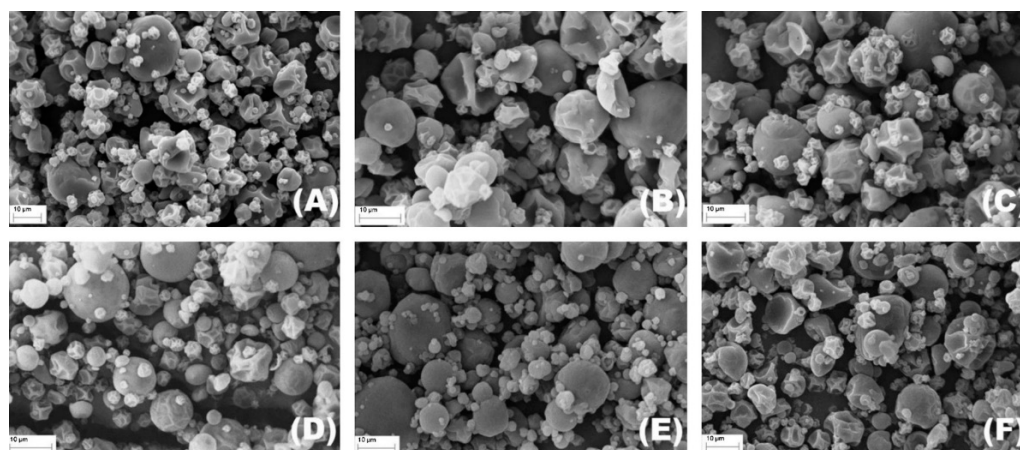


**Figure 20.** Scanning electron micrographs of the particles containing rosemary essential oil [203]. (A): arabic gum; (B): arabic gum/maltodextrin; (C): arabic gum/inulin; (D): starch; (E): modified starch/maltodextrin; (F): modified starch/inulin.

A group of researchers compared the release properties of three different microcapsules, namely gelatin microcapsules loaded with holy basil essential oil (HBEO) (designated as UC), UC coated with aluminium carboxymethylcellulose (CC), and UC coated with aluminium compound carboxymethyl cellulose–beeswax (CB) [204]. To be applied as a feed additive, the HBEO was encapsulated in order to be a potential alternative to antibiotic growth promoters (AGP). However, its benefits depend on the available amount in the gastrointestinal tract.

The SEM technique was used to characterise the internal and external factors of the microcapsule surface morphology. According to Figure 21, UC microcapsules (Figure 21a) are almost spherical in shape and after coating, the CC (Figure 21b) and CB (Figure 21c) microcapsules are more spherical. Upon magnification of these micrographs, it was possible to verify that UC microcapsules have a spongy structure (Figure 21d) and that CC (Figure 21e) and CB (Figure 21) microcapsules are denser. When cut transversely, UC microcapsules seem to have a gelatinous morphology (Figure 21g), whereas the CC (Figure 21h) and CB microcapsules (Figure 21i) reveal a thicker and more compact outer coating layer with a honeycomb structure. This method of encapsulation demonstrated an effective process for improving HBEO efficacy for pathogen reduction in the distal region of the intestine.

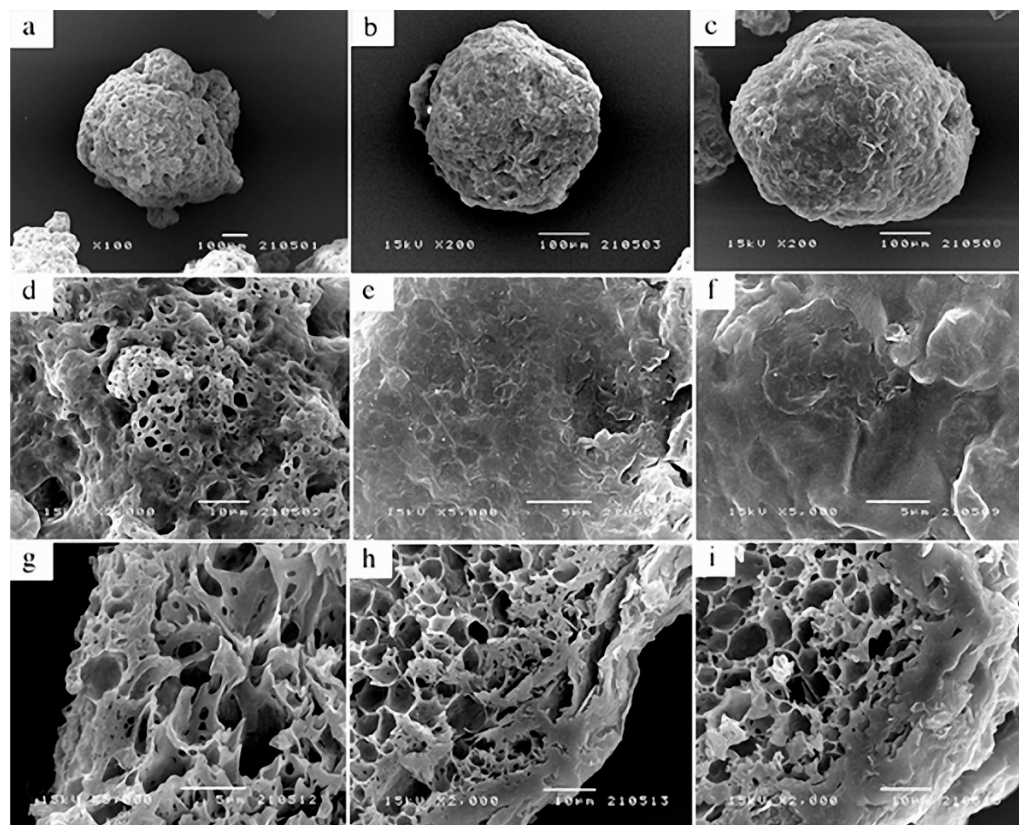


**Figure 21.** SEM micrographs of UC, CC, and CB gelatin-based microcapsules: (a) whole UC; (b) whole CC; (c) whole CB; (d) external surface of UC; (e) external surface of CC; (f) external surface of CB; (g) inner edge of UC; (h) inner edge of CC; (i) inner edge of CB [204].

Regarding food safety, the use of antimicrobial packaging materials offers the potential to retard the growth rate of spoilage microorganisms. The physical and antimicrobial properties of nanofibres manufactured for active packaging systems were studied by Munhuweyi et al. [205]. Microcapsules and active nanofibres derived from the precipitation of  $\beta$ -cyclodextrin ( $\beta$ -CD) with essential oils of cinnamon and oregano were developed and their antifungal activity in vitro against *Botrytis* sp. was examined. To induce microencapsulation, the solutions were subjected to co-precipitation. It was verified that cinnamon microcapsules have greater antimicrobial efficacy when compared to oregano. As food preservatives, this microencapsulation system could have promising applications in the development of active packaging systems.

Using the thermogravimetric analysis (TGA) technique, the initial weight loss for simple  $\beta$ -CD occurred at  $\sim 100$  °C and the greatest weight loss at  $\sim 330$  °C (Figure 22a). The degradation temperature of  $\beta$ -CD in the CIN/ $\beta$ -CD and OREG/ $\beta$ -CD complexes decreased from  $\sim 330$  °C to  $\sim 270$  °C (Figure 22b,c). Comparing the TGA curves, there is

a difference between them, demonstrating the presence of chemical and guest molecule interaction in the complex.

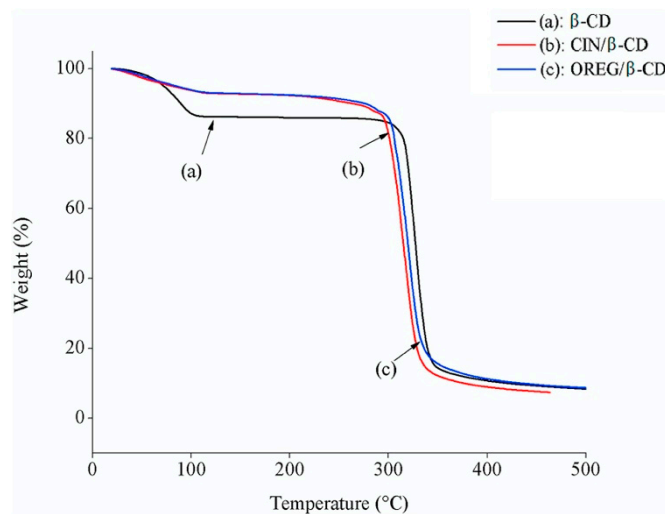


**Figure 22.** TGA curves of (a) plain  $\beta$ -cyclodextrin ( $\beta$ -CD), (b) microencapsulated cinnamon (CIN/ $\beta$ -CD), and (c) oregano (OREG/ $\beta$ -CD) [205].

Using the simple coacervation method, Leimann et al. encapsulated lemongrass, which is known for its broad spectrum antimicrobial activity [206]. Poly(vinyl alcohol) crosslinked with glutaraldehyde was used as the wall-forming polymer. The influence of the agitation rate and the fraction of oil volume on the microcapsule size distribution was evaluated. Sodium dodecyl sulphate (SDS) and poly(vinyl pyrrolidone) were tested to prevent the agglomeration of microcapsules during the process. The microcapsules did not show agglomeration when 0.03% by weight of SDS was used. The composition and antimicrobial properties of the encapsulated oil were determined, demonstrating that the microencapsulation process did not deteriorate the encapsulated essential oil.

Cyclodextrins (CDs) are important supramolecular microcapsule hosts in foods and other fields, and the essential oil of *Laurus nobilis* (LEO) has natural antioxidant properties in food due to its main constituents being terpenic alcohols and phenols. For these reasons, Li et al. isolated LEO by microwave-assisted hydrodistillation [207]. The authors prepared chitosan (CS) microcapsules loaded with citrus essential oils (CEOs: D-limonene, linalool,  $\alpha$ -terpinene, myrcene, and  $\alpha$ -pinene) using six different emulsifiers (Tween 20, Tween 40, Tween 60, Tween 60/Tween 20/Span 80 1:1, Tween 20/sodium dodecyl benzene sulfonate (SDBS) 1:1, Span 80) through an emulsion gelation technique [208]. After preparing  $\beta$ -cyclodextrin ( $\beta$ -CD) microcapsules and their derivatives, several affecting factors were examined in detail.

Figure 23 shows the total antioxidant activity of LEO. LEO caused Mo (VI) to be deoxidised to become Mo (V) through a mechanism of total antioxidant activity. Mo (V) exhibits maximum absorption at 695 nm and has a stronger antioxidant activity; the greater the concentration of Mo (V) solution, the greater the absorbency of the solution. With the increase in absorbance of the solutions, there was an increase in the concentrations of the sample, causing the antioxidant activity to increase significantly.

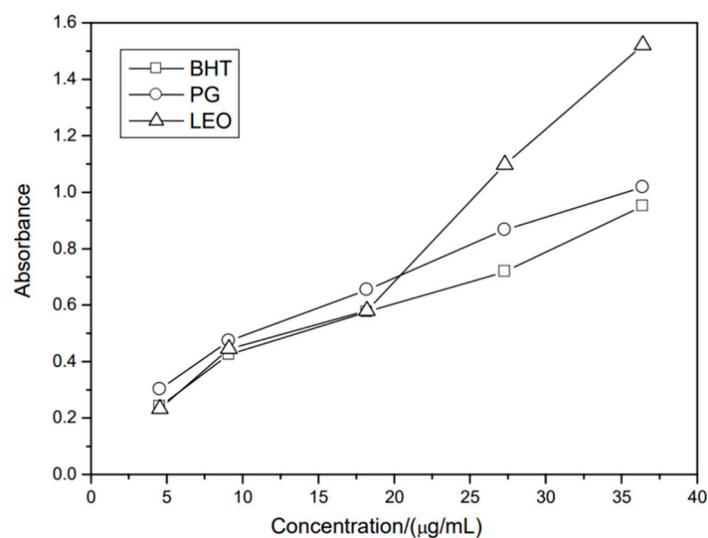


**Figure 23.** Absorbance of antioxidants in different concentrations of 2,6-ditert-butylphenol (BHT, square), propyl gallate (PG, circle) and *Laurus nobilis* essential oil (LEO, triangle) [207].

The microcapsules were analysed and the results indicate that the choice of emulsifier significantly affects the size and effectiveness of incorporating the microcapsules.

Figure 24a presents the FTIR spectra observed in CS, CEOs, and four groups of microcapsules prepared with different emulsifiers. In the CEOs curve, the peak at  $886\text{ cm}^{-1}$  corresponds to the absorption of limonene. The strong methylene/methyl band occurs at  $1435\text{ cm}^{-1}$ , and at  $1646\text{ cm}^{-1}$ , the C=O stretching vibration appears. Peaks corresponding to the asymmetric and symmetrical modes of the  $\text{CH}_2$  elongation vibration appear for Span 80 and Tween 60, and the new connections can be seen at  $2922\text{ cm}^{-1}$ . Through these results, it was possible to observe that the CEOs were incorporated in the microcapsules, showing benefits for inhibiting them from oxidation and volatilisation.

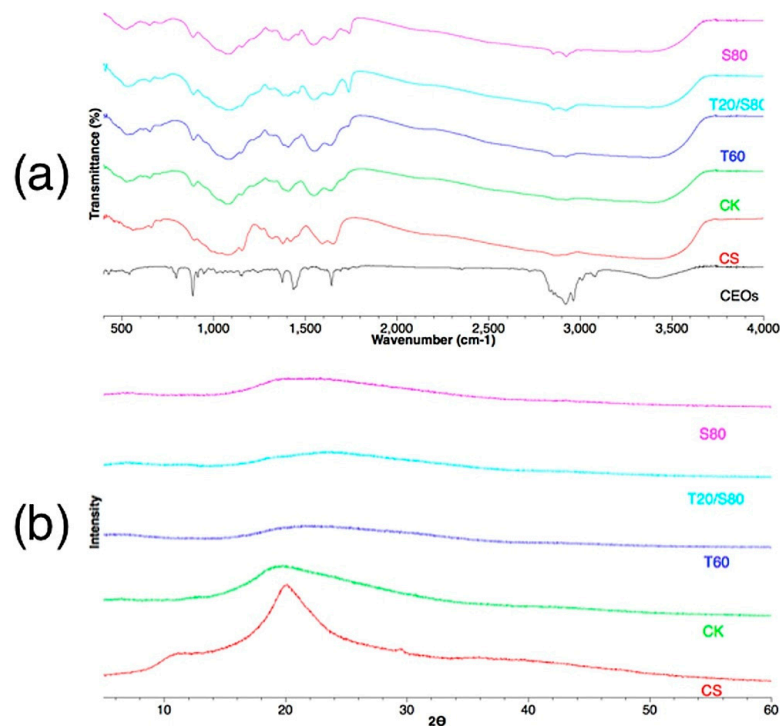


**Figure 24.** (a) FTIR spectroscopy, (b) X-ray diffraction of pure chitosan (CS), control group (CK), Tween 60, Tween 20/Span 80, and Span 80 [208].



A second step in the characterisation of the microcapsules was the analysis of the crystallographic structure. Through X-ray diffraction (XRD) analysis (Figure 24b), it was possible to observe that CS exhibits a diffraction pattern with a broad band centred at  $2\theta$   $20^\circ$ , thus indicating the existence of an amorphous structure. Comparing the CS with the microcapsule groups, the latter exhibit a significant reduction in this broad band. This reduction in intensity is due to the destruction of the CS structure, which can be attributed to a change in the arrangement of the molecules in the crystalline chain.

To develop a new use of functional EOs, Karimi Sani et al. studied the influence of process parameters on the characteristics of microencapsulated essential oil *Melissa officinalis* using whey protein isolate (WPI) and sodium caseinate (NaCS). The impacts of these variables were examined using the response surface methodology. Smaller particle sizes were obtained for higher amounts of WPI with the lowest level of applied sonication power. The results of the desirability function indicate that the maximum amount of WPI with an ultrasound power of 50 W led to the smallest particle size and the lowest zeta potential and turbidity. In this study, the ultrasonic technique showed potential in the use of milk proteins to produce microparticles with OEs. The obtained results showed that the microcapsules loaded with *Melissa officinalis* can preserve the bioactive compounds and induce flavour stability, enabling their use in food formulations and pharmaceutical products.

Mehran et al. carried out a study of the microencapsulation of spearmint essential oil (SEO), using a mixture of inulin and arabic gum as wall material in order to be used in the food and pharmaceutical industry [209]. The technique used for the formation of the microcapsules was spray drying. The microcapsules were characterised for oil retention, encapsulation efficiency, hygroscopicity, and carbon content, having as ideal conditions 35% solid wall, 4% essential oil concentration, and  $110^\circ\text{C}$  inlet temperature, with maximum retention of 91% of oil. To confirm that the SEO was encapsulated, this group of researchers used differential scanning calorimetry (DSC) and FTIR characterisation techniques.

The infrared spectra of pure SEO, pure matrix (containing inulin and arabic gum), and microcapsules are shown in Figure 25. In the SEO spectrum, the characteristic peaks at  $801\text{ cm}^{-1}$  and  $894\text{ cm}^{-1}$  are ascribed to  $=\text{CH}$  vibrations. The C-O-C elongation corresponds to the peak at  $1109\text{ cm}^{-1}$  and the C=O elongation corresponds to the peak  $1675\text{ cm}^{-1}$ . In the matrix spectrum, a wide band at  $3392\text{ cm}^{-1}$  is related to the hydroxylated group. In relation to the peak at  $1030\text{ cm}^{-1}$ , it can be associated with the strong absorption bands of the C-O-C elongation. In the microcapsule spectrum, it can be observed that it is quite similar to the matrix, and that the peaks related to the SEO disappear or are absent, which may be related to the overlap of the peaks of the matrix and SEO due to the low weight fraction of SEO in the total weight of the microcapsules. Through this spectrum, it was possible to verify the successful encapsulation of the SEO (peaks at  $1673\text{ cm}^{-1}$  and  $900\text{ cm}^{-1}$ ).

The double barrier release system is a method used for essential oils that have antifungal activity, even against drug-resistant fungi. However, there are some limitations due to the sensitivity to pH, temperature, and light. Adepu et al. encapsulated three essential oils (thymol, eugenol, and carvacrol) in a polylactic acid shell with high encapsulation efficiency to achieve their synergistic antifungal activity using the coacervation phase separation method. These were incorporated into bacterial cellulose (a nanofibre fibrous hydrogel) [210]. An antifungal test was performed on the *Candida albicans* fungus model (a cause of common oral and vaginal infections). Another test was carried out—a transvaginal drug release study in vitro—to compare the release of microcapsules like colloids and composites, where the latter exhibited a controlled release. Through several studies, such as the SEM technique, it was found that the average size and size distribution of the microcapsules depends on the concentration of the used polymer (poly(lactic acid)) and surfactant (poloxamer).

SEM images of BC loaded with microcapsules demonstrate a regular distribution and spherical shape, appearing to be well separated and stable in the stages of the preparation

process (Figure 26). From the highest magnification image, it was observed that the microcapsules were anchored to the nanofibre matrix.

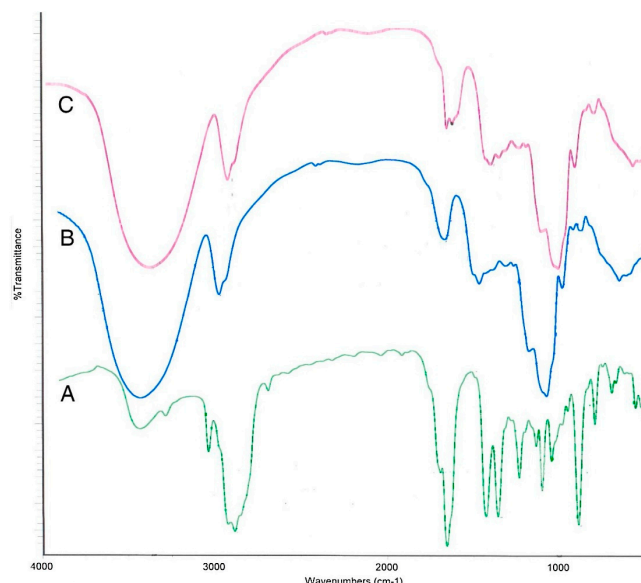


**Figure 25.** FTIR spectra of (A) pure SEO, (B) pure matrix, and (C) inulin and arabic gum-based microcapsules [209].

Repellent essential oils are becoming increasingly widespread due to their low toxicity and customer approval. Its application in textile materials has been widely developed. To optimise their application efficiency, it is important to develop long-lasting repellent textiles using OEs. Specos et al. obtained citronella-loaded gelatin microcapsules through the complex coacervation method, which were applied to cotton fabrics in order to study the repellent effectiveness of the obtained fabrics [70]. The release of citronella by the treated tissues was monitored and the repellent activity evaluated by exposing a human hand and arm covered with the treated tissues to *Aedes aegypti* mosquitoes.

It was found that the tissues treated with citronella microcapsules present greater and more lasting protection against insects in comparison to fabrics sprayed with an ethanol solution of essential oil. Repellent textiles were obtained by filling cotton fabrics with microcapsule sludge, using a conventional drying method. This methodology does not require additional investments for the textile finishing industries, which is a desirable factor in developing countries. Figure 27A shows the morphology of blackberry-type microcapsules in a fresh paste with diameters ranging from 25 to 100  $\mu\text{m}$ , while Figure 27B shows SEM micrographs of spray-dried microcapsules revealing two types of structures, with small spherical units of less than 10  $\mu\text{m}$  and clusters ranging from 25 to 100  $\mu\text{m}$ .

In 2016, Ribeiro et al. investigated the functionalisation of photocatalytic titanium dioxide nanoparticles on the surface of polymeric microcapsules as a way to control the release of citronella by solar radiation, thus obtaining a release of a repellent without mechanical intervention [211]. These authors used a modified hydrothermal sol-gel method to synthesise  $\text{TiO}_2$  nanoparticles. Through several characterisation techniques, these authors were able to observe the surface of the microcapsules and the release efficiency. Using in vitro biological assays with live mosquitoes, the controlled release repellence effect of these photocatalytic microcapsules was reinforced by the inhibition of these vectors. According to the results, it was shown that functionalising the microcapsules with photocatalytic nanoparticles on the surface, and then exposing them to ultraviolet radiation, effectively increased the emission of citronella into the air, repelling mosquitoes. Table 6 shows an overview of illustrative examples of EO microencapsulation oils, wall materials, and microencapsulation methods with industrial importance.

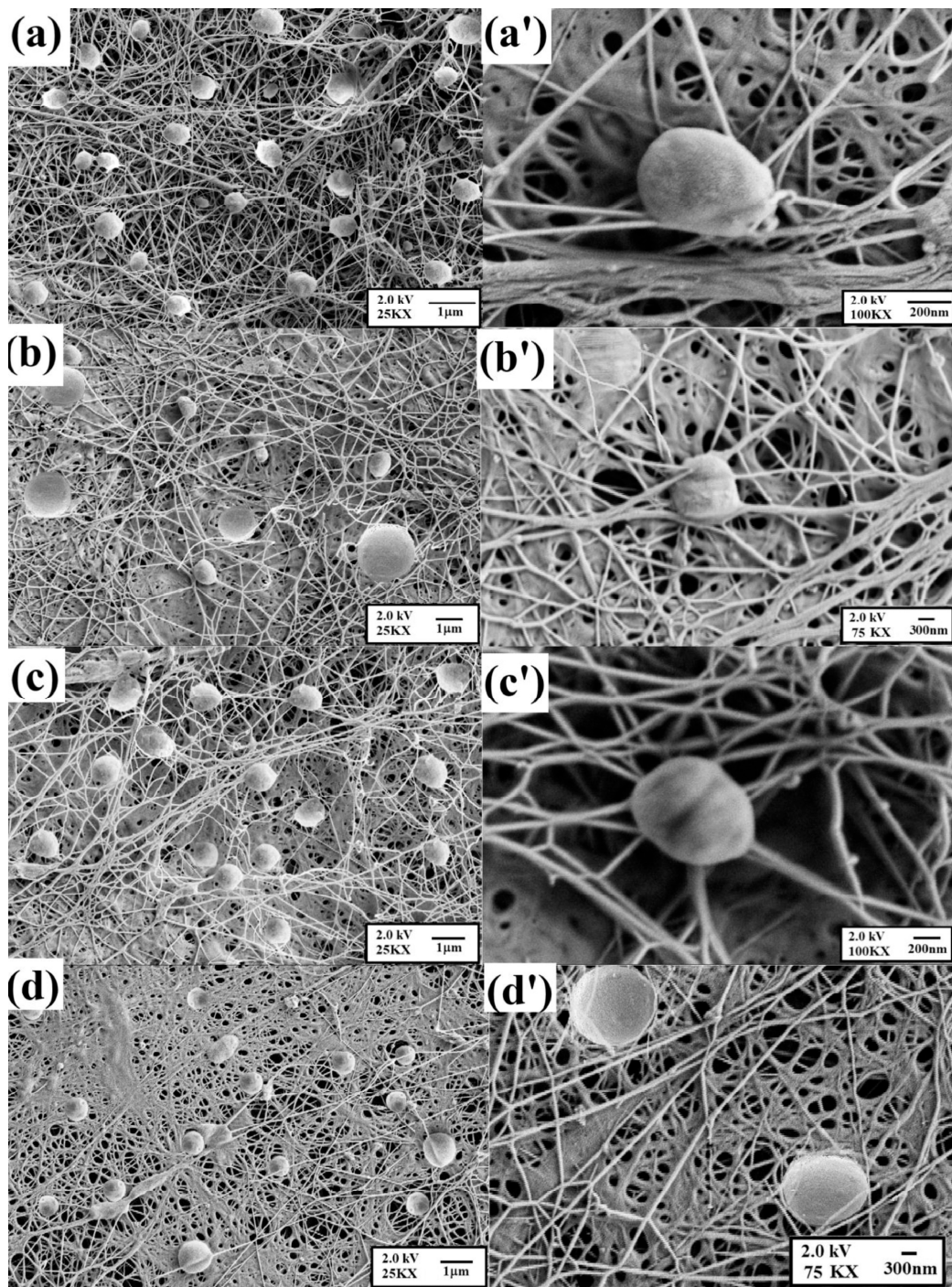


**Figure 26.** Low- and high-magnification SEM micrographs of (a,a') BC-PLA<sub>1.5</sub>-Pol<sub>5.0</sub>, (b,b') BC-PLA<sub>1.5</sub>-Pol<sub>2.5</sub>, (c,c') BC-PLA<sub>3.0</sub>-Pol<sub>5.0</sub>, and (d,d') BC-PLA<sub>3.0</sub>-Pol<sub>2.5</sub> [210].

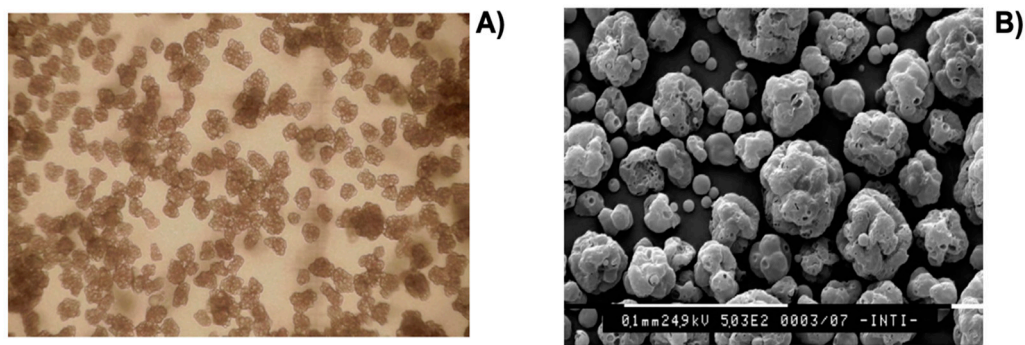


**Figure 27.** (A) Optical micrographs of gelatin microcapsules containing citronella essential oil (100× magnification) and (B) SEM microphotographs of spray-dried microcapsules containing citronella essential oil (500× magnification) [70].

**Table 6.** Overview of essential oil microencapsulation, methods, wall materials, and industrial applications.

| Microencapsulation Method | Wall Material(s)  | Essential Oil/Source  | Applications                         | Reference    |
|---------------------------|---|-----------------------|--------------------------------------|--------------|
| Emulsification            | Hydroxypropyl methyl cellulose/<br>chitosan/silica                | Peppermint oil        | Medical                              | [212]        |
|                           | Polydopamine  | Turpentine            | Agrochemical                         | [213]        |
|                           | β-cyclodextrin  | Thyme                 | Food                                 | [214]        |
|                           | β-cyclodextrin/sugar beet pectin                                  | Garlic                | Food                                 | [215]        |
| Ionic Gelation            | Cassava starch/poly(butylene adipate-co-terephthalate)            | Oregano               | Food                                 | [216]        |
| Simple Coacervation       | Gelatin   | Basil                 | Agrochemical                         | [217]        |
|                           | Poly(vinyl alcohol)   | Lemongrass            | Food and pharmaceutical              | [206]        |
|                           | Gelatin/gum arabic  | Citronella            | Anti-mosquito textile                | [149]        |
| Complex Coacervation      | Gelatin/sodium alginate   | Citronella            | Anti-mosquito textile                | [218]        |
|                           | Gelatin/gum arabic  | Lavender              | Cosmetics                            | [219]        |
|                           | Chitosan/gum arabic/maltodextrin                                  | Peppermint            | Cosmetics                            | [220]        |
|                           | Chitosan/k-carrageenan  | <i>Pimenta dioica</i> | Food                                 | [221]        |
|                           | Gelatin/chia mucilage   | Oregano               | Food                                 | [222]        |
|                           | Mung bean protein isolate/apricot peel pectin                     | Rose                  | Food                                 | [223]        |
|                           | Sichuan pepper seed soluble dietary fibre/soybean protein isolate | Sichuan pepper        | Food                                 | [224]        |
|                           | Whey protein isolate/arabic gum                                   | Orange                | Food                                 | [225]        |
|                           | Interfacial Polymerization  | Polyurea              | Lemongrass, lavender, sage and thyme | Agrochemical |

Table 6. Cont.

| Microencapsulation Method      | Wall Material(s)   | Essential Oil/Source      | Applications                       | Reference |
|--------------------------------|--|---------------------------|------------------------------------|-----------|
| In situ polymerisation         | Silicon dioxide/poly(melamine formaldehyde)                      | Cinnamon                  | Agrochemical                       | [226]     |
|                                | Melamine/formaldehyde  | Thyme                     | Food                               | [169]     |
|                                | Melamine/formaldehyde  | Lavandin and tea tree     | Paints                             | [227]     |
| Extrusion                      | Sodium alginate  | Nutmeg                    | Pharmaceutical                     | [228]     |
|                                | Sodium alginate  | Rosemary                  | Agrochemical                       | [229]     |
| Spray Drying                   | Acacia gum   | Citronella                | Cosmetics                          | [230]     |
|                                | Palm trunk/ chitosan   | Ginger                    | Food                               | [231]     |
|                                | Maltodextrin   | Citrus                    | Food                               | [232]     |
|                                | Gum arabic/maltodextrin/sodium alginate/whey protein concentrate | Juniper berry             | Food                               | [233]     |
|                                | Whey protein isolate/maltodextrin/sodium alginate                | Cinnamon                  | Food                               | [234]     |
|                                | Hydroxypropyl methyl cellulose/maltodextrin                      | Oregano                   | Food                               | [235]     |
|                                | Gelatin/arabic gum   | Citronella                | Textile                            | [70]      |
|                                | Gum arabic/starch/maltodextrin/inulin                            | Rosemary                  | Food                               | [203]     |
|                                | Gum arabic/modified starch                                       | Black pepper              | Food                               | [236]     |
|                                | Gum arabic/maltodextrin/whey protein isolate                     | Basil                     | Food                               | [237]     |
| Freeze-drying                  | Urushiol   | Not mentioned             | Medical and pharmaceutical         | [238]     |
|                                | $\beta$ -cyclodextrin  | <i>Litsea cubeba</i>      | Cosmetics and pharmaceutical       | [239]     |
|                                | Maltodextrin/gelation  | Lemongrass                | Cosmetics, pharmaceutical and food | [240]     |
|                                | Gum arabic/collagen hydrolysate                                  | <i>Origanum onites</i> L. | Environmental                      | [241]     |
|                                | Whey protein isolate/carboxymethylcellulose                      | Orange                    | Food                               | [242]     |
| Supercritical Fluid Technology | Starch   | Oregano                   | Food                               | [243]     |
|                                | n-octenyl succinic/modified starches                             | Lavandin                  | Agrochemical                       | [244]     |
|                                | Modified starch  | Limonene                  | Food                               | [245]     |

## 5. Conclusions

This review summarises different types of EO structures and describes their extraction and application methodology. In addition, different techniques for microencapsulating essential oils are described and some reports are presented to provide a basis for research and industrial development.

As described in this paper, EOs are used in several applications in the pharmaceutical, cosmetic, agricultural, and food industries, as they are natural metabolites produced by plants with interesting properties. Furthermore, EOs are being explored as an alternative to synthetic products due to their ecological factors and the fact that their characteristics are different from the corresponding synthetic product. For example, synthesised oil may have the same odour as natural oils, but may not have the same therapeutic characteristics.

Currently, there is growing interest in the application of EO microencapsulation, making it an effective and important tool in the preparation of high-quality products, improving their chemical, oxidative, and thermal stability. Besides these advantages, the shelf life, biological activity, functional activity, controlled release, physicochemical properties, and general quality of oils can also be improved with microencapsulation technology.

Based on the scientific studies available and presented throughout this paper, it can be concluded that the microencapsulation of EOs is an emerging trend for industrial applications. However, this development has limitations, such as the low diversity of wall materials and their incompatibility with microencapsulation methods. Many of the encapsulating agents available present a high cost for production on an industrial scale. In future research, microencapsulation must also be directed to encapsulate a different mixture of oils by different techniques, in order to disguise the flavour of the oils and to improve safety, quality, and nutritional value.

**Funding:** Vânia I. Sousa and Joana F. Parente are grateful to the Project ReleaseME-POCI-01-0247-FEDER-033268, for their research grants from the Agência Nacional de Inovação, co-funded by the European Regional Development Fund (ERDF), through the Operational Programme for Competitiveness and Internationalisation (COMPETE 2020), under the PORTUGAL 2020 Partnership Agreement. Juliana F. Marques and Marta A. Forte are grateful to the Fundação para a Ciência e Tecnologia (FCT) of Portugal for their Ph.D. grants, SFRH/BD/112868/2015 and PD/BD/128491/2017, respectively. The authors also acknowledge the funding from FCT/PIDDAC through the Strategic Funds project reference UIDB/04650/2020-2023. This research was funded by the project Repel+: New solutions for mosquito repellence as an application for malaria control (project number 47036) from the Agência Nacional de Inovação, co-funded by the European Regional Development Fund (ERDF), through the Operational Programme for Competitiveness and Internationalisation (COMPETE 2020), under the PORTUGAL 2020 Partnership Agreement.

**Data Availability Statement:** The raw/processed data required to reproduce these findings cannot be shared at this time due to technical or time limitations.

**Conflicts of Interest:** The authors declare no conflict of interest.

## References

1. Benchaar, C.; Greathead, H. Essential oils and opportunities to mitigate enteric methane emissions from ruminants. *Anim. Feed Sci. Technol.* **2011**, *166–167*, 338–355. [CrossRef]
2. Benchaar, C.; Calsamiglia, S.; Chaves, A.V.; Fraser, G.R.; Colombatto, D.; McAllister, T.A.; Beauchemin, K.A. A review of plant-derived essential oils in ruminant nutrition and production. *Anim. Feed Sci. Technol.* **2008**, *145*, 209–228. [CrossRef]
3. Raut, J.S.; Karuppayil, S.M. A status review on the medicinal properties of essential oils. *Ind. Crops Prod.* **2014**, *62*, 250–264. [CrossRef]
4. Lubbe, A.; Verpoorte, R. Cultivation of medicinal and aromatic plants for specialty industrial materials. *Ind. Crop. Prod.* **2011**, *34*, 785–801. [CrossRef]
5. daCunha, A.P.; Nogueira, M.T.; Rodrigues Roque, O.; Barroso, J.M.G. *Plantas Aromáticas e Óleos Essenciais: Composição e Aplicações*; Fundação Calouste Gulbenkian: Lisbon, Portugal, 2012; ISBN 978-972-31-1450-8.
6. Teixeira, B.; Marques, A.; Ramos, C.; Neng, N.R.; Nogueira, J.M.F.; Saraiva, J.A.; Nunes, M.L. Chemical composition and antibacterial and antioxidant properties of commercial essential oils. *Ind. Crops Prod.* **2013**, *43*, 587–595. [CrossRef]
7. Sacchetti, G.; Maietti, S.; Muzzoli, M.; Scaglianti, M.; Manfredini, S.; Radice, M.; Bruni, R. Comparative evaluation of 11 essential oils of different origin as functional antioxidants, antiradicals and antimicrobials in foods. *Food Chem.* **2005**, *91*, 621–632. [CrossRef]
8. Bakkali, F.; Averbeck, S.; Averbeck, D.; Idaomar, M. Biological effects of essential oils—A review. *Food Chem. Toxicol.* **2008**, *46*, 446–475. [CrossRef]
9. Warnke, P.H.; Becker, S.T.; Podschun, R.; Sivananthan, S.; Springer, I.N.; Russo, P.A.J.; Wiltfang, J.; Fickenscher, H.; Sherry, E. The battle against multi-resistant strains: Renaissance of antimicrobial essential oils as a promising force to fight hospital-acquired infections. *J. Cranio-Maxillofac. Surg.* **2009**, *37*, 392–397. [CrossRef]

10. De Billerbeck, V.G. Huiles essentielles et bactéries résistantes aux antibiotiques. *Phytotherapie* **2007**, *5*, 249–253. [CrossRef]
11. Burt, S. Essential oils: Their antibacterial properties and potential applications in foods—A review. *Int. J. Food Microbiol.* **2004**, *94*, 223–253. [CrossRef]
12. Nakatsu, T.; Lupo, A.T.; Chinn, J.W.; Kang, R.K.L. Biological activity of essential oils and their constituents. *Stud. Nat. Prod. Chem.* **2000**, *21*, 571–631. [CrossRef]
13. Dima, C.; Dima, S. Essential oils in foods: Extraction, stabilization, and toxicity. *Curr. Opin. Food Sci.* **2015**, *5*, 29–35. [CrossRef]
14. Hogenbom, J.; Jones, A.; Wang, H.V.; Pickett, L.J.; Faraone, N. Synthesis and characterization of  $\beta$ -cyclodextrin-essential oil inclusion complexes for tick repellent development. *Polymers* **2021**, *13*, 1892. [CrossRef] [PubMed]
15. Ponce Cevallos, P.A.; Buera, M.P.; Elizalde, B.E. Encapsulation of cinnamon and thyme essential oils components (cinnamaldehyde and thymol) in  $\beta$ -cyclodextrin: Effect of interactions with water on complex stability. *J. Food Eng.* **2010**, *99*, 70–75. [CrossRef]
16. Saberi-Riseh, R.; Moradi-Pour, M.; Mohammadinejad, R.; Thakur, V.K. Biopolymers for biological control of plant pathogens: Advances in microencapsulation of beneficial microorganisms. *Polymers* **2021**, *13*, 1938. [CrossRef]
17. Lengyel, M.; Kállai-Szabó, N.; Antal, V.; Laki, A.J.; Antal, I. Microparticles, microspheres, and microcapsules for advanced drug delivery. *Sci. Pharm.* **2019**, *87*, 20. [CrossRef]
18. Council of Europe (Ed.) European Directorate for the Quality of Medicines & HealthCare (EDQM). In *European Pharmacopoeia*, 10th ed.; EDQM: Strasbourg, France, 2021.
19. Svoboda, K.P.; Greenaway, R.I. Investigation of volatile oil glands of *Satureja hortensis* L. (*summer savory*) and phytochemical comparison of different varieties. *Int. J. Aromather.* **2003**, *13*, 196–202. [CrossRef]
20. Dajic Stevanovic, Z.; Sieniawska, E.; Glowniak, K.; Obradovic, N.; Pajic-Lijakovic, I. Natural Macromolecules as Carriers for Essential Oils: From Extraction to Biomedical Application. *Front. Bioeng. Biotechnol.* **2020**, *8*, 1–24. [CrossRef]
21. Figueiredo, A.C.; Pedro, L.G.; Barroso, J.G. Plantas aromáticas e medicinais: Factores que afetam a produção. In *Potencialidades e Aplicações das Plantas Aromáticas e Medicinais*; Plant Biotechnology Center—Faculty of Sciences of the University of Lisbon: Lisbon, Portugal, 2007; ISBN 978-972-9348-16-7.
22. Peixoto, L.R.; Rosalen, P.L.; Ferreira, G.L.S.; Freires, I.A.; de Carvalho, F.G.; Castellano, L.R.; de Castro, R.D. Antifungal activity, mode of action and anti-biofilm effects of *Laurus nobilis* Linnaeus essential oil against *Candida* spp. *Arch. Oral Biol.* **2017**, *73*, 179–185. [CrossRef]
23. Eslahi, H.; Fahimi, N.; Sardarian, A.R. Chemical Composition of Essential Oils: Chemistry, Safety and Applications. In *Essential Oils in Food Processing: Chemistry, Safety and Applications*; Hashemi, S.M.B., Khaneghah, A.M., de Souza Sant’Ana, A., Eds.; Wiley: Hoboken, NJ, USA, 2017; pp. 119–171. ISBN 9781119149392.
24. Dhifi, W.; Bellili, S.; Jazi, S.; Bahloul, N.; Mnif, W. Essential Oils’ Chemical Characterization and Investigation of Some Biological Activities: A Critical Review. *Medicines* **2016**, *3*, 25. [CrossRef]
25. Chang, T.H.; Hsieh, F.L.; Ko, T.P.; Teng, K.H.; Liang, P.H.; Wang, A.H.J. Structure of a heterotetrameric geranyl pyrophosphate synthase from mint (*Mentha piperita*) reveals intersubunit regulation. *Plant Cell* **2010**, *22*, 454–467. [CrossRef] [PubMed]
26. Noriega, P. Terpenes in Essential Oils: Bioactivity and Applications. In *Terpenes and Terpenoids—Recent Advances*; Perveen, S., Al-Taweel, A.M., Eds.; Licensee IntechOpen: London, UK, 2020.
27. Neelam; Khatkar, A.; Sharma, K.K. Phenylpropanoids and its derivatives: Biological activities and its role in food, pharmaceutical and cosmetic industries. *Crit. Rev. Food Sci. Nutr.* **2020**, *60*, 2655–2675. [CrossRef] [PubMed]
28. Liu, H.-W.B.; Begley, T.P. *Comprehensive Natural Products III*, 3rd ed.; Elsevier: Amsterdam, The Netherlands, 2020; ISBN 978-0-08-102691-5.
29. Grassmann, J.; Elstner, E.F. Essential Oils—Properties and Uses. In *Encyclopedia of Food Sciences and Nutrition*; Caballero, B., Ed.; Academic Press: Cambridge, MA, USA, 2003; ISBN 978-0-12-227055-0.
30. Stratakos, A.; Koidis, A. Essential Oils in Food Preservation, Flavor and Safety. In *Methods for Extracting Essential Oils*; Preedy, V.R., Ed.; Academic Press: Cambridge, MA, USA, 2016; pp. 31–38.
31. Silva, M.G.F. Atividade antioxidante e antimicrobiana in vitro de óleos essenciais e extratos hidroalcoólicos de manjerona (*Origanum majorana* L.) e manjerição (*Ocimum basilicum* L.). Bachelor’s Thesis, Graduation Conclusion Work. Federal Technological University of Paraná, Londrina, Brazil, December 2011.
32. Sartor, R.B. *Modelagem, Simulação e Otimização de uma Unidade Industrial de Extração de Óleos Essenciais por Arraste a Vapor*; Universidade Federal do Rio Grande do Sul: Porto Alegre, Brazil, 2009.
33. Masango, P. Cleaner production of essential oils by steam distillation. *J. Clean. Prod.* **2005**, *13*, 833–839. [CrossRef]
34. Luque de Castro, M.D.; García-Ayuso, L.E. Soxhlet extraction of solid materials: An outdated technique with a promising innovative future. *Anal. Chim. Acta* **1998**, *369*, 1–10. [CrossRef]
35. Elyemni, M.; Louaste, B.; Nechad, I.; Elkamli, T.; Bouia, A.; Taleb, M.; Chaouch, M.; Eloutassi, N. Extraction of Essential Oils of *Rosmarinus officinalis* L. by Two Different Methods: Hydrodistillation and Microwave Assisted Hydrodistillation. *Sci. World J.* **2019**, *2019*, 3659432. [CrossRef]
36. Rezaei, K.; Hashemi, N.B.; Sahraee, S. Use of Hydrodistillation as a Green Technology to Obtain Essential Oils From Several Medicinal Plants Belonging to Lamiaceae (Mint) Family. In *Phytopharmaceuticals*; Wiley: Hoboken, NJ, USA, 2021; pp. 59–75. [CrossRef]
37. Atti-Santos, A.C.; Rossato, M.; Serafini, L.A.; Cassel, E.; Moyna, P. Extraction of essential oils from lime (*Citrus latifolia* tanaka) by hydrodistillation and supercritical carbon dioxide. *Brazilian Arch. Biol. Technol.* **2005**, *48*, 155–160. [CrossRef]

38. Baldin, V.P.; Bertin de Lima Scodro, R.; Mariano Fernandez, C.M.; Ieque, A.L.; Caleffi-Ferracioli, K.R.; Dias Siqueira, V.L.; de Almeida, A.L.; Gonçalves, J.E.; Garcia Cortez, D.A.; Cardoso, R.F. Ginger essential oil and fractions against *Mycobacterium* spp. *J. Ethnopharmacol.* **2019**, *244*, 112095. [CrossRef]
39. Fitriady, M.A.; Sulaswatty, A.; Agustian, E.; Salahuddin; Aditama, D.P.F. Steam distillation extraction of ginger essential oil: Study of the effect of steam flow rate and time process. *AIP Conf. Proc.* **2017**, *1803*, 020032-1–020032-10. [CrossRef]
40. Jeliaskova, E.; Zheljaskov, V.D.; Kačaniova, M.; Astatkie, T.; Tekwani, B.L. Sequential elution of essential oil constituents during steam distillation of hops (*Humulus lupulus* L.) and influence on oil yield and antimicrobial activity. *J. Oleo Sci.* **2018**, *67*, 871–883. [CrossRef]
41. Gavahian, M.; Chu, Y.H. Ohmic accelerated steam distillation of essential oil from lavender in comparison with conventional steam distillation. *Innov. Food Sci. Emerg. Technol.* **2018**, *50*, 34–41. [CrossRef]
42. Donelian, A.; Carlson, L.H.C.; Lopes, T.J.; Machado, R.A.F. Comparison of extraction of patchouli (*Pogostemon cablin*) essential oil with supercritical CO<sub>2</sub> and by steam distillation. *J. Supercrit. Fluids* **2009**, *48*, 15–20. [CrossRef]
43. Guzmán, E.; Lucia, A. Essential Oils and Their Individual Components in Cosmetic Products. *Cosmetics* **2021**, *8*, 114. [CrossRef]
44. Sharmeen, J.B.; Mahomoodally, F.M.; Zengin, G.; Maggi, F. Essential oils as natural sources of fragrance compounds for cosmetics and cosmeceuticals. *Molecules* **2021**, *26*, 666. [CrossRef] [PubMed]
45. Carvalho, I.T.; Estevinho, B.N.; Santos, L. Application of microencapsulated essential oils in cosmetic and personal healthcare products—A review. *Int. J. Cosmet. Sci.* **2016**, *38*, 109–119. [CrossRef] [PubMed]
46. Asbahani, A.E.; Miladi, K.; Badri, W.; Sala, M.; Addi, E.H.A.; Casabianca, H.; Mousadik, A.E.; Hartmann, D.; Jilale, A.; Renaud, F.N.R.; et al. Essential oils: From extraction to encapsulation. *Int. J. Pharm.* **2015**, *483*, 220–243. [CrossRef] [PubMed]
47. Li, G.; Xiang, S.; Pan, Y.; Long, X.; Cheng, Y.; Han, L.; Zhao, X. Effects of Cold-Pressing and Hydrodistillation on the Active Non-volatile Components in Lemon Essential Oil and the Effects of the Resulting Oils on Aging-Related Oxidative Stress in Mice. *Front. Nutr.* **2021**, *8*, 1–15. [CrossRef]
48. Menichini, F.; Tundis, R.; Bonesi, M.; De Cindio, B.; Loizzo, M.R.; Conforti, F.; Statti, G.A.; Menabeni, R.; Bettini, R.; Menichini, F. Chemical composition and bioactivity of *Citrus medica* L. cv. Diamante essential oil obtained by hydrodistillation, cold-pressing and supercritical carbon dioxide extraction. *Nat. Prod. Res.* **2011**, *25*, 789–799. [CrossRef] [PubMed]
49. Ferhat, M.A.; Meklati, B.Y.; Chemat, F. Comparison of different isolation methods of essential oil from Citrus fruits: Cold pressing, hydrodistillation and microwave ‘dry’ distillation. *Flavour Fragr. J.* **2007**, *22*, 494–504. [CrossRef]
50. Yousefi, M.; Rahimi-Nasrabadi, M.; Pourmortazavi, S.M.; Wysokowski, M.; Jesionowski, T.; Ehrlich, H.; Mirsadeghi, S. Supercritical fluid extraction of essential oils. *TrAC—Trends Anal. Chem.* **2019**, *118*, 182–193. [CrossRef]
51. De Corato, U.; Maccioni, O.; Trupo, M.; Di Sanzo, G. Use of essential oil of *Laurus nobilis* obtained by means of a supercritical carbon dioxide technique against post harvest spoilage fungi. *Crop Prot.* **2010**, *29*, 142–147. [CrossRef]
52. Irmak, S.; Solakyildirim, K.; Hesenov, A.; Erbatur, O. Study on the stability of supercritical fluid extracted rosemary (*Rosmarinus Officinalis* L.) essential oil. *J. Anal. Chem.* **2010**, *65*, 899–906. [CrossRef]
53. Glisic, S.; Ivanovic, J.; Ristic, M.; Skala, D. Extraction of sage (*Salvia officinalis* L.) by supercritical CO<sub>2</sub>: Kinetic data, chemical composition and selectivity of diterpenes. *J. Supercrit. Fluids* **2010**, *52*, 62–70. [CrossRef]
54. Uquiche, E.; Cirano, N.; Millao, S. Supercritical fluid extraction of essential oil from *Leptocarpha rivularis* using CO<sub>2</sub>. *Ind. Crops Prod.* **2015**, *77*, 307–314. [CrossRef]
55. Zhao, S.; Zhang, D. Supercritical fluid extraction and characterisation of *Moringa oleifera* leaves oil. *Sep. Purif. Technol.* **2013**, *118*, 497–502. [CrossRef]
56. Martínez-Abad, A.; Ramos, M.; Hamzaoui, M.; Kohnen, S.; Jiménez, A.; Garrigós, M.C. Optimisation of sequential microwave-assisted extraction of essential oil and pigment from lemon peels waste. *Foods* **2020**, *9*, 1493. [CrossRef]
57. Ferhat, M.A.; Meklati, B.Y.; Smadja, J.; Chemat, F. An improved microwave Clevenger apparatus for distillation of essential oils from orange peel. *J. Chromatogr. A* **2006**, *1112*, 121–126. [CrossRef]
58. Bayramoglu, B.; Sahin, S.; Sumnu, G. Extraction of essential oil from laurel leaves by using microwaves. *Sep. Sci. Technol.* **2009**, *44*, 722–733. [CrossRef]
59. Lucchesi, M.E.; Smadja, J.; Bradshaw, S.; Louw, W.; Chemat, F. Solvent free microwave extraction of *Elletaria cardamomum* L.: A multivariate study of a new technique for the extraction of essential oil. *J. Food Eng.* **2007**, *79*, 1079–1086. [CrossRef]
60. Filly, A.; Fernandez, X.; Minuti, M.; Visinoni, F.; Cravotto, G.; Chemat, F. Solvent-free microwave extraction of essential oil from aromatic herbs: From laboratory to pilot and industrial scale. *Food Chem.* **2014**, *150*, 193–198. [CrossRef]
61. Okoh, O.O.; Sadimenko, A.P.; Afolayan, A.J. Comparative evaluation of the antibacterial activities of the essential oils of *Rosmarinus officinalis* L. obtained by hydrodistillation and solvent free microwave extraction methods. *Food Chem.* **2010**, *120*, 308–312. [CrossRef]
62. Lucchesi, M.E.; Chemat, F.; Smadja, J. Solvent-free microwave extraction of essential oil from aromatic herbs: Comparison with conventional hydro-distillation. *J. Chromatogr. A* **2004**, *1043*, 323–327. [CrossRef] [PubMed]
63. Sandhu, H.K.; Sinha, P.; Emanuel, N.; Kumar, N.; Sami, R.; Khojah, E.; Al-Mushhin, A.A.M. Effect of ultrasound-assisted pretreatment on extraction efficiency of essential oil and bioactive compounds from citrus waste by-products. *Separations* **2021**, *8*, 244. [CrossRef]
64. Zheng, S.; Zhang, G.; Wang, H.J.; Long, Z.; Wei, T.; Li, Q. Progress in ultrasound-assisted extraction of the value-added products from microorganisms. *World J. Microbiol. Biotechnol.* **2021**, *37*, 1–14. [CrossRef] [PubMed]



65. Ramos, C.; Teixeira, B.; Batista, I.; Matos, O.; Serrano, C.; Neng, N.R.; Nogueira, J.M.F.; Nunes, M.L.; Marques, A. Antioxidant and antibacterial activity of essential oil and extracts of bay laurel *Laurus nobilis* Linnaeus (*Lauraceae*) from Portugal. *Nat. Prod. Res.* **2012**, *26*, 518–529. [CrossRef]
66. Dadalioglu, I.; Evrendilek, G.A. Chemical compositions and antibacterial effects of essential oils of Turkish oregano (*Origanum minutiflorum*), bay laurel (*Laurus nobilis*), Spanish lavender (*Lavandula stoechas* L.), and fennel (*Foeniculum vulgare*) on common foodborne pathogens. *J. Agric. Food Chem.* **2004**, *52*, 8255–8260. [CrossRef]
67. Shaaya, E.; Ravid, U.; Paster, N.; Juven, B.; Zisman, U.; Pissarev, V. Fumigant toxicity of essential oils against four major stored-product insects. *J. Chem. Ecol.* **1991**, *17*, 499–504. [CrossRef]
68. Cosimi, S.; Rossi, E.; Cioni, P.L.; Canale, A. Bioactivity and qualitative analysis of some essential oils from Mediterranean plants against stored-product pests: Evaluation of repellency against *Sitophilus zeamais* Motschulsky, *Cryptolestes ferrugineus* (Stephens) and *Tenebrio molitor* (L.). *J. Stored Prod. Res.* **2009**, *45*, 125–132. [CrossRef]
69. Lawless, J. *The Encyclopedia of Essential Oils: The Complete Guide to the Use of Aromatic Oils In Aromatherapy, Herbalism, Health, and Well Being*; Conari Press: Newburyport, MA, USA, 2013; ISBN 9780007145188.
70. Specos, M.M.M.; Garcia, J.J.; Tornesello, J.; Marino, P.; Vecchia, D.M.; Tesoriero, D.M.V.; Hermida, L.G. Microencapsulated citronella oil for mosquito repellent finishing of cotton textiles. *Trans. R. Soc. Trop. Med. Hyg.* **2010**, *104*, 653–658. [CrossRef]
71. Sakulku, U.; Nuchuchua, O.; Uawongyart, N.; Puttipipatkachorn, S.; Soottitantawat, A.; Ruktanonchai, U. Characterization and mosquito repellent activity of citronella oil nanoemulsion. *Int. J. Pharm.* **2009**, *372*, 105–111. [CrossRef]
72. Tawatsin, A.; Wratten, S.D.; Scott, R.R.; Thavara, U.; Techadamrongsin, Y. Repellency of volatile oils from plants against three mosquito vectors. *J. Vectory Ecol.* **2001**, *26*, 76–82.
73. Nakahara, K.; Alzoreky, N.S.; Yoshihashi, T.; Nguyen, H.T.T.; Trakoontivakorn, G. Chemical Composition and Antifungal Activity of Essential Oil from *Cymbopogon nardus* (*Citronella* Grass). *Jpn. Agric. Res. Q.* **2003**, *37*, 249–252. [CrossRef]
74. Andrade, M.A.; Das Graças Cardoso, M.; Batista, L.R.; Mallet, A.C.T.; Machado, S.M.F. Essential oils of *Cinnamomum zeylanicum*, *Cymbopogon nardus* and *Zingiber officinale*: Composition, antioxidant and antibacterial activities. *Rev. Ciência Agronômica* **2012**, *43*, 399–408. [CrossRef]
75. Simpson, W.J.; Smith, A.R.W. Factors affecting antibacterial activity of hop compounds and their derivatives. *J. Appl. Bacteriol.* **1992**, *72*, 327–334. [CrossRef] [PubMed]
76. Zanolli, P.; Zavatti, M. Pharmacognostic and pharmacological profile of *Humulus lupulus* L. *J. Ethnopharmacol.* **2008**, *116*, 383–396. [CrossRef]
77. Miranda, C.L.; Stevens, J.F.; Helmrich, A.; Henderson, M.C.; Rodriguez, R.J.; Yang, Y.H.; Deinzer, M.L.; Barnes, D.W.; Buhler, D.R. Antiproliferative and cytotoxic effects of prenylated flavonoids from hops (*Humulus lupulus*) in human cancer cell lines. *Food Chem. Toxicol.* **1999**, *37*, 271–285. [CrossRef]
78. Reher, T.; Van Kerckvoorde, V.; Verheyden, L.; Wenseleers, T.; Beliën, T.; Bylemans, D.; Martens, J.A. Evaluation of hop (*Humulus lupulus*) as a repellent for the management of *Drosophila suzukii*. *Crop Prot.* **2019**, *124*, 104839. [CrossRef]
79. Bedini, S.; Flamini, G.; Girardi, J.; Cosci, F.; Conti, B. Not just for beer: Evaluation of spent hops (*Humulus lupulus* L.) as a source of eco-friendly repellents for insect pests of stored foods. *J. Pest Sci.* **2015**, *88*, 583–592. [CrossRef]
80. Abdel-Naime, W.A.; Fahim, J.R.; Fouad, M.A.; Kamel, M.S. Antibacterial, antifungal, and GC–MS studies of *Melissa officinalis*. *S. Afr. J. Bot.* **2019**, *124*, 228–234. [CrossRef]
81. Shakeri, A.; Sahebkar, A.; Javadi, B. *Melissa officinalis* L.—A review of its traditional uses, phytochemistry and pharmacology. *J. Ethnopharmacol.* **2016**, *188*, 204–228. [CrossRef]
82. Moradkhani, H.; Sargsyan, E.; Bibak, H.; Naseri, B.; Sadat-Hosseini, M.; Fayazi-Barjin, A.; Meftahizade, H. *Melissa officinalis* L., a valuable medicine plant: A review. *J. Med. Plants Res.* **2010**, *4*, 2753–2759.
83. Vitalini, S.; Tomè, F.; Fico, G. Traditional uses of medicinal plants in Valvestino (Italy). *J. Ethnopharmacol.* **2009**, *121*, 106–116. [CrossRef] [PubMed]
84. Biswas, K.; Banerjee, R.K.; Bandyopadhyay, U.; Chattopadhyay, I. Biological activities and medicinal properties of Neem (*Azadirachta indica*). *Curr. Sci.* **2001**, *82*, 1336–1445.
85. Schmutterer, H. Properties and Potential of Natural Pesticides from Neem Tree, *Azadirachta Indica*. *Anu. Rev. Entomol.* **1990**, *35*, 271–297. [CrossRef] [PubMed]
86. Rao, A.; Sukumar, S.; Paramasivam, T.; Kamalakshi, S.; Parashuraman, M.; Shantha, A.R. Study of antiviral activity of tender leaves of Margosa tree (*Melia azadirachta*) on vaccinia and variola virus: A preliminary report. *Indian J Med Res.* **1969**, *57*, 495–502. [PubMed]
87. Chopra, I.; Gupta, K.; Nazir, B. Preliminary study of anti-bacterial substances from *Melia azadirachta*. *Indian J. Med. Res.* **1952**, *40*, 511–515. [PubMed]
88. Almas, K. The antimicrobial effects of extracts of *Azadirachta indica* (Neem) and *Salvadora persica* (Arak) chewing sticks. *Indian J. Dent. Res.* **1999**, *10*, 23–26. [PubMed]
89. Salem, N.; Sriti, J.; Bachrouh, O.; Msaada, K.; Khammassi, S.; Hammami, M.; Selmi, S.; Boushah, E.; Ouertani, M.; Hachani, N.; et al. Phenological stage effect on phenolic composition and repellent potential of *Mentha pulegium* against *Tribolium castaneum* and *Lasioderma serricorne*. *Asian Pac. J. Trop. Biomed.* **2018**, *8*, 207–216. [CrossRef]

90. Salem, N.; Bachrouch, O.; Sriti, J.; Msaada, K.; Khammassi, S.; Hammami, M.; Selmi, S.; Boushah, E.; Koorani, S.; Abderraba, M.; et al. Fumigant and repellent potentials of *Ricinus communis* and *Mentha pulegium* essential oils against *Tribolium castaneum* and *Lasioderma serricornis*. *Int. J. Food Prop.* **2018**, *20*, 2899–2913. [CrossRef]
91. Soares, S.F.; Borges, L.M.F.; de Sousa Braga, R.; Ferreira, L.L.; Louly, C.C.B.; Tresvenzol, L.M.F.; de Paula, J.R.; Ferri, P.H. Repellent activity of plant-derived compounds against *Amblyomma cajennense* (Acari: Ixodidae) nymphs. *Vet. Parasitol.* **2010**, *167*, 67–73. [CrossRef]
92. Brahmi, F.; Abdenour, A.; Bruno, M.; Silvia, P.; Alessandra, P.; Danilo, F.; Drifa, Y.G.; Fahmi, E.M.; Khodir, M.; Mohamed, C. Chemical composition and in vitro antimicrobial, insecticidal and antioxidant activities of the essential oils of *Mentha pulegium* L. and *Mentha rotundifolia* (L.) Huds growing in Algeria. *Ind. Crops Prod.* **2016**, *88*, 96–105. [CrossRef]
93. Teixeira, B.; Marques, A.; Ramos, C.; Batista, I.; Serrano, C.; Matos, O.; Neng, N.R.; Nogueira, J.M.F.; Saraiva, J.A.; Nunes, M.L. European pennyroyal (*Mentha pulegium*) from Portugal: Chemical composition of essential oil and antioxidant and antimicrobial properties of extracts and essential oil. *Ind. Crops Prod.* **2012**, *36*, 81–87. [CrossRef]
94. Ait-Ouazzou, A.; Lorán, S.; Arakrak, A.; Laglaoui, A.; Rota, C.; Herrera, A.; Pagán, R.; Conchello, P. Evaluation of the chemical composition and antimicrobial activity of *Mentha pulegium*, *Juniperus phoenicea*, and *Cyperus longus* essential oils from Morocco. *Food Res. Int.* **2012**, *45*, 313–319. [CrossRef]
95. Khaled-Khodja, N.; Boulekbache-Makhlouf, L.; Madani, K. Phytochemical screening of antioxidant and antibacterial activities of methanolic extracts of some Lamiaceae. *Ind. Crops Prod.* **2014**, *61*, 41–48. [CrossRef]
96. Pehlivan Karakaş, F.; Yildirim, A.; Türker, A. Biological screening of various medicinal plant extracts for antibacterial and antitumor activities. *Turk. J. Biol.* **2012**, *36*, 641–652. [CrossRef]
97. Lee, S.W.; Li, G.; Lee, K.S.; Jung, J.S.; Xu, M.L.; Seo, C.S.; Chang, H.W.; Kim, S.K.; Song, D.K.; Son, J.K. Preventive Agents against Sepsis and New Phenylpropanoid Glucosides from the Fruits of *Illicium verum*. *Planta Med.* **2003**, *69*, 861–864. [CrossRef]
98. Ohira, H.; Torii, N.; Aida, T.M.; Watanabe, M.; Smith, R.L. Rapid separation of shikimic acid from Chinese star anise (*Illicium verum* Hook. f.) with hot water extraction. *Sep. Purif. Technol.* **2009**, *69*, 102–108. [CrossRef]
99. Yang, J.F.; Yang, C.H.; Chang, H.W.; Yang, C.S.; Wang, S.M.; Hsieh, M.C.; Chuang, L.Y. Chemical composition and antibacterial activities of *Illicium verum* against antibiotic-resistant pathogens. *J. Med. Food* **2010**, *13*, 1254–1262. [CrossRef]
100. Padmashree, A.; Roopa, N.; Semwal, A.D.; Sharma, G.K.; Agathian, G.; Bawa, A.S. Star-anise (*Illicium verum*) and black caraway (*Carum nigrum*) as natural antioxidants. *Food Chem.* **2007**, *104*, 59–66. [CrossRef]
101. Xin, S.; Xiongmin, L.; Chunlin, F.; Qiuxia, L. Extraction, characterization and antitumor effect of the polysaccharides from star anise (*Illicium verum* Hook. f.). *J. Med. Plants Res.* **2010**, *4*, 2666–2673. [CrossRef]
102. Lee, J.S.; Park, M.A.; Yoon, C.S.; Na, J.H.; Han, J. Characterization and Preservation Performance of Multilayer Film with Insect Repellent and Antimicrobial Activities for Sliced Wheat Bread Packaging. *J. Food Sci.* **2019**, *84*, 3194–3203. [CrossRef]
103. Park, M.A.; Chang, Y.; Choi, I.; Bai, J.; Ja-hyun, N.; Han, J. Development of A Comprehensive Biological Hazard-Proof Packaging Film with Insect-Repellent, Antibacterial, and Antifungal Activities. *J. Food Sci.* **2018**, *83*, 3035–3043. [CrossRef] [PubMed]
104. Brown, J. *Valeriana officinalis*. *Aust. J. Herb. Med.* **2012**, *24*, 136–139. [CrossRef]
105. *Joanne Barnes Herbal Medicines: A Guide for Health Care Professionals*, 2nd ed.; Pharmaceutical Press: London, UK, 1996; ISBN 0853692890.
106. Grant, K.L. Patient education and herbal dietary supplements. *Am. J. Health Pharm.* **2000**, *57*, 1997–2003. [CrossRef] [PubMed]
107. Wang, J.; Zhao, J.; Liu, H.; Zhou, L.; Liu, Z.; Wang, J.; Han, J.; Yu, Z.; Yang, F. Chemical analysis and biological activity of the essential oils of two valerianaceous species from China: *Nardostachys chinensis* and *valeriana officinalis*. *Molecules* **2010**, *15*, 6411–6422. [CrossRef] [PubMed]
108. Khademian, R.; Karimzadeh, F.; Moradi, P.; Asghari, B. Anti-microbial Properties of *Valeriana officinalis*, *Satureja bachtiarica* and *Thymus daenensis* Methanolic Extracts against *Helicobacter pylori*. *J. Pharm. Res. Int.* **2019**, *26*, 1–7. [CrossRef]
109. Holubec, H.; Baines, A.T.; Bayse, J.L.; Waite, S.; Bhattacharyya, A.K.; Clark, L.C.; Payne, C.M.; Earnest, D.L.; Nelson, M.A. Chemoprevention of colon carcinogenesis by dietary selenomethionine. *Gastroenterology* **1998**, *114*, A612.
110. Trombetta, D.; Castelli, F.; Sarpietro, M.G.; Venuti, V.; Cristani, M.; Daniele, C.; Saija, A.; Mazzanti, G.; Bisignano, G. Mechanisms of antibacterial action of three monoterpenes. *Antimicrob. Agents Chemother.* **2005**, *49*, 2474–2478. [CrossRef]
111. Khan, M.T.H.; Ather, A.; Thompson, K.D.; Gambari, R. Extracts and molecules from medicinal plants against herpes simplex viruses. *Antivir. Res.* **2005**, *67*, 107–119. [CrossRef] [PubMed]
112. Peana, A.T.; D’Aquila, P.S.; Panin, F.; Serra, G.; Pippia, P.; Moretti, M.D.L. Anti-inflammatory activity of linalool and linalyl acetate constituents of essential oils. *Phytomedicine* **2002**, *9*, 721–726. [CrossRef]
113. Ziegler, H.L.; Jensen, T.H.; Christensen, J.; Stärk, D.; Hägerstrand, H.; Sittie, A.A.; Olsen, C.E.; Staalsø, T.; Ekpe, P.; Jaroszewski, J.W. Possible artefacts in the in vitro determination of antimalarial activity of natural products that incorporate into lipid bilayer: Apparent antiplasmodial activity of dehydroabietinol, a constituent of *Hyptis suaveolens*. *Planta Med.* **2002**, *68*, 547–549. [CrossRef]
114. Sienkiewicz, M.; Głowacka, A.; Poznańska-Kurowska, K.; Kaszuba, A.; Urbaniak, A.; Kowalczyk, E. The effect of clary sage oil on staphylococci responsible for wound infections. *Postep. Dermatol. I Alergol.* **2015**, *32*, 21–26. [CrossRef] [PubMed]
115. Fujita, K.I.; Chavasiri, W.; Kubo, I. Anti-Salmonella Activity of Volatile Compounds of Vietnam Coriander. *Phyther. Res.* **2015**, *29*, 1081–1087. [CrossRef] [PubMed]

116. Wan, J.; Wilcock, A.; Coventry, M.J. The effect of essential oils of basil on the growth of *Aeromonas hydrophila* and *Pseudomonas fluorescens*. *J. Appl. Microbiol.* **1998**, *84*, 152–158. [CrossRef] [PubMed]
117. Takarada, K.; Kimizuka, R.; Takahashi, N.; Honma, K.; Okuda, K.; Kato, T. A comparison of the antibacterial efficacies of essential oils against oral pathogens. *Oral Microbiol. Immunol.* **2004**, *19*, 61–64. [CrossRef] [PubMed]
118. Hammer, K.A.; Dry, L.; Johnson, M.; Michalak, E.M.; Carson, C.F.; Riley, T.V. Susceptibility of oral bacteria to *Melaleuca alternifolia* (tea tree) oil in vitro. *Oral Microbiol. Immunol.* **2003**, *18*, 389–392. [CrossRef]
119. Hammer, K.A.; Carson, C.F.; Riley, T.V. Antifungal activity of the components of *Melaleuca alternifolia* (tea tree) oil. *J. Appl. Microbiol.* **2003**, *95*, 853–860. [CrossRef]
120. Deans, S.G.; Ritchie, G. Antibacterial properties of plant essential oils. *Int. J. Food Microbiol.* **1987**, *5*, 165–180. [CrossRef]
121. Samber, N.; Khan, A.; Varma, A.; Manzoor, N. Synergistic anti-candidal activity and mode of action of *Mentha piperita* essential oil and its major components. *Pharm. Biol.* **2015**, *53*, 1496–1504. [CrossRef]
122. Mejía-Garibay, B.; Palou, E.; López-Malo, A. Composition, Diffusion, and Antifungal Activity of Black Mustard (*Brassica nigra*) Essential Oil When Applied by Direct Addition or Vapor Phase Contact. *J. Food Prot.* **2015**, *78*, 843–848. [CrossRef]
123. Prakash, B.; Singh, P.; Goni, R.; Raina, A.K.P.; Dubey, N.K. Efficacy of *Angelica archangelica* essential oil, phenyl ethyl alcohol and  $\alpha$ -terpineol against isolated molds from walnut and their anti-aflatoxigenic and antioxidant activity. *J. Food Sci. Technol.* **2015**, *52*, 2220–2228. [CrossRef]
124. Trindade, L.A.; de Araújo Oliveira, J.; de Castro, R.D.; de Oliveira Lima, E. Inhibition of adherence of *C. albicans* to dental implants and cover screws by *Cymbopogon nardus* essential oil and citronellal. *Clin. Oral Investig.* **2015**, *19*, 2223–2231. [CrossRef] [PubMed]
125. Barkatullah; Ibrar, M.; Muhammad, N.; De Feo, V. Chemical composition and biological activities of the essential oil of *Skimmia laureola* leaves. *Molecules* **2015**, *20*, 4735–4745. [CrossRef] [PubMed]
126. Mahboubi, M.; Kazempour, N. The antifungal activity of *Artemisia sieberi* essential oil from different localities of Iran against dermatophyte fungi. *J. Mycol. Med.* **2015**, *25*, 65–71. [CrossRef] [PubMed]
127. Baratta, M.T.; Damien, H.J.; Deans, S.G.; Biondi, D.M.; Ruberto, G. Chemical composition, antimicrobial and antioxidative activity of laurel, sage, rosemary, oregano and coriander essential oils. *J. Essent. Oil Res.* **1998**, *10*, 618–627. [CrossRef]
128. Gkinis, G.; Tzakou, O.; Iliopoulou, D.; Roussis, V. Chemical Composition and Biological Activity of *Nepeta parnassica* Oils and Isolated Nepetalactones. *Z. Für Nat. C.* **2003**, *58*, 681–686. [CrossRef]
129. Grunfeld, E.; Gresty, M.A. Relationship between motion sickness, migraine and menstruation in crew members of a “round the world” yacht race. *Brain Res. Bull.* **1998**, *47*, 433–436. [CrossRef]
130. Howes, M.-J.R.; Houghton, P.J.; Barlow, D.J.; Pocock, V.J.; Milligan, S.R. Assessment of estrogenic activity in some common essential oil constituents. *J. Pharm. Pharmacol.* **2010**, *54*, 1521–1528. [CrossRef]
131. Ali, B.; Al-Wabel, N.A.; Shams, S.; Ahamad, A.; Khan, S.A.; Anwar, F. Essential oils used in aromatherapy: A systemic review. *Asian Pac. J. Trop. Biomed.* **2015**, *5*, 601–611. [CrossRef]
132. Bhalla, Y.; Gupta, V.K.; Jaitak, V. Anticancer activity of essential oils: A review. *J. Sci. Food Agric.* **2013**, *93*, 3643–3653. [CrossRef]
133. Edris, A.E. Pharmaceutical and Therapeutic Potentials of Essential Oils and Their Individual Volatile Constituents: A Review. *Phyther. Res.* **2007**, *21*, 308–323. [CrossRef]
134. Jaganathan, S.K.; Supriyanto, E. Antiproliferative and Molecular Mechanism of Eugenol-Induced Apoptosis in Cancer Cells. *Molecules* **2012**, *17*, 6290–6304. [CrossRef] [PubMed]
135. Gupta, S.; Khan, S.; Muzafar, M.; Kushwaha, M.; Yadav, A.K.; Gupta, A.P. Encapsulation: Entrapping essential oil/flavors/aromas in food. In *Encapsulations*; Grumezescu, A.M., Ed.; Elsevier: Amsterdam, The Netherlands, 2016; pp. 229–268. ISBN 9780128043073.
136. Reis, D.R.; Ambrosi, A.; Luccio, M. Di Encapsulated essential oils: A perspective in food preservation. *Future Foods* **2022**. [CrossRef]
137. Ribeiro-Santos, R.; Andrade, M.; Sanches-Silva, A. Application of encapsulated essential oils as antimicrobial agents in food packaging. *Curr. Opin. Food Sci.* **2017**, *14*, 78–84. [CrossRef]
138. Zinoviadou, K.G.; Koutsoumanis, K.P.; Biliaderis, C.G. Physico-chemical properties of whey protein isolate films containing oregano oil and their antimicrobial action against spoilage flora of fresh beef. *Meat Sci.* **2009**, *82*, 338–345. [CrossRef]
139. Suppakul, P.; Sonneveld, K.; Bigger, S.W.; Miltz, J. Efficacy of polyethylene-based antimicrobial films containing principal constituents of basil. *LWT—Food Sci. Technol.* **2008**, *41*, 779–788. [CrossRef]
140. Vu, K.D.; Hollingsworth, R.G.; Leroux, E.; Salmieri, S.; Lacroix, M. Development of edible bioactive coating based on modified chitosan for increasing the shelf life of strawberries. *Food Res. Int.* **2011**, *44*, 198–203. [CrossRef]
141. De Melo, A.A.M.; Geraldine, R.M.; Silveira, M.F.A.; Lopes, M.C.; Silva, C.; Fernandes, T.H.; Oliveira, A.N. De Microbiological Quality and Other Characteristics of Refrigerated Chicken Meat in Contact with Cellulose Acetate-based Film Incorporated with Rosemary Essential Oil. *Braz. J. Microbiol.* **2012**, *16*, 1419–1427. [CrossRef]
142. Souza, A.C.; Goto, G.E.O.; Mainardi, J.A.; Coelho, A.C.V.; Tadini, C.C. Cassava starch composite films incorporated with cinnamon essential oil: Antimicrobial activity, microstructure, mechanical and barrier properties. *LWT—Food Sci. Technol.* **2013**, *54*, 346–352. [CrossRef]
143. Aburjai, T.; Natsheh, F.M. Plants Used in Cosmetics. *Phyther. Res.* **2003**, *17*, 987–1000. [CrossRef]
144. Minozzo, M.; Steffens, J.; Backes, G.T.; Paroul, N.; Cansian, R.L. Biological potential and microencapsulation of *Cinnamomum cassia* essential oil as an alternative for pest control in stored maize. *Res. Soc. Dev.* **2021**, *10*, e530101422334. [CrossRef]

145. Malešević, V.K.; Vaštag, Ž.; Radulović-Popović, L.; Senka, M.P.; Peričin-Starčević, I. Microencapsulation technology and essential oil pesticides for food plant production. In *Essential Oils in Food Preservation, Flavor and Safety*; Preedy, V.R., Ed.; Academic Press: Cambridge, MA, USA, 2016; pp. 123–129. ISBN 9780124166448.
146. Govindarajan, M.; Sivakumar, R. Laboratory evaluation of Indian medicinal plants as repellents against malaria, dengue, and filariasis vector mosquitoes. *Parasitol. Res.* **2015**, *114*, 601–612. [CrossRef] [PubMed]
147. Khanna, S.; Chakraborty, J.N. Mosquito repellent activity of cotton functionalized with inclusion complexes of  $\beta$ -cyclodextrin citrate and essential oils. *Fash. Text.* **2018**, *5*, 1–18. [CrossRef]
148. Soroh, A.; Owen, L.; Rahim, N.; Masania, J.; Abioye, A.; Qutachi, O.; Goodyer, L.; Shen, J.; Laird, K. Microemulsification of essential oils for the development of antimicrobial and mosquito repellent functional coatings for textiles. *J. Appl. Microbiol.* **2021**, *131*, 2808–2820. [CrossRef] [PubMed]
149. Bezerra, F.M.; Carmona, O.G.; Carmona, C.G.; Lis, M.J.; de Moraes, F.F. Controlled release of microencapsulated citronella essential oil on cotton and polyester matrices. *Cellulose* **2016**, *23*, 1459–1470. [CrossRef]
150. Sarişik, M.; Kartal, G.E.; Erkan, G.; Etkeser, S. Alternative methods for transferring mosquito repellent capsules containing bio-based citronella oil to upholstery fabrics: Coating and printing. *J. Coat. Technol. Res.* **2022**, *19*, 323–336. [CrossRef]
151. Singh, M.N.; Hemant, K.S.Y.; Ram, M.; Shivakumar, H.G. Microencapsulation: A promising technique for controlled drug delivery. *Res. Pharm. Sci.* **2010**, *5*, 65–77.
152. Gonçalves, A.; Estevinho, B.N.; Rocha, F. Microencapsulation of vitamin A: A review. *Trends Food Sci. Technol.* **2016**, *51*, 76–87. [CrossRef]
153. Dubey, R.; Shami, T.C.; Rao, K.U.B. Microencapsulation Technology and Applications. *Def. Sci. J.* **2009**, *59*, 82–95. [CrossRef]
154. Paulo, F.; Santos, L. Design of experiments for microencapsulation applications: A review. *Mater. Sci. Eng. C* **2017**, *77*, 1327–1340. [CrossRef]
155. Mehta, N.; Kumar, P.; Verma, A.K.; Umaraw, P.; Kumar, Y.; Malav, O.P.; Sazili, A.Q.; Lorenzo, J.M. Microencapsulation as a Noble Technique for the Application of Bioactive Compounds in the Food Industry: A Comprehensive Review. *Appl. Sci.* **2022**, *12*, 1424. [CrossRef]
156. Nesterenko, A.; Alric, I.; Silvestre, F.; Durrieu, V. Vegetable proteins in microencapsulation: A review of recent interventions and their effectiveness. *Ind. Crops Prod.* **2013**, *42*, 469–479. [CrossRef]
157. Petrusic, S.; Koncar, V. Controlled release of active agents from microcapsules embedded in textile structures. In *Smart Textiles and Their Applications*; Koncar, V., Ed.; Elsevier: Amsterdam, The Netherlands, 2016; pp. 89–114. ISBN 9780081005835.
158. Zhang, Y.; Rochefort, D. Characterisation and applications of microcapsules obtained by interfacial polycondensation. *J. Microencapsul.* **2012**, *29*, 636–649. [CrossRef] [PubMed]
159. Hoyos-Leyva, J.D.; Bello-Pérez, L.A.; Alvarez-Ramirez, J.; Garcia, H.S. Microencapsulation using starch as wall material: A review. *Food Rev. Int.* **2018**, *34*, 148–161. [CrossRef]
160. Jamekhorshid, A.; Sadrameli, S.M.; Farid, M. A review of microencapsulation methods of phase change materials (PCMs) as a thermal energy storage (TES) medium. *Renew. Sustain. Energy Rev.* **2014**, *31*, 531–542. [CrossRef]
161. Fang, Z.; Bhandari, B. Encapsulation of polyphenols—A review. *Trends Food Sci. Technol.* **2010**, *21*, 510–523. [CrossRef]
162. McClements, D.J.; Decker, E.A.; Park, Y.; Weiss, J. Structural design principles for delivery of bioactive components in nutraceuticals and functional foods. *Crit. Rev. Food Sci. Nutr.* **2009**, *49*, 577–606. [CrossRef]
163. Augustin, M.A.; Sanguansri, L.; Bode, O. Maillard reaction products as encapsulants for fish oil powders. *J. Food Sci.* **2006**, *71*, E25–E32. [CrossRef]
164. Li, M.; Rouaud, O.; Poncelet, D. Microencapsulation by solvent evaporation: State of the art for process engineering approaches. *Int. J. Pharm.* **2008**, *363*, 26–39. [CrossRef]
165. O'Donnell, P.B.; McGinity, J.W. Preparation of microspheres by the solvent evaporation technique. *Adv. Drug Deliv. Rev.* **1997**, *28*, 25–42. [CrossRef]
166. Bakry, A.M.; Abbas, S.; Ali, B.; Majeed, H.; Abouelwafa, M.Y.; Mousa, A.; Liang, L. Microencapsulation of Oils: A Comprehensive Review of Benefits, Techniques, and Applications. *Compr. Rev. Food Sci. Food Saf.* **2016**, *15*, 143–182. [CrossRef]
167. Timilsena, Y.P.; Akanbi, T.O.; Khalid, N.; Adhikari, B.; Barrow, C.J. Complex coacervation: Principles, mechanisms and applications in microencapsulation. *Int. J. Biol. Macromol.* **2019**, *121*, 1276–1286. [CrossRef] [PubMed]
168. Hwang, J.; Kim, J.; Wee, Y.; Yun, J.; Jang, H.; Kim, S.; Ryu, H. Preparation and characterization of melamine-formaldehyde resin microcapsules containing fragrant oil. *Biotechnol. Bioprocess Eng.* **2006**, *11*, 332–336. [CrossRef]
169. Chung, S.K.; Seo, J.Y.; Lim, J.H.; Park, H.H.; Yea, M.J.; Park, H.J. Microencapsulation of essential oil for insect repellent in food packaging system. *J. Food Sci.* **2013**, *78*, E709–E714. [CrossRef] [PubMed]
170. Sánchez-Navarro, M.M.; Cuesta-Garrote, N.; Arán-Áis, F.; Orgilés-Barceló, C. Microencapsulation of melaleuca alternifolia (tea tree) oil as biocide for footwear applications. *J. Dispers. Sci. Technol.* **2011**, *32*, 1722–1727. [CrossRef]
171. Long, Y.; York, D.; Zhang, Z.; Preece, J.A. Microcapsules with low content of formaldehyde: Preparation and characterization. *J. Mater. Chem.* **2009**, *19*, 6882–6887. [CrossRef]
172. Bansode, S.S.; Banarjee, S.K.; Gaikwad, D.D.; Jadhav, S.L.; Thorat, R.M. Microencapsulation: A review. *Int. J. Pharm. Sci. Rev. Res.* **2010**, *1*, 38–43.
173. Lam, P.L.; Gambari, R. Advanced progress of microencapsulation technologies: In vivo and in vitro models for studying oral and transdermal drug deliveries. *J. Control. Release* **2014**, *178*, 25–45. [CrossRef]

174. Huang, H.J.; Chen, X.D.; Yuan, W.K. Microencapsulation based on emulsification for producing pharmaceutical products: A literature review. *Dev. Chem. Eng. Miner. Process.* **2006**, *14*, 515–544. [CrossRef]
175. Estevinho, B.N.; Rocha, F.; Santos, L.; Alves, A. Microencapsulation with chitosan by spray drying for industry applications—A review. *Trends Food Sci. Technol.* **2013**, *31*, 138–155. [CrossRef]
176. Gharsallaoui, A.; Roudaut, G.; Chambin, O.; Voilley, A.; Saurel, R. Applications of spray-drying in microencapsulation of food ingredients: An overview. *Food Res. Int.* **2007**, *40*, 1107–1121. [CrossRef]
177. Mohammed, N.K.; Tan, C.P.; Manap, Y.A.; Muhiadin, B.J.; Hussin, A.S.M. Spray Drying for the Encapsulation of Oils—A Review. *Molecules* **2020**, *25*, 3873. [CrossRef] [PubMed]
178. Hazarika, U.; Gosztola, B. Lyophilization and its Effects on the Essential Oil Content and Composition of Herbs and Spices—A Review. *Acta Sci. Pol. Technol. Aliment.* **2020**, *19*, 467–473. [CrossRef]
179. Gardeli, C.; Evageliou, V.; Poulos, C.; Yanniotis, S.; Komaitis, M. Drying of fennel plants: Oven, freeze drying, effect of freeze-drying time, and use of biopolymers. *Dry. Technol.* **2010**, *28*, 542–549. [CrossRef]
180. Vujanović, M.D.; Đurović, S.D.; Radojković, M.M. Chemical Composition of Essential Oils of Elderberry (*Sambucus Nigra* L.) Flowers and Fruits. *Acta Period. Technol.* **2021**, *52*, 229–237. [CrossRef]
181. de Araújo, J.S.F.; de Souza, E.L.; Oliveira, J.R.; Gomes, A.C.A.; Kotzebue, L.R.V.; da Silva Agostini, D.L.; de Oliveira, D.L.V.; Mazzetto, S.E.; da Silva, A.L.; Cavalcanti, M.T. Microencapsulation of sweet orange essential oil (*Citrus aurantium* var. *dulcis*) by lyophilization using maltodextrin and maltodextrin/gelatin mixtures: Preparation, characterization, antimicrobial and antioxidant activities. *Int. J. Biol. Macromol.* **2020**, *143*, 991–999. [CrossRef] [PubMed]
182. Sebaaly, C.; Greige-Gerges, H.; Stainmesse, S.; Fessi, H.; Charcosset, C. Effect of composition, hydrogenation of phospholipids and lyophilization on the characteristics of eugenol-loaded liposomes prepared by ethanol injection method. *Food Biosci.* **2016**, *15*, 1–10. [CrossRef]
183. Cocero, M.J.; Martín, Á.; Mattea, F.; Varona, S. Encapsulation and co-precipitation processes with supercritical fluids: Fundamentals and applications. *J. Supercrit. Fluids* **2009**, *47*, 546–555. [CrossRef]
184. Jyothi, N.V.N.; Prasanna, P.M.; Sakarkar, S.N.; Prabha, K.S.; Ramaiah, P.S.; Srawan, G.Y. Microencapsulation techniques, factors influencing encapsulation efficiency. *J. Microencapsul.* **2010**, *27*, 187–197. [CrossRef]
185. Zhang, S.; Kawakami, K.; Yamamoto, M.; Masaoka, Y.; Kataoka, M.; Yamashita, S.; Sakuma, S. Coaxial electrospray formulations for improving oral absorption of a poorly water-soluble drug. *Mol. Pharm.* **2011**, *8*, 807–813. [CrossRef]
186. Koo, S.Y.; Cha, K.H.; Song, D.G.; Chung, D.; Pan, C.H. Microencapsulation of peppermint oil in an alginate-pectin matrix using a coaxial electrospray system. *Int. J. Food Sci. Technol.* **2014**, *49*, 733–739. [CrossRef]
187. Zhang, L.; Huang, J.; Si, T.; Xu, R.X. Coaxial electrospray of microparticles and nanoparticles for biomedical applications. *Expert Rev. Med. Devices* **2012**, *9*, 595–612. [CrossRef] [PubMed]
188. Lastow, O.; Balachandran, W. Numerical simulation of electrohydrodynamic (EHD) atomization. *J. Electrostat.* **2006**, *64*, 850–859. [CrossRef]
189. Anwar, S.H.; Kunz, B. The influence of drying methods on the stabilization of fish oil microcapsules: Comparison of spray granulation, spray drying, and freeze drying. *J. Food Eng.* **2011**, *105*, 367–378. [CrossRef]
190. Teunou, E.; Poncelet, D. Fluid-Bed Coating. In *Encapsulated and Powdered Foods*; Onwulata, C., Ed.; Taylor & Francis: Abingdon, UK, 2005; p. 18. ISBN 9780429120152.
191. Desai, K.G.H.; Jin Park, H. Recent developments in microencapsulation of food ingredients. *Dry. Technol.* **2005**, *23*, 1361–1394. [CrossRef]
192. Sadovoy, A.V.; Lomova, M.V.; Antipina, M.N.; Braun, N.A.; Sukhorukov, G.B.; Kiryukhin, M.V. Layer-by-layer assembled multilayer shells for encapsulation and release of fragrance. *ACS Appl. Mater. Interfaces* **2013**, *5*, 8948–8954. [CrossRef] [PubMed]
193. Xie, Y.L.; Wang, M.J.; Yao, S.J. Preparation and characterization of biocompatible microcapsules of sodium cellulose sulfate/chitosan by means of layer-by-layer self-assembly. *Langmuir* **2009**, *25*, 8999–9005. [CrossRef] [PubMed]
194. Ge, L.; Tan, X.; Sheng, R.; Xiao, J. Layer-by-layer self-assembly of giant polyelectrolyte microcapsules templated by microbubbles as potential hydrophilic or hydrophobic drug delivery system. *Colloids Interface Sci. Commun.* **2022**, *47*. [CrossRef]
195. Zhang, Z.; Zhang, S.; Su, R.; Xiong, D.; Feng, W.; Chen, J. Controlled Release Mechanism and Antibacterial Effect of Layer-By-Layer Self-Assembly Thyme Oil Microcapsule. *J. Food Sci.* **2019**, *84*, 1427–1438. [CrossRef]
196. Pan, H.M.; Subramanian, A.; Ochs, C.J.; Dewavrin, J.Y.; Beyer, S.; Trau, D.W. Edible polyelectrolyte microcapsules with water-soluble cargo assembled in organic phase. *RSC Adv.* **2014**, *4*, 35163–35166. [CrossRef]
197. Verma, G.; Hassan, P.A. Self assembled materials: Design strategies and drug delivery perspectives. *Phys. Chem. Chem. Phys.* **2013**, *15*, 17016–17028. [CrossRef]
198. Aguiar, M.C.S.; das Graças Fernandes da Silva, M.F.; Fernandes, J.B.; Forim, M.R. Evaluation of the microencapsulation of orange essential oil in biopolymers by using a spray-drying process. *Sci. Rep.* **2020**, *10*, 1–11. [CrossRef] [PubMed]
199. Martins, I.M.; Barreiro, M.F.; Coelho, M.; Rodrigues, A.E. Microencapsulation of essential oils with biodegradable polymeric carriers for cosmetic applications. *Chem. Eng. J.* **2014**, *245*, 191–200. [CrossRef]
200. Scarfato, P.; Avallone, E.; Iannelli, P.; De Feo, V.; Acierno, D. Synthesis and characterization of polyurea microcapsules containing essential oils with antigerminative activity. *J. Appl. Polym. Sci.* **2007**, *105*, 3568–3577. [CrossRef]
201. Bagle, A.V.; Jadhav, R.S.; Gite, V.V.; Hundiwal, D.G.; Mahulikar, P.P. Controlled release study of phenol formaldehyde microcapsules containing neem oil as an insecticide. *Int. J. Polym. Mater. Polym. Biomater.* **2013**, *62*, 421–425. [CrossRef]

202. Ahsaei, S.M.; Rodríguez-Rojo, S.; Salgado, M.; Cocero, M.J.; Talebi-Jahromi, K.; Amoabediny, G. Insecticidal activity of spray dried microencapsulated essential oils of *Rosmarinus officinalis* and *Zataria multiflora* against *Tribolium confusum*. *Crop Prot.* **2020**, *128*, 104996. [CrossRef]
203. Fernandes, R.V.D.B.; Borges, S.V.; Botrel, D.A. Gum arabic/starch/maltodextrin/inulin as wall materials on the microencapsulation of rosemary essential oil. *Carbohydr. Polym.* **2014**, *101*, 524–532. [CrossRef]
204. Chitprasert, P.; Sutaphanit, P. Holy basil (*ocimum sanctum* linn.) Essential oil delivery to swine gastrointestinal tract using gelatin microcapsules coated with aluminum carboxymethyl cellulose and beeswax. *J. Agric. Food Chem.* **2014**, *62*, 12641–12648. [CrossRef]
205. Munhuweyi, K.; Caleb, O.J.; van Reenen, A.J.; Opara, U.L. Physical and antifungal properties of  $\beta$ -cyclodextrin microcapsules and nanofibre films containing cinnamon and oregano essential oils. *LWT—Food Sci. Technol.* **2018**, *87*, 413–422. [CrossRef]
206. Leimann, F.V.; Gonçalves, O.H.; Machado, R.A.F.; Bolzan, A. Antimicrobial activity of microencapsulated lemongrass essential oil and the effect of experimental parameters on microcapsules size and morphology. *Mater. Sci. Eng. C* **2009**, *29*, 430–436. [CrossRef]
207. Li, R.; Jiang, S.; Jiang, Z.T.  $\beta$ -Cyclodextrin supramolecular microcapsules and antioxidant activity of *Laurus nobilis* essential oil. *J. Essent. Oil-Bear. Plants* **2017**, *20*, 1511–1524. [CrossRef]
208. Li, Y.; Wu, C.; Wu, T.; Wang, L.; Chen, S.; Ding, T.; Hu, Y. Preparation and characterization of citrus essential oils loaded in chitosan microcapsules by using different emulsifiers. *J. Food Eng.* **2018**, *217*, 108–114. [CrossRef]
209. Mehran, M.; Masoum, S.; Memarzadeh, M. Microencapsulation of *Mentha spicata* essential oil by spray drying: Optimization, characterization, release kinetics of essential oil from microcapsules in food models. *Ind. Crops Prod.* **2020**, *154*, 112694. [CrossRef]
210. Adepu, S.; Khandelwal, M. Bacterial cellulose with microencapsulated antifungal essential oils: A novel double barrier release system. *Materialia* **2020**, *9*, 100585. [CrossRef]
211. Ribeiro, A.D.; Marques, J.; Forte, M.; Correia, F.C.; Parpot, P.; Oliveira, C.; Pereira, A.I.; Andrade, L.; Azenha, C.; Mendes, A.; et al. Microencapsulation of citronella oil for solar-activated controlled release as an insect repellent. *Appl. Mater. Today* **2016**, *5*, 90–97. [CrossRef]
212. Lai, H.; Liu, Y.; Huang, G.; Chen, Y.; Song, Y.; Ma, Y.Q.; Yue, P. Fabrication and antibacterial evaluation of peppermint oil-loaded composite microcapsules by chitosan-decorated silica nanoparticles stabilized Pickering emulsion templating. *Int. J. Biol. Macromol.* **2021**, *183*, 2314–2325. [CrossRef]
213. Tang, C.; Li, Y.; Pun, J.; Mohamed Osman, A.S.; Tam, K.C. Polydopamine microcapsules from cellulose nanocrystal stabilized Pickering emulsions for essential oil and pesticide encapsulation. *Colloids Surf. A Physicochem. Eng. Asp.* **2019**, *570*, 403–413. [CrossRef]
214. Cai, C.; Ma, R.; Duan, M.; Lu, D. Preparation and antimicrobial activity of thyme essential oil microcapsules prepared with gum arabic. *RSC Adv.* **2019**, *9*, 19740–19747. [CrossRef]
215. Emadzadeh, B.; Ghorani, B.; Naji-Tabasi, S.; Charpashlo, E.; Molaveisi, M. Fate of  $\beta$ -cyclodextrin-sugar beet pectin microcapsules containing garlic essential oil in an acidic food beverage. *Food Biosci.* **2021**, *42*, 101029. [CrossRef]
216. de Medeiros, J.A.S.; Blick, A.P.; Galindo, M.V.; Alvim, I.D.; Yamashita, F.; Ueno, C.T.; Shirai, M.A.; Grosso, C.R.F.; Corradini, E.; Sakanaka, L.S. Incorporation of Oregano Essential Oil Microcapsules in Starch-Poly (Butylene Adipate Co-Terephthalate) (PBAT) Films. *Macromol. Symp.* **2019**, *383*, 1800052. [CrossRef]
217. Ngamekaue, N.; Chitprasert, P. Effects of beeswax-carboxymethyl cellulose composite coating on shelf-life stability and intestinal delivery of holy basil essential oil-loaded gelatin microcapsules. *Int. J. Biol. Macromol.* **2019**, *135*, 1088–1097. [CrossRef]
218. De Matos, E.F.; Scopel, B.S.; Dettmer, A. Citronella essential oil microencapsulation by complex coacervation with leather waste gelatin and sodium alginate. *J. Environ. Chem. Eng.* **2018**, *6*, 1989–1994. [CrossRef]
219. Xiao, Z.; Liu, W.; Zhu, G.; Zhou, R.; Niu, Y. Production and characterization of multinuclear microcapsules encapsulating lavender oil by complex coacervation. *Flavour Fragr. J.* **2014**, *29*, 166–172. [CrossRef]
220. Baiocco, D.; Preece, J.A.; Zhang, Z. Microcapsules with a fungal chitosan-gum Arabic-maltodextrin shell to encapsulate health-beneficial peppermint oil. *Food Hydrocoll. Health* **2021**, *1*, 100016. [CrossRef]
221. Dima, C.; Cotârlet, M.; Alexe, P.; Dima, S. Microencapsulation of essential oil of pimento [*Pimenta dioica* (L) Merr.] by chitosan/k-carrageenan complex coacervation method. *Innov. Food Sci. Emerg. Technol.* **2014**, *22*, 203–211. [CrossRef]
222. Hernández-Nava, R.; López-Malo, A.; Palou, E.; Ramírez-Corona, N.; Jiménez-Munguía, M.T. Encapsulation of oregano essential oil (*Origanum vulgare*) by complex coacervation between gelatin and chia mucilage and its properties after spray drying. *Food Hydrocoll.* **2020**, *109*, 106077. [CrossRef]
223. Qiu, L.; Zhang, M.; Adhikari, B.; Chang, L. Microencapsulation of rose essential oil in mung bean protein isolate-apricot peel pectin complex coacervates and characterization of microcapsules. *Food Hydrocoll.* **2022**, *124*, 107366. [CrossRef]
224. Chen, K.; Zhang, M.; Adhikari, B.; Wang, M. Microencapsulation of Sichuan pepper essential oil in soybean protein isolate-Sichuan pepper seed soluble dietary fiber complex coacervates. *Food Hydrocoll.* **2022**, *125*, 107421. [CrossRef]
225. Rojas-Moreno, S.; Cárdenas-Bailón, F.; Osorio-Revilla, G.; Gallardo-Velázquez, T.; Proal-Nájera, J. Effects of complex coacervation-spray drying and conventional spray drying on the quality of microencapsulated orange essential oil. *J. Food Meas. Charact.* **2018**, *12*, 650–660. [CrossRef]
226. Li, Y.; Liu, J.; He, X.; Kong, D.; Zhou, C.; Wu, H.; Yang, Z.; Yang, Z.; Hu, Y. Preparation of Cinnamon Oil-Loaded Antibacterial Composite Microcapsules by In Situ Polymerization of Pickering Emulsion Templates. *Macromol. Mater. Eng.* **2020**, *305*, 1900851. [CrossRef]

227. Revuelta, M.V.; Bogdan, S.; Gámez-Espinosa, E.; Deyá, M.C.; Romagnoli, R. Green antifungal waterborne coating based on essential oil microcapsules. *Prog. Org. Coat.* **2021**, *151*, 106101. [CrossRef]
228. Matulyte, I.; Kasparaviciene, G.; Bernatoniene, J. Development of new formula microcapsules from nutmeg essential oil using sucrose esters and magnesium aluminometasilicate. *Pharmaceutics* **2020**, *12*, 628. [CrossRef] [PubMed]
229. Dolça, C.; Ferrándiz, M.; Capablanca, L.; Franco, E.; Mira, E.; López, F.; García, D. Microencapsulation of Rosemary Essential Oil by Co-Extrusion/Gelling Using Alginate as a Wall Material. *J. Encapsulation Adsorpt. Sci.* **2015**, *5*, 121–130. [CrossRef]
230. Yingngam, B.; Kacha, W.; Rungseevijitprapa, W.; Sudta, P.; Prasitpuriprecha, C.; Brantner, A. Response surface optimization of spray-dried citronella oil microcapsules with reduced volatility and irritation for cosmetic textile uses. *Powder Technol.* **2019**, *355*, 372–385. [CrossRef]
231. Maulidna; Wirjosentono, B.; Tamrin; Marpaung, L. Microencapsulation of ginger-based essential oil (*Zingiber cassumunar roxb*) with chitosan and oil palm trunk waste fiber prepared by spray-drying method. *Case Stud. Therm. Eng.* **2020**, *18*, 100606. [CrossRef]
232. Ren, W.; Tian, G.; Zhao, S.; Yang, Y.; Gao, W.; Zhao, C.; Zhang, H.; Lian, Y.; Wang, F.; Du, H.; et al. Effects of spray-drying temperature on the physicochemical properties and polymethoxyflavone loading efficiency of citrus oil microcapsules. *LWT—Food Sci. Technol.* **2020**, *133*, 109954. [CrossRef]
233. Bajac, J.; Nikolovski, B.; Lončarević, I.; Petrović, J.; Bajac, B.; Đurović, S.; Petrović, L. Microencapsulation of juniper berry essential oil (*Juniperus communis* L.) by spray drying: Microcapsule characterization and release kinetics of the oil. *Food Hydrocoll.* **2022**, *125*, 107430. [CrossRef]
234. Hu, Q.; Li, X.; Chen, F.; Wan, R.; Yu, C.W.; Li, J.; McClements, D.J.; Deng, Z. Microencapsulation of an essential oil (cinnamon oil) by spray drying: Effects of wall materials and storage conditions on microcapsule properties. *J. Food Process. Preserv.* **2020**, *44*, e14805. [CrossRef]
235. Asensio, C.M.; Paredes, A.J.; Martin, M.P.; Allemandi, D.A.; Nepote, V.; Grosso, N.R. Antioxidant Stability Study of Oregano Essential Oil Microcapsules Prepared by Spray-Drying. *J. Food Sci.* **2017**, *82*, 2864–2872. [CrossRef]
236. Shaikh, J.; Bhosale, R.; Singhal, R. Microencapsulation of black pepper oleoresin. *Food Chem.* **2006**, *94*, 105–110. [CrossRef]
237. Ozdemir, N.; Bayrak, A.; Tat, T.; Yanuk, Z.N.; Altay, F.; Halkman, A.K. Fabrication and characterization of basil essential oil microcapsule-enriched mayonnaise and its antimicrobial properties against *Escherichia coli* and *Salmonella Typhimurium*. *Food Chem.* **2021**, *359*, 129940. [CrossRef]
238. Qi, Z.; Zhou, H.; Xue, X.; Zhang, C.; Chen, H.; Yuan, H.; Wang, C. Fabrication of epoxy sustained-release coatings loaded with urushiol microcapsules containing essential oil for inhibition on drug-resistant *Helicobacter pylori* and *Staphylococcus aureus*. *Prog. Org. Coat.* **2021**, *161*, 106459. [CrossRef]
239. Yang, Y.H.; Li, X.Z.; Zhang, S. Preparation methods and release kinetics of: *Litsea cubeba* essential oil microcapsules. *RSC Adv.* **2018**, *8*, 29980–29987. [CrossRef]
240. Martins, W.S.; de Araújo, J.S.F.; Feitosa, B.F.; Oliveira, J.R.; Kotzebue, L.R.V.; Agostinic, D.L.S.; Oliveira, D.L.V.; Mazzetto, S.E.; Cavalcanti, M.T.; daSilva, A.L. Lemongrass (*Cymbopogon citratus* DC. Stapf) essential oil microparticles: Development, characterization, and antioxidant potential. *Food Chem.* **2021**, *355*, 129644. [CrossRef]
241. Ocak, B. Gum arabic and collagen hydrolysate extracted from hide fleshing wastes as novel wall materials for microencapsulation of *Origanum onites* L. essential oil through complex coacervation. *Environ. Sci. Pollut. Res.* **2020**, *27*, 42727–42737. [CrossRef] [PubMed]
242. Rojas-Moreno, S.; Osorio-Revilla, G.; Gallardo-Velázquez, T.; Cárdenas-Bailón, F.; Meza-Márquez, G. Effect of the cross-linking agent and drying method on encapsulation efficiency of orange essential oil by complex coacervation using whey protein isolate with different polysaccharides. *J. Microencapsul.* **2018**, *35*, 165–180. [CrossRef]
243. Almeida, A.P.; Rodríguez-Rojo, S.; Serra, A.T.; Vila-Real, H.; Simplicio, A.L.; Delgadillo, I.; Beirão Da Costa, S.; Beirão Da Costa, L.; Nogueira, I.D.; Duarte, C.M.M. Microencapsulation of oregano essential oil in starch-based materials using supercritical fluid technology. *Innov. Food Sci. Emerg. Technol.* **2013**, *20*, 140–145. [CrossRef]
244. Varona, S.; Kareth, S.; Martín, Á.; Cocero, M.J. Formulation of lavandin essential oil with biopolymers by PGSS for application as biocide in ecological agriculture. *J. Supercrit. Fluids* **2010**, *54*, 369–377. [CrossRef]
245. Machado, L.C.; Pelegati, V.B.; Oliveira, A.L. Study of simple microparticles formation of limonene in modified starch using PGSS—Particles from gas-saturated suspensions. *J. Supercrit. Fluids* **2016**, *107*, 260–269. [CrossRef]

## Article

# Sensitive Non-Enzymatic Glucose Electrochemical Sensor Based on Electrochemically Synthesized PANI/Bimetallic Oxide Composite

Anish Khan <sup>1,2,\*</sup>, Aftab Aslam Parwaz Khan <sup>1,2</sup>, Hadi M. Marwani <sup>1,2</sup>, Maha Moteb Alotaibi <sup>2</sup>, Abdullah M. Asiri <sup>1,2</sup>, Ayyar Manikandan <sup>3</sup>, Suchart Siengchin <sup>4</sup> and Sanjay Mavinkere Rangappa <sup>4</sup>

<sup>1</sup> Center of Excellence for Advanced Materials Research, King Abdulaziz University, Jeddah 21589, Saudi Arabia; draapk@gmail.com (A.A.P.K.); hmarwani@kau.edu.sa (H.M.M.); aasiri2@gmail.com (A.M.A.)

<sup>2</sup> Chemistry Department, Faculty of Science, King Abdulaziz University, Jeddah 21589, Saudi Arabia; mmsalotaibi@kau.edu.sa

<sup>3</sup> Department of Chemistry, Bharath Institute of Higher Education and Research (BIHER), Bharath University, Chennai 600073, India; manikandana.che@bharathuniv.ac.in

<sup>4</sup> Natural Composites Research Group Lab, Department of Materials and Production Engineering, The Sirindhorn International Thai-German Graduate School of Engineering (TGGS), King Mongkut's University of Technology North Bangkok (KMUTNB), Bangkok 10800, Thailand; suchart.s.pe@tggs-bangkok.org (S.S.); mavinkere.r.s@op.kmutnb.ac.th (S.M.R.)

\* Correspondence: akrkhan@kau.edu.sa

**Abstract:** The development of a sensitive glucose monitoring system is highly important to protect human lives as high blood-glucose level-related diseases continue to rise globally. In this study, a glucose sensor based on polyaniline-bimetallic oxide (PANI-MnBaO<sub>2</sub>) was reported. PANI-MnBaO<sub>2</sub> was electrochemically synthesized on the glassy carbon electrode (GCE) surface. The as-prepared PANI-MnBaO<sub>2</sub> was characterized by field emission scanning electron microscopy, Fourier transform infrared spectroscopy, energy dispersive X-ray spectroscopy, cyclic voltammetry, and electrochemical impedance spectroscopy. Glucose sensing on PANI-MnBaO<sub>2</sub> is based on the electrocatalytic oxidation of glucose to the glucolactone, which gives oxidation current. The oxidation potential for glucose was 0.83 V, with a limit of detection of 0.06 μM in the linear and in the concentration range of 0.05 μM–1.6 mM. The generated current densities displayed excellent stability in terms of repeatability and reproducibility with fast response. The development of a sensitive glucose sensor as obtained in the current study would ensure human health safety and protection through timely and accurate glucose detection and monitoring.

**Keywords:** electrochemical sensor; glucose sensor; PANI-MnBaO<sub>2</sub>; conducting polymer composite; cyclic voltammetry; linear sweep voltammetry

**Citation:** Khan, A.; Khan, A.A.P.; Marwani, H.M.; Alotaibi, M.M.; Asiri, A.M.; Manikandan, A.; Siengchin, S.; Rangappa, S.M. Sensitive Non-Enzymatic Glucose Electrochemical Sensor Based on Electrochemically Synthesized PANI/Bimetallic Oxide Composite. *Polymers* **2022**, *14*, 3047. <https://doi.org/10.3390/polym14153047>

Academic Editor: Cristina Cazan

Received: 4 June 2022

Accepted: 15 July 2022

Published: 27 July 2022

**Publisher's Note:** MDPI stays neutral with regard to jurisdictional claims in published maps and institutional affiliations.



**Copyright:** © 2022 by the authors. Licensee MDPI, Basel, Switzerland. This article is an open access article distributed under the terms and conditions of the Creative Commons Attribution (CC BY) license (<https://creativecommons.org/licenses/by/4.0/>).

## 1. Introduction

Cases of diabetes have been increasing rapidly in the last decades globally, and the International Diabetic Federation has projected that by 2035, cases of diabetes will reach 600 million globally [1]. High blood-glucose levels in the human system are the major cause of diabetic cases. The glucose level in the human system exceeding 6.5 mM is a signal of the onset of diabetes [2,3]. In addition, high glucose levels in the human body could lead to malfunction or damage to the vital organs such as the heart, eyes, kidneys, tissues, and blood vessels [4–6]. Therefore, there is a great need for accurate and timely detection of glucose to protect and save human lives. In the past and till now, several analytical techniques have been used to determine glucose level/concentration. These techniques include colometric, spectroscopic and electrochemical methods. Electrochemical-based sensing of glucose is very attractive among the techniques because it provides low-cost,



accurate detection in a short time and is a simple process. Electrochemical glucose sensing can be categorized into enzymatic and non-enzymatic detection. Non-enzymatic detection offers much more affordable, selectivity, sensitivity, and performance reproducibility [7–9].

Previously, researchers have explored the use of nanomaterials based on metal oxides, metal phosphides, metal sulfides, double-layered hydroxides, etc., for non-enzymatic glucose detection. Similarly, the use of conducting polymer-based materials such as PANI, polypyrrole composites have been reported. For instance, PANI microtube-modified electrode exhibited glucose detection in the linear range of 0.004–0.8 mM and a limit of detection (LOD) of 0.8  $\mu$ M [10]. Wenwei et al., tried to increase the linear range of glucose using PANI by incorporating TiO<sub>2</sub> into PANi film. The obtained linear range stretched from 0.02–6 mM and LOD of 6.31  $\mu$ M [11]. Similarly, the incorporation of NiFe nanoparticles into PANI yielded LOD of 0.5  $\mu$ M in the linear range of 10  $\mu$ M–1 mM [12]. Recently, Liu et al., synthesized PANI fibers with CuO nanoparticle fillers for the detection of glucose at LOD of 0.11  $\mu$ M [13]. In a recent study by Varghese et al., PANI doped Ag nanoparticle was synthesized and applied as a non-enzymatic glucose sensor. Their procedure achieved a detection limit of 1.3  $\mu$ M in the linear range of 100  $\mu$ M to 10 mM [14]. However, despite several studies on glucose electrochemical detection, there is a need for improvement of sensor performance in terms of selectivity, sensitivity, stability, and response time [14–16]. To address these challenges, this study reports the synthesis of PANI-MnBaO<sub>2</sub> for glucose detection. Selection of conducting polymer such as PANI in composite with manganous and barium oxide is conceived because of their individual unique properties which include high electrical conductivity, high catalytic property, and chemical stability. PANI has excellent electrochemical properties, biocompatibility, and ease of synthesis which prompt its use as an electrode surfaces modifier [17]. It also has conjugated pi-electron in the backbone of its carbon chain. This conjugated electron affords it high electron mobility which accounts for its high chemical stability, and electrical and catalytic properties. In addition, manganous oxide (MnO) is a transition metal oxide with high catalytic properties as a result of partially filled d-orbital in Mn., and also has good electrical conductivity [18]. Likewise, barium oxide (BaO) is a stable metal oxide with good chemical stability [19]. It is thought that composting these materials would result in a highly effective catalyst and a sensing material that could be suitable for non-enzymatic oxidation of glucose as a means of its detection.

Consequently, the aim of the current study is to develop sensitive and reliable electrochemical sensors for glucose determination using affordable and readily available materials. To the best of the authors' knowledge, PANI-MnBaO<sub>2</sub> has never been synthesized before and has never been applied for glucose sensing. This makes this study original, important, and a major contribution to glucose sensing technology.

## 2. Materials and Methods

### 2.1. Reagents

The reagents used for this study were used as purchased without purification except for aniline, which was distilled before use. The reagents used include aniline hydrochloride, manganese II sulfate, barium nitrate, potassium chloride, potassium nitrate, potassium dihydrogen phosphate, dipotassium hydrogen phosphate, glucose, fructose, uric acid, ascorbic acid, nitrite, zinc sulfate, copper sulfate, nitrite, human serum albumin and deionized water. All the reagents used are analytical grades and were sourced from Sigma-Aldrich, St. Louis, MO, USA.

### 2.2. Apparatus

The following apparatus was used for this study: field emission scanning electron microscopy (FESEM) (JEOL JSAM 6300, Jeol, Tokyo, Japan), energy dispersive X-ray spectrometer (XEDS) (X-Max Oxford, Oxford Instruments, Abingdon, UK), Fourier transform Infrared spectrometer (Thermo Scientific, Waltham, MA, USA powered by Vision software). Others include an electrochemical workstation by Autolab Model AUT85887 (Utrecht,

The Netherlands), a three-electrode system made up of a reference electrode (Ag/AgCl-3M (in KCl)), a working electrode made of glassy carbon electrode (bare or coated with PANI-MnBaO<sub>2</sub> and counter electrode (Pt wire-3 mm diameter).

### 2.3. Experimental

#### 2.3.1. Synthesis of PANI

PANI was synthesized by the electrochemical method, specifically, by the chronoamperometric method. The choice of the chronoamperometric method was informed because of its advantages such as ease of formation of controllable film thickness as well as fast and rapid synthesis [20,21]. Before the synthesis, the electrochemical cell was saturated with nitrogen gas to remove dissolved oxygen, or any other gaseous bubbles and this process was repeated in every electrochemical measurement. In order to ascertain the oxidation potential of aniline, the potentiodynamic method (cyclic voltammetry) was employed. A potentiostatic voltage of 1.0 V (gotten from the cyclic voltammetric method) at room temperature was applied to the electrochemical cell containing 0.1 M H<sub>2</sub>SO<sub>4</sub> and 0.5 M aniline using a scan rate of 75 mV/s. The formation of PANI was monitored closely as the synthesis proceeded with special attention to the accompanying color change. After the deposition of PANI on the GCE surface, the modified GCE was gently washed with de-ionized water to remove unpolymerized aniline and oligomers.

#### 2.3.2. Deposition of MnO and BaO on the PANI Support

After the completion of the deposition of the polymerized aniline substrate, the modified electrode was cleaned thoroughly and air-dried. The as-prepared electrode was then immersed in a solution containing 0.1 M manganese sulfate and 0.1 M KNO<sub>3</sub> (supporting electrolyte). The electrochemical setup was subjected to a potentiodynamic sweep from 0 V to -1.0 V at a scan rate of 75 mV/s for 10 cycles. The same procedure was reported for the deposition of Ba<sup>2+</sup> in a solution containing 0.1 M Ba (NO<sub>3</sub>)<sub>2</sub> and 0.1 M KNO<sub>3</sub>. The modified GCE was then immersed in a solution containing 0.1 M NaOH to convert the Mn<sup>2+</sup> and Ba<sup>2+</sup> to their corresponding oxides, MnO and BaO respectively. The modified GCE was later then washed thoroughly with de-ionized water to remove unadsorbed ions. The as-prepared PANI-MnBaO<sub>2</sub> was used for the subsequent experiment.

#### 2.3.3. Characterization Technique

The structure and morphology of the synthesized PANI-MnBaO<sub>2</sub> were investigated using field emission scanning electron microscopy. The functionalities in the synthesized PANI composite were investigated with FTIR in the spectrum range of 400–4000 cm<sup>-1</sup> (FTIR-ATR). Moreover, the elemental analysis to identify elemental composition was carried out with x-ray energy dispersive spectroscopy (XEDS) fitted with FESEM. Electrochemical properties of the synthesized composite were assessed with Autolab potentiostat with the aid of cyclic voltammetry (CV) and electrochemical impedance spectroscopy (EIS). CV was conducted in the potential window of 0.1 V to 1.2 V, with a scan rate of 75 mV/s and an amplitude of 10 mV. EIS was carried out at a potential of 400 mV.

#### 2.3.4. Application for Glucose Sensing

Electrochemical sensing of glucose was conducted using cyclic voltammetry (CV) and linear sweep voltammetry (LSV) with the following applied parameters. CV: potential window: 0.1 to 1.2 V, scan rate of 75 mV/s, amplitude of 0.005 V; LSV: potential window of 0.1 to 1.2 V, scan rate of 75 mV/s, and amplitude of 5 mV.

## 3. Results and Discussion

### 3.1. Synthesis of PANI

Before the electropolymerization, the color of aniline was white yellowish; but gradually changed to dark green (especially at the near working electrode region) upon passage of a constant potential of 1.0 V. This potential was selected based on obtained oxidation

potential for aniline oxidation. A gradual rise in current was observed from 10 s which continued to rise till 120 s (Figure 1a). The increment in the current response (from about 10 s) was due to the gradual deposition of PANI which led to the observed increasing current. At about 120 s, the current started decreasing going forward, which could be attributed to the exhaustion of active sites on the glassy carbon electrode (Figure 1a). This phenomenon signified a successful synthesis of a conducting material (PANI).

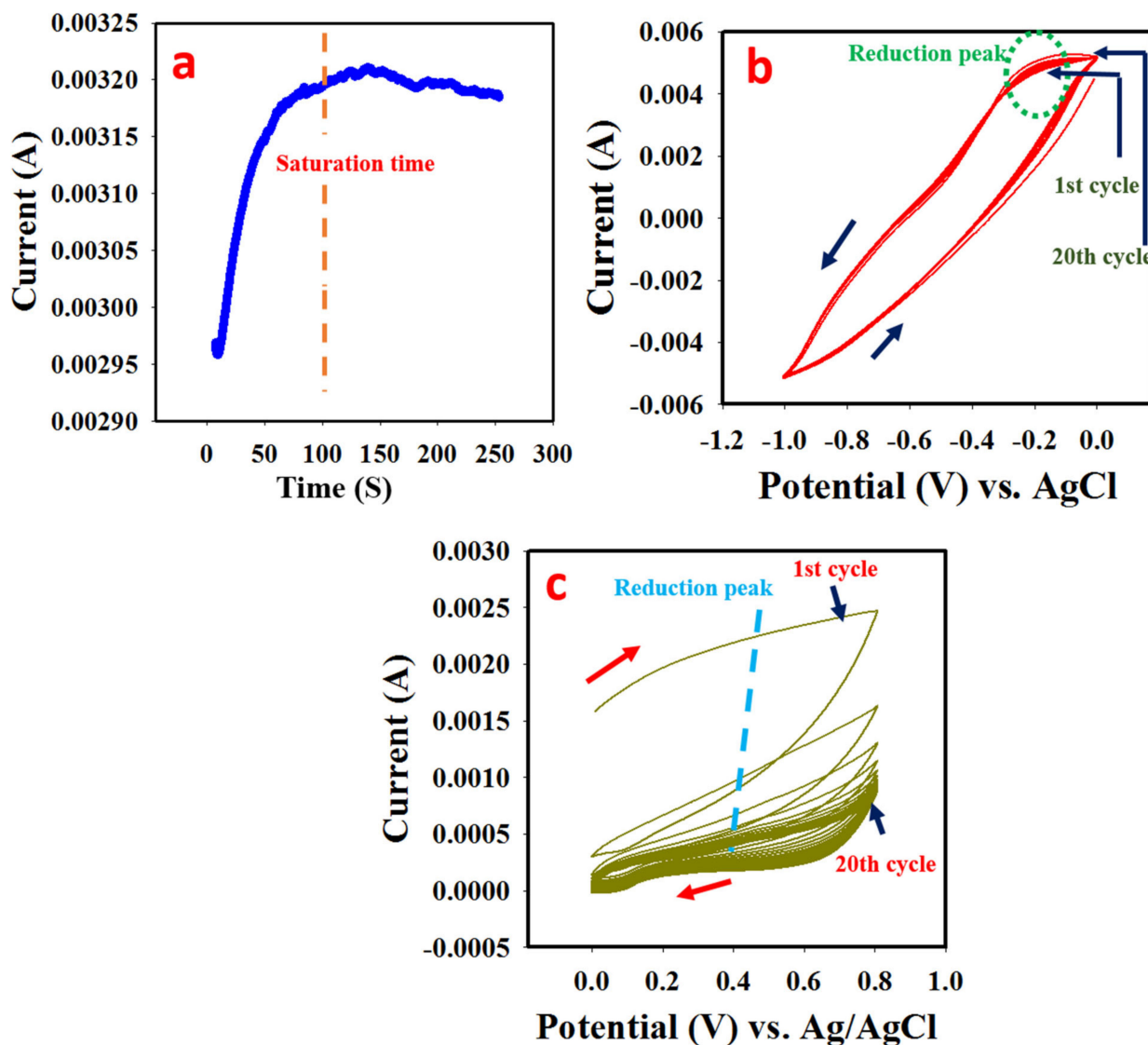
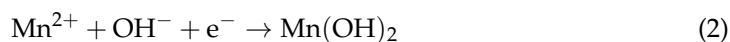


**Figure 1.** (a) Chronoamperogram obtained during synthesis of PANI at a constant potential of 1.0 V. (b) Cyclic voltammogram obtained during deposition of MnO on PANI coated GCE in a solution containing 0.1 M  $\text{MnSO}_4$ /0.1 M  $\text{KNO}_3$  at a scan rate of 75 mV/s. (c) Cyclic voltammogram obtained during deposition of BaO on PANI–MnO coated GCE in a solution containing 0.1 M  $\text{Ba}(\text{NO}_3)_2$ /0.1 M  $\text{KNO}_3$  at a scan rate of 75 mV/s.

### 3.2. Electrodeposition of MnO

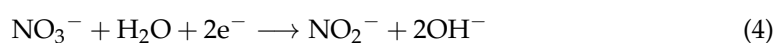
The obtained cyclic voltammogram in 0.1 M manganese II sulfate is presented in Figure 1b. At 0.28 V, a peak could be observed which kept reducing with increasing cyclic sweep. At this potential, reduction of  $\text{Mn}^{2+}$  to Mn is suggested; The reduction peak decreased until the active sites on the substrate (PANI) were exhausted and therefore remained constant. It should be noted also that, the higher the cyclic sweep during the electro-deposition process, the higher the deposited materials and vice versa. The

proposed equation of the reaction is presented in Equations (1)–(3) as adapted from the literature [22–24].



### 3.3. Electrodeposition of BaO

The as-prepared PANI-MnO was immersed in 0.1 M Ba (NO<sub>3</sub>)<sub>2</sub>/0.1 M KNO<sub>3</sub> resulting in the obtained cyclic voltammogram shown in Figure 1c. At the potential of 0.36 V, a reduction process of Ba<sup>2+</sup> was observed with the diminishing current response as the sweep increased. The deposited Ba (s) was converted to their respective oxides by a cyclic sweep in 0.1 M NaOH. The proposed equation of the reaction is presented in Equations (4) and (5) as adapted from the literature [22–24].



Ba ions precipitate with the hydroxyl anions and are spontaneously dehydrated into BaO.



### 3.4. Morphological Studies

The structural and morphological image as captured by FESEM is presented in Figure 2. The image revealed a homogeneously coated surface. The deposit exhibits a non-porous amorphous look. However, upon deposition of MnBaO<sub>2</sub>, some agglomerated particles could be seen sparsely distributed on the PANI surface. The deposited particles (Figure 2c,d) suggest that particle growth predominated nucleation during the electro-synthesis of MnBaO<sub>2</sub>. At higher magnification, the deposited bimetallic oxide exhibited a crystalline sheet-like material with an average size of 15 nm.

First, the bare glassy carbon electrode as shown in Figure 2a revealed a plain and uncoated surface, slightly marred with little lining, which possibly arose from the electrode polishing. Upon deposition of PANI, a new semi-amorphous structure could be observed. The crystallinity of the deposited material was enhanced upon doping with MnBaO<sub>2</sub> fillers (Figure 2b–d).

### 3.5. Functionalities and Elemental Analysis

The FTIR study was conducted to elucidate the functional groups in the synthesized materials. The obtained spectrum is shown in Figure 3a. Successful formation of PANI was confirmed with the following characteristic peaks peculiar to PANI. These characteristic peaks are 3400 cm<sup>-1</sup> (N-H stretching vibration); 2910 cm<sup>-1</sup> (C-H aromatic stretch); 1560 cm<sup>-1</sup> (N = Q = N quinod stretch); 1290 cm<sup>-1</sup> and 1230 cm<sup>-1</sup> (C-N aromatic amine stretch); 1120 cm<sup>-1</sup> and 990 cm<sup>-1</sup> (protonated PANI—C-N<sup>+</sup> stretch) [25–27]. Moreover, a distinct peak at 1600 cm<sup>-1</sup> could be associated with Ba-O while the peaks at the fingerprint region (680 cm<sup>-1</sup> and 550 cm<sup>-1</sup>) are typical of Mn-O vibration [28,29]. The obtained data from the FTIR spectrum confirms the successful synthesis of PANI and highly suggests successful MnO and BaO doping. This claim is further substantiated by the XEDS spectrum (Figure 3b) which revealed the presence of carbon, nitrogen, oxygen, manganese, and barium in the prepared material, which are the elemental features of the synthesized PANI-MnBaO<sub>2</sub>.

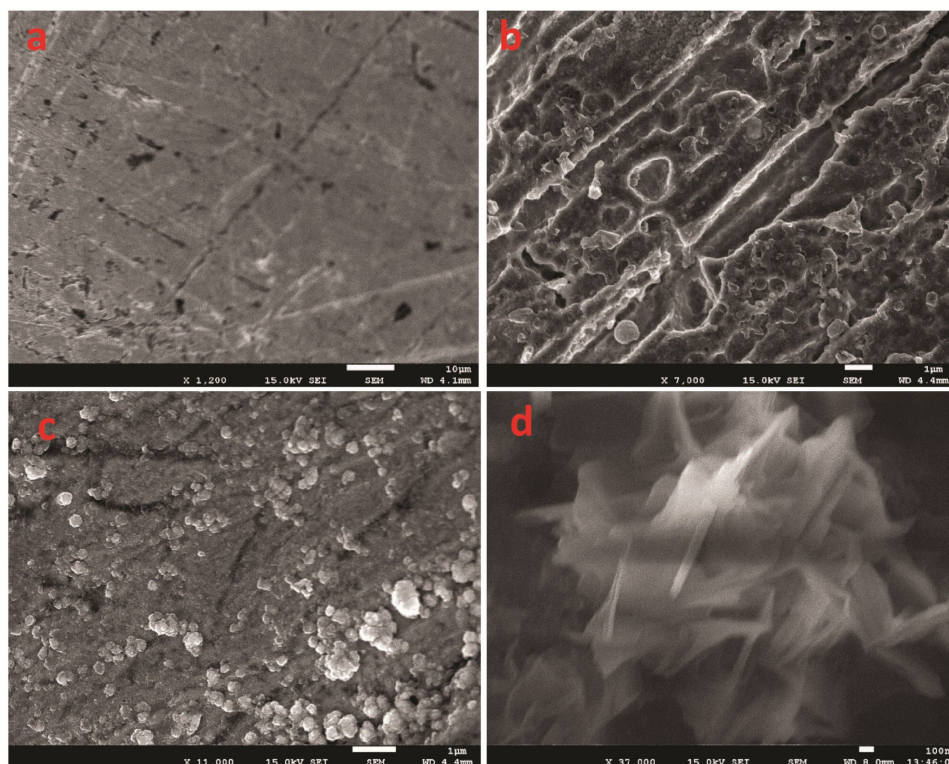


**Figure 2.** (a) Image of unmodified GCE (before electropolymerization). (b) Image of deposited PANI of GCE surface. (c) Image of PANI@MnBaO<sub>2</sub> (low magnification). (d) Focus on MnBaO<sub>2</sub> nanostructure (high magnification).

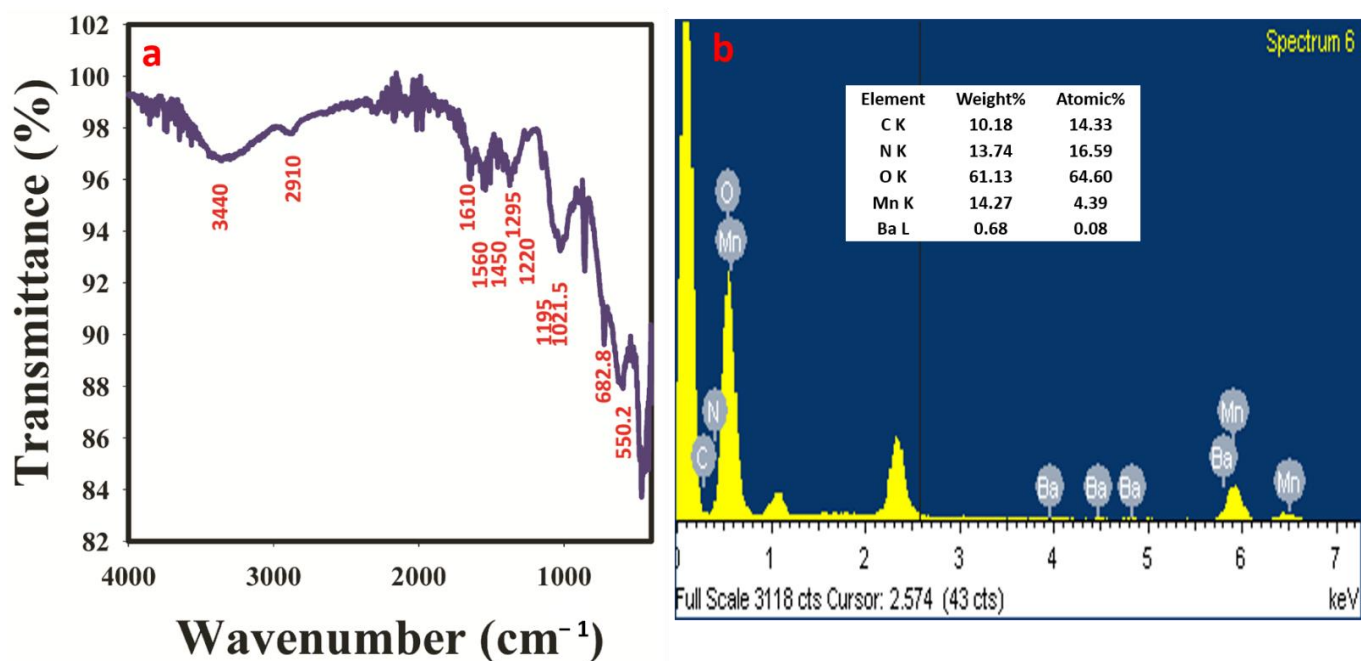


**Figure 3.** (a) FTIR spectrum of the synthesized PANI–MnBaO<sub>2</sub> composite. (b) XEDS spectrum of the PANI–MnBaO<sub>2</sub> composite.

### 3.6. Material Characterization with Cyclic Voltammetry and EIS

The electron mobility, which translates to the electrical conductivity of PANI–MnBaO<sub>2</sub> was assessed with cyclic voltammetry using potassium ferricyanide as the supporting electrolyte. The obtained cyclic voltammogram obtained in 0.1 mM Fe(CN)<sub>6</sub><sup>3−/4−</sup> is presented

in Figure 4a. Information related to electron mobility and electrical conductivity can be inferred from the cyclic voltammogram. From Figure 4a, the oxidation peak current of PANI–MnBaO<sub>2</sub> modified GCE was four times higher than that of bare GCE. Compared to PANI modified GCE only, improved electron mobility is observed with MnBaO<sub>2</sub> doped PANI. In addition, anodic/cathodic peak separation potential is also smaller for the PANI–MnBaO<sub>2</sub> modified GCE (101 mV), as compared to the bare GCE (149 mV). These phenomena are indications of improved electron mobility and electrical conductivity of the PANI–MnBaO<sub>2</sub>.

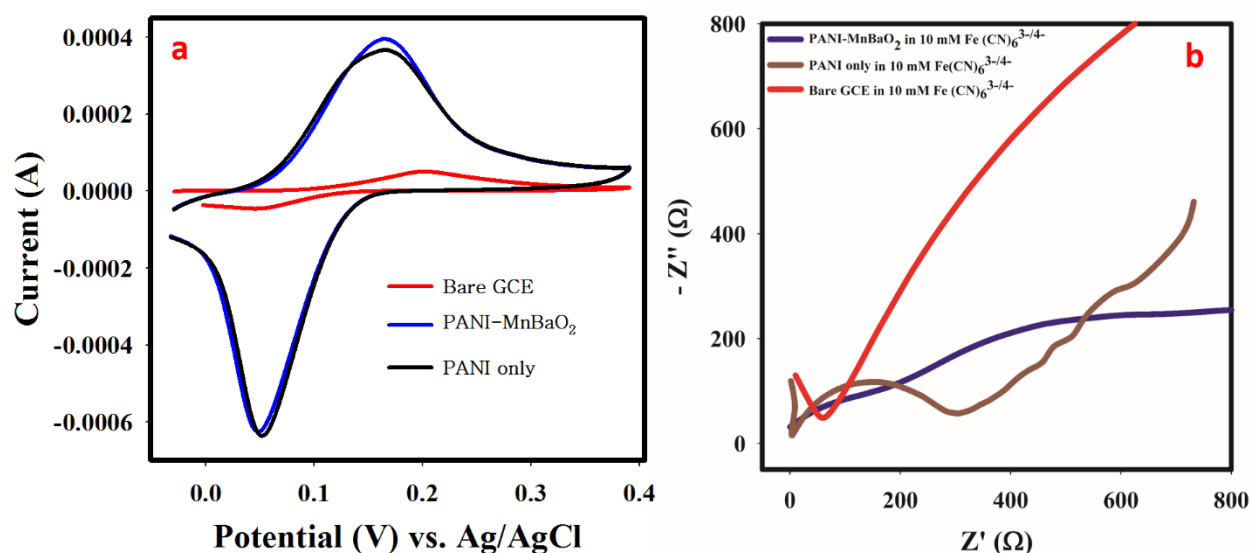


**Figure 4.** (a) Cyclic voltammogram obtained in 0.1 mM Fe(CN)<sub>6</sub><sup>3-/4-</sup> at a scan rate of 75 mV/s. (b) EIS spectrum obtained in 10 mM Fe(CN)<sub>6</sub><sup>3-/4-</sup>.

Electrochemical impedance spectroscopy was conducted purposely to investigate interfacial electron/charge transfer between the modified electrode surface and electrolyte. The Nyquist plot is useful to elucidate information on the resistance on the electrode surface which can be revealed by the charge transfer resistance (R<sub>ct</sub>) denoted by the semi-circle of the Nyquist plot [30,31]. A semi-circle or segment with a smaller radius or diameter has a better interfacial electron transfer compared to a bigger one. As given in Figure 4b and Table S2, PANI-MnBaO<sub>2</sub> modified GCE displayed a reduced segment (R<sub>ct</sub>) (198 Ω) compared to the unmodified PANI (403 Ω) and bare GCE (1.47 kΩ) at high frequency. The reduced charge transfer resistance value of PANI-MnBaO<sub>2</sub> indicates better electrochemical property than unmodified PANI and bare GCE. The equivalent circuit diagram for the reaction process with values of circuit parameters is given in ESI-S1.

### 3.7. Electrochemical Response to Glucose

#### 3.7.1. Control Study and Optimization

In order to establish a response from PANI-MnBaO<sub>3</sub> towards glucose, a controlled study was used, involving bare GCE and modified GCE in glucose solution. PANI-MnBaO<sub>2</sub> gives an oxidation peak at 0.83 V while bare GCE did not show any peak at this potential. Moreover, in the absence of glucose solution, PANI-MnBaO<sub>3</sub> showed very little or no peak at 0.83 V. The obtained results indicate that PANI-MnBaO<sub>2</sub> is responsible for the oxidation peak observed (Figure 5a). This suggests that PANI-MnBaO<sub>2</sub> catalyzed the oxidation of glucose to gluconolactone due to its unique catalytic property. In order to optimize the glucose oxidation (basis of glucose sensing), supporting electrolyte optimization/effect was studied. From the result, the optimum supporting electrolyte for glucose oxidation was 0.1 M NaOH (pH 10) because it has the highest oxidation current at the lowest potential

(Figure 5b). The result suggests that the oxidation of glucose was enhanced in the alkaline medium compared to the acidic medium.

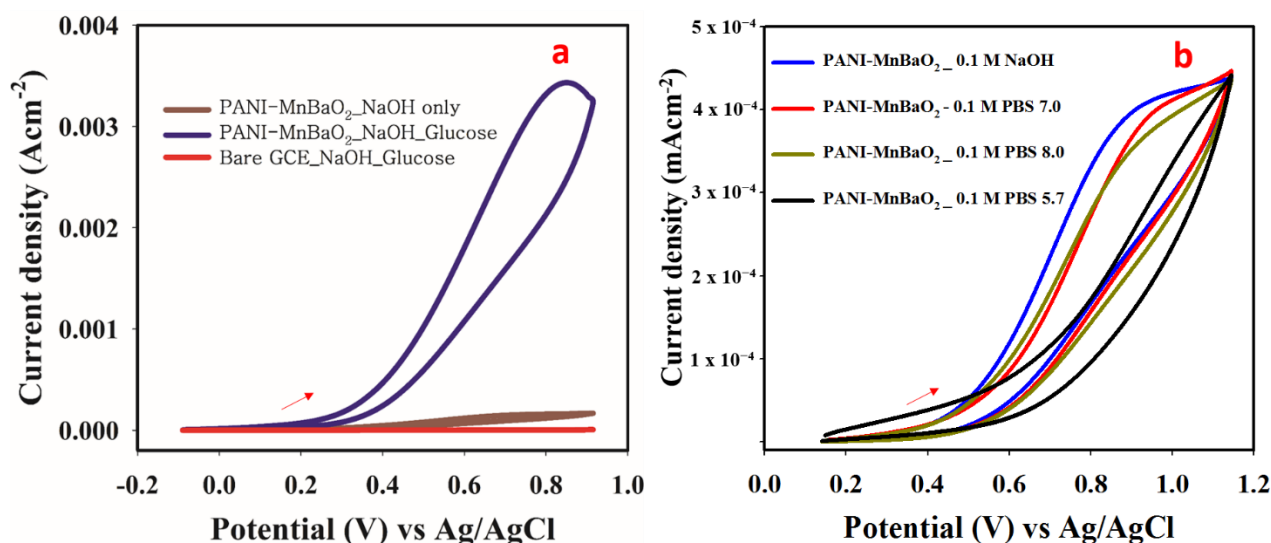


**Figure 5.** (a) Cyclic voltammogram obtained in a solution containing 20 mM glucose and 0.1 M NaOH at a scan rate of 75 mV/s. (b) Cyclic voltammogram obtained in a solution containing 0.2 mM glucose and different pH/supporting electrolyte.

### 3.7.2. Calibration Curve, Scan Rate, and Response Stability

The behavior of PANI-MnBaO<sub>2</sub> towards glucose concentration is shown in Figure 6a. The linear sweep voltammogram showed that an increasing oxidation peak was observed from the addition of 0.1  $\mu$ M glucose to 10 mM. The calibration curve (Figure 6b) with the equation of the graph (i) and (ii) has a good correlation and as presented in Equations (6) and (7).

$$i_p(\text{ox}) = 0.0004 \times C (\mu\text{M} (\pm 0.000109)) - 0.003 (\pm 0.000104) \quad (6)$$

$$i_p(\text{ox}) = 0.00672 \times C (\mu\text{M} (\pm 0.00039)) + 0.005 (\pm 0.00003) \quad (7)$$

Figure 6c presents the cyclic voltammogram obtained at different scan rates (25 mV/s–550 mV/s). The effect of scan rate on the current response of an electrode material could give information about the diffusivity of the reaction on the electrode surface. The linear increase in scan rate and corresponding current portrays a diffusion-controlled reaction (as given in Figure 6d). Specifically, the slope of the plot of the logarithm of scan rate against the logarithm of peak current emphatically dictates whether a reaction is a fully diffusion-controlled or partial diffusion. As given in the literature [21], the slope of plot of logarithm of current against logarithm of scan rate < 0.4 denotes a fully diffusion-controlled reaction; 0.4–0.6 denotes a partial diffusion-controlled reaction; while >0.6 denotes adsorption-controlled reaction [31,32]. For this study, the plot of the square root of the scan rate is linearly proportional to the peak current which suggests a diffusion-controlled reaction.

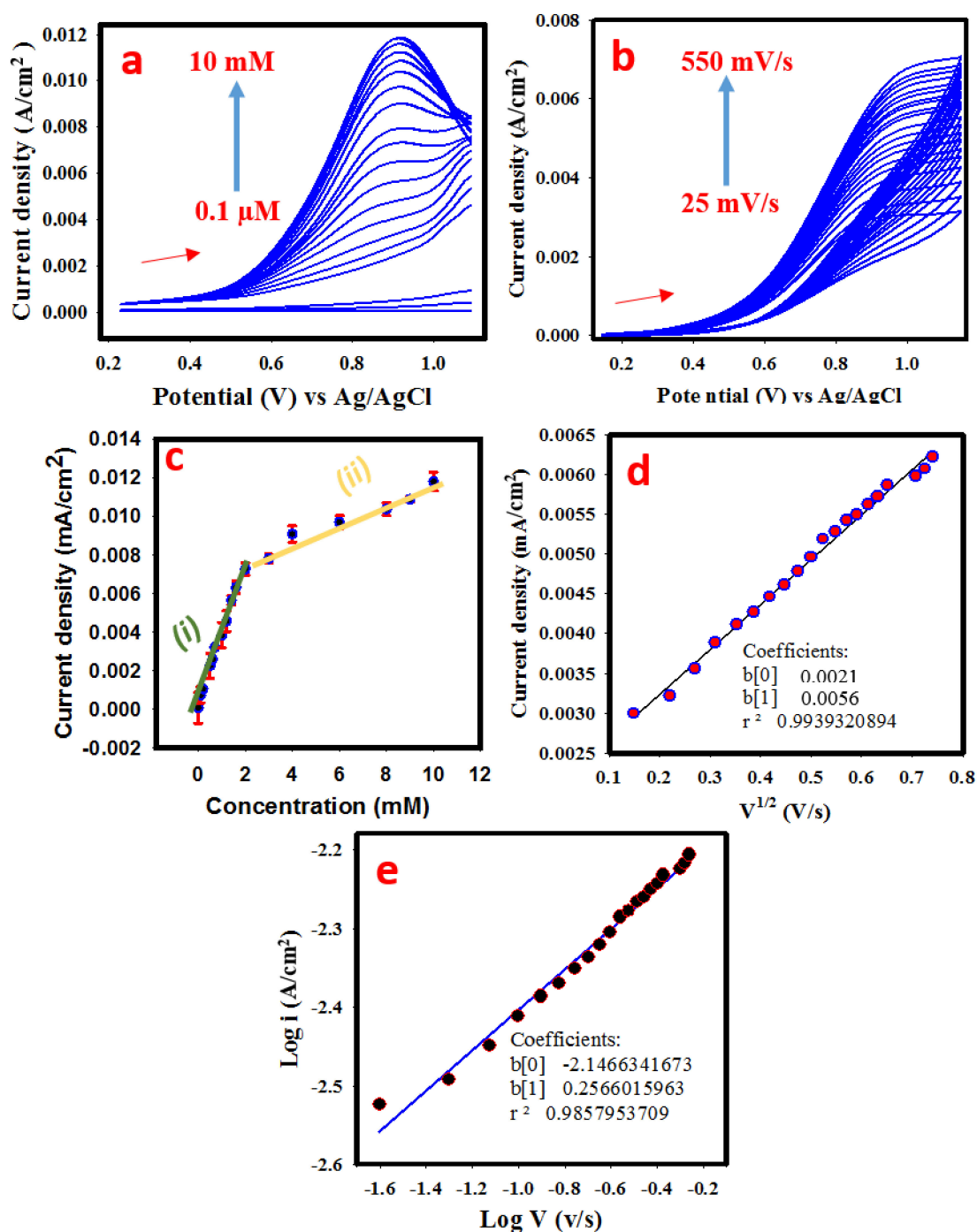


**Figure 6.** (a) Linear sweep voltammogram obtained at different glucose concentrations at the scan rate of  $75 mV/s$ . (b) Cyclic voltammogram obtained in  $2 mM$  glucose/ $0.1 M$  NaOH solution at the scan rate of  $25 mV/s$  to  $550 mV/s$ . (c) calibration plot with error bars. (d) Linear regression graph of oxidation current density against the square root of the scan rate. (e) Plot of the logarithm of oxidation current density against the logarithm of the scan rate.

From the calibration plot, the analytical performance of the electrode (sensor) was determined in terms of limit of detection (LOD), limit of quantification (LOQ), sensitivity,



linear response, and dynamic range. The LOD, LOQ, and sensitivity were estimated using Equations (8)–(10), respectively.

$$\text{LOD} = \frac{3 \times \text{Sd (standard deviation of the blank)}}{\text{slope of the calibration}} \quad (8)$$

$$\text{LOQ} = \frac{10 \times \text{Sd (standard deviation of the blank)}}{\text{slope of the calibration}} \quad (9)$$

$$\text{Sensitivity} = \frac{\text{Slope of the calibration}}{\text{GCE surface area}} \quad (10)$$

The values obtained for LOD, LOQ, and sensitivity are 0.06  $\mu\text{M}$ , 0.199  $\mu\text{M}$ , and 128  $\mu\text{AmM}^{-1} \text{cm}^{-2}$  respectively. The linear response was recorded in the range of 0.05–1.6 mM while the full dynamic response was in the range of 0.05–10 mM.

In addition, the response of PANI-MnBaO<sub>2</sub> modified GCE towards glucose sensing was assessed in terms of repeatability, reproducibility, interference effect, and fast response time. The obtained results for stability testing are presented in Figure 7. For the repeatability study, ten successive measurements (current density) at 0.83 V were taken (Figure 7a). The relative standard deviation in the measurements was 2.2%, which suggests high stability. Current density reproducibility was also carried out by recording the current density produced by PANI-MnBaO<sub>2</sub> modified GCE over the period of 30 days (Figure 7b). It was observed that only 4% of the current density decayed after 30 days. The relative standard deviation of the recorded current density response among the GCEs was 5.2%. The obtained results indicate that PANI-MnBaO<sub>2</sub> is a highly stable and effective sensing material for glucose.

The effect of likely interferents was assessed and the result is presented in Figure 7c. From the result, it could be observed that upon the addition of 10 mM of fructose, ascorbic acid, uric acid, dopamine, and Zn (II) ion. The oxidation peak was unaffected in terms of strength, but little potential drift upon the addition of dopamine. The obtained oxidation peak current upon addition of the listed interferents has a relative standard deviation of 4.8%. Since this value is less than 5%, it could be well assumed that the listed interferents did not interfere with the current density of PANI-MnBaO<sub>2</sub> in the glucose solution.

Moreover, the response time of the PANI-MnBaO<sub>2</sub> modified GCE towards oxidation of glucose was examined using the I-V method. The prepared PANI-MnBaO<sub>2</sub> showed increasing oxidation as early as 2 s and became steady at <10 s (Figure 7d). The fast response time of PANI-MnBaO<sub>2</sub> modified GCE is extremely important in the real application of the prepared electrode for real-life glucose detection as a point of care device.

### 3.7.3. Real Sample Analysis

For real sample analysis, human serum (procured from Sigma Aldrich) was used for the study. The obtained result is summarized in Table 1.

**Table 1.** Result of real sample analysis.

| Sample              | Replicate Number | Spiked Concentration (mM) | Detected Concentration (mM) | Bias  | RSD (%) | Recovery (%) |
|---------------------|------------------|---------------------------|-----------------------------|-------|---------|--------------|
| Human serum Albumin | 3                | 0.5                       | 0.38 ± 0.02                 | −0.12 | 5.2     | 76           |
|                     | 3                | 1                         | 0.85 ± 0.019                | −0.15 | 2.2     | 85           |
|                     | 3                | 2                         | 2.2 ± 0.07                  | 0.2   | 3.18    | 110          |

The percentage recovery of spiked glucose concentration ranged from 76–110%. The obtained result supports good potential use in real determination of glucose in human systems.

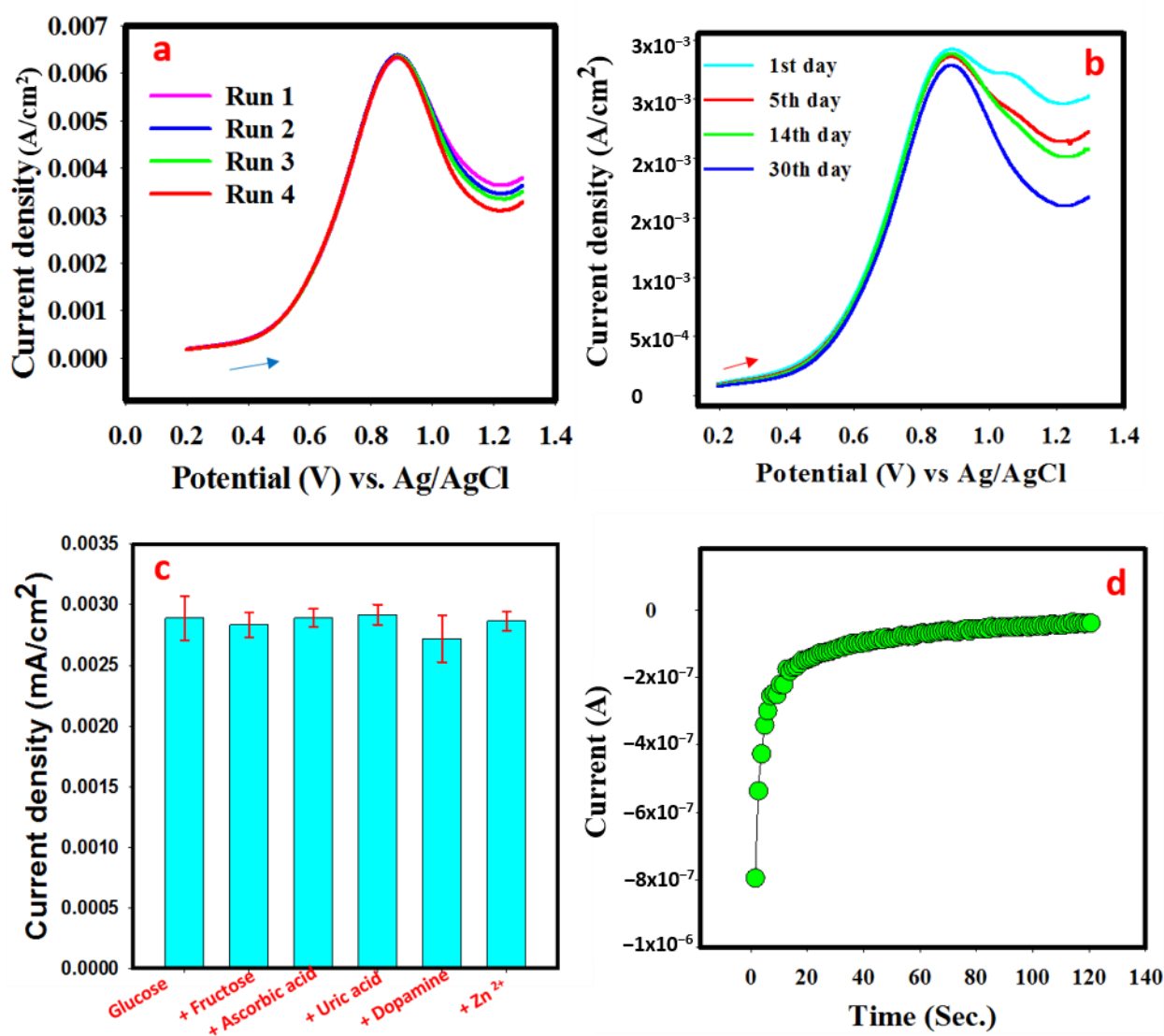


**Figure 7.** (a) Current density response of PANI-MnBaO<sub>2</sub> in 4 mM glucose performed at five consecutive times. (b) LSV response of PANI-MnBaO<sub>2</sub> in 2 mM glucose obtained over a period of 30 days. (c) Peak current density in 2 mM glucose (with and without likely interferents). (d) the obtained response time in 2 mM glucose solution.

### 3.8. Comparison with Earlier Reported Glucose Electrochemical Sensor

It is imperative to state that most of the reported glucose electrochemical sensing is based on enzyme-aided processes. Due to the limitations of enzymatic-based detection such as high cost, unstable performance, and complicated procedures, a non-enzymatic procedure such as the one used in the current study is preferred [16]. Therefore, this study reports a non-enzymatic method, which is easier, cost-effective, straight forward with better analytical performance. As shown in Table 2, the as-prepared PANI-MnBaO<sub>2</sub> compared very well with the literature, and even out-performed others. The observed improved glucose sensing performance by PANI-MnBaO<sub>2</sub> could be ascribed to the combination of unique electrical and catalytic properties of PANI, manganese oxide, and barium oxide. Therefore, this developed approach is a promising analytical technique for glucose determination.

**Table 2.** Reported current density of the bioanode in the literature.

| Electrode Materials                   | LR (mM)  | FDR (mM) | LOD ( $\mu\text{M}$ ) | Sensitivity ( $\mu\text{AmM}^{-1} \text{cm}^{-2}$ ) | Ref        |
|---------------------------------------|----------|----------|-----------------------|---|------------|
| PANI/GO/CuO                           | 0–13     | 0–20     | 1.5                   | 1252  | [33]       |
| PDDA-graphene/CuO                     | 0.04–4   | 0.04–4   | 0.2                   | 4982.2  | [34]       |
| Au NPs/PANI                           | 0.01–10  | 0.01–10  | 3.05                  | 150   | [35]       |
| Graphene/polyaniline-co-diphenylamine | 0.001–1  | 0.001–1  | 0.1                   | 500   | [36]       |
| CuO/NiO/PANI                          | 0.02–2.5 | 0.02–2.5 | 2.0                   | -   | [37]       |
| PANI/CuNi                             | 1–7      | 1–10     | 0.2                   | 1030  | [38]       |
| Ni2(dihydroxyterephthalic acid) MOFs  | 0.04–0.8 | 0.04–6   | 1.46                  | 40.95   | [39]       |
| Polypyrrole-MOFs                      | 0.02–0.5 | 0.02–3   | 1.13                  | 1805  | [40]       |
| MXene-Cu <sub>2</sub> O               | 0.01–30  | -        | 2.83                  | 11.061  | [41]       |
| PANi/MnBaO <sub>2</sub> /GCE          | 0.05–1.6 | 0.05–10  | 0.06                  | 128   | This Study |

#### 4. Conclusions

This study has presented a new material (PANI-MnBaO<sub>2</sub> composite) for application in glucose electrochemical sensing. The prepared PANI-MnBaO<sub>2</sub> was characterized morphologically, optically, and electrochemically. PANI-MnBaO<sub>2</sub> exhibited good performance in glucose electrochemical sensing in terms of sensitivity, response reproducibility, response repeatability, and fast response time. Therefore, the results obtained in this study reveal that PANI-MnBaO<sub>2</sub> nanocomposite is a promising electrode material for sensitive detection of glucose in the human system for human health monitoring and protection.

**Supplementary Materials:** The following are available online at <https://www.mdpi.com/article/10.3390/polym14153047/s1>, Figure S1: The equivalent circuit diagram, Table S1: Values of electrochemical circuit parameters for bare GE, Table S2: Values of electrochemical circuit parameters for PANI-MnBaO<sub>2</sub> modified GCE.

**Author Contributions:** Conceptualization, A.K. and A.A.P.K.; methodology, A.M.A. and H.M.M.; data validation, M.M.A. and S.S.; formal analysis, S.M.R. and A.M.; investigation, A.K.; resources, A.M.A.; data curation, A.K.; writing—original draft preparation, A.K.; writing—review and editing, A.K. All authors have read and agreed to the published version of the manuscript.

**Funding:** The authors extend their appreciation to the Deputyship for Research & Innovation, Ministry of Education in Saudi Arabia for funding this research work through the project number IFPRC-030-130-2020 and King Abdulaziz University, DSR, Jeddah, Saudi Arabia.

**Institutional Review Board Statement:** Not applicable.

**Informed Consent Statement:** Not applicable.

**Data Availability Statement:** The authors of this article confirm that all the associated data related to this article are included in this manuscript and its Supplementary Materials. Raw data supporting this article is available from the corresponding author upon request.

**Conflicts of Interest:** There are no conflicts in this research work.

#### References




1. Monami, M.; Dicembrini, I.; Nardini, C.; Fiordelli, I.; Mannucci, E. Glucagon-like peptide-1 receptor agonists and pancreatitis: A meta-analysis of randomized clinical trials. *Diabetes Res. Clin. Pract.* **2014**, *103*, 269–275. [CrossRef]
2. Hindmarsh, P.C.; Geertsma, K. Chapter 19—Glucose and Cortisol. In *Congenit Adrenal Hyperplasia*; Academic Press: Cambridge, MA, USA, 2017; pp. 219–230. [CrossRef]
3. Baura, G. (Ed.) Chapter 20—Artificial pancreas. In *Medical Device Technologies: A Systems Based Overview Using Engineering Standards*, 2nd ed.; Academic Press: Cambridge, MA, USA, 2021; pp. 503–537. [CrossRef]
4. Arnone, D.; Chabot, C.; Heba, A.-C.; Kökten, T.; Caron, B.; Hansmannel, F.; Dreumont, N.; Ananthakrishnan, A.N.; Quilliot, D.; Peyrin-Biroulet, L. Sugars and Gastrointestinal Health. *Clin. Gastroenterol. Hepatol.* **2021**, *in press*. [CrossRef] [PubMed]
5. World Health Organization. *World Health Statistics*; World Health Organization: Geneva, Switzerland, 2012.
6. Centers for Disease Control and Prevention. *National Diabetes Fact Sheet: National Estimates and General Information on Diabetes and Prediabetes in the United States*; US. Department of Health and Human Services: Atlanta, GA, USA, 2012.

7. Wei, M.; Qiao, Y.; Zhao, H.; Liang, J.; Li, T.; Luo, Y.; Lu, S.; Shi, X.; Lu, W.; Sun, X. Electrochemical non-enzymatic glucose sensors: Recent progress and perspectives. *Chem. Commun.* **2020**, *56*, 14553–14569. [CrossRef] [PubMed]
8. Hwang, D.-W.; Lee, S.; Seo, M.; Chung, T.D. Recent advances in electrochemical non-enzymatic glucose sensors—A review. *Anal. Chim. Acta* **2018**, *1033*, 1–34. [CrossRef] [PubMed]
9. Jia, H.; Shang, N.; Feng, Y.; Ye, H.; Zhao, J.; Wang, H.; Wang, C.; Zhang, Y. Facile preparation of Ni nanoparticle embedded on mesoporous carbon nanorods for non-enzymatic glucose detection. *J. Colloid Interface Sci.* **2021**, *583*, 310–320. [CrossRef]
10. Zhang, L.; Zhou, C.; Luo, J.; Long, Y.; Wang, C.; Yu, T.; Xiao, D. A polyaniline microtube platform for direct electron transfer of glucose oxidase and biosensing applications. *J. Mater. Chem. B* **2015**, *3*, 1116–1124. [CrossRef] [PubMed]
11. Tang, W.; Li, L.; Zeng, X. A glucose biosensor based on the synergistic action of nanometer-sized TiO<sub>2</sub> and polyaniline. *Talanta* **2015**, *131*, 417–423. [CrossRef] [PubMed]
12. Lakhdari, D.; Guittoum, A.; Benbrahim, N.; Belgherbi, O.; Berkani, M.; Vasseghian, Y.; Lakhdari, N. A novel non-enzymatic glucose sensor based on NiFe(NPs)-polyaniline hybrid materials. *Food Chem. Toxicol.* **2021**, *151*, 112099. [CrossRef] [PubMed]
13. Liu, T.; Guo, Y.; Zhang, Z.; Miao, Z.; Zhang, X.; Su, Z. Fabrication of hollow CuO/PANI hybrid nanofibers for non-enzymatic electrochemical detection of H<sub>2</sub>O<sub>2</sub> and glucose. *Sens. Actuators B Chem.* **2019**, *286*, 370–376. [CrossRef]
14. Varghese, E.V.; Saidu, F.K.; Schwandt, C.; Thomas, G.; Joseph, A. Non-Enzymatic Electrochemical Biosensing of Glucose Using Nanocomposites of Polyaniline Nanofibers and Silver. *ChemistrySelect* **2022**, *7*, e202103518. [CrossRef]
15. Yassin, M.A.; Shrestha, B.K.; Ahmad, R.; Shrestha, S.; Park, C.H.; Kim, C.S. Exfoliated nanosheets of Co<sub>3</sub>O<sub>4</sub> webbed with polyaniline nanofibers: A novel composite electrode material for enzymeless glucose sensing application. *J. Ind. Eng. Chem.* **2019**, *73*, 106–117. [CrossRef]
16. Osuna, V.; Vega-Rios, A.; Zaragoza-Contreras, E.A.; Estrada-Moreno, I.A.; Dominguez, R.B. Progress of Polyaniline Glucose Sensors for Diabetes Mellitus Management Utilizing Enzymatic and Non-Enzymatic Detection. *Biosensors* **2022**, *12*, 137. [CrossRef]
17. Du, X.; Chen, Y.; Dong, W.; Han, B.; Liu, M.; Chen, Q.; Zhou, J. A nanocomposite-based electrochemical sensor for non-enzymatic detection of hydrogen peroxide. *Oncotarget* **2017**, *8*, 13039–13047. [CrossRef] [PubMed]
18. Selvakumar, K.; Kumar, S.S.; Thangamuthu, R.; Kruthika, G.; Murugan, P. Development of shape-engineered  $\alpha$ -MnO<sub>2</sub> materials as bi-functional catalysts for oxygen evolution reaction and oxygen reduction reaction in alkaline medium. *Int. J. Hydrogen Energy* **2014**, *39*, 21024–21036. [CrossRef]
19. Renukadevi, R.; Sundaram, R.; Kasinathan, K. Barium oxide nanoparticles with robust catalytic, photocatalytic and humidity sensing properties. *J. Nanostruct.* **2020**, *10*, 167–176. [CrossRef]
20. Inamuddin; Kashmery, H.A. Ternary graphene@polyaniline-TiO<sub>2</sub> composite for glucose biofuel cell anode application. *Int. J. Hydrogen Energy* **2019**, *44*, 22173–22180. [CrossRef]
21. Adeosun, W.A.; Asiri, A.M.; Marwani, H.M. Sensitive determination of 2-nitrophenol using electrochemically deposited poly-methyl red film for healthcare and environmental safety. *Synth. Met.* **2020**, *261*, 116321. [CrossRef]
22. Yoshida, T.; Komatsu, D.; Shimokawa, N.; Minoura, H. Mechanism of cathodic electrodeposition of zinc oxide thin films from aqueous zinc nitrate baths. *Thin Solid Films* **2004**, *451–452*, 166–169. [CrossRef]
23. Prasad, B.E.; Kamath, P.V.; Ranganath, S. Electrodeposition of ZnO coatings from aqueous Zn(NO<sub>3</sub>)<sub>2</sub> baths: Effect of Zn concentration, deposition temperature, and time on orientation. *J. Solid State Electrochem.* **2012**, *16*, 3715–3722. [CrossRef]
24. Cruickshank, A.C.; Tay, S.E.R.; Illy, B.N.; Da Campo, R.; Schumann, S.; Jones, T.S.; Heutz, S.; McLachlan, M.A.; McComb, D.W.; Riley, D.J.; et al. Electrodeposition of ZnO Nanostructures on Molecular Thin Films. *Chem. Mater.* **2011**, *23*, 3863–3870. [CrossRef]
25. Kondawar, S.B.; Deshpande, M.D.; Agrawal, S.P. Transport Properties of Conductive Polyaniline Nanocomposites Based on Carbon Nanotubes. *Int. J. Compos. Mater.* **2012**, *2*, 32–36. [CrossRef]
26. Shadi, L.; Karimi, M.; Entezami, A.A.; Safa, K.D. A facile synthesis of polyaniline/polyethylene glycol/polyaniline terpolymers: Preparation of electrospun conducting nanofibers by blending of the terpolymers with polycaprolactone. *Polym. Bull.* **2013**, *70*, 3529–3545. [CrossRef]
27. Shaikh, S.F.; Shaikh, F.F.; Shaikh, A.V.; Ubaidullah, M.; Al-Enizi, A.M.; Pathan, H.M. Electrodeposited more-hydrophilic nano-nest polyaniline electrodes for supercapacitor application. *J. Phys. Chem. Solids* **2020**, *149*, 109774. [CrossRef]
28. Haque, S.U.; Nasar, A.; Inamuddin; Asiri, A.M. Preparation and characterization of a bioanode (GC/MnO<sub>2</sub>/PSS/Gph/Frt/GOx) for biofuel cell application. *Int. J. Hydrogen Energy* **2019**, *44*, 7308–7319. [CrossRef]
29. Ahmad, N.; Wahab, R.; Alam, M. Facile Growth of Barium Oxide Nanorods: Structural and Optical Properties. *J. Nanosci. Nanotechnol.* **2014**, *14*, 5342–5346. [CrossRef]
30. Ghanei-Motlagh, M.; Taher, M.A.; Fayazi, M.; Baghayeri, M.; Hosseiniifar, A. Non-Enzymatic Amperometric Sensing of Hydrogen Peroxide Based on Vanadium Pentoxide Nanostructures. *J. Electrochem. Soc.* **2019**, *166*, B367–B372. [CrossRef]
31. Asiri, A.M.; Adeosun, W.A.; Marwani, H.M. Electrocatalytic reduction of 2, 6-dinitrophenol on polycongo red decorated glassy carbon electrode for sensing application. *J. Environ. Chem. Eng.* **2020**, *8*, 104378. [CrossRef]
32. Goseer, D.K. *Cyclic Voltammetry-Simulation and Analysis of Reaction*; VCH: New York, NY, USA, 1993.
33. Fang, L.; Zhu, Q.; Cai, Y.; Liang, B.; Ye, X. 3D porous structured polyaniline/reduced graphene oxide/copper oxide decorated electrode for high performance nonenzymatic glucose detection. *J. Electroanal. Chem.* **2019**, *841*, 1–9. [CrossRef]
34. Yang, J.; Lin, Q.; Yin, W.; Jiang, T.; Zhao, D.; Jiang, L. A novel nonenzymatic glucose sensor based on functionalized PDDA-graphene/CuO nanocomposites. *Sens. Actuators B Chem.* **2017**, *253*, 1087–1095. [CrossRef]

35. Xu, M.; Song, Y.; Ye, Y.; Gong, C.; Shen, Y.; Wang, L.; Wang, L. A novel flexible electrochemical glucose sensor based on gold nanoparticles/polyaniline arrays/carbon cloth electrode. *Sens. Actuators B Chem.* **2017**, *252*, 1187–1193. [CrossRef]
36. Muthusankar, E.; Ragupathy, D. Graphene/Poly(aniline-co-diphenylamine) nanohybrid for ultrasensitive electrochemical glucose sensor. *Nano-Struct. Nano-Objects* **2019**, *20*, 100390. [CrossRef]
37. Ghanbari, K.; Babaei, Z. Fabrication and characterization of non-enzymatic glucose sensor based on ternary NiO/CuO/polyaniline nanocomposite. *Anal. Biochem.* **2016**, *498*, 37–46. [CrossRef] [PubMed]
38. Bilal, S.; Ullah, W.; Shah, A.-U.A. Polyaniline@CuNi nanocomposite: A highly selective, stable and efficient electrode material for binder free non-enzymatic glucose sensor. *Electrochim. Acta* **2018**, *284*, 382–391. [CrossRef]
39. Lopa, N.S.; Rahman, M.; Jang, H.; Sutradhar, S.C.; Ahmed, F.; Ryu, T.; Kim, W. A glassy carbon electrode modified with poly(2,4-dinitrophenylhydrazine) for simultaneous detection of dihydroxybenzene isomers. *Mikrochim. Acta* **2017**, *185*, 23. [CrossRef] [PubMed]
40. Chen, S.; Liu, D.; Song, N.; Wang, C.; Lu, X. Promoting non-enzymatic electrochemical sensing performance toward glucose by the integration of conducting polypyrrole with metal-organic framework. *Compos. Commun.* **2022**, *30*, 101074. [CrossRef]
41. Gopal, T.S.; Jeong, S.K.; Alrebdi, T.A.; Pandiaraj, S.; Alodhayb, A.; Muthuramamoorthy, M.; Grace, A.N. MXene-based composite electrodes for efficient electrochemical sensing of glucose by non-enzymatic method. *Mater. Today Chem.* **2022**, *24*, 100891. [CrossRef]

## Article

# Development of Polymeric-Based Formulation as Potential Smart Colonic Drug Delivery System

Mohammad F. Bayan <sup>1,\*</sup>, Saeed M. Marji <sup>1</sup>, Mutaz S. Salem <sup>1,2</sup>, M. Yasmin Begum <sup>3</sup>,  
Kumarappan Chidambaram <sup>4,\*</sup> and Balakumar Chandrasekaran <sup>1,5</sup>

<sup>1</sup> Faculty of Pharmacy, Philadelphia University, P.O. Box 1, Amman 19392, Jordan

<sup>2</sup> Faculty of Pharmacy, Jordan University of Science and Technology, P.O. Box 3030, Irbid 22110, Jordan

<sup>3</sup> Department of Pharmaceutics, School of Pharmacy, King Khalid University, Abha 61421, Saudi Arabia

<sup>4</sup> Department of Pharmacology, School of Pharmacy, King Khalid University, Abha 62529, Saudi Arabia

<sup>5</sup> Department of Pharmaceutical Chemistry, School of Pharmacy, ITM University, Gwalior 474001, India

\* Correspondence: mbayan01@qub.ac.uk (M.F.B.); kumarappan@kku.edu.sa (K.C.)

**Abstract:** Conventional oral formulations are mainly absorbed in the small intestine. This limits their use in the treatment of some diseases associated with the colon, where the drug has to act topically at the inflammation site. This paved the way for the development of a smart colonic drug delivery system, thereby improving the therapeutic efficacy, reducing the dosing frequency and potential side effects, as well as improving patient acceptance, especially in cases where enemas or other topical preparations may not be effective alone in treating the inflammation. In healthy individuals, it takes an oral medication delivery system about 5 to 6 h to reach the colon. A colonic drug delivery system should delay or prohibit the medication release during these five to six hours while permitting its release afterward. The main aim of this study was to develop a smart drug delivery system based on pH-sensitive polymeric formulations, synthesized by a free-radical bulk polymerization method, using different monomer and crosslinker concentrations. The formulations were loaded with 5-amino salicylic acid as a model drug and Capmul MCM C8 as a bioavailability enhancer. The glass transition temperature (T<sub>g</sub>), tensile strength, Young's modulus, and tensile elongation at break were all measured as a part of the dried films' characterization. In vitro swelling and release studies were performed to assess the behavior of the produced formulations. The in vitro swelling and release evaluation demonstrated the potential ability of the developed system to retard the drug release at conditions mimicking the stomach and small intestine while triggering its release at conditions mimicking the colon, which indicates its promising applicability as a potential smart colonic drug delivery system.

**Keywords:** 5-amino salicylic acid; smart delivery system; sustainable polymers; triggered drug delivery; ulcerative colitis

**Citation:** Bayan, M.F.; Marji, S.M.; Salem, M.S.; Begum, M.Y.; Chidambaram, K.; Chandrasekaran, B. Development of Polymeric-Based Formulation as Potential Smart Colonic Drug Delivery System. *Polymers* **2022**, *14*, 3697. <https://doi.org/10.3390/polym14173697>

Academic Editors: Cristina Cazan, Carlos Guerrero Sanchez and Dimitrios Bikiaris

Received: 21 July 2022

Accepted: 31 August 2022

Published: 5 September 2022

**Publisher's Note:** MDPI stays neutral with regard to jurisdictional claims in published maps and institutional affiliations.



**Copyright:** © 2022 by the authors. Licensee MDPI, Basel, Switzerland. This article is an open access article distributed under the terms and conditions of the Creative Commons Attribution (CC BY) license (<https://creativecommons.org/licenses/by/4.0/>).

## 1. Introduction

Orally delivered dosage forms are the most commonly used dosage forms, due to the ease of administration and convenience. The aim of any successful oral drug delivery system is to deliver the therapeutic agent to the site of action with proper dosing and timing [1]. This can be guaranteed through developing a smart delivery system, which elicits a stimulus-responsive drug release. In these systems, an external or internal stimuli, such as pH change, can trigger the drug release. As a consequence, this can reduce the required doses, reduce potential side effects, increase patient compliance, and improve therapeutic efficacy [2]. The development of such a system requires an understanding of the mechanism of action of the drug, site of action, physicochemical properties, residence time, and the environment that the dosage unit will pass through after administration, so the system can be developed to trigger the drug depending on its environment within the

body. The pH and residence time vary within the gastrointestinal tract. The pH changes from acidic in the stomach to relatively basic in the small and large intestines [3]. The drug residence time is estimated to be 1–4 h in the stomach, around 4 h in the small intestine, and around 10 h in the large intestine [2]. These changes have paved the way to develop a pH–time-dependent drug delivery system aiming to deliver the drug in the intestine, for example. This can be achieved via employing polymers that retard the drug in the acidic environment while permitting its release at the basic environment, where the polymer swells or dissolves. Increased attention has been given to these systems to treat some diseases, such as inflammatory bowel disease, which can affect specific parts of the large intestine. Conventional oral dosage forms are mainly absorbed in the small intestine, and this limits their use in the treatment of colon disorders, where the topical effect of the medicinal agent is important at the inflammation sites [4]. This advocated the need to fabricate a colonic oral delivery system especially in some severe and specific cases, where the topical dosage form (such as an enema) may not be effective alone in treating the inflammation. This smart delivery can be achieved using a pH–time-dependent system that employs a polymer capable of preventing/retarding the drug release in the upper gastrointestinal tract (stomach and small intestine) while permitting its release in the lower gastrointestinal tract. The importance of developing a smart colonic delivery system is not justified only for the local treatment of colonic disorders, but it is also extended to the systemic delivery of some agents, such as peptides, proteins, and anti-diabetic and anti-hypertensive agents. Crohn’s disease and ulcerative colitis are the main inflammatory bowel disorders, where the first can affect any part of the intestine, while the second is mainly affecting the colon [5]. Persons affected with this disease have to use a lifelong remedy as there is no permanent treatment for this condition. Additionally, the available remedies are not always effective and can cause severe side effects [6]. Ulcerative colitis is usually treated using 5-amino salicylic acid (also called mesalamine), prescribed as oral and topical dosage forms, as a first choice, for the local treatment of the inflamed parts of the large intestine. 5-amino salicylic acid is considered as class IV in the Biopharmaceutical Classification System (this class characterized by low solubility and low permeability) [7]. The majority of oral-marketed 5-amino salicylic acid dosage forms employs a pH-sensitive polymer coating to withstand the drug release in the stomach while permitting it in the intestine, such as in Asacol<sup>®</sup>, Lialda<sup>®</sup>, Apriso<sup>®</sup>, and Claversal<sup>®</sup>, which use the Eudragit<sup>®</sup> coating that dissolves at the intestinal pH [8]. The employment of a pH-sensitive polymer can improve the oral delivery of the 5-amino salicylic acid through the pH-dependent swelling, which results in a high concentration gradient and rapid release, as well as high mucoadhesivity, and higher absorption. The pH approach alone may fail to achieve a colonic-triggered delivery of the 5-amino salicylic acid. This is attributed to the inter/intra pH variations and the similarity in the pH of the colon and small intestine. This paved the way to employ a combined pH–time-dependent approach to achieve a colonic-specific delivery [9].

Rehman et al. [10] reported the use of polymers, based on long hydrophobic chains, as a promising large intestinal delayed drug delivery system. The carrier was loaded with 5-amino salicylic and Ibuprofen as the model drugs. The developed system demonstrated a relatively higher in vitro drug release in the simulated large intestinal environment compared to the simulated gastric and small intestinal environments. Another delayed drug delivery system was developed by Mirabbasi et al. [11]. This system employed a polyurethane-grafted chitosan nanoparticle loaded with 5-amino salicylic acid. The in vitro release evaluations had shown the ability of the system to retard the drug release, with a less than 60% cumulative release achieved after 8 h and no burst effect. Synthetic monomers are preferred to be used over the natural monomers in synthesizing crosslinked polymers for pharmaceutical purposes because they permit the flexibility and easiness of modifying the structure of the produced polymer as well as the capability to obtain a large-scale production with uniform and reproducible characteristics [12]. Hydroxyethyl methacrylate has been reported as a biocompatible, chemically and thermally stable synthetic monomer. It is the first and most widely used synthetic monomer in biomedical and pharmaceutical

applications [13]. Roointan et al. [14] reported the development of a pH-sensitive drug delivery system based on a cationic polymeric carrier, synthesized using hydroxyethyl methacrylate crosslinked with a dimethylaminoethyl methacrylate monomer, as a promising anti-cancer-specific drug delivery system. Polyethylene glycol diacrylate was used as a crosslinker and doxorubicin as a model drug. This system was developed to trigger the drug release at the acidic pH (the cancer site). In vitro evaluations were conducted in different pH medias, simulating the healthy and cancer sites (pH 7.4 and pH 5.5, respectively). A significant higher drug release was obtained at pH 5.5 compared to that at pH 7.4, which encourages their use as a potential anti-cancer-specific delivery system. Zia et al. [15] investigated the use of hydroxyethyl methacrylate in the development of an anionic polymeric carrier for the potential oral delivery of nonsteroidal anti-inflammatory drugs. The in vitro studies demonstrated a significant higher swelling and release in the simulated intestinal fluid compared to the simulated gastric fluid. The main aim of our study was to develop a smart drug delivery system based on pH-sensitive polymeric formulations, synthesized by free-radical bulk polymerization method, using different monomer and crosslinker concentrations. The formulations were loaded with 5-amino salicylic acid as a model drug and Capmul MCM C8 as a bioavailability enhancer. In vitro swelling and release studies were performed for the produced formulations.

## 2. Materials and Methods

### 2.1. Materials

Hydroxyethyl methacrylate (HEMA), Methacrylic acid (MAA), Dimethylaminoethyl methacrylate (DMAEMA), 5-amino salicylic acid, ethylene glycol dimethacrylate (EGDMA), disodium hydrogen phosphate dodecahydrate, azobisisobutyronitrile (AIBN), potassium chloride, sodium chloride, potassium dihydrogen phosphate, BRAND<sup>®</sup> stopcock grease, sodium dodecyl sulphate, and sodium hydroxide were purchased from Sigma-Aldrich. Capmul<sup>®</sup> MCM C8 was purchased from ABITEC. Hydrochloric acid (37%) was purchased from Biosolve Chimie. HPLC-grade water was used in all experiments. The purchased materials were used as supplied with no modification.

### 2.2. Methods

#### 2.2.1. Preparation of Smart Polymeric Formulations

A free-radical thermal bulk polymerization method was used to synthesize 18 copolymerized formulations (Table 1), based on HEMA, MAA, and/or DMAEMA monomers, using different concentrations of EGDMA as a crosslinker, and loaded with capmul MCM C8 and 5-amino salicylic acid, as a dissolution enhancer and model drug, respectively. AIBN was used as a thermoinitiator. A 10 g copolymerized film was produced for each formulation. During preparation, the components of each formulation (in ratios as described in Table 1) were blended together in a 30 mL amber glass bottle, at room temperature, with stirring for 45 min. A 20 mL syringe was used to inject the prepared mixture in a premade mold, designed for all formulations, and then transferred to the oven (preheated to 60 °C), where the polymerization process occurred at 60 °C for 18 h. The mold was made using a medical-grade rubbery silicone tubing (0.76 mm internal diameter, 1.65 external diameter, and 0.445 mm wall thickness), two borosilicate glass sheets (215 × 215 × 3 mm), 8 32 mm-foldback clips, and silicon-coated release liner. The silicone coated sheet was spread onto the glass sheets and the borders of the mold were drawn using the silicone tube on one of the glass sheets, where the other one was flipped onto it and the two sheets held together vertically using the foldback clips. At the end of the synthesis process, each film was soaked in HPLC-grade water placed in a storage box covered with aluminum foil. The water was changed daily to rinse the prepared film and remove any unreacted or unwanted species remaining from the polymerization process. A UV-vis spectrophotometer (Spectroscan 80 D, Biotech Engineering Ltd., London, UK) was used to monitor the washing step. A cork borer no. 1 (5 mm) was used to pierce the produced swollen film into uniform small discs, which were then dried in the oven at 60 °C until reaching a constant weight.



The drug entrapment efficiency (EE%) of the produced formulations was calculated using the following formula:  $EE\% = \text{Actual content} / \text{theoretical content} \times 100\%$ . The theoretical content represents the initial drug concentration used during the preparation (5 % w/w), while the actual content represents the analyzed drug content of each formulation.

**Table 1.** The compositions of the synthesized copolymerized formulations.

| Formula | HEMA<br>(% w/w) | MAA<br>(% w/w) | DMAEMA<br>(% w/w) | EGDMA<br>(% w/w) | Capmul<br>MCM C8<br>(% w/w) | AIBN<br>(% w/w) | 5-Amino<br>Salicylic Acid<br>(% w/w) |
|---------|-----------------|----------------|-------------------|------------------|-----------------------------|-----------------|--------------------------------------|
| D1      | 98              | -              | -                 | 1                | -                           | 1               | -                                    |
| D2      | 78              | -              | -                 | 1                | 20                          | 1               | -                                    |
| D3      | 68              | 10             | -                 | 1                | 20                          | 1               | -                                    |
| D4      | 58              | 20             | -                 | 1                | 20                          | 1               | -                                    |
| D5      | 54              | 20             | -                 | 5                | 20                          | 1               | -                                    |
| D6      | 49              | 20             | -                 | 10               | 20                          | 1               | -                                    |
| D7      | 88              | -              | 10                | 1                | -                           | 1               | -                                    |
| D8      | 68              | -              | 10                | 1                | 20                          | 1               | -                                    |
| D9      | 58              | -              | 20                | 1                | 20                          | 1               | -                                    |
| F1      | 93              | -              | -                 | 1                | -                           | 1               | 5                                    |
| F2      | 73              | -              | -                 | 1                | 20                          | 1               | 5                                    |
| F3      | 63              | 10             | -                 | 1                | 20                          | 1               | 5                                    |
| F4      | 53              | 20             | -                 | 1                | 20                          | 1               | 5                                    |
| F5      | 49              | 20             | -                 | 5                | 20                          | 1               | 5                                    |
| F6      | 44              | 20             | -                 | 10               | 20                          | 1               | 5                                    |
| F7      | 83              | -              | 10                | 1                | -                           | 1               | 5                                    |
| F8      | 63              | -              | 10                | 1                | 20                          | 1               | 5                                    |
| F9      | 53              | -              | 20                | 1                | 20                          | 1               | 5                                    |

### 2.2.2. Dynamic Mechanical Thermal (DMT) Analysis

The glass transition temperature of the produced formulations was obtained using Q800 DMT analyzer. The discs were analyzed at a range of 35–160 °C, 1 Hz, and a rate of 3 °C/min. The glass transition temperature was defined as the peak of Tan  $\delta$  curve. Three replicates were carried out. The mean and the standard deviation were calculated. The data were analyzed statistically using a one-way analysis of variance, followed by Tukey's multiple comparisons test ( $n = 3, p < 0.05$ ).

### 2.2.3. Mechanical Properties

The mechanical properties of the produced polymeric formulations were characterized using a TA-XT plus texture analyzer. The dried films (25 × 10 mm) were clamped between the grips, leaving a constant length of the films below stress (20 mm). The upper clamp was lifted at a constant speed of 0.5 mm/s until fracturing the film. The tensile strength, Young's modulus, and tensile elongation at break were determined from the stress–strain curve. Three replicates were carried out. The mean and the standard deviation were calculated. The data were analyzed statistically using a one-way analysis of variance, followed by Tukey's multiple comparisons test ( $n = 3, p < 0.05$ ).

### 2.2.4. In Vitro Swelling Evaluation

The in vitro swelling behavior of the produced polymeric discs was evaluated in a biobase thermostatic shaking water bath SWB-A, at 37 °C in buffers of equal ionic strength, at pH 1.2 and pH 7.4. Three replicates of each formulation as dried discs were initially weighed and placed in amber glass vials. Each vial was then filled with 10 mL buffer, previously kept at 37 °C in the thermostatic shaking bath. The discs were withdrawn from the vials at predetermined time points using forceps and placed on a thick medical tissue, where they were blotted gently before weighing and immersing them back in their vials in the thermostatic shaking bath. The equilibrium swelling ratio and the swelling

behavior of the produced formulations were investigated via plotting the swelling ratios obtained at each time point (calculated using Equation (1)) versus the time. The swelling rate of each formulation was investigated via fitting the swelling ratios of the first 7 h to the Korsmeyer–Peppas model. All data were analyzed statistically using a two-way analysis of variance test, followed by Tukey's multiple comparisons test ( $n = 3, p < 0.05$ ). The statistical tests and the graphs were made using a GraphPad Prism software version 9.4.0.

$$\text{Swelling ratio (\%)} = \left[ \frac{\text{The weight of the swollen disc} - \text{The initial weight of the dried disc}}{\text{The weight of the swollen disc}} \right] \times 100\% \quad (1)$$

### 2.2.5. In Vitro Drug Release Studies

The in vitro release of the model drug (5-amino salicylic acid) was investigated, using a modified method of Heelan and Corrigan, in a biobase thermostatic shaking water bath SWB-A, operating at 100 round per minute and 37 °C in buffers of equal ionic strength, at pH 1.2 and pH 7.4 [16]. Three replicates of each formulation were placed in 28 mL McCartney bottles. Each bottle was then filled with 20 mL buffer, previously kept at 37 °C in the thermostatic shaking bath. A 0.5 mL sample was withdrawn at predetermined time points and replaced with 0.5 mL fresh buffer. The 0.45 µm syringe filters were used to filter the withdrawn samples prior measuring their absorbance in the UV–vis spectrophotometer at 300 nm (pH 1.2) and 330 nm (pH 7.4). Fully validated calibration curves were constructed at the two pH values to determine the concentration of the model drug. The release profiles of 5-amino salicylic acid were constructed via plotting the cumulative release percentage achieved at each time point versus the time. The release rate and mechanism of the drug release were examined after fitting the first 60% of the release data to the Korsmeyer–Peppas model. All data were analyzed statistically using a two-way analysis of variance test, followed by Tukey's multiple comparisons test ( $n = 3, p < 0.05$ ). The statistical tests and the graphs were made using a GraphPad Prism software version 9.4.0.

## 3. Results and Discussion

### 3.1. Preparation of Smart Polymeric Formulations

The main objective of this work was to develop a smart oral drug delivery system capable of delivering drugs with poor solubility and/or poor permeability to their site of action, selectively, with proper dosing and timing. To develop this system, a pH–time-dependent approach was designed, based on copolymerized formulations crosslinked by EGDMA and loaded with capmul MCM C8 (dissolution/bioavailability enhancer). The polymeric smart system was based on HEMA, HEMA copolymerized with MAA, or HEMA copolymerized with DMAEMA. The optimization of this smart system was studied in this work to achieve a colon-specific drug delivery, thereby improving the therapeutic efficacy, reducing the dosing frequency and potential side effects, as well as improving patient acceptance. Capmul<sup>®</sup> MCM products are usually obtained from the esterification of vegetable-sourced acids with glycerin. They have been extensively used in food products, such as confectionery, ice creams, bakery, and chewing gums. They can improve the dissolution/permeability of poorly soluble/absorbed drugs [17]. Shailendrakumar et al. [18] employed a capmul<sup>®</sup> MCM product with palm oil to improve the oral bioavailability of pentoxifylline. In another work, Bayan et al. [19] reported the potential use of capmul MCM C8 to improve the dissolution of poorly soluble drugs. The produced polymeric formulations (Table 1) were loaded with 5-amino salicylic acid as a model drug, which is characterized by poor solubility/permeability and used as a first-choice drug in the treatment of inflammatory bowel diseases that affect mainly the colon. A free-radical thermal polymerization technique was used to successfully synthesize eighteen polymeric formulations using AIBN as a thermal initiator. The drug-loaded formulations showed a satisfactory drug entrapment efficiency of ~92% (Table 2).

**Table 2.** The EE% values of the produced formulations.

| Formulation | EE%          |
|-------------|--------------|
| F1          | 90.11 ± 1.84 |
| F2          | 92.73 ± 2.45 |
| F3          | 92.79 ± 1.97 |
| F4          | 93.79 ± 1.16 |
| F5          | 92.48 ± 2.01 |
| F6          | 91.92 ± 3.07 |
| F7          | 91.05 ± 0.53 |
| F8          | 92.31 ± 1.42 |
| F9          | 92.20 ± 1.38 |

### 3.2. Dynamic Mechanical Thermal (DMT) Analysis

The Tg values of the produced formulations are summarized in Table 3. All formulations had Tg values between 120 and 130 °C. The employment of the drug demonstrated an insignificant effect on the Tg value of the polymer. The used concentration of the bioavailability enhancer, capmul MCM C8, had no significant effect on the Tg value of the polymer as there was no significant difference between D1 and D2, F1 and F2, D7 and D8, as well as F7 and F8. The Tg value was reduced significantly with an increasing concentration of the crosslinker (EGDMA), as demonstrated by D4, D5, and D6 and F4, F5, and F6. This indicates the formation of a more rigid structure upon increasing the crosslinker concentration. Increasing the MAA and DMAEMA concentrations had no significant effect on the Tg value, as demonstrated between D3 and D4, F3 and F4, D8 and D9, as well as F8 and F9.

**Table 3.** The Tg values of the produced polymeric films.

| Formulation | Tg (°C)      |
|-------------|--------------|
| D1          | 127.4 ± 1.27 |
| D2          | 126.6 ± 0.66 |
| D3          | 123.4 ± 0.95 |
| D4          | 120.3 ± 0.78 |
| D5          | 122.6 ± 0.81 |
| D6          | 125.1 ± 1.15 |
| D7          | 129.5 ± 1.04 |
| D8          | 128.1 ± 1.18 |
| D9          | 128.4 ± 0.71 |
| F1          | 126.3 ± 0.91 |
| F2          | 126.0 ± 1.10 |
| F3          | 122.9 ± 0.87 |
| F4          | 121.8 ± 1.31 |
| F5          | 123.0 ± 1.17 |
| F6          | 125.4 ± 0.57 |
| F7          | 129.2 ± 1.39 |
| F8          | 128.6 ± 1.22 |
| F9          | 129.8 ± 0.62 |

### 3.3. Mechanical Properties

The mechanical properties (tensile strength, Young's modulus, and tensile elongation at break) of the produced formulations are summarized in Table 4. The employment of the drug demonstrated an insignificant effect on the mechanical properties of the polymer. The used concentration of the bioavailability enhancer, capmul MCM C8, had no significant effect on the mechanical properties of the polymer as there was no significant difference between D1 and D2, F1 and F2, D7 and D8, as well as F7 and F8 in the values of the tensile strength, Young's modulus, and tensile elongation at break. The tensile strength and Young's modulus values were increased significantly, while the tensile elongation-at-break value reduced significantly, with an increasing concentration of the crosslinker (EGDMA),

as demonstrated by D4, D5, and D6 and F4, F5, and F6. This indicates the formation of a more rigid structure upon increasing the crosslinker concentration. Increasing the MAA concentrations had reduced the tensile strength and Young's modulus values, while it increased the tensile elongation-at-break value, as demonstrated between D3 and D4 as well as F3 and F4. Increasing the DMAEMA concentrations had increased the tensile strength and Young's modulus values, while it reduced the tensile elongation-at-break value, as demonstrated between D3 and D4 as well as F3 and F4.

**Table 4.** The mechanical properties of the produced polymeric films.

| Formulation | Tensile Strength (MPa) | Young's Modulus (MPa) | Tensile Elongation at Break (%) |
|-------------|------------------------|-----------------------|---------------------------------|
| D1          | 5.34 ± 0.52            | 33.02 ± 0.87          | 2.38 ± 0.19                     |
| D2          | 5.06 ± 0.19            | 31.07 ± 0.49          | 2.08 ± 0.29                     |
| D3          | 4.67 ± 0.43            | 28.47 ± 0.79          | 2.62 ± 0.12                     |
| D4          | 4.40 ± 0.24            | 23.99 ± 1.26          | 3.97 ± 0.32                     |
| D5          | 5.05 ± 0.20            | 27.42 ± 0.71          | 3.25 ± 0.21                     |
| D6          | 5.45 ± 0.30            | 33.76 ± 0.36          | 2.35 ± 0.25                     |
| D7          | 5.79 ± 0.22            | 36.64 ± 1.76          | 2.07 ± 0.58                     |
| D8          | 5.30 ± 0.41            | 33.21 ± 0.77          | 2.52 ± 0.31                     |
| D9          | 6.10 ± 0.32            | 37.79 ± 2.60          | 2.15 ± 0.60                     |
| F1          | 5.10 ± 0.45            | 32.00 ± 0.50          | 2.38 ± 0.38                     |
| F2          | 5.89 ± 1.05            | 30.99 ± 0.79          | 1.92 ± 0.10                     |
| F3          | 5.57 ± 0.43            | 26.86 ± 0.90          | 2.93 ± 0.50                     |
| F4          | 4.66 ± 0.41            | 25.09 ± 0.64          | 3.87 ± 0.23                     |
| F5          | 4.94 ± 0.29            | 27.60 ± 1.04          | 3.18 ± 0.27                     |
| F6          | 5.37 ± 0.17            | 31.61 ± 1.28          | 2.43 ± 0.29                     |
| F7          | 5.84 ± 0.34            | 36.48 ± 1.95          | 2.15 ± 0.47                     |
| F8          | 5.65 ± 0.41            | 33.98 ± 1.35          | 2.60 ± 0.23                     |
| F9          | 6.08 ± 0.07            | 37.06 ± 3.00          | 2.07 ± 0.50                     |

### 3.4. In Vitro Swelling Evaluation

The swelling behavior of a polymer in a fluid is an intrinsic property of the polymeric structure, which occurs as a result of the penetration of the liquid into the voids between the polymeric chains. This behavior is governed by the polymer–fluid and polymer–polymer interactions [20]. The maximum or equilibrium swelling ratio is reached when a balance takes place between these interactions, and it can be affected by some triggers, such as ionic strength, temperature, and pH. The swelling behavior of a polymeric carrier plays an important role in controlling the drug release as it can facilitate the diffusion of the drug through the polymeric matrix as well as the erosion of the polymer [2]. The in vitro swelling behavior of the synthesized polymers was investigated at pH 1.2 and pH 7.4, simulating the pH conditions the drug will face during its way to the colon. The in vitro swelling profile and equilibrium swelling ratio of the synthesized polymers at each pH are presented in Figures 1–3 and Supplementary Materials (Figures S1–S11). Table 5 shows the swelling rate constants (*k*) at each pH, estimated after fitting to the Korsmeyer–Peppas equation. The used concentration of the bioavailability enhancer, capmul MCM C8, had no significant effect on the swelling behavior of the polymers, as there was no significant difference between D1 and D2 as well as D7 and D8 at each pH. The swelling ratio and rate were reduced significantly with an increasing concentration of the crosslinker (EGDMA), as demonstrated by the significant differences in the swelling behavior between D4, D5, and D6 at each pH. This can be attributed to the reduced polymer's elasticity and the formation of a more rigid structure upon increasing the crosslinker concentration [21]. Polymers, based on HEMA without MAA or DMAEMA, displayed statistically similar swelling profiles at the two pH values, as demonstrated for D1 and D2 at the two pH values. This can be contributed to the absence of ionizable pendant groups in these polymers, so they exist in the neutral form at the simulated gastric and intestinal fluids. Polymers, based on HEMA-co-MAA and HEMA-co-DMAEMA, displayed a pH-responsive swelling. Regarding the

HEMA-co-MAA formulations, a significant higher swelling profile was observed at pH 7.4 compared to that at pH 1.2. This can be contributed to the greater ionization of the anionic pendant groups (MAA) in these polymers at the simulated intestinal fluid compared to that at the simulated gastric fluid, so greater electrostatic repulsions between the pendant groups and enhanced swelling [22]. Regarding the HEMA-co-DMAEMA formulations, a significant higher swelling profile was observed at pH 1.2 compared to that at pH 7.4. This can be contributed to the greater ionization of the cationic pendant group (DMAEMA) in these polymers at the simulated gastric fluid compared to that at the simulated intestinal fluid [14]. Increasing the DMAEMA concentration had no significant effect on the swelling profile at the two pH values, as demonstrated between D8 and D9. Increasing the MAA concentration had no significant effect on the swelling profile pH 1.2, while it increased the swelling significantly at pH 7.4, as demonstrated between D3 and D4. The equilibrium swelling ratios of the polymers, based on HEMA and HEMA-co-DMAEMA, were reached within 24 h at the two pH values. The equilibrium swelling ratios of polymers, based on HEMA-co-MAA, were reached within 24 h at pH 1.2 and 72 h at pH 7.4. equilibrium ratios of ~30, ~25, ~19, and ~55% were obtained for D1–D4, D5, D6, and D7–D9, respectively, at pH 1.2. At pH 7.4, equilibrium ratios of ~30% were obtained for polymers, based on HEMA and HEMA-co-DMAEMA. The HEMA-co-MAA-based polymers exhibited a pH-responsive swelling at pH 7.4 with ~70, ~80, ~67, and ~54% equilibrium ratios obtained for D3, D4, D5, and D6, respectively.

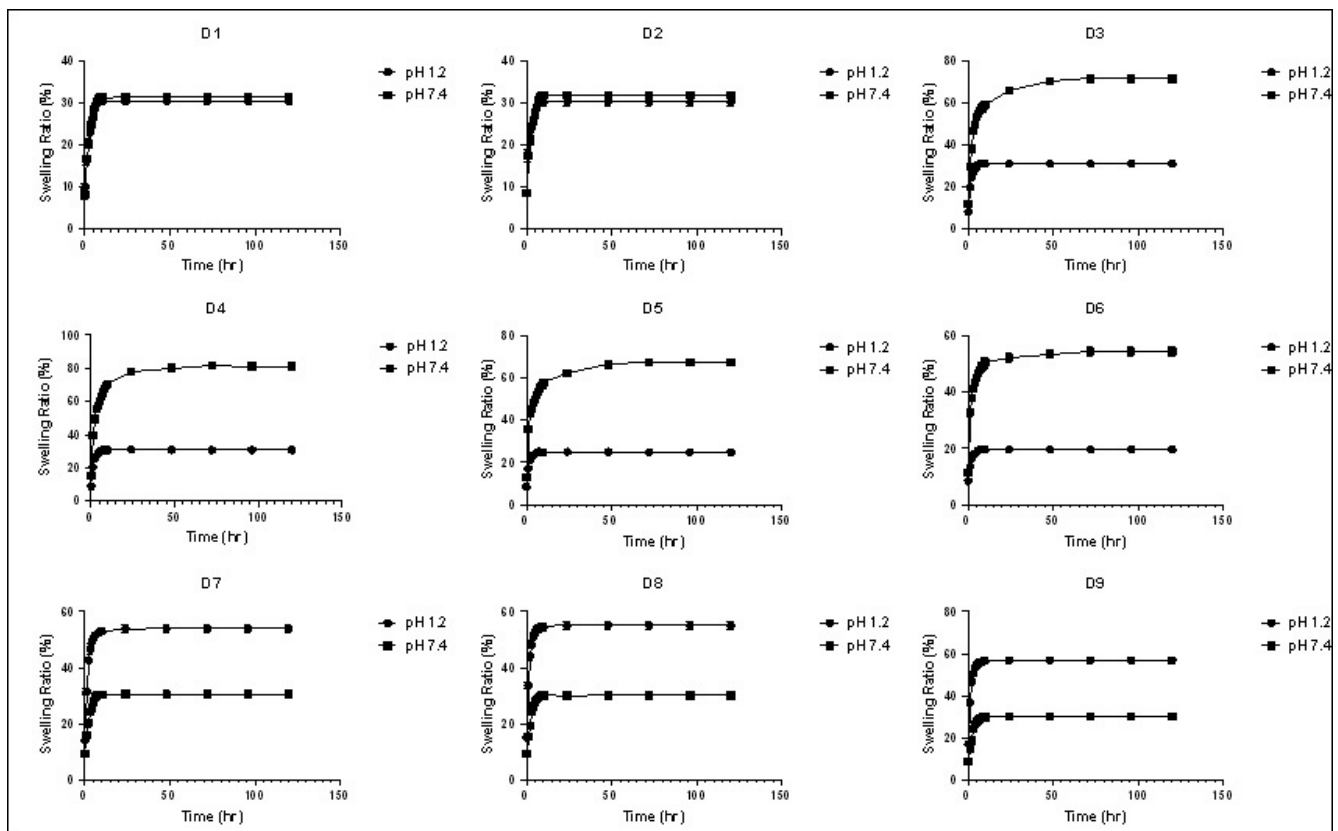


Figure 1. The swelling profiles of the polymeric formulations (mean  $\pm$  SD,  $n = 3$ ) at pH 1.2 and pH 7.4.

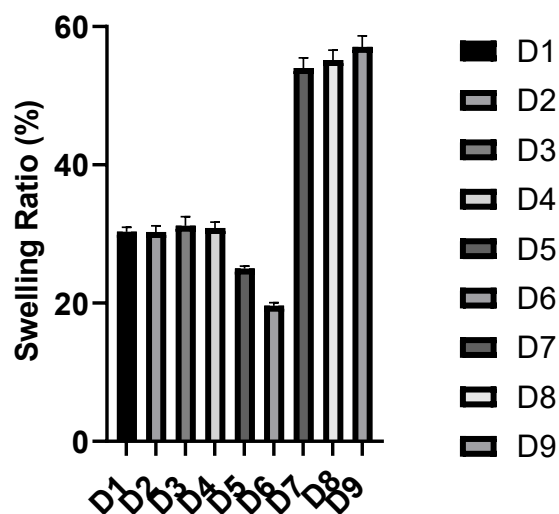


Figure 2. The equilibrium swelling ratios of the polymeric formulations (mean ± SD, *n* = 3) at pH 1.2.

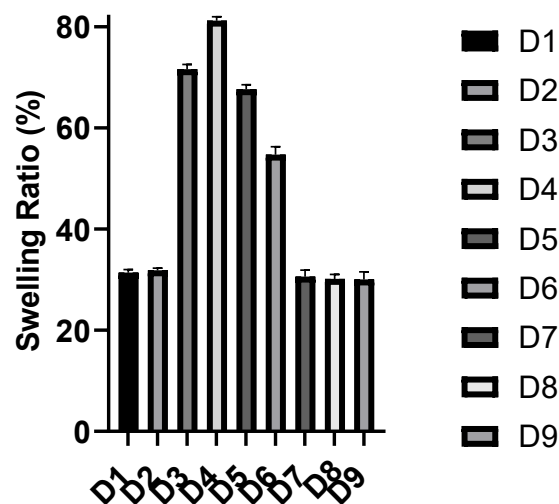


Figure 3. The equilibrium swelling ratios of the polymeric formulations (mean ± SD, *n* = 3) at pH 7.4.

Table 5. The swelling rate constants (*k*) and  $R^2$  obtained from fitting to the Korsmeyer–Peppas model.

| Formulation | $R^2$ | <i>k</i> |
|-------------|-------|----------|
| D1 pH 1.2   | 0.987 | 0.177    |
| D2 pH 1.2   | 0.999 | 0.176    |
| D3 pH 1.2   | 0.982 | 0.185    |
| D4 pH 1.2   | 0.979 | 0.191    |
| D5 pH 1.2   | 0.980 | 0.165    |
| D6 pH 1.2   | 0.994 | 0.138    |
| D7 pH 1.2   | 0.982 | 0.314    |
| D8 pH 1.2   | 0.982 | 0.331    |
| D9 pH 1.2   | 0.979 | 0.355    |
| D1 pH 7.4   | 0.997 | 0.171    |
| D2 pH 7.4   | 0.998 | 0.175    |
| D3 pH 7.4   | 0.995 | 0.297    |
| D4 pH 7.4   | 0.985 | 0.369    |
| D5 pH 7.4   | 0.969 | 0.313    |
| D6 pH 7.4   | 0.965 | 0.280    |
| D7 pH 7.4   | 0.985 | 0.176    |
| D8 pH 7.4   | 0.973 | 0.174    |
| D9 pH 7.4   | 0.971 | 0.168    |

### 3.5. In Vitro Drug Release Studies

The in vitro release of the 5-amino salicylic acid from the prepared polymeric formulations was investigated at pH 1.2 and pH 7.4, simulating the environmental conditions that it will face the formulation during its transit through the GI to the colon. The calibration curve of 5-amino salicylic acid at each pH is presented in the Supplementary Materials (Figures S12 and S13). The in vitro release profiles of the 5-amino salicylic acid from the synthesized polymers at each pH are shown in Figure 4 and Supplementary Materials (Figures S14–S24). Table 6 displays the  $R^2$ ,  $n$  values, and release rate constants ( $k$ ) at each pH, estimated after fitting the release data to the Korsmeyer–Peppas model. The used concentration of the bioavailability enhancer, capmul MCM C8, has significantly increased the release profile of the 5-amino salicylic acid, as demonstrated by D1, D2 and D7, D8 at each pH. This can be contributed to forming micelles within the polymeric matrix by the capmul<sup>®</sup> MCM C8, thus enhancing the dissolution and release of the 5-amino salicylic acid [19]. The release profile of the model drug was also decreased significantly with an increasing concentration of the crosslinker (EGDMA), as demonstrated by F4, F5, and F6 at each pH. This agrees with the in vitro swelling finding, and it is contributed to the reduced polymer's elasticity and the formation of a more rigid structure [21]. At pH 1.2, the F1–F6 polymeric formulations (based on HEMA and HEMA-co-MAA) demonstrated a higher ability to retard the release of the model drug compared with the HEMA-co-DMAEMA polymeric formulations (F7–F9). After 5 h, a less than ~25% cumulative release was achieved for F1–F6, while a more than ~35% cumulative release was reached for F7–F9 at pH 1.2. This can be justified by the existence of the HEMA- and HEMA-co-MAA-based polymers in a neutral form in the simulated gastric fluid, while the existence of the HEMA-co-DMAEMA-based polymers in the ionized form is due to the ionization of the cationic pendant groups (DMAEMA). This results in greater electrostatic repulsions between the pendant groups (DMAEMA) and exhibits a pH-responsive swelling and release. At pH 7.4, the HEMA-co-MAA-based formulations (F3–F6) demonstrated a higher release rate compared with the other formulations. This can be explained by the presence of these formulations in the ionized form, due to the ionization of the anionic pendant groups (MAA), thus eliciting a pH-responsive swelling and release. F4 achieved the highest cumulative drug release at pH 7.4 with a ~75% cumulative release achieved after 12 h. This formulation also achieved a ~25% cumulative release after 5 h at pH 1.2. An oral drug delivery system is estimated to reach the colon after 5–6 h of administration in healthy persons. A colonic drug delivery system should prevent/retard the drug release during these 5–6 h while permitting its release afterward. The in vitro release studies demonstrated the potential ability of F4 to retard the release of the 5-amino salicylic acid during its residence in the stomach and small intestine while triggering the payload to the colon. This indicates their potential applicability as a smart colonic delivery system. The mechanism of the drug release from a polymeric carrier is usually controlled through diffusion, swelling, and/or chemical cleavage [23]. The first 60% of the release data at the two pH values were fitted to the Korsmeyer–Peppas model.

$$F = k t^n \quad (2)$$

This exponential model (Equation (2):  $F$  represents the fraction of drug released at a specific time,  $k$  represents the release rate constant,  $t$  is time in hours, and  $n$  is the release exponent) is widely used with polymeric formulations to investigate  $k$  and the mechanism of the drug release. Plotting  $\log F$  versus  $t$  will result in a linear relationship, where the  $n$  value represents the slope of the line, and its value indicates the mechanism of the drug release. The antilog of the y intercept represents  $k$ . The mechanism of the drug release is interpreted as a Fickian diffusion if  $n$  is less than or equal to 0.5, interpreted as an anomalous release if  $n$  is less than 1.0 and greater than 0.5, interpreted as a case 2 transport if  $n$  equals 1, and interpreted as a super case 2 transport if  $n$  is greater than 1 [24]. As described in Table 6, all the polymeric formulations at pH 7.4 and F7–F9 at pH 1.2 had an  $n$  value greater than 0.5 and less than 1, which refers to an anomalous mechanism of the drug release. This means that the release of the 5-amino salicylic acid in these formulations is controlled by

the diffusion and swelling of the polymer. Other formulations (F1–F6) at pH 1.2 had an  $n$  value less than 0.5, which refers to a Fickian diffusion mechanism.

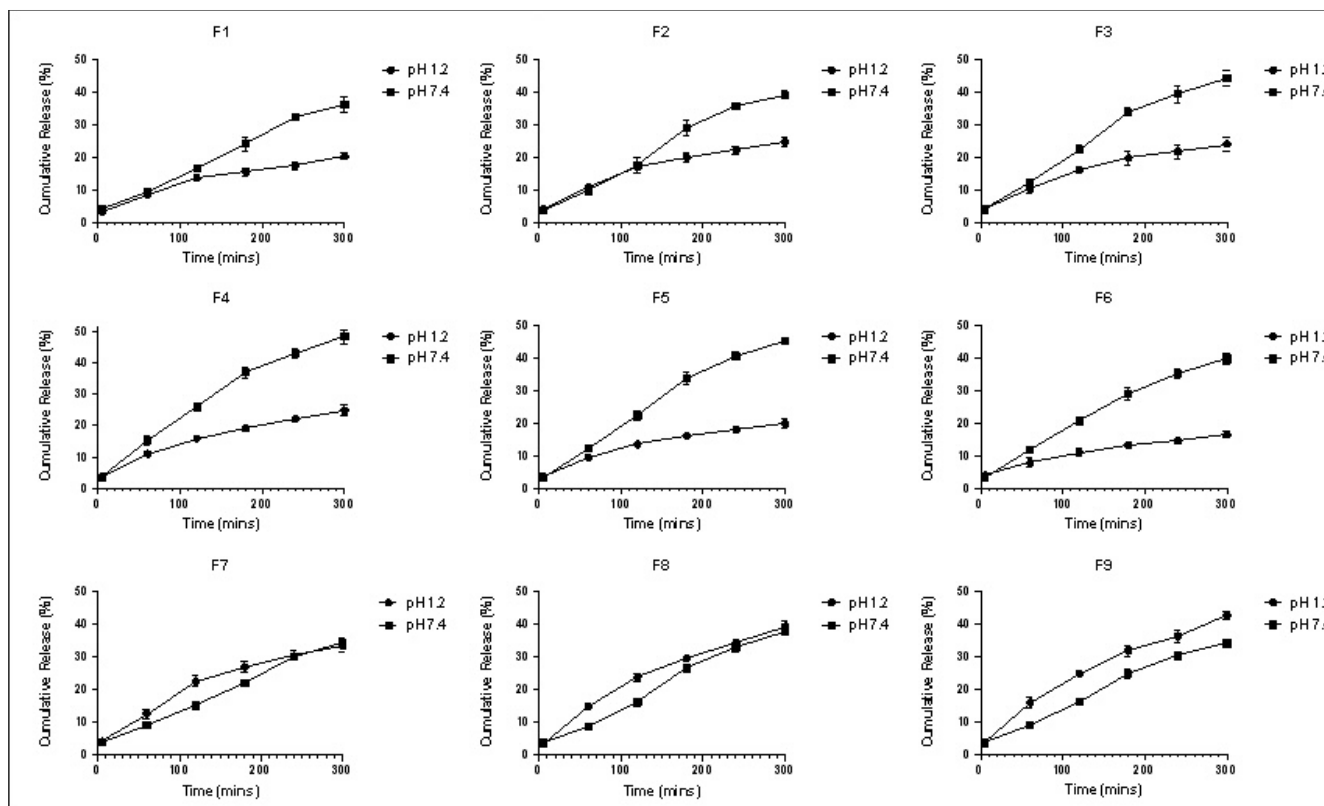


Figure 4. The release profiles of the polymeric formulations (mean  $\pm$  SD,  $n = 3$ ) at pH 1.2 and pH 7.4.

Table 6.  $R^2$ ,  $n$ , and  $k$  obtained from fitting the release data to the Korsmeyer–Peppas model.

| Formulation | $R^2$ | $n$   | $k$   |
|-------------|-------|-------|-------|
| F1 pH 1.2   | 0.989 | 0.444 | 0.095 |
| F2 pH 1.2   | 0.994 | 0.450 | 0.119 |
| F3 pH 1.2   | 0.993 | 0.453 | 0.115 |
| F4 pH 1.2   | 0.998 | 0.449 | 0.117 |
| F5 pH 1.2   | 0.997 | 0.398 | 0.103 |
| F6 pH 1.2   | 0.983 | 0.343 | 0.090 |
| F7 pH 1.2   | 0.990 | 0.518 | 0.147 |
| F8 pH 1.2   | 0.994 | 0.585 | 0.154 |
| F9 pH 1.2   | 0.999 | 0.598 | 0.162 |
| F1 pH 7.4   | 0.965 | 0.556 | 0.133 |
| F2 pH 7.4   | 0.969 | 0.586 | 0.138 |
| F3 pH 7.4   | 0.985 | 0.606 | 0.159 |
| F4 pH 7.4   | 0.997 | 0.634 | 0.172 |
| F5 pH 7.4   | 0.989 | 0.639 | 0.153 |
| F6 pH 7.4   | 0.993 | 0.610 | 0.142 |
| F7 pH 7.4   | 0.964 | 0.541 | 0.128 |
| F8 pH 7.4   | 0.961 | 0.587 | 0.131 |
| F9 pH 7.4   | 0.972 | 0.570 | 0.127 |

#### 4. Conclusions

This research work has investigated the development of a smart drug delivery system capable of achieving a colonic-specific drug delivery. A free-radical polymerization method was used to successfully synthesize polymeric formulations loaded with 5-amino salicylic acid as a model drug. The drug-loaded formulations showed a satisfactory drug



entrapment efficiency of ~92%. These formulations were based on copolymerized formulations (HEMA, HEMA-co-MAA, or HEMA-co-DMAEMA) crosslinked by EGDMA and loaded with capmul MCM C8 (dissolution/bioavailability enhancer). The optimization of this smart system was investigated in this work to achieve a colon-specific drug delivery, thereby improving the therapeutic efficacy, reducing the dosing frequency and potential side effects, as well as improving patient acceptance. Polymers, based on HEMA-co-MAA, exhibited a significant higher swelling profile at pH 7.4 compared to that at pH 1.2, which is contributed to the greater ionization of the anionic pendant groups (MAA) in these polymers. The *in vitro* release studies of F4 have also demonstrated the potential ability of this carrier to delay the release of 5-amino salicylic acid during its stay in the stomach and small intestine while triggering the payload to the colon. This makes it promising to achieve a colonic-specific delivery for the potential treatment of colon-associated diseases, such as inflammatory bowel diseases, and to improve the bioavailability of BSC class IV drugs. Further work will assess the *in vivo* behavior, biocompatibility, and safety of this system.

**Supplementary Materials:** The following supporting information can be downloaded at: <https://www.mdpi.com/article/10.3390/polym14173697/s1>, Figure S1: The swelling profile of the polymeric formulations (mean  $\pm$  SD,  $n = 3$ ) at pH 1.2; Figure S2: The swelling profile of the polymeric formulations (mean  $\pm$  SD,  $n = 3$ ) at pH 7.4; Figure S3: The swelling profile of D1 (mean  $\pm$  SD,  $n = 3$ ) at each pH; Figure S4: The swelling profile of D2 (mean  $\pm$  SD,  $n = 3$ ) at each pH; Figure S5: The swelling profile of D3 (mean  $\pm$  SD,  $n = 3$ ) at each pH; Figure S6: The swelling profile of D4 (mean  $\pm$  SD,  $n = 3$ ) at each pH; Figure S7: The swelling profile of D5 (mean  $\pm$  SD,  $n = 3$ ) at each pH; Figure S8: The swelling profile of D6 (mean  $\pm$  SD,  $n = 3$ ) at each pH; Figure S9: The swelling profile of D7 (mean  $\pm$  SD,  $n = 3$ ) at each pH; Figure S10: The swelling profile of D8 (mean  $\pm$  SD,  $n = 3$ ) at each pH; Figure S11: The swelling profile of D9 (mean  $\pm$  SD,  $n = 3$ ) at each pH; Figure S12: Calibration curve of 5-amino salicylic acid at pH 1.2; Figure S13: Calibration curve of 5-amino salicylic acid at pH 7.4; Figure S14: The release profile of the polymeric formulations (mean  $\pm$  SD,  $n = 3$ ) at pH 1.2.; Figure S15: The release profile of the polymeric formulations (mean  $\pm$  SD,  $n = 3$ ) at pH 7.4.; Figure S16: The release profile of F1 (mean  $\pm$  SD,  $n = 3$ ) at each pH; Figure S17: The release profile of F2 (mean  $\pm$  SD,  $n = 3$ ) at each pH; Figure S18: The release profile of F3 (mean  $\pm$  SD,  $n = 3$ ) at each pH; Figure S19: The release profile of F4 (mean  $\pm$  SD,  $n = 3$ ) at each pH; Figure S20: The release profile of F5 (mean  $\pm$  SD,  $n = 3$ ) at each pH; Figure S21: The release profile of F6 (mean  $\pm$  SD,  $n = 3$ ) at each pH; Figure S22: The release profile of F7 (mean  $\pm$  SD,  $n = 3$ ) at each pH; Figure S23: The release profile of F8 (mean  $\pm$  SD,  $n = 3$ ) at each pH; Figure S24: The release profile of F9 (mean  $\pm$  SD,  $n = 3$ ) at each pH.

**Author Contributions:** M.F.B.: conceptualization, project administration, methodology design, writing, review, editing, and supervision; S.M.M. and M.Y.B.: methodology, review, and editing; M.S.S.: review and editing; K.C.: supervision, review, and editing; B.C.: review and editing. All authors have read and agreed to the published version of the manuscript.

**Funding:** This research was funded by Philadelphia University, Amman, Jordan. Grant No. 511/34/100 PU.

**Institutional Review Board Statement:** Not applicable.

**Informed Consent Statement:** Not applicable.

**Data Availability Statement:** The data presented in this study are available on request from the corresponding author.

**Acknowledgments:** The authors extend their appreciation to the Deanship of Scientific Research at King Khalid University for funding this work through the Research Group (Large) (Project number RGP.2/31/43).

**Conflicts of Interest:** The authors declare no conflict of interest.

## References

- Xu, Y.; Shrestha, N.; Pr eat, V.; Beloqui, A. Overcoming the intestinal barrier: A look into targeting approaches for improved oral drug delivery systems. *J. Control. Release* **2020**, *322*, 486–508. [CrossRef] [PubMed]
- Bayan, M.F.; Bayan, R.F. Recent advances in mesalamine colonic delivery systems. *Futur. J. Pharm. Sci.* **2020**, *6*, 1–7. [CrossRef]
- Ruan, W.; Engevik, M.A.; Spinler, J.K.; Versalovic, J. Healthy Human Gastrointestinal Microbiome: Composition and Function After a Decade of Exploration. *Dig. Dis. Sci.* **2020**, *65*, 695–705. [CrossRef]
- Bayan, M.F.; Salem, M.S.; Bayan, R.F. Development and In Vitro Evaluation of a Large-Intestinal Drug Delivery System. *Res. J. Pharm. Technol.* **2022**, *15*, 35–39. [CrossRef]
- Guo, Y.; Zong, S.; Pu, Y.; Xu, B.; Zhang, T.; Wang, B. Advances in pharmaceutical strategies enhancing the efficiencies of oral colon-targeted delivery systems in inflammatory bowel disease. *Molecules* **2018**, *23*, 1622. [CrossRef] [PubMed]
- Ginwala, R.; Bhavsar, R.; Chigbu, D.G.I.; Jain, P.; Khan, Z.K. Potential Role of Flavonoids in Treating Chronic Inflammatory Diseases with a Special Focus on the Anti-Inflammatory Activity of Apigenin. *Antioxidants* **2019**, *8*, 35. [CrossRef]
- Veloso, P.M.; Machado, R.; Nobre, C. Mesalazine and inflammatory bowel disease—From well-established therapies to progress beyond the state of the art. *Eur. J. Pharm. Biopharm.* **2021**, *167*, 89–103. [CrossRef] [PubMed]
- Bak, A.; Ashford, M.; Brayden, D.J. Local delivery of macromolecules to treat diseases associated with the colon. *Adv. Drug Deliv. Rev.* **2018**, *136*, 2–7. [CrossRef]
- Sardou, H.S.; Akhgari, A.; Mohammadpour, A.H.; Namdar, A.B.; Kamali, H.; Jafarian, A.H.; Garekani, H.A.; Sadeghi, F. Optimization study of combined enteric and time-dependent polymethacrylates as a coating for colon targeted delivery of 5-ASA pellets in rats with ulcerative colitis. *Eur. J. Pharm. Sci.* **2021**, *168*, 106072. [CrossRef]
- Rehman, F.; Rahim, A.; Airoidi, C.; Volpe, P.L. Preparation and characterization of glycidyl methacrylate organo bridges grafted mesoporous silica SBA-15 as ibuprofen and mesalamine carrier for controlled release. *Mater. Sci. Eng. C* **2016**, *59*, 970–979. [CrossRef]
- Mirabbasi, F.; Dorkoosh, F.A.; Moghimi, A.; Shahsavari, S.; Babanejad, N.; Seifirad, S. Preparation of Mesalamine Nanoparticles Using a Novel Polyurethane-Chitosan Graft Copolymer. *Pharm. Nanotechnol.* **2018**, *5*, 230–239. [CrossRef] [PubMed]
- Englert, C.; Brendel, J.C.; Majdanski, T.C.; Yildirim, T.; Schubert, S.; Gottschaldt, M.; Windhab, N.; Schubert, U.S. Pharmapolymers in the 21st century: Synthetic polymers in drug delivery applications. *Prog. Polym. Sci.* **2018**, *87*, 107–164.
- Tomić, S.; Nikodinović-Runić, J.; Vukomanović, M.; Babić, M.M.; Vuković, J.S. Novel Hydrogel Scaffolds Based on Alginate, Gelatin, 2-Hydroxyethyl Methacrylate, and Hydroxyapatite. *Polymers* **2021**, *13*, 932. [CrossRef] [PubMed]
- Roointan, A.; Farzanfar, J.; Mohammadi-Samani, S.; Behzad-Behbahani, A.; Farjadian, F. Smart pH responsive drug delivery system based on poly (HEMA-co-DMAEMA) nanohydrogel. *Int. J. Pharm.* **2018**, *552*, 301–311. [CrossRef] [PubMed]
- Zia, M.A.; Sohail, M.; Minhas, M.U.; Sarfraz, R.M.; Khan, S.; de Matas, M.; Hussain, Z.; Abbasi, M.; Shah, S.A.; Kousar, M.; et al. HEMA based pH-sensitive semi IPN microgels for oral delivery; A rationale approach for ketoprofen. *Drug Dev. Ind. Pharm.* **2020**, *46*, 272–282. [CrossRef]
- Obaidat, R.M.; Tashtoush, B.M.; Bayan, M.F.; Al Bustami, R.T.; Alnaief, M. Drying Using Supercritical Fluid Technology as a Potential Method for Preparation of Chitosan Aerogel Microparticles. *AAPS PharmSciTech* **2015**, *16*, 1235–1244. [CrossRef]
- Li, S.; Madan, P.; Lin, S. Application of Capmul MCM and caprylic acid for the development of danazol-loaded SEDDS. *Pharm. Dev. Technol.* **2014**, *20*, 886–896. [CrossRef]
- Shailendrakumar, A.M.; Ghate, V.M.; Kinra, M.; Lewis, S.A. Improved Oral Pharmacokinetics of Pentoxifylline with Palm Oil and Capmul®MCM Containing Self-Nano-Emulsifying Drug Delivery System. *AAPS PharmSciTech* **2020**, *21*, 1–12.
- Bayan, M.F. Drug release control and enhancement using carriers with different concentrations of Capmul®MCM c8. *Int. J. Appl. Pharm.* **2021**, *13*, 249–252. [CrossRef]
- Saraydin, D.; Çaldiran, Y. In vitro dynamic swelling behaviors of polyhydroxamic acid hydrogels in the simulated physiological body fluids. *Polym. Bull.* **2001**, *46*, 91–98. [CrossRef]
- Garnica-Palafox, I.M.; Sánchez-Arévalo, F.M. Influence of natural and synthetic crosslinking reagents on the structural and mechanical properties of chitosan-based hybrid hydrogels. *Carbohydr. Polym.* **2016**, *151*, 1073–1081. [CrossRef] [PubMed]
- Khan, H.; Chaudhary, J.P.; Meena, R. Anionic carboxymethylagarose-based pH-responsive smart superabsorbent hydrogels for controlled release of anticancer drug. *Int. J. Biol. Macromol.* **2019**, *124*, 1220–1229. [CrossRef] [PubMed]
- Onoyima, C.C.; Okibe, F.G.; Sholadoye, Q.O. Kinetics and mechanisms of doxorubicin release from hydroxyapatite-sodium alginate nanocomposite. *Niger. J. Pharm. Appl. Sci. Res.* **2020**, *9*, 7–13.
- de Stéfano, J.C.Q.; Abundis-Correa, V.; Herrera-Flores, S.D.; Alvarez, A.J. pH-sensitive starch-based hydrogels: Synthesis and effect of molecular components on drug release behavior. *Polymers* **2020**, *12*, 1974. [CrossRef] [PubMed]



MDPI  
St. Alban-Anlage 66  
4052 Basel  
Switzerland  
Tel. +41 61 683 77 34  
Fax +41 61 302 89 18  
[www.mdpi.com](http://www.mdpi.com)

*Polymers* Editorial Office  
E-mail: [polymers@mdpi.com](mailto:polymers@mdpi.com)  
[www.mdpi.com/journal/polymers](http://www.mdpi.com/journal/polymers)





MDPI  
St. Alban-Anlage 66  
4052 Basel  
Switzerland  
Tel: +41 61 683 77 34  
[www.mdpi.com](http://www.mdpi.com)



ISBN 978-3-0365-7370-0